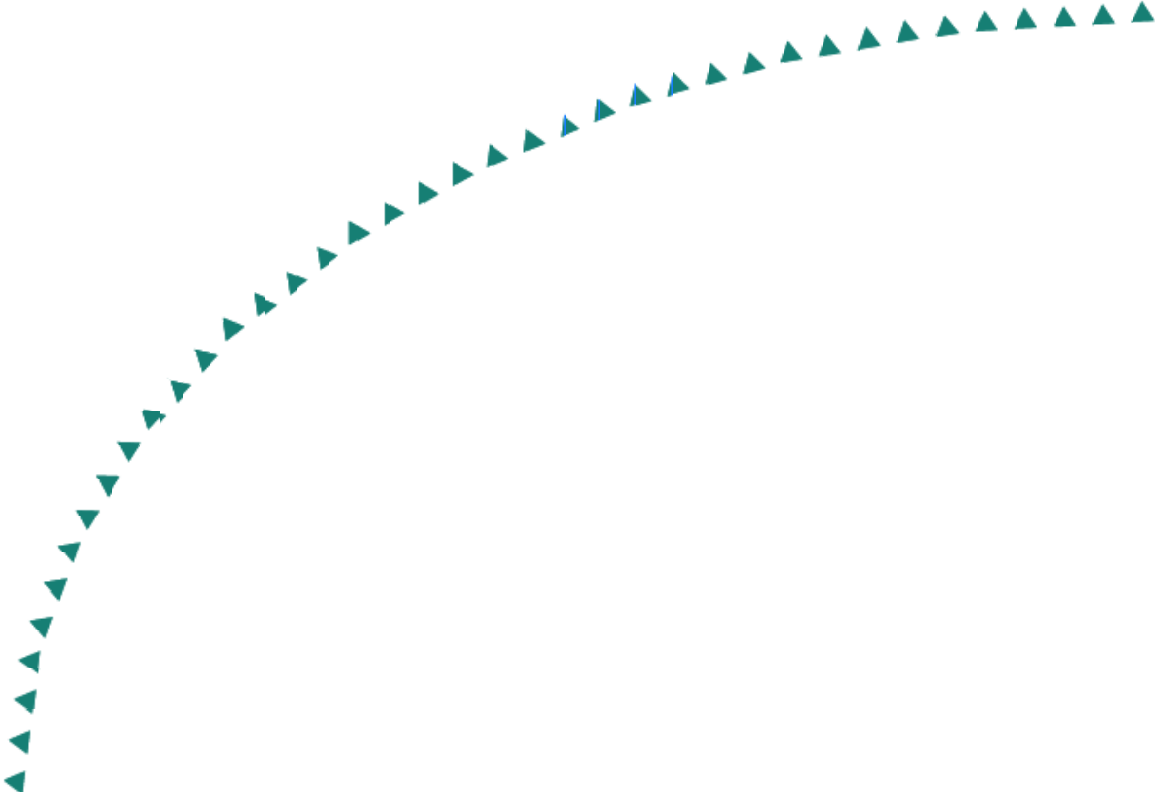


2006-40

Final Report

Load Rating of Composite Steel Curved I-Girder Bridges through Load Testing with Heavy Trucks



Technical Report Documentation Page

1. Report No. MN/RC-2006-40	2.	3. Recipients Accession No.	
4. Title and Subtitle Load Rating of Composite Steel Curved I-Girder Bridges through Load Testing with Heavy Trucks		5. Report Date October 2006	6.
7. Author(s) Dan P. Krzmarzick and Jerome F. Hajjar		8. Performing Organization Report No.	
9. Performing Organization Name and Address Department of Civil Engineering 500 Pillsbury Drive SE University of Minnesota Minneapolis, MN 55455-0220		10. Project/Task/Work Unit No.	11. Contract (C) or Grant (G) No. (c) 81655 (wo) 60
12. Sponsoring Organization Name and Address Minnesota Department of Transportation 395 John Ireland Boulevard Mail Stop 330 St. Paul, Minnesota 55155		13. Type of Report and Period Covered Final Report; 2003-2006	14. Sponsoring Agency Code
15. Supplementary Notes http://www.lrrb.org/PDF/200640.pdf			
16. Abstract (Limit: 200 words) Current techniques for rating of horizontally curved composite steel I-girder bridges often use approximate methods of analysis based on assessment of individual straight girders with altered properties to account for member curvature. This project investigates the behavior and rating of these bridges through load testing with heavy trucks. A five-span continuous two-girder horizontally curved steel I-girder bridge was load tested. Strain and displacement measurements were obtained for the main girders, diaphragms, lateral wind bracing, bearings, composite interaction, and areas of high strain concentrations near stiffener details. Forty-three static tests with different truck load patterns were conducted along with thirteen dynamic tests to assess the bridge response. A linear elastic grillage-based model of the bridge was used to simulate the load patterns. A sensitivity study was carried out based on the tested bridge along with simulations of two other bridges previously tested elsewhere so as to assess the robustness of grillage analysis for use in load rating of horizontally curved steel I-girder bridges. Recommendations are made outlining rating of horizontally curved composite steel I-girder bridges through the use of grillage-based analysis, with and without the use of load testing, and within the context of the AASHTO Load and Resistance Factor Rating (LRFR) and Load Factor Rating (LFR) procedures.			
17. Document Analysis/Descriptors Bridges Curved Steel I-girder Load Rating Load Testing LRFR Torsion		Diaphragm Lateral Wind Bracing Composite Deck Warping Load Distribution Grillage Analysis	18. Availability Statement No restrictions. Document available from: National Technical Information Services, Springfield, Virginia 22161
19. Security Class (this report) Unclassified	20. Security Class (this page) Unclassified	21. No. of Pages 546	22. Price

Load Rating of Composite Steel Curved I-Girder Bridges through Load Testing with Heavy Trucks

Final Report

Prepared by:

Dan P. Krzmarzick

Department of Civil Engineering

University of Minnesota

Minneapolis, Minnesota 55455

Jerome F. Hajjar

Department of Civil and Environmental Engineering

University of Illinois at Urbana-Champaign

Urbana, Illinois 61801

October 2006

Published by:

Minnesota Department of Transportation
Research Services Section
395 John Ireland Boulevard, MS 330
St. Paul, Minnesota 55155-1899

This report represents the results of research conducted by the authors and does not necessarily represent the views or policies of the Minnesota Department of Transportation and/or the Center for Transportation Studies. This report does not contain a standard or specified technique.

The authors and the Minnesota Department of Transportation and/or Center for Transportation Studies do not endorse products or manufacturers. Trade or manufacturers' names appear herein solely because they are considered essential to this report.

Acknowledgements

The authors would like to thank the Offices of Bridges and Structures and Research Administration at the Minnesota Department of Transportation, including G. Peterson, E. Wol Howe, E. Lutgen, L. Johnson, K. Obeidat, D. Davidson, P. Wilson, P. Rowekamp, and B. Loida. Special thanks go to R. Dexter for his work in the initial phase of this research project, to C. Freisinger for her help in the development of the load test, and to M. Brice for his assistance with data collection and assessment. The authors would also like to thank P. Bergson, M. Christensen, J. Ocel, J. Zimmerman, A. Dornbusch, A. Nesvold, C. Tort, B. Erkmen, A. Askarihatamabadi, and S. LaFore from the University of Minnesota for their assistance with this research. Funding for this research was provided by the Minnesota Department of Transportation, the Center for Transportation Studies, and the University of Minnesota. This support is gratefully acknowledged.

Findings, conclusions, and recommendations expressed in this publication are those of the authors and do not necessarily reflect the views of the Minnesota Department of Transportation or the Center for Transportation Studies.

Table of Contents

Chapter 1 Introduction	1
1.1 Objectives	2
1.2 Scope.....	2
1.3 Outline of Report	3
Chapter 2 Literature Review.....	5
2.1 Historical Overview	5
2.2 Load Rating.....	5
2.3 Load Testing	8
2.3.1 Diagnostic Load Tests.....	9
2.3.2 Proof Load Tests	11
2.3.3 Dynamic Load Tests	12
2.4 Analysis.....	13
Chapter 3 Bridge Overview	19
3.1 Overview of Bridge No. 69824.....	19
3.2 Details of Bridge 69824 Unit 2	19
3.2.1 Steel I-Girders	20
3.2.2 Concrete Deck.....	21
3.2.3 Diaphragms	21
3.2.4 Lateral Wind Bracing.....	22
3.2.5 Gusset Plate Details	22
3.2.6 Bearings	22
Chapter 4 Grillage Analysis of Curved Girder Bridge	33
4.1 Verification of UMN Program.....	33
4.2 Modifications to UMN Program	35
4.3 Analysis of Mn/DOT Bridge No. 69824 Unit 2	35
4.3.1 Basis Model for the Bridge	35
4.3.2 Load Distribution: TRUCKLOADS	37
4.4 Comparison between MDX and UMN Program	37
4.4.1 Differences in Analytical Methods	38
4.4.2 Comparisons based on Specific Loading	39
4.4.2.1 Dead Load Comparisons.....	39
4.4.2.2 Live Load Comparisons.....	41
4.4.3 Conclusions.....	42
Chapter 5 Bridge Testing	60
5.1 Instrumentation Plan	60
5.1.1 Instruments.....	60
5.1.1.1 Campbell CR9000 Data logger.....	60
5.1.1.2 Strain Measurements.....	61
5.1.1.3 Displacement Measurements	61
5.1.1.4 Instrument Precision	61

5.1.2 Instrument Locations	62
5.1.2.1 Main Girder Strains.....	62
5.1.2.2 Secondary Location Strains	63
5.1.2.3 Displacements	63
5.2 Truck Test Plan	63
5.2.1 Test Trucks.....	64
5.2.2 Test Configurations.....	64
5.2.2.1 Static Tests	65
5.2.2.2 Dynamic Tests	65
5.3 Reduction of Data	65
5.3.1 Data Recording Process	66
5.3.2 Recording Issues and Erratic Gages	66
5.3.3 Removal of Thermal Strains	67
5.3.4 Conversion from Strains and Voltages to Stresses and Displacements.....	68
5.4 Post-Test Inspection Summary	69
 Chapter 6 Evaluation of Bridge Properties	92
6.1 Composite Section Properties	92
6.1.1 Girder Strain Profile.....	92
6.1.2 Interface Slip.....	93
6.1.3 Neutral Axis	94
6.1.4 Concrete Contribution.....	95
6.2 Load Distribution	97
6.3 Bearing Fixity	99
6.4 Dynamic Impact Factor.....	100
6.4.1 Calculation of the Dynamic Impact Factor.....	100
6.4.2 Dynamic Impact Factors for Bridge No. 69824.....	101
6.4.3 Effects due to Centrifugal Forces	102
6.4.4 Error due to Transverse Position of Vehicle.....	104
6.4.5 Summary of Dynamic Impact Factor for Mn/DOT Bridge No. 69824	105
 Chapter 7 Comparison of Bridge Behavior with Computed Results.....	127
7.1 Analysis Models for Computed Results	127
7.2 Discussion of Measured and Computed Results.....	128
7.2.1 Displacements	129
7.2.2 Girder Stresses	130
7.2.2.1 Bending Stresses at Girder Gage Locations BC, TC, and W.....	130
7.2.2.2 Warping Stresses at Girder Gage Locations BI, BE, TI, and TE.....	131
7.2.3 Diaphragm Stresses.....	133
7.2.4 Lateral Wind Bracing Stresses.....	134
7.3 Measured Fatigue Detail Stresses	135
7.3.1 Gusset Plate Tip	135
7.3.2 Web Gap	137
 Chapter 8 Sensitivity Study of Curved Girder Bridge Analysis and Rating.....	161
8.1 Bridge Descriptions	161

8.1.1 Mn/DOT Bridge No. 69824 Unit 2.....	161
8.1.2 Mn/DOT Bridge No. 27998	162
8.1.3 FHWA Test Specimen	163
8.1.4 Comments about the Bridge Base Models and Analysis with UMN Program.....	163
8.2 Method for Comparisons	164
8.3 Sensitivity Studies.....	166
8.3.1 Study 1: Beam Diaphragm Stiffness due to Knee Brace Region.....	167
8.3.2 Study 2: Vertical Rigid Offsets for Diaphragm Beam Elements	168
8.3.3 Study 3: Composite Action of Beam Diaphragms.....	168
8.3.4 Study 4: Cross-frame Member Size.....	169
8.3.5 Study 5: Lateral Wind Bracing Members	170
8.3.6 Study 6: Diaphragm Spacing	172
8.3.7 Study 7: Transverse Concrete Deck Beams.....	173
8.3.8 Study 8: Rotational DOFs for Transverse Concrete Deck Beams	174
8.3.9 Study 9: Girder Axial DOFs at Piers	175
8.3.10 Study 10: Composite Torsion Constant	176
8.3.11 Study 11: Thickness of Concrete Slab	177
8.3.12 Study 12: Effective Concrete Width for Girder Flexure.....	178
8.3.13 Study 13: Modular Ratio.....	179
8.3.14 Study 14: Bridge Radius of Curvature.....	180
8.3.15 Study 15: Longitudinal Distribution of Loads and Stress Calculations.....	181
8.3.16 Study 16: Restraint of Warping Stress Approximation	182
 Chapter 9 Bridge Rating	225
9.1 Current Mn/DOT Rating of Bridge No. 69824.....	225
9.2 Proposed Rating Procedure.....	226
9.2.1 Grillage Analysis	227
9.2.2 Code Provisions for Load Rating of Curved Steel I-girder Bridges.....	227
9.2.3 Load Testing	227
9.3 Initial Rating for Spans 9-8 and 8-7 of Mn/DOT Bridge No. 69824.....	229
9.3.1 Computational Model IMR	229
9.3.2 Applied Loads for Initial Rating	230
9.3.3 Results of Initial Pretest Load Rating	231
9.4 Final Rating of Mn/DOT Bridge No. 69824.....	232
9.4.1 Computational Model FMR	232
9.4.2 Applied Loads for Final Rating	232
9.4.3 Results of Final Load Rating	233
9.5 Discussion on the Various Load Ratings	234
 Chapter 10 Conclusions	256
10.1 Summary of Methodology	256
10.2 Summary of Research Findings	258
10.2.1 Test Results	258
10.2.2 Computational Analysis Results	260
10.2.3 Modeling Parameter Study Results.....	263
10.2.4 Load Rating Results	267

10.3 Recommendations for Load Rating with and without Load Testing.....	268
10.4 Recommendations for Future Research.....	270
References.....	271
Appendix A: Distribution of Vertical Loads for Grillage Analysis	
Appendix B: Instrumentation Plan	
Appendix C: Truck Weights, Dimensions, and Original Testing Sequence	
Appendix D: Static Test Raw Data and Thermal Strain Plots	
Appendix E: Dynamic Test Data	
Appendix F: Results for Computed and Measured Static Test Data	
Appendix G: Strength Check Procedures of Composite Steel Curved Girder Bridge Components for Load Rating	

List of Tables

Table 2-1: LRFR Load Factors for Steel Bridges	17
Table 3-1: Girder Span Lengths for Bridge 69824 Unit 2	23
Table 3-2: Girder C Properties along the Arc Length.....	23
Table 3-3: Girder A Properties along the Arc Length	24
Table 4-1: Non-Composite Girder Comparison between UMN Program and Differential Equations	43
Table 4-2: Composite Girder Comparison between UMN Program and Differential Equations.....	44
Table 4-3: Dead Load Pier Reaction Comparisons.....	45
Table 4-4: Total Girder Dead Load Distribution Comparison.....	45
Table 4-5: Dead Load Shear Comparisons	46
Table 4-6: Dead Load Moment Comparisons.....	47
Table 4-7: Midspan Dead Load Deflection Comparisons	48
Table 4-8: Dead Load Stress Comparisons for Interior Girder C	49
Table 4-9: Dead Load Stress Comparisons for Exterior Girder A	50
Table 4-10: Live Load Moment Comparison between UMN Program and MDX.....	51
Table 5-1: Instrumentation Labeling Scheme.....	70
Table 5-2: Cross-References between Test Groupings.....	71
Table 5-3: Static Tests	72
Table 5-4: Dynamic Tests.....	72
Table 5-5: Strain Gages Not Recorded for Zero1, T42, T45, T46, T47, and T54	73
Table 5-6: Strain Gages Not Recorded for T45, T50, T52, T54, and T56	73
Table 5-7: Strain Gages Modified for Thermal Strain Effects for T1 through T19	74
Table 6-1: Interior Girder C Neutral Axis Locations.....	106
Table 6-2: Exterior Girder A Neutral Axis Locations	106
Table 6-3: Diaphragm Neutral Axis Locations.....	106
Table 6-4: Measured Effective Widths and Moments of Inertia for Girders using N = 6	107
Table 6-5: Measured Effective Widths and Moments of Inertia for Diaphragms using N = 6 ..	107
Table 6-6: GDFs for Loads Centered on Pier 9	107
Table 6-7: GDFs for Loads Centered on Span 9-8	108
Table 6-8: GDFs for Loads Centered on Pier 8	109
Table 6-9: GDFs for Loads Centered on Span 8-7	110
Table 6-10: GDFs for Loads Shifted to Interior Girder on Span 9-8	110
Table 6-11: GDFs for Loads Shifted to Exterior Girder on Span 9-8	111
Table 6-12: GDFs for Loads Shifted to Interior Girder on Span 9-8 and Exterior Girder on Span 8-7	111
Table 6-13: GDFs: for Loads Shifted to Exterior Girder on Span 98 and Interior Girder on Span 8-7	112
Table 6-14: Average GDFs at Point of Loading.....	112

Table 7-1: Measured versus Computed Comparison for Displacements.....	139
Table 7-2: Measured versus FM Computed Comparison for Bottom Flange Gage BC.....	139
Table 7-3: Measured versus FMR Computed Comparison for Bottom Flange Gage BC	140
Table 7-4: Measured versus FM Computed Comparison for Top Flange Gage TC	140
Table 7-5: Measured versus FMR Computed Comparison for Top Flange Gage TC.....	141
Table 7-6: Measured versus FM Computed Comparison for Girder Web Gage W	141
Table 7-7: Measured versus FMR Computed Comparison for Girder Web Gage W	142
Table 7-8: Measured versus FM Computed Comparison for Bottom Flange Tip Gages BI, BE.....	142
Table 7-9: Measured versus FMR Computed Comparison for Bottom Flange Tip Gages BI, BE.....	143
Table 7-10: Measured versus FM Computed Comparison for Top Flange Tip Gages TI, TE	143
Table 7-11: Measured versus FMR Computed Comparison for Top Flange Tip Gages TI, TE	144
Table 7-12: Measured versus Computed Comparison for Diaphragm Gages	144
Table 7-13: Measured versus Computed Comparison for Lateral Wind Bracing Gages	145
Table 7-14: Fatigue Detail Stress Ranges for Dynamic Tests	145
 Table 8-1: Grillage Model Base Parameters	185
Table 8-2: Study 1 Diaphragm Knee Brace Stiffness versus No Knee Brace Stiffness	186
Table 8-3: Study 2 Diaphragm Vertical Offsets versus No Vertical Offsets.....	186
Table 8-4: Study 3 Diaphragm $b_{eff} = 7$ inches versus $b_{eff} = 0$ inches.....	187
Table 8-5: Study 3 Diaphragm $b_{eff} = 7$ inches versus $b_{eff} = 54$ inches.....	187
Table 8-6: Study 4 Cross-frame Members with Half Area	188
Table 8-7: Study 4 Cross-frame Members with Double Area	189
Table 8-8: Study 5 Excluding Lateral Wind Bracing	189
Table 8-9: Study 5 Lateral Wind Bracing Member Area Cut in Half	190
Table 8-10: Study 5 Lateral Wind Bracing Member Area Doubled.....	190
Table 8-11: Study 6 Diaphragm Spacing Approximately Doubled.....	191
Table 8-12: Study 7 Transverse Concrete Deck Beams	192
Table 8-13: Study 8 Rotational DOFs for Transverse Concrete Deck Beams	193
Table 8-14: Study 9 Girder Axial DOFs at Piers.....	194
Table 8-15: Study 10 Composite Torsion Constant J with Half of b_{eff}	195
Table 8-16: Study 10 Composite Torsion Constant J with the Full b_{eff}	196
Table 8-17: Study 11 Concrete Slab Thickness Plus 1 inch	197
Table 8-18: Study 11 Concrete Slab Thickness Plus $\frac{1}{2}$ inch	198
Table 8-19: Study 11 Concrete Slab Thickness Minus $\frac{1}{2}$ inch.....	199
Table 8-20: Study 11 Concrete Slab Thickness Minus 1 inch.....	200
Table 8-21: Study 12 Effective Concrete Width 20% Larger.....	201
Table 8-22: Study 12 Effective Concrete Width 10% Larger.....	202
Table 8-23: Study 12 Effective Concrete Width 10% Smaller.....	203
Table 8-24: Study 12 Effective Concrete Width 20% Smaller.....	204
Table 8-25: Study 13 Modular Ratio Minus 2	205
Table 8-26: Study 13 Modular Ratio Minus 1	206
Table 8-27: Study 13 Modular Ratio Plus 1	207

Table 8-28: Study 13 Modular Ratio Plus 2	208
Table 8-29: Study 14 Radius of Curvature 10 Times Greater	209
Table 8-30: Study 15 Longitudinal Load Distribution and Stress Calculation NC-NC	210
Table 8-31: Study 15 Longitudinal Load Distribution and Stress Calculation C-NC	211
Table 8-32: Study 15 Longitudinal Load Distribution and Stress Calculation C-RC	212
Table 9-1: Summary of Rating Factors for Mn/DOT Bridge No. 69824	237

List of Figures

Figure 2-1: HS20-44 Truck (AASHTO, 2002).....	17
Figure 2-2: HS20-44 Lane Loading (AASHTO, 2002).....	17
Figure 2-3: HL-93 Loading (AASHTO, 2003b).....	18
Figure 2-4: Example Grillage Assemblage.....	18
Figure 3-1: Plan View of Bridge 69824 in Duluth, Minnesota (Mn/DOT Design Specifications)	25
Figure 3-2: Access Road between Pier 9 and Pier 8 beneath Bridge 69824 (TH 35 NB is on the Right).....	25
Figure 3-3: Unit 2 Framing Plan from Pier 10 to Midspan 8-7 (Mn/DOT Design Specifications)	26
Figure 3-4: Unit 2 Framing Plan from Midspan 8-7 to Pier 5 (Mn/DOT Design Specifications)	27
Figure 3-5: Flange Property Transition (Butt Weld on Bottom Flange)	28
Figure 3-6: Unit 2 Cross-section (Mn/DOT Design Specifications)	28
Figure 3-7: Unit 2 Bridge Deck and Diaphragm	28
Figure 3-8: Typical Diaphragm on Unit 2 of Bridge 69824 (Mn/DOT Design Specifications)...	29
Figure 3-9: Diaphragm and Lateral Wind Bracing at Pier 8.....	29
Figure 3-10: Lateral Bracing and Gusset Plate Details (Mn/DOT Design Specifications)	30
Figure 3-11: Gusset Plate Connection	30
Figure 3-12: Gusset Plate Retrofit from Exterior Face	31
Figure 3-13: Gusset Plate Retrofit (arrow) from Interior Face	31
Figure 3-14: Expansion Bearing at Pier 9	32
Figure 3-15: Fixed Bearing at Pier 8.....	32
Figure 4-1: Non-composite and Composite Flexural Section Dimensions	52
Figure 4-2: Composite Section Torsion Properties.....	52
Figure 4-3: UMN Program Finite Element Mesh of Bridge 69824 Unit 2.....	53
Figure 4-4: Interior Girder C Total Dead Load Shear Comparison.....	54
Figure 4-5: Exterior Girder A Total Dead Load Shear Comparison	54
Figure 4-6: Interior Girder C Total Dead Load Moment Comparison	55
Figure 4-7: Exterior Girder A Total Dead Load Moment Comparison	55
Figure 4-8: Interior Girder C Total Dead Load Deflection Comparison	56
Figure 4-9: Exterior Girder A Total Dead Load Deflection Comparison.....	56
Figure 4-10: Interior Girder C Non-composite Dead Load Stress Comparison	57
Figure 4-11: Exterior Girder A Non-composite Dead Load Stress Comparison.....	57
Figure 4-12: Interior Girder C Superimposed Dead Load Stress Comparison	58
Figure 4-13: Exterior Girder A Superimposed Dead Load Stress Comparison.....	58
Figure 4-14: Interior Girder C Total Dead Load Stress Comparison	59
Figure 4-15: Exterior Girder A Total Dead Load Stress Comparison	59
Figure 5-1: Types of Strain Gages used for Test Measurements.....	74
Figure 5-2: Weldable Strain Gage being Installed.....	75

Figure 5-3: Tiltmeter, String Potentiometer, and LVDT used for Test Displacement Measurements	75
Figure 5-4: LVDTs at Pier 9 to Measure Movement of Expansion Bearings	76
Figure 5-5: LVDT to Measure Slip between Top Flange and Concrete Slab.....	76
Figure 5-6: Cross-section Labeling Scheme	77
Figure 5-7: Main Girder Strain Gages	78
Figure 5-8: Typical Two Strain Gage per Girder Section.....	79
Figure 5-9: Typical Seven Strain Gage per Girder Section	79
Figure 5-10: Secondary Location Strain Gages	80
Figure 5-11: Typical Diaphragm Gage Locations	81
Figure 5-12: Typical Lateral Wind Bracing Gage Locations	81
Figure 5-13: Typical Web Gap Gage Location (gage positioned vertically).....	82
Figure 5-14: Gages to Determine Stress Concentration at Gusset Plate Attachment	82
Figure 5-15: Rosette on Gusset Plate.....	82
Figure 5-16: Displacement Instrumentation	83
Figure 5-17: Average Properties from the Quad-Axle Dump Trucks Used for Testing	84
Figure 5-18: Static Test Configurations.....	85
Figure 5-19: Static Test Configurations (continued)	86
Figure 5-20: Static Test Configurations (continued)	87
Figure 5-21: Static Test Configurations (continued)	88
Figure 5-22: Dynamic Test Configurations	89
Figure 5-23: Zero Load Readings throughout Test Period	90
Figure 5-24: Plot Showing Thermal Effects at 9N-GA-TC	90
Figure 5-25: Measured and Thermal Strains for Static Tests at Section 9N Girder A	91
Figure 5-26: Small Crack in Weld at Diaphragm Connection South of Pier 8 on Girder C	91
 Figure 6-1: Linear Strain Profile Section 9B-GA	113
Figure 6-2: Linear Strain Profile Section 9J-GA	113
Figure 6-3: Linear Strain Profile Section 8D-GC	114
Figure 6-4: Linear Strain Profile Section 8D-GA.....	114
Figure 6-5: Nonlinear Strain Profile Section 9B-GC	115
Figure 6-6: Nonlinear Strain Profile Section 9J-GC.....	115
Figure 6-7: Nonlinear Strain Profile Section 9O-GC	116
Figure 6-8: Nonlinear Strain Profile Section 9O-GA	116
Figure 6-9: Slip at Steel Top Flange and Concrete Deck Interface	117
Figure 6-10: Relative Magnitude of Slip and Rotation at Section 9B-GA	117
Figure 6-11: Effective Width Calculation.....	118
Figure 6-12: Measured Bearing Movement along Longitudinal Direction at Pier 9	118
Figure 6-13: Relative Magnitude of Bearing Movement at 9A-GA and Rotation at Section 9B-GA.....	119
Figure 6-14: Generic Strain Profile for Gages during Dynamic Tests	119
Figure 6-15: Exponential Decrease in DIF with Increase in Peak Strain	120
Figure 6-16: Girder Dynamic Impact Factors.....	120
Figure 6-17: Interior Girder C DIF by Test	121
Figure 6-18: Exterior Girder A DIF by Test.....	121
Figure 6-19: DIF for Tests D1-D3	122

Figure 6-20: Average Girder DIF for Each Cross-Section	122
Figure 6-21: Diaphragm Dynamic Impact Factors	123
Figure 6-22: Average Diaphragm Dynamic Impact Factors.....	123
Figure 6-23: Lateral Bracing Dynamic Impact Factors	124
Figure 6-24: Average Lateral Bracing Dynamic Impact Factors.....	124
Figure 6-25: Web Gap and Gusset Plate Tip Dynamic Impact Factors.....	125
Figure 6-26: Average Web Gap and Gusset Plate Tip Dynamic Impact Factors	125
Figure 6-27: Girder DIF Adjusted for Centrifugal Effects	126
Figure 6-28: Girder DIF for D1-D3 Adjusted for Centrifugal Effects	126
 Figure 7-1: FM Analysis versus Measured at Section 8C Girder C	146
Figure 7-2: FMR Analysis versus Measured at Section 8C Girder C.....	146
Figure 7-3: Interior Girder C Bending Stresses for Test S19	147
Figure 7-4: Exterior Girder A Bending Stresses for Test S19	147
Figure 7-5: Interior Girder C Bending Stresses for Test S24	148
Figure 7-6: Exterior Girder A Bending Stresses for Test S24	148
Figure 7-7: Interior Girder C Bending Stresses for Test S28	149
Figure 7-8: Exterior Girder A Bending Stresses for Test S28	149
Figure 7-9: Interior Girder C Bending Stresses for Tests S39	150
Figure 7-10: Exterior Girder A Bending Stresses for Test S39	150
Figure 7-11: Interior Girder C Bending Stresses for Test S43	151
Figure 7-12: Exterior Girder A Bending Stresses for Test S43	151
Figure 7-13: Warping Stresses on Interior Girder C for Test S24.....	152
Figure 7-14: Warping Stresses on Exterior Girder A for Test S24.....	152
Figure 7-15: Bottom Flange Warping Comparisons at Section 9B	153
Figure 7-16: Bottom Flange Warping Comparisons at Section 9J	153
Figure 7-17: Bottom Flange Warping Comparisons at Section 9O	154
Figure 7-18: Bottom Flange Warping Comparisons at Section 8D	154
Figure 7-19: Measured versus Computed Diaphragm Stresses at Section 9F-D-QI	155
Figure 7-20: Measured versus Computed Diaphragm Stresses at Section 8A-D-QI.....	155
Figure 7-21: Comparison of Five Lateral Bracing Gages at Section 9E-LBU	156
Figure 7-22: Tensile Lateral Wind Bracing Behavior on Span 8-7	156
Figure 7-23: Tensile Lateral Wind Bracing Behavior on Span 9-8 and Span 8-7	157
Figure 7-24: Well Correlated Lateral Wind Bracing Behavior	157
Figure 7-25: Photograph of Gusset Plate Tip Strain Gage	158
Figure 7-26: Gusset Plate Stress Comparison.....	158
Figure 7-27: Stress Concentration Factors for Gusset Plate Detail	159
Figure 7-28: Out-of-Plane Web Gap Distortion	159
Figure 7-29: Photograph of Web Gap Strain Gage Vertically Aligned on Web	160
Figure 7-30: Measured Web Gap Stresses.....	160
 Figure 8-1: Mn/DOT Bridge No. 27998 Grillage Model	213
Figure 8-2: FHWA Test Specimen Grillage Model.....	214
Figure 8-3: Study 16 Warping Stress Comparison Bridge 69824 Girder C Span 10-9 Loaded.	214
Figure 8-4: Study 16 Warping Stress Comparison Bridge 69824 Girder C Span 9-8 Loaded...	215
Figure 8-5: Study 16 Warping Stress Comparison Bridge 69824 Girder C Span 8-7 Loaded...	215

Figure 8-6: Study 16 Warping Stress Comparison Bridge 69824 Girder C Span 7-6 Loaded...	216
Figure 8-7: Study 16 Warping Stress Comparison Bridge 69824 Girder C Span 6-5 Loaded...	216
Figure 8-8: Study 16 Warping Stress Comparison Bridge 69824 Girder A Span 10-9 Loaded.	217
Figure 8-9: Study 16 Warping Stress Comparison Bridge 69824 Girder A Span 9-8 Loaded...	217
Figure 8-10: Study 16 Warping Stress Comparison Bridge 69824 Girder A Span 8-7 Loaded.	218
Figure 8-11: Study 16 Warping Stress Comparison Bridge 69824 Girder A Span 7-6 Loaded.	218
Figure 8-12: Study 16 Warping Stress Comparison Bridge 69824 Girder A Span 6-5 Loaded.	219
Figure 8-13: Study 16 Warping Stress Comparison Bridge 27998 Girder 1 Span I Loaded.....	219
Figure 8-14: Study 16 Warping Stress Comparison Bridge 27998 Girder 1 Span II Loaded ...	220
Figure 8-15: Study 16 Warping Stress Comparison Bridge 27998 Girder 2 Span I Loaded.....	220
Figure 8-16: Study 16 Warping Stress Comparison Bridge 27998 Girder 2 Span II Loaded	221
Figure 8-17: Study 16 Warping Stress Comparison Bridge 27998 Girder 3 Span I Loaded.....	221
Figure 8-18: Study 16 Warping Stress Comparison Bridge 27998 Girder 3 Span II Loaded	222
Figure 8-19: Study 16 Warping Stress Comparison Bridge 27998 Girder 4 Span I Loaded.....	222
Figure 8-20: Study 16 Warping Stress Comparison Bridge 27998 Girder 4 Span II Loaded	223
Figure 8-21: Study 16 Warping Stress Comparison FHWA Test Specimen Girder 1 Midspan Loaded	223
Figure 8-22: Study 16 Warping Stress Comparison FHWA Test Specimen Girder 2 Midspan Loaded	224
Figure 8-23: Study 16 Warping Stress Comparison FHWA Test Specimen Girder 3 Midspan Loaded	224
 Figure 9-1: Interior Girder C Unfactored Dead Load Deflections	238
Figure 9-2: Exterior Girder A Unfactored Dead Load Deflections	238
Figure 9-3: Interior Girder C Unfactored Dead Load Shears	239
Figure 9-4: Exterior Girder A Unfactored Dead Load Shears	239
Figure 9-5: Interior Girder C Unfactored Dead Load Moments	240
Figure 9-6: Exterior Girder A Unfactored Dead Load Moments	240
Figure 9-7: Interior Girder C Unfactored DC Flange Stresses	241
Figure 9-8: Exterior Girder A Unfactored DC Flange Stresses	241
Figure 9-9: Interior Girder C Unfactored DW Flange Stresses	242
Figure 9-10: Exterior Girder A Unfactored DW Flange Stresses	242
Figure 9-11: Interior Girder C Unfactored Total Dead Load Flange Stresses.....	243
Figure 9-12: Exterior Girder A Unfactored Total Dead Load Flange Stresses	243
Figure 9-13: Interior Girder C LL+IM Deflection Envelope and Limits for HL-93 Loading....	244
Figure 9-14: Exterior Girder A LL+IM Deflection Envelope and Limits for HL-93 Loading ..	244
Figure 9-15: Interior Girder C Unfactored LL+IM Shear Envelope for HL-93 Loading.....	245
Figure 9-16: Exterior Girder A Unfactored LL+IM Shear Envelope for HL-93 Loading	245
Figure 9-17: Interior Girder C Factored Total Shears and Capacities with Rating Factors for LRFR	246
Figure 9-18: Exterior Girder A Factored Total Shears and Capacities with Rating Factors for LRFR	246
Figure 9-19: Interior Girder C Unfactored LL+IM Moment Envelope for HL-93 Loading	247
Figure 9-20: Exterior Girder A Unfactored LL+IM Moment Envelope for HL-93 Loading	247
Figure 9-21: Interior Girder C Maximum Unfactored LL+IM Flange Stresses for LRFR	248
Figure 9-22: Exterior Girder A Maximum Unfactored LL+IM Flange Stresses for LRFR	248

Figure 9-23: Interior Girder C Factored Total Flange Stresses for LRFR.....	249
Figure 9-24: Exterior Girder A Factored Total Flange Stresses for LRFR	249
Figure 9-25: Interior Girder C Bottom Flange Factored Stresses, Capacities, and RF for LRFR.....	250
Figure 9-26: Exterior Girder A Bottom Flange Factored Stresses, Capacities, and RF for LRFR.....	250
Figure 9-27: Interior Girder C Bottom Flange Factored Stresses, Reduced Capacities, and RF for LRFR	251
Figure 9-28: Exterior Girder A Bottom Flange Factored Stresses, Reduced Capacities, and RF for LRFR.....	251
Figure 9-29: Interior Girder C Unfactored LL+IM Moment Envelope for HS20 Loading.....	252
Figure 9-30: Exterior Girder A Unfactored LL+IM Moment Envelope for HS20 Loading	252
Figure 9-31: Interior Girder C Maximum Unfactored LL+IM Flange Stresses for LFR	253
Figure 9-32: Exterior Girder A Maximum Unfactored LL+IM Flange Stresses for LFR.....	253
Figure 9-33: Interior Girder C Factored Total Flange Stresses for LFR	254
Figure 9-34: Exterior Girder A Factored Total Flange Stresses for LFR	254
Figure 9-35: Interior Girder C Bottom Flange Factored Stresses, Capacities, and RF for LFR.....	255
Figure 9-36: Exterior Girder A Bottom Flange Factored Stresses, Capacities, and RF for LFR.....	255

Executive Summary

The load rating of horizontally curved composite steel I-girder bridges is presently performed with simplified analysis methods that roughly estimate the effects of curvature. For example, line girder analysis of a straight girder is combined with flange yield strength reductions that approximately account for the secondary moments and the restraint of warping stresses that occur in curved bridges. In addition to the simplified analysis methods, conservative assumptions are typically made concerning the behavior of these complex structures when load rating. In particular, composite action of the concrete deck is typically underestimated and load distribution between the girders and along the length of the bridge is approximated. Thus, to utilize the capacity of horizontally curved steel I-girder bridges, the integration of more accurate methods of analysis and load rating are necessary.

This research was conducted in an effort to improve the accuracy of load ratings for horizontally curved composite steel I-girder bridges. The focus of this work is on the use of grillage finite element analysis combined with procedures for both load and resistance factor rating (LRFR) and load factor rating (LFR) for the load rating of bridges. The objectives of this research are to:

1. Conduct a literature review of current bridge rating, load testing, and computational analysis specifically applicable to horizontally curved steel I-girder bridges.
2. Load test a horizontally curved steel I-girder bridge, assess the load test results, and calibrate a computational grillage model of the bridge based on the assessment.
3. Perform a sensitivity study of bridge and grillage modeling parameters to identify accurate methods of analysis for rating of these types of structures.
4. Develop recommendations for load rating of horizontally curved steel I-girder bridges with and without the use of load testing within the context of current LRFR and LFR provisions, and provide a more accurate load rating for the tested bridge.

A two-girder five-span continuous horizontally curved steel I-girder bridge was load tested using forty-three static truck configurations with up to eight 72,000 lbs quad-axle dump trucks. In addition, thirteen dynamic load tests were conducted with individual trucks driving along the centerline of the bridge at a constant speed, driving over a wood 2x4, or quickly applying brakes. High load level tests loaded the bridge to a total stress (i.e., dead load + live load) near 75% of yield stress to provide bridge behavior at anticipated load rating levels. Composite action was verified in the positive and negative moment regions for the girders and for the beam diaphragms at all load levels, although the girders do not have shear connectors in these regions (the diaphragms do, however). Slip between the concrete deck and the steel girders in the negative moment regions remained elastic even at high load levels, validating the inclusion of composite action in the negative moment regions for analysis. A more appropriate modular ratio N of 6 was identified for the bridge versus the design value of 8. A large scatter in measured concrete effective widths for the girders was calculated. Nonetheless, effective concrete widths for the girders based on AASHTO (2004) provisions provided good correlation with test results. Calculated girder distribution factors indicated that the girder with the larger radius of curvature carried approximately 55% of the total moment at cross sections near the applied loads when the loads were transversely centered between the two girders. Away from the location of the applied loads, especially on adjacent spans, the girder distribution factors varied significantly demonstrating the need for a system-based analytical technique for horizontally curved I-girder bridges versus a line girder analysis, as is currently done. Calculations of dynamic impact factors

for the dynamic tests showed that the values recommended by the *Guide Specifications for Horizontally Curved Steel Girder Highway Bridges* (AASHTO, 2003a) for trucks of 1.25 for the girders and 1.30 for the diaphragms and lateral wind bracing are reasonable values.

Analysis of the test bridge was conducted using an updated version of UMN Program, a linear elastic grillage-based finite element program which was previously written at the University of Minnesota for studying curved steel I-girder bridges. In addition, select comparisons were also made between UMN Program and MDX, a commercially available bridge analysis program, and indicate that MDX can provide reasonable predictions for many basic configurations of horizontally curved steel I-girder bridges. Using the load test evaluations from above along with considerations from a grillage analysis sensitivity study (as discussed later), two calibrated analysis models of the test bridge were created with UMN Program. The first calibrated model was termed the Final Model, or FM. Longitudinal distribution of the truck loads and stress checks were based on the full composite section properties of the girders in both the positive and negative moment regions (i.e., the concrete was assumed to provide tensile resistance in the negative moment regions). This method of load distribution and stress calculation provided the most accurate representation of the experimental data for all test load levels. The second analysis model termed Final Model – Rating, or FMR, was created as a more conservative model to be used for rating analysis of the bridge. FMR was identical to FM except that for girder flexural stress calculations in the negative moment regions, FMR conservatively assumed that the concrete was cracked and thus, only included the reinforcement for the stress calculations. Comparisons between the measured and UMN Program computed values for the static load tests generally showed good correlation for the girder flexural stresses and displacements, diaphragm stresses, and lateral wind bracing stresses. Correlations for the restraint of warping stresses were more sporadic due largely to a high strain gradient near the installed instruments, but magnitudes for measured and computed values were comparable. Error between measured and computed values increased for the girder restraint of warping stresses, diaphragm stresses, and lateral wind bracing stresses for gages near the applied loads because of the inability of UMN Program to capture localized bending effects in the slab due to approximations used for applying the truck loads in the analysis model.

A series of parametric studies were conducted to determine the sensitivity of grillage analysis with the intent of expanding the scope of the analysis for rating horizontally curved composite steel I-girder bridges. Two other previously tested horizontally curved composite steel I-girder bridges were used along with the test bridge to determine the extent to which various bridge and modeling parameters affect the live load computational response of these complex bridges using UMN Program. Selected recommendations for more accurate yet conservative grillage analysis based on the parametric study results and findings from a literature review include:

- Grillage analyses that use open-walled section beam elements (7 DOFs per node) for the girders are recommended since they more accurately reflect the effects of restraint of warping on stiffness and stress. Analysis with frame elements (6 DOFs per node) for the girders with the incorporation of approximate equations for restraint of warping stresses, such as used in the commercially available program MDX, may provide reasonable results for bridges with simple layouts, but are less reliable for bridges with skewed supports, non-uniform diaphragm spacing, small radii of curvature, changes in curvature, and other more complex geometries.

- Lateral wind bracing, if present, should be modeled at the correct vertical offset to obtain accurate representation of the transverse load distribution between girders and the overall torsional stiffness of the structure. Not including the lateral wind bracing in the analysis will tend to result in over prediction of stresses and displacements on the girder with the largest radius of curvature, and under predictions on the girder with the smallest radius of curvature.
- The AASHTO (2004) recommended equations for effective concrete widths provide for reasonable approximations of the composite behavior so long as an appropriate modular ratio is used. It is recommended that the modular ratio be based on the current strength of the concrete versus the design strength, which is typically much lower. Additional stiffness due to curbs and/or parapets should be included where appropriate by increasing the effective width by the area of the additional concrete divided by the slab thickness, or by using half of that value as recommended by AASHTO (2004) for a more conservative assessment.
- Web distortion effects should be taken into consideration by ignoring the contribution of the concrete deck to the composite torsion constant and/or releasing the rotational DOFs of transverse concrete slab members from the girder DOFs. See Chang et al. (2005) for similar recommendations when modeling the deck using shell elements.
- Longitudinal load distribution for rating should generally assume the concrete in the negative moment regions to be effective in tension unless inspections or testing indicate considerable levels of deterioration and/or slip at the flange to deck interface. Stresses in these regions should be conservatively checked based on non-composite properties, or on composite properties including the reinforcement only, although it may be noted that computing stresses assuming full action of the concrete will often be more accurate (just not as consistently conservative).

Using the calibrated grillage analysis model FMR and load rating procedures for both LFR and LRFR, final load ratings at the inventory level with two lanes loaded were determined for the test bridge. The controlling load rating factor for LFR was 0.73 and for LRFR was 0.63. The old inventory load rating of the bridge using LFR methodology was approximately 0.81 and was based on line girder analysis of straight girders with approximate yield strength reductions to account for secondary moments and restraint of warping stresses due to the horizontal curvature of the bridge. The two primary factors that account for the discrepancies between the old and new load ratings are that analysis for the old load rating does not accurately model the transverse load distribution between the girders and the old load rating assumes the concrete deck and reinforcement in the negative moment regions to be ineffective.

The findings of this research project show that grillage analysis can generally be relied upon to provide accurate and efficient load ratings of horizontally curved composite steel I-girder bridges so long as modeling assumptions used are handled appropriately. Therefore, the need for load testing of these complex structures for load rating is greatly reduced. Some cases where load testing could be used to complement computational analysis or to improve the rating of a bridge include:

- To confirm composite action at high load levels in regions without shear connectors.
- To determine the benefits of large curbs and/or parapets along edge girders so as to calibrate an effective width for the girders.

- To verify longitudinal and transverse load distributions.
- To prove a certain load carrying capacity or stiffness for deteriorated components.
- To verify computational methods for bridges with highly non-uniform girder or diaphragm spacing, or for bridges with a reversal in the direction of curvature.

For some types of bridge behavior, load testing may not be beneficial for the purposes of load rating horizontally curved steel I-girder bridges. Load tests to verify or quantify unintended bearing fixity in an attempt to increase the load rating of a curved steel bridge are not advantageous. The use of loads tests on curved steel I-girder bridges with the sole intent of determining an effective concrete width to use in analysis is also not warranted (except noted above for large curbs and/or parapets). The *Guide Manual for Condition Evaluation and Load and Resistance Factor Rating of Highway Bridges* (AASHTO, 2003b) provides additional guidance on when to and when not to load test for the purpose of load rating.

Chapter 1

Introduction

As urban areas have become more congested and highway interchanges more complex, horizontally curved steel I-girder bridges have become an essential component in highway infrastructure. These types of bridges are key to providing smooth transitions from one highway to the next, allowing for a seamless flow of traffic. However, continually increasing vehicle load levels combined with simplified, and typically conservative, methods of analysis and load rating have resulted in a wide scatter in safety factors for these complex structures. In order to fully utilize the capacity of horizontally curved steel I-girder bridges while also preventing premature damage to them, the integration of more accurate methods of analysis and load rating are necessary.

The load rating of a bridge involves the determination of the safe maximum live load capacity for the structure. Typically, it involves analytical calculations based on the current state of the bridge, including actual member properties and configurations, effects due to deterioration and/or rehabilitation, and current load levels (both dead and live). Load tests may also be implemented and used to aid in the determination of the load rating if the structural performance of the bridge is questionable. The AASHTO *Manual for Condition Evaluation of Bridges* (AASHTO, 1994) and the *Guide Manual for Condition Evaluation and Load and Resistance Factor Rating of Highway Bridges* (AASHTO, 2003b) provide guidelines for the load rating of bridges using the load factor rating (LFR) and load and resistance factor rating (LRFR) philosophies, respectively.

The load rating of horizontally curved steel I-girder bridges is presently performed with simplified analysis methods that roughly estimate the effects of curvature. For example, line girder analysis of a straight girder is combined with yield strength reductions that approximately account for the secondary moments and the restraint of warping stresses that occur in curved bridges. Horizontally curved bridges built prior to 1980 and the first edition of the AASHTO *Guide Specifications for Horizontally Curved Highway Bridges* (1980) were also designed with similar simplified methods and were not necessarily detailed for the complex behavior inherent with these types of structures. In addition to the simplified analysis methods, conservative assumptions are typically made concerning the behavior of these complex structures when load rating. In particular, composite action of the concrete deck is typically underestimated and load distribution between the girders and along the length of the bridge is approximated. More refined analytical methods, such as grillage methods, now exist that can provide more accurate predictions of the behavior for curved girder bridges. Grillage methods have been successfully used by a number of researchers (Galambos et al., 2000; McElwain and Laman, 2000; Nevling, 2003; Chang et al., 2005) to predict the experimentally measured behavior of horizontally curved steel I-girder bridges.

This research was conducted in an effort to improve the accuracy of load ratings for horizontally curved composite steel I-girder bridges. The focus herein is on the use of grillage models combined with procedures for both LRFR and LFR for the load rating of bridges. A literature review was conducted to identify past and current load rating, load testing, and analysis

procedures for horizontally curved steel bridges. An extensive load test was completed on a two-girder five-span continuous horizontally curved steel I-girder bridge at total (dead + live) girder stress levels nearing 75% of the yield stress. Results from the load test were used to both verify and calibrate a grillage model of the structure. A sensitivity study using grillage analysis models of the tested bridge and two other bridges from literature was conducted on a series of bridge and grillage modeling parameters to help identify more accurate methods of analysis. A new rating of the test bridge was calculated using the calibrated grillage model with LRFR and LFR procedures and compared to the previous rating. Finally, recommendations pertaining to load rating of horizontally curved steel I-girder bridges with and without the use of load testing are presented.

The objectives and scope of this project are defined below followed by an outline briefly summarizing the contents of each chapter and appendix in this report.

1.1 Objectives

The objectives of this research are to:

1. Conduct a literature review of current bridge rating, load testing, and computational analysis specifically applicable to horizontally curved steel I-girder bridges.
2. Develop a testing strategy utilizing heavy trucks, and load test a horizontally curved steel I-girder bridge.
3. Assess the load test results and calibrate a computational grillage model of the bridge based on the assessment.
4. Perform a sensitivity study of bridge and grillage modeling parameters to identify accurate methods of analysis for rating of these types of structures.
5. Develop recommendations for load rating of horizontally curved steel I-girder bridges with and without the use of load testing within the context of current LRFR and LFR provisions, and use these recommendations to provide a more accurate load rating for the tested bridge.

The benefit of this research is the development of a procedure for providing more accurate load ratings of horizontally curved steel I-girder bridges. The more accurate bridge ratings resulting from this research will improve the efficiency of these structures while helping to prevent future damage. This will result in direct and significant economic benefits.

1.2 Scope

The general methodology developed as part of this research project for load rating of horizontally curved steel I-girder bridges is generally applicable to a wide range of bridges. The inclusion in the parametric studies of analysis models for two other curved bridges, both with significantly different configurations than the bridge tested as part of this project, helps to expand this scope of applicability. However, the specific relations between the load testing and analysis results determined herein may only be applicable to bridges similar to that tested. The tested bridge was a two-girder five-span continuous horizontally curved steel I-girder bridge with a minimum radius of curvature of approximately 566 feet, composite beam diaphragms at approximately 12 foot spacing, and lateral wind bracing near the bottom flange of the girders.

The centerline span lengths vary between approximately 79 feet and 149 feet, and composite action of the girders is provided for with shear connectors only in the positive moment regions of the bridge.

1.3 Outline of Report

Chapter 2 provides a literature review discussing load rating, load testing, and computational analysis pertaining to horizontally curved steel I-girder bridges. Rating procedures for load and resistance factor rating and load factor rating are discussed. Diagnostic, proof, and dynamic load tests are explained along with examples of each from literature. Various types of computational analysis for horizontally curved steel I-girder bridges are also presented.

Chapter 3 provides an overview of the bridge load tested as part of this research project. Member properties, overall bridge layout, and connection details are presented for Mn/DOT Bridge No. 69824.

Chapter 4 discusses the grillage-based computational software, UMN Program, which was used for the bulk of the analysis in this research project. Results from UMN Program for a single curved girder beam are verified against solutions based on the differential equations governing the linear elastic behavior of curved beams. The grillage mesh and overall model of Mn/DOT Bridge No. 69824 are presented. Finally, comparisons are made between UMN Program and MDX, a commercially available bridge design and rating analysis program.

Chapter 5 provides details of the bridge testing. The instrumentation plan is discussed, providing information on the location and purpose for each of the strain and displacement measurement devices used to obtain data for the test. The trucks used for the test are presented along with the test configurations for each of the forty-three static and thirteen dynamic load tests. The reduction of the measured data is then explained, including discussion of erratic gages, the removal of thermal strains, and the conversion of the raw data to stresses and displacements.

Chapter 6 contains the evaluation of the bridge properties as determined from the load test data. Composite action of the girders and diaphragms is discussed detailing the measured neutral axes and corresponding moments of inertia and concrete effective widths. Load distribution between girders is quantified based on the transverse location of the applied loads. Dynamic impact factors are determined for the girders, diaphragms, and lateral wind bracing.

Chapter 7 presents the comparisons between the measured bridge behavior and the computed results. Calibration of the UMN Program analysis models based on the measured results is discussed followed by comparisons for each of the measured displacements and stresses for the forty-three static load tests. Measured fatigue detail stresses are also presented for the gusset plate connection and web gap regions.

Chapter 8 provides a sensitivity study on a series of parameters for grillage analysis of horizontally curved composite steel I-girder bridges. UMN Program analysis for two other previously tested bridges from other research projects were included along with Mn/DOT Bridge No. 69824 in the sensitivity study. Parameters such as diaphragm and lateral wind bracing stiffness, composite action for flexural and torsional properties, diaphragm spacing, radius of

curvature, and longitudinal load distribution are investigated, among others. Recommendations are made pertaining to grillage analysis of these complex structures.

Chapter 9 discusses load rating of horizontally curved bridges using load tests and grillage-based computational analysis within the context of LRFR and LFR. The current rating of Mn/DOT Bridge No. 69824 is presented along with the pretest rating and final rating of the bridge using the proposed method.

Chapter 10 contains a summary of this research project along with findings and conclusions. Recommendations are made pertaining to the load rating of horizontally curved composite steel I-girder bridges with and without the use of load testing.

Appendix A outlines the process used to distribute applied vertical loads to the model nodes for use in the grillage analysis software UMN Program.

Appendix B provides the instrumentation plan used for the load testing of Mn/DOT Bridge No. 69824. The locations of all strain and displacement instruments are supplied along with the naming convention utilized.

Appendix C displays the axle spacings and weights for the eight quad-axle dump trucks used in the testing of Mn/DOT Bridge No. 69824. In addition, the truck configurations are provided for the original sequence of load tests as they occurred during the test.

Appendix D provides plots of the raw data as a function of time for all instruments. On the plots, thermal strains are also plotted for strain gages which were determined to be strongly influenced by cooling of the bridge at nightfall.

Appendix E shows plots of the dynamic test data for tests D1, D2, and D3 that were used in determining the neutral axis locations for the girders and diaphragms. In addition, tables are provided showing the calculated dynamic impact factors for the various bridge locations and dynamic tests.

Appendix F provides plots of the measured static test data versus the UMN Program computed values for each of the instruments along with tables of the same data including calculated percent errors for the computed values.

Appendix G lists the various components of Mn/DOT Bridge No. 69824 along with the LRFR and LFR strength design equations used for rating of this composite steel I-girder bridge. This appendix was originally published in Freisinger et al. (2004) and is provided here for reference.

Chapter 2

Literature Review

In order to provide background information on topics covered in this research project, a literature review was conducted. The focus of this literature review was on past research pertaining to load rating, load testing, and analysis of steel bridges, with an emphasis on horizontally curved steel girder bridges. This chapter provides a summary of each of these research areas, preceded by a brief historical overview of the design of horizontally curved steel girder bridges in the United States.

2.1 Historical Overview

Due to the complex interaction between bending and torsion for horizontally curved steel girder bridges, the development of analytical tools and codes for these types of bridges has significantly lagged behind that of common straight bridges. However, with a considerable increase in the use of curved steel bridges in the United States beginning in the 1960s, reliable and consistent methods for designing these structures became a necessity. To this end, a number of large-scale research projects were funded over the years, and several of which are briefly described in the next paragraph.

In order to develop specifications for the design of horizontally curved steel girder bridges, twenty-five states along with the Federal Highway Administration (FHWA) created the Consortium of University Research Teams (CURT) project beginning in 1969. Theoretical, analytical, and experimental work within the CURT project resulted in allowable stress design (ASD) specifications for curved steel bridges in 1976. Combined with load factor design (LFD) specifications funded by the American Iron and Steel Institute (AISI) during the mid-1970s (Stegmann and Galambos, 1976), the ASD specifications were printed by the American Association of State Highway and Transportation Officials (AASHTO) in 1980 as the *Guide Specifications for Horizontally Curved Highway Bridges* (AASHTO, 1980). During the 1980s and early 1990s, several modifications to these specifications were made, and in 1993 a second edition was printed (AASHTO, 1993). Under Project 12-38 of the National Cooperative Highway Research Program (NCHRP), begun in 1993, improved design specifications were developed for curved steel bridges based solely on LFD, and were adopted by AASHTO in 1999. In 2003, these specifications were printed as the *Guide Specifications for Horizontally Curved Steel Girder Highway Bridges* (AASHTO, 2003a). Load and resistance factor design (LRFD) specifications for curved bridges created under NCHRP Project 12-52 have recently been published, but are beyond the scope of this research. See Linzell et al. (2004a) for more in-depth background information.

2.2 Load Rating

Load rating involves the determination of the safe load capacity for a structure at a given point in time. Typically, it involves analytical calculations based on the current state of the bridge, including actual member properties and configurations, effects due to deterioration and/or rehabilitation, and current load levels (both dead and live). A bridge rating occurs each time

routine inspections report a change in any of the above parameters. If the structural performance of a bridge is unknown, load tests can also be conducted on the bridge and used to aid in the determination of the load rating.

The *Manual for Condition Evaluation of Bridges* (AASHTO, 1994) provides guidelines for the load rating of straight bridges using the allowable stress design and load factor design philosophies. Two options for rating levels, inventory and operating, are described in the manual. The inventory rating correlates to the level of live load that can safely traverse a bridge for an indefinite amount of time without causing damage, and generally corresponds to the design level stresses. On the other hand, the operating rating provides the maximum permissible live load to which the bridge can be subject. Unrestricted truck usage at the operating level may shorten the life of a bridge. The inventory rating thus provides a higher level of reliability than does the operating level.

The general rating equation used for both inventory and operating levels is:

$$RF = \frac{C - A_1 D}{A_2 L(1+I)} \quad (2-1)$$

where,

RF = the rating factor for the live-load carrying capacity

C = the capacity of the member

D = dead load effect on the member

L = live load effect on the member

I = impact factor to be used with the live load effect

A_1 = factor for dead loads

A_2 = factor for live loads

Live load effects for each member are determined based on the maximum value resulting from either HS20 truck or lane loading, which are shown in Figure 2-1 and Figure 2-2, respectively. The final bridge rating is then the lowest obtained from all member ratings.

When using Equation (2-1) with ASD, the load factors A_1 and A_2 are both 1.0 for inventory and operating ratings. For LFD rating, A_1 equals 1.3 and A_2 equals 2.17 for inventory and 1.30 for operating levels. It is evident that the variation in reliability between inventory and operating levels for LFD is due to load factor A_2 . As for ASD, the variation in reliability occurs due to higher allowable capacities C for the operating level as compared to the inventory level.

The recently released *Guide Manual for Condition Evaluation and Load and Resistance Factor Rating of Highway Bridges* (AASHTO, 2003b), hereafter referred to as the *LRFR Manual*, extends the capabilities of straight bridge load rating to LRFD philosophy. The *LRFR Manual* was developed as part of NCHRP Project 12-46. An excellent overview of the manual is presented in Minervino et al. (2004).

Three load rating levels are defined in the *LRFR Manual*: 1) design, 2) legal, and 3) permit. The design rating level contains two levels of reliability (reliability index β of 3.5 and 2.5), which are generally comparable to the inventory and operating levels previously described for the *Manual for Condition Evaluation of Bridges* (AASHTO, 1994). However, the *LRFR Manual* uses HL-93

design loading (see Figure 2-3), which tends to produce slightly higher load effects, thus resulting in lower ratings than those using the older HS20 truck or lane loads. Strength I and Service II limit states as defined by the *LRFD Bridge Design Specifications* (AASHTO, 1998) are used for the design level ratings, with an optional fatigue check available. The legal rating level is used to determine a single safe load capacity for AASHTO and State legal loads. The primary concern is the Strength I limit state, which here has the live load factor modified based on the average daily truck traffic (ADTT). The results from the legal level rating can be used to determine bridge load postings or needs for bridge strengthening. The final load rating level is the permit level. It is used to rate a bridge for specific truck loads and configurations that are above those determined with the legal rating level. The Strength II limit state is the primary concern, and live load factors are determined based on the specific permit truck used for the rating and the site traffic conditions.

The general load rating equation used in the *LRFR Manual* (AASHTO, 2003b) is:

$$RF = \frac{C - (\gamma_{DC})(DC) - (\gamma_{DW})(DW) \pm (\gamma_P)(P)}{(\gamma_L)(LL + IM)}, \quad (2-2)$$

where,

RF = rating factor

C = capacity = $\varphi_c \varphi_s \varphi R_n$

DC = dead load effect due to structural components and attachments

DW = dead load effect due to wearing surface and utilities

P = permanent loads other than dead loads

LL = live load effect

IM = dynamic load allowance

γ_{DC} = LRFD load factor for structural components and attachments

γ_{DW} = LRFD load factor for wearing surface and utilities

γ_P = LRFD load factor for permanent loads other than dead loads

γ_L = LRFD load factor for live load

φ_c = condition factor

φ_s = system factor

φ = LRFD member resistance factor

R_n = nominal member resistance

Ratings are carried out for all members in the bridge structure using the loading defined by the rating level (i.e., design, legal, or permit), with the minimum member rating governing the system. Table 2-1 shows the load factors for the various rating levels and limit states to be used with rating of steel bridges.

The condition factor φ_c and the system factor φ_s used in the determination of capacity C for Equation (2-2) are new rating factors that are introduced in the *LRFR Manual*. The condition factor takes into account the increased uncertainty in the strength of a member due to deterioration. It varies from 1.0 for good condition to 0.85 for poor condition. The system factor is used to penalize flexural and axial member capacities in non-redundant systems. Recommended values in the *LRFR Manual* range from 0.85 for welded members in two-girder bridges to 1.0 for fully redundant systems. At the discretion of the evaluator, the system factor may be replaced by a value corresponding to the *LRFD Bridge Design Specifications* (AASHTO,

1998) load modifier η_i , which accounts for ductility, redundancy, and operational importance of the structure. In general, the system factors suggested in the *LRFR Manual* are more conservative than those determined using the load modifier from the *LRFD Bridge Design Specifications* (AASHTO, 1998).

Currently, both rating manuals are written specifically within the context of straight bridges and are therefore, not directly applicable to the rating of horizontally curved steel girder bridges. However, Article 6.1.6 of the *Manual for Condition Evaluation of Bridges* (AASHTO, 1994) and Article 6.1.9 of the *LRFR Manual* (AASHTO, 2003b), suggest that each manual can serve as general guidance in the rating of complex structures, such as horizontally curved steel girder bridges. Both manuals recommend that special analysis methods and procedures be used in addition to those set forth in the manuals to provide accurate ratings for these types of complex structures.

Since there are no specific rating guidelines for horizontally curved steel girder bridges, bridge owners, such as state departments of transportation, have needed to create their own approaches for rating these bridges. For example, the Minnesota Department of Transportation (Mn/DOT) combines line girder analysis provided by AASHTO BARS (Bridge Analysis and Rating System) with flange yield strength (F_y) reductions based on research done by Gillespie (1968). In this procedure, the flange yield strength is reduced based on the secondary moments induced by bridge curvature and the approximated warping stresses. A line girder analysis is then completed for each girder using the reduced flange yield strength to obtain the final rating based on criteria for straight girders. Updates to BARS were discontinued in 1995, so the most recent code specifications are not utilized for these ratings. Therefore, Mn/DOT is investigating alternative procedures for future rating of their curved bridge inventory.

An alternate option for rating curved bridges that has recently become popular with many state departments of transportation is the commercial design and rating package MDX (see www.mdxsoftware.com or MDX, 2004). For horizontally curved bridge rating, MDX uses system analytical methods, such as grid or grillage analysis, to include the effects of curvature and girder-diaphragm interaction. Girder curvature is provided by piecewise-linear segments and warping stresses are approximated using methods provided in the *Highway Structures Design Handbook* Volume II, Section 6 (AISC, 1986). The most current codes guiding curved bridge design (i.e., the 2003 *Guide Specifications for Horizontally Curved Steel Girder Highway Bridges* for LFD and the 1993 *Guide Specifications for Horizontally Curved Highway Bridges* for ASD) are utilized in determining bridge ratings. LRFD rating of horizontally curved bridges using MDX is not yet available since design equations have only recently been published.

2.3 Load Testing

In general, load testing involves the addition of load to a bridge while monitoring the response (strains/stresses and displacements) to obtain information about the behavior and capacity of the structure. Section 8 of the *LRFR Manual* (AASHTO, 2003b), which is based on NCHRP Project 12-28(13)A and reported in the *NCHRP Research Results Digest 234* (Beal, 1998), describes two particular types of static load tests that are typically used in the load testing of bridges. These two test types are diagnostic and proof tests. In addition to the static test types, dynamic load tests are

commonly made on bridges, and are also described in the *LRFR Manual*. All three of these test types are discussed below, including corresponding tests from literature.

2.3.1 Diagnostic Load Tests

Diagnostic load tests are used to determine the behavior of a bridge at load levels below the capacity of the structure. Response characteristics such as load distribution, member stiffness, and support fixity are typically investigated. These characteristics are then used to determine the level of composite action, participation of non-structural and secondary members, and boundary conditions, among other things. Diagnostic tests can also be used to confirm or calibrate analytical methods and/or computer models.

The *LRFR Manual* (AASHTO, 2003b) provides a simple method for correlating diagnostic load tests and bridge ratings. The following equation is provided to modify the original load rating by test results:

$$RF_r = RF_c \times K \quad (2-3)$$

where,

RF_r = the rating factor for the live-load capacity based on the load test result

RF_c = the rating factor based on calculations prior to testing

K = adjustment factor resulting from comparison of measured test behavior and the analytical model

Care should be taken when extrapolating test data to anticipated rating load levels. In order for a modified rating based on a diagnostic test to be realistic, the applied test loads should be high enough to accurately determine the behavior of the bridge up to the rating load levels.

Chajes et al. (1997) used diagnostic load testing to show that the posting limit on a straight steel girder bridge was unnecessary. Testing of the nine-girder three-span simply supported bridge revealed a high level of composite action between the steel girders and concrete slab, although the bridge was designed non-composite (i.e., no shear connectors). Unintended bearing restraint was also confirmed through the test, however it was deemed unreliable for use in improving the bridge rating. A finite element model (FEM) was created for the bridge and calibrated based on the test results. The FEM was used to rate the bridge and revealed a significant rating increase as compared to that prior to testing.

Elhelbawey et al. (1999) used diagnostic load tests to investigate the participation of the concrete slab on four in-service steel girder bridges. Determination of the neutral axis location provided insight into the effective flange width and modular ratio. Testing revealed that the slab participation was higher than prescribed by design code. It was recommended that the modular ratio be decreased to reflect this increase in slab participation, thus utilizing the actual strength of the concrete versus the design strength. It was also concluded that parapets added stiffness to the edge girders, significant composite action was developed in the negative moment regions of continuous span bridges, and the transverse location of the loading vehicle affected the level of slab participation, with higher participation for girders directly beneath the vehicle.

A systematic approach for separating and quantifying the contributions from various effects that resist load during a bridge test is presented in Barker (2001). Diagnostic loading testing of a straight four-girder three-span bridge was used to demonstrate the procedures developed. Effects such as actual impact factors, actual section dimensions, unaccounted system stiffness, actual lateral and longitudinal live load distribution, bearing restraint, and unintended composite action were investigated. An equation was developed that allows for the modification of the bridge rating based on observed behavior during testing. The equation allows for beneficial effects to increase the rating and unreliable effects, such as unintended composite action and bearing restraint, to be excluded. An increase in the inventory rating of 39% was achieved for the test bridge.

Some of the earliest field testing of horizontally curved steel bridges was done in the state of New York during the 1970s. Beal (1978) summarizes the results of diagnostic field tests on four curved steel bridges; two single-span I-girder bridges, one two-span continuous I-girder bridge, and one two-span continuous box girder bridge were tested. Tests were specifically aimed at determining general behavior of these complex structures and verification of design procedures. Analysis models were verified, preliminary design aids were developed, and an improved approximation method for the lateral bending effects was created based on the results of the bridge tests.

As part of a multi-stage research project, a four-girder two-span steel curved bridge in Minnesota was tested at all stages of construction and at low diagnostic levels by Galambos et al. (1996), and then also at higher diagnostic levels by Galambos et al. (2000) and Hajjar et al. (2001). The bridge was designed as composite in the positive moment regions and non-composite over the negative moment region. In the low level tests, two dump trucks weighing approximately 50 kips each were placed on the bridge in a number of configurations to provide insight into the live load behavior of the bridge. High level loads were produced by using up to nine 50-kip trucks in various configurations. Results from the tests were used to verify and calibrate a grillage-based analytical model. Results showed that a modular ratio of 6, which was based on the actual compressive strength of the concrete deck, used in the analytical model provided better correlation with test data than the design specified modular ratio of 8. Also reported was that the negative moment region showed full composite behavior at all truck load levels, even though no shear connectors were provided there.

Huang (2004) determined the load rating of a horizontally curved box girder bridge based on diagnostic load tests. The four-span continuous bridge consisted of two parallel box girders integral with a composite concrete deck. A number of different truck configurations were tested using two flatbed trucks and incrementally applied steel blocks. The analytical models of the bridge were modified based on the test results and then used to provide a new load rating that was at least 17% higher than the previous rating determined in 1988.

In 1992, the Federal Highway Administration (FHWA) instigated the Curved Steel Bridge Research Project (CSBRP). The main experimental focus of the project was a large-scale laboratory test of a three-girder single-span horizontally curved steel bridge. A number of papers have been written on the project including Zureick et al. (2000), Linzell et al. (2004b), Chang et al. (2005), and Jung et al. (2005). An extensive array of instrumentation was applied to fully monitor the behavior of the bridge from construction through ultimate load testing of the final

composite system. Part of the project included diagnostic load testing of the bridge in the non-composite and composite state (Jung et al., 2005). Besides providing data for design code provisions, results from the tests were also used to verify analytical models of the bridge. Final results and conclusions from this project should be available in the near future.

2.3.2 Proof Load Tests

Proof load testing provides an alternative method to the analytical load rating of a bridge. It can also be used to prove the ability of a bridge to support a specific load. For this type of bridge test, load is incrementally applied until a predetermined maximum load is attained or the bridge begins to show signs of distress or nonlinear behavior. Good candidate bridges for proof load tests are those with low calculated ratings or that have unknown structural properties and therefore, cannot be analytically rated.

To provide a margin of safety for bridge ratings determined by proof load tests, the applied test load must be greater than the desired unfactored load level. The *LRFR Manual* (AASHTO, 2003b) provides guidance in determining the magnified load, referred to as the target proof load, which must be supported by the bridge in order to obtain the desired rating level. A target adjusted live load factor X_{pA} is used to scale the desired proof load to obtain the target proof load. X_{pA} is determined by adjusting the target live load factor X_p by factors accounting for the condition of the bridge, bridge details, and average daily truck traffic, among other things. The calculation is as follows:

$$X_{pA} = X_p \cdot \left(1 + \frac{\Sigma \%}{100} \right) \quad (2-4)$$

where,

X_{pA} = target adjusted live load factor

X_p = target live load factor (recommended value of 1.4)

$\Sigma \%$ = net percent increase in X_p due to adjustment factors

The target proof load L_T to be applied for the test is then found from:

$$L_T = X_{pA} L_R (1 + IM) \quad (2-5)$$

where,

L_T = target proof load

L_R = unfactored live load due to the rating vehicle for the lanes loaded

IM = dynamic load allowance

X_{pA} = target adjusted live load factor

After carrying out the proof load test, the operating level capacity is determined based on the actual maximum proof live load L_p that was attained during the test, where L_p is equal to or less than L_T . The operating level capacity is calculated by (AASHTO, 2003b):

$$OP = \frac{k_o L_p}{X_{pA}} \quad (2-6)$$

where,

OP = the operating level capacity
 k_o = factor accounting for termination point of test
 X_{pA} = target adjusted live load factor

The corresponding operating rating factor is then:

$$RF_o = \frac{OP}{L_R(1+IM)} \quad (2-7)$$

where,

RF_o = the rating factor at the operating level
 OP = the operating level capacity
 L_R = unfactored live load due to the rating vehicle for the lanes loaded
 IM = dynamic load allowance

The operating capacity, in tons, can then be calculated by multiplying RF_o by the test vehicle weight, in tons. If an inventory level rating is required, a reasonable approximation can be achieved by multiplying the operating capacity by 0.73, which is based on the typical ratio of operating to inventory safety factors (Beal, 1998).

Literature pertaining to proof load tests on steel bridges, and more specifically on horizontally curved steel bridges, are sparse. In general, this is because steel bridges, unlike concrete bridges, have few unknown, or hidden, properties that would make them difficult to analytically rate. If design drawings are unavailable, field inspections can typically be used to provide dimensions and properties necessary to create a realistic analytical rating of a steel bridge. Calibration of the analytical model through diagnostic testing is then a more suitable approach than proof load testing.

There have been some proof load tests done on straight steel girder bridges. Nowak and Saraf (1996) and Saraf and Nowak (1998) discuss the proof load testing of three deteriorated steel girder bridges, one of which had recently been retrofitted. The tests were done according to the procedures set forth in the final draft of *Bridge Rating through Nondestructive Load Testing* (Lichtenstein, 1993), which is the basis for the previously described method in the *LRFR Manual* (AASHTO, 2003b). All three bridges were single-span concrete slab on steel girder bridges and were built during the 1920s and early 1930s. The proof load for all three bridges was set to the maximum allowable legal load in Michigan, which is approximately 154 kips. Operating ratings for this load prior to the tests were as low as 0.45. Tests revealed significant amounts of composite action, although the bridges were designed non-composite, and also showed contributions to the flexural stiffness from nonstructural elements such as the concrete façade, parapets, and railings. In addition, effects due to partial bearing fixity were observed. The proof load tests revealed that all three bridges were adequate to carry the maximum Michigan legal loads.

2.3.3 Dynamic Load Tests

Three types of dynamic load tests are defined by the *LRFR Manual* (AASHTO, 2003b): weigh-in-motion (WIM), dynamic response, and vibration tests. WIM tests survey the actual truck spectra on a bridge and are used to determine site-specific loading models or made use of in

fatigue calculations. Dynamic response tests provide bridge specific dynamic load allowance and live-load stress ranges for fatigue details. Vibration tests are utilized in the determination of dynamic characteristics, such as frequencies of vibration, mode shapes, and damping.

Dynamic response tests, which are of most interest to this research project, can be conducted under ordinary traffic or using specific test vehicles during controlled conditions. The *LRFR Manual* (AASHTO, 2003b) recommends a variety of vehicle types, speeds, weights, and transverse positions be used to obtain appropriate dynamic response values. Dynamic load allowance can be obtained by comparing the peak dynamic strain to the peak static strain for vehicles in the same transverse position on the bridge. Strain gages attached near fatigue details can be used to provide realistic live-load stress ranges for fatigue-life calculations.

Armstrong (1972) tested a four-girder single-span horizontally curved steel bridge with a single truck simulating a HS20-44 design load. Multiple passes were made with the truck at various speeds and transverse positions. Impact runs were also conducted where the truck drove over a ramp with a 2 inch drop. Strain measurements were used to determine neutral axis locations, which revealed noticeable shifts with the truck in different transverse positions. Maximum impact factors of 26.4% and 76.0% were determined for the standard passes and impact runs, respectively. Frequencies of vibration were observed at 4.1 Hz and 6.5 Hz during testing and verified using a variation generator exciting the bridge. A logarithmic decrement was estimated at 0.07 based on oscillograph records from several runs.

Three horizontally curved steel girder bridges were dynamically tested to determine their impact factors by McElwain and Laman (2000). A six-girder two-span continuous, a four-girder single-span, and a five-girder three-span continuous bridge were tested. All were in good condition with smooth roadway to bridge deck transitions. A single tandem axle vehicle was passed over each bridge at various load levels, speeds, and transverse positions. Plots of the bending dynamic load allowance (DLA) versus the peak static strain revealed a nonlinear decrease in DLA with increasing peak static strain. Two of the bridges exhibited DLA limits of 20% at high strain levels, while the third bridge was near 30%.

2.4 Analysis

Horizontally curved steel I-girder bridges are more complicated to analyze than corresponding straight bridges because vertical loads induce torsion as well as flexure in these complex structures. Chapter 4 of the *Guide Specifications for Horizontally Curved Steel Girder Highway Bridges* (AASHTO, 2003a), hereafter referred to as the *2003 Curved Guide Specification*, provides guidance on the structural analysis of these bridge types. In the simplest case, line girder analysis can be used to determine the vertical bending moment in the girders when all of the following conditions are met:

1. Girders are concentric,
2. Bearing lines are not skewed more than 10 degrees from radial, and
3. The girder arc span L_{as} divided by the girder radius R is less than 0.06 radians, where
 - For simple spans: L_{as} equals the arc length
 - For end spans of continuous members: L_{as} equals 0.9 times the arc length
 - For interior spans of continuous members: L_{as} equals 0.8 times the arc length

If the above conditions are met, the lateral bending moment in the I-girder flanges due to curvature can be approximated by:

$$M_{lat} = \frac{6Ml^2}{5RD} \quad (2-8)$$

where,

M_{lat} = lateral flange bending moment (k-ft)

M = vertical bending moment (k-ft)

l = unbraced length (ft)

R = girder radius (ft)

D = web depth (in)

When any of the aforementioned conditions are not met, more rigorous analytical techniques are warranted. The *2003 Curved Guide Specification* (AASHTO, 2003a) recommends that either approximate methods or refined methods be used. Approximate methods, such as the V-load method (AISC, 1986) or those presented by Gillespie (1968) and Ketchek (1969), tend to be limited in scope and are typically used only for the preliminary design of curved bridges. Final designs and bridge ratings are commonly performed using refined methods, which usually resemble some form of computer-based analysis. A comprehensive overview of approximate and refined analysis methods pertaining to horizontally curved steel I-girder bridges can be found in Zureick and Naqib (1999). Chang et al. (2005) provides general descriptions of various analytical tools currently employed in practice, along with their assessments based on comparisons from a bridge test.

To date, the most accurate methods for predicting the behavior of horizontally curved steel I-girder bridges are those that utilize three-dimensional (3D) finite element computer analysis. In general, 3D FEMs incorporate shell, beam, and truss elements in modeling the three-dimensional nature of these complex structures. Solid elements are typically not used for horizontally curved steel girder bridges, because they drastically increase the computing power and time necessary for analysis with little improvement in results as compared to shell elements. Rigid or spring links are used when necessary to connect elements in their actual 3D configurations.

Recent examples of 3D FEM analysis for horizontally curved steel girder bridges can be found in Simpson (2000), Nevling (2003), and Chang et al. (2005). Simpson (2000) used the commercially available program ANSYS to create linear elastic models and nonlinear geometric models to study the behavior of a proposed non-composite horizontally curved steel girder bridge test frame. The three-girder single-span curved bridge was modeled using four node shell elements for the girders and both beam and truss elements for the diaphragms. Simpson (2000) also used ANSYS to create a linear elastic model of Mn/DOT Bridge No. 27998, a four-girder two-span horizontally curved steel girder bridge that was previously tested by the University of Minnesota (Galambos et al., 2000). Shell elements were used to model the steel girders and the concrete deck, beam elements modeled the concrete barrier walls, and truss elements were used to model the diaphragms. Comparisons with the test results showed reasonable correlation, although a low magnitude of loading made some comparisons difficult.

Nevling (2003) used the commercial program SAP2000 to create a 3D FEM model of a composite five-girder three-span horizontally curved steel bridge and compared it to field test

results. The model used four node shell elements for the concrete deck and girder webs, and beam elements for the girder flanges and diaphragms. Good correlation was found between the predicted and measured bending moments. However, the correlation was poor for diaphragm forces and lateral bending of the flanges.

Chang et al. (2005) created three 3D FEM models in ABAQUS for a composite three-girder single-span curved bridge, which had a similar steel structure as the test frame studied by Simpson (2000), and compared them with test data. The models were denoted by S-BS, S-B, and S-BR. The S-BS model utilized shell elements for the concrete slab and girder webs, beam elements for the girder flanges, and beam and truss elements for the diaphragms. Rigid offsets were used to tie elements together where necessary. The S-B and the S-BR models used shell elements for the slab, open-walled section beam elements (i.e., beam elements with an additional degree of freedom at each end for warping) for the girders, and beam and truss elements for the diaphragms. Rigid offsets were also used for these two models to tie elements together, except that the rotational degrees of freedom (DOFs) for the rigid link between the slab and the girder were released in the S-BR model. These releases were applied because it was found that the torsional and lateral bending stiffness of the slab over-constrained the girder twisting and bottom flange lateral bending for open-walled section beam elements, thus leading to analyses that underestimated the girder deflections and bottom flange lateral bending stresses. In essence, the use of the rotational releases in model S-BR provided a conservative approximation of the web distortion effects which occur over the depth of the girder. Comparisons with experimental data revealed that the S-BS model provided the most accurate predictions, followed by the S-BR model, then the S-B model. The main problem with the S-B model was that it drastically underestimated the diaphragm forces and the lateral bending stress in the bottom flange due to its inability to include web distortion effects. The S-BR model provided much better results than the S-B model, except that it slightly overestimated the diaphragm forces.

Although three-dimensional finite element methods currently provide the most accurate prediction of horizontally curved steel girder bridge behavior, they tend to be time consuming to create and utilize. Thus, they are currently more suited for research applications than industry. The design and rating sectors of the bridge market require more efficient methods of analysis. Grillage, or grid, methods have been successfully implemented for this role. Linear elastic grillage models are especially useful for bridge rating since loads must remain in the linear elastic range.

Grillage models exist in many forms and levels of refinement. Generally, they model the bridge elements as an assemblage of beam and truss elements, an example of which can be seen in Figure 2-4. The neutral axes of all girder elements are normally assumed to coincide in a single plane, known as the grillage plane, and rigid links are typically used to connect diaphragms, lateral wind bracing, and transverse deck beams at their actual vertical offsets.

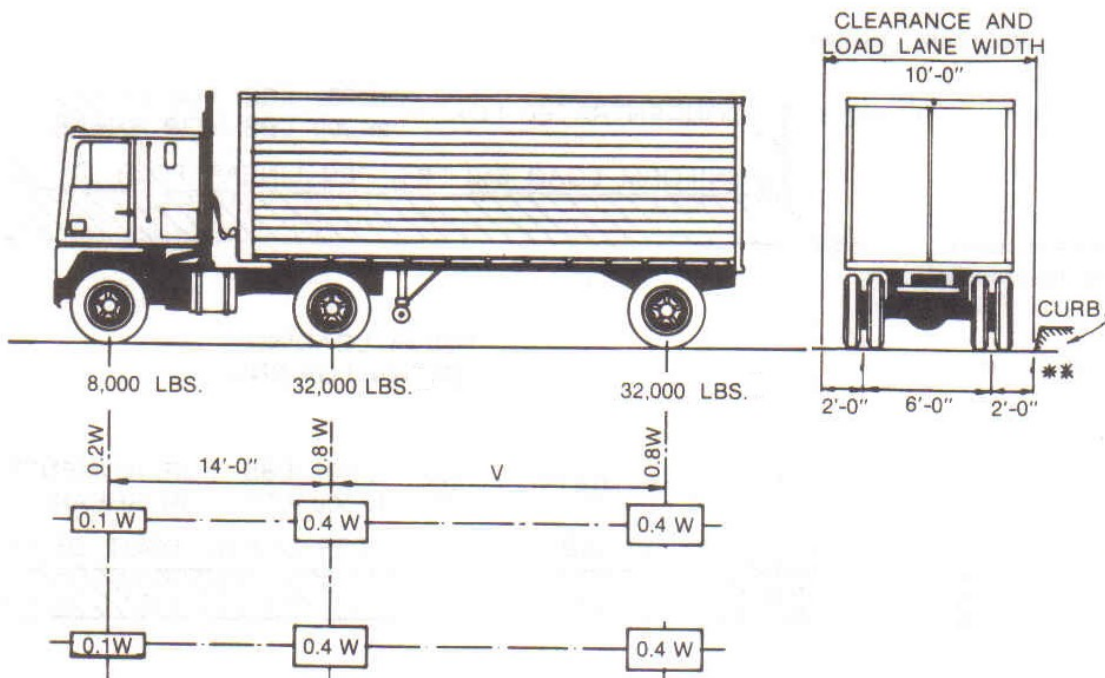
It is standard in a grillage model to use beam and/or truss elements to model the diaphragms, lateral wind bracing, and transverse deck beams. In some cases, cross-frame diaphragms are converted to equivalent beams to make analysis more simplistic. Weissman (1970) provides a procedure for this conversion. Girders in grillage models are generally modeled in one of three ways. The simplest method is to use conventional beam elements that have 3 DOFs per node: a vertical DOF and the two in-plane rotational DOFs. A similar, but more refined method utilizes

frame elements with 6 DOFs per node: three displacements and three rotations. These two methods approximate the curvature of the girders by using piece-wise linear segments. Bottom flange lateral bending is approximated by making use of equations similar to Equation (2-8). The most refined grillage method for modeling the curved girders is by using open-walled section beam elements that include 7 DOFs per node: three displacements and three rotations, plus a DOF for cross-sectional warping. These elements are typically derived from the differential equations governing curved beam behavior, thus providing for effects of curvature and the direct calculation of the flange lateral bending stresses, otherwise known as restraint of warping stresses.

Comparisons between grillage models and more refined 3D finite element models have shown that grillage models can be used effectively to predict behavior nearly as accurately as 3D finite element methods, although with less detail (Simpson, 2000; Nevling, 2003; Chang et al., 2005). Comparisons between load tests and grillage models have also proven the capabilities of grillage models to accurately predict the behavior of these types of structures (Galambos et al., 2000; McElwain and Laman, 2000; Nevling, 2003; Chang et al., 2005). Galambos et al. (2000) used grillage analysis in the UMN Program (Huang, 1996) to predict the construction and live load stresses of a four-girder two-span composite horizontally curved steel girder bridge. McElwain and Laman (2000) created grillage models of three horizontally curved steel girder bridges in SAP2000 and compared them with experimental data based on trucks passing over the bridges. Nevling (2003) made grillage models in SAP2000 and MDX of a five-girder three-span continuous curved steel bridge and made comparisons with field test data. In addition, Chang et al. (2005) compared test data for a three-girder single-span curved steel bridge with five different grillage models using the program GT-SABRE (Chang et al., 2005). All of these grillage models were able to provide reasonable correlation with the corresponding bridge test results.

Limit State	Dead Load DC	Dead Load DW	Design Load		Legal Load LL	Permit Load LL
			Inventory	Operating		
			LL	LL		
Strength I	1.25	1.50	1.75	1.35	1.4 to 1.8	-
Strength II	1.25	1.50	--	--	--	1.10 to 1.85
Service II	1.00	1.00	1.30	1.00	1.30	1.00
Fatigue	0.00	0.00	0.75	--	--	--

Table 2-1: LRFR Load Factors for Steel Bridges



W = COMBINED WEIGHT ON THE FIRST TWO AXLES WHICH IS THE SAME AS FOR THE CORRESPONDING H TRUCK.

V = VARIABLE SPACING — 14 FEET TO 30 FEET INCLUSIVE. SPACING TO BE USED IS THAT WHICH PRODUCES MAXIMUM STRESSES.

Figure 2-1: HS20-44 Truck (AASHTO, 2002)

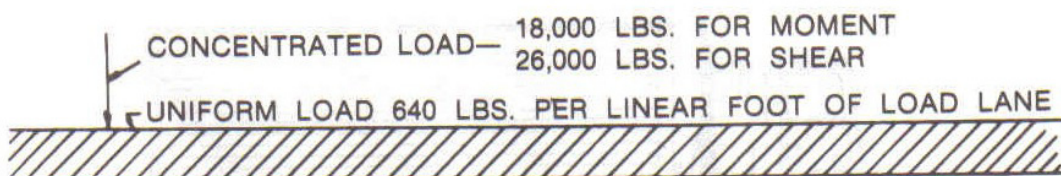
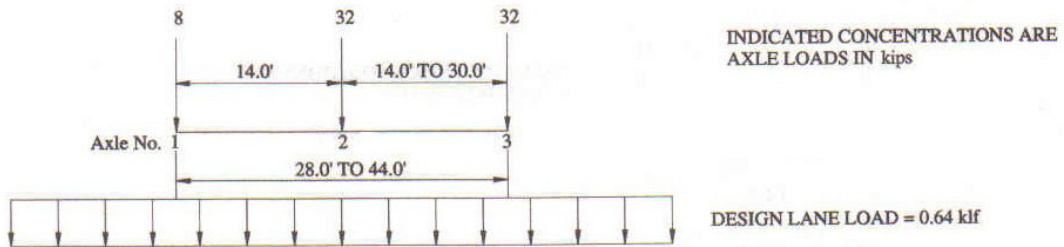


Figure 2-2: HS20-44 Lane Loading (AASHTO, 2002)

DESIGN TRUCK = 72 kips (36 tons)



DESIGN TANDEM = 50 kips (25 tons)



ADDITIONAL LOAD MODEL FOR NEGATIVE MOMENT AND INTERIOR REACTION
(REDUCE ALL LOADS TO 90%)

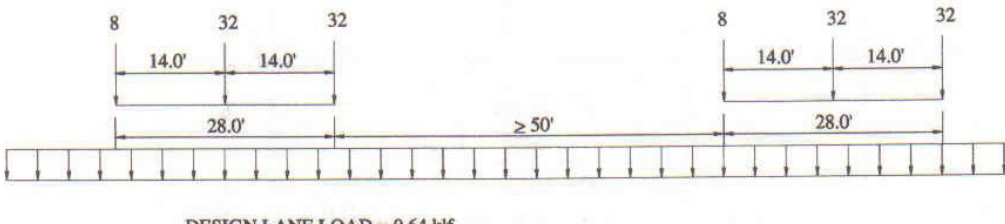


Figure 2-3: HL-93 Loading (AASHTO, 2003b)

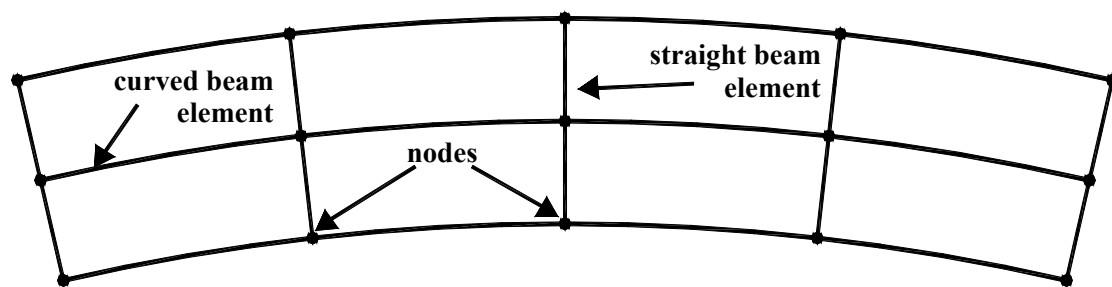


Figure 2-4: Example Grillage Assemblage

Chapter 3

Bridge Overview

In order to investigate and validate the procedure for using grillage-based analysis to rate horizontally curved steel I-girder bridges, the University of Minnesota researchers, along with the bridge rating department at the Minnesota Department of Transportation (Mn/DOT) identified a bridge to load test and rate. The bridge chosen was selected based on a number of criteria. First, the bridge had to be representative of typical curved bridges in the bridge inventory of Mn/DOT. Second, it had to be reasonably accessible in terms of attaching instrumentation and establishing traffic control during the testing. Finally, it was desirable that load testing of the selected bridge would potentially result in an increase in the bridge rating.

3.1 Overview of Bridge No. 69824

The bridge selected for load testing was Mn/DOT Bridge No. 69824 on the southern outskirts of Duluth, MN. It is an off-ramp that connects Trunk Highway (TH) 35 SB with TH 535 NB. Refer to Figure 3-1 for the bridge plan view. Bridge No. 69824 spans TH 35 NB, a ramp from TH 535 SB to TH 35 SB, and several railroad tracks and access roads. It was designed in the late 1960s using the 1965 American Association of State Highway Officials (AASHO) design code utilizing HS20 loading. The bridge was built in 1969 using 4 ksi concrete and 36 ksi steel, common structural materials at that time. In 1982, a 2 inch low-slump concrete overlay was added to the bridge roadway. In the mid-1990s, 1 inch diameter holes were drilled through the girder webs in the positive moment regions to eliminate stress concentrations due to tri-axial welds at the junction of the gusset plate, diaphragm connection stiffener, and girder web. No other structural retrofits have been completed on the bridge.

Bridge 69824 is just over 1400 feet in length and consists of eighteen unequal spans broken into five distinct units. These units are separated by expansion joints, which provide hinges in the otherwise continuous structure. Unit 1 is 200 feet long with four spans, and consists of three nearly straight 30 inch WF sections. Unit 2 is 563 feet long with five spans, and contains two curved welded plate girders with typical web heights of 78 inches. Unit 3 is 237 feet long with three spans, and consists of three curved 36 inch WF sections. Unit 4 is 346 feet in length with five spans, and contains three nearly straight 36 inch WF sections. Unit 5 is a single simply supported span 54 feet in length composed of three 36 inch WF sections. All units have a cast in place deck that was originally 7½ inches thick, but with the addition of the overlay (1982) is now closer to 9 inches. All piers consist of a single round column with a hammer head cap that is radially aligned with the center of curvature.

3.2 Details of Bridge 69824 Unit 2

The focus of this research project for testing, analyzing, and rating was limited to Unit 2. This unit was selected because it is representative of a number of similar horizontally curved steel I-girder bridges in Minnesota, especially around the Duluth area. It also provided relatively easy access for instrumentation on the spans between Piers 9 and 8 and Piers 8 and 7, hereafter referred to as Span 9-8 and Span 8-7, respectively. Refer to Figure 3-2 for an elevation of Span

9-8. In addition, testing of the bridge could be completed with minimal disruption to traffic. This two-girder system provided a realistic but not overly complicated set of details for modeling, thus enabling excellent opportunity for comparing measured and computed results. In addition, through the use of the grillage method, more detailed accounting for the effects of girder curvature, diaphragms, lateral wind bracing, unknown composite behavior, boundary conditions, and other related modeling improvements (relative to current common rating procedures) all provided the potential for an increase in the bridge rating capacity.

Note that throughout the remainder of this report, references to Bridge No. 69824 are specific to Unit 2 of the bridge.

3.2.1 Steel I-Girders

The original Mn/DOT bridge specifications refer to the interior girder as Girder C and the exterior girder as Girder A. Note that Unit 2 does not have a Girder B, whereas Units 1, 3, 4, and 5 contain three girders each with the middle one being Girder B. The convention set up by the specifications using Girder C and Girder A for Unit 2 will be maintained in this report.

As mentioned previously, Unit 2 of Bridge 69824 is composed of two continuous horizontally curved steel I-girders that span six piers. On the south end of Pier 10, the girders cantilever approximately 10 feet to the expansion joint connecting to Unit 3. To the north of Pier 5, the girders cantilever approximately 5 feet to the expansion joint connecting with Unit 1. The longest span occurs between Pier 8 and Pier 7 and is about 149 feet along the centerline.

Figure 3-3 and Figure 3-4 provide the framing plans for the bridge which, among other things, detail the span lengths and dimensions for each welded steel plate girder. Because the clarity of the numerical values in these two figures is questionable, Table 3-1, Table 3-2, and Table 3-3 have been included. Table 3-1 provides detailed span lengths for each girder and the distance along each girder from the south end expansion joint to each pier. Table 3-2 and Table 3-3 summarize the property changes along the length for Girder C and Girder A, respectively. Note that lengths on these three tables are the arc lengths. Figure 3-3 and Figure 3-4 also indicate that the radius of curvature for Girder C from the south expansion joint to Pier 6 is 565.96 feet, while that of Girder A is 583.96 feet. From Pier 6 to the north expansion joint, Girder C has a radius of curvature of 1630.02 feet and that for Girder A is 1648.02 feet. This gives a constant girder spacing of 18 feet along the length of the bridge.

As the above referenced figures and tables show, the flange thicknesses change significantly between the positive and negative moment regions of the bridge. The minimum flange thickness is 0.875 inches and is common in most positive moment regions for both girders, while the maximum thickness of 2.625 inches occurs on Girder A at Pier 8 and Pier 7. Unlike the other units of the bridge, cover plates are not used to provide thicker flanges in Unit 2 of Bridge 69824. Instead, at flange property changes the two different thickness plates are connected with a butt weld and ground smooth to provide a soft transition along the flange as shown in Figure 3-5. Flange properties are symmetric in all locations except along the exterior Girder A between Pier 8 and Pier 7, where the bottom flange is thicker than the top so as to more efficiently resist the large positive moments in this region. Also, the web for both girders is 78 inches deep except

between Pier 6 and the north expansion joint where it linearly tapers down to 26 inches at the joint.

Composite action is provided in the positive moment regions of the bridge through the use of C4x7.25 channels. These channels are welded to the top of the girder and each have a length of 9 inches. No shear lugs are provided along the girders in the negative moment regions, which are denoted as region *A* in Figure 3-3 and Figure 3-4.

3.2.2 Concrete Deck

Figure 3-6 shows the cast-in-place concrete deck, curb, and railing that were initially designed for the bridge. The deck was poured first and allowed to harden before the curb and railing were set. Stirrups made from #4 bars at 12 inch spacing along with a rough concrete surface provide the connection between the deck and curb. The original Mn/DOT bridge specifications indicate that four ksi concrete ($N = 8$) was specified for all concrete deck elements.

The thickness of the deck was originally 7½ inches between the two girders and slightly thicker in the overhang regions as shown in the figure. The haunch between the top flange and the bottom of the deck is typically 3 inches for the 0.875 inch thick top flange, but decreases as the top flange thickness increases. In 1982, a low-slump concrete overlay was added to the bridge. In the process of adding the overlay, approximately ½ inch of the original deck was ground away to provide a fresh, rough surface to which the overlay could bond. Therefore, the current thickness of the deck between the girders is approximately 9 inches. The overhang width from the center of the girders is 44 inches.

Two layers of steel reinforcement are provided in both the longitudinal and transverse directions. Both layers of the longitudinal steel consist of #7 bars at 6 inch spacing. The top layer centroid is located approximately 5.563 inches above the bottom surface of the deck and the bottom layer centroid is approximately 1.438 inches above the bottom surface. In the transverse direction, both layers are composed of #5 bars at 8 inch spacing, which is measured along the exterior edge of the slab (due to curvature the spacing along the interior edge will be smaller than 8 inches). The top and bottom layer centroids reside at approximately 4.813 inches and 2.188 inches above the bottom surface of the deck.

Super-elevation is provided to the deck by means of slanted pier caps. On average, the deck above the exterior girder sits 1.06 feet higher than that above the interior girder. For a girder spacing of 18 feet, that correlates to a super-elevation of 3.3° for the roadway surface.

As Figure 3-6 and Figure 3-7 show, the width available for roadway surface is 21½ feet. Although this width could provide for two lanes of traffic based on current code, Bridge 69824 is a one way ramp and is only striped for one lane. This lane is centered 7 feet from the interior girder and has a highway speed limit of 35 mph.

3.2.3 Diaphragms

The diaphragms for Unit 2 consist of a W21x55 rolled section with knee bracing on each end. Refer to Figure 3-8 for a diagram and Figure 3-9 for a photograph of a typical diaphragm. The

flanges for the knee bracing are $8\frac{1}{4} \times \frac{1}{2}$ inch plate and the web is 0.375 inches thick. The height of the knee bracing varies depending on the depth of the girder, but always attaches to the gusset plate at the bottom, which is about $3\frac{1}{2}$ inches above the top surface of the bottom flange. Gusset plate details are provided in Section 3.2.5

Two rows of bolts connect the diaphragm webs to the connection stiffeners, which are welded to the webs of the girders. Copes on the corners of the stiffeners near the girder longitudinal welds are approximately $\frac{3}{4}$ inch and a welded connection is made only to the compression flange.

Composite action is supplied to the diaphragms by C4x7.25 channels at 6 inch spacing. They are welded to the top flange and are 9 inches in length. The haunch height above the diaphragms varies with the girder depths, but is typically 3 inches.

3.2.4 Lateral Wind Bracing

Lateral wind bracing is provided throughout the length of Unit 2. It is composed of WT4x8.5 rolled sections. The framing plan, Figure 3-3 and Figure 3-4, show the layout for the lateral bracing. The spacing is consistent with that of the diaphragms and creates an X pattern when viewed from below. See Figure 3-9 for a photograph of the lateral wind bracing and Figure 3-10 for diagrams of the connection details.

3.2.5 Gusset Plate Details

The gusset plates provide the connection point to the main girders for the lateral wind bracing and the bottom flange of the diaphragm knee bracing. See Figure 3-10 for drawings and Figure 3-11 for a photograph of a gusset plate. The bracing and diaphragm are bolted to the gusset plate, while the connection to the main girders is provided by a single-bevel groove weld utilizing a backer bar, which was left in place. The gusset plate is made from $\frac{1}{2}$ inch steel plate and has a connection weld of approximately 20 inches to the girder web.

The gussets plate details in the positive moment regions of Unit 2 have had a retrofit applied to them as shown in Figure 3-12 and Figure 3-13. One inch diameter holes were drilled through the exterior face of the girder webs on each side of the connection stiffener at the gusset plate. This was done to remove fracture prone details created by tri-axial welds where the gusset plate-to-stiffener, stiffener-to-girder web, and gusset plate-to-girder web welds intersect.

3.2.6 Bearings

Fixed and expansion rocker plate assemblies are used for bearings on Unit 2 of Bridge 69824. The expansion assemblies consist of a guided, lubricated bronze plate as shown in Figure 3-14. The expansion bearings occur at Piers 10, 9, 6, and 5. These bearings are oriented at an angle of up to 14° from the tangent of the girder longitudinal axis to allow for thermal expansion, which for curved bridges has components in both the longitudinal and radial directions of the girders. Also, all expansion bearings prevent motion in the transverse direction. The fixed assemblies at Piers 8 and 7 are similar to that shown in Figure 3-15 and prevent longitudinal and radial movement.

Interior Girder C			Exterior Girder A	
Location	distance to (ft)	span length (ft)	distance to (ft)	span length (ft)
South Joint	0.00		0.00	
		9.88		10.19
Pier 10	9.88		10.19	
		94.11		97.14
Pier 9	103.99		107.33	
		111.63		115.18
Pier 8	215.61		222.51	
		146.19		150.84
Pier 7	361.81		373.35	
		111.65		115.13
Pier 6	473.45		488.48	
		78.66		79.53
Pier 5	552.11		568.02	
		4.98		5.04
North Joint	557.09		573.05	

Table 3-1: Girder Span Lengths for Bridge 69824 Unit 2

Interior Girder C Properties				
distance to (ft)	length (ft)	t _{bf} (inches)	t _{tf} (inches)	d _w (inches)
0.00				
	85.01	0.875	0.875	78.0
85.01				
	38.03	1.000	1.000	78.0
123.04				
	78.61	0.875	0.875	78.0
201.65				
	26.00	1.875	1.875	78.0
227.65				
	123.17	0.875	0.875	78.0
350.82				
	23.50	1.750	1.750	78.0
374.32				
	99.15	0.875	0.875	78.0
473.47				78.0
	83.67	0.875	0.875	linear
557.14				26.0
$b_{bf} = b_{tf} = 18$ inches, $t_w = 0.5$ inches				

Table 3-2: Girder C Properties along the Arc Length

Exterior Girder A Properties				
distance to (ft)	length (ft)	t _{bf} (inches)	t _{tf} (inches)	d _w (inches)
0.00				
	101.26	0.875	0.875	78.0
101.26				
	12.50	1.375	1.375	78.0
113.76				
	86.68	0.875	0.875	78.0
200.44				
	9.00	1.500	1.500	78.0
209.44				
	23.00	2.625	2.625	78.0
232.44				
	8.00	1.500	1.500	78.0
240.44				
	13.09	0.875	0.875	78.0
253.53				
	12.78	0.875	1.000	78.0
266.31				
	61.00	1.625	1.000	78.0
327.31				
	14.91	0.875	1.000	78.0
342.22				
	14.09	0.875	0.875	78.0
356.31				
	8.00	1.500	1.500	78.0
364.31				
	22.00	2.625	2.625	78.0
386.31				
	9.00	1.500	1.500	78.0
395.31				
	87.12	0.875	0.875	78.0
482.43				
	6.00	1.125	1.125	78.0
488.43				
	6.00	1.125	1.125	linear
494.43				linear
	78.59	0.875	0.875	linear
573.02				26.0
$b_{bf} = b_{tf} = 18$ inches, $t_w = 0.5$ inches				

Table 3-3: Girder A Properties along the Arc Length

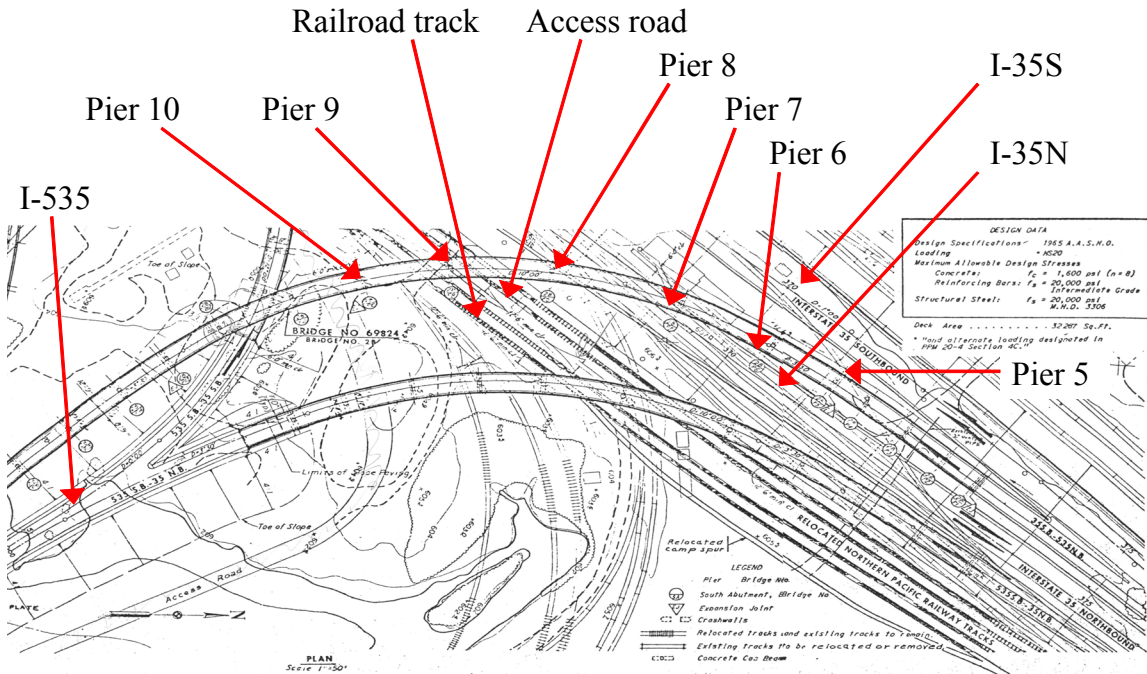


Figure 3-1: Plan View of Bridge 69824 in Duluth, Minnesota (Mn/DOT Design Specifications)



Figure 3-2: Access Road between Pier 9 and Pier 8 beneath Bridge 69824 (TH 35 NB is on the Right)

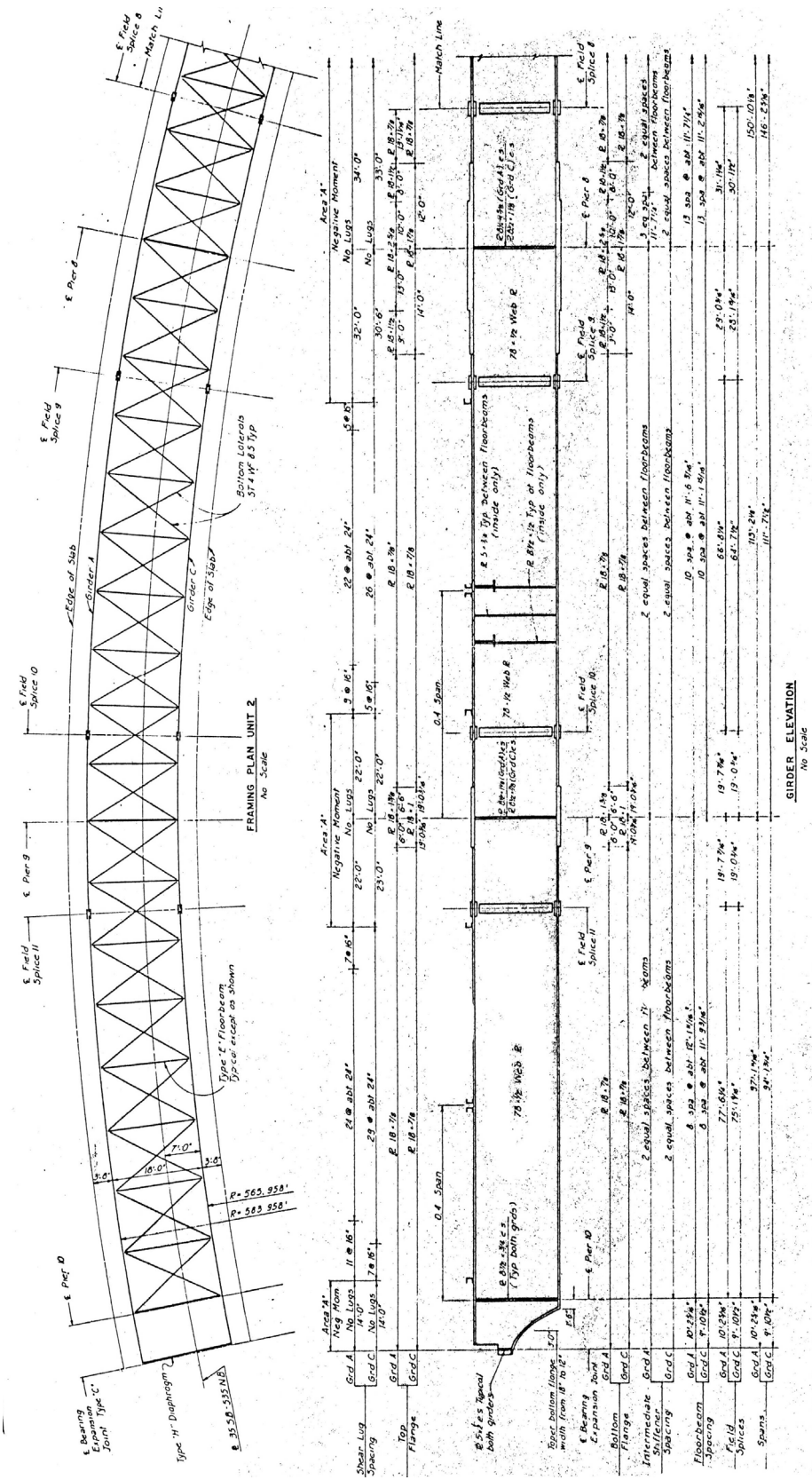


Figure 3-3: Unit 2 Framing Plan from Pier 10 to Midspan 8-7 (Mn/DOT Design Specifications)

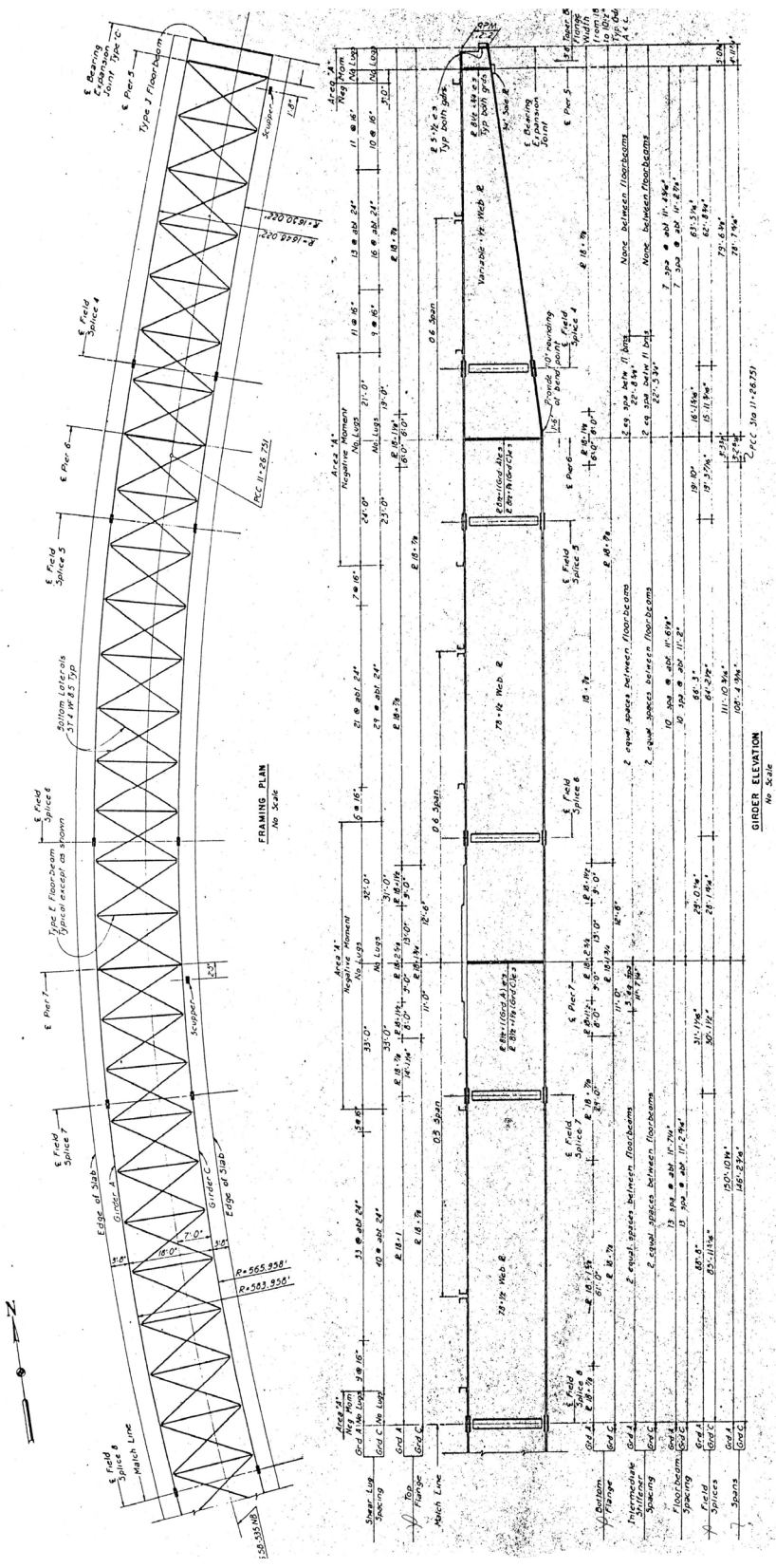


Figure 3-4: Unit 2 Framing Plan from Midspan 8-7 to Pier 5 (Mn/DOT Design Specifications)

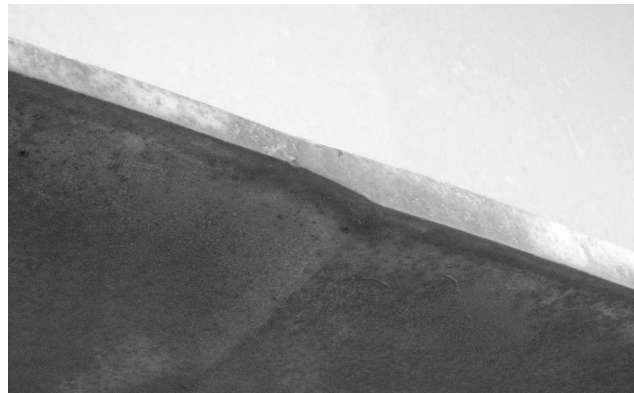


Figure 3-5: Flange Property Transition (Butt Weld on Bottom Flange)

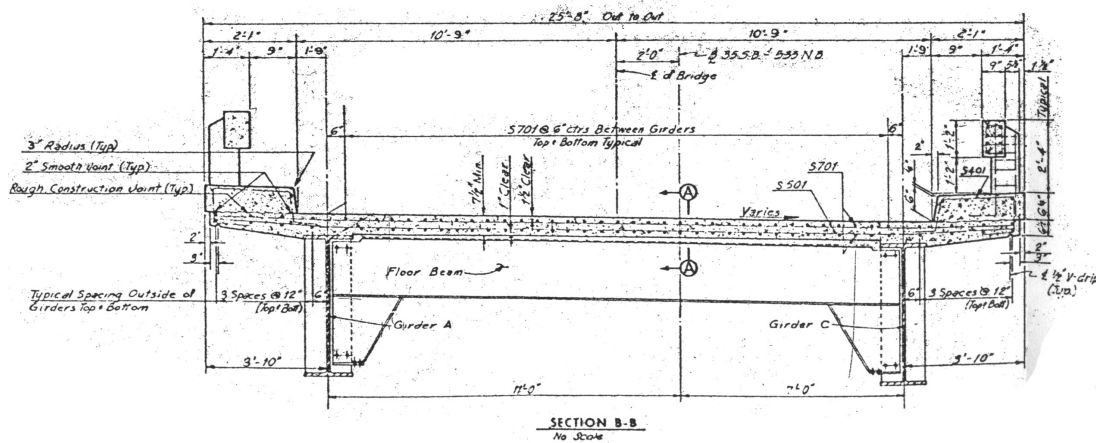


Figure 3-6: Unit 2 Cross-section (Mn/DOT Design Specifications)

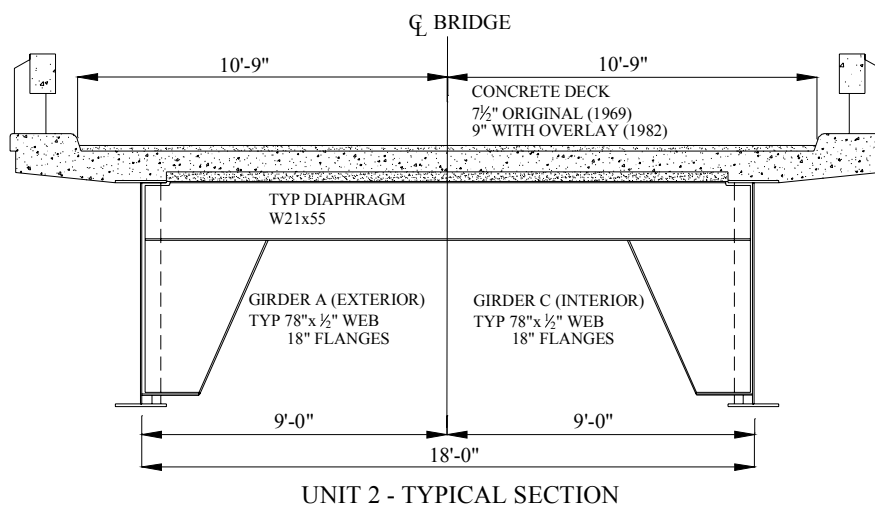


Figure 3-7: Unit 2 Bridge Deck and Diaphragm

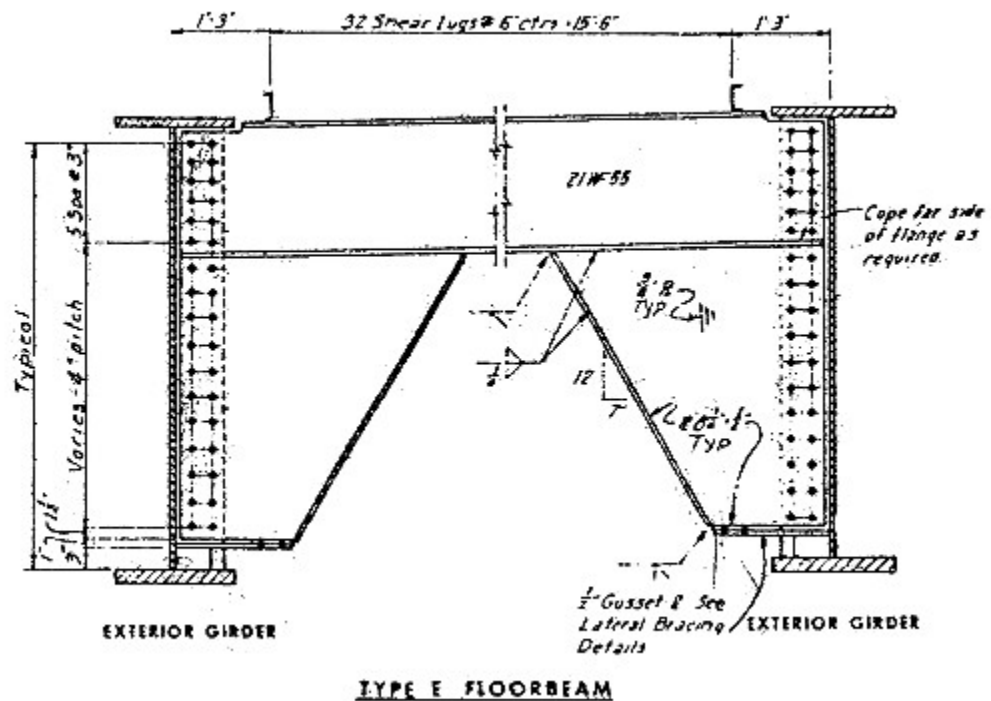


Figure 3-8: Typical Diaphragm on Unit 2 of Bridge 69824 (Mn/DOT Design Specifications)



Figure 3-9: Diaphragm and Lateral Wind Bracing at Pier 8

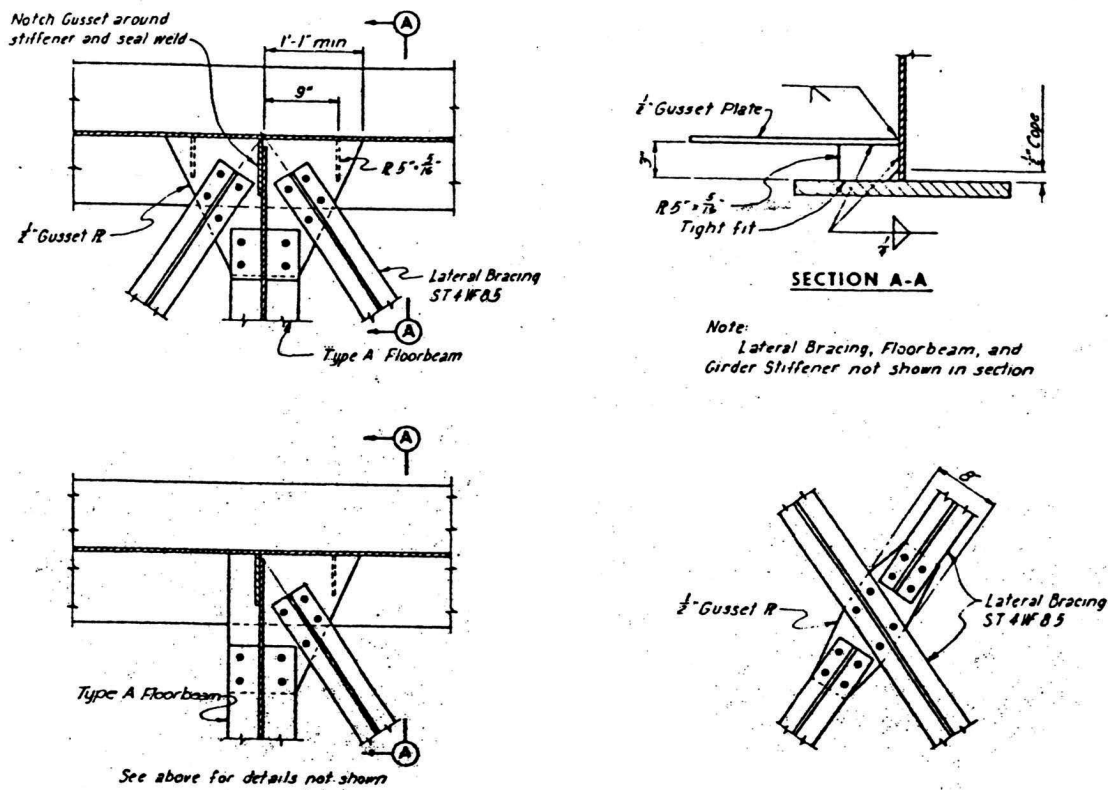


Figure 3-10: Lateral Bracing and Gusset Plate Details (Mn/DOT Design Specifications)



Figure 3-11: Gusset Plate Connection



Figure 3-12: Gusset Plate Retrofit from Exterior Face



Figure 3-13: Gusset Plate Retrofit (arrow) from Interior Face



Figure 3-14: Expansion Bearing at Pier 9



Figure 3-15: Fixed Bearing at Pier 8

Chapter 4

Grillage Analysis of Curved Girder Bridge

Due to its ease of application and availability in commercial programs, the grillage method was chosen for the analytical models in this research project. UMN Program, which was previously written at the University of Minnesota for studying curved steel girder bridges, was used for the bulk of the analysis. The commercial design and rating package MDX was also used for comparative purposes. For more information, refer to the literature review in Chapter 2.

This chapter discusses the verification process used for UMN Program and modifications made to it, followed by a description of the base model created for the tested bridge. The chapter ends with a comparison between UMN Program and MDX.

4.1 Verification of UMN Program

In order to provide greater freedom and accuracy in modeling the test bridge for this project, it was determined that modifications to UMN Program were necessary. The original FORTRAN 77 source code, as written by Huang (1996) using *Microsoft Fortran 77 Version 5.1*, contained data storage structures that were not compatible with the new compiler, *Compaq Visual Fortran 6.6*. Therefore, minor updates to the source code were made so that the program would run with the new compiler.

To ensure that the program was not inadvertently modified by the updates to the source code, comparisons were made using the original data files from the research done at the University of Minnesota in 1996. For these comparisons, the input file was run using the old version of the program and the newly compiled version. For all cases, the results were identical, thus verifying that the upgrade to the new compiler did not alter the internal workings of UMN Program.

To provide further confidence that the newly compiled UMN Program was providing practical results, comparisons were made between the UMN Program results and solutions based on the differential equations governing the linear elastic behavior of horizontally curved beams as developed by Vlasov (1961). Freisinger et al. (2004) derives and discusses the specific solutions used for comparisons in this research project.

Five cases based on the boundary conditions of a single span curved beam were used for the comparisons. Each case was done using non-composite and composite girder properties providing a total of ten comparisons. All cases had a uniform line load applied to the girder of 0.135 kips/inch, which was approximately the dead weight of the steel and concrete deck.

The non-composite girder properties were based on the interior girder of the test bridge between Pier 9 and Pier 8. This span included a radius of curvature just under 566 feet and a steel girder with a 78 inch x $\frac{1}{2}$ inch web and 18 inch x 0.875 inch flanges. The left side of Figure 4-1 shows the non-composite section.

The composite girder properties were based on the above steel girder plus a 7.5 inch concrete deck with an effective flange width b_{eff} of 90.5 inches. Composite flexure properties were

calculated in the typical fashion by transforming the concrete deck to an equivalent area of steel by dividing b_{eff} by N , the ratio of the modulus of elasticity for steel to that of the concrete. The right side of Figure 4-1 presents the transformed flexural section. The composite torsion properties were calculated by the process described in Heins and Kuo (1972) for these comparisons and are shown in Figure 4-2.

The boundary conditions for each case, which were identical on both ends of the beam (except for Case 5), were as follows:

Case 1:

Bending – pinned:	no vertical displacement no moment
Torsion – pinned:	no twist free warping

Case 2:

Bending – fixed:	no vertical displacement no displacement gradient
Torsion – fixed:	no twist no twist gradient

Case 3:

Bending – pinned:	no vertical displacement no moment
Torsion – fixed:	no twist no twist gradient

Case 4:

Bending – fixed:	no vertical displacement no displacement gradient
Torsion – pinned:	no twist free warping

Case 5:

Bending – variable:	no vertical displacement variable moment
Torsion – variable:	variable twist variable warping

For Case 5, UMN Program was used to analyze a five span continuous girder, where one of the spans corresponded to the beam being analyzed using the differential equations. For the boundary conditions at each end of the beam, the moment, twist angle, and bimoment from the analysis using UMN Program were entered into the differential equation solution, which was then solved for the remaining values.

Comparisons for the non-composite cases are provided in Table 4-1. The maximum percent difference for all compared quantities was 1.29%. Table 4-2 shows the same comparisons for the composite cases. Excluding values that are relatively small, and therefore not representative of

the results as a whole, the largest percent difference is at 4.00% for the composite cases. These comparisons indicate that the finite element formulation for horizontally curved beams in UMN Program provides nearly exact correlation with linear elastic horizontally curved beam theory.

4.2 Modifications to UMN Program

Throughout the course of this project, a number of modifications were applied to UMN Program. The code was cleared of any unnecessary portions and re-commented to make it more understandable. Steel reinforcement (i.e., rebar) in the concrete deck was added to the flexural properties of the composite sections for both positive and negative moment regions of the bridge. Multiple methods of load distribution and stress calculation (e.g., non-composite, composite with rebar only, and composite with rebar and concrete deck section properties) along the length of the bridge were added to provide analysis methods recommended by design and rating codes. Modifications were made to the calculation of the torsion constant J for composite sections to allow for adjustments in the effective flange width used. The number of input parameters for the diaphragm rigid offsets and the deck haunch heights was increased to make them more accurate. Minor adjustments were made to the input file to account for the additions and subtractions discussed above. Finally, the output files were significantly altered to provide more efficient compatibility with *Microsoft Excel*.

No alterations were made to the shape functions or general solution process of the program as discussed in Huang (1996).

4.3 Analysis of Mn/DOT Bridge No. 69824 Unit 2

The bulk of the analysis for Bridge 69824 was done using UMN Program. The basis model that was used to provide the computational data within this report is detailed below. Also, the load distribution method for applying the truck axle weights to the model nodes is described.

4.3.1 Basis Model for the Bridge

After a number of preliminary models with varying degrees of refinement, the grillage mesh displayed in Figure 4-3 was chosen to provide the analytical data for the bridge tested as part of this project. Four hundred thirty-two girder elements, 159 diaphragm elements, 150 transverse deck beam elements, and 96 lateral wind bracing elements comprise the mesh. The transverse deck beams are not displayed in Figure 4-3 for clarity purposes, but are located radially between the two girders at the quarter points and midpoint between diaphragms. Note that there is not a transverse deck beam at the diaphragm locations, since the concrete in this region is already used to provide composite action for the diaphragm elements. Girder elements were modeled with open-walled section beam elements including a seventh nodal degree of freedom (DOF) to account for cross-section warping. Diaphragm and transverse concrete deck elements were modeled with straight beams. Lateral wind bracing was modeled using truss elements. Rigid offsets provided the vertical eccentricities between the grillage plane (i.e., the location of the girder element centroids) and the diaphragm, transverse deck, and lateral wind bracing elements.

Nodes were placed along the girders so that between each diaphragm there were four curved girder elements. Additional girder nodes were placed at locations of flange property changes (as listed in Chapter 3) and at splice plates. Nodes for the diaphragms were placed so that most diaphragms were broken into three elements. In this way, the additional stiffness due to the knee bracing at the ends of the diaphragms could be included if so desired. In addition, two diaphragms had extra nodes which were included for comparisons with test data. Nodes were not included at the intersection of lateral wind bracing elements. Therefore, these elements acted independently of one another in the model, whereas some minor interaction would be expected in the real structure.

All three displacements, three rotations, and the warping DOF at each node were allowed to displace except as listed below:

- Vertical and radial displacements at all six piers were fixed
- Longitudinal (i.e., axial) displacements at Pier 8 and Pier 7 were fixed
- Torsional rotations at Pier 10 and Pier 5 were fixed
- Warping DOF on the diaphragm nodes without girders connected were fixed

The minor axis DOF for the diaphragm elements where they connect to the girders was released to better model the connection detail there. In addition, all rotational DOFs at the ends of the transverse deck beam elements were released to prevent over-constraining of girder twisting and lateral bending of the girder flanges. These releases on the transverse deck elements were implemented based on observations by Chang et al. (2005) mentioned briefly in Chapter 2 and results from the sensitivity study in Chapter 8 of this report.

The above boundary conditions were applied to most accurately model the conditions as they were designed for the real structure. However, some approximations in the boundary conditions had to be made and are explained below:

1. Because UMN Program does not provide for skewed support alignments, the in-plane restraints at the piers were approximated as radial (i.e., perpendicular to bridge curvature) and longitudinal (i.e., tangent to bridge curvature). Also, the support conditions in the model had to be applied at the grillage plane, not at the bottom flange where they actually exist.
2. The actual bridge has additional bridge units attached to the north and south cantilevered ends that provide some level of restraint. It was not possible to include the full extent of this restraint. However, to prevent the two cantilevered ends of the bridge from twisting unrealistically, the torsion rotations at the adjacent piers were fixed.
3. Because the straight beam elements used for the diaphragms do not include warping stiffness, the warping DOFs had to be fixed at all internal diaphragm nodes (i.e., away from the girder elements) to prevent singularities in the matrix solution process.

Member properties for area A , major axis moment of inertia I_x , minor axis moment of inertia I_y , torsion constant J , and warping constant C_w of the steel sections were calculated based upon assuming a linear elastic homogeneous isotropic material. The composite section properties were calculated as previously mentioned in Section 4.1 and shown in Figure 4-2, where the process

described in Heins and Kuo (1972) was used for the composite torsion properties. The only modification to the composite torsion properties was that either half of b_{eff} was used in the calculation for the torsion constant J as recommended in C4.6.3.3 of the AASHTO LRFD 3rd Edition (2004) or the concrete deck was ignored and J was based solely on the steel girder as recommended by Chang et al. (2005). The effective width used for the transverse concrete deck beams was 34 inches, which is approximately the tributary width for each element.

Because UMN Program does not allow for linearly varying dimensions along the length of a member, some approximations were made for the web heights of the diaphragms and the girders. In particular, the varying depth portion of the diaphragm knee bracing was divided so that two-thirds of it was given the larger end dimension (75 inches), while the remaining third was given the web height of the W21 x 55 beam (19.76 inches). The linear varying web height of the girders between Pier 6 and the north end expansion joint was modeled by breaking the girders into approximately 12 foot long sections and using the average web height for each section to provide a stepwise approximation.

Some aspects of the model, such as the degree of composite action (i.e., N and b_{eff}), have not been discussed in this section because they vary depending on the purpose of the analysis (e.g., test comparisons or bridge rating). These additional details are provided as needed in each section of this report that contains computational data.

4.3.2 Load Distribution: TRUCKLOADS

The distribution of point loads on the bridge deck was accomplished by use of a secondary program, TRUCKLOADS, which was specifically written for this purpose. To use TRUCKLOADS, an input file describing the bridge configuration, the dimensions and weights of the loading vehicles and the locations of the vehicles on the bridge deck was made and then run. TRUCKLOADS then created an output file describing the corresponding nodal loads in a format useable by UMN Program.

The process by which vehicle axle loads are distributed to the girder nodes in TRUCKLOADS is described in Appendix A. The method is similar to that originally used by Huang (1996), except that the axle weights are now distributed individually instead of being lumped together as one large load at the center of gravity of the truck. Only vertical components are included (i.e., local torques and moments due to the eccentricity of the loads from the nearby nodes are ignored).

4.4 Comparison between MDX and UMN Program

As part of this research project, the bridge rating department at the Minnesota Department of Transportation was interested in the capabilities of MDX to predict the behavior of horizontally curved steel girder bridges. The direct use of MDX to make the live load comparisons of each specific loading configuration for the bridge test was not practical. This is because MDX, when provided with a specific loading pattern, runs a number of analyses with the loading pattern at all possible locations on the bridge deck and reports the worst case member effects, as would be needed for the design or rating of the bridge. Locating the output data from MDX for a specific loading pattern at a particular location, as would be needed for a test comparison, is thus difficult

and time consuming. Since UMN Program utilizes an analysis method (i.e., linear elastic grillage) similar to MDX, but offers more flexibility in the output, it was chosen as the main analytical tool for this research.

To show that MDX and UMN Program predict similar behavior for horizontally curved steel girder bridges, and thus to provide a relationship between the test data and MDX, models of Mn/DOT Bridge No. 69824 were created with each program and used to make comparisons for specific loads. The differences in analytical methods and load comparisons between MDX and UMN Program are provided below, followed by conclusions.

4.4.1 Differences in Analytical Methods

Key differences between MDX and UMN Program as they pertain to the analysis used for the comparisons in the next section are mentioned below:

1. For this comparison, the girder mesh refinement using MDX was one element between each diaphragm connection resulting in approximately 12 foot elements for this bridge, while for UMN Program there were typically four girder elements between each diaphragm connection.
2. Slope-deflection equations for a straight beam are used as the displacement shape functions in MDX, while UMN Program utilizes a combination of hyperbolic and trigonometric functions derived from the differential equations for a curved beam.
3. Flange warping normal stresses due to restraint of warping are approximated based on the major axis flexure in MDX using an equation similar to Equation 2-8, whereas UMN Program calculates them directly from the additional warping degree of freedom.
4. MDX uses a concrete plate (i.e., 2D shell) and eccentric beam grillage model, while UMN Program uses a beam grillage model with modified section properties to reflect the composite action of the deck along with transverse concrete deck beams to provide the axial stiffness of the concrete slab between the top flanges of adjacent girders.
5. MDX does not include the stiffness of the lateral wind bracing, but UMN Program does.
6. MDX uses weighted average properties for the steel beams where flange properties change within a beam element, while UMN Program has a finer mesh that provides for exact property change locations.
7. For the stress calculation at each node, MDX only checks based on the element properties on one side of a node, whereas UMN Program checks stress for the elements on both sides of a node.
8. The diaphragms in MDX do not include additional stiffness due to the knee bracing, nor do they have rigid offsets to provide for the vertical eccentricity from the girder elements. UMN Program includes both.

9. MDX directly accounts for the linearly varying web height of the girders between Pier 6 and the north expansion joint, while UMN Program uses a stepwise approximation along the length.
10. To get around the modeling assumption in MDX that the ends of the bridge are supported by abutments, one additional diaphragm had to be added between the cantilever tip and the pier at the south end of the bridge. This additional diaphragm was not included in the UMN Program model. Also due to this assumption in MDX, the abutment boundary conditions had to be manually released at both cantilever tips of the bridge so that the desired conditions could be achieved.

4.4.2 Comparisons based on Specific Loading

The non-composite (steel and wet concrete) and superimposed (curb, railing, and overlay) dead load analyses provided by MDX were readily available for comparisons with UMN Program. Christensen (2005) provides the original comparison between the dead load analyses from MDX and UMN Program. These comparisons are repeated here using updated UMN Program analyses based on the final bridge mesh as described previously and shown in Figure 4-3. One live load comparison based on the maximum loading configuration for the bridge test was also completed and details are provided below.

In the following comparisons, differences are calculated by:

$$\text{Percent Difference} = \frac{\text{UMN}_{\text{result}} - \text{MDX}_{\text{result}}}{\text{UMN}_{\text{result}}} * 100\% \quad (4-1)$$

The following classification of results was used to show the correlation between UMN Program and MDX:

- Strong – Difference less than 10%
- Moderate – Difference between 10% and 30%
- Weak – Difference greater than 30%
- Intermediate – very small values with difference greater than 10%

The intermediate classification is included to prevent comparisons of small values from unreasonably skewing the correlation results.

4.4.2.1 Dead Load Comparisons

The calculation of dead loads used for the UMN Program analyses are described in Chapter 9, and are similar to those used by MDX for these comparisons. No load factors were applied for any of these comparisons. The non-composite dead load analysis for both programs included the self-weight of the steel along with the wet weight of the deck acting on the steel members only. The superimposed dead load analysis included the weight of the curb, railing, and 2 inch overlay acting on the long-term composite system. The long-term composite system utilized an effective flange width of 90.5 inches, modular ratio of 24, slab thickness of 7.0 inches, and typical haunch height of 3.0 inches for each girder. Because the calculations in MDX assumed the minimum

amount of reinforcement steel in the deck, the UMN Program reinforcement ratio was decreased from the actual value near 2.8% to 1.0% for comparison purposes. The composite torsion constant J was calculated using one-half of b_{eff} for UMN Program in these comparisons since that is the value typically used by MDX. Loads on the composite section were distributed assuming full composite action everywhere. However, stresses in the negative moment regions (i.e., at piers) were calculated based on the steel girder section only as typically recommended for design or rating in this region when shear connectors are not provided.

Prior to any comparisons, it should be noted that the total dead load in each program was virtually identical; 2952.84 kips for UMN Program and 2953.07 kips for MDX. This is less than a 0.01% difference.

Table 4-3 displays the comparisons for the pier reactions of the non-composite, superimposed, and total (non-composite + superimposed) dead loads for both girders. The correlation is quite strong with the maximum difference being only 3.82%. Summing up the reactions along each girder, Table 4-4 shows the total dead load distributed to each girder as determined by the different programs. On average, UMN Program distributed approximately 2% more dead load to the exterior girder than did MDX for this bridge. Since the total dead load within each program was virtually identical and the loads were applied in a similar fashion for each program (uniform line loads on the girders), it was concluded that UMN Program exhibits a greater load transfer from the interior girder to the exterior girder than MDX.

The total dead load shear comparison plots for Girder C and Girder A are shown in Figure 4-4 and Figure 4-5, respectively. One item to note on these two plots is that at each end of the bridge, MDX drops off toward zero shear prior to the tip of the cantilever. If only line loads were applied this would make sense; however, point loads are applied at the tips to simulate the dead load of the adjacent bridge units. Therefore, there should be an offset shear at the ends, as UMN Program correctly shows. This problem is due to #10 in Section 4.4.1, and was unavoidable. Table 4-5 provides the percent differences between UMN Program and MDX for the shears at each pier. All shear correlations at the piers are strong, with the highest difference being 4.39%.

Moment comparison plots are provided in Figure 4-6 and Figure 4-7 for the total dead load on Girder C and Girder A, respectively. Table 4-6 breaks down the percent differences between the two programs for each dead load moment at the piers and midspans. The non-composite dead load moments correlate strongly at all locations, while the superimposed dead load moments deviate at the cantilevered ends, especially at the south end near Pier 10. Like the shears, the moment deviation at the cantilevered ends goes back to #10 in Section 4.4.1. Because both girders at Pier 10 have significantly higher moments in MDX for the superimposed loads and not the non-composite loads, it is hypothesized that the plate elements used for the concrete deck in MDX and the additional diaphragm introduce relatively high bridge stiffness at the cantilevered end as compared to UMN Program. Thus more load was attracted to Pier 10 in MDX than UMN Program.

Figure 4-8 and Figure 4-9 show the total dead load deflection comparisons for each girder. Midspan deflection percent differences are provided in Table 4-7. In general, UMN Program tends to predict larger deflections than MDX. This is because UMN Program includes the warping DOF, which slightly decreases the stiffness of the girder elements as compared to the

MDX counterparts. At 4.91% for the interior girder and 2.04% for the exterior girder, the overall correlation for maximum total dead load deflections is still strong.

The most important comparison between the two programs is the longitudinal stress. For both programs, the stress presented in the plots and charts that follow includes the maximum flexural stress at the flange surface plus the maximum warping stress at the flange tip. Recall from Section 4.4.1 that UMN Program calculates the warping stress directly from the warping DOF, while MDX approximates it based on the vertical moment at the cross-section. Also, for both programs the calculation of stress in the negative moment regions for the superimposed dead loads ignores the concrete deck and reinforcement since shear connectors are not provided here.

Figure 4-10 and Figure 4-11 plot the comparisons for the non-composite dead load stress for the top flange (TF) and bottom flange (BF) of Girder C and Girder A, while Figure 4-12 and Figure 4-13 do likewise for the superimposed dead load stress. Figure 4-14 and Figure 4-15 provide the plots of the total dead load stress for each girder. Table 4-8 and Table 4-9 tabulate the percent differences for each type of dead load for the Interior Girder C and the Exterior Girder A, respectively. Besides showing a generally strong correlation for the stresses between the two programs, the above figures and tables reveal a number of interesting details. First of all, the stress at Pier 10 for the superimposed dead loads had the same issues as previously discussed for the moments there. Second, due to #6 and #7 in Section 4.4.1, a great deal of accuracy was lost in the MDX results, especially in the negative moment regions where there were a lot of girder property changes. This typically caused unconservative results, but could have been rectified by adding additional nodes to the element mesh in MDX. Third, because the warping stress for MDX is calculated independent of torsion at a given section, it cannot provide a detailed warping stress profile as UMN Program does.

4.4.2.2 Live Load Comparisons

Although retrieving specific live load results in MDX was difficult, it was decided that at least one comparison should be made from the truck configurations for the bridge test. The overall maximum load case with four trucks on Span 9-8 and four trucks on Span 8-7 was chosen to provide the correlation between MDX and UMN Program for live load behavior. The composite section used for UMN Program consisted of an effective flange width of 99.5 inches, modular ratio of 8, slab thickness of 8.5 inches, and typical haunch height of 3.0 inches. Similar to the composite dead load calculations, the reinforcement ratio for UMN Program was also reduced to 1.0% for this comparison. Loads were distributed based on full composite action along the entire length of the bridge.

The only data that was retrieved from the MDX output, and thus was available for comparison with UMN Program, was the moment along the length of the interior girder. Table 4-10 compares the maximum moments at the piers and near the middle of the spans for each program. In the region where the loads are applied, between Pier 9 and Pier 7, the correlation of maximum moments is within 5.75% for all values. Outside of this region where the values are much smaller, the maximum difference bumps up to 16.3%, excluding the comparisons between the extremely low moments at Pier 10 and Pier 5. Because moment tended to be a good indicator of the general correlation between the two programs for the dead load comparisons, it was concluded that the overall correlation for this live load case was strong.

4.4.3 Conclusions

Overall, the results from these comparisons show that there is a strong analytical correlation between MDX and UMN Program for Mn/DOT Bridge No. 69824. However, for bridges with skewed supports, non-uniform diaphragm spacing, small radii of curvature, changes in curvature, and other generally more complex geometries this correlation will likely degrade due to the approximate methods used in MDX for modeling the restraint of warping behavior. In particular, MDX does not directly account for the stiffness due to restraint of warping, and the approximate equation used for calculating the restraint of warping stresses makes generalizing assumptions that limit its applicability. Refer to Section 2.4 of this report for a summary of these limits as provided by AASHTO (2003a).

Note that only the analysis engine for MDX was investigated for this project. No claims are herein made concerning the code checking capabilities of MDX.

Comparison between UMN Program and Differential Equations for Cases 1-5
SINGLE SPAN NONCOMPOSITE GIRDER

Span Length Radius	Distance (inches) from left end of girder					Fractional Distance				
	Left (L)	Quarter (LQ)	Middle (M)	Quarter (RQ)	Right (R)	Left (L)	Quarter (LQ)	Middle (M)	Quarter (RQ)	Right (R)
111.63 ft 565.96 ft	0	267.6	669.1	1069.9	1339.5	0.000	0.200	0.500	0.799	1.000

MOMENT (k-ft)

CASE	UMN Program					Differential Equations					Percent Difference (UMN as base)				
	L	LQ	M	RQ	R	L	LQ	M	RQ	R	L	LQ	M	RQ	R
1	0	1620	2530	1620	0	0	1627	2543	1627	0	0.00%	-0.43%	-0.51%	-0.43%	0.00%
2	-2070	-456	451	-456	-2070	-2072	-457	452	-457	-2072	-0.10%	-0.25%	-0.16%	-0.25%	-0.10%
3	0	1620	2530	1620	0	0	1627	2543	1627	0	0.00%	-0.43%	-0.51%	-0.43%	0.00%
4	-2020	-408	499	-408	-2020	-2031	-410	502	-410	-2031	-0.54%	-0.55%	-0.59%	-0.55%	-0.54%
5	-232	-44	50	-82	-296	-232	-44	50	-82	-296	0.00%	-0.51%	0.54%	-0.45%	0.00%

BIMOMENT (k-ft²)

CASE	UMN Program					Differential Equations					Percent Difference (UMN as base)				
	L	LQ	M	RQ	R	L	LQ	M	RQ	R	L	LQ	M	RQ	R
1	0	2160	3620	2160	0	0	2175	3644	2175	0	0.00%	-0.69%	-0.66%	-0.69%	0.00%
2	110	-106	162	-106	110	111	-107	163	-107	111	-1.29%	-0.66%	-0.64%	-0.66%	-1.29%
3	-3360	-185	1780	-185	-3360	-3387	-187	1795	-187	-3387	-0.80%	-0.94%	-0.84%	-0.94%	-0.80%
4	0	-129	184	-129	0	0	-130	185	-130	0	0.00%	-0.88%	-0.52%	-0.88%	0.00%
5	-137	-116	-75	-141	-146	-137	-117	-75	-141	-146	0.00%	-0.46%	-0.55%	0.07%	0.00%

DEFLECTION (inches)

CASE	UMN Program					Differential Equations					Percent Difference (UMN as base)				
	L	LQ	M	RQ	R	L	LQ	M	RQ	R	L	LQ	M	RQ	R
1	0.00	40.70	69.30	40.70	0.00	0.00	41.18	70.02	41.18	0.00	0.00%	-1.19%	-1.04%	-1.19%	0.00%
2	0.00	0.31	0.83	0.31	0.00	0.00	0.32	0.84	0.32	0.00	0.00%	-0.64%	-0.48%	-0.64%	0.00%
3	0.00	11.70	20.60	11.70	0.00	0.00	11.81	20.82	11.81	0.00	0.00%	-0.94%	-1.05%	-0.94%	0.00%
4	0.00	0.32	0.86	0.32	0.00	0.00	0.32	0.86	0.32	0.00	0.00%	-0.94%	-0.94%	-0.94%	0.00%
5	0.00	-2.20	-3.68	-2.36	0.00	0.00	-2.20	-3.69	-2.36	0.00	0.00%	-0.14%	-0.30%	0.00%	0.00%

TORSION ANGLE (radians)

CASE	UMN Program					Differential Equations					Percent Difference (UMN as base)				
	L	LQ	M	RQ	R	L	LQ	M	RQ	R	L	LQ	M	RQ	R
5	0.026	0.087	0.124	0.108	0.054	0.026	0.087	0.124	0.108	0.054	0.00%	0.00%	0.00%	0.00%	0.00%

*Torsion angle was not compared in cases 1-4

CASE 1 - Bending PINNED, Torsion PINNED

CASE 2 - Bending FIXED, Torsion FIXED

CASE 3 - Bending PINNED, Torsion FIXED

CASE 4 - Bending FIXED, Torsion PINNED

CASE 5 - Bending VARIABLE, Torsion VARIABLE

Table 4-1: Non-Composite Girder Comparison between UMN Program and Differential Equations

Comparison between UMN Program and Differential Equations for Cases 1-5
SINGLE SPAN COMPOSITE GIRDER

Span Length	111.63 ft	Distance (inches) from left end of girder					Fractional Distance				
Radius	565.96 ft	Left (L)	Quarter (LQ)	Middle (M)	Quarter (RQ)	Right (R)	Left (L)	Quarter (LQ)	Middle (M)	Quarter (RQ)	Right (R)
		0	267.6	669.1	1069.9	1339.5	0.000	0.200	0.500	0.799	1.000

MOMENT (k-ft)

CASE	UMN Program					Differential Equations					Percent Difference (UMN as base)				
	L	LQ	M	RQ	R	L	LQ	M	RQ	R	L	LQ	M	RQ	R
1	0	1620	2530	1620	0	0	1627	2543	1627	0	0.00%	-0.43%	-0.51%	-0.43%	0.00%
2	-1820	-206	701	-206	-1820	-1828	-207	705	-207	-1828	-0.44%	-0.60%	-0.62%	-0.60%	-0.44%
3	0	1620	2530	1620	0	0	1627	2543	1627	0	0.00%	-0.43%	-0.51%	-0.43%	0.00%
4	-1820	-205	702	-205	-1820	-1827	-206	706	-207	-1829	-0.38%	-0.58%	-0.53%	-1.20%	-0.49%
5	-1770	-298	393	-733	-2490	-1770	-300	393	-732	-2490	0.00%	-0.60%	0.10%	0.10%	0.00%

BIMOMENT (k-ft²)

CASE	UMN Program					Differential Equations					Percent Difference (UMN as base)				
	L	LQ	M	RQ	R	L	LQ	M	RQ	R	L	LQ	M	RQ	R
1	0.0	84.2	133.0	84.2	0.0	0.0	84.7	133.7	84.7	0.0	0.00%	-0.55%	-0.56%	-0.55%	0.00%
2	1.7	-11.9	35.0	-11.9	1.7	1.9	-12.0	35.2	-12.0	1.9	-10.71%	-0.70%	-0.58%	-0.70%	-10.88%
3	-891.0	68.6	133.0	68.6	-891.0	-896.8	69.1	133.7	69.1	-896.8	-0.65%	-0.69%	-0.50%	-0.69%	-0.65%
4	0.0	-11.9	35.0	-11.9	0.0	0.0	-12.0	35.2	-12.0	0.0	0.00%	-0.50%	-0.65%	-1.07%	0.00%
5	-71.2	-18.2	18.5	-41.4	-105.0	-71.2	-18.3	18.4	-41.4	-105.0	0.00%	-0.36%	0.39%	0.04%	0.00%

DEFLECTION (inches)

CASE	UMN Program					Differential Equations					Percent Difference (UMN as base)				
	L	LQ	M	RQ	R	L	LQ	M	RQ	R	L	LQ	M	RQ	R
1	0.00	1.48	2.51	1.48	0.00	0.00	1.50	2.53	1.49	0.00	0.00%	-1.08%	-0.80%	-0.41%	0.00%
2	0.00	0.13	0.31	0.13	0.00	0.00	0.13	0.31	0.13	0.00	0.00%	-0.80%	-0.64%	-0.80%	0.00%
3	0.00	1.35	2.29	1.35	0.00	0.00	1.36	2.31	1.36	0.00	0.00%	-0.67%	-1.00%	-0.67%	0.00%
4	0.00	0.13	0.31	0.13	0.00	0.00	0.13	0.31	0.12	0.00	0.00%	-0.80%	-0.64%	0.80%	0.00%
5	0.00	-0.18	-0.27	-0.30	0.00	0.00	-0.18	-0.27	-0.30	0.00	0.00%	-0.56%	0.00%	0.00%	0.00%

TORSION ANGLE (radians)

CASE	UMN Program					Differential Equations					Percent Difference (UMN as base)				
	L	LQ	M	RQ	R	L	LQ	M	RQ	R	L	LQ	M	RQ	R
5	0.0003	0.0043	0.0070	0.0125	0.0108	0.0003	0.0043	0.0070	0.0120	0.0110	1.20%	-0.23%	-0.14%	4.00%	-1.85%

*Torsion angle was not compared in cases 1-4

CASE 1 - Bending PINNED, Torsion PINNED
CASE 2 - Bending FIXED, Torsion FIXED
CASE 3 - Bending PINNED, Torsion FIXED
CASE 4 - Bending FIXED, Torsion PINNED
CASE 5 - Bending VARIABLE, Torsion VARIABLE

Table 4-2: Composite Girder Comparison between UMN Program and Differential Equations

Non-Composite Dead Load Pier Reactions								
Bridge Location	Interior Girder C				Exterior Girder A			
	UMN (kips)	MDX (kips)	Percent Difference	Correlation	UMN (kips)	MDX (kips)	Percent Difference	Correlation
Pier 10	129.96	130.72	-0.58%	strong	143.08	142.34	0.52%	strong
Pier 9	182.76	187.28	-2.47%	strong	190.81	187.57	1.70%	strong
Pier 8	250.50	256.64	-2.45%	strong	265.80	257.58	3.09%	strong
Pier 7	247.30	252.93	-2.28%	strong	267.60	260.16	2.78%	strong
Pier 6	177.25	179.47	-1.25%	strong	175.69	173.67	1.15%	strong
Pier 5	84.83	86.41	-1.86%	strong	87.40	89.34	-2.22%	strong
Superimposed Dead Load Pier Reactions								
Bridge Location	Interior Girder C				Exterior Girder A			
	UMN (kips)	MDX (kips)	Percent Difference	Correlation	UMN (kips)	MDX (kips)	Percent Difference	Correlation
Pier 10	46.61	47.73	-2.40%	strong	50.62	50.89	-0.53%	strong
Pier 9	62.36	63.17	-1.30%	strong	65.14	62.65	3.82%	strong
Pier 8	83.58	85.46	-2.25%	strong	87.51	85.95	1.78%	strong
Pier 7	82.82	84.60	-2.15%	strong	88.07	85.86	2.51%	strong
Pier 6	61.23	62.13	-1.47%	strong	61.04	60.73	0.51%	strong
Pier 5	30.06	29.47	1.96%	strong	30.82	30.32	1.62%	strong
Total Dead Load Pier Reactions								
Bridge Location	Interior Girder C				Exterior Girder A			
	UMN (kips)	MDX (kips)	Percent Difference	Correlation	UMN (kips)	MDX (kips)	Percent Difference	Correlation
Pier 10	176.57	178.45	-1.06%	strong	193.70	193.23	0.24%	strong
Pier 9	245.12	250.45	-2.17%	strong	255.95	250.22	2.24%	strong
Pier 8	334.08	342.10	-2.40%	strong	353.31	343.53	2.77%	strong
Pier 7	330.12	337.53	-2.24%	strong	355.67	346.02	2.71%	strong
Pier 6	238.48	241.60	-1.31%	strong	236.73	234.40	0.98%	strong
Pier 5	114.89	115.88	-0.86%	strong	118.22	119.66	-1.22%	strong

Table 4-3: Dead Load Pier Reaction Comparisons

Total Girder Dead Load Distribution								
Bridge Location	Interior Girder C			Exterior Girder A			UMN (kips)	MDX (kips)
	UMN (kips)	MDX (kips)	Percent Difference	UMN (kips)	MDX (kips)	Percent Difference		
Non-Composite:	1072.60	1093.45	-1.94%	1130.38	1110.66	1.74%		
Superimposed:	366.66	372.56	-1.61%	383.20	376.40	1.77%		
Total Dead Load:	1439.26	1466.01	-1.86%	1513.58	1487.06	1.75%		

Table 4-4: Total Girder Dead Load Distribution Comparison

Non-Composite Dead Load Shear									
Bridge Location		Interior Girder C				Exterior Girder A			
		UMN (kips)	MDX (kips)	Percent Difference	Correlation	UMN (kips)	MDX (kips)	Percent Difference	Correlation
Pier 10	South	-60.75	-60.11	1.05%	strong	-62.44	-61.59	1.36%	strong
	North	69.21	69.37	-0.23%	strong	80.64	81.31	-0.83%	strong
Pier 9	South	-93.34	-93.51	-0.18%	strong	-102.50	-102.69	-0.19%	strong
	North	89.42	89.81	-0.44%	strong	88.31	88.16	0.17%	strong
Pier 8	South	-120.50	-119.94	0.46%	strong	-119.30	-118.59	0.60%	strong
	North	130.00	129.27	0.56%	strong	146.50	145.73	0.53%	strong
Pier 7	South	-128.50	-127.01	1.16%	strong	-146.80	-145.85	0.65%	strong
	North	118.80	118.38	0.35%	strong	120.80	121.17	-0.31%	strong
Pier 6	South	-89.76	-89.85	-0.10%	strong	-86.99	-85.98	1.16%	strong
	North	87.49	87.97	-0.55%	strong	88.70	88.67	0.03%	strong
Pier 5	South	-49.42	-50.45	-2.08%	strong	-51.63	-53.12	-2.89%	strong
	North	35.41	35.55	-0.40%	strong	35.77	35.93	-0.45%	strong
Superimposed Dead Load Shear									
Bridge Location		Interior Girder C				Exterior Girder A			
		UMN (kips)	MDX (kips)	Percent Difference	Correlation	UMN (kips)	MDX (kips)	Percent Difference	Correlation
Pier 10	South	-22.39	-22.34	0.22%	strong	-23.06	-22.97	0.39%	strong
	North	24.22	24.89	-2.77%	strong	27.56	28.24	-2.47%	strong
Pier 9	South	-31.88	-31.22	2.07%	strong	-34.58	-33.57	2.92%	strong
	North	30.48	30.64	-0.52%	strong	30.56	30.17	1.28%	strong
Pier 8	South	-39.89	-39.71	0.45%	strong	-39.29	-39.34	-0.13%	strong
	North	43.69	43.37	0.73%	strong	48.22	48.84	-1.29%	strong
Pier 7	South	-43.32	-42.65	1.55%	strong	-48.40	-48.42	-0.04%	strong
	North	39.50	39.56	-0.15%	strong	39.67	39.69	-0.05%	strong
Pier 6	South	-30.75	-30.74	0.03%	strong	-30.28	-29.84	1.45%	strong
	North	30.48	30.81	-1.08%	strong	30.76	31.25	-1.59%	strong
Pier 5	South	-17.98	-17.19	4.39%	strong	-18.60	-17.90	3.76%	strong
	North	12.08	11.93	1.24%	strong	12.22	12.12	0.82%	strong
Total Dead Load Shear									
Bridge Location		Interior Girder C				Exterior Girder A			
		UMN (kips)	MDX (kips)	Percent Difference	Correlation	UMN (kips)	MDX (kips)	Percent Difference	Correlation
Pier 10	South	-83.14	-82.45	0.83%	strong	-85.50	-84.56	1.10%	strong
	North	93.43	94.26	-0.89%	strong	108.20	109.55	-1.25%	strong
Pier 9	South	-125.22	-124.73	0.39%	strong	-137.08	-136.26	0.60%	strong
	North	119.90	120.45	-0.46%	strong	118.87	118.33	0.45%	strong
Pier 8	South	-160.39	-159.65	0.46%	strong	-158.59	-157.93	0.42%	strong
	North	173.69	172.64	0.60%	strong	194.72	194.57	0.08%	strong
Pier 7	South	-171.82	-169.66	1.26%	strong	-195.20	-194.27	0.48%	strong
	North	158.30	157.94	0.23%	strong	160.47	160.86	-0.24%	strong
Pier 6	South	-120.51	-120.59	-0.07%	strong	-117.27	-115.82	1.24%	strong
	North	117.97	118.78	-0.69%	strong	119.46	119.92	-0.39%	strong
Pier 5	South	-67.40	-67.64	-0.36%	strong	-70.23	-71.02	-1.12%	strong
	North	47.49	47.48	0.02%	strong	47.99	48.05	-0.13%	strong

Table 4-5: Dead Load Shear Comparisons

Non-Composite Dead Load Moment								
Bridge Location	Interior Girder C				Exterior Girder A			
	UMN (kip-ft)	MDX (kip-ft)	Percent Difference	Correlation	UMN (kip-ft)	MDX (kip-ft)	Percent Difference	Correlation
Pier 10	-514.70	-509.18	1.07%	strong	-545.80	-539.22	1.21%	strong
Midspan 10-9	840.90	843.58	-0.32%	strong	1168.00	1187.16	-1.64%	strong
Pier 9	-1533.00	-1542.62	-0.63%	strong	-1690.00	-1682.36	0.45%	strong
Midspan 9-8	585.50	586.35	-0.15%	strong	429.70	412.89	3.91%	strong
Pier 8	-2947.00	-2944.26	0.09%	strong	-3540.00	-3574.78	-0.98%	strong
Midspan 8-7	1484.00	1455.59	1.91%	strong	2244.00	2203.52	1.80%	strong
Pier 7	-2870.00	-2821.63	1.69%	strong	-3574.00	-3656.26	-2.30%	strong
Midspan 7-6	600.60	622.20	-3.60%	strong	476.10	439.75	7.63%	strong
Pier 6	-1558.00	-1545.51	0.80%	strong	-1576.00	-1545.92	1.91%	strong
Midspan 6-5	487.70	501.07	-2.74%	strong	536.60	562.02	-4.74%	strong
Pier 5	-156.50	-154.39	1.35%	strong	-159.80	-157.51	1.43%	strong
Superimposed Dead Load Moment								
Bridge Location	Interior Girder C				Exterior Girder A			
	UMN (kip-ft)	MDX (kip-ft)	Percent Difference	Correlation	UMN (kip-ft)	MDX (kip-ft)	Percent Difference	Correlation
Pier 10	-189.60	-250.10	-31.91%	weak	-202.90	-275.89	-35.97%	weak
Midspan 10-9	292.40	257.28	12.01%	moderate	376.70	349.54	7.21%	strong
Pier 9	-521.00	-525.68	-0.90%	strong	-573.60	-565.34	1.44%	strong
Midspan 9-8	200.70	207.70	-3.49%	strong	175.90	160.37	8.83%	strong
Pier 8	-980.60	-964.66	1.63%	strong	-1144.00	-1180.47	-3.19%	strong
Midspan 8-7	536.00	515.81	3.77%	strong	759.50	789.82	-3.99%	strong
Pier 7	-960.30	-925.98	3.57%	strong	-1152.00	-1184.99	-2.86%	strong
Midspan 7-6	203.60	208.92	-2.61%	strong	186.10	164.91	11.39%	moderate
Pier 6	-533.80	-536.02	-0.42%	strong	-546.20	-547.00	-0.15%	strong
Midspan 6-5	181.00	197.13	-8.91%	strong	191.50	214.10	-11.80%	moderate
Pier 5	-52.58	-53.20	-1.18%	strong	-53.75	-54.47	-1.34%	strong
Total Dead Load Moment								
Bridge Location	Interior Girder C				Exterior Girder A			
	UMN (kip-ft)	MDX (kip-ft)	Percent Difference	Correlation	UMN (kip-ft)	MDX (kip-ft)	Percent Difference	Correlation
Pier 10	-704.30	-759.28	-7.81%	strong	-748.70	-815.11	-8.87%	strong
Midspan 10-9	1133.30	1100.86	2.86%	strong	1544.70	1536.70	0.52%	strong
Pier 9	-2054.00	-2068.30	-0.70%	strong	-2263.60	-2247.70	0.70%	strong
Midspan 9-8	786.20	794.05	-1.00%	strong	605.60	573.26	5.34%	strong
Pier 8	-3927.60	-3908.92	0.48%	strong	-4684.00	-4755.25	-1.52%	strong
Midspan 8-7	2020.00	1971.40	2.41%	strong	3003.50	2993.34	0.34%	strong
Pier 7	-3830.30	-3747.61	2.16%	strong	-4726.00	-4841.25	-2.44%	strong
Midspan 7-6	804.20	831.12	-3.35%	strong	662.20	604.66	8.69%	strong
Pier 6	-2091.80	-2081.53	0.49%	strong	-2122.20	-2092.92	1.38%	strong
Midspan 6-5	668.70	698.20	-4.41%	strong	728.10	776.12	-6.60%	strong
Pier 5	-209.08	-207.59	0.71%	strong	-213.55	-211.98	0.74%	strong

Table 4-6: Dead Load Moment Comparisons

Non-Composite Dead Load Deflections								
Bridge Location	Interior Girder C				Exterior Girder A			
	UMN (inches)	MDX (inches)	Percent Difference	Correlation	UMN (inches)	MDX (inches)	Percent Difference	Correlation
Midspan 10-9	0.544	0.551	-1.31%	strong	0.826	0.852	-3.21%	strong
Midspan 9-8	0.184	0.202	-9.78%	strong	-0.064	-0.077	-20.77%	intermediate
Midspan 8-7	1.989	1.953	1.81%	strong	2.467	2.463	0.16%	strong
Midspan 7-6	0.200	0.229	-14.27%	moderate	0.008	-0.035	558.00%	intermediate
Midspan 6-5	0.628	0.631	-0.46%	strong	0.715	0.735	-2.87%	strong
Superimposed Dead Load Deflections								
Bridge Location	Interior Girder C				Exterior Girder A			
	UMN (inches)	MDX (inches)	Percent Difference	Correlation	UMN (inches)	MDX (inches)	Percent Difference	Correlation
Midspan 10-9	0.110	0.074	32.54%	intermediate	0.153	0.108	29.60%	moderate
Midspan 9-8	0.039	0.071	-80.52%	intermediate	0.010	0.045	-360.36%	intermediate
Midspan 8-7	0.429	0.346	19.31%	moderate	0.503	0.446	11.24%	moderate
Midspan 7-6	0.040	0.071	-75.35%	intermediate	0.020	0.046	-130.23%	intermediate
Midspan 6-5	0.124	0.097	21.96%	intermediate	0.136	0.108	20.30%	moderate
Total Dead Load Deflections								
Bridge Location	Interior Girder C				Exterior Girder A			
	UMN (inches)	MDX (inches)	Percent Difference	Correlation	UMN (inches)	MDX (inches)	Percent Difference	Correlation
Midspan 10-9	0.654	0.625	4.38%	strong	0.979	0.960	1.93%	strong
Midspan 9-8	0.223	0.273	-22.24%	moderate	-0.054	-0.032	40.72%	intermediate
Midspan 8-7	2.418	2.299	4.91%	strong	2.970	2.909	2.04%	strong
Midspan 7-6	0.241	0.300	-24.54%	moderate	0.028	0.011	60.18%	intermediate
Midspan 6-5	0.752	0.728	3.24%	strong	0.850	0.843	0.82%	strong

Table 4-7: Midspan Dead Load Deflection Comparisons

Interior Girder C Non-composite Dead Load Stress								
Bridge Location	Top Flange				Bottom Flange			
	UMN (ksi)	MDX (ksi)	Percent Difference	Correlation	UMN (ksi)	MDX (ksi)	Percent Difference	Correlation
Pier 10	3.79	3.75	1.06%	strong	-3.75	-3.75	0.00%	strong
Midspan 10-9	-6.21	-6.48	-4.35%	strong	6.64	6.48	2.41%	strong
Pier 9	10.46	9.75	6.79%	strong	-9.99	-9.75	2.40%	strong
Midspan 9-8	-4.62	-4.46	3.46%	strong	4.47	4.46	0.22%	strong
Pier 8	12.52	11.33	9.50%	strong	-11.20	-11.33	-1.16%	strong
Midspan 8-7	-10.71	-10.59	1.12%	strong	11.18	10.59	5.28%	strong
Pier 7	12.78	11.50	10.02%	moderate	-11.71	-11.50	1.79%	strong
Midspan 7-6	-4.72	-4.73	-0.21%	strong	4.59	4.73	-3.05%	strong
Pier 6	11.55	11.11	3.81%	strong	-10.85	-11.11	-2.40%	strong
Midspan 6-5	-5.66	-5.60	1.06%	strong	5.49	5.60	-2.00%	strong
Pier 5	4.08	3.55	12.99%	moderate	-4.15	-3.55	14.46%	moderate
Interior Girder C Superimposed Dead Load Stress								
Bridge Location	Top Flange				Bottom Flange			
	UMN (ksi)	MDX (ksi)	Percent Difference	Correlation	UMN (ksi)	MDX (ksi)	Percent Difference	Correlation
Pier 10	1.32	1.70	-28.79%	moderate	-1.37	-1.88	-37.23%	weak
Midspan 10-9	-0.78	-0.63	19.23%	moderate	1.88	1.75	6.91%	strong
Pier 9	3.31	3.17	4.23%	strong	-3.58	-3.79	-5.87%	strong
Midspan 9-8	-0.54	-0.53	1.85%	strong	1.25	1.37	-9.60%	strong
Pier 8	3.85	3.51	8.83%	strong	-3.97	-3.91	1.51%	strong
Midspan 8-7	-1.33	-1.24	6.77%	strong	3.26	3.32	-1.84%	strong
Pier 7	3.94	3.54	10.15%	moderate	-4.17	-4.01	3.84%	strong
Midspan 7-6	-0.54	-0.52	3.70%	strong	1.27	1.39	-9.45%	strong
Pier 6	3.72	3.59	3.49%	strong	-3.94	-3.99	-1.27%	strong
Midspan 6-5	-0.63	-0.61	3.17%	strong	1.62	1.91	-17.90%	moderate
Pier 5	1.36	1.16	14.71%	moderate	-1.38	-1.28	7.25%	strong
Interior Girder C Total Dead Load Stress								
Bridge Location	Top Flange				Bottom Flange			
	UMN (ksi)	MDX (ksi)	Percent Difference	Correlation	UMN (ksi)	MDX (ksi)	Percent Difference	Correlation
Pier 10	5.11	5.45	-6.65%	strong	-5.15	-5.63	-9.32%	strong
Midspan 10-9	-6.99	-7.11	-1.72%	strong	8.52	8.23	3.40%	strong
Pier 9	13.77	12.92	6.17%	strong	-13.56	-13.54	0.15%	strong
Midspan 9-8	-5.16	-4.99	3.29%	strong	5.74	5.83	-1.57%	strong
Pier 8	16.37	14.84	9.35%	strong	-15.38	-15.24	0.91%	strong
Midspan 8-7	-12.04	-11.83	1.74%	strong	14.44	13.91	3.67%	strong
Pier 7	16.72	15.04	10.05%	moderate	-15.65	-15.51	0.89%	strong
Midspan 7-6	-5.26	-5.25	0.19%	strong	5.84	6.12	-4.79%	strong
Pier 6	15.27	14.70	3.73%	strong	-14.80	-15.10	-2.03%	strong
Midspan 6-5	-6.29	-6.21	1.27%	strong	7.11	7.51	-5.63%	strong
Pier 5	5.44	4.71	13.42%	moderate	-4.07	-4.83	-18.67%	moderate

Table 4-8: Dead Load Stress Comparisons for Interior Girder C

Exterior Girder A Non-composite Dead Load Stress								
Bridge Location	Top Flange				Bottom Flange			
	UMN (ksi)	MDX (ksi)	Percent Difference	Correlation	UMN (ksi)	MDX (ksi)	Percent Difference	Correlation
Pier 10	4.03	3.98	1.24%	strong	-4.06	-3.98	1.97%	strong
Midspan 10-9	-8.78	-9.15	-4.21%	strong	9.12	9.15	-0.33%	strong
Pier 9	9.03	8.34	7.64%	strong	-9.55	-8.34	12.67%	moderate
Midspan 9-8	-3.38	-3.15	6.80%	strong	3.25	3.15	3.08%	strong
Pier 8	11.27	10.30	8.61%	strong	-11.10	-10.30	7.21%	strong
Midspan 8-7	-13.97	-13.66	2.22%	strong	11.03	10.57	4.17%	strong
Pier 7	11.22	10.53	6.15%	strong	-11.42	-10.53	7.79%	strong
Midspan 7-6	-3.70	-3.36	9.19%	strong	3.63	3.36	7.44%	strong
Pier 6	9.73	9.23	5.14%	strong	-10.10	-9.23	8.61%	strong
Midspan 6-5	-6.18	-6.29	-1.78%	strong	6.07	6.29	-3.62%	strong
Pier 5	4.19	3.62	13.60%	moderate	-4.26	-3.62	15.02%	moderate
Exterior Girder A Superimposed Dead Load Stress								
Bridge Location	Top Flange				Bottom Flange			
	UMN (ksi)	MDX (ksi)	Percent Difference	Correlation	UMN (ksi)	MDX (ksi)	Percent Difference	Correlation
Pier 10	1.41	1.89	-34.04%	weak	-1.49	-2.06	-38.26%	weak
Midspan 10-9	-1.04	-0.85	18.27%	moderate	2.38	2.39	-0.42%	strong
Pier 9	2.87	2.63	8.36%	strong	-3.01	-2.98	1.00%	strong
Midspan 9-8	-0.46	-0.44	4.35%	strong	1.09	1.04	4.59%	strong
Pier 8	3.36	3.24	3.57%	strong	-3.41	-3.56	-4.40%	strong
Midspan 8-7	-1.79	-1.78	0.56%	strong	3.11	3.50	-12.54%	moderate
Pier 7	3.32	3.15	5.12%	strong	-3.49	-3.68	-5.44%	strong
Midspan 7-6	-0.48	-0.45	6.25%	strong	1.16	1.07	7.76%	strong
Pier 6	3.17	3.04	4.10%	strong	-3.27	-3.39	-3.67%	strong
Midspan 6-5	-0.67	-0.66	1.49%	strong	1.72	2.08	-20.93%	moderate
Pier 5	1.39	1.18	15.11%	moderate	-1.44	-1.31	9.03%	strong
Exterior Girder A Total Dead Load Stress								
Bridge Location	Top Flange				Bottom Flange			
	UMN (ksi)	MDX (ksi)	Percent Difference	Correlation	UMN (ksi)	MDX (ksi)	Percent Difference	Correlation
Pier 10	5.44	5.87	-7.90%	strong	-5.56	-6.04	-8.63%	strong
Midspan 10-9	-9.82	-10.00	-1.83%	strong	11.48	11.54	-0.52%	strong
Pier 9	11.90	10.97	7.82%	strong	-12.57	-11.32	9.94%	strong
Midspan 9-8	-3.84	-3.59	6.51%	strong	4.34	4.19	3.46%	strong
Pier 8	14.63	13.54	7.45%	strong	-14.73	-13.86	5.91%	strong
Midspan 8-7	-15.76	-15.44	2.03%	strong	14.14	14.07	0.50%	strong
Pier 7	14.54	13.68	5.91%	strong	-14.91	-14.21	4.69%	strong
Midspan 7-6	-4.18	-3.81	8.85%	strong	4.80	4.43	7.71%	strong
Pier 6	12.90	12.27	4.88%	strong	-13.37	-12.62	5.61%	strong
Midspan 6-5	-6.85	-6.95	-1.46%	strong	7.79	8.37	-7.45%	strong
Pier 5	5.58	4.80	13.98%	moderate	-4.19	-4.93	-17.66%	moderate

Table 4-9: Dead Load Stress Comparisons for Exterior Girder A

Maximum Live Load Moments:				
4 trucks at Midspan 9-8 and 4 trucks at Midspan 8-7				
Bridge Location	Interior Girder C			
	UMN (kip-ft)	MDX (kip-ft)	Percent Difference	Correlation
Pier 10	-3.23	-0.67	79.22%	intermediate
Span 10-9	-331.80	-326.11	1.71%	strong
Pier 9	-765.10	-809.09	-5.75%	strong
Span 9-8	1254.00	1191.93	4.95%	strong
Pier 8	-2752.00	-2800.69	-1.77%	strong
Span 8-7	1758.00	1748.97	0.51%	strong
Pier 7	-1406.00	-1352.51	3.80%	strong
Span 7-6	-461.50	-386.47	16.26%	moderate
Pier 6	319.90	275.69	13.82%	moderate
Span 6-5	164.20	151.39	7.80%	strong
Pier 5	0.70	0.57	18.50%	intermediate

Table 4-10: Live Load Moment Comparison between UMN Program and MDX

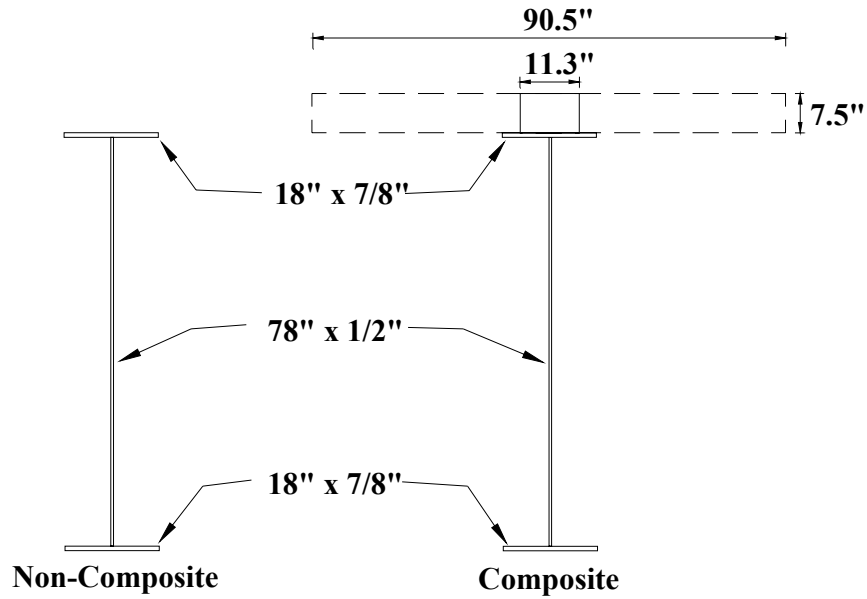


Figure 4-1: Non-composite and Composite Flexural Section Dimensions

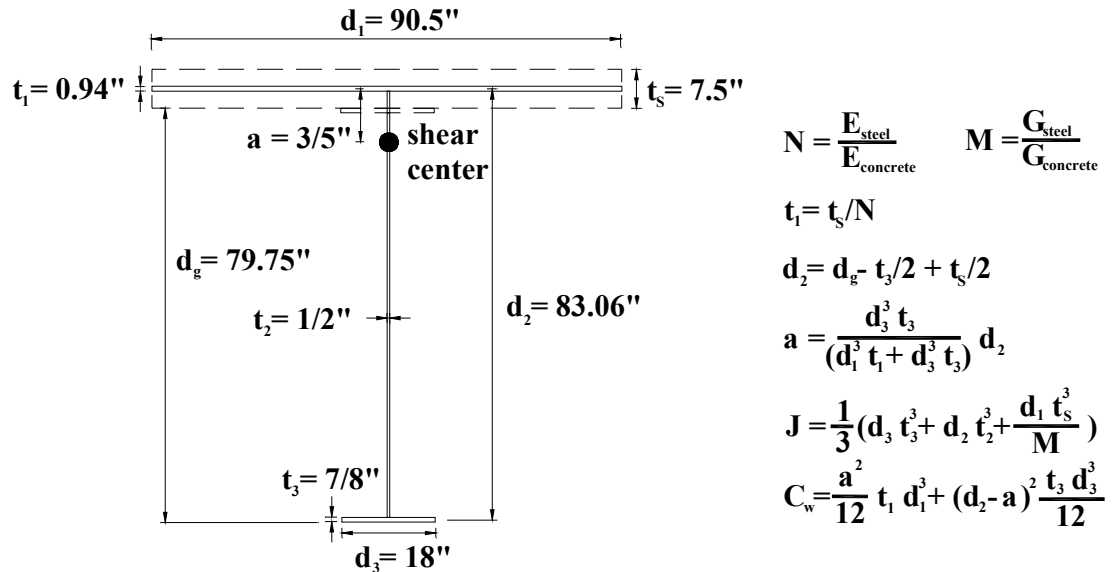


Figure 4-2: Composite Section Torsion Properties

Grillage Model for Mn/DOT Bridge No 69824 Unit 2

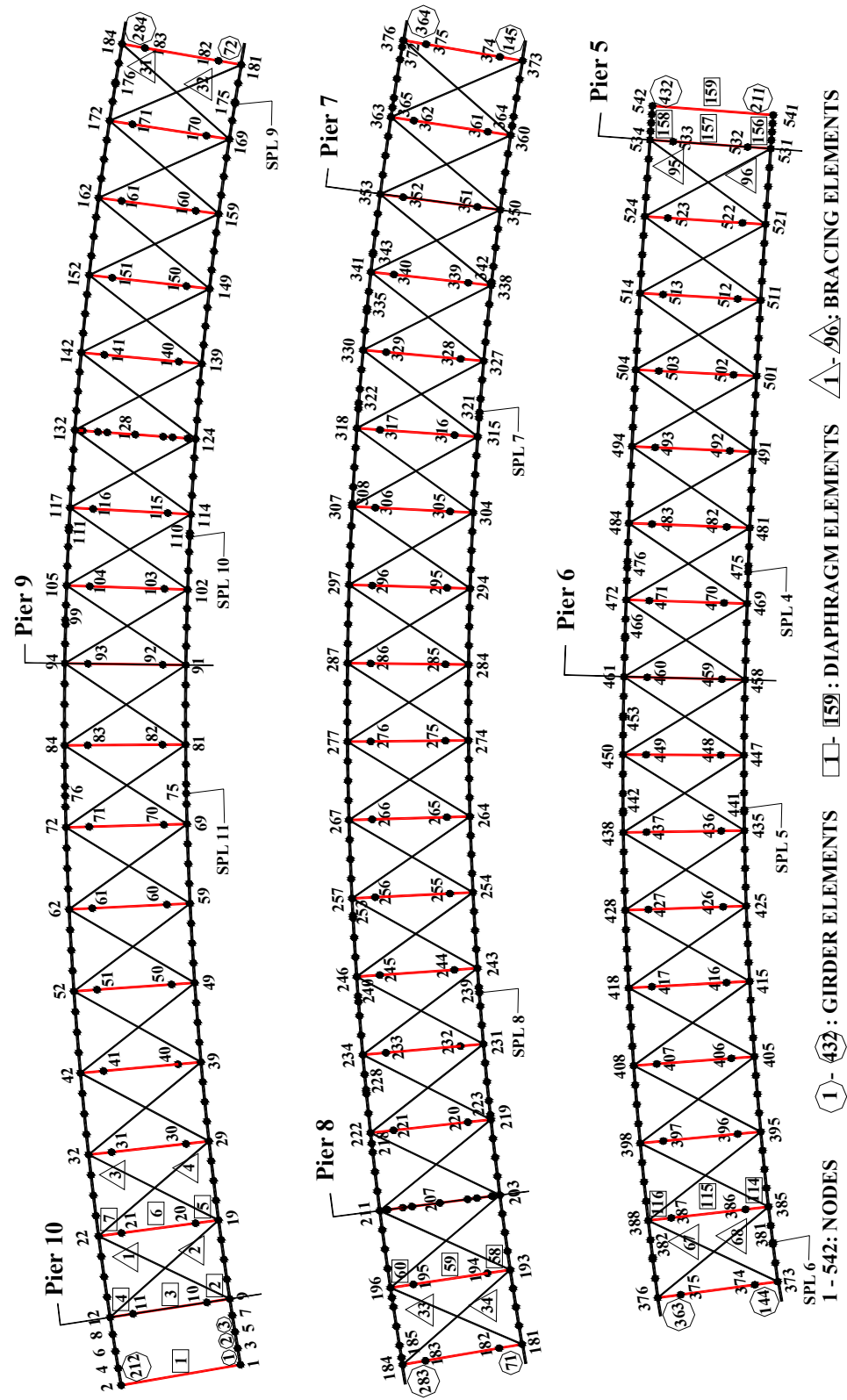


Figure 4-3: UMN Program Finite Element Mesh of Bridge 69824 Unit 2

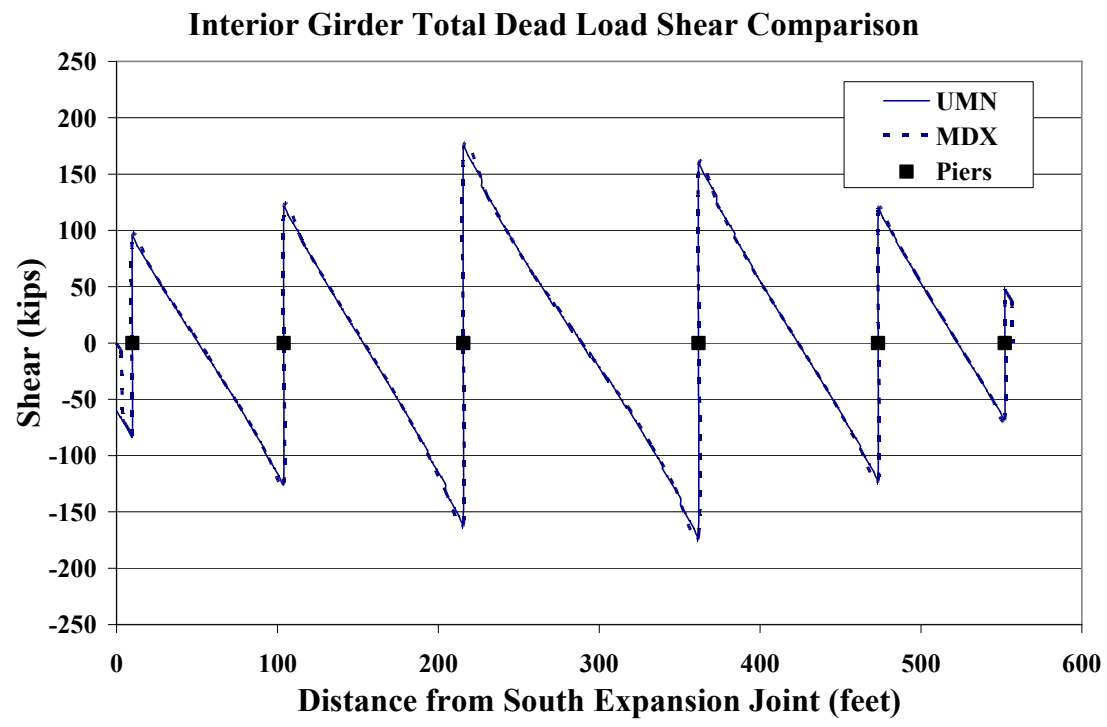


Figure 4-4: Interior Girder C Total Dead Load Shear Comparison



Figure 4-5: Exterior Girder A Total Dead Load Shear Comparison

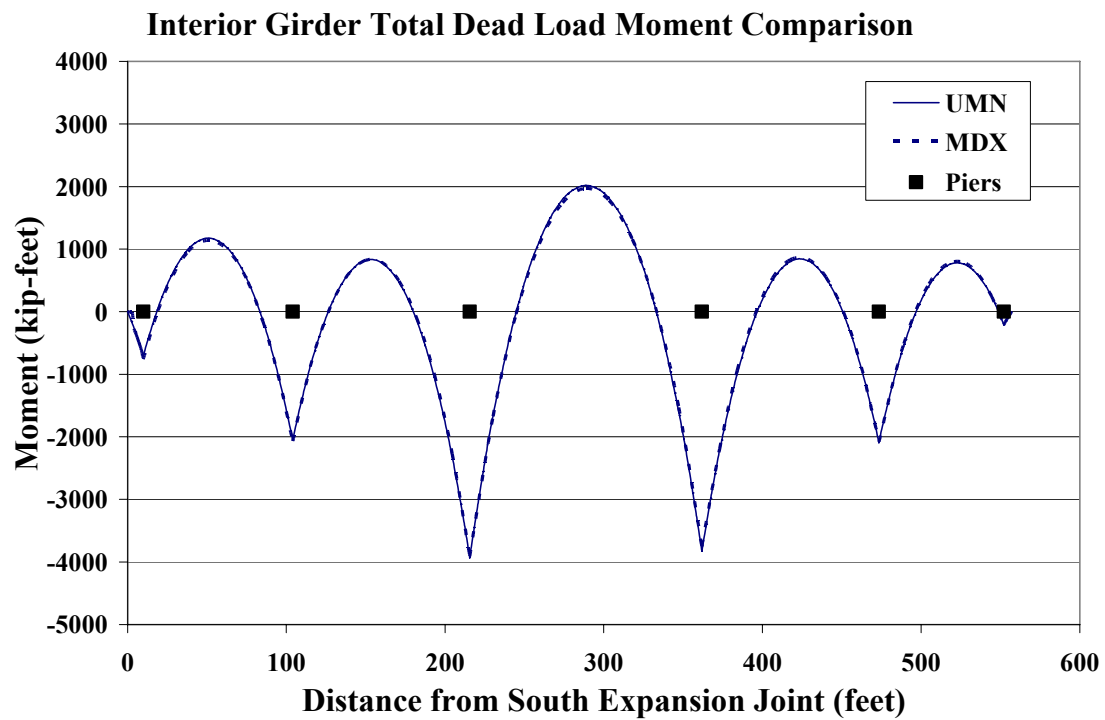


Figure 4-6: Interior Girder C Total Dead Load Moment Comparison

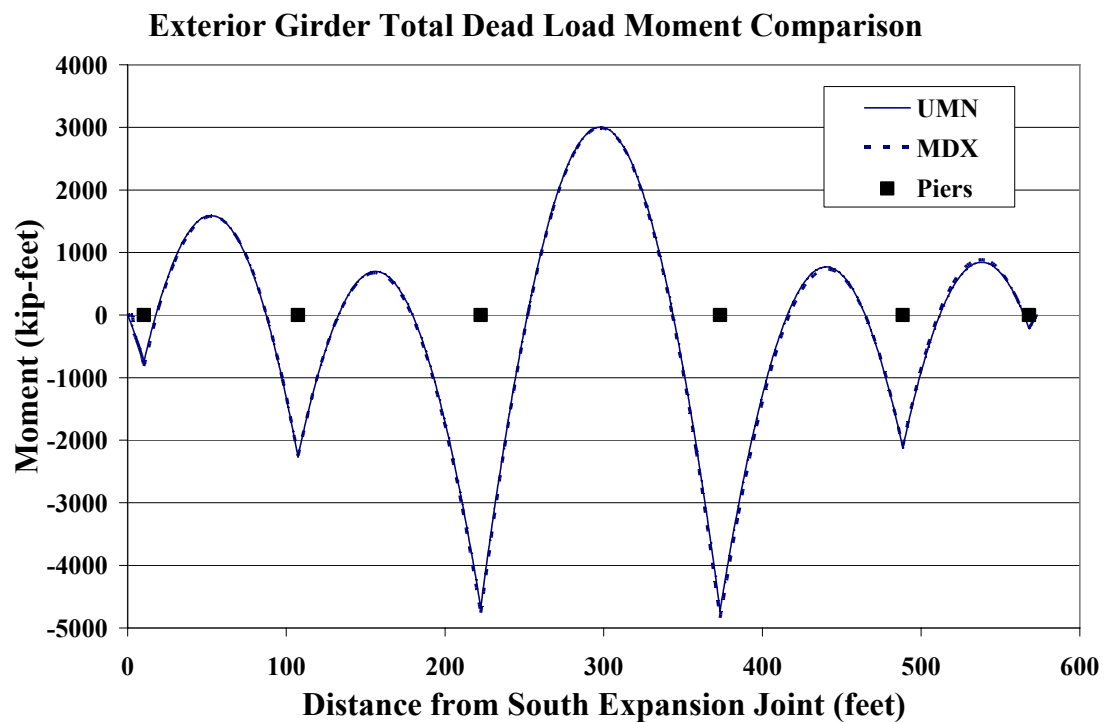


Figure 4-7: Exterior Girder A Total Dead Load Moment Comparison

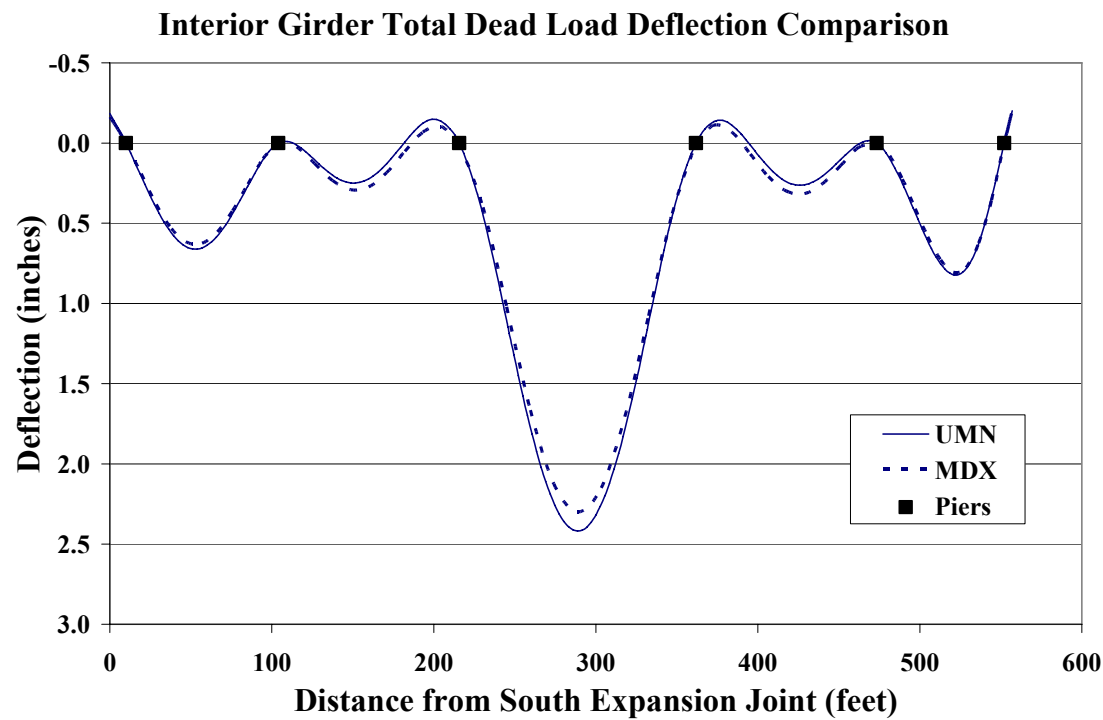


Figure 4-8: Interior Girder C Total Dead Load Deflection Comparison

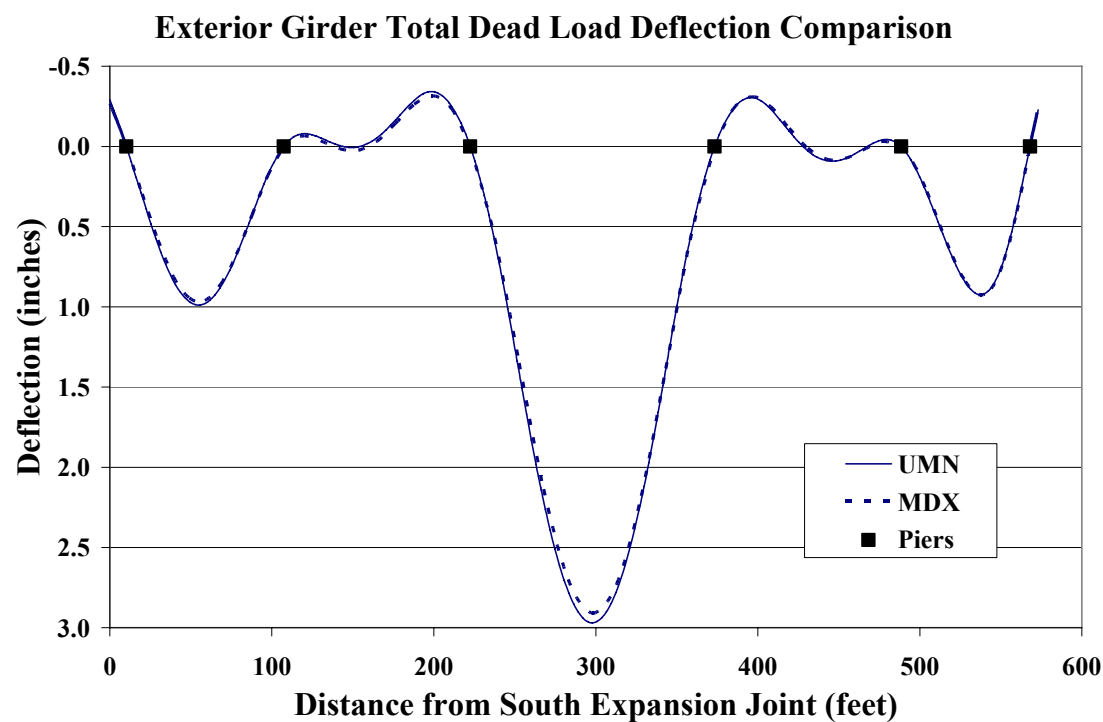


Figure 4-9: Exterior Girder A Total Dead Load Deflection Comparison

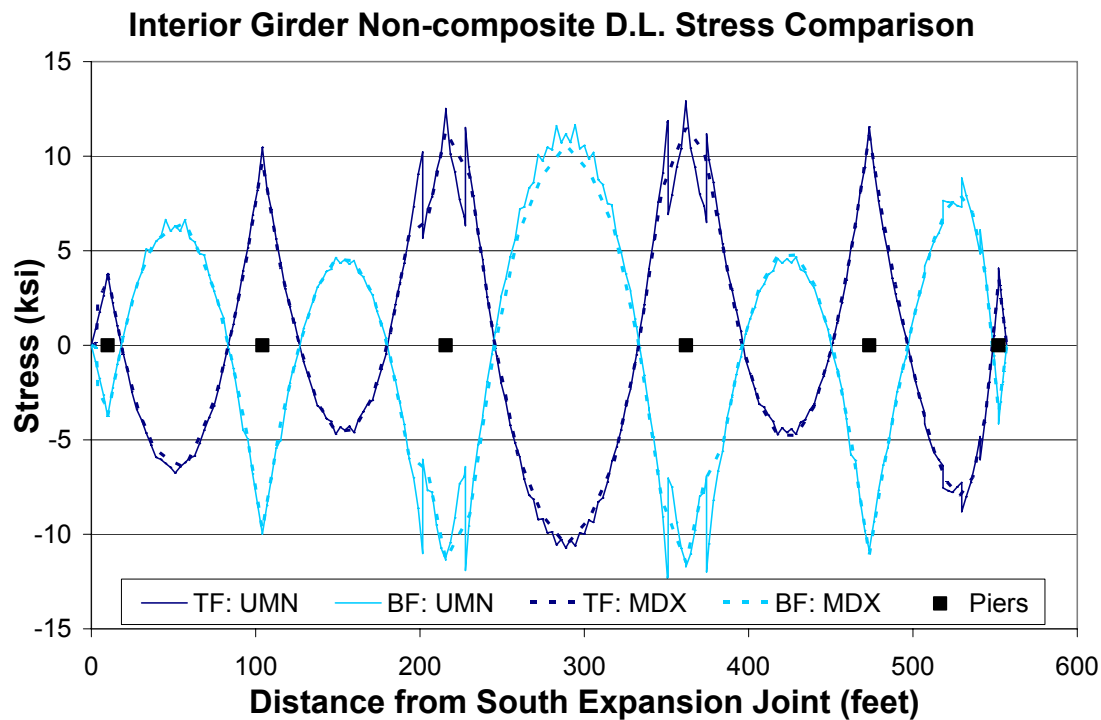


Figure 4-10: Interior Girder C Non-composite Dead Load Stress Comparison

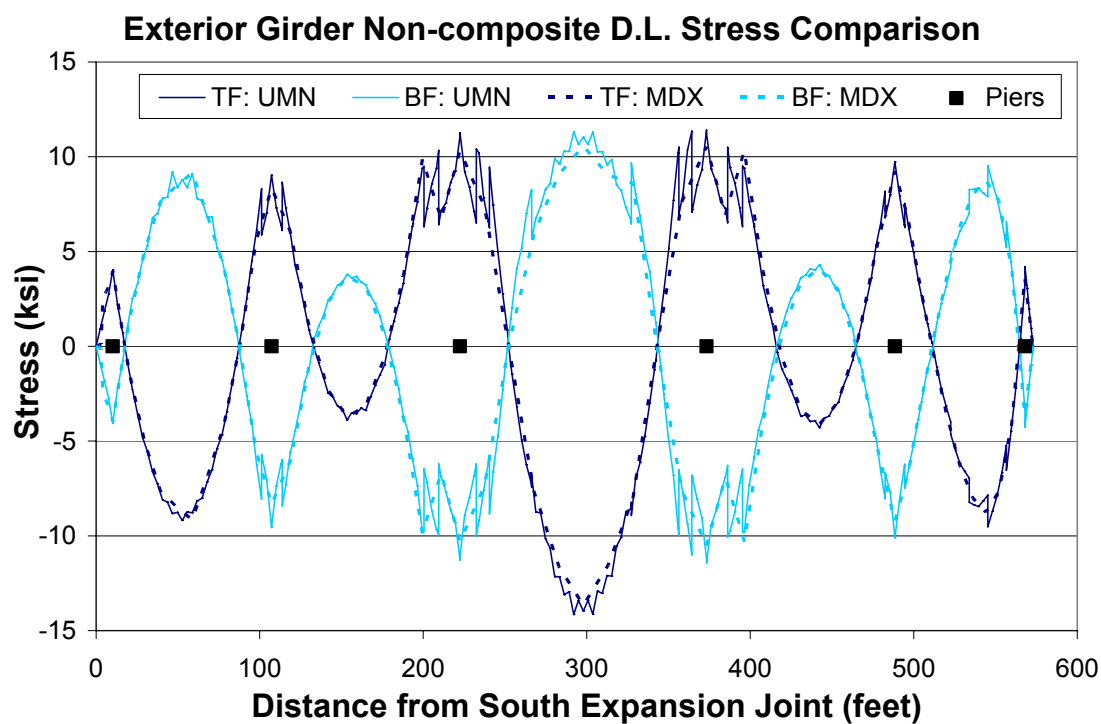


Figure 4-11: Exterior Girder A Non-composite Dead Load Stress Comparison

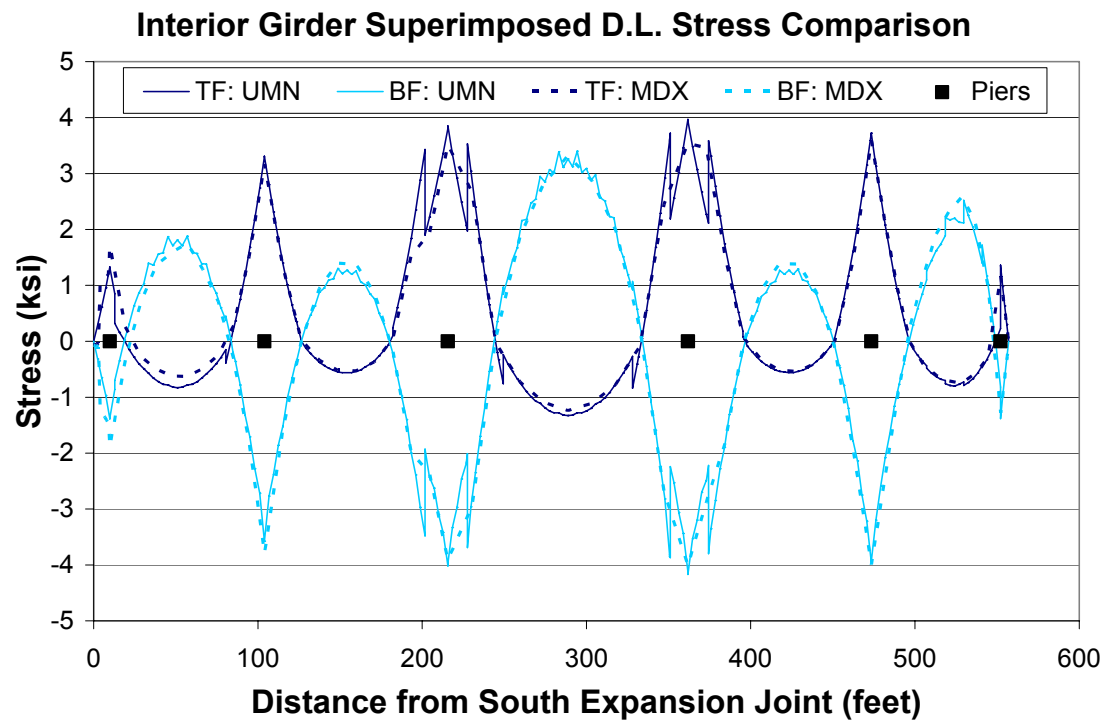


Figure 4-12: Interior Girder C Superimposed Dead Load Stress Comparison

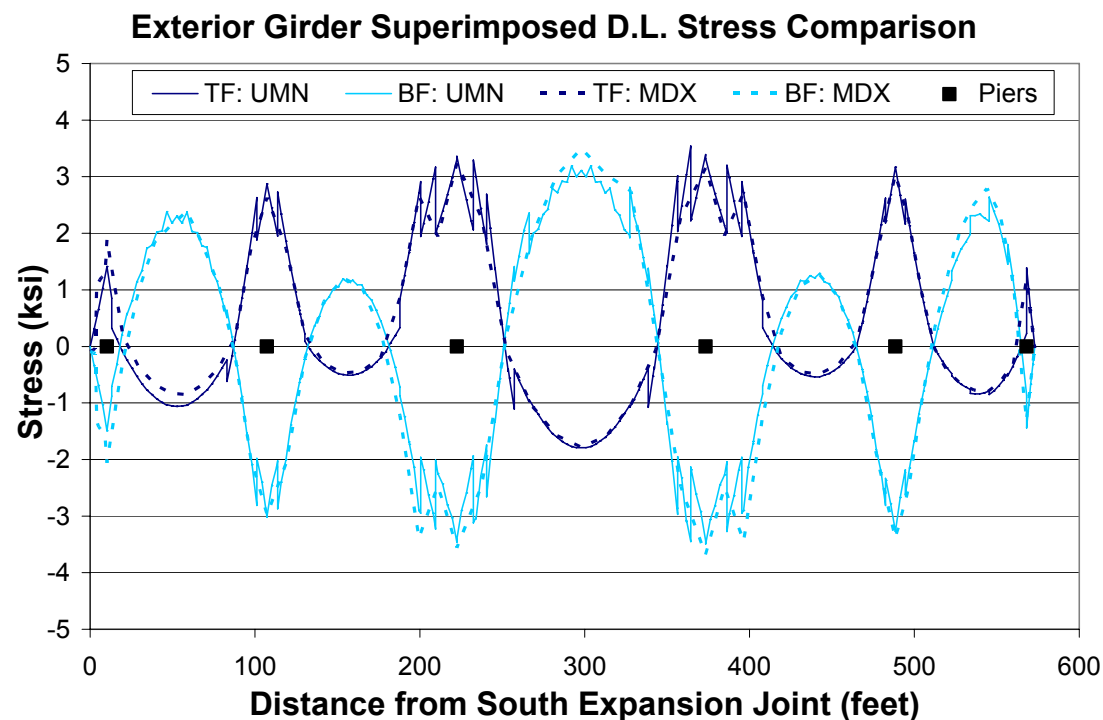


Figure 4-13: Exterior Girder A Superimposed Dead Load Stress Comparison

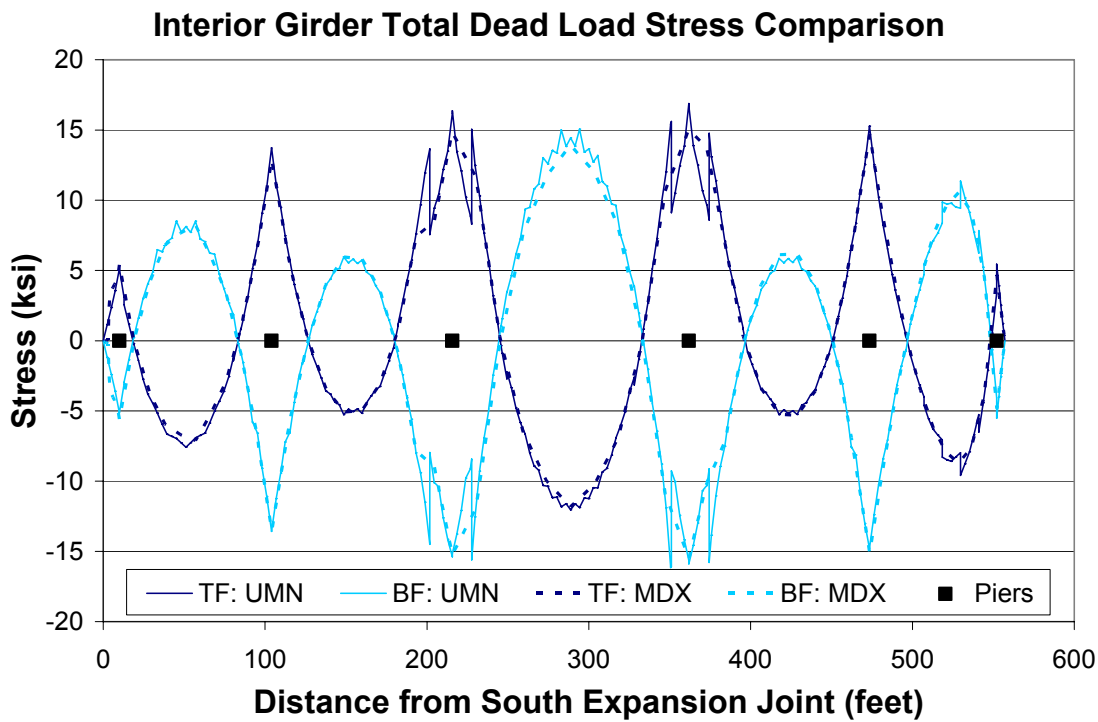


Figure 4-14: Interior Girder C Total Dead Load Stress Comparison

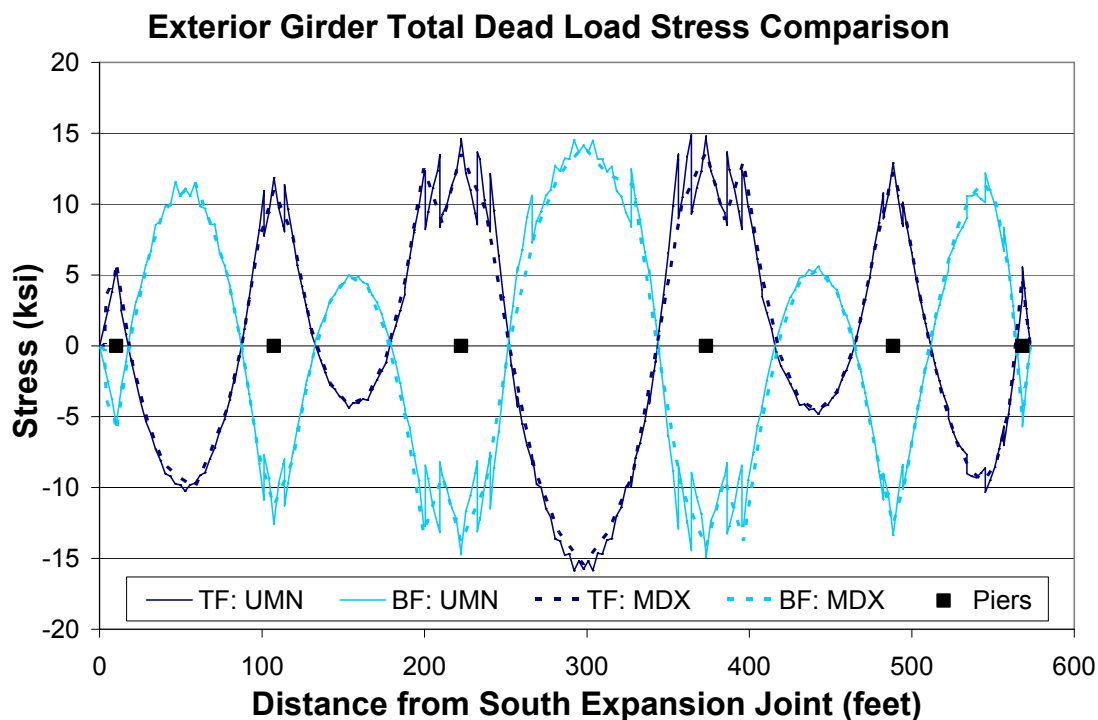


Figure 4-15: Exterior Girder A Total Dead Load Stress Comparison

Chapter 5

Bridge Testing

The main purpose of the load test was to assess the behavior of the two-girder, horizontally curved steel bridge at various load levels and loading configurations. Some of the behavior that was to be documented in the field test included:

- Girder, diaphragm, and lateral bracing strains/stresses
- Vertical and rotational girder displacements
- Actual girder and diaphragm stiffness
- Web gap distortional strains/stresses
- Strains/forces at gusset plate connection
- Unintended composite action in the negative moment region
- Expansion bearing displacements

This chapter describes the instrumentation plan used for recording data on Mn/DOT Bridge No. 69824, the truck test plan that was implemented, and the reduction of raw data. In addition, a brief summary of a post-test inspection of the bridge is provided.

5.1 Instrumentation Plan

To accomplish the goals of the load test, an extensive array of instrumentation was developed to maximize the data collected from the field. Twelve displacement devices and one hundred twenty-eight strain gages were installed on Mn/DOT Bridge No. 69824 in the region just south of Pier 9 to Midspan 8-7 (i.e., between Pier 8 and Pier 7). This region of the bridge was determined to be the most easily accessible for instrumentation while also allowing critical regions of the bridge to be tested.

The rest of this section details the instruments used for testing and their locations on the bridge.

5.1.1 Instruments

Each of the instruments used for the testing of Mn/DOT Bridge No. 69824 are described below. All connections between data loggers and instruments were made using *Belden* 8730 wire, which has two pairs of shielded wire. Moisture resistant *3M Scotchlok* UY splice connectors were used to connect strain gage lead wires to the *Belden* wire.

5.1.1.1 Campbell CR9000 Data logger

Two *Campbell* CR9000 Dataloggers were used to record the measurements made during the field test. Using Ethernet cables and NL105 Ethernet Modules, each data logger was connected to a laptop running PC9000 software (the basic interface provided by *Campbell* for the CR9000s). This setup provided immediate data recording to the laptops, which allowed for real-time monitoring of the measurements. The PC9000 software also offered streamlined setup for data labeling along with automatic conversion of resistance measurements to strains.

5.1.1.2 Strain Measurements

Strain measurements were made using three different types of strain gages, all of which can be seen in Figure 5-1 along with their specification sheets. The most common gage used was the *Vishay Micro-Measurements* weldable strain gage (LWK-06-W250B-350). These gages came mounted on a thin stainless steel carrier that was spot welded to the bridge using a *Vishay Micro-Measurements* Model 700 Portable Strain Gage Welding and Soldering Unit. See Figure 5-2 for a photograph of a gage being installed. One hundred and nine of these gages were installed.

Seven smaller, glueable strain gages were installed at hot spot locations (i.e., web gaps and gusset plate tips) to provide more precise measurements. *Texas Instruments, Inc.* single element foil strain gages (FLA-3-350-11-3LT) were used for this purpose. Four (glueable) *Texas Instruments, Inc.* 45°/90° 3-element rosettes (FRA-3-350-11-3LT) were also installed to obtain plane strain behavior on the exterior girder near Pier 8 and on a gusset plate.

5.1.1.3 Displacement Measurements

String potentiometers, linear voltage differential transducers (LVDTs), tiltmeters, and total stations were used to make the displacement measurements during the test. All are pictured in Figure 5-3 except the total stations.

Four *UniMeasure, Inc.* P510-3 string potentiometers were used to measure vertical girder deflections on Span 9-8. Because the base of the girders was approximately 45 feet above ground on this span, steel fishing line was used to connect the string potentiometers at ground level to mounts glued to the center of the bottom flange for each girder.

Due to close proximity of traffic from TH 35 NB during the test, string potentiometers could not be used for vertical deflections on Span 8-7. Therefore, two *Geodimeter* System 400 total stations were used there to measure vertical deflections. These total stations were set up on the inside of the horizontal curvature approximately 60 feet from the bridge. Prism targets were mounted to the girder bottom flanges to provide accurate sites for measurements.

Applied Geomechanics Model 800 tiltmeters were used on each girder near Pier 9 to measure major axis rotations. Magnets were used to mount the tiltmeters to the girder webs at mid-height.

Expansion bearing movements and slip between the top girder flange and concrete deck were measured using four *Schaevitz Sensors* GCD-121-500 LVDTs. These sensors were mounted to the concrete pier cap using nylon and wooden blocks bonded with epoxy as modeled in Figure 5-4 for expansion bearing movements. To measure slip due to possible non-composite action in the negative moment regions, the LVDTs were mounted in nylon blocks glued to the top flange, while wooden blocks were attached to the concrete slab as shown in Figure 5-5 to provide a reference point for measurement.

5.1.1.4 Instrument Precision

Typical noise levels for each of the instruments during the static load tests were used to determine the accuracy of the measurements for the field test. Strain gage measurements were

determined to be accurate to within $\pm 1.5 \mu\text{strain}$ (0.044 ksi), vertical displacements to within ± 0.05 inches, rotations to within $\pm 0.00025^\circ$ (0.0000044 radians), and slip and bearing movements to within ± 0.0001 inches. Common measured values for strain gages were around 200 μstrain , those for vertical displacements were around 0.75 inches, those for rotations were around 0.043° (0.00075 radians), and those for slip were near 0.003 inches. All of these instruments provided for accurate measurements. The only measurements that were close to the accuracy range, and were therefore questionable, were those for the bearing movements with typical values being around 0.0005 inches.

5.1.2 Instrument Locations

The complete set of drawings depicting all instrument locations is provided in Appendix B. Portions are included here to provide the reader an understanding of where the instruments were installed on the bridge.

In general terms, each instrument is labeled by X-Y-Z, where X refers to the bridge section, Y to the member type, and Z to the location of the instrument on the member. Table 5-1 details each of the symbols used for Y and Z, while Figure 5-6 shows the labels used for the instrumented sections of the bridge, or X. For example, 9B-GA-BI would be located at Section 9B on the exterior girder (A) bottom flange tip on the interior side of horizontal curvature.

The instrumentation has been broken down into three categories: Main Girder Strains, Secondary Location Strains, and Displacements. Each is described below.

5.1.2.1 Main Girder Strains

Strain gages were applied to the girders in the longitudinal direction at ten sections along the length of the testing region as shown in Figure 5-7. All ten of these sections were located at a quarter-point between adjacent diaphragms. This location was chosen to avoid as much as possible any local effects due to the diaphragms and the intermediate stiffeners, which are located halfway between diaphragms. All girder strain gages were of the weldable type unless otherwise noted.

At a minimum, each of the instrumented girder cross sections had two gages, one on the web 3 inches from the top flange and another on the web 3 inches from the bottom flange. Refer to Figure 5-8 for a depiction. These two gages were used to determine major axis flexure behavior in the girders.

Some sections also contained an additional gage on the web midway between the flanges and up to four additional gages placed on the flange tips, positioned 1 inch from the edge. This type of section can be seen in Figure 5-9. The web gage on these sections was used in conjunction with the two flexure gages to better understand the bending strain profile, while the flange tip gages were used to document longitudinal strains due to restraint of warping. It should be noted that Section 8D Girder A exterior tip gages TE and BE were originally planned but could not be installed due to unavoidable close proximity of traffic during gage installation.

On the exterior girder near Pier 8 (Section 9O), three glueable rosettes were attached to the web in place of the three major axis flexure gages. In addition to the flexure behavior, these rosettes provided shear strains and principal strain directions at the pier.

5.1.2.2 Secondary Location Strains

All the remaining strain gages (i.e., those not included in the Main Girder Strains) fall into this category. This includes gages on the diaphragms, lateral wind bracing, web gaps, and gusset plate connections at the sections shown in Figure 5-10.

Weldable strain gages were applied to two diaphragms in the configuration shown in Figure 5-11. These gages were used in the same manner as the two flexure gages on the girders to determine major axis flexure behavior along the length of the diaphragms.

The lateral wind bracing gages were attached as shown in Figure 5-12. All of the instrumented lateral wind bracing were equipped with a gage at the neutral axis, approximately $\frac{1}{2}$ inch above the flange. This was done so that bending strains (which were anticipated to be small) would not interfere with the desired axial strain. One lateral bracing was also instrumented with four additional gages so that flexural effects could be determined and used to justify the use of the neutral axis location for the other lateral wind bracing.

Because the diaphragm connection stiffeners were not attached to the tension flange, five glueable strain gages were attached at various web gap locations to quantify distortional out-of-plane strains. These gages were all attached vertically on the backside of the connection stiffeners at approximately the top of the web gap. Refer to Figure 5-13.

The remaining strain gages were attached to the gusset plate region on the exterior girder at Section 9F. Two glueable gages were placed on the girder web as close to the weld toe of the gusset plate as possible to pick up any stress concentrations due to the gusset plate detail. See Figure 5-14 for a diagram. One glueable rosette was also attached to the gusset plate as shown in Figure 5-15 to measure load transfer into the gusset plate attachment.

5.1.2.3 Displacements

The location of displacement instrumentation along the length of the bridge is detailed in Figure 5-16. Vertical deflections were measured at the midspan of Span 9-8 and the quarter-point between midspan and Pier 8 using string potentiometers. Total stations were used to measure vertical deflections near midspan of Span 8-7. Tiltmeters near Pier 9 provided flexure rotations for each of the girders, while LVDTs mounted to the pier cap as previously shown in Figure 5-4 supplied axial displacements of the expansion bearings there. LVDTs were also used to provide slip at the steel girder-to-concrete deck interface as shown in Figure 5-5 on the exterior girder near Pier 9 and Pier 8.

5.2 Truck Test Plan

The truck test plan was developed to provide a wide variety of load levels and truck configurations. Low load levels were designed to mimic typical loading seen on the bridge, while

high load levels were designed to load the bridge to a Mn/DOT specified total stress (i.e., dead load + live load) limit of 75% of yield stress, or 27 ksi for this bridge. A preliminary finite element model of the bridge was made using the UMN Program to estimate the dead load and predict the live load for each test configuration. To ensure that the limit was not surpassed during testing, strain levels were monitored as the load was incremented from low to high levels. All test load levels and configurations originally planned were implemented.

This section describes the trucks used for testing along with the various truck loading configurations that were implemented.

5.2.1 Test Trucks

Eight quad-axle dump trucks were used for the testing of the bridge. Figure 5-17 shows the average dimensions and weights for the trucks, while Appendix C provides the data for each of the individual trucks. As Figure 5-17 shows, the average gross vehicle weight (GVW) was approximately 72,000 lbs and the front axle to rear axle distance was approximately 21 ½ feet.

It is important to note that the trucks used for this test are similar to the HS20 trucks (without load factors applied) used for Load Factor Rating and Load and Resistance Factor Rating as described in Chapter 2. The average test truck weight of 72,000 lbs is identical to that of the HS20 truck, and the average test truck front-to-rear axle spacing of 21 ½ feet is smaller than the 28 foot minimum length for the HS20 truck. Thus, the trucks used for the bridge test are actually more demanding on the bridge than the HS20 trucks. Both rating procedures also use lane loads of 640 lbs per linear foot per highway lane. For Span 8-7 of Bridge 69824, which is the longest span on the bridge, this lane load amounts to approximately 95,000 lbs of load distributed along the length of each lane. The LRFR combination of HS20 truck and lane loads are more demanding than the LFR loads, and require both the HS20 truck and the lane load on each designated highway lane. Two test trucks end-to-end at midspan provide slightly less load than the LRFR loads, but provide similar deflections and moments as the LRFR loading since the test truck loading is more concentrated near the midspan. Therefore, the bridge tests described below with two trucks per lane are very good indicators of the behavior of the bridge that can be anticipated for typical rating level loads.

5.2.2 Test Configurations

The original testing sequence was designed to minimize the total time for the test while still providing enough data to achieve the goals. Appendix C provides descriptions and truck locations for each test in the original testing sequence that the tests occurred. Also included is a table reporting the time for each test and zero reading.

However, to present the test data and future analytical comparisons in a more convenient manner, the load tests have been broken down into Static Tests and Dynamic Tests. They have also been regrouped based on the objective of the loading configuration. Throughout this document, the following prefixes are used to distinguish between the various test groupings:

- T -- refers to the original testing sequence
- S -- refers to the static tests

- D -- refers to the dynamic tests

For example, T1, S1, and D1 are the first tests in the original testing sequence, the static tests, and the dynamic tests, respectively. Table 5-2 provides the cross-references between the test groups.

5.2.2.1 Static Tests

There were forty-three static tests completed as part of the testing of Mn/DOT Bridge No. 69824. Table 5-3 briefly describes each of the tests, while Figure 5-18 through Figure 5-21 provide diagrams of the actual truck positions for each test. For the configuration diagrams in these figures:

- Trucks face toward the left (i.e., from Pier 7 toward Pier 9)
- All L_i distances are arcs measured along the interior edge of the roadway
- All R_i distances are measured radially outward from the interior edge of the roadway
- The interior edge of the roadway for this bridge coincides with the interior curb edge
- The numbers in parenthesis refer to the original testing sequence as in Appendix C

As Table 5-3 shows, the static tests were subdivided into nine sets based on testing objectives. The first two sets provided light and heavy load influence lines for one and four trucks, respectively, positioned at locations along the bridge testing region. The third set focused on positive moment stresses on Span 9-8, while the fourth set did the same for Span 8-7. Negative moment stresses at Pier 8 were the objective of the fifth set. The sixth and seventh sets dealt with load transversely positioned on Span 9-8 above the exterior girder and interior girder, respectively. The last two sets provided twisting cases where the loads on Span 9-8 and Span 8-7 were on opposing girders.

5.2.2.2 Dynamic Tests

Thirteen dynamic tests utilizing one truck per test were also carried out on the bridge. Table 5-4 describes each of the tests, while Figure 5-22 provides diagrams for them. The same comments apply to these diagrams as those stated for the static configuration diagrams mentioned in the last section.

The dynamic tests were subdivided into three sets: constant velocity, constant velocity over 2x4, and constant velocity then braking. The constant velocity dynamic tests consisted of an individual truck driving along the centerline of the bridge at a constant velocity. The constant velocity over 2x4 dynamic tests consisted of a truck driving over a 2x4 placed at midspan between Pier 9 and Pier 8. The constant velocity then braking dynamic tests had a truck quickly apply its brakes as it passed over Pier 8 and onto Span 9-8. All of the dynamic tests were done at a variety of vehicle speeds.

5.3 Reduction of Data

This section provides the manner in which data was recorded and processed to the final values that are used for analysis in later chapters.

5.3.1 Data Recording Process

The testing officially began at 8:37 p.m. on July 14th, 2004, and went until 4:09 a.m. on July 15th. Due to the 7½ hour testing period, it was impractical to record all instruments for the entire test period. Therefore, for static tests, trucks were moved into position at low speeds one at a time until the test configuration was complete, and then data was recorded for approximately 30 seconds using a 5 Hz sampling frequency while the trucks remained stationary. At the higher load levels, some additional data was recorded while trucks were moving into position to ensure that maximum stress limits were not being exceeded. Average values were then calculated for each gage per test. For each of the dynamic tests, data was recorded at a 50 Hz sampling frequency while the truck traveled along the bridge.

Prior to the first test, while no vehicles were on the bridge, all strain gages were set to an initial value of zero strain. Then, four times during the test, readings were taken with no load on the bridge to determine if the gages returned to the zero strain condition. These readings are referred to as Zero 1, Zero 2, Zero 3, and Zero 4 and occurred at 12:03 a.m., 12:53 a.m., 2:43 a.m., and 4:09 a.m., respectively. Following Zero 1, significant levels of strain remained in a number of strain gages. To prevent these strain accumulations from perpetuating throughout the remaining test data, the strain gages were all reset to a value of zero strain. Large strain accumulations were not noticed for the remaining zero readings, and therefore resetting to zero values was not necessary again. However, to provide a clean start for the dynamic tests which followed the Zero 3 reading, the strain gages were again reset to zero strain.

5.3.2 Recording Issues and Erratic Gages

This section documents issues that arose with the data recording. First, a handful of the tests were not recorded for one or both of the *Campbell* CR9000 units. This was especially a problem for the dynamic tests. After testing, it was determined that the transfer of data from the CR9000 units to the laptop was likely not fast enough to keep up with the pace for testing. Practice data recording runs did not reveal this issue, because they were limited in scope and duration. In all, portions of one zero reading (Zero 1), one static test reading (T56) and seven dynamic test readings (T42, T45, T46, T47, T50, T52, and T54) were not recorded. Table 5-5 and Table 5-6 provide the list of gages that were not recorded for each test.

The second issue with the data recording was that six of the one hundred twenty-eight strain gages provided either no data or erratic data. Gages 10Z-GA-BC, 9B-GA-TI, 9B-GA-TC, and 9J-GA-TI all gave infinite resistance throughout the test night, meaning that they had an open-loop circuit (i.e., somewhere the wire was disconnected). Gages 8D-GA-TI and 8A-D-BI had large strain jumps at different points during the test that were not supported by other nearby gages. It is hypothesized that these two gages may not have been properly welded to their respective members. These six gages are marked in the drawings in Appendix B with a ~~double strikethrough~~ font.

One last data recording issue was that the string potentiometer at 9I-GC-DF did not provide enough range for the vertical deflection experienced by the girder. For tests T10, T18, T19, T25, T26, and T56, this string potentiometer achieved its maximum measurement at approximately ½

inch of deflection, although the actual girder deflection was larger. These six unreliable displacement values are marked with an X on all plots containing data for 9I-GC-DF.

5.3.3 Removal of Thermal Strains

Section 5.3.1 mentioned that strain accumulations were recorded in Zero 1, but did not occur in any of the remaining zero readings. Figure 5-23 shows all strain values that were recorded for each of the four zero readings, and reveals the relatively large magnitudes for Zero 1. The gages have been grouped based on their location on the bridge, such as interior girder, exterior girder, diaphragm, lateral bracing, and web gap and gusset plate. Also, in the key for this plot each of the zero readings has an additional label, such as T19+ for Zero 1. These additional labels are included to show when the readings occurred relative to the tests in the original testing sequence. The + in T19+, T27+, T41+, and T56+ means that the zero reading occurred after T19, T27, T41, and T56, respectively.

Of particular interest in Figure 5-23 is that all of the highest magnitudes are from strain gages located on the exterior girder. Plots of the measured strain for locations on the exterior girder reveal a nonlinear change in strain with the majority of change occurring between the beginning of the test at 8:37 p.m. and approximately 10:00 p.m. (around T13). The change is most obvious in plots of top flange gages since they are located near the neutral axis and generally have low strains due to the applied loading. Figure 5-24 shows the strain accumulation for top flange gage 9N-GA-TC, as an example. Although the load test magnitudes are similar for tests before and after Zero 1 (12:03 a.m.), the strain magnitudes are clearly different.

Initial concerns were that yielding had occurred in the bridge and was the cause of the observed nonlinear strain accumulation. However, this was ruled out for a number of reasons. First, top and bottom gages at a given cross-section revealed similar profiles and magnitudes, which would not be the case if yielding occurred. Second, the exterior girder showed larger magnitudes than the interior girder even though their total stress (dead + live) levels were similar. Third and most important, the change in strain was observed predominately during low level load tests.

After yielding was ruled out as the source of the change in strain over time, it was determined that cooling of the exterior girder due to the setting of the sun around 9 p.m. resulted in the observed strain accumulations. Thermal straining explains why the profiles were similar for top and bottom flange gages. It also fits with the observed time period of the change in strain. Since the sun was only shining on the exterior girder for the latter part of the afternoon and evening, the change in temperature was larger for it than the interior girder, and therefore explains why the observed strain accumulations observed were much greater in the exterior girder.

Since the focus of this research project was on truck loading and not thermal effects, it was necessary to quantify the thermal strains in the data prior to Zero 1 (12:03 a.m.), so that they could be removed from the measured data for tests T1 through T19. To accomplish this task, the following procedure was followed:

1. Similar live load cases (same pattern and location, but different trucks) were identified before and after the resetting of the strain gage values to zero following the Zero 1

reading at 12:03 p.m. Test T7 was duplicated by T55, T10 by T25 and T56, T13 by T20, and T17 by T20.

2. Strains from post-Zero 1 duplicate cases (i.e., T20, T25, T55, T56) were subtracted from the pre-Zero 1 recordings (i.e., T7, T10, T13, T17), and the resultants were identified as the thermal strains for each case. For T10, which had two post-Zero 1 duplicate cases, the available values from the two cases (recall from Section 5.3.1 that some of the gage data for T56 was missing) were averaged.
3. Using the above four data points, plus the initial zero point at 8:37 p.m. and the available Zero 1 values at 12:03 p.m. (recall from Section 5.3.1 that some of the gage data for Zero 1 was missing), thermal strain curves as a function of time were defined using linear interpolation between these data points for each gage. Where values did not exist for Zero 1, the thermal strain magnitude from the previous data point was used (thus providing a constant thermal strain between T17 and Zero 1).
4. Gages (except on lateral bracing and diaphragms) that had any of the thermal strains as defined in #3 with a magnitude greater than $\pm 15 \mu\text{strain}$ were modified by subtracting the thermal strain curves (thermal strain as a function of time as created from #3 above) from the original test data (strain as a function of time) for tests T1 through T19. Lateral bracing and diaphragm measurements were not modified for thermal strains because the thermal curves created by #3 did not reveal consistent patterns like those for gages on the girders.

Figure 5-25 shows the thermal strains, as determined using the above procedure, with the measured strains for the top (TC) and bottom (BC) flanges of Girder A at Section 9N. As can be seen, the thermal strains are a significant percentage of the measured strains, especially for the top flange. The full set of plots for all measured values for the static test cases is provided in Appendix D. Where thermal strains have been determined to play a significant role in the measured strain as defined in #4 above, they are plotted along with the measured values in Appendix D.

It should be noted that the thermal strain values defined in the above procedure are a combination of two effects. The first effect is that the thermal coefficients of expansion for the strain gages and the steel girders are not identical. Therefore, a change in temperature will cause a strain to develop in the gage. The second effect is that mechanical bending and axial strains develop in the bridge due to unintended bearing restraint and the indeterminate nature of the curved bridge system as the bridge tries to expand or contract due to thermal changes. Since these thermal behaviors are beyond the scope of this project, no further attempt was made to investigate them.

5.3.4 Conversion from Strains and Voltages to Stresses and Displacements

Once the strain data was cleared of unwanted thermal strains, all strains were converted to stresses. The single-element gage strain readings were converted to stress by multiplying by the modulus of elasticity of steel (29,000 ksi). Hooke's law was used to convert the strains from the three-element rosettes into stresses.

To convert the voltage readings for the displacement instruments (except the total stations) into actual displacements, offset values had to be determined for each gage. For the raw data plots in

Appendix D this was done by using the average of the four zero readings for each displacement instrument. These offset values were subtracted from the readings per instrument for each test. In this manner, the progression of each displacement instrument can be traced throughout the testing period. However, this method proved to be somewhat inaccurate due to slight variations in the zero readings throughout the nearly eight hour test period. To provide more accurate values for comparisons with computational results, the displacements presented for the final experimental data in Appendix F are calculated by using offset values equal to the closest zero reading value following each test. For example, T9 uses the offset values from Zero 1 and T35 uses values from Zero 3. In this way, voltage changes due to other factors, such as temperature changes and modifications to the software running the data loggers, do not propagate throughout the entire set of displacement data and corrupt comparisons with computational data. Once the offset values were removed from the readings, conversion factors provided by the manufacturer of each displacement instrument were used to convert the voltage readings to displacements. Total station measurements were converted to displacements using trigonometry.

Appendix F provides tables and plots of the final stresses and displacements for all static tests and compares them to analytical values as determined in Chapter 7.

5.4 Post-Test Inspection Summary

Immediately following the load test, key details on the steel girders located within the test region were inspected to determine if any significant damage had occurred. Two key findings are worth mention. First, in both negative moment regions of Span 9-8, freshly exposed paint at the bearing surface of the diaphragm connection stiffeners and the top flange of the girders indicated recent out-of-plane bending of the girder webs in these regions. Magnetic particle testing at the diaphragm just south of Pier 8 on the Interior Girder C located a small crack approximately 0.25 inches in length that likely occurred during the test. See Figure 5-26 for a photograph of the crack location. The second significant finding from the post-test inspection was that four lateral wind bracing shelf plate connections in the positive moment region of Span 9-8 showed signs of separation between the top of the backer bar and the bottom of the shelf plate. The separation was indicated by freshly exposed paint along the interface. No cracks were found in any of these shelf plate locations. Neither of these findings was determined to be of significance for the function or rating of the bridge.

X: denotes the bridge section (9B, 9J, 8C, etc.)

Y: denotes the bridge member as described below:

GA	Girder A (exterior)
GC	Girder C (interior)
LBU	Lateral Bracing at 45° angle counter-clockwise from centerline of roadway
LBD	Lateral Bracing at 45° angle clockwise from centerline of roadway
D	Diaphragm
GPA	Gusset Plate region on girder A
GPC	Gusset Plate region on girder C

Z: denotes the location of instrument on the bridge member as described below:

T	Top of the member or section
B	Bottom of the member or section
W	Mid-depth of the web of the main girder
C	Center of flange on web
CN	Centroid of lateral bracing section
E	Exterior of the member or section in reference to the center of radius of the bridge
QE	Quarter point of the diaphragm closest to the exterior girder
M	Mid-point of the diaphragm
QI	Quarter point of the diaphragm closest to the interior girder
I	Interior of the member or section in reference to the center of radius if the bridge
V	Vertical strain gage in rosette
H	Horizontal strain gage in rosette
TR	Strain gage in rosette orientated in the transverse direction of the main girder
LO	Strain gage in rosette orientated in the longitudinal direction of the main girder
45	45° diagonal (clockwise from horizontal gage in rosette) strain gage in rosette
W9	Main girder web location nearest Pier 9 at the gusset plate weld toe
W8	Main girder web location nearest Pier 8 at the gusset plate weld toe
WG	Web gap location on the main girder at the bottom of the stiffener
DF	Vertical deflection
BM	Bearing movement
SM	Slip movement
RM	Rotation movement
TS	Total Station vertical deflection measurement

Table 5-1: Instrumentation Labeling Scheme

Original Testing Sequence				Static Tests				Dynamic Tests	
T1	S1	T29	S30	S1	T1	S23	T13	D1	T42
T2	S2	T30	S36	S2	T2	S24	T17	D2	T43
T3	S3	T31	S31	S3	T3	S25	T11	D3	T44
T4	S4	T32	S32	S4	T4	S26	T14	D4	T45
T5	S5	T33	S33	S5	T5	S27	T15	D5	T46
T6	S6	T34	S40	S6	T6	S28	T16	D6	T50
T7	S20	T35	S34	S7	T20	S29	T28	D7	T47
T8	S35	T36	S41	S8	T21	S30	T29	D8	T48
T9	S15	T37	S37	S9	T22	S31	T31	D9	T49
T10	S16	T38	S38	S10	T23	S32	T32	D10	T54
T11	S25	T39	S39	S11	T24	S33	T33	D11	T51
T12	S22	T40	S42	S12	T25	S34	T35	D12	T52
T13	S23	T41	S43	S13	T26	S35	T8	D13	T53
T14	S26	T42	D1	S14	T27	S36	T30		
T15	S27	T43	D2	S15	T9	S37	T37		
T16	S28	T44	D3	S16	T10	S38	T38		
T17	S24	T45	D4	S17	T56	S39	T39		
T18	S18	T46	D5	S18	T18	S40	T34		
T19	S19	T47	D7	S19	T19	S41	T36		
T20	S7	T48	D8	S20	T7	S42	T40		
T21	S8	T49	D9	S21	T55	S43	T41		
T22	S9	T50	D6	S22	T12				
T23	S10	T51	D11						
T24	S11	T52	D12						
T25	S12	T53	D13						
T26	S13	T54	D10						
T27	S14	T55	S21						
T28	S29	T56	S17						

Table 5-2: Cross-References between Test Groupings

<u>Test No</u>	<u>Objective</u>	<u>Truck Locations</u>
S1 - S6	Influence line (light load)	1 static truck at 6 different locations along the bridge going from midspan 8-7 to pier 9
S7 - S14	Influence line (heavy load)	Group of 4 static trucks at 8 different locations along the bridge going from midspan 8-7 to pier 9
S15	Maximum stresses at midspan 9-8	2 trucks at midspan 9-8
S16		4 trucks at midspan 9-8 (Pre-test)
S17		4 trucks at midspan 9-8 (Post-test)
S18		5 trucks at midspan 9-8
S19		6 trucks at midspan 9-8
S20		2 trucks at midspan 8-7 (Pre-test)
S21	Maximum stresses at midspan 8-7	2 trucks at midspan 8-7 (Post-test)
S22		3 trucks at midspan 8-7
S23		4 trucks at midspan 8-7
S24		4 trucks at midspan 8-7 (Redo of Test S23)
S25		2 trucks at midspan 9-8 and 2 trucks at midspan 8-7
S26	Maximum stresses at pier 8	4 trucks at midspan 9-8 and 2 trucks at midspan 8-7
S27		4 trucks at midspan 9-8 and 3 trucks at midspan 8-7
S28		4 trucks at midspan 9-8 and 4 trucks at midspan 8-7
S29	Maximum load on exterior lane 9-8	1 truck at midspan 9-8 along exterior lane
S30		2 trucks at midspan 9-8 along exterior lane
S31		3 trucks at midspan 9-8 along exterior lane
S32	Maximum load on interior lane 9-8	1 truck at midspan 9-8 along interior lane
S33		2 trucks at midspan 9-8 along interior lane
S34		3 trucks at midspan 9-8 along interior lane
S35	Maximum twist due to loads on exterior 9-8 and interior 8-7	1 truck at midspan 9-8 (Ext) and 1 truck at midspan of 8-7 (Int)
S36		2 trucks at midspan 9-8 (Ext) and 1 truck at midspan 8-7 (Int)
S37		2 trucks at midspan 9-8 (Ext) and 2 trucks at midspan 8-7 (Int)
S38		3 trucks at midspan 9-8 (Ext) and 2 trucks at midspan 8-7 (Int)
S39		3 trucks at midspan 9-8 (Ext) and 3 trucks at midspan 8-7 (Int)
S40	Maximum twist due to loads on interior 9-8 and exterior 8-7	2 trucks at midspan 9-8 (Int) and 1 truck at midspan 8-7 (Ext)
S41		2 trucks at midspan 9-8 (Int) and 2 trucks at midspan 8-7 (Ext)
S42		3 trucks at midspan 9-8 (Int) and 2 trucks at midspan 8-7 (Ext)
S43		3 trucks at midspan 9-8 (Int) and 3 trucks at midspan 8-7 (Ext)

Table 5-3: Static Tests

<u>Test No</u>	<u>Objective</u>	<u>Truck Locations</u>
D1	Constant Velocity	1 truck driving across bridge at 10 mph
D2		1 truck driving across bridge at 20 mph
D3		1 truck driving across bridge at 35 mph
D4		1 truck driving across bridge at 35 mph
D5	Constant Velocity over 2x4	1 truck driving across bridge at 10 mph with 2x4 on midspan 9-8
D6		1 truck driving across bridge at 10 mph with 2x4 on midspan 9-8
D7		1 truck driving across bridge at 20 mph with 2x4 on midspan 9-8
D8		1 truck driving across bridge at 24 mph with 2x4 on midspan 9-8
D9		1 truck driving across bridge at 25 mph with 2x4 on midspan 9-8
D10		1 truck driving across bridge at 35 mph with 2x4 on midspan 9-8
D11	Constant Velocity then Braking	1 truck driving at 10 mph, then applying brakes at midspan 9-8
D12		1 truck driving at 20 mph, then applying brakes at midspan 9-8
D13		1 truck driving at 35 mph, then applying brakes at midspan 9-8

Table 5-4: Dynamic Tests

Strain Gages Not Recorded for Zero 1, T42, T45, T46, T47, and T54					
<u>Exterior Girder</u>		<u>Interior Girder</u>		<u>Diaphragm</u>	<u>Lateral Bracing</u>
10Z-GA-TC		10Z-GC-TC		9F-D-TI	9E-LBU-CN
10Z-GA-BC		10Z-GC-BC		9F-D-BI	9E-LBU-BC
9B-GA-TI		9B-GC-TI		9F-D-TQI	9E-LBU-BE
9B-GA-TC		9B-GC-TC		9F-D-BQI	9E-LBU-BI
9B-GA-TE		9B-GC-TE		9F-D-TM	9E-LBU-TC
9B-GA-W		9B-GC-W		9F-D-BM	9E-LBD-CN
9B-GA-BI		9B-GC-BI		9F-D-TQE	9G-LBU-CN
9B-GA-BC		9B-GC-BC		9F-D-BQE	9G-LBD-CN
9B-GA-BE		9B-GC-BE		9F-D-TE	9K-LBD-CN
9C-GA-TC		9C-GC-TC		9F-D-BE	
9C-GA-BC		9C-GC-BC			<u>Gusset Plate</u>
9H-GA-TC		9H-GC-TC			9F-GPA-LO
9H-GA-BC		9H-GC-BC			9F-GPA-TR
9J-GA-TI		9J-GC-TI			9F-GPA-45
9J-GA-TC		9J-GC-TC			9F-GPA-W9
9J-GA-TE		9J-GC-TE			9F-GPA-W8
9J-GA-W		9J-GC-W			
9J-GA-BI		9J-GC-BI			
9J-GA-BC		9J-GC-BC			
9J-GA-BE		9J-GC-BE			

Table 5-5: Strain Gages Not Recorded for Zero1, T42, T45, T46, T47, and T54

Strain Gages Not Recorded for T45, T50, T52, T54, and T56					
<u>Exterior Girder</u>		<u>Interior Girder</u>		<u>Diaphragm</u>	
9L-GA-TC	9O-GA-BI	9L-GC-TC		8A-D-TI	
9L-GA-BC	9O-GA-BCH	9L-GC-BC		8A-D-BI	
9N-GA-TC	9O-GA-BC45	9N-GC-TC		8A-D-TQI	
9N-GA-BC	9O-GA-BCV	9N-GC-BC		8A-D-BQI	
9O-GA-TI	9O-GA-BE	9O-GC-TI		8A-D-TM	
9O-GA-TCH	8C-GA-TC	9O-GC-TC		8A-D-BM	
9O-GA-TC45	8C-GA-BC	9O-GC-TE		8A-D-TQE	
9O-GA-TCV	8D-GA-TI	9O-GC-W		8A-D-BQE	
9O-GA-TE	8D-GA-TC	9O-GC-BI		8A-D-TE	
9O-GA-WH	8D-GA-W	9O-GC-BC		8A-D-BE	
9O-GA-W45	8D-GA-BI	9O-GC-BE			<u>Web Gap</u>
9O-GA-WV	8D-GA-BC	8C-GC-TC			9I-GPC-WG
		8C-GC-BC			8E-GPC-WG
<u>Lateral Bracing</u>		8D-GC-TI			9I-GPA-WG
9K-LBU-CN		8D-GC-TC			
9O-LBD-CN		8D-GC-TE			
8B-LBU-CN		8D-GC-W			
8D-LBU-CN		8D-GC-BI			
8F-LBD-CN		8D-GC-BC			
		8D-GC-BE			

Table 5-6: Strain Gages Not Recorded for T45, T50, T52, T54, and T56

Strain Gages Modified for Thermal Strain Effects for T1-T19				
<u>Exterior Girder</u>		<u>Interior Girder</u>		<u>Web Gap</u>
10Z-GA-TC	9O-GA-TCH	9B-GC-TI		9I-GPC-WG
9B-GA-W	9O-GA-TC45	9B-GC-TE		8E-GPC-WG
9B-GA-BC	9O-GA-TCV	9B-GC-BE		9I-GPA-WG
9B-GA-BE	9O-GA-W45	9J-GC-BI		
9C-GA-BC	9O-GA-WV	9J-GC-BC		
9H-GA-TC	9O-GA-BCH	9J-GC-BE		
9H-GA-BC	9O-GA-BC45	9N-GC-TC		
9J-GA-TC	9O-GA-BCV	9N-GC-BC		
9J-GA-W	9O-GA-BE	9O-GC-W		
9J-GA-BI	8C-GA-TC	8C-GC-BC		
9J-GA-BC	8C-GA-BC	8D-GC-TI		
9J-GA-BE	8D-GA-TI	8D-GC-TE		
9L-GA-TC	8D-GA-TC	8D-GC-BI		
9L-GA-BC	8D-GA-W			
9N-GA-TC	8D-GA-BI			
9N-GA-BC	8D-GA-BC			

Table 5-7: Strain Gages Modified for Thermal Strain Effects for T1 through T19

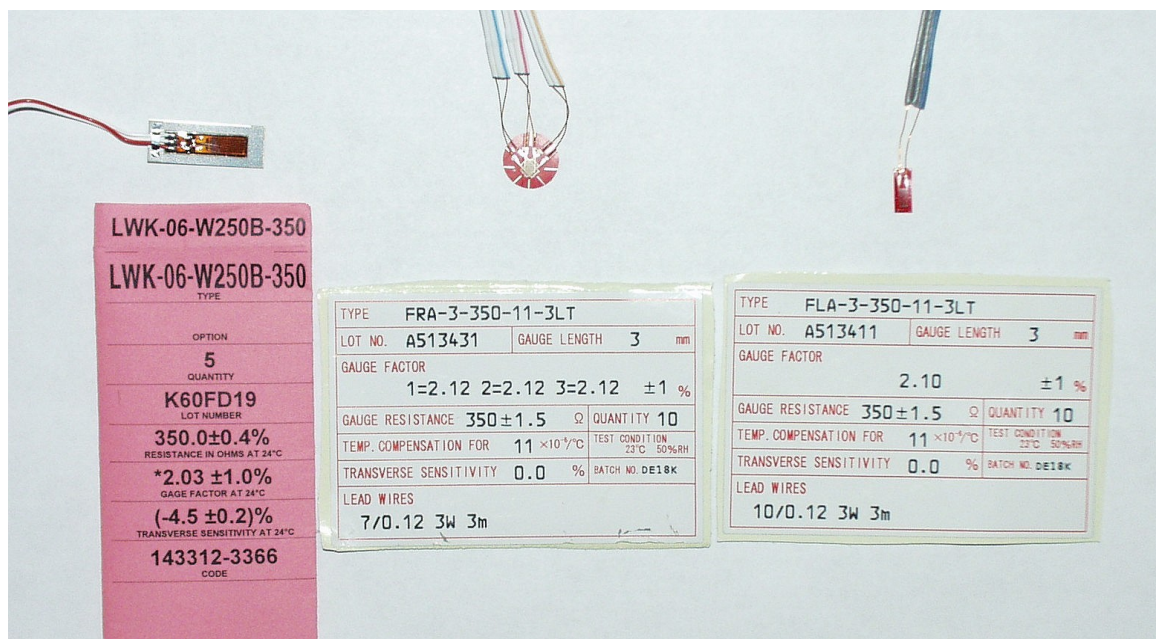


Figure 5-1: Types of Strain Gages used for Test Measurements



Figure 5-2: Weldable Strain Gage being Installed

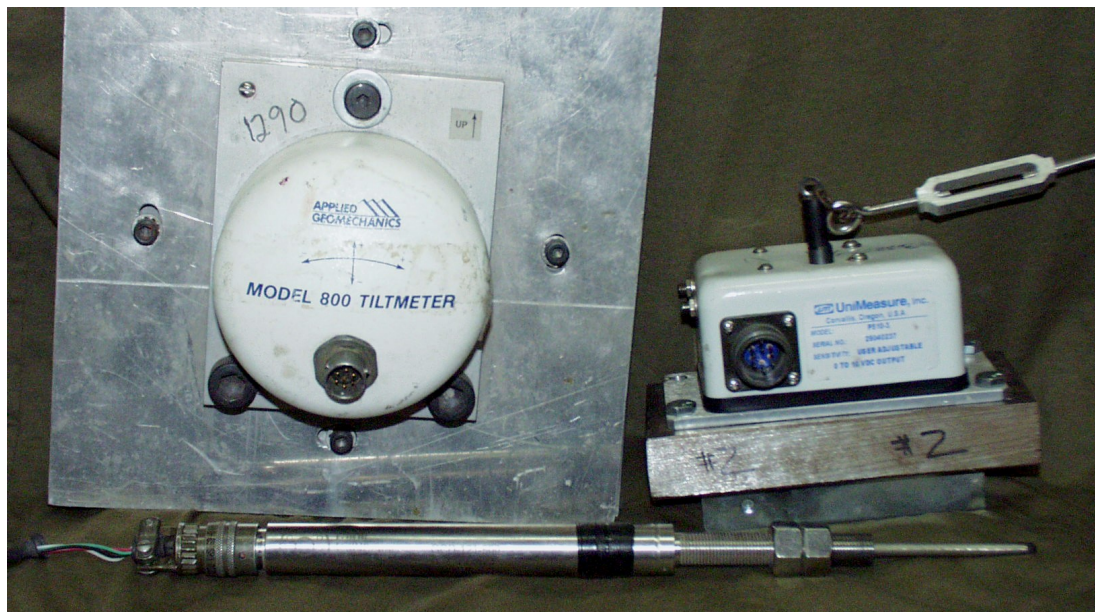


Figure 5-3: Tiltmeter, String Potentiometer, and LVDT used for Test Displacement Measurements

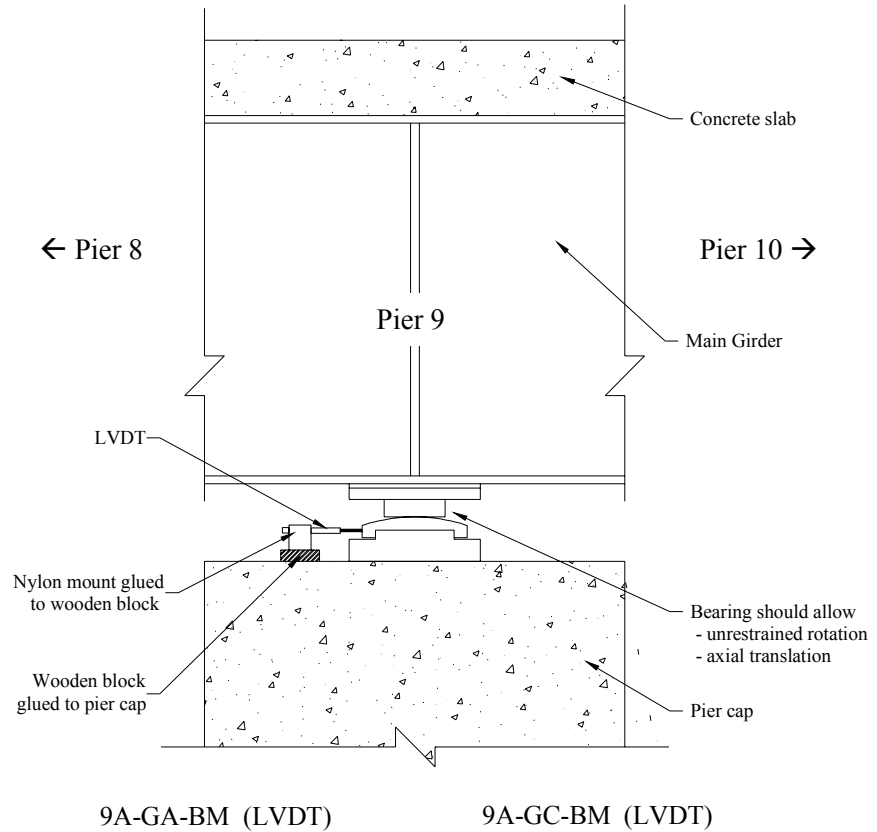


Figure 5-4: LVDTs at Pier 9 to Measure Movement of Expansion Bearings

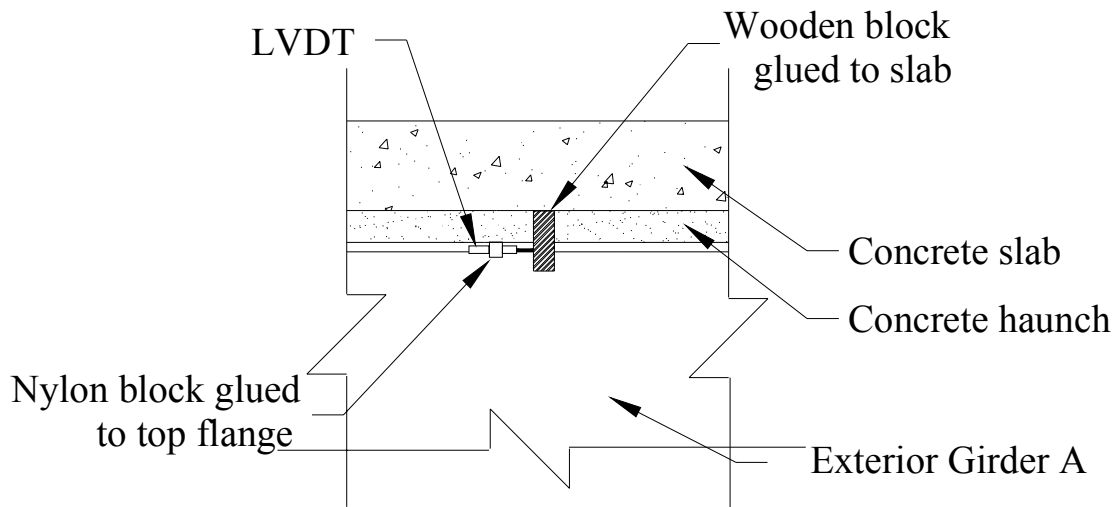


Figure 5-5: LVDT to Measure Slip between Top Flange and Concrete Slab

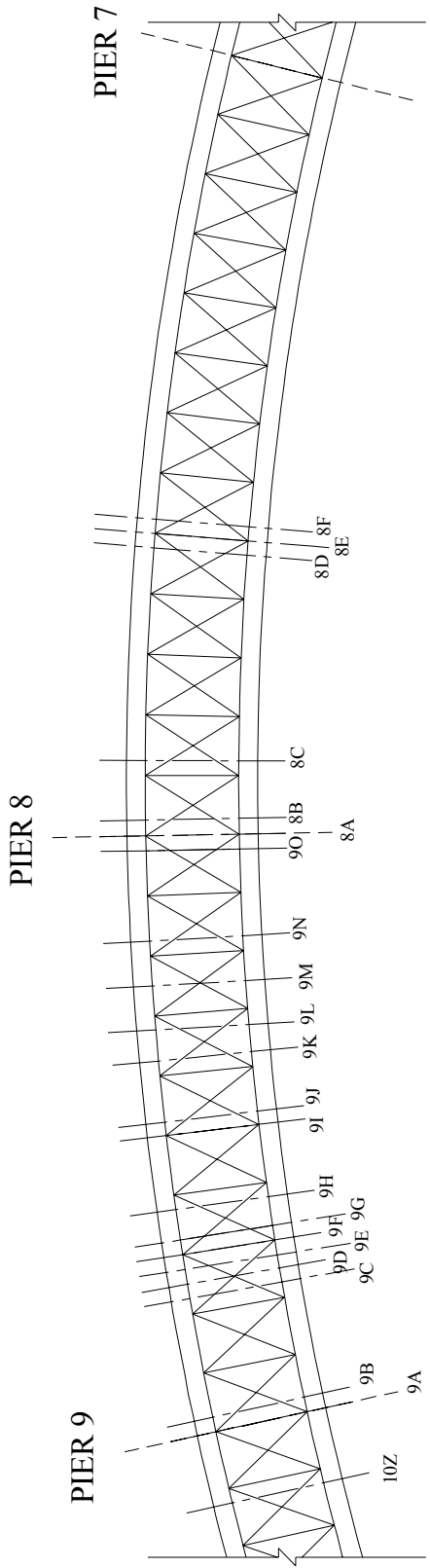


Figure 5-6: Cross-section Labeling Scheme

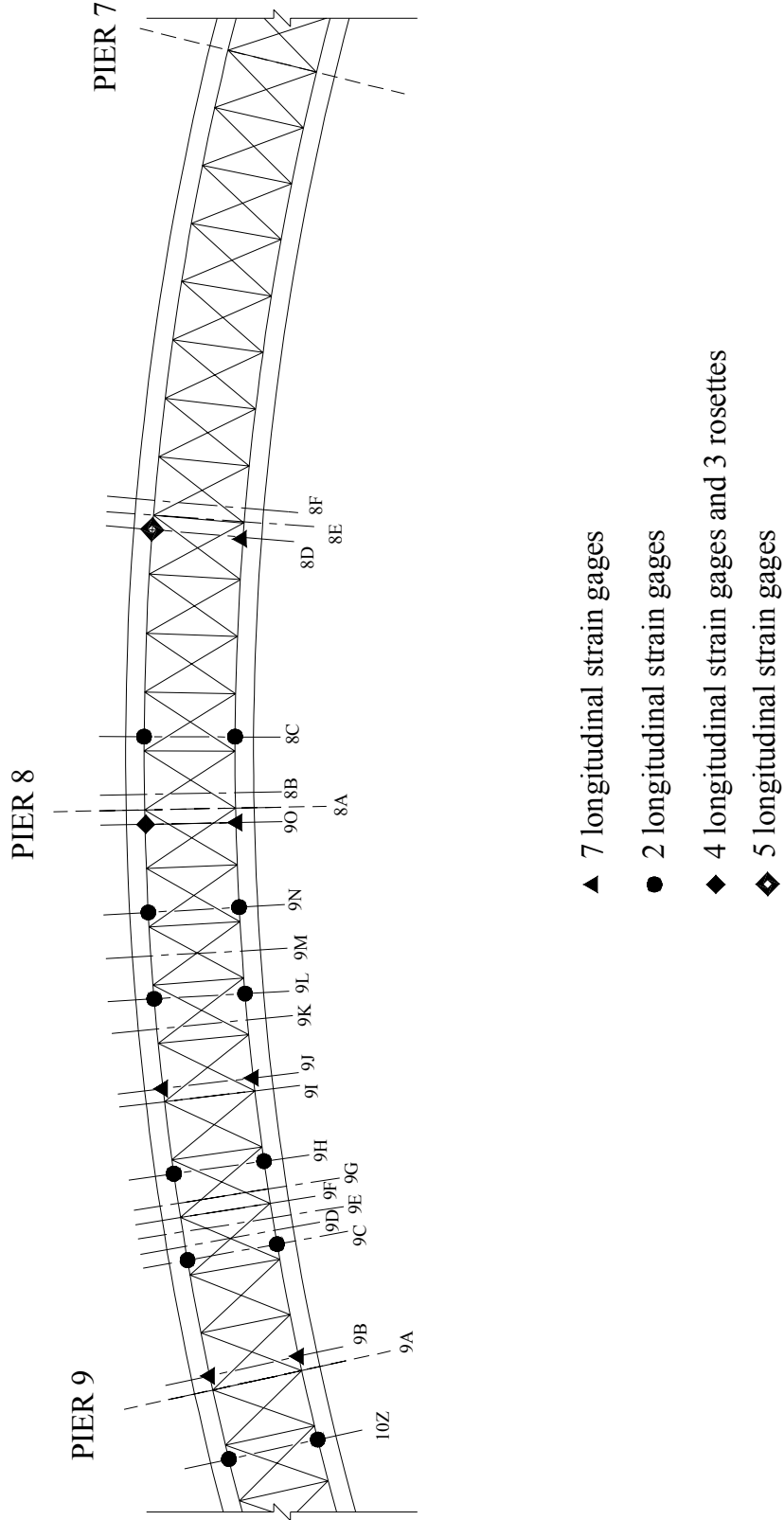


Figure 5-7: Main Girder Strain Gages

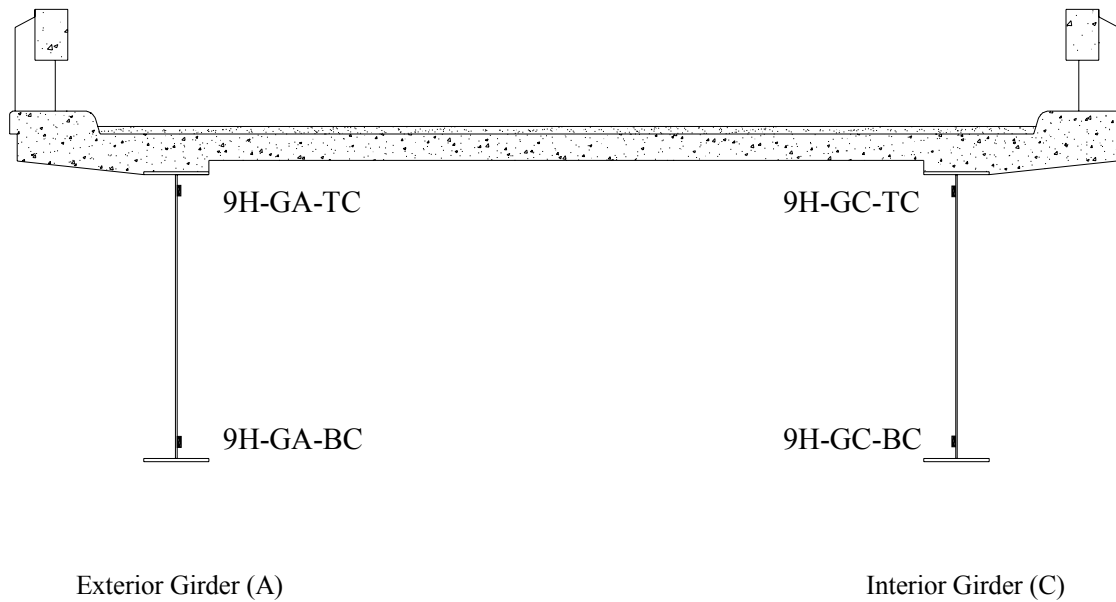


Figure 5-8: Typical Two Strain Gage per Girder Section

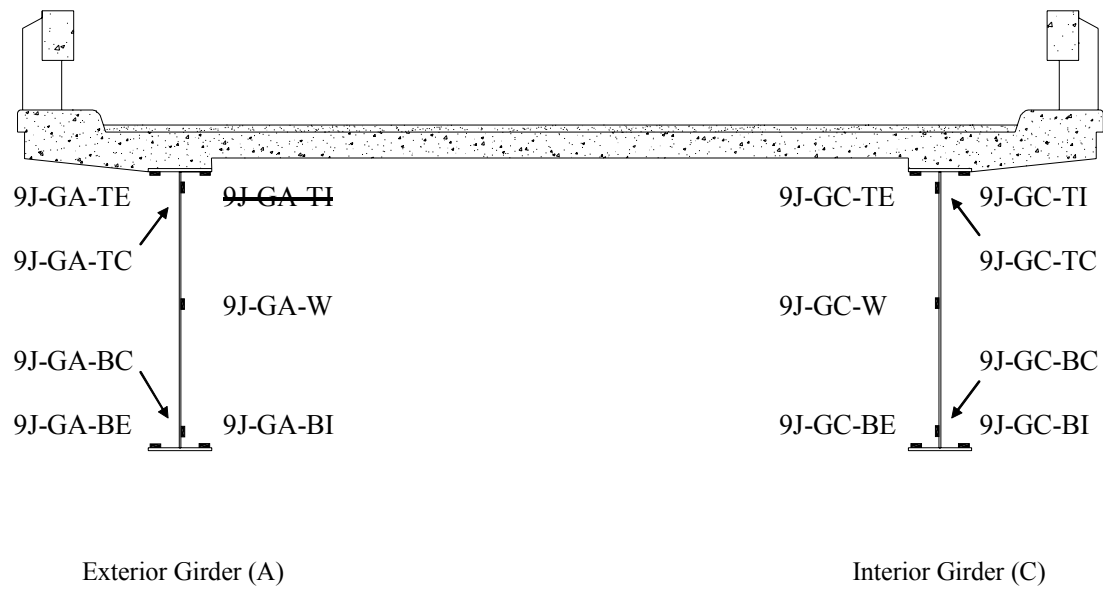


Figure 5-9: Typical Seven Strain Gage per Girder Section

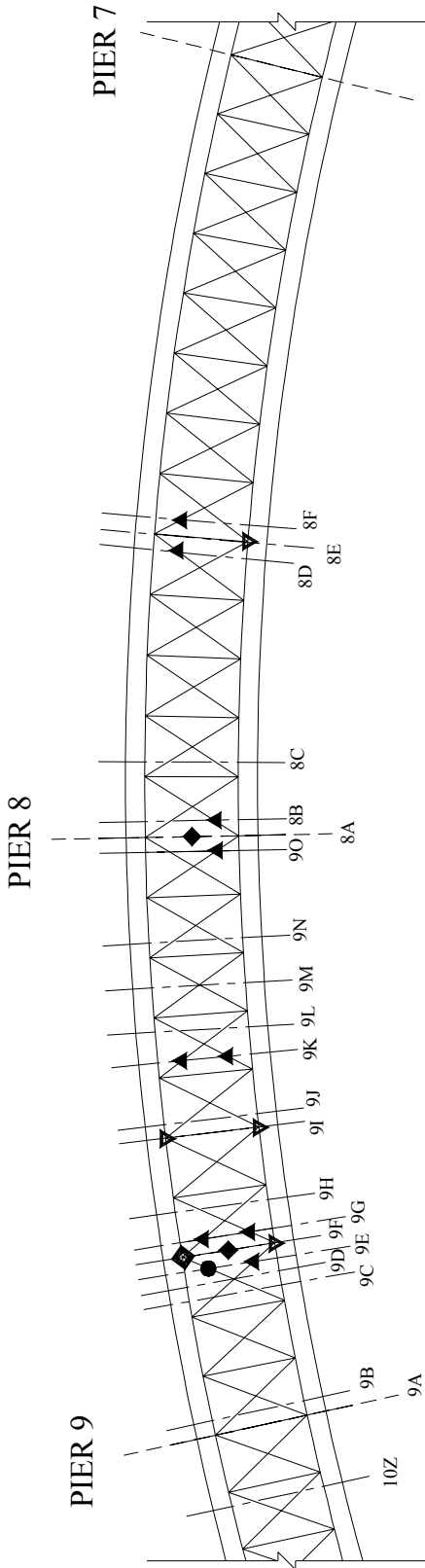


Figure 5-10: Secondary Location Strain Gages

- ▲ 1 longitudinal strain gage on lateral bracing
- 5 longitudinal strain gages on lateral bracing
- ◆ 10 longitudinal strain gages on diaphragm
- ◆ 2 longitudinal strain gages and 1 rosette on gusset plate connection,
plus 1 vertical strain gage at the web gap location
- ▼ 1 vertical strain gage at the web gap location

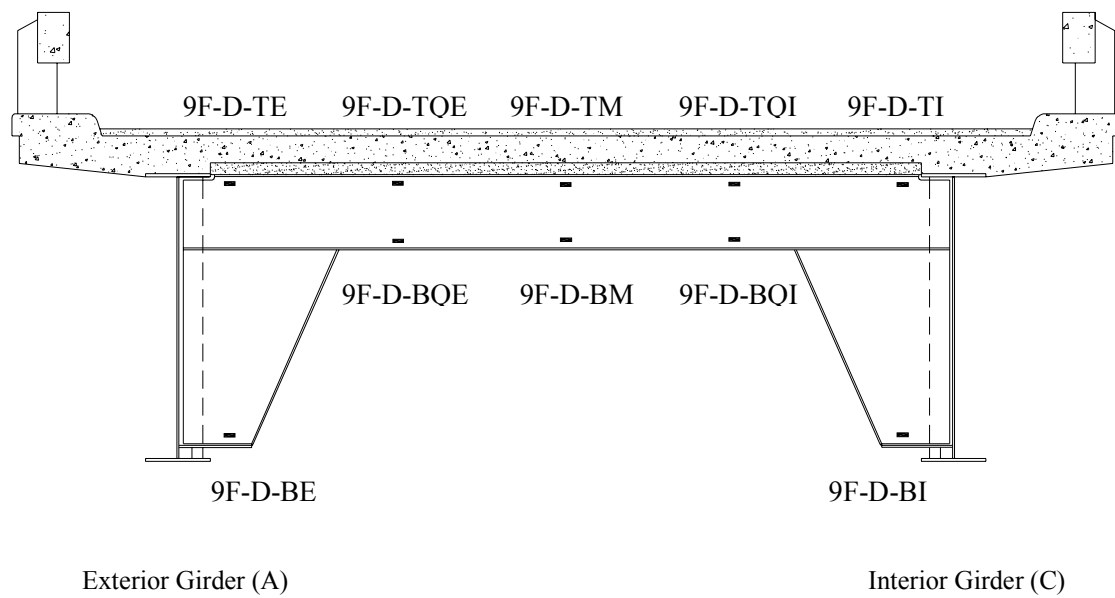


Figure 5-11: Typical Diaphragm Gage Locations

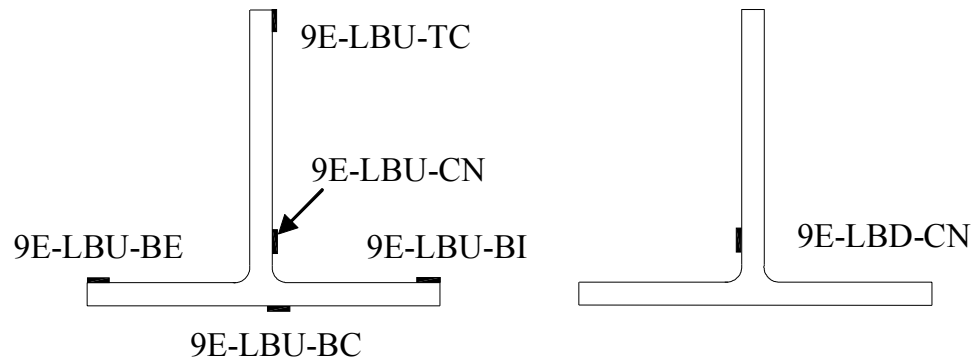


Figure 5-12: Typical Lateral Wind Bracing Gage Locations

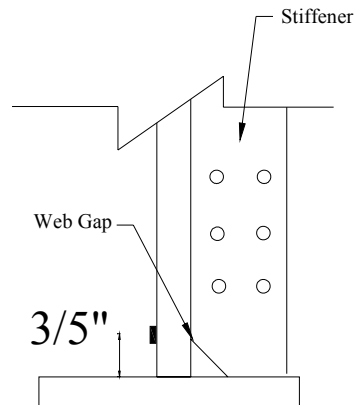


Figure 5-13: Typical Web Gap Gage Location (gage positioned vertically)

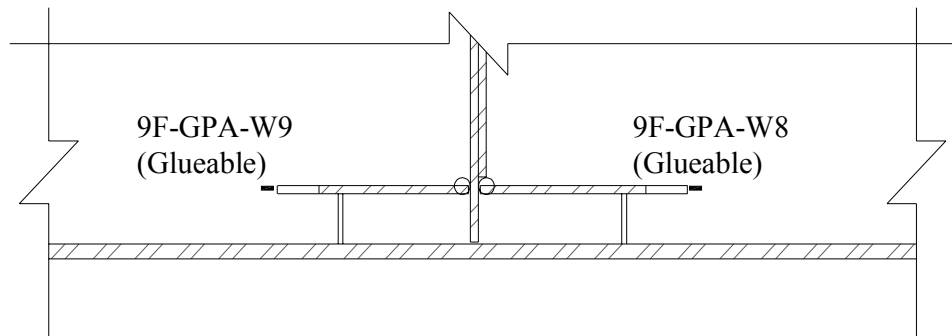


Figure 5-14: Gages to Determine Stress Concentration at Gusset Plate Attachment

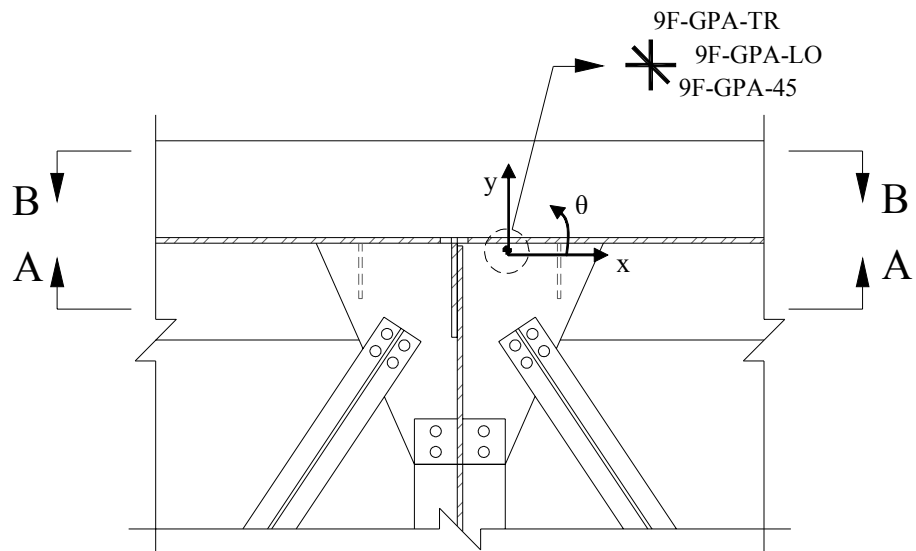


Figure 5-15: Rosette on Gusset Plate

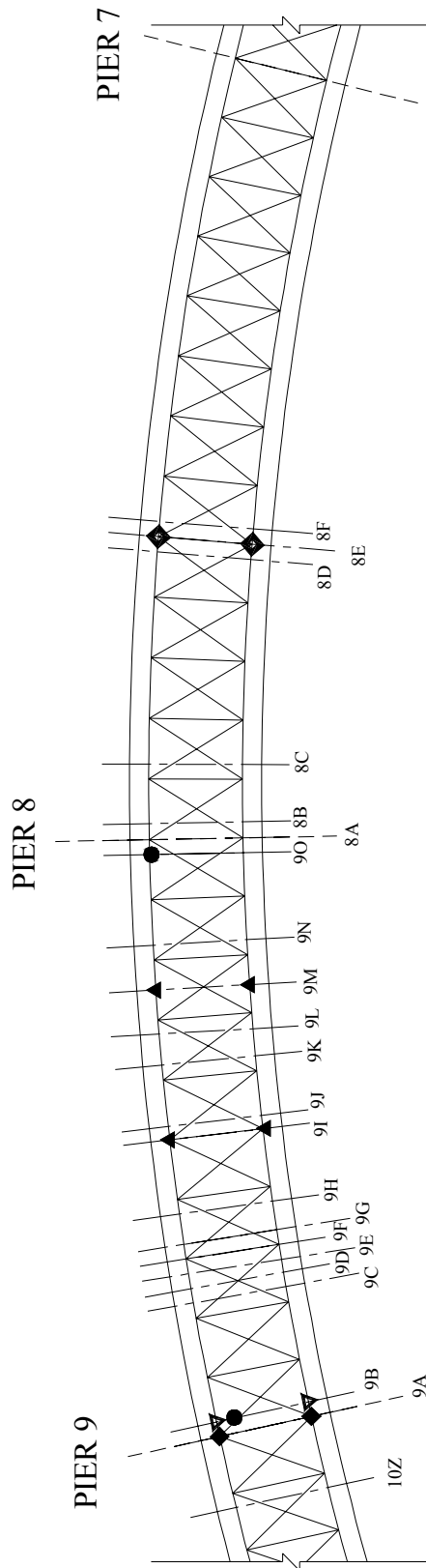


Figure 5-16: Displacement Instrumentation

- ▲ String potentiometer to measure girder vertical deflection
- LVDT to measure slip between concrete slab and steel top flange
- ◆ LVDT to measure translational slide bearing movement
- ◆ Total Station to measure girder vertical deflection
- ▼ Tiltmeter to measure girder rotation

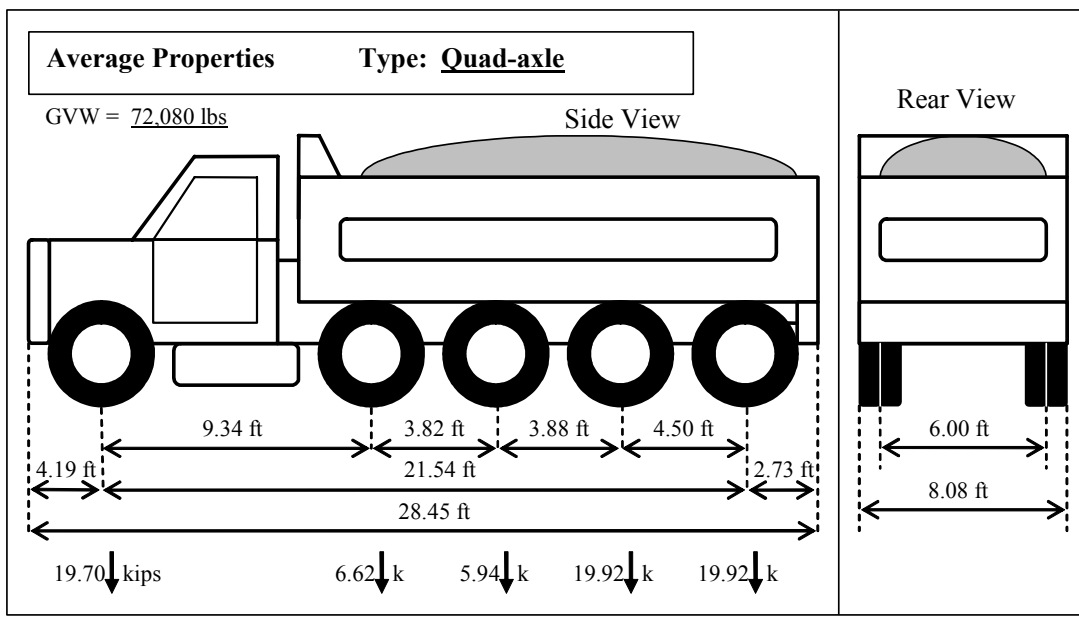
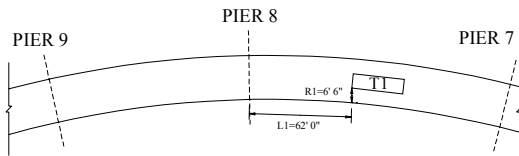
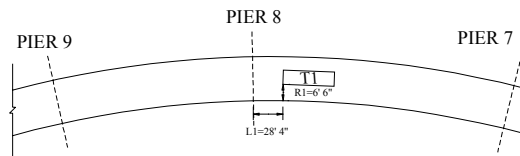


Figure 5-17: Average Properties from the Quad-Axle Dump Trucks Used for Testing

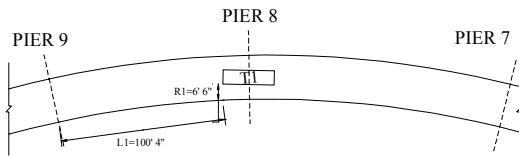
TEST S1 (T1):



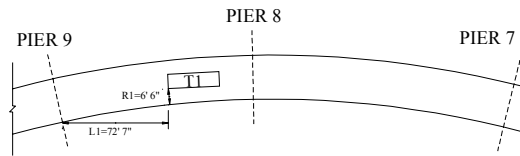
TEST S2 (T2):



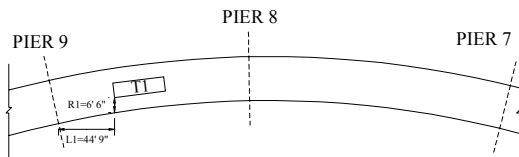
TEST S3 (T3):



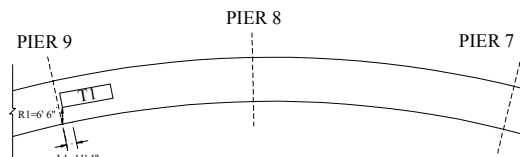
TEST S4 (T4):



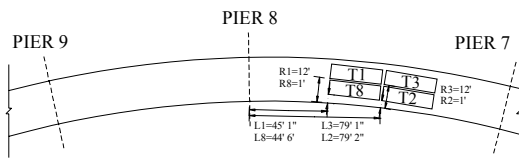
TEST S5 (T5):



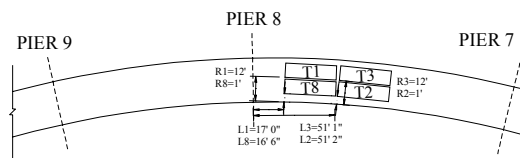
TEST S6 (T6):



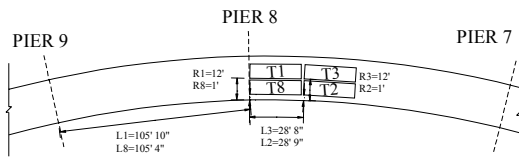
TEST S7 (T20):



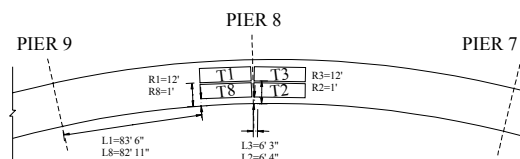
TEST S8 (T21):



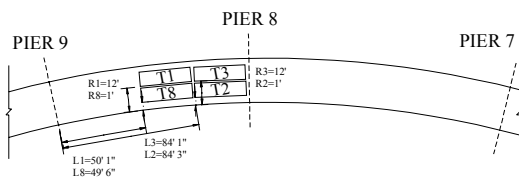
TEST S9 (T22):



TEST S10 (T23):



TEST S11 (T24):



TEST S12 (T25):

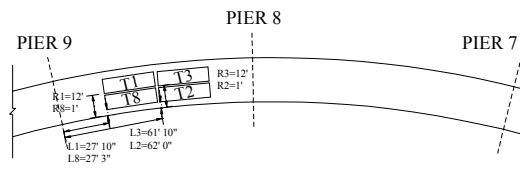
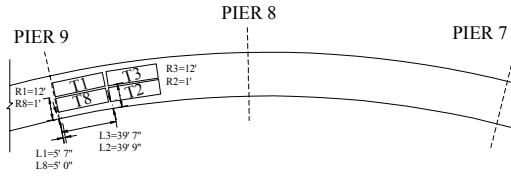
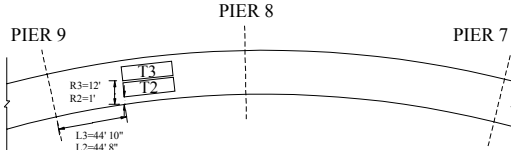


Figure 5-18: Static Test Configurations

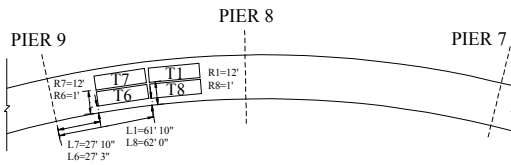
TEST S13 (T26):



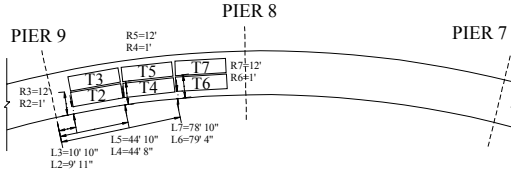
TEST S15 (T9):



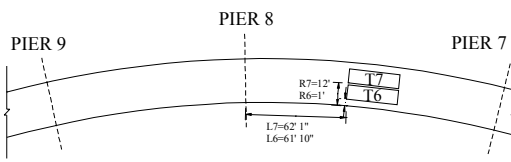
TEST S17 (T56):



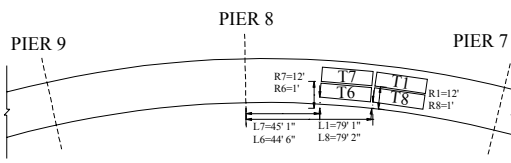
TEST S19 (T19):



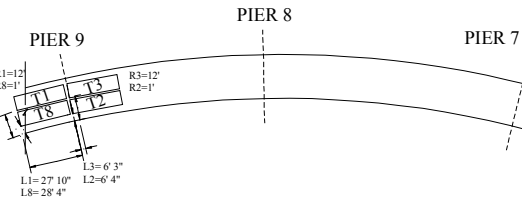
TEST S21 (T55):



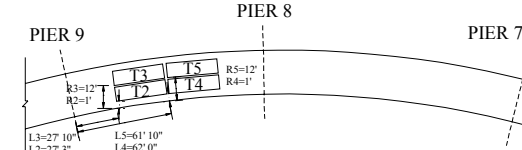
TEST S23 (T13):



TEST S14 (T27):



TEST S16 (T10):

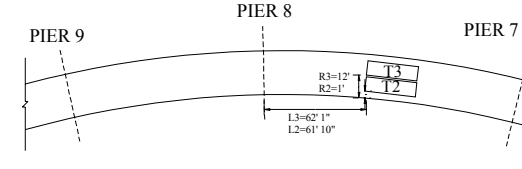


TEST S17 (T56):

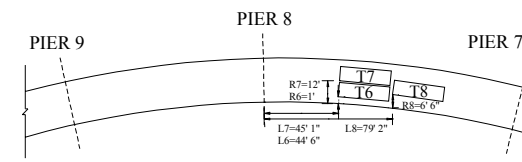


The diagram illustrates Pier 9's location between PIER 8 and PIER 7. Pier 9 has a total length of 12' and a radius of 6' 6". It features two main sections: one section is 10' long with a radius of 4' 11", and another section is 11' long with a radius of 12' 2". The overall width of Pier 9 is 9' 11". Pier 9 is positioned such that its center is 10' 10" from Pier 8 and 9' 11" from Pier 7.

TEST S20 (T7):



TEST S22 (T12):



TEST S24 (T17):

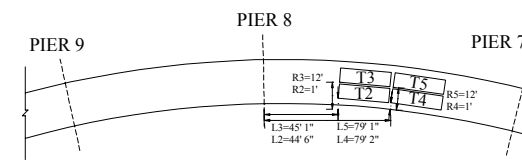
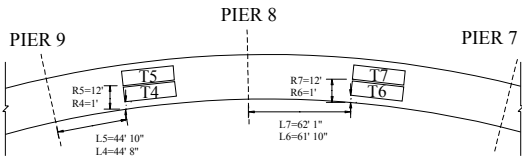
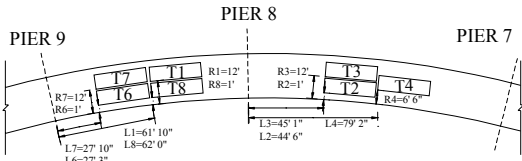


Figure 5-19: Static Test Configurations (continued)

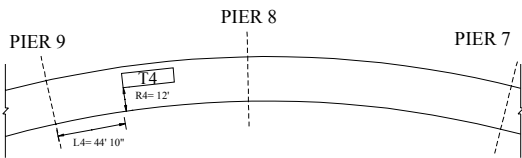
TEST S25 (T11):



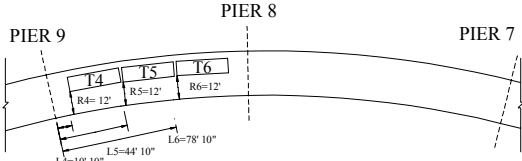
TEST S27 (T15):



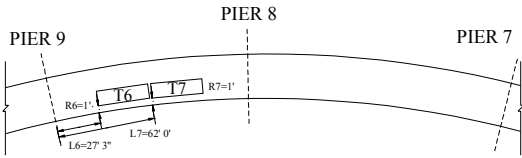
TEST S29 (T28):



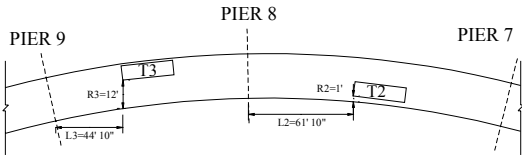
TEST S31 (T31):



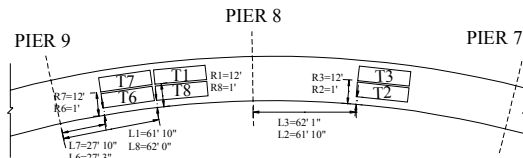
TEST S33 (T33):



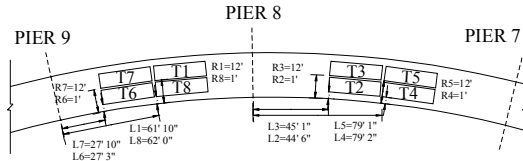
TEST S35 (T8):



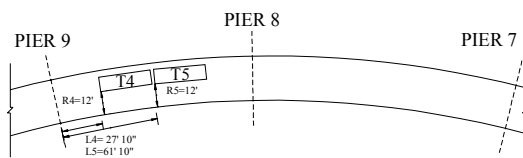
TEST S26 (T14):



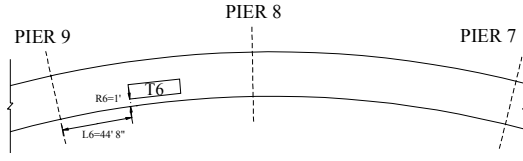
TEST S28 (T16):



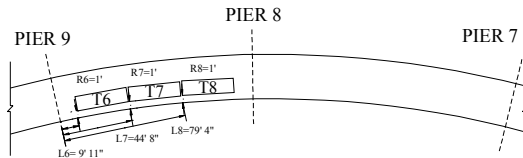
TEST S30 (T29):



TEST S32 (T32):



TEST S34 (T35):



TEST S36 (T30):

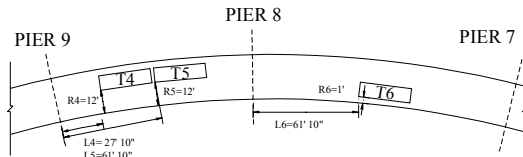
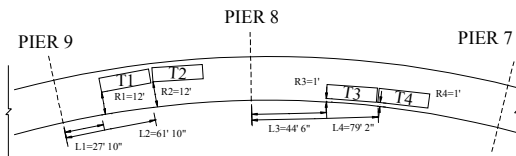
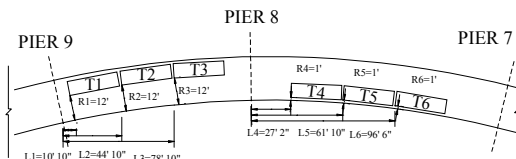


Figure 5-20: Static Test Configurations (continued)

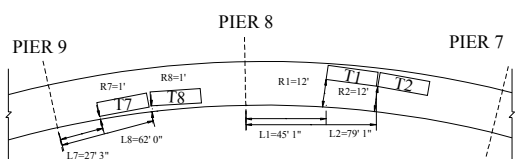
TEST S37 (T37):



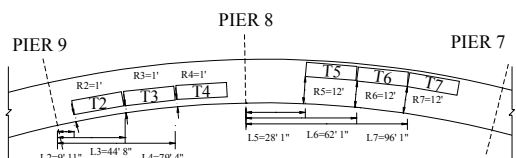
TEST S39 (T39):



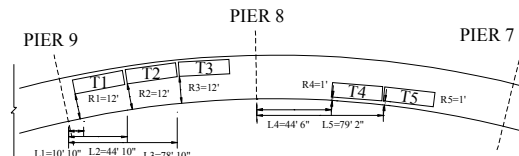
TEST S41 (T36):



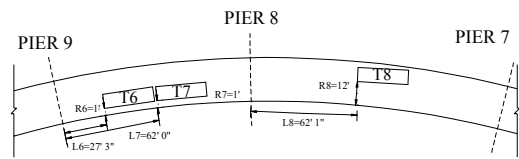
TEST S43 (T41):



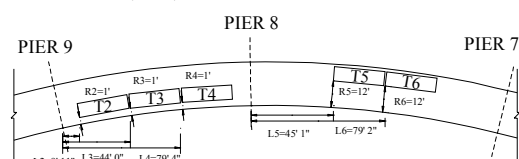
TEST S38 (T38):



TEST S40 (T34):

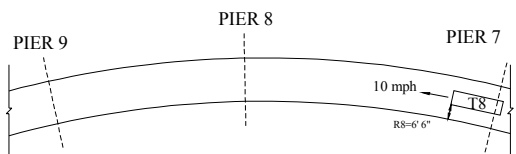


TEST S42 (T40):

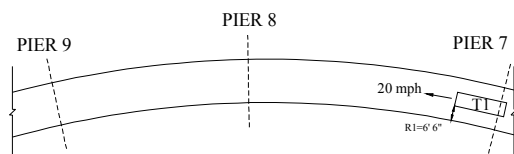


Configurations (continued)

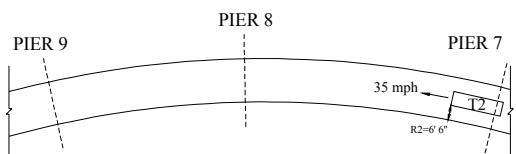
TEST D1 (T42):



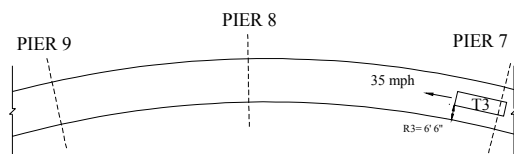
TEST D2 (T43):



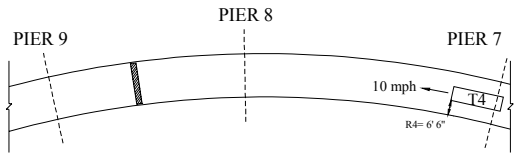
TEST D3 (T44):



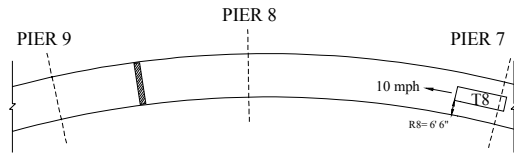
TEST D4 (T45):



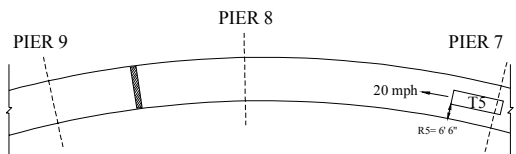
TEST D5 (T46):



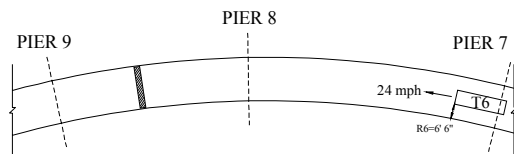
TEST D6 (T50):



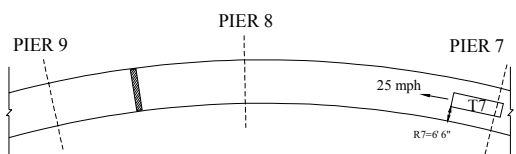
TEST D7 (T47):



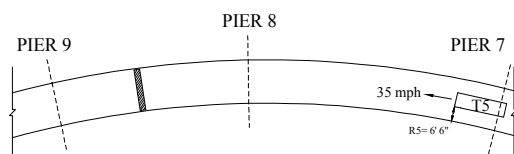
TEST D8 (T48):



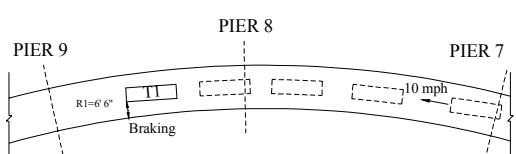
TEST D9 (T49):



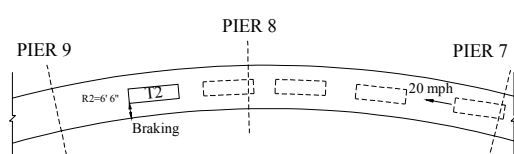
TEST D10 (T54):



TEST D11 (T51):



TEST P12 (T52):



TEST P13 (T53):

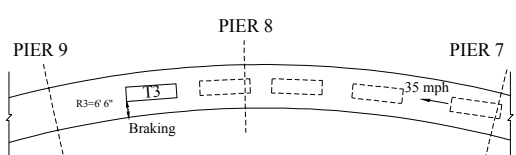


Figure 5-22: Dynamic Test Configurations

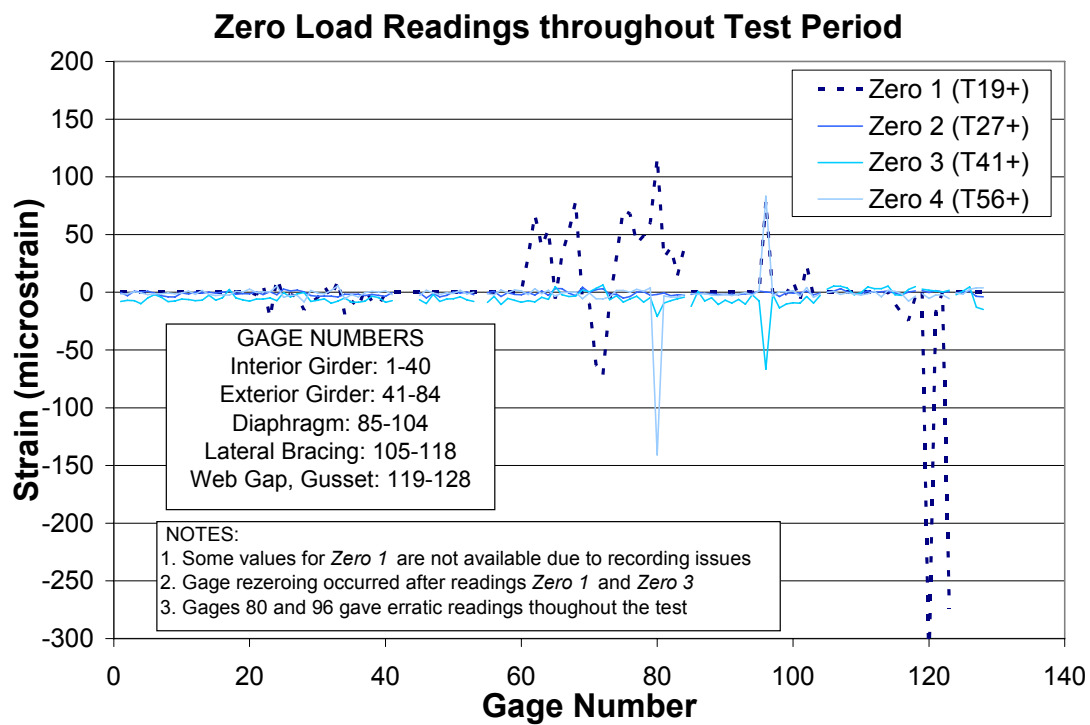


Figure 5-23: Zero Load Readings throughout Test Period

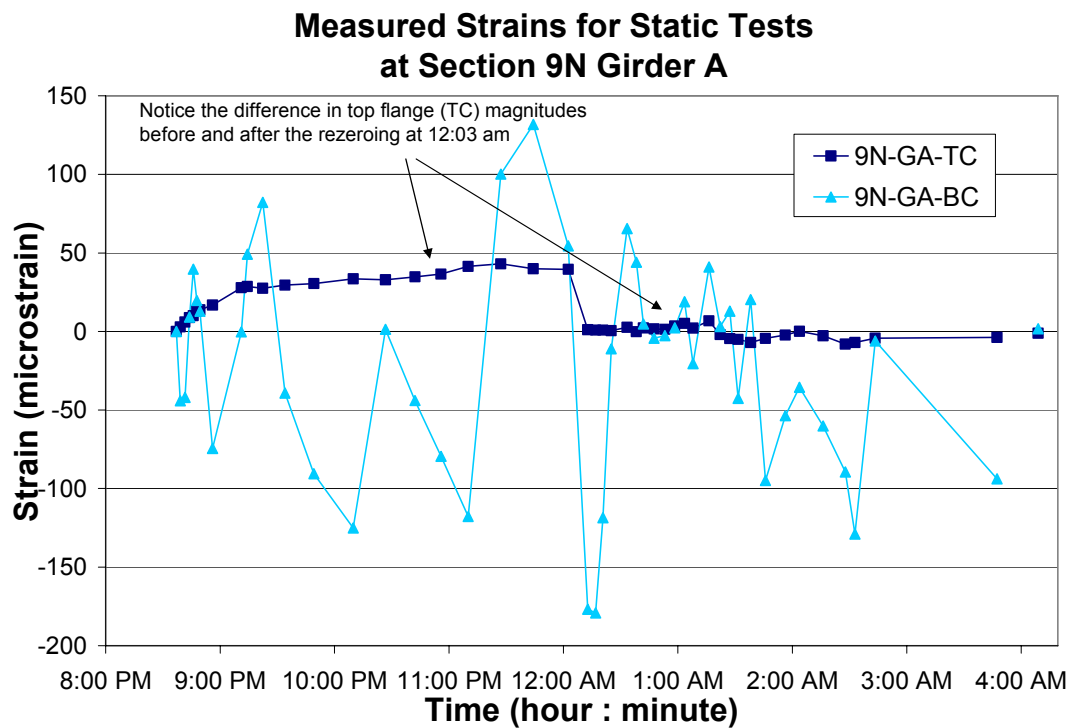


Figure 5-24: Plot Showing Thermal Effects at 9N-GA-TC

**Measured and Thermal Strains for Static Tests
at Section 9N Girder A**

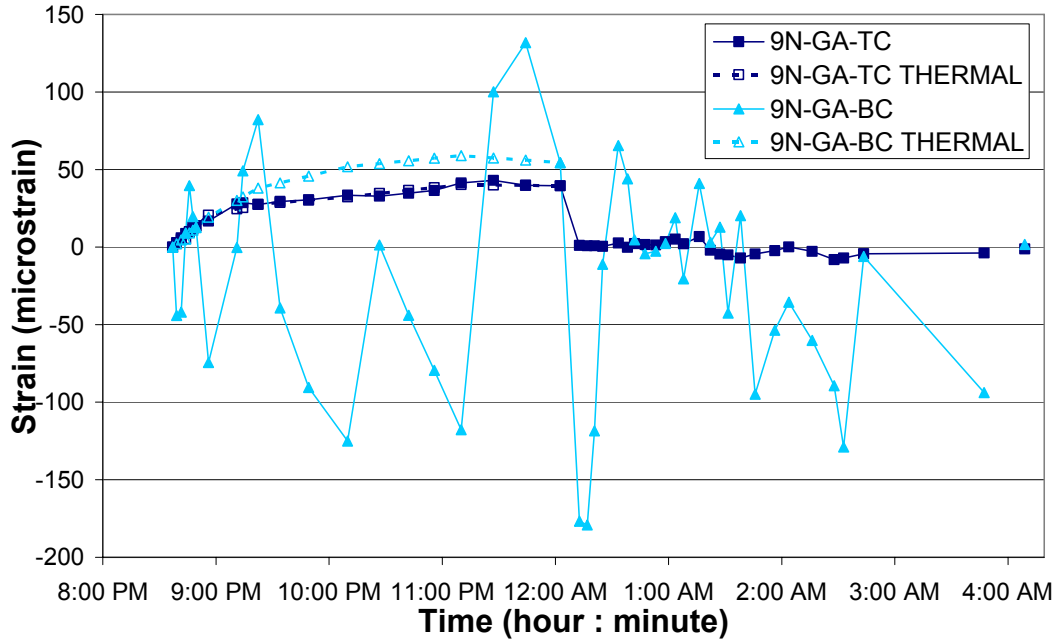


Figure 5-25: Measured and Thermal Strains for Static Tests at Section 9N Girder A

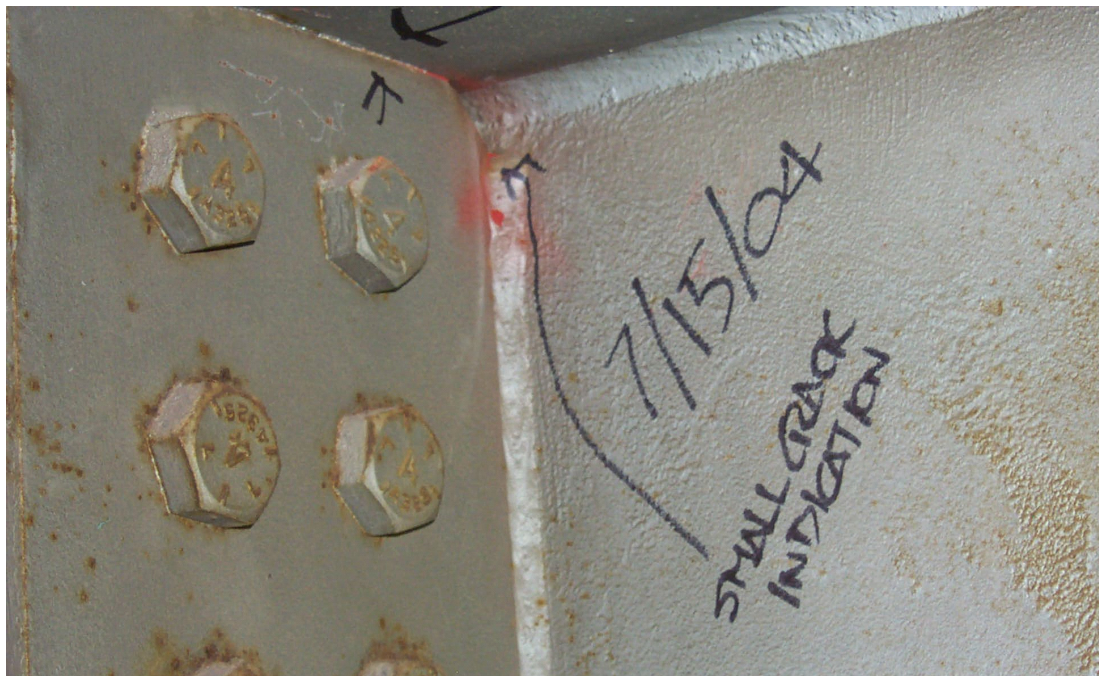


Figure 5-26: Small Crack in Weld at Diaphragm Connection South of Pier 8 on Girder C

Chapter 6

Evaluation of Bridge Properties

Observed experimental behavior of the tested bridge is discussed and quantified in this chapter. Of particular interest are composite section properties, load distribution, bearing fixity, and dynamic impact factor. Specific discussions on the stresses and displacements from the load test are provided in Chapter 7, where comparisons are made to analysis.

The static test data used for these calculations is provided in Appendix F. The dynamic data is located in Appendix E.

6.1 Composite Section Properties

One of the most important properties necessary for accurate predictions of bridge behavior is the level of composite action that occurs between the steel girders and the concrete deck. This tends to be difficult to predict because there are a number of unknown parameters, such as the modular ratio N , the effective width of concrete b_{eff} , and added stiffness due to curbs and parapets. To compound all of this, the amount of shear transfer, and thus composite action that can occur, is dependent on the mechanical shear connectors, friction, and/or adhesion at the deck-to-girder interface. For girders with built up sections, composite action can also be influenced by mechanical interlock between the deck and the top flange due to abrupt changes in flange thickness. Negative moment regions are typically influenced by localized cracks which can significantly decrease the amount of composite action observed at the crack locations.

Recall from Chapter 3 that Mn/DOT Bridge No. 69824 has shear connectors in the positive moment regions and on all diaphragms. There are however, no shear connectors provided on the girders in the negative moment regions. Other research projects have reported that bridges without shear connectors in the negative moment regions have shown conclusive evidence of composite action during load tests (Burdette and Goodpasture, 1988; Nowak and Saraf, 1996; Galambos et al., 2000; Jáuregui et al., 2002).

The remainder of this section uses the experimental data for the girders and diaphragms to calculate the level of composite action at each of the gaged sections.

6.1.1 Girder Strain Profile

In order to investigate the girder strain profiles for the tested bridge, each girder had two positive moment regions (Sections 9J and 8D) and two negative moment regions (Section 9B and 9O) instrumented with three strain gages down the web (refer to Figure 5-9). One gage was located near the top flange (TC), one near the bottom flange (BC), and one was at mid-height (W) of the steel girder. Because the W gage was located halfway between the TC and BC gages, for a linear strain profile it should provide a strain that is halfway between the TC and BC values. The four cross-sections (9B-GA, 9J-GA, 8D-GC, and 8D-GA) plotted in Figure 6-1 through Figure 6-4 generally show this type of behavior. However, the other four sections (9B-GC, 9J-GC, 9O-GC,

and 9O-GA) which are plotted in Figure 6-5 through Figure 6-8, do not show linear profiles for either high or low level load cases.

In all four of the sections with nonlinear strain profiles, comparisons with theoretical neutral axis locations based on composite section properties indicate that the mid-height gage W is providing the anomalous results. For the three nonlinear profiles near piers (9B-GC, 9O-GC, and 9O-GA), the W gages exhibited a magnitude that departed increasingly from linear behavior the higher the applied loads and the closer the loads were to the respective piers. In all likelihood, the webs at these locations are exhibiting some form of out-of-plane bending due to the large shear and compression forces and/or torsional loads acting on the curved web cross-section. These out-of-plane bending effects are not observed for the TC and BC gages because their locations are laterally stiffened by the flanges. It is interesting to note that the remaining gaged pier section, Section 9B-GA, does provide a reasonably linear strain profile. The only observed difference between Section 9B-GA and the other three gaged negative moment sections is that the expansion bearing near 9B-GA showed small signs of movement (see Section 6.3 for details), whereas for the other sections there was none. It is possible that axial forces due to bearing fixity played a role in the observed distorted web gage values on the three sections with nonlinear strain profiles near piers. As for the remaining section that showed a nonlinear strain profile, Section 9J-GC, torsional distortion and oil-canning of the web are plausible explanations for the observed behavior.

Although some of the cross-sections as mentioned above revealed nonlinear strain profiles, it was determined that for major axis flexure the typical assumption of a linear girder strain profile was adequate for further analysis of this bridge. This assumption is backed up by the ability of this computational approach to predict top and bottom flange stresses in this bridge as shown in Chapter 7 of this report. It must be noted however, that factors other than major axis bending may be affecting the measured strains in the webs and are not predicted by grillage-based analysis.

6.1.2 Interface Slip

Instruments attached between the exterior girder top flange and the concrete deck at Sections 9B and 9O revealed relative displacements as shown in Figure 6-9. With a maximum value just over 0.005 inches, the displacements were small. They were also elastic, that is, they always returned to their original position when load was removed. In fact, it is very likely that these slip measurements were not measuring interface slip at all, but were instead providing an indirect measurement of the girder rotations due to the physical setup of the instruments (see Chapter 5 or Appendix B for setup diagrams). This correlation is made because the relative magnitude of the slip measurement at Section 9B-GA follows almost the exact same profile as the rotation 9B-GA-RM at the same cross-section. Figure 6-10 depicts this correlation. If this is the case, little to no interface slip is actually occurring, and the deck is acting as a fully composite section in the negative moment regions. Fully composite behavior in the negative moment regions is also supported by physical investigations of the girder-deck interface which revealed no indications of slip, and strain gage measurements.

One other issue to note is that the slip measurement at 9O generally is lower in magnitude than that at 9B. This is likely due to two factors. First, the cross-section at 9O is much stiffer than that

at 9B and should have a smaller rotation and therefore less interaction at the girder-deck interface. Second, the presence of multiple layers of top flange thickness changes near Pier 8 provide a means for mechanical interlock that helps prevent interface slip from occurring there.

6.1.3 Neutral Axis

In order to determine the level of composite action adding to the stiffness of the steel girders, a number of calculations were made to determine the neutral axis of the girders at various cross-sections. Calculations were also made to determine the neutral axis and composite action of the diaphragms. Ten sections along each girder and five sections along each of the two instrumented diaphragms were investigated. Assuming a linear strain profile, the following equation can be used to determine the location of the neutral axis from the base of the girder or diaphragm:

$$y_{NA-m} = d_{bf-g} + D_g \frac{BC}{BC - TC}, \quad (6-1)$$

where,

y_{NA-m} = distance from the base of the girder to the measured neutral axis (inches)

d_{bf-g} = distance from base of the girder to the BC gage (inches)

D_g = distance between the two gages (inches)

BC = stress or strain value at the bottom flange gage (ksi or $\mu\epsilon$)

TC = stress or strain value at the top flange gage (ksi or $\mu\epsilon$)

When using the above equation for the girders, D_g is 72 inches for all cross-sections. For diaphragms, D_g is either 13.76 inches for the middle three sets of gages or 69 inches for the two sets of gages in the knee-brace regions near the girders. The value of d_{bf-g} is 3 inches plus the thickness of the bottom flange for all cross-sections.

Average values were calculated for the neutral axis based on the calculated values for each section due to all 43 of the static tests and then again for the dynamic tests that were simulating normal traffic (i.e., tests D1-D3). See Appendix F for static test data and Appendix E for dynamic test data used for these calculations. To prevent low strain/stress levels from skewing the data, values were only incorporated from a test if the stress in the BC gage was more than 1 ksi for the girders or 0.5 ksi for the diaphragms.

Measured neutral axis results for the Interior Girder C are shown in Table 6-1 for each gaged cross-section, while those for the Exterior Girder A are in Table 6-2. Sections 10Z and 9B for the exterior girder had only one gage with useable strain profile data, so neutral axis locations could not be calculated. For both girders, the combined average from the static and dynamic averages is also provided in these tables, since these values are used later for quantifying the level of composite action at each section.

The calculated neutral axes for the two instrumented diaphragms are provided in Table 6-3. As the table shows, the neutral axis location for all four knee-brace regions could not be quantified. This was because the strain values near the gusset plates were small or unreliable and those near the deck where influenced by the cope in the diaphragm top flange near the connection to the

girders (see Chapter 7 for more discussion on the diaphragm stresses). For QI at Section 8A, the values were too small to provide a reasonable value for the neutral axis.

For both the girders and the diaphragms, measured neutral axis locations indicated that significant amounts of composite action with the concrete deck were occurring in both positive and negative moment regions. The following sections quantify the contribution from the deck to the overall girder and diaphragm stiffness.

6.1.4 Concrete Contribution

With the neutral axis determined for each of the cross-sections, the amount of concrete necessary to raise the neutral axis to the measured level can be determined. If the slab is assumed to have a constant thickness (i.e., the height offset of the curb and railing is ignored), the following equation can be used to determine the neutral axis of the composite sections:

$$y_{NA} = \frac{A_s \cdot y_s + \frac{A_c}{N} \cdot y_c}{A_s + \frac{A_c}{N}}, \quad (6-2)$$

where,

y_{NA} = vertical distance from the base of the section to the neutral axis

A_s = total area of steel girder/diaphragm at cross-section

y_s = vertical distance from base of section to the centroid of the steel section

N = modular ratio $E_{steel}/E_{concrete}$

A_c = effective area of concrete deck at cross-section

y_c = vertical distance from base of section to centroid of concrete deck

If the measured neutral axis is used with the above equation and A_c is replaced by the slab thickness t_s times the effective width parameter b_{eff} , the equation can be solved for the two remaining unknowns, b_{eff} and N :

$$\frac{b_{eff}}{N} = \frac{A_s(y_{NA-m} - y_s)}{t_s(y_c - y_{NA-m})} \quad (6-3)$$

The original design over thirty years ago used a modular ratio of 8, which corresponds to a concrete compressive strength between 3.6 and 4.6 ksi for normal weight concrete according to Article C6.10.1.1b of the *LRFD 3rd Edition* (AASHTO, 2004). Although adequate at the time of design, a modular ratio of 8 likely no longer accurately represents the concrete stiffness of this bridge. A more realistic value of 6 has been identified for this bridge. This value was chosen based on the measured results from this bridge test and internal testing at Mn/DOT that has consistently provided cylinder tests with compressive strengths of more than 7 ksi for similar concrete decks built in Duluth during the same time period as Bridge No. 69824. AASHTO (2004) recommends a modular ratio of 6 for compressive strengths over 6 ksi.

Using a modular ratio of 6 and Equation (6-3), the effective widths for each of the girder and diaphragm cross-sections can be calculated. The *Combined Average* values from Table 6-1, Table 6-2, and Table 6-3 are used as the measured neutral axes for the calculations of b_{eff} presented in Table 6-4 and Table 6-5. As Table 6-4 shows for the girders, there is a large spread in the calculated effective widths; the minimum value is 57.2 inches while the maximum is 414.1 inches. The total measured moments of inertia I_{total} are also presented in Table 6-4 and Table 6-5, and indicate that the measured values are 2 to 3 times larger than the moments of inertia I_{steel} for the steel alone. Although shear connectors are not present in the negative moment regions (Sections 10Z, 9B, 9N, 9O, and 8C), it is obvious from these calculations that a significant amount of composite action is occurring there.

An average value for all girder sections was calculated to be 166 inches with a standard deviation of 97 inches. Recalling from Chapter 3 that the spacing between the two girders is 18 feet and the overhang dimension is 44 inches, the available deck width for each of the girders is only 152 inches, which is close to the calculated average value. For the cross-sections with much larger effective widths, other factors are influencing the measured stiffness. Some of these influences, such as thickness variations in the deck, rebar lap-splice locations, and actual concrete strength, are difficult to quantify without in-depth measurements and material testing. The most obvious factor that is creating additional girder stiffness is the influence of the curb and railing. The curb is continuous and well anchored to the deck, thus able to provide for composite action anywhere along the deck length. The railing, on the other hand, is a series of discontinuous beams approximately 10 to 22 feet in length that are each supported on two or three small columns. With the center of mass of the railing beams approximately 2 feet above the deck, large neutral axis shifts could result if load is transferred through the column supports to the beams. Inspection of the railings indicated severe cracking and spalling at the base of many column supports. This damage is likely due to cyclic loading of the railing support columns through shear transfer from the deck. Harsh Minnesota freeze-thaw conditions help to increase the rate of deterioration of these concrete columns. The discontinuous nature of the railings and locations of severe damage likely explain the large variation seen in the measured neutral axes and calculated effective widths. Localized cracks in the negative moment regions explain the lower b_{eff} calculated at some of these regions.

In general, the calculated b_{eff} are similar to those determined using Article 4.6.2.6.1 of the *LRFD Bridge Design Specifications* (AASHTO, 2004). For this bridge, all cross-sections were governed by:

$$b_{eff} = 6t_s + b_{tf} / 4 + w_{OH} \quad (6-4)$$

where,

b_{eff} = effective width of concrete deck

t_s = thickness of the slab

b_{tf} = width of top flange of steel girder

w_{OH} = width of overhang

The overhang dimension of the bridge is 44 inches; however, this region for both girders included significantly thicker slabs than the 9 inches for the slab between the girders. Therefore,

the width of overhang w_{OH} was calculated by dividing the total area of the overhang region by the slab thickness of 9 inches. The area of the curb was included in this calculation, but the area for the railings was not included since its effectiveness is unreliable. Both girders had similar overhang dimensions, so only one overhang width was calculated. See Figure 6-11 for a diagram showing the procedure. The result of this process is an overhang width of 64.5 inches. Using a slab thickness of 9 inches and a top flange width of 18 inches, the resulting effective width of concrete deck is 123 inches. This value is about 74% of the average calculated value of 166 inches. However, it is a more reasonable value since the measured average is skewed by the unrealistically large effective width values at some cross-sections. The overhang region of the deck in the negative moment regions contained a number of cracks which provide poor resistance to the tensile deck loads in these regions. Therefore, the overhang dimension in the negative moment regions was limited to the actual dimension of 44 inches, thus providing a total b_{eff} of 102.5 inches. The b_{eff} values of 102.5 inches in the negative moment regions and 123 inches in the positive moment regions of Mn/DOT Bridge No. 69824 along with a modular ratio of 6 are reasonable values for this bridge and provide good analytical correlation with test results as shown in Chapter 7.

The calculated moments of inertia based on the measured neutral axis locations for the diaphragms indicate an average increase of 2.66 times the moment of inertia for the steel beam alone. The range for the effective width to attain the measured neutral axis locations was between 2.16 inches and 14.24 inches with an average value of 6.63 inches. This value is somewhat smaller than the 54 inch effective width that was calculated using the AASHTO LRFD (2004), which for these diaphragms was governed by the $L/4$ provision with L equal to the girder spacing of 18 feet. Based on this information, an effective width of 7 inches is recommended for the diaphragms on this bridge.

6.2 Load Distribution

The load distribution at a given cross-section can be quantified using girder distribution factors (GDFs) that describe the percentage of load that is resisted by each girder. To do so, the moment that each girder develops at a cross-section is divided by the total moment at that cross-section. For the two-girder bridge in this project, the following equation is used:

$$GDF_i = \frac{M_i}{\sum_{j=1}^n M_j}, \quad (6-5)$$

where,

GDF_i = girder distribution factor for girder i at cross-section

M_i, M_j = moment for girder i, j at cross-section

n = total number of girders at cross-section

The basic equation for flexural stress at a given depth on a cross-section can be rearranged to solve for the moment at the cross-section as shown below:

$$M = \frac{\sigma_k \cdot I}{y_k}, \quad (6-6)$$

where,

M = moment at cross-section

σ_k = flexural stress at location k on the cross-section

I = moment of inertia of the cross-section

y_k = distance between the neutral axis and the location k

Using the measured data from the 43 static tests, GDFs have been calculated for eight cross-sections along the length of the bridge (Section 10Z and 9B could not be calculated because data was unavailable for the exterior girder at these locations). The total measured moments of inertia presented in Table 6-4, the combined average neutral axis locations in Table 6-1 and Table 6-2, and the BC gage stresses from Appendix F are used to calculate the GDFs. In the following tables, the Static Test cases have been grouped based on the longitudinal (Pier 9, Span 9-8, Pier 8, etc.) and transverse (Centered or Shifted) positions of the center of gravity of the truck configurations:

- Table 6-6: GDFs for Loads Centered on Pier 9
- Table 6-7: GDFs for Loads Centered on Span 9-8
- Table 6-8: GDFs for Loads Centered on Pier 8
- Table 6-9: GDFs for Loads Centered on Span 8-7
- Table 6-10: GDFs for Loads Shifted to Interior Girder on Span 9-8
- Table 6-11: GDFs for Loads Shifted to Exterior Girder on Span 9-8
- Table 6-12: GDFs for Loads Shifted to Interior Girder on Span 9-8 and Exterior Girder on Span 8-7
- Table 6-13: GDFs: for Loads Shifted to Exterior Girder on Span 98 and Interior Girder on Span 8-7

In general, GDFs are used to determine the amount of load to apply to each girder during analysis. For this purpose, Table 6-14 was created. In this table, the average GDF for each girder was calculated using only the GDFs at the cross-section of the applied load using all applicable tests for each transverse position. The results show that for trucks centered between the two girders, 45% of the load goes to the interior girder while 55% is taken up by the exterior girder at the point of loading. For cases where the load is transversely positioned 5.5 ft closer to the interior girder, the interior girder takes 66% of the load while the exterior takes 34%. This correlates to a 21% load shift for each girder as compared to the centered case. On the other hand, when the load is transversely positioned 5.5 ft closer to the exterior girder, the percentages are 23% for the interior girder and 77% for the exterior girder. This is a 22% shift from the transversely centered position. As can be seen, an equal shift (5.5 ft) in the transverse position from center results in an equal percentage change (approximately 21.5%) in the GDFs. Equations for the girder distribution factors based on these values and assuming a linear profile were created for the test bridge as shown:

$$\begin{aligned} GDF_{Int} \% &= 88 - 4.78 \cdot x_{Int} \\ GDF_{Ext} \% &= 98 - 4.78 \cdot x_{Ext} \end{aligned} \quad (6-7)$$

where,

$GDF_{Int,Ext}\%$ = percent of total load carried by the interior, exterior girder

$x_{Int,Ext}$ = transverse distance from the interior, exterior girder to the load center (ft)

These GDF values are specific to the point of load application (i.e., the longitudinal position of trucks), and are good for distributing the loads to nearby girder nodes when using a system-based analysis technique. They are not recommended for line girder-based analysis, since one set of GDFs along the length of the bridge does not accurately define the load distribution. This is evident from Table 6-6 through Table 6-13, where the GDFs consistently vary along the length of the bridge, especially from span to span. Because of this, it is recommended that curved bridge analysis be done using a system-based analytical technique to provide a more accurate representation for load path.

6.3 Bearing Fixity

Pretest inspections of the expansion bearings at Pier 10 and Pier 9 revealed no indications of movement. Uncracked paint dating back to the original painting in 1971 could be seen in a number of locations along the slide interfaces of the bearings, indicating the lack of movement. This is somewhat surprising since the yearly temperature range in Duluth, MN, is over 100°F and should provide a reasonable amount of movement for the thermal expansion and contraction of the bridge.

In order to verify the functionality of the expansion bearings at Pier 9, displacement readings were taken along the axis of each bearing pad. Figure 6-12 shows the results of these measurements for the 43 static tests. The interior girder measurements (9A-GC-BM) show virtually no movement. Although small, the exterior girder measurements (9A-GA-BM) do show some displacement. It should be noted that the plot in Figure 6-12 for 9A-GA-BM does not accurately display the initial offset value, which should be near zero at the beginning of the tests. This is because the method used to determine the offset values for the voltage-based instruments (see Chapter 5) assumes that all four of the zero readings are at similar values. This was not the case for instrument 9A-GA-BM, which showed a drift pattern throughout the test period. However, 9A-GA-BM was plotted in Figure 6-12 using this offset determination method for consistency purposes, since this method provided reasonable values for all other voltage-based displacement instruments. Even accounting for this discrepancy, the plot for 9A-GA-BM does show some displacement relative to the expansion bearing on the interior girder.

Similar to the comparison made between the interface slip and rotation measurements in Section 6.1.2 above, a relative magnitude comparison is shown in Figure 6-13 between the rotation at Section 9B-GA and the bearing displacement at Section 9A-GA, the gages for which were approximately 3 ft apart. Two observations may be made. First, the displacements show similar profiles; therefore the bearing displacement measurements are real bridge responses and not faulty data. And second, there is an obvious drift in the bearing measurement with time. This drift could be due to thermal expansion/contraction of the bridge or could be an accumulation of displacement due to bearing friction preventing the return to the original position after loads are removed.

Inspection of the slide interface after the test for the bearing at 9A-GA-BM revealed no indications of movement, such as fresh paint or paint cracking. Therefore, it is believed that the measured values may be due to other displacements at the bearing assembly. For example, the

entire assembly, which rests on a thin lead pad and is bolted to the concrete piercap with two bolts, could be sliding along the lead pad or could be rocking as the girder rotates. It would not take much movement from either of these mechanisms to produce the 0.002 inches of total accumulated displacement measured for 9A-GA-BM.

6.4 Dynamic Impact Factor

To provide basic information on the dynamic behavior of the horizontally curved bridge in this project, a limited number of dynamic tests were completed as described in Chapter 5. The primary focus of these dynamic tests was the dynamic impact factor (DIF). This section provides the results of the investigation into the dynamic impact factor for Mn/DOT Bridge No. 69824.

6.4.1 Calculation of the Dynamic Impact Factor

In order to include the dynamic effects due to moving loads on a bridge, DIFs are used to increase the weight of a vehicle for use in static analyses. To determine the DIFs for the test bridge in this project, the dynamic test data was compared to a subset of static test data (typically tests S1-S6) for each strain gage using:

$$DIF = \frac{\text{Peak Dynamic Strain}}{\text{Peak Static Strain}} \quad (6-8)$$

For most instruments two dynamic impact factors were calculated; one for peak positive strain and one for peak negative strain. In the event that an instrument experienced only positive or negative values throughout the dynamic and static tests, only one DIF was calculated. For cases where the peak dynamic and the peak static strains were of opposite signs, the DIFs were neglected since in all of these cases the measured values were of small magnitude.

Because the static test subset is based on a series of discrete truck locations, a full continuum of static data for a truck along the length is not available. To provide reasonable values for the DIF, the truck locations for the static test subset were chosen in an attempt to provide the maximum strain or displacement for each instrument that would occur if a full continuum of static tests were completed. Some error is involved in this process. In general, the maximum values from the subset of static data are lower than would occur from a continuum of static data for a truck at locations along the length of the bridge. This is especially true for the gages on the diaphragms and lateral bracing, which were difficult to predict the worst case truck position along the length. Since the peak static strains used in Equation (6-8) may be lower than actually exist, the DIFs calculated for this bridge could be slightly high. This was determined to be acceptable since it results in conservative values from a rating or design perspective.

In order to provide accurate dynamic impact factors for the braking tests, the static test subset had to be limited. Contrary to the trucks in the constant velocity tests and the constant velocity tests driving over a 2x4 (see Chapter 5 for descriptions), the trucks for the constant velocity test that included braking did not fully cross over the bridge as part of the test. This is because the trucks for the braking tests came to a stop somewhere between Pier 8 and the midspan between Pier 8 and Pier 9 (the final stopped locations are unknown). Therefore, directly comparing the

dynamic data for these tests to the full static subset (S1-S6) is not accurate since the trucks for these dynamic tests never reached the position for static test S6, and possibly that for test S5. For this reason, the static test subset for determining the DIF for braking tests D11 – D13 is limited to tests S1-S5. Although the dynamic test trucks may not have quite reached the location for static test S5 for tests D11 – D13, data for S5 is included in the static test subset. The result of this is a large scatter in dynamic impact factors for the braking tests, especially for the gages near Pier 9.

Also, note that all data for the dynamic impact factors is based on loads transversely centered on the bridge. This was done due to a limited time frame for dynamic tests and the fact that typical highway traffic on this bridge is located near the transverse center of the bridge.

6.4.2 Dynamic Impact Factors for Bridge No. 69824

As the trucks for the dynamic tests drove along the bridge, the strain at each gage varied in a pattern similar to that in Figure 6-14. A maximum strain (most tensile) and minimum strain (most compressive) were obtained. Appendix E provides tables of the maximum and minimum strains for each gage per test, along with the corresponding dynamic impact factors. The dynamic impact factors are only shown if the peak static test strain was above a minimum threshold magnitude of 25 microstrain. Otherwise, the column for the DIF is marked by the phrase *low static*. This limit of 25 microstrain was set so that small magnitude strains would not unfairly skew the dynamic impact factors. The value of 25 microstrain was determined from a plot of the associated dynamic impact factors for all of the dynamic data as represented in the tables in Appendix E. Figure 6-15 shows this plot of data along with the recommended girder impact factor from the *Guide Specifications for Horizontally Curved Steel Girder Highway Bridges* (AASHTO, 2003a), and the limit of 25 microstrain. As the figure shows, there is an exponential decrease in the dynamic impact factor as the magnitude of strain increases. The threshold value of 25 microstrain was chosen because for larger magnitudes of peak static strain the dynamic impact factor remains relatively constant.

In nearly all cases for the dynamic impact factor calculations of the girders, the top flange gage had a magnitude less than the limit of 25 microstrain. Therefore, all DIFs for the girders are based solely on data from the BC gage.

The calculated girder dynamic impact factors using the process described in Section 6.4.1 are plotted for each girder in Figure 6-16 using all available dynamic test data. Data is provided at each of the ten instrumented sections along the bridge length. The average values for each girder are also provided to show how the two girders compare with one another. In general, the calculated girder dynamic impact factors using Equation (6-8) for the exterior girder are higher than those for the interior girder. The average DIF of the average cross-section values for the interior girder is 1.25, while that for the exterior girder is 1.37. Calculated dynamic impact factors less than unity are not included in the calculation of the average values. Further discussion of the difference in DIFs for the girders is delayed until Section 6.4.3 where centrifugal effects are discussed.

A breakdown of the dynamic impact factors by test is provided for the Interior Girder C in Figure 6-17 and for Exterior Girder A in Figure 6-18 . Triangular shapes are used to plot data for

the constant velocity tests, squares are used for the constant velocity over 2x4 tests, and circles are used for the constant velocity then braking tests. For both girders there is a relatively consistent range for the constant velocity tests and a wide scatter for both the constant velocity over 2x4 tests and the constant velocity then braking tests. Since the 2x4 and braking tests are more intense than what typically occurs on the bridge for dynamic impact, Figure 6-19 was created using only the data for the constant velocity tests (D1-D3) to provide a more realistic view of the typical dynamic impact for this bridge.

The recommended girder dynamic impact factor from the *Guide Specifications for Horizontally Curved Steel Girder Highway Bridges* (AASHTO, 2003a) is 1.25. This one value is specified to be used for all girders. To provide a comparison of this bridge with the code recommended value, the average values for all gages (i.e., for both girders) at each cross-section is provided in Figure 6-20 along with values for one and two standard deviations from the average. The average value of all dynamic impact factors greater than unity is 1.30. This value is slightly higher than the 1.25 recommended by code. However, recall from Section 6.4.1 that the resulting DIFs were expected to be slightly high from these calculations since the static subset used for determining the DIFs was based on a limited number of locations along the bridge length.

The calculated dynamic impact factors for the diaphragms are limited since the strains were small for almost all gages on the two diaphragms instrumented. There were only four diaphragm gages at Section 9F that had strains higher than the limit of 25 microstrain and none at Section 8A. Dynamic impact factors for the four gages are provided by test in Figure 6-21. The average values at each gage along with values at one and two standard deviations are provided in Figure 6-22. These two figures show a scatter between approximately 1.0 and 1.7 in the DIFs for the diaphragms. The average of these values greater than or equal to unity is 1.31. This value happens to be quite close to the code recommended value of 1.30 for diaphragms (AASHTO, 2003a).

The calculated lateral wind bracing dynamic impact factors are provided in Figure 6-23 for each dynamic test. Figure 6-24 shows the average values and the values for one and two standard deviations. The average value for values greater than or equal to unity is 1.55 (since there were five gages at bracing 9E-LBU, only one value is included in this average value so as not to unjustly skew the average value). This value is skewed upward due to large impact factors for the 2x4 tests for lateral bracing near the midspan between Pier 8 and Pier 9, which is where the 2x4 was placed. Dynamic impact factors up to approximately 2.4 were achieved at Section 9G for the 2x4 tests. However, it should be kept in mind that the use of a full continuum of static test locations for the trucks would decrease these values significantly.

Dynamic impact factors for the web gap details and those for the gusset plate tips are shown in Figure 6-25. The average values along with values for one and two standard deviations are provided in Figure 6-26. The web gap details average a dynamic impact factor near 1.30, while that for the gusset plate tips is closer to 1.5.

6.4.3 Effects due to Centrifugal Forces

Centrifugal forces generated as a moving vehicle travels along a curved bridge create an overturning moment on the vehicle that shifts the weight of the vehicle toward the exterior

wheels (i.e., those furthest from the bridge center of curvature). The overturning moment due to centrifugal force is:

$$M_{ot} = \frac{W \cdot v^2}{g \cdot R} H \quad (6-9)$$

where,

M_{ot} = overturning moment

W = weight of vehicle

v = velocity of vehicle

g = acceleration of gravity

R = radius of curvature to vehicle center of mass

H = vertical height from roadway surface to vehicle center of mass

Since centrifugal forces are dependent on velocity and go to zero as the velocity goes to zero, the dynamic tests include centrifugal effects, while the static tests do not. The direct comparison between dynamic and static test values for DIFs as done using Equation (6-8) does not take into account this key difference. This results in higher calculated DIFs for the exterior girder as compared to the interior girder, since centrifugal effects in the dynamic tests increase the load on the exterior girder while decreasing it on the interior girder. This is not an effect of dynamic impact and should be removed to get a more accurate picture of the dynamic impact for each girder.

The following approximate method was employed to remove centrifugal effects from the dynamic impact factors for the girders:

1. A transverse shift in the location of the vehicle weight was determined for velocities of 10, 20, 24.5, and 35 mph with $H = 6$ ft and $R = 575$ ft using:

$$\Delta = \left(\frac{M_{ot}}{w} \cdot \frac{1}{W} \right) \cdot w = \frac{M_{ot}}{W} = \frac{v^2 \cdot H}{g \cdot R} \quad (6-10)$$

where,

Δ = radial shift in weight

w = width of vehicle between wheel centroids

M_{ot} , W , v , g , R , H as described above

The resulting shifts for 10, 20, 24.5, and 35 mph are 0.07, 0.28, 0.42, and 0.85 feet, respectively.

2. The fractional change in girder distribution factor for each girder was calculated for each shift assuming the vehicle is transversely centered between the girders. The slope defined in Equation (6-7) was used along with the transversely centered distribution factors of 45% for the interior girder and 55% for the exterior girder to define the fractional changes in GDF due to the centrifugal force shift as:

$$\begin{aligned}\delta GDF_{Int} &= \frac{4.78 \cdot \Delta}{45} \\ \delta GDF_{Ext} &= \frac{4.78 \cdot \Delta}{55}\end{aligned}\quad (6-11)$$

The resulting fractional changes in GDF on the interior girder for 10, 20, 24.5, and 35 mph are 0.007, 0.030, 0.044, and 0.091, respectively. Similarly for the exterior girder, the fractional changes are 0.006, 0.024, 0.036, and 0.074, respectively.

3. Since the change in girder distribution factor is directly proportional to a change in moment for each girder, which is directly proportional to a change in strain, which is directly proportional to a change in the dynamic impact factor, the fractional changes calculated above were multiplied by the dynamic impact factors determined in Section 6.4.2 to remove the effects of centrifugal force. This was accomplished on the interior girder by increasing the calculated DIF by the fractional changes determined for each velocity. On the exterior girder, the DIFs were decreased by the fractional changes determined for each velocity. For example, if the original DIF on the exterior girder at a velocity of 35 mph was 28%, the new value with centrifugal effects removed is 28% - 0.074 (28%) = 25.9%.

The result of this process is that the impact factors for the interior girder and exterior girder draw closer to one another after the centrifugal effects have been removed. This can be seen by comparing the before and after plots of the girder dynamic impact factors as shown by Figure 6-16 and Figure 6-27, respectively. The new average value for the interior girder is 1.30, while that for the exterior girder is 1.32. These values are slightly higher than the code recommended value of 1.25 (AASHTO, 2003a). Figure 6-28 provides the values for the constant velocity tests (D1-D3) only. This plot clearly shows the convergence of the dynamic impact factors for the two girders once centrifugal effects have been removed.

6.4.4 Error due to Transverse Position of Vehicle

Some error inherently exists in the determination of the dynamic impact factors since the exact transverse position of the vehicle in the dynamic tests is not known. The truck operators were given instructions to travel along the center of the roadway (i.e., midway between the girders). However, maintaining this position while driving along a curve at speeds up to 35 mph was not an easy task. Variances up to a foot may have occurred in either direction. As for the transverse position of the vehicles in the static tests used for determining the DIF, the value was known to within a few inches.

The error due to the difference in transverse positioning of the moving vehicles versus the static ones can be approximated using Steps 2 and 3 from Section 6.4.3 . With a Δ of ± 1 foot, the percent change for the interior girder is $\pm 10.6\%$, while that for the exterior girder is $\pm 8.7\%$. These are significant values and are on par with those for the centrifugal effects. However, it is expected that these contributions would somewhat average out due to the equal likelihood that the trucks shifted slightly in and out.

6.4.5 Summary of Dynamic Impact Factor for Mn/DOT Bridge No. 69824

The results of this limited investigation into the dynamic behavior of Mn/DOT Bridge No. 69824 indicate that the recommended dynamic impact factors for horizontally curved steel I-girder bridges by the *Guide Specifications for Horizontally Curved Steel Girder Highway Bridges* (AASHTO, 2003a) are reasonable. The calculated average value of 1.30 and the modified values of 1.30 and 1.32 with the removal of centrifugal effects compare well with the recommended value of 1.25 for the girders. If a full continuum of static test data along the bridge length was available, these values would compare even better since the calculated values would decrease. As for the diaphragms, it is difficult to make conclusions based on so few data points, but from what is available from the tests, the recommended dynamic impact factor of 1.30 is a rational value. Although the code (AASHTO, 2003a) does not specifically recommend dynamic impact factors for lateral wind bracing, it is recommended that the higher values used for cross-frames and diaphragms be used as well for the lateral wind bracing.

Interior Girder C: Neutral Axis Locations from Base of Girder (inches)									
Section	Static Tests				Dynamic Tests				Combined Average
	Min	Max	Average	St. Dev.	Min	Max	Average	St. Dev.	
10Z	64.9	85.1	70.5	4.7	66.7	75.5	71.4	1.9	70.9
9B	55.3	84.6	65.1	6.5	58.0	74.6	65.5	3.7	65.3
9C	64.4	74.9	70.3	2.8	66.9	77.6	71.6	2.6	71.0
9H	66.2	89.8	73.6	3.8	67.4	77.0	72.2	1.9	72.9
9J	65.7	81.6	74.3	3.3	67.4	78.9	72.5	1.9	73.4
9L	70.8	77.0	74.2	1.6	67.4	80.3	73.4	2.2	73.8
9N	58.1	98.7	76.3	9.9	66.0	80.0	74.6	2.0	75.5
9O	59.0	77.6	67.5	4.1	65.0	81.5	72.9	2.3	70.2
8C	72.3	88.7	83.3	2.7	70.7	89.2	81.5	2.6	82.4
8D	64.5	85.4	74.6	4.7	63.2	85.7	73.9	2.8	74.2

Table 6-1: Interior Girder C Neutral Axis Locations

Exterior Girder A: Neutral Axis Locations from Base of Girder (inches)									
Section	Static Tests				Dynamic Tests				Combined Average
	Min	Max	Average	St. Dev.	Min	Max	Average	St. Dev.	
10Z	*	*	*	*	*	*	*	*	*
9B	*	*	*	*	*	*	*	*	*
9C	58.9	75.9	69.9	4.8	69.0	88.7	75.6	3.2	72.8
9H	64.5	84.7	77.3	4.4	75.4	91.1	81.7	3.1	79.5
9J	65.2	83.8	79.3	3.2	74.9	90.9	82.9	3.0	81.1
9L	68.1	96.0	75.7	4.6	69.5	88.5	77.5	2.7	76.6
9N	74.8	90.8	78.7	3.6	71.2	85.3	79.5	2.3	79.1
9O	62.1	85.6	68.7	4.6	56.6	65.0	61.2	1.6	65.0
8C	75.0	95.9	79.7	4.7	73.3	88.0	80.3	3.2	80.0
8D	59.0	85.8	69.5	4.6	67.6	80.2	72.8	2.2	71.2

* incomplete data

Table 6-2: Exterior Girder A Neutral Axis Locations

Diaphragms: Neutral Axis Locations from Base of Diaphragm (inches)									
Section	Static Tests				Dynamic Tests				Combined Average
	Min	Max	Average	St. Dev.	Min	Max	Average	St. Dev.	
9F: I	**	**	**	**	**	**	**	**	**
QI	13.1	18.2	14.7	1.9	19.4	23.2	21.3	1.2	18.0
M	11.1	15.0	12.6	1.2	12.3	16.6	14.2	1.0	13.4
QE	15.2	19.7	16.9	1.4	22.2	26.8	24.4	1.5	20.6
E	**	**	**	**	**	**	**	**	**
8A: I	**	**	**	**	**	**	**	**	**
QI	**	**	**	**	**	**	**	**	**
M	14.1	24.0	17.9	3.9	12.3	15.3	13.3	0.5	15.6
QE	11.9	16.5	14.4	1.2	15.6	18.2	17.0	0.7	15.7
E	**	**	**	**	**	**	**	**	**

** unreliable data

Table 6-3: Diaphragm Neutral Axis Locations

Measured Effective Widths and Moments of Inertia for Composite Girders using N = 6													
Section	Girder	t _{bf}	t _{tf}	A _s	haunch	y _s	y _c	y _{NA-m}	b _{eff} /N	I _{steel}	I _{total}	I _{total} /I _{steel}	b _{eff} (in)
		(in)	(in)	(in ²)	(in)	(in)	(in)	(in)	(in)	(in ⁴)	(in ⁴)		
10Z	Int. C	1.00	1.00	75.00	2.88	40.00	87.38	70.94	15.68	75945	186822	2.5 **	94.1 **
	Ext. A	0.88	0.88	70.50	3.00	39.88	87.25	*	**	68767	**		
9B	Int. C	1.00	1.00	75.00	2.88	40.00	87.38	65.28	9.53	75945	166329	2.2 **	57.2 **
	Ext. A	1.38	1.38	88.50	2.50	40.38	87.75	*	**	97748	**		
9C	Int. C	0.88	0.88	70.50	3.00	39.88	87.25	70.99	14.99	68767	173610	2.5 2.6	90.0 106.6
	Ext. A	0.88	0.88	70.50	3.00	39.88	87.25	72.76	17.77	68767	179668		
9H	Int. C	0.88	0.88	70.50	3.00	39.88	87.25	72.89	18.01	68767	180129	2.6 3.0	108.1 240.9
	Ext. A	0.88	0.88	70.50	3.00	39.88	87.25	79.51	40.14	68767	203600		
9J	Int. C	0.88	0.88	70.50	3.00	39.88	87.25	73.42	18.99	68767	181947	2.6 3.0	114.0 315.2
	Ext. A	0.88	0.88	70.50	3.00	39.88	87.25	81.10	52.54	68767	209657		
9L	Int. C	0.88	0.88	70.50	3.00	39.88	87.25	73.82	19.80	68767	183349	2.7 2.8	118.8 161.6
	Ext. A	0.88	0.88	70.50	3.00	39.88	87.25	76.57	26.93	68767	192974		
9N	Int. C	0.88	0.88	70.50	3.00	39.88	87.25	75.46	23.65	68767	189071	2.7 2.6	141.9 272.4
	Ext. A	1.50	1.50	93.00	2.38	40.50	87.88	79.09	45.39	105107	277888		
9O	Int. C	1.88	1.88	106.50	2.00	40.88	88.25	70.20	19.23	127456	276598	2.2 1.9	115.4 86.5
	Ext. A	2.63	2.63	133.50	1.25	41.63	89.00	64.98	14.42	173399	321979		
8C	Int. C	0.88	0.88	70.50	3.00	39.88	87.25	82.42	69.01	68767	215061	3.1 2.7	414.1 309.2
	Ext. A	1.50	1.50	93.00	2.38	40.50	87.88	79.96	51.54	105107	282106		
8D	Int. C	0.88	0.88	70.50	3.00	39.88	87.25	74.22	20.65	68767	184738	2.7 2.8	123.9 122.3
	Ext. A	1.63	1.00	86.25	2.88	35.37	88.00	71.16	20.38	91843	255588		
For all: b _{bf} = b _{tf} = 18 inches, dw = 78 inches, tw = 0.5 inches, ts = 9 inches												Average:	2.62
*data not available ** calculation not possible												St.Dev.:	166.22 96.90

Table 6-4: Measured Effective Widths and Moments of Inertia for Girders using N = 6

Measured Effective Widths and Moments of Inertia for Composite Diaphragms (N = 6)													
Section	t _{bf}	t _{tf}	A _s	haunch	y _s	y _c	y _{NA-m}	b _{eff} /N	I _{steel}	I _{total}	I _{total} /I _{steel}	b _{eff} (in)	
	(in)	(in)	(in ²)	(in)	(in)	(in)	(in)	(in)	(in)	(in ⁴)	(in ⁴)		
9F:	QI	0.52	0.52	15.99	3.00	10.40	28.30	18.00	1.31	1123	3377	3.01 1.79 3.74	7.86 2.16 14.24
	M	0.52	0.52	15.99	3.00	10.40	28.30	13.42	0.36	1123	2008		
	QE	0.52	0.52	15.99	3.00	10.40	28.30	20.64	2.37	1123	4197		
8A:	QI	0.52	0.52	15.99	3.00	10.40	28.30	*	*	1123	*	2.38 2.39	4.42 4.49
	M	0.52	0.52	15.99	3.00	10.40	28.30	15.64	0.74	1123	2669		
	QE	0.52	0.52	15.99	3.00	10.40	28.30	15.71	0.75	1123	2688		
Note: knee brace regions I and E not computed due to low strain levels												Average:	2.66
For all: b _{bf} = b _{tf} = 8.22 in., dw = 19.76 in., tw = 0.375 in., ts = 9 in.												St.Dev.:	6.63 4.22
*data not available													

Table 6-5: Measured Effective Widths and Moments of Inertia for Diaphragms using N = 6

GDFs for Loads Centered on Pier 9								
Interior Girder								
Test	<u>9C</u>	<u>9H</u>	<u>9J</u>	<u>9L</u>	<u>9N</u>	<u>9O</u>	<u>8C</u>	<u>8D</u>
S14	0.56	0.52	0.46	0.48	0.47	0.55	0.51	0.42
Average =	0.56	0.52	0.46	0.48	0.47	0.55	0.51	0.42
Exterior Girder								
Test	<u>9C</u>	<u>9H</u>	<u>9J</u>	<u>9L</u>	<u>9N</u>	<u>9O</u>	<u>8C</u>	<u>8D</u>
S14	0.44	0.48	0.54	0.52	0.53	0.45	0.49	0.58
Average =	0.44	0.48	0.54	0.52	0.53	0.45	0.49	0.58

Table 6-6: GDFs for Loads Centered on Pier 9

GDFs for Loads Centered on Span 98								
Interior Girder								
Test	<u>9C</u>	<u>9H</u>	<u>9J</u>	<u>9L</u>	<u>9N</u>	<u>9O</u>	<u>8C</u>	<u>8D</u>
S4	0.43	0.43	0.40	0.46	0.50	0.57	0.51	0.38
S5	0.48	0.46	0.43	0.47	0.44	0.54	0.50	0.39
S6	0.53	0.46	0.40	0.43	**	0.64	0.52	0.40
S11	0.47	0.48	0.45	0.46	0.46	0.48	0.48	0.39
S12	0.49	0.49	0.43	0.46	0.47	0.48	0.48	0.39
S13	0.50	0.48	0.44	0.47	0.40	0.49	0.48	0.39
S15	0.51	0.48	0.42	0.49	0.44	0.48	0.48	0.39
S16	0.51	0.50	0.44	0.48	0.47	0.48	0.48	0.39
S17	0.50	0.49	0.44	*	*	*	*	*
S18	0.52	0.50	0.44	0.48	0.47	0.50	0.49	0.42
S19	0.52	0.50	0.44	0.48	0.47	0.50	0.48	0.42
Average =	0.50	0.48	0.43	0.47	0.46	0.52	0.49	0.40
Exterior Girder								
Test	<u>9C</u>	<u>9H</u>	<u>9J</u>	<u>9L</u>	<u>9N</u>	<u>9O</u>	<u>8C</u>	<u>8D</u>
S4	0.57	0.57	0.60	0.54	0.50	0.43	0.49	0.62
S5	0.52	0.54	0.57	0.53	0.56	0.46	0.50	0.61
S6	0.47	0.54	0.60	0.57	**	0.36	0.48	0.60
S11	0.53	0.52	0.55	0.54	0.54	0.52	0.52	0.61
S12	0.51	0.51	0.57	0.54	0.53	0.52	0.52	0.61
S13	0.50	0.52	0.56	0.53	0.60	0.51	0.52	0.61
S15	0.49	0.52	0.58	0.51	0.56	0.52	0.52	0.61
S16	0.49	0.50	0.56	0.52	0.53	0.52	0.52	0.61
S17	0.50	0.51	0.56	*	*	*	*	*
S18	0.48	0.50	0.56	0.52	0.53	0.50	0.51	0.58
S19	0.48	0.50	0.56	0.52	0.53	0.50	0.52	0.58
Average =	0.50	0.52	0.57	0.53	0.54	0.48	0.51	0.60
* Data unavailable								
** GDF not possible since girder moments have opposite signs								

Table 6-7: GDFs for Loads Centered on Span 9-8

GDFs for Loads Centered on Pier 8								
Interior Girder								
<u>Test</u>	<u>9C</u>	<u>9H</u>	<u>9J</u>	<u>9L</u>	<u>9N</u>	<u>9O</u>	<u>8C</u>	<u>8D</u>
S3	0.25	0.22	0.17	0.26	0.30	0.80	0.54	0.38
S10	0.70	0.62	0.52	0.58	**	0.49	0.51	0.47
S25	0.53	0.52	0.45	0.72	0.43	0.47	0.50	0.42
S26	0.52	0.51	0.45	0.53	0.42	0.48	0.50	0.40
S27	0.52	0.51	0.46	0.59	0.43	0.48	0.50	0.41
S28	0.52	0.52	0.46	0.70	0.43	0.47	0.50	0.40
Average =	0.51	0.48	0.42	0.56	0.40	0.53	0.51	0.41
Exterior Girder								
<u>Test</u>	<u>9C</u>	<u>9H</u>	<u>9J</u>	<u>9L</u>	<u>9N</u>	<u>9O</u>	<u>8C</u>	<u>8D</u>
S3	0.75	0.78	0.83	0.74	0.70	0.20	0.46	0.62
S10	0.30	0.38	0.48	0.42	**	0.51	0.49	0.53
S25	0.47	0.48	0.55	0.28	0.57	0.53	0.50	0.58
S26	0.48	0.49	0.55	0.47	0.58	0.52	0.50	0.60
S27	0.48	0.49	0.54	0.41	0.57	0.52	0.50	0.59
S28	0.48	0.48	0.54	0.30	0.57	0.53	0.50	0.60
Average =	0.49	0.52	0.58	0.44	0.60	0.47	0.49	0.59
** GDF not possible since girder moments have opposite signs								

Table 6-8: GDFs for Loads Centered on Pier 8

GDFs for Loads Centered on Span 87								
Interior Girder								
<u>Test</u>	<u>9C</u>	<u>9H</u>	<u>9J</u>	<u>9L</u>	<u>9N</u>	<u>9O</u>	<u>8C</u>	<u>8D</u>
S1	0.64	0.43	0.40	0.43	0.44	0.48	0.56	0.41
S2	0.67	0.44	0.40	0.43	0.44	0.49	0.69	0.44
S7	0.53	0.44	0.39	0.42	0.43	0.47	0.52	0.41
S8	0.51	0.44	0.39	0.42	0.44	0.48	0.56	0.42
S9	0.51	0.43	0.39	0.42	0.44	0.48	**	0.44
S20	0.68	0.43	0.40	0.42	0.43	0.47	0.54	0.41
S21	0.76	0.44	0.40	0.43	0.43	0.48	0.54	0.41
S22	**	0.36	0.41	0.41	0.44	0.47	0.54	0.42
S23	**	0.38	0.39	0.41	0.43	0.47	0.52	0.41
S24	**	0.36	0.39	0.40	0.43	0.47	0.52	0.39
Average =	0.61	0.42	0.40	0.42	0.44	0.48	0.56	0.41
Exterior Girder								
<u>Test</u>	<u>9C</u>	<u>9H</u>	<u>9J</u>	<u>9L</u>	<u>9N</u>	<u>9O</u>	<u>8C</u>	<u>8D</u>
S1	0.36	0.57	0.60	0.57	0.56	0.52	0.44	0.59
S2	0.33	0.56	0.60	0.57	0.56	0.51	0.31	0.56
S7	0.47	0.56	0.61	0.58	0.57	0.53	0.48	0.59
S8	0.49	0.56	0.61	0.58	0.56	0.52	0.44	0.58
S9	0.49	0.57	0.61	0.58	0.56	0.52	**	0.56
S20	0.32	0.57	0.60	0.58	0.57	0.53	0.46	0.59
S21	0.24	0.56	0.60	0.57	0.57	0.52	0.46	0.59
S22	**	0.64	0.59	0.59	0.56	0.53	0.46	0.58
S23	**	0.62	0.61	0.59	0.57	0.53	0.48	0.59
S24	**	0.64	0.61	0.60	0.57	0.53	0.48	0.61
Average =	0.39	0.58	0.60	0.58	0.56	0.52	0.44	0.59
** GDF not possible since girder moments have opposite signs								

Table 6-9: GDFs for Loads Centered on Span 8-7

GDFs for Loads Shifted to Interior Girder on Span 98								
Interior Girder								
<u>Test</u>	<u>9C</u>	<u>9H</u>	<u>9J</u>	<u>9L</u>	<u>9N</u>	<u>9O</u>	<u>8C</u>	<u>8D</u>
S32	0.55	0.65	0.61	0.60	0.49	0.67	0.58	0.41
S33	0.62	0.64	0.58	0.62	0.63	0.70	0.59	0.41
S34	0.66	0.63	0.59	0.61	0.69	0.70	0.58	0.41
Average =	0.61	0.64	0.59	0.61	0.60	0.69	0.58	0.41
Exterior Girder								
<u>Test</u>	<u>9C</u>	<u>9H</u>	<u>9J</u>	<u>9L</u>	<u>9N</u>	<u>9O</u>	<u>8C</u>	<u>8D</u>
S32	0.45	0.35	0.39	0.40	0.51	0.33	0.42	0.59
S33	0.38	0.36	0.42	0.38	0.37	0.30	0.41	0.59
S34	0.34	0.37	0.41	0.39	0.31	0.30	0.42	0.59
Average =	0.39	0.36	0.41	0.39	0.40	0.31	0.42	0.59

Table 6-10: GDFs for Loads Shifted to Interior Girder on Span 9-8

GDFs for Loads Shifted to Exterior Girder on Span 98							
Interior Girder							
Test	<u>9C</u>	<u>9H</u>	<u>9J</u>	<u>9L</u>	<u>9N</u>	<u>9O</u>	<u>8C</u>
S29	0.38	0.35	0.32	0.38	0.49	0.34	0.42
S30	0.34	0.34	0.31	0.34	0.31	0.31	0.40
S31	0.32	0.33	0.30	0.33	0.25	0.31	0.40
Average =	0.35	0.34	0.31	0.35	0.35	0.32	0.41
Exterior Girder							
Test	<u>9C</u>	<u>9H</u>	<u>9J</u>	<u>9L</u>	<u>9N</u>	<u>9O</u>	<u>8C</u>
S29	0.62	0.65	0.68	0.62	0.51	0.66	0.58
S30	0.66	0.66	0.69	0.66	0.69	0.69	0.60
S31	0.68	0.67	0.70	0.67	0.75	0.69	0.60
Average =	0.65	0.66	0.69	0.65	0.65	0.68	0.59

Table 6-11: GDFs for Loads Shifted to Exterior Girder on Span 9-8

GDFs for Loads Shifted to Interior Girder on Span 98 and to Exterior Girder on Span 87							
Interior Girder							
Test	<u>9C</u>	<u>9H</u>	<u>9J</u>	<u>9L</u>	<u>9N</u>	<u>9O</u>	<u>8C</u>
S40	0.62	0.68	0.64	0.82	0.19	0.54	0.52
S41	0.63	0.73	0.76	**	0.30	0.48	0.49
S42	0.64	0.68	0.70	**	0.19	0.49	0.49
S43	0.64	0.71	0.80	**	0.26	0.46	0.49
Average =	0.63	0.70	0.73	0.82	0.24	0.49	0.50
Exterior Girder							
Test	<u>9C</u>	<u>9H</u>	<u>9J</u>	<u>9L</u>	<u>9N</u>	<u>9O</u>	<u>8C</u>
S40	0.38	0.32	0.36	0.18	0.81	0.46	0.48
S41	0.37	0.27	0.24	**	0.70	0.52	0.51
S42	0.36	0.32	0.30	**	0.81	0.51	0.51
S43	0.36	0.29	0.20	**	0.74	0.54	0.51
Average =	0.37	0.30	0.27	0.18	0.76	0.51	0.50
** GDF not possible since girder moments have opposite signs							

Table 6-12: GDFs for Loads Shifted to Interior Girder on Span 9-8 and Exterior Girder on Span 8-7

GDFs for Loads Shifted to Exterior Girder on Span 98 and Interior Girder on Span 87								
Interior Girder								
<u>Test</u>	<u>9C</u>	<u>9H</u>	<u>9J</u>	<u>9L</u>	<u>9N</u>	<u>9O</u>	<u>8C</u>	<u>8D</u>
S35	0.46	0.32	0.18	0.15	0.53	0.46	0.51	0.60
S36	0.34	0.32	0.28	0.26	0.61	0.43	0.48	0.77
S37	0.31	0.29	0.22	**	0.56	0.46	0.52	0.61
S38	0.31	0.29	0.23	0.07	0.64	0.46	0.50	0.66
S39	0.31	0.28	0.19	**	0.60	0.48	0.52	0.62
Average =	0.35	0.30	0.22	0.16	0.59	0.46	0.51	0.65
Exterior Girder								
<u>Test</u>	<u>9C</u>	<u>9H</u>	<u>9J</u>	<u>9L</u>	<u>9N</u>	<u>9O</u>	<u>8C</u>	<u>8D</u>
S35	0.54	0.68	0.82	0.85	0.47	0.54	0.49	0.40
S36	0.66	0.68	0.72	0.74	0.39	0.57	0.52	0.23
S37	0.69	0.71	0.78	**	0.44	0.54	0.48	0.39
S38	0.69	0.71	0.77	0.93	0.36	0.54	0.50	0.34
S39	0.69	0.72	0.81	**	0.40	0.52	0.48	0.38
Average =	0.65	0.70	0.78	0.84	0.41	0.54	0.49	0.35
** GDF not possible since girder moments have opposite signs								

Table 6-13: GDFs: for Loads Shifted to Exterior Girder on Span 98 and Interior Girder on Span 87

Average GDFs at Point of Loading			
<u>Girder</u>	<u>Transverse Load Position</u>		
	Centered between Girders	Shifted 5.5 ft toward Interior Girder	Shifted 5.5 ft toward Exterior Girder
Interior	0.45	0.66	0.23
Exterior	0.55	0.34	0.77

Table 6-14: Average GDFs at Point of Loading

Measured Stress for Static Tests at Section 9B Girder A

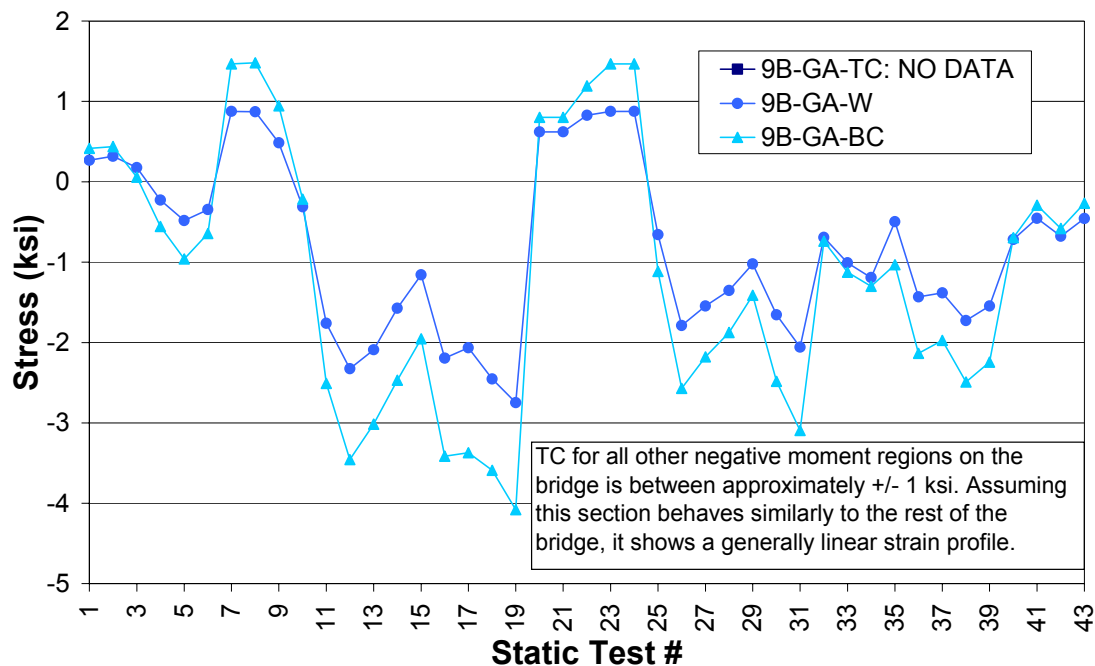


Figure 6-1: Linear Strain Profile Section 9B-GA

Measured Stress for Static Tests at Section 9J Girder A

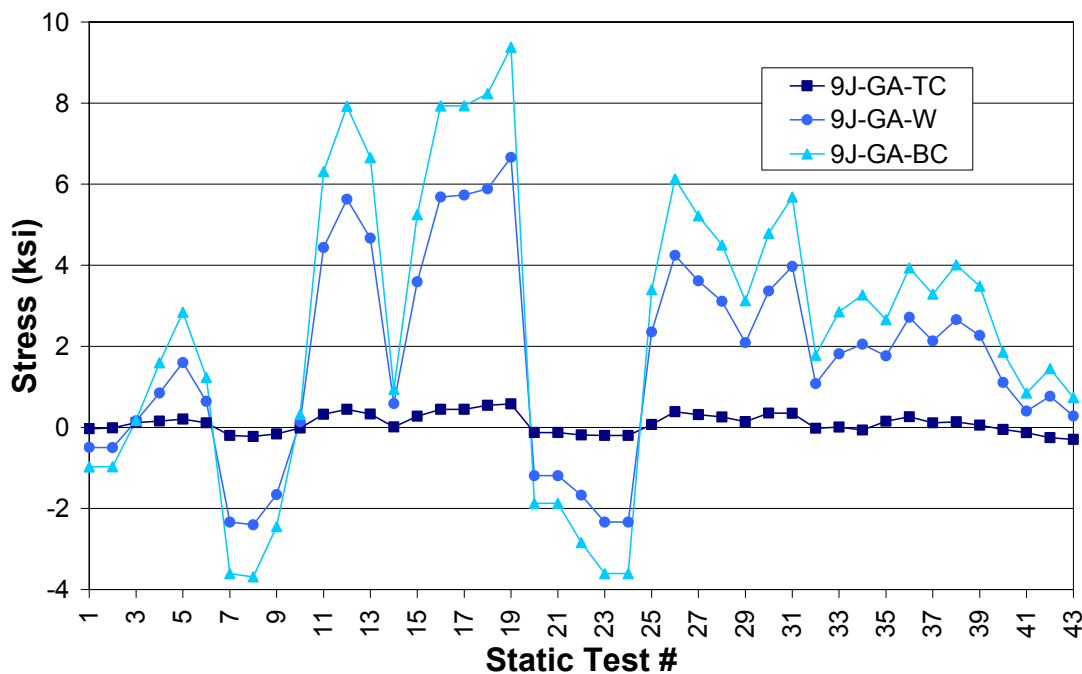


Figure 6-2: Linear Strain Profile Section 9J-GA

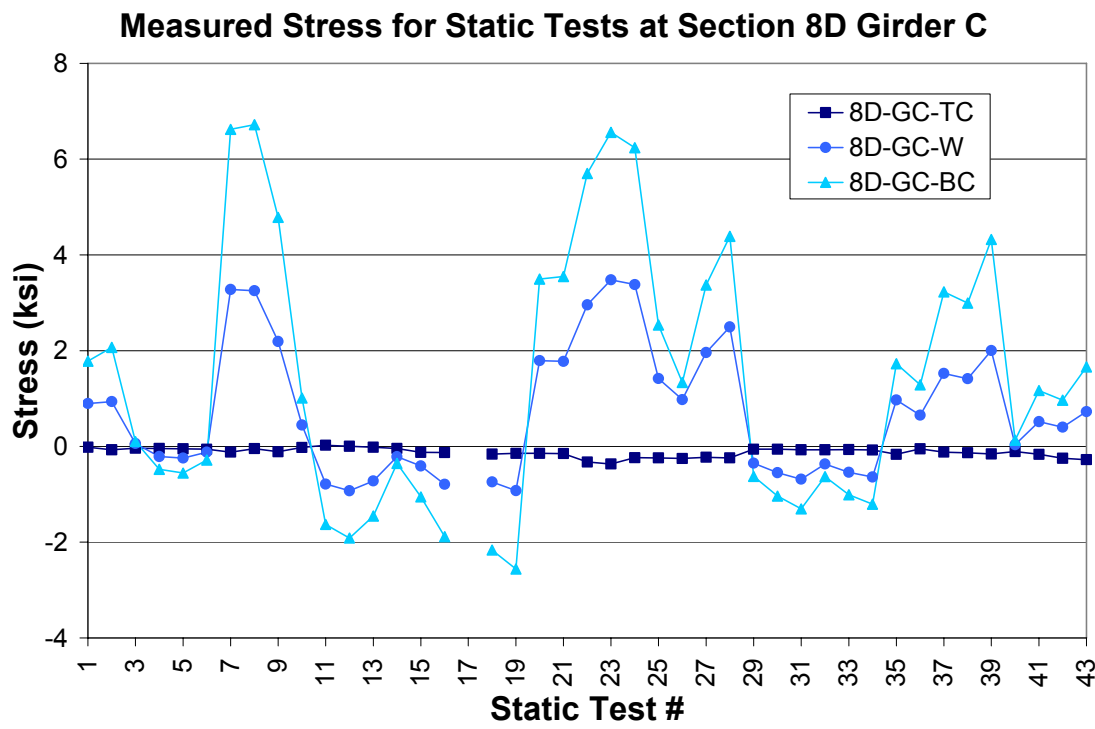


Figure 6-3: Linear Strain Profile Section 8D-GC

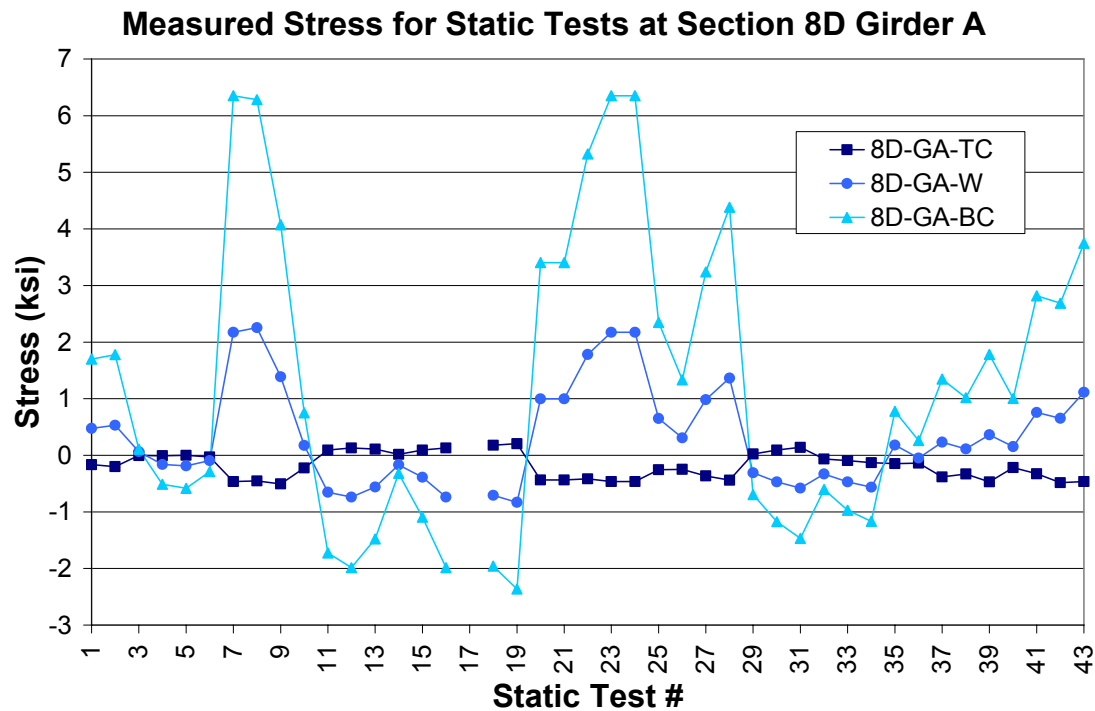


Figure 6-4: Linear Strain Profile Section 8D-GA

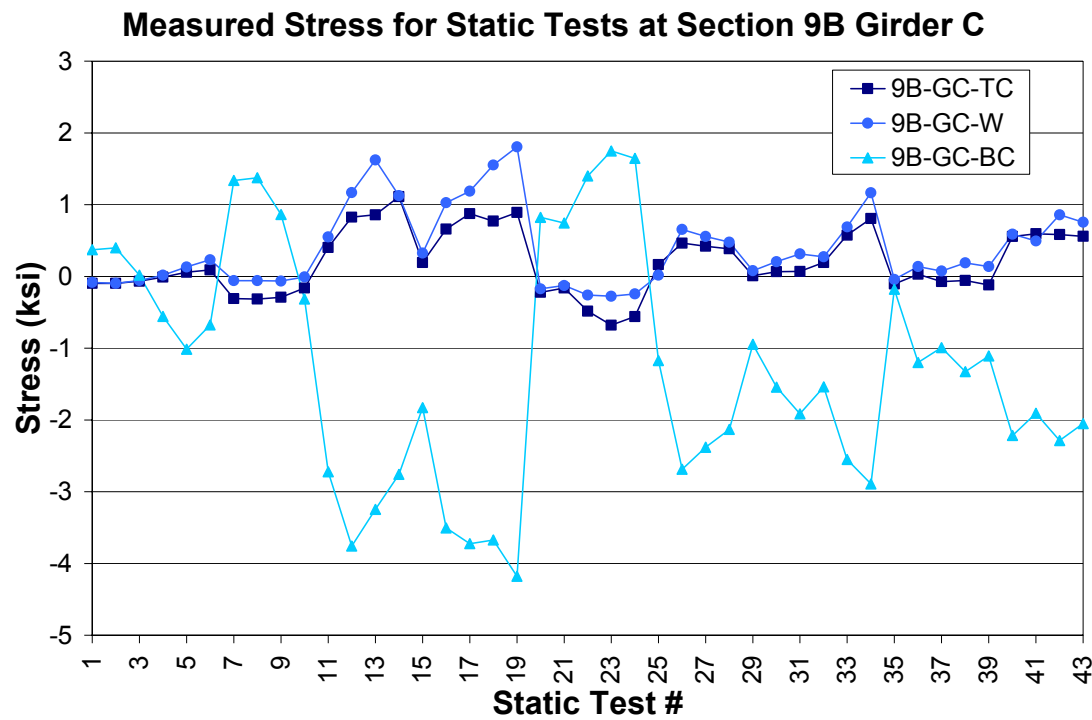


Figure 6-5: Nonlinear Strain Profile Section 9B-GC

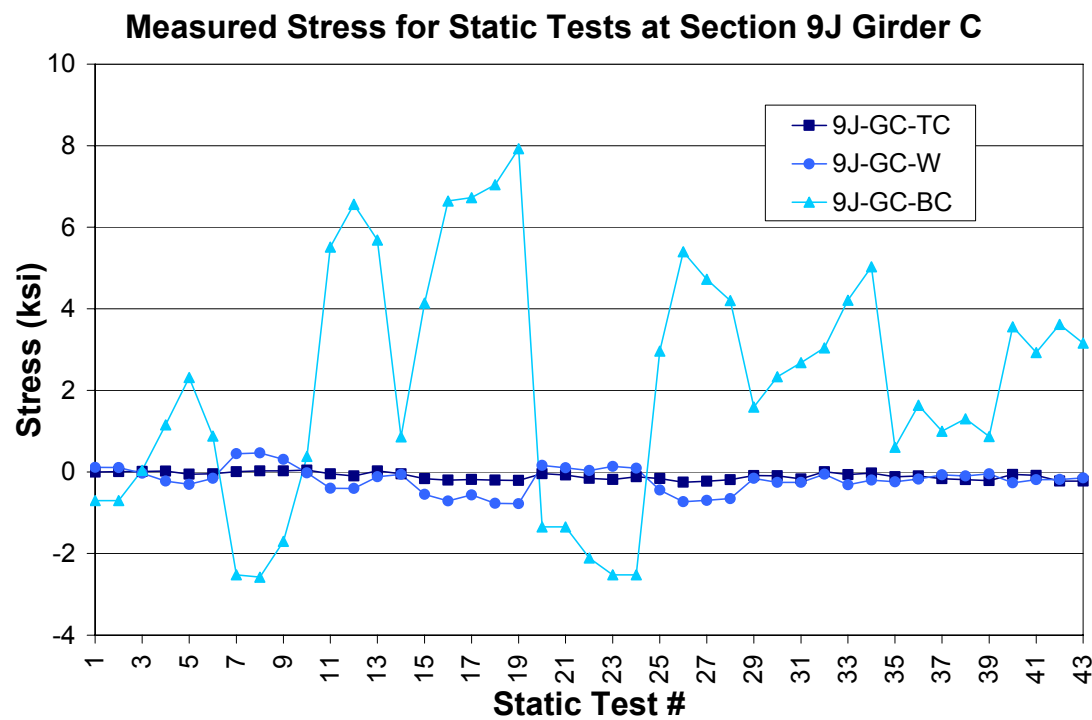


Figure 6-6: Nonlinear Strain Profile Section 9J-GC

Measured Stress for Static Tests at Section 9O Girder C

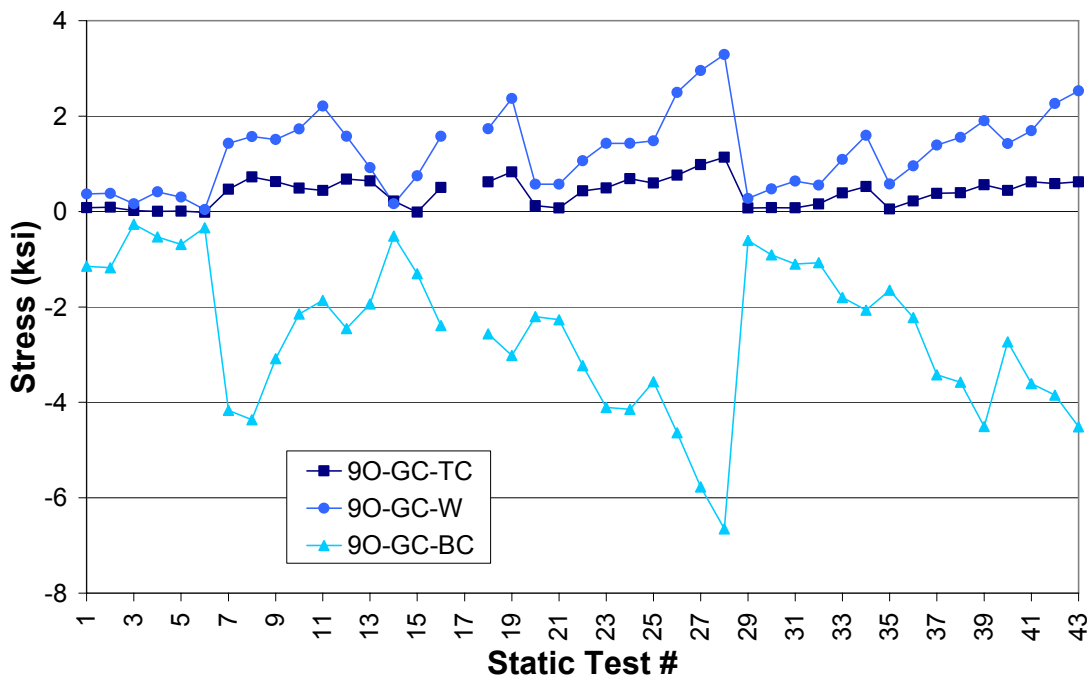


Figure 6-7: Nonlinear Strain Profile Section 9O-GC

Measured Stress for Static Tests at Section 9O Girder A

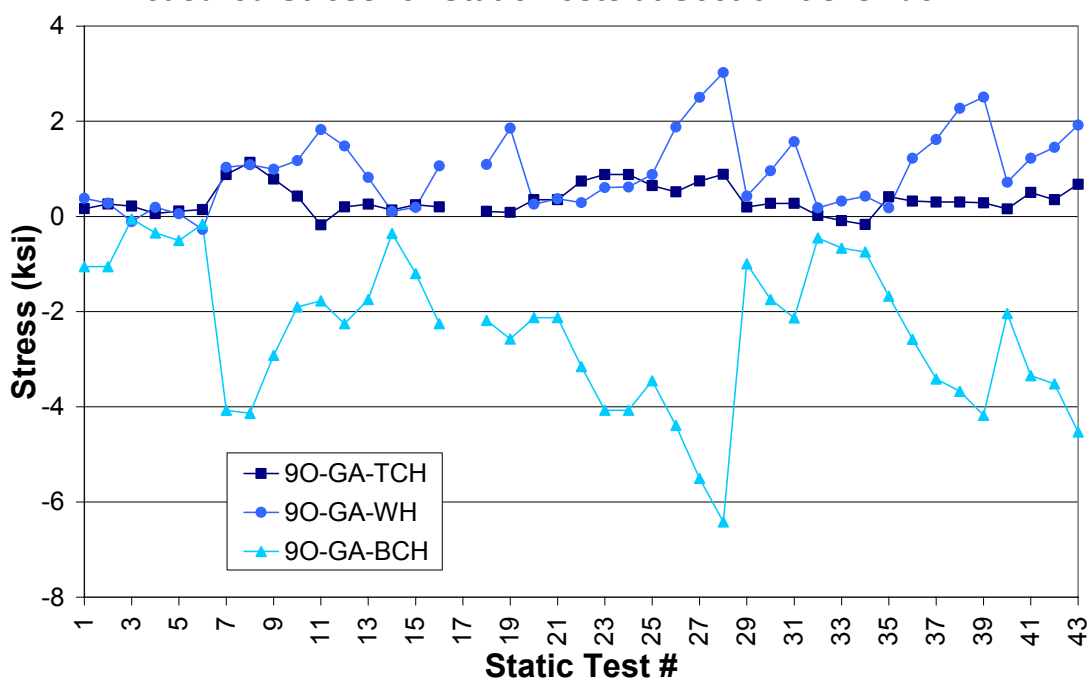


Figure 6-8: Nonlinear Strain Profile Section 9O-GA

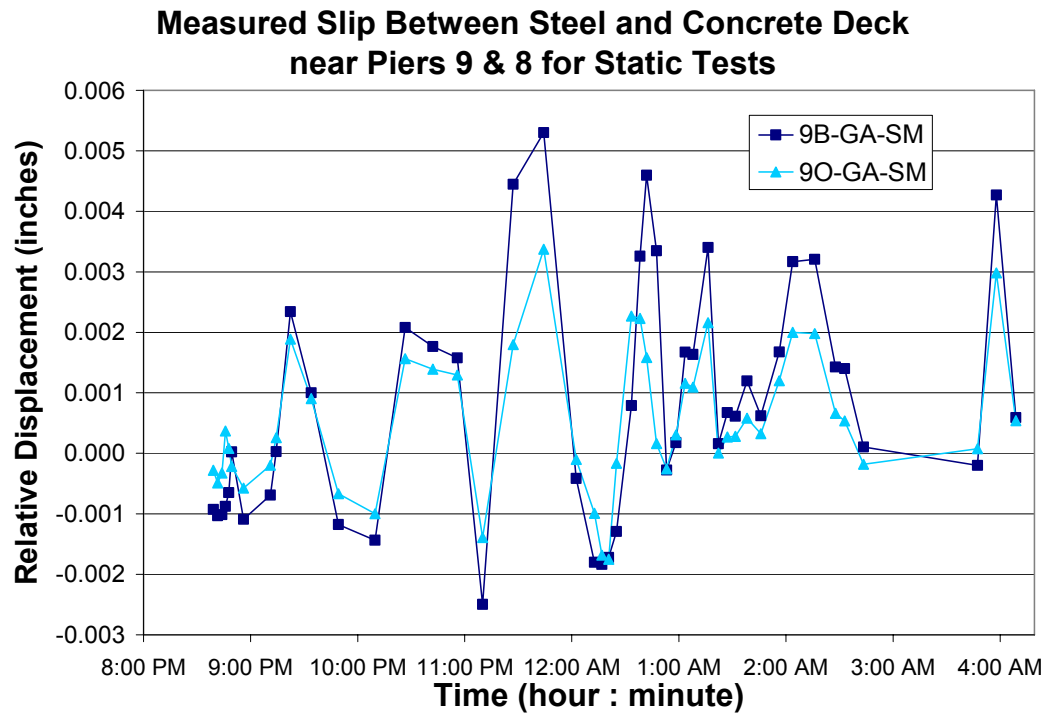


Figure 6-9: Slip at Steel Top Flange and Concrete Deck Interface

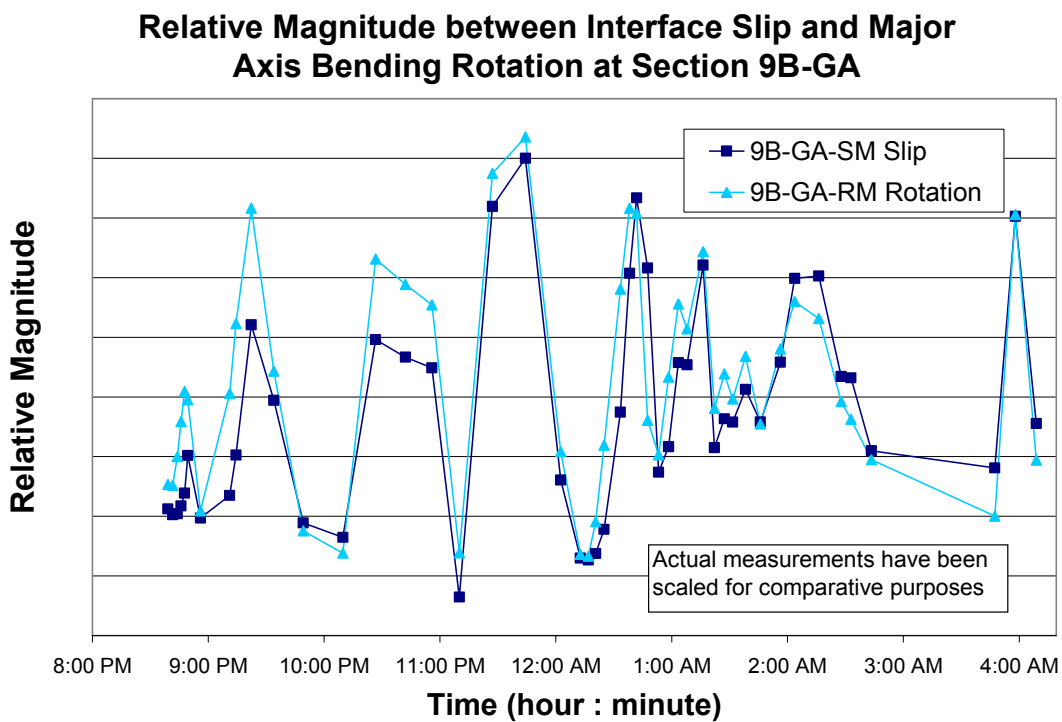


Figure 6-10: Relative Magnitude of Slip and Rotation at Section 9B-GA

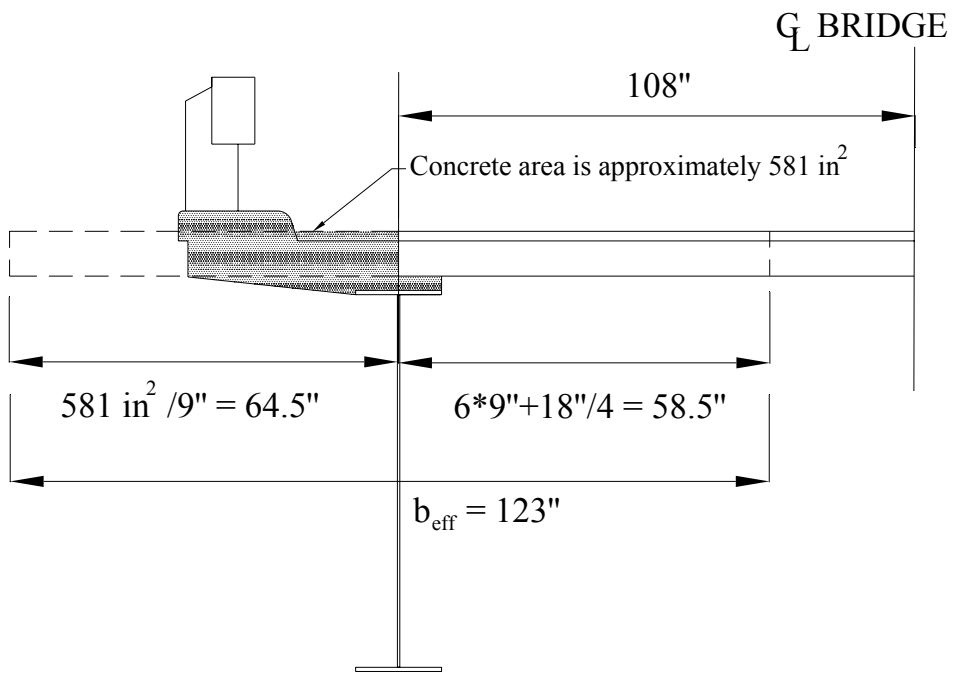


Figure 6-11: Effective Width Calculation

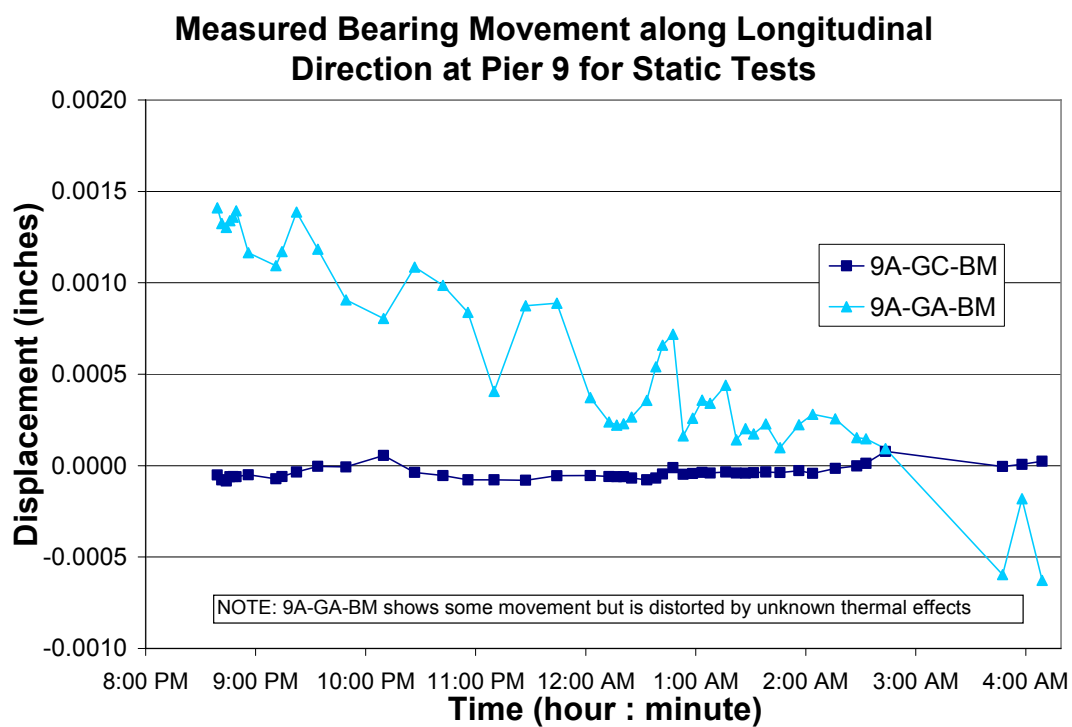


Figure 6-12: Measured Bearing Movement along Longitudinal Direction at Pier 9

Relative Magnitudes for Bearing Movement at 9A-GA and Major Axis Bending Rotation at 9B-GA

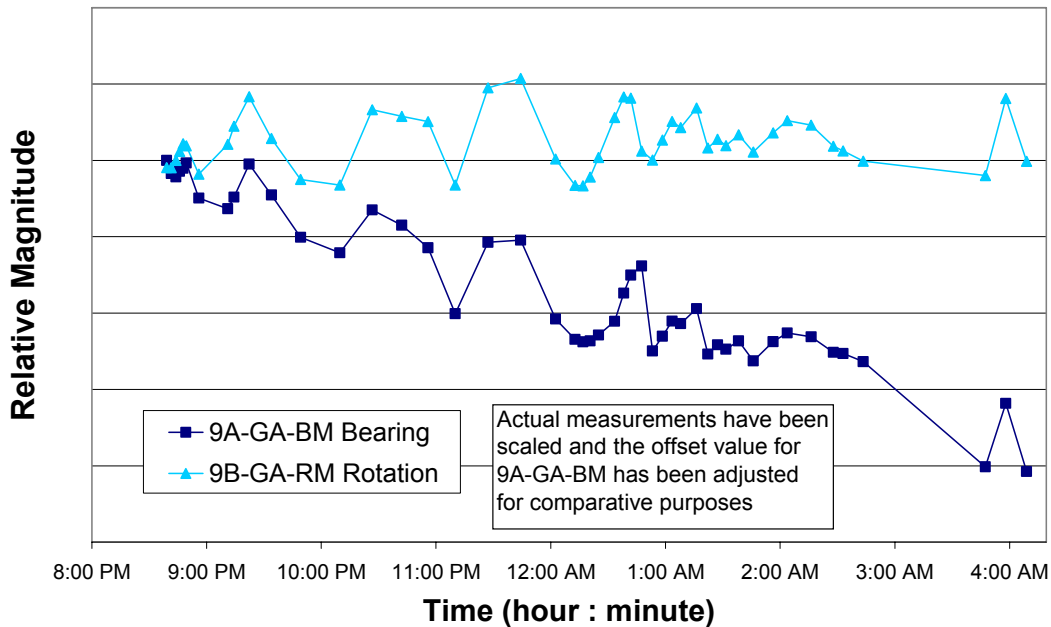


Figure 6-13: Relative Magnitude of Bearing Movement at 9A-GA and Rotation at Section 9B-GA

Generic Strain Profile for Gages During Dynamic Tests

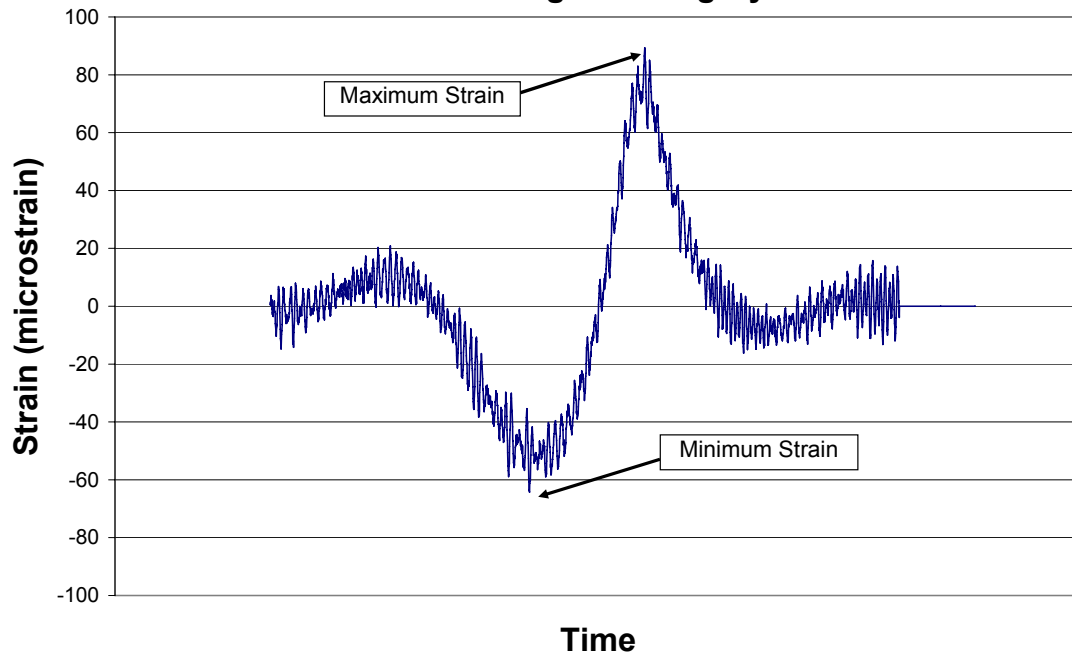


Figure 6-14: Generic Strain Profile for Gages during Dynamic Tests

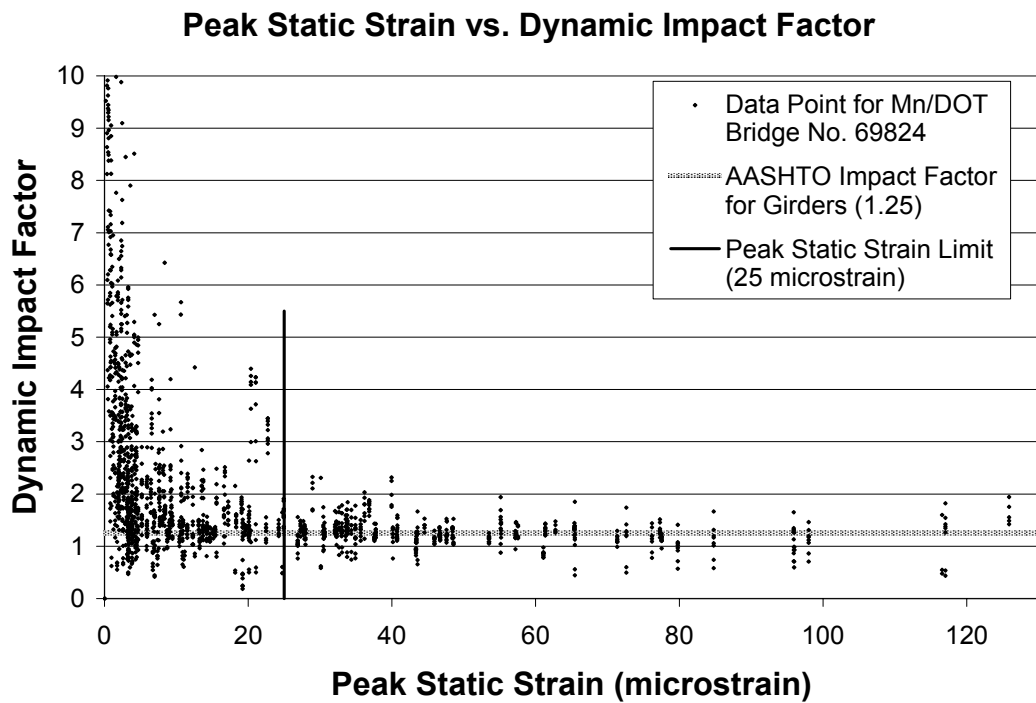


Figure 6-15: Exponential Decrease in DIF with Increase in Peak Strain

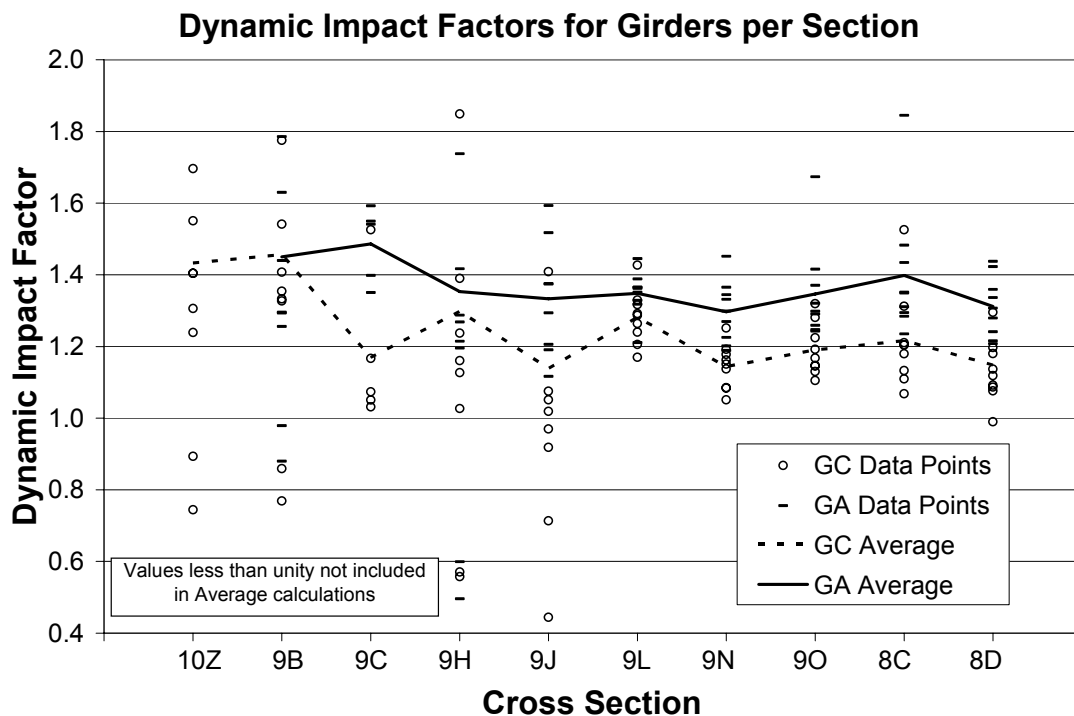


Figure 6-16: Girder Dynamic Impact Factors

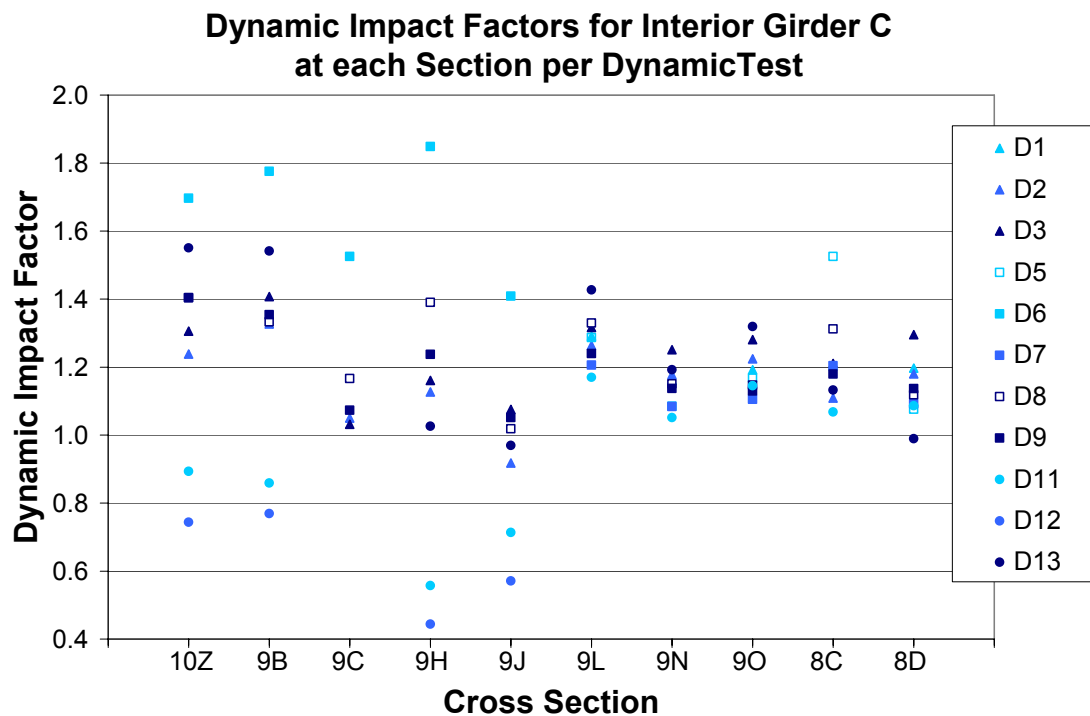


Figure 6-17: Interior Girder C DIF by Test

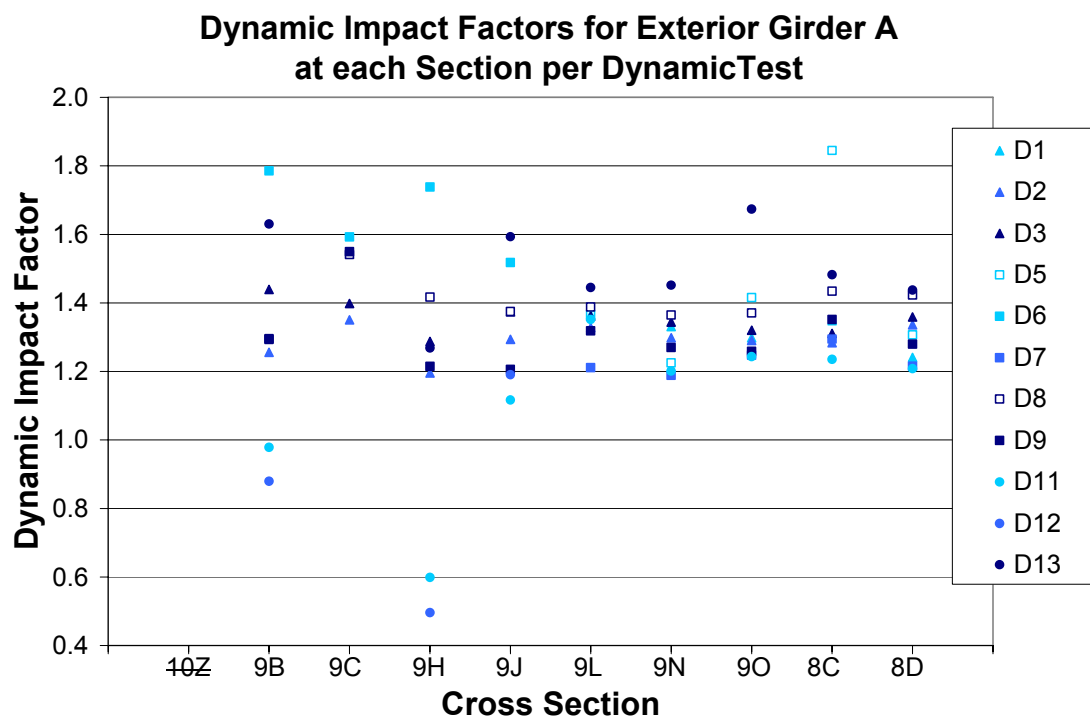


Figure 6-18: Exterior Girder A DIF by Test

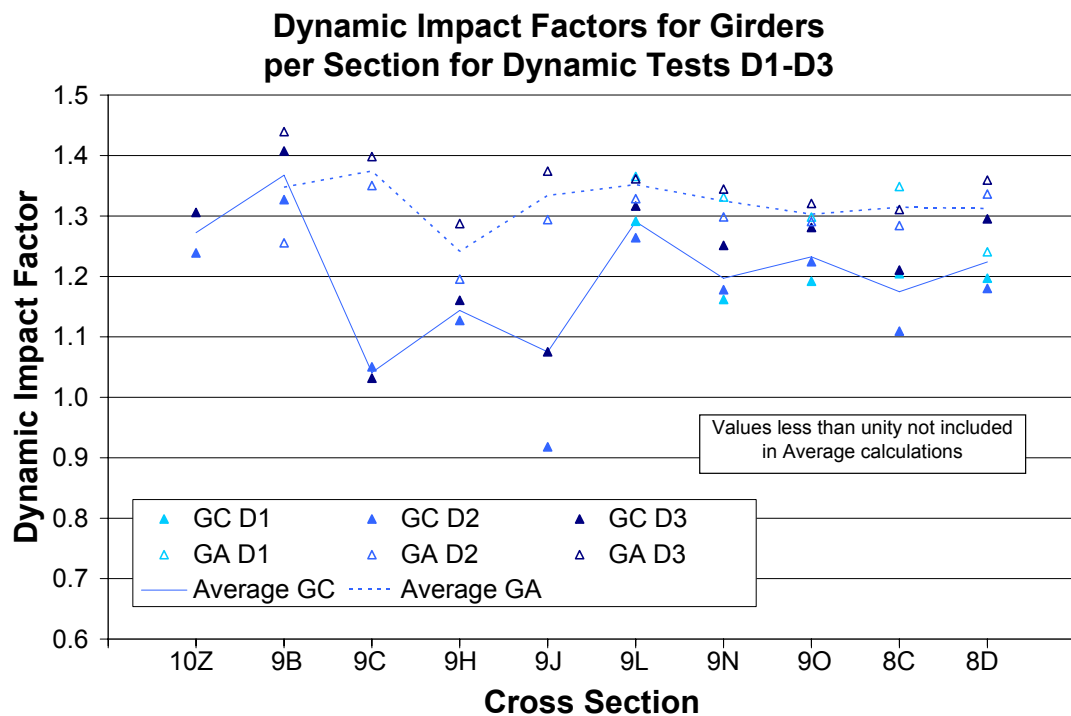


Figure 6-19: DIF for Tests D1-D3

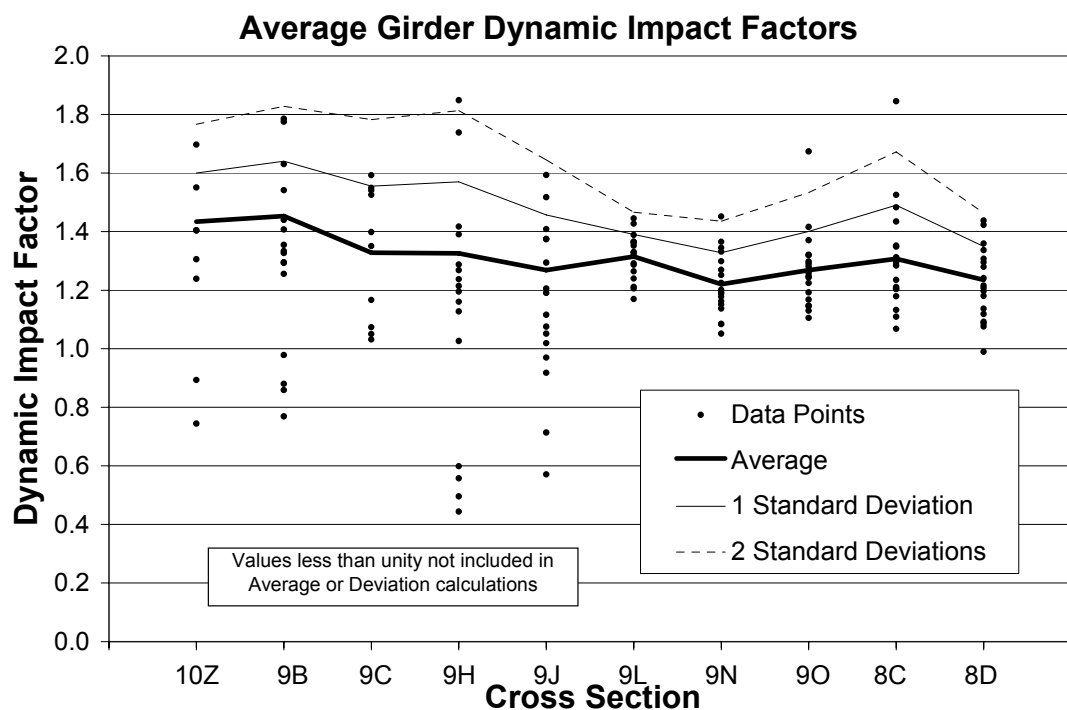


Figure 6-20: Average Girder DIF for Each Cross-Section

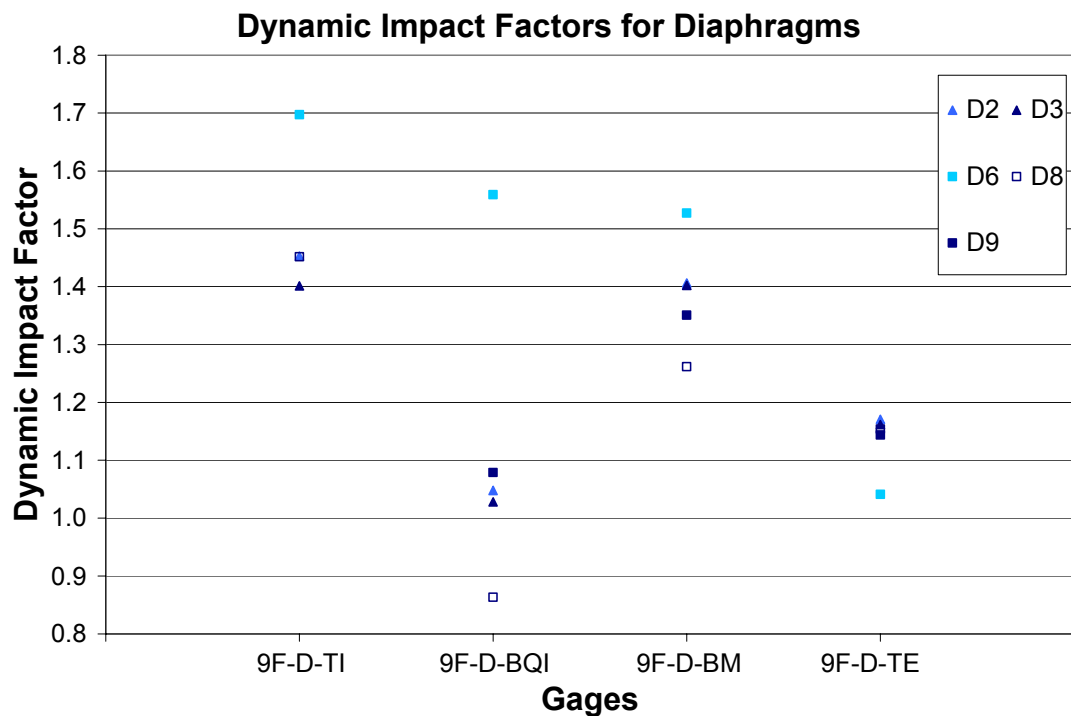


Figure 6-21: Diaphragm Dynamic Impact Factors

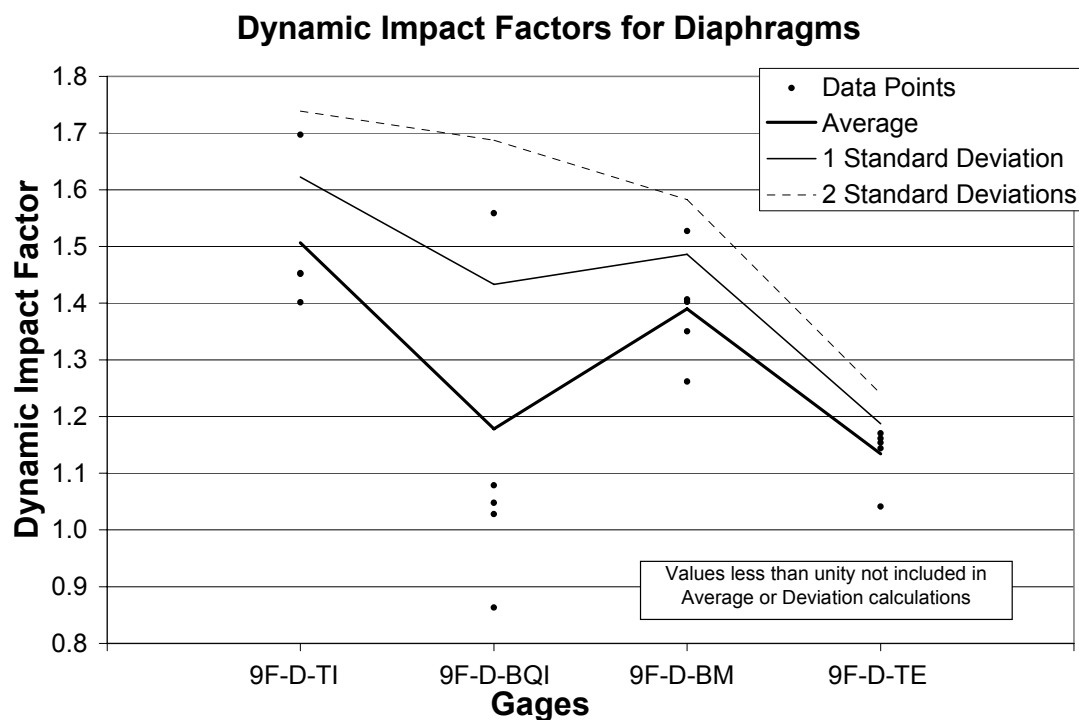


Figure 6-22: Average Diaphragm Dynamic Impact Factors

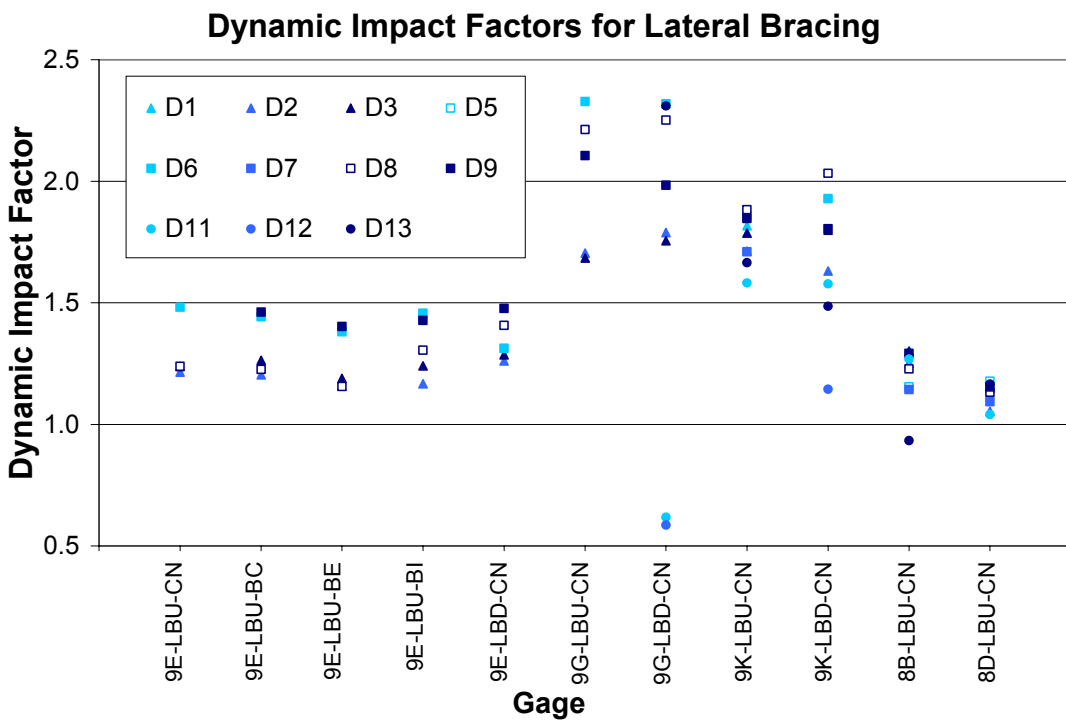


Figure 6-23: Lateral Bracing Dynamic Impact Factors

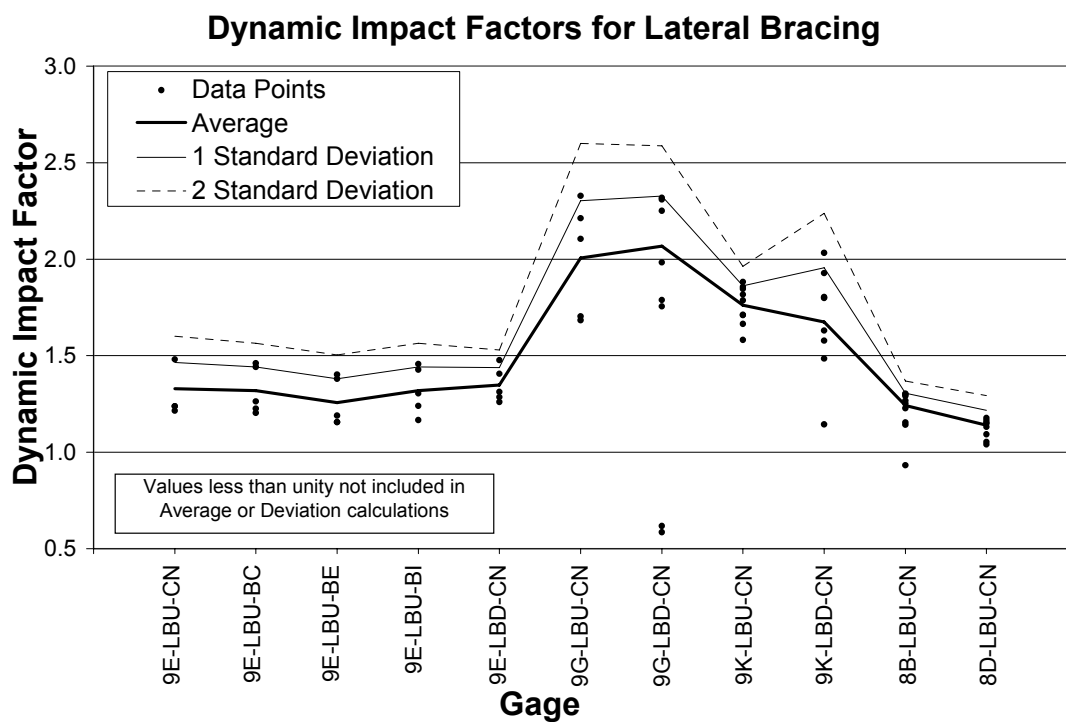


Figure 6-24: Average Lateral Bracing Dynamic Impact Factors

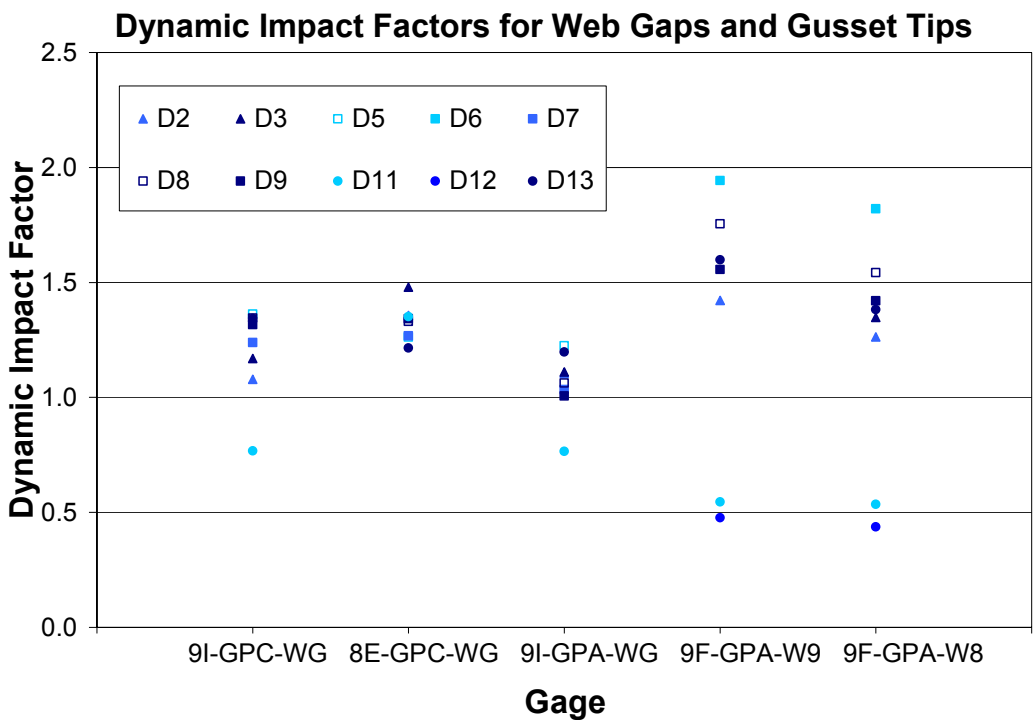


Figure 6-25: Web Gap and Gusset Plate Tip Dynamic Impact Factors

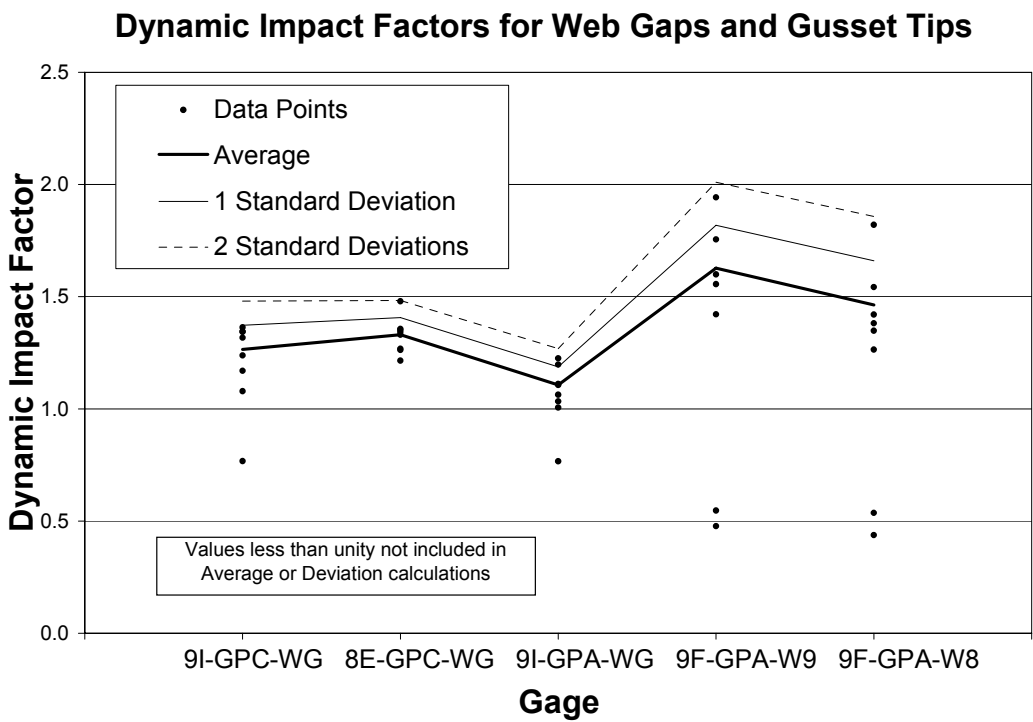


Figure 6-26: Average Web Gap and Gusset Plate Tip Dynamic Impact Factors

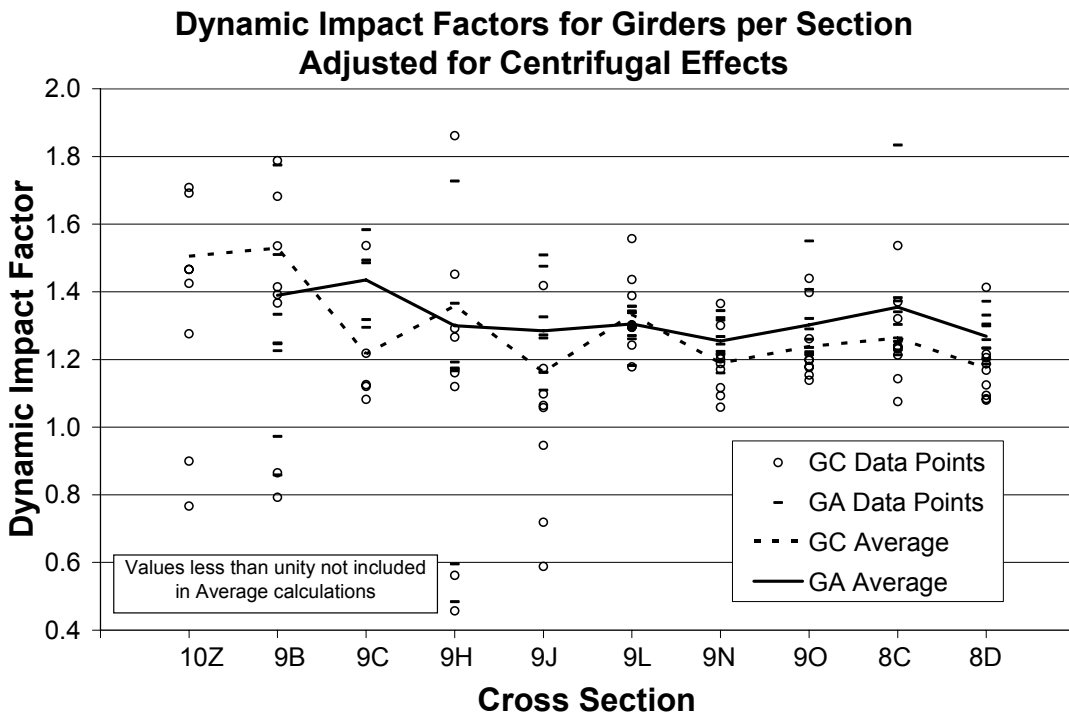


Figure 6-27: Girder DIF Adjusted for Centrifugal Effects

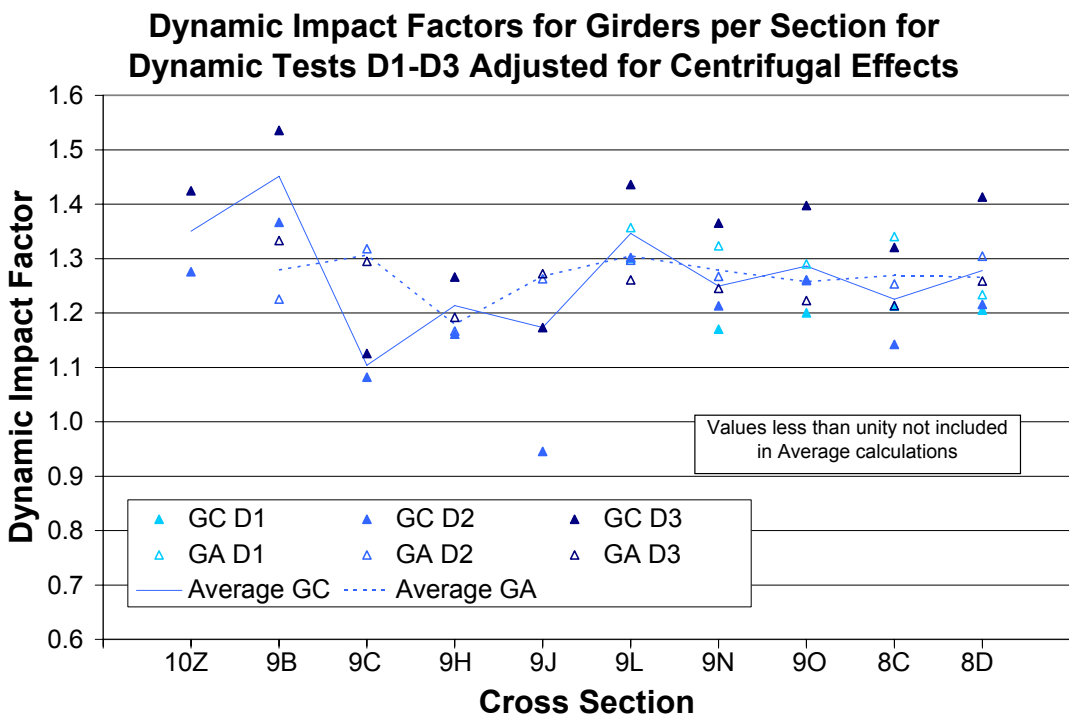


Figure 6-28: Girder DIF for D1-D3 Adjusted for Centrifugal Effects

Chapter 7

Comparison of Bridge Behavior with Computed Results

Comparisons are made between measured bridge responses and computed results based on calibrated analysis models of the tested horizontally curved steel I-girder bridge. Discussion of girder displacements and stresses, diaphragm stresses, and lateral wind bracing stresses is also provided, along with comments as to the effectiveness or ineffectiveness of the computer analysis to capture these behaviors. The final section of the chapter presents fatigue data for the gusset plate tip and web gap details along with a brief assessment of each.

7.1 Analysis Models for Computed Results

The bridge properties determined in Chapter 6 were used to create a calibrated model of the bridge utilizing the UMN Program model described in Chapter 4. This calibrated model is referred to as the Final Model, or FM. For the Final Model, the modular ratio was 6 and the effective concrete width for the girders was set to 123.0 inches in the positive moment regions and 102.5 inches in the negative moment regions as discussed in Chapter 6. Longitudinal distribution of the loads and stress checks were based on the full composite section properties in both the positive and negative moment regions (i.e., the concrete was assumed to provide tensile resistance in the negative moment regions). The effective width for the composite action of the diaphragms was set to 7.0 inches as determined in Chapter 6. Although measurements of the bearing displacements at Pier 9 indicated little to no movement, the axial displacements at the pier locations for the Final Model were allowed to displace. This was done primarily because the axial degree of freedom in UMN Program is located at the neutral axis of the beam and not at the flange where the restraint occurs. Similar to many grillage analysis programs, UMN Program does not provide for restraint at locations other than the neutral axis of the bridge members.

As the ensuing comparisons show, the Final Model provides for a good representation of the behavior of the tested bridge. However, there were some instances where the FM analysis provided unconservative results. In some cases for the negative moment regions, measured girder top flange flexural stresses were up to twice as large as those predicted with the FM analytical model. Also, for some cross-sections in the negative moment regions, especially Section 8C, the Final Model consistently under predicted the bottom flange flexural stresses by up to approximately 20% of the measured values. Localized cracks in the concrete deck are likely responsible for both of these discrepancies. As the tensile load increases on the deck in these regions and cracks appear, the stiffness of the section decreases. Load can no longer travel through the concrete and is confined to the rebar and top flange of the girder. This results in the neutral axis dropping toward the center of the steel section, significantly increasing the magnitude of stress at the top flange and to a lesser extent the stress at the bottom flange.

In order to ensure that the new rating of the bridge determined in Chapter 9 will be reasonably conservative, a second analysis model was created using UMN Program which takes into account the possible increase in stress due to cracks in the deck of the negative moment regions. The Final Model – Rating (FMR) was created identical to FM, except that girder flexural stresses in the negative moment regions were checked based on the section modulus for only the steel

girder and reinforcement (i.e., concrete was assumed ineffective, or cracked, in these regions for stress calculations). As with the Final Model, longitudinal load distribution was still accomplished using the full composite properties (assuming concrete is effective in both tension and compression) for both the positive and negative moment regions. This manner of analysis is typical for straight and curved bridges where shear connectors are provided in the negative moment regions. Although this bridge does not have shear connectors on the girders in the negative moment regions, the testing of the bridge at rating level loads done as part of this project along with visual inspection of the deck-to-girder interface in the negative moment regions of the bridge validate its composite nature and warrant the inclusion of the rebar for stress checks in these regions. Friction, adhesion, and the shear connectors on the diaphragms in the negative moment regions provide enough resistance for composite action to develop. If future inspections of the bridge reveal significant deterioration of the girder-to-deck interface or if loads higher than those used for the testing of this bridge are anticipated, the currently recommended inclusion of the rebar for the stress checks in the negative moment regions should be reevaluated.

7.2 Discussion of Measured and Computed Results

The final measured results for the static tests S1-S43 are provided in Appendix F (note that thermal effects have been removed for this data as described in Chapter 5). Plots showing the measured displacements and stresses along with the FM computed values are provided for each test for each instrument. Plots with the measured and FMR computed values are also presented, but only where the FMR values differ from the FM values; namely Sections 10Z, 9B, 9N, 9O, and 8C in the negative moment regions for the girders. Figure 7-1 and Figure 7-2 show an example of the difference in results between the FM and FMR analysis models. Figure 7-1 provides the measured versus FM computed values for the forty-three static tests for the TC and BC gages on Girder C at Section 8C, while Figure 7-2 shows the same data but with the FMR computed values. As the figures show, the FM values for the BC gage consistently under predict the measured values by approximately 20% of the measured value, while the FMR values match the measured data almost exactly. For the TC gage, the FMR analysis significantly over predicts the measured behavior, but this is generally acceptable for bridge rating since the bottom flange is the critical location in the negative moment regions.

Appendix F also provides tables that list the measured, FM computed, FMR computed, and percent error for each instrument by test. The percent error for these tables was calculated using:

$$\text{Percent Error} = \frac{\text{Computed} - \text{Measured}}{\text{Measured}} \cdot 100\% \quad (7-1)$$

Therefore, positive percent errors reflect an over prediction by the analysis and negative values represent under predictions. Percent errors with magnitudes greater than -100% indicate that the measured and computed values are of opposite signs.

Percent error calculations were made for each measured-to-computed comparison that had the measured value greater than a minimum magnitude. The minimum magnitude was set at 0.0001 radians for rotations, 0.10 inches for girder deflections, and 0.30 ksi for stresses. Comparisons with values smaller than these minimum limits were found to consistently result in unrealistically

high percent errors that unjustly skewed the resulting measured-to-computed comparisons. For each instrument, the maximum and minimum percent errors were also tabulated in Appendix F along with the average and standard deviation of the calculated percent error values.

The resulting maximum, minimum, average, and standard deviation values for the percent errors from the tables in Appendix F are included in this chapter along with the number of data used to determine those values out of the 43 static tests (i.e., the number of tests that the measured value of the instrument was above the minimum limit). A correlation is also assigned for each instrument based on the measured-to-FM computed and measured-to-FMR computed percent errors. Correlations are classified as *strong*, *moderate*, or *weak*. *Strong* correlations have at least 10 number of data above the limit, the magnitude of the average percent error less than 20%, and a standard deviation for percent error less than 40%. *Weak* correlations have at least 10 number of data above the limit and the magnitude of the average percent error more than 40%. All other instruments are classified as *moderate*. The *moderate* correlation generally includes those instruments that had low response magnitudes throughout the testing. This data has been organized into tables by instrument type and are individually discussed in the following sections.

7.2.1 Displacements

As expected for a horizontally curved bridge, the measured vertical deflections were greatest on the exterior girder during the test. The maximum measured deflection on the exterior girder for Span 9-8 was 0.72 inches, while that for Span 8-7 was 1.11 inches. Note that the maximum deflection on Span 8-7 would have actually been slightly larger than 1.11 inches since the deflection measurement for that span was made at approximately $0.4L_{arc}$, where L_{arc} is the arc length of the girder between bearing supports, instead of at midspan due to traffic constraints during testing. Service live load deflections (including impact) for each girder are limited by $L_{arc}/800$ for horizontally curved steel girder bridges (AASHTO, 2003a). If a girder impact factor of 1.25 is used, the limit for static truck tests then becomes $L_{arc}/1000$. For exterior girder arc lengths of approximately 115 ft and 151 ft on Span 9-8 and Span 8-7, respectively, the deflection limits are 1.40 inches and 1.81 inches. The measured values are well below these limits. For comparison purposes, the corresponding interior girder maximum deflections were 0.66 inches and 0.97 inches for Span 9-8 and Span 8-7, respectively. These values also fall well below the deflection limits based on the slightly shorter interior girder arc length.

The major axis bending rotations near Pier 9 and the deflections of Span 9-8 and Span 8-7 were predicted well by the FM and FMR analyses (displacement values were identical for both models). In general, the predicted exterior girder displacements correlated better with the experimental data than those for the interior girder. Table 7-1 provides a summary of the percent errors for each of the displacements that where computed. (Note that no predictions were attempted for the bearing displacements at Pier 9 or the slip displacement at the concrete-to-steel interface near Pier 9 and Pier 8). The Exterior Girder A provided *strong* correlations for all four displacement comparisons while the Interior Girder C had two *moderates* and two *strongs*. For all three interior girder displacements on Span 9-8, the analysis under predicted the actual behavior, while the displacement on Span 8-7 was over predicted.

The largest discrepancies between the computed and measured results for the displacements occurred for the twist cases S35 through S43. For these cases, trucks were shifted radially in on

one span and out on the adjacent span. For example, test S43 had three trucks shifted toward the interior girder on Span 9-8 and three trucks shifted toward the exterior girder on Span 8-7. This type of loading resulted in complicated interactions between the girders over Pier 8. Although the percent errors for displacements were slightly higher for these tests, UMN Program was still able to provide reasonable predictions. See Appendix F for the plots and tables of measured versus computed values.

7.2.2 Girder Stresses

The girder stresses have been separated into two categories: bending stresses at girder gage locations BC, TC, and W and warping stresses at girder gage locations BI, BE, TI, and TE. Each is discussed below.

7.2.2.1 Bending Stresses at Girder Gage Locations BC, TC, and W

Ten cross-sections along the length of the bridge were instrumented to obtain bending stress data for each girder. Generally speaking, the FM analysis using UMN Program provides excellent correlation with the measured bending stress data. To show this relationship, the bending stress data for the five most heavily loaded tests has been plotted along the girder length for each of the girders and is shown in Figure 7-3 through Figure 7-12. The plots are for tests S19, S24, S28, S39, and S43 and show the measured, FM computed, and FMR computed values for the TC and BC gages, which are located on the girder web 3 inches from the top and bottom flanges, respectively. Pier 9 at around 110 feet and Pier 8 near 220 feet are shown in the plots by small black squares to provide reference for the bending action of the girders. Brief descriptions of the tests are provided on the plots while the specific truck test configurations are located in Chapter 5.

The BC gages, located on the web near the bottom flange, provided the best correlation between measured and computed results. Table 7-2 and Table 7-3 provide summaries of the correlations for the FM and FMR analyses for the ten BC gages located on each girder. For the FM analysis, eighteen of the nineteen functioning gages provided *strong* correlation between the measured and computed data (note that gage 10Z-GA-BC did not function during the test). The remaining BC gage had a *moderate* rating and was just slightly above the maximum percent error limit of $\pm 20\%$ for the *strong* correlation. As expected for the FMR analysis correlations with measured data, the correlations for the negative moment regions were more conservative than those for the FM analysis. The range for the average percent errors for the FMR comparisons was between -3.7% and 20.4%, while for the FM analysis it was -20.6% and 18.8%. In general, the average percent errors and standard deviations were consistently lower for the BC gages than for any other group of measured values. The most compressive and tensile measured BC gage stresses due to the test truck loads were -9.07 ksi and 9.38 ksi, respectively.

In general terms, the TC gages were mostly predicted accurately by the FM analysis. This can be seen by the closeness of the plotted data for the measured and FM computed values in Figure 7-3 through Figure 7-12. However, since the magnitude of stress for the TC gages was rather small due to the closeness of these gages to the neutral axes of the composite sections, percent error calculations indicate somewhat misleading correlations. The percent error correlations for the

FM analysis are provided in Table 7-4 and show one *strong*, fourteen *moderate*, and four *weak* correlations (note that gage 9B-GA-TC did not function during the test). The large percentage of moderate correlations for the TC gages attests to the fact that the stresses were low in these gages. Also note that a number of the TC gages have average percent errors with magnitudes greater than -100%, indicating that the predicted and measured values are of opposite signs. This is not surprising due to closeness of the TC gages to the neutral axes. For the FMR analysis correlations provided in Table 7-5, the average percent errors for the gages in the negative moment regions tend to be much larger in magnitude than those for the FM analysis. This is because the FMR analysis predicts stresses using a much smaller bending section, which ignores the contribution of the concrete. Figure 7-3 through Figure 7-12 show the conservative nature of the FMR analysis for predicting the TC stresses in the negative moment regions. The most compressive and tensile measured TC gage stresses were -0.72 ksi and 1.14 ksi, respectively.

The web gage W that was attached at the mid-height of the steel girder web also provided bending stress data. Four cross-sections were instrumented for each girder along the length at the W location. Percent error correlations for these eight gages are provided in Table 7-6 for the FM analysis. They result in one *strong*, two *moderate*, and five *weak* correlations. For the FMR analysis correlations in Table 7-7, the average percent errors show a slight improvement. Because of the inherent curvature of the web and the large girder depth, the measured behavior of the web gages is strongly influenced by out-of-plane web distortion, especially near the piers. It is not surprising that these gages do not correlate as well with the computed results, since these out-of-plane effects are not considered in the analysis provided by UMN Program.

7.2.2.2 Warping Stresses at Girder Gage Locations BI, BE, TI, and TE

Torsion of restrained open section beams, such as the case for curved I-girder bridges, results in lateral bending of the flanges. This bending leads to longitudinal stresses in the flanges known as restraint of warping stresses. For typical beams with the web centered on the flanges, the warping stress is zero at the web and has maximum positive and negative values at the opposing tips of the flange.

For this bridge test, warping stresses were measured at four cross-sections for each of the girders. For most of these cross sections, two gages were attached near the edges of the top flange (TI and TE) and two near the edges of the bottom flange (BI and BE). For Section 8D on Girder A, only one gage was placed on each flange (TI and BI) due to accessibility issues during instrumentation.

The measured values for each of these gages include a component of flexural bending stress along with stress due to the restraint of warping. Correlations between total measured stresses for these gages were made with the FM and FMR computed values (both of which also include flexural bending and warping stresses) in Table 7-8 and Table 7-9 for the bottom flange and Table 7-10 and Table 7-11 for the top flange. For the bottom flange gages BI and BE in Table 7-8 for the FM analysis, there are twelve *strong* and three *moderate* correlations. The FMR analysis correlations in Table 7-9 are more conservative for gages in the negative moment regions than those for the FM analysis. The top flange gages TI and TE in Table 7-10 provide eight *moderate* and four *weak* correlations (note that gages 9B-GA-TI and 9J-GA-TI did not function during the test and gage 8D-GA-TI was unreliable). The FMR correlations in Table

7-11 for the top flange gages are similar except that they are more conservative for the gages in the negative moment regions. These correlations are very similar to those for the previously discussed TC and BC gages, which only included flexural bending stress. The reason for this is explained in the next paragraph regarding the magnitude of the measured restraint of warping stresses.

In order to get a more accurate assessment of the warping stresses, the bending stresses were removed from the measured data. For flanges that had two gages providing tip stresses (e.g., BI and BE or TI and TE), the values were subtracted from one another and divided by 2 to get the magnitude of the average warping stress at the tip gage (located approximately 1 inch from the edge). When data from only one tip gage was available, the TC and BC gages at the cross-section were used to determine the bending stress at the height of the tip gage by assuming a linear strain profile in the web. This bending stress was then subtracted from the measured tip gage value to determine the component of warping stress. Figure 7-13 and Figure 7-14 show the results of this process for the bottom flange warping of each girder for test S24. The computed values (FM and FMR were identical) are shown continuously plotted along the length of the girders in these two plots to show the typical nature of the warping stresses in the girders, while the measured values are shown as points on each plot. Notice on these plots that the location of the measured values tends to be near an inflection point in the warping stress profile. These results show the difficulty of measuring warping stresses in this specific bridge. Ideally, the tip gages would have been located directly at a diaphragm or halfway between diaphragms, both of which are locations that have transverse stiffeners at the cross sections, instead of at the quarter points between diaphragms as chosen herein. However, locating the gages near the locations of transverse stiffeners would have strongly influenced the localized strain distributions. Thus, it is difficult to assess the accuracy or dominance of the restraint of warping stresses in this bridge. However, the accuracy of the prediction of the restraint of warping stresses in Figure 7-13 and Figure 7-14 and as described in the following paragraph indicates that the analysis may be used with some reliability to estimate the likely range of warping stresses. In this regard, the results are similar to those reported by Galambos et al. (2000).

Plots for the bottom flange warping (herein termed BW), with the measured values calculated using the procedure in the previous paragraph, are provided in Figure 7-15 through Figure 7-18 for each girder at Section 9B, 9J, 9O, and 8D for all forty-three static tests. Top flange warping (TW) stresses were considerably smaller and are not shown. In each of the four figures, solid squares represent measured stresses for the Interior Girder C, solid triangles represent measured stresses for the Exterior Girder A, and the hollow squares and triangles represent the computed stresses for the interior and exterior girders, respectively. The two plots for the bottom flange restraint of warping stresses near the piers, Figure 7-15 for Section 9B near Pier 9 and Figure 7-17 for Section 9O near Pier 8, reveal that the measured warping stresses were much higher than the predicted values. This is especially evident for tests S29-S43, where large twisting moments were induced on the bridge due to the asymmetrical loading patterns. For Section 9J near midspan of Span 9-8 and Section 8D near midspan of Span 8-7, the magnitudes of the measured and computed warping stresses as shown in Figure 7-16 and Figure 7-18, respectively, were generally quite similar. However, there are some measured values in these two plots that vary significantly from the computed values. In most cases, these large discrepancies occur for

tests with the trucks located at the given cross section. The largest measured restraint of warping stress was approximately 1.5 ksi.

There are a number of factors that play into the apparent weak correlation between the computed and measured restraint of warping stresses. The first of these was the choice of location for the warping measurements, as discussed earlier. The second factor is that, while UMN Program accounts well for restraint of warping in the presence of torsion, it is likely that local loading effects due to the location of the trucks between the girders may create additional localized torsion that is difficult to take into account in the computer analysis. This is likely the cause of the large discrepancies between some measured and computed values for the midspan warping stresses in Figure 7-16 and Figure 7-18. This behavior is further discussed in Section 7.2.4 with the lateral wind bracing. A third factor that adversely affects the correlation between the measured and computed warping stresses is that boundary conditions in the computer model do not necessarily reflect the actual arrangement in the structure. In particular, the bearing restraint at the piers in the radial direction significantly restricts the amount of torsion that can occur there, which increases the measured restraint of warping stresses there. This behavior is difficult to include in a grillage model unless boundary conditions can be introduced at the bottom flange location, which was not possible with UMN Program. This is likely the cause of the under prediction of the computed results near the piers as shown in Figure 7-16 and Figure 7-18. The final factor is related to the third and has to do with the inability of a grillage model to include effects due to the girder web distorting, including the influence of web distortion on the influence of the boundary conditions.

7.2.3 Diaphragm Stresses

Two beam diaphragms, the one at Section 9F and the one at Section 8A, were instrumented with strain gages at five sections along their lengths in order to assess the bending action in the diaphragms. Ten gages were installed on each diaphragm, with a gage on the web near the top flange and one near the bottom flange for each of the five sections along the diaphragm lengths. The end two gaged sections on the diaphragms were located close to the girders in the knee brace regions of the diaphragms, while the middle three sections were away from the knee brace region.

Percent error comparisons for the measured and computed values for the gages on the diaphragms at Sections 9F and 8A are provided in Table 7-12 (note that results for FM and FMR are identical). For the analysis comparisons, there are 8 *moderate* correlations and 11 *weak* correlations (note that gage 8A-D-BI was unreliable). The large number of *moderate* correlations for the diaphragms is due to the fact that the stress levels in the diaphragms were relatively low. The magnitude of the maximum measured diaphragm stress was around 2.0 ksi, which is less than one-fourth of the measured maximum girder stress.

In general, the analysis using UMN Program was able to provide a reasonable model for the diaphragm behavior. See Appendix F for plots and tables of all measured and computed values. Figure 7-19 provides a typical comparison between measured and computed results for the gages on the diaphragm at Section 9F for each of the 43 static tests. Notice in this figure that the bottom flange gage (9F-D-BQI) has significantly higher tensile stresses than predicted for a number of tests. This behavior is similar for all three of the gaged sections near the middle of the

diaphragm at Section 9F, while for the end two sections on this diaphragm the top flange gage has excessively high tensile loads for the same load tests. Correlating these tests with the locations of the trucks, it is apparent that this behavior occurs when a truck is directly over the diaphragm for the load test. The bending stresses created in the diaphragms due to vertical loads transferring through the diaphragms to the girders are significant for this bridge. Most grillage-based analytical programs, including UMN Program, do not take into account the diaphragm bending action due to truck loads above a given diaphragm since loads in the analysis programs are typically distributed to the girder nodes only; thus the reason for the discrepancy in the measured versus computed values.

The measured and computed results for the diaphragm at Section 8A (Pier 8) are generally more consistent than those for the diaphragm at Section 9F. This is because fewer load tests had trucks positioned directly over this diaphragm; thus reducing the local bending effects in the diaphragm. However, for tests with trucks over this diaphragm, similar bending behavior as described previously for the diaphragm at Section 9F does occur. The major discrepancy with the diaphragm at Pier 8 is that for the tests with asymmetrical loading (tests S29-S43), the measured and computed values diverge. This is evident in Figure 7-20 for the measured and computed values at Section 8A-D-QI. This divergence is likely due to the inability of UMN Program to accurately model the boundary conditions for the bottom flange at the pier at which this diaphragm is located. This is similar to the issue discussed previously for the girder restraint of warping stresses.

7.2.4 Lateral Wind Bracing Stresses

The primary function of lateral wind bracing in a bridge is to provide axial resistance between the bottom flanges of adjacent girders. The strain gages for this bridge test were welded on the stem of the lateral bracing tee sections at the theoretical elastic neutral axis to prevent bending stresses from contributing to the desired stress due to axial forces. In order to provide evidence that the chosen gage location was indeed providing measurements due to the axial force only, one lateral wind bracing at Section 9E-LBU was instrumented with five gages. Gage 9E-LBU-BC was located on the outer surface of the flange across from the stem, gages 9E-LBU-BI and 9E-LBU-BE were on the inner surface of the flange near the tips, gage 9E-LBU-TC was on the tip of the stem, and gage 9E-LBU-CN was located at the theoretical neutral axis. Figure 7-21 shows the measured stresses for these five gages along with the FM computed value for each of the forty-three static tests. The gage responses consistently reveal a pattern of bending with a neutral axis close to the (-CN) gage location. Therefore, the computed (axial forces only) and measured values can be confidently compared with one another.

Ten lateral wind bracing were instrumented for the bridge test. The maximum measured compression stress was -5.0 ksi, while the maximum measured tensile stress was 5.4 ksi. The results of the percent error comparisons between the measured and FM computed values (FMR values are identical) are provided in Table 7-13. One gage resulted in a *strong* correlation, seven in *moderate*, and the remaining two in *weak* correlations. Inspection of the lateral wind bracing behavior in the plots in Appendix F reveals that measured data correlates well with computed data when the trucks are located away from a specific lateral bracing. Also, the measured data for lateral wind bracing is consistently more tensile than predicted when trucks are located in the

vicinity of a lateral bracing. To show this behavior, Figure 7-22 and Figure 7-23 have been included. A box labeled with *Trucks* is placed in both of these figures next to lateral bracing that had trucks on the concrete slab directly above them. Figure 7-22 shows the measured versus computed stresses for the ten lateral wind bracing for test S24. For this test, the trucks were located near midspan on Span 8-7 and the measured lateral bracing stresses near the trucks were significantly more tensile than computed. Figure 7-23 provides the same data but for test S28, where trucks were located near midspan of Span 9-8 and midspan of Span 8-7. This data clearly shows the increase in tensile forces for the lateral wind bracing beneath the trucks. For the previous two cases, the trucks were located transversely on the bridge so that the center of gravity was halfway between the girders. A third figure, Figure 7-24, has been provided to show the behavior of the lateral wind bracing for a case where the loads are not located between the girders, but are instead shifted above the Exterior Girder A on Span 9-8. For this case, all ten of the lateral bracing are predicted reasonably well, with little notable increase in the tensile behavior of the lateral bracing beneath the trucks.

It has been concluded herein that localized bending in the slab at the point of load application is the cause for the increase in tensile forces seen in the lateral wind bracing. Application of loads between the girders creates torsional rotations that draw the top flanges of the girders together and attempt to spread the bottom girder flanges. However, the lateral bracing near the bottom flanges develop tensile forces and prevent the flanges from rotating apart. When the load is applied directly above a single girder, such as the case in Figure 7-24 for test S31, the addition of tensile forces in the lateral bracing is not as appreciable since bending in the slab has been minimized. This behavior also influences diaphragm forces and restraint of warping stresses in the girder near the applied truck loads.

7.3 Measured Fatigue Detail Stresses

Two details on the bridge were identified as possible fatigue problem regions and were instrumented with the intention of capturing data useful for fatigue assessment. The first of these details was the gusset plate tips, while the second was the vertical stiffener web gap. Diagrams of these details along with the locations of the instruments on them can be located in Chapter 5 or in Appendix B. The following two sections take a closer look at these two fatigue details along with the test results for each.

7.3.1 Gusset Plate Tip

The gusset plate tip refers to the region of the girder web at the edge of the welded gusset plate connection. Welded attachments to the web of a girder, such as the approximately 20 inch wide gusset plates located at the base of each diaphragm for the tested bridge, are known to draw significant amounts of load from the web and create hot spot regions at the ends of the attachments. In addition, out-of-plane loads from the lateral wind bracing and diaphragms can intensify the stress in the web at these locations. When these attachments are located in tension regions of the web, fatigue problems can arise.

The gusset plate region on the exterior girder at Section 9F was instrumented with strain gages (gages 9F-GPA-W9 and 9F-GPA-W8) on the girder web as close to the gusset plate tip weld toe

as possible. See Figure 7-25 for a photograph of an attached gage. The gages were oriented longitudinally to pick up the concentration of stress in the girder web at these locations. Also, gage 9F-GPA-LO was located on the gusset plate near the weld to the web and oriented in the longitudinal direction to measure the longitudinal stress transferred through the web and into the gusset plate.

Figure 7-26 contains the plotted data for each of the three gages on the gusset plate detail for the forty-three static tests. Also included in the plot is the FM computed value for the web ignoring the gusset plate effects and the average value of the measured BC gages at Sections 9C and 9H. Since the location of the BC gage was at nearly the same height on the web as the gusset plate, and Sections 9C and 9H were equal distance away from the gusset plate in opposite directions, the average of their values for each test provides a reasonable approximation for the measured stress that would exist in the web at Section 9F if the gusset plate was not there. As the figure shows, the stresses at each of the gusset tips were nearly identical and were significantly higher than those assuming no effects due to the attachment. The maximum measured hot spot stress due to the live load alone was slightly over 15 ksi and occurred for test S19, where six trucks were located on Span 9-8.

The data in Figure 7-26 was used to define stress concentration factors (SCF) for the instrumented locations on the girder web near the edge of the weld for the gusset plate. The SCFs were calculated by dividing both of the gusset tip gage values by the FM computed value and also by the average of the 9C and 9H measured values for each static test. Figure 7-27 shows the four resulting plots of data from this process. The stress concentration factors range from approximately 1.5 to 3.0 with the majority of the SCF values falling between 2.0 and 2.5. Therefore, it can be expected that the stresses in the web near the gusset plate attachments for this bridge will be around 3 times higher than the expected nominal stress ignoring the gusset plate and weld. Note that as the gage location moves closer to the weld, this value could increase somewhat and results for other gusset plates may vary to some degree.

Stress ranges for individual test trucks weighing approximately 72,000 lbs each were determined for the gusset plate detail using the dynamic load testing. Ranges were calculated by subtracting the minimum stress (most compression) from the maximum stress (most tensile) that occurred for each of the thirteen dynamic tests. The resulting stress ranges are provided in Table 7-14 along with the tensile component for each of the stress ranges. The largest measured stress range was 9.6 ksi (7.1 ksi tensile) and occurred for test D6, where the truck drove over a 2x4. For the three tests D1 through D3 that mimicked normal traffic, the largest stress range was 8.0 ksi (5.4 ksi tensile).

Chapter 7 of the *LRFR Manual* (AASHTO, 2003b) provides a procedure that can be used to predict the fatigue life of various details and is similar to other procedures provided by AASHTO (1998, 2002, and 2004). For the procedure, either measured or computed nominal stress ranges based on a 54 kip fatigue truck driving along the bridge are compared to stress (S) versus number of cycles to failure (N) curves to estimate the life expectancy of a detail. Details are broken down into various categories depending on the severity of the detail to fatigue. The fatigue curves are base on experimental tests and already include effects due to stress concentrations: thus, using measured hot spot stresses would provide a highly conservative assessment. With this in mind, a conservative estimate was made based on a stress range of 75% of the 8.0 ksi hot spot stress

range measured above for the 72 kip test trucks. Note that 75% of the measured hot spot stress range was used to correlate the stress range of the 72 kip test truck to that for a 54 kip fatigue truck. Using the average daily truck traffic (ADTT) of 338 for the bridge, the result was a life expectancy for this Category E gusset plate detail of approximately 41 years. A second calculation of the life expectancy was made based solely on the in-plane nominal stress range (i.e., ignoring stress concentrations and out-of-plane stress generated from forces in the lateral wind bracing and/or diaphragms) in the web near the gusset plate height as is typically done during the design of a bridge. The largest measured nominal stress range for an individual 72 kip test truck driving along the bridge at maximum speed for dynamic test D3 was approximately 4.8 ksi (3.4 ksi tensile) near midspan of Span 9-8 on the exterior girder (gage 9J-GA-BC). Using 75% percent of this stress range to correlate to a 54 kip fatigue truck, a life expectancy of 190 years was calculated. In reality, the fatigue life of the gusset plate tip details for this bridge will fall somewhere between these two values. Based on the very conservative life expectancy of 41 years and the more realistic value of 190 years, it is unlikely that fatigue cracks will develop at the gusset plate tips within a typical 75 year design life for this bridge, assuming truck weights and the ADTT do not increase considerably.

7.3.2 Web Gap

Since connection stiffeners welded to the web of a girder are typically coped at the ends to provide clearance for the girder web-to-flange welds or the k-region of a rolled beam, small distances of unstiffened web exist near the flanges of the girder. These regions are called web gaps. Fatigue problems can occur at the web gap regions when the connection stiffener is not bolted or welded to the girder flange. The problem is depicted in Figure 7-28 and results when diaphragm, lateral bracing, or other loads near the flange cause relative displacements between the flange and the connection stiffener. Large amounts of displacement are forced to occur over the small web gap height creating significant levels of stress.

For a number of years, bridge designers stayed away from welding to the tension flange of girders thinking that the welds would create unwanted fatigue issues and lead to fractures in the girder flanges. This thinking led to the design and construction of a number of bridges without welds between the connection stiffeners and the tension flanges. This resulted in a number of fatigue issues due to the out-of-plane distortion of the web gaps in these bridges. Current bridge codes now recommend the attachment of connection stiffeners to both flanges with the intent of eliminating web gap fatigue problems (AASHTO, 2003a).

The tested bridge for this project did not have the connection stiffener welded to the tension flange. Therefore, five web gaps in positive moment regions were instrumented with vertically aligned strain gages (see Figure 7-29 for a photograph of an attached gage) near the bottom flange to capture the out-of-plane bending stress created by the displacement of the girder web relative to the bottom flange. Web gaps near the top flange in the negative moment regions were not instrumented since the composite nature of the beam diaphragm with the concrete deck prevents out-of-plane displacements of the diaphragm connection stiffener there. The five measured web gap stresses are plotted for the forty-three static tests in Figure 7-30. The values range between approximately +3.3 and -3.5 ksi for these tests. Similar to the gusset plate tip details, stress ranges were also calculated for each of the five web gap details using the dynamic

test data and are listed in Table 7-14 along with the component of the stress range due to tensile stress. The maximum measured stress range based on an individual 72 kip test truck was 2.0 ksi. This is a small maximum stress range and will likely not result in any fatigue problems for the web gap details on this bridge.

Gage	Minimum % Error	Maximum % Error	Standard Deviation	Average % Error	# of Data above Limit	Correlation
9B-GC-RM	-58.5%	24.2%	16.2%	-17.2%	41	Strong
9B-GA-RM	-95.3%	24.1%	23.2%	-2.6%	41	Strong
9I-GC-DF	-93.2%	31.2%	24.2%	-23.9%	38	Moderate
9I-GA-DF	-32.7%	11.5%	9.2%	-3.0%	36	Strong
9M-GC-DF	-57.2%	21.8%	18.4%	-21.2%	31	Moderate
9M-GA-DF	-41.6%	13.9%	13.6%	-5.0%	32	Strong
8E-GC-TS	-27.8%	50.1%	18.2%	7.0%	35	Strong
8E-GA-TS	-87.8%	84.7%	39.4%	2.1%	36	Strong

Correlation

Strong: # of Data above Limit > 9, |Average| < 20%, and Standard Deviation < 40%

Moderate: do not fit criteria for Strong or Weak

Weak: # of Data above Limit > 9 and |Average| > 40%

Table 7-1: Measured versus Computed Comparison for Displacements

Gage	Minimum % Error	Maximum % Error	Standard Deviation	Average % Error	# of Data above Limit	Correlation
10Z-GC-BC	-64.6%	36.6%	24.6%	3.4%	40	Strong
9B-GC-BC	-98.2%	29.6%	30.6%	-1.3%	41	Strong
9C-GC-BC	-39.9%	32.0%	14.2%	0.3%	30	Strong
9H-GC-BC	-37.9%	32.8%	12.6%	-3.7%	41	Strong
9J-GC-BC	-51.8%	29.2%	15.4%	2.4%	42	Strong
9L-GC-BC	-48.5%	138.2%	27.6%	4.8%	38	Strong
9N-GC-BC	-60.8%	22.8%	18.8%	-5.7%	34	Strong
9O-GC-BC	-45.7%	16.9%	14.0%	-0.5%	41	Strong
8C-GC-BC	-46.4%	-2.2%	10.3%	-20.6%	41	Moderate
8D-GC-BC	-32.2%	27.4%	13.2%	6.4%	39	Strong
10Z-GA-BC*	--	--	--	--	--	*No Data
9B-GA-BC	-105.2%	25.8%	22.2%	1.4%	39	Strong
9C-GA-BC	0.3%	36.5%	9.7%	18.8%	30	Strong
9H-GA-BC	-12.1%	31.0%	8.8%	12.2%	41	Strong
9J-GA-BC	-57.9%	19.6%	14.0%	-1.0%	42	Strong
9L-GA-BC	-36.8%	76.6%	21.9%	13.8%	41	Strong
9N-GA-BC	-50.6%	28.5%	16.6%	-2.1%	35	Strong
9O-GA-BCH	-38.3%	29.7%	11.8%	-3.6%	40	Strong
8C-GA-BC	-34.3%	18.4%	12.9%	-3.4%	39	Strong
8D-GA-BC	-33.0%	42.2%	16.0%	6.8%	39	Strong

Correlation

Strong: # of Data above Limit > 9, |Average| < 20%, and Standard Deviation < 40%

Moderate: do not fit criteria for Strong or Weak

Weak: # of Data above Limit > 9 and |Average| > 40%

Table 7-2: Measured versus FM Computed Comparison for Bottom Flange Gage BC

<u>Gage</u>	Minimum % Error	Maximum % Error	Standard Deviation	Average % Error	# of Data above Limit	Correlation
10Z-GC-BC	-59.6%	59.4%	28.9%	20.4%	40	Moderate
9B-GC-BC	-98.2%	51.5%	35.8%	15.1%	41	Strong
9C-GC-BC	-39.9%	32.0%	14.2%	0.3%	30	Strong
9H-GC-BC	-37.9%	32.8%	12.6%	-3.7%	41	Strong
9J-GC-BC	-51.8%	29.2%	15.4%	2.4%	42	Strong
9L-GC-BC	-48.5%	138.2%	27.6%	4.8%	38	Strong
9N-GC-BC	-54.1%	44.8%	22.2%	11.0%	34	Strong
9O-GC-BC	-37.9%	30.8%	15.6%	11.2%	41	Strong
8C-GC-BC	-37.8%	15.3%	12.3%	-6.4%	41	Strong
8D-GC-BC	-32.2%	27.4%	13.2%	6.4%	39	Strong
10Z-GA-BC*	--	--	--	--	--	*No Data
9B-GA-BC	-106.9%	43.7%	25.5%	15.9%	39	Strong
9C-GA-BC	0.3%	36.5%	9.7%	18.8%	30	Strong
9H-GA-BC	-12.1%	31.0%	8.8%	12.2%	41	Strong
9J-GA-BC	-57.9%	19.6%	14.0%	-1.0%	42	Strong
9L-GA-BC	-36.8%	76.6%	21.9%	13.8%	41	Strong
9N-GA-BC	-44.7%	47.2%	19.2%	11.3%	35	Strong
9O-GA-BCH	-31.7%	41.2%	12.9%	5.1%	40	Strong
8C-GA-BC	-24.4%	35.0%	14.4%	9.7%	39	Strong
8D-GA-BC	-33.0%	42.2%	16.0%	6.8%	39	Strong

Correlation

Strong: # of Data above Limit > 9, |Average| < 20%, and Standard Deviation < 40%

Moderate: do not fit criteria for Strong or Weak

Weak: # of Data above Limit > 9 and |Average| > 40%

Table 7-3: Measured versus FMR Computed Comparison for Bottom Flange Gage BC

<u>Gage</u>	Minimum % Error	Maximum % Error	Standard Deviation	Average % Error	# of Data above Limit	Correlation
10Z-GC-TC	-70.3%	-57.4%	3.9%	-63.7%	7	Moderate
9B-GC-TC	-89.7%	-69.8%	5.6%	-78.4%	22	Weak
9C-GC-TC	-94.7%	-90.5%	1.6%	-93.6%	5	Moderate
9H-GC-TC	0.0%	0.0%	--	--	0	Moderate
9J-GC-TC	0.0%	0.0%	--	--	0	Moderate
9L-GC-TC	0.0%	0.0%	--	--	0	Moderate
9N-GC-TC	-142.6%	-84.4%	17.5%	-105.5%	12	Weak
9O-GC-TC	-70.4%	0.9%	20.1%	-35.4%	26	Moderate
8C-GC-TC	-179.5%	-79.9%	31.5%	-128.9%	23	Weak
8D-GC-TC	-105.5%	-100.0%	2.7%	-102.7%	2	Moderate
10Z-GA-TC	-113.5%	-89.7%	9.9%	-100.2%	3	Moderate
9B-GA-TC*	--	--	--	--	--	*No Data
9C-GA-TC	-110.4%	-106.4%	1.6%	-108.3%	3	Moderate
9H-GA-TC	0.0%	0.0%	--	--	0	Moderate
9J-GA-TC	-148.9%	-122.3%	7.8%	-131.8%	11	Weak
9L-GA-TC	-134.7%	-127.1%	3.8%	-130.9%	2	Moderate
9N-GA-TC	0.0%	0.0%	--	--	0	Moderate
9O-GA-TCH	-43.6%	66.2%	31.9%	-4.7%	20	Strong
8C-GA-TC	-138.8%	-136.8%	1.0%	-137.8%	2	Moderate
8D-GA-TC	-95.9%	-18.4%	24.8%	24.8%	16	Moderate

Correlation

Strong: # of Data above Limit > 9, |Average| < 20%, and Standard Deviation < 40%

Moderate: do not fit criteria for Strong or Weak

Weak: # of Data above Limit > 9 and |Average| > 40%

Table 7-4: Measured versus FM Computed Comparison for Top Flange Gage TC

<u>Gage</u>	Minimum % Error	Maximum % Error	Standard Deviation	Average % Error	# of Data above Limit	Correlation
10Z-GC-TC	407.8%	532.9%	37.3%	470.8%	7	Moderate
9B-GC-TC	57.6%	346.5%	83.8%	213.0%	22	Weak
9C-GC-TC	-94.7%	-90.5%	1.6%	-93.6%	5	Moderate
9H-GC-TC	0.0%	0.0%	--	--	0	Moderate
9J-GC-TC	0.0%	0.0%	--	--	0	Moderate
9L-GC-TC	0.0%	0.0%	--	--	0	Moderate
9N-GC-TC	-885.9%	209.3%	309.0%	-251.1%	12	Weak
9O-GC-TC	105.8%	604.3%	141.6%	348.7%	26	Weak
8C-GC-TC	-885.8%	-75.3%	183.8%	-637.5%	23	Weak
8D-GC-TC	-105.5%	-100.0%	2.7%	-102.7%	2	Moderate
10Z-GA-TC	-427.2%	-100.0%	138.4%	-238.1%	3	Moderate
9B-GA-TC*	--	--	--	--	--	*No Data
9C-GA-TC	-110.4%	-106.4%	1.6%	-108.3%	3	Moderate
9H-GA-TC	0.0%	0.0%	--	--	0	Moderate
9J-GA-TC	-148.9%	-122.3%	7.8%	-131.8%	11	Weak
9L-GA-TC	-134.7%	-127.1%	3.8%	-130.9%	2	Moderate
9N-GA-TC	0.0%	0.0%	--	--	0	Moderate
9O-GA-TCH	186.4%	737.6%	160.8%	381.4%	20	Weak
8C-GA-TC	-358.5%	-349.6%	4.5%	-354.1%	2	Moderate
8D-GA-TC	-95.9%	-18.4%	24.8%	24.8%	16	Moderate

Correlation

Strong: # of Data above Limit > 9, |Average| < 20%, and Standard Deviation < 40%

Moderate: do not fit criteria for Strong or Weak

Weak: # of Data above Limit > 9 and |Average| > 40%

Table 7-5: Measured versus FMR Computed Comparison for Top Flange Gage TC

<u>Gage</u>	Minimum % Error	Maximum % Error	Standard Deviation	Average % Error	# of Data above Limit	Correlation
9B-GC-W	-425.7%	-200.4%	52.4%	-284.8%	19	Weak
9J-GC-W	-109.8%	-85.7%	5.4%	-103.9%	16	Weak
9O-GC-W	-288.8%	-138.0%	37.4%	-200.0%	38	Weak
8D-GC-W	-26.9%	54.8%	19.1%	11.7%	36	Strong
9B-GA-W	-144.8%	13.1%	32.5%	-35.2%	40	Moderate
9J-GA-W	-32.1%	0.1%	7.0%	-21.9%	40	Moderate
9O-GA-WH	-384.3%	-138.9%	62.0%	-208.6%	31	Weak
8D-GA-W	-33.0%	157.7%	37.4%	58.2%	31	Weak

Correlation

Strong: # of Data above Limit > 9, |Average| < 20%, and Standard Deviation < 40%

Moderate: do not fit criteria for Strong or Weak

Weak: # of Data above Limit > 9 and |Average| > 40%

Table 7-6: Measured versus FM Computed Comparison for Girder Web Gage W

<u>Gage</u>	Minimum % Error	Maximum % Error	Standard Deviation	Average % Error	# of Data above Limit	Correlation
9B-GC-W	-272.9%	-153.3%	27.8%	-197.8%	19	Weak
9J-GC-W	-109.8%	-85.7%	5.4%	-103.9%	16	Weak
9O-GC-W	-181.3%	-116.3%	16.1%	-143.1%	38	Weak
8D-GC-W	-26.9%	54.8%	19.1%	11.7%	36	Strong
9B-GA-W	-120.8%	-46.5%	15.5%	-69.0%	40	Weak
9J-GA-W	-32.1%	0.1%	7.0%	-21.9%	40	Moderate
9O-GA-WH	-206.6%	-114.5%	23.3%	-140.6%	31	Weak
8D-GA-W	-33.0%	157.7%	37.4%	58.2%	31	Weak

Correlation

Strong: # of Data above Limit > 9, |Average| < 20%, and Standard Deviation < 40%

Moderate: do not fit criteria for Strong or Weak

Weak: # of Data above Limit > 9 and |Average| > 40%

Table 7-7: Measured versus FMR Computed Comparison for Girder Web Gage W

<u>Gage</u>	Minimum % Error	Maximum % Error	Standard Deviation	Average % Error	# of Data above Limit	Correlation
9B-GC-BE	-100.0%	31.7%	27.9%	-9.2%	41	Strong
9J-GC-BE	-60.5%	15.5%	14.6%	-8.6%	42	Strong
9O-GC-BE	-52.5%	67.6%	22.0%	-5.4%	41	Strong
8D-GC-BE	-38.6%	26.5%	13.5%	1.8%	39	Strong
9B-GC-BI	-97.9%	155.0%	54.4%	16.5%	41	Moderate
9J-GC-BI	-51.6%	27.1%	15.3%	-0.9%	42	Strong
9O-GC-BI	-64.7%	79.4%	29.8%	1.3%	42	Strong
8D-GC-BI	-27.6%	33.1%	14.8%	2.7%	40	Strong
9B-GA-BE	-137.4%	80.7%	43.0%	0.3%	41	Moderate
9J-GA-BE	-54.3%	24.3%	14.2%	-0.7%	42	Strong
9O-GA-BE	-52.4%	56.8%	24.3%	8.9%	40	Strong
9B-GA-BI	-74.5%	146.5%	34.3%	19.7%	38	Strong
9J-GA-BI	-52.2%	48.8%	18.1%	30.6%	41	Moderate
9O-GA-BI	-20.8%	59.9%	18.3%	8.0%	38	Strong
8D-GA-BI	-29.6%	39.1%	15.5%	12.6%	39	Strong

Correlation

Strong: # of Data above Limit > 9, |Average| < 20%, and Standard Deviation < 40%

Moderate: do not fit criteria for Strong or Weak

Weak: # of Data above Limit > 9 and |Average| > 40%

Table 7-8: Measured versus FM Computed Comparison for Bottom Flange Tip Gages BI, BE

Gage	Minimum % Error	Maximum % Error	Standard Deviation	Average % Error	# of Data above Limit	Correlation
9B-GC-BE	-98.0%	56.5%	33.0%	8.2%	41	Strong
9J-GC-BE	-60.5%	15.5%	14.6%	-8.6%	42	Strong
9O-GC-BE	-46.2%	91.2%	25.1%	8.1%	41	Strong
8D-GC-BE	-38.6%	26.5%	13.5%	1.8%	39	Strong
9B-GC-BI	-97.4%	205.6%	65.2%	38.9%	41	Moderate
9J-GC-BI	-51.6%	27.1%	15.3%	-0.9%	42	Strong
9O-GC-BI	-59.9%	105.0%	34.1%	15.4%	42	Strong
8D-GC-BI	-27.6%	33.1%	14.8%	2.7%	40	Strong
9B-GA-BE	-144.7%	112.3%	50.6%	17.1%	41	Moderate
9J-GA-BE	-54.3%	24.3%	14.2%	-0.7%	42	Strong
9O-GA-BE	-46.6%	74.9%	27.0%	21.5%	40	Moderate
9B-GA-BI	-74.5%	186.7%	40.4%	39.4%	38	Moderate
9J-GA-BI	-52.2%	48.8%	18.1%	30.6%	41	Moderate
9O-GA-BI	-12.2%	77.8%	20.4%	20.1%	38	Moderate
8D-GA-BI	-29.6%	39.1%	15.5%	12.6%	39	Strong

Correlation

Strong: # of Data above Limit > 9, |Average| < 20%, and Standard Deviation < 40%

Moderate: do not fit criteria for Strong or Weak

Weak: # of Data above Limit > 9 and |Average| > 40%

Table 7-9: Measured versus FMR Computed Comparison for Bottom Flange Tip Gages BI, BE

Gage	Minimum % Error	Maximum % Error	Standard Deviation	Average % Error	# of Data above Limit	Correlation
9B-GC-TE	-78.7%	-56.7%	6.3%	-68.2%	24	Weak
9J-GC-TE	-53.8%	-18.1%	12.6%	-40.3%	9	Moderate
9O-GC-TE	-65.2%	68.2%	31.7%	-21.8%	27	Moderate
8D-GC-TE	-200.3%	122.8%	79.5%	-57.1%	12	Weak
9B-GC-TI	-77.6%	-29.8%	9.0%	-63.3%	23	Weak
9J-GC-TI	-55.8%	17.7%	24.0%	-30.2%	8	Moderate
9O-GC-TI	-87.1%	26.0%	25.3%	-34.8%	29	Moderate
8D-GC-TI	-58.9%	61.4%	36.9%	-13.8%	7	Moderate
9B-GA-TE	-63.1%	36.4%	21.4%	-42.9%	19	Weak
9J-GA-TE	-97.4%	35.0%	46.5%	-25.9%	8	Moderate
9O-GA-TE	-58.8%	33.8%	18.3%	-29.4%	31	Moderate
9B-GA-TI*	--	--	--	--	--	*No Data
9J-GA-TI*	--	--	--	--	--	*No Data
9O-GA-TI	-56.9%	-10.3%	11.5%	-36.2%	32	Moderate
8D-GA-TI**	-123.6%	-28.0%	25.5%	-72.2%	27	**Unreliable

Correlation

Strong: # of Data above Limit > 9, |Average| < 20%, and Standard Deviation < 40%

Moderate: do not fit criteria for Strong or Weak

Weak: # of Data above Limit > 9 and |Average| > 40%

Table 7-10: Measured versus FM Computed Comparison for Top Flange Tip Gages TI, TE

<u>Gage</u>	Minimum % Error	Maximum % Error	Standard Deviation	Average % Error	# of Data above Limit	Correlation
9B-GC-TE	74.7%	271.8%	61.4%	159.6%	24	Weak
9J-GC-TE	-53.8%	-18.1%	12.6%	-40.3%	9	Moderate
9O-GC-TE	94.0%	793.0%	169.9%	320.2%	27	Weak
8D-GC-TE	-200.3%	122.8%	79.5%	-57.1%	12	Weak
9B-GC-TI	84.1%	464.5%	68.2%	206.8%	23	Weak
9J-GC-TI	-55.8%	17.7%	24.0%	-30.2%	8	Moderate
9O-GC-TI	-25.8%	570.6%	132.6%	248.2%	29	Weak
8D-GC-TI	-58.9%	61.4%	36.9%	-13.8%	7	Moderate
9B-GA-TE	158.2%	799.7%	138.8%	292.1%	19	Weak
9J-GA-TE	-97.4%	35.0%	46.5%	-25.9%	8	Moderate
9O-GA-TE	73.9%	478.0%	78.9%	202.4%	31	Weak
9B-GA-TI*	--	--	--	--	--	*No Data
9J-GA-TI*	--	--	--	--	--	*No Data
9O-GA-TI	83.1%	268.6%	50.1%	167.1%	32	Weak
8D-GA-TI**	-123.6%	-28.0%	25.5%	-72.2%	27	**Unreliable

Correlation

Strong: # of Data above Limit > 9, |Average| < 20%, and Standard Deviation < 40%

Moderate: do not fit criteria for Strong or Weak

Weak: # of Data above Limit > 9 and |Average| > 40%

Table 7-11: Measured versus FMR Computed Comparison for Top Flange Tip Gages TI, TE

<u>Gage</u>	Minimum % Error	Maximum % Error	Standard Deviation	Average % Error	# of Data above Limit	Correlation
9F-D-TI	-154.9%	-108.1%	11.9%	-122.0%	25	Weak
9F-D-BI	-156.7%	-122.0%	10.7%	-137.7%	10	Weak
9F-D-TQI	-78.7%	-75.2%	1.8%	-76.9%	2	Moderate
9F-D-BQI	-155.8%	24.0%	63.7%	-58.5%	17	Weak
9F-D-TM	-111.6%	-39.2%	16.2%	-65.6%	23	Weak
9F-D-BM	-217.3%	-115.5%	25.0%	-159.6%	16	Weak
9F-D-TQE	-112.5%	-112.5%	0.0%	-112.5%	1	Moderate
9F-D-BQE	-179.2%	176.0%	86.9%	3.9%	23	Moderate
9F-D-TE	-116.6%	-101.0%	5.1%	-107.2%	19	Weak
9F-D-BE	-102.4%	-18.3%	35.8%	-69.4%	10	Weak
8A-D-TI	-98.2%	19.7%	41.7%	-43.5%	7	Moderate
8A-D-BI**	-125.4%	-37.7%	29.2%	-88.3%	24	**Unreliable
8A-D-TQI	-132.4%	-39.4%	29.0%	-95.0%	15	Weak
8A-D-BQI	-85.5%	20.0%	25.5%	-40.9%	18	Weak
8A-D-TM	0.0%	0.0%	--	--	0	Moderate
8A-D-BM	-96.4%	64.1%	50.7%	-22.7%	10	Moderate
8A-D-TQE	-176.1%	-137.8%	11.0%	-150.6%	10	Weak
8A-D-BQE	-34.0%	147.7%	39.0%	28.2%	30	Moderate
8A-D-TE	-110.3%	-82.3%	10.6%	-99.6%	6	Moderate
8A-D-BE	-166.5%	67.7%	66.0%	-50.8%	17	Weak

Correlation

Strong: # of Data above Limit > 9, |Average| < 20%, and Standard Deviation < 40%

Moderate: do not fit criteria for Strong or Weak

Weak: # of Data above Limit > 9 and |Average| > 40%

Table 7-12: Measured versus Computed Comparison for Diaphragm Gages

Gage	Minimum % Error	Maximum % Error	Standard Deviation	Average % Error	# of Data above Limit	Correlation
9E-LBU-CN	-248.1%	223.9%	108.7%	-23.8%	34	Moderate
9E-LBD-CN	-85.4%	133.0%	39.3%	-5.0%	36	Strong
9G-LBU-CN	-145.9%	429.0%	118.8%	-18.6%	32	Moderate
9G-LBD-CN	-84.3%	171.0%	62.3%	-9.3%	37	Moderate
9K-LBU-CN	-91.4%	153.8%	63.3%	2.5%	32	Moderate
9K-LBD-CN	-459.8%	524.6%	188.8%	-32.5%	31	Moderate
9O-LBD-CN	-296.5%	180.7%	86.3%	6.1%	32	Moderate
8B-LBU-CN	-337.6%	199.3%	90.6%	19.2%	32	Moderate
8D-LBU-CN	-126.9%	137.1%	81.0%	-48.0%	25	Weak
8F-LBD-CN	-78.8%	0.8%	15.8%	-62.2%	20	Weak

Correlation

Strong: # of Data above Limit > 9, |Average| < 20%, and Standard Deviation < 40%

Moderate: do not fit criteria for Strong or Weak

Weak: # of Data above Limit > 9 and |Average| > 40%

Table 7-13: Measured versus Computed Comparison for Lateral Wind Bracing Gages

Test	Fatigue Detail Stress Ranges for Dynamic Tests (ksi)															
	Web Gaps					Gusset Plate										
	9F-GPC-WG		9I-GPC-WG		8E-GPC-WG		9F-GPA-WG		9I-GPA-WG		9F-GPA-LO		9F-GPA-W9		9F-GPA-W8	
Test	Tensile	Total	Tensile	Total	Tensile	Total	Tensile	Total	Tensile	Total	Tensile	Total	Tensile	Total	Tensile	Total
D1	--	--	0.41	1.84	0.32	1.42	--	--	0.35	1.14	--	--	--	--	--	--
D2	0.31	0.96	0.39	1.64	0.41	1.50	0.16	0.74	0.24	1.11	1.12	1.73	5.19	7.46	4.29	6.43
D3	0.31	0.96	0.39	1.75	0.35	1.54	0.17	0.73	0.30	1.17	1.17	1.84	5.44	8.02	4.58	7.17
D5	--	--	0.43	2.02	0.35	1.36	0.00	--	0.29	1.24	--	--	--	--	--	--
D6	0.31	1.29	--	--	--	--	0.14	0.90	--	--	1.54	2.18	7.09	9.62	6.18	8.69
D7	--	--	0.32	1.76	0.24	1.26	--	--	0.33	1.14	--	--	--	--	--	--
D8	0.32	1.06	0.38	1.95	0.26	1.32	0.13	0.81	0.31	1.14	1.37	2.05	6.41	8.93	5.23	7.69
D9	0.33	1.04	0.33	1.86	0.29	1.37	0.14	0.73	0.19	0.97	1.38	2.04	5.68	8.27	4.82	7.24
D11	0.10	0.34	0.31	1.21	0.27	1.36	0.05	0.30	0.15	0.75	0.43	0.66	1.85	2.53	1.82	2.46
D12	0.10	0.29	--	--	--	--	0.06	0.27	--	--	0.35	0.58	1.61	2.48	1.48	2.25
D13	0.24	0.85	0.39	1.96	0.22	1.20	0.13	0.74	0.32	1.25	1.18	1.72	5.41	7.24	4.69	6.46
Maximum:	0.33	1.29	0.43	2.02	0.41	1.54	0.17	0.90	0.35	1.25	1.54	2.18	7.09	9.62	6.18	8.69
Average:	0.26	0.90	0.37	1.78	0.30	1.37	0.11	0.65	0.28	1.10	1.07	1.60	4.83	6.82	4.14	6.05

-- no data recorded

Table 7-14: Fatigue Detail Stress Ranges for Dynamic Tests

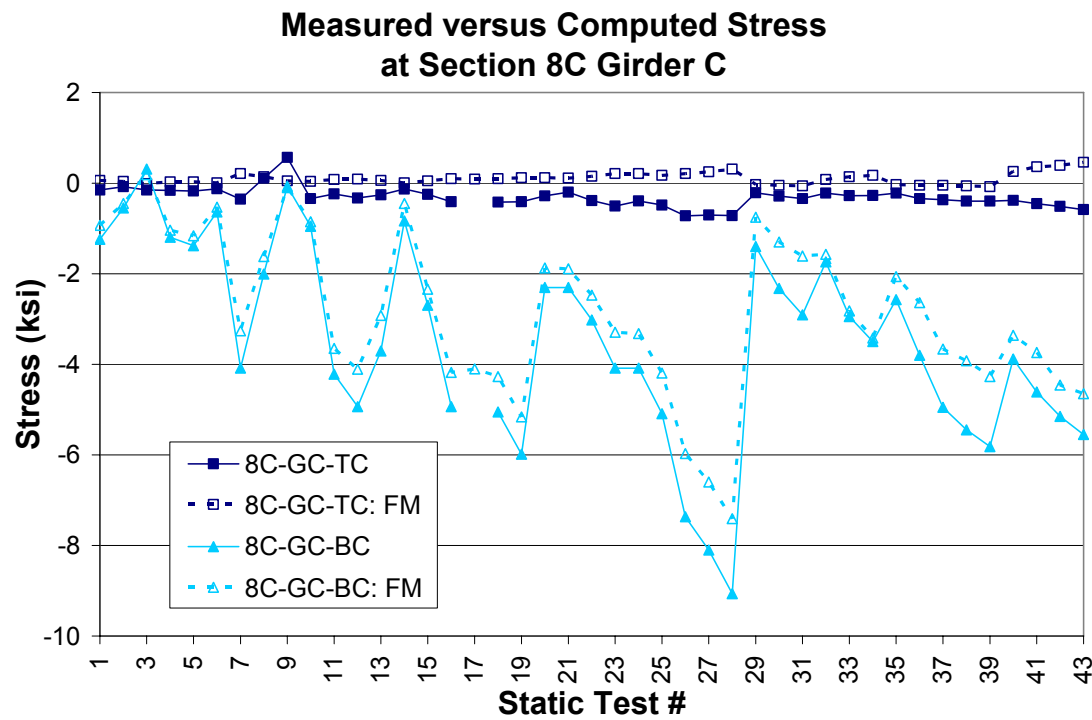


Figure 7-1: FM Analysis versus Measured at Section 8C Girder C

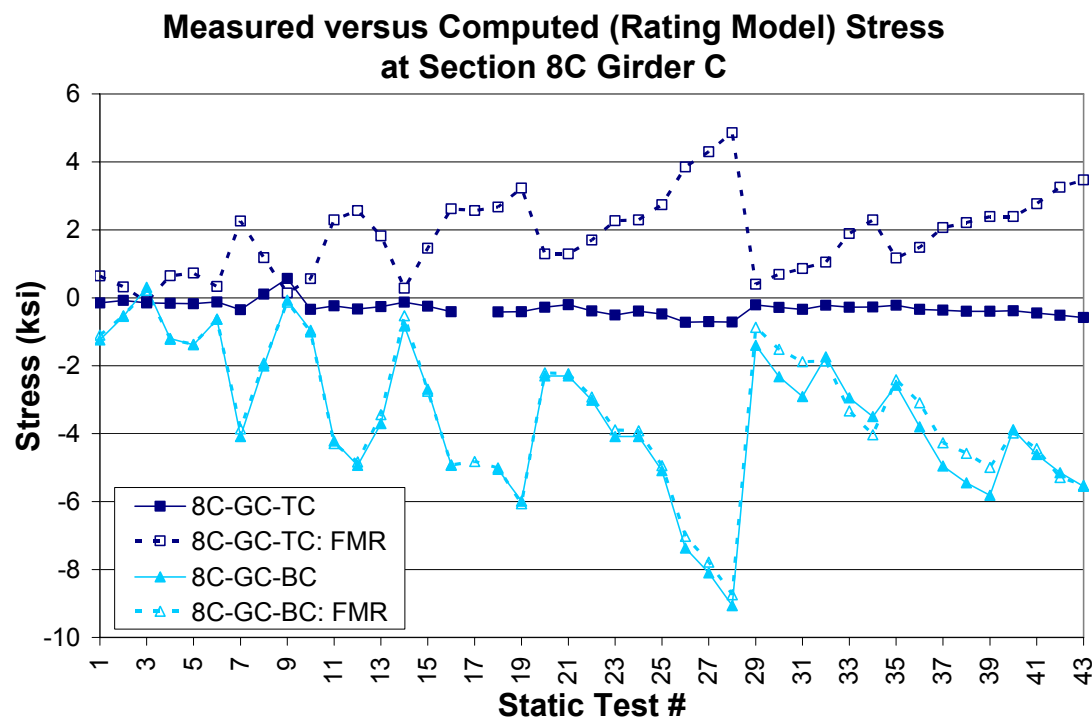


Figure 7-2: FMR Analysis versus Measured at Section 8C Girder C

Comparison for Gage Locations TC and BC of Girder C

Test S19 (T19): Maximum Load on Midspan 98

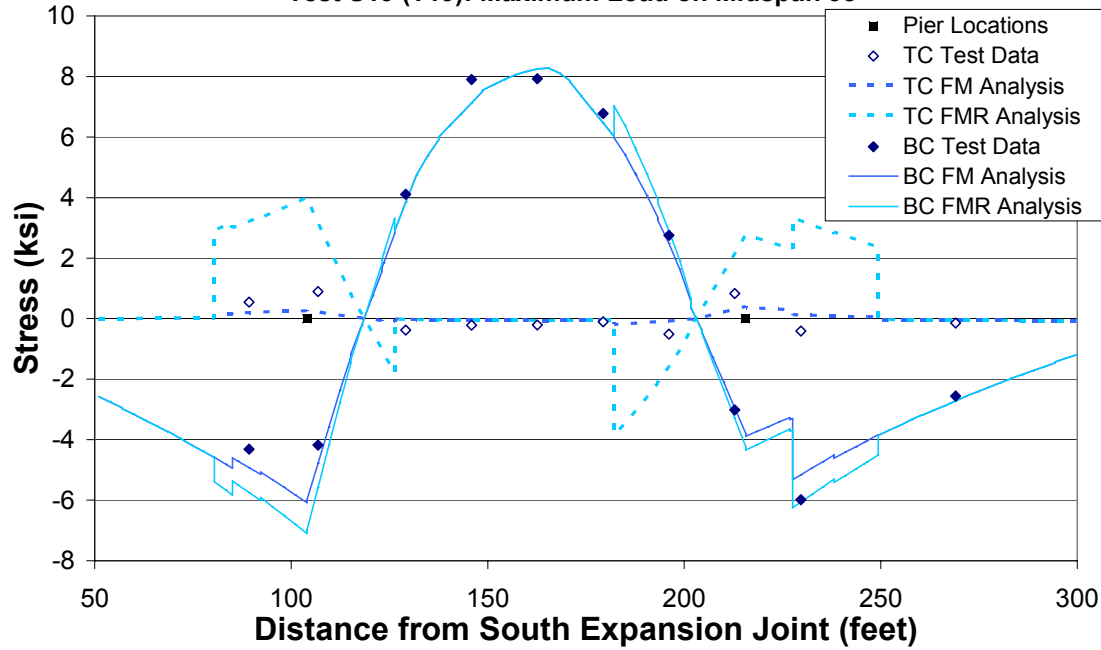


Figure 7-3: Interior Girder C Bending Stresses for Test S19

Comparison for Gage Locations TC and BC of Girder A

Test S19 (T19): Maximum Load on Midspan 98

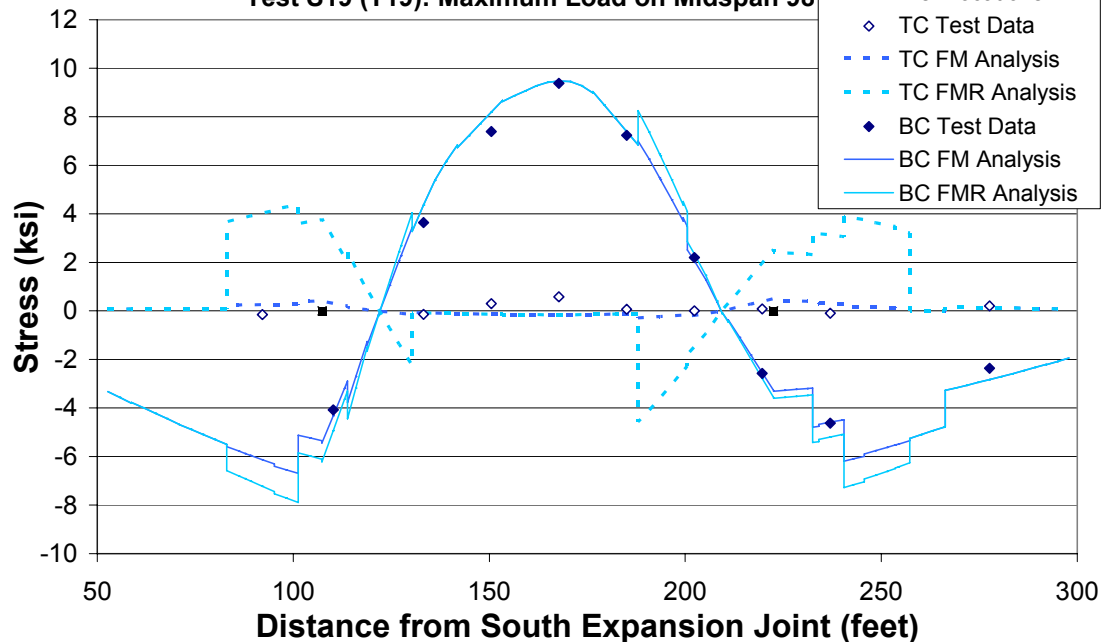


Figure 7-4: Exterior Girder A Bending Stresses for Test S19

Comparison for Gage Locations TC and BC of Girder C

Test S24 (T17): Maximum Load on Midspan 87

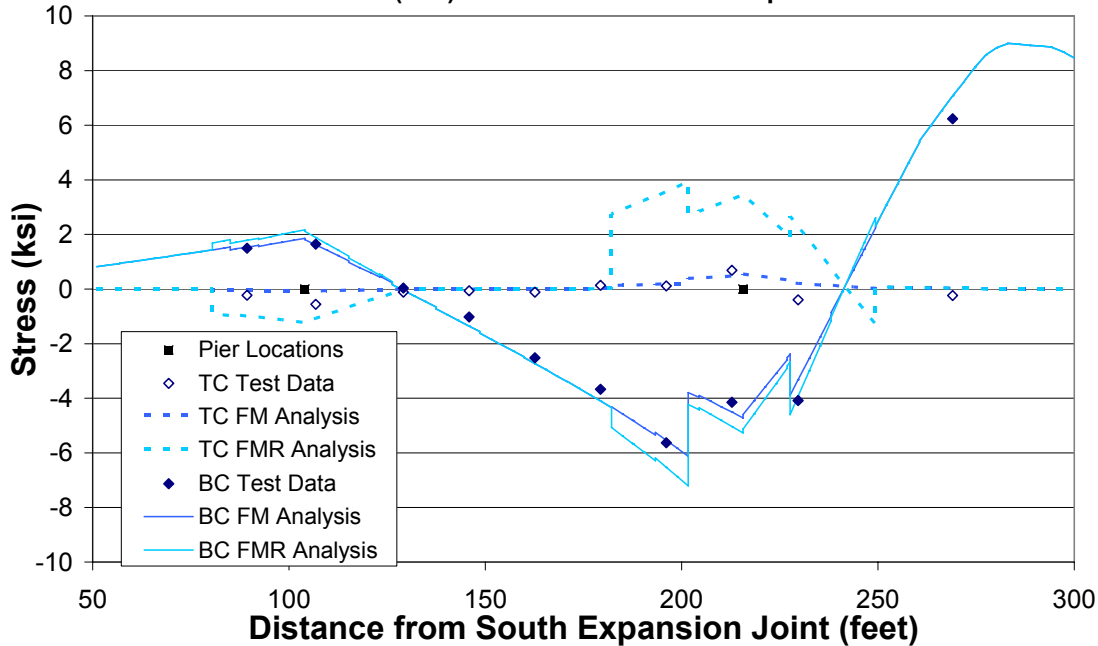


Figure 7-5: Interior Girder C Bending Stresses for Test S24

Comparison for Gage Locations TC and BC of Girder A

Test S24 (T17): Maximum Load on Midspan 87

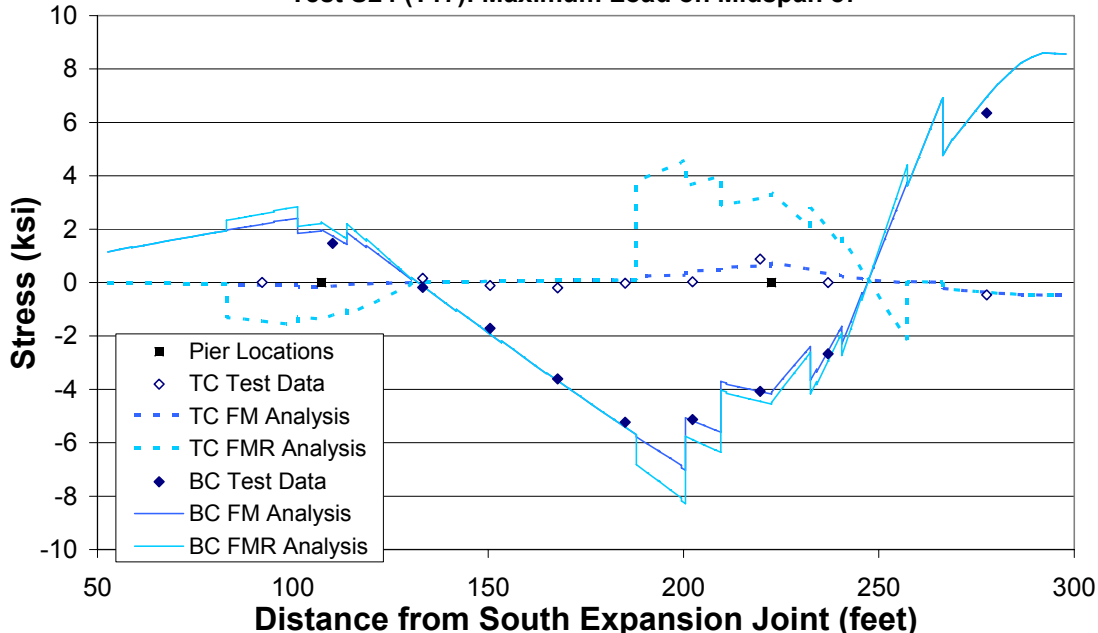


Figure 7-6: Exterior Girder A Bending Stresses for Test S24

Comparison for Gage Locations TC and BC of Girder C

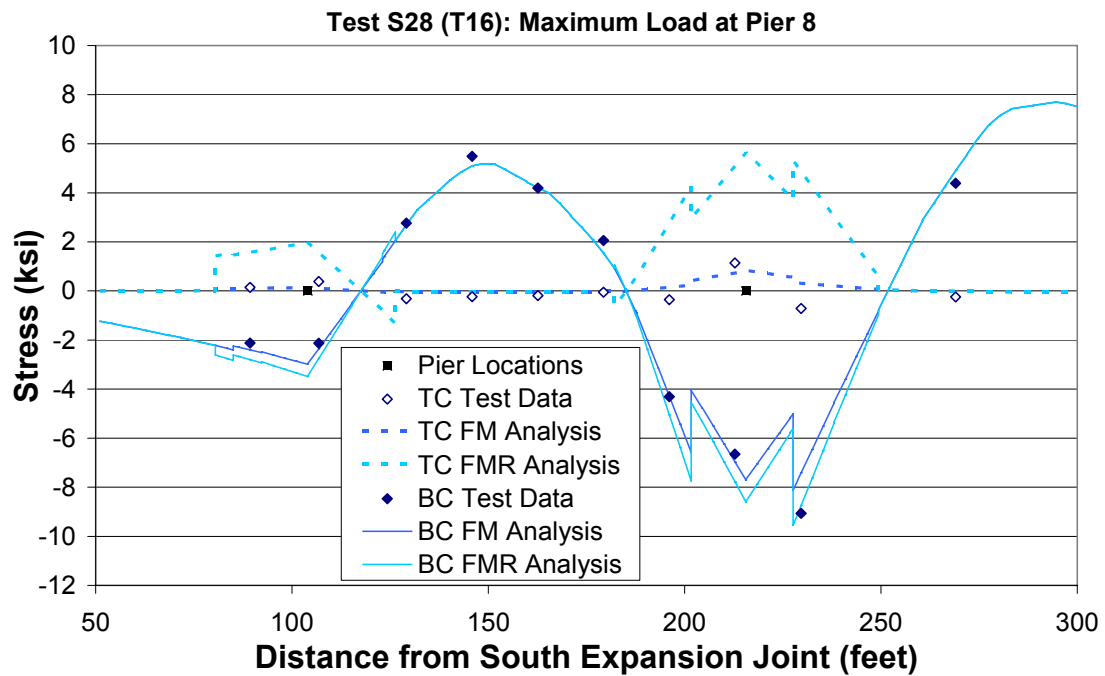


Figure 7-7: Interior Girder C Bending Stresses for Test S28

Comparison for Gage Locations TC and BC of Girder A

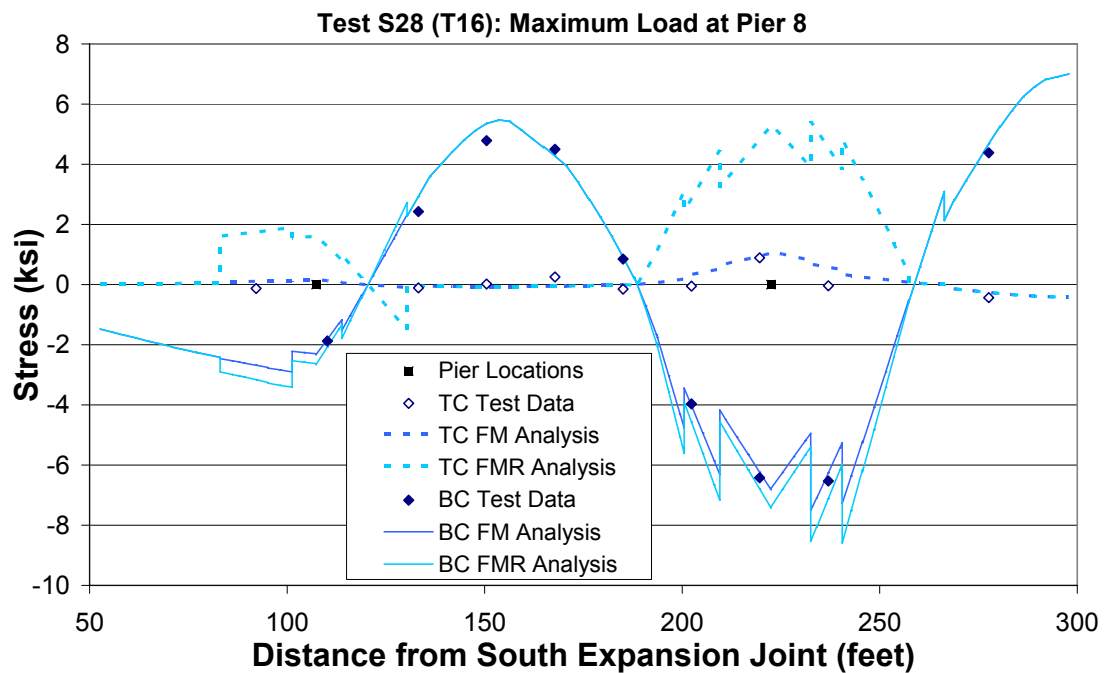


Figure 7-8: Exterior Girder A Bending Stresses for Test S28

Comparison for Gage Locations TC and BC of Girder C

Test S39 (T39): Maximum Twist over Pier 8

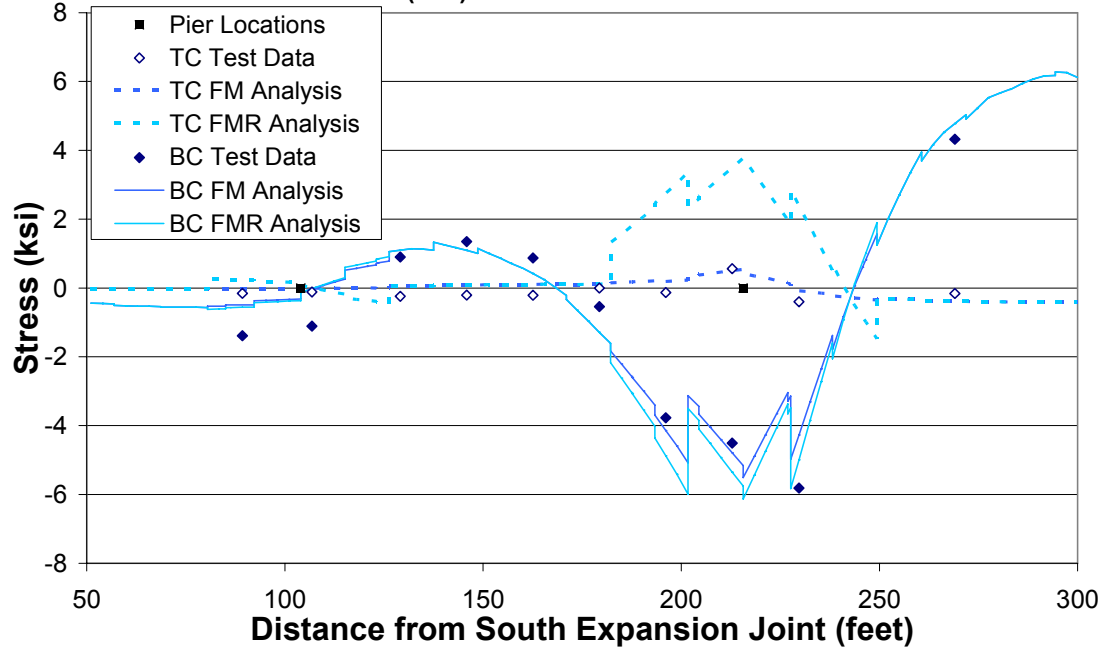


Figure 7-9: Interior Girder C Bending Stresses for Tests S39

Comparison for Gage Locations TC and BC of Girder A

Test S39 (T39): Maximum Twist over Pier 8

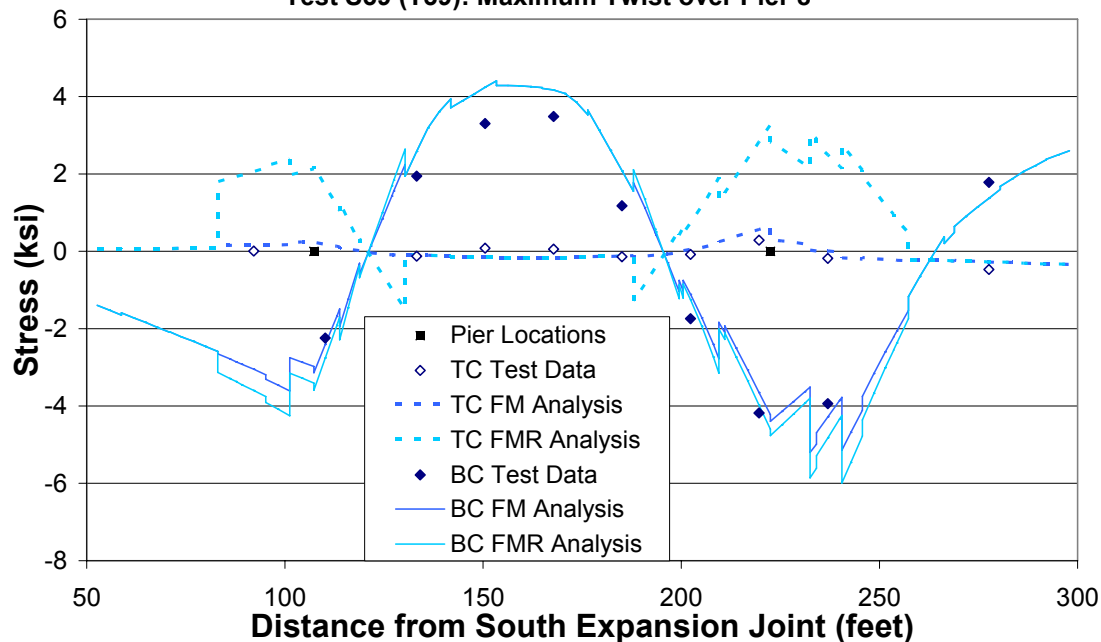


Figure 7-10: Exterior Girder A Bending Stresses for Test S39

Comparison for Gage Locations TC and BC of Girder C

Test S43 (T41): Maximum Twist over Pier 8

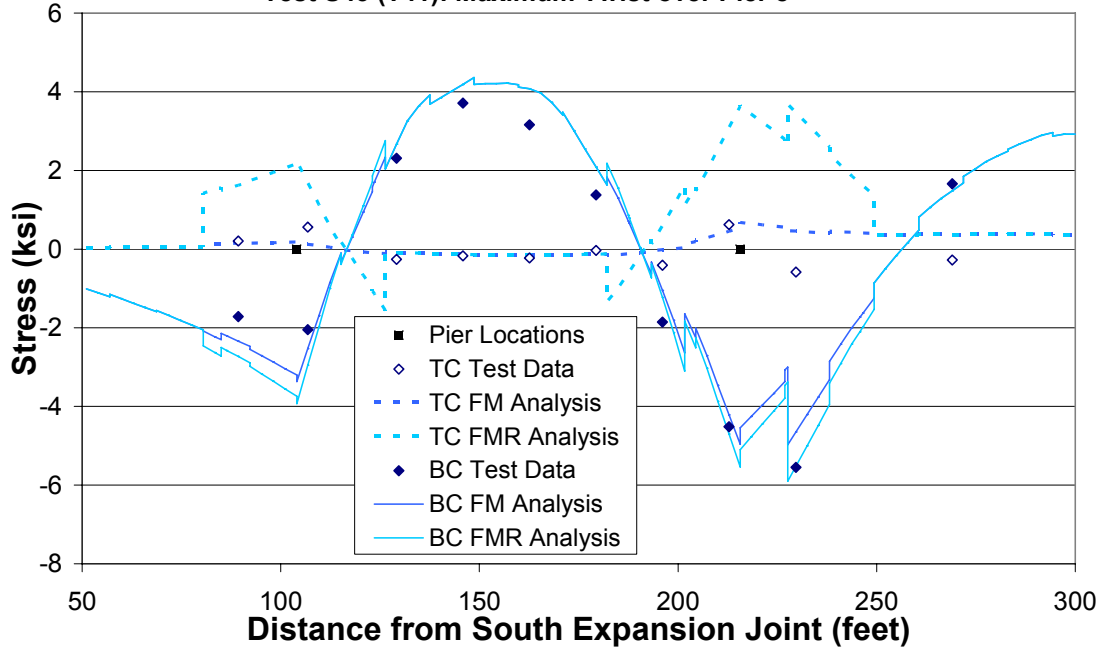


Figure 7-11: Interior Girder C Bending Stresses for Test S43

Comparison for Gage Locations TC and BC of Girder A

Test S43 (T41): Maximum Twist over Pier 8

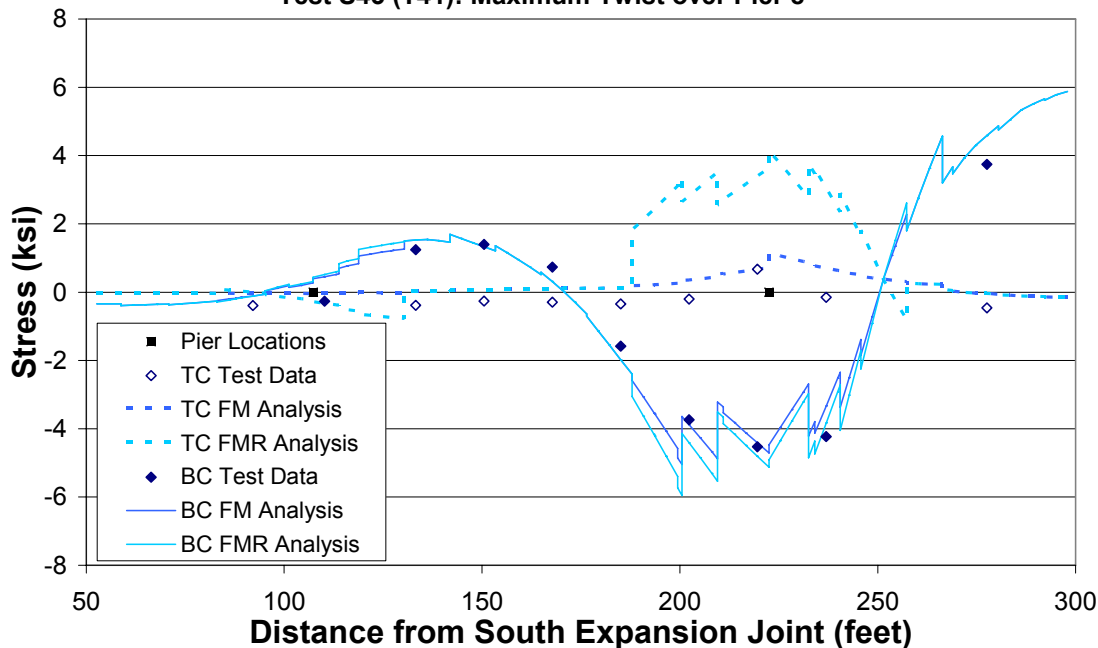


Figure 7-12: Exterior Girder A Bending Stresses for Test S43

Comparison for Bottom Flange Tip Warping of Girder C

Test S24 (T17): Maximum Load on Midspan 87

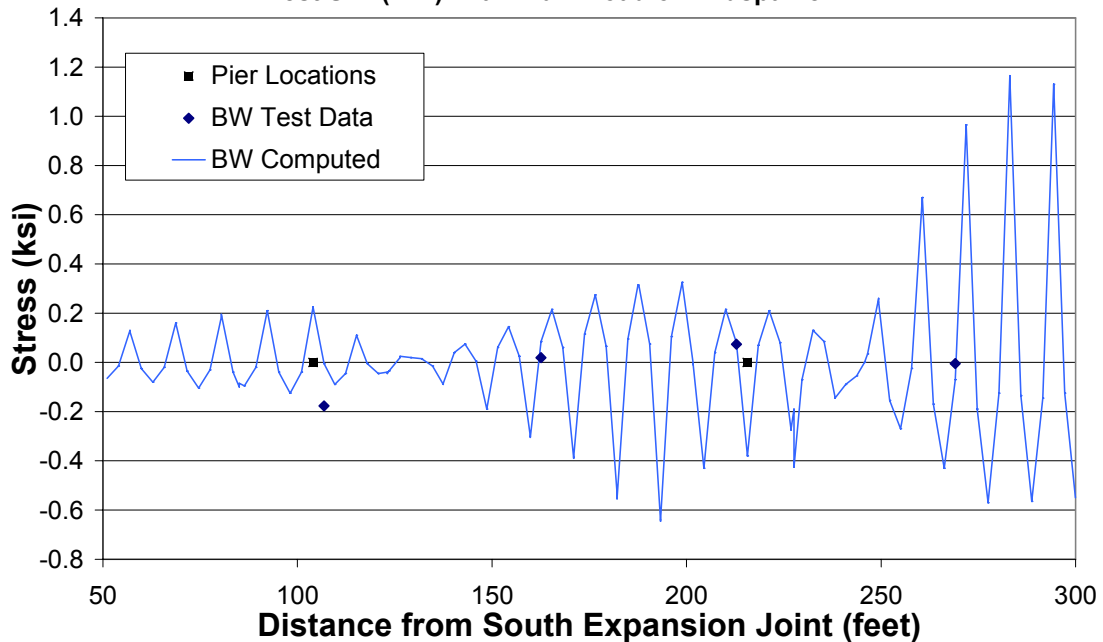


Figure 7-13: Warping Stresses on Interior Girder C for Test S24

Comparison for Bottom Flange Tip Warping of Girder A

Test S24 (T17): Maximum Load on Midspan 87

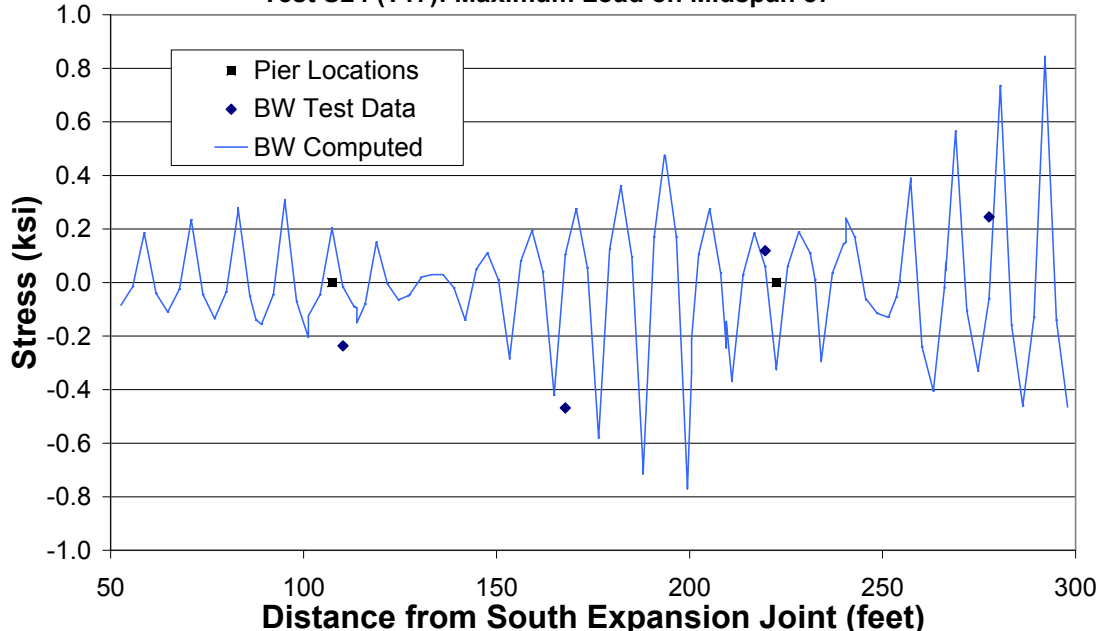


Figure 7-14: Warping Stresses on Exterior Girder A for Test S24

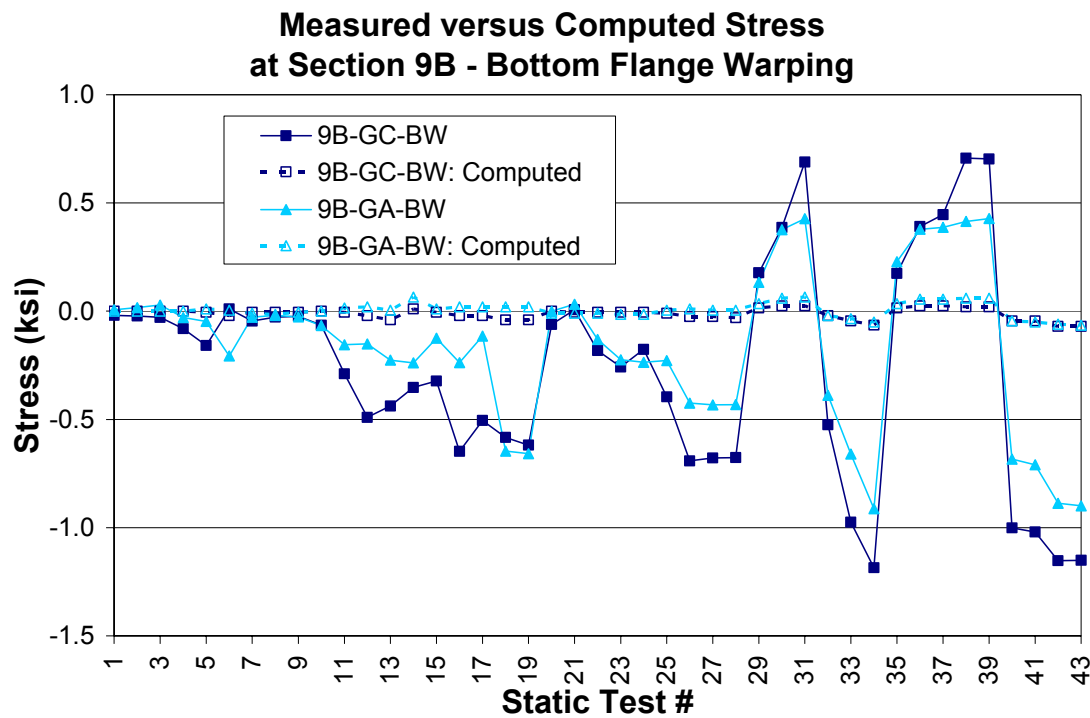


Figure 7-15: Bottom Flange Warping Comparisons at Section 9B

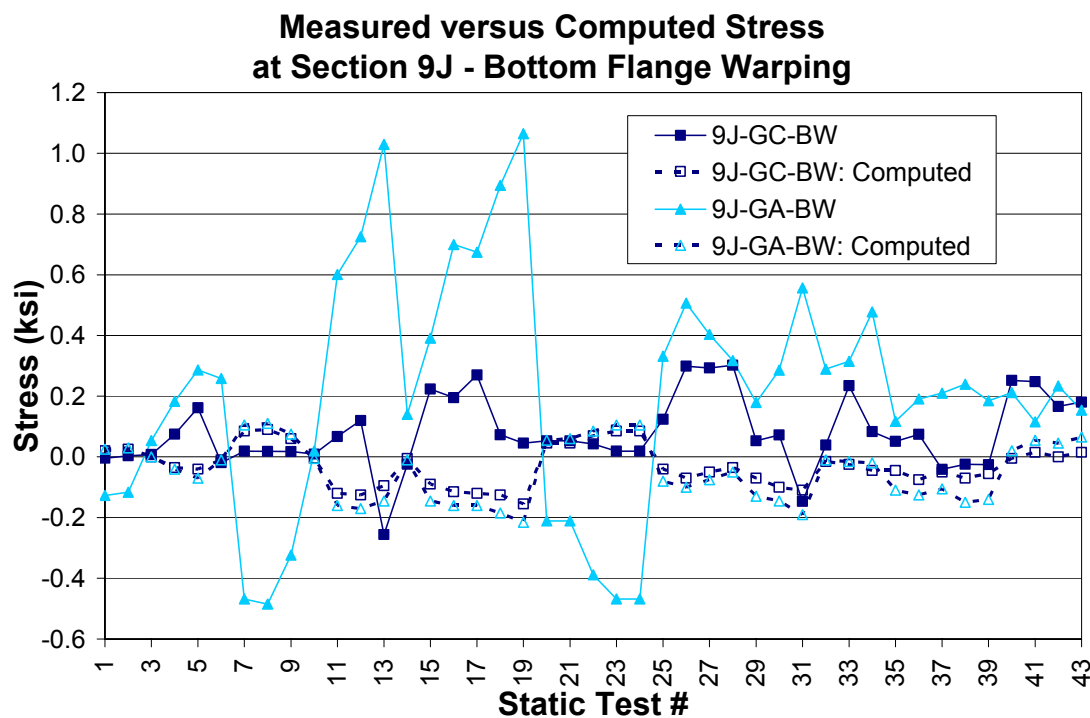


Figure 7-16: Bottom Flange Warping Comparisons at Section 9J

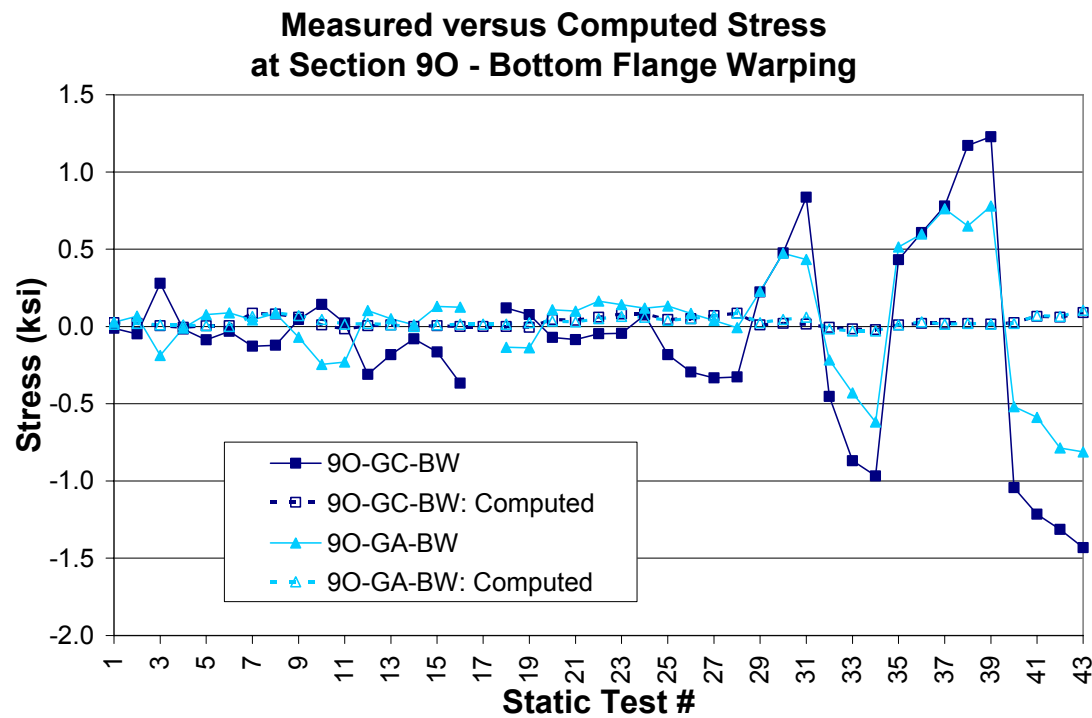


Figure 7-17: Bottom Flange Warping Comparisons at Section 9O

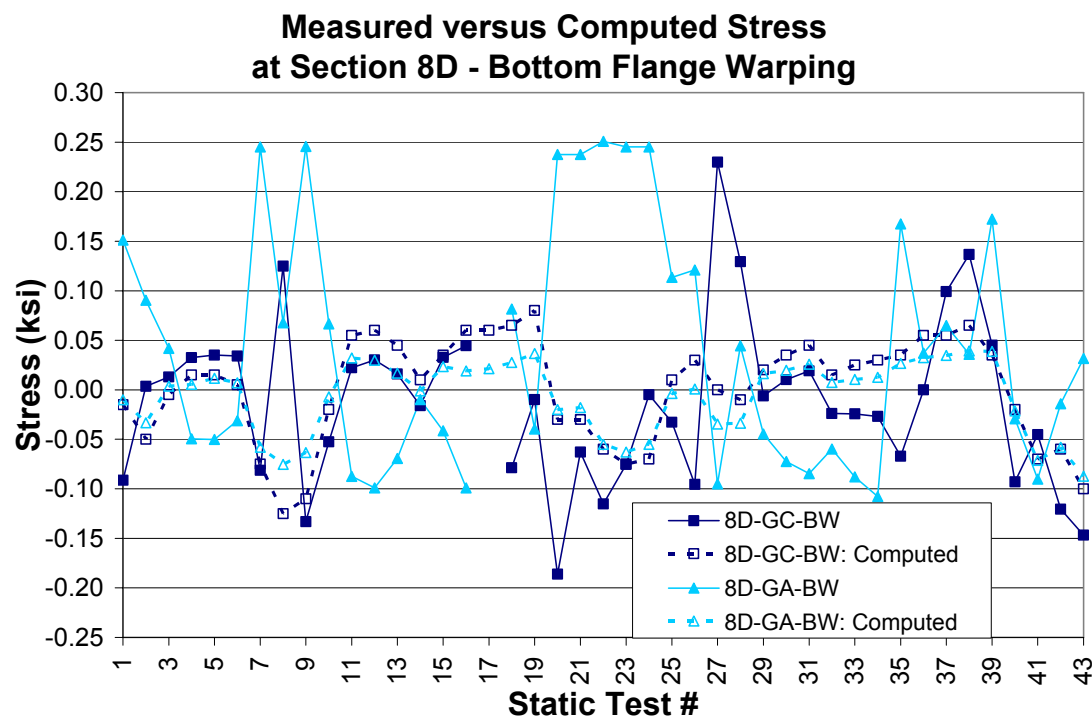


Figure 7-18: Bottom Flange Warping Comparisons at Section 8D

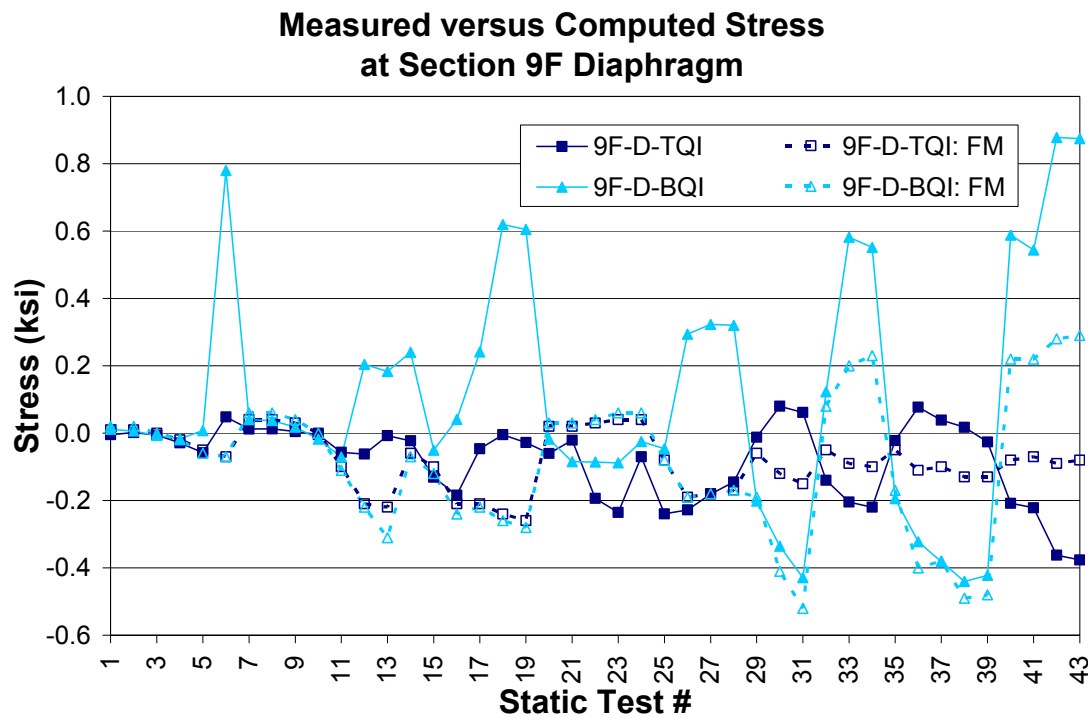


Figure 7-19: Measured versus Computed Diaphragm Stresses at Section 9F-D-QI

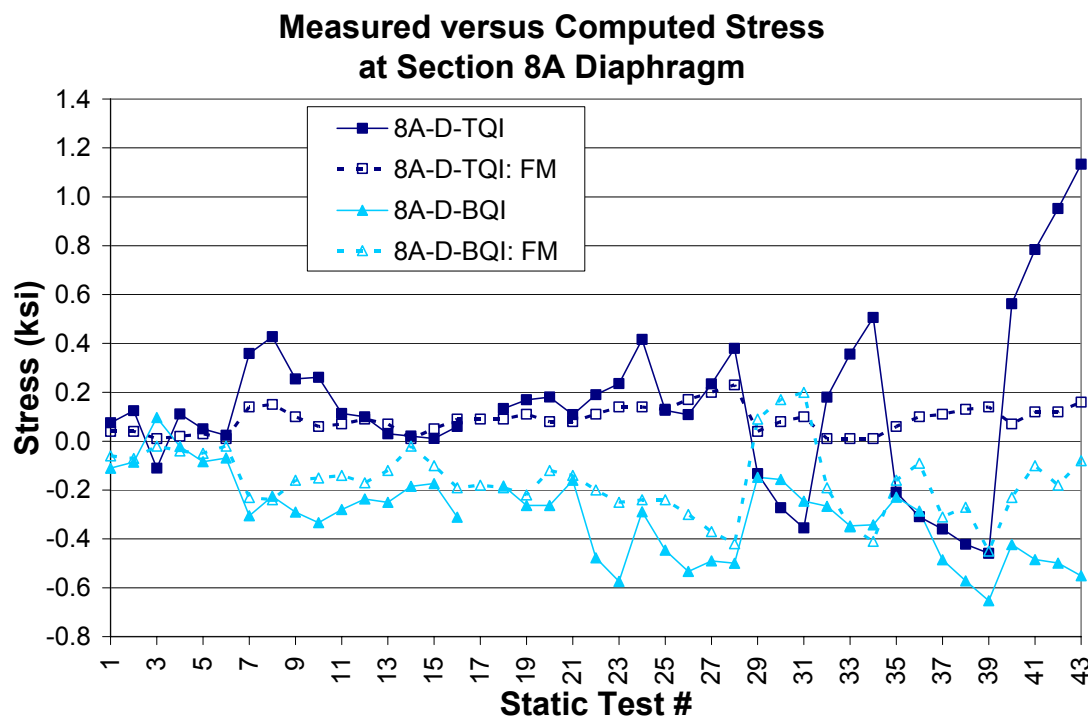


Figure 7-20: Measured versus Computed Diaphragm Stresses at Section 8A-D-QI

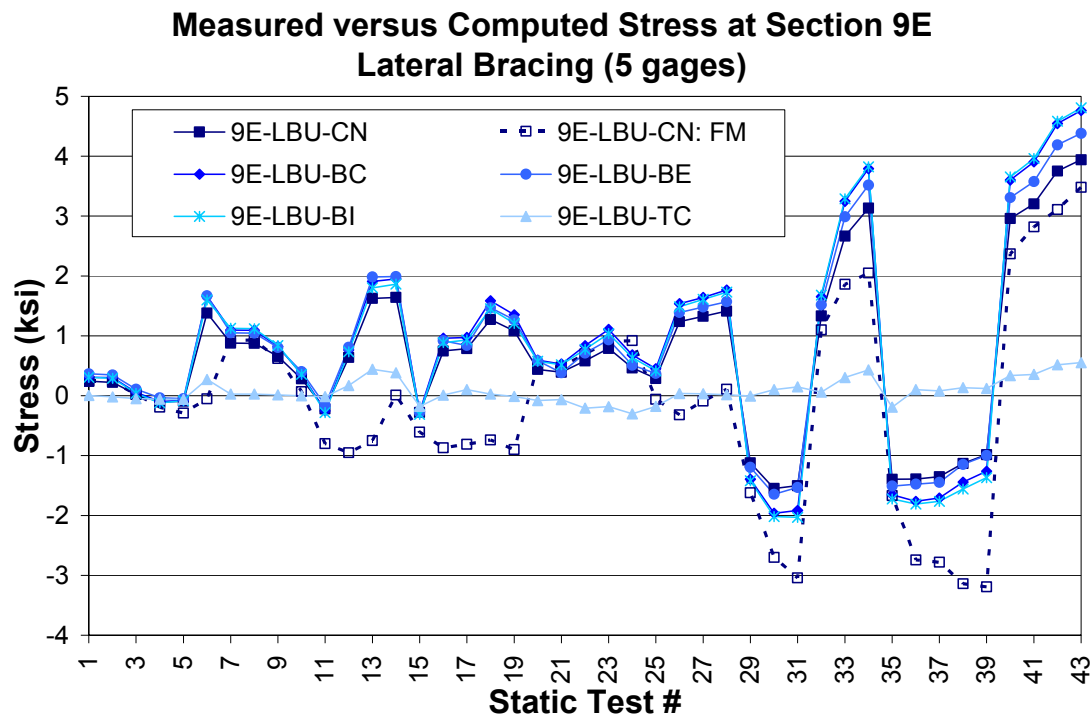


Figure 7-21: Comparison of Five Lateral Bracing Gages at Section 9E-LBU

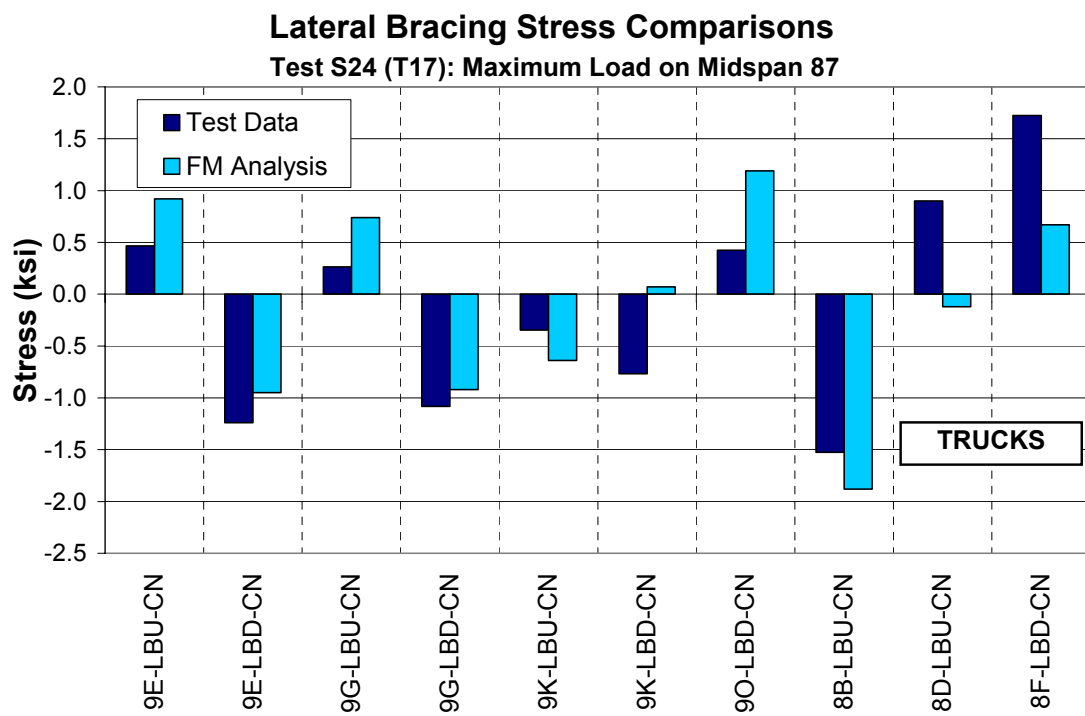


Figure 7-22: Tensile Lateral Wind Bracing Behavior on Span 8-7

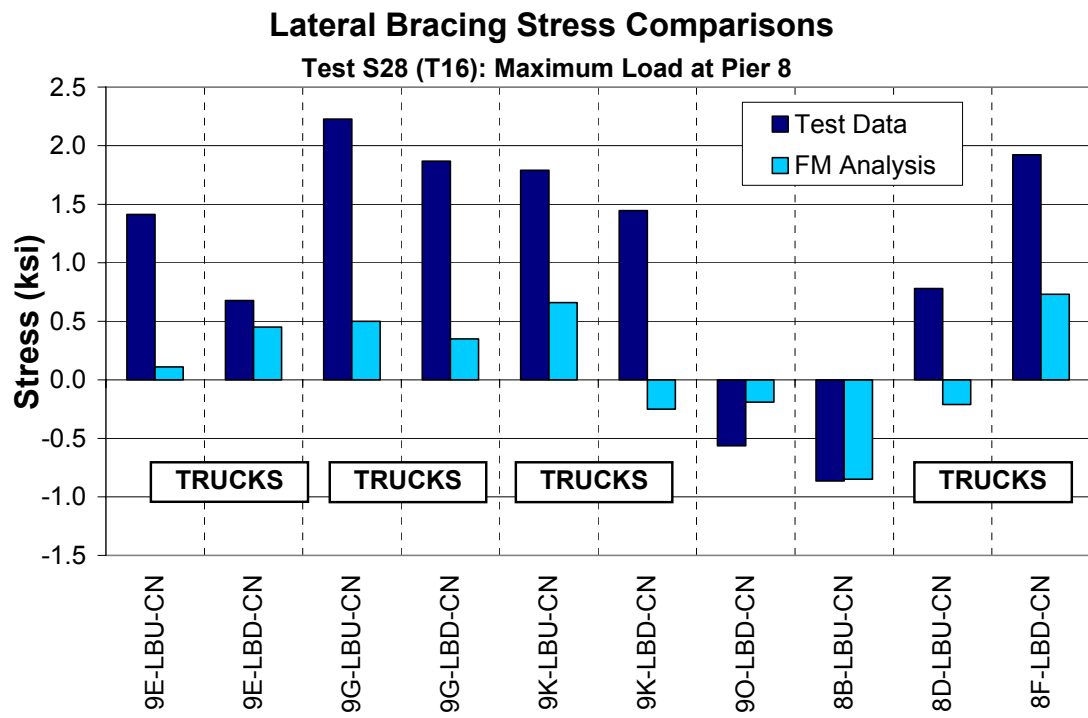


Figure 7-23: Tensile Lateral Wind Bracing Behavior on Span 9-8 and Span 8-7

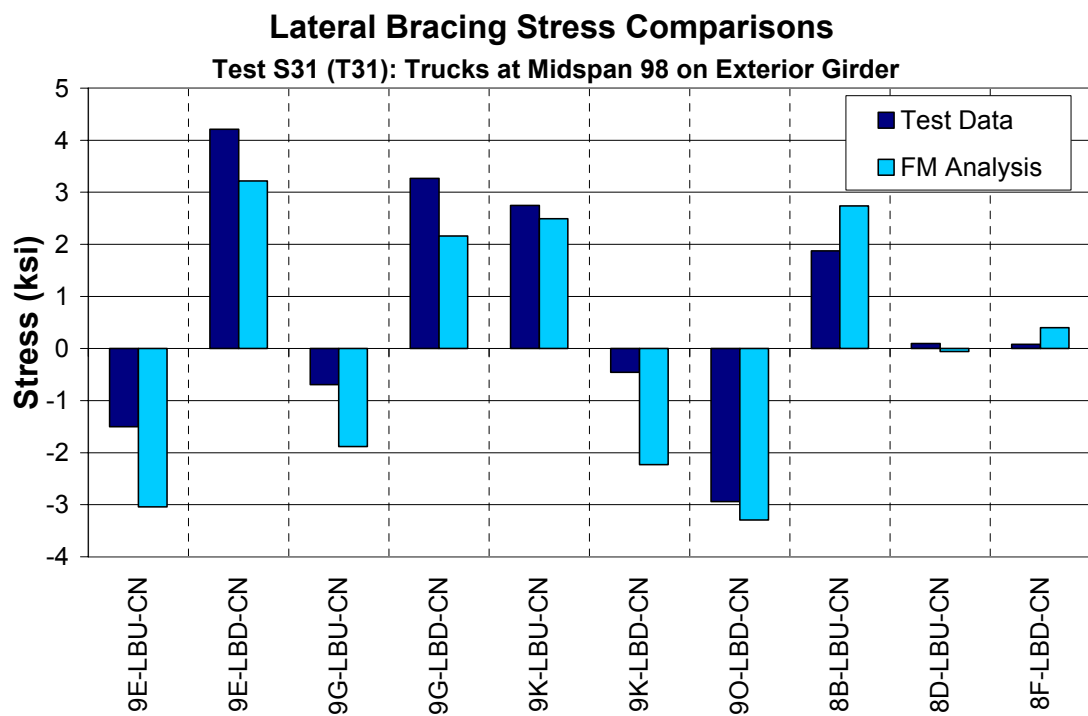


Figure 7-24: Well Correlated Lateral Wind Bracing Behavior



Figure 7-25: Photograph of Gusset Plate Tip Strain Gage

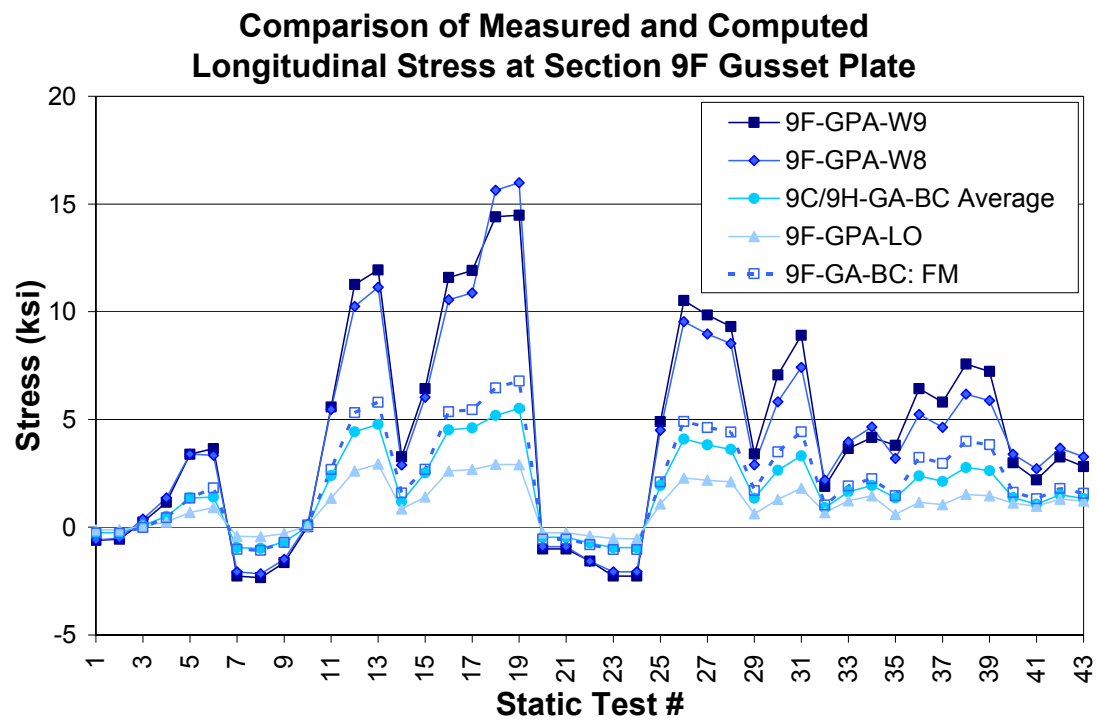


Figure 7-26: Gusset Plate Stress Comparison

Stress Concentration Factors for Longitudinal Stress at Section 9F Gusset Plate Tips

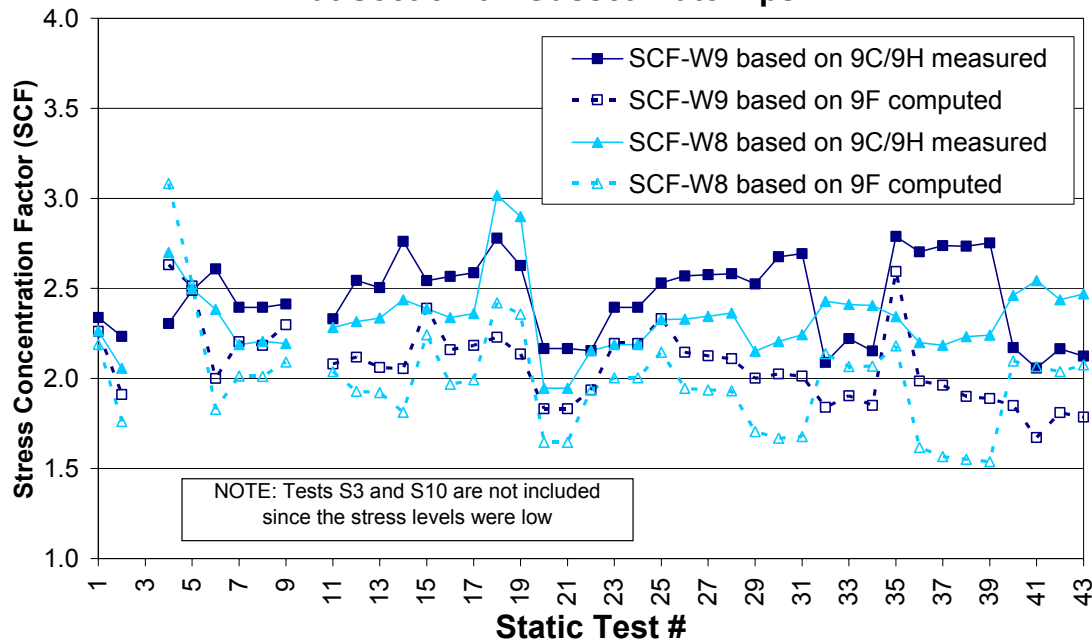


Figure 7-27: Stress Concentration Factors for Gusset Plate Detail

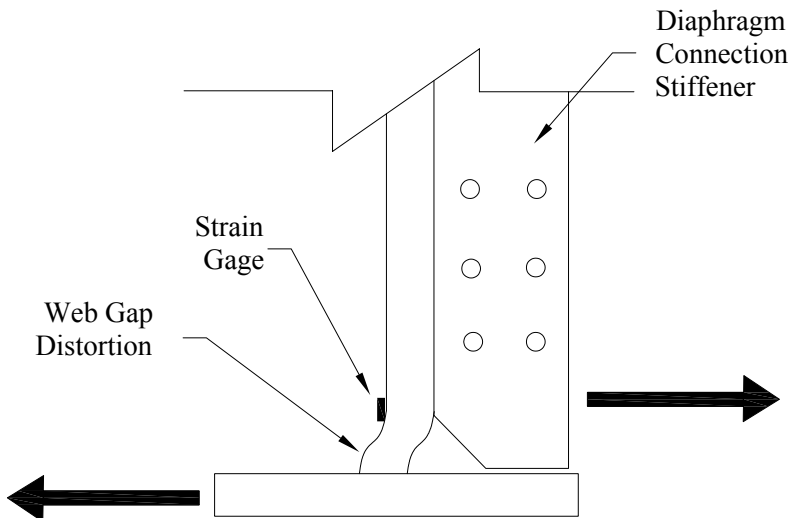


Figure 7-28: Out-of-Plane Web Gap Distortion



Figure 7-29: Photograph of Web Gap Strain Gage Vertically Aligned on Web

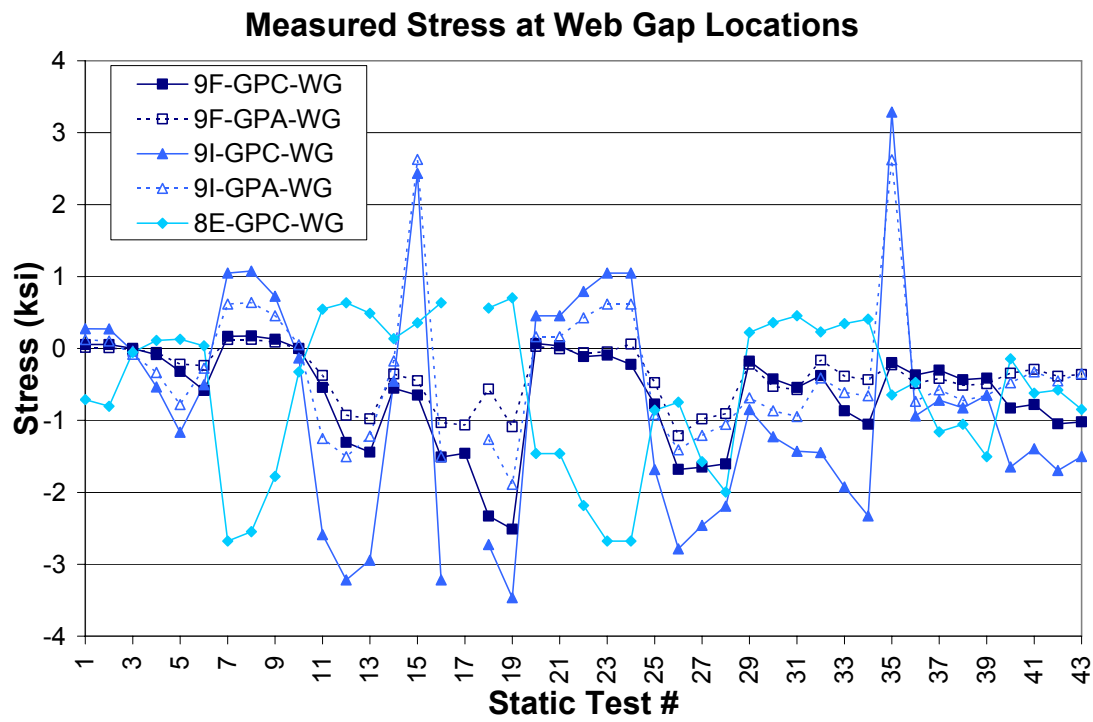


Figure 7-30: Measured Web Gap Stresses

Chapter 8

Sensitivity Study of Curved Girder Bridge Analysis and Rating

To expand the scope of the employed grillage method for the purpose of load rating horizontally curved composite steel I-girder bridges, a series of parametric studies were conducted to determine the sensitivity of the analysis method for these types of bridges. Two other previously tested horizontally curved steel I-girder bridges, Mn/DOT Bridge No. 27998 and the Federal Highway Administration (FHWA) Test Specimen, were used along with the test bridge (Mn/DOT Bridge No. 69824) to determine the extent to which various bridge and modeling parameters affect the live load computational response of these complex bridges.

The chapter begins by briefly describing each of the three bridges used for the parametric study. A series of parametric studies using grillage models created and analyzed with UMN Program are then presented focusing on the deflection, axial force, shear, moment, and stress responses of the different bridge elements when parameters are varied one at a time. Comments are made following each study discussing the significance of the findings.

8.1 Bridge Descriptions

Each of the three bridges is briefly discussed below. Layout details for each bridge are provided along with information relevant to the parametric study. Specific details of all bridge members for each bridge are not provided in this chapter, but references are given for documents that supply the specific details for each bridge.

8.1.1 Mn/DOT Bridge No. 69824 Unit 2

Mn/DOT Bridge No. 69824 Unit 2, the bridge whose response is documented in this report, is a two-girder five-span continuous composite steel I-girder bridge with an average girder radius of curvature of approximately 575 feet from Pier 10 through Pier 6 and approximately 1639 feet from Pier 6 to Pier 5. The longest girder span arc length is about 151 feet and the girder spacing is 18 feet. Both girders typically have 78 inch x 0.5 inch webs with 18 inch x 0.875 inch flanges. Flange thicknesses increase up 2.625 inches in the negative moment regions. All supports are radially positioned. The bridge deck is 9 inches thick and has a typical haunch height (distance from bottom surface of concrete deck to top surface of top flange) of 3 inches. The edges of the roadway consist of a curb and beam-column railings (i.e., beams supported on small columns). The diaphragms are radially positioned between the girders at a nearly consistent spacing of about 12 feet, and consist of W-shape beams directly beneath the concrete deck with knee bracing at the connections to the girders that extend the full depth of the girders. Between each pair of diaphragms in an X-shaped pattern are lateral wind bracing attached to gusset plates near the bottom flanges of the girders.

This bridge was the focus of the load tests carried out as part of this research project and full bridge details are provided within this document. Figure 4-3 provides the general layout of the bridge along with the UMN Program model nodes showing the mesh refinement of the bridge elements. See Chapter 3 for a more thorough description of the bridge. See Chapter 4, Chapter 6,

and Chapter 7 for more information on the computational model. The base model used here is the same as used for the Final Model (FM) analysis in Chapter 7. Although some of the computed values in the sensitivity study below would be different for the FM and the Final Model – Rating (FMR) analysis, the results determined as a percent change would be the same for both models. This is due to the similarity of the models and the fact that all differences between the two models have constant ratios, which have no effect on the result of a percent change calculation. Recall from Chapter 7 that the only difference between the FM and FMR analyses is that for the FMR analysis girder flexural stresses in the negative moment region are calculated using section properties for the steel girder and reinforcement, while for the FM analysis the concrete is also included in the section properties. Load distribution and member forces (i.e., shears, moments, axial forces, etc.) are the same for both models. Thus, the results below based on the FM computational analysis are directly applicable to the FMR analysis. The exception for this is Study 15 below, which directly compares the differences between the FM and the FMR analyses.

8.1.2 Mn/DOT Bridge No. 27998

Mn/DOT Bridge No. 27998 is a four-girder two-span continuous composite steel I-girder bridge with an average girder radius of curvature of approximately 286 feet and a girder spacing of 9 feet. The longest girder arc span is slightly over 155 feet. The girder webs are all 0.625 inches thick and have depths of 50 inches, 56 inches, 62 inches and 70 inches, going from the girder with the smallest radius of curvature to that with the largest. The width of the flanges is either 20 inches or 24 inches and the thicknesses range between 1.25 inches and 3.0 inches. All three supports are skewed from the radial direction at angles up to 40 degrees. The bridge deck is 9 inches thick with a typical haunch height of 1 inch. The roadway edges consist of J-barriers with heights of 2 feet 10 inches and 3 feet 8 inches on the interior (edge with smaller radius of curvature) and exterior edges, respectively. The diaphragms are radially positioned between the girders except at the two end abutments where they are aligned with the abutments. Diaphragms are typically spaced at approximately 16 ft increments along the interior edge of the bridge, except at the center pier where two additional diaphragms are included. X-frames with top and bottom chords make up all diaphragms except the end abutment diaphragms, which are beams.

This bridge was part of previous University of Minnesota research that focused on bridge loads throughout the construction of a horizontally curved steel I-girder bridge, along with effects due to truck live loads. More information on the bridge is provided in Galambos et al. (1996), Galambos et al. (2000), and Hajjar et al. (2001). Figure 8-1 provides a layout of the bridge along with key parameters and the UMN Program model nodes showing the mesh refinement of the bridge elements. Boundary conditions in the computational model consist of fixed vertical deflection, radial deflection, and torsional rotation at nodes 1, 2, 3, 4, 77, 84, 91, 98, 169, 170, 171, and 172 along with fixed axial displacement at nodes 77, 84, 91, and 98. In order to obtain more information on the warping behavior of the girders for this project, the UMN Program model of this bridge has been redone using twice the girder mesh refinement as compared to the original model created for the aforementioned research projects.

8.1.3 FHWA Test Specimen

The FHWA Test Specimen (FHWA TS) is a three-girder single-span composite steel I-girder bridge with an average girder radius of curvature of 200 feet. The longest girder arc span length is slightly less than 94 feet and the girder spacing is 8.75 feet. The girder webs are all approximately 48 inches deep with thicknesses between 0.323 inches and 0.362 inches. The flange widths vary between 12.2 inches and 24.2 inches, while the thicknesses are between 0.88 inches and 1.39 inches. Both end supports are radially positioned. The bridge deck is 8 inches thick with a haunch height of approximately 2 inches. There are no barriers or curbs on the outer edges of this bridge test specimen, although the thickness of the deck increases slightly in the overhang regions. The diaphragms are radially aligned between the girders and are K-shaped cross-frames including top chords.

This bridge was part of a multi-stage test performed by the FHWA at the Turner-Fairbank Highway Research Center in McLean, Virginia. Specific information on this bridge for the purposes of this project was obtained through research at the Georgia Institute of Technology (Chang et al., 2005). Figure 8-2 provides a layout of the bridge along with some key parameters and the UMN Program model nodes showing the mesh refinement of the bridge elements. Boundary conditions in the computational model consist of fixed vertical deflection at nodes 1, 3, 5, 57, 59, and 61, fixed radial deflection at nodes 3 and 59, and fixed axial displacements at nodes 29, 31, and 33.

8.1.4 Comments about the Bridge Base Models and Analysis with UMN Program

The base models for each bridge were created using the dimensions and properties defined within their respective documents mentioned above. Other key modeling parameters were determined as follows. The modular ratios N were determined using values appropriate for the actual strength of the concrete, not the design strength. The thickness of the deck t_{slab} includes the thickness of the overlay. The effective width for the girders in flexure was determined by using both the AASHTO LRFD recommendations (AASHTO, 2004) and bridge test data. For the edge girders in the positive moment regions, the overhang contribution to b_{eff} was calculated by taking the area of the slab and curb/parapet (for Mn/DOT Bridge No. 69824 the beam and column areas were not included) in the overhang region and dividing by the typical thickness of the slab. In the negative moment regions for the edge girders, the contribution to b_{eff} due to the overhang was taken as the width of the overhang. The main parameters for the base models of all three bridges are summarized in Table 8-1.

The same limitations and modeling techniques for UMN Program as described for Mn/DOT Bridge No. 69824 in Chapter 4 apply to the models for Mn/DOT Bridge No. 27998 and the FHWA Test Specimen. In particular, the boundary conditions are applied at the neutral axes of the girder elements and must be oriented in the radial or tangential directions. Rigid offsets are used to position the truss elements (i.e., axial load only) forming the X-shaped and K-shaped diaphragms for the Mn/DOT Bridge No. 27998 model and the FHWA Test Specimen model, respectively. The torsion constant J ignores contribution from the concrete deck for all girder elements in the base models. Truck axle loads are converted to nodal loads using the program TRUCKLOADS based on composite girder properties for the base models. Also, all rotational degrees of freedom for the transverse concrete deck beams spanning between the top flanges of

the girders are released for the base models. Refer to Chapter 4 for more discussion on these topics.

8.2 Method for Comparisons

In order to obtain results for a variety of bridge span lengths and end support conditions, such as continuous or pinned, each of the eight bridge spans from the three bridges were isolated for comparisons in the parametric study. For the computational analysis of each span, between fifteen and twenty-one different load cases were applied to the span and used to generate deflection, axial force, shear, moment, and stress maximum response envelopes for the various bridge elements. For each parametric study, computational analysis was completed and envelopes were created for both the base model and each of the modified models (i.e., the models with the alternate values for the current parameter under investigation) using the same load cases. The largest magnitude responses from the envelopes for a number of key bridge components and regions were then compared between the base model and the modified model for each individual span that was loaded. These comparisons were tabulated and are provided for each of the parametric studies in this chapter. The following paragraphs provide further details on the implementation of this process.

For the FHWA Test Specimen, which had both ends of the simply supported span pinned, fifteen load cases were used. These load cases consisted of a single HS20 truck with 14 foot rear axle spacing located at different longitudinal and transverse positions near midspan. Three transverse positions were used: radially centered on the roadway surface, shifted radially in one-half of a roadway lane width, and shifted radially out one-half of a roadway lane width. Note that a typical roadway lane width is 12 feet. Longitudinally, five different positions for the HS20 truck were used: truck center of gravity at midspan, at ± 10 feet from midspan, and ± 20 feet from midspan. These fifteen load cases focused on maximizing the positive moment region responses of the bridge span.

In addition to the same fifteen load cases used for the single span of the FHWA Test Specimen, the remaining seven bridge spans included three additional load cases for each end of the span that was continuous. Therefore, the two spans of Mn/DOT Bridge No. 27998 and the two outer spans (Span 10-9 and Span 6-5) of Mn/DOT Bridge No. 69824 had a total of 18 load cases used to generate the maximum response envelopes, while the three inner spans (Spans 9-8, 8-7, and 7-6) of Bridge No. 69824 had 21 load cases. At each continuous end of these spans, the additional load cases consisted of one HS20 truck on each side of the pier with 50 feet between the rear axle of the first truck and the front axle of the second truck. The weight of these two trucks was reduced to 90% to reflect the analogous load case defined for LRFD bridge design and rating (AASHTO, 2004). The same three transverse positions as mentioned previously for the positive moment regions were used for positioning these two trucks. Note that for Mn/DOT Bridge No. 69824, the roadway lane width was reduced from 12 feet to 10.75 feet due to physical limitations of the roadway surface on this bridge. The only longitudinal position used for these additional load cases was with the center of gravity of the two truck pair centered at the pier. These additional load cases at each interior pier focused on maximizing the negative moment region responses of the bridge span.

Of particular interest to the rating of bridges is how the overall maximum responses (i.e., the largest values from the response envelopes) for bridge components change for different values of a parameter, since this will have a direct influence on the final bridge rating. A number of key bridge components and responses were identified and used to narrow down the vast quantity of data available from the response envelopes created using the analyses described in the previous paragraphs. Comparisons between the base models and the modified models were divided into two main categories for each bridge: girders and diaphragms/bracing. Girders were further divided into a middle of span region and two support regions, one near each pier at the ends of the span, to show how both the positive and negative moment regions of the span are affected by each parameter. For the middle of span region, comparisons were made for vertical deflection, torsional rotation, flexural moment, and bottom flange stresses due to flexure and restraint of warping for each bridge girder. In each of the support regions for the girders, comparisons were made for flexural shear, flexural moment, and bottom flange stresses due to flexure and restraint of warping. The diaphragm/bracing category was divided into two subcategories, one that made comparisons based on response envelope data for all of the members in the current span being investigated and one that only used data for the members near midspan of that span. Comparisons based on the midspan only subcategory were used to identify changes in the transverse load distribution between girders near midspan, while the category using data for all of the members in the span was used to observe how the overall maximum diaphragm/bracing forces changed in the span as parameters were varied. Comparisons for the beam diaphragms in Mn/DOT Bridge No. 69824 focused on the axial force, shear, and moment transferred at each of the bridge girders, while the members composing the X-shaped and K-shaped diaphragms for Mn/DOT Bridge No. 27998 and the FHWA Test Specimen, respectively, had comparisons for the axial loads in the chords. Comparisons for the lateral wind bracing on Bridge No. 69824 were made for both the maximum tension and maximum compression forces. Note that the component breakdown in this paragraph describes the general layout of Table 8-2 through Table 8-32, which provide the results for each of the parametric studies that follow below. An additional note on the tables is that for the results of the X-shaped and K-shaped diaphragms, U, L, and M stand for Upper, Lower, and Middle, and are used to describe the various chords in the diaphragms. For example, U1-L2 refers to the X-shaped frame chord that goes from Upper Girder 1 to Lower Girder 2, while M-U3 refers to the K-shaped frame chord from the Middle of the bottom chord to Upper Girder 3.

For each bridge span used in a particular parametric study, comparisons were quantified by calculating the percent change from the base model to the modified model as $(Modified - Base) / Base \cdot 100\%$ using the maximum magnitude values from the response envelopes in each of the regions identified in the previous paragraph. For example, using the response envelopes generated for loads applied to Span 8-7 of Bridge No. 69824, the maximum compression force from all 26 of the lateral wind bracing in that span would be compared for base model and modified model analyses to obtain the percent change for the maximum compression response for these elements in that span. Note that the location, or lateral wind bracing element in this case, of the maximum force could be different for the base and modified models, but this is acceptable since the goal here is to focus on the consequences for bridge rating, which is concerned with changes in overall maximum values, not how values change at each specific location. Positive percent change values indicate that the modified model value is larger than the base model value, while negative percent change values generally mean that the

modified model value is smaller. In cases where the percent change is greater than negative 100%, the maximum response has changed from the base model to the modified model from a tension force to a compression force, or vice versa. For example, a percent difference of -200% means that the base model and the modified model have the same magnitude response (i.e., absolute value) but different signs, while a percent difference of -300% means that the magnitude of the modified model response is twice that of the base model and has an opposite sign. These occurrences are an outcome of the process chosen for making comparisons in this sensitivity study. In particular, the base model and modified model values with the largest magnitudes in a specific region were used for comparisons regardless of sign, while comparisons were calculated including the signs. Thus, for elements or regions that were not dominated by tension or compression values, these sign reversals occasionally happened. They typically do not indicate a significant finding and must be taken in context of the remaining values for other spans in the study.

Note that the large radius of curvature and short span length for Span 6-5 of Mn/DOT Bridge No. 69824 generally reduces the effects of horizontal curvature on this span as compared to the other bridge spans in the parametric study. In particular, the magnitude of the torsional rotations, diaphragm forces, lateral wind bracing forces, and restraint of warping stresses in this span are lower. In addition, the web depth for both girders in this region tapers from 78 inches near Pier 6 to 26 inches near Pier 5. This linear taper in the web depth is modeled in UMN Program using stepwise increments at approximately 12 feet. This modeling approximation introduces discontinuities in the analysis of this span that may lead to unrealistic percent changes in the parametric study, especially when the effect of these discontinuities is coupled with the small magnitude of the horizontal curvature effects in this span. Caution and good judgment must be used when evaluating the comparison results for the torsional rotations, diaphragm forces, lateral wind bracing forces, and restraint of warping stresses in this span. For these reasons, in the discussions below for the parametric studies, the results for these particular responses in Span 6-5 are neglected when generalizing comments are made about the typical response for a particular study. However, results for vertical deflection, girder moment, and bottom flange flexural stress are included for this span in generalizing comments since they are not as sensitive to low magnitude forces or the discontinuities due to the web taper approximation.

8.3 Sensitivity Studies

A series of parametric studies are presented below that provide insight into the sensitivity of grillage models for horizontally curved composite steel I-girder bridges to various parameters. The parameters investigated are:

1. Beam Diaphragm Stiffness due to Knee Brace Region
2. Vertical Rigid Offsets for Diaphragm Beam Elements
3. Composite Action of Beam Diaphragms
4. Cross-frame Member Size
5. Lateral Wind Bracing Members
6. Diaphragm Spacing
7. Transverse Concrete Deck Beams
8. Rotational DOFs for Transverse Concrete Deck Beams
9. Girder Axial DOFs at Piers

10. Composite Torsion Constant
11. Thickness of Concrete Slab
12. Effective Concrete Width for Girder Flexure
13. Modular Ratio
14. Bridge Radius of Curvature
15. Longitudinal Distribution of Loads and Stress Calculations
16. Restraint of Warping Stress Approximation

8.3.1 Study 1: Beam Diaphragm Stiffness due to Knee Brace Region

Bridges Investigated: Mn/DOT 69824

Overview:

The diaphragms on Mn/DOT Bridge No. 69824 consist of 18 foot W21x55 beams with 75 inch deep knee brace regions at the ends which significantly stiffen the beams where they connect to each girder. Some commercial grillage-based analysis programs only allow for a single beam element to model the diaphragms. Therefore, this study was conducted to determine the extent to which ignoring the end region knee bracing affects the overall bridge analysis.

A modified model of Bridge 69824 was created that uses a single W21x55 section for the diaphragms and was compared to the base model, which includes the higher stiffness for the beam elements at the ends of the diaphragms to simulate the knee brace regions.

Results: see Table 8-2

Not including the additional stiffness provided by the knee brace regions of the diaphragms for Mn/DOT Bridge No 69824 primarily results in less transfer of load from the Interior Girder C to the Exterior Girder A. This is indicated by a decrease in maximum shear in the diaphragms near midspan of up to 6.0% and a decrease in the diaphragm moments at Girder C by approximately 23.0%. In addition, maximum axial forces in the diaphragms decreased by approximately 3.0%. For the bridge girders, this results in up to 1.4% larger deflections and up to 1.1% larger moments on Girder C, while the maximum deflections only slightly increase by approximately 0.1% and the moments by up to 0.3% on the midspan of Girder A. Restraint of warping stresses on the bottom flange for Girder C decreased by up to 3.0% near midspan and up to 9.1% at the piers, while there was little change for these stresses on Girder A.

Comments:

Analysis for Mn/DOT Bridge No. 69824 ignoring the additional stiffness of the diaphragms due to the knee brace regions provides satisfactory results for the girders, although restraint of warping stresses on the interior girder may be slightly under predicted. Calculated forces in the diaphragms, however, are significantly different. If accurate forces in the diaphragms are essential, such as for bridges with diaphragms governing the overall bridge rating, the additional stiffness of the knee braces should be included in the analysis.

8.3.2 Study 2: Vertical Rigid Offsets for Diaphragm Beam Elements

Bridges Investigated: Mn/DOT 69824

Overview:

Not all grillage-based analysis programs permit the modeling of the vertical offsets that can exist between the rotational center of the girder elements and the neutral axis of the beam diaphragms. This study was conducted to identify the effects of ignoring the vertical offset of the girder and diaphragm elements for Mn/DOT Bridge No 69824.

A modified model of Bridge 69824 was created that ignores the vertical offset of the diaphragms in relation to the girders. Analyses using this model were compared to the base model values, which utilize rigid offsets to account for the vertical separation of these two bridge elements.

Results: see Table 8-3

The axial force in the diaphragms goes almost completely away when the offset is ignored, which is indicated by a reduction in axial force in the diaphragms of almost 90.0% as compared to the base model. Diaphragm moments at Girder C decrease by up to 27.3% near midspan, while those at Girder A increase by up to 32.2%. On the other hand, the major axis shear transfer through the diaphragms is nearly unchanged with the maximum percent change being only 0.1%. The major axis moments and deflections of the girders also remain nearly unchanged with their maximum percent changes being only 0.1% and 0.2%, respectively. The only noticeable effect to the girders is that the torsional rotations and warping stresses change slightly. The magnitude of most of the percent changes for the girder torsional rotations and restraint of warping stresses are less than 1.0%, with a handful being up to 5.0%.

Comments:

For Mn/DOT Bridge No 69824, ignoring the vertical offset of the diaphragms relative to the girders significantly alters the axial force and moment in the diaphragms, but has minimal impact on the behavior of the girders and the shear transfer through the diaphragms. Similar to Study 1 above, the vertical offset between the diaphragm and girder elements does not need to be precise unless accurate assessment of the diaphragms is important.

8.3.3 Study 3: Composite Action of Beam Diaphragms

Bridges Investigated: Mn/DOT 69824

Overview:

Each of the beam diaphragms on Mn/DOT Bridge No 69824 has shear connectors welded along the length and embedded into the concrete deck to provide composite action in resisting the torsional loads induced due to bridge curvature. Bridge test data as reported in Chapter 6 indicated moments of inertia for the diaphragms that were between 1.8 and 3.7 times higher than those for the W21x55 steel section alone. For composite action, this roughly amounts to an effective width b_{eff} of 7.0 inches for a modular ratio of $N = 6$ and a haunch height of 3.0 inches. If

the *LRFD* (AASHTO, 2004) is used to calculate an effective width for the diaphragms, the limiting factor is one-fourth of the effective span length. Assuming an effective length equal to the girder spacing of 18 feet, the resulting effective width for the diaphragms is 54.0 inches, almost 8 times greater than that calculated from test data. This study was conducted to investigate the variation in using the calculated test value, the *LRFD* value, or ignoring the composite action of the diaphragms altogether.

Two comparisons, one with $b_{eff} = 0$ inches and one with $b_{eff} = 54.0$, were made and compared to the base model case with $b_{eff} = 7.0$ inches. Note that the ratios of the moments of inertia for the diaphragms are approximately 1:3:5 for b_{eff} of 0 inches, 7 inches, and 54 inches, respectively.

Results: see Table 8-4 and Table 8-5

Reducing the amount of composite action on the diaphragms from $b_{eff} = 7$ inches to 0 inches, results in up to a 4.4% decrease in the amount of shear load transferred through the diaphragms near midspan, along with approximately 10% increase in diaphragm moment at Girder C and 20% decrease at Girder A. The maximum vertical deflections on the interior girder increase by up to 1.0%, while the increase in maximum deflections on the exterior girder is only around 0.1%. Maximum midspan girder moments increase by up to 0.8% on the interior girder and by up to 0.2% on the exterior girder.

Increasing the level of composite action on the diaphragms from $b_{eff} = 7$ inches to 54 inches, results in an increase in shear transfer through the diaphragms up to 1.4% near midspan. The maximum diaphragm moment near midspan decreases at Girder C by approximately 22%, while that at Girder A increases by approximately 29%. Maximum percent changes for girder vertical displacements, shears, moments, and flexural stresses are minimal with the highest magnitude at 0.3%. Changes in the restraint of warping stress are varied, with the largest increase being at 3.0% and the largest decrease at 1.4%.

Comments:

Comparing Table 8-4 and Table 8-5, the magnitude of most effects from b_{eff} going from 7 inches to 0 inches are 2 to 3 times greater than those for b_{eff} going from 7 inches to 54 inches. This is because the ratio of moments of inertia is greater for b_{eff} going from 7 inches to 0 inches than it is for b_{eff} going from 7 inches to 54 inches. Thus, it is more important that composite action be included than b_{eff} be exactly right. Therefore, in absence of test data for the composite action of beam diaphragms, the typical equations for girders (AASHTO, 2004) are recommended for determining the effective width of the diaphragms.

8.3.4 Study 4: Cross-frame Member Size

Bridges Investigated: Mn/DOT 27998, FHWA TS

Overview:

Study 1 and Study 3 looked specifically at the effects resulting from varying the stiffness of beam diaphragms. This study, in contrast, investigates the bridge response with varying stiffness

of the X-shaped and K-shaped cross-frames on Mn/DOT Bridge No 27998 and the FHWA Test Specimen, respectively.

Two modified models of Bridge No. 27998 and FHWA TS were created with the cross-sectional areas of the cross-frame members cut in half for one case and doubled for the other. Both cases were then compared to the corresponding bridge base models, which were based on the original areas of the cross-frame members.

Results: see Table 8-6 and Table 8-7

Decreasing the areas of the cross-frame members by a factor of 2 resulted in increased maximum girder vertical deflections up to 9.8% on Bridge 27998 and 5.1% on FHWA TS. In addition, maximum girder torsional rotations increased up to 23.7% on Bridge 27998 and 13.0% on FHWA TS. Many of the maximum cross-frame forces in both bridges had decreases of approximately 30%. Changes in the maximum bottom flange flexure stresses near midspan were between -0.6% and 2.8% for Bridge 27998 and between -0.3% and 1.1% for FHWA TS. Girder warping stresses near midspan had more significant differences with values for Bridge 27998 decreasing by up to 10.3% and those for FHWA TS decreasing by up to 2.5%.

Increasing the areas of the cross-frame members by a factor of 2 resulted in decreased girder deflections by up to 9.8% on Bridge 27998 and 2.7% on FHWA TS. Maximum torsional rotations on Bridge 27998 decreased by up to 17.2%, while those for FHWA TS decreased by 6.9%. Common increases in the maximum diaphragm forces for Bridge No. 27998 were around 70%. Changes in girder flexural moments at midspan varied between a decrease of 4.0% and an increase of 0.1%. Maximum bottom flange warping stresses near midspan increased by up to 6.8% on Bridge 27998, while those for FHWA TS increased by up to 1.4%.

Comments:

Similar patterns of bridge response are observed for these two bridges as for Mn/DOT Bridge No. 69824 when varying the stiffness of the diaphragms. However, the magnitude for percent changes was much larger for these two bridges. This is due to the larger span length-to-radius of curvature ratios for Bridge No. 27998 and FHWA TS, which results in larger effects due to horizontal curvature and greater demand on the diaphragms. In addition, the lateral wind bracing on Bridge No. 69824 provides an additional level of overall bridge stiffness that reduces the sensitivity of the bridge to diaphragm properties as compared to the bridges without lateral wind bracing.

In general, decreasing the areas of the cross-frame members, and therefore the overall stiffness of the diaphragms, results in less transfer of force through the diaphragms and an increase in the overall displacements of the bridge, while an increase in stiffness has the opposite effects. Therefore, for accurate assessment of load distribution between the girders and bridge displacements, it is important to account for the actual stiffness of the cross-frame members.

8.3.5 Study 5: Lateral Wind Bracing Members

Bridges Investigated: Mn/DOT 69824

Overview:

Mn/DOT Bridge No 69824 contains lateral wind bracing at the bottom flanges of the girders in an X-shaped pattern between diaphragms. Some commercial grillage-based programs do not allow for the inclusion of these members. Therefore, this study was conducted to determine the effects of analyzing the bridge excluding the lateral wind bracing members. Additional comparisons were made to determine the effects of varying the axial stiffness of the lateral wind bracing members.

Three modified models of Bridge 69824 were analyzed with lateral wind bracing excluded, with the area of the lateral wind bracing members cut in half, and with the area of the lateral wind bracing doubled. All three of these models were then compared with the base model, which had lateral wind bracing with the original area as specified by bridge documents.

Results: see Table 8-8, Table 8-9, and Table 8-10

Removing the lateral wind bracing results in up to a 14.8% increase in maximum vertical deflections on Girder C and up to 31.6% on Girder A. Torsional rotations nearly double for both girders. Maximum girder flexural moments near midspan increase on Girder C by approximately 12%, while those on Girder A increase by approximately 20%. The maximum beam diaphragm shears decrease by approximately 40%, while the diaphragm moments at each girder decrease between approximately 30% and 40%. Maximum bottom flange restraint of warping stresses on Girder C increase by up to 29.4%, while those on Girder A decrease by up to 28.8%.

Cutting the area of the lateral wind bracing in half has the same pattern of effects as for completely excluding the lateral wind bracing, although the percent differences as compared to the base model are 3 to 4 times smaller than when the lateral wind bracing was completely ignored. The maximum lateral wind bracing forces are approximately 28% lower when only half of the area is used for the lateral wind bracing members. Doubling the area of the lateral wind bracing has nearly identical magnitudes of effects as cutting the area in half, except that decreases are now increases and vice versa.

Comments:

Excluding the lateral wind bracing members causes a considerable shift in the load resistance mechanism of Bridge No. 69824, along with a significant loss in overall bridge stiffness. The girders resist more of the load while the role of the diaphragms is decreased. Without the lateral wind bracing to stabilize the torsional rotation of the bridge, the transverse load distribution between girders shifts towards the exterior girder. Girder deflections and rotations increase considerably. Because of these significant effects, it is highly recommended that lateral wind bracing be included in the computational analysis of horizontally curved bridges. Not doing so will result in significant under predictions for the diaphragm forces along with grossly conservative results for the girder flexural behavior, for both displacements and forces. Restraint of warping stresses may be under predicted as well.

8.3.6 Study 6: Diaphragm Spacing

Bridges Investigated: Mn/DOT 69824, Mn/DOT 27998, and FHWA TS

Overview:

The spacing of the diaphragms in horizontally curved steel I-girder bridges has a significant impact on the magnitude of the warping stresses that develop in the flanges of the girders. Diaphragms limit girder torsional rotations. The restraint, however, induces longitudinal warping stresses in the girders. As indicated by the formula in Equation 2-8, warping stresses are generally understood to be proportional to the square of the diaphragm spacing. This study was conducted to determine if this holds true for doubling the diaphragm spacing for the bridges investigated here.

Modified models of each the bridges were created that had approximately every other diaphragm removed as compared to the base models. For the FHWA Test Specimen, the diaphragms extending along the cross-sections from nodes 15 and 43 were removed. For Bridge 27998, the diaphragms originating from nodes 13, 30, 46, 66, 107, 127, 143, and 160 were all removed. Adapting the model for Bridge 69824 was more complicated since Span 8-7 and Span 6-5 had odd numbers of diaphragms. Because of this, the spacing of the diaphragms on these two spans for the modified model was slightly less than double that for the base model. The modified model of Bridge 69824 included diaphragms at all the piers and every other diaphragm as compared to the base model for Span 10-9, Span 9-8, and Span 7-6. For Span 8-7 and Span 6-5, all of the original diaphragms as in the base model were removed between piers and new ones were added radially extending from nodes 229, 249, 270, 290, 311, 331, 479, 497, and 515. Lateral wind bracing was kept in the model of Bridge 69824, except that it was repositioned to align with the new diaphragm locations. This resulted in a reduction of the number of lateral wind braces from 96 for the base model to 50 for the modified model. Also, due to modeling difficulties in relocating the diaphragm nodes for Span 8-7 and Span 6-5, the base model and the modified model for comparisons in this study use single element diaphragms for Bridge 69824. These diaphragms are similar to those used in the modified model created for Study 1.

Results: see Table 8-11

Approximately doubling the spacing of the diaphragms results in increases of the maximum bottom flange restraint of warping stresses at midspan of up to 337.4%, 380.2%, and 316.5% for Bridge 69824, Bridge 27998, and the FHWA Test Specimen, respectively. Restraint of warping stresses at the piers increase by up to 342.6% and 184.1% for Bridge 69824 and Bridge 27998, respectively.

Comments:

These calculated increases in restraint of warping stress are on par with the expected approximate value of 300% derived from Equation 2-8 for double the diaphragm spacing.

8.3.7 Study 7: Transverse Concrete Deck Beams

Bridges Investigated: Mn/DOT 69824, Mn/DOT 27998, and FHWA TS

Overview:

Grillage-based analysis programs used for horizontally curved steel I-girder bridges vary widely in the method by which the concrete deck is modeled. Simple analysis programs only use the concrete deck properties to increase the flexural and torsional properties of the composite beam sections and ignore the continuity that the deck provides between the top flanges of the girders, while higher level analysis programs can go so far as to use 2D shell elements to simulate all facets of the deck.

In addition to composite flexural and torsional properties for the girder elements, the base models of all three bridges using UMN Program utilize transverse concrete deck beams with vertical offsets (using rigid links) to model the continuity between the top flanges of the girders. These transverse beams are positioned radially between the girders with 1 (Bridge 27998) or 3 (Bridge 69824 and FHWA) transverse beams occurring between consecutive diaphragms. The element rotational DOFs at the ends of each of these elements are all released (discussed and investigated in Study 8 below) to prevent over stiffening of the bridge system. Therefore, the transverse concrete deck beams only provide torsional restraint of the bridge by effectively locking together the radial displacement of the top flanges of the girders using the axial stiffness of the deck beams. This study was conducted to determine the effects of not including the transverse concrete deck beams.

Modified models of each of the three bridges were created that do not include transverse concrete deck beams. The results from these models were compared to the base models which include transverse concrete deck beams with the element rotational DOFs released where they frame into the girder nodes.

Results: see Table 8-12

Removing the concrete deck beams on Bridge 69824 resulted in up to a 2.1% decrease in the maximum torsional rotations of Girder C and an increase up to 2.2% on Girder A. There was minimal change for the maximum vertical deflections, shears, moments, and stresses for the girders. The maximum diaphragm axial forces and moments changed by magnitudes up to 56.1% at midspan, while the diaphragm shears had no change. Maximum tension forces in the lateral wind bracing for all members in the span decreased by approximately 1%, while the maximum compression forces increased by approximately 1%.

For Bridge 27998 and FHWA TS, the differences were more pronounced when the concrete deck beams were removed. Torsional rotations on the girder with the largest radius of curvature increased by up to 56.9% on Bridge 27998 and 37.1% on FHWA. Vertical deflections for these same girders increased by up to 19.2% on Bridge 27998 and 13.4% on FHWA. Maximum girder flexure stresses increased by up to 5.1%. Girder restraint of warping stresses varied between an increase of 17.2% and a decrease of 15.1% on these two bridges. Cross-frames had top and

bottom member forces that changed significantly, while the diagonal members revealed maximum shear transfer forces changing by magnitudes up to 33.8%.

Comments:

Excluding the transverse concrete deck beams from the models results in less torsionally stiff structures. The girders have more freedom to rotate since the top flanges are no longer tied together. For all three bridges, the girders with the larger radii of curvature tend to have significantly higher increases in torsional rotations, while those with smaller radii of curvature tend to have rotations that either decrease or only increase slightly. This pattern occurs because the higher torsional loads induced on the girders with the larger radii of curvature no longer have a load path back to the other girders so that the torsion can be shared more uniformly across the bridge. It is interesting to note that Bridge 69824 sees significantly smaller effects due to removing the transverse deck beams. This is because the lateral wind bracing on Bridge 69824 provides an alternate load path for the bridge girders to share the torsional loads.

The large percent changes for the vertical deflections, torsional rotations, restraint of warping stresses, and diaphragm forces on Bridge 27998 and FHWA TS indicate that inclusion of the concrete deck as a transverse load path at the top of the girders is important for the analysis of horizontally curved I-girder bridges, especially those without lateral wind bracing.

8.3.8 Study 8: Rotational DOFs for Transverse Concrete Deck Beams

Bridges Investigated: Mn/DOT 69824, Mn/DOT 27998, and FHWA TS

Overview:

The transverse concrete deck beams used by UMN Program for all three of the bridges included releases of the three rotational DOFs at each end of the elements. This effectively reduced the transverse deck beams to axial members. This was done based on observations made as part of this research project along with research reported by Chang et al. (2005), which is discussed in Chapter 2. The comparison in this study was completed to show the difference in bridge responses when the rotational DOFs of the transverse concrete deck beams are released from or fixed to those of the girders.

A modified model of each of the three bridges was created with the rotational DOFs fixed to the DOFs of the girders. The results were compared with each of the base models, which all have the rotational DOFs at the ends of the transverse deck beams released.

Results: see Table 8-13

Fixing the rotational DOFs for the transverse concrete deck beams to the DOFs of the girders results in decreases for girder torsional rotations up to 2.7%, 19.5%, and 14.4% for Bridge 69824, Bridge 27998, and FHWA TS, respectively. Girder vertical deflections decrease by up to 0.9%, 9.4%, and 9.2% for each of the bridges. Maximum diaphragm shear forces near midspan decrease by up to 10.3%, 63.7%, and 60.4% for Bridge 69824, Bridge 27998, and FHWA TS, respectively. Maximum girder moments decrease on the outermost girders by values up to 0.7%,

5.0%, and 4.9% for Bridge 69824, Bridge 27998, and FHWA TS, respectively. On Bridge 69824 and Bridge 27998 the predicted maximum restraint of warping stresses are lower by percent changes up to 14.5% and 62.8%, respectively. For FHWA TS, the torsional constraint provided by the deck beams is so great that the maximum flange warping actually changes direction on Girder 1 and Girder 2, while on Girder 3 the restraint of warping stress is decreased by 42.1%.

Comments:

Chang et al. (2005) found that due to web distortion effects, fixing the rotational DOFs of the concrete slab to those of the girders modeled as open-walled section beam elements, such as in UMN Program, over-constrains the girder twisting and bottom flange lateral bending leading to unconservative results for deflections and restraint of warping stresses in horizontally curved girder bridges. They recommended releasing the slab rotational DOFs from the girder DOFs to improve results and to provide a conservative approximation of the web distortion effects over the depth of the girders. The results in Table 8-13 indicate that the base model analyses with the rotational DOFs for the transverse concrete deck beams released from those for the girders provides higher predictions for nearly all bridge responses, especially for deflections and restraint of warping stresses. Thus, analysis with these DOFs released can be used to provide a more conservative analysis and is recommended when using grillage analysis with open-walled section beam elements for the curved bridge girders.

8.3.9 Study 9: Girder Axial DOFs at Piers

Bridges Investigated: Mn/DOT 69824, Mn/DOT 27998, and FHWA TS

Overview:

Investigation and testing of Mn/DOT Bridge 69824 revealed minimal movement at the sliding expansion bearings located at Piers 10, 9, 6, and 5. Accurate representation of these fixities would require an analysis program to apply the fixities at the bottom flange of the girders, and would generate moments in the girders due to the eccentricity of the girder neutral axes to the bearing restraint. This effect tends to decrease overall bridge deflections and moments, improving the load carrying capacity of a bridge. However, UMN Program and many grillage-based analysis tools are not equipped to include boundary conditions at locations other than the neutral axes of the girders. This study was conducted to determine the extent to which fixing the axial DOFs, which are located at the girder neutral axes for these studies, at the piers with expansion bearings changes the computational results.

Modified models of all three bridges were made with the axial DOFs at all piers fixed. The results of these analyses were then compared to the base model results. The base model for Bridge 69824 has the axial DOFs fixed at Pier 7 and Pier 8. The base model for Bridge 27998 has the axial DOFs fixed at the center pier. The base model for FHWA TS has no axial DOFs fixed at either pier.

Results: see Table 8-14

Fixing the axial DOFs at all piers has nearly no effect on the computational responses of Bridge 27998 and FHWA TS. For Bridge 69824 however, a slight torsional stiffening of the bridge occurs, likely due to an increase in constraint on the lateral wind bracing. The torsional rotation of the girders for Bridge 69824 decreases by up to 5.6%. Vertical loads shift slightly toward Girder C as shown by the greater magnitude reductions in deflection and moment on Girder A as compared to Girder C. Maximum diaphragm forces for Bridge 69824 shift slightly with the maximum percent change being 2.5%, while overall maximum lateral wind bracing forces increase by up to 12.7%.

Comments:

For grillage analyses that apply support fixities at the neutral axes of the girder elements, the use of axial restraints to simulate frozen bearings has minor influence on overall analysis results. To obtain more realistic results from these fixities for comparisons with load test data, the inclusion of rotational springs or the application of the axial restraints using a vertical offset must be incorporated in the analysis. However, the extra load capacity provided by frozen axial bearings is generally not accepted as a reliable source of strength, especially at higher load levels (AASHTO, 2003b). For the purpose of bridge rating therefore, a complex application of these restraints may not be warranted.

8.3.10 Study 10: Composite Torsion Constant

Bridges Investigated: Mn/DOT 69824, Mn/DOT 27998, and FHWA TS

Overview:

Overestimation of the composite torsion constant can result in under predictions of longitudinal restraint of warping stresses. This is because high torsional shear stiffness, which is defined by J , attracts more load and reduces the load demand on warping. Common formulas for composite torsion constants such as that provided by Heins and Kuo (1972) tend to increase the torsion constant by orders of magnitude as compared to the steel section alone for typical composite girders in bridges today. In the commentary of the *LRFD Specification* (AASHTO, 2004), using one-half of the effective width of the concrete deck for calculating the composite torsion constant for I-girders is recommended. Researchers such as Chang et al. (2005) have gone so far as to recommend ignoring the contribution of the concrete deck in the determination of the torsion constant to ensure a conservative prediction of the restraint of warping stresses. This study was conducted to investigate the variance in computational results for different values of the torsion constant J .

Two modified models of each of the three bridges were created. One model used the *LRFD* recommended torsion constant with one-half of the effective width of the concrete deck. The other model used the composite torsion constant based on the full effective width of the concrete deck. These models were then compared to the base model, which conservatively ignored the contribution from the concrete deck and simply used the steel girder to calculate the torsion constant as recommended by Chang et al. (2005). Note that for all of these models the warping constant C_w was calculated using the full effective width of the concrete.

Results: see Table 8-15 and Table 8-16

Increasing the torsion constant from a non-composite value to a composite value using half of the effective concrete width generally decreased the girder displacements and the calculated restraint of warping stresses. Rotations for the three bridges decreased by values up to 13.4%, while deflections decreased by up to 7.7%. Maximum bottom flange restraint of warping stresses near midspan decreased more significantly with values on Bridge 69824, Bridge 27998, and FHWA TS decreasing by up to 25.5%, 11.7%, and 29.6%, respectively.

Increasing the torsion constant from the non-composite value in the base model to including the full effective concrete width had an even more drastic effect. In general, the magnitude of the percent changes was typically around twice that as described for using half of the effective concrete width above.

Comments:

As suggested by Chang et al. (2005) and confirmed by the results in Table 8-15 and Table 8-16, ignoring the contribution of the concrete slab on the torsion constant is an effective method for adding conservatism to a grillage analysis without grossly overestimating the response of a curved bridge. It is the preferred method used in this research project.

8.3.11 Study 11: Thickness of Concrete Slab

Bridges Investigated: Mn/DOT 69824, Mn/DOT 27998, and FHWA TS

Overview:

Renovation of concrete decks or the application of a new wearing course may sometimes conceal the true thickness of the deck. This study was conducted to determine the effect on the response of the curved bridges when the thickness of the concrete bridge deck is varied.

Four modified models of each of the three bridges were constructed with the thickness of the deck varying from the base model thickness by plus 1 inch, plus $\frac{1}{2}$ inch, minus $\frac{1}{2}$ inch, and minus 1 inch. Each of these models was then compared with the corresponding bridge base model.

Results: see Table 8-17, Table 8-18, Table 8-19, and Table 8-20

Adding an inch to the concrete slab thickness resulted in slightly more stiff structures, both for vertical deflections and torsional rotations. Percent decreases in maximum vertical deflections for the girders ranged between 2.6% and 4.2%, while maximum torsional rotations decreased by up to 4.3%. Typical decreases in the bottom flange flexural stresses were around 1.6% and decreases in the maximum restraint of warping stresses were up to 2.7%. Percent changes in maximum girder moments and lateral wind bracing forces were typically less than 1%, while overall changes to the maximum diaphragm forces were generally small with a few changing by up to 6.9%.

Adding only one-half of an inch to the deck thickness resulted in approximately half the percent change magnitudes as compared to adding a full inch to the slab thickness. Subtracting one-half inch or a full inch provided nearly identical magnitudes of response changes as for adding one-half inch or a full inch, respectively, except that the percent changes were in the opposite direction.

Comments:

These results indicate that for typical girder sizes and concrete deck thicknesses on horizontally curved composite steel I-girder bridges, small variations in the thickness of the concrete deck result in relatively small deviations for the computational results. For a change in concrete thickness of ± 1 inch, maximum vertical deflections and torsional rotations vary by approximately $\pm 4\%$, while maximum bottom flange flexural stresses vary by approximately $\pm 2\%$. Most other bridge responses are minimally affected. Note that for bridges with smaller girders, these effects would increase.

8.3.12 Study 12: Effective Concrete Width for Girder Flexure

Bridges Investigated: Mn/DOT 69824, Mn/DOT 27998, and FHWA TS

Overview:

When the concrete deck on a bridge is approximated in an analysis program by using composite section properties for the girder elements, an effective width for the deck must be determined. Typical values for the effective width are based on the girder spacing, span length, and slab thickness as provided in *LRFD* (AASHTO, 2004). Some bridge guide manuals such as the *Guide Specification for Horizontally Curved Steel Girder Highway Bridges* (AASHTO, 2003a), simply recommend the effective width be equal to the girder spacing. To complicate matters, overhang regions of bridges typically provide additional stiffness to the girders, which further increases the effective width to be used in the computational model. This study was conducted to determine the degree to which changing the effective width for the girders varies the resulting computational response of horizontally curved I-girder bridges.

Four modified models of each of the three bridges were created with the effective concrete width for all girder elements increased as compared to the base model values by 10% or 20%, or decreased by 10% or 20%. The results for each were compared with the base model computational results.

Results: see Table 8-21, Table 8-22, Table 8-23, and Table 8-24

Decreasing the effective concrete width of the girders by 20% as compared to the values used for the base model increased both the displacements and the calculated stresses in the bridges. Maximum torsional rotations increased by up to 15.8%, 4.2%, and 5.1% and vertical deflections increased by up to 8.1%, 4.8%, and 5.4% for Bridge 69824, Bridge 27998, and FHWA TS, respectively. Maximum bottom flange flexural stresses were up to 4.1% higher and calculated maximum restraint of warping stresses increased by up to 9.8%. Changes in the maximum

diaphragm forces were varied for each bridge, while maximum lateral wind bracing forces on Bridge 69824 decreased by up to 13.8%.

Reducing the effective width by only 10% resulted in roughly half the magnitude of the percent changes as for a reduction in effective width of 20% mentioned previously. Increasing the effective width by 20% produced magnitudes for percent difference that were between approximately 60% and 80% of those for decreasing the effective width by the same percentage. Increasing the effective width by only 10% gave percent changes around half of those for the 20% increase in effective width.

Comments:

The results shown here indicate that changing the effective width has a much larger influence on the displacements of the bridge than on the stresses. In addition, the sensitivity of these bridges to changes in the concrete effective width is relatively small for a reasonable range of effective widths, such as used above. Thus, attempting to narrow in on an exact value for the effective width for analysis is not warranted. It is interesting to note that Bridge 69824 showed higher sensitivity to the effective width than the other two bridges, likely due to the overall lower stiffness of this bridge as compared to the other bridges with more girders. For higher percent changes in the effective width, such as can occur for edge girders with large concrete curbs or parapets, the additional stiffness should not be ignored since it can have a significant impact on the bridge response.

8.3.13 Study 13: Modular Ratio

Bridges Investigated: Mn/DOT 69824, Mn/DOT 27998, and FHWA TS

Overview:

The modular ratio provides the ratio of material stiffness between the steel beam and the concrete slab and is used for determining the properties of a composite section. The stiffness of concrete is a function of the concrete strength; thus, the modular ratio is also a function of the concrete strength. Since the strength of concrete can vary significantly from its specified design strength, especially as it ages, the modular ratio varies as well. This study was conducted to determine the extent to which varying the modular ratio affects the resulting computational response of curved composite bridges.

Four modified models of each bridge were created that use modular ratios that are values of 1.0 and 2.0 higher than and 1.0 and 2.0 lower than the modular ratios used in the base models. The results were compared with the computational results for the base models.

Results: see Table 8-25, Table 8-26, Table 8-27, and Table 8-28

Reducing the modular ratios by 2.0 as compared to the base model values increased the overall stiffness of the bridge structures and reduced the stresses on the bridge girders. Maximum girder rotations decreased by at most 10.6% and vertical deflections decreased between 4.4% and 7.4%. Flexural stresses decreased by up to 2.9% and warping stresses decreased by up to 6.8%.

Decreasing the modular ratio by 1.0 as compared to the base model values had similar responses as for a reduction by 2.0, except that the magnitudes were approximately half. Increasing the modular ratios had opposite percent changes as decreasing them and had slightly lower magnitudes.

Comments:

Decreasing the modular ratio to better reflect the actual strength of the concrete, which is typically much higher than the originally specified design strength, can be an effective method for slightly improving the computational response and rating of a bridge, especially for stiffness controlled bridges. If available, tests of concrete cylinders from the original pour can be used to identify the actual strength of the concrete, or cores can be drilled and tested for older bridges.

8.3.14 Study 14: Bridge Radius of Curvature

Bridges Investigated: Mn/DOT 69824, Mn/DOT 27998, and FHWA TS

Overview:

Bridge curvature creates longitudinal warping stresses in the girders and shifts load from the innermost girders to those with the larger radii of curvature. Previous methods of designing and rating horizontally curved bridges have analyzed girders as straight members and used reduction factors to account for curvature effects. This study was conducted to provide insight into the magnitude of change for the analysis of a bridge as straight or curved.

Modified models of each of the three bridges were made with the radius of curvature of the centerline of the girders increased by a factor of 10. This factor of 10 puts all spans of the three bridges herein outside of the requirement set in the *Guide Specifications for Horizontally Curved Highway Bridges* (AASHTO, 2003a) for being able to neglect curvature effects on the girder moments. The values from the modified bridges were compared with the corresponding curved bridge base models.

Results: see Table 8-29

Straightening the bridges caused drastic changes in the distribution of loads between the girders and lowered the warping stresses for all girders. Maximum vertical deflections on the innermost girders increased by values up to 19.3%, 82.2%, and 64.0% for Bridge 69284, Bridge 27998, and the FHWA Test Specimen, respectively. On the other hand, vertical deflections on the outermost girders decreased by values up to 13.7%, 45.7%, and 49.0%. Average reductions in maximum bottom flange restraint of warping stresses for each of the bridges were approximately 90% on Bridge 69824, 60% on Bridge 27998, and 80% on FHWA TS. It is not surprising that the reduction in warping stresses on Bridge 27998 was not as high as for the other two bridges since the skewed piers for this bridge also generate torsion in the girders. For all three bridges, the maximum diaphragm forces decreased significantly. Maximum lateral wind bracing forces on Bridge 69824 decreased on average by approximately 20%.

Comments:

These results point out the importance of including the effects of curvature for analyzing horizontally curved I-girder bridges. Note that the effects of horizontal curvature were lower for Bridge 69824 due to its larger radius of curvature and the lateral wind bracing, which help to stabilize the bridge against the torsional forces.

8.3.15 Study 15: Longitudinal Distribution of Loads and Stress Calculations

Bridges Investigated: Mn/DOT 69824, Mn/DOT 27998

Overview:

The longitudinal distribution of loads on continuous composite bridges is dependent on the effectiveness of the concrete and steel reinforcement in the negative moment regions (i.e., at the pier locations) to handle tensile loads. Estimation of this distribution is further complicated when shear connectors are not provided in this region. Bridge tests, such as that conducted as part of this research project, typically show high levels of tensile resistance and composite action in the negative moment regions of bridges without shear connectors in these regions. However, at load levels higher than those tested or as deterioration occurs over time, the resistance is not guaranteed to exist. This study was conducted to determine the extent to which load distribution based on composite and non-composite properties in the negative moment regions differs, and to see how the corresponding predictions of stresses change.

Three modified models of Bridge 69824 and Bridge 27998 were created: one with the loads distributed with non-composite properties in the negative moment regions and the flexural stresses in these regions calculated based on the non-composite properties (NC-NC), one with the loads distributed with composite properties (assuming the deck is effective in tension) in the negative moment regions and the flexural stresses in these regions checked based on the non-composite properties (C-NC), and one with the loads distributed with the composite properties in the negative moment regions and flexural stresses in these regions calculated based on the section properties defined by the steel girder and the rebar in the deck (C-R). For all three modified models, the positive moment regions distributed loads and calculated stresses based on the composite section properties. Each modified model was compared to the corresponding base model, which distributed loads and calculated stresses in both the positive and negative moment regions using the composite section properties. Note that for Mn/DOT Bridge No. 69824, the C-R model is the same as the FMR analysis model discussed in Chapter 7 and the base model is the same as the FM analysis model. Thus, comparisons between the base model and the C-R model below highlight the differences between the FM and FMR analysis models.

The FHWA Test Specimen was not included in this study since it is a single simply supported span and does not have any negative moment regions.

Results: see Table 8-30, Table 8-31, and Table 8-32

Using the NC-NC model significantly lowers the stiffness of the bridge and alters the distribution of flexural moments along the bridge length. Maximum vertical displacements on Bridge 69824 increase by percent changes up to 41.1%, while on Bridge 27998 they increase by up to 10.4%. It is expected that the influence on Bridge 27998 would be less since only one end of each of its

two spans are negative moment regions. Positive region moments on Bridge 69824 increase by up to 16.6% and on Bridge 27998 increase by up to 5.4%. The largest reduction in maximum negative region moments for Bridge 69824 is 27.3% and for Bridge 27998 is 18.5%. Calculated maximum bottom flange flexural stresses in the negative moment regions for the NC-NC model are between 0% and 9.2% higher than those for the base model, which distributes and checks stresses using full composite section properties. These relatively small increases in negative moment flexural stress are due to the large reduction in moments distributed to the negative moment regions.

The only difference between the C-NC and C-R modified models and the base model are the section properties used to check the girder flexural stresses in the negative moment regions. For all three of these models the displacements, positive moment forces and stresses, diaphragm forces, and lateral wind bracing forces are identical, as are the moments in the negative moment regions. For the C-NC modified model, the calculated maximum bottom flange flexural stresses at the piers are up to 43.6% higher for Bridge 69824 and up to 22.8% higher for Bridge 27998 than the base model values. The average increase in negative moment stresses for both bridges using the C-R models is around 20%. Note that the larger difference between the C-NC and C-R models for Bridge 69824 compared to Bridge 27998 are due to a greater steel reinforcement ratio in the deck for Bridge 69824.

Comments:

The results above indicate that for continuous bridges without shear connectors in the negative moment regions, assuming non-composite properties in those regions for load distribution and stress calculations is not necessarily the most conservative method of analysis. In particular, predictions for negative moment region bottom flange stresses for both the C-NC and C-R models were more conservative than those for the NC-NC models for both of these bridges. For this reason and the fact that test data presented in Chapter 6 for Bridge 69824 indicates composite action in the negative moment regions, the preferred model for analysis of Bridge 69824 distributes loads based on full composite properties in the negative moment regions. Both the FM and FMR analyses discussed in Chapter 7 use this approach for Bridge No. 69824. As long as a bridge does not indicate a loss of bond in the negative moment regions, either by visual inspection of the deck-to-girder interface or by load test, it is recommended that loads be distributed based on full composite properties along the length of the bridge.

8.3.16 Study 16: Restraint of Warping Stress Approximation

Bridges Investigated: Mn/DOT 69824, Mn/DOT 27998, FHWA TS

Overview:

Computer analysis programs for curved composite steel I-girder bridges that do not include a seventh degree of freedom for use in determining the restraint of warping stresses generally rely on an approximate equation for estimating these stresses. Lateral bending moments in the bottom flange are approximated such as by using Equation 2-8 and then divided by the bending modulus of the bottom flange in the lateral direction to obtain the tip stresses due to restraint of warping.

This method approximates the magnitude of the maximum restraint of warping stresses along the length of the girders, while providing little insight into the local behavior of these stresses.

Using the bridge properties and the vertical bending moment envelopes for the base model analyses for each of the three bridges, the approximate maximum restraint of warping stress along each girder was calculated for the various spans being loaded. Equation 2-8, excluding the 6/5 factor, was used to calculate the lateral bending moments in the bottom flange. The section web depth D in Equation 2-8 for the composite girders was calculated as the distance from the mid-thickness of the bottom flange to the mid-thickness of the concrete slab. The approximate equation results were then plotted against the base model restraint of warping stress envelopes from the finite element method analysis for the bottom flange. Note that the absolute values are plotted for both, since the approximate equation does not provide directionality.

Results: see Figure 8-3 through Figure 8-23

The results on Bridge 69824 are plotted along the length for Girder C and Girder A in Figure 8-3 through Figure 8-7 and Figure 8-8 through Figure 8-12, respectively. Results for each of the five different spans being loaded are provided. The dark oscillating line in the plots shows the absolute value of the finite element analysis envelopes for maximum restraint of warping stress, while the light line shows the calculated values for the approximate equation. The black squares along the horizontal axis indicate support locations (i.e., piers). For the approximate equation to be conservative as compared to the finite element method results, all points on the dark line must lie below those for the light line. The results for both girders of Bridge 69824 generally show good correlation. Comparing the peak stresses near midspan of the loaded span indicate that for Girder C the approximate equation is typically unconservative by around 10% of the FEM value, while for Girder A it is usually conservative by about 10%.

Results for each of the four girders of Bridge 27998 are plotted in Figure 8-13 through Figure 8-20. For each girder, plots are provided for the two different spans of the bridge being loaded. Comparing the peak midspan stresses for the loaded span indicate that the approximate equation results are unconservative for Girder 1, Girder 2, and Girder 3 by around 10% of the FEM value. For the outermost girder, Girder 4, the approximate equation results are conservative by about 25% of the FEM value. Note that around the support regions of this bridge the approximate equation values and the FEM values generally do not correlate well. This is because the approximate equation can not accurately incorporate the effects of the skewed support angles and change in diaphragm spacing at these locations.

The results for the three girders of the FHWA Test Specimen are shown in Figure 8-21 through Figure 8-23. For Girder 1, the peak midspan region restraint of warping stress is underestimated using the approximate equation by approximately 7% of the FEM value. For Girder 2, it is underestimated by around 16% of the FEM value. The outermost girder, Girder 3, is overestimated using the approximate equation by about 17% of the FEM value.

Comments:

The use of the approximate equation for estimating restraint of warping stresses on the bottom flange of curved girders is shown for these bridges to be reasonably accurate as compared to the

FEM values. However, near skewed supports and non-uniform diaphragm spacing, the approximate equation provided poor estimates of the warping behavior due to assumptions in the formulation of the equation. On all three bridges, the results for the girders with the largest radius of curvature were slightly conservative. On the other hand, the approximate equation slightly underestimated the FEM value for all other girders. Conservative measures, such as the inclusion of the 6/5 factor as in Equation 2-8 or limiting the flange couple depth D for composite sections to the height of the steel girder, can be taken to avoid under prediction of the restraint of warping stresses on the bridge girders with the smaller radii of curvature.

Grillage Model Base Parameters

Bridge Span	Mn/DOT 69824					Mn/DOT 27998		FHWA
	Span 10-9	Span 9-8	Span 8-7	Span 7-6	Span 6-5	Span I	Span II	
Number of Girders	2	2	2	2	2	4	4	3
R _{min} ¹ (ft)	565.96	565.96	565.96	565.96	1630.02	272.02	272.02	191.25
Girder Spacing (ft)	18.00	18.00	18.00	18.00	18.00	9.00	9.00	8.75
L _{arc_max} ² (ft)	97.14	115.18	150.84	115.13	79.53	155.40	149.57	93.94
Diaphragm Type	beam	beam	beam	beam	beam	X	X	K
D _{max} ³ (ft)	12.14	11.52	11.60	11.51	11.36	17.59	17.59	23.48
N (Modular Ratio)	6	6	6	6	6	6	6	8
b _{eff} - Interior ⁴ (+/-) ⁵ (in)	123.0/102.5	123.0/102.5	123.0/102.5	123.0/102.5	123.0/102.5	138.5/92.5	138.5/92.5	105.0/NA
b _{eff} - Middle ⁶ (+/-) ⁵ (in)	NA	NA	NA	NA	NA	108.0/108.0	108.0/108.0	105.0/NA
b _{eff} - Exterior ⁷ (+/-) ⁵ (in)	123.0/102.5	123.0/102.5	123.0/102.5	123.0/102.5	123.0/102.5	152.5/92.5	152.5/92.5	105.0/NA
t _{slab} (in)	9.0	9.0	9.0	9.0	9.0	9.0	9.0	8.0
Composite Deck ⁸ (+/-) ⁵	yes/yes	yes/yes	yes/yes	yes/yes	yes/yes	yes/yes	yes/yes	yes/NA
Lateral Wind Bracing?	yes	yes	yes	yes	yes	no	no	no
Deck Beams Included?	yes	yes	yes	yes	yes	yes	yes	yes

KEY:

- 1 minimum radius of curvature for all girders in the current span
- 2 maximum arc span length for all girders in the current span
- 3 maximum diaphragm spacing for all girders in the current span
- 4 girder with smallest radius of curvature
- 5 (positive moment region) / (negative moment region)
- 6 girders between Interior and Exterior girders
- 7 girder with largest radius of curvature
- 8 stiffness and stress assume deck is effective in tension

NA not applicable

Table 8-1: Grillage Model Base Parameters

Study 1: Beam Diaphragm Stiffness due to Knee Brace Region															
Percent Change for Maximum Responses from Analysis using: Base Model with knee brace stiffness to: Modified Model without knee brace stiffness															
Mn/DOT Bridge No. 69824															
Girder															
Span Loaded		Middle of Span					Left Support				Right Support				
		Vertical Deflection	Torsional Rotation	Flexural Moment	Bottom Flange Stress	Flexural Shear	Flexural Moment	Bottom Flange Stress	Flexural Shear	Flexural Moment	Bottom Flange Stress	Flexure	Warping	Flexure	Warping
		Flexure	Warping	Flexure	Warping	Flexure	Warping	Flexure	Warping	Flexure	Warping	Flexure	Warping	Flexure	Warping
GC	10-9	1.4%	-2.2%	1.0%	0.9%	-1.7%	0.7%	Pinned	Pinned	Pinned	0.5%	1.0%	1.1%	-9.1%	
	9-8	1.3%	-1.7%	1.0%	1.2%	-1.9%	0.3%	1.0%	1.1%	-9.1%	0.3%	0.8%	1.0%	-2.3%	
	8-7	1.4%	-0.1%	1.1%	1.3%	-0.8%	0.3%	0.8%	1.0%	-6.1%	0.3%	0.9%	1.0%	-2.5%	
	7-6	1.2%	-1.5%	0.9%	0.8%	-2.8%	0.3%	0.9%	1.0%	-2.4%	0.2%	0.8%	1.0%	-8.3%	
	6-5	0.6%	-4.6%	0.6%	0.5%	-3.0%	0.4%	0.8%	1.0%	-8.3%	0.1%	Pinned	Pinned	Pinned	
GA	10-9	0.1%	-0.5%	0.2%	0.3%	0.9%	0.1%	Pinned	Pinned	Pinned	0.0%	0.2%	0.3%	-200.0%	
	9-8	0.1%	-0.5%	0.2%	0.3%	1.1%	0.0%	0.2%	0.3%	1.6%	0.0%	0.0%	0.3%	0.0%	
	8-7	0.0%	0.4%	0.0%	0.2%	6.8%	0.0%	0.0%	-0.4%	-1.6%	0.1%	0.0%	0.0%	0.0%	
	7-6	0.1%	-0.4%	0.2%	0.3%	0.0%	0.1%	0.0%	0.0%	0.0%	0.2%	0.4%	0.5%	-1.6%	
	6-5	0.2%	-1.6%	0.3%	0.2%	5.0%	0.2%	0.4%	0.5%	-1.6%	0.0%	Pinned	Pinned	Pinned	

Beam Diaphragm and Lateral Wind Bracing															
Span Loaded		Diaphragm Forces at Girder C			Diaphragm Forces at Girder A			Lateral Wind Bracing Forces							
		Axial	Shear	Moment	Axial	Shear	Moment	Axial Tension	Axial Compression	Axial Tension	Axial Compression	Axial Tension	Axial Compression	Axial Tension	Axial Compression
All Members in Span	10-9	-2.9%	-193.6%	-23.0%	-2.9%	-193.6%	-209.8%	-1.0%	0.2%						
	9-8	-1.9%	-13.6%	-18.6%	-1.9%	-13.6%	-194.7%	-0.9%	0.2%						
	8-7	-3.1%	-4.7%	-24.3%	-3.1%	-4.7%	18.3%	-0.8%	-0.8%						
	7-6	-3.2%	-13.8%	-19.2%	-3.2%	-13.8%	-194.9%	-1.3%	1.5%						
	6-5	2.8%	-15.4%	-28.9%	2.8%	-15.4%	-0.2%	0.7%	-5.2%						
Only Members near Midspan	10-9	-2.9%	-5.6%	-23.0%	-2.9%	-5.6%	14.7%	-7.6%	2.2%						
	9-8	-3.2%	-6.0%	-23.2%	-3.2%	-6.0%	14.0%	-5.9%	-0.6%						
	8-7	-3.1%	-4.7%	-24.3%	-3.1%	-4.7%	18.3%	0.8%	1.9%						
	7-6	-3.2%	-6.0%	-23.3%	-3.2%	-6.0%	14.2%	-4.2%	-0.3%						
	6-5	2.8%	-3.1%	-211.1%	2.8%	-3.1%	10.8%	-2.5%	0.0%						

Table 8-2: Study 1 Diaphragm Knee Brace Stiffness versus No Knee Brace Stiffness

Study 2: Vertical Rigid Offsets for Beam Diaphragms															
Percent Change for Maximum Responses from Analysis using: Base Model with vertical offsets to: Modified Model without vertical offsets															
Mn/DOT Bridge No. 69824															
Span Loaded		Middle of Span					Left Support				Right Support				
		Vertical Deflection	Torsional Rotation	Flexural Moment	Bottom Flange Stress	Flexural Shear	Flexural Moment	Bottom Flange Stress	Flexural Shear	Flexural Moment	Bottom Flange Stress	Flexure	Warping	Flexure	Warping
		Flexure	Warping	Flexure	Warping	Flexure	Warping	Flexure	Warping	Flexure	Warping	Flexure	Warping	Flexure	Warping
GC	10-9	0.1%	-1.1%	0.1%	0.0%	0.0%	0.0%	Pinned	Pinned	Pinned	0.0%	0.1%	0.3%	0.0%	
	9-8	0.0%	-0.7%	0.1%	0.0%	0.0%	0.0%	0.1%	0.3%	0.0%	0.0%	0.1%	0.3%	0.0%	
	8-7	0.1%	-0.4%	0.2%	0.3%	-0.8%	0.0%	0.1%	0.3%	1.5%	0.0%	0.1%	0.0%	2.5%	
	7-6	0.1%	-0.7%	0.1%	0.0%	0.0%	0.0%	0.1%	0.0%	0.0%	0.0%	0.1%	0.0%	1.2%	
	6-5	0.1%	-2.3%	0.1%	0.2%	-1.5%	0.0%	0.1%	1.2%	0.0%	Pinned	Pinned	Pinned	Pinned	
GA	10-9	0.1%	1.0%	0.1%	0.0%	0.9%	0.0%	Pinned	Pinned	Pinned	0.0%	0.1%	0.0%	-1.6%	
	9-8	0.1%	0.8%	0.1%	0.0%	0.0%	0.0%	0.1%	0.0%	0.0%	0.1%	0.3%	0.0%	0.0%	
	8-7	0.0%	0.4%	0.0%	0.2%	0.0%	0.0%	0.1%	0.0%	-1.6%	0.0%	0.0%	0.0%	0.0%	
	7-6	0.1%	0.8%	0.1%	0.0%	1.1%	0.0%	0.0%	0.0%	0.0%	0.1%	0.0%	0.0%	-1.6%	
	6-5	0.1%	2.3%	0.1%	0.2%	5.0%	0.0%	0.1%	0.0%	-1.6%	0.0%	Pinned	Pinned	Pinned	

Beam Diaphragm and Lateral Wind Bracing															
Span Loaded		Diaphragm Forces at Girder C			Diaphragm Forces at Girder A			Lateral Wind Bracing Forces							
		Axial	Shear	Moment	Axial	Shear	Moment	Axial Tension	Axial Compression	Axial Tension	Axial Compression	Axial Tension	Axial Compression	Axial Tension	Axial Compression
All Members in Span	10-9	-89.0%	-0.1%	-182.4%	-89.0%	-0.1%	-223.1%	-0.8%	1.0%						
	9-8	-111.1%	0.0%	-7.5%	-111.1%	0.0%	7.8%	0.0%	0.2%						
	8-7	-76.9%	0.0%	-177.0%	-76.9%	0.0%	32.2%	-1.0%	-1.0%						
	7-6	-88.4%	0.0%	-8.1%	-88.4%	0.0%	8.3%	0.0%	0.0%						
	6-5	-87.7%	-0.1%	-20.1%	-87.7%	-0.1%	22.4%	-3.0%	0.2%						
Only Members near Midspan	10-9	-89.0%	0.0%	-24.6%	-89.0%	0.0%	28.6%	-7.3%	9.3%						
	9-8	-88.7%	0.0%	-24.3%	-88.7%	0.0%	28.2%	-4.0%	3.7%						
	8-7	-76.9%	0.0%	-27.3%	-76.9%	0.0%	32.2%	-1.1%	1.0%						
	7-6	-88.4%	-0.1%	-24.4%	-88.4%	-0.1%	28.4%	-3.1%	3.4%						
	6-5	-87.7%	-0.1%	-237.3%	-87.7%	-0.1%	31.1%	-2.3%	2.9%						

Table 8-3: Study 2 Diaphragm Vertical Offsets versus No Vertical Offsets

Study 3: Composite Action of Beam Diaphragms														
Percent Change for Maximum Responses from Analysis using: Base Model with $b_{eff} = 7$ inches for beam diaphragms to: Modified Model with no composite action for beam diaphragms														
Mn/DOT Bridge No. 69824														
Girder														
Span Loaded		Middle of Span					Left Support				Right Support			
		Vertical Deflection	Torsional Rotation	Flexural Moment	Bottom Flange Stress		Flexural Shear	Flexural Moment	Bottom Flange Stress		Flexural Shear	Flexural Moment	Bottom Flange Stress	
					Flexure	Warping			Flexure	Warping			Flexure	Warping
GC	10-9	1.0%	-1.4%	0.7%	0.6%	-1.7%	0.5%	Pinned	Pinned	Pinned	0.3%	0.7%	0.8%	-7.1%
	9-8	0.9%	-1.1%	0.7%	0.9%	-1.0%	0.3%	0.7%	0.8%	-7.1%	0.2%	0.6%	0.7%	-2.3%
	8-7	0.9%	0.0%	0.8%	1.0%	-0.8%	0.2%	0.6%	0.7%	-3.0%	0.2%	0.6%	0.6%	-1.3%
	7-6	0.8%	-1.0%	0.6%	0.6%	-1.9%	0.2%	0.6%	0.6%	-2.4%	0.2%	0.6%	0.7%	-7.1%
	6-5	0.6%	-4.0%	0.5%	0.5%	6.0%	0.3%	0.6%	0.7%	-7.1%	0.4%	Pinned	Pinned	Pinned
GA	10-9	0.1%	-0.5%	0.2%	0.0%	0.9%	0.1%	Pinned	Pinned	Pinned	0.0%	0.1%	0.0%	-198.4%
	9-8	0.1%	-0.5%	0.2%	0.0%	1.1%	0.0%	0.1%	0.0%	0.0%	0.0%	0.0%	0.3%	0.0%
	8-7	0.0%	0.3%	0.0%	0.2%	4.1%	0.0%	0.0%	-0.4%	-1.6%	0.0%	0.0%	0.0%	0.0%
	7-6	0.1%	-0.4%	0.2%	0.3%	0.0%	0.0%	0.0%	0.0%	0.0%	0.2%	0.3%	0.3%	-1.6%
	6-5	0.2%	-2.4%	0.2%	0.4%	10.0%	0.1%	0.3%	0.3%	-1.6%	0.2%	Pinned	Pinned	Pinned
Beam Diaphragm and Lateral Wind Bracing														
Span Loaded		Diaphragm Forces at Girder C				Diaphragm Forces at Girder A				Lateral Wind Bracing Forces				
		Axial	Shear	Moment		Axial	Shear	Moment		Axial Tension	Axial Compression			
All Members in Span	10-9	2.9%	-195.1%	8.9%	2.9%	-195.1%	-21.6%	-21.6%	-21.6%	-0.7%	0.0%			
	9-8	0.6%	-10.2%	-202.0%	0.6%	-10.2%	-14.9%	-14.9%	-14.9%	-0.7%	0.0%			
	8-7	0.2%	-3.4%	11.6%	0.2%	-3.4%	-181.2%	-181.2%	-181.2%	-0.5%	-0.5%			
	7-6	2.8%	-10.4%	-202.2%	2.8%	-10.4%	-15.4%	-15.4%	-15.4%	-0.9%	1.1%			
	6-5	1.6%	-11.5%	-6.6%	1.6%	-11.5%	-23.8%	-23.8%	-23.8%	-2.3%	-4.1%			
Only Members near Midspan	10-9	2.9%	-4.1%	8.9%	2.9%	-4.1%	-19.2%	-19.2%	-19.2%	-4.4%	0.4%			
	9-8	2.8%	-4.4%	8.4%	2.8%	-4.4%	-19.3%	-19.3%	-19.3%	-3.7%	-0.9%			
	8-7	0.2%	-3.4%	11.6%	0.2%	-3.4%	-21.1%	-21.1%	-21.1%	0.8%	1.5%			
	7-6	2.8%	-4.3%	8.5%	2.8%	-4.3%	-19.3%	-19.3%	-19.3%	-2.6%	-0.8%			
	6-5	1.6%	-0.4%	29.3%	1.6%	-0.4%	-177.1%	-177.1%	-177.1%	-2.3%	-1.3%			

Table 8-4: Study 3 Diaphragm $b_{eff} = 7$ inches versus $b_{eff} = 0$ inches

Study 3: Composite Action of Beam Diaphragms														
Percent Change for Maximum Responses from Analysis using: Base Model with $b_{eff} = 7$ inches for beam diaphragms to: Modified Model with $b_{eff} = 54$ inches for beam diaphragms														
Mn/DOT Bridge No. 69824														
Span Loaded		Middle of Span					Left Support				Right Support			
		Vertical Deflection	Torsional Rotation	Flexural Moment	Bottom Flange Stress		Flexural Shear	Flexural Moment	Bottom Flange Stress		Flexural Shear	Flexural Moment	Bottom Flange Stress	
					Flexure	Warping			Flexure	Warping			Flexure	Warping
GC	10-9	-0.3%	0.7%	-0.2%	-0.3%	0.0%	-0.2%	Pinned	Pinned	Pinned	-0.1%	-0.2%	-0.3%	3.0%
	9-8	-0.2%	0.5%	-0.2%	-0.3%	1.0%	-0.1%	-0.2%	-0.3%	3.0%	-0.1%	-0.2%	0.0%	0.0%
	8-7	-0.3%	0.1%	-0.2%	-0.3%	0.8%	-0.1%	-0.2%	0.0%	0.0%	-0.1%	-0.2%	-0.3%	0.0%
	7-6	-0.2%	0.5%	-0.2%	-0.3%	0.0%	-0.1%	-0.2%	-0.3%	0.0%	-0.1%	-0.2%	-0.2%	2.4%
	6-5	-0.2%	1.5%	-0.2%	-1.5%	-0.1%	-0.2%	-0.2%	-0.2%	2.4%	-0.1%	Pinned	Pinned	Pinned
GA	10-9	0.0%	-0.1%	-0.1%	0.0%	0.9%	0.0%	Pinned	Pinned	Pinned	0.0%	-0.1%	0.0%	0.0%
	9-8	0.0%	-0.1%	-0.1%	-0.3%	0.0%	0.0%	-0.1%	0.0%	0.0%	0.0%	0.0%	0.0%	0.0%
	8-7	0.0%	-0.2%	0.0%	0.0%	-1.4%	0.0%	0.0%	0.0%	0.0%	0.0%	0.0%	0.0%	0.0%
	7-6	-0.1%	-0.1%	-0.1%	0.0%	0.0%	0.0%	0.0%	0.0%	0.0%	-0.1%	-0.1%	-0.3%	0.0%
	6-5	-0.1%	0.5%	-0.1%	0.0%	0.0%	0.0%	-0.1%	-0.3%	0.0%	-0.1%	Pinned	Pinned	Pinned
Beam Diaphragm and Lateral Wind Bracing														
Span Loaded		Diaphragm Forces at Girder C				Diaphragm Forces at Girder A				Lateral Wind Bracing Forces				
		Axial	Shear	Moment		Axial	Shear	Moment		Axial Tension	Axial Compression			
All Members in Span	10-9	-189.0%	4.7%	-187.1%	-189.0%	4.7%	-223.1%	0.2%	-0.2%	-0.2%	0.0%			
	9-8	-2.5%	3.8%	-5.3%	-2.5%	3.8%	13.2%	0.2%	0.2%	0.2%	0.0%			
	8-7	-1.9%	1.1%	-1.9%	-1.9%	1.1%	32.5%	0.3%	0.3%	0.3%	0.0%			
	7-6	-197.3%	3.9%	-5.9%	-197.3%	3.9%	14.0%	0.6%	0.6%	0.6%	-0.7%			
	6-5	-4.3%	4.2%	-15.0%	-4.3%	4.2%	26.0%	1.6%	1.6%	1.6%	1.7%			
Only Members near Midspan	10-9	-13.3%	1.3%	-22.0%	-13.3%	1.3%	28.5%	2.9%	2.9%	2.9%	-1.8%			
	9-8	-13.9%	1.4%	-21.7%	-13.9%	1.4%	28.2%	2.4%	2.4%	2.4%	-0.3%			
	8-7	-1.9%	1.1%	-25.5%	-1.9%	1.1%	32.5%	0.5%	0.5%	0.5%	-0.7%			
	7-6	-13.8%	1.3%	-21.8%	-13.8%	1.3%	28.5%	2.3%	2.3%	2.3%	-0.6%			
	6-5	-4.3%	1.3%	-243.0%	-4.3%	1.3%	34.3%	1.2%	1.2%	1.2%	-0.3%			

Table 8-5: Study 3 Diaphragm $b_{eff} = 7$ inches versus $b_{eff} = 54$ inches

Study 4: Cross-frame Member Size															
Percent Change for Maximum Responses from Analysis using: Base Model to: Modified Model with half the area for cross-frame members															
Mn/DOT Bridge No. 27998															
Girder															
Span Loaded		Middle of Span				Left Support				Right Support					
		Vertical Deflection	Torsional Rotation	Flexural Moment	Bottom Flange Stress	Flexural Shear	Flexural Moment	Bottom Flange Stress	Flexural Shear	Flexural Moment	Bottom Flange Stress	Flexure	Warping		
G1		I	5.2%	13.7%	-0.3%	0.0%	-7.9%	-1.0%	Pinned	Pinned	Pinned	-0.4%	1.9%		
		II	5.0%	14.4%	0.0%	0.0%	-5.7%	-0.4%	1.9%	2.1%	-164.8%	1.6%	2.1%		
G2		I	7.0%	15.3%	2.3%	2.2%	-4.1%	0.9%	Pinned	Pinned	Pinned	-0.3%	2.2%		
		II	7.0%	16.4%	2.0%	2.4%	-10.3%	-0.3%	2.2%	2.1%	-195.9%	-3.2%	2.1%		
G3		I	6.1%	18.7%	1.7%	1.5%	-3.3%	-3.6%	Pinned	Pinned	Pinned	-3.3%	-1.0%		
		II	6.8%	20.3%	-0.6%	-0.8%	-7.3%	-10.4%	-1.0%	-0.8%	-230.8%	-6.3%	-0.8%		
G4		I	7.9%	22.2%	2.7%	2.7%	-6.8%	-0.1%	Pinned	Pinned	Pinned	-2.1%	2.0%		
		II	9.8%	23.7%	2.8%	2.9%	-5.2%	0.3%	2.0%	2.4%	19.8%	-1.7%	2.4%		
X - shaped Diaphragm															
Span Loaded		Axial Forces between G1 and G2				Axial Forces between G2 and G3				Axial Forces between G3 and G4					
		Top	Bottom	U1-L2	L1-U2	Top	Bottom	U2-L3	L2-U3	Top	Bottom	U3-L4	L3-U4		
All Members in Span		I	-163.7%	-42.1%	-35.0%	1.6%	-33.0%	-37.3%	-7.4%	-3.0%	-23.8%	-33.0%	-31.8%	-36.2%	
		II	-40.6%	-45.8%	-4.8%	-169.7%	-29.4%	-39.4%	-4.8%	-160.8%	-31.2%	5.3%	-162.0%	-41.5%	
Only Members near Midspan		I	-163.7%	19.4%	-9.5%	1.6%	-33.0%	10.4%	-4.3%	-3.0%	-23.8%	6.3%	2.3%	-6.5%	
		II	-40.6%	12.8%	-4.8%	2.6%	-29.4%	17.8%	-4.8%	-2.3%	-15.7%	5.3%	3.0%	-6.4%	
FHWA Test Specimen															
Girder		Middle of Span				Left Support				Right Support					
Span Loaded		Vertical Deflection	Torsional Rotation	Flexural Moment	Bottom Flange Stress	Flexural Shear	Flexural Moment	Bottom Flange Stress	Flexural Shear	Flexural Moment	Bottom Flange Stress	Flexure	Warping		
G1		1	5.1%	4.5%	0.3%	0.2%	-1.2%	0.1%	Pinned	Pinned	Pinned	0.1%	Pinned		
		G2	1	1.7%	9.7%	-0.3%	-0.3%	-2.5%	0.2%	Pinned	Pinned	Pinned	0.1%	Pinned	
		G3	1	4.6%	13.0%	1.1%	1.1%	-2.2%	0.9%	Pinned	Pinned	Pinned	0.9%	Pinned	
K - shaped Diaphragm															
Span Loaded		Axial Forces between G1 and G2					Axial Forces between G2 and G3								
		Top	Bottom 1	Bottom 2	U1-M	M-U2	Top	Bottom 2	Bottom 3	U2-M	M-U3				
All Members in Span		1	-30.9%	1.1%	-1.6%	-4.5%	-4.6%	-33.4%	1.8%	3.8%	0.9%	0.3%			
		Only Members near Midspan	1	-30.9%	1.1%	-1.6%	-4.5%	-4.6%	-33.4%	1.8%	3.8%	0.9%	0.3%		

Table 8-6: Study 4 Cross-frame Members with Half Area

Study 4: Cross-frame Member Size														
Percent Change for Maximum Responses from Analysis using: Base Model to: Modified Model with area doubled for cross-frame members														
Mn/DOT Bridge No. 27998														
Girder														
Span Loaded	Middle of Span					Left Support				Right Support				
	Vertical Deflection	Torsional Rotation	Flexural Moment	Bottom Flange Stress	Flexure Warping	Flexural Shear	Flexural Moment	Bottom Flange Stress	Flexure Warping	Flexural Shear	Flexural Moment	Bottom Flange Stress	Flexure Warping	
G1	I	-4.2%	-11.7%	-0.3%	0.0%	2.9%	0.5%	Pinned	Pinned	Pinned	0.3%	-2.0%	-2.1%	-12.6%
	II	-4.1%	-13.3%	-0.4%	-0.5%	4.1%	0.3%	-2.0%	-2.1%	-7.3%	-2.8%	Pinned	Pinned	Pinned
G2	I	-5.3%	-12.3%	-2.4%	-2.7%	0.8%	1.9%	Pinned	Pinned	Pinned	-0.8%	-1.9%	-2.1%	11.4%
	II	-5.3%	-14.1%	-2.2%	-1.8%	6.8%	-0.8%	-1.9%	-2.1%	-12.3%	3.0%	Pinned	Pinned	Pinned
G3	I	-6.3%	-13.9%	-2.6%	-2.9%	-1.1%	6.7%	Pinned	Pinned	Pinned	2.0%	0.4%	0.8%	-27.1%
	II	-7.8%	-15.9%	-1.5%	-1.6%	3.7%	3.8%	0.4%	-1.7%	-13.5%	9.2%	Pinned	Pinned	Pinned
G4	I	-7.7%	-15.5%	-4.0%	-4.0%	1.0%	0.6%	Pinned	Pinned	Pinned	1.9%	-1.7%	-1.8%	-13.5%
	II	-9.8%	-17.2%	-4.0%	-3.4%	5.2%	-0.5%	-1.7%	-1.8%	-13.5%	1.9%	Pinned	Pinned	Pinned
X - shaped Diaphragm														
Span Loaded	Axial Forces between G1 and G2					Axial Forces between G2 and G3				Axial Forces between G3 and G4				
	Top	Bottom	U1-L2	L1-U2		Top	Bottom	U2-L3	L2-U3	Top	Bottom	U3-L4	L3-U4	
All Members in Span	I	74.8%	67.4%	70.1%	67.0%	56.2%	77.0%	76.6%	11.1%	-248.6%	83.4%	80.3%	62.7%	
	II	68.2%	71.6%	-223.4%	75.8%	47.2%	67.1%	6.1%	71.5%	44.3%	51.7%	67.7%	63.1%	
Only Members near Midspan	I	74.8%	-26.2%	11.4%	-1.1%	56.2%	-24.5%	4.6%	3.7%	39.8%	-12.2%	-0.7%	7.6%	
	II	68.2%	-29.8%	2.9%	-5.0%	47.2%	-22.9%	6.1%	2.4%	28.7%	-7.0%	1.2%	6.8%	
FHWA Test Specimen														
Girder														
Span Loaded	Middle of Span					Left Support				Right Support				
	Vertical Deflection	Torsional Rotation	Flexural Moment	Bottom Flange Stress	Flexure Warping	Flexural Shear	Flexural Moment	Bottom Flange Stress	Flexure Warping	Flexural Shear	Flexural Moment	Bottom Flange Stress	Flexure Warping	
G1	1	-2.6%	-2.6%	-0.3%	-0.2%	0.4%	0.0%	Pinned	Pinned	Pinned	0.0%	Pinned	Pinned	Pinned
G2	1	-0.9%	-5.4%	0.1%	0.0%	1.4%	-0.2%	Pinned	Pinned	Pinned	-0.3%	Pinned	Pinned	Pinned
G3	1	-2.7%	-6.9%	-0.8%	-0.8%	0.9%	-0.8%	Pinned	Pinned	Pinned	-0.8%	Pinned	Pinned	Pinned
K - shaped Diaphragm														
Span Loaded	Axial Forces between G1 and G2					Axial Forces between G2 and G3				Axial Forces between G3 and G4				
	Top	Bottom	1	Bottom 2	U1-M	M-U2	Top	Bottom	2	Bottom 3	U2-M	M-U3		
All Members in Span	1	58.0%	-2.5%	-3.4%	2.7%	2.8%	64.5%	-3.8%	-6.3%	0.3%	0.4%			
Only Members near Midspan	1	58.0%	-2.5%	-3.4%	2.7%	2.8%	64.5%	-3.8%	-6.3%	0.3%	0.4%			

Table 8-7: Study 4 Cross-frame Members with Double Area

Study 5: Lateral Wind Bracing Members														
Percent Change for Maximum Responses from Analysis using: Base Model to: Modified Model without lateral wind bracing members														
Mn/DOT Bridge No. 69824														
Girder														
Span Loaded	Middle of Span					Left Support				Right Support				
	Vertical Deflection	Torsional Rotation	Flexural Moment	Bottom Flange Stress	Flexure Warping	Flexural Shear	Flexural Moment	Bottom Flange Stress	Flexure Warping	Flexural Shear	Flexural Moment	Bottom Flange Stress	Flexure Warping	
GC	10-9	11.6%	77.1%	11.9%	12.5%	19.8%	5.1%	Pinned	Pinned	Pinned	3.6%	6.6%	6.8%	11.1%
	9-8	10.7%	79.8%	11.7%	12.5%	20.0%	2.7%	6.6%	6.8%	11.1%	2.1%	6.7%	6.6%	15.1%
	8-7	14.8%	100.1%	17.9%	20.6%	29.4%	2.1%	6.7%	6.6%	19.7%	2.2%	6.9%	6.7%	16.5%
	7-6	11.7%	82.0%	12.3%	13.3%	21.3%	2.2%	6.9%	6.7%	16.5%	2.3%	7.1%	7.5%	14.3%
	6-5	14.2%	77.7%	13.4%	12.8%	35.8%	3.1%	7.1%	7.5%	14.3%	5.2%	Pinned	Pinned	Pinned
GA	10-9	25.0%	66.2%	20.4%	22.1%	-2.8%	8.2%	Pinned	Pinned	Pinned	6.1%	10.2%	10.4%	-195.1%
	9-8	26.9%	71.9%	20.1%	21.6%	-6.5%	7.0%	10.2%	10.4%	-4.8%	4.7%	8.7%	18.9%	-12.0%
	8-7	31.6%	100.6%	19.8%	14.9%	-28.8%	4.7%	8.7%	26.8%	0.0%	5.5%	8.7%	27.6%	1.6%
	7-6	26.8%	73.9%	20.1%	22.1%	-5.3%	5.5%	8.7%	18.4%	-10.8%	6.9%	9.3%	9.6%	-9.8%
	6-5	19.4%	55.2%	17.0%	15.6%	-80.0%	4.1%	9.3%	9.6%	-9.8%	6.5%	Pinned	Pinned	Pinned
Beam Diaphragm and Lateral Wind Bracing														
Span Loaded	Diaphragm Forces at Girder C					Diaphragm Forces at Girder A				Lateral Wind Bracing Forces				
	Axial	Shear	Moment	Axial	Shear	Moment	Axial	Shear	Moment	Axial Tension	Axial Compression			
All Members in Span	10-9	-1.1%	-156.9%	-39.6%	-1.1%	-156.9%	-164.8%	-	-100.0%	-	-100.0%			
	9-8	-202.6%	-40.0%	-35.9%	-202.6%	-40.0%	-33.2%	-	-100.0%	-	-100.0%			
	8-7	31.1%	-41.1%	-42.0%	31.1%	-41.1%	-31.4%	-	-100.0%	-	-100.0%			
	7-6	5.0%	-41.2%	-36.7%	5.0%	-41.2%	-34.5%	-	-100.0%	-	-100.0%			
	6-5	-145.0%	-62.6%	-60.8%	-145.0%	-62.6%	-55.0%	-	-100.0%	-	-100.0%			
Only Members near Midspan	10-9	-1.1%	-42.6%	-39.6%	-1.1%	-42.6%	-32.3%	-	-100.0%	-	-100.0%			
	9-8	4.9%	-41.7%	-40.9%	4.9%	-41.7%	-31.6%	-	-100.0%	-	-100.0%			
	8-7	31.1%	-41.1%	-42.0%	31.1%	-41.1%	-31.4%	-	-100.0%	-	-100.0%			
	7-6	5.0%	-41.3%	-41.3%	5.0%	-41.3%	-31.0%	-	-100.0%	-	-100.0%			
	6-5	-82.6%	-78.0%	-72.5%	-82.6%	-78.0%	-79.3%	-	-100.0%	-	-100.0%			

Table 8-8: Study 5 Excluding Lateral Wind Bracing

Study 5: Lateral Wind Bracing Members														
Percent Change for Maximum Responses from Analysis using: Base Model to: Modified Model with half the area for lateral wind bracing members														
Mn/DOT Bridge No. 69824														
Girder														
Span Loaded		Middle of Span				Left Support				Right Support				
		Vertical Deflection	Torsional Rotation	Flexural Moment	Bottom Flange Stress	Flexural Shear	Flexural Moment	Bottom Flange Stress	Flexural Shear	Flexural Moment	Bottom Flange Stress	Flexural Shear	Flexural Moment	
		Flexure	Warping	Flexure	Warping	Flexure	Warping	Flexure	Warping	Flexure	Warping	Flexure	Warping	
GC	10-9	3.1%	20.8%	3.3%	3.4%	6.0%	1.6%	Pinned	Pinned	Pinned	1.1%	2.2%	2.2%	4.0%
	9-8	2.7%	20.0%	3.2%	3.5%	5.7%	0.9%	2.2%	2.2%	4.0%	0.7%	2.2%	2.3%	4.7%
	8-7	3.7%	24.6%	4.8%	5.5%	8.4%	0.7%	2.2%	2.3%	6.1%	0.8%	2.3%	2.2%	6.3%
	7-6	2.9%	20.4%	3.3%	3.4%	5.6%	0.8%	2.3%	2.2%	4.7%	0.9%	2.5%	2.7%	7.1%
	6-5	4.2%	22.9%	4.1%	4.0%	11.9%	0.9%	2.5%	2.7%	7.1%	1.7%	Pinned	Pinned	Pinned
GA	10-9	6.6%	17.3%	5.6%	6.1%	-0.9%	2.5%	Pinned	Pinned	Pinned	1.7%	3.3%	3.5%	-3.3%
	9-8	6.5%	17.4%	5.3%	5.5%	-2.2%	1.8%	3.3%	3.5%	-1.6%	1.6%	2.8%	4.6%	-2.7%
	8-7	7.5%	23.5%	5.0%	3.9%	-8.2%	1.6%	2.8%	6.4%	1.6%	1.8%	2.8%	6.8%	1.6%
	7-6	6.5%	17.9%	5.2%	5.7%	-1.1%	1.8%	2.8%	4.5%	-2.7%	1.4%	3.2%	3.3%	-3.3%
	6-5	5.5%	15.6%	5.0%	4.7%	-25.0%	1.2%	3.2%	3.3%	-3.3%	2.1%	Pinned	Pinned	Pinned
Beam Diaphragm and Lateral Wind Bracing														
Span Loaded		Diaphragm Forces at Girder C			Diaphragm Forces at Girder A			Lateral Wind Bracing Forces						
		Axial	Shear	Moment	Axial	Shear	Moment	Axial Tension	Axial Compression	Axial Tension	Axial Compression	Axial Tension	Axial Compression	
All Members in Span	10-9	-5.0%	-186.1%	-15.0%	-5.0%	-186.1%	-185.0%	-28.6%	-28.3%					
	9-8	-4.0%	-14.9%	-16.4%	-4.0%	-14.9%	-13.4%	-27.2%	-27.0%					
	8-7	-176.0%	-13.1%	-14.2%	-176.0%	-13.1%	-11.9%	-27.8%	-27.1%					
	7-6	-4.6%	-15.4%	-16.8%	-4.6%	-15.4%	-13.9%	-26.7%	-26.9%					
	6-5	-29.9%	-23.3%	-24.5%	-29.9%	-23.3%	-21.9%	-33.2%	-30.5%					
Only Members near Midspan	10-9	-5.0%	-13.2%	-15.0%	-5.0%	-13.2%	-11.2%	-34.2%	-32.4%					
	9-8	-4.5%	-13.5%	-15.1%	-4.5%	-13.5%	-11.6%	-32.4%	-31.6%					
	8-7	-28.3%	-13.1%	-14.2%	-28.3%	-13.1%	-11.9%	-29.3%	-24.8%					
	7-6	-4.6%	-13.1%	-14.8%	-4.6%	-13.1%	-11.2%	-32.6%	-31.9%					
	6-5	-29.9%	-26.3%	-24.7%	-29.9%	-26.3%	-27.6%	-32.9%	-33.8%					

Table 8-9: Study 5 Lateral Wind Bracing Member Area Cut in Half

Study 5: Lateral Wind Bracing Members														
Percent Change for Maximum Responses from Analysis using: Base Model to: Modified Model with double the area for lateral wind bracing members														
Mn/DOT Bridge No. 69824														
Girder														
Span Loaded		Middle of Span				Left Support				Right Support				
		Vertical Deflection	Torsional Rotation	Flexural Moment	Bottom Flange Stress	Flexural Shear	Flexural Moment	Bottom Flange Stress	Flexural Shear	Flexural Moment	Bottom Flange Stress	Flexural Shear	Flexural Moment	
		Flexure	Warping	Flexure	Warping	Flexure	Warping	Flexure	Warping	Flexure	Warping	Flexure	Warping	
GC	10-9	-2.7%	-18.1%	-3.0%	-3.4%	-5.2%	-1.6%	Pinned	Pinned	Pinned	-1.2%	-2.3%	-2.2%	-6.1%
	9-8	-2.3%	-16.7%	-2.9%	-3.2%	-5.7%	-1.0%	-2.3%	-2.2%	-6.1%	-0.8%	-2.3%	-2.3%	-3.5%
	8-7	-3.2%	-20.2%	-4.2%	-4.8%	-7.6%	-0.8%	-2.3%	-2.3%	-7.6%	-0.9%	-2.4%	-2.2%	-6.3%
	7-6	-2.4%	-17.1%	-2.9%	-3.1%	-6.5%	-0.9%	-2.4%	-2.2%	-3.5%	-1.1%	-2.8%	-2.9%	-7.1%
	6-5	-4.1%	-179.4%	-4.0%	-4.2%	-11.9%	-1.0%	-2.8%	-2.9%	-7.1%	-1.8%	Pinned	Pinned	Pinned
GA	10-9	-5.6%	-14.7%	-4.9%	-5.3%	0.9%	-2.4%	Pinned	Pinned	Pinned	-1.6%	-3.4%	-3.7%	1.6%
	9-8	-5.4%	-14.5%	-4.7%	-5.0%	1.1%	-1.8%	-3.4%	-3.7%	0.0%	-1.1%	-2.9%	-3.6%	2.7%
	8-7	-6.0%	-18.7%	-4.2%	-3.4%	6.8%	-1.1%	-2.9%	-5.7%	-3.2%	-1.0%	-3.0%	-4.7%	-1.6%
	7-6	-5.4%	-14.8%	-4.5%	-4.9%	1.1%	-1.0%	-3.0%	-3.9%	2.7%	-1.2%	-3.4%	-3.6%	1.6%
	6-5	-5.2%	-14.5%	-4.7%	-4.7%	25.0%	-1.1%	-3.4%	-3.6%	1.6%	-2.1%	Pinned	Pinned	Pinned
Beam Diaphragm and Lateral Wind Bracing														
Span Loaded		Diaphragm Forces at Girder C			Diaphragm Forces at Girder A			Lateral Wind Bracing Forces						
		Axial	Shear	Moment	Axial	Shear	Moment	Axial Tension	Axial Compression	Axial Tension	Axial Compression	Axial Tension	Axial Compression	
All Members in Span	10-9	6.8%	19.8%	-218.3%	6.8%	19.8%	18.5%	25.3%	25.0%					
	9-8	4.7%	17.6%	18.5%	4.7%	17.6%	16.6%	29.8%	24.6%					
	8-7	17.8%	13.6%	13.9%	17.8%	13.6%	13.3%	26.8%	25.0%					
	7-6	6.5%	18.3%	20.2%	6.5%	18.3%	17.3%	31.0%	26.9%					
	6-5	32.5%	26.8%	27.4%	32.5%	26.8%	26.3%	38.5%	30.3%					
Only Members near Midspan	10-9	6.8%	13.1%	14.2%	6.8%	13.1%	11.8%	36.4%	35.6%					
	9-8	6.4%	14.4%	15.3%	6.4%	14.4%	13.3%	34.8%	33.9%					
	8-7	17.8%	13.6%	13.9%	17.8%	13.6%	13.3%	25.8%	20.6%					
	7-6	6.5%	13.8%	14.8%	6.5%	13.8%	12.8%	35.8%	35.0%					
	6-5	32.5%	32.5%	-242.3%	32.5%	32.5%	34.3%	35.3%	36.9%					

Table 8-10: Study 5 Lateral Wind Bracing Member Area Doubled

Study 6: Diaphragm Spacing														
Percent Change for Maximum Responses from Analysis using: Base Model to: Modified Model with approximately double the diaphragm spacing														
Mn/DOT Bridge No. 69824														
Girder														
Span Loaded	Middle of Span				Left Support				Right Support					
	Vertical Deflection	Torsional Rotation	Flexural Moment	Bottom Flange Stress	Flexural Shear	Flexural Moment	Bottom Flange Stress	Flexural Shear	Flexural Moment	Flexural Shear	Flexural Moment	Bottom Flange Stress		
GC	10-9	2.6%	13.2%	1.4%	1.4%	288.6%	2.2%	Pinned	Pinned	Pinned	0.4%	0.8%	0.8%	245.6%
	9-8	2.0%	13.0%	1.5%	1.4%	266.0%	-1.1%	0.8%	0.8%	245.6%	-1.1%	0.8%	0.7%	-328.6%
	8-7	2.4%	11.1%	2.1%	2.5%	293.2%	-1.1%	0.8%	0.7%	274.2%	-1.1%	0.8%	0.6%	201.3%
	7-6	1.9%	12.5%	1.3%	1.4%	273.3%	-1.1%	0.8%	0.6%	348.2%	-1.2%	1.2%	1.2%	214.3%
	6-5	2.2%	9.7%	2.0%	0.9%	116.9%	0.2%	1.2%	1.2%	214.3%	1.3%	Pinned	Pinned	Pinned
GA	10-9	4.6%	78.1%	2.4%	2.5%	337.4%	1.1%	Pinned	Pinned	Pinned	0.8%	1.7%	1.7%	326.2%
	9-8	3.6%	58.6%	1.2%	1.3%	308.5%	0.4%	1.7%	1.7%	312.7%	0.4%	1.2%	-1.3%	145.3%
	8-7	3.1%	35.7%	0.7%	-2.0%	264.1%	0.4%	1.2%	2.9%	341.0%	0.7%	1.2%	2.9%	342.6%
	7-6	3.3%	58.2%	0.9%	0.8%	322.3%	0.7%	1.2%	-1.0%	154.1%	0.2%	1.5%	1.5%	210.0%
	6-5	2.7%	30.8%	2.2%	1.1%	304.8%	0.5%	1.5%	1.5%	261.7%	1.1%	Pinned	Pinned	Pinned
Beam Diaphragm and Lateral Wind Bracing														
Span Loaded	Diaphragm Forces at Girder C				Diaphragm Forces at Girder A				Lateral Wind Bracing Forces					
	Axial	Shear	Moment		Axial	Shear	Moment		Axial Tension	Axial Compression				
All Members in Span	10-9	213.3%	71.5%	64.2%	213.3%	71.5%	77.1%		23.5%		7.5%			
	9-8	-392.4%	-257.7%	54.6%	-392.4%	-257.7%	69.8%		21.1%		29.8%			
	8-7	197.4%	76.7%	71.1%	197.4%	76.7%	80.9%		21.9%		16.8%			
	7-6	208.1%	-261.8%	52.7%	208.1%	-261.8%	73.1%		23.1%		29.2%			
	6-5	-274.0%	42.8%	37.3%	-274.0%	42.8%	47.3%		17.0%		23.0%			
Only Members near Midspan	10-9	213.3%	71.5%	64.2%	213.3%	71.5%	77.1%		88.2%		35.2%			
	9-8	203.0%	63.6%	55.6%	203.0%	63.6%	69.8%		55.9%		25.7%			
	8-7	197.4%	76.7%	71.1%	197.4%	76.7%	80.9%		52.8%		13.6%			
	7-6	208.1%	67.2%	59.6%	208.1%	67.2%	73.1%		54.0%		24.2%			
	6-5	67.6%	43.8%	51.0%	67.6%	43.8%	50.2%		-15.5%		-4.7%			
Mn/DOT Bridge No. 27998														
Girder														
Span Loaded	Middle of Span				Left Support				Right Support					
	Vertical Deflection	Torsional Rotation	Flexural Moment	Bottom Flange Stress	Flexural Shear	Flexural Moment	Bottom Flange Stress	Flexural Shear	Flexural Moment	Flexural Shear	Flexural Moment	Bottom Flange Stress		
G1	I	10.2%	13.4%	-0.3%	0.0%	255.0%	5.7%	Pinned	Pinned	Pinned	-2.9%	1.3%	1.6%	154.0%
	II	10.9%	13.2%	0.3%	0.0%	277.0%	-2.9%	1.3%	1.6%	-233.9%	11.7%	Pinned	Pinned	Pinned
G2	I	11.5%	30.3%	1.2%	1.1%	259.5%	2.3%	Pinned	Pinned	Pinned	2.7%	3.7%	3.4%	184.1%
	II	11.6%	34.5%	1.6%	1.8%	244.4%	2.7%	3.7%	3.4%	-271.2%	6.5%	Pinned	Pinned	Pinned
G3	I	8.7%	51.6%	0.3%	0.0%	259.3%	-2.5%	Pinned	Pinned	Pinned	-0.9%	-0.7%	-0.8%	75.0%
	II	8.6%	54.5%	-3.4%	-3.2%	200.0%	-3.1%	-0.7%	-0.8%	-261.5%	-11.7%	Pinned	Pinned	Pinned
G4	I	9.8%	69.2%	0.1%	0.0%	343.7%	3.4%	Pinned	Pinned	Pinned	-3.8%	2.5%	2.9%	111.5%
	II	11.0%	71.9%	1.4%	1.5%	380.2%	-0.8%	2.5%	2.9%	111.5%	-6.7%	Pinned	Pinned	Pinned
X - shaped Diaphragm														
Span Loaded	Axial Forces between G1 and G2				Axial Forces between G2 and G3				Axial Forces between G3 and G4					
	Top	Bottom	U1-L2	L1-U2	Top	Bottom	U2-L3	L2-U3	Top	Bottom	U3-L4	L3-U4		
All Members in Span	I	-227.1%	-3.7%	17.0%	93.3%	28.0%	10.0%	67.9%	85.6%	39.3%	22.5%	31.2%	58.9%	
	II	12.7%	4.8%	68.0%	-231.8%	28.0%	14.7%	84.2%	-219.7%	-3.5%	105.6%	-219.8%	12.0%	
Only Members near Midspan	I	-227.1%	113.9%	62.8%	93.3%	28.0%	91.7%	73.6%	85.6%	39.3%	94.3%	96.8%	78.3%	
	II	12.7%	124.5%	68.0%	88.2%	28.0%	108.0%	84.2%	92.3%	57.3%	105.6%	98.9%	84.3%	
FHWA Test Specimen														
Girder														
Span Loaded	Middle of Span				Left Support				Right Support					
	Vertical Deflection	Torsional Rotation	Flexural Moment	Bottom Flange Stress	Flexural Shear	Flexural Moment	Bottom Flange Stress	Flexural Shear	Flexural Moment	Flexural Shear	Flexural Moment	Bottom Flange Stress		
G1	1	110.3%	500.4%	-3.4%	-3.3%	255.8%	5.3%	Pinned	Pinned	Pinned	4.7%	Pinned	Pinned	
	1	51.9%	142.2%	8.8%	8.8%	300.8%	9.4%	Pinned	Pinned	Pinned	8.3%	Pinned	Pinned	
	1	55.8%	291.8%	5.3%	5.2%	316.5%	-4.2%	Pinned	Pinned	Pinned	-4.1%	Pinned	Pinned	
K - shaped Diaphragm														
Span Loaded	Axial Forces between G1 and G2						Axial Forces between G2 and G3							
	Top	Bottom 1	Bottom 2	U1-M	M-U2		Top	Bottom 2	Bottom 3	U2-M	M-U3			
All Members in Span	1	68.1%	80.3%	74.0%	82.3%	81.8%	69.2%	67.7%	93.1%	92.8%	91.0%			
	1	68.1%	80.3%	74.0%	82.3%	81.8%	69.2%	67.7%	93.1%	92.8%	91.0%			

Table 8-11: Study 6 Diaphragm Spacing Approximately Doubled

Study 7: Transverse Concrete Deck Beams													
Percent Change for Maximum Responses from Analysis using: Base Model with deck beams to: Modified Model without deck beams													
Mn/DOT Bridge No. 69824													
Girder													
Span Loaded	Middle of Span				Left Support				Right Support				
	Vertical Deflection	Torsional Rotation	Flexural Moment	Bottom Flange Stress	Flexural Shear	Flexural Moment	Bottom Flange Stress	Flexural Shear	Flexural Moment	Flexural Shear	Flexural Moment	Bottom Flange Stress	
GC	10-9	0.0%	-2.1%	0.0%	0.0%	0.0%	Pinned	Pinned	Pinned	0.0%	0.0%	0.0%	-1.0%
	9-8	0.0%	-1.4%	0.0%	0.0%	0.0%	0.0%	0.0%	-1.0%	0.0%	0.0%	0.0%	0.0%
	8-7	0.0%	-0.8%	0.1%	0.3%	0.0%	0.0%	0.0%	-1.5%	0.0%	0.0%	0.0%	0.0%
	7-6	0.0%	-1.5%	0.0%	0.0%	-0.9%	0.0%	0.0%	0.0%	0.0%	0.0%	0.0%	0.0%
	6-5	0.0%	-2.4%	0.0%	0.0%	-1.5%	0.0%	0.0%	0.0%	0.0%	Pinned	Pinned	Pinned
GA	10-9	0.1%	2.2%	0.0%	0.0%	1.9%	0.0%	Pinned	Pinned	Pinned	0.0%	0.0%	0.0%
	9-8	0.1%	1.6%	0.0%	0.0%	1.1%	0.0%	0.0%	1.6%	0.0%	0.0%	0.0%	0.0%
	8-7	0.1%	1.0%	0.0%	0.0%	0.0%	0.0%	0.0%	0.0%	0.0%	0.0%	0.4%	1.6%
	7-6	0.1%	1.7%	0.0%	0.0%	1.1%	0.0%	0.0%	0.0%	1.4%	0.0%	0.0%	-1.6%
	6-5	0.1%	2.4%	0.1%	0.0%	10.0%	0.0%	0.0%	0.0%	-1.6%	0.0%	Pinned	Pinned
Beam Diaphragm and Lateral Wind Bracing													
Span Loaded	Diaphragm Forces at Girder C			Diaphragm Forces at Girder A			Lateral Wind Bracing Forces						
	Axial	Shear	Moment	Axial	Shear	Moment	Axial Tension	Axial Compression					
All Members in Span	10-9	-191.6%	0.0%	-197.8%	-191.6%	0.0%	-207.9%	-0.7%				0.9%	
	9-8	0.4%	0.1%	0.2%	0.4%	0.1%	0.1%	-0.9%				0.9%	
	8-7	-173.2%	0.0%	-184.0%	-173.2%	0.0%	19.5%	-0.3%				0.0%	
	7-6	-196.5%	0.2%	0.2%	-196.5%	0.2%	0.1%	-0.9%				1.1%	
	6-5	-171.6%	0.0%	0.0%	-171.6%	0.0%	0.0%	-0.7%				0.8%	
Only Members near Midspan	10-9	-56.1%	0.0%	-10.9%	-56.1%	0.0%	12.7%	-5.8%				7.6%	
	9-8	-54.5%	0.0%	-10.7%	-54.5%	0.0%	12.4%	-3.2%				3.2%	
	8-7	-54.8%	0.0%	-16.5%	-54.8%	0.0%	19.5%	-1.9%				1.7%	
	7-6	-53.0%	0.0%	-10.5%	-53.0%	0.0%	12.2%	-2.3%				3.1%	
	6-5	-45.7%	0.0%	-224.3%	-45.7%	0.0%	15.4%	-1.6%				1.8%	
Mn/DOT Bridge No. 27998													
Girder													
Span Loaded	Middle of Span				Left Support				Right Support				
	Vertical Deflection	Torsional Rotation	Flexural Moment	Bottom Flange Stress	Flexural Shear	Flexural Moment	Bottom Flange Stress	Flexural Shear	Flexural Moment	Flexural Shear	Flexural Moment	Bottom Flange Stress	
G1	I	2.1%	-11.7%	-2.7%	-2.7%	-4.3%	-3.8%	Pinned	Pinned	Pinned	-1.1%	0.5%	0.5% 17.2%
	II	1.2%	-13.9%	-3.2%	-2.9%	-4.1%	-1.1%	0.5%	-161.8%	-1.9%	Pinned	Pinned	Pinned
G2	I	4.1%	5.3%	5.2%	4.9%	4.1%	6.7%	Pinned	Pinned	Pinned	0.0%	2.7%	2.8% 13.6%
	II	3.9%	4.6%	4.3%	4.2%	0.9%	0.0%	2.7%	2.8%	-15.1%	2.9%	Pinned	Pinned
G3	I	4.9%	34.0%	5.2%	5.1%	5.5%	6.1%	Pinned	Pinned	Pinned	-2.4%	-1.8%	-1.7% -8.3%
	II	5.5%	34.0%	0.1%	-1.6%	4.9%	-5.3%	-1.8%	-1.7%	-11.5%	1.7%	Pinned	Pinned
G4	I	18.7%	59.6%	4.3%	4.0%	-2.9%	5.2%	Pinned	Pinned	Pinned	2.6%	5.0%	4.7% -3.1%
	II	19.2%	55.4%	2.8%	3.4%	1.0%	1.8%	5.0%	4.7%	-3.1%	0.9%	Pinned	Pinned
X-shaped Diaphragm													
Span Loaded	Axial Forces between G1 and G2				Axial Forces between G2 and G3				Axial Forces between G3 and G4				
	Top	Bottom	U1-L2	L1-U2	Top	Bottom	U2-L3	L2-U3	Top	Bottom	U3-L4	L3-U4	
All Members in Span	I	45.4%	-240.0%	-11.5%	-3.2%	-353.8%	37.5%	-13.3%	-11.6%	-499.0%	36.7%	33.8%	4.2%
	II	-282.2%	-19.9%	2.0%	-15.1%	-397.5%	15.3%	-22.1%	-24.9%	-334.7%	105.8%	24.1%	-4.1%
Only Members near Midspan	I	45.4%	238.1%	-10.5%	-9.2%	-353.8%	142.4%	-15.1%	-11.6%	-499.0%	116.9%	-18.4%	-7.9%
	II	-223.7%	-396.6%	-23.8%	-8.0%	-362.8%	160.3%	-22.1%	-12.7%	-556.7%	105.8%	-11.8%	-9.0%
FHWA Test Specimen													
Girder													
Span Loaded	Middle of Span				Left Support				Right Support				
	Vertical Deflection	Torsional Rotation	Flexural Moment	Bottom Flange Stress	Flexural Shear	Flexural Moment	Bottom Flange Stress	Flexural Shear	Flexural Moment	Flexural Shear	Flexural Moment	Bottom Flange Stress	
G1	1	1.4%	-7.9%	-0.8%	-0.9%	-0.2%	-1.0%	Pinned	Pinned	Pinned	-0.9%	Pinned	Pinned
	1	-0.9%	11.1%	4.5%	4.2%	4.3%	4.4%	Pinned	Pinned	Pinned	3.8%	Pinned	Pinned
	1	13.4%	37.1%	3.6%	3.6%	1.9%	2.8%	Pinned	Pinned	Pinned	2.7%	Pinned	Pinned
K-shaped Diaphragm													
Span Loaded	Axial Forces between G1 and G2						Axial Forces between G2 and G3						
	Top	Bottom 1	Bottom 2	U1-M	M-U2	Top	Bottom 2	Bottom 3	U2-M	M-U3			
All Members in Span	1	-271.5%	17.8%	24.6%	-3.6%	-3.7%	-367.4%	-227.2%	35.1%	0.7%	0.5%		
	1	-271.5%	17.8%	24.6%	-3.6%	-3.7%	-367.4%	-227.2%	35.1%	0.7%	0.5%		

Table 8-12: Study 7 Transverse Concrete Deck Beams

Study 8: Rotational DOFs for Transverse Concrete Deck Beams															
Percent Change for Maximum Responses from Analysis using: Base Model with rotational DOFs released to: Modified Model without rotational releases															
Mn/DOT Bridge No. 69824															
Girder															
Span Loaded	Middle of Span					Left Support					Right Support				
	Vertical Deflection	Torsional Rotation	Flexural Moment	Bottom Flange Stress	Flexure Warping	Flexural Shear	Flexural Moment	Bottom Flange Stress	Flexure Warping	Flexural Shear	Flexural Moment	Bottom Flange Stress	Flexure	Warping	
GC	10-9	-0.5%	-2.0%	-0.4%	-0.6%	-12.9%	0.1%	Pinned	Pinned	Pinned	-0.1%	-0.2%	-0.3%	-13.1%	
	9-8	-0.4%	-2.1%	-0.4%	-0.3%	-11.4%	0.2%	-0.2%	-0.3%	-13.1%	0.3%	-0.2%	0.0%	-11.6%	
	8-7	-0.4%	-2.1%	-0.4%	-0.3%	-11.8%	0.3%	-0.2%	-0.2%	-13.6%	0.2%	-0.2%	-0.3%	-11.4%	
	7-6	-0.4%	-2.1%	-0.4%	-0.3%	-12.0%	0.2%	-0.2%	-0.3%	-11.8%	0.2%	-0.3%	-0.2%	-13.1%	
	6-5	-0.7%	-1.9%	-0.6%	-0.5%	-17.9%	0.0%	-0.3%	-0.2%	-13.1%	0.3%	Pinned	Pinned	Pinned	
GA	10-9	-0.9%	-2.7%	-0.6%	-0.5%	-11.3%	0.1%	Pinned	Pinned	Pinned	-0.1%	-0.3%	-0.3%	-186.9%	
	9-8	-0.8%	-2.5%	-0.6%	-0.5%	-10.8%	0.0%	-0.3%	-0.3%	-11.3%	0.0%	-0.2%	-0.3%	-12.0%	
	8-7	-0.7%	-2.2%	-0.4%	-0.5%	-9.6%	0.0%	-0.2%	-0.7%	-14.5%	0.0%	-0.3%	-0.4%	-13.1%	
	7-6	-0.8%	-2.5%	-0.6%	-0.5%	-10.6%	0.0%	-0.3%	-0.6%	-12.2%	-0.1%	-0.3%	-0.3%	-13.1%	
	6-5	-0.9%	-3.0%	-0.7%	-0.7%	-15.0%	0.0%	-0.3%	-0.3%	-13.1%	0.3%	Pinned	Pinned	Pinned	
Beam Diaphragm and Lateral Wind Bracing															
Span Loaded	Diaphragm Forces at Girder C					Diaphragm Forces at Girder A					Lateral Wind Bracing Forces				
	Axial	Shear	Moment	Axial	Shear	Moment	Axial	Shear	Moment	Axial	Axial Tension	Axial Compression			
All Members in Span	10-9	-3.8%	-9.0%	-9.7%	-3.8%	-9.0%	-9.3%	0.3%	0.0%	0.3%	0.0%	0.0%	0.0%		
	9-8	-4.4%	-8.6%	-8.5%	-4.4%	-8.6%	-8.7%	0.7%	0.2%	0.5%	-0.3%	-0.3%	-0.2%		
	8-7	-2.9%	-10.0%	-9.4%	-2.9%	-10.0%	-10.7%	-0.5%	-0.5%	-0.5%	-0.5%	-0.5%	-0.5%		
	7-6	-3.6%	-8.6%	-8.5%	-3.6%	-8.6%	-8.8%	0.4%	0.4%	0.4%	-0.2%	-0.2%	-0.2%		
	6-5	-5.8%	-9.0%	-8.6%	-5.8%	-9.0%	-9.3%	-0.5%	-0.5%	-0.5%	-0.8%	-0.8%	-0.8%		
Only Members near Midspan	10-9	-3.8%	-10.3%	-9.7%	-3.8%	-10.3%	-11.1%	1.1%	1.1%	1.1%	-3.1%	-3.1%	-3.1%		
	9-8	-3.7%	-10.1%	-9.6%	-3.7%	-10.1%	-10.8%	0.8%	0.8%	0.8%	-1.4%	-1.4%	-1.4%		
	8-7	-2.9%	-10.0%	-9.4%	-2.9%	-10.0%	-10.7%	0.0%	0.0%	0.0%	-1.0%	-1.0%	-1.0%		
	7-6	-3.6%	-10.2%	-9.6%	-3.6%	-10.2%	-10.8%	0.5%	0.5%	0.5%	-2.0%	-2.0%	-2.0%		
	6-5	-5.8%	-12.3%	-187.2%	-5.8%	-12.3%	-11.7%	-0.7%	-0.7%	-0.7%	-2.1%	-2.1%	-2.1%		
Mn/DOT Bridge No. 27998															
Girder															
Span Loaded	Middle of Span					Left Support					Right Support				
	Vertical Deflection	Torsional Rotation	Flexural Moment	Bottom Flange Stress	Flexure Warping	Flexural Shear	Flexural Moment	Bottom Flange Stress	Flexure Warping	Flexural Shear	Flexural Moment	Bottom Flange Stress	Flexure	Warping	
G1	I	-5.3%	-19.2%	-2.3%	-2.2%	-25.0%	4.2%	Pinned	Pinned	Pinned	3.7%	-1.7%	-1.6%	-181.6%	
	II	-6.0%	-19.5%	-2.8%	-2.9%	-23.8%	3.7%	-1.7%	-1.6%	13.9%	-0.4%	Pinned	Pinned	Pinned	
G2	I	-5.4%	-18.7%	-2.5%	-2.2%	-62.8%	2.3%	Pinned	Pinned	Pinned	-1.3%	-2.8%	-2.8%	-247.7%	
	II	-6.1%	-19.4%	-2.6%	-1.8%	-62.4%	-1.3%	-2.8%	-2.8%	31.5%	1.4%	Pinned	Pinned	Pinned	
G3	I	-6.4%	-17.7%	-1.1%	-0.7%	-54.9%	7.6%	Pinned	Pinned	Pinned	1.3%	0.1%	0.0%	-10.4%	
	II	-7.7%	-18.6%	-1.6%	-1.6%	-52.4%	-2.3%	0.1%	0.0%	55.8%	12.7%	Pinned	Pinned	Pinned	
G4	I	-7.6%	-15.9%	-4.2%	-3.6%	-23.3%	1.4%	Pinned	Pinned	Pinned	5.6%	-2.2%	-1.8%	-17.7%	
	II	-9.4%	-17.1%	-5.0%	-3.9%	-19.8%	-0.4%	-2.2%	-1.8%	-17.7%	1.7%	Pinned	Pinned	Pinned	
X - shaped Diaphragm															
Span Loaded	Axial Forces between G1 and G2					Axial Forces between G2 and G3					Axial Forces between G3 and G4				
	Top	Bottom	U1-L2	L1-U2		Top	Bottom	U2-L3	L2-U3		Top	Bottom	U3-L4	L3-U4	
All Members in Span	I	1.1%	38.9%	-6.6%	-37.4%	-0.2%	20.9%	-4.1%	-43.9%	-3.1%	9.8%	-10.8%	-16.9%		
	II	13.5%	11.8%	-41.1%	0.8%	0.0%	14.4%	-48.4%	-7.0%	-13.7%	11.6%	-23.2%	-11.4%		
Only Members near Midspan	I	1.1%	6.7%	-52.9%	-59.3%	-0.2%	-2.7%	-48.9%	-60.8%	-3.1%	-8.0%	-45.0%	-63.7%		
	II	-1.4%	0.5%	-55.6%	-60.2%	-7.2%	-7.8%	-48.4%	-60.5%	-5.0%	-9.4%	-44.9%	-62.2%		
FHWA Test Specimen															
Girder															
Span Loaded	Middle of Span					Left Support					Right Support				
	Vertical Deflection	Torsional Rotation	Flexural Moment	Bottom Flange Stress	Flexure Warping	Flexural Shear	Flexural Moment	Bottom Flange Stress	Flexure Warping	Flexural Shear	Flexural Moment	Bottom Flange Stress	Flexure	Warping	
G1	1	-9.2%	-10.7%	-0.7%	-0.7%	-145.9%	-3.7%	Pinned	Pinned	Pinned	-1.3%	Pinned	Pinned	Pinned	
	2	-5.4%	-12.7%	1.2%	1.1%	-122.4%	4.3%	Pinned	Pinned	Pinned	4.9%	Pinned	Pinned	Pinned	
	3	-6.5%	-14.4%	-4.9%	-4.4%	-42.1%	1.7%	Pinned	Pinned	Pinned	1.9%	Pinned	Pinned	Pinned	
K - shaped Diaphragm															
Span Loaded	Axial Forces between G1 and G2					Axial Forces between G2 and G3					Axial Forces between G3 and G4				
	Top	Bottom 1	Bottom 2	U1-M	M-U2	Top	Bottom 2	Bottom 3	U2-M	M-U3					
All Members in Span	1	-10.8%	-65.1%	-36.0%	-55.9%	-55.8%	-8.7%	-204.5%	-37.6%	-60.4%	-60.3%				
	2	-10.8%	-65.1%	-36.0%	-55.9%	-55.8%	-8.7%	-204.5%	-37.6%	-60.4%	-60.3%				

Table 8-13: Study 8 Rotational DOFs for Transverse Concrete Deck Beams

Study 9: Girder Axial DOFs Fixed at Piers													
Percent Change for Maximum Responses from Analysis using: Base Model to: Modified Model with all axial DOFs fixed at pier locations													
Mn/DOT Bridge No. 69824													
Girder													
Span Loaded	Middle of Span				Left Support				Right Support				
	Vertical Deflection	Torsional Rotation	Flexural Moment	Bottom Flange Stress	Flexural Shear	Flexural Moment	Bottom Flange Stress	Flexural Shear	Flexural Moment	Flexural Shear	Flexural Moment	Bottom Flange Stress	
GC	10-9	-0.7%	-4.9%	-0.5%	-0.9%	0.0%	-0.1%	Pinned	Pinned	Pinned	-0.2%	-0.3%	0.0% 0.0%
	9-8	-0.7%	-5.6%	-0.7%	-1.2%	0.0%	-0.4%	-0.3%	0.0%	0.0%	-0.2%	0.0%	1.2% 0.0%
	8-7	-0.1%	-1.6%	0.0%	0.0%	0.0%	0.0%	-0.2%	0.0%	-1.5%	0.0%	-0.2%	-0.3% 0.0%
	7-6	-0.8%	-5.3%	-0.8%	-1.4%	0.0%	0.0%	-0.2%	-0.3%	0.0%	-0.1%	0.0%	1.2% 0.0%
	6-5	-0.4%	-2.3%	-0.3%	-0.4%	0.0%	0.0%	-0.1%	0.0%	1.2%	-0.3%	Pinned	Pinned Pinned
GA	10-9	-1.6%	-4.0%	-1.2%	1.0%	-1.9%	-0.3%	Pinned	Pinned	Pinned	-0.4%	-0.4%	-1.4% -3.3%
	9-8	-1.9%	-4.9%	-1.3%	1.1%	-3.2%	-0.3%	-0.4%	-1.4%	-3.2%	0.0%	-0.3%	2.0% 4.0%
	8-7	-0.6%	-1.4%	-0.2%	-0.5%	0.0%	0.0%	-0.3%	1.8%	-1.6%	0.0%	-0.3%	2.2% -1.6%
	7-6	-1.7%	-4.7%	-1.3%	1.3%	-2.1%	0.0%	-0.3%	1.9%	-2.7%	-0.2%	-0.2%	-0.5% -1.6%
	6-5	-0.7%	-1.9%	-0.6%	0.0%	0.0%	0.1%	-0.2%	-0.5%	-1.6%	-0.5%	Pinned	Pinned Pinned
Beam Diaphragm and Lateral Wind Bracing													
Span Loaded	Diaphragm Forces at Girder C				Diaphragm Forces at Girder A				Lateral Wind Bracing Forces				
	Axial	Shear	Moment		Axial	Shear	Moment		Axial Tension	Axial Compression			
All Members in Span	10-9	1.9%	-200 4%	1.0%	1.9%	-200 4%	0.4%	6.9%	6.2%				
	9-8	-200.0%	0.4%	0.4%	-200.0%	0.4%	0.4%	11.5%	10.8%				
	8-7	-0.1%	-0.1%	-0.1%	-0.1%	-0.1%	0.0%	-0.5%	-0.2%				
	7-6	2.5%	0.4%	0.4%	2.5%	0.4%	0.3%	12.7%	11.4%				
	6-5	0.4%	0.5%	0.6%	0.4%	0.5%	0.6%	-4.2%	6.0%				
Only Members near Midspan	10-9	1.9%	1.3%	1.0%	1.9%	1.3%	1.6%	-0.4%	-2.7%				
	9-8	2.3%	1.3%	1.1%	2.3%	1.3%	1.7%	0.3%	-1.4%				
	8-7	-0.1%	-0.1%	-0.1%	-0.1%	-0.1%	0.0%	-0.3%	-0.7%				
	7-6	2.5%	1.4%	1.1%	2.5%	1.4%	1.8%	-1.8%	-3.6%				
	6-5	0.4%	-0.1%	-0.2%	0.4%	-0.1%	-0.2%	7.1%	7.6%				
Mn/DOT Bridge No. 27998													
Girder													
Span Loaded	Middle of Span				Left Support				Right Support				
	Vertical Deflection	Torsional Rotation	Flexural Moment	Bottom Flange Stress	Flexural Shear	Flexural Moment	Bottom Flange Stress	Flexural Shear	Flexural Moment	Flexural Shear	Flexural Moment	Bottom Flange Stress	
G1	I	0.0%	-0.1%	0.0%	0.4%	0.0%	0.0%	Pinned	Pinned	Pinned	0.0%	0.0%	0.0% 0.0%
	II	-0.1%	-0.2%	0.0%	0.5%	0.0%	0.0%	0.0%	0.0%	0.6%	0.3%	Pinned	Pinned Pinned
G2	I	0.0%	0.0%	0.0%	0.0%	0.0%	0.0%	Pinned	Pinned	Pinned	0.0%	0.0%	0.0% 0.0%
	II	0.0%	-0.2%	0.0%	0.0%	0.0%	0.0%	0.0%	0.0%	-1.4%	-0.3%	Pinned	Pinned Pinned
G3	I	0.0%	0.0%	0.0%	0.0%	0.0%	0.0%	Pinned	Pinned	Pinned	0.0%	0.0%	0.0% 0.0%
	II	-0.1%	-0.2%	-0.1%	-0.8%	0.0%	-0.1%	0.0%	0.0%	0.0%	0.0%	Pinned	Pinned Pinned
G4	I	0.0%	-0.1%	-0.1%	0.0%	-1.0%	0.0%	Pinned	Pinned	Pinned	0.0%	0.0%	0.0% 0.0%
	II	-0.1%	-0.2%	-0.1%	0.5%	0.0%	0.0%	0.0%	0.0%	0.0%	0.2%	Pinned	Pinned Pinned
X - shaped Diaphragm													
Span Loaded	Axial Forces between G1 and G2				Axial Forces between G2 and G3				Axial Forces between G3 and G4				
	Top	Bottom	U1-L2	L1-U2	Top	Bottom	U2-L3	L2-U3	Top	Bottom	U3-L4	L3-U4	
All Members in Span	I	0.0%	-0.1%	0.0%	0.0%	0.0%	0.0%	0.0%	0.0%	0.0%	0.2%	-0.1%	0.0%
	II	-0.1%	0.1%	-0.1%	0.2%	0.0%	0.0%	-0.1%	0.0%	0.1%	-0.1%	-0.1%	0.0%
Only Members near Midspan	I	0.0%	0.0%	0.0%	0.0%	0.0%	0.0%	0.0%	0.0%	0.0%	0.0%	0.0%	0.0%
	II	-0.1%	0.1%	-0.1%	-0.1%	-0.1%	-0.1%	-0.1%	0.0%	0.1%	-0.1%	-0.1%	0.0%
FHWA Test Specimen													
Girder													
Span Loaded	Middle of Span				Left Support				Right Support				
	Vertical Deflection	Torsional Rotation	Flexural Moment	Bottom Flange Stress	Flexural Shear	Flexural Moment	Bottom Flange Stress	Flexural Shear	Flexural Moment	Flexural Shear	Flexural Moment	Bottom Flange Stress	
G1	1	0.0%	0.0%	0.0%	0.0%	-0.1%	0.0%	Pinned	Pinned	Pinned	0.0%	Pinned	Pinned
	1	0.0%	0.0%	0.0%	0.0%	0.0%	0.0%	Pinned	Pinned	Pinned	0.0%	Pinned	Pinned
	1	0.0%	0.0%	0.0%	-0.3%	0.1%	0.0%	Pinned	Pinned	Pinned	0.0%	Pinned	Pinned
G2	1	0.0%	0.0%	0.0%	0.0%	0.0%	0.0%	Pinned	Pinned	Pinned	0.0%	Pinned	Pinned
	1	0.0%	0.0%	0.0%	0.0%	0.0%	0.0%	Pinned	Pinned	Pinned	0.0%	Pinned	Pinned
	1	0.0%	0.0%	0.0%	-0.3%	0.1%	0.0%	Pinned	Pinned	Pinned	0.0%	Pinned	Pinned
K - shaped Diaphragm													
Span Loaded	Axial Forces between G1 and G2						Axial Forces between G2 and G3						
	Top	Bottom 1	Bottom 2	U1-M	M-U2		Top	Bottom 2	Bottom 3	U2-M	M-U3		
All Members in Span	1	0.0%	0.0%	0.0%	0.0%	0.0%	0.0%	0.0%	0.0%	0.0%	0.0%	0.0%	0.0%
	1	0.0%	0.0%	0.0%	0.0%	0.0%	0.0%	0.0%	0.0%	0.0%	0.0%	0.0%	0.0%
Only Members near Midspan	1	0.0%	0.0%	0.0%	0.0%	0.0%	0.0%	0.0%	0.0%	0.0%	0.0%	0.0%	0.0%
	1	0.0%	0.0%	0.0%	0.0%	0.0%	0.0%	0.0%	0.0%	0.0%	0.0%	0.0%	0.0%

Table 8-14: Study 9 Girder Axial DOFs at Piers

Study 10: Composite Torsion Constant															
Percent Change for Maximum Responses from Analysis using: Base Model ignoring concrete contribution to: Modified Model using half of the effective concrete width															
Mn/DOT Bridge No. 69824															
Girder															
Span Loaded	Middle of Span					Left Support					Right Support				
	Vertical Deflection	Torsional Rotation	Flexural Moment	Bottom Flange Stress		Flexural Shear	Flexural Moment	Bottom Flange Stress		Flexural Shear	Flexural Moment	Bottom Flange Stress		Flexure	Warping
GC	10-9	-0.5%	-3.8%	-0.5%	-0.6%	-4.3%	-0.3%	Pinned	Pinned	Pinned	-0.3%	-0.3%	-0.3%	-0.3%	-2.0%
	9-8	-0.4%	-3.1%	-0.4%	-0.3%	-2.9%	-0.2%	-0.3%	-0.3%	-2.0%	-0.1%	-0.3%	0.0%	0.0%	-2.3%
	8-7	-0.4%	-3.4%	-0.5%	-0.5%	-1.7%	-0.1%	-0.3%	0.0%	-3.0%	-0.2%	-0.3%	-0.3%	0.0%	0.0%
	7-6	-0.4%	-3.3%	-0.4%	-0.6%	-3.7%	-0.2%	-0.3%	-0.3%	-2.4%	-0.2%	-0.5%	-0.5%	1.2%	
	6-5	-1.2%	-6.6%	-1.0%	-1.3%	31.3%	-0.5%	-0.5%	1.2%	-0.9%	Pinned	Pinned	Pinned	Pinned	Pinned
GA	10-9	-1.1%	-3.9%	-0.9%	-0.8%	-25.5%	-0.6%	Pinned	Pinned	Pinned	-0.6%	-0.5%	-0.6%	-0.6%	-173.8%
	9-8	-1.0%	-3.2%	-0.8%	-0.8%	-24.7%	-0.6%	-0.5%	-0.6%	-19.4%	-0.3%	-0.3%	-0.7%	-0.7%	-25.3%
	8-7	-1.0%	-3.2%	-0.6%	-0.5%	-21.9%	-0.3%	-0.3%	-1.1%	-17.7%	-0.2%	-0.3%	-0.7%	-0.7%	-16.4%
	7-6	-1.0%	-3.2%	-0.8%	-0.8%	-24.5%	-0.2%	-0.3%	-1.0%	-25.7%	-0.3%	-0.6%	-0.5%	-0.5%	-26.2%
	6-5	-1.5%	-6.3%	-1.2%	-1.6%	-110.0%	-0.6%	-0.6%	-0.5%	-26.2%	-1.1%	Pinned	Pinned	Pinned	Pinned
Beam Diaphragm and Lateral Wind Bracing															
Span Loaded	Diaphragm Forces at Girder C					Diaphragm Forces at Girder A					Lateral Wind Bracing Forces				
	Axial	Shear	Moment	Axial	Shear	Moment	Axial	Shear	Moment	Axial	Axial Tension	Axial Compression			
All Members in Span	10-9	-1.3%	3.1%	3.2%	-1.3%	3.1%	3.3%	-3.7%	-3.7%	-3.7%	-3.6%	-3.6%			
	9-8	-2.7%	2.9%	2.8%	-2.7%	2.9%	2.9%	-2.6%	-2.6%	-2.6%	-2.6%	-2.6%			
	8-7	-0.9%	3.5%	3.2%	-0.9%	3.5%	3.9%	-2.8%	-2.8%	-2.8%	-2.8%	-2.8%			
	7-6	-1.2%	2.9%	2.9%	-1.2%	2.9%	3.0%	-2.8%	-2.8%	-2.8%	-2.8%	-2.8%			
	6-5	-1.5%	3.5%	3.2%	-1.5%	3.5%	3.9%	-5.7%	-5.7%	-5.7%	-3.9%	-3.9%			
Only Members near Midspan	10-9	-1.3%	3.4%	3.2%	-1.3%	3.4%	3.7%	-2.9%	-2.9%	-2.9%	-4.0%	-4.0%			
	9-8	-1.3%	3.5%	3.3%	-1.3%	3.5%	3.9%	-2.4%	-2.4%	-2.4%	-2.9%	-2.9%			
	8-7	-0.9%	3.5%	3.2%	-0.9%	3.5%	3.9%	-3.2%	-3.2%	-3.2%	-3.2%	-3.2%			
	7-6	-1.2%	3.5%	3.2%	-1.2%	3.5%	3.9%	-2.6%	-2.6%	-2.6%	-3.4%	-3.4%			
	6-5	-1.5%	18.8%	20.8%	-1.5%	18.8%	17.2%	-5.3%	-5.3%	-5.3%	-6.0%	-6.0%			
Mn/DOT Bridge No. 27998															
Span Loaded	Middle of Span					Left Support					Right Support				
	Vertical Deflection	Torsional Rotation	Flexural Moment	Bottom Flange Stress		Flexural Shear	Flexural Moment	Bottom Flange Stress		Flexural Shear	Flexural Moment	Bottom Flange Stress		Flexure	Warping
G1	I	-1.5%	-7.8%	-1.7%	-1.3%	-10.7%	-2.2%	Pinned	Pinned	Pinned	-0.3%	-0.7%	-0.5%	-4.6%	
	II	-1.9%	-6.9%	-1.8%	-1.9%	-9.0%	-0.3%	-0.7%	-0.5%	-18.8%	-1.0%	Pinned	Pinned	Pinned	Pinned
G2	I	-0.5%	-7.5%	-1.1%	-1.1%	-6.6%	-2.0%	Pinned	Pinned	Pinned	-0.7%	-0.5%	-0.7%	-4.5%	
	II	-0.9%	-6.5%	-1.5%	-1.2%	-12.0%	-0.7%	-0.5%	-0.7%	0.0%	1.2%	Pinned	Pinned	Pinned	Pinned
G3	I	-2.2%	-7.2%	-0.3%	-0.7%	-4.4%	-1.0%	Pinned	Pinned	Pinned	-0.6%	-0.6%	0.0%	-2.1%	
	II	-2.3%	-6.2%	-0.4%	-0.8%	-4.9%	-3.5%	-0.6%	0.0%	0.0%	-1.9%	Pinned	Pinned	Pinned	Pinned
G4	I	-3.4%	-7.2%	-2.3%	-2.2%	-11.7%	-2.4%	Pinned	Pinned	Pinned	-1.2%	-0.8%	-0.6%	-6.3%	
	II	-3.2%	-6.1%	-2.1%	-2.0%	-11.5%	-0.7%	-0.8%	-0.6%	-6.3%	-0.4%	Pinned	Pinned	Pinned	Pinned
X - shaped Diaphragm															
Span Loaded	Axial Forces between G1 and G2					Axial Forces between G2 and G3					Axial Forces between G3 and G4				
	Top	Bottom	U1-L2	L1-U2		Top	Bottom	U2-L3	L2-U3		Top	Bottom	U3-L4	L3-U4	
All Members in Span	I	-4.3%	2.5%	-1.0%	1.7%	-4.7%	-1.4%	-0.7%	1.6%	-5.6%	-3.0%	-2.8%	-1.6%		
	II	-2.9%	-3.8%	15.7%	-1.3%	-3.7%	-4.8%	-9.4%	-2.8%	-3.7%	-5.1%	-3.7%	-3.7%		
Only Members near Midspan	I	-4.3%	1.5%	-8.7%	1.7%	-4.7%	-1.8%	-9.1%	1.6%	-5.6%	-5.4%	-5.5%	1.0%		
	II	-2.9%	1.1%	-8.0%	1.2%	-3.7%	-2.3%	-9.4%	1.3%	-4.8%	-5.1%	1.7%	0.7%		
FHWA Test Specimen															
Span Loaded	Middle of Span					Left Support					Right Support				
	Vertical Deflection	Torsional Rotation	Flexural Moment	Bottom Flange Stress		Flexural Shear	Flexural Moment	Bottom Flange Stress		Flexural Shear	Flexural Moment	Bottom Flange Stress		Flexure	Warping
G1	1	-3.0%	-11.9%	-1.6%	-1.5%	-29.6%	-1.0%	Pinned	Pinned	Pinned	-0.8%	Pinned	Pinned	Pinned	Pinned
	1	-4.6%	-12.7%	-1.1%	-1.1%	-15.1%	-0.9%	Pinned	Pinned	Pinned	-0.8%	Pinned	Pinned	Pinned	Pinned
	1	-7.7%	-13.4%	-5.9%	-6.0%	-26.6%	-4.4%	Pinned	Pinned	Pinned	-4.2%	Pinned	Pinned	Pinned	Pinned
K - shaped Diaphragm															
Span Loaded	Axial Forces between G1 and G2					Axial Forces between G2 and G3					Axial Forces between G3 and G4				
	Top	Bottom 1	Bottom 2	U1-M	M-U2	Top	Bottom 2	Bottom 3	U2-M	M-U3					
All Members in Span	1	-8.5%	1.1%	-12.9%	-8.0%	-8.2%	-10.7%	1.0%	-15.9%	4.3%	4.2%				
	1	-8.5%	1.1%	-12.9%	-8.0%	-8.2%	-10.7%	1.0%	-15.9%	4.3%	4.2%				

Table 8-15: Study 10 Composite Torsion Constant J with Half of b_{eff}

Study 10: Composite Torsion Constant														
Percent Change for Maximum Responses from Analysis using: Base Model ignoring concrete contribution to: Modified Model using the full effective concrete width														
Mn/DOT Bridge No. 69824														
Girder														
Span Loaded		Middle of Span				Left Support				Right Support				
		Vertical Deflection	Torsional Rotation	Flexural Moment	Bottom Flange Stress	Flexural Shear	Flexural Moment	Bottom Flange Stress	Flexural Shear	Flexural Moment	Flexural Shear	Flexural Moment	Bottom Flange Stress	
		Flexure	Warping	Flexure	Warping	Flexure	Warping	Flexure	Flexure	Warping	Flexure	Warping	Flexure	
GC	10-9	-1.0%	-7.2%	-1.0%	-1.1%	-6.9%	-0.7%	Pinned	Pinned	Pinned	-0.6%	-0.5%	-0.5%	-3.0%
	9-8	-0.7%	-6.1%	-0.8%	-0.9%	-4.8%	-0.4%	-0.5%	-0.5%	-0.3%	-0.3%	-0.5%	-0.3%	-4.7%
	8-7	-0.8%	-6.5%	-1.1%	-0.8%	-3.4%	-0.3%	-0.5%	-0.3%	-0.4%	-0.5%	-0.5%	-0.6%	-1.3%
	7-6	-0.8%	-6.3%	-0.9%	-0.8%	-5.6%	-0.3%	-0.5%	-0.6%	-3.5%	-0.5%	-1.0%	-1.0%	3.6%
	6-5	-2.1%	-12.0%	-1.8%	-2.4%	52.2%	-0.8%	-1.0%	-1.0%	3.6%	-1.6%	Pinned	Pinned	Pinned
GA	10-9	-2.2%	-7.2%	-1.7%	-1.5%	-44.3%	-1.2%	Pinned	Pinned	Pinned	-1.1%	-0.9%	-0.9%	-157.4%
	9-8	-2.0%	-6.1%	-1.5%	-1.6%	-44.1%	-1.1%	-0.9%	-0.9%	-35.5%	-0.5%	-0.7%	-1.3%	-44.0%
	8-7	-1.9%	-6.1%	-1.2%	-1.2%	-39.7%	-0.5%	-0.7%	-1.8%	-30.6%	-0.4%	-0.7%	-1.4%	-31.1%
	7-6	-2.0%	-6.2%	-1.5%	-1.3%	-43.6%	-0.4%	-0.7%	-1.6%	-44.6%	-0.6%	-1.1%	-1.0%	-44.3%
	6-5	-2.8%	-11.2%	-2.3%	-2.8%	-130.0%	-1.1%	-1.1%	-1.0%	-44.3%	-2.0%	Pinned	Pinned	Pinned
Beam Diaphragm and Lateral Wind Bracing														
Span Loaded		Diaphragm Forces at Girder C			Diaphragm Forces at Girder A			Lateral Wind Bracing Forces						
		Axial	Shear	Moment	Axial	Shear	Moment	Axial	Shear	Moment	Axial Tension	Axial Compression		
All Members in Span	10-9	-2.5%	6.1%	6.1%	-2.5%	6.1%	6.5%	-7.0%	-7.2%					
	9-8	-195.4%	5.7%	5.6%	-195.4%	5.7%	5.8%	-5.0%	-5.3%					
	8-7	-1.8%	6.8%	6.2%	-1.8%	6.8%	7.6%	-5.5%	-5.4%					
	7-6	-2.3%	5.8%	5.7%	-2.3%	5.8%	5.9%	-5.2%	-5.5%					
	6-5	-3.1%	6.9%	6.4%	-3.1%	6.9%	7.6%	-10.2%	-7.6%					
Only Members near Midspan	10-9	-2.5%	6.6%	6.1%	-2.5%	6.6%	7.2%	-5.1%	-8.0%					
	9-8	-2.4%	6.9%	6.4%	-2.4%	6.9%	7.6%	-4.8%	-5.7%					
	8-7	-1.8%	6.8%	6.2%	-1.8%	6.8%	7.6%	-6.2%	-6.1%					
	7-6	-2.3%	6.8%	6.3%	-2.3%	6.8%	7.5%	-5.0%	-6.4%					
	6-5	-3.1%	36.6%	-241.7%	-3.1%	36.6%	32.9%	-9.9%	-11.0%					
Mn/DOT Bridge No. 27998														
Girder														
Span Loaded		Middle of Span				Left Support				Right Support				
		Vertical Deflection	Torsional Rotation	Flexural Moment	Bottom Flange Stress	Flexural Shear	Flexural Moment	Bottom Flange Stress	Flexural Shear	Flexural Moment	Flexural Shear	Flexural Moment	Bottom Flange Stress	
		Flexure	Warping	Flexure	Warping	Flexure	Warping	Flexure	Flexure	Warping	Flexure	Warping	Flexure	
G1	I	-2.8%	-14.5%	-3.3%	-3.1%	-17.9%	-4.2%	Pinned	Pinned	Pinned	-0.5%	-1.3%	-1.1%	-6.9%
	II	-3.5%	-12.9%	-3.5%	-3.4%	-16.4%	-0.5%	-1.3%	-1.1%	-149.1%	-2.4%	Pinned	Pinned	Pinned
G2	I	-1.0%	-14.0%	-2.2%	-2.2%	-12.4%	-3.8%	Pinned	Pinned	Pinned	-1.4%	-0.9%	-1.4%	11.4%
	II	-1.5%	-12.1%	-2.8%	-2.4%	-17.9%	-1.4%	-0.9%	-1.4%	1.4%	1.4%	Pinned	Pinned	Pinned
G3	I	-4.1%	-13.5%	-0.5%	-0.7%	-8.8%	-1.9%	Pinned	Pinned	Pinned	-1.2%	-1.1%	-0.8%	-8.3%
	II	-4.3%	-11.6%	-0.7%	-0.8%	-7.3%	-6.7%	-1.1%	-0.8%	-1.9%	-3.3%	Pinned	Pinned	Pinned
G4	I	-6.4%	-13.4%	-4.2%	-4.5%	-22.3%	-4.5%	Pinned	Pinned	Pinned	-2.3%	-1.5%	-1.2%	-12.5%
	II	-6.0%	-11.5%	-4.0%	-3.9%	-22.9%	-1.4%	-1.5%	-1.2%	-12.5%	-1.0%	Pinned	Pinned	Pinned
X - shaped Diaphragm														
Span Loaded		Axial Forces between G1 and G2				Axial Forces between G2 and G3				Axial Forces between G3 and G4				
		Top	Bottom	U1-L2	L1-U2	Top	Bottom	U2-L3	L2-U3	Top	Bottom	U3-L4	L3-U4	
All Members in Span	I	-8.0%	4.3%	-1.9%	3.3%	-8.8%	-3.0%	-1.3%	3.0%	-10.4%	-5.9%	-5.2%	-3.1%	
	II	-5.6%	-7.4%	26.1%	-2.5%	-6.9%	-9.0%	-14.2%	-5.3%	-7.0%	-9.9%	-6.9%	-6.9%	
Only Members near Midspan	I	-8.0%	3.0%	-16.3%	3.3%	-8.8%	-3.6%	-16.9%	3.0%	-10.4%	-10.1%	-3.1%	1.8%	
	II	-5.6%	2.0%	-15.1%	2.9%	-6.9%	-4.3%	-17.5%	2.6%	-9.1%	-9.9%	3.8%	1.3%	
FHWA Test Specimen														
Girder														
Span Loaded		Middle of Span				Left Support				Right Support				
		Vertical Deflection	Torsional Rotation	Flexural Moment	Bottom Flange Stress	Flexural Shear	Flexural Moment	Bottom Flange Stress	Flexural Shear	Flexural Moment	Flexural Shear	Flexural Moment	Bottom Flange Stress	
		Flexure	Warping	Flexure	Warping	Flexure	Warping	Flexure	Flexure	Warping	Flexure	Warping	Flexure	
G1	1	-4.7%	-20.6%	-3.0%	-3.1%	-41.7%	-2.0%	Pinned	Pinned	Pinned	-1.6%	Pinned	Pinned	Pinned
	2	-7.9%	-21.1%	-1.7%	-1.7%	-23.8%	-1.3%	Pinned	Pinned	Pinned	-1.2%	Pinned	Pinned	Pinned
	3	-13.2%	-22.3%	-10.3%	-10.2%	-43.4%	-7.5%	Pinned	Pinned	Pinned	-7.2%	Pinned	Pinned	Pinned
K - shaped Diaphragm														
Span Loaded		Axial Forces between G1 and G2						Axial Forces between G2 and G3						
		Top	Bottom 1	Bottom 2	U1-M	M-U2	Top	Bottom 2	Bottom 3	U2-M	M-U3			
All Members in Span	1	-14.3%	2.8%	-22.6%	-4.8%	-5.0%	-18.4%	2.2%	-27.9%	8.0%	7.9%			
	2	-14.3%	2.8%	-22.6%	-4.8%	-5.0%	-18.4%	2.2%	-27.9%	8.0%	7.9%			
Only Members near Midspan	1	-14.3%	2.8%	-22.6%	-4.8%	-5.0%	-18.4%	2.2%	-27.9%	8.0%	7.9%			

Table 8-16: Study 10 Composite Torsion Constant J with the Full b_{eff}

Study 11: Concrete Slab Thickness															
Percent Change for Maximum Responses from Analysis using: Base Model to: Modified Model with 1.0 inch thicker concrete slab															
Mn/DOT Bridge No. 69824															
Girder															
Span Loaded	Middle of Span					Left Support					Right Support				
	Vertical Deflection	Torsional Rotation	Flexural Moment	Bottom Flange Stress	Flexure Warping	Flexural Shear	Flexural Moment	Bottom Flange Stress	Flexure Warping	Flexural Shear	Flexural Moment	Bottom Flange Stress	Flexure	Warping	
GC	10-9	-3.1%	-4.0%	-0.2%	-1.7%	-0.9%	-0.1%	Pinned	Pinned	Pinned	0.0%	-0.1%	-1.4%	-1.0%	
	9-8	-3.2%	-4.2%	-0.2%	-1.4%	0.0%	-0.1%	-0.1%	-1.4%	-1.0%	0.0%	-0.1%	-1.3%	-1.2%	
	8-7	-3.1%	-4.0%	-0.2%	-1.3%	0.0%	0.0%	-0.1%	-1.3%	-1.5%	0.0%	-0.1%	-1.3%	0.0%	
	7-6	-3.2%	-4.2%	-0.2%	-1.7%	-0.9%	0.0%	-0.1%	-1.3%	-1.2%	-0.1%	-0.2%	-1.7%	0.0%	
	6-5	-3.8%	-4.3%	0.0%	-2.4%	-1.5%	-0.1%	-0.2%	-1.7%	0.0%	0.1%	Pinned	Pinned	Pinned	
GA	10-9	-3.3%	-3.9%	-0.3%	-1.8%	-0.9%	-0.1%	Pinned	Pinned	Pinned	-0.1%	-0.1%	-1.4%	-1.6%	
	9-8	-3.4%	-4.1%	-0.3%	-1.8%	-1.1%	-0.1%	-0.1%	-1.4%	0.0%	0.0%	-0.1%	-1.7%	-2.7%	
	8-7	-3.3%	-3.8%	-0.2%	-1.7%	-2.7%	0.0%	-0.1%	-1.8%	-1.6%	0.0%	-0.1%	-1.4%	-1.6%	
	7-6	-3.4%	-4.1%	-0.4%	-1.6%	-1.1%	0.0%	-0.1%	-1.6%	-1.4%	-0.1%	-0.2%	-1.5%	-1.6%	
	6-5	-3.9%	-4.3%	-0.1%	-2.5%	0.0%	0.0%	-0.2%	-1.5%	-1.6%	0.1%	Pinned	Pinned	Pinned	
Beam Diaphragm and Lateral Wind Bracing															
Span Loaded	Diaphragm Forces at Girder C					Diaphragm Forces at Girder A					Lateral Wind Bracing Forces				
	Axial	Shear	Moment	Axial	Shear	Moment	Axial	Shear	Moment	Axial	Tension	Axial	Compression		
All Members in Span	10-9	0.8%	0.6%	-0.6%	0.8%	0.6%	1.4%	0.3%	0.3%	0.3%	0.3%	0.3%	0.3%	0.3%	0.3%
	9-8	0.1%	0.6%	0.2%	0.1%	0.6%	0.9%	0.7%	0.7%	0.7%	0.7%	0.4%	0.4%	0.4%	0.4%
	8-7	-1.0%	0.3%	-0.9%	-1.0%	0.3%	1.6%	-0.5%	-0.5%	-0.5%	-0.5%	-0.3%	-0.3%	-0.3%	-0.3%
	7-6	0.8%	0.6%	0.2%	0.8%	0.6%	0.9%	0.4%	0.4%	0.4%	0.4%	0.4%	0.4%	0.4%	0.4%
	6-5	-1.2%	0.2%	-0.6%	-1.2%	0.2%	1.2%	-0.5%	-0.5%	-0.5%	-0.5%	-0.6%	-0.6%	-0.6%	-0.6%
Only Members near Midspan	10-9	0.8%	0.3%	-0.6%	0.8%	0.3%	1.5%	0.0%	0.0%	0.0%	0.0%	-0.9%	-0.9%	-0.9%	-0.9%
	9-8	0.8%	0.3%	-0.7%	0.8%	0.3%	1.4%	0.3%	0.3%	0.3%	0.3%	-0.6%	-0.6%	-0.6%	-0.6%
	8-7	-1.0%	0.3%	-0.9%	-1.0%	0.3%	1.6%	0.3%	0.3%	0.3%	0.3%	-1.0%	-1.0%	-1.0%	-1.0%
	7-6	0.8%	0.3%	-0.7%	0.8%	0.3%	1.4%	0.0%	0.0%	0.0%	0.0%	-0.8%	-0.8%	-0.8%	-0.8%
	6-5	-1.2%	0.3%	-1.6%	-1.2%	0.3%	1.7%	-0.2%	-0.2%	-0.2%	-0.2%	-0.8%	-0.8%	-0.8%	-0.8%
Mn/DOT Bridge No. 27998															
Span Loaded	Middle of Span					Left Support					Right Support				
	Vertical Deflection	Torsional Rotation	Flexural Moment	Bottom Flange Stress	Flexure Warping	Flexural Shear	Flexural Moment	Bottom Flange Stress	Flexure Warping	Flexural Shear	Flexural Moment	Bottom Flange Stress	Flexure	Warping	
G1	I	-3.7%	-2.9%	0.1%	-1.3%	-1.4%	-0.1%	Pinned	Pinned	Pinned	0.0%	0.2%	-1.6%	-1.1%	
	II	-3.5%	-2.7%	0.1%	-1.9%	0.0%	0.0%	0.2%	-1.6%	-1.2%	-0.1%	Pinned	Pinned	Pinned	
G2	I	-3.5%	-2.5%	0.2%	-1.6%	-0.8%	0.0%	Pinned	Pinned	Pinned	0.0%	0.2%	-1.4%	-2.3%	
	II	-3.3%	-2.3%	0.3%	-1.2%	-0.9%	0.0%	0.2%	-1.4%	-2.7%	-0.5%	Pinned	Pinned	Pinned	
G3	I	-3.2%	-2.2%	0.2%	-1.5%	-1.1%	-0.2%	Pinned	Pinned	Pinned	0.0%	0.1%	-0.8%	-2.1%	
	II	-2.9%	-2.0%	0.3%	-1.6%	-1.2%	0.3%	0.1%	-0.8%	-1.9%	-0.5%	Pinned	Pinned	Pinned	
G4	I	-2.9%	-1.9%	0.3%	-0.9%	0.0%	0.1%	Pinned	Pinned	Pinned	0.0%	0.2%	-0.6%	-1.0%	
	II	-2.6%	-1.7%	0.6%	-1.0%	0.0%	0.1%	0.2%	-0.6%	-1.0%	0.1%	Pinned	Pinned	Pinned	
X - shaped Diaphragm															
Span Loaded	Axial Forces between G1 and G2					Axial Forces between G2 and G3					Axial Forces between G3 and G4				
	Top	Bottom	U1-L2	L1-U2	Top	Bottom	U2-L3	L2-U3	Top	Bottom	U3-L4	L3-U4			
All Members in Span	I	-6.9%	-4.2%	-3.0%	-0.3%	-5.0%	-3.3%	-2.6%	-0.5%	-6.4%	-2.8%	-2.9%	-2.6%	-2.6%	
	II	-1.1%	-2.2%	-0.4%	-1.8%	-0.5%	-2.1%	-0.4%	-2.1%	-2.9%	0.8%	-1.9%	-2.1%	-2.1%	
Only Members near Midspan	I	-6.9%	0.9%	-1.0%	-0.3%	-5.0%	0.8%	-0.5%	-0.5%	-6.4%	0.7%	-0.5%	-0.7%	-0.7%	
	II	-6.4%	0.3%	-0.4%	-0.1%	-4.4%	1.7%	-0.4%	-0.3%	-6.7%	0.8%	-0.2%	-0.5%	-0.5%	
FHWA Test Specimen															
Span Loaded	Middle of Span					Left Support					Right Support				
	Vertical Deflection	Torsional Rotation	Flexural Moment	Bottom Flange Stress	Flexure Warping	Flexural Shear	Flexural Moment	Bottom Flange Stress	Flexure Warping	Flexural Shear	Flexural Moment	Bottom Flange Stress	Flexure	Warping	
G1	1	-3.9%	-4.0%	0.0%	-1.9%	-1.0%	0.0%	Pinned	Pinned	Pinned	0.0%	Pinned	Pinned	Pinned	Pinned
	1	-4.2%	-3.6%	0.0%	-2.0%	-0.9%	0.1%	Pinned	Pinned	Pinned	0.0%	Pinned	Pinned	Pinned	Pinned
	1	-4.0%	-3.3%	0.2%	-1.5%	-0.4%	0.1%	Pinned	Pinned	Pinned	0.1%	Pinned	Pinned	Pinned	Pinned
K - shaped Diaphragm															
Span Loaded	Axial Forces between G1 and G2					Axial Forces between G2 and G3					Axial Forces between G3 and G4				
	Top	Bottom 1	Bottom 2	U1-M	M-U2	Top	Bottom 2	Bottom 3	U2-M	M-U3					
All Members in Span	1	-5.2%	-0.4%	-0.7%	-0.3%	-0.4%	-3.5%	-0.1%	-0.4%	-0.1%	-0.1%	-0.4%	-0.1%	-0.1%	-0.1%
	1	-5.2%	-0.4%	-0.7%	-0.3%	-0.4%	-3.5%	-0.1%	-0.4%	-0.1%	-0.4%	-0.1%	-0.1%	-0.1%	-0.1%

Table 8-17: Study 11 Concrete Slab Thickness Plus 1 inch

Study 11: Concrete Slab Thickness													
Percent Change for Maximum Responses from Analysis using: Base Model to: Modified Model with 0.5 inch thicker concrete slab													
Mn/DOT Bridge No. 69824													
Girder													
Span Loaded	Middle of Span				Left Support				Right Support				
	Vertical Deflection	Torsional Rotation	Flexural Moment	Bottom Flange Stress	Flexural Shear	Flexural Moment	Bottom Flange Stress	Flexural Shear	Flexural Moment	Flexural Shear	Flexural Moment	Bottom Flange Stress	
GC	10-9	-1.6%	-2.1%	-0.1%	-0.9%	0.0%	0.0%	Pinned	Pinned	Pinned	0.0%	0.0%	-0.5% 0.0%
	9-8	-1.6%	-2.2%	-0.1%	-0.9%	0.0%	0.0%	0.0%	-0.5%	0.0%	0.0%	0.0%	-0.7% 0.0%
	8-7	-1.6%	-2.1%	-0.1%	-0.8%	0.0%	0.0%	0.0%	-0.7%	-1.5%	0.0%	0.0%	-0.6% 0.0%
	7-6	-1.6%	-2.2%	-0.1%	-0.8%	-0.9%	0.0%	0.0%	-0.6%	-1.2%	-0.1%	-0.1%	-0.7% 0.0%
	6-5	-2.0%	-2.2%	0.0%	-1.3%	0.0%	0.0%	-0.1%	-0.7%	0.0%	0.0%	Pinned	Pinned Pinned
GA	10-9	-1.7%	-2.0%	-0.2%	-0.8%	0.0%	0.0%	Pinned	Pinned	Pinned	0.0%	-0.1%	-0.9% -1.6%
	9-8	-1.7%	-2.1%	-0.2%	-0.8%	-1.1%	0.0%	-0.1%	-0.9%	0.0%	0.0%	0.0%	-0.7% -1.3%
	8-7	-1.7%	-1.9%	-0.1%	-0.7%	-1.4%	0.0%	0.0%	-1.1%	-1.6%	0.0%	-0.1%	-0.7% 0.0%
	7-6	-1.8%	-2.1%	-0.2%	-0.8%	0.0%	0.0%	-0.1%	-1.0%	0.0%	0.0%	-0.1%	-0.8% -1.6%
	6-5	-2.0%	-2.2%	0.0%	-1.2%	-5.0%	0.0%	-0.1%	-0.8%	-1.6%	0.0%	Pinned	Pinned Pinned
Beam Diaphragm and Lateral Wind Bracing													
Span Loaded	Diaphragm Forces at Girder C				Diaphragm Forces at Girder A				Lateral Wind Bracing Forces				
	Axial	Shear	Moment		Axial	Shear	Moment		Axial Tension	Axial Compression			
All Members in Span	10-9	0.4%	0.3%	-0.3%	0.4%	0.3%	0.7%		0.2%	0.2%			
	9-8	0.1%	0.3%	0.1%	0.1%	0.3%	0.5%		0.4%	0.2%			
	8-7	-0.5%	0.1%	-0.4%	-0.5%	0.1%	0.8%		-0.2%	-0.2%			
	7-6	0.4%	0.3%	0.1%	0.4%	0.3%	0.5%		0.2%	0.2%			
	6-5	-0.6%	0.1%	-0.3%	-0.6%	0.1%	0.6%		-0.2%	-0.2%			
Only Members near Midspan	10-9	0.4%	0.2%	-0.3%	0.4%	0.2%	0.7%		0.0%	-0.4%			
	9-8	0.4%	0.1%	-0.3%	0.4%	0.1%	0.7%		0.3%	-0.3%			
	8-7	-0.5%	0.1%	-0.4%	-0.5%	0.1%	0.8%		0.3%	-0.5%			
	7-6	0.4%	0.1%	-0.3%	0.4%	0.1%	0.7%		0.0%	-0.6%			
	6-5	-0.6%	0.1%	-0.8%	-0.6%	0.1%	0.8%		0.0%	-0.3%			
Mn/DOT Bridge No. 27998													
Girder													
Span Loaded	Middle of Span				Left Support				Right Support				
	Vertical Deflection	Torsional Rotation	Flexural Moment	Bottom Flange Stress	Flexural Shear	Flexural Moment	Bottom Flange Stress	Flexural Shear	Flexural Moment	Flexural Shear	Flexural Moment	Bottom Flange Stress	
G1	I	-1.9%	-1.5%	0.0%	-0.9%	-1.4%	0.0%	Pinned	Pinned	Pinned	0.0%	0.1%	-0.5% 0.0%
	II	-1.8%	-1.4%	0.1%	-1.0%	0.0%	0.0%	0.1%	-0.5%	-0.6%	0.0%	Pinned	Pinned Pinned
G2	I	-1.8%	-1.2%	0.1%	-0.5%	-0.8%	0.0%	Pinned	Pinned	Pinned	0.0%	0.1%	-0.7% -2.3%
	II	-1.7%	-1.2%	0.2%	-0.6%	-0.9%	0.0%	0.1%	-0.7%	-1.4%	-0.2%	Pinned	Pinned Pinned
G3	I	-1.6%	-1.1%	0.1%	-0.7%	-1.1%	-0.1%	Pinned	Pinned	Pinned	0.0%	0.0%	-0.8% 0.0%
	II	-1.5%	-1.0%	0.1%	-0.8%	0.0%	0.1%	0.0%	-0.8%	-1.9%	-0.2%	Pinned	Pinned Pinned
G4	I	-1.5%	-1.0%	0.2%	-0.4%	0.0%	0.1%	Pinned	Pinned	Pinned	0.0%	0.1%	-0.6% 0.0%
	II	-1.3%	-0.8%	0.3%	-0.5%	0.0%	0.0%	0.1%	-0.6%	0.0%	0.1%	Pinned	Pinned Pinned
X-shaped Diaphragm													
Span Loaded	Axial Forces between G1 and G2				Axial Forces between G2 and G3				Axial Forces between G3 and G4				
	Top	Bottom	U1-L2	L1-U2	Top	Bottom	U2-L3	L2-U3	Top	Bottom	U3-L4	L3-U4	
All Members in Span	I	-3.5%	-2.1%	-1.5%	-0.2%	-2.6%	-1.7%	-1.3%	-0.2%	-3.4%	-1.4%	-1.5%	-1.3%
	II	-1.5%	-1.1%	-0.2%	-0.9%	-0.3%	-1.1%	-0.2%	-1.1%	-1.4%	0.5%	-1.1%	-1.1%
Only Members near Midspan	I	-3.5%	0.5%	-0.5%	-0.2%	-2.6%	0.5%	-0.3%	-0.2%	-3.4%	0.4%	-0.3%	-0.3%
	II	-3.3%	0.2%	-0.2%	-0.1%	-2.3%	0.9%	-0.2%	-0.2%	-3.5%	0.5%	-0.1%	-0.2%
FHWA Test Specimen													
Girder													
Span Loaded	Middle of Span				Left Support				Right Support				
	Vertical Deflection	Torsional Rotation	Flexural Moment	Bottom Flange Stress	Flexural Shear	Flexural Moment	Bottom Flange Stress	Flexural Shear	Flexural Moment	Flexural Shear	Flexural Moment	Bottom Flange Stress	
G1	1	-2.0%	-2.0%	0.0%	-0.9%	-0.5%	0.0%	Pinned	Pinned	Pinned	0.0%	Pinned	Pinned Pinned
	1	-2.2%	-1.9%	0.0%	-0.8%	-0.6%	0.1%	Pinned	Pinned	Pinned	0.0%	Pinned	Pinned Pinned
	1	-2.1%	-1.7%	0.1%	-0.8%	-0.1%	0.1%	Pinned	Pinned	Pinned	0.1%	Pinned	Pinned Pinned
K-shaped Diaphragm													
Span Loaded	Axial Forces between G1 and G2						Axial Forces between G2 and G3						
	Top	Bottom 1	Bottom 2	U1-M	M-U2		Top	Bottom 2	Bottom 3	U2-M	M-U3		
All Members in Span	1	-2.7%	-0.2%	-0.3%	-0.2%	-1.8%	-0.1%	-0.2%	0.0%	-0.1%	-0.2%	0.0%	-0.1%
	1	-2.7%	-0.2%	-0.3%	-0.2%	-1.8%	-0.1%	-0.2%	0.0%	-0.2%	0.0%	0.0%	-0.1%

Table 8-18: Study 11 Concrete Slab Thickness Plus $\frac{1}{2}$ inch

Study 11: Concrete Slab Thickness													
Percent Change for Maximum Responses from Analysis using: Base Model to: Modified Model with 0.5 inch thinner concrete slab													
Mn/DOT Bridge No. 69824													
Girder													
Span Loaded	Middle of Span				Left Support				Right Support				
	Vertical Deflection	Torsional Rotation	Flexural Moment	Bottom Flange Stress	Flexural Shear	Flexural Moment	Bottom Flange Stress	Flexural Shear	Flexural Moment	Flexural Shear	Flexural Moment	Bottom Flange Stress	
GC	10-9	1.7%	2.2%	0.1%	0.6%	0.9%	0.0%	Pinned	Pinned	Pinned	0.0%	0.0%	0.8% 0.0%
	9-8	1.7%	2.3%	0.1%	0.9%	0.0%	0.0%	0.0%	0.0%	0.0%	0.0%	0.0%	0.7% 0.0%
	8-7	1.7%	2.2%	0.1%	0.8%	0.8%	0.0%	0.0%	0.0%	0.7%	0.0%	0.0%	0.6% 0.0%
	7-6	1.7%	2.3%	0.1%	0.8%	0.0%	0.0%	0.0%	0.0%	0.6%	0.0%	0.1%	0.7% 1.2%
	6-5	2.0%	2.3%	0.0%	1.3%	1.5%	0.0%	0.1%	0.7%	1.2%	0.0%	Pinned	Pinned Pinned
GA	10-9	1.8%	2.2%	0.2%	0.8%	0.9%	0.0%	Pinned	Pinned	Pinned	0.0%	0.1%	0.6% 0.0%
	9-8	1.8%	2.3%	0.2%	0.8%	0.0%	0.0%	0.1%	0.6%	1.6%	0.0%	0.1%	1.0% 1.3%
	8-7	1.8%	2.1%	0.1%	1.0%	1.4%	0.0%	0.1%	0.7%	0.0%	0.0%	0.0%	1.1% 1.6%
	7-6	1.8%	2.3%	0.2%	0.8%	1.1%	0.0%	0.0%	0.6%	1.4%	0.0%	0.1%	0.8% 0.0%
	6-5	2.0%	2.3%	0.1%	1.2%	0.0%	0.0%	0.1%	0.8%	0.0%	0.0%	Pinned	Pinned Pinned
Beam Diaphragm and Lateral Wind Bracing													
Span Loaded	Diaphragm Forces at Girder C			Diaphragm Forces at Girder A			Lateral Wind Bracing Forces						
	Axial	Shear	Moment	Axial	Shear	Moment	Axial Tension	Axial Compression					
All Members in Span	10-9	-0.5%	-0.3%	0.3%	-0.5%	-0.3%	-0.7%	-0.3%	-0.7%	-0.3%	-0.2%	-0.2%	
	9-8	-0.1%	-0.3%	-0.2%	-0.1%	-0.3%	-0.5%	-0.4%	-0.5%	-0.4%	-0.4%	-0.4%	
	8-7	0.5%	-0.2%	0.4%	0.5%	-0.2%	-0.9%	0.2%	0.2%	0.2%	0.2%	0.2%	
	7-6	-0.5%	-0.3%	-0.2%	-0.5%	-0.3%	-0.5%	-0.2%	-0.2%	-0.2%	-0.4%	-0.4%	
	6-5	0.5%	-0.2%	0.2%	0.5%	-0.2%	-0.6%	0.4%	0.4%	0.4%	0.4%	0.4%	
Only Members near Midspan	10-9	-0.5%	-0.2%	0.3%	-0.5%	-0.2%	-0.8%	-0.4%	-0.4%	-0.4%	0.9%	0.9%	
	9-8	-0.5%	-0.2%	0.3%	-0.5%	-0.2%	-0.7%	0.0%	0.0%	0.0%	0.3%	0.3%	
	8-7	0.5%	-0.2%	0.4%	0.5%	-0.2%	-0.9%	-0.3%	-0.3%	-0.3%	0.5%	0.5%	
	7-6	-0.5%	-0.2%	0.3%	-0.5%	-0.2%	-0.7%	0.0%	0.0%	0.0%	0.3%	0.3%	
	6-5	0.5%	-0.2%	0.8%	0.5%	-0.2%	-1.0%	0.2%	0.2%	0.2%	0.3%	0.3%	
Mn/DOT Bridge No. 27998													
Girder													
Span Loaded	Middle of Span				Left Support				Right Support				
	Vertical Deflection	Torsional Rotation	Flexural Moment	Bottom Flange Stress	Flexural Shear	Flexural Moment	Bottom Flange Stress	Flexural Shear	Flexural Moment	Flexural Shear	Flexural Moment	Bottom Flange Stress	
G1	I	2.0%	1.5%	0.0%	0.9%	0.0%	0.0%	Pinned	Pinned	Pinned	0.0%	-0.1%	1.1% 0.0%
	II	1.8%	1.5%	-0.1%	0.5%	0.8%	0.0%	-0.1%	1.1%	1.2%	0.0%	Pinned	Pinned Pinned
G2	I	1.9%	1.4%	-0.1%	0.5%	0.0%	0.0%	Pinned	Pinned	Pinned	0.0%	-0.1%	0.7% 0.0%
	II	1.8%	1.2%	-0.2%	0.6%	0.0%	0.0%	-0.1%	0.7%	-21.9%	0.3%	Pinned	Pinned Pinned
G3	I	1.7%	1.2%	-0.1%	0.7%	0.0%	0.1%	Pinned	Pinned	Pinned	0.1%	0.0%	0.8% 0.0%
	II	1.6%	1.0%	-0.1%	0.0%	0.0%	-0.2%	0.0%	0.8%	1.9%	0.2%	Pinned	Pinned Pinned
G4	I	1.6%	1.0%	-0.2%	0.4%	0.0%	-0.1%	Pinned	Pinned	Pinned	0.0%	-0.1%	0.6% 0.0%
	II	1.4%	0.9%	-0.3%	0.5%	1.0%	0.0%	-0.1%	0.6%	0.0%	-0.1%	Pinned	Pinned Pinned
X - shaped Diaphragm													
Span Loaded	Axial Forces between G1 and G2				Axial Forces between G2 and G3				Axial Forces between G3 and G4				
	Top	Bottom	U1-L2	L1-U2	Top	Bottom	U2-L3	L2-U3	Top	Bottom	U3-L4	L3-U4	
All Members in Span	I	3.7%	2.2%	1.6%	0.1%	2.7%	1.7%	1.4%	0.3%	3.7%	1.5%	1.6%	1.4%
	II	3.5%	1.1%	0.2%	1.0%	2.4%	1.1%	0.2%	1.1%	1.5%	-0.5%	1.1%	1.1%
Only Members near Midspan	I	3.7%	-0.6%	0.5%	0.1%	2.7%	-0.5%	0.3%	0.3%	3.7%	-0.5%	0.3%	0.4%
	II	3.5%	-0.2%	0.2%	0.1%	2.4%	-1.0%	0.2%	0.2%	3.9%	-0.5%	0.2%	0.3%
FHWA Test Specimen													
Girder													
Span Loaded	Middle of Span				Left Support				Right Support				
	Vertical Deflection	Torsional Rotation	Flexural Moment	Bottom Flange Stress	Flexural Shear	Flexural Moment	Bottom Flange Stress	Flexural Shear	Flexural Moment	Flexural Shear	Flexural Moment	Bottom Flange Stress	
G1	1	2.1%	2.2%	0.0%	1.0%	0.5%	0.0%	Pinned	Pinned	Pinned	0.0%	Pinned	Pinned Pinned
	1	2.3%	2.0%	0.0%	0.8%	0.6%	0.0%	Pinned	Pinned	Pinned	-0.1%	Pinned	Pinned Pinned
	1	2.2%	1.8%	-0.1%	0.8%	0.3%	-0.1%	Pinned	Pinned	Pinned	-0.1%	Pinned	Pinned Pinned
K - shaped Diaphragm													
Span Loaded	Axial Forces between G1 and G2						Axial Forces between G2 and G3						
	Top	Bottom 1	Bottom 2	U1-M	M-U2	Top	Bottom 2	Bottom 3	U2-M	M-U3			
All Members in Span	1	3.0%	0.2%	0.3%	0.2%	1.8%	0.1%	0.2%	0.1%	0.1%	0.1%	0.1%	0.1%
	1	3.0%	0.2%	0.3%	0.2%	1.8%	0.1%	0.2%	0.2%	0.2%	0.1%	0.1%	0.1%

Table 8-19: Study 11 Concrete Slab Thickness Minus ½ inch

Study 11: Concrete Slab Thickness													
Percent Change for Maximum Responses from Analysis using: Base Model to: Modified Model with 1.0 inch thinner concrete slab													
Mn/DOT Bridge No. 69824													
Girder													
Span Loaded	Middle of Span				Left Support				Right Support				
	Vertical Deflection	Torsional Rotation	Flexural Moment	Bottom Flange Stress	Flexural Shear	Flexural Moment	Bottom Flange Stress	Flexural Shear	Flexural Moment	Flexural Shear	Flexural Moment	Bottom Flange Stress	
GC	10-9	3.4%	4.7%	0.2%	1.4%	0.9%	0.1%	Pinned	Pinned	Pinned	0.0%	0.1%	1.6% 0.0%
	9-8	3.5%	4.8%	0.3%	1.7%	1.0%	0.0%	0.1%	1.6%	0.0%	0.0%	0.1%	1.3% 0.0%
	8-7	3.5%	4.7%	0.3%	1.5%	0.8%	0.0%	0.1%	1.3%	0.0%	0.0%	0.1%	1.3% 1.3%
	7-6	3.6%	4.8%	0.3%	1.7%	0.0%	0.0%	0.1%	1.3%	1.2%	0.1%	0.2%	1.7% 1.2%
	6-5	4.1%	4.8%	0.1%	2.6%	1.5%	0.0%	0.2%	1.7%	1.2%	0.0%	Pinned	Pinned Pinned
GA	10-9	3.7%	4.5%	0.4%	1.8%	1.9%	0.1%	Pinned	Pinned	Pinned	0.1%	0.1%	1.4% 0.0%
	9-8	3.8%	4.7%	0.4%	1.6%	1.1%	0.1%	0.1%	1.4%	1.6%	0.0%	0.1%	2.0% 1.3%
	8-7	3.7%	4.3%	0.2%	2.0%	1.4%	0.0%	0.1%	1.4%	0.0%	0.0%	0.1%	1.8% 1.6%
	7-6	3.8%	4.7%	0.4%	1.8%	1.1%	0.0%	0.1%	1.6%	2.7%	0.1%	0.2%	1.5% 0.0%
	6-5	4.2%	4.8%	0.1%	2.5%	5.0%	0.0%	0.2%	1.5%	0.0%	0.0%	Pinned	Pinned Pinned
Beam Diaphragm and Lateral Wind Bracing													
Span Loaded	Diaphragm Forces at Girder C				Diaphragm Forces at Girder A				Lateral Wind Bracing Forces				
	Axial	Shear	Moment		Axial	Shear	Moment		Axial Tension	Axial Compression			
All Members in Span	10-9	-1.0%	-0.7%	0.5%	-1.0%	-0.7%	-1.5%		-0.8%	-0.5%			
	9-8	-0.2%	-0.7%	-0.4%	-0.2%	-0.7%	-1.0%		-0.9%	-0.9%			
	8-7	1.0%	-0.4%	0.8%	1.0%	-0.4%	-1.8%		0.3%	0.2%			
	7-6	-1.1%	-0.6%	-0.4%	-1.1%	-0.6%	-1.0%		-0.6%	-0.9%			
	6-5	1.0%	-0.4%	0.4%	1.0%	-0.4%	-1.3%		0.5%	0.6%			
Only Members near Midspan	10-9	-1.0%	-0.5%	0.5%	-1.0%	-0.5%	-1.6%		-0.7%	1.3%			
	9-8	-1.1%	-0.4%	0.6%	-1.1%	-0.4%	-1.5%		-0.3%	0.6%			
	8-7	1.0%	-0.4%	0.8%	1.0%	-0.4%	-1.8%		-0.5%	1.0%			
	7-6	-1.1%	-0.4%	0.6%	-1.1%	-0.4%	-1.5%		0.0%	0.6%			
	6-5	1.0%	-0.4%	1.5%	1.0%	-0.4%	-1.9%		0.2%	0.5%			
Mn/DOT Bridge No. 27998													
Girder	Middle of Span				Left Support				Right Support				
	Span Loaded	Vertical Deflection	Torsional Rotation	Flexural Moment	Bottom Flange Stress	Flexural Shear	Flexural Moment	Bottom Flange Stress	Flexural Shear	Flexural Moment	Bottom Flange Stress		
G1	I	4.0%	3.2%	0.0%	1.8%	0.7%	0.0%	Pinned	Pinned	Pinned	0.0%	-0.2%	1.6% 1.1%
	II	3.8%	3.0%	-0.1%	1.5%	1.6%	0.0%	-0.2%	1.6%	1.8%	0.1%	Pinned	Pinned Pinned
G2	I	3.9%	2.8%	-0.3%	1.1%	0.8%	0.0%	Pinned	Pinned	Pinned	0.0%	-0.2%	1.4% 2.3%
	II	3.7%	2.5%	-0.3%	1.8%	0.9%	0.0%	-0.2%	1.4%	-20.5%	0.5%	Pinned	Pinned Pinned
G3	I	3.5%	2.4%	-0.3%	1.5%	1.1%	0.1%	Pinned	Pinned	Pinned	0.1%	-0.1%	1.7% 2.1%
	II	3.2%	2.2%	-0.3%	0.8%	0.0%	-0.4%	-0.1%	1.7%	5.8%	0.5%	Pinned	Pinned Pinned
G4	I	3.3%	2.0%	-0.4%	0.9%	0.0%	-0.1%	Pinned	Pinned	Pinned	0.0%	-0.2%	1.2% 0.0%
	II	2.9%	1.8%	-0.7%	0.5%	0.0%	-0.1%	-0.2%	1.2%	0.0%	-0.1%	Pinned	Pinned Pinned
X - shaped Diaphragm													
Span Loaded	Axial Forces between G1 and G2				Axial Forces between G2 and G3				Axial Forces between G3 and G4				
	Top	Bottom	U1-L2	L1-U2	Top	Bottom	U2-L3	L2-U3	Top	Bottom	U3-L4	L3-U4	
All Members in Span	I	7.7%	4.6%	3.3%	0.3%	5.5%	3.6%	2.9%	0.5%	7.7%	3.0%	3.2%	2.8%
	II	7.2%	2.3%	0.4%	2.0%	4.9%	2.2%	0.4%	2.3%	2.9%	-1.2%	2.4%	2.2%
Only Members near Midspan	I	7.7%	-1.3%	1.1%	0.3%	5.5%	-1.1%	0.5%	0.5%	7.7%	-1.1%	0.6%	0.8%
	II	7.2%	-0.5%	0.4%	0.1%	4.9%	-2.1%	0.4%	0.3%	8.3%	-1.2%	0.4%	0.6%
FHWA Test Specimen													
Girder	Middle of Span				Left Support				Right Support				
	Span Loaded	Vertical Deflection	Torsional Rotation	Flexural Moment	Bottom Flange Stress	Flexural Shear	Flexural Moment	Bottom Flange Stress	Flexural Shear	Flexural Moment	Bottom Flange Stress		
G1	1	4.3%	4.6%	0.0%	1.9%	1.0%	0.0%	Pinned	Pinned	Pinned	0.0%	Pinned	Pinned Pinned
	1	4.8%	4.1%	-0.1%	1.7%	1.2%	-0.1%	Pinned	Pinned	Pinned	-0.1%	Pinned	Pinned Pinned
	1	4.6%	3.7%	-0.2%	1.5%	0.4%	-0.1%	Pinned	Pinned	Pinned	-0.1%	Pinned	Pinned Pinned
K - shaped Diaphragm													
Span Loaded	Axial Forces between G1 and G2						Axial Forces between G2 and G3						
	Top	Bottom 1	Bottom 2	U1-M	M-U2		Top	Bottom 2	Bottom 3	U2-M	M-U3		
All Members in Span	1	6.2%	0.4%	0.7%	0.4%	0.5%	3.5%	0.1%	0.4%	0.1%	0.1%	0.1%	
	1	6.2%	0.4%	0.7%	0.4%	0.5%	3.5%	0.1%	0.4%	0.1%	0.1%	0.1%	
Only Members near Midspan	1	6.2%	0.4%	0.7%	0.4%	0.5%	3.5%	0.1%	0.4%	0.1%	0.1%	0.1%	

Table 8-20: Study 11 Concrete Slab Thickness Minus 1 inch

Study 12: Effective Concrete Width for Girders

Percent Change for Maximum Responses from Analysis using: Base Model
to: Modified Model with 20% larger effective widths

Mn/DOT Bridge No. 69824

Girder

Span Loaded	Middle of Span					Left Support				Right Support			
	Vertical Deflection	Torsional Rotation	Flexural Moment	Bottom Flange Stress		Flexural Shear	Flexural Moment	Bottom Flange Stress		Flexural Shear	Flexural Moment	Bottom Flange Stress	
				Flexure	Warping			Flexure	Warping			Flexure	Warping
GC	10-9	-3.8%	-9.2%	-0.8%	-1.7%	0.0%	-0.3%	Pinned	Pinned	-0.2%	-0.3%	-1.1%	1.0%
	9-8	-3.8%	-9.4%	-1.0%	-1.7%	1.0%	-0.1%	-0.3%	-1.1%	0.0%	-0.2%	-1.0%	0.0%
	8-7	-3.6%	-8.0%	-0.8%	-1.3%	0.0%	0.0%	-0.2%	-1.0%	0.0%	-0.2%	-1.3%	1.3%
	7-6	-3.8%	-9.3%	-1.0%	-1.7%	0.0%	0.0%	-0.2%	-1.3%	0.0%	-0.3%	-1.2%	1.2%
	6-5	-3.7%	-7.5%	-0.9%	-1.6%	1.5%	-0.2%	-0.3%	-1.2%	1.2%	Pinned	Pinned	Pinned
GA	10-9	-4.9%	-8.0%	-1.6%	-2.3%	-3.8%	-0.5%	Pinned	Pinned	-0.5%	-0.5%	-1.4%	-195.1%
	9-8	-5.2%	-8.6%	-1.6%	-2.4%	-5.4%	-0.5%	-0.5%	-1.4%	-4.8%	-0.2%	-2.3%	-5.3%
	8-7	-4.7%	-7.2%	-0.8%	-2.2%	-4.1%	-0.2%	-0.3%	-2.1%	-4.8%	-0.1%	-2.2%	-3.3%
	7-6	-5.0%	-8.4%	-1.6%	-2.3%	-4.3%	-0.1%	-0.3%	-2.3%	-5.4%	-0.2%	-0.4%	-1.3%
	6-5	-4.1%	-6.5%	-1.2%	-1.8%	-15.0%	-0.2%	-0.4%	-1.3%	-3.3%	-0.3%	Pinned	Pinned

Beam Diaphragm and Lateral Wind Bracing

	Span Loaded	Diaphragm Forces at Girder C			Diaphragm Forces at Girder A			Lateral Wind Bracing Forces		
		Axial	Shear	Moment	Axial	Shear	Moment	Axial Tension	Axial Compression	
All Members in Span	10-9	-1.1%	2.0%	1.9%	-1.1%	2.0%	1.9%	6.4%	6.7%	
	9-8	0.0%	1.9%	2.1%	0.0%	1.9%	1.6%	7.2%	7.3%	
	8-7	-3.3%	1.5%	1.2%	-3.3%	1.5%	1.9%	2.0%	2.5%	
	7-6	-1.1%	1.8%	2.1%	-1.1%	1.8%	1.6%	7.1%	7.9%	
	6-5	-0.8%	1.9%	2.0%	-0.8%	1.9%	1.9%	5.3%	3.3%	
Only Members near Midspan	10-9	-1.1%	2.1%	1.9%	-1.1%	2.1%	2.2%	3.6%	3.6%	
	9-8	-1.2%	1.7%	1.6%	-1.2%	1.7%	1.8%	4.8%	4.3%	
	8-7	-3.3%	1.5%	1.2%	-3.3%	1.5%	1.9%	4.3%	1.7%	
	7-6	-1.1%	1.7%	1.6%	-1.1%	1.7%	1.9%	4.4%	3.6%	
	6-5	-0.8%	2.9%	3.5%	-0.8%	2.9%	2.5%	3.2%	3.4%	

Mn/DOT Bridge No. 27998

Girder

Span Loaded	Middle of Span					Left Support				Right Support			
	Vertical Deflection	Torsional Rotation	Flexural Moment	Bottom Flange Stress		Flexural Shear	Flexural Moment	Bottom Flange Stress		Flexural Shear	Flexural Moment	Bottom Flange Stress	
				Flexure	Warping			Flexure	Warping			Flexure	Warping
G1	I	-3.4%	-3.3%	-0.1%	-0.9%	-1.4%	-0.3%	Pinned	Pinned	0.0%	0.3%	-0.5%	0.0%
	II	-3.3%	-3.0%	-0.1%	-1.0%	0.0%	0.0%	0.3%	-0.5%	-1.8%	-0.3%	Pinned	Pinned
G2	I	-3.4%	-2.5%	0.4%	-0.5%	0.0%	0.3%	Pinned	Pinned	0.0%	0.2%	-0.7%	-2.3%
	II	-3.2%	-2.2%	0.5%	0.0%	0.0%	0.2%	Pinned	Pinned	-0.4%	-0.4%	Pinned	Pinned
G3	I	-3.4%	-1.9%	0.5%	-0.7%	0.0%	0.2%	Pinned	Pinned	-0.1%	0.0%	-0.8%	0.0%
	II	-3.0%	-1.6%	0.2%	-0.8%	-1.2%	0.4%	0.0%	-0.8%	-3.8%	-0.1%	Pinned	Pinned
G4	I	-3.0%	-1.3%	0.5%	-0.4%	1.0%	0.3%	Pinned	Pinned	0.1%	0.4%	-0.6%	0.0%
	II	-2.5%	-1.1%	0.8%	0.0%	1.0%	0.2%	0.4%	-0.6%	0.0%	0.2%	Pinned	Pinned

X - shaped Diaphragm

Span Loaded	Axial Forces between G1 and G2				Axial Forces between G2 and G3				Axial Forces between G3 and G4				
	Top	Bottom	U1-L2	L1-U2	Top	Bottom	U2-L3	L2-U3	Top	Bottom	U3-L4	L3-U4	
All Members in Span	I	-9.8%	-3.1%	-2.9%	0.3%	-7.5%	-2.4%	-2.6%	-0.5%	-10.1%	-2.2%	-2.5%	-2.9%
	II	-2.3%	-2.1%	-0.7%	-2.5%	-2.9%	-1.5%	-0.6%	-2.5%	-4.2%	3.0%	-2.3%	-2.2%
Only Members near Midspan	I	-9.8%	4.3%	-1.6%	0.3%	-7.5%	3.7%	-0.6%	-0.5%	-10.1%	3.1%	-0.3%	-1.2%
	II	-9.3%	2.9%	-0.7%	0.7%	-6.5%	5.0%	-0.6%	-0.3%	-10.1%	3.0%	0.0%	-1.0%

FHWA Test Specimen

Girder

Span Loaded	Middle of Span					Left Support				Right Support			
	Vertical Deflection	Torsional Rotation	Flexural Moment	Bottom Flange Stress		Flexural Shear	Flexural Moment	Bottom Flange Stress		Flexural Shear	Flexural Moment	Bottom Flange Stress	
				Flexure	Warping			Flexure	Warping			Flexure	Warping
G1	1	-3.0%	-3.6%	0.0%	-0.7%	-0.1%	0.0%	Pinned	Pinned	0.0%	Pinned	Pinned	Pinned
	2	-3.9%	-3.0%	0.2%	-0.6%	0.0%	0.2%	Pinned	Pinned	0.1%	Pinned	Pinned	Pinned
G2	1	-3.4%	-2.3%	0.3%	-0.5%	0.8%	0.2%	Pinned	Pinned	0.2%	Pinned	Pinned	Pinned
	2	-3.0%	-2.0%	0.3%	-0.5%	0.8%	0.2%	Pinned	Pinned	0.2%	Pinned	Pinned	Pinned
G3	1	-3.4%	-2.3%	0.3%	-0.5%	0.8%	0.2%	Pinned	Pinned	0.2%	Pinned	Pinned	Pinned
	2	-3.0%	-2.0%	0.3%	-0.5%	0.8%	0.2%	Pinned	Pinned	0.2%	Pinned	Pinned	Pinned

K - shaped Diaphragm

Span Loaded	Axial Forces between G1 and G2					Axial Forces between G2 and G3					
	Top	Bottom 1	Bottom 2	U1-M	M-U2	Top	Bottom 2	Bottom 3	U2-M	M-U3	
All Members in Span	1	-7.3%	0.3%	0.2%	-0.6%	-0.7%	-5.1%	0.1%	0.9%	-0.2%	-0.3%
Only Members near Midspan	1	-7.3%	0.3%	0.2%	-0.6%	-0.7%	-5.1%	0.1%	0.9%	-0.2%	-0.3%

Table 8-21: Study 12 Effective Concrete Width 20% Larger

Study 12: Effective Concrete Width for Girders															
Percent Change for Maximum Responses from Analysis using: Base Model to: Modified Model with 10% larger effective widths															
Mn/DOT Bridge No. 69824															
Girder															
Span Loaded	Middle of Span					Left Support					Right Support				
	Vertical Deflection	Torsional Rotation	Flexural Moment	Bottom Flange Stress		Flexural Shear	Flexural Moment	Bottom Flange Stress		Flexural Shear	Flexural Moment	Bottom Flange Stress		Flexure	Warping
GC	10-9	-2.1%	-5.2%	-0.5%	-1.1%	0.0%	-0.2%	Pinned	Pinned	Pinned	-0.1%	-0.2%	-0.5%	1.0%	
	9-8	-2.1%	-5.3%	-0.5%	-0.9%	0.0%	-0.1%	-0.2%	-0.5%	1.0%	0.0%	-0.1%	-0.7%	0.0%	
	8-7	-2.0%	-4.4%	-0.5%	-0.5%	0.0%	0.0%	-0.1%	-0.7%	0.0%	0.0%	-0.1%	-0.6%	0.0%	
	7-6	-2.1%	-5.2%	-0.6%	-1.1%	-0.9%	0.0%	-0.1%	-0.6%	0.0%	-0.1%	-0.2%	-0.7%	1.2%	
	6-5	-2.0%	-4.3%	-0.5%	-0.9%	1.5%	-0.1%	-0.2%	-0.7%	1.2%	-0.1%	Pinned	Pinned	Pinned	
GA	10-9	-2.7%	-4.5%	-0.9%	-1.3%	-1.9%	-0.3%	Pinned	Pinned	Pinned	-0.3%	-0.3%	-0.9%	-3.3%	
	9-8	-2.8%	-4.8%	-0.9%	-1.3%	-3.2%	-0.3%	-0.3%	-0.9%	-3.2%	-0.1%	-0.2%	-1.0%	-2.7%	
	8-7	-2.5%	-3.9%	-0.5%	-1.2%	-1.4%	-0.1%	-0.2%	-1.4%	-3.2%	0.0%	-0.3%	-1.1%	-1.6%	
	7-6	-2.8%	-4.7%	-0.9%	-1.3%	-2.1%	0.0%	-0.3%	-1.3%	-2.7%	-0.1%	-0.2%	-0.8%	-3.3%	
	6-5	-2.3%	-3.6%	-0.7%	-1.1%	-10.0%	-0.1%	-0.2%	-0.8%	-3.3%	-0.2%	Pinned	Pinned	Pinned	
Beam Diaphragm and Lateral Wind Bracing															
Span Loaded	Diaphragm Forces at Girder C					Diaphragm Forces at Girder A					Lateral Wind Bracing Forces				
	Axial	Shear	Moment	Axial	Shear	Moment	Axial	Shear	Moment	Axial	Axial Tension	Axial Compression			
All Members in Span	10-9	-0.6%	1.2%	1.2%	-0.6%	1.2%	1.2%	-0.6%	1.2%	1.2%	3.7%	3.8%			
	9-8	0.0%	1.1%	1.2%	0.0%	1.1%	0.9%	0.0%	1.1%	1.2%	4.1%	4.2%			
	8-7	-1.8%	0.9%	0.7%	-1.8%	0.9%	1.1%	-1.8%	0.9%	1.1%	1.2%	1.3%			
	7-6	-0.6%	1.1%	1.2%	-0.6%	1.1%	0.9%	-0.6%	1.1%	1.2%	4.1%	4.6%			
	6-5	-0.5%	1.2%	1.2%	-0.5%	1.2%	1.1%	-0.5%	1.2%	1.1%	3.2%	1.9%			
Only Members near Midspan	10-9	-0.6%	1.2%	1.2%	-0.6%	1.2%	1.3%	-0.6%	1.3%	1.3%	2.2%	2.2%			
	9-8	-0.7%	1.0%	1.0%	-0.7%	1.0%	1.1%	-0.7%	1.0%	1.1%	2.9%	2.6%			
	8-7	-1.8%	0.9%	0.7%	-1.8%	0.9%	1.1%	-1.8%	0.9%	1.1%	2.4%	1.0%			
	7-6	-0.6%	1.0%	0.9%	-0.6%	1.0%	1.2%	-0.6%	1.0%	1.2%	2.6%	2.2%			
	6-5	-0.5%	1.7%	2.1%	-0.5%	1.7%	1.5%	-0.5%	1.7%	1.5%	1.8%	1.8%			
Mn/DOT Bridge No. 27998															
Span Loaded	Middle of Span					Left Support					Right Support				
	Vertical Deflection	Torsional Rotation	Flexural Moment	Bottom Flange Stress		Flexural Shear	Flexural Moment	Bottom Flange Stress		Flexural Shear	Flexural Moment	Bottom Flange Stress		Flexure	Warping
G1	I	-1.9%	-1.8%	-0.1%	-0.4%	-0.7%	-0.2%	Pinned	Pinned	Pinned	0.0%	0.2%	-0.5%	0.0%	
	II	-1.8%	-1.6%	0.0%	-0.5%	0.0%	0.0%	0.2%	-0.5%	-1.2%	-0.1%	Pinned	Pinned	Pinned	
G2	I	-1.8%	-1.3%	0.2%	-0.5%	-0.8%	0.1%	Pinned	Pinned	Pinned	0.0%	0.1%	-0.7%	0.0%	
	II	-1.7%	-1.2%	0.3%	0.0%	0.0%	0.0%	0.1%	-0.7%	-1.4%	-0.2%	Pinned	Pinned	Pinned	
G3	I	-1.9%	-1.0%	0.3%	0.0%	0.0%	0.1%	Pinned	Pinned	Pinned	0.0%	0.0%	0.0%	0.0%	
	II	-1.6%	-0.8%	0.1%	-0.8%	-1.2%	0.2%	0.0%	0.0%	-1.9%	-0.1%	Pinned	Pinned	Pinned	
G4	I	-1.6%	-0.7%	0.2%	-0.4%	0.0%	0.1%	Pinned	Pinned	Pinned	0.1%	0.2%	0.0%	0.0%	
	II	-1.3%	-0.6%	0.4%	0.0%	0.0%	0.1%	0.2%	0.0%	0.0%	0.1%	Pinned	Pinned	Pinned	
X - shaped Diaphragm															
Span Loaded	Axial Forces between G1 and G2					Axial Forces between G2 and G3					Axial Forces between G3 and G4				
	Top	Bottom	U1-L2	L1-U2	Top	Bottom	U2-L3	L2-U3	Top	Bottom	U3-L4	L3-U4			
All Members in Span	I	-5.1%	-1.7%	-1.6%	0.2%	-4.0%	-1.3%	-1.4%	-0.2%	-5.5%	-1.2%	-1.3%	-1.5%		
	II	-2.1%	-1.1%	-0.3%	-1.3%	-1.6%	-0.8%	-0.3%	-1.3%	-2.2%	1.7%	-1.2%	-1.1%		
Only Members near Midspan	I	-5.1%	2.3%	-0.8%	0.2%	-4.0%	2.0%	-0.3%	-0.2%	-5.5%	1.7%	-0.2%	-0.6%		
	II	-4.8%	1.5%	-0.3%	0.3%	-3.4%	2.7%	-0.3%	-0.2%	-5.6%	1.7%	-0.1%	-0.5%		
FHWA Test Specimen															
Span Loaded	Middle of Span					Left Support					Right Support				
	Vertical Deflection	Torsional Rotation	Flexural Moment	Bottom Flange Stress		Flexural Shear	Flexural Moment	Bottom Flange Stress		Flexural Shear	Flexural Moment	Bottom Flange Stress		Flexure	Warping
G1	1	-1.6%	-1.9%	0.0%	-0.3%	-0.1%	0.0%	Pinned	Pinned	Pinned	0.0%	Pinned	Pinned	Pinned	
	1	-2.1%	-1.6%	0.1%	-0.6%	0.0%	0.1%	Pinned	Pinned	Pinned	0.1%	Pinned	Pinned	Pinned	
	1	-1.9%	-1.2%	0.2%	-0.3%	0.4%	0.1%	Pinned	Pinned	Pinned	0.1%	Pinned	Pinned	Pinned	
K - shaped Diaphragm															
Span Loaded	Axial Forces between G1 and G2					Axial Forces between G2 and G3					Axial Forces between G3 and G4				
	Top	Bottom 1	Bottom 2	U1-M	M-U2	Top	Bottom 2	Bottom 3	U2-M	M-U3					
All Members in Span	1	-3.9%	0.2%	0.1%	-0.3%	-0.4%	-2.6%	0.0%	0.4%	-0.1%	-0.1%	-0.1%			
	1	-3.9%	0.2%	0.1%	-0.3%	-0.4%	-2.6%	0.0%	0.4%	-0.1%	-0.1%	-0.1%			

Table 8-22: Study 12 Effective Concrete Width 10% Larger

Study 12: Effective Concrete Width for Girders															
Percent Change for Maximum Responses from Analysis using: Base Model to: Modified Model with 10% smaller effective widths															
Mn/DOT Bridge No. 69824															
Girder															
Span Loaded	Middle of Span					Left Support					Right Support				
	Vertical Deflection	Torsional Rotation	Flexural Moment	Bottom Flange Stress		Flexural Shear	Flexural Moment	Bottom Flange Stress		Flexural Shear	Flexural Moment	Bottom Flange Stress		Flexural Warping	
GC	10-9	2.5%	6.8%	0.7%	1.1%	0.0%	0.2%	Pinned	Pinned	Pinned	0.1%	0.2%	0.8%	-1.0%	
	9-8	2.5%	6.8%	0.7%	1.2%	0.0%	0.1%	0.2%	0.8%	-1.0%	0.0%	0.2%	1.0%	0.0%	
	8-7	2.3%	5.2%	0.6%	1.0%	0.0%	0.0%	0.2%	1.0%	-1.5%	0.0%	0.2%	0.6%	0.0%	
	7-6	2.6%	6.7%	0.7%	1.1%	0.0%	0.0%	0.2%	0.6%	0.0%	0.1%	0.2%	0.7%	0.0%	
	6-5	2.5%	5.5%	0.7%	1.1%	-1.5%	0.1%	0.2%	0.7%	0.0%	0.2%	Pinned	Pinned	Pinned	
GA	10-9	3.5%	5.9%	1.2%	1.8%	3.8%	0.4%	Pinned	Pinned	Pinned	0.4%	0.4%	0.9%	3.3%	
	9-8	3.5%	6.2%	1.2%	1.6%	3.2%	0.4%	0.4%	0.9%	4.8%	0.1%	0.3%	1.7%	4.0%	
	8-7	3.0%	4.8%	0.6%	1.7%	2.7%	0.1%	0.3%	1.1%	3.2%	0.1%	0.3%	1.4%	3.3%	
	7-6	3.4%	6.1%	1.1%	1.6%	3.2%	0.1%	0.3%	1.3%	4.1%	0.2%	0.4%	0.8%	1.6%	
	6-5	2.8%	4.8%	0.9%	1.2%	10.0%	0.2%	0.4%	0.8%	1.6%	0.2%	Pinned	Pinned	Pinned	
Beam Diaphragm and Lateral Wind Bracing															
Span Loaded	Diaphragm Forces at Girder C				Diaphragm Forces at Girder A				Lateral Wind Bracing Forces						
	Axial	Shear	Moment		Axial	Shear	Moment		Axial Tension	Axial Compression					
All Members in Span	10-9	0.8%	-1.8%	-1.6%	0.8%	-1.8%	-1.7%		-5.4%	-5.1%					
	9-8	-0.2%	-1.4%	-1.7%	-0.2%	-1.4%	-1.2%		-5.4%	-5.5%					
	8-7	2.1%	-1.2%	-1.0%	2.1%	-1.2%	-1.4%		-1.3%	-1.6%					
	7-6	0.7%	-1.5%	-1.7%	0.7%	-1.5%	-1.2%		-4.9%	-6.3%					
	6-5	0.5%	-1.8%	-1.8%	0.5%	-1.8%	-1.7%		-3.7%	-2.5%					
Only Members near Midspan	10-9	0.8%	-1.7%	-1.6%	0.8%	-1.7%	-1.9%		-3.3%	-3.1%					
	9-8	0.8%	-1.5%	-1.4%	0.8%	-1.5%	-1.6%		-4.0%	-3.7%					
	8-7	2.1%	-1.2%	-1.0%	2.1%	-1.2%	-1.4%		-3.2%	-1.2%					
	7-6	0.7%	-1.5%	-1.4%	0.7%	-1.5%	-1.6%		-3.4%	-3.6%					
	6-5	0.5%	-2.6%	-3.0%	0.5%	-2.6%	-2.3%		-2.3%	-2.9%					
Mn/DOT Bridge No. 27998															
Girder															
Span Loaded	Middle of Span					Left Support					Right Support				
	Vertical Deflection	Torsional Rotation	Flexural Moment	Bottom Flange Stress		Flexural Shear	Flexural Moment	Bottom Flange Stress		Flexural Shear	Flexural Moment	Bottom Flange Stress		Flexural Warping	
G1	I	2.1%	2.0%	0.1%	0.9%	0.0%	0.1%	Pinned	Pinned	Pinned	0.0%	-0.2%	0.5%	0.0%	
	II	2.1%	1.8%	0.0%	0.5%	0.8%	0.0%	-0.2%	0.5%	1.2%	0.1%	Pinned	Pinned	Pinned	
G2	I	2.2%	1.6%	-0.3%	0.0%	-0.8%	-0.2%	Pinned	Pinned	Pinned	0.0%	-0.1%	0.0%	0.0%	
	II	2.1%	1.3%	-0.3%	0.6%	0.0%	0.0%	-0.1%	0.0%	-21.9%	0.3%	Pinned	Pinned	Pinned	
G3	I	2.1%	1.2%	-0.3%	0.0%	-1.1%	-0.2%	Pinned	Pinned	Pinned	0.0%	0.0%	0.8%	0.0%	
	II	1.8%	1.0%	-0.1%	0.0%	-0.3%	0.0%	Pinned	Pinned	Pinned	0.1%	Pinned	Pinned	Pinned	
G4	I	1.8%	0.7%	-0.4%	0.0%	-1.0%	-0.1%	Pinned	Pinned	Pinned	-0.1%	-0.2%	0.6%	0.0%	
	II	1.6%	0.6%	-0.5%	0.0%	0.0%	-0.1%	-0.2%	0.6%	0.0%	-0.1%	Pinned	Pinned	Pinned	
X - shaped Diaphragm															
Span Loaded	Axial Forces between G1 and G2				Axial Forces between G2 and G3				Axial Forces between G3 and G4						
	Top	Bottom	U1-L2	L1-U2	Top	Bottom	U2-L3	L2-U3	Top	Bottom	U3-L4	L3-U4			
All Members in Span	I	5.9%	1.9%	1.8%	-0.2%	4.3%	1.5%	1.6%	0.3%	6.2%	1.4%	1.5%	1.7%		
	II	5.5%	1.2%	0.3%	1.5%	3.7%	0.8%	0.3%	1.5%	1.9%	-1.9%	1.4%	1.3%		
Only Members near Midspan	I	5.9%	-2.7%	0.9%	-0.2%	4.3%	-2.2%	0.3%	0.3%	6.2%	-1.9%	0.2%	0.7%		
	II	5.5%	-1.8%	0.3%	-0.4%	3.7%	-3.2%	0.3%	0.2%	6.5%	-1.9%	0.1%	0.6%		
FHWA Test Specimen															
Girder															
Span Loaded	Middle of Span					Left Support					Right Support				
	Vertical Deflection	Torsional Rotation	Flexural Moment	Bottom Flange Stress		Flexural Shear	Flexural Moment	Bottom Flange Stress		Flexural Shear	Flexural Moment	Bottom Flange Stress		Flexural Warping	
G1	1	1.9%	2.3%	0.0%	0.5%	0.1%	0.0%	Pinned	Pinned	Pinned	0.0%	Pinned	Pinned	Pinned	Pinned
	1	2.5%	1.9%	-0.1%	0.3%	0.0%	-0.1%	Pinned	Pinned	Pinned	-0.1%	Pinned	Pinned	Pinned	Pinned
	1	2.2%	1.5%	-0.2%	0.3%	-0.3%	-0.1%	Pinned	Pinned	Pinned	-0.1%	Pinned	Pinned	Pinned	Pinned
K - shaped Diaphragm															
Span Loaded	Axial Forces between G1 and G2						Axial Forces between G2 and G3								
	Top	Bottom 1	Bottom 2	U1-M	M-U2	Top	Bottom 2	Bottom 3	U2-M	M-U3					
All Members in Span	1	4.4%	-0.2%	-0.1%	0.4%	0.4%	2.6%	0.0%	-0.5%	0.1%	0.2%				
	1	4.4%	-0.2%	-0.1%	0.4%	0.4%	2.6%	0.0%	-0.5%	0.1%	0.2%				
Only Members near Midspan	1	4.4%	-0.2%	-0.1%	0.4%	0.4%	2.6%	0.0%	-0.5%	0.1%	0.2%				

Table 8-23: Study 12 Effective Concrete Width 10% Smaller

Study 12: Effective Concrete Width for Girders													
Percent Change for Maximum Responses from Analysis using: Base Model to: Modified Model with 20% smaller effective widths													
Mn/DOT Bridge No. 69824													
Girder													
Span Loaded	Middle of Span				Left Support				Right Support				
	Vertical Deflection	Torsional Rotation	Flexural Moment	Bottom Flange Stress	Flexural Shear	Flexural Moment	Bottom Flange Stress	Flexural Shear	Flexural Moment	Flexural Shear	Flexural Moment	Bottom Flange Stress	
GC	10-9	5.7%	15.8%	1.5%	2.6%	-0.9%	0.6%	Pinned	Pinned	Pinned	0.4%	0.6%	1.9% -2.0%
	9-8	5.7%	15.6%	1.6%	2.6%	-1.0%	0.2%	0.6%	1.9%	-2.0%	0.0%	0.4%	2.0% 0.0%
	8-7	5.2%	11.7%	1.2%	1.8%	0.0%	0.0%	0.4%	2.0%	-3.0%	0.0%	0.5%	1.9% -1.3%
	7-6	5.8%	15.4%	1.7%	2.8%	-0.9%	0.0%	0.5%	1.9%	0.0%	0.2%	0.5%	1.7% -1.2%
	6-5	5.6%	13.0%	1.5%	2.6%	-4.5%	0.3%	0.5%	1.7%	-1.2%	0.4%	Pinned	Pinned
GA	10-9	7.9%	13.8%	2.9%	4.1%	8.5%	0.9%	Pinned	Pinned	Pinned	0.8%	1.0%	2.3% 9.8%
	9-8	8.1%	14.2%	2.7%	3.9%	7.5%	0.9%	1.0%	2.3%	9.7%	0.3%	0.7%	3.6% 6.7%
	8-7	6.7%	10.5%	1.2%	3.4%	4.1%	0.3%	0.7%	2.9%	6.5%	0.3%	0.7%	3.2% 6.6%
	7-6	7.8%	14.0%	2.6%	3.6%	7.4%	0.3%	0.7%	3.2%	8.1%	0.4%	0.8%	2.0% 3.3%
	6-5	6.3%	11.1%	2.0%	3.0%	25.0%	0.5%	0.8%	2.0%	3.3%	0.6%	Pinned	Pinned
Beam Diaphragm and Lateral Wind Bracing													
Span Loaded	Diaphragm Forces at Girder C				Diaphragm Forces at Girder A				Lateral Wind Bracing Forces				
	Axial	Shear	Moment		Axial	Shear	Moment		Axial Tension	Axial Compression			
All Members in Span	10-9	1.8%	-4.4%	-4.0%	1.8%	-4.4%	-4.1%		-12.4%		-12.3%		
	9-8	-199.4%	-3.5%	-4.1%	-199.4%	-3.5%	-2.9%		-13.0%		-13.2%		
	8-7	4.6%	-2.8%	-2.3%	4.6%	-2.8%	-3.4%		-3.0%		-3.3%		
	7-6	1.6%	-3.5%	-4.2%	1.6%	-3.5%	-2.9%		-11.8%		-13.8%		
	6-5	1.1%	-4.4%	-4.6%	1.1%	-4.4%	-4.2%		-9.2%		-6.4%		
Only Members near Midspan	10-9	1.8%	-4.2%	-4.0%	1.8%	-4.2%	-4.5%		-8.4%		-7.6%		
	9-8	1.7%	-3.6%	-3.4%	1.7%	-3.6%	-3.9%		-9.8%		-9.2%		
	8-7	4.6%	-2.8%	-2.3%	4.6%	-2.8%	-3.4%		-6.5%		-2.9%		
	7-6	1.6%	-3.7%	-3.4%	1.6%	-3.7%	-3.9%		-8.6%		-8.7%		
	6-5	1.1%	-6.3%	-7.2%	1.1%	-6.3%	-5.6%		-6.0%		-6.8%		
Mn/DOT Bridge No. 27998													
Girder	Middle of Span				Left Support				Right Support				
	Span Loaded	Vertical Deflection	Torsional Rotation	Flexural Moment	Bottom Flange Stress	Flexural Shear	Flexural Moment	Bottom Flange Stress	Flexural Shear	Flexural Moment	Bottom Flange Stress		
G1	I	4.7%	4.2%	0.1%	1.3%	0.7%	0.2%	Pinned	Pinned	Pinned	0.0%	-0.4%	1.1% -1.1%
	II	4.6%	3.8%	0.0%	1.0%	1.6%	0.0%	-0.4%	1.1%	2.4%	0.3%	Pinned	Pinned
G2	I	4.8%	3.4%	-0.5%	0.5%	0.0%	-0.3%	Pinned	Pinned	Pinned	-0.1%	-0.3%	0.7% 0.0%
	II	4.5%	2.9%	-0.6%	0.6%	0.0%	-0.1%	-0.3%	0.7%	-19.2%	0.6%	Pinned	Pinned
G3	I	4.7%	2.5%	-0.7%	0.7%	-1.1%	-0.3%	Pinned	Pinned	Pinned	0.0%	-0.1%	1.7% 2.1%
	II	4.1%	2.1%	-0.3%	0.8%	0.0%	-0.7%	-0.1%	1.7%	5.8%	0.2%	Pinned	Pinned
G4	I	4.0%	1.6%	-0.8%	0.0%	-1.9%	-0.3%	Pinned	Pinned	Pinned	-0.2%	-0.4%	1.2% -1.0%
	II	3.4%	1.2%	-1.1%	0.0%	0.0%	-0.2%	-0.4%	1.2%	-1.0%	-0.2%	Pinned	Pinned
X - shaped Diaphragm													
Span Loaded	Axial Forces between G1 and G2				Axial Forces between G2 and G3				Axial Forces between G3 and G4				
	Top	Bottom	U1-L2	L1-U2	Top	Bottom	U2-L3	L2-U3	Top	Bottom	U3-L4	L3-U4	
All Members in Span	I	12.2%	4.2%	4.0%	-0.4%	9.2%	3.3%	3.6%	0.6%	13.7%	3.0%	3.2%	3.7%
	II	11.5%	2.4%	0.5%	3.1%	7.8%	1.6%	0.5%	3.2%	3.8%	-4.0%	2.9%	2.8%
Only Members near Midspan	I	12.2%	-5.7%	1.9%	-0.4%	9.2%	-4.8%	0.6%	0.6%	13.7%	-4.3%	0.5%	1.4%
	II	11.5%	-4.0%	0.5%	-0.8%	7.8%	-7.0%	0.5%	0.4%	14.8%	-4.3%	0.4%	1.3%
FHWA Test Specimen													
Girder	Middle of Span				Left Support				Right Support				
	Span Loaded	Vertical Deflection	Torsional Rotation	Flexural Moment	Bottom Flange Stress	Flexural Shear	Flexural Moment	Bottom Flange Stress	Flexural Shear	Flexural Moment	Bottom Flange Stress		
G1	1	4.3%	5.1%	0.0%	1.0%	0.2%	0.0%	Pinned	Pinned	Pinned	0.0%	Pinned	Pinned
	1	5.4%	4.3%	-0.2%	0.6%	0.0%	-0.2%	Pinned	Pinned	Pinned	-0.2%	Pinned	Pinned
	1	4.9%	3.4%	-0.4%	0.7%	-0.8%	-0.3%	Pinned	Pinned	Pinned	-0.3%	Pinned	Pinned
K - shaped Diaphragm													
Span Loaded	Axial Forces between G1 and G2						Axial Forces between G2 and G3						
	Top	Bottom 1	Bottom 2	U1-M	M-U2		Top	Bottom 2	Bottom 3	U2-M	M-U3		
All Members in Span	1	9.6%	-0.4%	-0.2%	0.8%	1.0%	5.2%	0.0%	-0.9%	0.3%	0.4%		
	1	9.6%	-0.4%	-0.2%	0.8%	1.0%	5.2%	0.0%	-0.9%	0.3%	0.4%		

Table 8-24: Study 12 Effective Concrete Width 20% Smaller

Study 13: Modular Ratio																
Percent Change for Maximum Responses from Analysis using: Base Model to: Modified Model with modular ratio lowered by 2																
Mn/DOT Bridge No. 69824																
Girder																
Span Loaded	Middle of Span					Left Support					Right Support					
	Vertical Deflection	Torsional Rotation	Flexural Moment	Bottom Flange Stress		Flexural Shear	Flexural Moment	Bottom Flange Stress		Flexural Shear	Flexural Moment	Bottom Flange Stress		Flexure	Warping	
GC	10-9	-6.3%	-10.0%	-0.7%	-2.3%	0.0%	-0.2%	Pinned	Pinned	Pinned	-0.1%	-0.1%	-1.9%	1.0%		
	9-8	-6.4%	-10.6%	-0.9%	-2.3%	0.0%	-0.1%	-0.1%	-1.9%	1.0%	0.0%	0.0%	-1.6%	0.0%		
	8-7	-6.4%	-10.4%	-0.9%	-2.0%	0.0%	0.0%	0.0%	-1.6%	-1.5%	0.0%	-0.1%	-1.9%	1.3%		
	7-6	-6.3%	-10.5%	-0.9%	-2.3%	-0.9%	0.0%	-0.1%	-1.9%	0.0%	-0.1%	-0.1%	-1.9%	1.2%		
	6-5	-6.2%	-8.7%	-0.8%	-2.6%	0.0%	0.0%	-0.1%	-1.9%	1.2%	-0.2%	Pinned	Pinned	Pinned		
GA	10-9	-7.0%	-9.0%	-1.3%	-2.8%	-2.8%	-0.3%	Pinned	Pinned	Pinned	-0.3%	-0.3%	-2.0%	-3.3%		
	9-8	-7.4%	-9.8%	-1.4%	-2.9%	-3.2%	-0.3%	-0.3%	-2.0%	-3.2%	0.0%	-0.1%	-3.0%	-4.0%		
	8-7	-7.4%	-9.3%	-0.7%	-2.9%	-4.1%	0.0%	-0.1%	-2.9%	-3.2%	0.0%	-0.1%	-2.5%	-1.6%		
	7-6	-7.3%	-9.7%	-1.3%	-2.6%	-3.2%	0.0%	-0.1%	-2.9%	-4.1%	-0.2%	-0.2%	-1.8%	-1.6%		
	6-5	-6.4%	-7.9%	-1.0%	-2.6%	-10.0%	0.0%	-0.2%	-1.8%	-1.6%	-0.3%	Pinned	Pinned	Pinned		
Beam Diaphragm and Lateral Wind Bracing																
Span Loaded	Diaphragm Forces at Girder C					Diaphragm Forces at Girder A					Lateral Wind Bracing Forces					
	Axial	Shear	Moment	Axial	Shear	Moment	Axial	Shear	Moment	Axial	Axial Tension	Axial Compression				
All Members in Span	10-9	1.9%	1.8%	-2.3%	1.9%	1.8%	4.5%				3.5%		3.6%			
	9-8	-199.6%	1.7%	0.4%	-199.6%	1.7%	3.0%				4.3%		4.4%			
	8-7	-4.2%	1.1%	-2.9%	-4.2%	1.1%	5.8%				0.5%		0.7%			
	7-6	2.0%	1.6%	0.2%	2.0%	1.6%	3.0%				4.5%		4.1%			
	6-5	0.2%	1.3%	-1.7%	0.2%	1.3%	4.8%				1.6%		1.7%			
Only Members near Midspan	10-9	1.9%	1.2%	-2.3%	1.9%	1.2%	5.3%				1.8%		0.4%			
	9-8	1.9%	0.9%	-2.5%	1.9%	0.9%	4.9%				1.9%		0.9%			
	8-7	-4.2%	1.1%	-2.9%	-4.2%	1.1%	5.8%				3.0%		-1.2%			
	7-6	2.0%	0.9%	-2.5%	2.0%	0.9%	4.9%				1.3%		0.3%			
	6-5	0.2%	1.2%	-204.2%	0.2%	1.2%	6.3%				2.8%		2.9%			
Mn/DOT Bridge No. 27998																
Girder																
Span Loaded	Middle of Span					Left Support					Right Support					
	Vertical Deflection	Torsional Rotation	Flexural Moment	Bottom Flange Stress		Flexural Shear	Flexural Moment	Bottom Flange Stress		Flexural Shear	Flexural Moment	Bottom Flange Stress		Flexure	Warping	
G1	I	-7.0%	-6.8%	-0.3%	-1.8%	-1.4%	-0.6%	Pinned	Pinned	Pinned	0.1%	0.7%	-1.6%	0.0%		
	II	-6.7%	-6.4%	-0.2%	-1.9%	-0.8%	0.1%	0.7%	-1.6%	-4.8%	-0.6%	Pinned	Pinned	Pinned		
G2	I	-7.0%	-5.2%	0.8%	-1.1%	0.0%	0.6%	Pinned	Pinned	Pinned	0.0%	0.5%	-1.4%	-2.3%		
	II	-6.6%	-4.8%	1.0%	-0.6%	-0.9%	0.0%	0.5%	-1.4%	-6.8%	-0.7%	Pinned	Pinned	Pinned		
G3	I	-7.1%	-4.0%	1.1%	-0.7%	0.0%	0.5%	Pinned	Pinned	Pinned	-0.2%	0.0%	-1.7%	0.0%		
	II	-6.3%	-3.5%	0.4%	-1.6%	-1.2%	0.8%	0.0%	-1.7%	-5.8%	-0.2%	Pinned	Pinned	Pinned		
G4	I	-6.2%	-2.9%	1.1%	-0.4%	1.9%	0.5%	Pinned	Pinned	Pinned	0.3%	0.8%	-1.2%	0.0%		
	II	-5.4%	-2.4%	1.4%	0.0%	3.1%	0.3%	0.8%	-1.2%	0.0%	0.3%	Pinned	Pinned	Pinned		
X - shaped Diaphragm																
Span Loaded	Axial Forces between G1 and G2					Axial Forces between G2 and G3					Axial Forces between G3 and G4					
	Top	Bottom	U1-L2	L1-U2		Top	Bottom	U2-L3	L2-U3		Top	Bottom	U3-L4	L3-U4		
All Members in Span	I	-20.1%	-6.4%	-5.8%	0.7%	-15.0%	-5.0%	-4.5%	-1.0%	-18.9%	-4.5%	-6.1%	-5.6%			
	II	-3.0%	-4.4%	-2.1%	-5.2%	-4.4%	-3.4%	-1.1%	-5.1%	-9.2%	5.5%	-4.1%	-4.3%			
Only Members near Midspan	I	-20.1%	8.5%	-3.4%	0.7%	-15.0%	7.4%	-1.2%	-1.0%	-19.0%	6.0%	-0.4%	-2.4%			
	II	-19.2%	5.6%	-2.1%	1.3%	-13.9%	9.2%	-1.1%	-0.7%	-19.5%	5.5%	0.4%	-2.1%			
FHWA Test Specimen																
Girder																
Span Loaded	Middle of Span					Left Support					Right Support					
	Vertical Deflection	Torsional Rotation	Flexural Moment	Bottom Flange Stress		Flexural Shear	Flexural Moment	Bottom Flange Stress		Flexural Shear	Flexural Moment	Bottom Flange Stress		Flexure	Warping	
G1	1	-4.4%	-5.4%	0.0%	-1.2%	-0.1%	0.0%	Pinned	Pinned	Pinned	0.0%	Pinned	Pinned	Pinned	Pinned	
	2	-5.8%	-4.4%	0.3%	-1.1%	0.0%	0.3%	Pinned	Pinned	Pinned	0.2%	Pinned	Pinned	Pinned	Pinned	
	3	-5.1%	-3.3%	0.5%	-0.8%	1.2%	0.4%	Pinned	Pinned	Pinned	0.4%	Pinned	Pinned	Pinned	Pinned	
K - shaped Diaphragm																
Span Loaded	Axial Forces between G1 and G2					Axial Forces between G2 and G3					Axial Forces between G3 and G4					
	Top	Bottom 1	Bottom 2	U1-M	M-U2	Top	Bottom 2	Bottom 3	U2-M	M-U3						
All Members in Span	1	-10.6%	0.5%	0.3%	-0.8%	-1.1%	-7.6%	0.1%	1.3%	-0.1%	-0.4%					
	2	-10.6%	0.5%	0.3%	-0.8%	-1.1%	-7.6%	0.1%	1.3%	-0.1%	-0.4%					
Only Members near Midspan	1	-10.6%	0.5%	0.3%	-0.8%	-1.1%	-7.6%	0.1%	1.3%	-0.1%	-0.4%					

Table 8-25: Study 13 Modular Ratio Minus 2

Study 13: Modular Ratio													
Percent Change for Maximum Responses from Analysis using: Base Model to: Modified Model with modular ratio lowered by 1													
Mn/DOT Bridge No. 69824													
Girder													
Span Loaded	Middle of Span				Left Support				Right Support				
	Vertical Deflection	Torsional Rotation	Flexural Moment	Bottom Flange Stress	Flexural Shear	Flexural Moment	Bottom Flange Stress	Flexural Shear	Flexural Moment	Flexural Shear	Flexural Moment	Bottom Flange Stress	
GC	10-9	-3.0%	-4.9%	-0.3%	-1.1%	0.0%	-0.1%	Pinned	Pinned	Pinned	-0.1%	-0.1%	-0.8% 1.0%
	9-8	-3.1%	-5.1%	-0.4%	-1.2%	1.0%	-0.1%	-0.1%	-0.2%	-0.8%	1.0%	0.0%	-0.7% 0.0%
	8-7	-3.1%	-5.1%	-0.4%	-0.8%	0.0%	0.0%	0.0%	0.0%	-0.7%	0.0%	0.0%	-1.0% 1.3%
	7-6	-3.1%	-5.1%	-0.4%	-1.1%	0.0%	0.0%	0.0%	0.0%	-1.0%	-1.2%	0.0%	-0.1% 1.2%
	6-5	-2.9%	-4.2%	-0.4%	-1.1%	0.0%	0.0%	-0.1%	-1.0%	1.2%	-0.1%	Pinned	Pinned Pinned
GA	10-9	-3.4%	-4.4%	-0.6%	-1.3%	-0.9%	-0.1%	Pinned	Pinned	Pinned	-0.1%	-0.2%	-0.9% -1.6%
	9-8	-3.5%	-4.8%	-0.6%	-1.3%	-1.1%	-0.2%	-0.2%	-0.9%	-1.6%	0.0%	0.0%	-1.3% -1.3%
	8-7	-3.5%	-4.4%	-0.3%	-1.2%	-2.7%	0.0%	0.0%	-1.4%	-1.6%	0.0%	-0.1%	-1.1% -1.6%
	7-6	-3.5%	-4.7%	-0.6%	-1.3%	-1.1%	0.0%	-0.1%	-1.6%	-1.4%	-0.1%	-0.1%	-1.0% -1.6%
	6-5	-3.1%	-3.8%	-0.5%	-1.2%	-5.0%	0.0%	-0.1%	-1.0%	-1.6%	-0.1%	Pinned	Pinned Pinned
Beam Diaphragm and Lateral Wind Bracing													
Span Loaded	Diaphragm Forces at Girder C				Diaphragm Forces at Girder A				Lateral Wind Bracing Forces				
	Axial	Shear	Moment		Axial	Shear	Moment		Axial Tension	Axial Compression			
All Members in Span	10-9	0.9%	0.9%	-0.9%	0.9%	0.9%	2.1%		1.7%		1.9%		
	9-8	-0.4%	0.8%	0.2%	-0.4%	0.8%	1.3%		2.2%		2.2%		
	8-7	-2.0%	0.5%	-1.3%	-2.0%	0.5%	2.6%		0.2%		0.3%		
	7-6	0.9%	0.8%	0.2%	0.9%	0.8%	1.4%		2.2%		2.0%		
	6-5	0.1%	0.7%	-0.7%	0.1%	0.7%	2.2%		0.9%		1.0%		
Only Members near Midspan	10-9	0.9%	0.6%	-0.9%	0.9%	0.6%	2.3%		0.7%		0.4%		
	9-8	0.8%	0.4%	-1.0%	0.8%	0.4%	2.2%		1.1%		0.6%		
	8-7	-2.0%	0.5%	-1.3%	-2.0%	0.5%	2.6%		1.3%		-0.5%		
	7-6	0.9%	0.5%	-1.0%	0.9%	0.5%	2.2%		0.8%		0.3%		
	6-5	0.1%	0.6%	-199.5%	0.1%	0.6%	2.8%		1.4%		1.3%		
Mn/DOT Bridge No. 27998													
Girder													
Span Loaded	Middle of Span				Left Support				Right Support				
	Vertical Deflection	Torsional Rotation	Flexural Moment	Bottom Flange Stress	Flexural Shear	Flexural Moment	Bottom Flange Stress	Flexural Shear	Flexural Moment	Flexural Shear	Flexural Moment	Bottom Flange Stress	
G1	I	-3.4%	-3.3%	-0.1%	-0.9%	-1.4%	-0.3%	Pinned	Pinned	Pinned	0.0%	0.3%	-0.5% 0.0%
	II	-3.2%	-3.0%	-0.1%	-1.0%	0.0%	0.0%	0.3%	-0.5%	-1.8%	-0.3%	Pinned	Pinned Pinned
G2	I	-3.3%	-2.5%	0.4%	-0.5%	0.0%	0.2%	Pinned	Pinned	Pinned	0.0%	0.2%	-0.7% -2.3%
	II	-3.2%	-2.3%	0.5%	0.0%	0.0%	0.0%	0.2%	-0.7%	-4.1%	-0.4%	Pinned	Pinned Pinned
G3	I	-3.4%	-2.0%	0.5%	-0.7%	0.0%	0.2%	Pinned	Pinned	Pinned	-0.1%	0.0%	-0.8% 0.0%
	II	-3.0%	-1.8%	0.2%	-0.8%	-1.2%	0.4%	0.0%	-0.8%	-1.9%	-0.1%	Pinned	Pinned Pinned
G4	I	-3.0%	-1.4%	0.5%	-0.4%	1.0%	0.2%	Pinned	Pinned	Pinned	0.1%	0.3%	-0.6% 0.0%
	II	-2.5%	-1.2%	0.7%	0.0%	1.0%	0.1%	0.3%	-0.6%	0.0%	0.1%	Pinned	Pinned Pinned
X-shaped Diaphragm													
Span Loaded	Axial Forces between G1 and G2				Axial Forces between G2 and G3				Axial Forces between G3 and G4				
	Top	Bottom	U1-L2	L1-U2	Top	Bottom	U2-L3	L2-U3	Top	Bottom	U3-L4	L3-U4	
All Members in Span	I	-9.3%	-3.1%	-2.7%	0.3%	-6.8%	-2.4%	-2.6%	-0.4%	-9.1%	-2.2%	-3.0%	-2.7%
	II	-2.4%	-2.1%	-0.9%	-2.5%	-1.9%	-1.6%	-0.4%	-2.3%	-3.8%	2.7%	-2.4%	-2.0%
Only Members near Midspan	I	-9.3%	4.0%	-1.5%	0.3%	-6.8%	3.4%	-0.5%	-0.4%	-9.1%	2.9%	-0.2%	-1.1%
	II	-8.8%	2.6%	-0.9%	0.6%	-6.2%	4.3%	-0.4%	-0.3%	-9.6%	2.7%	0.1%	-0.9%
FHWA Test Specimen													
Girder													
Span Loaded	Middle of Span				Left Support				Right Support				
	Vertical Deflection	Torsional Rotation	Flexural Moment	Bottom Flange Stress	Flexural Shear	Flexural Moment	Bottom Flange Stress	Flexural Shear	Flexural Moment	Flexural Shear	Flexural Moment	Bottom Flange Stress	
G1	1	-2.1%	-2.6%	0.0%	-0.5%	-0.1%	0.0%	Pinned	Pinned	Pinned	0.0%	Pinned	Pinned Pinned
	1	-2.8%	-2.2%	0.1%	-0.6%	0.0%	0.2%	Pinned	Pinned	Pinned	0.1%	Pinned	Pinned Pinned
	1	-2.5%	-1.7%	0.2%	-0.4%	0.7%	0.2%	Pinned	Pinned	Pinned	0.2%	Pinned	Pinned Pinned
K-shaped Diaphragm													
Span Loaded	Axial Forces between G1 and G2						Axial Forces between G2 and G3						
	Top	Bottom 1	Bottom 2	U1-M	M-U2	Top	Bottom 2	Bottom 3	U2-M	M-U3			
All Members in Span	1	-5.1%	0.2%	0.1%	-0.4%	-0.5%	-3.3%	0.0%	0.6%	-0.1%	-0.2%		
	1	-5.1%	0.2%	0.1%	-0.4%	-0.5%	-3.3%	0.0%	0.6%	-0.1%	-0.2%		

Table 8-26: Study 13 Modular Ratio Minus 1

Study 13: Modular Ratio															
Percent Change for Maximum Responses from Analysis using: Base Model to: Modified Model with modular ratio increased by 1															
Mn/DOT Bridge No. 69824															
Girder															
Span Loaded	Middle of Span					Left Support					Right Support				
	Vertical Deflection	Torsional Rotation	Flexural Moment	Bottom Flange Stress		Flexural Shear	Flexural Moment	Bottom Flange Stress		Flexural Shear	Flexural Moment	Bottom Flange Stress		Flexural Shear	Flexural Moment
GC	10-9	2.8%	4.6%	0.3%	0.9%	0.0%	0.1%	Pinned	Pinned	Pinned	0.0%	0.1%	0.8%	-1.0%	
	9-8	2.8%	4.8%	0.4%	1.2%	1.0%	0.0%	0.1%	0.8%	-1.0%	0.0%	0.0%	1.0%	1.2%	
	8-7	2.8%	4.7%	0.4%	1.0%	0.0%	0.0%	0.0%	1.0%	-1.5%	0.0%	0.1%	0.6%	0.0%	
	7-6	2.9%	4.8%	0.4%	0.8%	-0.9%	0.0%	0.1%	0.6%	0.0%	0.0%	0.1%	0.7%	0.0%	
	6-5	2.7%	4.0%	0.3%	1.1%	1.5%	0.0%	0.1%	0.7%	0.0%	0.1%	Pinned	Pinned	Pinned	
GA	10-9	3.2%	4.2%	0.6%	1.0%	1.9%	0.1%	Pinned	Pinned	Pinned	0.1%	0.1%	0.9%	1.6%	
	9-8	3.3%	4.5%	0.6%	1.1%	1.1%	0.1%	0.1%	0.9%	1.6%	0.0%	0.1%	1.3%	1.3%	
	8-7	3.3%	4.2%	0.3%	1.5%	0.0%	0.0%	0.1%	1.1%	1.6%	0.0%	0.1%	1.4%	1.6%	
	7-6	3.2%	4.4%	0.6%	1.3%	1.1%	0.0%	0.1%	1.0%	1.4%	0.1%	0.1%	0.8%	0.0%	
	6-5	2.8%	3.6%	0.4%	1.2%	5.0%	0.0%	0.1%	0.8%	0.0%	0.1%	Pinned	Pinned	Pinned	
Beam Diaphragm and Lateral Wind Bracing															
Span Loaded	Diaphragm Forces at Girder C					Diaphragm Forces at Girder A					Lateral Wind Bracing Forces				
	Axial	Shear	Moment	Axial	Shear	Moment	Axial	Shear	Moment	Axial	Axial Tension	Axial Compression			
All Members in Span	10-9	-0.8%	-0.8%	0.6%	-0.8%	-0.8%	-1.7%	-1.8%	-1.7%						
	9-8	0.3%	-0.7%	-0.3%	0.3%	-0.7%	-1.1%	-2.0%	-2.0%						
	8-7	1.8%	-0.5%	0.9%	1.8%	-0.5%	-2.2%	-0.3%	-0.3%						
	7-6	-0.8%	-0.7%	-0.3%	-0.8%	-0.7%	-1.1%	-1.5%	-2.0%						
	6-5	0.0%	-0.7%	0.4%	0.0%	-0.7%	-1.9%	-0.7%	-0.8%						
Only Members near Midspan	10-9	-0.8%	-0.6%	0.6%	-0.8%	-0.6%	-1.9%	-1.1%	-1.1%						
	9-8	-0.8%	-0.5%	0.7%	-0.8%	-0.5%	-1.8%	-1.1%	-1.1%						
	8-7	1.8%	-0.5%	0.9%	1.8%	-0.5%	-2.2%	-1.3%	-1.3%						
	7-6	-0.8%	-0.5%	0.7%	-0.8%	-0.5%	-1.8%	-0.8%	-0.8%						
	6-5	0.0%	-0.6%	1.6%	0.0%	-0.6%	-2.4%	-1.2%	-1.2%						
Mn/DOT Bridge No. 27998															
Girder															
Span Loaded	Middle of Span					Left Support					Right Support				
	Vertical Deflection	Torsional Rotation	Flexural Moment	Bottom Flange Stress		Flexural Shear	Flexural Moment	Bottom Flange Stress		Flexural Shear	Flexural Moment	Bottom Flange Stress		Flexural Shear	Flexural Moment
G1	I	3.2%	2.9%	0.1%	0.9%	0.0%	0.2%	Pinned	Pinned	Pinned	0.0%	-0.2%	0.5%	0.0%	
	II	3.0%	2.7%	0.0%	0.5%	0.8%	0.0%	-0.2%	0.5%	1.8%	0.2%	Pinned	Pinned	Pinned	
G2	I	3.2%	2.4%	-0.3%	0.5%	0.0%	-0.2%	Pinned	Pinned	Pinned	0.0%	-0.2%	0.7%	0.0%	
	II	3.0%	2.1%	-0.4%	0.6%	0.0%	0.0%	-0.2%	0.7%	-21.9%	0.4%	Pinned	Pinned	Pinned	
G3	I	3.2%	1.9%	-0.4%	0.0%	-1.1%	-0.2%	Pinned	Pinned	Pinned	0.1%	0.0%	0.8%	0.0%	
	II	2.8%	1.6%	-0.2%	0.0%	0.0%	-0.4%	0.0%	0.8%	3.8%	0.1%	Pinned	Pinned	Pinned	
G4	I	2.8%	1.3%	-0.5%	0.0%	-1.0%	-0.2%	Pinned	Pinned	Pinned	-0.1%	-0.2%	0.6%	0.0%	
	II	2.4%	1.1%	-0.7%	0.0%	0.0%	-0.1%	-0.2%	0.6%	0.0%	-0.1%	Pinned	Pinned	Pinned	
X - shaped Diaphragm															
Span Loaded	Axial Forces between G1 and G2					Axial Forces between G2 and G3					Axial Forces between G3 and G4				
	Top	Bottom	U1-L2	L1-U2		Top	Bottom	U2-L3	L2-U3		Top	Bottom	U3-L4	L3-U4	
All Members in Span	I	7.9%	2.8%	2.5%	-0.3%	5.7%	2.2%	2.4%	0.4%	8.4%	2.1%	2.8%	2.5%		
	II	7.4%	1.8%	0.6%	2.1%	5.1%	1.4%	0.3%	2.1%	2.7%	-2.6%	2.2%	1.8%		
Only Members near Midspan	I	7.9%	-3.6%	1.3%	-0.3%	5.7%	-2.9%	0.4%	0.4%	8.4%	-2.7%	0.3%	0.9%		
	II	7.4%	-2.4%	0.6%	-0.5%	5.1%	-3.9%	0.3%	0.2%	9.3%	-2.6%	0.1%	0.8%		
FHWA Test Specimen															
Girder															
Span Loaded	Middle of Span					Left Support					Right Support				
	Vertical Deflection	Torsional Rotation	Flexural Moment	Bottom Flange Stress		Flexural Shear	Flexural Moment	Bottom Flange Stress		Flexural Shear	Flexural Moment	Bottom Flange Stress		Flexural Shear	Flexural Moment
G1	1	2.1%	2.5%	0.0%	0.5%	0.1%	0.0%	Pinned	Pinned	Pinned	0.0%	Pinned	Pinned	Pinned	Pinned
	1	2.6%	2.1%	-0.1%	0.3%	0.2%	-0.1%	Pinned	Pinned	Pinned	-0.1%	Pinned	Pinned	Pinned	Pinned
	1	2.5%	1.6%	-0.2%	0.4%	-0.4%	-0.1%	Pinned	Pinned	Pinned	-0.2%	Pinned	Pinned	Pinned	Pinned
K - shaped Diaphragm															
Span Loaded	Axial Forces between G1 and G2					Axial Forces between G2 and G3					Axial Forces between G3 and G4				
	Top	Bottom 1	Bottom 2	U1-M	M-U2	Top	Bottom 2	Bottom 3	U2-M	M-U3					
All Members in Span	1	4.6%	-0.2%	-0.1%	0.4%	0.5%	2.6%	0.0%	-0.5%	0.1%	0.2%				
	1	4.6%	-0.2%	-0.1%	0.4%	0.5%	2.6%	0.0%	-0.5%	0.1%	0.2%				
Only Members near Midspan	1	4.6%	-0.2%	-0.1%	0.4%	0.5%	2.6%	0.0%	-0.5%	0.1%	0.2%				

Table 8-27: Study 13 Modular Ratio Plus 1

Study 13: Modular Ratio															
Percent Change for Maximum Responses from Analysis using: Base Model to: Modified Model with modular ratio increased by 2															
Mn/DOT Bridge No. 69824															
Girder															
Span Loaded	Middle of Span					Left Support					Right Support				
	Vertical Deflection	Torsional Rotation	Flexural Moment	Bottom Flange Stress		Flexural Shear	Flexural Moment	Bottom Flange Stress		Flexural Shear	Flexural Moment	Bottom Flange Stress		Flexural Shear	Flexural Moment
GC	10-9	5.4%	9.0%	0.6%	1.7%	0.0%	0.2%	Pinned	Pinned	Pinned	0.1%	0.1%	1.6%	-1.0%	
	9-8	5.5%	9.4%	0.7%	2.0%	0.0%	0.1%	0.1%	1.6%	-1.0%	0.0%	0.1%	1.6%	0.0%	
	8-7	5.5%	9.0%	0.7%	1.8%	0.8%	0.0%	0.1%	1.6%	-1.5%	0.0%	0.1%	1.6%	0.0%	
	7-6	5.5%	9.3%	0.7%	2.0%	0.0%	0.0%	0.1%	1.6%	0.0%	0.0%	0.1%	1.4%	0.0%	
	6-5	5.2%	7.8%	0.7%	2.0%	1.5%	0.0%	0.1%	1.4%	0.0%	0.2%	Pinned	Pinned	Pinned	
GA	10-9	6.2%	8.1%	1.1%	2.3%	2.8%	0.2%	Pinned	Pinned	Pinned	0.2%	0.3%	1.7%	3.3%	
	9-8	6.4%	8.7%	1.1%	2.4%	2.2%	0.3%	0.3%	1.7%	3.2%	0.1%	0.2%	2.6%	2.7%	
	8-7	6.3%	8.1%	0.6%	2.4%	2.7%	0.1%	0.2%	2.1%	1.6%	0.0%	0.2%	2.5%	3.3%	
	7-6	6.3%	8.6%	1.1%	2.3%	2.1%	0.0%	0.2%	2.3%	2.7%	0.1%	0.2%	1.5%	0.0%	
	6-5	5.5%	7.0%	0.9%	2.1%	5.0%	0.0%	0.2%	1.5%	0.0%	0.2%	Pinned	Pinned	Pinned	
Beam Diaphragm and Lateral Wind Bracing															
Span Loaded	Diaphragm Forces at Girder C					Diaphragm Forces at Girder A					Lateral Wind Bracing Forces				
	Axial	Shear	Moment	Axial	Shear	Moment	Axial	Shear	Moment	Axial	Axial Tension	Axial Compression			
All Members in Span	10-9	-1.5%	-1.6%	0.9%	-1.5%	-1.6%	-3.2%	-3.5%	-3.4%						
	9-8	0.7%	-1.4%	-0.7%	0.7%	-1.4%	-2.1%	-3.9%	-4.0%						
	8-7	3.4%	-1.0%	1.7%	3.4%	-1.0%	-4.1%	-0.7%	-0.7%						
	7-6	-1.6%	-1.3%	-0.6%	-1.6%	-1.3%	-2.1%	-3.0%	-3.9%						
	6-5	-0.1%	-1.3%	0.6%	-0.1%	-1.3%	-3.4%	-1.8%	-1.6%						
Only Members near Midspan	10-9	-1.5%	-1.2%	0.9%	-1.5%	-1.2%	-3.6%	-2.2%	-0.4%						
	9-8	-1.6%	-0.9%	1.2%	-1.6%	-0.9%	-3.3%	-2.1%	-1.1%						
	8-7	3.4%	-1.0%	1.7%	3.4%	-1.0%	-4.1%	-2.7%	0.7%						
	7-6	-1.6%	-1.0%	1.1%	-1.6%	-1.0%	-3.4%	-1.6%	-1.1%						
	6-5	-0.1%	-1.3%	2.6%	-0.1%	-1.3%	-4.5%	-2.3%	-2.6%						
Mn/DOT Bridge No. 27998															
Girder															
Span Loaded	Middle of Span					Left Support					Right Support				
	Vertical Deflection	Torsional Rotation	Flexural Moment	Bottom Flange Stress		Flexural Shear	Flexural Moment	Bottom Flange Stress		Flexural Shear	Flexural Moment	Bottom Flange Stress		Flexural Shear	Flexural Moment
G1	I	6.1%	5.6%	0.2%	1.8%	0.7%	0.3%	Pinned	Pinned	Pinned	0.0%	-0.4%	1.6%	0.0%	
	II	5.8%	5.1%	0.1%	1.5%	1.6%	0.0%	-0.4%	1.6%	3.6%	0.4%	Pinned	Pinned	Pinned	
G2	I	6.1%	4.6%	-0.6%	0.5%	-0.8%	-0.3%	Pinned	Pinned	Pinned	-0.1%	-0.3%	1.4%	2.3%	
	II	5.7%	4.1%	-0.8%	1.2%	0.0%	-0.1%	-0.3%	1.4%	-19.2%	0.7%	Pinned	Pinned	Pinned	
G3	I	6.1%	3.7%	-0.8%	0.7%	0.0%	-0.3%	Pinned	Pinned	Pinned	0.1%	0.0%	1.7%	0.0%	
	II	5.3%	3.1%	-0.4%	0.8%	0.0%	-0.8%	0.0%	1.7%	5.8%	0.3%	Pinned	Pinned	Pinned	
G4	I	5.4%	2.5%	-0.9%	0.4%	-1.9%	-0.4%	Pinned	Pinned	Pinned	-0.1%	-0.4%	1.2%	-1.0%	
	II	4.6%	2.1%	-1.3%	0.0%	-1.0%	-0.2%	-0.4%	1.2%	-1.0%	-0.2%	Pinned	Pinned	Pinned	
X - shaped Diaphragm															
Span Loaded	Axial Forces between G1 and G2					Axial Forces between G2 and G3					Axial Forces between G3 and G4				
	Top	Bottom	U1-L2	L1-U2		Top	Bottom	U2-L3	L2-U3		Top	Bottom	U3-L4	L3-U4	
All Members in Span	I	14.8%	5.4%	4.8%	0.2%	10.6%	4.3%	4.5%	0.7%	16.2%	4.0%	5.4%	4.7%		
	II	13.7%	3.4%	0.9%	4.0%	9.4%	2.7%	0.5%	3.9%	4.7%	-2.8%	4.2%	3.4%		
Only Members near Midspan	I	14.8%	-6.7%	2.3%	-0.5%	10.6%	-5.5%	0.7%	0.7%	16.2%	-5.1%	0.6%	1.8%		
	II	13.7%	-4.5%	0.9%	-1.0%	9.4%	-7.5%	0.5%	0.4%	18.1%	-5.2%	0.2%	1.5%		
FHWA Test Specimen															
Girder															
Span Loaded	Middle of Span					Left Support					Right Support				
	Vertical Deflection	Torsional Rotation	Flexural Moment	Bottom Flange Stress		Flexural Shear	Flexural Moment	Bottom Flange Stress		Flexural Shear	Flexural Moment	Bottom Flange Stress		Flexural Shear	Flexural Moment
G1	1	4.1%	4.9%	0.0%	1.0%	0.1%	0.0%	Pinned	Pinned	Pinned	0.0%	Pinned	Pinned	Pinned	Pinned
	1	5.2%	4.1%	-0.2%	0.6%	0.2%	-0.2%	Pinned	Pinned	Pinned	-0.2%	Pinned	Pinned	Pinned	Pinned
	1	4.7%	3.2%	-0.4%	0.7%	-1.0%	-0.3%	Pinned	Pinned	Pinned	-0.3%	Pinned	Pinned	Pinned	Pinned
K - shaped Diaphragm															
Span Loaded	Axial Forces between G1 and G2					Axial Forces between G2 and G3					Axial Forces between G3 and G4				
	Top	Bottom 1	Bottom 2	U1-M	M-U2	Top	Bottom 2	Bottom 3	U2-M	M-U3					
All Members in Span	1	8.9%	-0.4%	-0.2%	0.8%	0.9%	4.6%	0.0%	-0.9%	0.2%	0.3%				
	1	8.9%	-0.4%	-0.2%	0.8%	0.9%	4.6%	0.0%	-0.9%	0.2%	0.3%				
Only Members near Midspan	1	8.9%	-0.4%	-0.2%	0.8%	0.9%	4.6%	0.0%	-0.9%	0.2%	0.3%				

Table 8-28: Study 13 Modular Ratio Plus 2

Study 14: Radius of Curvature															
Percent Change for Maximum Responses from Analysis using: Base Model to: Modified Model with radius of curvature 10 times greater															
Mn/DOT Bridge No. 69824															
Girder															
Span Loaded	Middle of Span					Left Support					Right Support				
	Vertical Deflection	Torsional Rotation	Flexural Moment	Bottom Flange Stress		Flexural Shear	Flexural Moment	Bottom Flange Stress		Flexural Shear	Flexural Moment	Bottom Flange Stress		Flexure	Warping
GC	10-9	12.2%	-181.5%	5.5%	5.1%	-78.4%	4.9%	Pinned	Pinned	Pinned	3.1%	5.3%	5.4%	-70.7%	
	9-8	13.8%	-181.7%	5.8%	5.5%	-78.1%	1.8%	5.3%	5.4%	-70.7%	2.1%	5.9%	5.6%	-125.6%	
	8-7	19.3%	-206.0%	8.9%	10.1%	-77.3%	2.1%	5.9%	5.6%	-66.7%	2.0%	5.8%	5.4%	-72.2%	
	7-6	13.3%	-183.3%	5.7%	5.4%	-77.8%	2.0%	5.8%	5.4%	-125.9%	1.1%	3.0%	2.9%	-64.3%	
	6-5	4.6%	-204.7%	2.2%	2.0%	-55.2%	-0.1%	3.0%	2.9%	-64.3%	1.1%	Pinned	Pinned	Pinned	Pinned
GA	10-9	-12.8%	-25.7%	-5.0%	-4.8%	-100.9%	-4.3%	Pinned	Pinned	Pinned	-3.1%	-4.8%	-4.9%	-103.3%	
	9-8	-13.4%	-24.8%	-4.3%	-4.2%	-102.2%	-1.9%	-4.8%	-4.9%	-93.5%	-0.7%	-4.2%	-4.3%	-93.3%	
	8-7	-13.7%	-191.2%	-2.4%	-4.4%	-94.5%	-0.7%	-4.2%	-6.4%	-93.5%	-0.6%	-4.2%	-5.4%	-109.8%	
	7-6	-12.6%	-24.0%	-4.0%	-3.6%	-102.1%	-0.6%	-4.2%	-4.2%	-93.2%	-0.6%	-2.7%	-2.8%	-93.4%	
	6-5	-4.0%	-9.7%	-1.9%	-1.8%	-130.0%	-0.2%	-2.7%	-2.8%	-96.7%	-1.0%	Pinned	Pinned	Pinned	Pinned
Beam Diaphragm and Lateral Wind Bracing															
Span Loaded	Diaphragm Forces at Girder C					Diaphragm Forces at Girder A					Lateral Wind Bracing Forces				
	Axial	Shear	Moment	Axial	Shear	Moment	Axial	Shear	Moment	Axial	Axial Tension	Axial Compression			
All Members in Span	10-9	-14.5%	-32.0%	-169.7%	-14.5%	-32.0%	-33.2%	-20.1%	-22.3%						
	9-8	-184.7%	-35.3%	-30.2%	-184.7%	-35.3%	-40.5%	-18.7%	-23.3%						
	8-7	23.3%	-39.6%	-35.2%	23.3%	-39.6%	-44.7%	-10.4%	-23.2%						
	7-6	-12.8%	-30.1%	-24.5%	-12.8%	-30.1%	-165.1%	-18.3%	-22.9%						
	6-5	-5.1%	-22.7%	-20.0%	-5.1%	-22.7%	-175.5%	-5.7%	-7.4%						
Only Members near Midspan	10-9	-14.5%	-36.0%	-33.1%	-14.5%	-36.0%	-169.7%	-9.1%	-27.1%						
	9-8	-13.3%	-35.8%	-33.0%	-13.3%	-35.8%	-168.5%	-13.6%	-24.1%						
	8-7	23.3%	-39.6%	-35.2%	23.3%	-39.6%	-44.7%	24.7%	-18.4%						
	7-6	-12.8%	-36.2%	-33.5%	-12.8%	-36.2%	-167.8%	-13.1%	-23.8%						
	6-5	-5.1%	-12.0%	-208.2%	-5.1%	-12.0%	-10.1%	-5.5%	-7.3%						
Mn/DOT Bridge No. 27998															
Span Loaded	Middle of Span					Left Support					Right Support				
	Vertical Deflection	Torsional Rotation	Flexural Moment	Bottom Flange Stress		Flexural Shear	Flexural Moment	Bottom Flange Stress		Flexural Shear	Flexural Moment	Bottom Flange Stress		Flexure	Warping
G1	I	82.2%	-257.2%	43.6%	44.0%	-64.3%	46.9%	Pinned	Pinned	Pinned	10.2%	21.3%	21.6%	-75.9%	
	II	63.8%	-210.0%	31.5%	31.1%	-63.9%	10.2%	21.3%	21.6%	-78.2%	16.8%	Pinned	Pinned	Pinned	Pinned
G2	I	54.7%	-253.0%	26.4%	26.1%	-63.6%	44.7%	Pinned	Pinned	Pinned	7.9%	18.3%	17.9%	-45.5%	
	II	40.1%	-207.1%	19.2%	19.3%	-46.2%	7.9%	18.3%	17.9%	-13.7%	25.0%	Pinned	Pinned	Pinned	Pinned
G3	I	-32.2%	-245.4%	-1.5%	-1.5%	-54.9%	14.9%	Pinned	Pinned	Pinned	-211.5%	-9.1%	-9.2%	-162.5%	
	II	-32.1%	-202.2%	1.1%	0.8%	-48.8%	-11.3%	-9.1%	-9.2%	69.2%	16.6%	Pinned	Pinned	Pinned	Pinned
G4	I	-45.7%	-237.6%	-22.8%	-22.9%	-96.1%	-26.5%	Pinned	Pinned	Pinned	-21.3%	-16.5%	-16.5%	-202.1%	
	II	-41.3%	-197.1%	-17.2%	-17.1%	-62.5%	-9.9%	-16.5%	-16.5%	-70.8%	-17.2%	Pinned	Pinned	Pinned	Pinned
X - shaped Diaphragm															
Span Loaded	Axial Forces between G1 and G2					Axial Forces between G2 and G3					Axial Forces between G3 and G4				
	Top	Bottom	U1-L2	L1-U2		Top	Bottom	U2-L3	L2-U3		Top	Bottom	U3-L4	L3-U4	
All Members in Span	I	-267.7%	81.7%	79.6%	70.0%	-236.2%	76.8%	57.7%	-51.9%	-265.6%	72.7%	-14.4%	-50.1%		
	II	-213.5%	-44.2%	-245.8%	1.5%	-192.5%	-0.4%	-23.7%	-38.1%	-39.7%	11.0%	-43.4%	-42.0%		
Only Members near Midspan	I	-267.7%	-248.5%	-128.4%	-79.6%	-236.2%	-52.1%	-110.5%	-75.1%	-205.6%	-75.3%	-86.0%	-65.4%		
	II	-213.5%	-200.5%	-134.7%	-78.2%	-192.5%	-66.6%	-89.3%	-75.0%	-169.1%	-90.0%	-75.7%	-59.9%		
FHWA Test Specimen															
Span Loaded	Middle of Span					Left Support					Right Support				
	Vertical Deflection	Torsional Rotation	Flexural Moment	Bottom Flange Stress		Flexural Shear	Flexural Moment	Bottom Flange Stress		Flexural Shear	Flexural Moment	Bottom Flange Stress		Flexure	Warping
G1	1	64.0%	-169.6%	47.7%	47.7%	-78.7%	25.6%	Pinned	Pinned	Pinned	21.2%	Pinned	Pinned	Pinned	Pinned
	1	-34.3%	-164.4%	12.5%	12.4%	-72.0%	8.9%	Pinned	Pinned	Pinned	7.6%	Pinned	Pinned	Pinned	Pinned
	1	-49.0%	-158.2%	-25.5%	-25.4%	-93.2%	-16.9%	Pinned	Pinned	Pinned	-16.1%	Pinned	Pinned	Pinned	Pinned
K - shaped Diaphragm															
Span Loaded	Axial Forces between G1 and G2					Axial Forces between G2 and G3					Axial Forces between G3 and G4				
	Top	Bottom 1	Bottom 2	U1-M	M-U2	Top	Bottom 2	Bottom 3	U2-M	M-U3					
All Members in Span	1	-148.5%	-92.1%	-95.2%	-90.5%	-90.5%	-152.2%	-91.4%	-93.2%	-86.8%	-86.7%				
	1	-148.5%	-92.1%	-95.2%	-90.5%	-90.5%	-152.2%	-91.4%	-93.2%	-86.8%	-86.7%				

Table 8-29: Study 14 Radius of Curvature 10 Times Greater

Study 15: Longitudinal Load Distribution and Stress Calculation													
Percent Change for Maximum Responses from Analysis using: Base Model to: Modified Model NC-NC													
Mn/DOT Bridge No. 69824													
Girder													
Span Loaded	Middle of Span				Left Support				Right Support				
	Vertical Deflection	Torsional Rotation	Flexural Moment	Bottom Flange Stress	Flexural Shear	Flexural Moment	Bottom Flange Stress	Flexural Shear	Flexural Moment	Flexural Shear	Flexural Moment	Bottom Flange Stress	
GC	10-9	17.9%	29.0%	7.5%	7.1%	11.2%	4.5%	Pinned	Pinned	Pinned	-2.2%	-25.3%	4.6% -8.1%
	9-8	35.5%	48.7%	12.1%	12.2%	16.2%	-4.2%	-25.3%	4.6%	-8.1%	-4.6%	-15.0%	7.6% 3.0%
	8-7	32.8%	54.4%	13.5%	14.1%	16.8%	-4.6%	-15.0%	7.6%	3.0%	-5.2%	-15.8%	7.6% -8.9%
	7-6	33.7%	48.0%	10.9%	11.0%	14.8%	-5.2%	-15.8%	7.6%	-8.9%	-7.0%	-27.3%	4.3% 2.4%
	6-5	19.2%	28.4%	14.7%	10.4%	25.4%	-6.2%	-27.3%	4.3%	2.4%	5.9%	Pinned	Pinned Pinned
GA	10-9	21.1%	25.9%	9.0%	8.9%	14.2%	6.5%	Pinned	Pinned	Pinned	-0.5%	-20.5%	4.9% -32.2%
	9-8	39.8%	44.8%	14.9%	15.0%	47.3%	2.2%	-20.5%	4.9%	-24.2%	0.1%	-9.1%	9.2% -167.6%
	8-7	41.1%	51.2%	16.6%	19.3%	84.9%	0.1%	-9.1%	9.2%	-37.8%	1.1%	-9.5%	8.7% -33.3%
	7-6	38.3%	44.0%	13.8%	14.1%	43.6%	1.1%	-9.5%	8.7%	-33.3%	2.2%	-22.8%	5.3% -77.0%
	6-5	19.2%	24.4%	14.4%	10.5%	80.0%	-194.1%	-22.8%	5.3%	-34.4%	6.1%	Pinned	Pinned Pinned
Beam Diaphragm and Lateral Wind Bracing													
Span Loaded	Diaphragm Forces at Girder C			Diaphragm Forces at Girder A			Lateral Wind Bracing Forces						
	Axial	Shear	Moment	Axial	Shear	Moment	Axial Tension	Axial Compression					
All Members in Span	10-9	8.8%	-209.0%	9.8%	8.8%	-209.0%	8.5%	2.0%					-1.2%
	9-8	-217.3%	26.8%	-220.4%	-217.3%	26.8%	37.6%	31.1%					37.8%
	8-7	20.3%	-221.4%	13.4%	20.3%	-221.4%	-236.7%	22.8%					25.0%
	7-6	25.7%	21.8%	17.8%	25.7%	21.8%	33.3%	31.2%					38.0%
	6-5	9.0%	39.9%	-230.2%	9.0%	39.9%	53.5%	18.6%					8.9%
Only Members near Midspan	10-9	8.8%	9.9%	9.8%	8.8%	9.9%	10.0%	4.4%					3.6%
	9-8	20.0%	14.3%	14.3%	20.0%	14.3%	16.5%	18.4%					23.0%
	8-7	20.3%	12.6%	13.2%	20.3%	12.6%	11.9%	21.2%					28.2%
	7-6	25.7%	13.5%	13.4%	25.7%	13.5%	13.7%	15.1%					20.7%
	6-5	9.0%	-317.2%	141.1%	9.0%	-317.2%	-301.4%	-24.2%					51.0%
Mn/DOT Bridge No. 27998													
Girder													
Span Loaded	Middle of Span				Left Support				Right Support				
	Vertical Deflection	Torsional Rotation	Flexural Moment	Bottom Flange Stress	Flexural Shear	Flexural Moment	Bottom Flange Stress	Flexural Shear	Flexural Moment	Flexural Shear	Flexural Moment	Bottom Flange Stress	
G1	I	5.5%	8.4%	1.9%	2.2%	0.7%	1.1%	Pinned	Pinned	Pinned	-6.5%	-18.4%	0.5% -219.5%
	II	8.9%	7.3%	3.1%	2.9%	3.3%	-6.5%	-18.4%	0.5%	3.6%	1.3%	Pinned	Pinned
G2	I	6.5%	8.3%	2.5%	2.2%	0.8%	1.7%	Pinned	Pinned	Pinned	-8.5%	-18.5%	0.0% 2.3%
	II	10.4%	8.4%	3.0%	3.0%	1.7%	-8.5%	-18.5%	0.0%	8.2%	1.8%	Pinned	Pinned
G3	I	9.2%	8.1%	4.2%	4.4%	9.9%	2.2%	Pinned	Pinned	Pinned	-2.8%	-13.5%	3.3% -31.3%
	II	9.0%	11.4%	3.2%	3.2%	28.0%	-12.4%	-13.5%	3.3%	17.3%	1.8%	Pinned	Pinned
G4	I	8.6%	7.3%	5.6%	5.4%	11.7%	4.4%	Pinned	Pinned	Pinned	-4.1%	-9.3%	6.5% -231.3%
	II	9.3%	8.7%	2.4%	2.4%	37.5%	-1.6%	-9.3%	6.5%	-19.8%	1.2%	Pinned	Pinned
X-shaped Diaphragm													
Span Loaded	Axial Forces between G1 and G2				Axial Forces between G2 and G3				Axial Forces between G3 and G4				
	Top	Bottom	U1-L2	L1-U2	Top	Bottom	U2-L3	L2-U3	Top	Bottom	U3-L4	L3-U4	
All Members in Span	I	9.5%	11.3%	12.8%	12.4%	6.2%	13.1%	20.4%	1.8%	349.9%	13.1%	15.6%	13.5% 9.3%
	II	33.2%	21.0%	20.0%	20.3%	-507.6%	12.7%	15.3%	13.7%	8.5%	20.5%	9.5%	
Only Members near Midspan	I	9.5%	-0.9%	2.0%	5.0%	6.2%	0.5%	3.7%	1.8%	5.2%	3.1%	15.6%	1.4% 7.4%
	II	7.7%	9.3%	20.0%	2.3%	18.7%	51.0%	15.3%	3.7%	24.5%	20.5%	6.2%	

Table 8-30: Study 15 Longitudinal Load Distribution and Stress Calculation NC-NC

Study 15: Longitudinal Load Distribution and Stress Calculation													
Percent Change for Maximum Responses from Analysis using: Base Model to: Modified Model C-NC													
Mn/DOT Bridge No. 69824													
Girder													
Span Loaded		Middle of Span				Left Support				Right Support			
		Vertical Deflection	Torsional Rotation	Flexural Moment	Bottom Flange Stress	Flexural Shear	Flexural Moment	Bottom Flange Stress	Flexural Shear	Flexural Moment	Bottom Flange Stress	Flexure	Warping
GC	10-9	0.0%	0.0%	0.0%	0.0%	0.0%	Pinned	Pinned	Pinned	0.0%	0.0%	40.1%	0.0%
	9-8	0.0%	0.0%	0.0%	0.0%	0.0%	0.0%	40.1%	0.0%	0.0%	0.0%	26.3%	-1.5%
	8-7	0.0%	0.0%	0.0%	0.0%	0.0%	0.0%	26.3%	-1.5%	0.0%	0.0%	27.4%	0.0%
	7-6	0.0%	0.0%	0.0%	0.0%	0.0%	0.0%	27.4%	0.0%	0.0%	0.0%	43.6%	1.2%
	6-5	0.0%	0.0%	0.0%	0.0%	0.0%	0.0%	43.6%	1.2%	0.0%	Pinned	Pinned	Pinned
GA	10-9	0.0%	0.0%	0.0%	0.0%	0.0%	Pinned	Pinned	Pinned	0.0%	0.0%	37.2%	0.0%
	9-8	0.0%	0.0%	0.0%	0.0%	0.0%	0.0%	37.2%	0.0%	0.0%	0.0%	20.5%	0.0%
	8-7	0.0%	0.0%	0.0%	0.0%	0.0%	0.0%	20.5%	0.0%	0.0%	0.0%	25.1%	0.0%
	7-6	0.0%	0.0%	0.0%	0.0%	0.0%	0.0%	25.1%	0.0%	0.0%	0.0%	37.1%	0.0%
	6-5	0.0%	0.0%	0.0%	0.0%	0.0%	0.0%	37.1%	0.0%	0.0%	Pinned	Pinned	Pinned
Beam Diaphragm and Lateral Wind Bracing													
Span Loaded		Diaphragm Forces at Girder C			Diaphragm Forces at Girder A			Lateral Wind Bracing Forces					
		Axial	Shear	Moment	Axial	Shear	Moment	Axial Tension	Axial Compression				
All Members in Span	10-9	0.0%	0.0%	0.0%	0.0%	0.0%	0.0%	0.0%	0.0%	0.0%	0.0%	0.0%	0.0%
	9-8	0.0%	0.0%	0.0%	0.0%	0.0%	0.0%	0.0%	0.0%	0.0%	0.0%	0.0%	0.0%
	8-7	0.0%	0.0%	0.0%	0.0%	0.0%	0.0%	0.0%	0.0%	0.0%	0.0%	0.0%	0.0%
	7-6	0.0%	0.0%	0.0%	0.0%	0.0%	0.0%	0.0%	0.0%	0.0%	0.0%	0.0%	0.0%
	6-5	0.0%	0.0%	0.0%	0.0%	0.0%	0.0%	0.0%	0.0%	0.0%	0.0%	0.0%	0.0%
Only Members near Midspan	10-9	0.0%	0.0%	0.0%	0.0%	0.0%	0.0%	0.0%	0.0%	0.0%	0.0%	0.0%	0.0%
	9-8	0.0%	0.0%	0.0%	0.0%	0.0%	0.0%	0.0%	0.0%	0.0%	0.0%	0.0%	0.0%
	8-7	0.0%	0.0%	0.0%	0.0%	0.0%	0.0%	0.0%	0.0%	0.0%	0.0%	0.0%	0.0%
	7-6	0.0%	0.0%	0.0%	0.0%	0.0%	0.0%	0.0%	0.0%	0.0%	0.0%	0.0%	0.0%
	6-5	0.0%	0.0%	0.0%	0.0%	0.0%	0.0%	0.0%	0.0%	0.0%	0.0%	0.0%	0.0%
Mn/DOT Bridge No. 27998													
Girder													
Span Loaded		Middle of Span				Left Support				Right Support			
		Vertical Deflection	Torsional Rotation	Flexural Moment	Bottom Flange Stress	Flexural Shear	Flexural Moment	Bottom Flange Stress	Flexural Shear	Flexural Moment	Bottom Flange Stress	Flexure	Warping
G1	I	0.0%	0.0%	0.0%	0.0%	0.0%	Pinned	Pinned	Pinned	0.0%	0.0%	22.6%	0.0%
	II	0.0%	0.0%	0.0%	0.0%	0.0%	0.0%	22.6%	0.6%	0.0%	Pinned	Pinned	Pinned
G2	I	0.0%	0.0%	0.0%	0.0%	0.0%	Pinned	Pinned	Pinned	0.0%	0.0%	22.8%	0.0%
	II	0.0%	0.0%	0.0%	0.0%	0.0%	0.0%	22.8%	0.0%	0.0%	Pinned	Pinned	Pinned
G3	I	0.0%	0.0%	0.0%	0.0%	0.0%	Pinned	Pinned	Pinned	0.0%	0.0%	20.0%	0.0%
	II	0.0%	0.0%	0.0%	0.0%	0.0%	0.0%	20.0%	0.0%	0.0%	Pinned	Pinned	Pinned
G4	I	0.0%	0.0%	0.0%	0.0%	0.0%	Pinned	Pinned	Pinned	0.0%	0.0%	17.1%	0.0%
	II	0.0%	0.0%	0.0%	0.0%	0.0%	0.0%	17.1%	0.0%	0.0%	Pinned	Pinned	Pinned
X - shaped Diaphragm													
Span Loaded		Axial Forces between G1 and G2				Axial Forces between G2 and G3				Axial Forces between G3 and G4			
		Top	Bottom	U1-L2	L1-U2	Top	Bottom	U2-L3	L2-U3	Top	Bottom	U3-L4	L3-U4
All Members in Span	I	0.0%	0.0%	0.0%	0.0%	0.0%	0.0%	0.0%	0.0%	0.0%	0.0%	0.0%	0.0%
	II	0.0%	0.0%	0.0%	0.0%	0.0%	0.0%	0.0%	0.0%	0.0%	0.0%	0.0%	0.0%
Only Members near Midspan	I	0.0%	0.0%	0.0%	0.0%	0.0%	0.0%	0.0%	0.0%	0.0%	0.0%	0.0%	0.0%
	II	0.0%	0.0%	0.0%	0.0%	0.0%	0.0%	0.0%	0.0%	0.0%	0.0%	0.0%	0.0%

Table 8-31: Study 15 Longitudinal Load Distribution and Stress Calculation C-NC

Study 15: Longitudinal Load Distribution and Stress Calculation															
Percent Change for Maximum Responses from Analysis using: Base Model to: Modified Model C-R															
Mn/DOT Bridge No. 69824															
Girder															
Span Loaded		Middle of Span				Left Support				Right Support					
		Vertical Deflection	Torsional Rotation	Flexural Moment	Bottom Flange Stress	Flexural Shear	Flexural Moment	Bottom Flange Stress	Flexural Shear	Flexural Moment	Bottom Flange Stress	Flexural Shear	Flexural Moment		
		Flexure	Warping	Flexure	Warping	Flexure	Warping	Flexure	Warping	Flexure	Warping	Flexure	Warping		
GC		10-9	0.0%	0.0%	0.0%	0.0%	0.0%	Pinned	Pinned	Pinned	0.0%	0.0%	20.1%	0.0%	
		9-8	0.0%	0.0%	0.0%	0.0%	0.0%	0.0%	20.1%	0.0%	0.0%	0.0%	15.8%	0.0%	
		8-7	0.0%	0.0%	0.0%	0.0%	0.0%	0.0%	15.8%	0.0%	0.0%	0.0%	15.9%	0.0%	
		7-6	0.0%	0.0%	0.0%	0.0%	0.0%	0.0%	15.9%	0.0%	0.0%	0.0%	21.0%	1.2%	
		6-5	0.0%	0.0%	0.0%	0.0%	0.0%	0.0%	21.0%	1.2%	0.0%	0.0%	Pinned	Pinned	
GA		10-9	0.0%	0.0%	0.0%	0.0%	0.0%	0.0%	Pinned	Pinned	Pinned	0.0%	0.0%	17.6%	0.0%
		9-8	0.0%	0.0%	0.0%	0.0%	0.0%	0.0%	0.0%	17.6%	0.0%	0.0%	0.0%	13.2%	0.0%
		8-7	0.0%	0.0%	0.0%	0.0%	0.0%	0.0%	0.0%	13.2%	0.0%	0.0%	0.0%	13.1%	2.6%
		7-6	0.0%	0.0%	0.0%	0.0%	0.0%	0.0%	0.0%	13.1%	2.6%	0.0%	0.0%	19.3%	-1.6%
		6-5	0.0%	0.0%	0.0%	0.0%	0.0%	0.0%	0.0%	19.3%	-1.6%	0.0%	0.0%	Pinned	Pinned
Beam Diaphragm and Lateral Wind Bracing															
Span Loaded		Diaphragm Forces at Girder C			Diaphragm Forces at Girder A			Lateral Wind Bracing Forces							
		Axial	Shear	Moment	Axial	Shear	Moment	Axial Tension	Axial Compression						
All Members in Span		10-9	0.0%	0.0%	0.0%	0.0%	0.0%	0.0%	0.0%	0.0%					
		9-8	0.0%	0.0%	0.0%	0.0%	0.0%	0.0%	0.0%	0.0%					
		8-7	0.0%	0.0%	0.0%	0.0%	0.0%	0.0%	0.0%	0.0%					
		7-6	0.0%	0.0%	0.0%	0.0%	0.0%	0.0%	0.0%	0.0%					
		6-5	0.0%	0.0%	0.0%	0.0%	0.0%	0.0%	0.0%	0.0%					
Mn/DOT Bridge No. 27998															
Girder															
Span Loaded		Middle of Span				Left Support				Right Support					
		Vertical Deflection	Torsional Rotation	Flexural Moment	Bottom Flange Stress	Flexural Shear	Flexural Moment	Bottom Flange Stress	Flexural Shear	Flexural Moment	Bottom Flange Stress	Flexural Shear	Flexural Moment		
		Flexure	Warping	Flexure	Warping	Flexure	Warping	Flexure	Warping	Flexure	Warping	Flexure	Warping		
G1		I	0.0%	0.0%	0.0%	0.0%	0.0%	0.0%	Pinned	Pinned	Pinned	0.0%	0.0%	20.5%	0.0%
		II	0.0%	0.0%	0.0%	0.0%	0.0%	0.0%	0.0%	20.5%	0.6%	0.0%	Pinned	Pinned	
G2		I	0.0%	0.0%	0.0%	0.0%	0.0%	0.0%	Pinned	Pinned	Pinned	0.0%	0.0%	20.0%	0.0%
		II	0.0%	0.0%	0.0%	0.0%	0.0%	0.0%	0.0%	20.0%	0.0%	0.0%	Pinned	Pinned	
G3		I	0.0%	0.0%	0.0%	0.0%	0.0%	0.0%	Pinned	Pinned	Pinned	0.0%	0.0%	18.3%	0.0%
		II	0.0%	0.0%	0.0%	0.0%	0.0%	0.0%	0.0%	18.3%	0.0%	0.0%	Pinned	Pinned	
G4		I	0.0%	0.0%	0.0%	0.0%	0.0%	0.0%	Pinned	Pinned	Pinned	0.0%	0.0%	15.9%	0.0%
		II	0.0%	0.0%	0.0%	0.0%	0.0%	0.0%	0.0%	15.9%	0.0%	0.0%	Pinned	Pinned	
X - shaped Diaphragm															
Span Loaded		Axial Forces between G1 and G2				Axial Forces between G2 and G3				Axial Forces between G3 and G4					
		Top	Bottom	U1-L2	L1-U2	Top	Bottom	U2-L3	L2-U3	Top	Bottom	U3-L4	L3-U4		
All Members in Span		I	0.0%	0.0%	0.0%	0.0%	0.0%	0.0%	0.0%	0.0%	0.0%	0.0%	0.0%	0.0%	
		II	0.0%	0.0%	0.0%	0.0%	0.0%	0.0%	0.0%	0.0%	0.0%	0.0%	0.0%	0.0%	
Only Members near Midspan		I	0.0%	0.0%	0.0%	0.0%	0.0%	0.0%	0.0%	0.0%	0.0%	0.0%	0.0%	0.0%	
		II	0.0%	0.0%	0.0%	0.0%	0.0%	0.0%	0.0%	0.0%	0.0%	0.0%	0.0%	0.0%	

Table 8-32: Study 15 Longitudinal Load Distribution and Stress Calculation C-RC

Mn/DOT Bridge No. 27998 Grillage Model

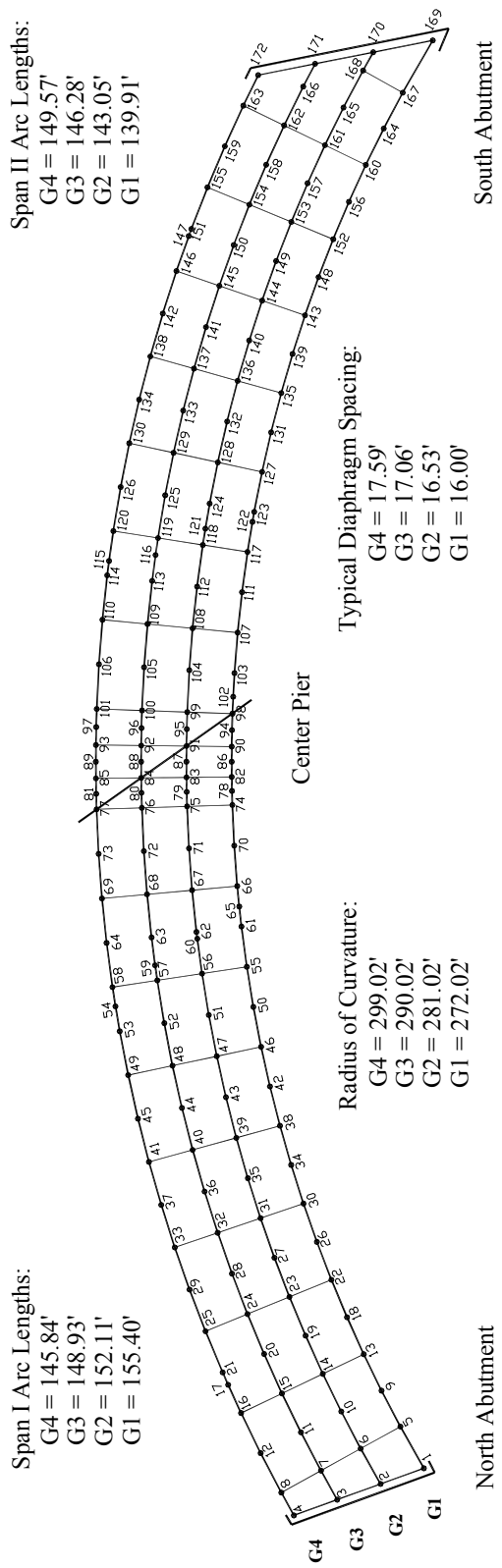


Figure 8-1: Mn/DOT Bridge No. 27998 Grillage Model

FHWA Test Specimen

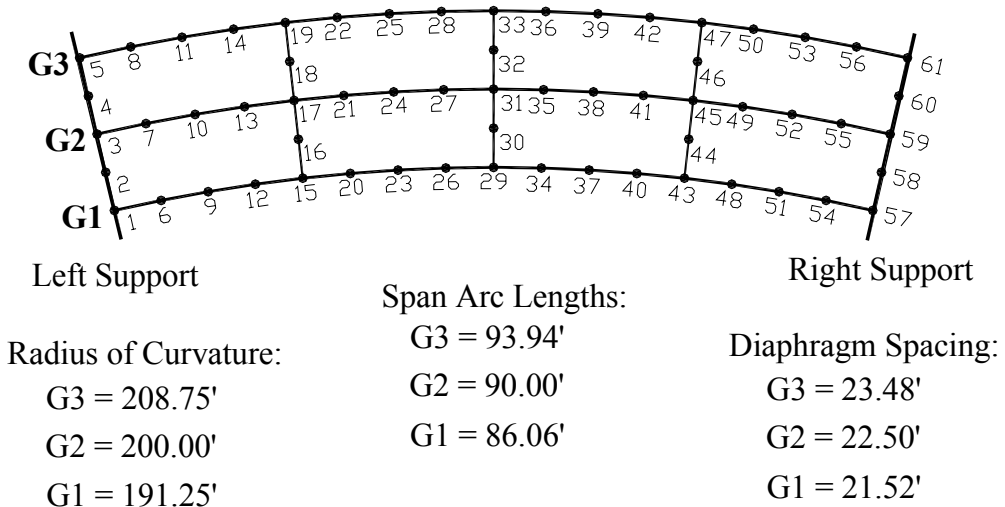


Figure 8-2: FHWA Test Specimen Grillage Model

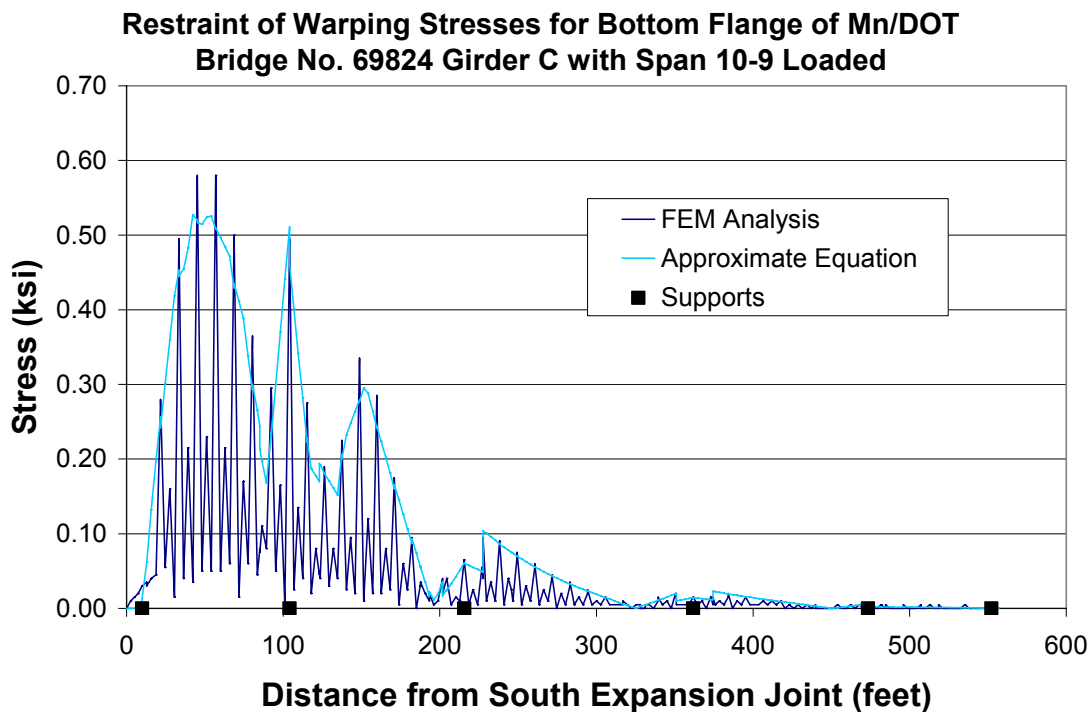


Figure 8-3: Study 16 Warping Stress Comparison Bridge 69824 Girder C Span 10-9 Loaded

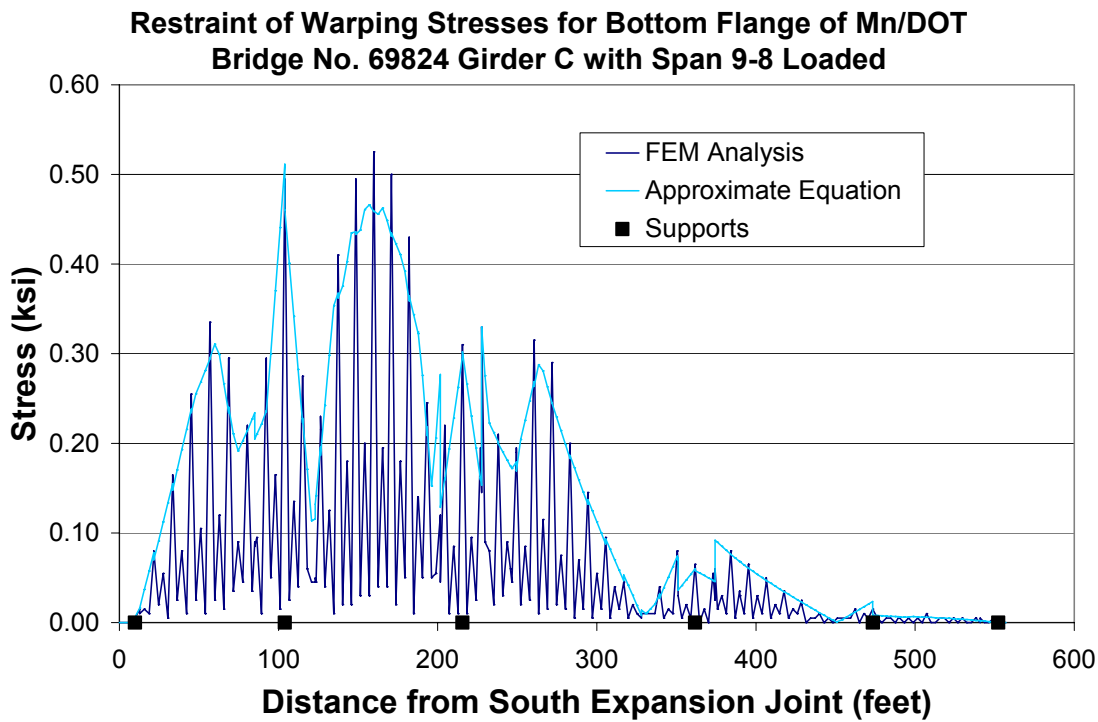


Figure 8-4: Study 16 Warping Stress Comparison Bridge 69824 Girder C Span 9-8 Loaded

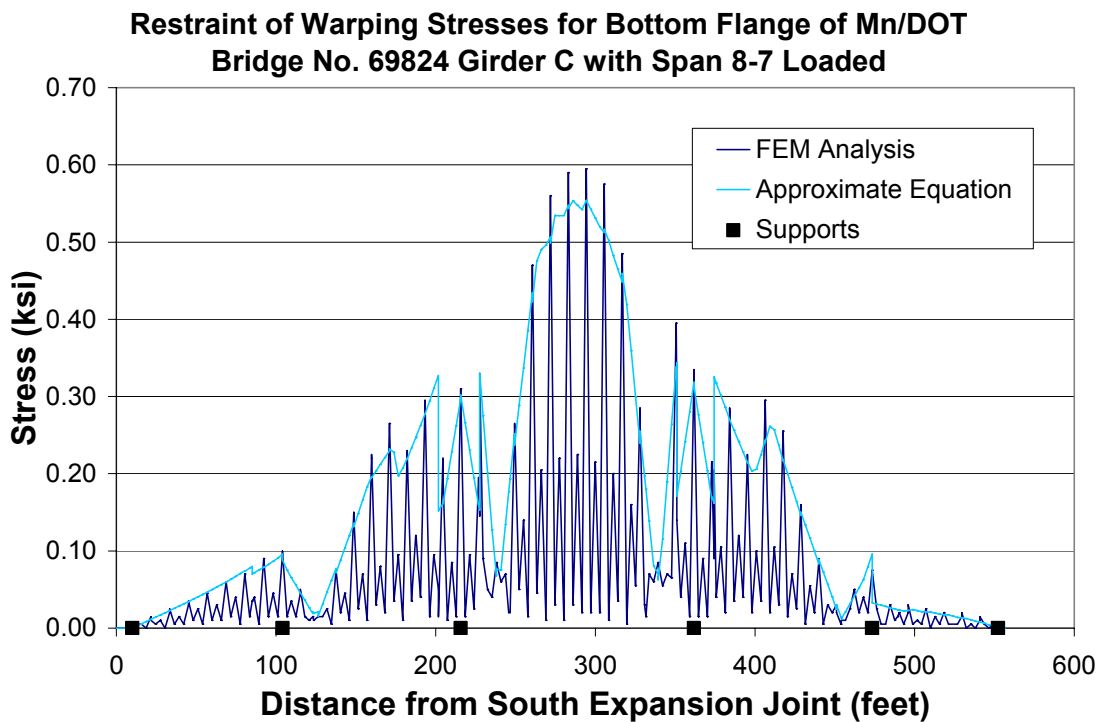


Figure 8-5: Study 16 Warping Stress Comparison Bridge 69824 Girder C Span 8-7 Loaded

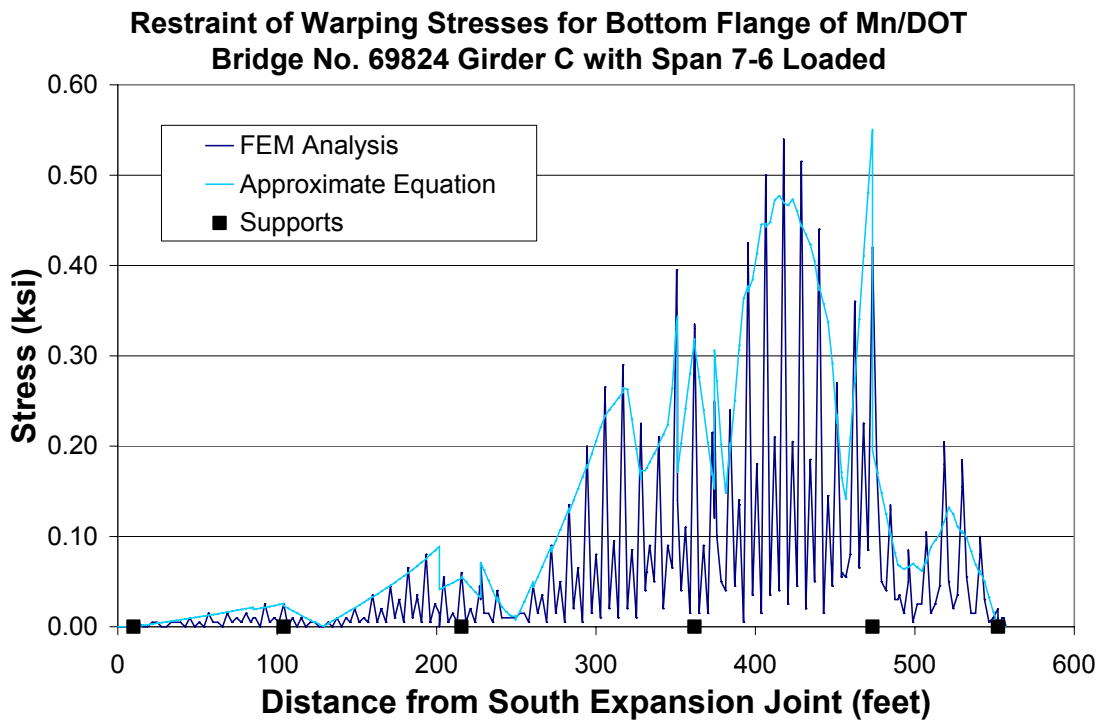


Figure 8-6: Study 16 Warping Stress Comparison Bridge 69824 Girder C Span 7-6 Loaded

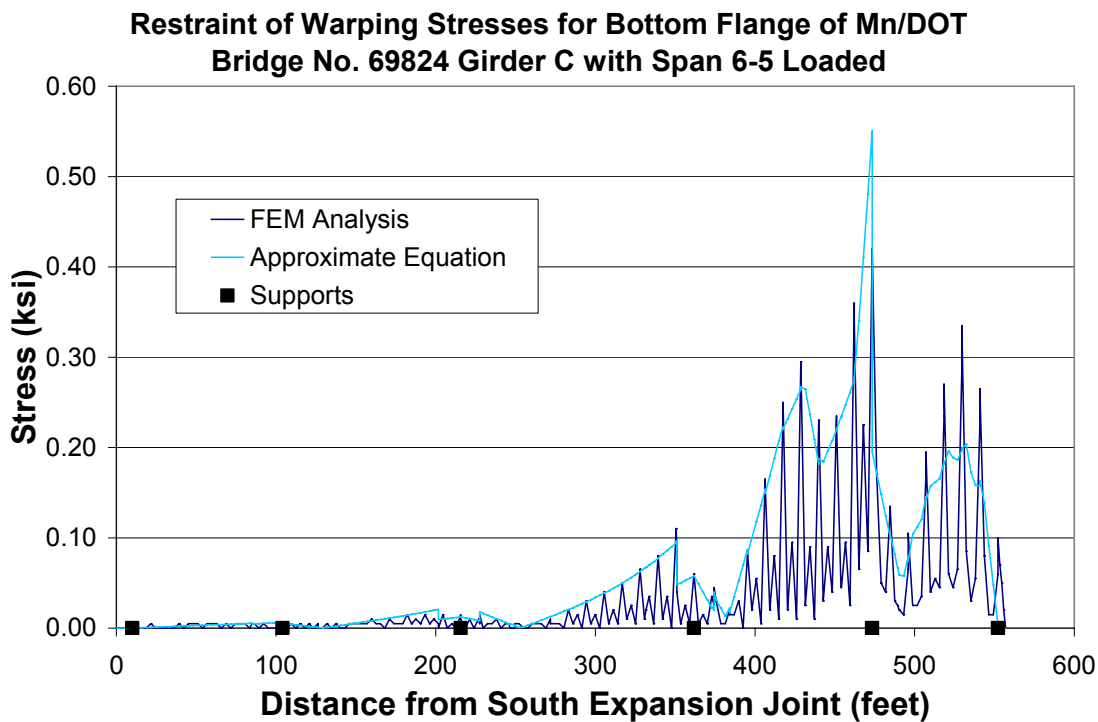


Figure 8-7: Study 16 Warping Stress Comparison Bridge 69824 Girder C Span 6-5 Loaded

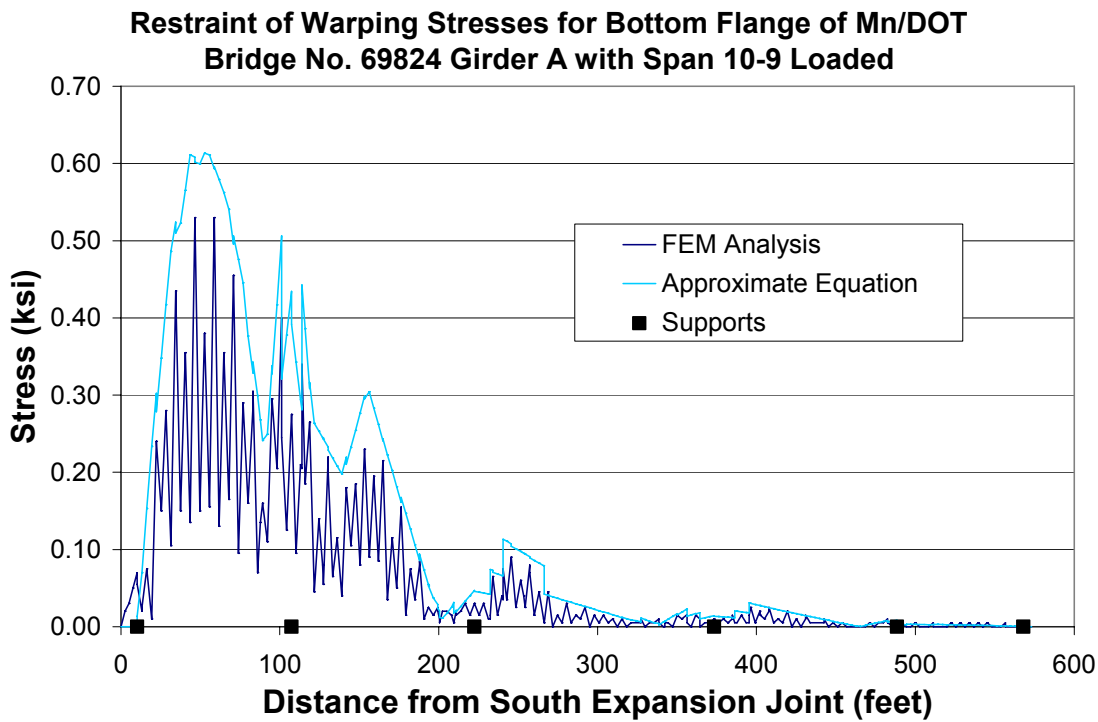


Figure 8-8: Study 16 Warping Stress Comparison Bridge 69824 Girder A Span 10-9 Loaded

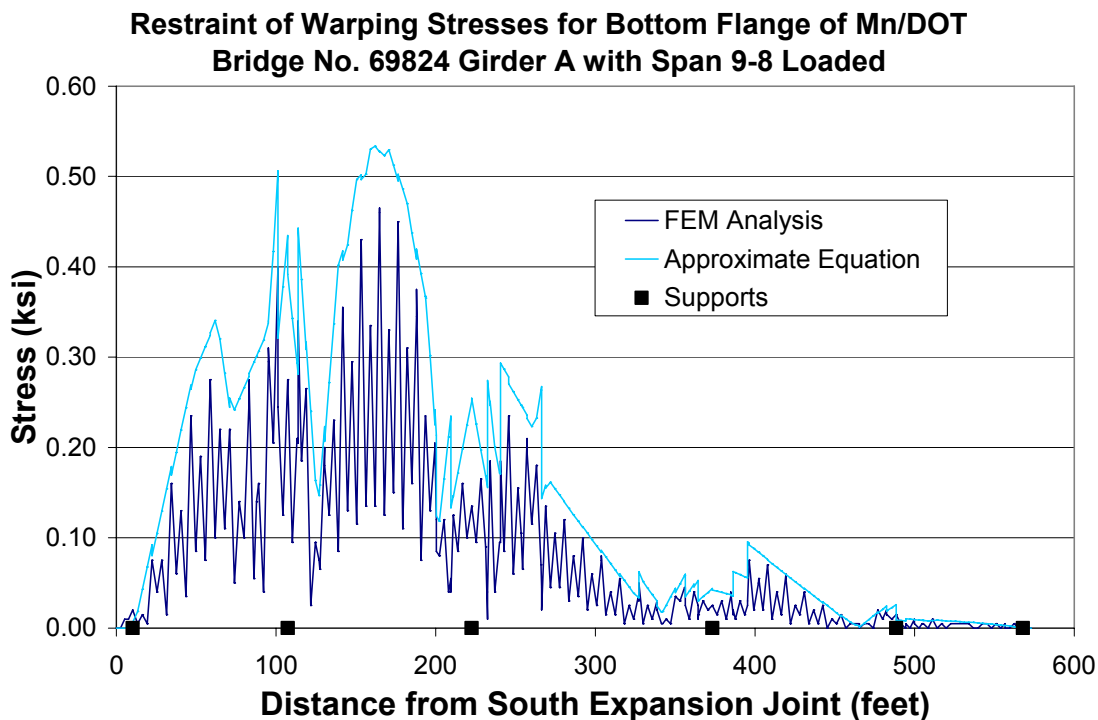


Figure 8-9: Study 16 Warping Stress Comparison Bridge 69824 Girder A Span 9-8 Loaded

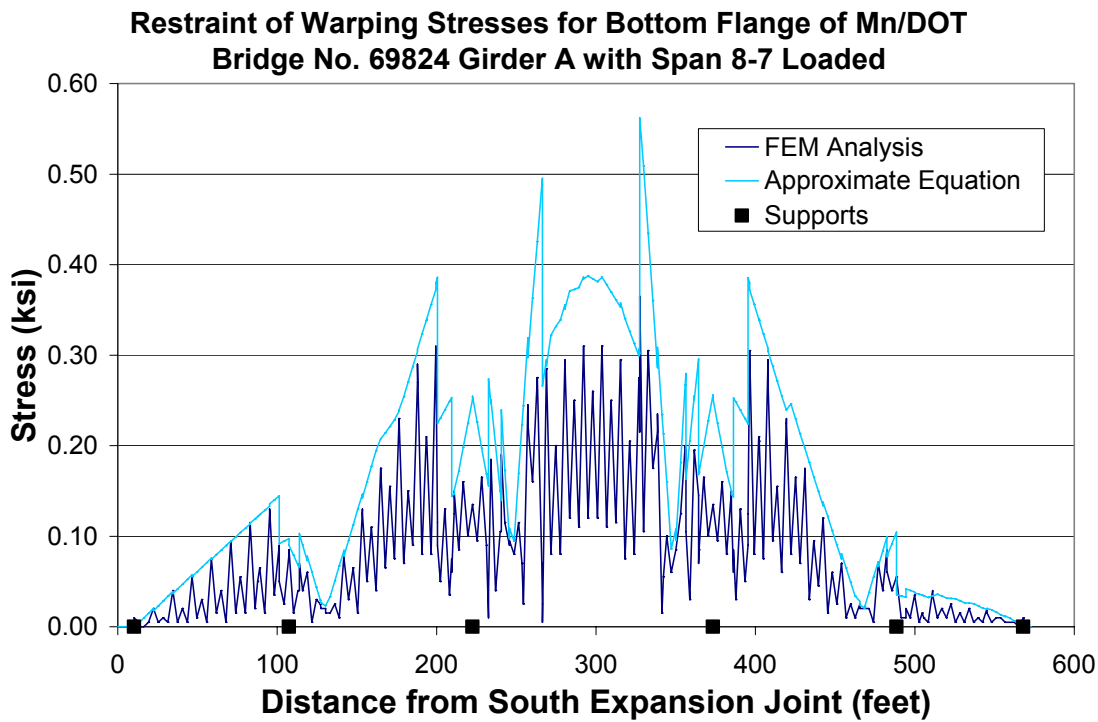


Figure 8-10: Study 16 Warping Stress Comparison Bridge 69824 Girder A Span 8-7 Loaded

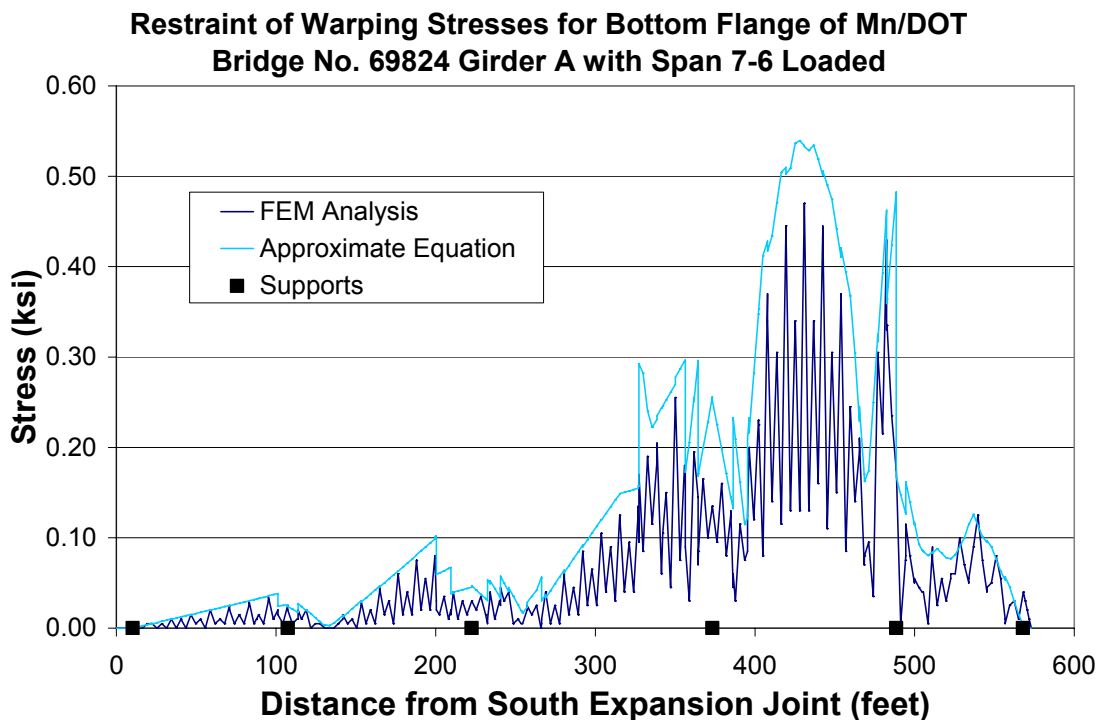


Figure 8-11: Study 16 Warping Stress Comparison Bridge 69824 Girder A Span 7-6 Loaded

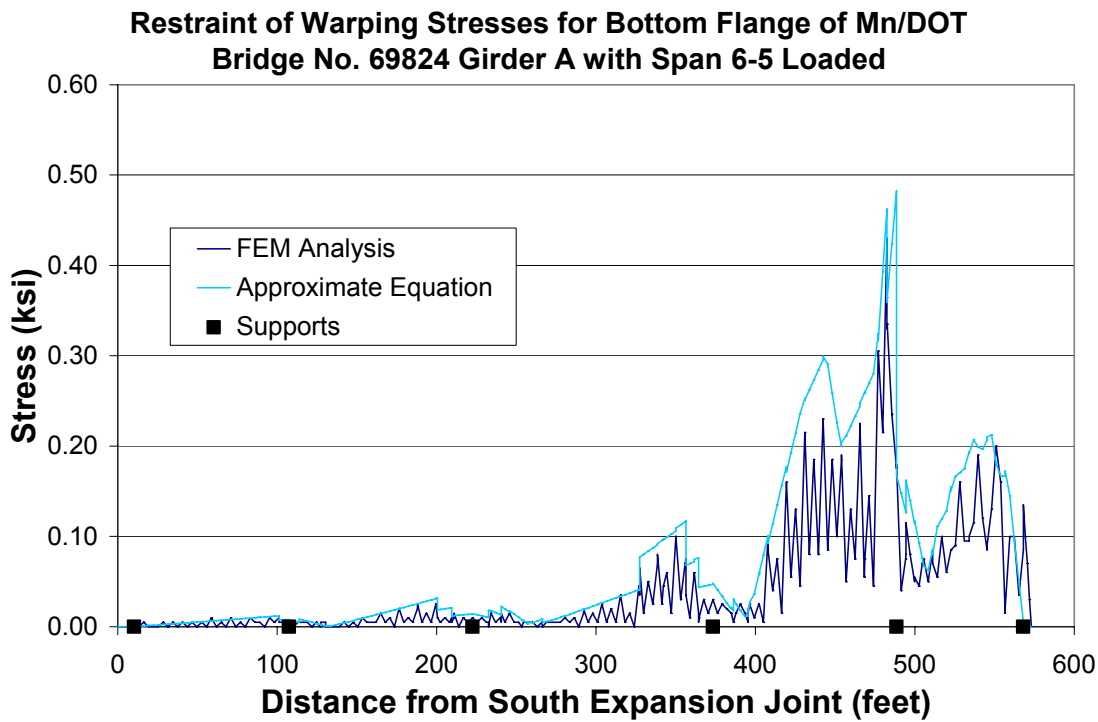


Figure 8-12: Study 16 Warping Stress Comparison Bridge 69824 Girder A Span 6-5 Loaded

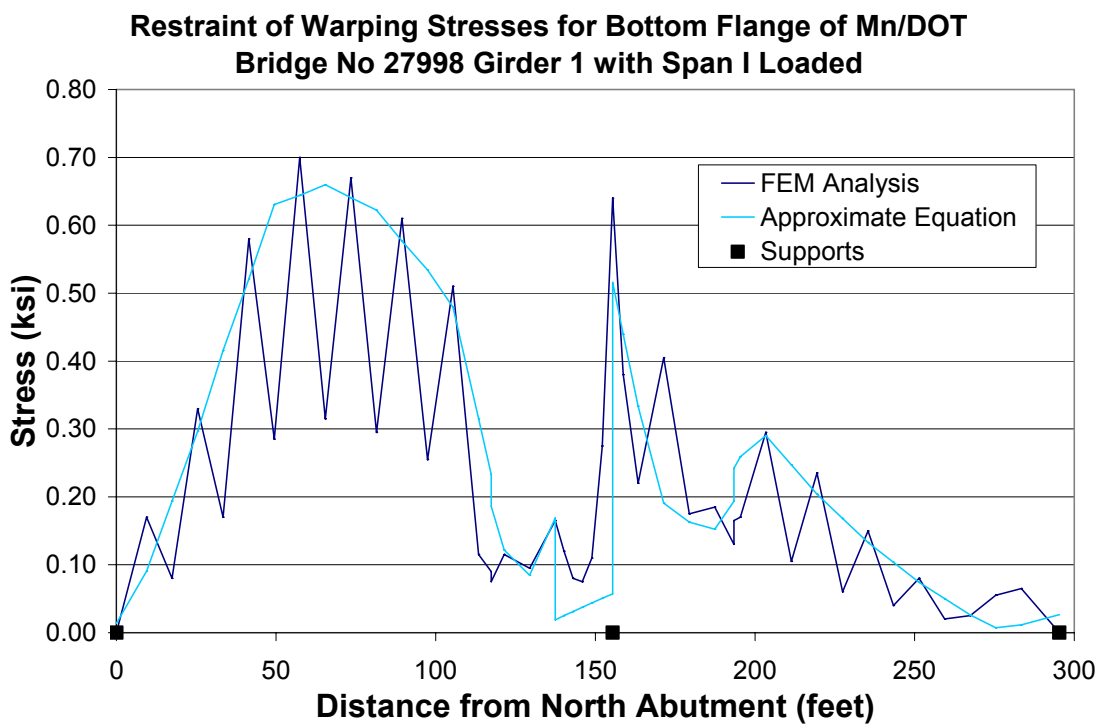


Figure 8-13: Study 16 Warping Stress Comparison Bridge 27998 Girder 1 Span I Loaded

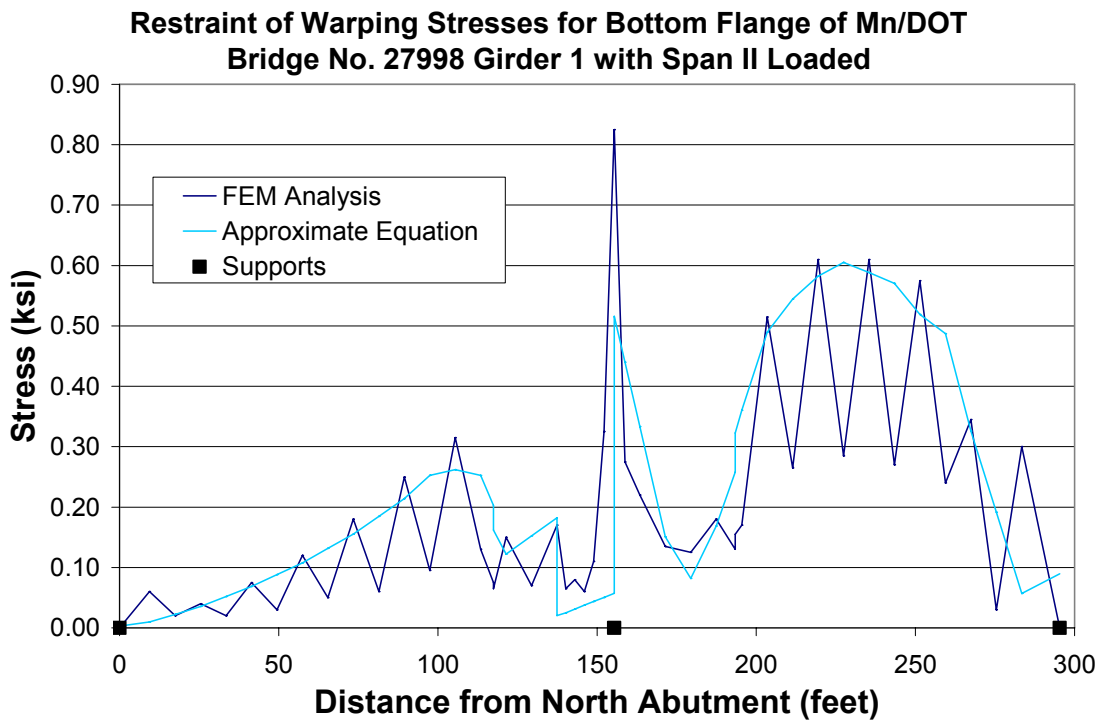


Figure 8-14: Study 16 Warping Stress Comparison Bridge 27998 Girder 1 Span II Loaded

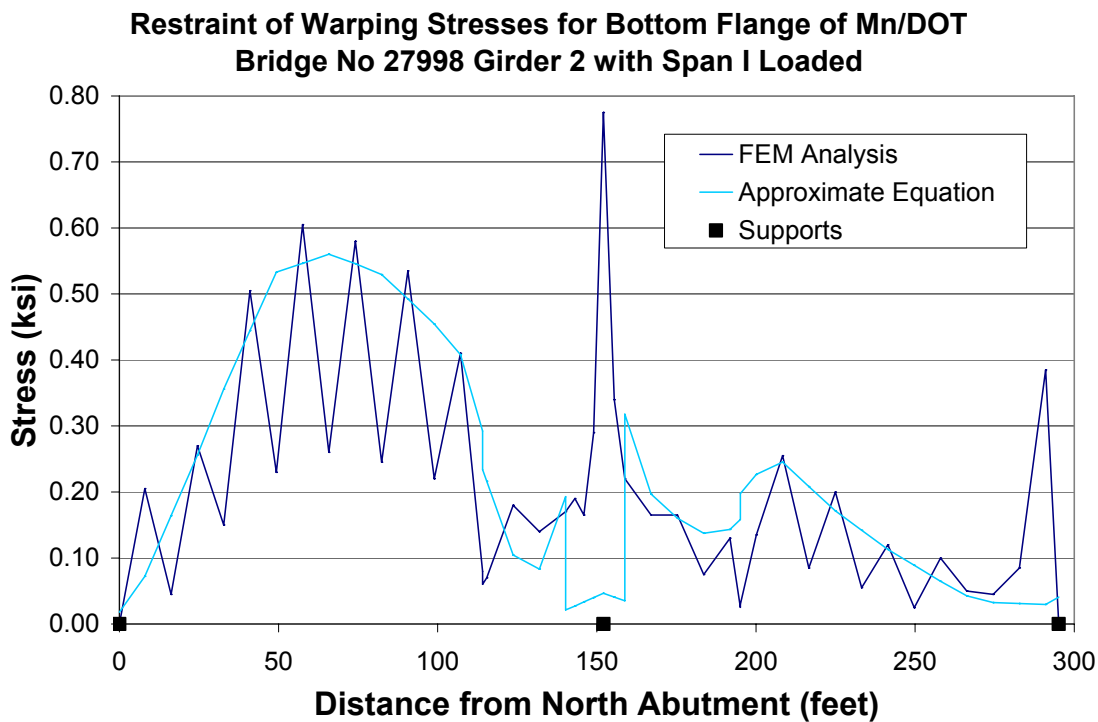


Figure 8-15: Study 16 Warping Stress Comparison Bridge 27998 Girder 2 Span I Loaded

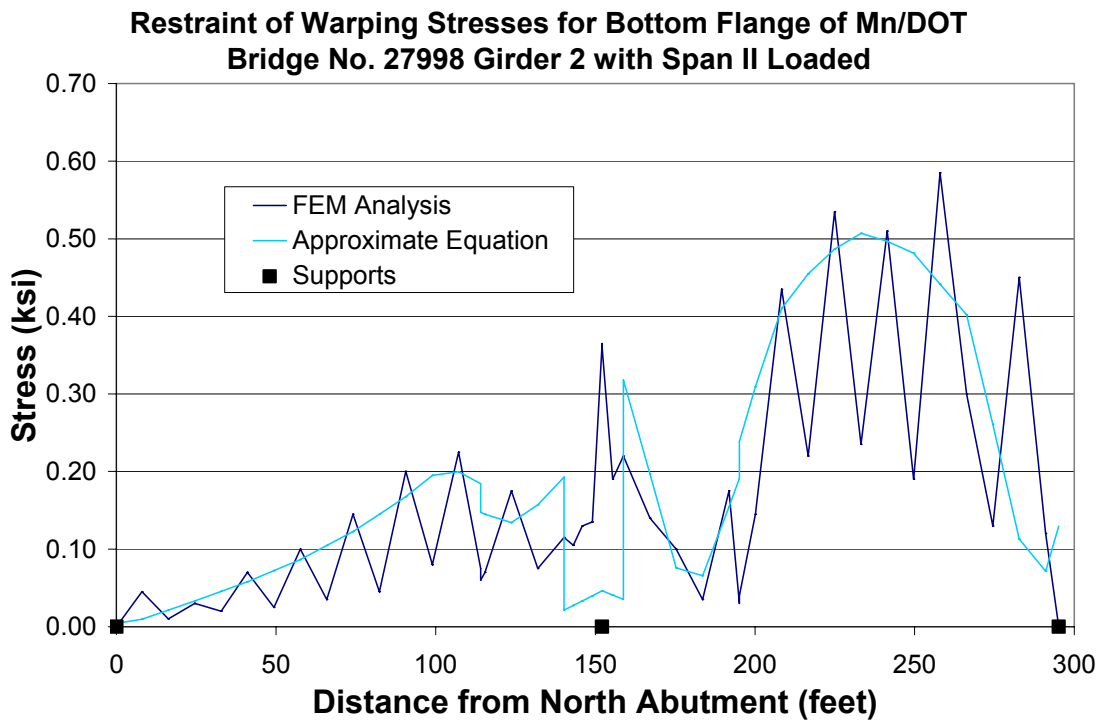


Figure 8-16: Study 16 Warping Stress Comparison Bridge 27998 Girder 2 Span II Loaded

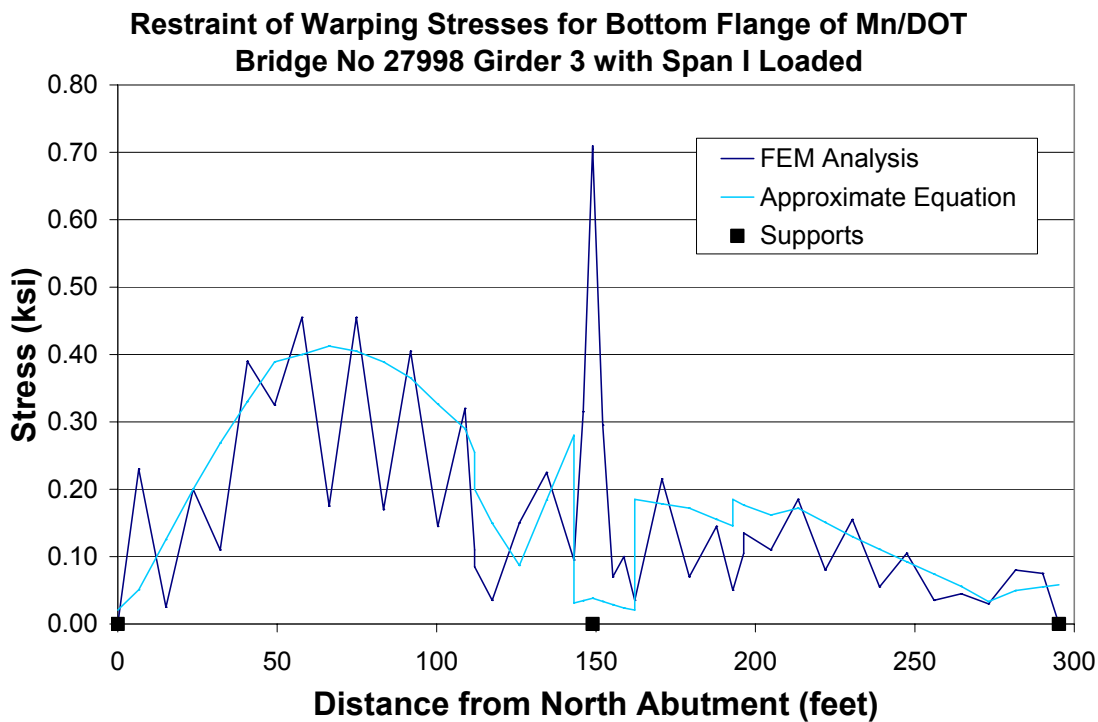


Figure 8-17: Study 16 Warping Stress Comparison Bridge 27998 Girder 3 Span I Loaded

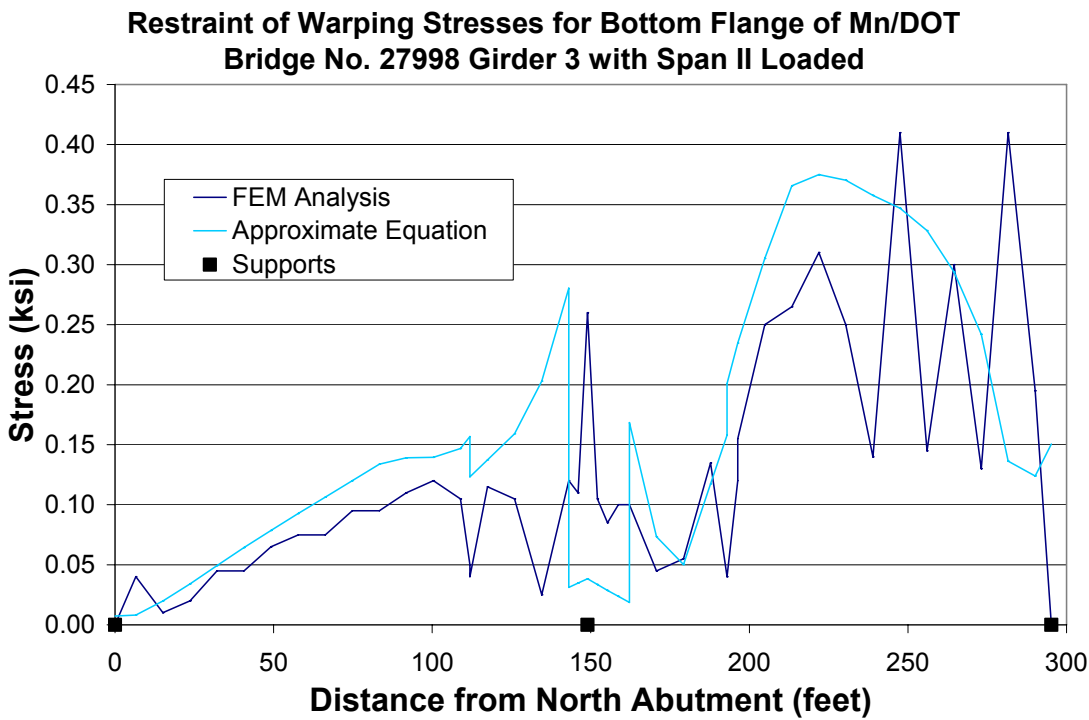


Figure 8-18: Study 16 Warping Stress Comparison Bridge 27998 Girder 3 Span II Loaded

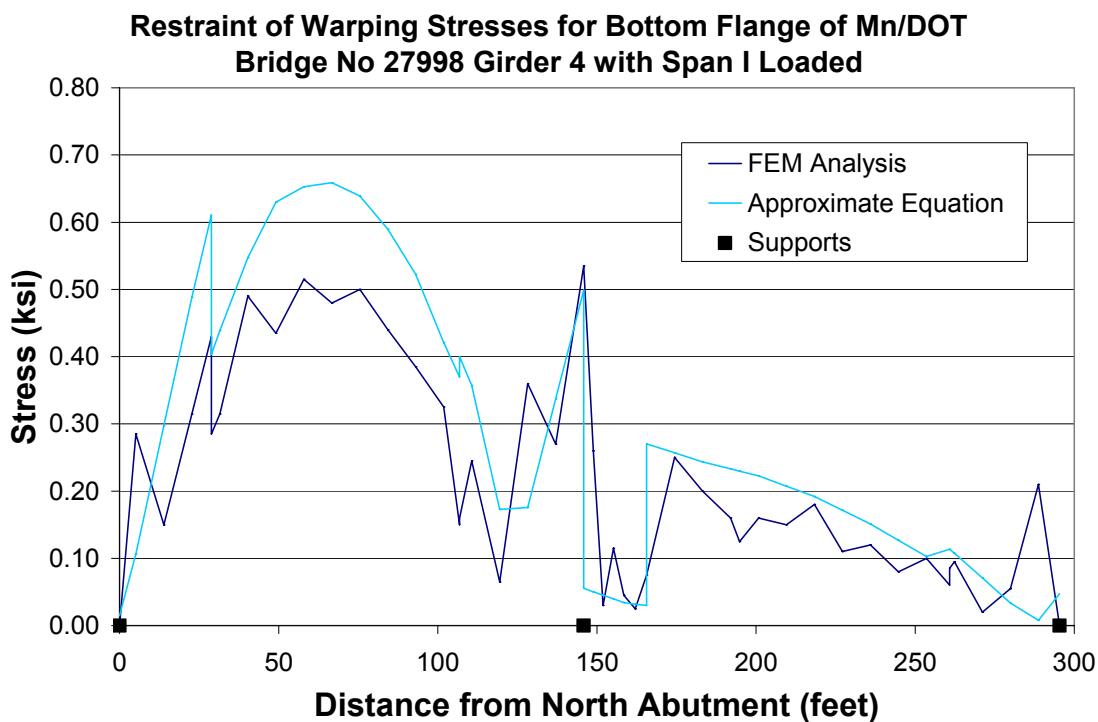


Figure 8-19: Study 16 Warping Stress Comparison Bridge 27998 Girder 4 Span I Loaded

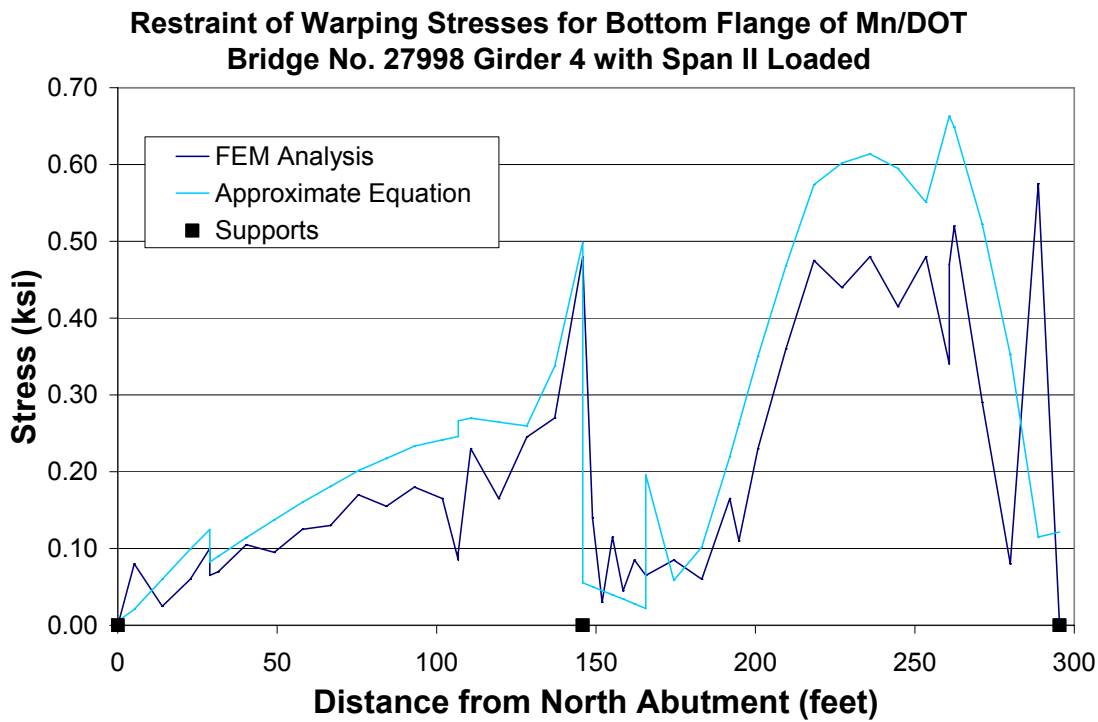


Figure 8-20: Study 16 Warping Stress Comparison Bridge 27998 Girder 4 Span II Loaded

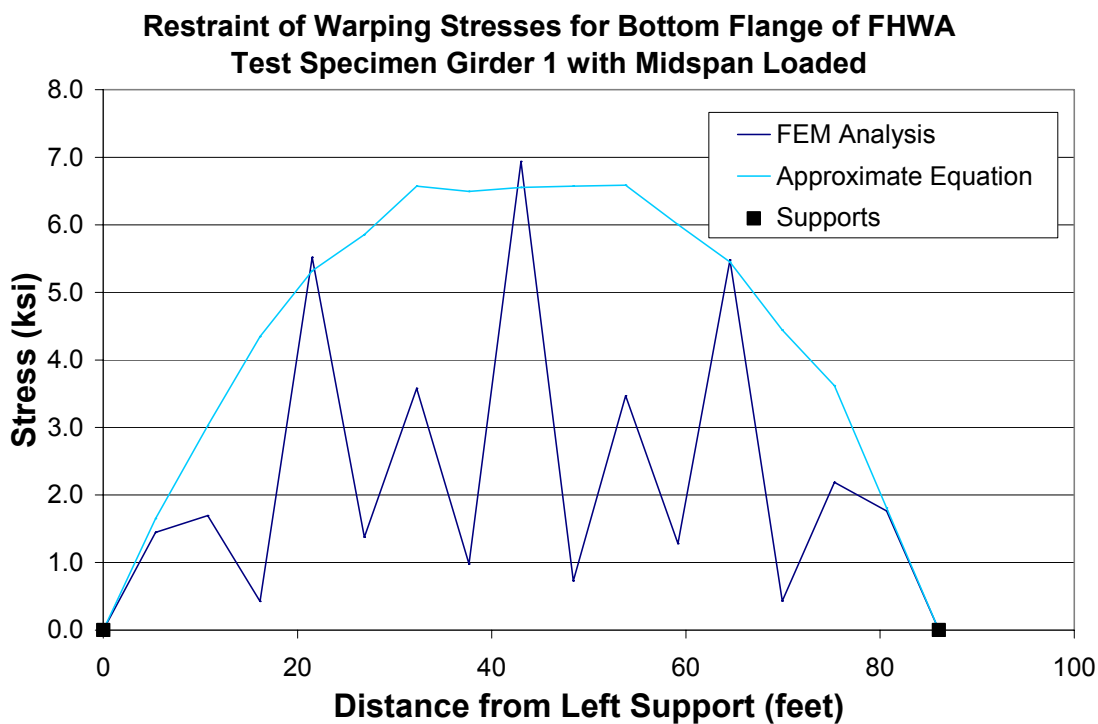


Figure 8-21: Study 16 Warping Stress Comparison FHWA Test Specimen Girder 1 Midspan Loaded

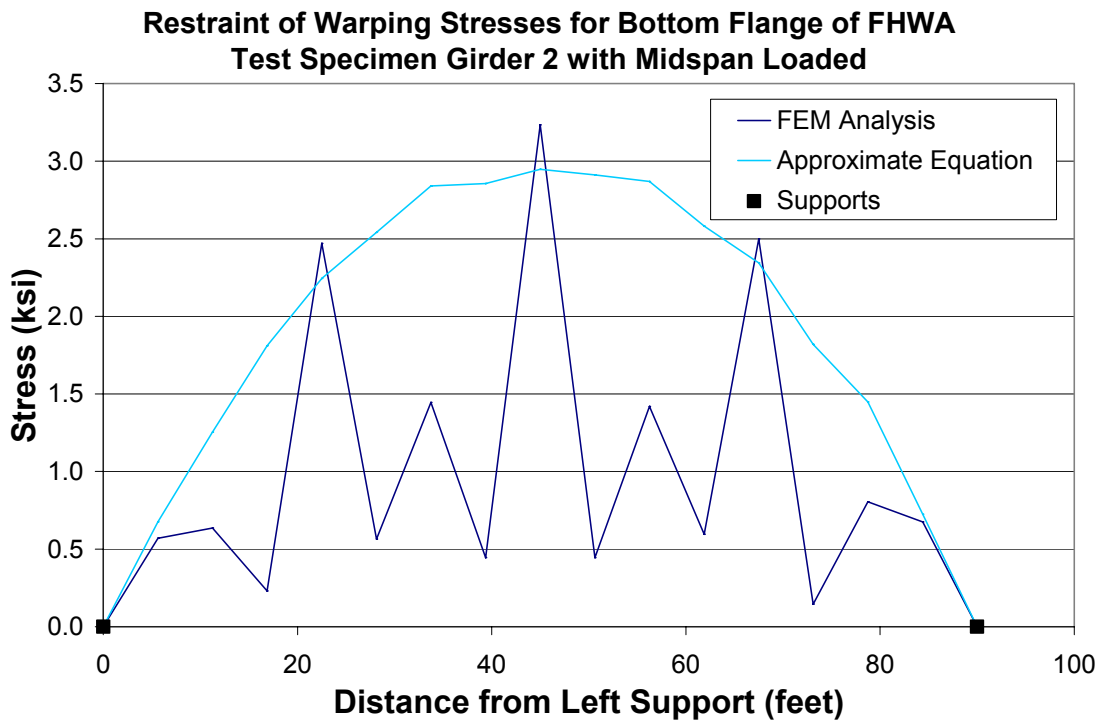


Figure 8-22: Study 16 Warping Stress Comparison FHWA Test Specimen Girder 2 Midspan Loaded

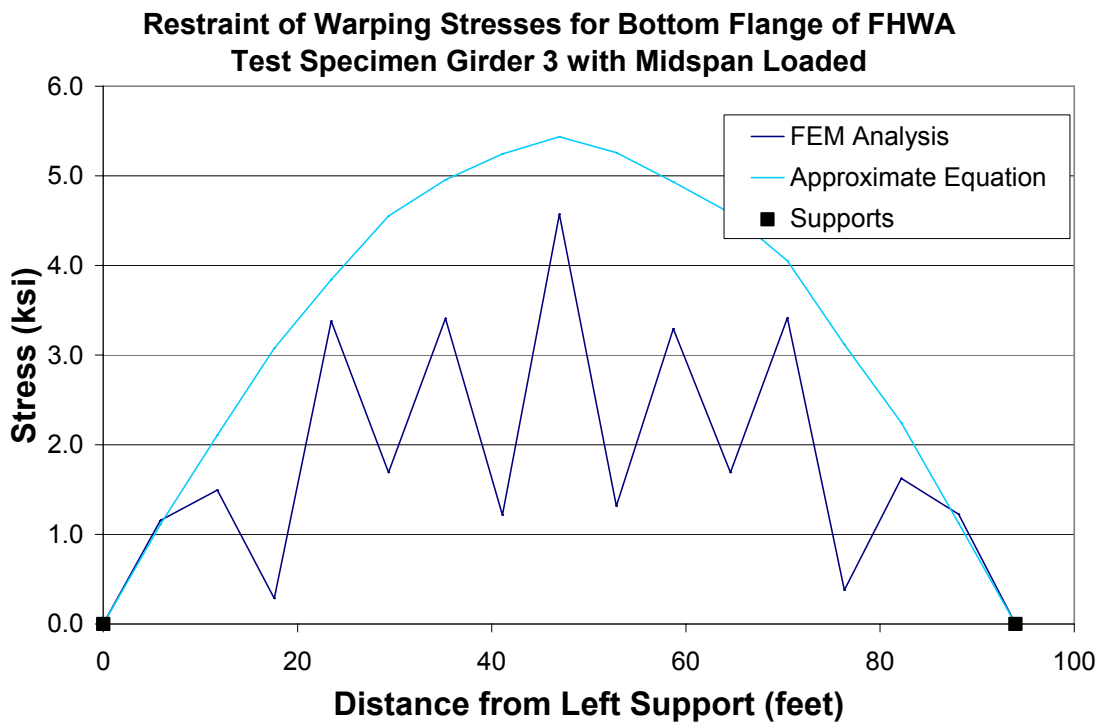


Figure 8-23: Study 16 Warping Stress Comparison FHWA Test Specimen Girder 3 Midspan Loaded

Chapter 9

Bridge Rating

A method for rating horizontally curved steel I-girder bridges is presented in this chapter that can be used to provide more reliable load ratings of curved steel bridges as compared to more common rating procedures that are currently in use. The chapter begins with a review of the current rating procedure utilized by Mn/DOT. This is followed by a description of the proposed rating method along with discussion on its applicability. An initial pretest rating for Span 9-8 and Span 8-7 of Mn/DOT Bridge No. 69824 based on the proposed rating method is then summarized. Next, results from the bridge test and the parametric study are integrated into the computational model of Bridge No. 69824 and used to provide a final rating of the bridge using the proposed rating procedure. Finally, comments are made concerning the current Mn/DOT rating, the initial pretest rating, and the final rating.

9.1 Current Mn/DOT Rating of Bridge No. 69824

As mentioned previously in Chapter 2, Mn/DOT currently rates their horizontally curved steel I-girder bridges using line girder analysis combined with yield strength reductions, which are used to account for the secondary bending moments and restraint of warping stresses attributable to horizontal curvature of the bridge. Secondary bending moments on the girders from load transfer through the diaphragms are approximated based on data curves provided in Gillespie (1968), which define a percent change in primary bending moment due to curvature for 3, 4, 5, and 8-girder systems. For bridges with a different number of girders, coefficients based on the V-load method (USS, 1984) are used to scale the curves from Gillespie (1968). Primary bending moment is defined as the moment that results from the analysis of a curved girder as an individual straight girder with span lengths equal to the curved girder arc lengths. By adding the primary moments from the straight girder analysis and the estimated secondary moments, the total bending moment in a curved girder is approximated. Flange stresses due to restraint of warping using the current Mn/DOT rating procedure are approximated by:

$$f_{lat} = \frac{12Ml^2}{RD} \left(\frac{6}{t_f b_f^2} \right) \quad (9-1)$$

where,

f_{lat} = flange lateral bending stress due to restraint of warping (ksi)

M = total vertical bending moment (k-ft)

l = unbraced length (ft)

R = girder radius (ft)

D = web depth (in)

t_f = thickness of flange (in)

b_f = width of flange (in)

The lateral bending stress f_{lat} is the approximated lateral bending moment in the flange due to restraint of warping (calculated similarly to Equation 2-8 but without the 6/5 factor) divided by the section modulus of the flange in the lateral direction. Because of uncertainties in the

approximation of the secondary moments and the restraint of warping stresses for this method, additional safety factors are applied at the discretion of the evaluator to both of these effects which increases each by approximately 5% to 15%.

For this rating method, an iterative process must be used to determine the final bridge rating since the secondary bending moments and restraint of warping stresses are dependent on the primary bending moments. To this end, the bridge girders are first analyzed and rated for moment and shear as individual straight girders within the context of load factor rating (LFR) using the AASHTO line girder analysis and rating software BARS (Bridge Analysis and Rating System) with HS20 loads. Adjustment factors for the flange yield stress are then determined based on approximated secondary bending moments and flange restraint of warping stresses at locations along the length of the girders. The line girder analysis is then rerun using the adjusted flange yield stresses, and new ratings are determined. This process is repeated until both the adjusted flange yield stresses and the rating factors along the length of the girder converge, and is typically only done for the girder determined by the bridge rating evaluator to be critical. The lowest rating factor calculated is used as the final rating for the bridge.

Results of this rating method for Mn/DOT Bridge No. 69824 indicated that the critical region for the bridge was at midspan of the Exterior Girder A on Span 8-7 due to positive moment bending for the Strength limit state. The resulting LFR rating factor for two lanes loaded at the inventory rating level was approximately 0.81. At this location, the steel yield stress was reduced from the actual value of 36 ksi to an adjusted value of 25.9 ksi to account for the effects of secondary bending moments and flange restraint of warping stresses. A key parameter to note in the computational model used for this rating besides those associated with the approximation of the curved girder as a straight girder is that the girder section properties in the negative moment regions were based on the non-composite section (i.e., the concrete and reinforcement at these locations were ignored for both load distribution along the length of the girders and for stress calculations). Also, the dynamic impact fractions used for this rating were based on the equation given for straight girder bridges in the *Standard Specifications for Highway Bridges*, 17th Edition (AASHTO, 2002), which is:

$$I = \frac{50}{L + 125} \leq 0.30 \quad (9-2)$$

where,

I = impact fraction

L = span arc length for curved girders (ft)

For Bridge No. 69824, this resulted in impact fractions between 0.181 and 0.3 for the various spans of the bridge. The same value was used for both the lane and the truck loads.

9.2 Proposed Rating Procedure

The proposed rating procedure for horizontally curved steel I-girder bridges consists of grillage computational analysis and load ratings based on LFR or LRFR philosophies as directed by the *Manual for Condition Evaluation of Bridges* (AASHTO, 1994) and the *LRFR Manual* (AASHTO, 2003b), respectively. Load testing may be used to supplement the rating procedure as discussed below.

9.2.1 Grillage Analysis

The primary tool for providing accurate yet efficient analysis for rating of horizontally curved steel I-girder bridges is a grillage-based analysis. This method provides for a complete system-based analysis that incorporates the interaction of the various elements in the bridge and has been shown in this project and others (Galambos et al., 2000; McElwain and Laman, 2000; Simpson, 2000; Nevling, 2001; Chang et al., 2005) to provide good correlation with load test results so long as the modeling assumptions used are handled appropriately. Caution must be used when selecting an analysis program since there are many levels of refinement for grillage analysis. See Chapter 2 for more information. Grillage analyses that use open-walled section beam elements (7 DOFs per node) are recommended, although frame elements (6 DOFs per node) can be used to provide reasonable results for simple layouts. All degrees of freedom should be included in the analysis due to the three-dimensional behavior of these complex structures. Diaphragms and lateral wind bracing, if present, should be modeled as accurately as possible since they play primary roles in the transverse load distribution and resistance mechanism of curved steel I-girder bridges. Web distortion effects should be taken into consideration by ignoring the contribution of the concrete deck to the composite torsion constant and/or releasing the rotational DOFs of concrete slab members from the girder DOFs. Longitudinal load distribution should generally assume the concrete in the negative moment regions to be effective in tension, while stresses in these regions should be checked based on non-composite properties or composite properties including the reinforcement only. See Chapter 8 for more discussion on these and a series of other grillage modeling assumptions and their influence on analysis results.

9.2.2 Code Provisions for Load Rating of Curved Steel I-girder Bridges

The load rating procedures outlined in Chapter 2 for the LFR and LRFR provide the general rating equations (Equation 2-1 and Equation 2-2) and methods to be followed for rating curved steel I-girder bridges. The LRFR equations in particular, which are relatively new in the industry, have been determined in this research to provide a strong basis for rating (Freisinger et al., 2004). Member capacities for both methods should be based on the most recent code provisions. The code provisions used for the bridge rating in this project follow the *Guide Specifications for Horizontally Curved Steel Girder Highway Bridges* (AASHTO, 2003a) for LFR checks and the *LRFD Bridge Design Specifications*, 2nd Ed. (AASHTO, 1998) for LRFR checks. The 1998 AASHTO LRFD provisions were augmented with a new section 6.10 for assessing the strength of the I-girders in this project. At the beginning of this project, the new section 6.10 had been balloted by AASHTO, but not yet published. It has since been published as part of the *LRFD Bridge Design Specifications*, 3rd Ed. (AASHTO, 2004). The 2005 interim provisions for the 2004 AASHTO LRFD including combined straight and curved girder equations are beyond the scope of this project. The code provisions used for this project were previously summarized and published in Freisinger et al. (2004). They are provided in Appendix G for reference.

9.2.3 Load Testing

Diagnostic load testing can be a valuable tool for calibrating and refining analytical models of a curved steel I-girder bridge in order to provide more accurate assessment of the bridge behavior for the purposes of load rating. Response characteristics such as load distribution, member

stiffness, and support fixity can be determined. These characteristics can be used to determine the level of composite action, participation of non-structural and secondary members, and boundary conditions, among other things. Care should be taken when extrapolating test data to rating load levels, since at higher load levels some of the observed benefits, such as unintended composite action or bearing fixity, may not exist. In order for a modified rating based on diagnostic test data to be realistic, the applied test loads should be high enough to accurately assess the behavior of the bridge up to the rating load levels.

The *LRFR Manual* (AASHTO, 2003b) provides general guidance on when to and when not to load test for the purpose of load rating. In general, load testing should only be conducted when pretest evaluations of the bridge indicate that load testing will likely provide an improved rating for the bridge. However, load testing should not be conducted if there is a possibility of sudden failure or if testing is impractical due to access difficulties or site traffic conditions. Bridge strengthening should always be investigated prior to load testing, since it is a more reliable method for increasing the load rating, and for some bridges it may be more cost effective.

Additional recommendations pertaining to the usefulness of load tests for load rating of horizontally curved steel I-girder bridges are made herein based on findings in this research project. As mentioned above, grillage analysis can generally be relied upon to provide accurate bridge ratings, thus reducing the need for load testing on most horizontally curved composite steel I-girder bridges. There are still some cases where load testing could be used to complement computational analysis or to improve the rating of a bridge. Load tests can be used to confirm composite action at high load levels in regions without shear connectors or to determine the benefits of large curbs and/or parapets along edge girders. This composite action can considerably increase a bridge rating, especially for stiffness (i.e., deflection) controlled bridges. Severely deteriorated steel or concrete components may need to be load tested to prove a certain load carrying capacity or stiffness; although, repair may be a better option unless the source of deterioration can also be removed. Load testing of curved steel I-girder bridges with slender girder webs may be useful for quantifying web distortion effects or proving load carrying capacity or overall bridge stiffness. Bridges with highly non-uniform girder or diaphragm spacing or with a reversal in the direction of curvature may require load testing to verify computational methods.

For some bridge behaviors, load testing may not be beneficial for the purposes of load rating horizontally curved steel I-girder bridges. Load tests to verify or quantify unintended bearing fixity in an attempt to increase the load rating of a curved steel bridge are not advantageous. There are two main reasons. First, this is generally not a reliable source of strength or stiffness, especially at higher load levels. And second, benefits due to bearing restraint on curved bridges should not be included unless detrimental effects due to increased thermal straining of the bridge are also taken into consideration. The use of loads tests on curved steel I-girder bridges with the sole intent of determining an effective concrete width to use in analysis is also not warranted. The sensitivity study in Chapter 8 shows that for a reasonable range of effective widths, the deflection and stress profiles of the bridge do not change much. Only small increases in the rating could be obtained. A more economical approach would be to test core samples from the bridge or review cylinder tests from the original pour of the concrete in order to decrease the modular ratio and increase the bridge stiffness and strength.

9.3 Initial Rating for Spans 9-8 and 8-7 of Mn/DOT Bridge No. 69824

Prior to load testing of Bridge No. 69824, a rating of the bridge was conducted for the two primary spans that were to be load tested. Span 9-8 and Span 8-7 were rated using the proposed rating procedure as outlined above in order to identify the controlling components of the bridge. In addition, the load rating of these two spans was used to determine a safe level (i.e., one that would not cause permanent damage to the bridge) for test loads that would encompass the behavior of the bridge at the anticipated load rating levels. The initial load ratings for Span 9-8 and Span 8-7 were conducted as part of an earlier segment of this research project and have been published in Freisinger et al. (2004). Checks were completed for all of the components as outlined in Appendix G. A summary of the computational model and loads used to obtain both the LFR and LRFR load ratings is provided below along with the key findings from the initial rating. As discussed below, the live loads used to generate the load ratings both for the initial pretest rating and the final rating were based on a subset of the full HS20 and HL-93 loadings due to the complexity of applying these loadings in UMN Program. In general, the subset of live loads used to determine the pretest load ratings were not as extensive as those used to determine the final bridge load ratings. The loads used for the initial LFR load rating were particularly low since they did not include the HS20 lane loading provisions.

9.3.1 Computational Model IMR

The UMN Program computational model used for the initial rating of Span 9-8 and Span 8-7 is herein termed the Initial Model – Rating (IMR). It was an earlier rendition of the Final Model – Rating (FMR) analysis model for Bridge 69824 that was discussed in Chapter 7 and is used below for the final rating of the bridge. Key differences between the IMR and FMR models were as follows. The mesh refinement for the girders in IMR was only 1 element between diaphragms instead of the 4 elements that were used for FMR. Transverse concrete deck beams were not included in the IMR analysis, but were included for the FMR analysis. The concrete deck and reinforcement in the negative moment regions for IMR were excluded for both stiffness (i.e., longitudinal load distribution) and stress calculations, since this is typical practice for bridges without shear connectors on the girders in these regions. For FMR, the concrete deck and reinforcement in the negative moment regions were both included for stiffness properties, while the rebar was included for stress calculations. Torsion section properties for the composite girders in IMR were calculated based on the equations from Heins and Kuo (1972) using the full effective width of concrete b_{eff} as described in Chapter 4, while for FMR the concrete was ignored for the calculation of the torsion constant J . For the composite section properties in IMR, the modular ratio N was 8 based on the design compressive strength of the concrete, the slab thickness was 7.0 inches for long-term dead load and 8.5 inches for live loads, and the effective concrete width was 90.5 inches for long-term dead load and 99.5 inches for live loads. For FMR, the modular ratio was 6, the slab thickness was 7.0 inches for long-term dead load and 9.0 inches for live loads, and the effective concrete width was 90.5 inches for long-term dead load and 102.5 inches in the negative moment regions and 123 inches in the positive moment regions for the live loads. The effective width of concrete for the composite diaphragms in IMR was 54.0 inches and in FMR it was 7.0 inches. Note that the changes from IMR to FMR were due to results from the load test as discussed in Chapter 6 and Chapter 7 in conjunction with the parametric studies in Chapter 8.

9.3.2 Applied Loads for Initial Rating

Loading was applied to the IMR model in three stages. First, the non-composite dead load was applied to the steel structure. This dead load, termed DC, included the steel weight of the girders, diaphragms, lateral wind bracing, various connection plates and bolts, along with the concrete weight for the original deck less $\frac{1}{2}$ inch thickness to account for the material ground away prior to the installation of the concrete overlay. Second, the long-term composite dead load, termed DW, was applied to the long-term composite system ($t_{slab} = 7.0$ inches and $3N = 24$). This second stage included loading from the 2 inch wearing coarse, the curbs, and the guard railings. Finally, the live load was applied to the final composite system ($t_{slab} = 8.5$ inches and $N = 8$).

Application locations and quantities for dead loads were determined using both the structural configuration of the bridge (i.e., cross-sectional dimensions, lengths, etc.) and the scheduled quantities from the original bridge specifications as provided by Mn/DOT. For the south and north ends of the bridge which cantilever past Pier 10 and Pier 5, respectively, DC and DW dead loads from the adjacent bridge units were approximated and applied as vertical point loads at the tips of the cantilevers in the analysis model. To determine the magnitude of these point loads, the girders for the adjacent spans were idealized as propped cantilevers with a uniformly distributed load applied. The vertical reactions at the propped ends were calculated for DC and DW loads and used for the corresponding vertical point loads in the analysis model.

The live loads used for load rating consist of truck and/or lane loads applied to the bridge to maximize the various member forces. The LRFR and LFR rating methods each have their own series of loads to apply. LRFR follows the HL-93 design loads as specified in the *LRFD Bridge Design Specifications* (AASHTO, 1998). LFR uses the standard HS20 truck or lane loads as defined in the *Manual for Condition Evaluation of Bridges* (AASHTO, 1994) or likewise, in the *Standard Specifications for Highway Bridges*, 17th Edition (AASHTO, 2002). These loadings were previously discussed in Chapter 2, where diagrams of each loading were also provided.

Although Bridge No. 69824 is only striped for a single lane, it was rated for two lanes. This was because both the LRFR and LFR methods consider a roadway width of 21 $\frac{1}{2}$ feet, which is the curb-to-curb clear distance for Bridge No. 69824, to be sufficiently wide enough for two lanes. In addition, the previous Mn/DOT rating of the bridge discussed above also rated the bridge for two lanes of load. For this bridge then, each lane was reduced from a standard 12 foot width down to 10 $\frac{3}{4}$ feet.

Both rating methods allow for truck and lane loads to be shifted both transversely and longitudinally on the roadway surface in an attempt to maximize various member forces. This results in a very large number of loading possibilities. Because the software (UMN Program) used for analysis required each load case to be individually entered as a series of point and uniformly distributed loads, the load cases considered for these ratings were reduced in an effort to simplify the analysis to those cases that were judged to be most critical.

To reduce the number of total load cases for analysis, truck loads were limited to a rear axle spacing of 14 feet (recall from Chapter 2 that it can vary between 14 feet and 30 feet) and were applied at select locations along the length of each span. The longitudinal load application points were conveniently chosen so that the center of gravity of the trucks was located at the diaphragm

locations. This method amounted to approximately 10 different truck load positions along the length of each span per lane. In addition, only two transverse positions for the trucks were used per lane: shifted as far in as possible and as far out as possible. Centrifugal forces on the trucks were not considered for the initial pretest load rating.

When lane loads were considered, they were patterned so as to produce the maximum response of the member in question. For example, when checking positive moment flexure, lane loads were applied to the current span being maximized and also to every alternate span extending out in both directions from the current span. For maximizing negative moment flexure at piers, both spans adjacent to the pier were loaded.

For the LRFR, truck/tandem loads and lane loads were combined to create maximum responses in members under consideration. One or two lanes were loaded, and one truck or tandem was applied per lane. A multiple presence factor (MP) of 1.2 was applied to the live load effect when only one lane was loaded. To maximize flexure at the interior piers of continuous spans, two trucks were applied per lane (one on each side of the pier), but only 90% of the total truck and lane loads was then considered for the live load effect. A dynamic impact fraction of 0.33 was applied to all truck and tandem loads for the LRFR.

The live loads for the initial pretest LFR rating were limited to the HS20 truck loads. No lane loads were considered for this initial LFR rating. As discussed later, lane loads were added for the final LFR bridge rating. A dynamic impact fraction of 0.25 was used for the truck loads in the LFR rating.

9.3.3 Results of Initial Pretest Load Rating

Results of the initial pretest load rating using Equation 2-1 and Equation 2-2 with capacities determined from the LFD and LRFD equations outlined in Appendix G indicated that the controlling components for Bridge No. 69824 were the longitudinal stress in the girders and the bearing resistance of the girders at the piers. The bearing resistance equations however, ignore the contribution of the robust diaphragms to the axial resistance of the pseudo-columns created by the combination of the bearing stiffeners and girder webs at the piers. In reality, the diaphragms on this bridge prevent lateral buckling of the girder webs and allow for much higher bearing resistances at the piers than is determined by the capacity equations. Thus, the bearing resistance at the piers was concluded to be sufficient and the longitudinal stress in the girders due to flexural and restraint of warping stresses was determined to be the controlling factor for the bridge. The rating factors for all other components, such as diaphragms, lateral wind bracing, welded and bolted connections, etc., were at a minimum approximately 3 times higher than the controlling rating factors for the stress in the girders. Thus, the focus for the final rating of Bridge No. 69824 was placed on the flexural and warping behavior of the girders.

The controlling rating factors on the Interior Girder C based on the LRFR provisions and Equation 2-2 with a conservative system factor φ_s of 0.85 were 0.50 for positive moment bending on Span 8-7 and 0.63 for negative moment bending at Pier 8. For the Exterior Girder A, the corresponding rating factors were 0.53 for positive moment bending on Span 8-7 and 0.65 for negative moment bending near Pier 8. Therefore, the controlling rating factor for the initial rating

for Span 9-8 and Span 8-7 using LRFR provisions was 0.50 for positive moment bending on Girder C of Span 8-7.

For the LFR provisions and Equation 2-1 the controlling rating factors on the Interior Girder C were 0.92 for positive moment bending on Span 8-7 and 1.53 for negative moment bending at Pier 8. On the Exterior Girder A, the rating factors were 0.99 for positive moment bending on Span 8-7 and 1.29 for negative moment bending at Pier 8. Note that these rating factors were based on the truck loads only from the HS20 Loadings. The lane loads for HS20 Loading were not included in determining the maximum component effects for this initial load rating.

There were two main reasons why the LRFR ratings were lower than the LFR ratings. First, the HL-93 loads used for the LRFR ratings are heavier than those used for the LFR ratings, since for LRFR ratings the effects of the truck and lane loads are added, while for the LFR ratings only one or the other is used. In addition, the LFR loads for this initial rating were low since the lane loads were not considered. Second, the system factor used for the LRFR ratings places an additional reduction on the LRFR ratings that is not utilized in the LFR ratings.

9.4 Final Rating of Mn/DOT Bridge No. 69824

The final rating of Bridge No. 69824 was completed taking into consideration the results from the load test and the parametric studies. The computational model and the applied loads are described below followed by the results for the final rating. Results focus on the rating based on LRFR criteria with HL-93 loading. Rating using LFR criteria and HS20 loading is provided for comparative purposes.

9.4.1 Computational Model FMR

The computational model for the final bridge rating using UMN Program has been termed Final Model – Rating, or FMR. FMR was calibrated based on the experimental data from the load tests (see Chapter 7) in conjunction with the parametric studies (see Chapter 8) to provide a more accurate computational model of the bridge. For a summary of the key parameters in the model, see Section 9.3.1 above, where FMR is compared with IMR.

9.4.2 Applied Loads for Final Rating

The applied loads for the final rating were the same as those for the initial rating previously discussed above, except for the following additions. The overturning effect of centrifugal forces based on a speed of 35 mph, which is the maximum posted speed for Bridge No. 69824, was included for truck and/or tandem loads when maximizing forces on the Exterior Girder A for both the final LRFR and LFR ratings. HS20 lane loads were added for the final LFR rating and had a dynamic impact fraction of 0.20 applied as per the *Guide Specifications for Horizontally Curved Steel Girder Highway Bridges* (AASHTO, 2003a). The HS20 lane loads included one point load per lane of 18 or 26 kips depending on moment or shear maximization, respectively. For moment at interior piers of continuous spans, two point loads were applied per HS20 lane, one on each side of the pier.

9.4.3 Results of Final Load Rating

In order to determine the load rating of the bridge, the bridge capacity consumed by the DC and DW dead loads on the structure had to be calculated. The dead load deflections of each girder for the unfactored DC, DW, and total dead (i.e., DC + DW) loads are shown in Figure 9-1 and Figure 9-2. Unfactored dead load shear forces for Girder C and Girder A are provided in Figure 9-3 and Figure 9-4, respectively, while Figure 9-5 and Figure 9-6 show the unfactored dead load moments for each girder. The unfactored dead load stresses in the top and bottom flanges are shown in Figure 9-7 through Figure 9-12. Figure 9-7 and Figure 9-8 provide the DC flange stresses for each girder, Figure 9-9 and Figure 9-10 the DW flange stresses, and Figure 9-11 and Figure 9-12 the total dead load flange stresses. *Top Flexure* and *Bottom Flexure* in the stress plots refer to the longitudinal stress at the extreme surface of the top and bottom flanges due to flexure, while *Top Warping* and *Bottom Warping* refer to the longitudinal restraint of warping stresses at the tips of the top and bottom flanges. Sharp changes in the *Flexure* flange stress profiles indicate a change in flange thickness. Sharp points in the *Warping* flange stress profiles are generally indicative of diaphragm locations. As Figure 9-11 and Figure 9-12 show, the unfactored total dead load stresses for each girder range between approximately ± 15 ksi for flexure and ± 1.5 ksi for restraint of warping.

The rating using LRFR was based on HL-93 loads and was conducted at the inventory level for the Strength I limit state. Load factors of 1.25 for DC, 1.50 for DW, and 1.75 for live load were used for factored loads. A dynamic impact factor of 1.33 was applied to all truck and tandem loads. Deflection envelopes due to unfactored live load including impact (LL+IM) for the HL-93 loads are shown in Figure 9-13 and Figure 9-14 for Interior Girder C and Exterior Girder A, respectively, along with the typical deflection limits of $L_{arc}/800$ (AASHTO, 1998 and 2003a). Deflections for both girders were governed by the midspan deflections on Span 8-7. Corresponding rating factors for deflections, which were calculated as the limit deflection divided by the maximum calculated deflection, were 1.73 for Girder C and 1.45 for Girder A. Unfactored LL+IM shear envelopes for the HL-93 loads are shown in Figure 9-15 and Figure 9-16. The LRFR factored total shears for each girder are provided in Figure 9-17 and Figure 9-18 along with rating factors based on Equation 2-2. The lowest rating factor for shear on Girder C was 1.15 at Pier 8 and on Girder A was 1.04 near Pier 7. The unfactored LL+IM moment envelopes for the HL-93 loads are shown in Figure 9-19 and Figure 9-20, while the corresponding top and bottom flange stresses are in Figure 9-21 and Figure 9-22. The unfactored restraint of warping stresses due to LL+IM are also plotted in Figure 9-21 and Figure 9-22. Note that the top flange restraint of warping stresses are close to zero due to the high resistance provided by the nearby concrete slab. Factored total flange stresses are shown in Figure 9-23 and Figure 9-24 for LRFR. Figure 9-25 and Figure 9-26 show the total factored stresses, including the component due to warping, and the LRFD capacities along the bridge length for the bottom flanges of each girder, which were the controlling components on the bridge. The capacities in these two plots were calculated using a system factor φ_s in Equation 2-2 of 0.952 based on the load modifier η_i equal to 1.05 as determined by AASHTO (1998) with values of 1.00 for ductility and importance factors and 1.05 for the non-redundant factor. These figures show that the controlling rating factor for Bridge No. 69824 is 0.63 and is located at the negative moment region of Interior Girder C at Pier 6. If a system factor φ_s of 0.85 based on the alternative values provided in the *LRFR Manual* (AASHTO, 2003b) is used instead, the capacities and LRFR

rating factors are reduced as shown in Figure 9-27 and Figure 9-28. The reduced rating factor at Pier 6 is now 0.48.

The rating using LFR was based on HS20 loads and was conducted at the inventory level for the Strength limit state. Load factors of 1.30 for DC and DW, and 2.17 for live load were used for factored loads. Dynamic impact factors of 1.25 and 1.20 were applied to truck loads and lane loads, respectively. The unfactored LL+IM moment envelopes for the HS20 loads are shown in Figure 9-29 and Figure 9-30. The corresponding top and bottom flange stresses are shown in Figure 9-31 and Figure 9-32. The unfactored restraint of warping stresses due to LL+IM are also plotted in these two figures. Factored total flange stresses are shown in Figure 9-33 and Figure 9-34 for LFR. Figure 9-35 and Figure 9-36 show the total factored stresses and the LFD capacities, minus the component due to warping, along the bridge length for the bottom flanges of each girder. Similar to the LRFR rating, these figures show that the controlling rating factor is located at the negative moment region of Interior Girder C at Pier 6. The corresponding rating factor RF was 0.73 for LFR.

A summary of the current, initial, and final load ratings for Mn/DOT Bridge No. 69824 is presented in Table 9-1. Inventory and operating level ratings are provided in the table for comparative purposes. The operating level ratings were determined by multiplying the inventory level ratings by the ratio of the inventory-to-operating live load factors previously discussed in Chapter 2. For LFR, the inventory ratings were multiplied by $2.17/1.30 = 1.669$ to obtain the operating ratings, while for LRFR, the inventory ratings were multiplied by $1.75/1.35 = 1.296$.

9.5 Discussion on the Various Load Ratings

There are several differences between the current Mn/DOT rating, the initial pretest rating, and the final load rating for Mn/DOT Bridge No. 69824. In particular, the different rating loads, capacity equations, and analysis methods and assumptions result in significantly different load ratings for the bridge. A series of key differences that are important to the rating of horizontally curved steel I-girder bridges are discussed in the following paragraphs based on the above load ratings for Bridge No. 69824.

Both the initial pretest rating and the final rating show that the controlling girder for Bridge No. 69824 is the Interior Girder C, while the current Mn/DOT rating has the Exterior Girder A as the controlling girder. This discrepancy is primarily due to the current Mn/DOT rating ignoring the effects of the lateral wind bracing on the transverse load distribution between the girders. AASHTO (2003a) warns against the use of approximate methods, such as the V-load method, for curved bridges with lateral wind bracing. The parametric study in Chapter 8 showed that the lateral wind bracing helps to equalize the vertical load between the girders. For Bridge No. 69824, vertical moments were significantly lower on the Interior Girder C as compared to Girder A in the parametric study when the lateral wind bracing was excluded from the computational model versus when it was included. Thus, the current Mn/DOT rating of Bridge No. 69824 underestimates the load on the interior girder and overestimates the load on the exterior girder by ignoring the influence of the lateral wind bracing.

The final rating found that the controlling location on Bridge No. 69824 was at the negative moment region of Pier 6, while both the current Mn/DOT rating and the initial pretest rating

showed that the positive moment region of Span 8-7 controlled. This key discrepancy is due to the difference in girder stiffness in the negative moment regions for longitudinal load distribution in the various computational analyses. The current Mn/DOT rating and the initial pretest rating assumed that the concrete deck and rebar would be ineffective in tension at rating level loads in the negative moment regions of the bridge since no shear connectors were provided on the girders in these regions. Based on the results of the load test which showed the deck to be effective in tension at rating load levels in the negative moment regions, the final rating included both the concrete deck and the rebar for girder stiffness and longitudinal load distribution. The parametric study in Chapter 8 showed that for Bridge No. 69824 the moments in the positive moment regions were approximately 15% higher and in the negative moment regions were approximately 20% lower when the stiffness of the deck was excluded in the negative moment regions for longitudinal load distribution versus when it was included. More load is carried by the negative moment regions when the stiffness there is higher. Hence, the current Mn/DOT rating underestimates the loads in the negative moment region by assuming the deck to be ineffective in tension at the rating level loads and overestimates the loads in the positive moment regions.

In general, the final LRFR rating factors are lower than those for the final LFR rating due to the higher loads for the HL-93 Loading versus the HS20 Loading. This was discussed earlier for the initial pretest rating, but is made clearer for the final ratings. In particular, a comparison between the unfactored LL+IM moment envelopes for the HL-93 Loading in Figure 9-19 and Figure 9-20 for each girder to those for the HS20 Loading in Figure 9-29 and Figure 9-30 show that the HL-93 loads are higher. The peak magnitudes in the positive moment regions for the unfactored LL+IM HL-93 loads are on average approximately 1.5 times those for the HS20 loads, while in the negative moment regions the HL-93 moments are on average approximately 1.65 times those for the HS20 loads. Accounting for the live load factors of 1.75 for LRFR and 2.17 for LFR, the previous values for the positive and negative moments decrease to approximately 1.21 and 1.33 times higher for the HL-93 factored live loads than the corresponding HS20 factored live loads. The higher LRFR loads can also be seen by comparing the total factored flange stresses for LRFR in Figure 9-23 and Figure 9-24 and the final LFR in Figure 9-33 and Figure 9-34. The *LRFR Manual* (AASHTO, 2003b) recognizes this inconsistency between the LRFR and LFR ratings in article C6.1.7.1.

Finally, the LFR rating at the Strength limit state based on the capacities from the *Guide Specifications for Horizontally Curved Steel Girder Highway Bridges* (AASHTO, 2003a) is restrictive on the negative moment region stresses in the compressive flange and the web of Bridge No. 69824, especially at Pier 6 for the Interior Girder C. There are two reasons. The first is that AASHTO (2003a) has limited the width-to-thickness ratio for compact compression flanges to 18 for all grades of steel less than or equal to Grade 50. This value is based on the equation provided in Article 6.10.4.1.3 of *AASHTO LRFD* (1998) for Grade 50 steel. Using this same equation but for Grade 36 steel, from which Bridge No. 69824 is made, the limit would be slightly over 21. At Pier 6 of Bridge No. 69824, the compression flange width is 18 inches and the thickness is 0.875 inches. This results in a width-to-thickness ratio of 20.6, which is noncompact by the AASHTO (2003a) limit but compact by the *AASHTO LRFD* (1998) limit. Following the AASHTO (2003a) provisions, a check of the compression flange at Pier 6 for Girder C as a compact flange leads to a limiting flange stress of 35.3 ksi, while checking as a

noncompact flange (as done for the load rating above) results in a lower limiting flange stress of 31.2 ksi. Second, including the rebar for the stress calculations in the negative moment regions of Bridge No. 69824 increases the depth of the web in compression D_c to a point where local bend-buckling of the web becomes a factor. This is handled in LRFR at the Strength I limit state by the inclusion of the web load-shedding factor R_b and in LFR based on AASHTO (2003a) at the Strength limit state by limiting the web longitudinal stress. The LFR provisions are more restrictive and result in a limiting compression web stress of 29.7 ksi on Girder C at Pier 6. In comparison, the web load-shedding factor for LRFR only reduces the available compressive strength of the Girder C bottom flange at Pier 6 from 36 ksi to 35.0 ksi. Reconsideration of the implementation of these two factors for the LFR load rating would result in a higher rating for Girder C at Pier 6 and thus, an overall higher rating for the bridge. These and other discrepancies are bound to arise when rating older bridges with newer code provisions. Bridge evaluators should be aware of these issues especially when utilizing computer programs that implement code provisions without consideration of the original codes from which a bridge was designed.

Summary of Rating Factors for Mn/DOT Bridge No. 69824					
Rating	Inventory Rating Factor		Operating Rating Factor		
	LFR	LRFR	LFR	LRFR	$\varphi_s = 0.85$
Current Mn/DOT	0.81	-	-	1.35	-
Initial (Pre-test)*	0.92	0.50	-	1.54	0.65
Final (Post-test)	0.73	0.48	0.63	1.22	0.62
	* Based only on Span 9-8 and Span 8-7				
	- Not available				

Table 9-1: Summary of Rating Factors for Mn/DOT Bridge No. 69824

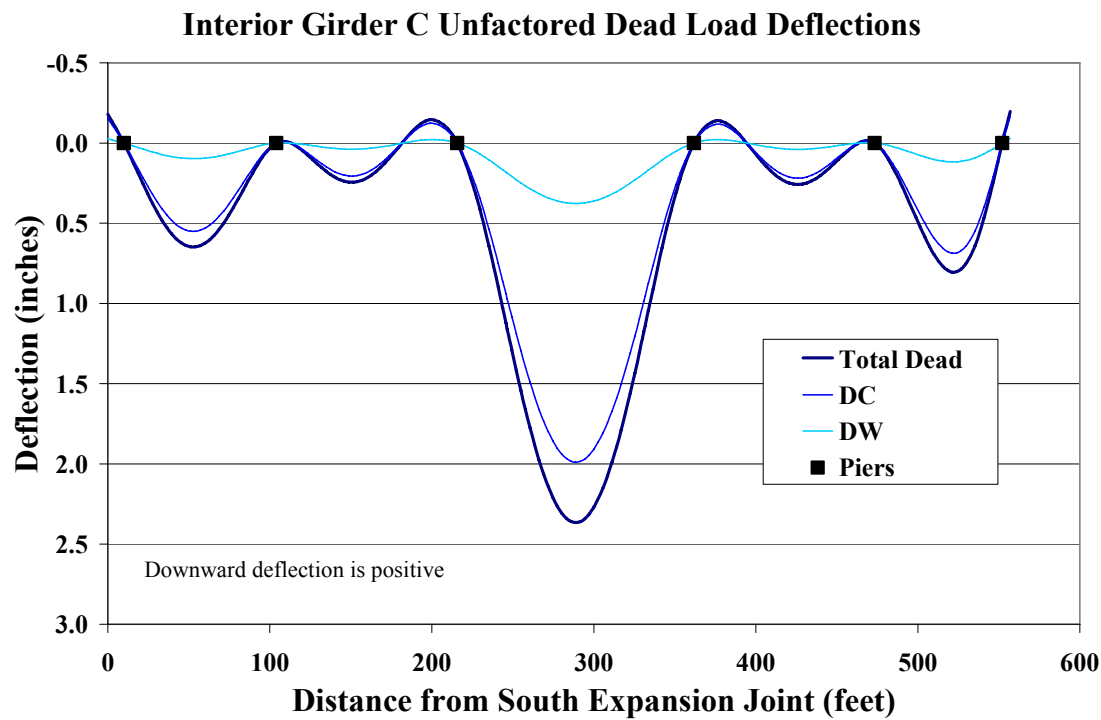


Figure 9-1: Interior Girder C Unfactored Dead Load Deflections

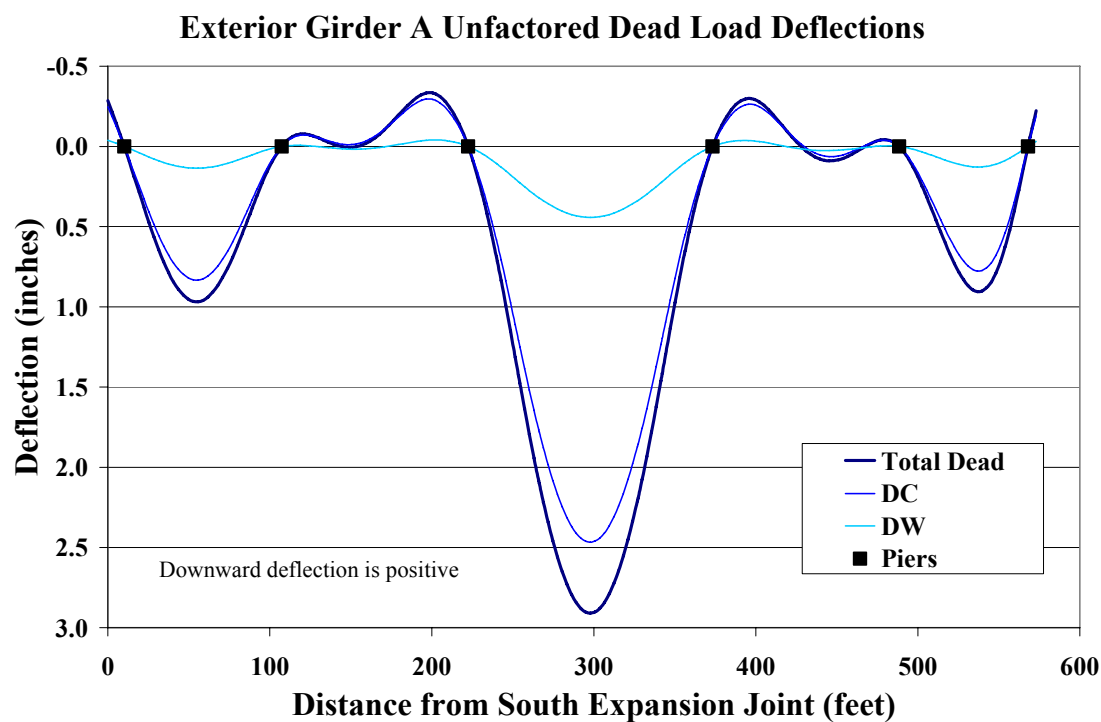


Figure 9-2: Exterior Girder A Unfactored Dead Load Deflections

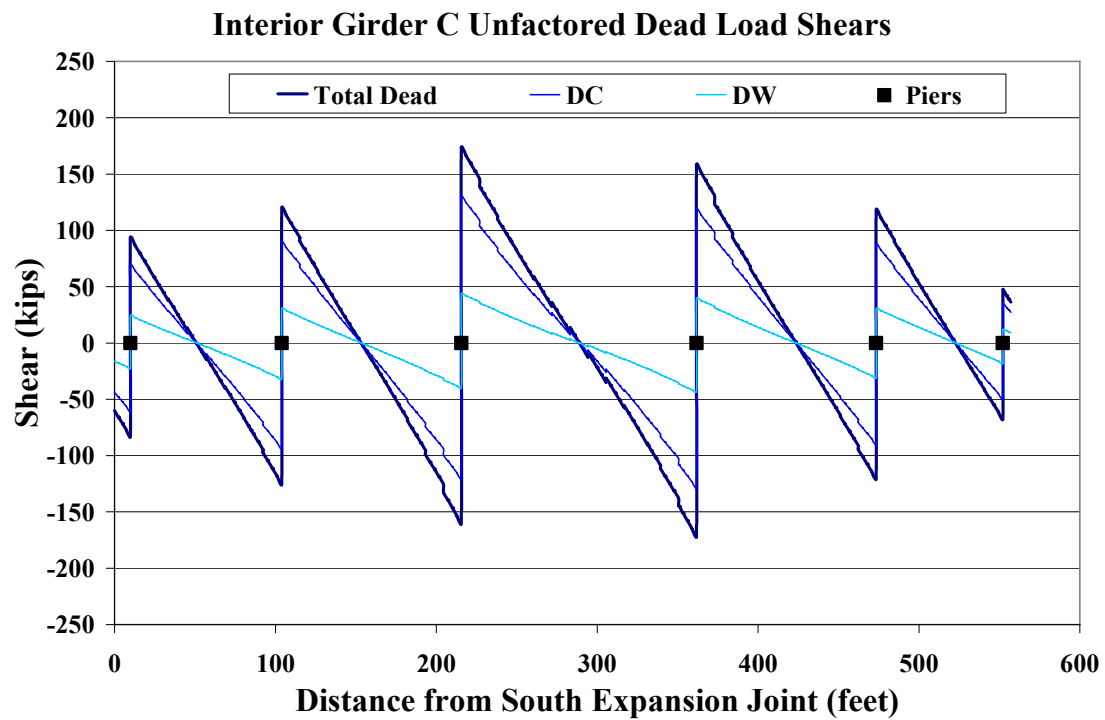


Figure 9-3: Interior Girder C Unfactored Dead Load Shears

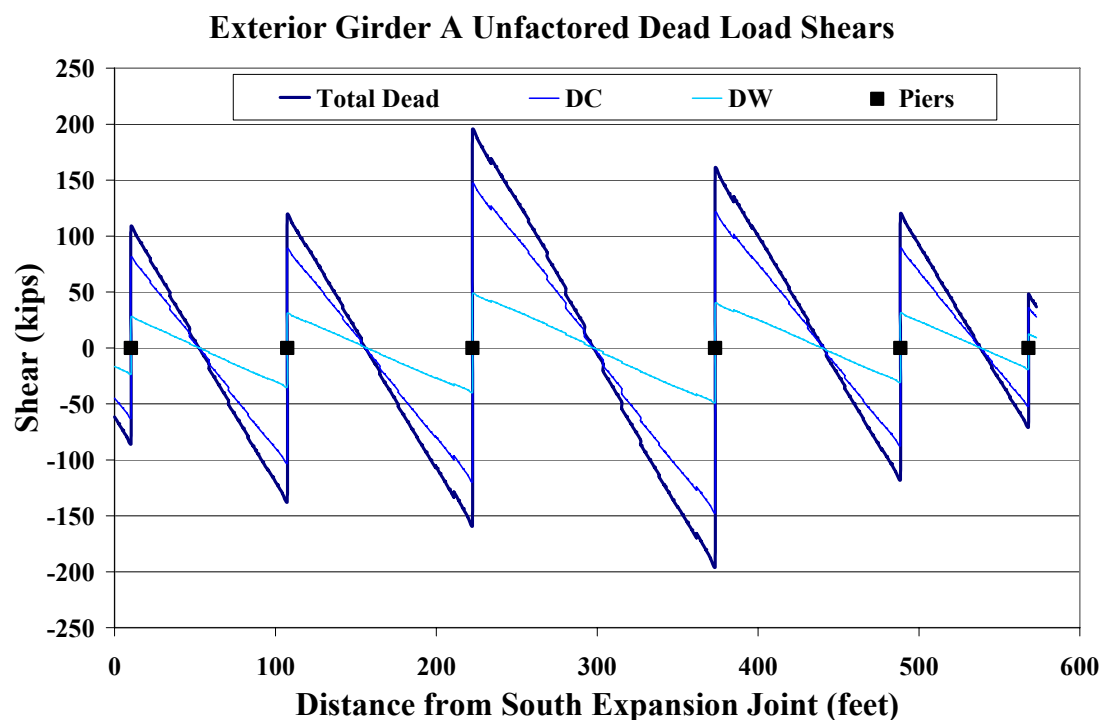


Figure 9-4: Exterior Girder A Unfactored Dead Load Shears

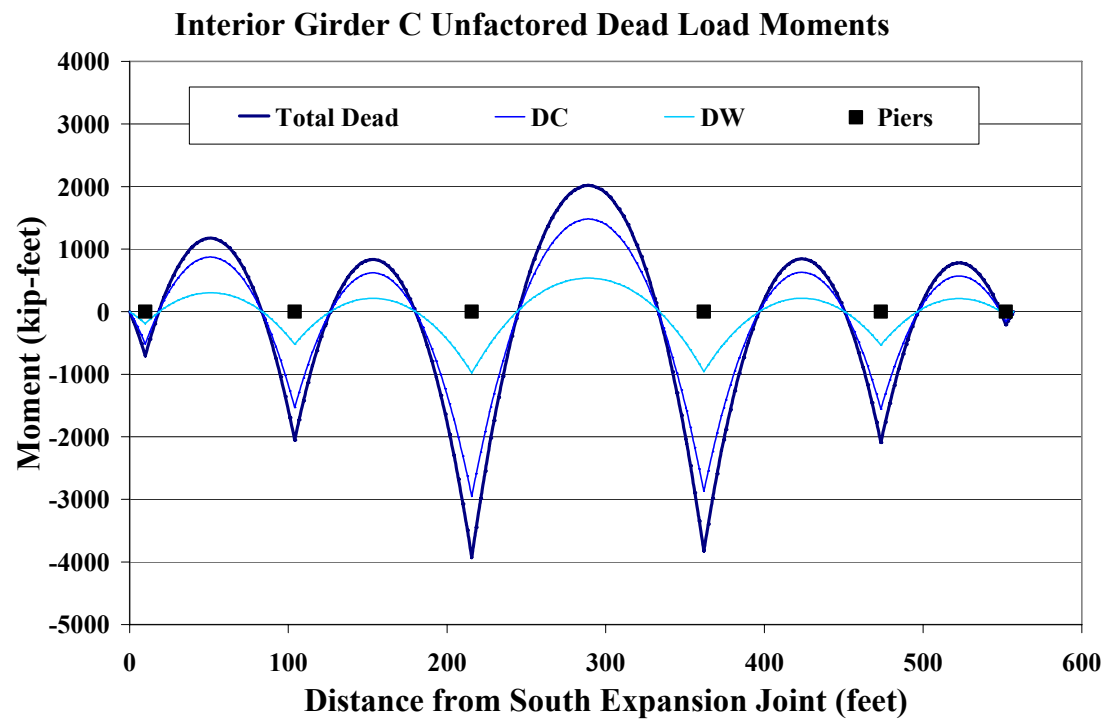


Figure 9-5: Interior Girder C Unfactored Dead Load Moments

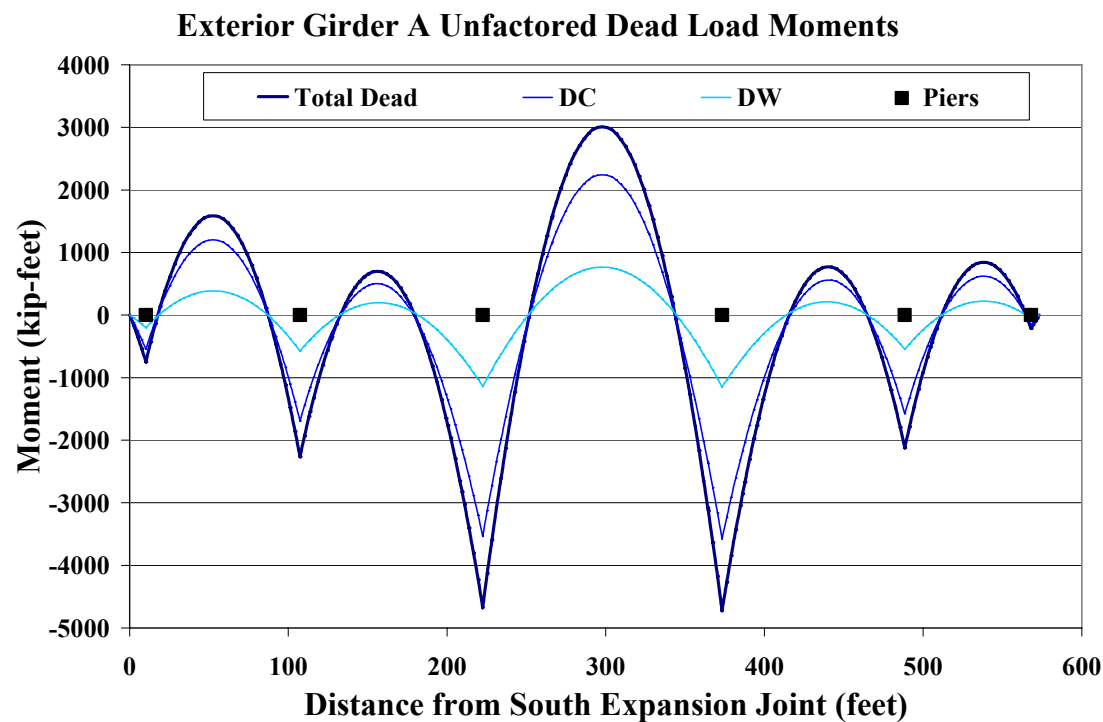


Figure 9-6: Exterior Girder A Unfactored Dead Load Moments

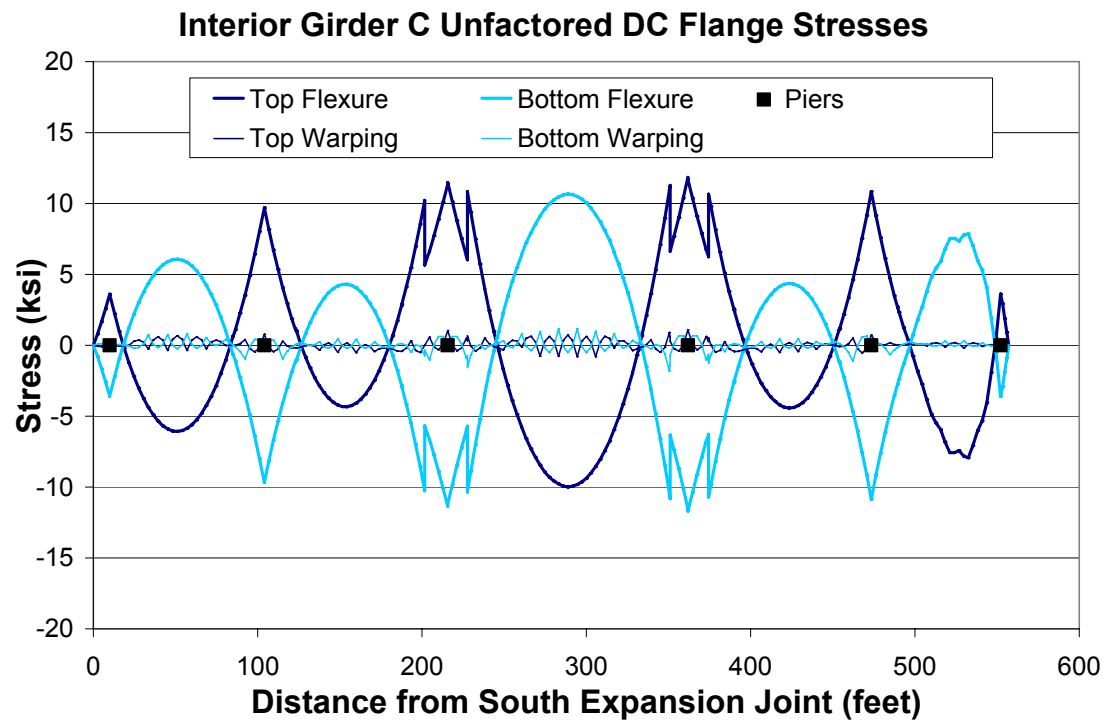


Figure 9-7: Interior Girder C Unfactored DC Flange Stresses

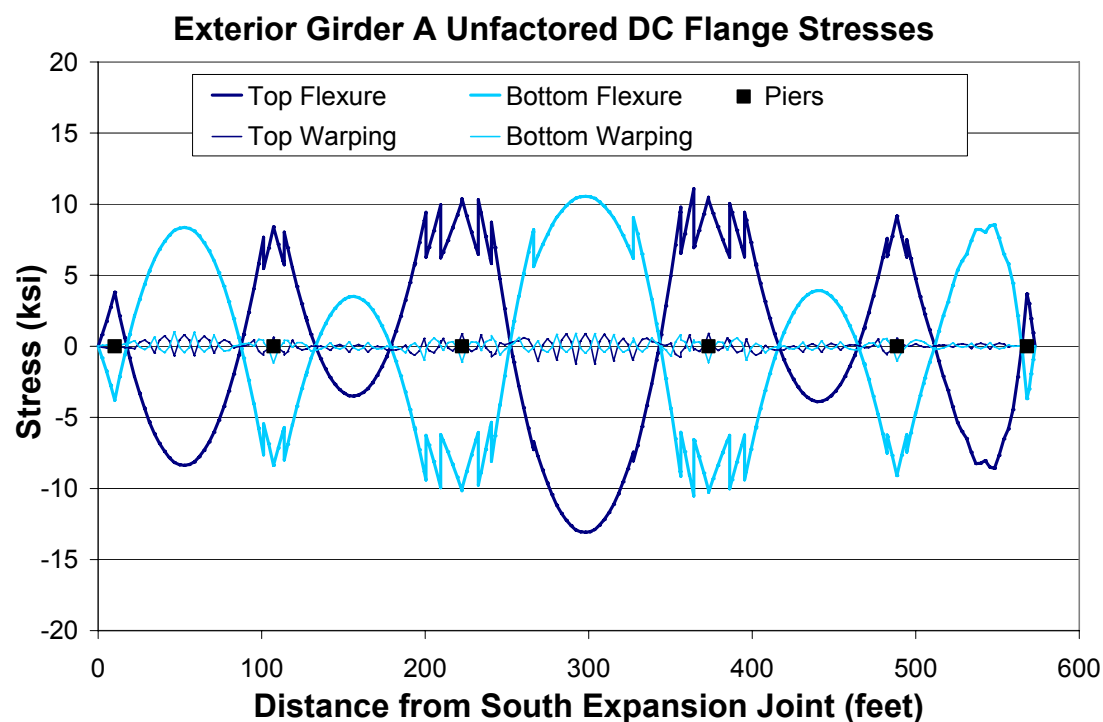


Figure 9-8: Exterior Girder A Unfactored DC Flange Stresses

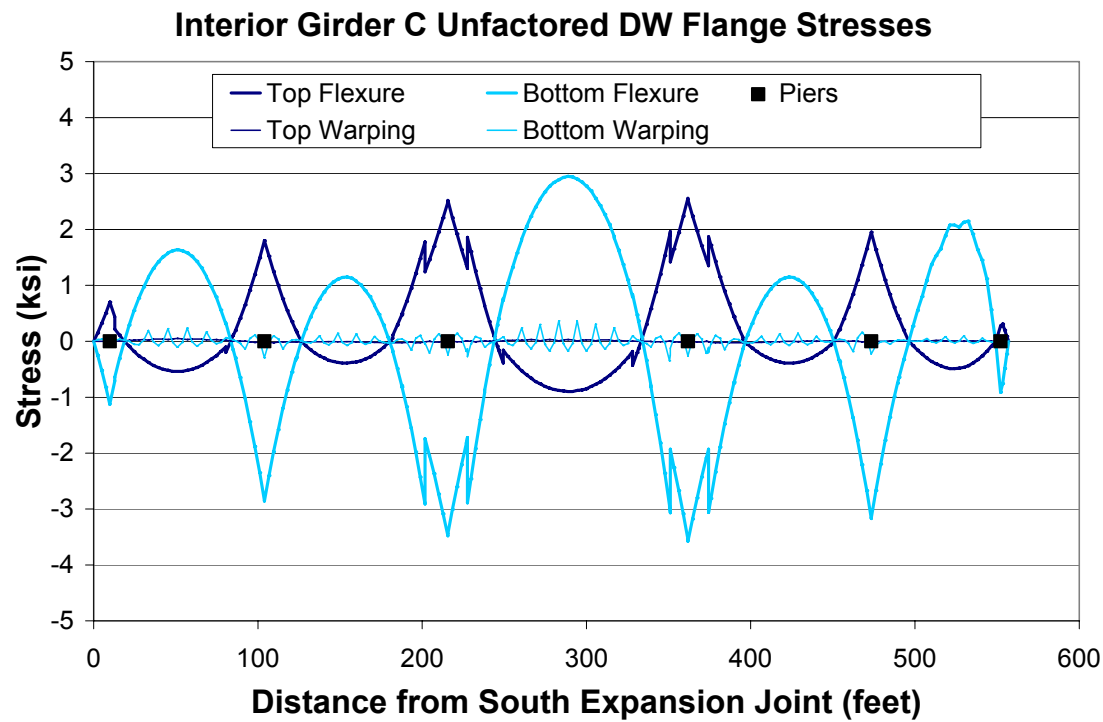


Figure 9-9: Interior Girder C Unfactored DW Flange Stresses

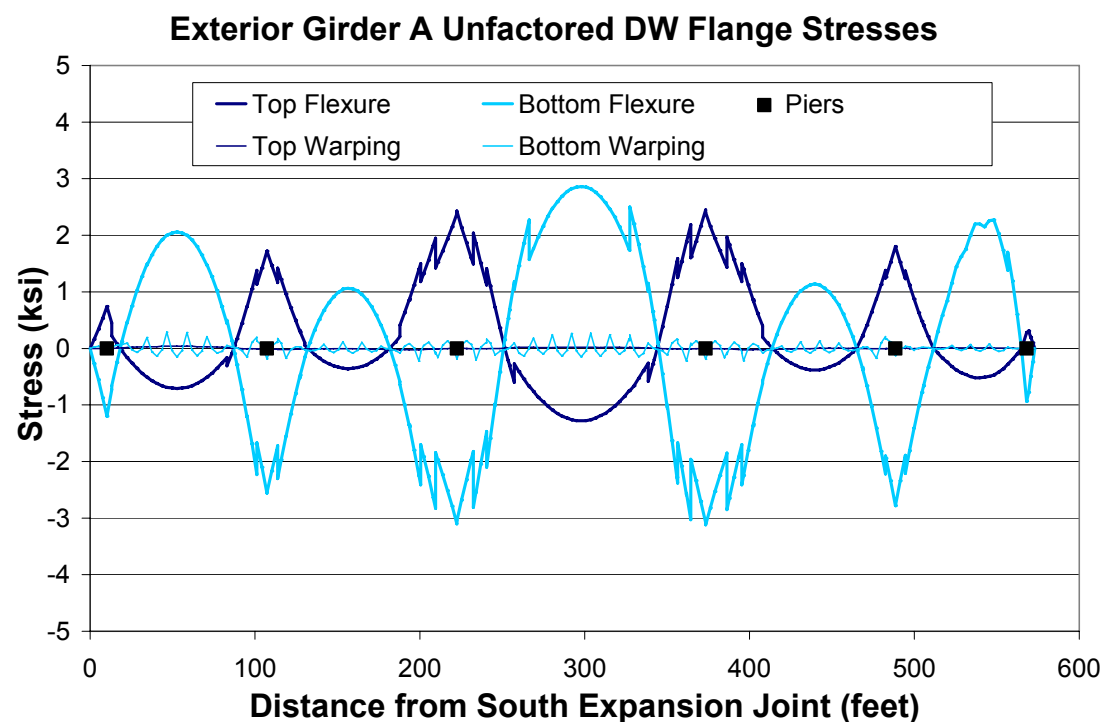


Figure 9-10: Exterior Girder A Unfactored DW Flange Stresses

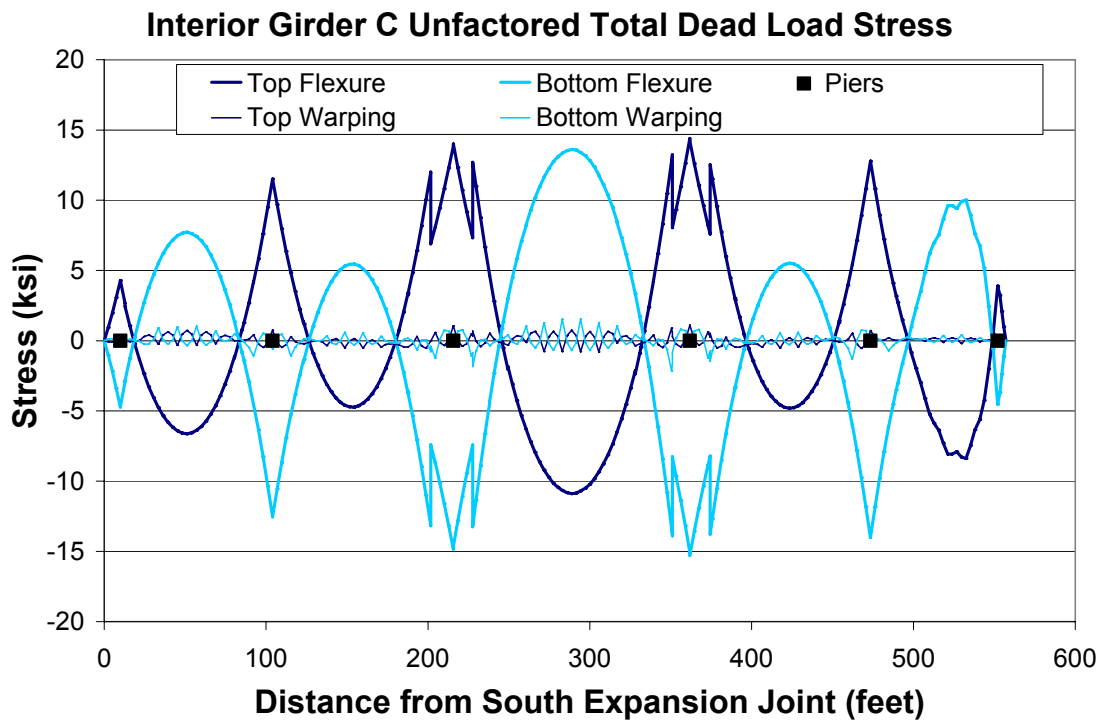


Figure 9-11: Interior Girder C Unfactored Total Dead Load Flange Stresses

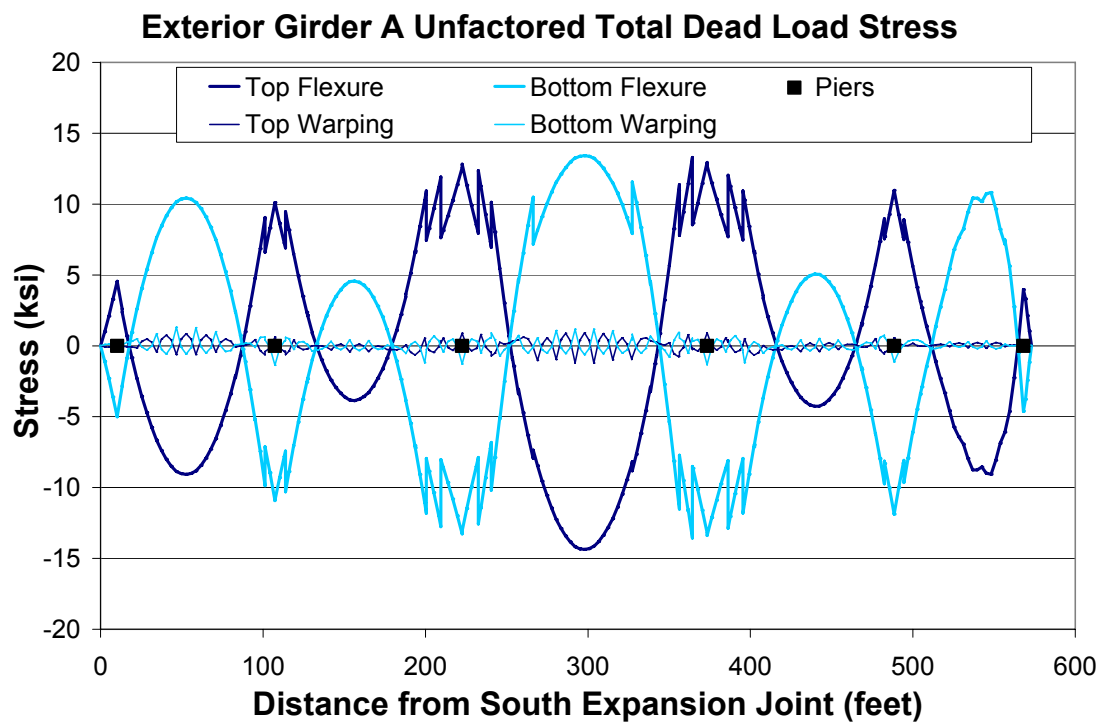


Figure 9-12: Exterior Girder A Unfactored Total Dead Load Flange Stresses

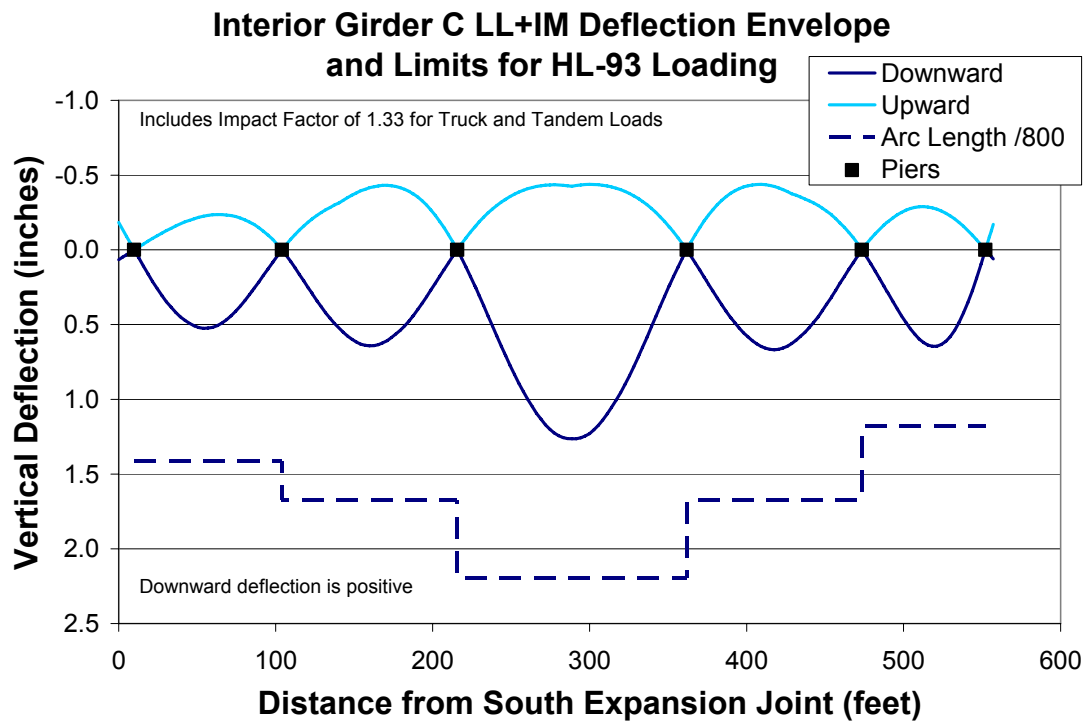


Figure 9-13: Interior Girder C LL+IM Deflection Envelope and Limits for HL-93 Loading

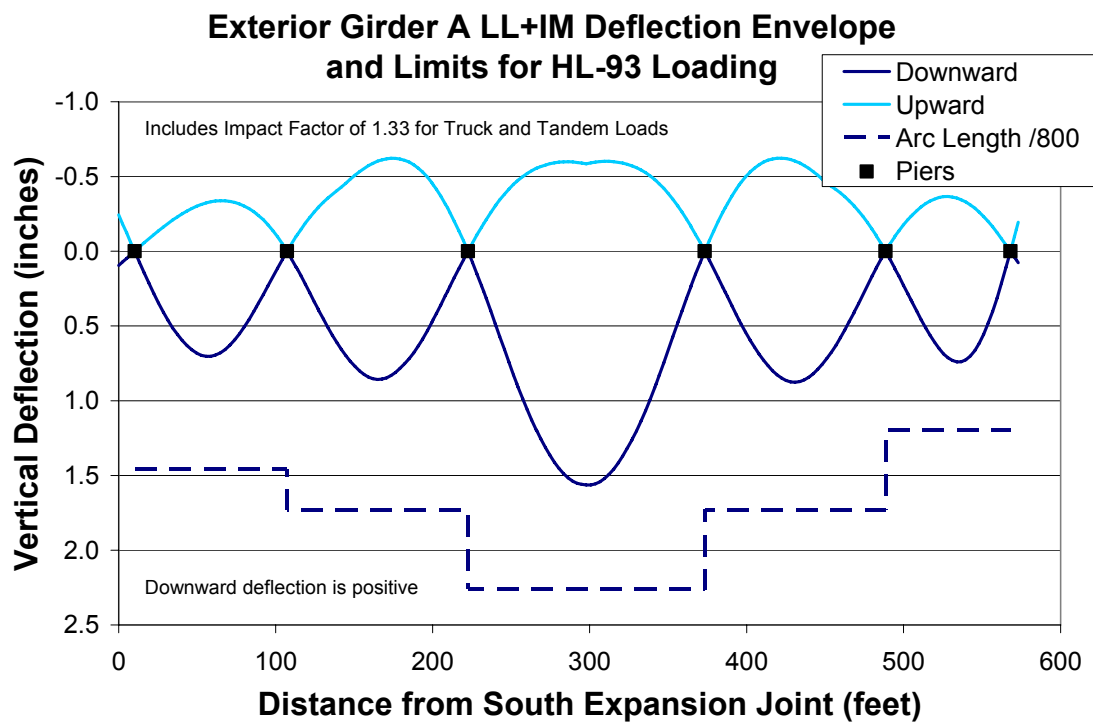


Figure 9-14: Exterior Girder A LL+IM Deflection Envelope and Limits for HL-93 Loading

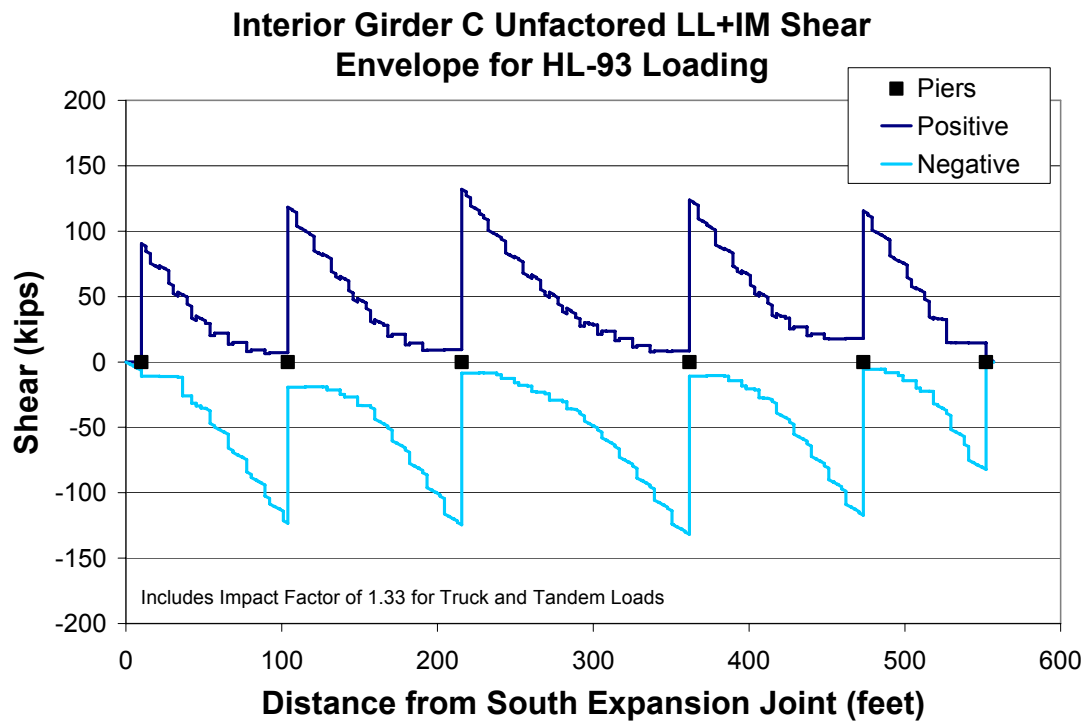


Figure 9-15: Interior Girder C Unfactored LL+IM Shear Envelope for HL-93 Loading

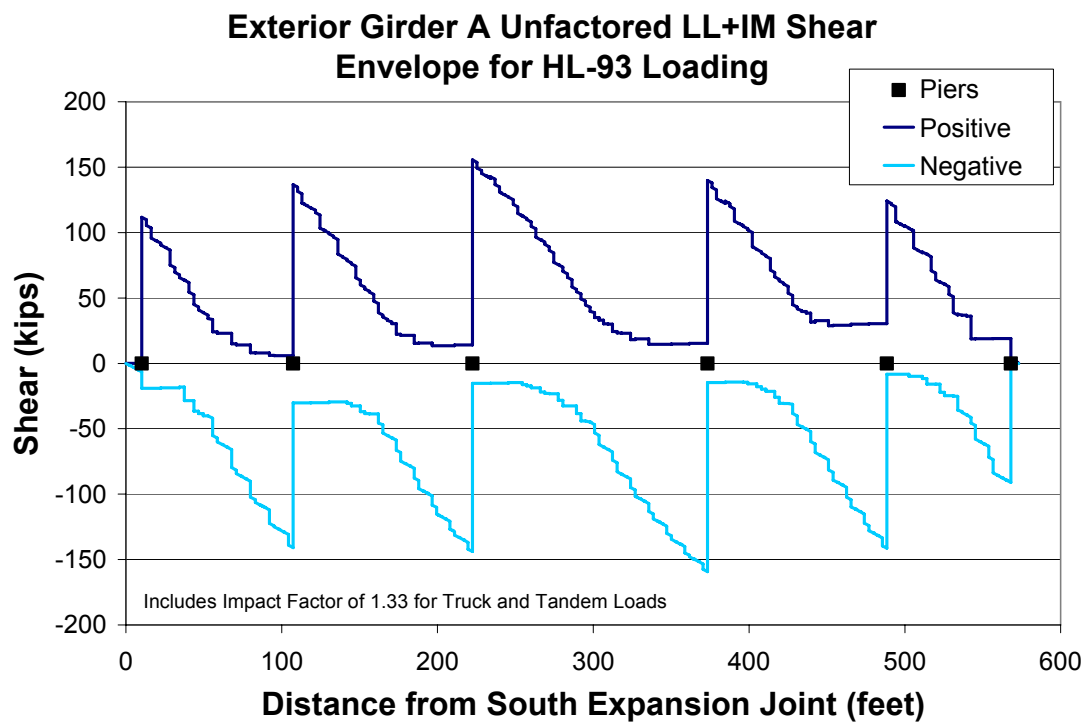


Figure 9-16: Exterior Girder A Unfactored LL+IM Shear Envelope for HL-93 Loading

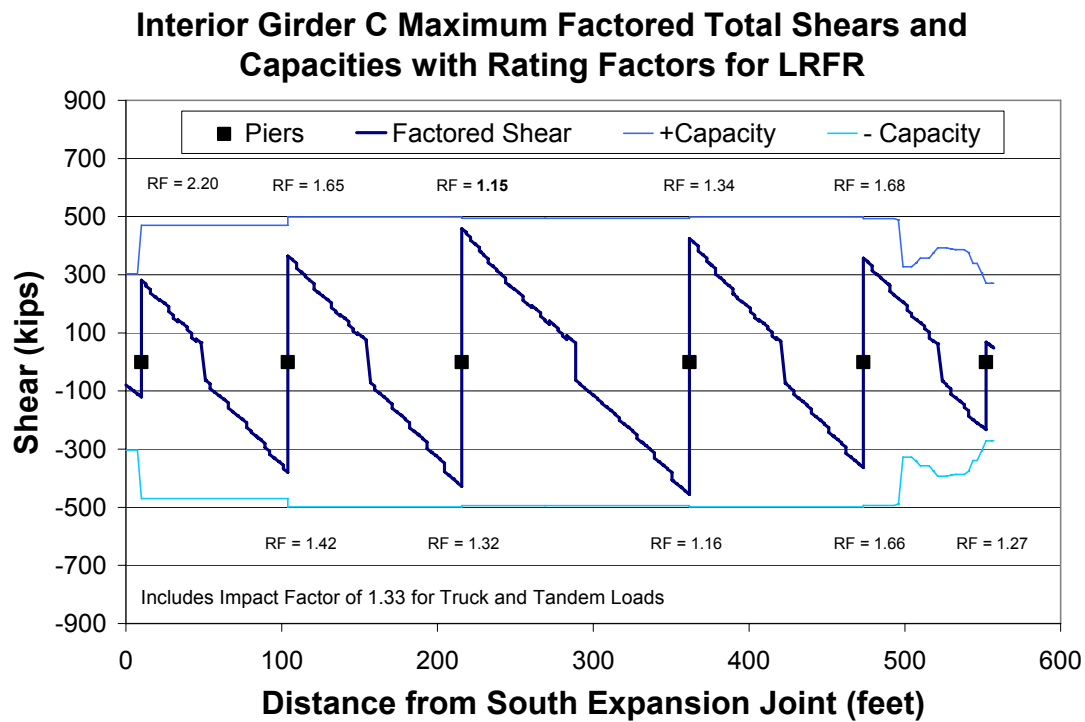


Figure 9-17: Interior Girder C Factored Total Shears and Capacities with Rating Factors for LRFR

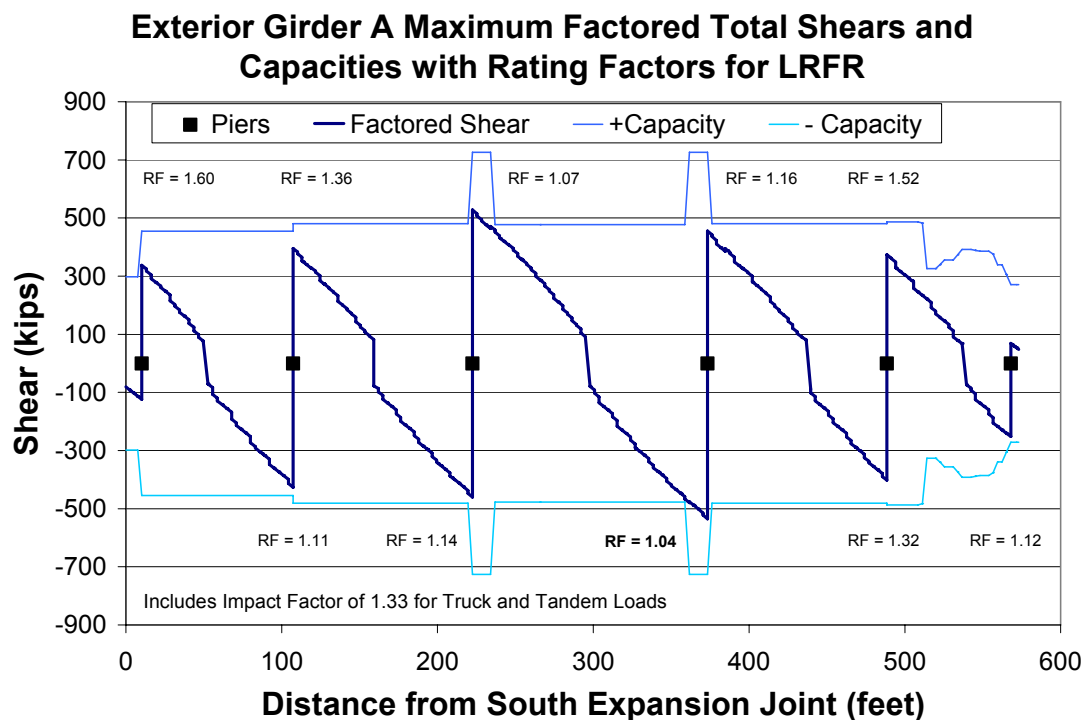


Figure 9-18: Exterior Girder A Factored Total Shears and Capacities with Rating Factors for LRFR

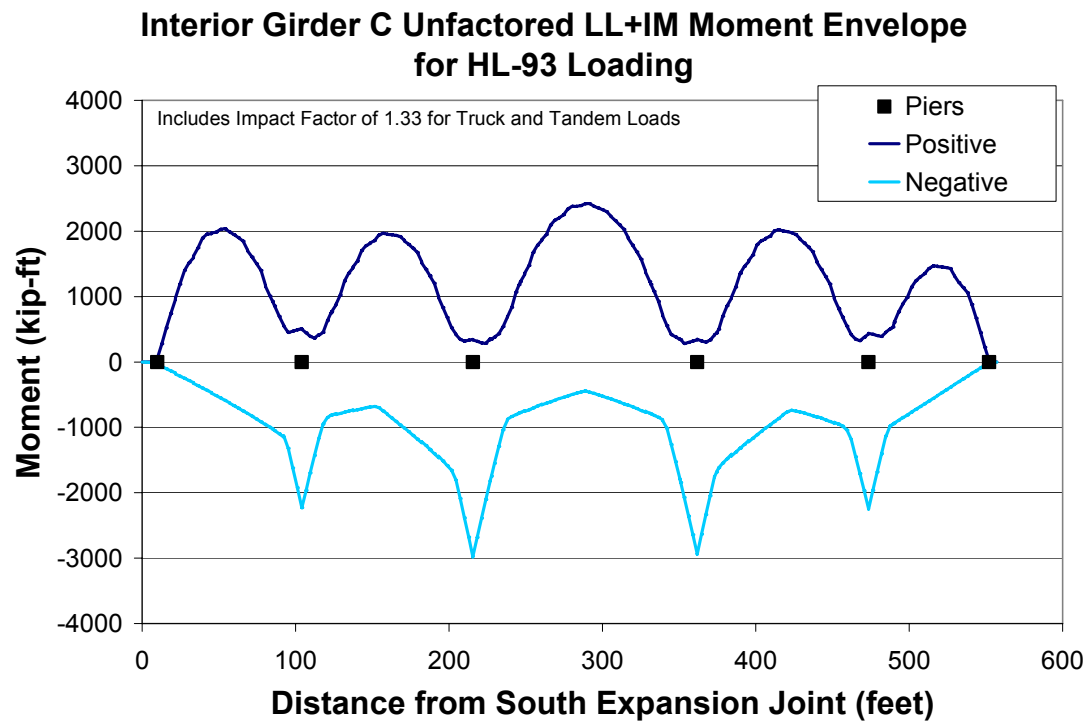


Figure 9-19: Interior Girder C Unfactored LL+IM Moment Envelope for HL-93 Loading

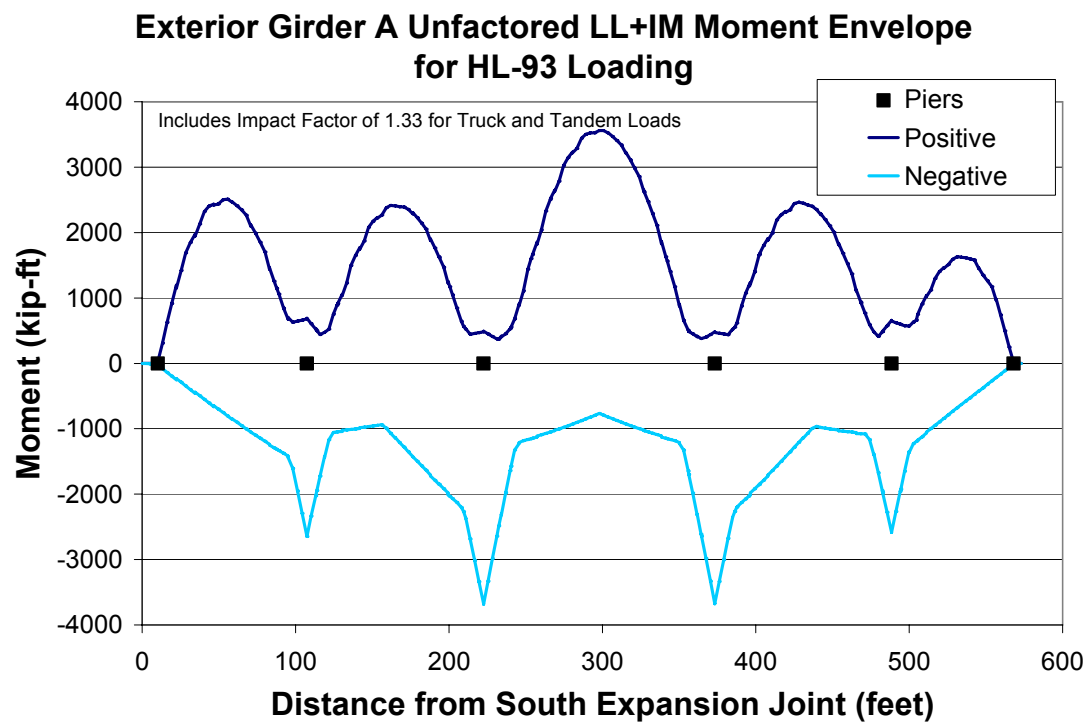


Figure 9-20: Exterior Girder A Unfactored LL+IM Moment Envelope for HL-93 Loading

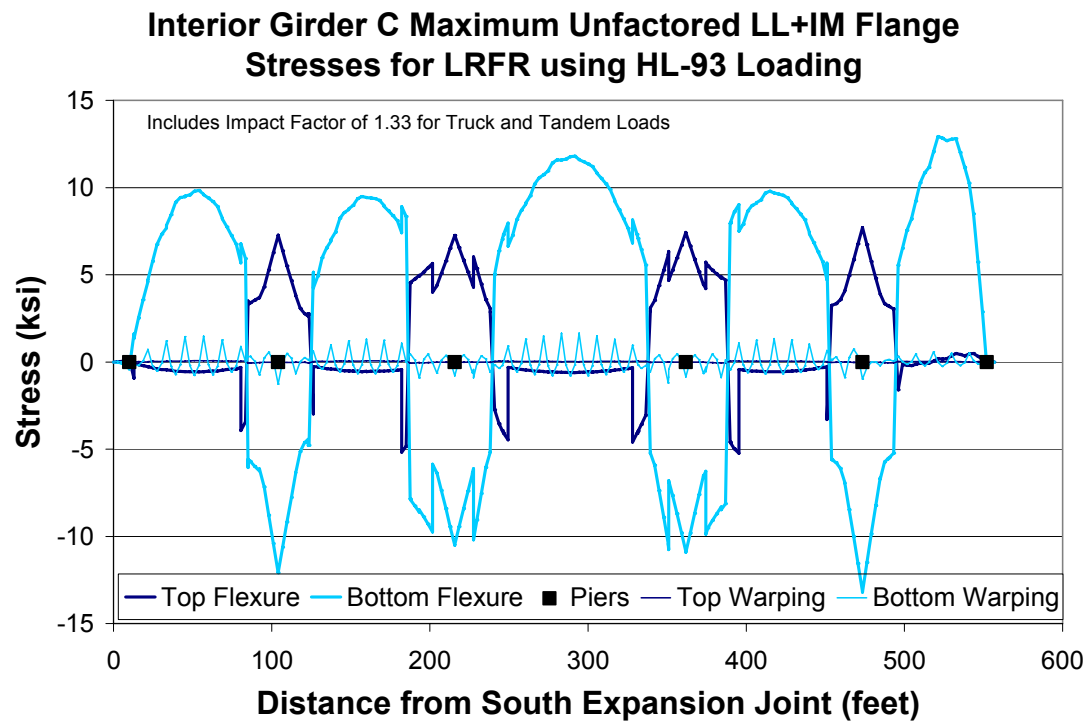


Figure 9-21: Interior Girder C Maximum Unfactored LL+IM Flange Stresses for LRFR

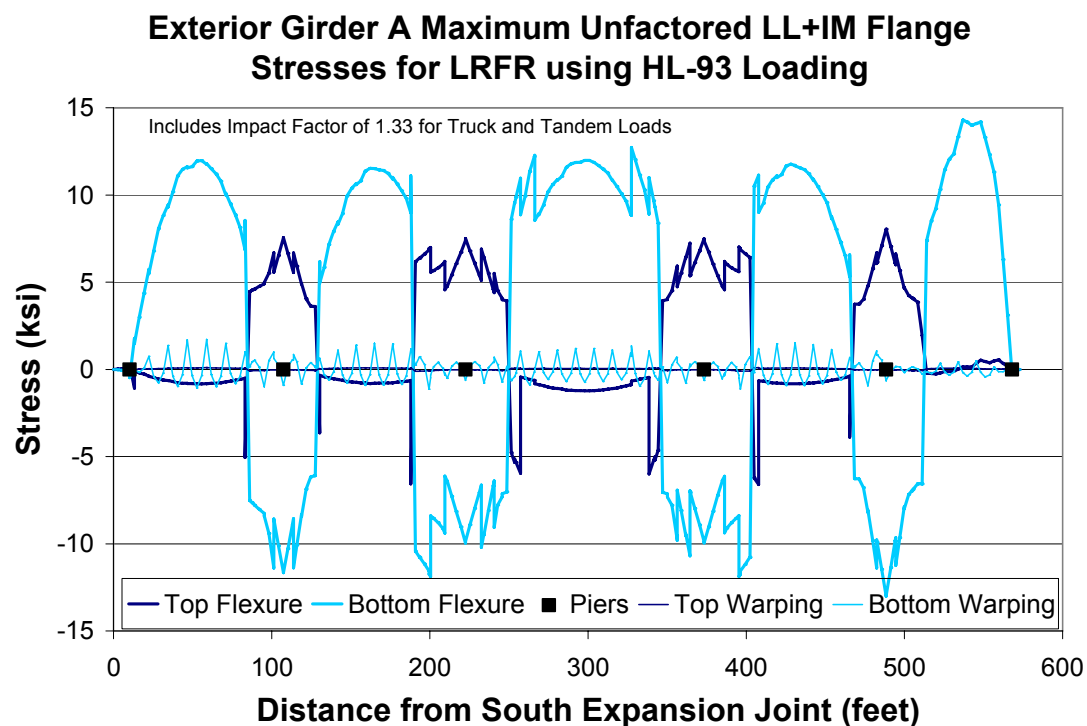


Figure 9-22: Exterior Girder A Maximum Unfactored LL+IM Flange Stresses for LRFR

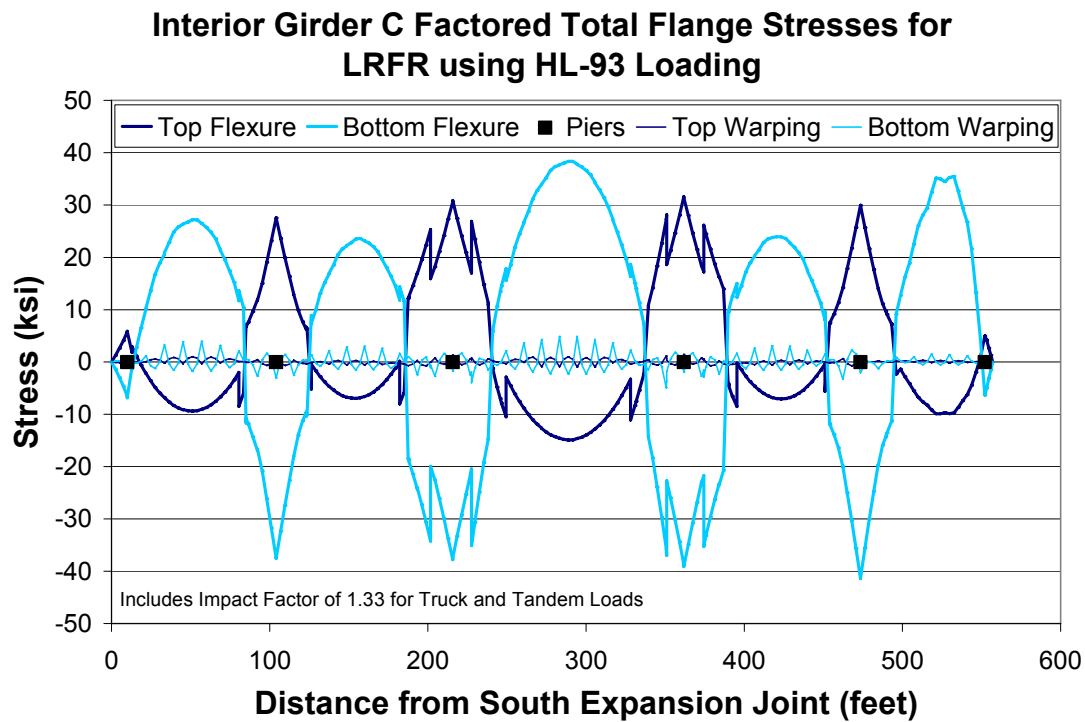


Figure 9-23: Interior Girder C Factored Total Flange Stresses for LRFR

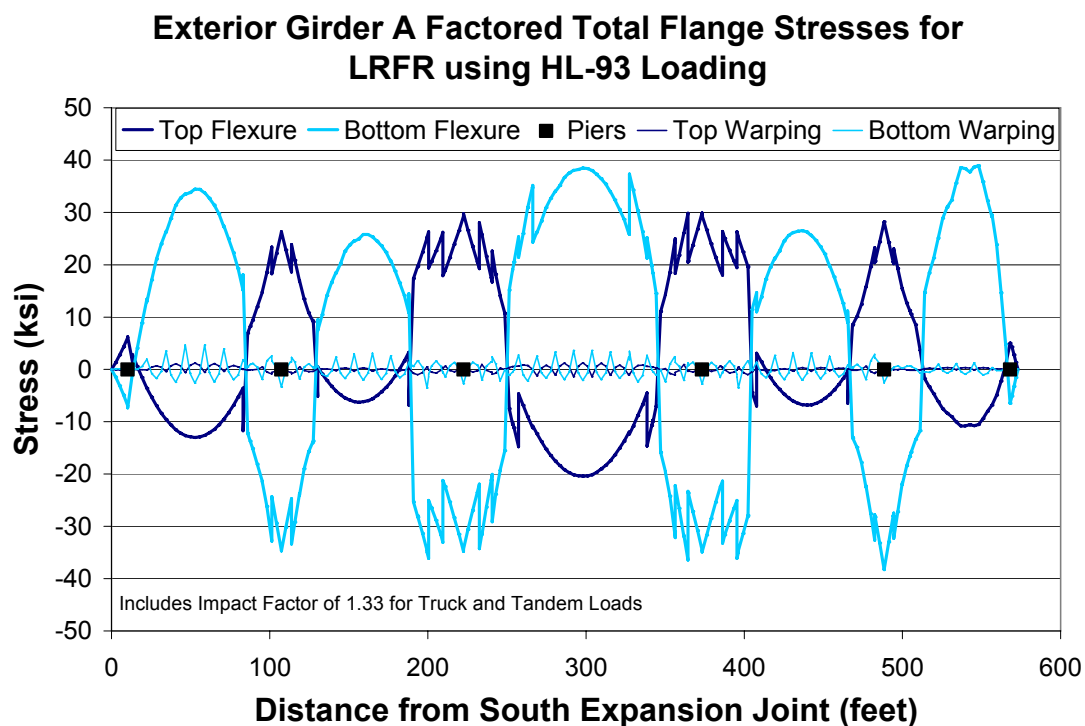


Figure 9-24: Exterior Girder A Factored Total Flange Stresses for LRFR

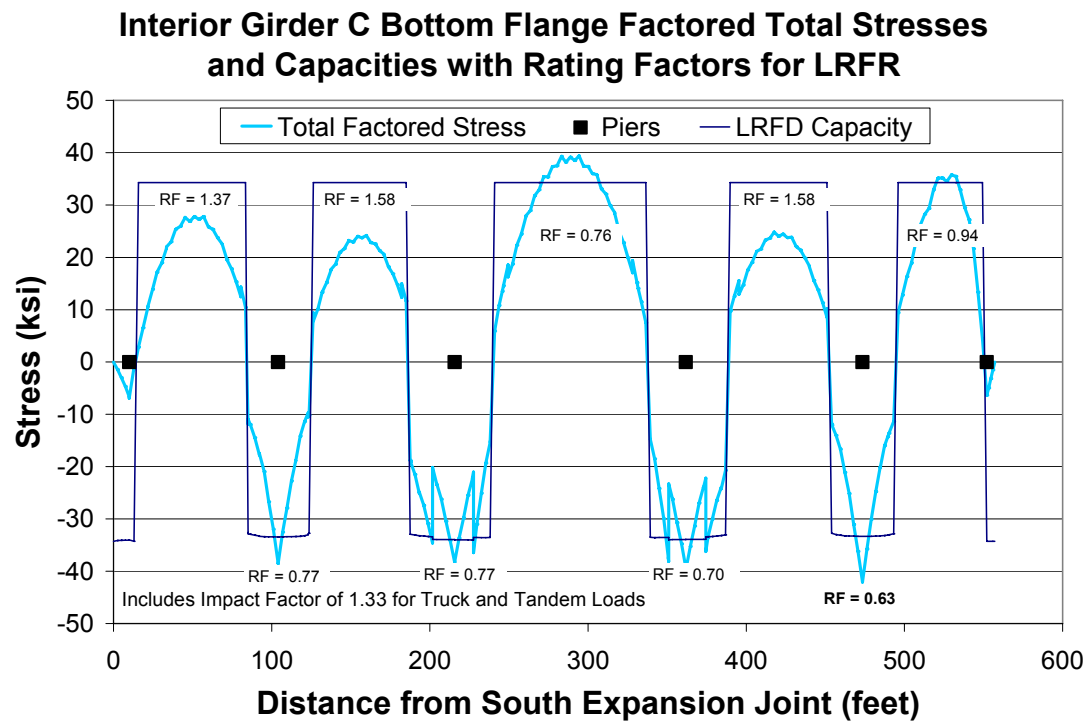


Figure 9-25: Interior Girder C Bottom Flange Factored Stresses, Capacities, and RF for LRFR

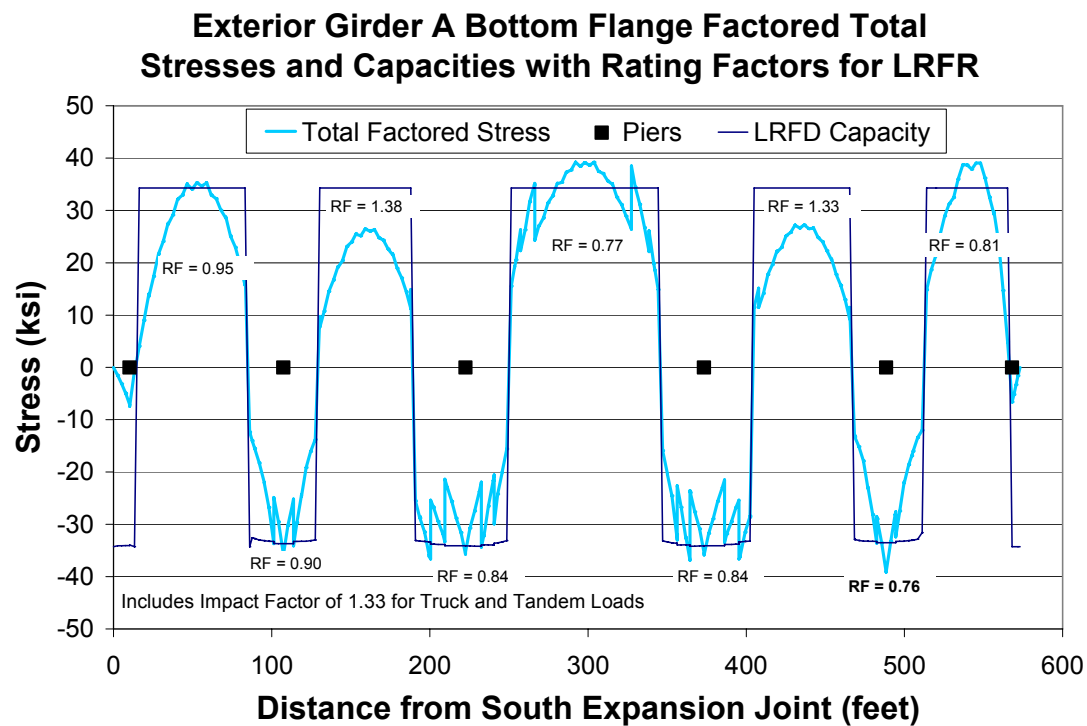


Figure 9-26: Exterior Girder A Bottom Flange Factored Stresses, Capacities, and RF for LRFR

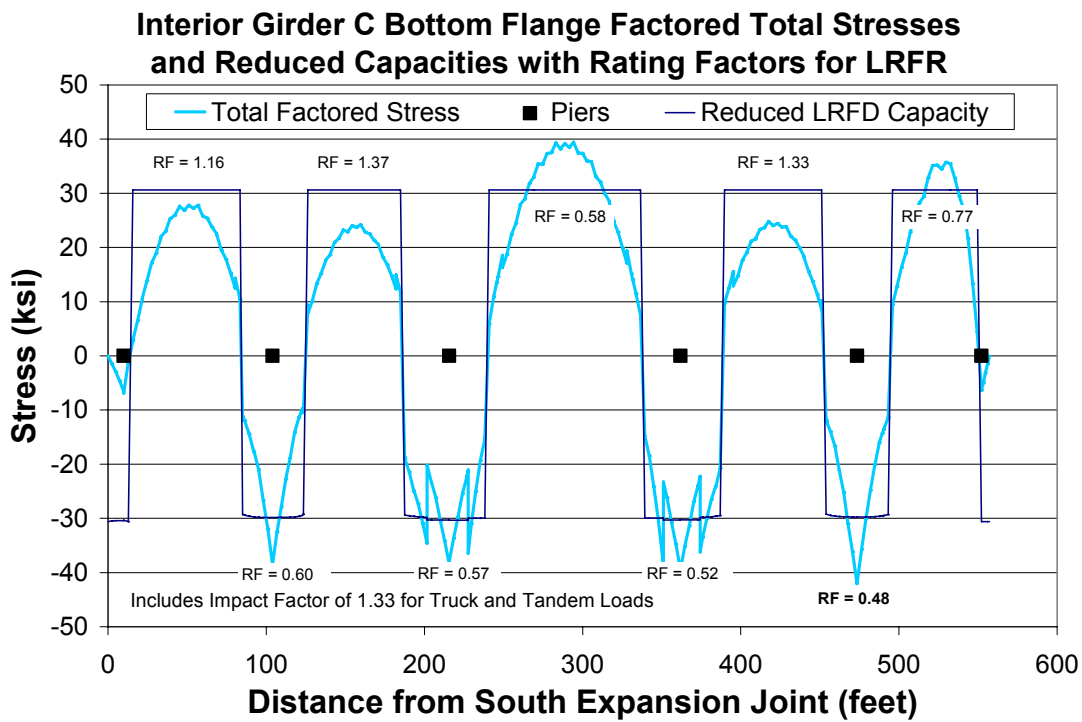


Figure 9-27: Interior Girder C Bottom Flange Factored Stresses, Reduced Capacities, and RF for LRFR

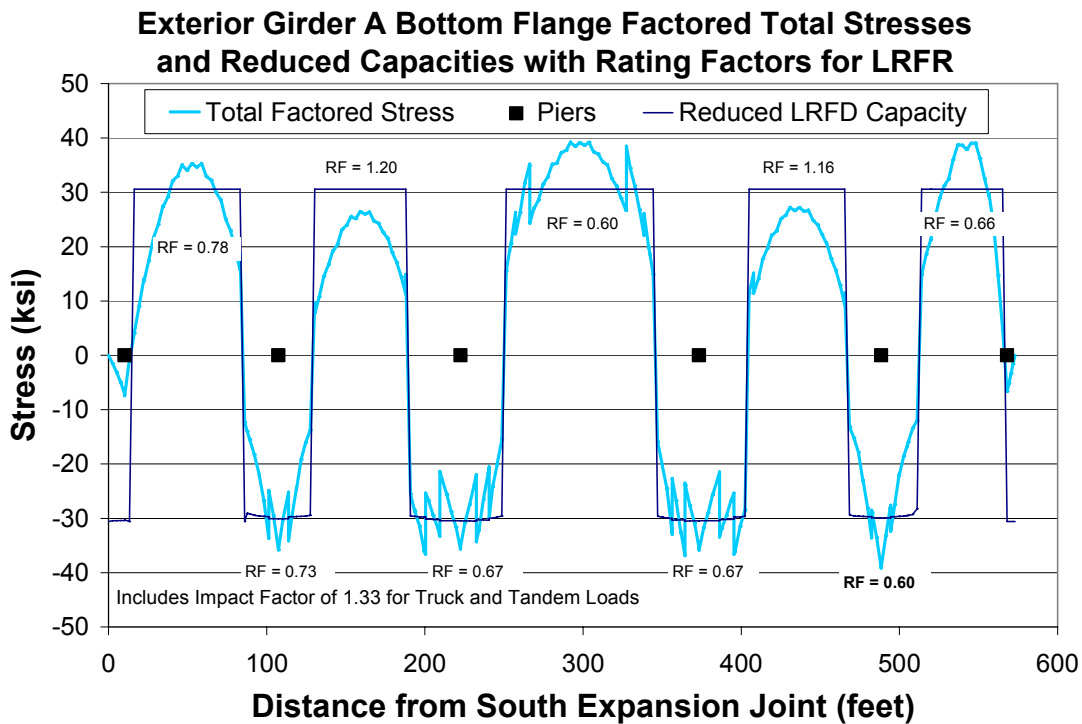


Figure 9-28: Exterior Girder A Bottom Flange Factored Stresses, Reduced Capacities, and RF for LRFR

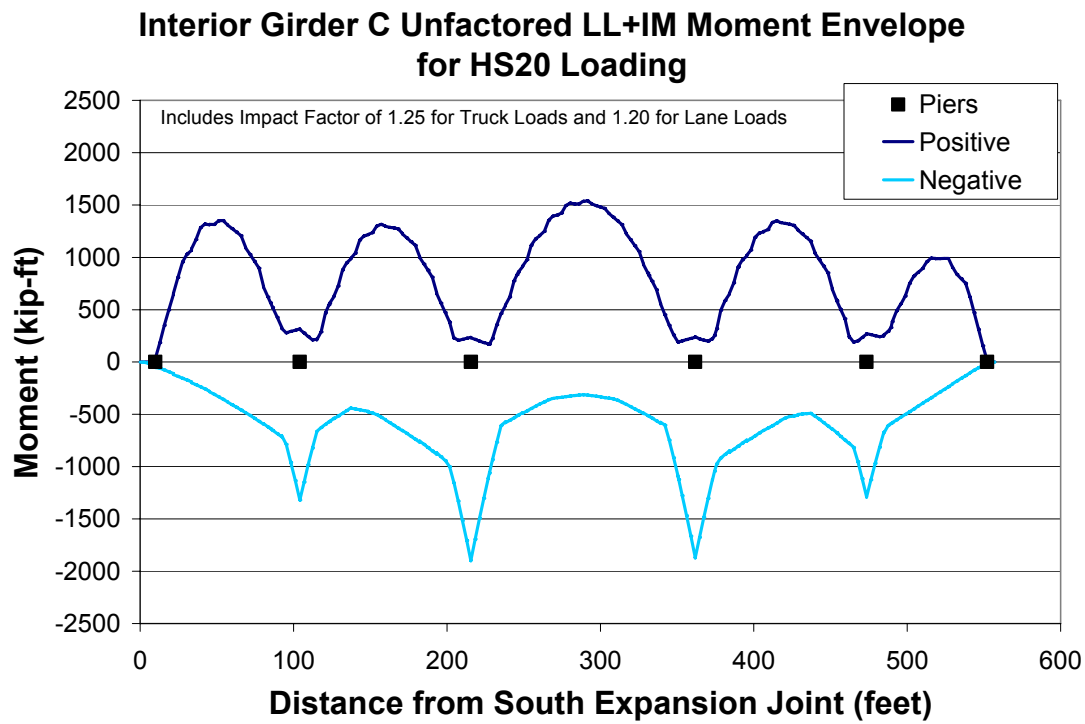


Figure 9-29: Interior Girder C Unfactored LL+IM Moment Envelope for HS20 Loading

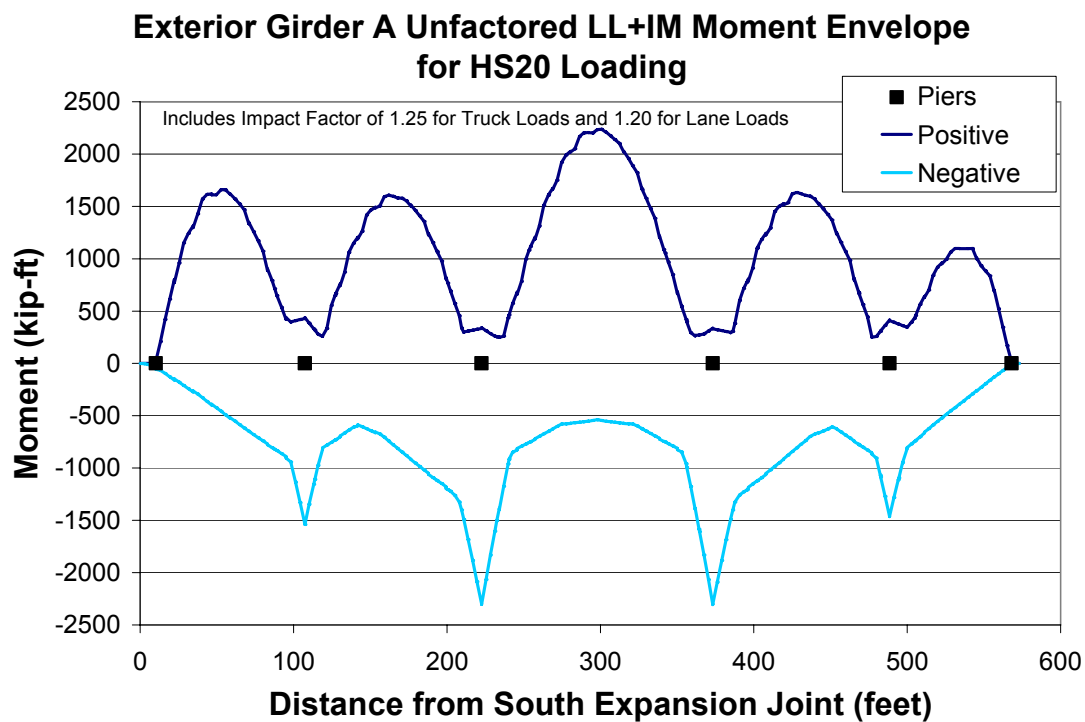


Figure 9-30: Exterior Girder A Unfactored LL+IM Moment Envelope for HS20 Loading

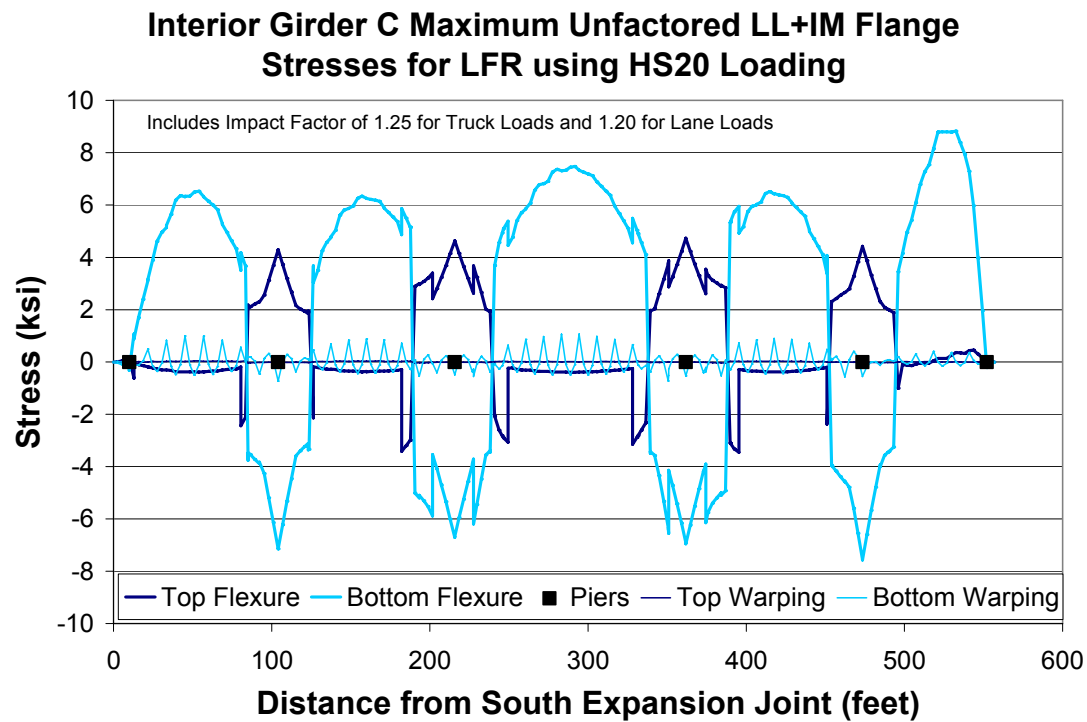


Figure 9-31: Interior Girder C Maximum Unfactored LL+IM Flange Stresses for LFR

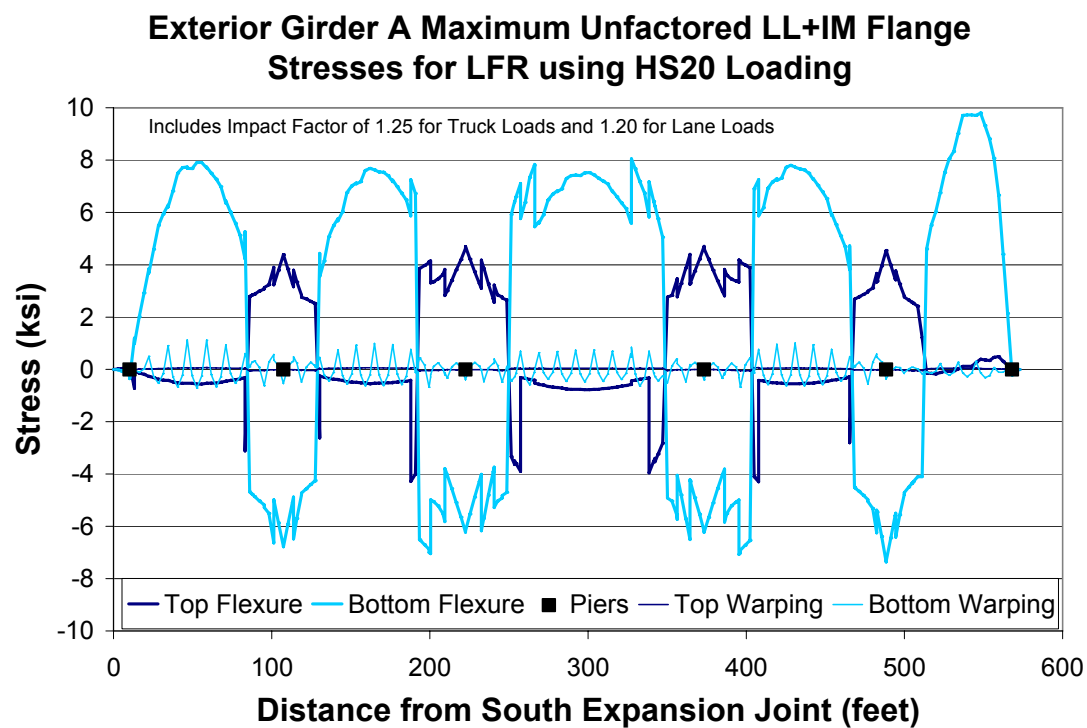


Figure 9-32: Exterior Girder A Maximum Unfactored LL+IM Flange Stresses for LFR

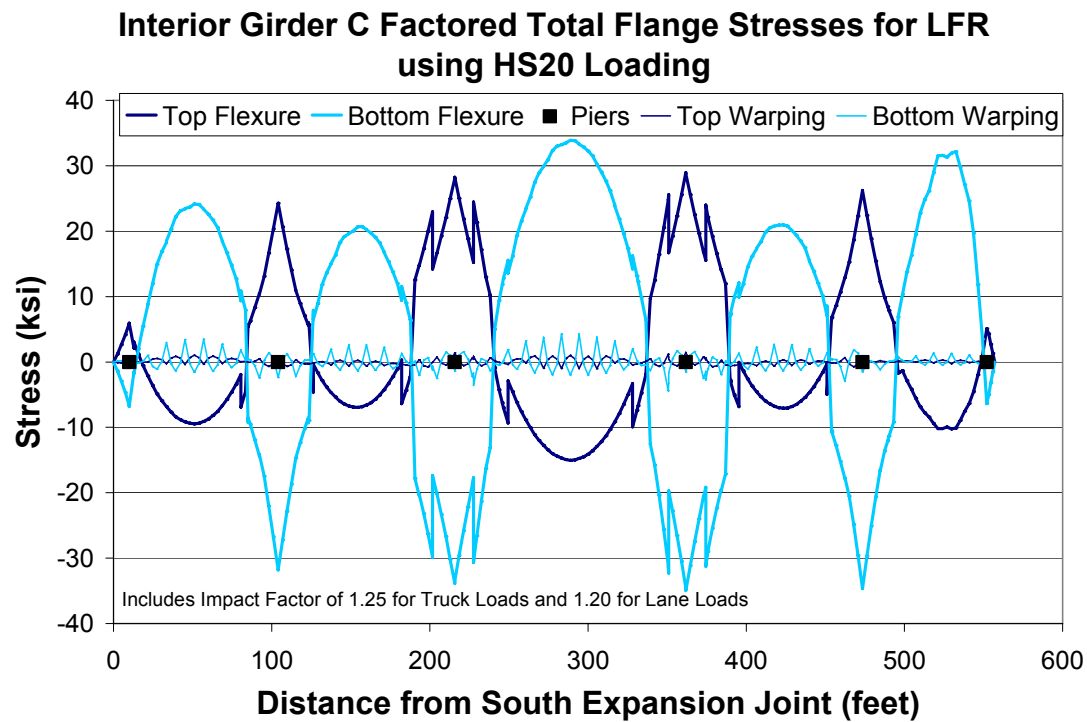


Figure 9-33: Interior Girder C Factored Total Flange Stresses for LFR

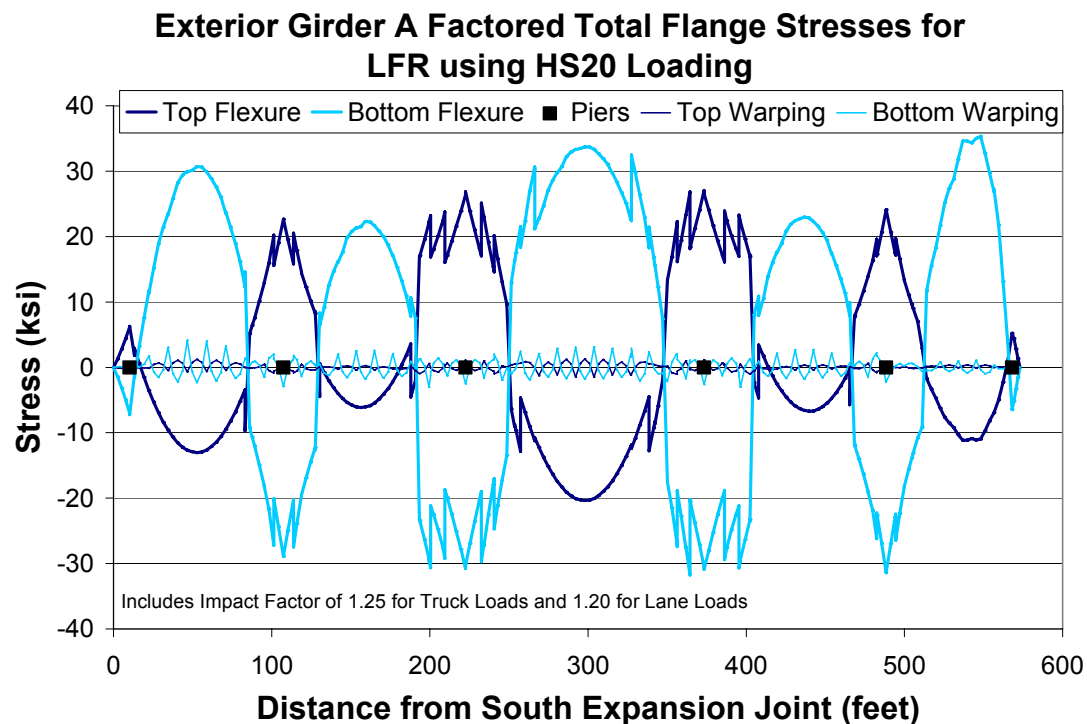


Figure 9-34: Exterior Girder A Factored Total Flange Stresses for LFR

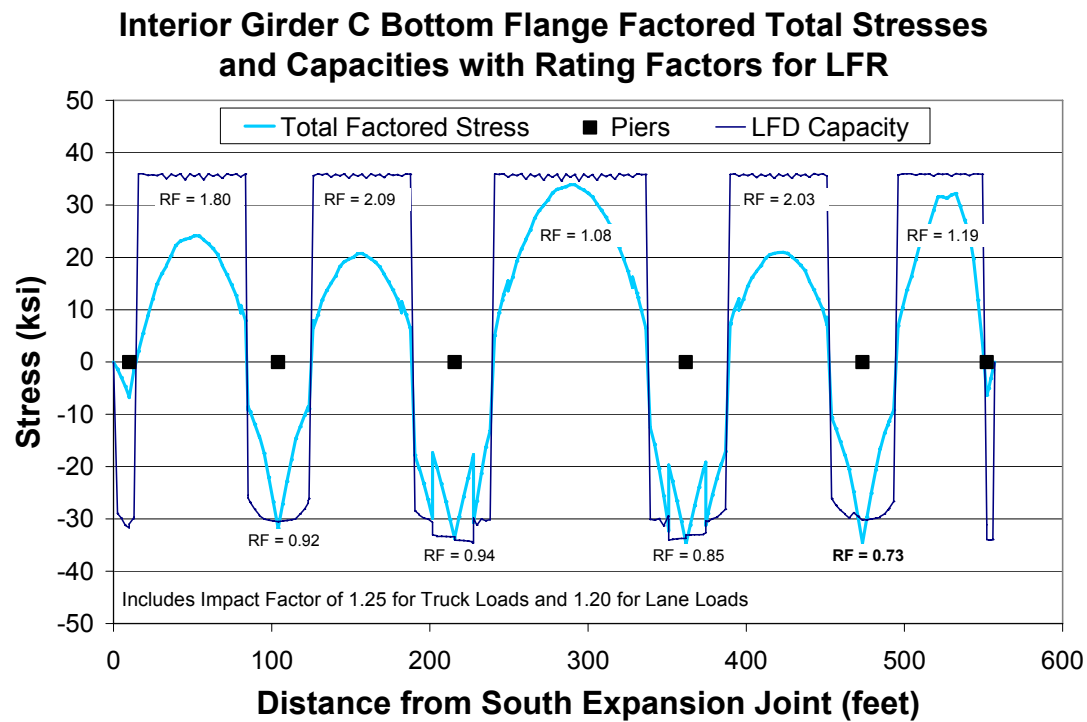


Figure 9-35: Interior Girder C Bottom Flange Factored Stresses, Capacities, and RF for LFR

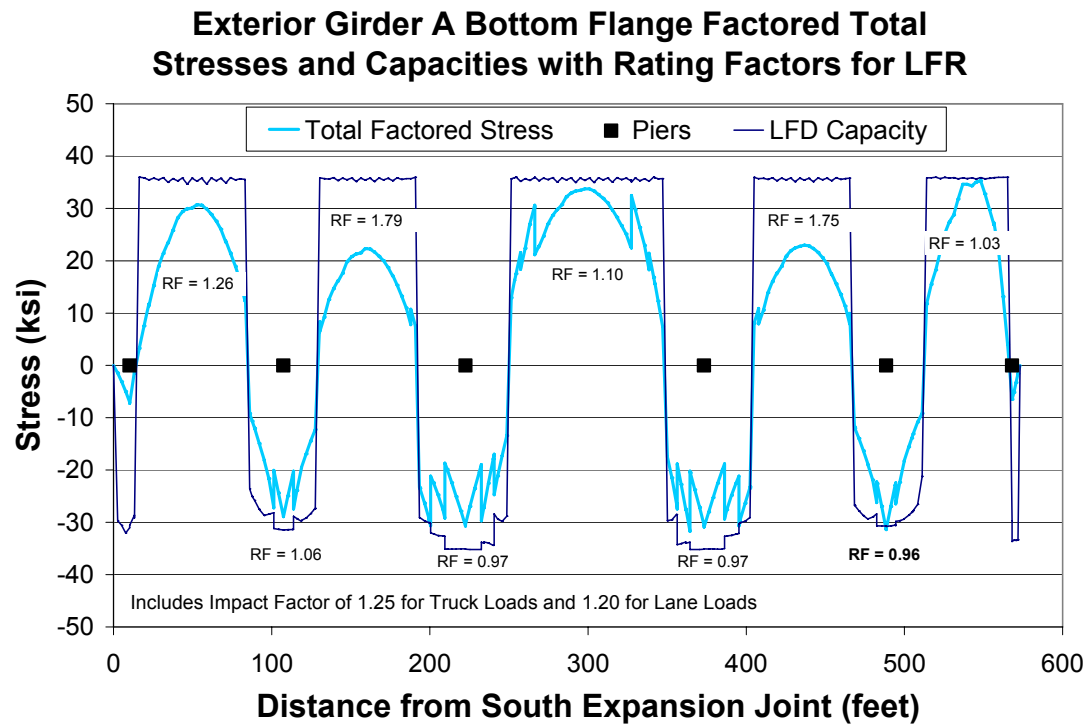


Figure 9-36: Exterior Girder A Bottom Flange Factored Stresses, Capacities, and RF for LFR

Chapter 10

Conclusions

This research project has outlined methods that can be used to provide more accurate load ratings of horizontally curved composite steel I-girder bridges. It has focused on the use of grillage computational analysis, load factor rating (LFR) and the new load and resistance factor rating (LRFR) methodologies, along with experimental results based on load tests with heavy trucks to improve the accuracy of load ratings for these complex structures. The following paragraphs provide a summary of this research project, highlighting key findings, conclusions, and recommendations.

10.1 Summary of Methodology

A literature review was conducted investigating load rating, load testing, and computational analysis of steel I-girder bridges, especially pertaining to bridges with horizontal curvature. Rating procedures for LFR and LRFR were presented, including discussion on the various levels of rating, the general rating equations, and the application of loads and factors for each methodology. It was noted that due to heavier rating loads (i.e., HL-93 Loading versus HS20 Loading) and the introduction of system and condition factors that add an additional level of safety to non-redundant and deteriorated bridges in the new LRFR methodology, load ratings for LRFR will generally be lower than for previous ratings based on LFR. Diagnostic, proof, and dynamic load tests were discussed and examples of each from literature were provided. Various types of computational analysis for horizontally curved steel I-girder bridges were also presented. In particular, linear elastic grillage analysis was shown to be useful for bridge rating since it is time efficient, readily available in commercial programs, has been used by a number of researchers to provide accurate predictions of experimental bridge tests (Galambos et al., 2000; McElwain and Laman, 2000; Nevling, 2003; Chang et al., 2005), and has shown good correlation with more refined 3D finite element methods (Simpson, 2000; Nevling, 2003; Chang et al., 2005).

Mn/DOT Bridge No. 69824, a two-girder five-span continuous horizontally curved steel I-girder bridge located in Duluth, Minnesota, was selected for analysis and load testing as part of this research project. The bridge was built in the late 1960s and was designed as composite in the positive moment regions only (i.e., the girders only have shear connectors in the positive moment regions). The typical radius of curvature for the bridge on the Interior Girder C is approximately 566 feet, and that on the Exterior Girder A is approximately 584 feet. All support columns are radially positioned. Diaphragms on the bridge are also radially positioned and are spaced at approximately 12 foot increments. The diaphragms consist of W21x55 rolled sections with shear connectors on the top flange embedded in the concrete deck for composite action and knee braces at the ends of the beams framing into the connection stiffeners on the girders. Lateral wind bracing forming an X-pattern between consecutive diaphragms is provided using WT sections connected to gusset plates near the bottom flanges of the girders. The deck was cast-in-place and has a typical thickness of 9 inches, 2 inches of which are from an overlay added in 1982. The edges of the roadway consist of curbs along with concrete rail beams supported every 10 to 14 feet by short concrete columns.

Bridge analysis in this research project was primarily conducted using UMN Program, a linear elastic grillage-based finite element program which was previously written at the University of Minnesota for studying curved steel I-girder bridges (Huang, 1996; Galambos et al., 1996). Curved girders are modeled in the program using open-walled section beam elements with seven degrees of freedom (DOFs) per node; three deflections, three rotations, and a cross-section warping DOF. The composite action of the concrete deck is primarily modeled in UMN Program by using composite properties for the girder and diaphragm elements when appropriate, although transverse concrete deck beams are included to provide the axial stiffness between the top flanges of adjacent girders. Straight beam and truss elements are used to model the diaphragms, transverse concrete deck beams, and lateral wind bracing, while rigid offsets are used to provide the vertical eccentricities between the various elements. The original source code for UMN Program was updated as part of this project so as to be more efficient and applicable to a wider range of bridges and bridge behavior. To provide confidence in the updated software, UMN Program results for a single curved girder with a variety of boundary conditions were successfully verified against solutions based on the differential equations governing the linear elastic behavior of a horizontally curved beam. In addition, comparisons primarily focusing on the non-composite dead and superimposed dead load behavior of Mn/DOT Bridge No. 69824 were made between results from UMN Program and MDX, a commercially available bridge design and rating analysis program. Comparisons between the two programs for vertical pier reactions, bending moment and shear, and longitudinal stress along the length of the bridge were generally strong with the majority of percent differences being less than 10%. Correlations for vertical deflections of the girders were somewhat lower between the two programs with percent differences being up to approximately 20% to 30%. Overall, the correlation between the two programs was strong for the dead load behavior of the bridge.

Load testing of Mn/DOT Bridge No. 69824 was conducted focusing primarily on the behavior of two spans, Span 9-8 and Span 8-7, which were readily accessible for instrumentation and had the longest centerline arc span lengths of the bridge at approximately 113 feet and 149 feet, respectively. An extensive array of instrumentation was developed to maximize the data collected from the field, including twelve displacement devices and one hundred twenty-eight strain gages. Measurements documented in the field test included:

- Girder, diaphragm, and lateral wind bracing strains/stresses
- Vertical and rotational girder displacements
- Web gap distortional strains/stresses
- Strains/stresses at gusset plate connection
- Slip at the interface of the girder top flange and the concrete deck in the negative moment regions
- Expansion bearing displacements

Forty-three static load tests and thirteen dynamic load tests were conducted on the bridge beginning shortly after 8 p.m. on July 14, 2004, and going until approximately 4 a.m. on July 15. The static load tests consisted of a series of truck configurations utilizing up to eight quad-axle dump trucks, each weighing approximately 72 kips. Low load level tests were designed to mimic typical loading seen on the bridge, while high load level tests were designed to load the bridge to a Mn/DOT specified total stress (i.e., dead load + live load) limit of 75% of yield stress to provide bridge behavior at anticipated load rating levels while also preventing damage to the

structure. The static tests were subdivided into nine sets based on testing objectives. The first two sets provided light and heavy load influence lines for one and four trucks, respectively, positioned at locations along the bridge testing region. The third set focused on positive moment stresses on Span 9-8, while the fourth set did the same for Span 8-7. Negative moment stresses at Pier 8 were the objective of the fifth set. The sixth and seventh sets dealt with load transversely positioned on Span 9-8 above the exterior girder and interior girder, respectively. The last two sets provided twisting cases where the loads on Span 9-8 and Span 8-7 were on opposing girders. The dynamic load tests consisted of individual trucks driving along the centerline of the bridge and were subdivided into three sets: constant velocity, constant velocity over 2x4, and constant velocity then braking. The constant velocity dynamic tests consisted of an individual truck driving along the centerline of the bridge at a constant velocity. The constant velocity over 2x4 dynamic tests consisted of a truck driving over a wood 2x4 placed at midspan between Pier 9 and Pier 8. The constant velocity then braking dynamic tests had a truck quickly apply its brakes as it passed over Pier 8 and onto Span 9-8. All of the dynamic tests were done at a variety of vehicle speeds up to the posted maximum speed of 35 mph for the bridge.

10.2 Summary of Research Findings

10.2.1 Test Results

Following the load test, the raw experimental test data was reduced to a useable form, including the removal of unwanted thermal strains that occurred over the first few hours of testing and the conversion from voltage changes and strains to displacements and stresses. A series of evaluations were conducted to determine various bridge properties and behavior. Findings include:

- Composite action was verified in the positive and negative moment regions for the girders and for the beam diaphragms at all load levels, although the girders do not have shear connectors in the negative moment regions. Friction, adhesion, and the shear connectors on the diaphragms were found to provide enough resistance for composite action to develop for the girders in the negative moment regions. Measured moments of inertia along the instrumented region of the bridge were 2 to 3 times higher than for the bare steel sections alone. Maximum interfacial slip measured between the top flange of the girders and the concrete deck near Pier 9 and Pier 8 was small at around 0.005 inches and remained elastic (i.e., it always returned to the original position when load was removed) even at higher load levels. This, plus the fact that pre- and post-test inspections of the negative moment regions revealed no indications of slip validate the inclusion of composite action in the negative moment regions of Mn/DOT Bridge No. 69824 for analytical purposes. A more appropriate modular ratio N of 6 was identified for the bridge based on the age of the structure and load test results. Assuming a linear strain profile and using the average neutral axis locations based on measured longitudinal strains near the top and bottom flanges, calculated effective concrete widths for the various girder cross sections ranged between approximately 57 inches and 414 inches. An average effective width for all girder sections was calculated to be 166 inches with a standard deviation of 97 inches. The large scatter in measured effective widths for the girders was largely due to influence from the discontinuous concrete guard railing on the

edges of the bridge. Effective concrete widths for the girders of 123 inches in the positive moment regions and 102.5 inches in the negative moment regions were recommended based on AASHTO (2004) provisions and good correlation with test results. The larger value for the effective width in the positive moment regions includes effects due to the concrete curb, while this contribution was determined to be unreliable in the negative moment regions due to effects of tensile cracking. Stiffening effects due to the guard railing were determined to be unreliable due to severe spalling and deterioration of the columns between the curbs and guard railings. An effective width of 7 inches was recommended for the composite beam diaphragms based on test results.

- Girder distribution factors (GDFs) were determined using measured test data as the percent of total moment on a girder at a given bridge cross section for various transverse positions of the center of gravity of the applied loads. GDFs for cross sections near the center of gravity of the applied loads were 45% for the Interior Girder C and 55% for the Exterior Girder A when the center of gravity of the loads was transversely (i.e., radially) positioned halfway between the two girders. For cases where the load was transversely positioned 5.5 feet closer to the interior girder, the interior girder carried 66% of the total moment while the exterior girder had 34%. This correlates to a 21% load shift for each girder as compared to the centered case. On the other hand, when the load was transversely positioned 5.5 feet closer to the exterior girder, the percentages were 23% for the interior girder and 77% for the exterior girder. This is a 22% shift from the transversely centered position. As can be seen, an equal shift (5.5 ft) in the transverse position from center results in an equal percentage change (approximately 21.5%) in the GDFs. These GDF values are specific to cross sections near the applied loads, and are useful for distributing the loads to nearby girder nodes when using a system-based analysis technique. They are not recommended for line girder analysis, since it was found that one set of GDFs along the length of the bridge did not accurately define the load distribution. Results showed that the GDFs vary along the length of the bridge, especially from span to span. Because of this, it is recommended that curved bridge analysis be done using a system-based analytical technique to provide a more accurate representation for load path.
- Expansion bearing measurements at Pier 9 for both girders revealed minimal amounts of movement. Post-test inspection of the bearings also showed no indications of movement validating the small measured values. A small accumulation of displacement on the order of 0.002 inches was noted for Girder A, and was likely due to shifting of the entire bearing assembly on the thin lead pad separating the concrete pier cap from the steel base plate. Visual inspection of other expansion bearings for the bridge indicated that most are likely frozen as was seen for the two at Pier 9. Due to frozen bearings and non-negligible thermal effects that were measured during the beginning hours of the load test (see Chapter 5), a thermal analysis of the bridge may be warranted. However, the bridge has sustained over 30 years of 100+ degree Fahrenheit annual temperature variations without problems. Thus, other mechanisms, such as displacement and rotation of the piers, may be providing enough release for the thermal strains generated in the bridge.
- Dynamic impact factors (DIFs) were determined for the girders, diaphragms, and lateral wind bracing as part of a limited investigation into the dynamic behavior of Mn/DOT Bridge No. 69824. To determine the DIFs for this project, the dynamic test data was compared to a subset of static test data that provided a piecewise influence line for an

individual truck along the length of the load test region for each strain gage. This method provided conservative DIFs, especially for the diaphragms and lateral wind bracing, since the maximum forces for a truck along the bridge length were not necessarily captured in the static data subset. Results indicate that the recommended dynamic impact factors for horizontally curved steel I-girder bridges by the *Guide Specifications for Horizontally Curved Steel Girder Highway Bridges* (AASHTO, 2003a) are reasonable. Average calculated DIFs from the load test of 1.30 and 1.32 for Girder C and Girder A, respectively, compare well with the recommended value of 1.25 for girders. If a full continuum of static test data along the bridge length was available, these values would compare even better since the calculated values would decrease. As for the diaphragms, it was difficult to make conclusions due to generally low strain values, but from what was available, the code recommended dynamic impact factor of 1.30 is a rational value. Although the code does not specifically address dynamic impact factors for lateral wind bracing, it is recommended from the results in this research that the slightly higher values used for cross-frames and diaphragms be used as well for the lateral wind bracing.

10.2.2 Computational Analysis Results

These evaluations along with considerations from a grillage analysis sensitivity study (as discussed later) were used to calibrate the analysis model in UMN Program to more accurately represent the measured behavior of Mn/DOT Bridge No. 69824. The calibrated model was termed the Final Model, or FM. Longitudinal distribution of the truck loads and stress checks were based on the full composite section properties of the girders in both the positive and negative moment regions (i.e., the concrete was assumed to provide tensile resistance in the negative moment regions). This method of load distribution and stress calculation provided the most accurate representation of the experimental data for all test load levels. A second analysis model termed Final Model – Rating, or FMR, was created as a slightly more conservative model to be used for rating analysis of the bridge. FMR was identical to FM except that for girder flexural stress calculations in the negative moment regions, FMR conservatively assumed that the concrete was cracked and thus, only included the reinforcement for the stress calculations. If future inspections of the bridge reveal significant deterioration of the girder-to-deck interface or if loads higher than those used for the testing of this bridge are anticipated, the currently recommended inclusion of the reinforcement for the stress checks in the negative moment regions should be reevaluated for future bridge ratings.

Grillage analysis was conducted with FM and FMR simulating each of the 43 static load tests. Comparisons were made between the measured and computed results. Findings from the load test for girder displacements and stresses, diaphragm stresses, and lateral wind bracing stresses are provided below, along with comments as to the effectiveness or ineffectiveness of the FM and FMR computer analyses for capturing these behaviors:

- The maximum measured vertical deflection on the exterior girder for Span 9-8 was 0.72 inches, while that for Span 8-7 was 1.11 inches. The corresponding interior girder maximum deflections were 0.66 inches and 0.97 inches for Span 9-8 and Span 8-7, respectively. These deflections along with the flexural bending rotations near Pier 9 were well predicted by the computer analyses (note that computed displacements for FM and

FMR were identical). In general, the predicted exterior girder displacements correlated better with the experimental data than those for the interior girder. The magnitude for the average percent errors between measured and computed displacements on Exterior Girder A were approximately 4%, while those for Interior Girder C were approximately 20%. The largest discrepancies between the computed and measured results for the displacements occurred for the twist cases S35 through S43 where trucks were shifted radially in on one span and out on the adjacent span. This type of loading resulted in complicated interactions between the girders over Pier 8. Although the percent errors between measured and computed displacements were slightly higher for these tests, UMN Program was still able to provide reasonable predictions.

- The FM analysis provided excellent correlation with the measured flexural bending stress data for the TC and BC gages, which were positioned longitudinally on the girder webs 3 inches from the top and bottom flanges. As expected for the FMR analysis, correlations with measured data in the negative moment regions were slightly more conservative than those for the FM analysis. In general, the average percent errors and standard deviations for percent error were lower for the BC gages than for any other group of measured values in the load test. The range for the average percent errors for the BC gages in the FM analysis was -20.6% to 18.8%, where (-) indicates an under-prediction by the analysis. For the FMR comparisons, the average percent error was between -3.7% and 20.4%, slightly more conservative than for FM. The most compressive and tensile measured BC gage stresses due to the test truck loads were -9.07 ksi and 9.38 ksi, respectively. The TC gages were generally predicted accurately by the FM analysis. However, since the magnitude of stress for the TC gages was small due to the closeness of these gages to the neutral axes of the composite sections, percent error calculations indicated somewhat misleading correlations. For the FMR analysis correlations, the average percent errors for the TC gages in the negative moment regions tended to be much larger in magnitude than those for the FM analysis. This was because the FMR analysis conservatively predicted stresses using a smaller bending section modulus, which ignored the contribution of the concrete. The most compressive and tensile measured TC gage stresses due to the truck loads were 0.72 ksi and 1.14 ksi, respectively.
- Maximum measured restraint of warping stresses at the bottom flange tips of the girders were up to approximately 1.5 ksi, while those for the top flanges were much lower due to restraint from the concrete deck. Computed restraint of warping stresses at the specific instrumented cross sections did not accurately predict the measured warping stresses there, especially for the gages near the piers. However, the magnitudes of the computed restraint of warping stresses at the diaphragms on either side of a gage were typically greater than the measured gage values. Thus, the analysis may be used with some reliability to capture the likely range of warping stresses. There were a number of factors determined for the apparent weak correlation between the computed and measured restraint of warping stresses. The first of these was the choice of location for the restraint of warping measurements. Girder cross sections for instrumentation were chosen to avoid localized strain distributions due to transverse stiffeners located at the diaphragms and halfway between diaphragms. Therefore, instruments were placed at quarter points between diaphragms. These locations happen to be regions of very high gradient for warping stresses, making accurate analytical predictions difficult. The second factor was

that, while UMN Program accounts well for restraint of warping in the presence of torsion, it is likely that local loading effects due to the location of the trucks between the girders created additional localized torsion that was difficult to take into account in the computer analysis. This was likely the cause of large discrepancies between some measured and computed values for gages near applied truck locations. This behavior is further discussed below for the diaphragms and lateral wind bracing. A third factor that adversely affected the correlation between the measured and computed warping stresses was that boundary conditions in the computer model do not necessarily reflect the actual arrangement in the structure. In particular, the bearing restraint at the piers in the radial direction significantly restricts the amount of torsion that can occur there, which increases the measured restraint of warping stresses there. This behavior is difficult to include in a grillage model unless boundary conditions can be introduced at the bottom flange location, which was not possible with UMN Program. This factor was likely the cause of under predictions in restraint of warping stresses near the piers. The final factor is related to the third and is the inability of a grillage model to include effects due to the girder web distorting, including the influence of web distortion on the influence of the boundary conditions.

- Two beam diaphragms, one near midspan of Span 9-8 and one at Pier 8, were instrumented with strain gages at five cross sections along their lengths in order to assess the bending action. The magnitude of the maximum measured diaphragm stress was approximately 2.0 ksi. In general, the analysis using UMN Program (note that results for FM and FMR were identical) was able to provide a reasonable model for the diaphragm behavior. Correlations between measured and computed values were good when the applied trucks were away from the instrumented diaphragms, and became worse the closer the trucks got to the diaphragms. The bending stresses generated in the composite beam diaphragms due to the truck loads transferring through the diaphragms to the girders resulted in the divergence between measured and computed results. Many grillage-based analytical programs, including UMN Program, do not take into account the local diaphragm bending action due to truck loads above a given diaphragm since loads in the analysis programs are typically distributed as vertical point loads to the girder nodes only; thus the reason for the discrepancy in the measured versus computed values. The measured and computed results for the diaphragm at Pier 8 were more consistent than those for the diaphragm near midspan of Span 9-8. This was because fewer load tests had trucks positioned directly over the diaphragm at Pier 8; thus reducing the local bending effects in the diaphragm results. The major discrepancy with the diaphragm at Pier 8 was that for the tests with asymmetrical loading (tests S29-S43), the measured and computed values diverged. This divergence was due to the inability of UMN Program to accurately model the boundary conditions for the bottom flange at the pier at which this diaphragm was located. This is similar to the issue discussed previously for the girder restraint of warping stresses at the pier. More accurate assessment could be attained by using a rotational spring or offset element to apply the boundary condition. One may be tempted to fix the torsional rotation of the girders at the piers, assuming that the combination of concrete deck at the top flanges and the bearings at the bottom flange rigidly fix these rotations. This is not a good assumption and will result in very low predicted stresses for the diaphragms at the pier, since its forces are generated primarily through the girder torsional rotations. It was seen in this bridge load

test, that the stresses in the diaphragm at the pier were as high or higher than those for the diaphragm near midspan.

- The maximum tensile and compressive axial stresses in the instrumented lateral wind bracing were 5.4 ksi and 5.0 ksi, respectively, due to the applied truck loads. Inspection of the lateral wind bracing behavior revealed that computed data correlated well with the measured results when the trucks were located away from a specific lateral bracing, similar to the behavior for the diaphragms as discussed previously. Also, the measured data for lateral wind bracing was consistently more tensile than predicted when trucks were located in the vicinity of a lateral bracing. It was concluded that localized bending in the slab at the point of load application was the cause for the increase in tensile forces seen in the lateral wind bracing. Application of loads between the girders creates torsional rotations that draw the top flanges of the two girders together and attempts to spread the bottom girder flanges. However, the lateral bracing near the bottom flanges develop tensile forces and prevent the flanges from rotating apart. This behavior was not predicted by the analysis because loads in UMN Program were only distributed as vertical point loads to the nearby girder nodes.

10.2.3 Modeling Parameter Study Results

A series of parametric studies were conducted to determine the sensitivity of grillage analysis with the intent of expanding the scope of the analysis for rating horizontally curved composite steel I-girder bridges. Two other previously tested horizontally curved composite steel I-girder bridges, Mn/DOT Bridge No. 27998 and the Federal Highway Administration (FHWA) Test Specimen, were used along with the test bridge (Mn/DOT Bridge No. 69824) to determine the extent to which various bridge and modeling parameters affect the live load computational response of these complex bridges using UMN Program. The sensitivity study focused on changes to the deflection, axial force, shear, moment, and stress responses of the different bridge elements when parameters were varied one at a time. Key findings from the parametric study and recommendations for more accurate yet conservative grillage analysis include:

- Analysis ignoring the additional bending stiffness of the diaphragms due to the knee brace regions for Mn/DOT Bridge No. 69824 provides satisfactory results for the girders, although restraint of warping stresses on the interior girder may be slightly under predicted. Calculated forces in the diaphragms, however, were significantly different. If accurate forces in the diaphragms are essential, such as for bridges with diaphragms governing the overall bridge rating, the additional stiffness of the knee braces should be included in the analysis.
- For Mn/DOT Bridge No 69824, ignoring the vertical offset of the diaphragms relative to the girders significantly alters the axial force and moment in the diaphragms, but has minimal impact on the overall behavior of the girders and the shear transfer through the diaphragms. The vertical offset between the diaphragm and girder elements does not need to be precise unless accurate assessment of the diaphragms is important.
- It was found that varying the composite action for the beam diaphragms for Bridge No. 69824 had minimal effects on the behavior of the girders, but, similar to the above two findings, altered the diaphragm forces significantly. The magnitude of percent change for most effects from b_{eff} going from 7 inches to 0 inches were 2 to 3 times greater than those for b_{eff} going from 7 inches to 54 inches. This was because the ratio of moments of

inertia was greater for b_{eff} going from 7 inches to 0 inches than it was for b_{eff} going from 7 inches to 54 inches. Thus, it was more important that composite action be included than b_{eff} be exactly right. In absence of test data for the composite action of beam diaphragms, the typical equations for girders (AASHTO, 2004) were found to provide reasonable effective widths for the diaphragms.

- Varying the axial stiffness of the X-shaped and K-shaped diaphragm members for Mn/DOT Bridge No. 27998 and the FHWA Test Specimen resulted in similar patterns of bridge response as for Mn/DOT Bridge No. 69824. However, the magnitude for percent changes was much larger for these two bridges. This was due to the larger span length-to-radius of curvature ratios for Bridge No. 27998 and FHWA Test Specimen, which results in larger effects due to horizontal curvature and greater demand on the diaphragms. In addition, the lateral wind bracing on Bridge No. 69824 provided an additional level of overall bridge stiffness that reduced the sensitivity of the bridge to diaphragm properties as compared to the bridges without lateral wind bracing. In general, decreasing the areas of the cross-frame members, and therefore the overall stiffness of the diaphragms, resulted in less transfer of force through the diaphragms and an increase in the overall displacements of the bridge, while an increase in stiffness had the opposite effects. Therefore, for accurate assessment of load distribution between the girders and bridge displacements, it is important to account for the actual stiffness of the cross-frame members.
- Excluding the lateral wind bracing members for Bridge No. 69824 caused a considerable shift in the load resistance mechanism, along with a significant loss in overall bridge stiffness. Without the lateral wind bracing to help stabilize the torsional rotations of the bridge, the transverse load distribution between girders shifted towards the exterior girder. Girder deflections and rotations increased considerably, especially on the exterior girder. Because of these significant effects, it is highly recommended that lateral wind bracing be included in the computational analysis of horizontally curved bridges. Not doing so will result in significant under predictions for the diaphragm forces along with grossly conservative results for the girder flexural behavior, for both displacements and forces. Restraint of warping stresses may be under predicted as well, especially for the exterior girder.
- Excluding the transverse concrete deck beams from the models resulted in less torsionally stiff structures. The girders had more freedom to rotate since the top flanges were no longer tied together. For all three bridges, the girders with the larger radii of curvature tended to have significantly higher increases in torsional rotations, while those with smaller radii of curvature tended to have rotations that either decreased or only increased slightly. This pattern occurred because the higher torsional loads induced on the girders with the larger radii of curvature no longer had a load path back to the other girders so that the torsion could be shared more uniformly across the bridge. It is interesting to note that Bridge No. 69824 saw significantly smaller effects due to removing the transverse deck beams. This was because the lateral wind bracing on Bridge No. 69824 provides an alternate load path for the bridge girders to share the torsional loads. Large percent changes for vertical deflections, torsional rotations, restraint of warping stresses, and diaphragm forces on Bridge No. 27998 and FHWA Test Specimen indicate that inclusion of the concrete deck as an axial transverse load

path at the top of the girders is important for the analysis of horizontally curved I-girder bridges, especially those without lateral wind bracing.

- Chang et al. (2005) found that due to web distortion effects, fixing the rotational DOFs of the concrete slab to those of the girders modeled as open-walled section beam elements, such as in UMN Program, over-constrains the girder twisting and bottom flange lateral bending leading to unconservative results for deflections and restraint of warping stresses in horizontally curved girder bridges. They recommended releasing the slab rotational DOFs from the girder DOFs to improve results and to provide a conservative approximation of the web distortion effects over the depth of the girders. Results from this sensitivity study indicate that the analyses with the rotational DOFs for the transverse concrete deck beams released from those for the girders provides somewhat higher predictions for nearly all bridge responses, especially for deflections and restraint of warping stresses. Thus, analysis with these DOFs released can be used to provide a more conservative analysis and is recommended when using grillage analysis with open-walled section beam elements for the curved bridge girders.
- For grillage analyses that apply support fixities at the neutral axes of the girder elements, the use of axial restraints to simulate frozen bearings has minor influence on overall analysis results. To obtain more realistic results from these fixities for comparisons with load test data, the inclusion of rotational springs or the application of the axial restraints using a vertical offset must be incorporated in the analysis. However, the extra load capacity provided by frozen axial bearings is generally not accepted as a reliable source of strength, especially at higher load levels (AASHTO, 2003b). For the purpose of bridge rating therefore, a complex application of these restraints may not be warranted.
- As suggested by Chang et al. (2005) and confirmed by the results in this sensitivity study, ignoring the contribution of the concrete slab on the torsion constant is an effective method for adding conservatism to a grillage analysis without grossly overestimating the response of a curved bridge. It is the preferred method used in this research project.
- Results indicate that for typical girder sizes and concrete deck thicknesses on horizontally curved composite steel I-girder bridges, small variations in the thickness of the concrete deck result in relatively small deviations for the computational results. For a change in concrete thickness of ± 1 inch, maximum vertical deflections and torsional rotations varied by approximately $\pm 4\%$, while maximum bottom flange flexural stresses varied by approximately $\pm 2\%$. Most other bridge responses were minimally affected. Note that for bridges with smaller steel girder cross-sections, these effects would increase since the concrete deck would have a greater influence on the bending stiffness of the composite section.
- Changing the effective width had a much larger influence on the displacements of the bridge than on the stresses. In addition, the sensitivity of the three modeled bridges to changes in the concrete effective width was relatively small for a $\pm 20\%$ range on the effective width. Thus, attempting to narrow in on an exact value for the effective width for analysis is not warranted. It is interesting to note that Bridge 69824 showed higher sensitivity to the effective width than the other two bridges, likely due to the overall lower stiffness of this bridge as compared to the other bridges with more girders. For possible higher percent changes in the effective width, such as can occur for edge girders

near large concrete curbs or parapets, the additional stiffness should not be ignored since it can have a significant impact on the bridge response.

- Decreasing the modular ratio to better reflect the actual strength of the concrete, which is typically much higher than the originally specified design strength, can be an effective method for slightly improving the computational response and rating of a bridge, especially for stiffness controlled bridges since the sensitivity to deflections was found to be at least 3 times that as for girder bottom flange stress. If available, tests of concrete cylinders from the original pour can be used to identify the actual strength of the concrete, or cores can be drilled and tested for older bridges. The structural integrity of the concrete should be verified to ensure deterioration of the concrete is not occurring.
- Investigations into curvature on the bridge behavior pointed out the importance of including the effects of curvature for analyzing horizontally curved I-girder bridges. Nearly all bridge responses are sensitive to the level of horizontal curvature of the bridge. Note that the effects of horizontal curvature were lower for Bridge 69824 due to its larger radius of curvature and the lateral wind bracing, which help to stabilize the bridge against the torsional forces generated due to curvature.
- It was found that for continuous bridges without shear connectors in the negative moment regions, assuming non-composite properties in those regions for load distribution and stress calculations was not necessarily the most conservative method of analysis, nor did it correlate with experimental data as discussed previously for Bridge No. 69824. In particular, predictions for negative moment region bottom flange stresses for both the C-NC and C-R models were more conservative than those for the NC-NC models for Bridge No. 69824 and Bridge No. 27998 (see Chapter 8 for a description of each of these models). For this reason and the fact that test data presented in Chapter 6 for Bridge 69824 indicated composite action in the negative moment regions, the preferred model for analysis of Bridge 69824 distributes loads based on full composite properties in the negative moment regions. As long as a bridge does not indicate a loss of bond in the negative moment regions, either by visual inspection of the deck-to-girder interface or by load test, it is recommended that loads be distributed based on full composite properties along the length of the bridge. Stress calculations in these regions should be based on the cracked composite section properties including the rebar or on non-composite section properties depending on whether experimental data is available to ensure composite properties at rating load levels.
- The use of approximate equations similar to Equation 2-8 for estimating restraint of warping stresses on the bottom flange of curved girders was shown for the bridges in this study to be reasonably accurate as compared to the values provided by UMN Program. On all three bridges, the results for the girders with the largest radius of curvature were slightly conservative. On the other hand, the approximate equation slightly underestimated the UMN program value for all other girders. Conservative measures, such as the inclusion of the 6/5 factor as in Equation 2-8 or limiting the flange couple depth D for composite sections to the height of the steel girder, are recommended to avoid under prediction of the restraint of warping stresses on the bridge girders with the smaller radii of curvature. Note that the approximate equation did not provide good results near changes in diaphragm spacing or skewed supports.

10.2.4 Load Rating Results

Using the calibrated grillage analysis model FMR and load rating procedures for both LFR and LRFR, final load ratings at the inventory level with two lanes loaded were determined for Mn/DOT Bridge No. 69824. The limiting component for both final ratings was determined to be the longitudinal stress in the bottom flange of Interior Girder C at Pier 6. The controlling load rating factor for LFR was 0.73 and for LRFR was 0.63. The current Mn/DOT inventory load rating of the bridge using LFR methodology was approximately 0.81 and was based on line girder analysis of straight girders with approximate flange yield strength reductions to account for secondary moments and restraint of warping stresses due to the horizontal curvature of the bridge. The limiting component for the current Mn/DOT rating was the bottom flange longitudinal stress at midspan of Exterior Girder A on Span 8-7. Primary reasons for the discrepancies between the old and new load ratings include:

- The new final ratings show that the controlling girder for Bridge No. 69824 is the Interior Girder C, while the current Mn/DOT rating has the Exterior Girder A as the controlling girder. This discrepancy is primarily due to the current Mn/DOT rating ignoring the effects of the lateral wind bracing on the transverse load distribution between the girders. AASHTO (2003a) warns against the use of approximate methods, such as the V-load method, for curved bridges with lateral wind bracing. The sensitivity study showed that the lateral wind bracing helps to equalize the vertical load between the girders. For Bridge No. 69824, vertical moments were significantly lower on the Interior Girder C as compared to Girder A in the parametric study when the lateral wind bracing was excluded from the computational model versus when it was included. Thus, the current Mn/DOT rating of Bridge No. 69824 underestimates the load on the interior girder and overestimates the load on the exterior girder by ignoring the influence of the lateral wind bracing.
- The final ratings found that the controlling location on Bridge No. 69824 was at the negative moment region of Pier 6, while the current Mn/DOT rating showed that the positive moment region of Span 8-7 controlled. This key discrepancy is due to the difference in girder stiffness in the negative moment regions for longitudinal load distribution for the computational analyses. The current Mn/DOT rating assumed that the concrete deck and rebar would be ineffective in tension at rating level loads in the negative moment regions of the bridge since no shear connectors were provided on the girders in these regions. Based on the results of the load test which showed the deck to be effective in tension at rating load levels in the negative moment regions, the final ratings included both the concrete deck and the rebar for girder stiffness and longitudinal load distribution. The sensitivity study showed that for Bridge No. 69824 the moments in the positive moment regions were approximately 15% higher and in the negative moment regions were approximately 20% lower when the stiffness of the deck was excluded in the negative moment regions for longitudinal load distribution versus when it was included. More load is carried by the negative moment regions when the stiffness there is higher. Hence, the current Mn/DOT rating underestimates the loads in the negative moment region by assuming the deck to be ineffective in tension at the rating level loads and overestimates the loads in the positive moment regions.

10.3 Recommendations for Load Rating with and without Load Testing

The findings of this research project show that grillage analysis can be used as a primary tool for providing accurate yet efficient analysis for the load rating of horizontally curved composite steel I-girder bridges. This method provides for a complete system-based analysis that incorporates the interaction of the various elements in the bridge and has been shown in this project and others (Galambos et al., 2000; McElwain and Laman, 2000; Simpson, 2000; Nevling, 2001; Chang et al., 2005) to provide good correlation with load test results so long as the modeling assumptions used are handled appropriately. Since there are many levels of refinement for grillage analysis, recommendations are made below to guide bridge rating evaluators toward more accurate analyses:

- Grillage analyses that use open-walled section beam elements (7 DOFs per node) for the girders are recommended since they more accurately reflect the effects of restraint of warping on stiffness and stress. Analysis with frame elements (6 DOFs per node) for the girders with the incorporation of approximate equations for restraint of warping stresses may provide reasonable results for bridges with simple layouts, but are less reliable for bridges with skewed supports, non-uniform diaphragm spacing, small radii of curvature, changes in curvature, and other more complex geometries.
- All degrees of freedom should be included in the analysis due to the three-dimensional behavior of these complex structures.
- The bending and shear stiffness due to beam diaphragms and/or cross-frames should be accurately modeled.
- Inclusion of the vertical offsets between the diaphragm and girder elements is important for obtaining accurate forces in the diaphragms; however, overall girder displacements and forces are minimally affected.
- Lateral wind bracing, if present, should be modeled at the correct vertical offset to obtain accurate representation of the transverse load distribution between girders and the overall torsional stiffness of the structure. Not including the lateral wind bracing in the analysis will tend to result in over prediction of stresses and displacements on the girder with the largest radius of curvature, and under predictions on the girder with the smallest radius of curvature.
- The AASHTO (2004) recommended equations for effective concrete widths provide for reasonable approximations of the composite behavior so long as an appropriate modular ratio is used. It is recommended that the modular ratio be based on the current strength of the concrete versus the design strength, which is typically much lower.
- Additional stiffness due to curbs and/or parapets should be included where appropriate by increasing the effective width by the area of the additional concrete divided by the slab thickness, or by using half of that value as recommended by AASHTO (2004) for a more conservative assessment.
- Web distortion effects should be taken into consideration by ignoring the contribution of the concrete deck to the composite torsion constant and/or releasing the rotational DOFs of transverse concrete slab members from the girder DOFs. See Chang et al. (2005) for similar recommendations when modeling the deck using shell elements.
- Longitudinal load distribution for rating should generally assume the concrete in the negative moment regions to be effective in tension unless inspections or testing indicate

considerable levels of deterioration and/or slip at the flange to deck interface. Stresses in these regions should be conservatively checked based on non-composite properties, or on composite properties including the reinforcement only, although it may be noted that computing stresses assuming full action of the concrete will often be more accurate (just not as consistently conservative).

- Boundary conditions should be applied as close to their actual locations and in the proper orientations as possible.
- Dynamic impact factors and centrifugal force effects should be included as per AASHTO (2003a and 2004). Note that centrifugal force effects should be considered at a variety of vehicle speeds, since for a given bridge, slower speeds will typically maximize forces on the girders with the smaller radii of curvature while faster speeds will maximize forces on the girders with the larger radii of curvature.

This research has found that grillage analysis can generally be relied upon to provide accurate bridge load ratings, thus reducing the need for load testing on most horizontally curved composite steel I-girder bridges. When load tests are completed for the purposes of load rating, the applied test loads should be high enough to accurately assess the behavior of the bridge near the rating load levels. Some cases where load testing could be used to complement computational analysis or to improve the rating of a bridge include:

- To confirm composite action at high load levels in regions without shear connectors.
- To determine the benefits of large curbs and/or parapets along edge girders so as to calibrate an effective width for the girders.
- To verify longitudinal and transverse load distributions.
- To prove a certain load carrying capacity or stiffness for severely deteriorated components.
- To verify computational methods for bridges with highly non-uniform girder or diaphragm spacing, or for bridges with a reversal in the direction of curvature.

For some types of bridge behavior, load testing may not be beneficial for the purposes of load rating horizontally curved steel I-girder bridges. Load tests to verify or quantify unintended bearing fixity in an attempt to increase the load rating of a curved steel bridge are not advantageous. There are two main reasons. First, this is generally not a reliable source of strength or stiffness, especially at higher load levels. Second, benefits due to bearing restraint on curved bridges should not be included unless detrimental effects due to increased thermal straining of the bridge are also taken into consideration. The use of load tests on curved steel I-girder bridges with the sole intent of determining an effective concrete width to use in analysis is not warranted. The sensitivity study in Chapter 8 shows that for a reasonable range of effective widths, the deflection and stress profiles of the bridge do not change much (except due to parapets, curbs, and other major sources of stiffness, which should be included in the effective width calculations). Only small increases in the rating are likely to be obtained for most composite bridges. A more economical approach would be to test core samples from the bridge or review cylinder tests from the original pour of the concrete in order to decrease the modular ratio and increase the bridge stiffness and strength.

The *LRFR Manual* (AASHTO, 2003b) provides additional guidance on when to and when not to load test for the purpose of load rating. In general, load testing should only be conducted when pretest evaluations of the bridge indicate that load testing will likely provide an improved rating

for the bridge. Load testing should not be conducted if there is a possibility of sudden failure or if testing is impractical due to access difficulties or site traffic conditions. Bridge strengthening should always be investigated prior to load testing, since for some bridges it may be more cost effective.

10.4 Recommendations for Future Research

Future research for load rating of horizontally curved steel I-girder bridges should focus on the incorporation of recently released combined straight and curved girder LRFD specifications. Additional load tests need to be completed to add to the available database for these structures, and should include a greater focus on the restraint of warping stresses and web distortion behavior. Load tests before and after retrofits for deteriorating guard railings, such as those on Mn/DOT Bridge No. 69824, could provide valuable insight into the effects of these so called nonstructural elements. The addition of lateral wind bracing to existing horizontally curved I-girder bridges could be explored as a method for improving the load rating of older bridges. Investigation into the effects of frozen support bearings on the thermal behavior of horizontally curved bridges may also prove to be beneficial for increasing the life expectancy of these structures. Finally, additional broad parametric studies should be conducted including a larger population of bridges than the three incorporated herein (e.g., other tested composite steel curved I-girder bridges, as they become available), along with comparisons between various commercial programs used for the analysis of these complex structures.

References

- American Institute of Steel Construction (AISC) (1986). *Highway Structures Design Handbook*. AISC Marketing Inc., Volume II, Section 6.
- American Association of State Highway and Transportation Officials (AASHTO) (1980). *Guide Specifications for Horizontally Curved Highway Bridges*, 1st Edition. AASHTO, Washington, D.C.
- AASHTO (1993). *Guide Specifications for Horizontally Curved Highway Bridges*, 2nd Edition. AASHTO, Washington, D.C.
- AASHTO (1994). *Manual for Condition Evaluation of Bridges*, 2nd Edition. AASHTO, Washington D.C.
- AASHTO (1998). *LRFD Bridge Design Specifications*, 2nd Edition. AASHTO, Washington, D.C.
- AASHTO (2002). *Standard Specifications for Highway Bridges*, 17th Edition. AASHTO, Washington, D.C.
- AASHTO (2003a). *Guide Specifications for Horizontally Curved Steel Girder Highway Bridges*, 3rd Edition. AASHTO, Washington, D.C.
- AASHTO (2003b). *Guide Manual for Condition Evaluation and Load and Resistance Factor Rating of Highway Bridges*. AASHTO, Washington, D.C.
- AASHTO (2004). *LRFD Bridge Design Specifications*, 3rd Edition. AASHTO, Washington, D.C.
- Armstrong, W. L. (1972). "Dynamic Testing of Curved Bridge – Huyck Stream." *Journal of the Structural Division*, ASCE, Vol. 98, No. ST9, pp. 2015-2030.
- Barker, M. G. (2001). "Quantifying Field-Test Behavior for Rating Steel Girder Bridges." *Journal of Bridge Engineering*, ASCE, Vol. 6, No. 4, pp. 254-261.
- Beal, D. B. (1978). *Research Report 61: Horizontally Curved Bridges - New York Field Testing and Design Studies*. New York State Department of Transportation, Albany, NY.
- Beal, D. B. (1998). *NCHRP Research Results Digest Number 234: Manual for Bridge Rating through Load Testing*. Transportation Research Board, National Research Council, Washington, D.C.
- Burdette, E. G., and Goodpasture, D. W. (1988). "Correlation of Bridge Load Capacity Estimates with Test Data," *NCHRP Report 306*, Transportation Research Board, National Research Council, Washington, D. C.

Chajes, M. J., Mertz, D. R., and Commander, B. (1997). "Experimental Load Rating of a Posted Bridge." *Journal of Bridge Engineering*, ASCE, Vol. 2, No. 1, pp. 1-10.

Chang C.-J. White, D. W., Beshah, F. and Wright, W. (2005). "Design Analysis of Curved I-Girder Bridge Systems – An Assessment of Modeling Strategies." *Structural Stability Research Council Annual Stability Conference Proceeding 2005*, SSRC, University of Missouri, Rolla, MO.

Christensen, M., and Hajjar, J. F. (2005). "Computer Analysis of a Horizontally Curved Composite Steel Girder Bridge," *Structural Engineering Report No. ST-05-01*, Department of Civil Engineering, University of Minnesota, Minneapolis, MN.

Elhelbawey, M., Fu, C. C., Sahin, M. A., and Schelling, D. R. (1999). "Determination of Slab Participation from Weigh-In-Motion Bridge Testing." *Journal of Bridge Engineering*, ASCE, Vol. 4, No. 3, pp. 165-173.

Freisinger, C. M., Krzmarzick, D., Hajjar, J. F., and Dexter, R. J. (2004). "Testing Strategy for Load Testing of a Horizontally Curved Composite Steel Girder Bridge," *Structural Engineering Report No. ST-04-01*, Department of Civil Engineering, University of Minnesota, Minneapolis, MN.

Galambos, T. V., Hajjar, J. F., Leon, R. T., Huang, W.-H., Pulver, B. E., and Rudie, B. J. (1996). *Mn/DOT Report No. MN/RC-96/28: Stresses in Steel Curved Girder Bridges*. Minnesota Department of Transportation, Saint Paul, MN.

Galambos, T. V., Hajjar, J. F., Huang, W.-H., Pulver, B. E., Leon, R. T., and Rudie, B. J. (2000). "Comparison of Measured and Computed Stresses in a Steel Curved Girder Bridge." *Journal of Bridge Engineering*, ASCE, Vol. 5, No. 3, pp. 191-199.

Gillespie, J. W. (1968). "Analysis of Horizontally Curved Bridges." *Engineering Journal*, AISC, Vol. 5, No. 4, pp. 137-143.

Hajjar, J. F., Ray, J. D., Wyffels, T. A., and Carlsson, M. L. R. (2001). *Mn/DOT Report No. MN/RC-2002/08: Live Load Stresses in Steel Curved Girder Bridges*. Minnesota Department of Transportation, Saint Paul, MN.

Heins, C. P., and Kuo, J. T. C. (1972). "Composite Beams in Torsion." *Journal of the Structural Division*, ASCE, Vol. 98., No. ST5, pp. 1105-1117.

Huang, D. (2004). "Field Test and Rating of Arlington Curved Steel Box Girder Bridge." *Proceedings of the 2004 Annual Meeting*, Transportation Research Board, Washington, D.C.

Huang, W.-H. (1996). "Curved I-Girder Systems," Ph.D. Dissertation. Department of Civil Engineering, University of Minnesota, Minneapolis, Minnesota.

Jáuregui, D. V., Yura, J. A., Frank, K. H., and Wood S. L. (2002). "Field Evaluation of Decommissioned Noncomposite Steel Girder Bridge." *Journal of Bridge Engineering*, Vol. 7, No. 1, pp. 39-49.

Jung S.-K. White, D. W., Beshah, F. and Wright, W. (2005). "Ultimate Strength of Horizontally Curved Composite I-Girder Bridge Structural Systems." *Structural Stability Research Council Annual Stability Conference Proceeding 2005*, SSRC, University of Missouri, Rolla, MO.

Ketchek, K. (1969). "Another Approach to Simplified Design of a Curved Steel Girder." *Engineering Journal*, AISC, Vol. 6, No. 4, pp. 116-123.

Lichtenstein, A. G. (1993). *NCHRP Rep. No. 12-28 (13)A: Bridge Rating Through Nondestructive Load Testing*. Transportation Research Board, National Research Council, Washington, D.C.

Lichtenstein, A. G. (2002). *NCHRP Report 12-28: Manual for Condition Evaluation and Load and Resistance Factor Rating of Highway Bridges*. Transportation Research Board, National Research Council, Washington, D.C.

Linzell, D., Hall, D. and White, D. (2004a). "Historical Perspective on Horizontally Curved I Girder Bridge Design in the United States." *Journal of Bridge Engineering*, ASCE, Vol. 9, No. 3, pp. 218-229.

Linzell, D., Leon, R. T., and Zureick, A. H. (2004b). "Experimental and Analytical Studies of a Horizontally Curved Steel I-Girder Bridge during Erection." *Journal of Bridge Engineering*, ASCE, Vol. 9, No. 6, pp. 521-530.

McElwain, B. A., and Laman, J. A. (2000). "Experimental Verification of Horizontally Curved I-Girder Bridge Behavior." *Journal of Bridge Engineering*, ASCE, Vol. 5, No. 4, pp. 284-292.

MDX (2004). "MDX Version 6 User Manual: Curved & Straight Steel Bridge Design & Rating, September 27 Edition." www.mdxsoftware.com.

Minervino, C., Sivakumar, B., Moses, F., Mertz, D., and Edberg, W. (2004). "New AASHTO Guide Manual for Load and Resistance Factor Rating of Highway Bridges." *Journal of Bridge Engineering*, ASCE, Vol. 9, No. 1, pp. 43-54.

Nevling, D. L. (2003). "Evaluation of Level of Analysis Methodologies for Horizontally Curved I-Girder Bridges through Comparison with Measured Response of an In-Service Structure," Masters Thesis. Pennsylvania State University, University Park, PA.

Nowak, A. S., and Saraf, V. K. (1996). *Research Report No. UMCEE 96-10: Load Testing of Bridges*. Department of Civil and Environmental Engineering, University of Michigan, Ann Arbor, MI.

Saraf, V. and Nowak, A. S. (1998). "Proof Load Testing of Deteriorated Steel Girder Bridges." *Journal of Bridge Engineering*, ASCE, Vol. 3, No. 2, pp. 82-89.

Senthilvasan, J., Thambiratnam, D. P., and Brameld, G.H. (2002). "Dynamic Response of a Curved Bridge under Moving Truck Load." *Engineering Structures*, Vol. 24, Issue 10, pp. 1283-1293.

Simpson, M. D. (2000). "Analytical Investigation of Curved Steel Girder Behavior," Ph.D. Dissertation. Department of Civil Engineering, University of Toronto, Ontario, Canada.

Stegmann, T. H., and Galambos, T. V. (1976). *Washington University Research Rep. No. 43: Load Factor Design Criteria for Curved Steel Girders of Open Cross Section*. Washington University, St. Louis, MO.

United States Steel Corporation (USS) (1984). "V-load Analysis: An Approximate Procedure, Simplified and Extended, for Determining Moments and Shears in Designing Horizontally-curved Open-Framed Highway Bridges." *Highway Structures Design Handbook*. United States Steel Corporation, Pittsburgh, PA.

Vlasov, V. Z. (1961). *Thin-Walled Elastic Beams, 2nd Ed.* Israel Program for Scientific Translations, Jerusalem, Israel.

Weissman, H. A. (1970). "Straight-Element Grid Analysis of Horizontally Curved Beam Systems." *Engineering Journal*, AISC, Vol. 7, No. 2, pp. 41-49.

Zureick, A. and Naqib, R. (1999). "Horizontally Curved Steel I-Girder State-of-the-Art Analysis Methods." *Journal of Bridge Engineering*, ASCE, Vol. 4, No. 1, pp. 38-47.

Zureick, A., Linzell, D., Leon, R. T., and Burrell, J. (2000). "Curved Steel I-Girder Bridges: Experimental and Analytical Studies." *Engineering Structures*, Vol. 22, pp. 180-190.

Appendix A
Distribution of Vertical Loads for Grillage Analysis

The analysis of a bridge using a grid or grillage based model consisting of nodes and line elements requires all loads to be applied as either point loads at the nodes or as distributed loads along the elements. In reality, vehicle axle loads rarely coincide with a node or girder element in the analysis model. Therefore, some auxiliary method for distributing the axle loads to the model nodes or elements is necessary for analysis.

The method of load distribution used in this research for horizontally curved bridges is based on two important assumptions: differential deflections do not occur between girders at a cross-section, and the cross-section rotates as a rigid body about its rigidity center. These assumptions are used to determine flexural and torsional distributions, which when combined provide the total load applied to each girder at a cross-section.

A.1 Flexural Distribution

The combination of diaphragms and concrete deck are assumed to be rigid enough to prevent differential deflections between the girders at a given cross-section. This assumption allows the load resisted by a girder to be taken as proportional to its flexural stiffness (i.e., moment of inertia I). Stated in equation form:

$$F_i = \frac{I_i}{\sum I} V, \quad (\text{A-1})$$

where F_i is the vertical load resisted by the i^{th} girder with stiffness I_i and V is the total applied load. Dividing both sides of Equation (A-1) by V , the fraction of load f_i resisted by each girder due to the flexural distribution is:

$$f_i = \frac{I_i}{\sum I} \quad (\text{A-2})$$

Equation (A-2) alone defines the distribution of load across the cross-section only when the load is positioned in a manner such that no rotation is created about the cross-section. Refer to Figure A-1 for an example. To find the location for zero rotation, set the sum of the torques due to the resistances F_i and the applied load V equal to zero. Using x_i as the distance from each girder to the interior girder (i.e. girder with smallest radius of curvature) and substituting for F_i using Equation (A-1), solve for X :

$$X = \frac{\sum (Ix)}{\sum I}, \quad (\text{A-3})$$

where X is the distance from the interior girder to the center of rotation, otherwise known as the rigidity center.

A.2 Torsional Distribution

When the applied load is not at the rigidity center, a second assumption must be made to complete the load distribution. It must now be assumed that the diaphragms and concrete slab are rigid enough that the cross-section rotates as a rigid body when the applied load V is offset from the rigidity center. Refer to Figure A-2. For a rigid rotation of small angle ϕ about the rigidity center, the vertical deflection y_i at each girder can be calculated from geometry as:

$$y_i = \phi d_i, \text{ where } d_i = X - x_i \quad (\text{A-4})$$

The absolute value of d_i is the distance between the i^{th} girder and the rigidity center. Using stiffness considerations (i.e., reaction = stiffness*displacement), the load R_i resisted by each girder due to the rotation is:

$$R_i = \frac{I_i}{\kappa} y_i, \text{ where } \kappa = \text{constant} \quad (\text{A-5})$$

Solving Equation (A-5) for y_i and setting it equal to Equation (A-4), an expression for R_i can be developed:

$$R_i = I_i d_i \theta, \text{ where } \theta = \frac{\phi}{\kappa} = \text{constant} \quad (\text{A-6})$$

For an applied load V that is offset some distance E_0 from the rigidity center, summing the moments about the rigidity center provides another expression for θ :

$$\theta = \frac{VE_0}{\sum(Id^2)} \quad (\text{A-7})$$

Placing Equation (A-7) into Equation (A-6) and dividing by V , the fraction of load resisted by each girder due to load eccentricity is then:

$$r_i = \frac{Id_i E_0}{\sum(Id^2)} \quad (\text{A-8})$$

A.3 Total Load Distribution

The total vertical load V_i resisted by each girder is then the sum of the flexural and rotational fractions f_i and r_i times the applied load V :

$$V_i = \left(\frac{I_i}{\sum I} + \frac{Id_i E_0}{\sum (Id^2)} \right) V \quad (\text{A-9})$$

The transfer of the vertical loads V_i to each girder at a cross-section provides half of the process for distributing the applied vertical load V to the surrounding model nodes. The second half of the process is to distribute the load to the nodes at the end of each girder segment. This is accomplished using a linear interpolation along the arc length of each girder. For example, if the load is located $\frac{1}{4}$ of the distance along the girder segment, the near node will receive $\frac{3}{4}$ of the load while the far node will receive $\frac{1}{4}$ of the load.

To recap the distribution process: the applied load V is distributed radially across the cross-section to each girder using Equation (A-9), then for each girder the load V_i is distributed to the end nodes using linear interpolation. Figure A-3 shows the general path in a multi-girder system for load distribution to the nodes surrounding an applied point load.

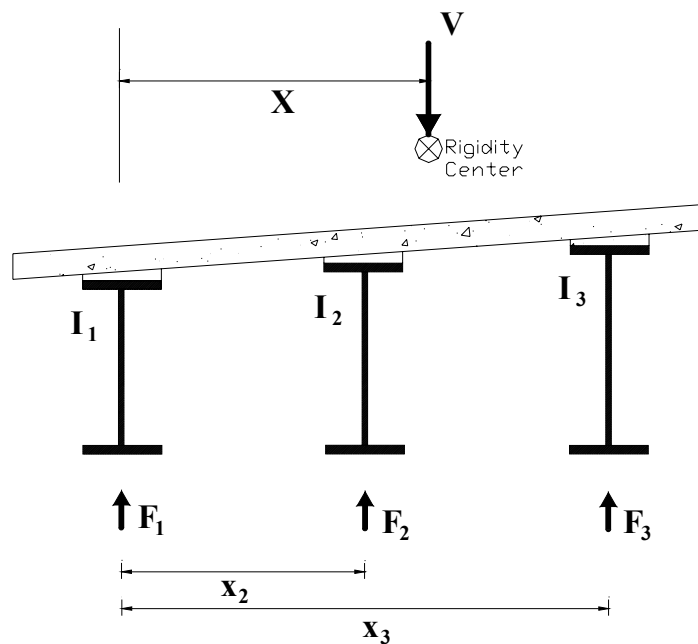


Figure A-1: Flexural Load Distribution

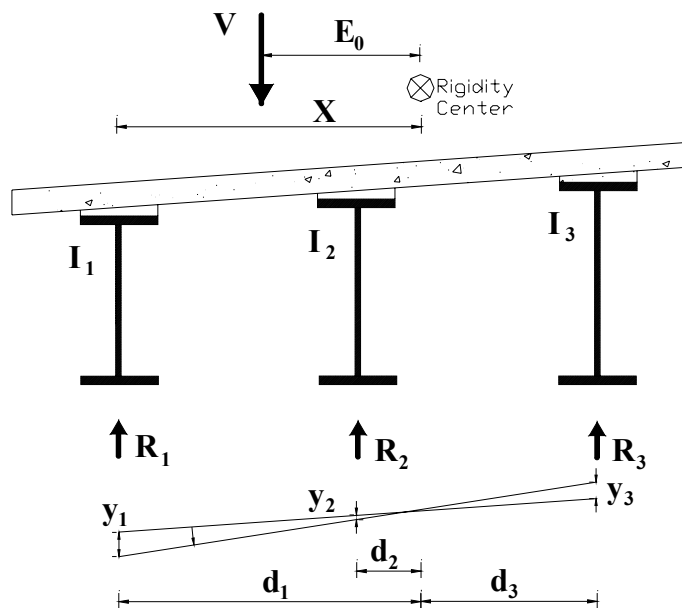


Figure A-2: Torsional Load Distribution

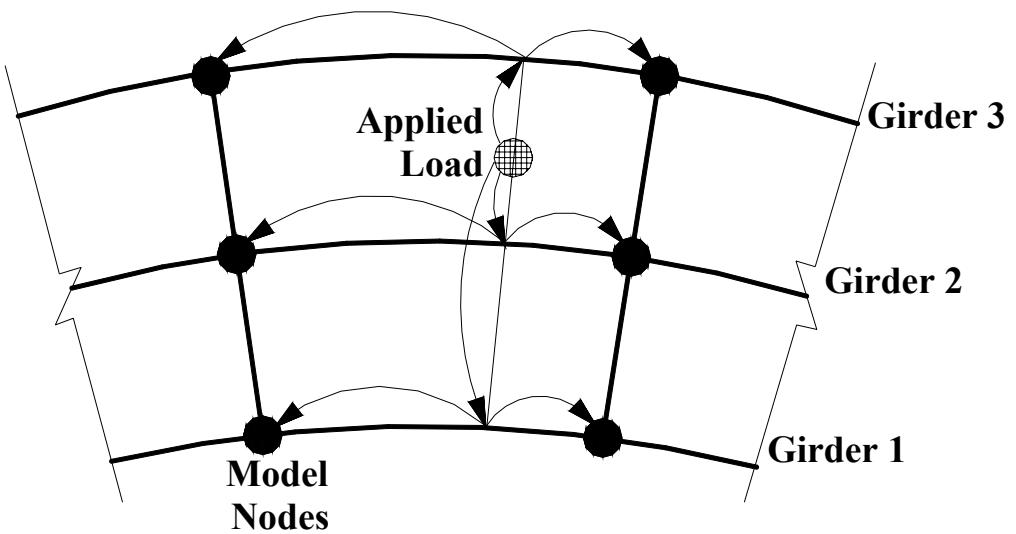


Figure A-3: Load Distribution Path

Appendix B

Instrumentation Plan

The instrumentation of Mn/DOT Bridge No. 69824 was composed of longitudinal strain gages (both weldable and glueable), glueable three-gage rosettes, string potentiometers, linear variable displacement transducers (LVDTs), tiltmeters, and total stations. This instrumentation was implemented to measure specific live load effects of the bridge, namely:

- Longitudinal strains on the flanges and web along both the interior and exterior girders
- Longitudinal strains on selected diaphragms and lateral bracing
- Plane strains on the exterior girder web at Pier 8 and at a gusset plate connection
- Web gap strains at selected diaphragm connection locations
- Vertical deflections of Span 9-8 and Span 8-7
- Major axis rotations of each girder at Pier 9
- Translational movement of the expansion bearings at Pier 9
- Slip along the concrete slab to steel girder interface in the negative moment regions at Pier 9 and Pier 8 for the exterior girder

The following set of drawings depicts the location of all instrumentation used in the load testing of Mn/DOT Bridge No. 69824. They are organized as described below:

- A table that describes the instrumentation labeling scheme for the location of each instrument on a given cross section.
- After the table, Figure B-1 and Figure B-2 show the exact location for gages on each member type.
- Figure B-3 is a layout showing the labeling scheme for the cross sections of the bridge that have instrumentation.
- The next three figures, Figure B-4 to Figure B-6, provide the locations along the length of the bridge for the main girder strain gages, the secondary location (i.e., lateral bracing, diaphragm, and gusset plate connection) strain gages, and the deflection instrumentation (i.e., string pots, LVDTs, tiltmeters, and total stations).
- The remaining figures go through each cross section and display the locations of all instruments on the cross section.

Other notes:

- All girder cross-section drawings are shown looking from south to north (i.e., from Pier 10 toward Pier 5).
- On the bridge sections, all instrumentation consists of weldable longitudinal strain gages unless otherwise noted.
- Instrumentation with double strikethrough font (e.g., ~~9B-GA-TC~~) did not provide data for the extent of the bridge test.
- Instrumentation with single strikethrough font (e.g., ~~8D-GA-TI~~) did not provide reliable data for the extent of the bridge test.
- Due to a lack of string potentiometers on test day, the originally planned instruments for Section 9D were not installed, and therefore Section 9D is not shown in the figures that follow.

In general terms, each instrument is labeled by **X-Y-Z**, where:

X: denotes the bridge section (9B, 9J, 8C, etc.)

Y: denotes the bridge member as described below:

GA	Girder A (exterior)
GC	Girder C (interior)
LBU	Lateral Bracing at 45° angle counter-clockwise from centerline of roadway
LBD	Lateral Bracing at 45° angle clockwise from centerline of roadway
D	Diaphragm
GPA	Gusset Plate region on girder A
GPC	Gusset Plate region on girder C

Z: denotes the location of instrument on the bridge member as described below:

T	Top of the member or section
B	Bottom of the member or section
W	Mid-depth of the web of the main girder
C	Center of flange on web
CN	Centroid of lateral bracing section
E	Exterior of the member or section in reference to the center of radius of the bridge
QE	Quarter point of the diaphragm closest to the exterior girder
M	Mid-point of the diaphragm
QI	Quarter point of the diaphragm closest to the interior girder
I	Interior of the member or section in reference to the center of radius if the bridge
V	Vertical strain gage in rosette
H	Horizontal strain gage in rosette
TR	Strain gage in rosette orientated in the transverse direction of the main girder
LO	Strain gage in rosette orientated in the longitudinal direction of the main girder
45	45° diagonal (clockwise from horizontal gage in rosette) strain gage in rosette
W9	Main girder web location nearest Pier 9 at the gusset plate weld toe
W8	Main girder web location nearest Pier 8 at the gusset plate weld toe
WG	Web gap location on the main girder at the bottom of the stiffener
DF	Vertical deflection
BM	Bearing movement
SM	Slip movement
RM	Rotation movement
TS	Total Station vertical deflection measurement

Table B-1: Instrumentation Labeling Scheme

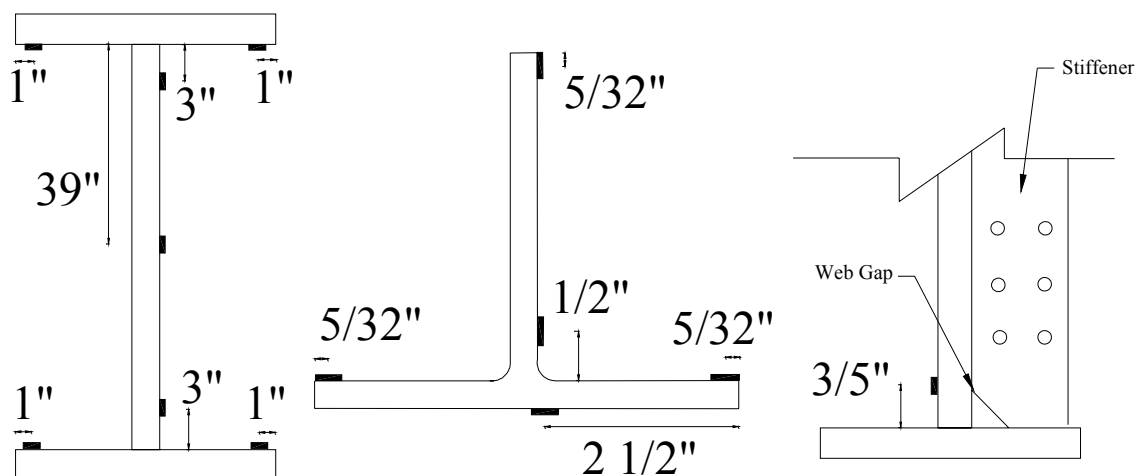


Figure B-1: Main Girder, Lateral Bracing, and Web Gap Gage Locations

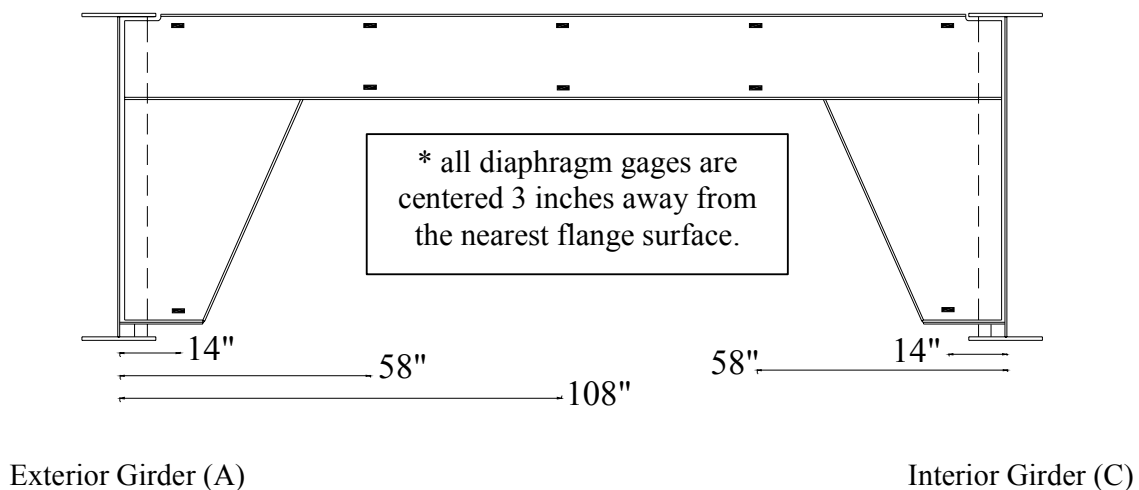


Figure B-2: Diaphragm Gage Locations

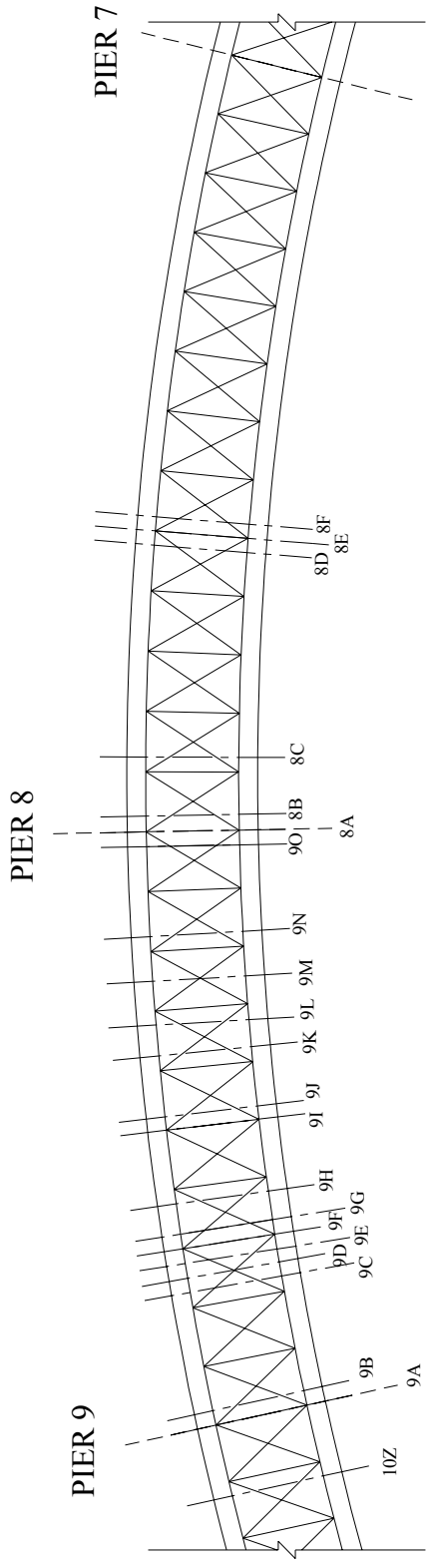


Figure B-3: Cross-section Labeling Scheme

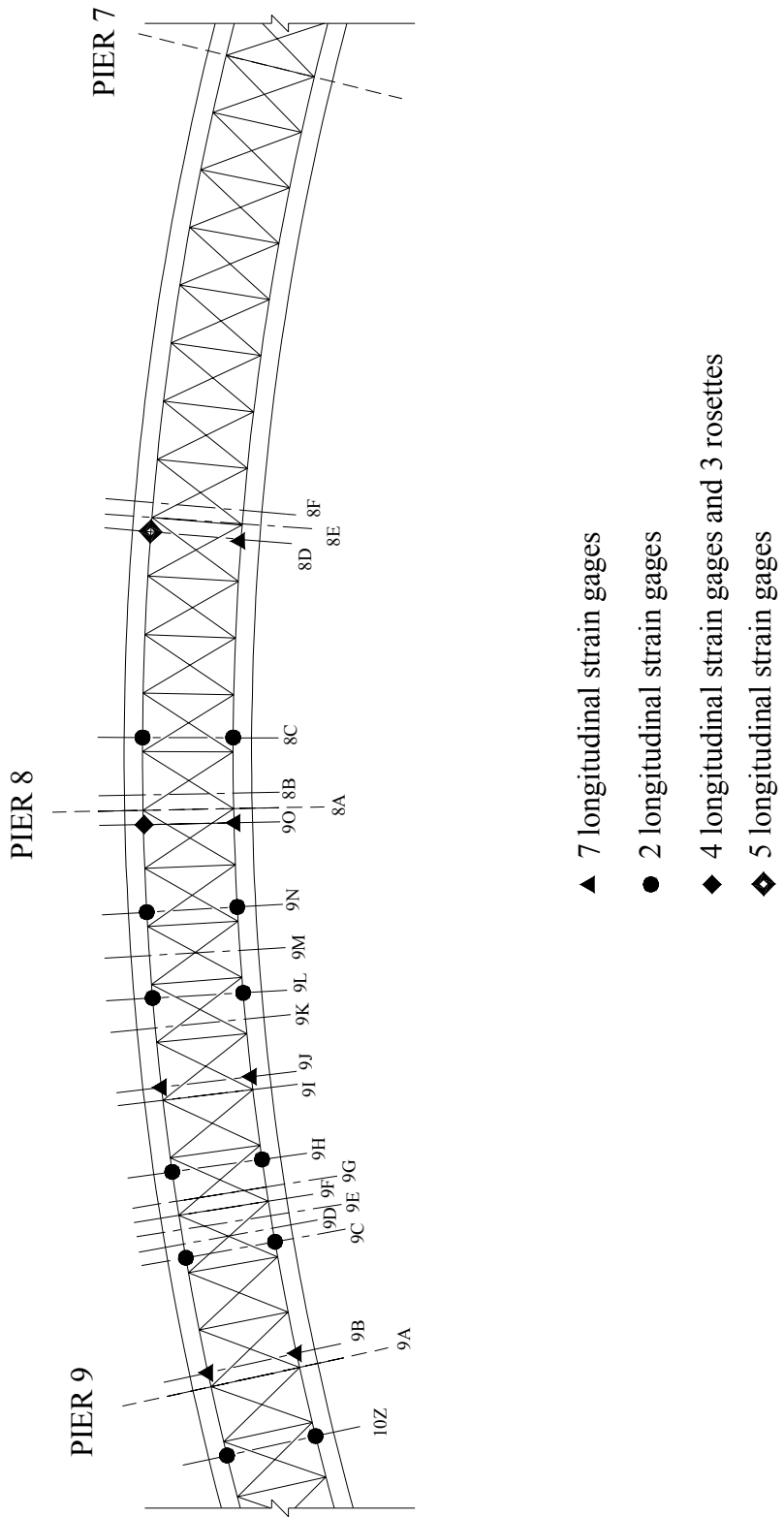
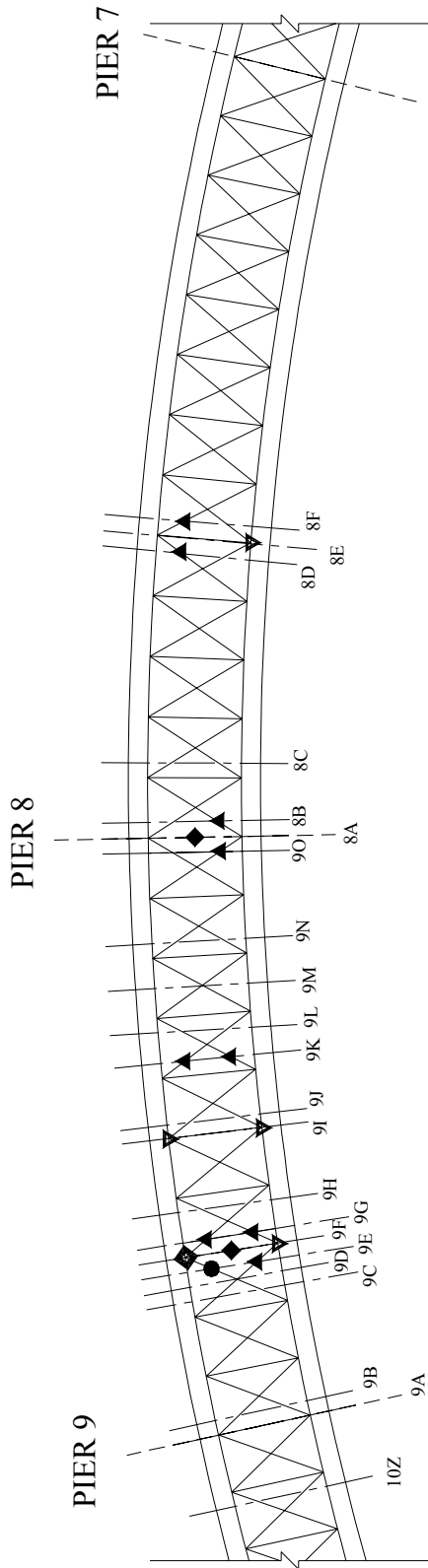


Figure B-4: Main Girder Strain Gages



- ▲ 1 longitudinal strain gage on lateral bracing
- 5 longitudinal strain gages on lateral bracing
- ◆ 10 longitudinal strain gages on diaphragm
- ◆ 2 longitudinal strain gages and 1 rosette on gusset plate connection,
plus 1 vertical strain gage at the web gap location
- ▼ 1 vertical strain gage at the web gap location

Figure B-5: Secondary Location Strain Gages

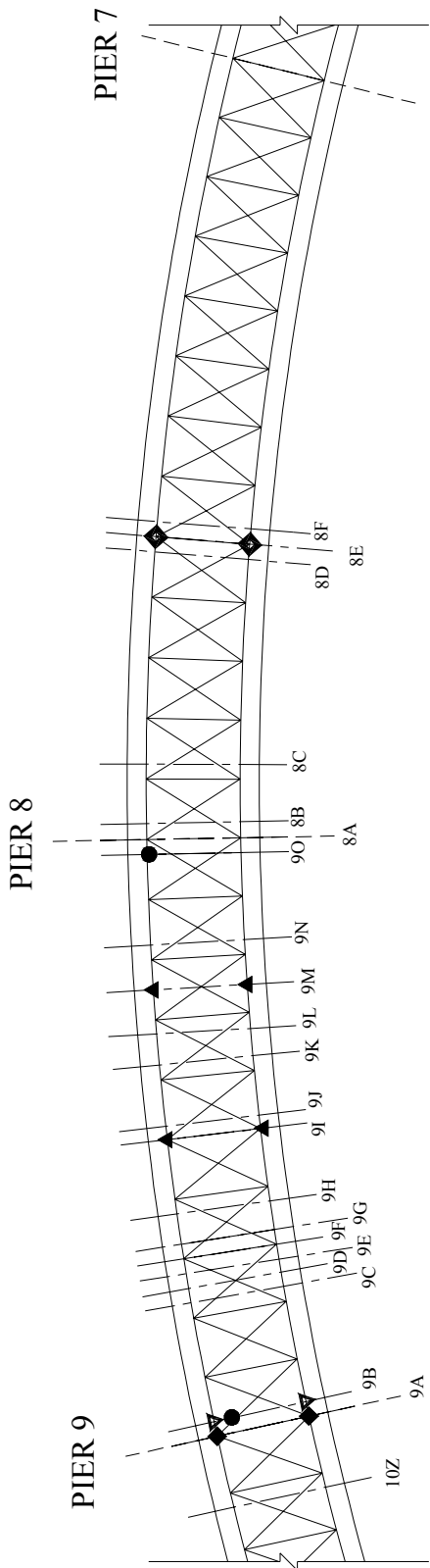
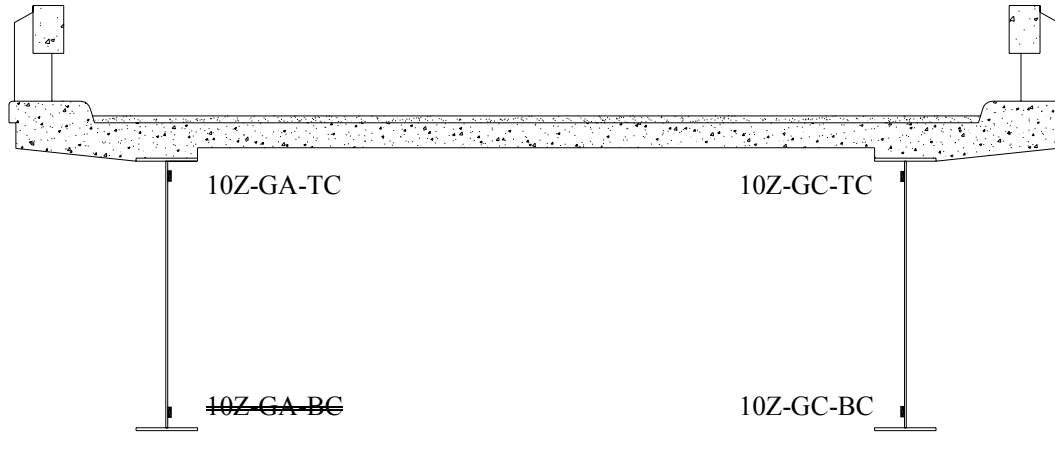


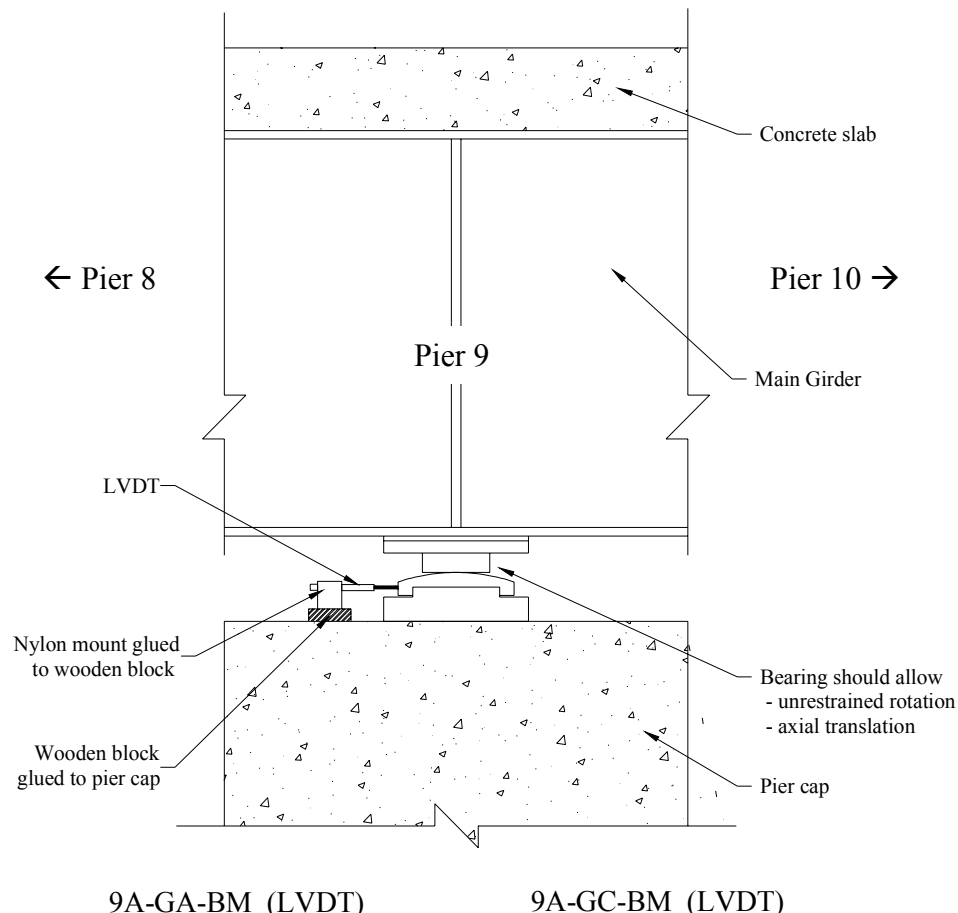
Figure B-6: Displacement Instrumentation



Exterior Girder (A)

Interior Girder (C)

Figure B-7: Gage Nomenclature for Section 10Z



9A-GA-BM (LVDT)

9A-GC-BM (LVDT)

Figure B-8: Gage Nomenclature for Section 9A

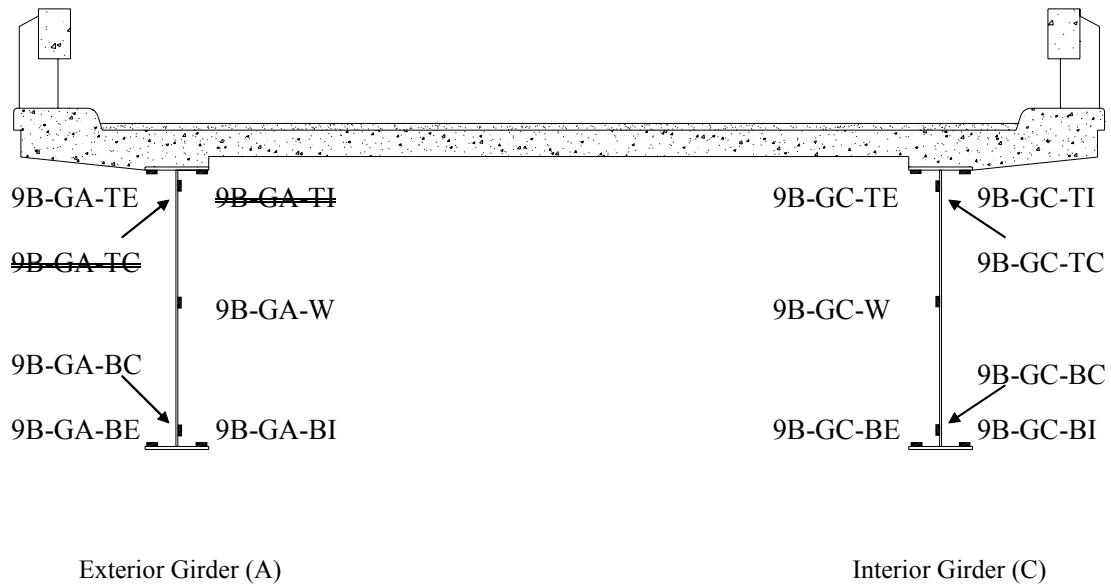


Figure B-9: Gage Nomenclature for Section 9B

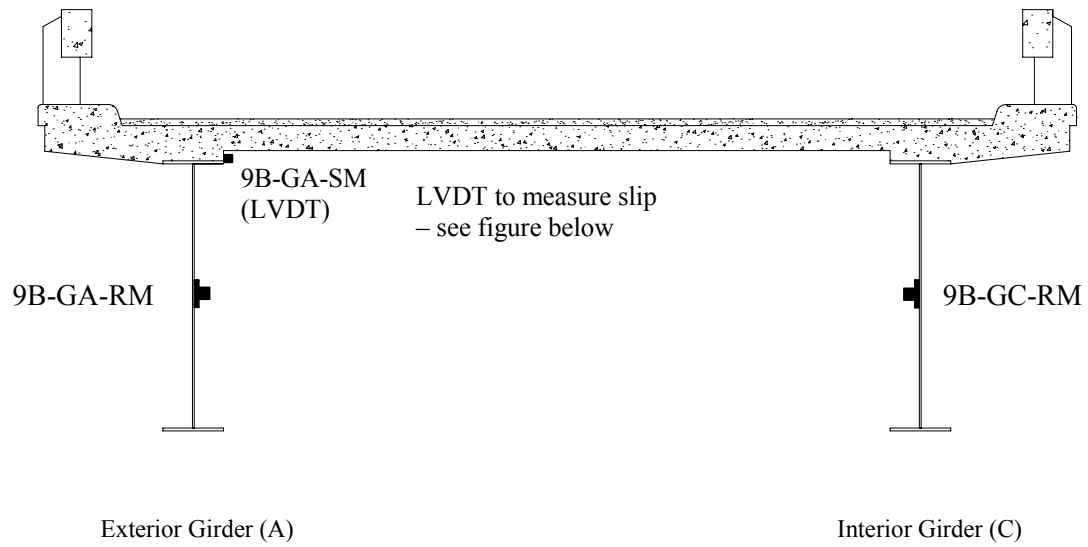


Figure B-10: Gage Nomenclature for Section 9B (continued)

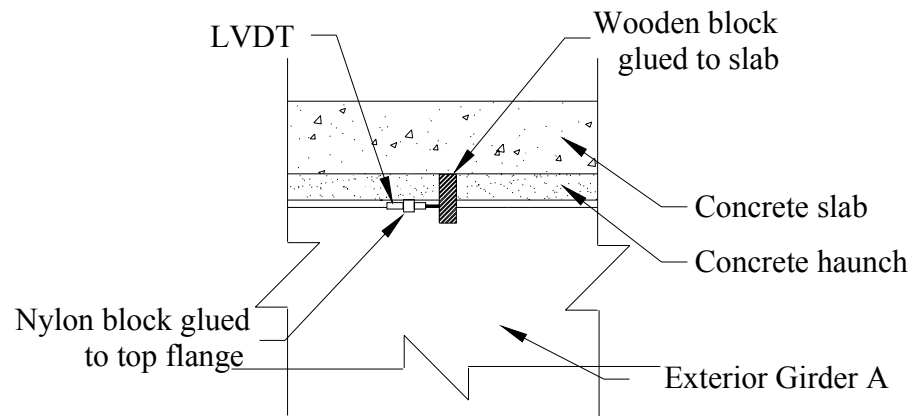


Figure B-11: Gage Nomenclature for Section 9B (continued)

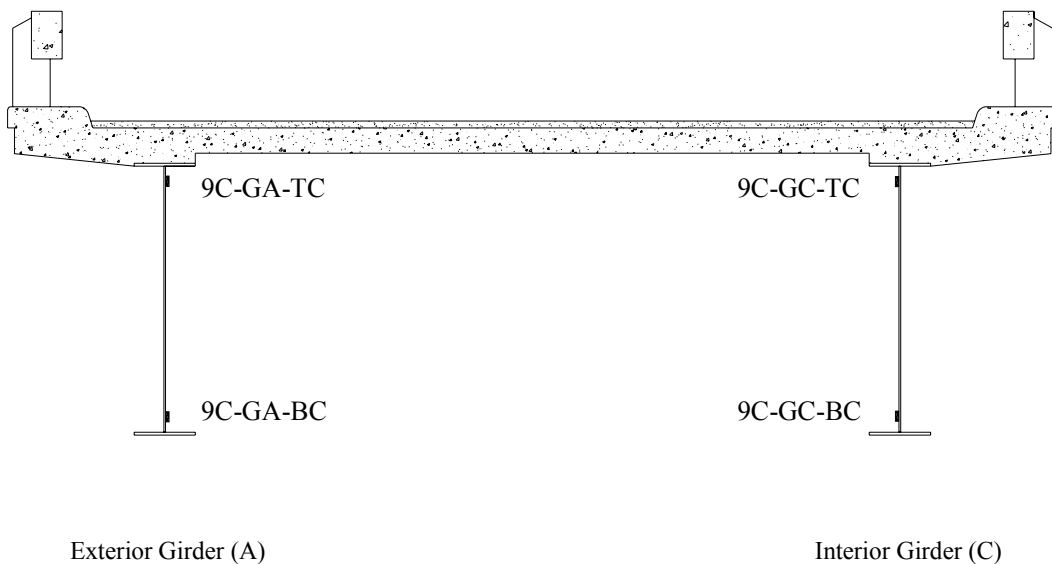


Figure B-12: Gage Nomenclature for Section 9C

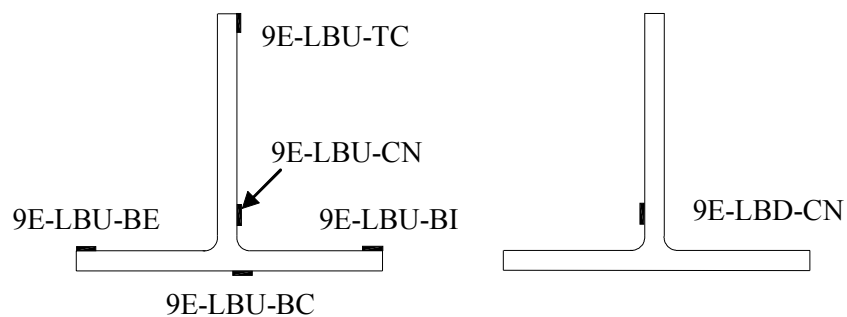


Figure B-13: Gage Nomenclature for Section 9E

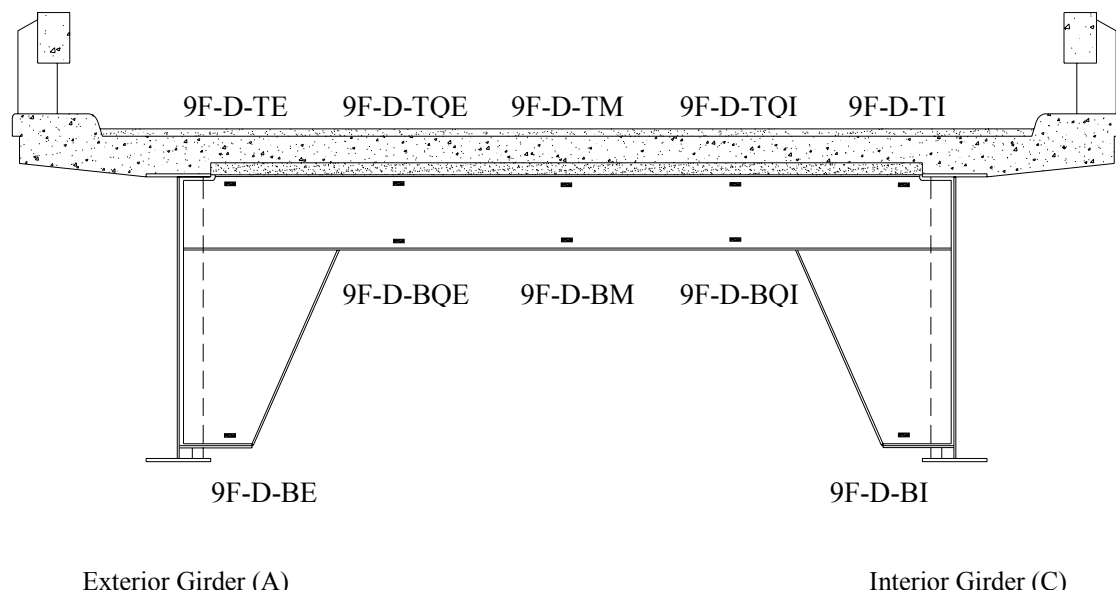


Figure B-14: Gage Nomenclature for Section 9F

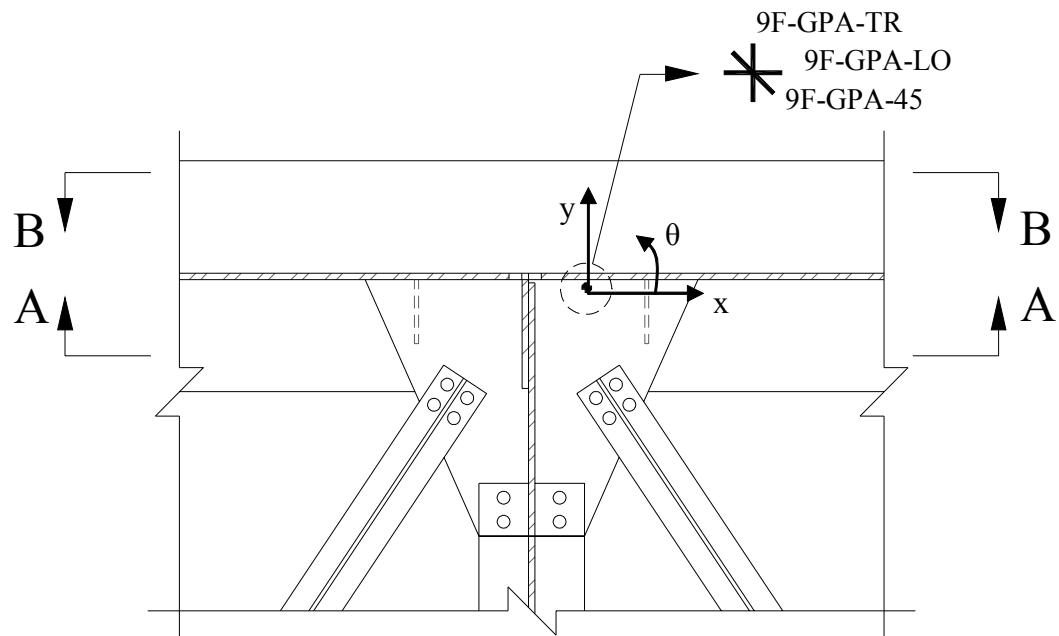


Figure B-15: Gage Nomenclature for Section 9F (continued)

Section AA:

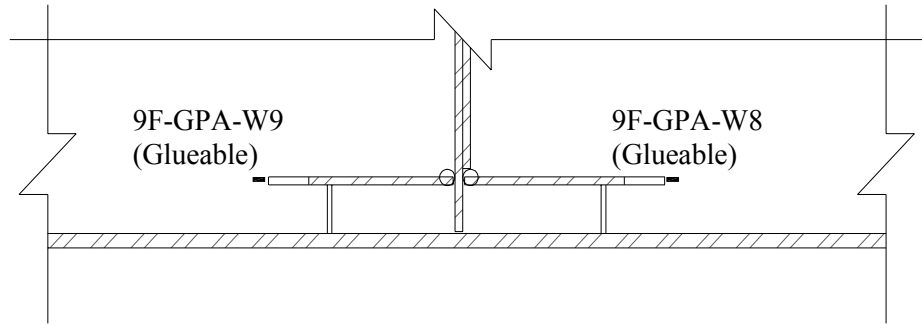


Figure B-16: Gage Nomenclature for Section 9F (continued)

Section BB (on the web gap on Girder A):

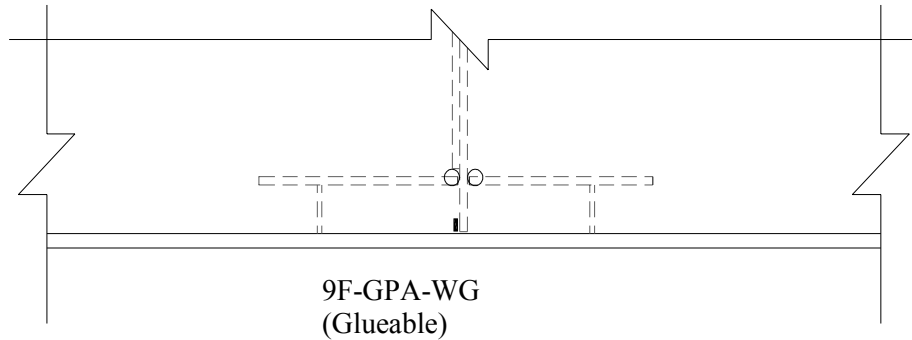


Figure B-17: Gage Nomenclature for Section 9F (continued)

Section BB (on the web gap on Girder C):

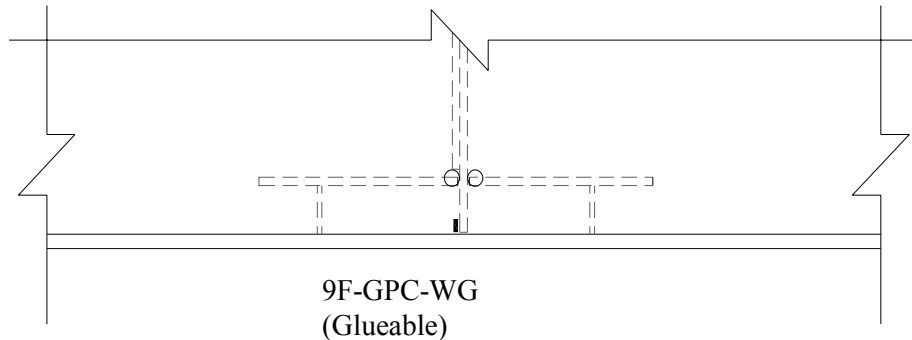


Figure B-18: Gage Nomenclature for Section 9F (continued)



Figure B-19: Gage Nomenclature for Section 9G

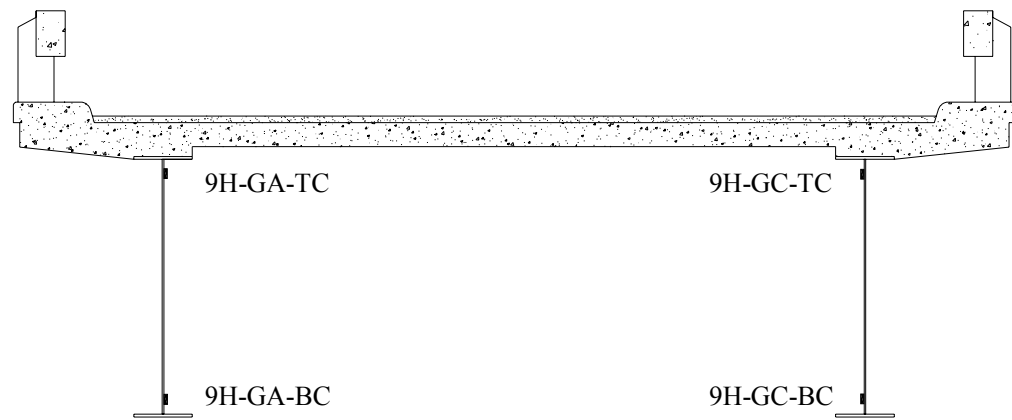


Figure B-20: Gage Nomenclature for Section 9H

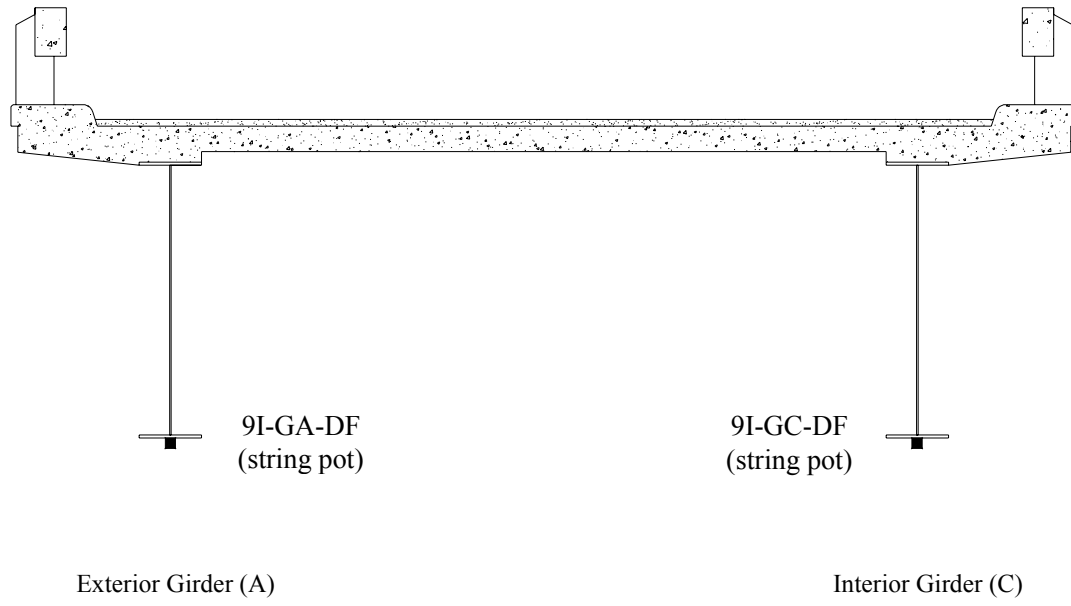


Figure B-21: Gage Nomenclature for Section 9I

Section BB (on the web gap on Girder A):

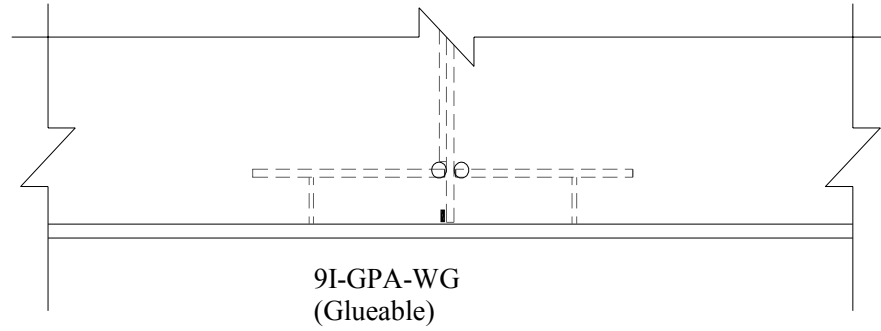


Figure B-22: Gage Nomenclature for Section 9I (continued)

Section BB (on the web gap on Girder C):

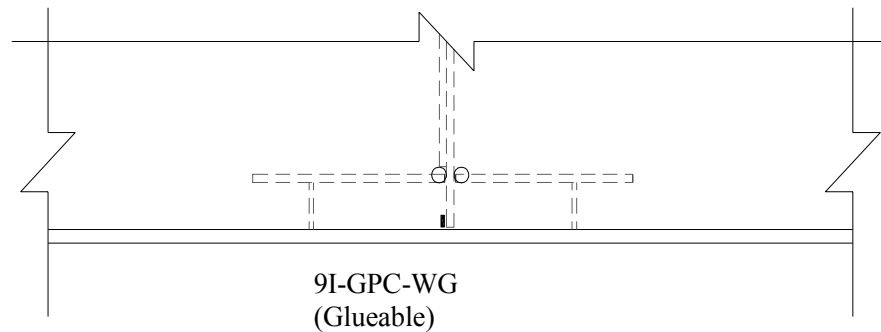


Figure B-23: Gage Nomenclature for Section 9I (continued)

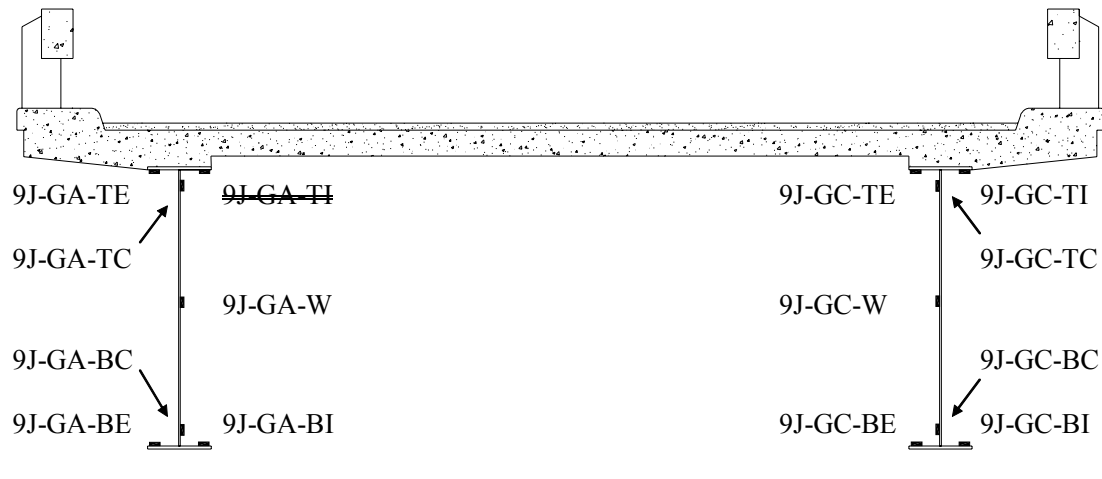


Figure B-24: Gage Nomenclature for Section 9J

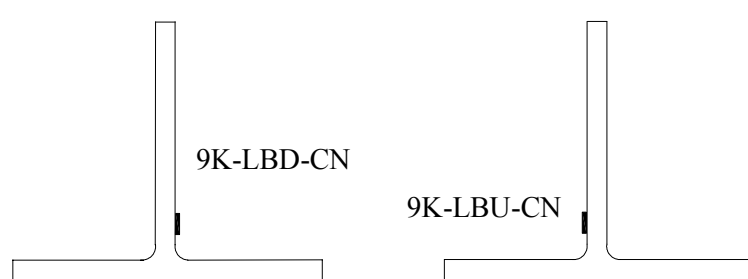


Figure B-25: Gage Nomenclature for Section 9K

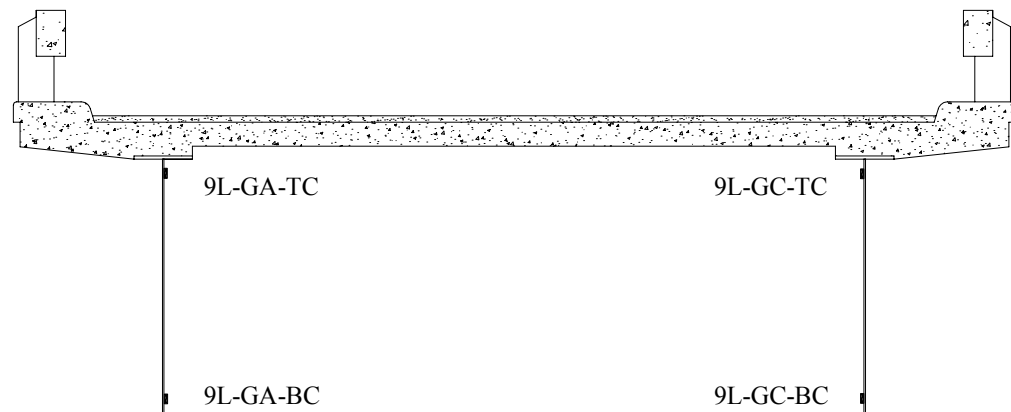
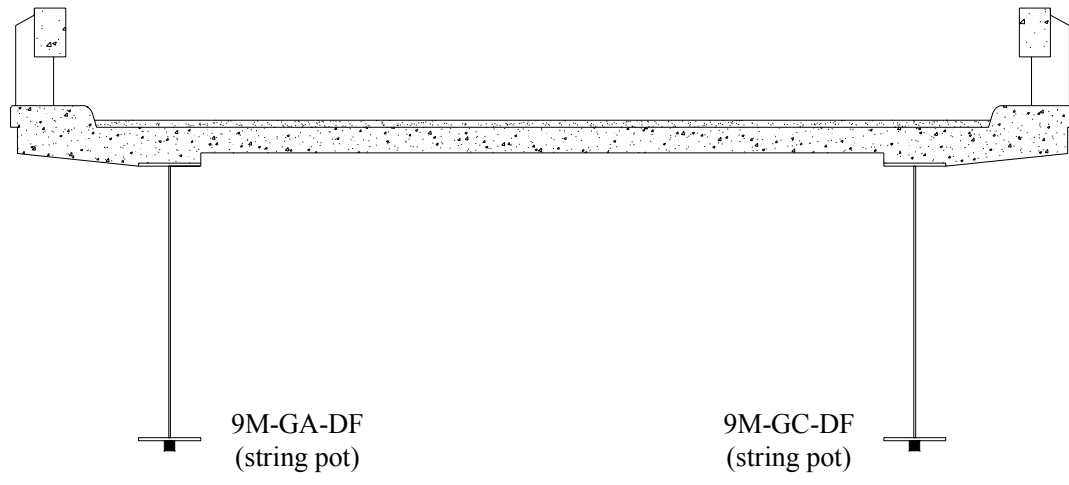


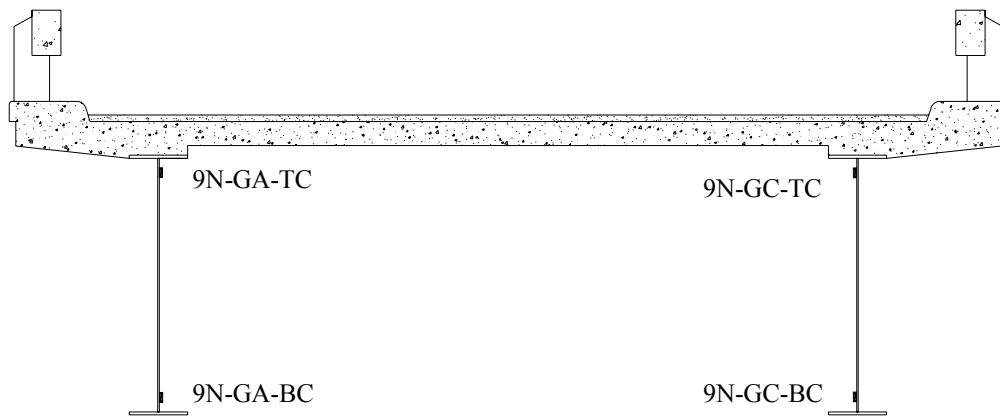
Figure B-26: Gage Nomenclature for Section 9L



Exterior Girder (A)

Interior Girder (C)

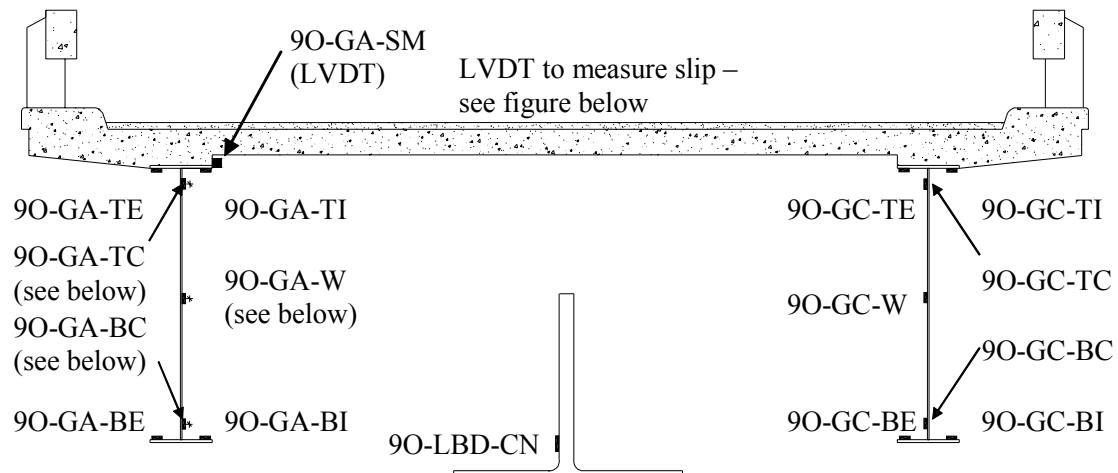
Figure B-27: Gage Nomenclature for Section 9M



Exterior Girder (A)

Interior Girder (C)

Figure B-28: Gage Nomenclature for Section 9N



Exterior Girder (A)

Interior Girder (C)

Rosettes: 9O-GA-TCV
 9O-GA-TCH
 9O-GA-TC45
 9O-GA-WV
 9O-GA-WH
 9O-GA-W45
 9O-GA-BCV
 9O-GA-BCH
 9O-GA-BC45

where,

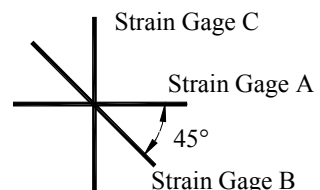
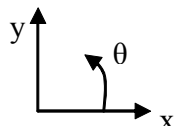


Figure B-29: Gage Nomenclature for Section 9O

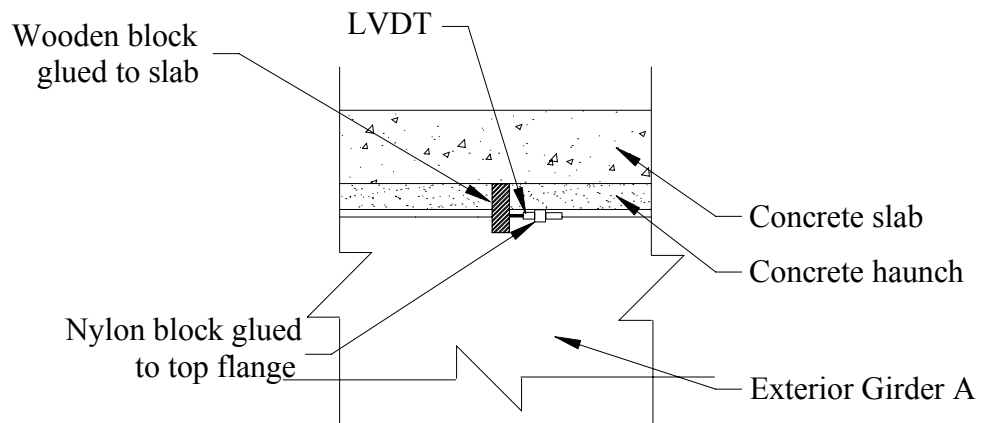
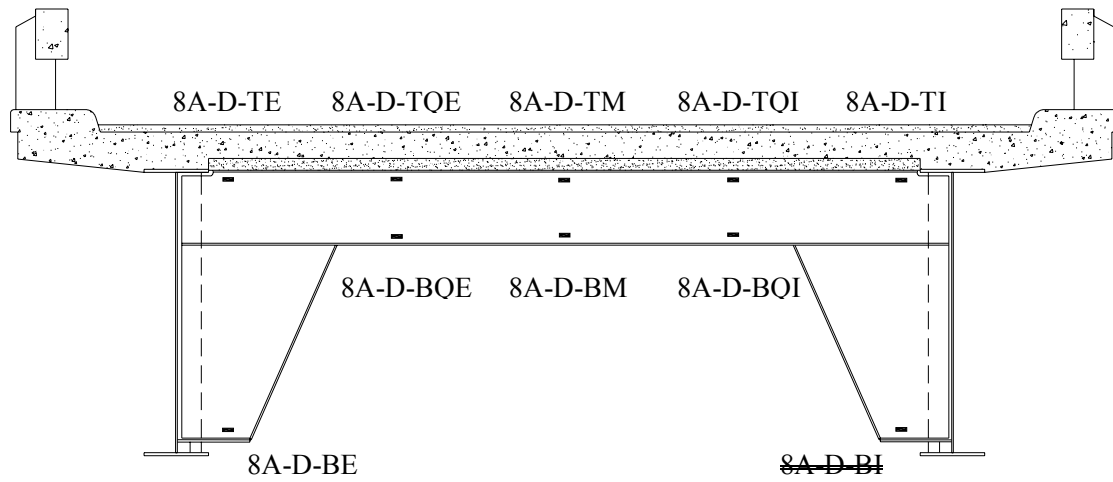


Figure B-30: Gage Nomenclature for Section 9O (continued)



Exterior Girder (A)

Interior Girder (C)

Figure B-31: Gage Nomenclature for Section 8A

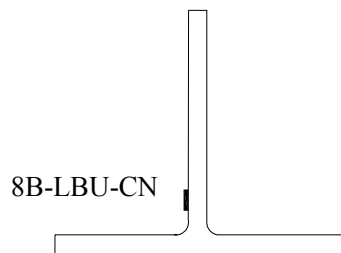
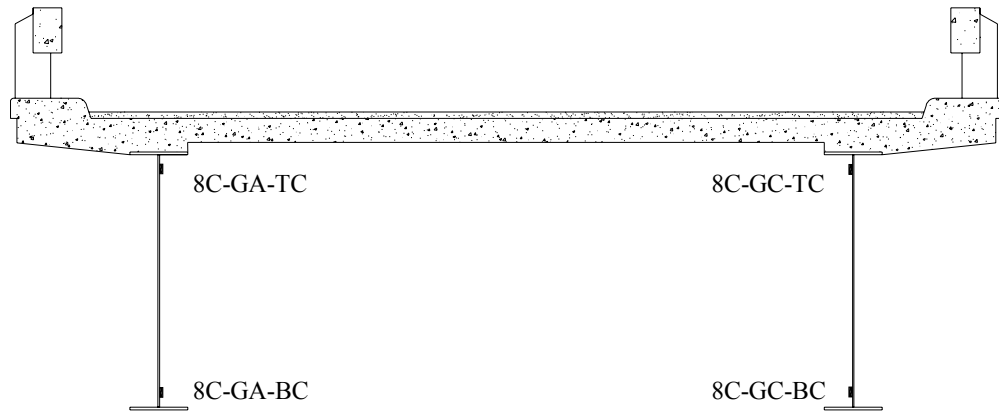


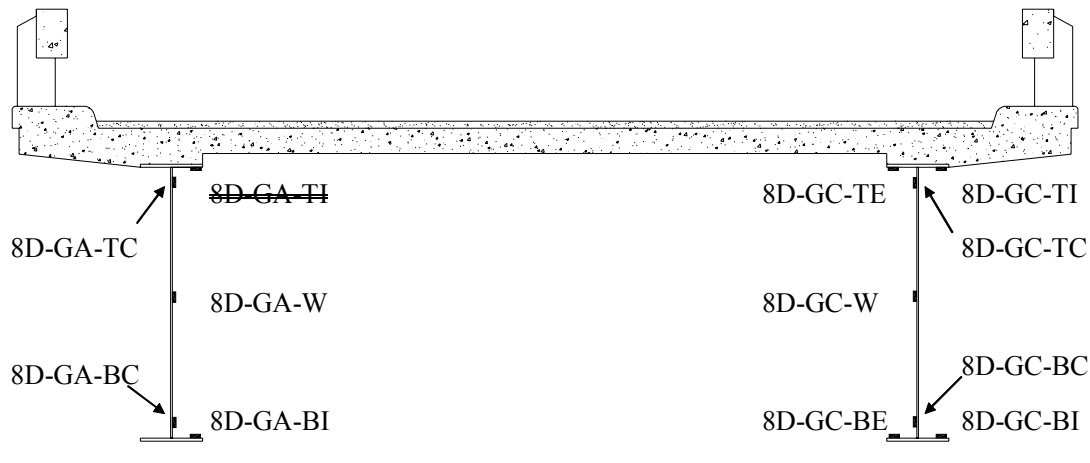
Figure B-32: Section 8B



Exterior Girder (A)

Interior Girder (C)

Figure B-33: Gage Nomenclature for Section 8C



Exterior Girder (A)

Interior Girder (C)

Figure B-34: Gage Nomenclature for Section 8D

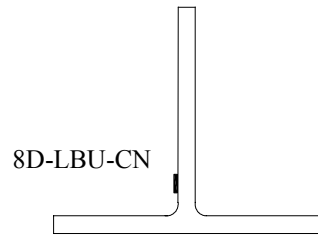
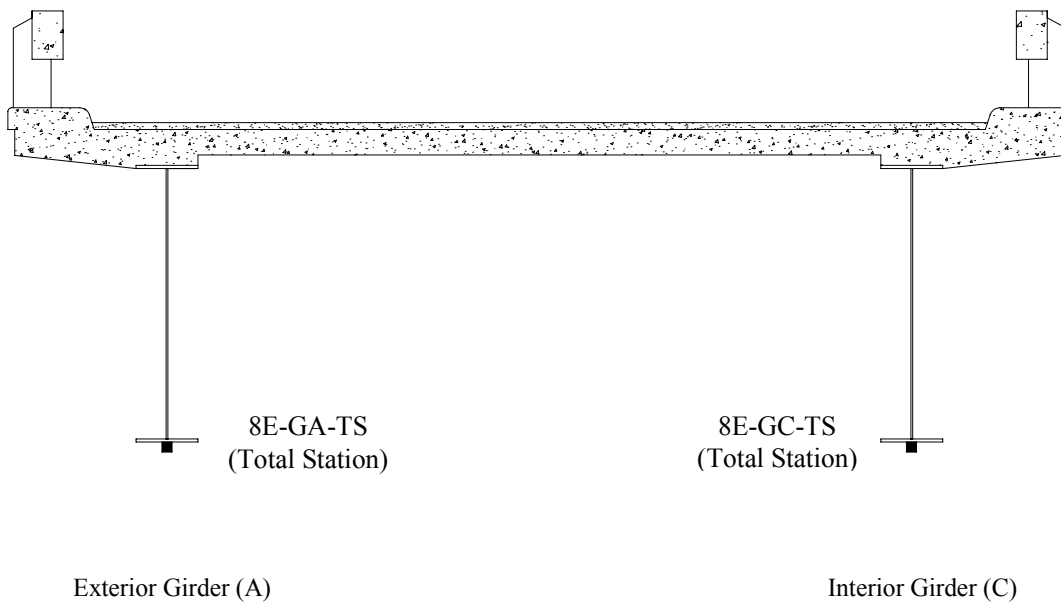


Figure B-35: Gage Nomenclature for Section 8D (continued)



Exterior Girder (A)

Interior Girder (C)

Figure B-36: Gage Nomenclature for Section 8E

Section BB (on the web gap on Girder C):

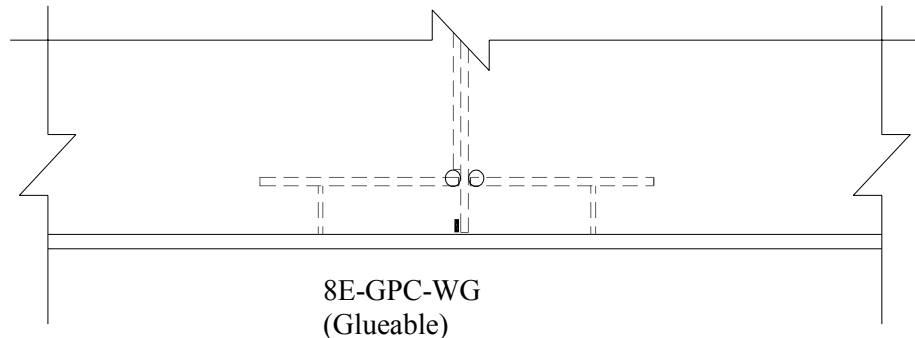


Figure B-37: Gage Nomenclature for Section 8E (continued)

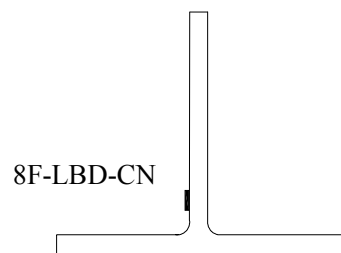


Figure B-38: Gage Nomenclature for Section 9F

Appendix C

Truck Weights, Dimensions, and Original Testing Sequence

Section C.1 of this appendix contains the dimensions and axle weights for the eight quad-axle dump trucks used for the testing of Mn/DOT Bridge No. 69824. Section C.2 provides the original truck testing sequence as it occurred for testing. Diagrams show the locations of the trucks for each test.

C.1 Truck Weights and Dimensions

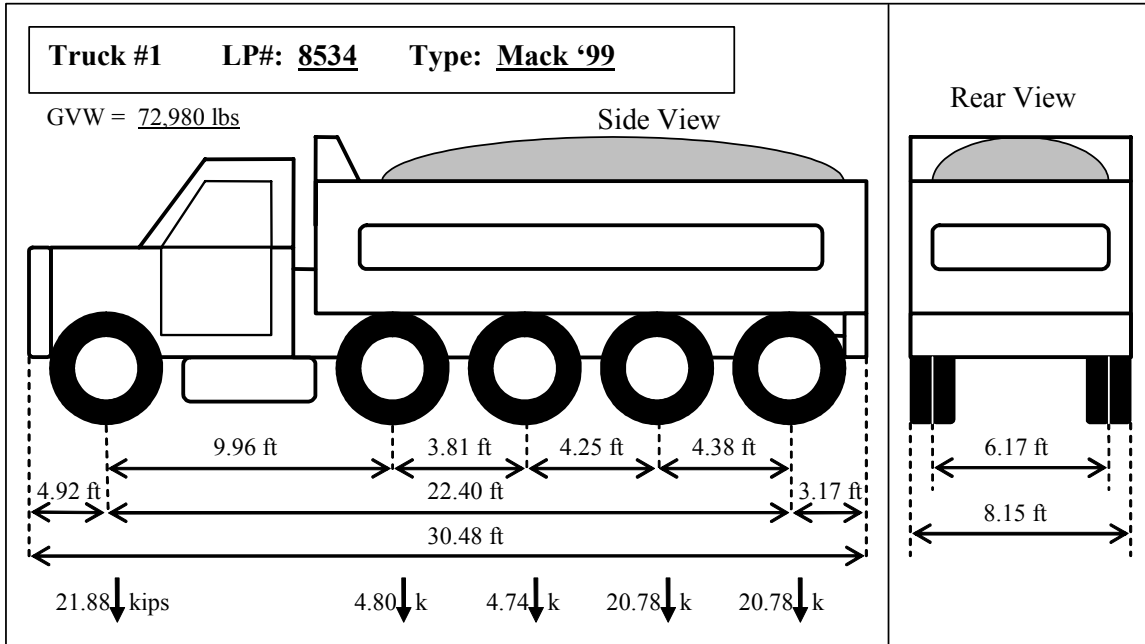


Figure C-1: Truck 1

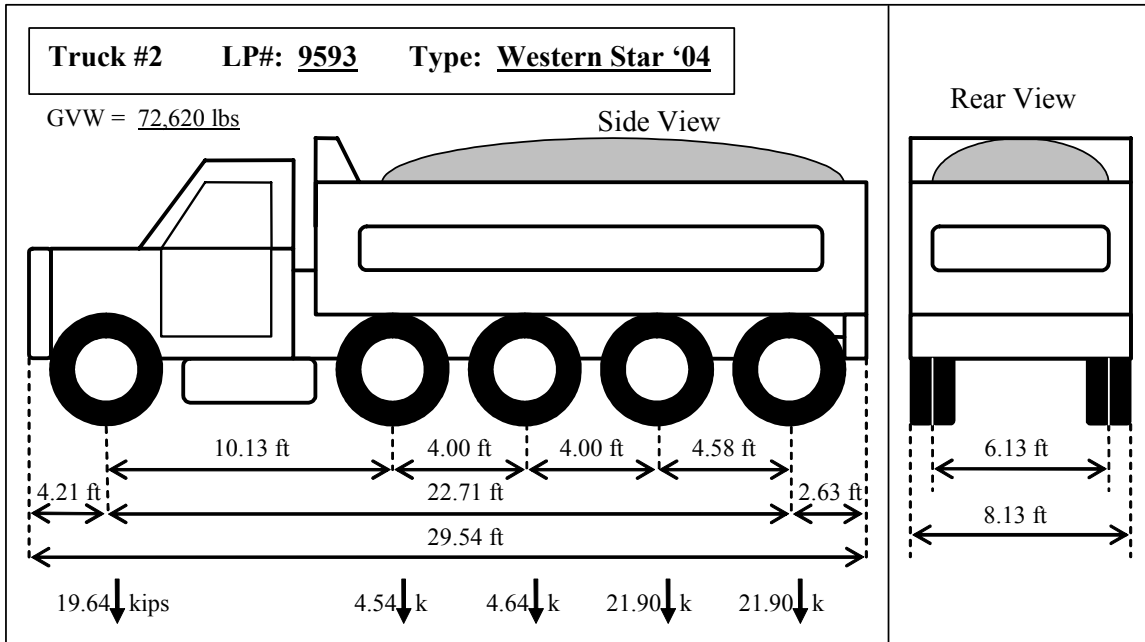


Figure C-2: Truck 2

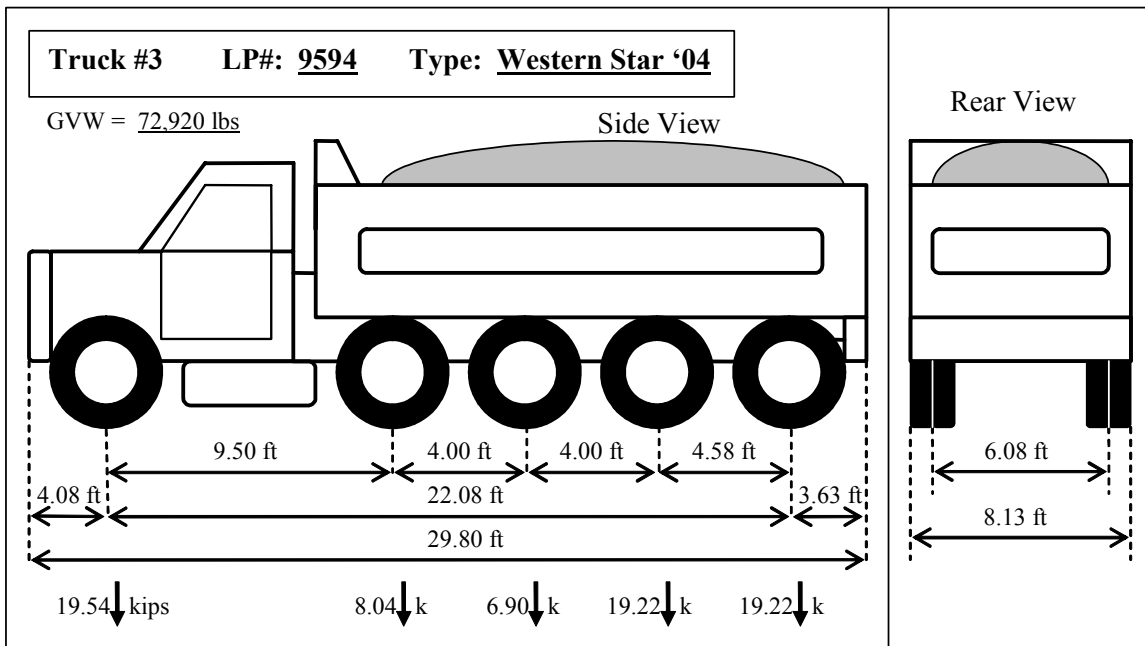


Figure C-3: Truck 3

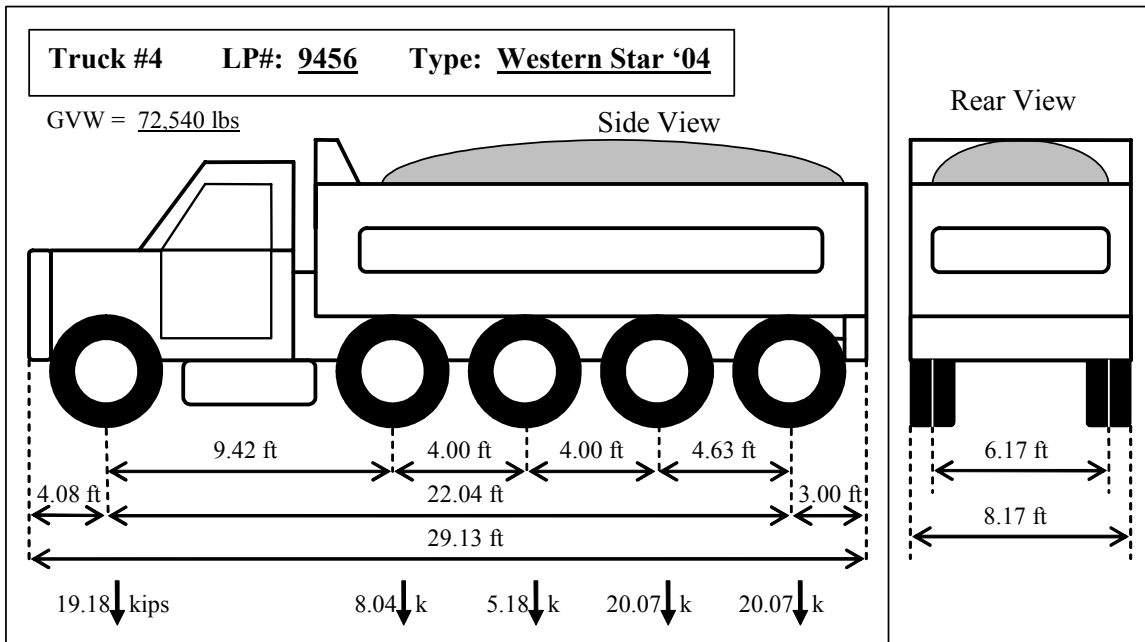


Figure C-4: Truck 4

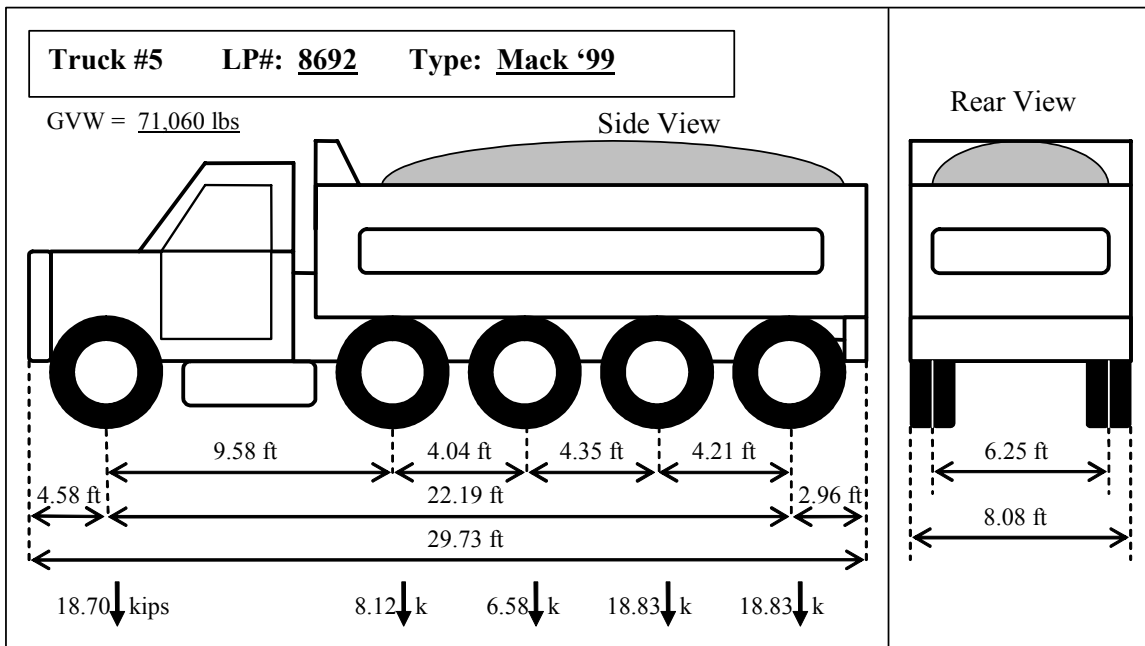


Figure C-5: Truck 5

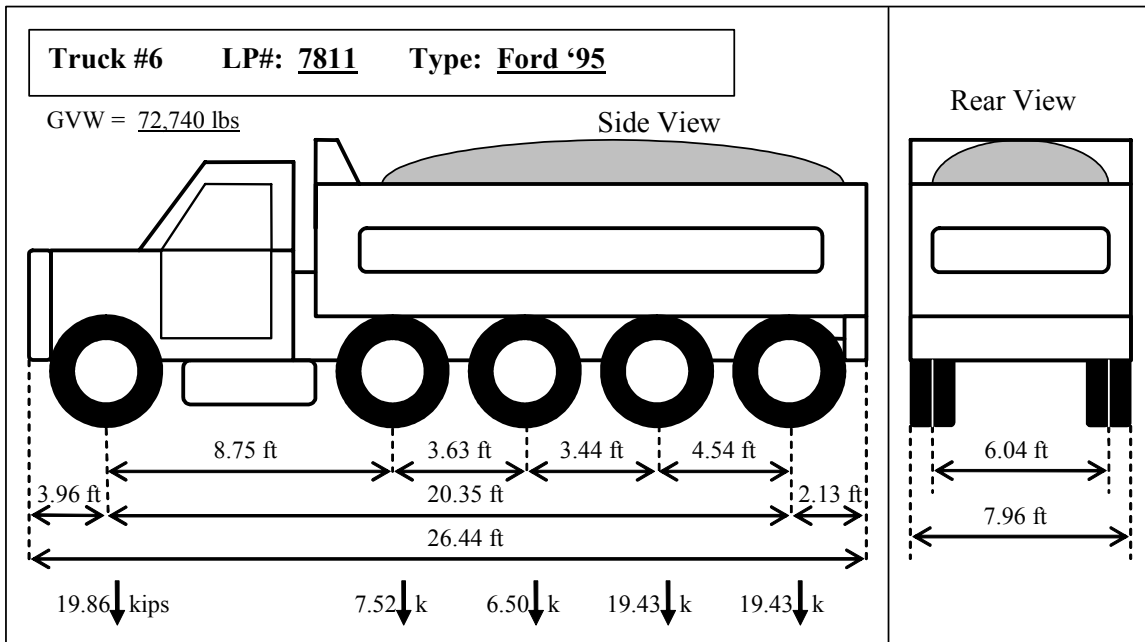


Figure C-6: Truck 6

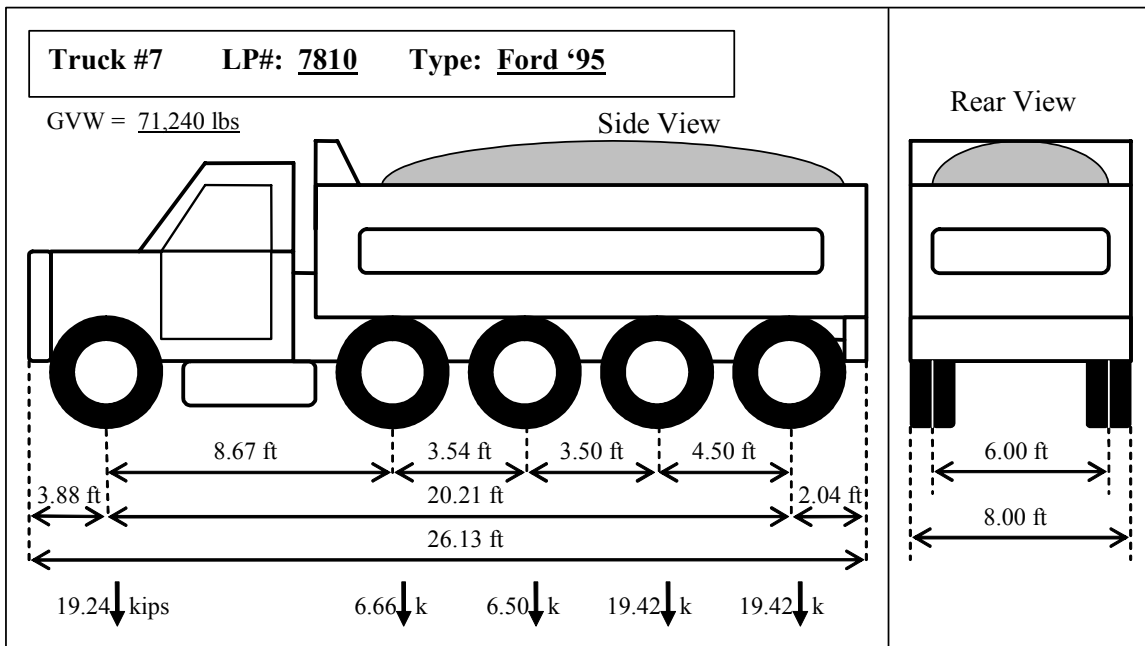


Figure C-7: Truck 7

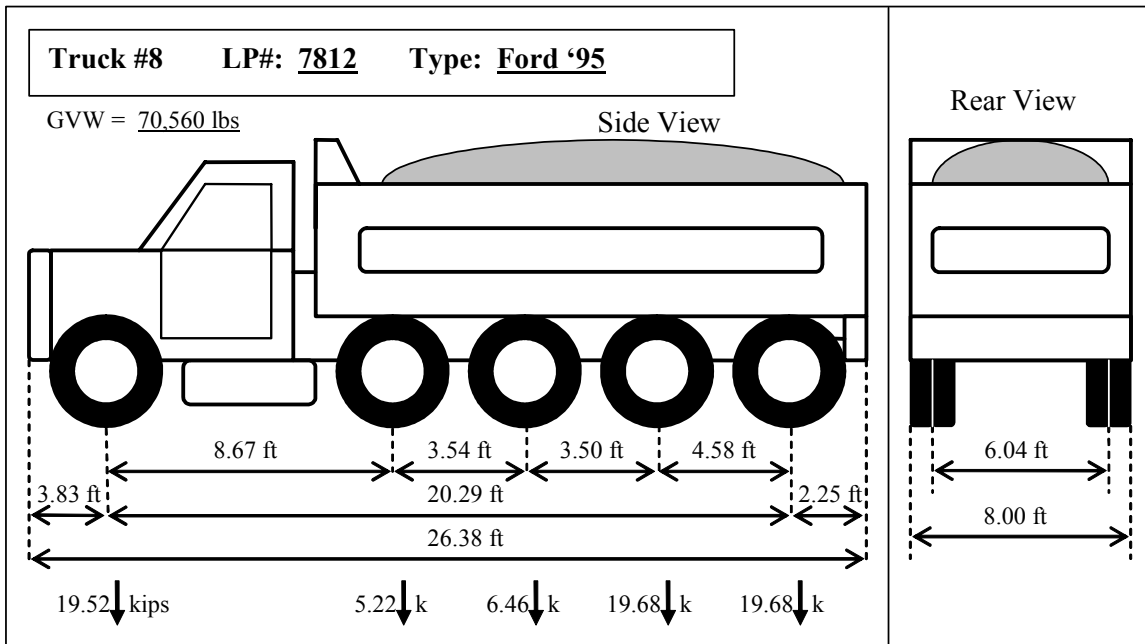


Figure C-8: Truck 8

C.2 Original Testing Sequence

Test No	Objective	Trucks
1-6	Low load level influence line	1 static truck at 6 different locations along the bridge going from midspan 8-7 to pier 9
7	Pretest bridge	2 trucks at midspan 8-7
8		1 truck at midspan 8-7 (Int) and 1 truck at midspan 9-8 (Ext)
9		2 trucks at midspan 9-8
10		4 trucks at midspan 9-8
11		2 trucks at midspan 8-7 and 2 trucks at midspan 9-8
12		3 trucks at midspan 8-7
13	Maximum stresses at midspan 8-7	4 trucks at midspan 8-7
14	Maximum stresses at Pier 8	2 trucks at midspan 8-7 and 4 trucks at midspan 9-8
15		3 trucks at midspan 8-7 and 4 trucks at midspan 9-8
16		4 trucks at midspan 8-7 and 4 trucks at midspan 9-8
17	Redo of Test 13	4 trucks at midspan 8-7
18	Maximum stresses at midspan 9-8	5 trucks at midspan 9-8
19		6 trucks at midspan 9-8
20-27	High load level influence line	Group of 4 static trucks at 8 different locations along the bridge going from midspan 8-7 to pier 9
28	Maximum forces in lateral bracing and diaphragms	1 truck at midspan 9-8 along exterior lane
29		2 trucks at midspan 9-8 along exterior lane
30		2 trucks at midspan 9-8 (Ext) and 1 truck at midspan 8-7 (Int)
31		3 trucks at midspan 9-8 along exterior lane
32		1 truck at midspan 9-8 along interior lane
33		2 trucks at midspan 9-8 along interior lane
34		2 trucks at midspan 9-8 (Int) and 1 truck at midspan 8-7 (Ext)
35		3 trucks at midspan 9-8 along interior lane
36		2 trucks at midspan 9-8 (Int) and 2 trucks at midspan 8-7 (Ext)
37		2 trucks at midspan 9-8 (Ext) and 2 trucks at midspan 8-7 (Int)
38		3 trucks at midspan 9-8 (Ext) and 2 trucks at midspan 8-7 (Int)
39		3 trucks at midspan 9-8 (Ext) and 3 trucks at midspan 8-7 (Int)
40		3 trucks at midspan 9-8 (Int) and 2 trucks at midspan 8-7 (Ext)
41		3 trucks at midspan 9-8 (Int) and 3 trucks at midspan 8-7 (Ext)
42	Dynamic testing	1 truck driving across bridge at 10 mph
43		1 truck driving across bridge at 20 mph
44		1 truck driving across bridge at 35 mph
45		1 truck driving across bridge at 35 mph
46	Dynamic testing with 2x4	1 truck driving across bridge with 2x4 at 10 mph
47		1 truck driving across bridge with 2x4 at 20 mph
48		1 truck driving across bridge with 2x4 at 24 mph
49		1 truck driving across bridge with 2x4 at 25 mph
50		1 truck driving across bridge with 2x4 at 10 mph
51	Braking Test	1 truck driving at 10 mph, brakes at midspan 9-8
52		1 truck driving at 20 mph, brakes at midspan 9-8
53		1 truck driving at 35 mph, brakes at midspan 9-8
54	Dynamic testing with 2x4	1 truck driving across bridge with 2x4 at 35 mph
55	Post-test bridge	2 trucks at midspan 8-7
56		4 trucks at midspan 9-8

Table C-1: Original Testing Sequence for Mn/DOT Bridge No. 69824

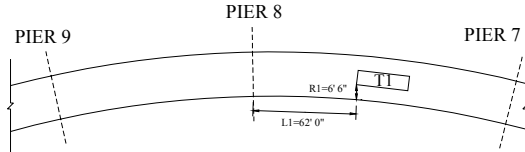
Test Times for Bridge No. 69824 on July 14 th -15 th , 2005			
Test #	Time	Test #	Time
Initial Zero	8:37:00 PM	29	1:03:31 AM
1	8:39:05 PM	30	1:07:55 AM
2	8:41:32 PM	31	1:16:20 AM
3	8:43:57 PM	32	1:22:11 AM
4	8:45:56 PM	33	1:27:13 AM
5	8:47:44 PM	34	1:31:37 AM
6	8:49:23 PM	35	1:38:12 AM
7	8:55:59 PM	36	1:45:55 AM
8	9:11:05 PM	37	1:56:16 AM
9	9:14:19 PM	38	2:03:46 AM
10	9:22:17 PM	39	2:16:09 AM
11	9:33:56 PM	40	2:27:47 AM
12	9:49:12 PM	41	2:32:53 AM
13	10:09:45 PM	Zero 3	2:43:28 AM
14	10:26:39 PM	42	2:55:00 AM
15	10:42:08 PM	43	2:57:37 AM
16	10:55:48 PM	44	2:59:45 AM
17	11:10:00 PM	45	3:01:33 AM
18	11:27:11 PM	46	3:09:30 AM
19	11:44:13 PM	47	3:13:32 AM
Zero 1	12:02:31 AM	48	3:16:11 AM
20	12:12:44 AM	49	3:18:30 AM
21	12:16:52 AM	50	3:21:32 AM
22	12:20:38 AM	51	3:26:33 AM
23	12:25:02 AM	52	3:28:50 AM
24	12:33:22 AM	53	3:31:58 AM
25	12:38:14 AM	54	3:39:36 AM
26	12:41:53 AM	55	3:47:21 AM
27	12:47:32 AM	56	3:57:56 AM
Zero 2	12:53:12 AM	Zero 4	4:08:52 AM
28	12:58:21 AM		

Table C-2: Original Test Sequence Times for Mn/DOT Bridge No. 69824

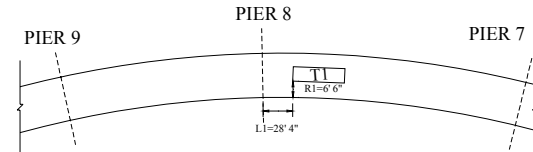
For all diagrams below:

- Trucks face toward the left (i.e., from pier 7 to pier 9)
 - All L _distances are arc lengths measured along the interior edge of the roadway
 - All R _distances are measured radially outward from the interior edge of the roadway
 - The interior edge of the roadway for this bridge coincides with the interior curb edge
 - The number in parenthesis refers to the Static or Dynamic numbering schemes

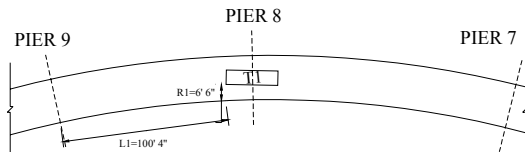
TEST #1 (S1):



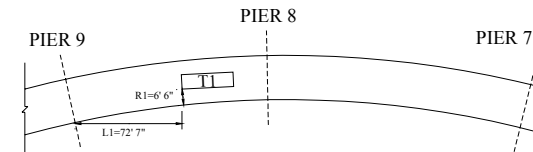
TEST #2 (S2):



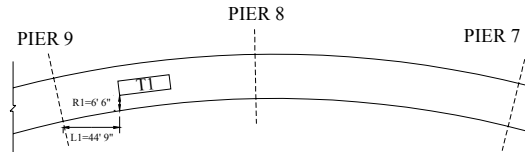
TEST #3 (S3):



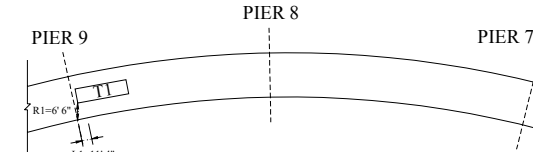
TEST #4 (S4):



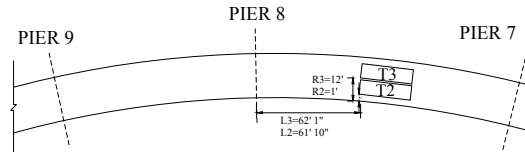
TEST #5 (S5):



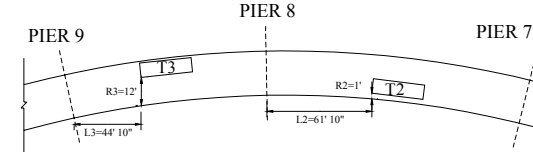
TEST #6 (S6):



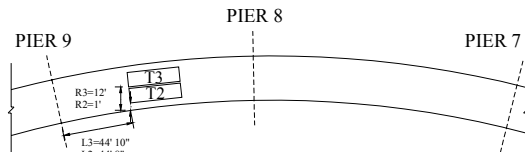
TEST #7 (S20):



TEST #8 (S35):



TEST #9 (S15):



TEST #10 (S16):

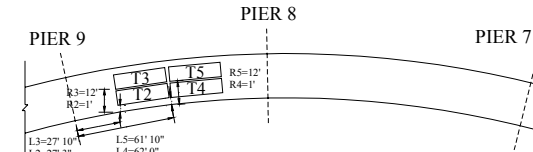
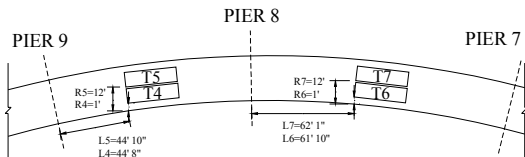
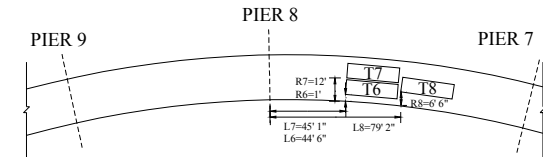


Figure C-9: Original Testing Sequence

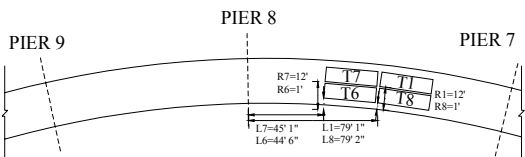
TEST #11 (S25):



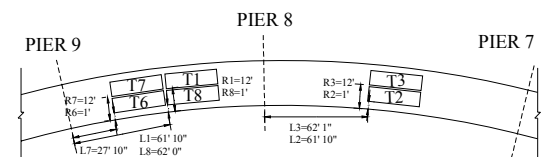
TEST #12 (S22):



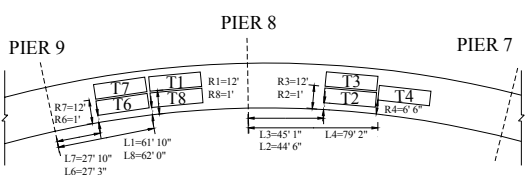
TEST #13 (S23):



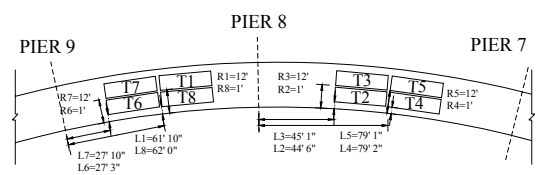
TEST #14 (S26):



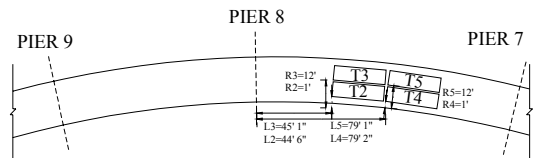
TEST #15 (S27):



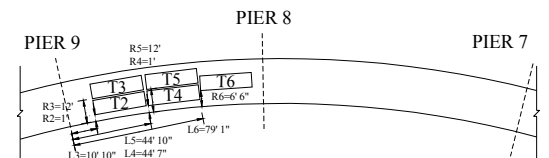
TEST #16 (S28):



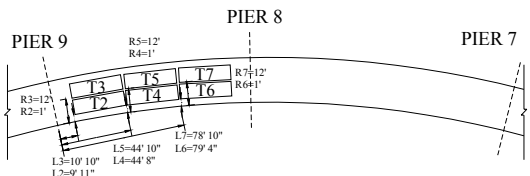
TEST #17 (S24):



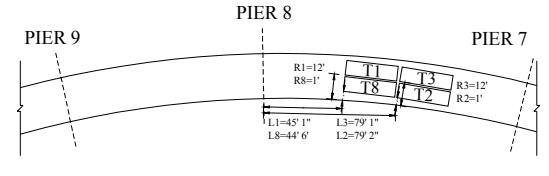
TEST #18 (S18):



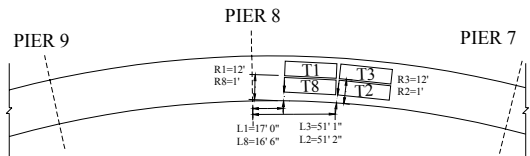
TEST #19 (S19):



TEST #20 (S7):



TEST #21 (S8):



TEST #22 (S9):

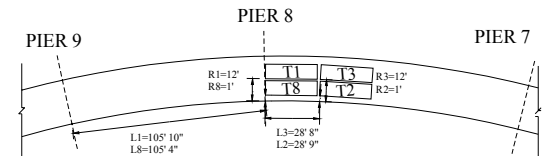
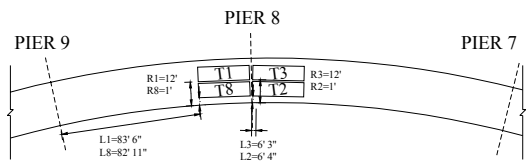
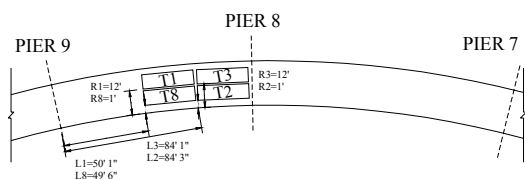


Figure C-10: Original Testing Sequence (continued)

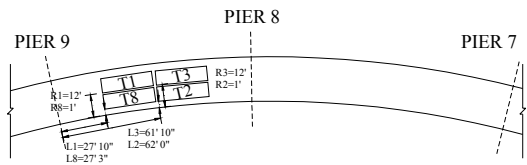
TEST #23 (S10):



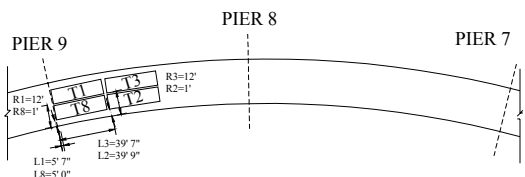
TEST #24 (S11):



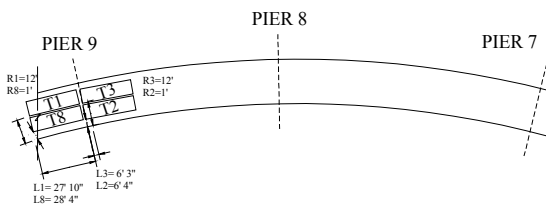
TEST #25 (S12):



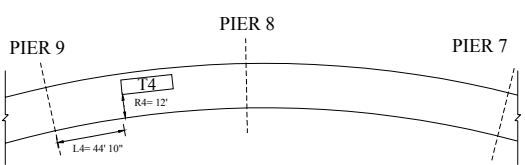
TEST #26 (S13):



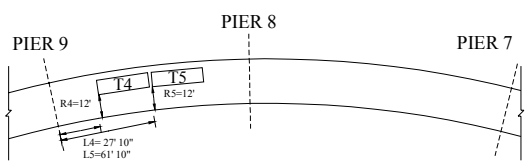
TEST #27 (S14):



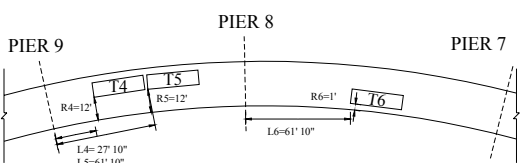
TEST #28 (S29):



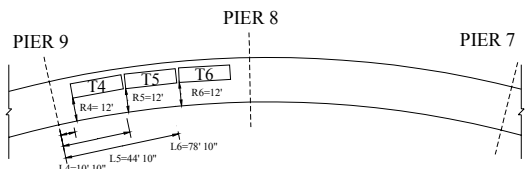
TEST #29 (S30):



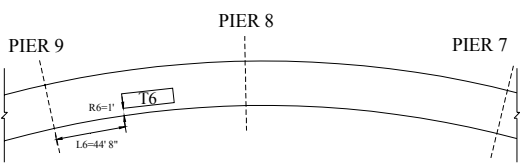
TEST #30 (S36):



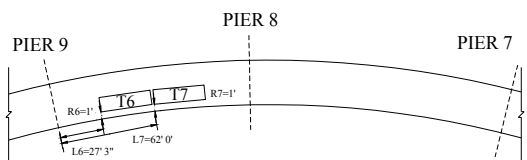
TEST #31 (S31):



TEST #32 (S32):



TEST #33 (S33):



TEST #34 (S40):

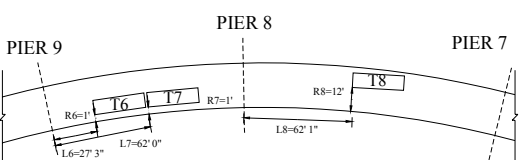
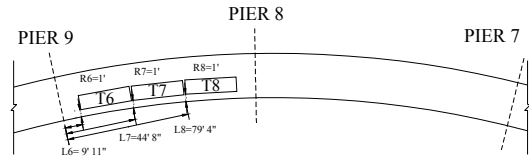
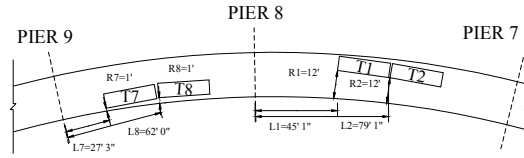


Figure C-11: Original Testing Sequence (continued)

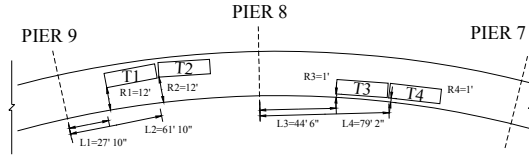
TEST #35 (S34):



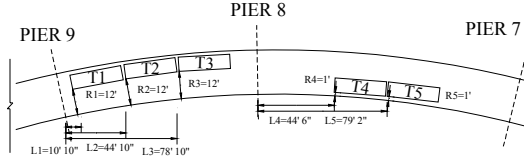
TEST #36 (S41):



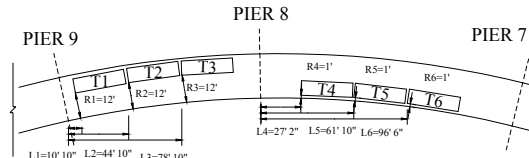
TEST #37 (S37):



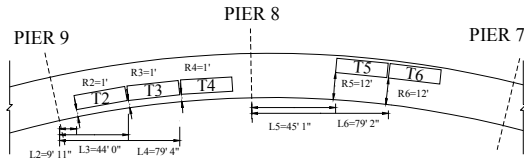
TEST #38 (S38):



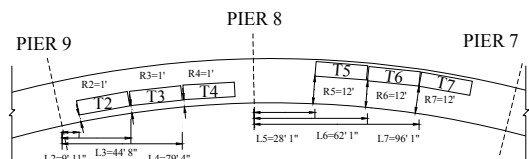
TEST #39 (S39):



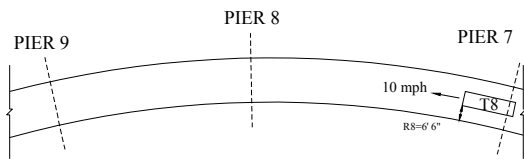
TEST #40 (S42):



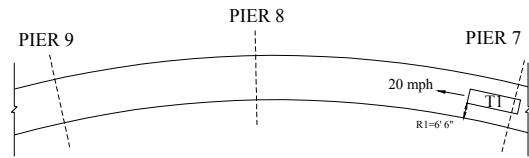
TEST #41 (S43):



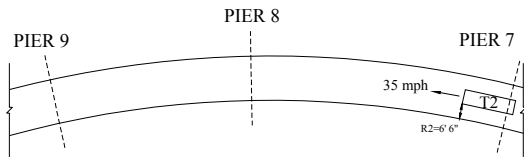
TEST #42 (D1):



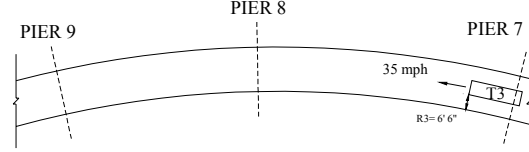
TEST #43 (D2):



TEST #44 (D3):



TEST #45 (D4):



TEST #46 (D5):

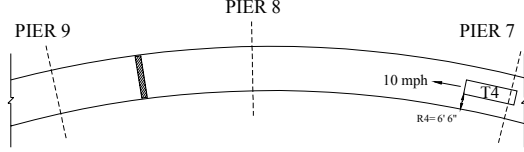
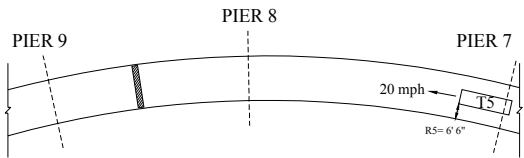
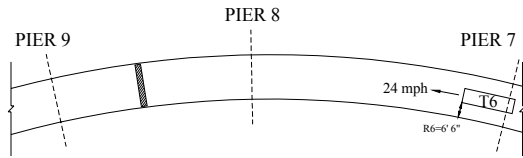


Figure C-12: Original Testing Sequence (continued)

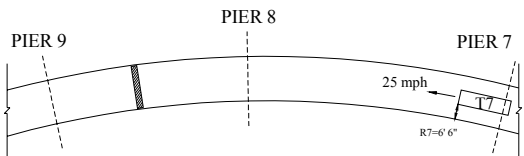
TEST #47 (D7):



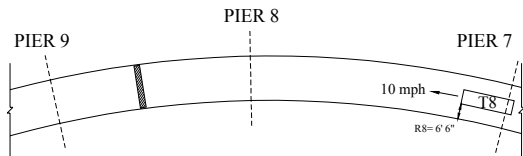
TEST #48 (D8):



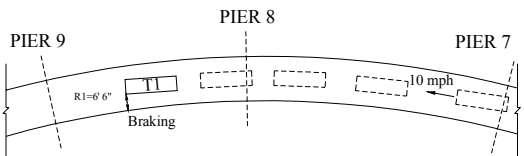
TEST #49 (D9):



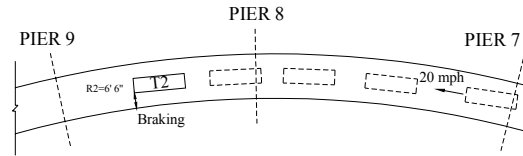
TEST #50 (D6):



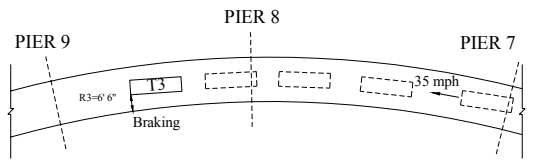
TEST #51 (D11):



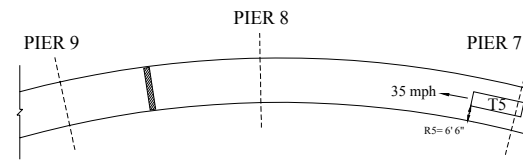
TEST #52 (D12):



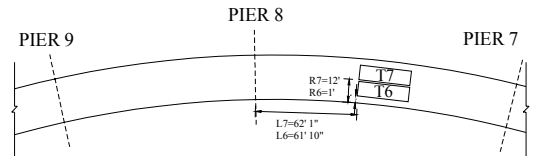
TEST #53 (D13):



TEST #54 (D10):



TEST #55 (S21):



TEST #56 (S17):

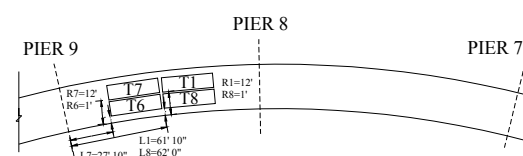


Figure C-13: Original Testing Sequence (continued)

Appendix D
Static Test Raw Data and Thermal Strain Plots

This appendix contains plots of the measured static test raw data for all instrumentation used during the testing of Mn/DOT Bridge No. 69824 in Duluth, Minnesota, on July 14th-15th, 2004. Where thermal strains have been determined to have a significant impact on the measured strain values (see Chapter 5 for details), they are plotted along with the measured strains. Measured static raw data are plotted per test (see Appendix C for configurations) using solid shapes and connected with solid lines, while thermal strains are plotted with hollow shapes and connected with dashed lines.

Since the displacement instruments only provided voltage readings (except the total stations), an offset value had to be subtracted from the readings for each test to determine the displacements. For these plots, a single offset value based on the average of the four zero readings is used per instrument for the entire test period. In this manner, the relative progression of the readings can be identified throughout the testing. Displacements from the total stations are calculated using trigonometry.

Due to unexpected data recording issues (see Chapter 5), approximately half of the strain gage data was not recorded at 12:02:31 a.m. (Zero 1) and likewise at 3:57:56 a.m. (T56). Missed data can be identified on these plots as a discontinuity in the line.

The plots are grouped as described below:

- Girder Rotations: Figure D-1
- Vertical Deflections: Figure D-2 to Figure D-4
- Steel-Concrete Slip: Figure D-5
- Bearing Movement: Figure D-6
- Girder Strains: Figure D-7 to Figure D-44
- Diaphragm Strains: Figure D-45 to Figure D-54
- Lateral Wind Bracing Strains: Figure D-55 to Figure D-59
- Gusset Plate Strains: Figure D-60 to Figure D-61
- Web Gap Strains: Figure D-62 to Figure D-63

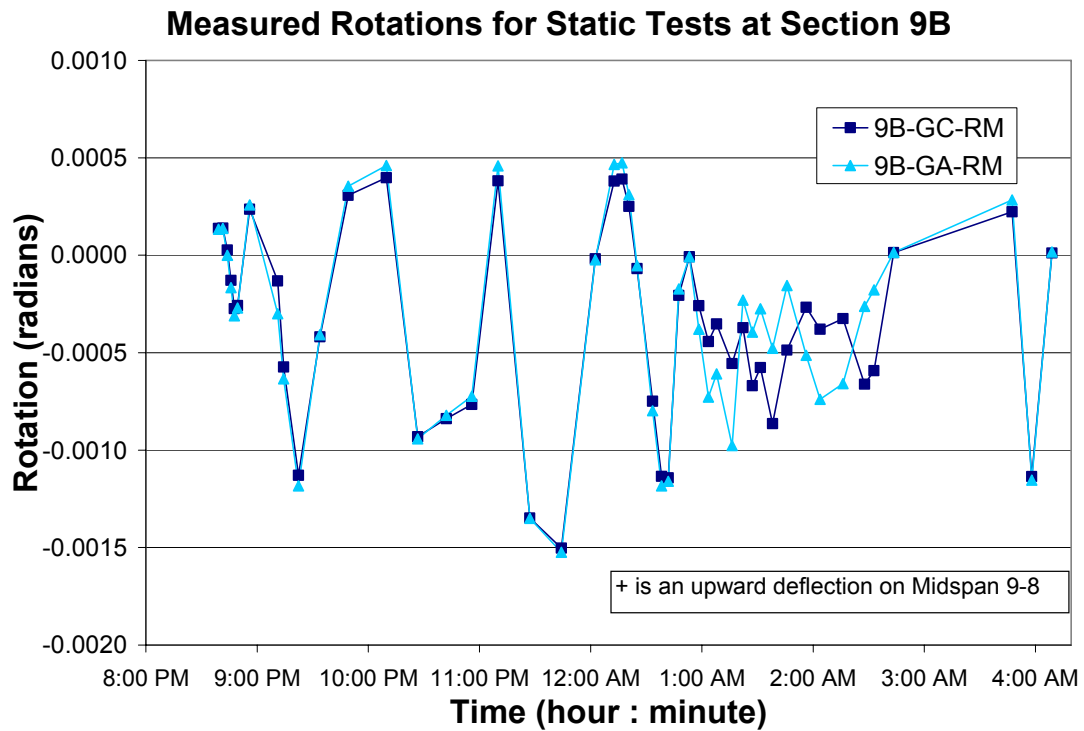


Figure D-1

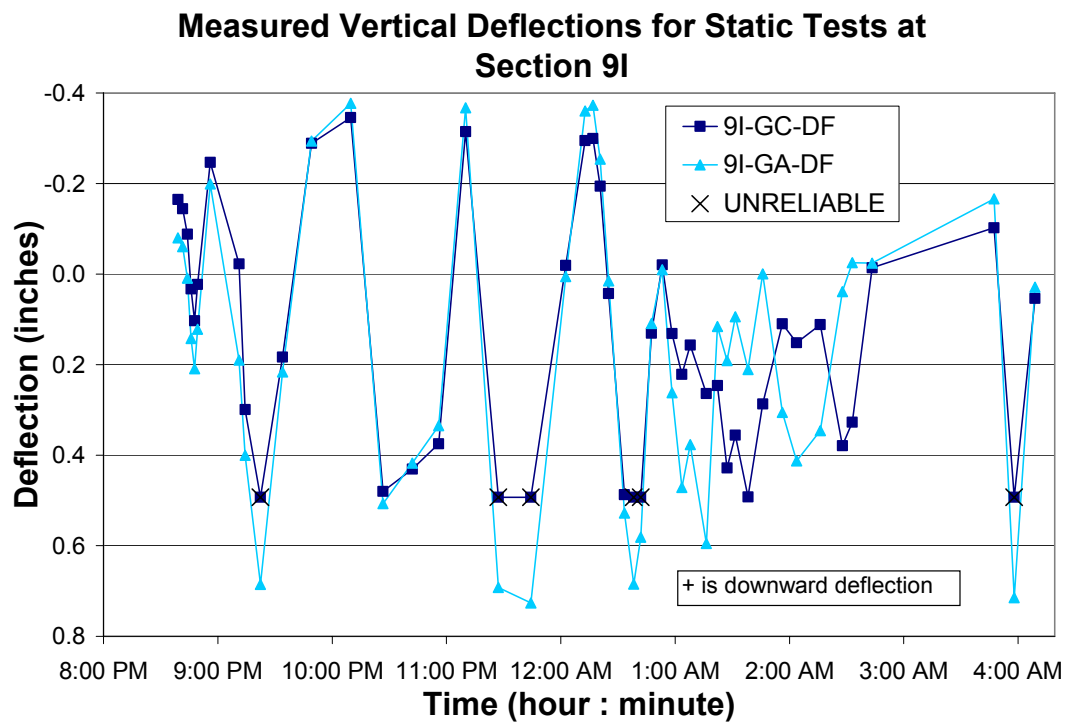


Figure D-2

Measured Vertical Deflections for Static Tests at Section 9M

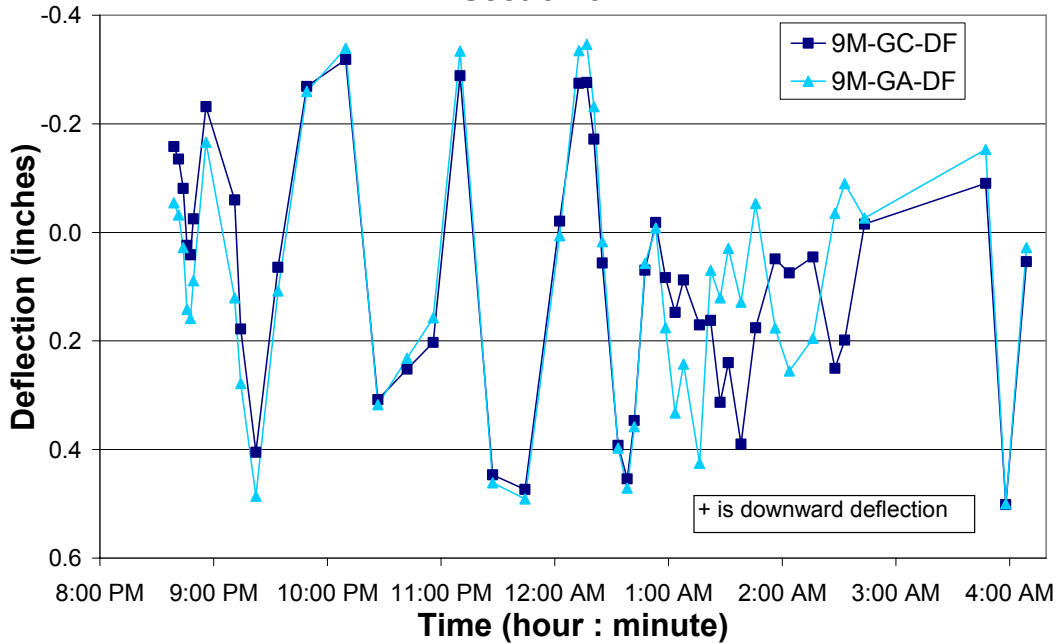


Figure D-3

Measured Vertical Deflections for Static Tests at Section 8E

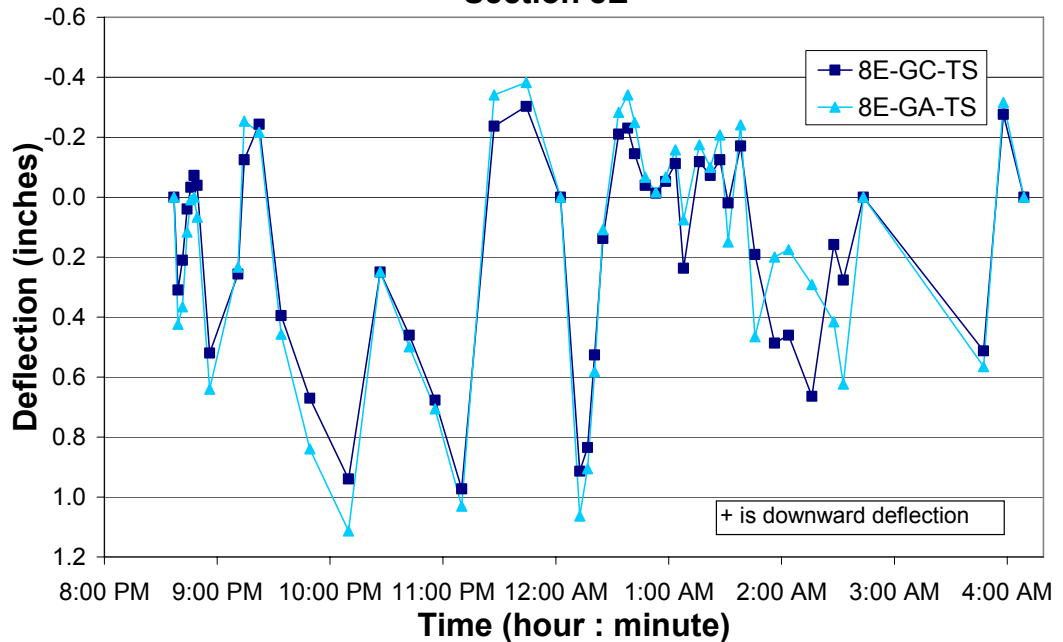


Figure D-4

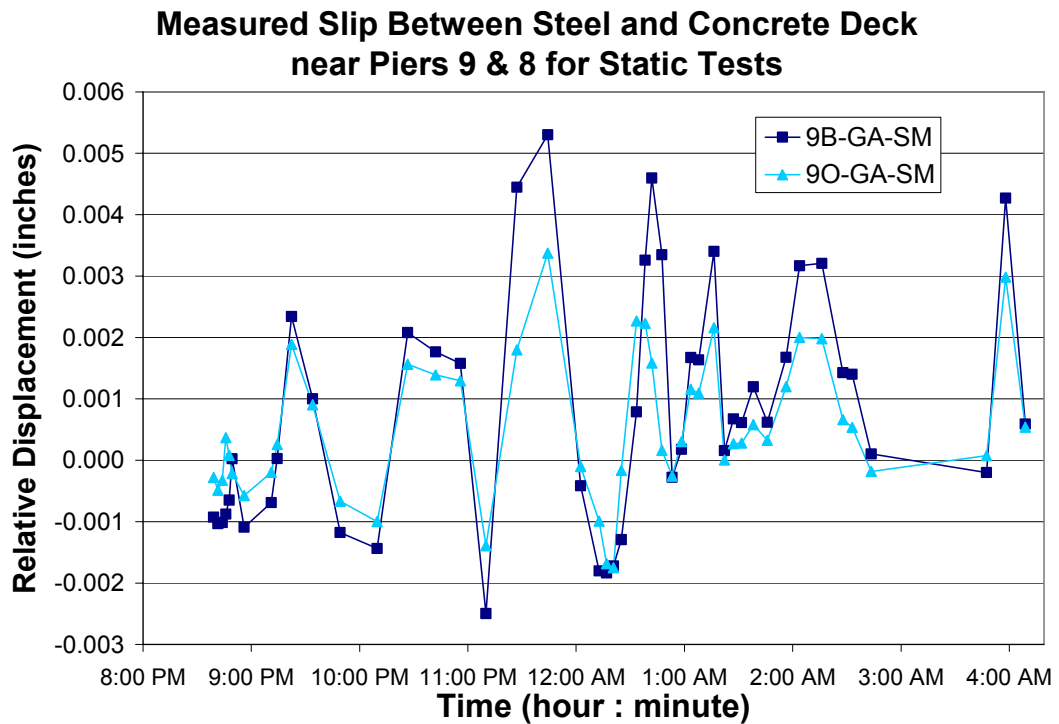


Figure D-5

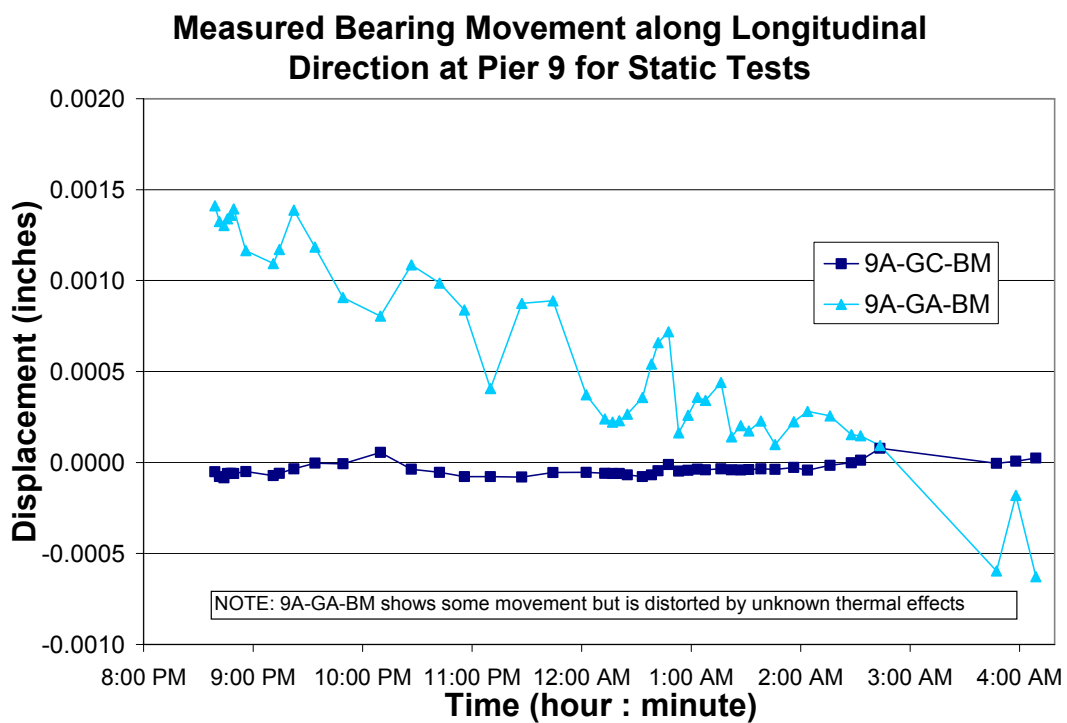


Figure D-6

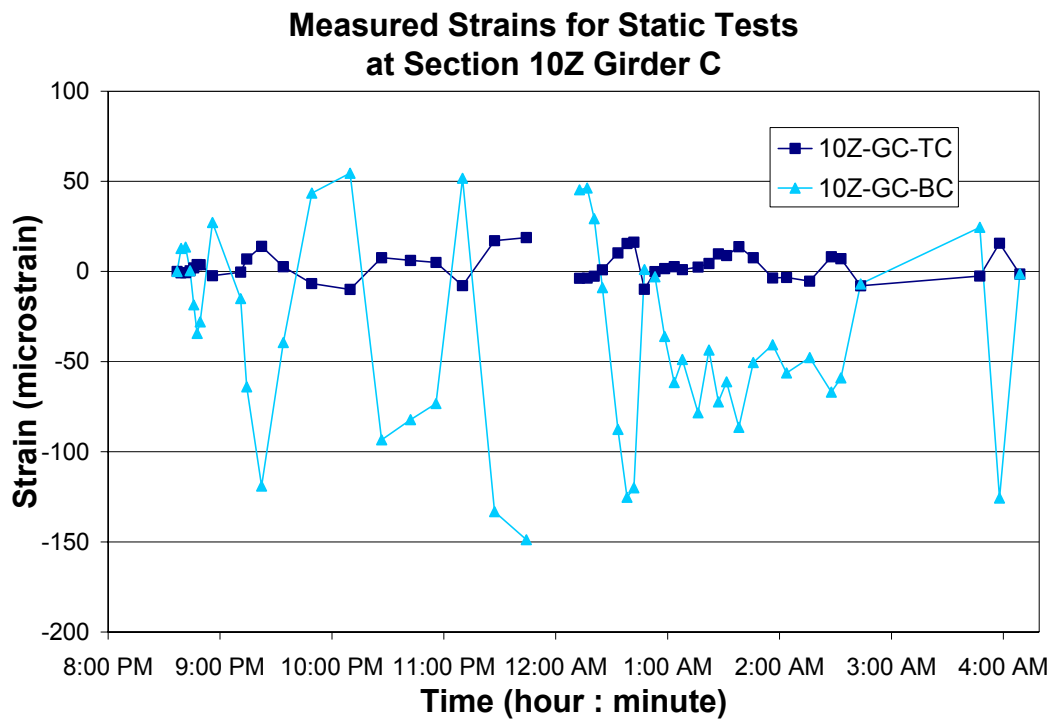


Figure D-7

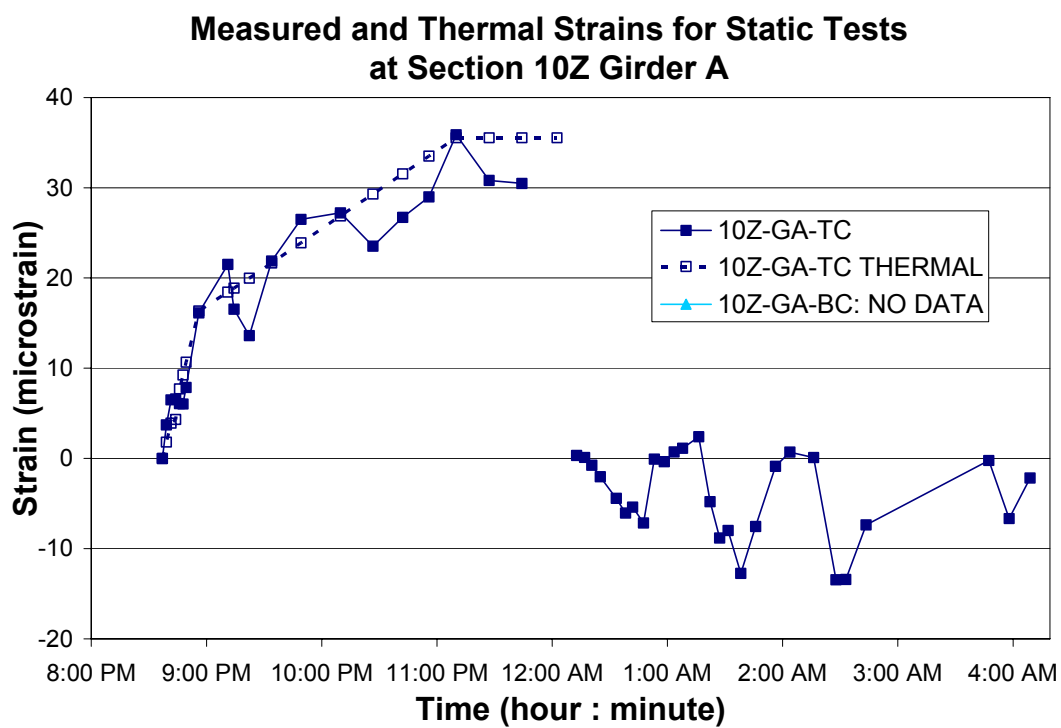


Figure D-8

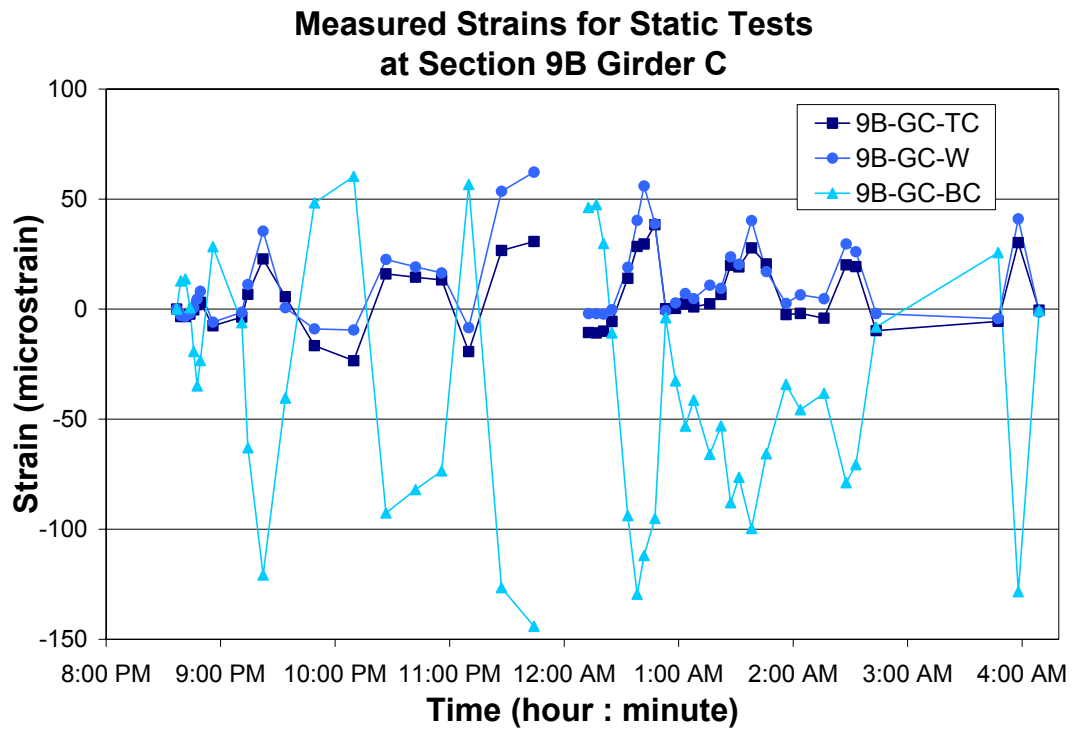


Figure D-9

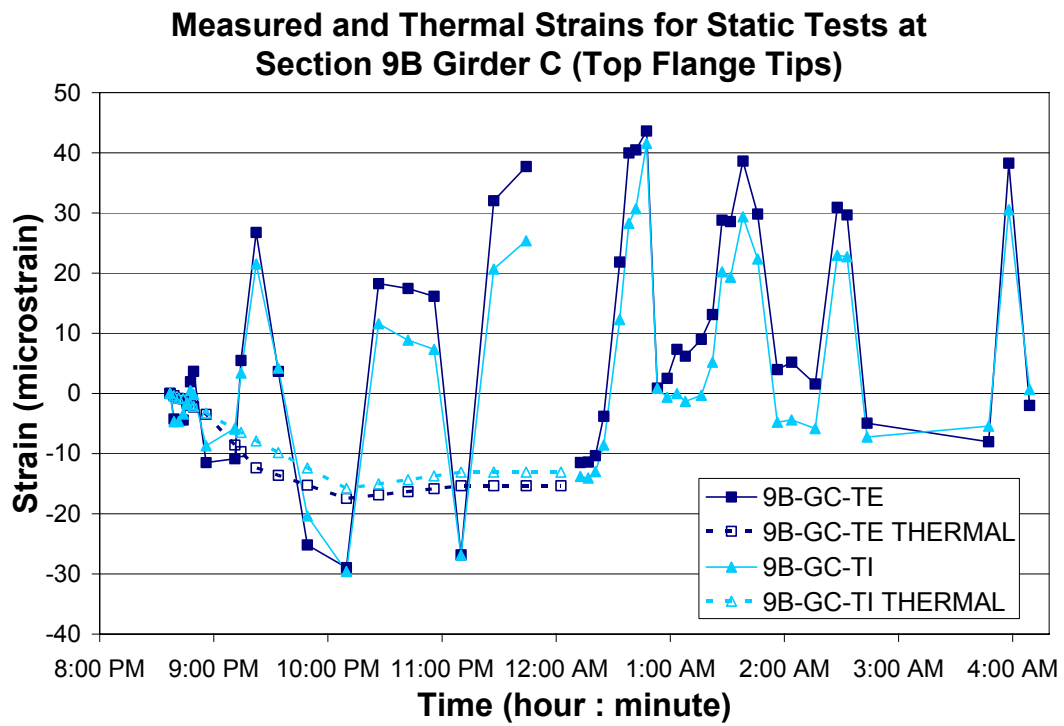


Figure D-10

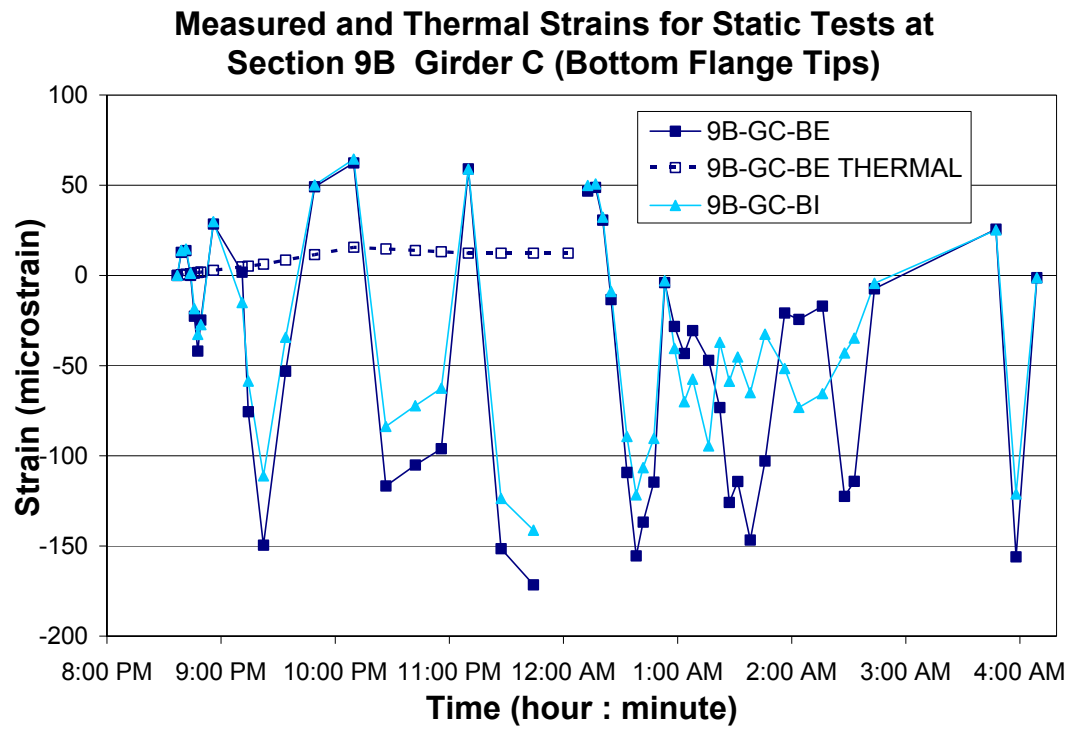


Figure D-11

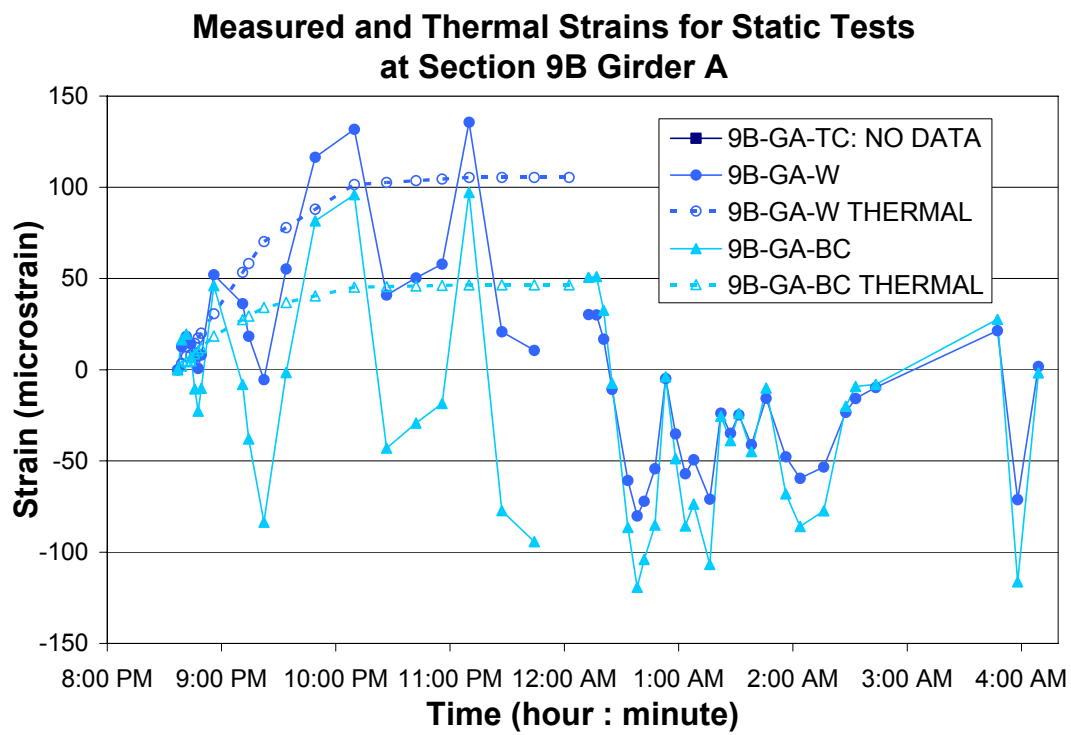


Figure D-12

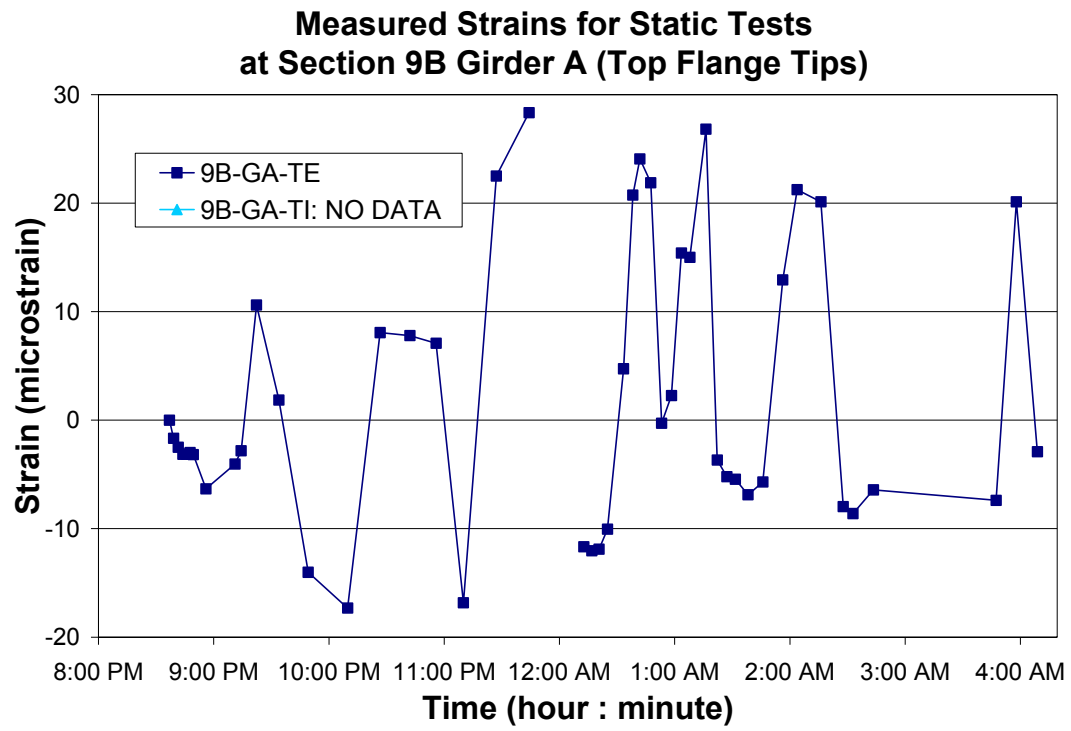


Figure D-13

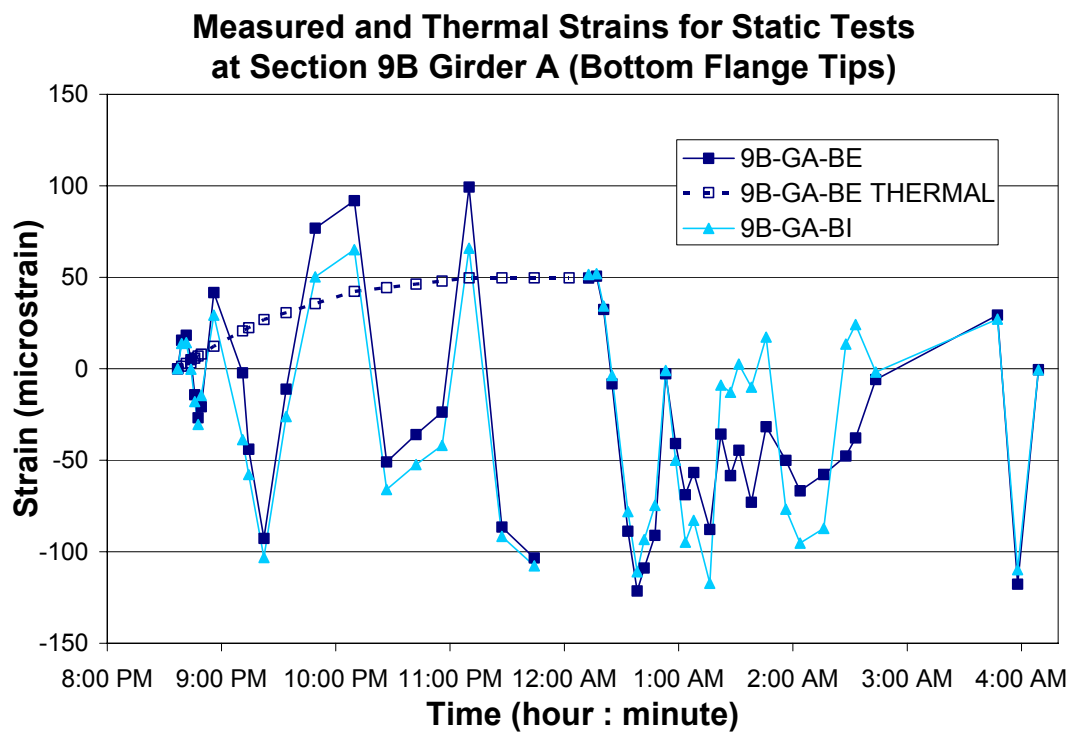


Figure D-14

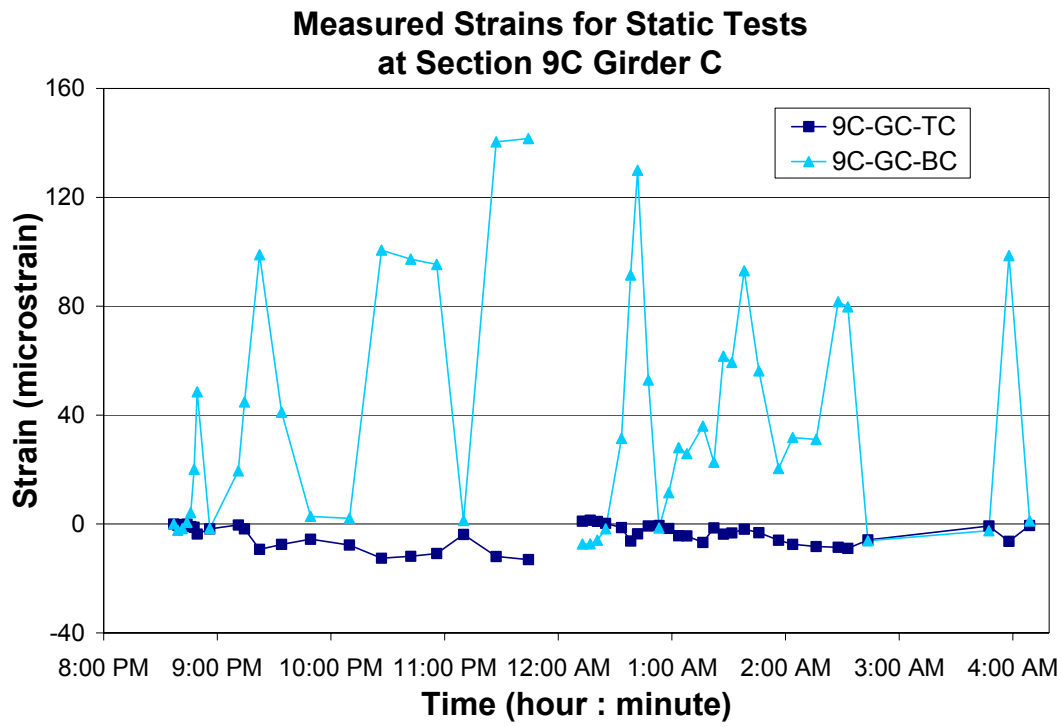


Figure D-15

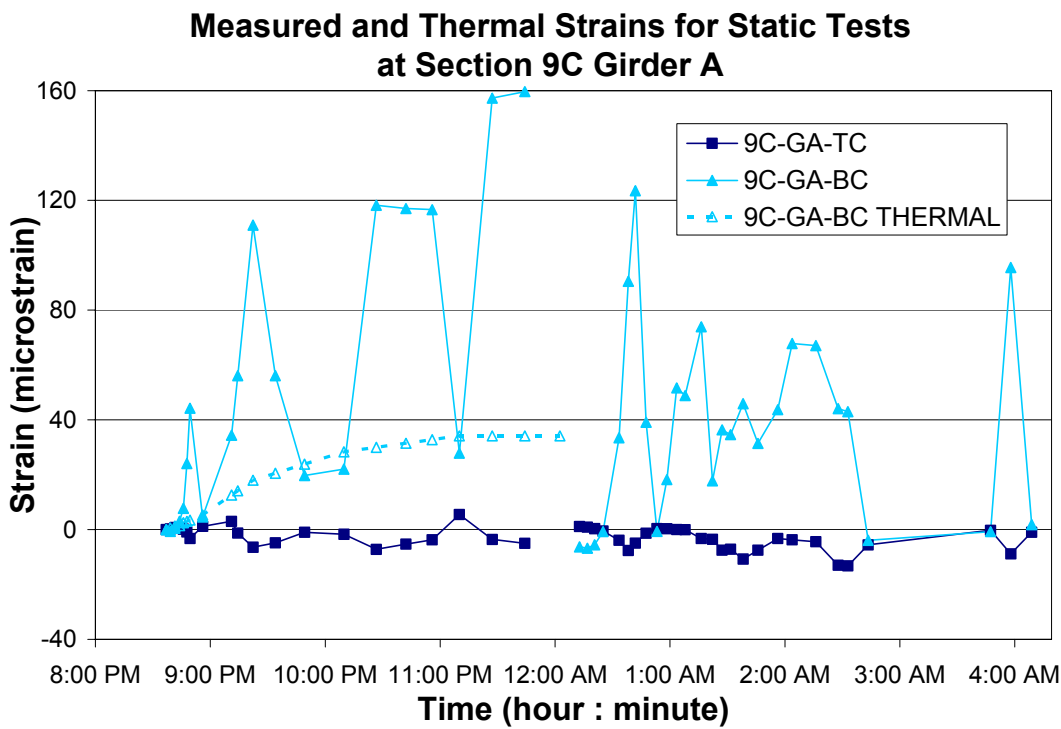


Figure D-16

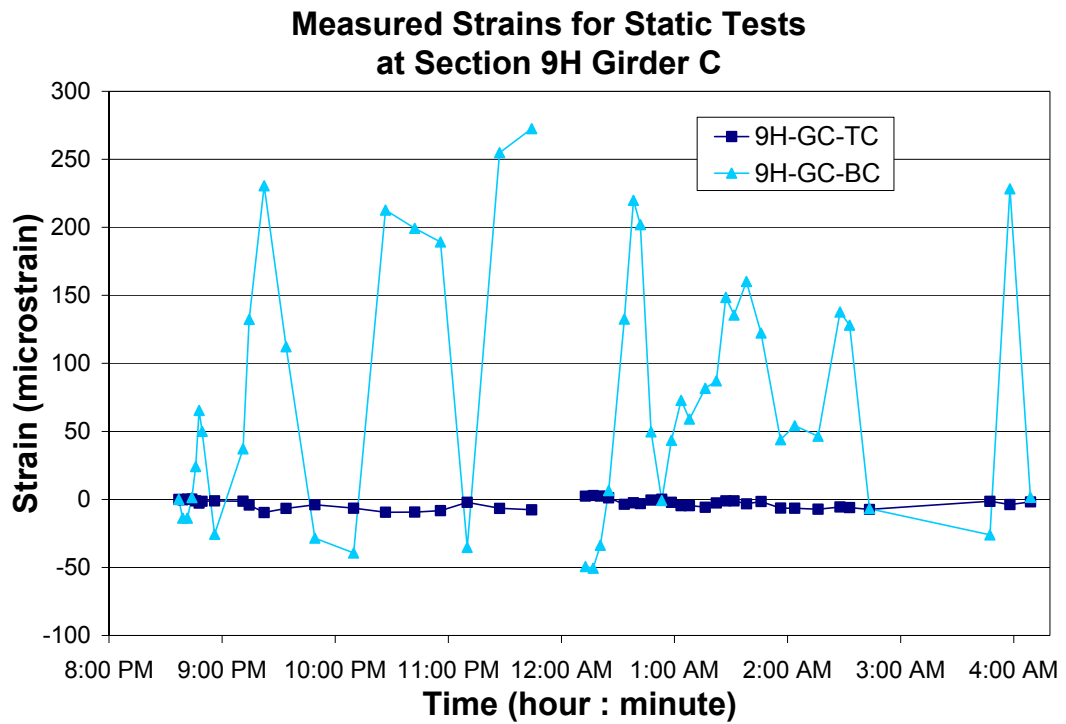


Figure D-17

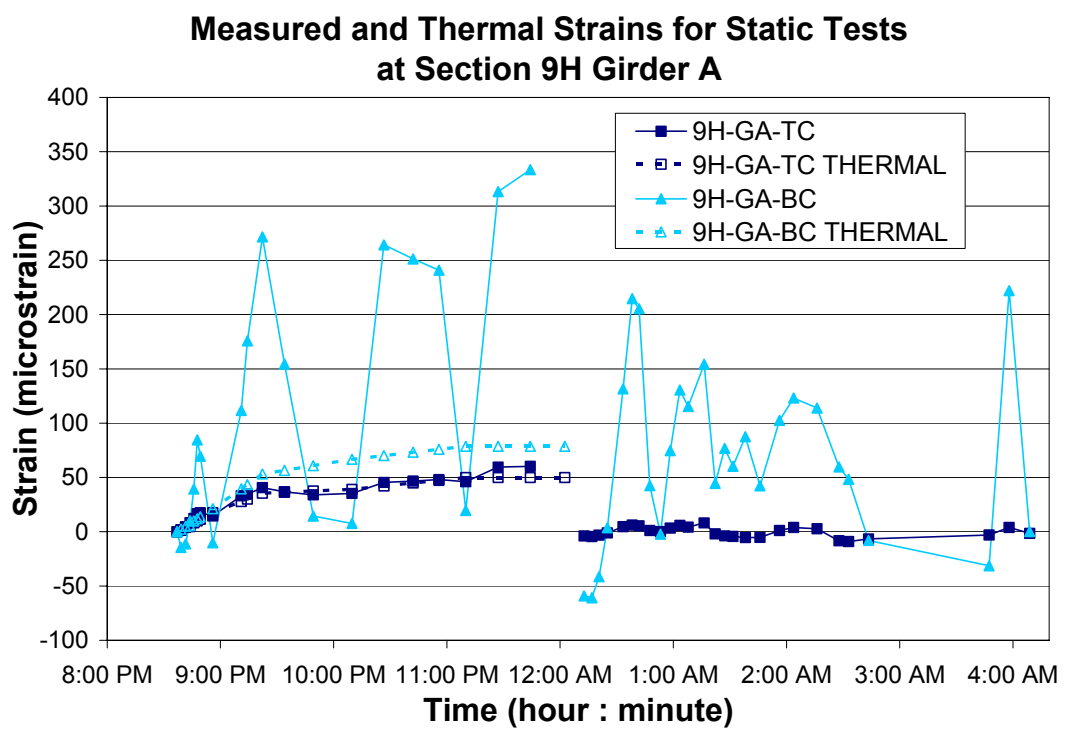


Figure D-18

**Measured and Thermal Strains for Static Tests
at Section 9J Girder C**

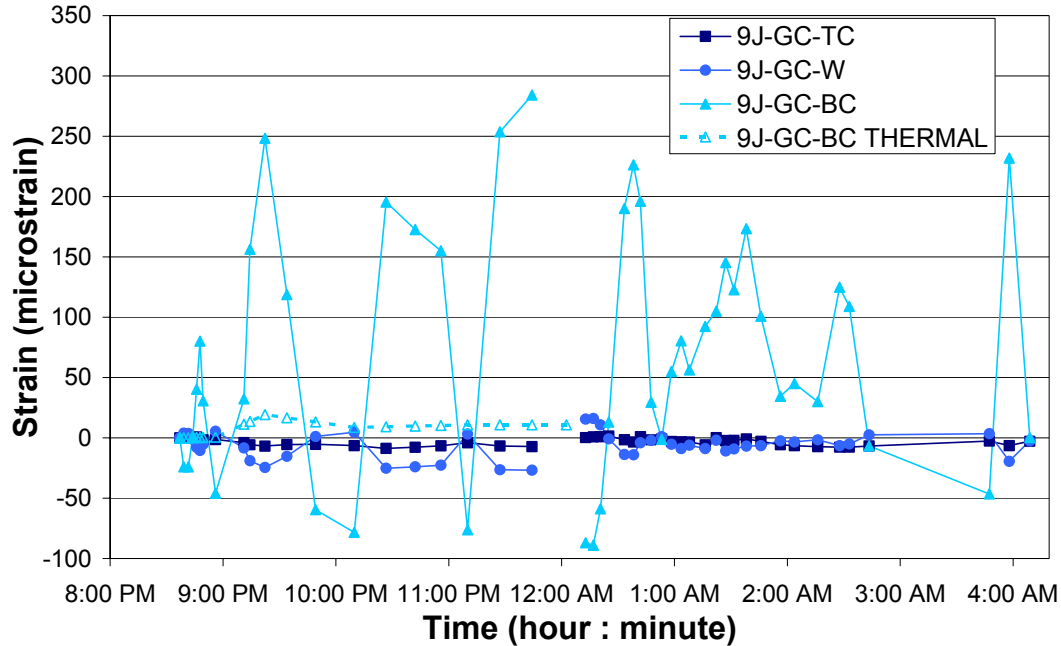


Figure D-19

**Measured Strains for Static Tests
at Section 9J Girder C (Top Flange Tips)**

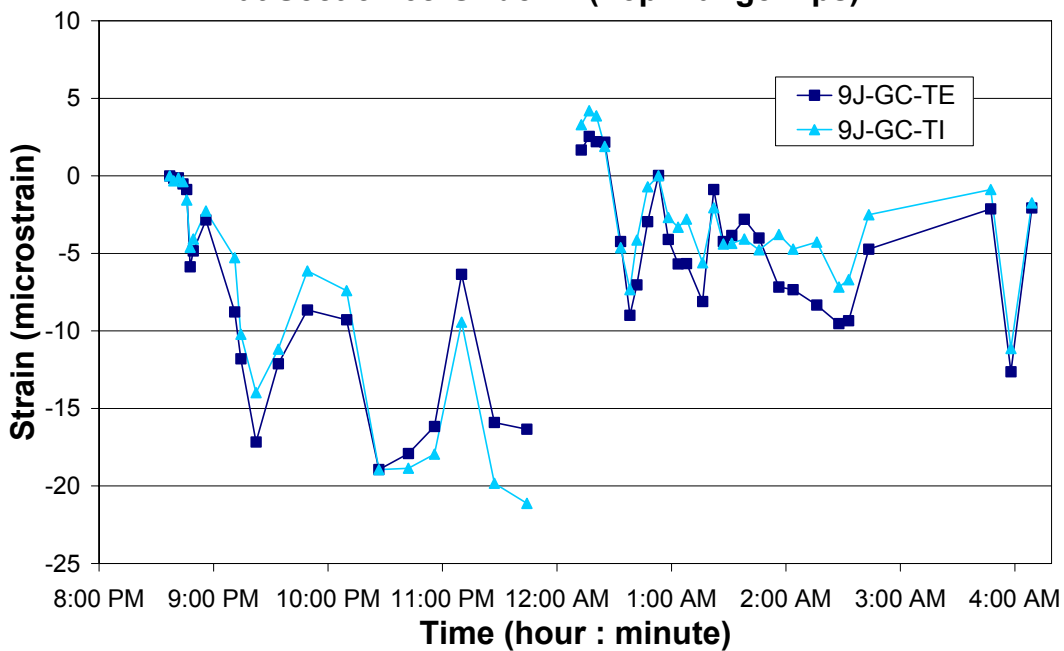


Figure D-20

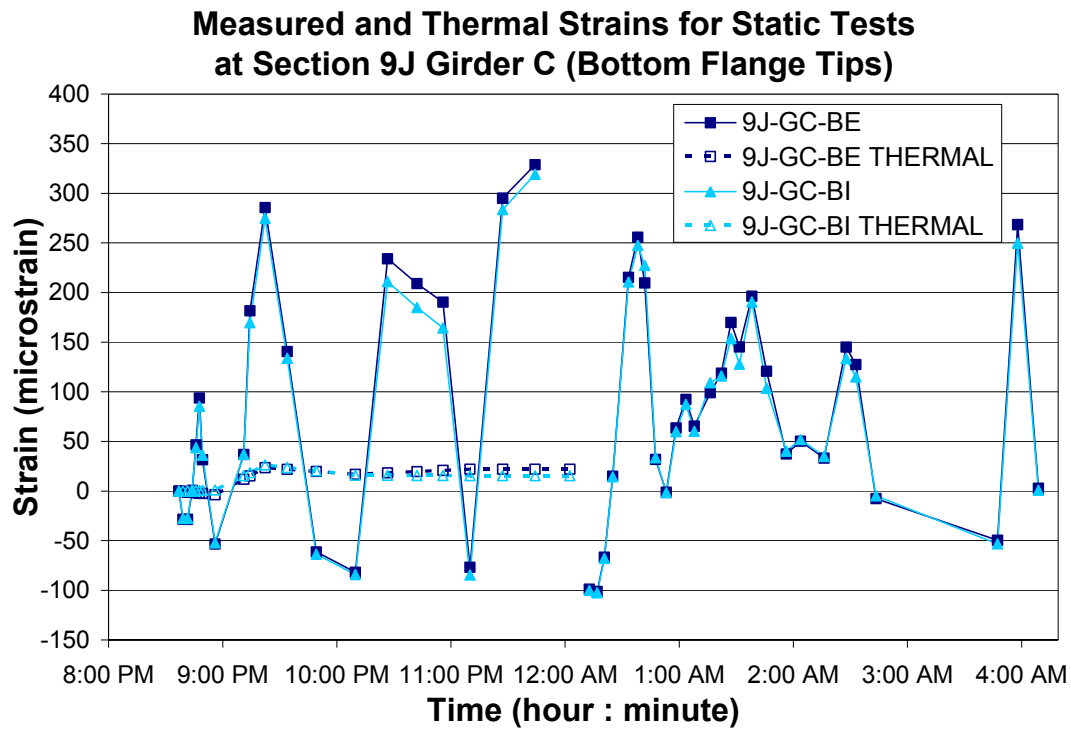


Figure D-21

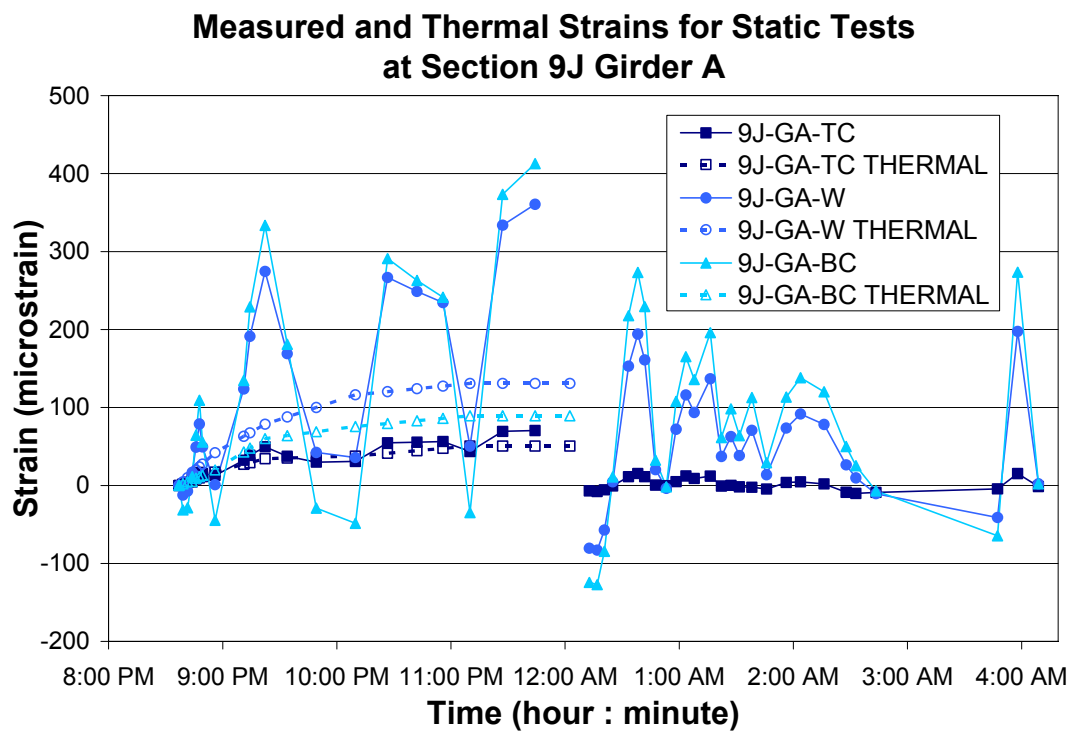


Figure D-22

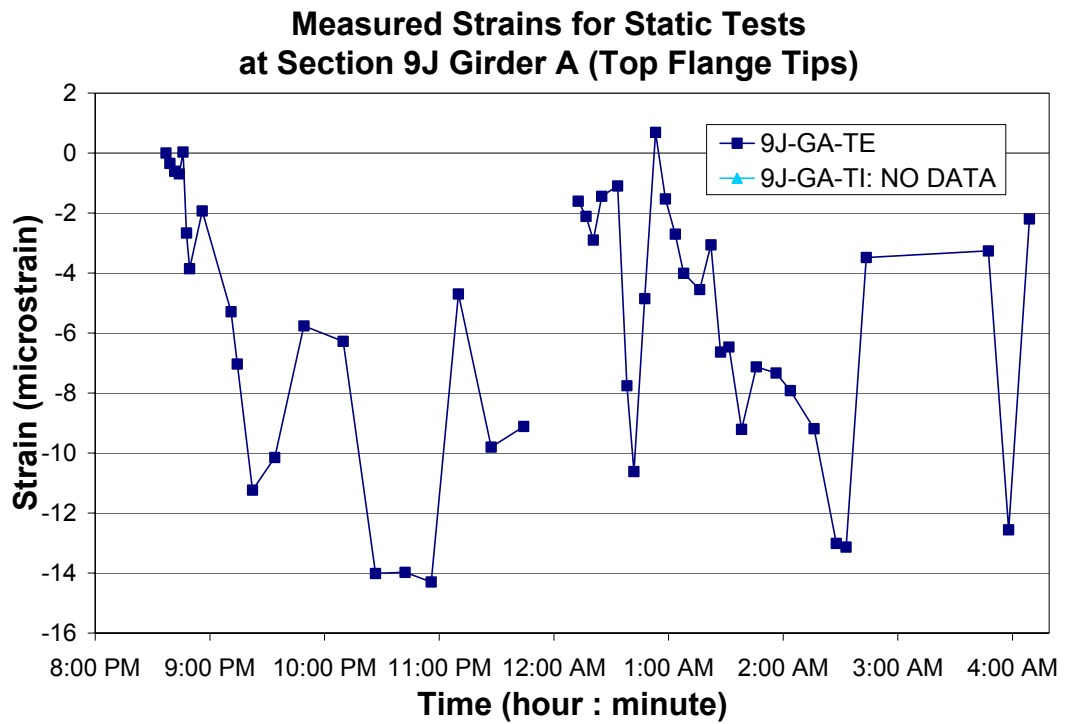


Figure D-23

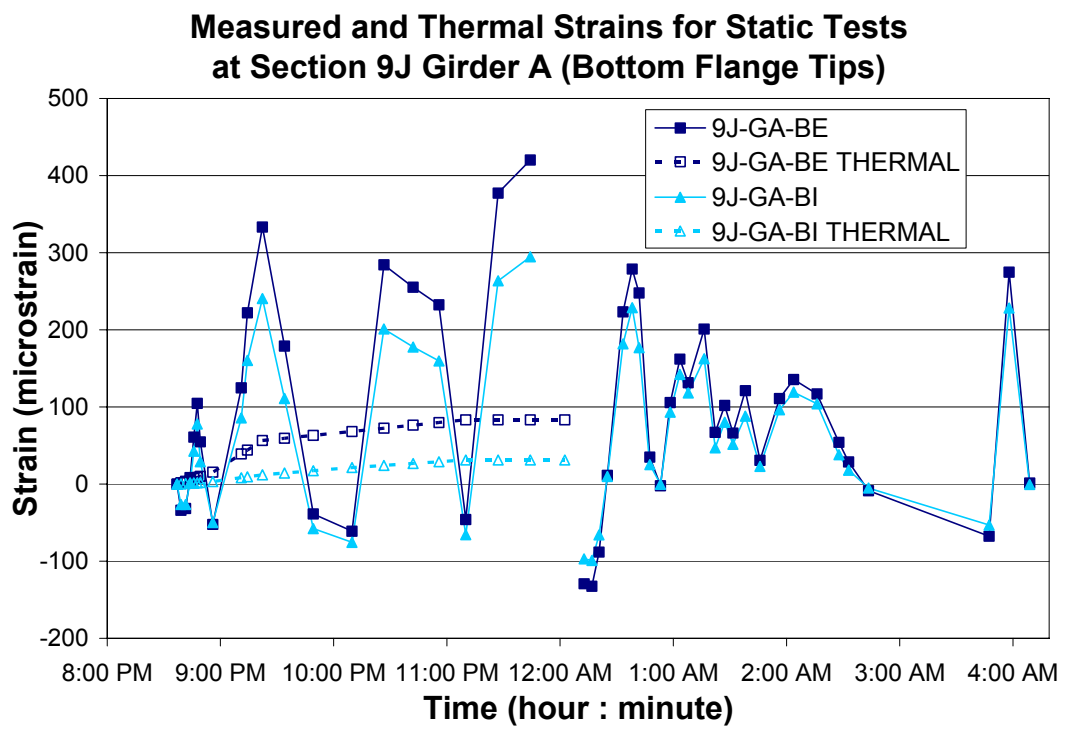


Figure D-24

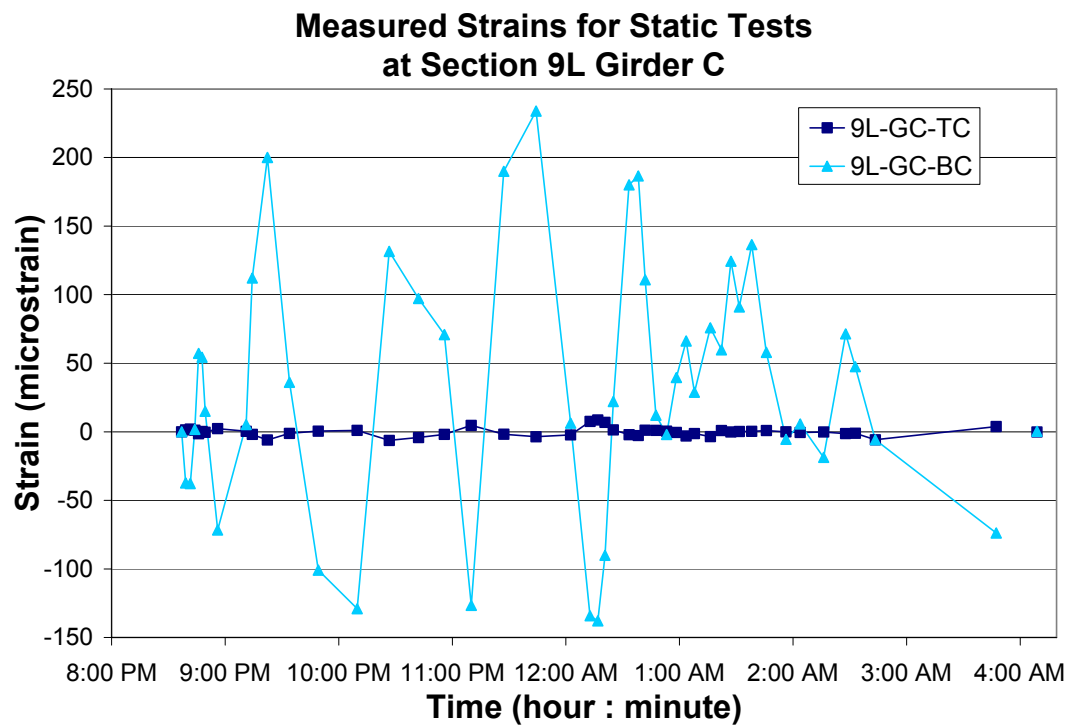


Figure D-25

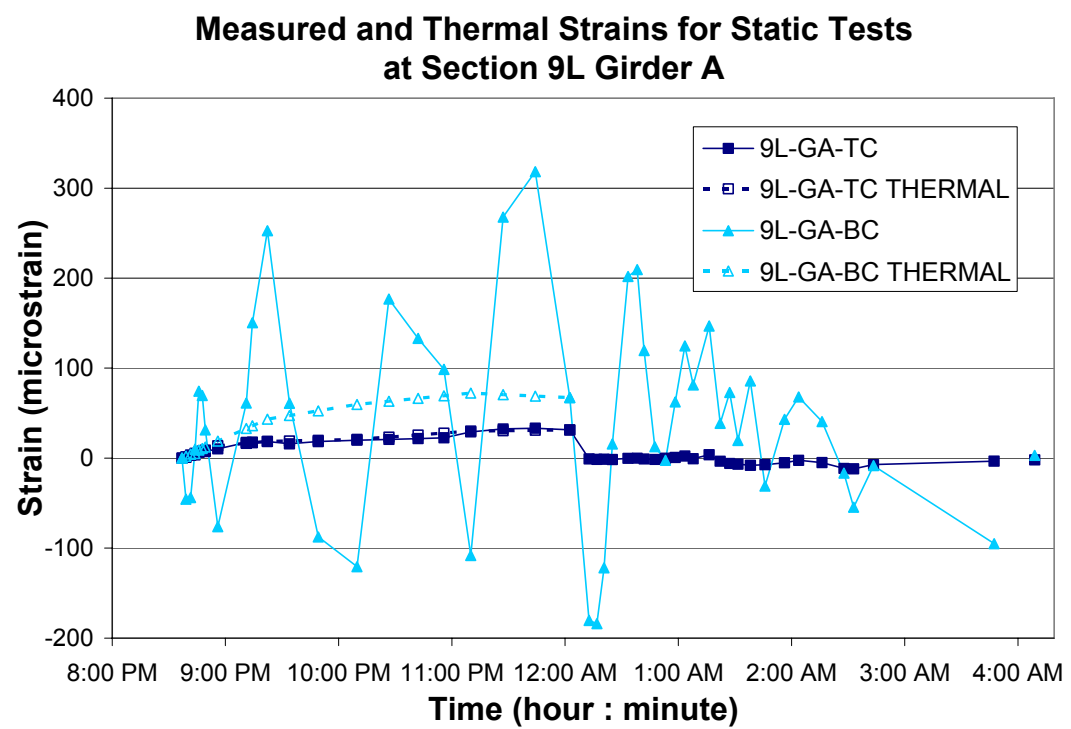


Figure D-26

**Measured and Thermal Strains for Static Tests
at Section 9N Girder C**

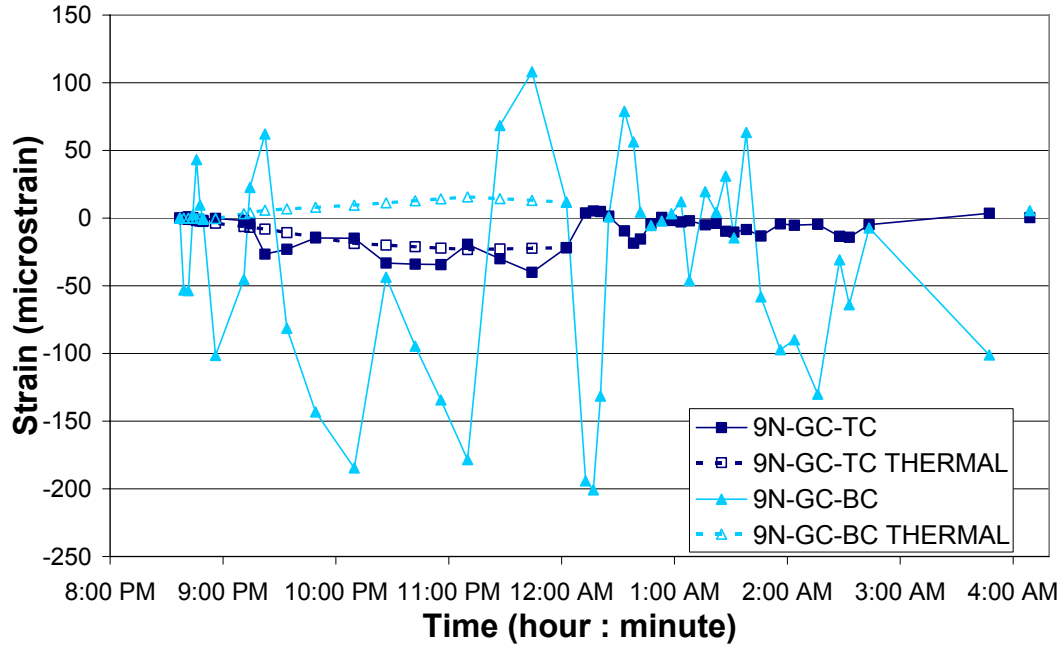


Figure D-27

**Measured and Thermal Strains for Static Tests
at Section 9N Girder A**

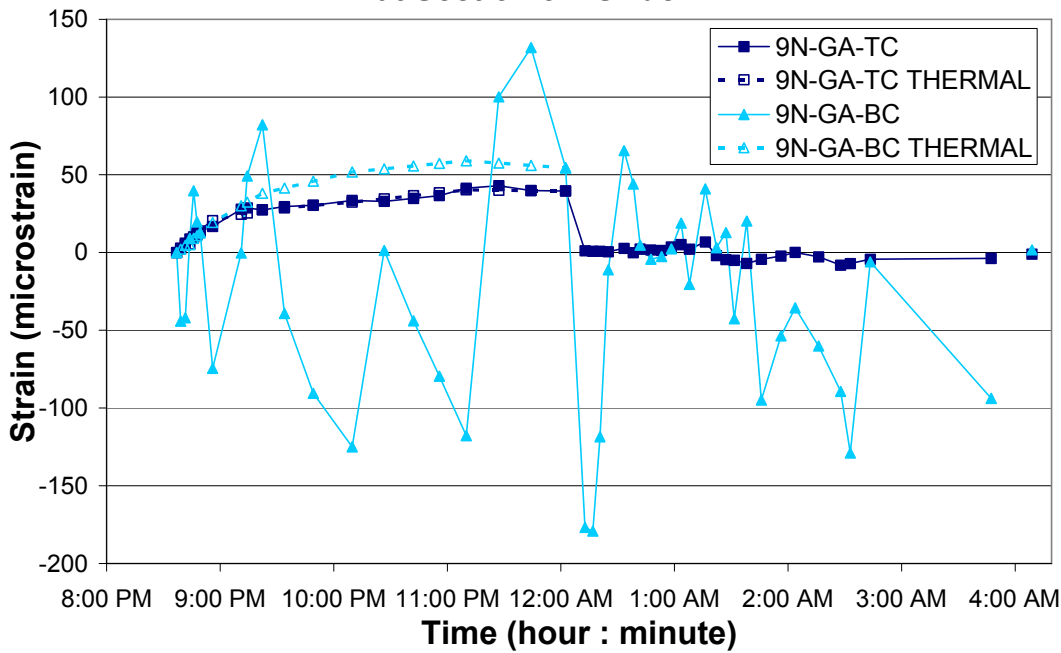


Figure D-28

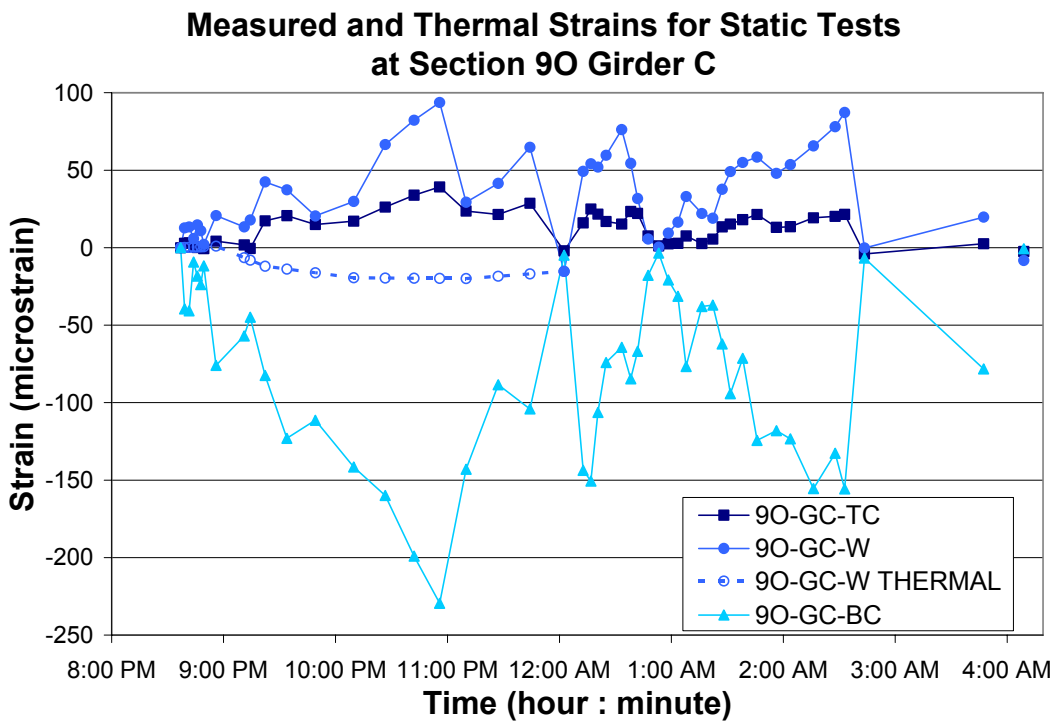


Figure D-29

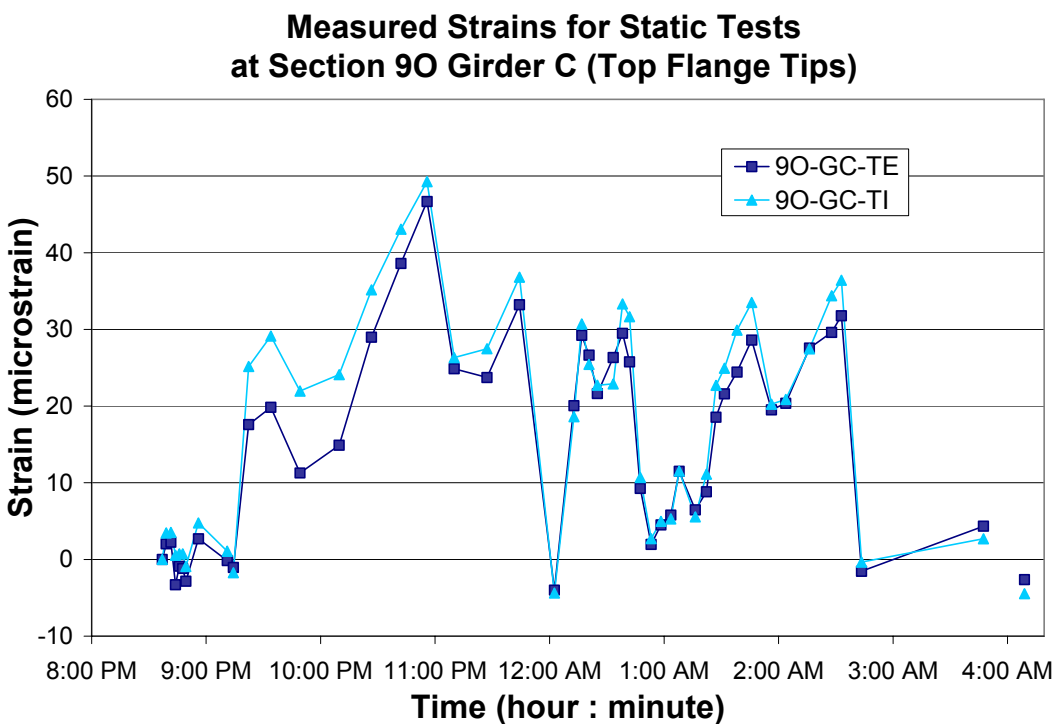


Figure D-30

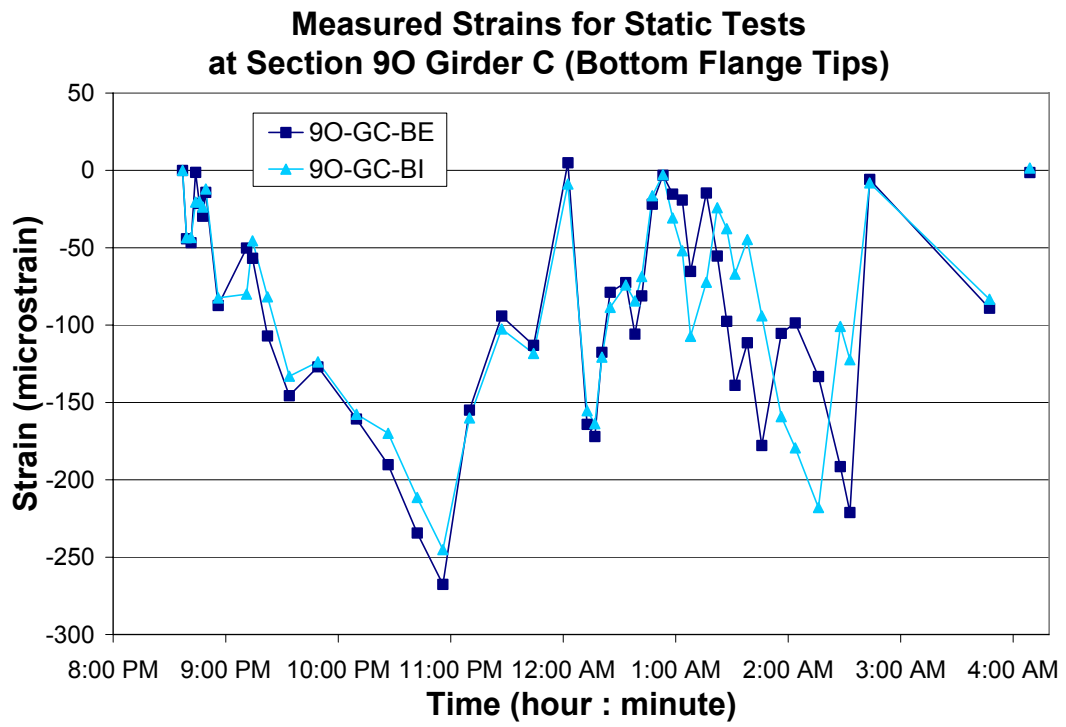


Figure D-31

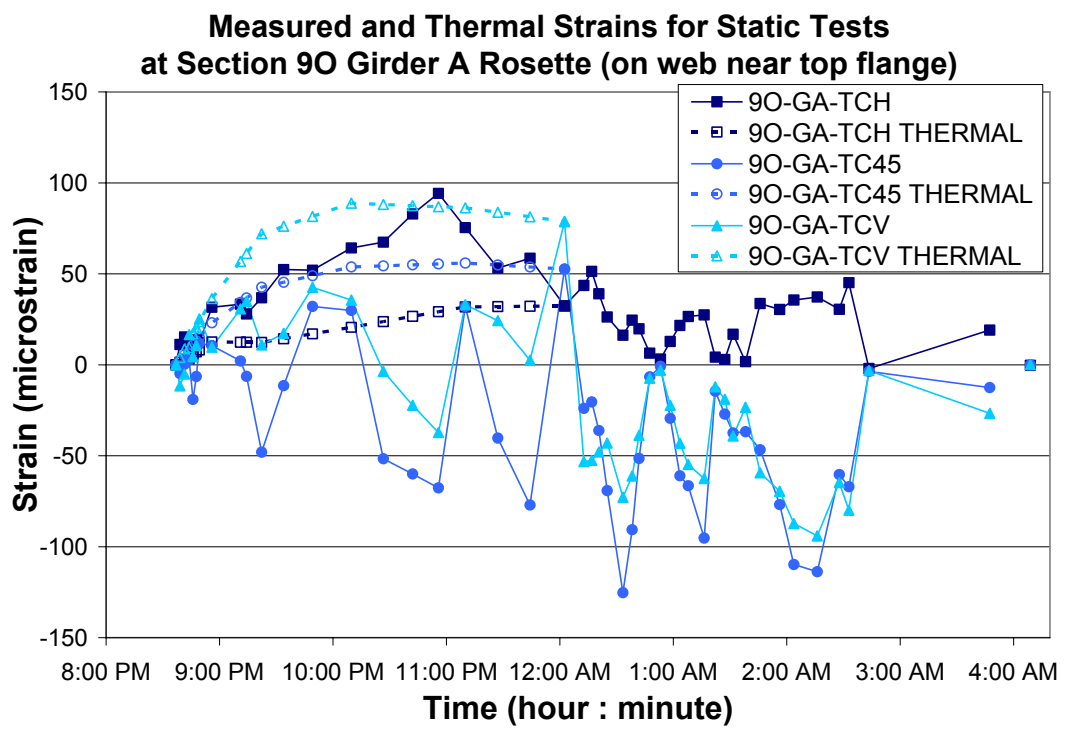


Figure D-32

**Measured and Thermal Strains for Static Tests
at Section 9O Girder A Rosette (on web at mid-height)**

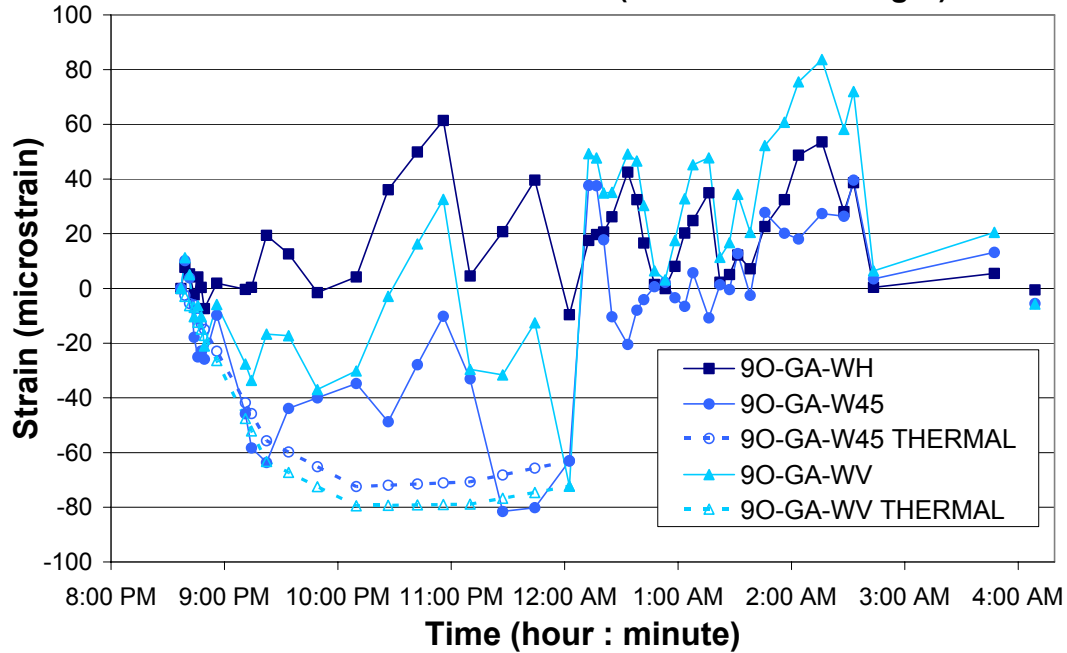


Figure D-33

**Measured and Thermal Strains for Static Tests
at Section 9O Girder A Rosette (on web near bottom)**

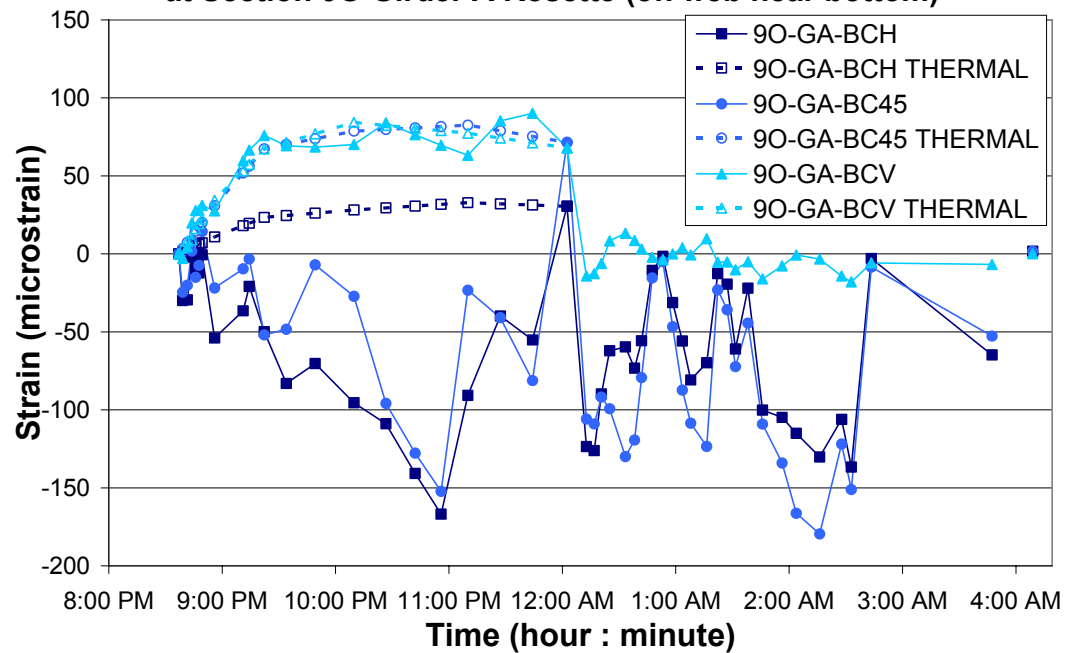


Figure D-34

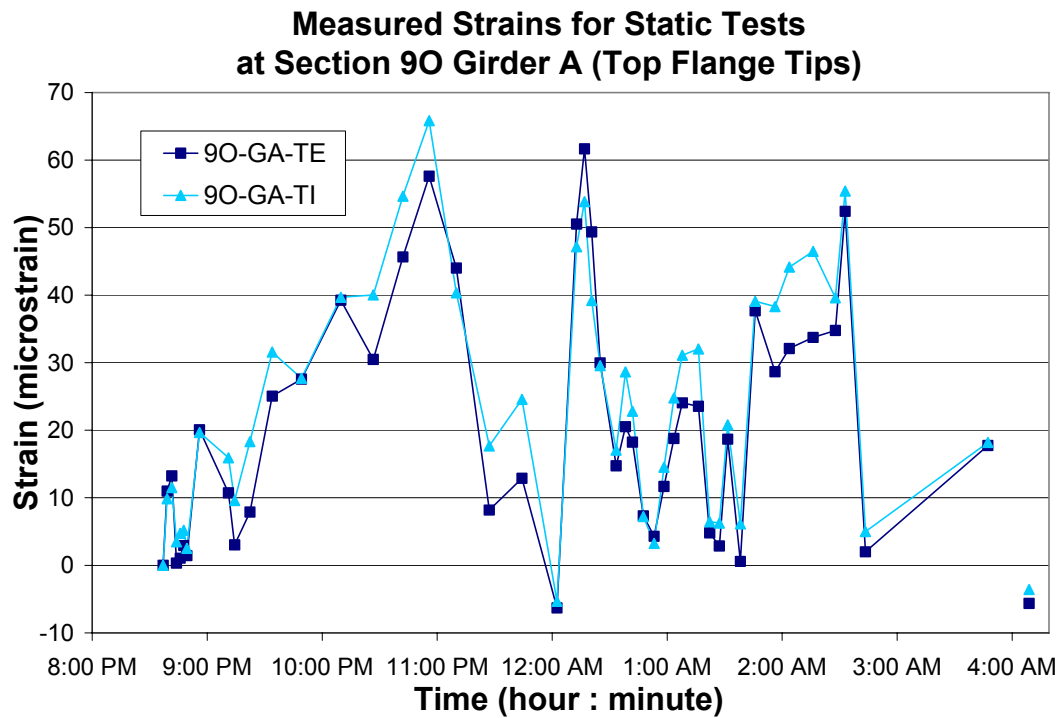


Figure D-35

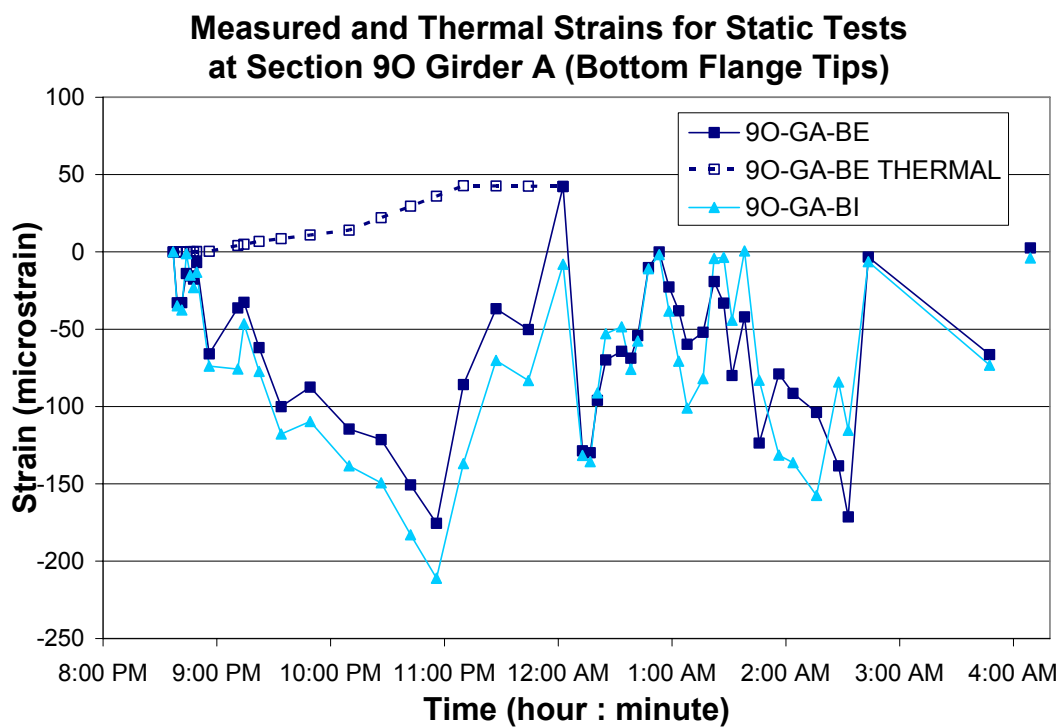


Figure D-36

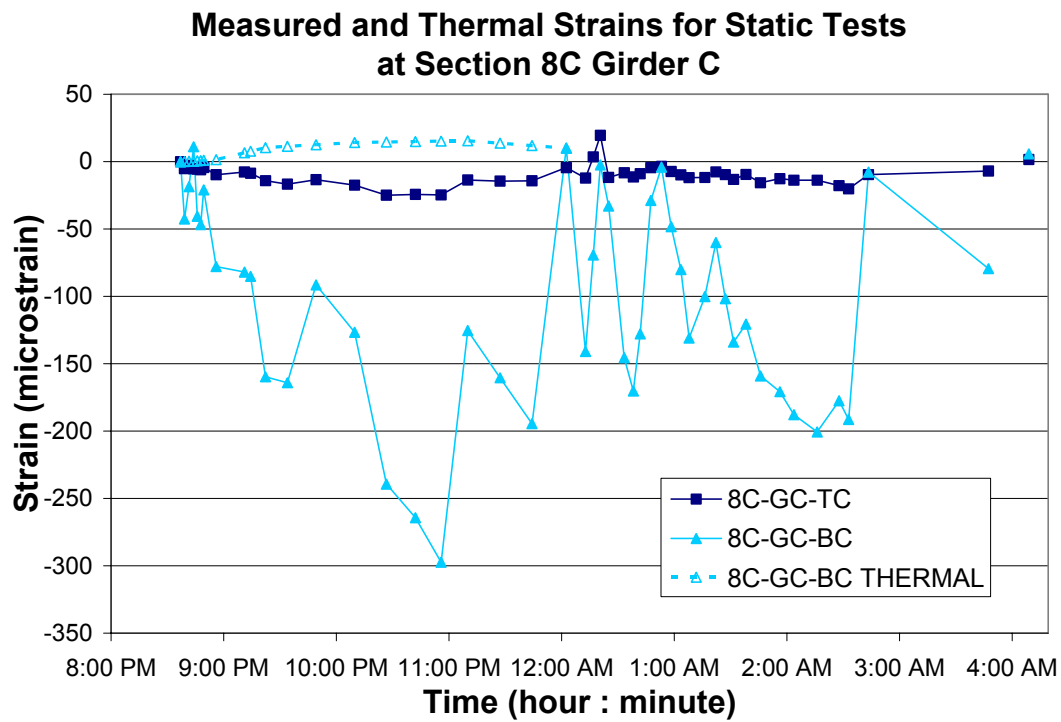


Figure D-37

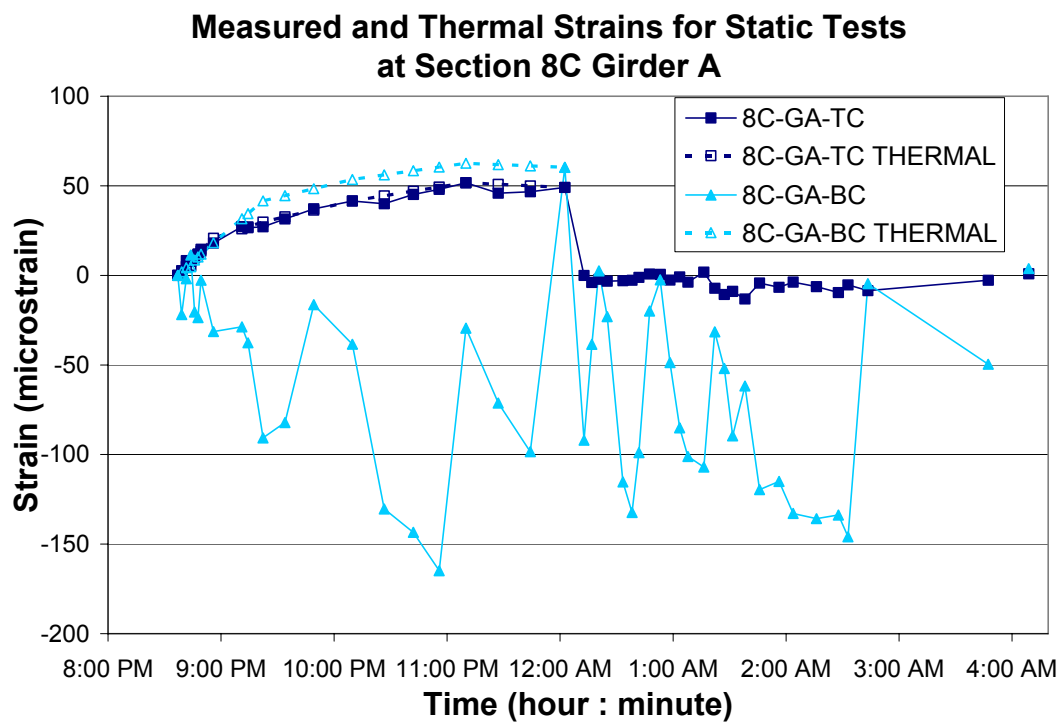


Figure D-38

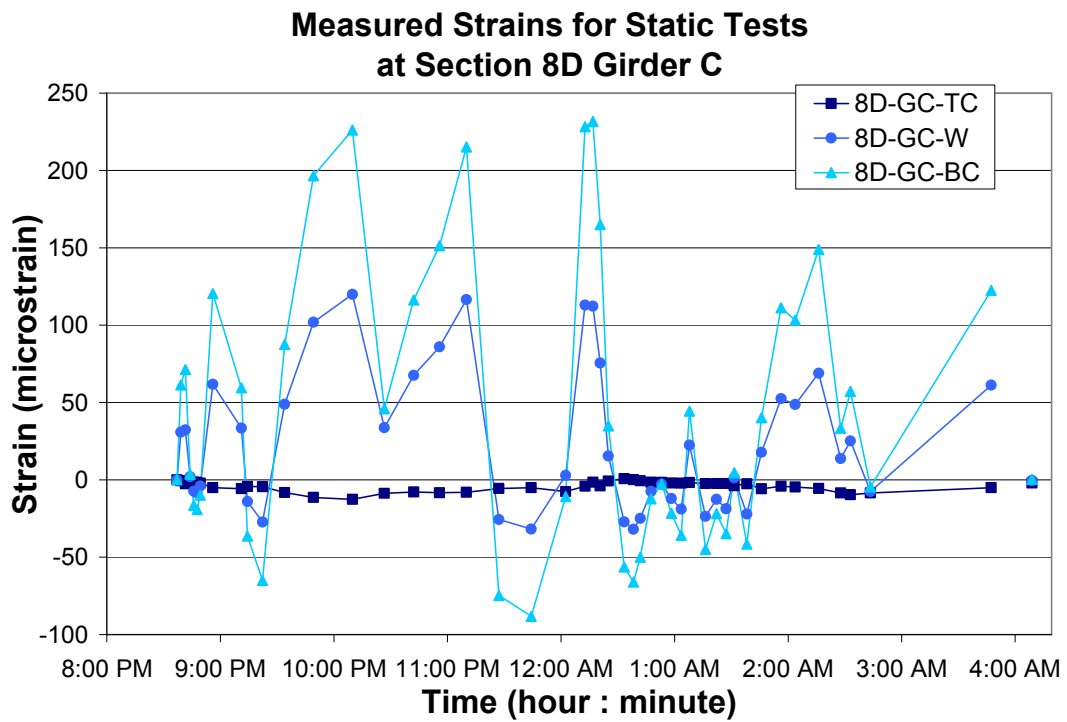


Figure D-39

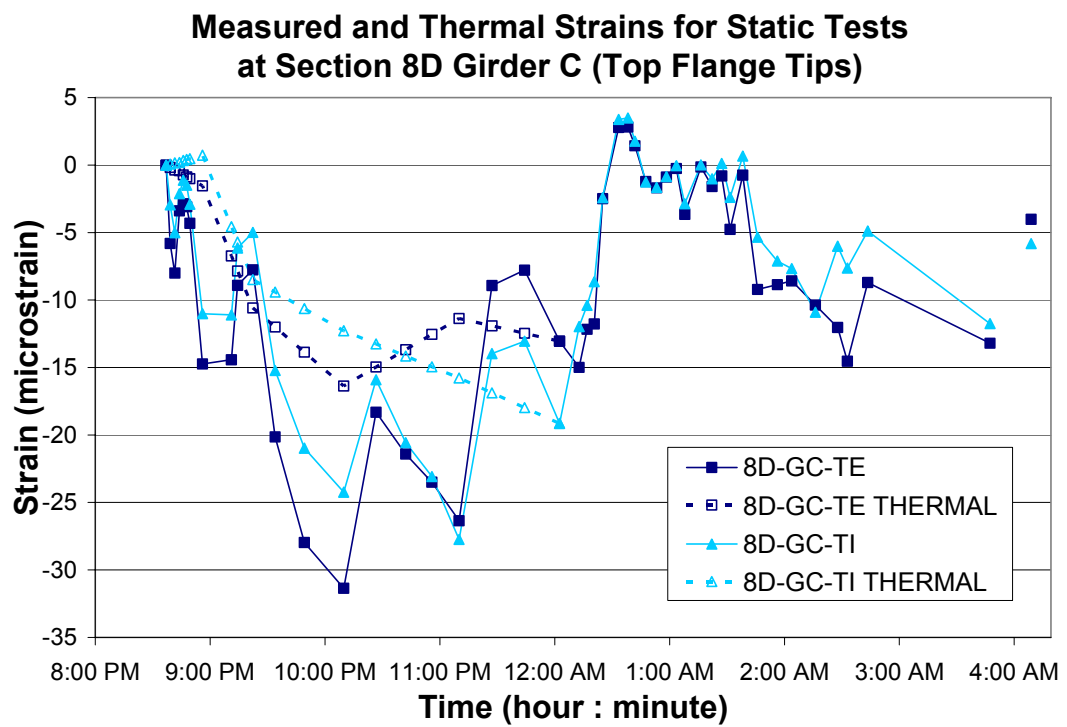


Figure D-40

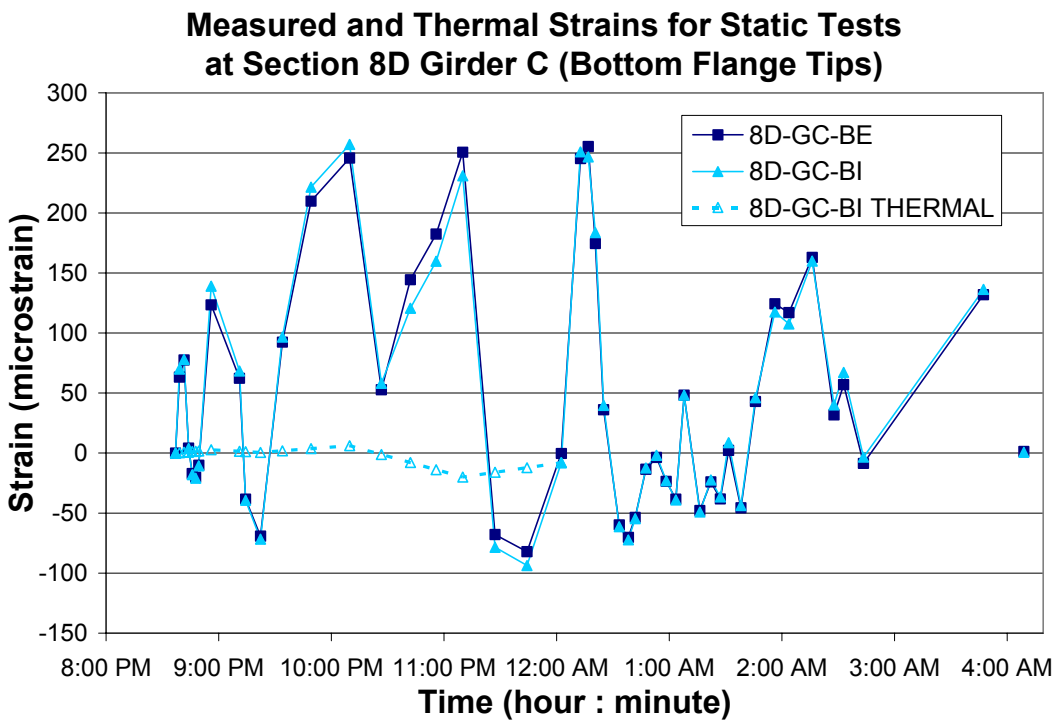


Figure D-41

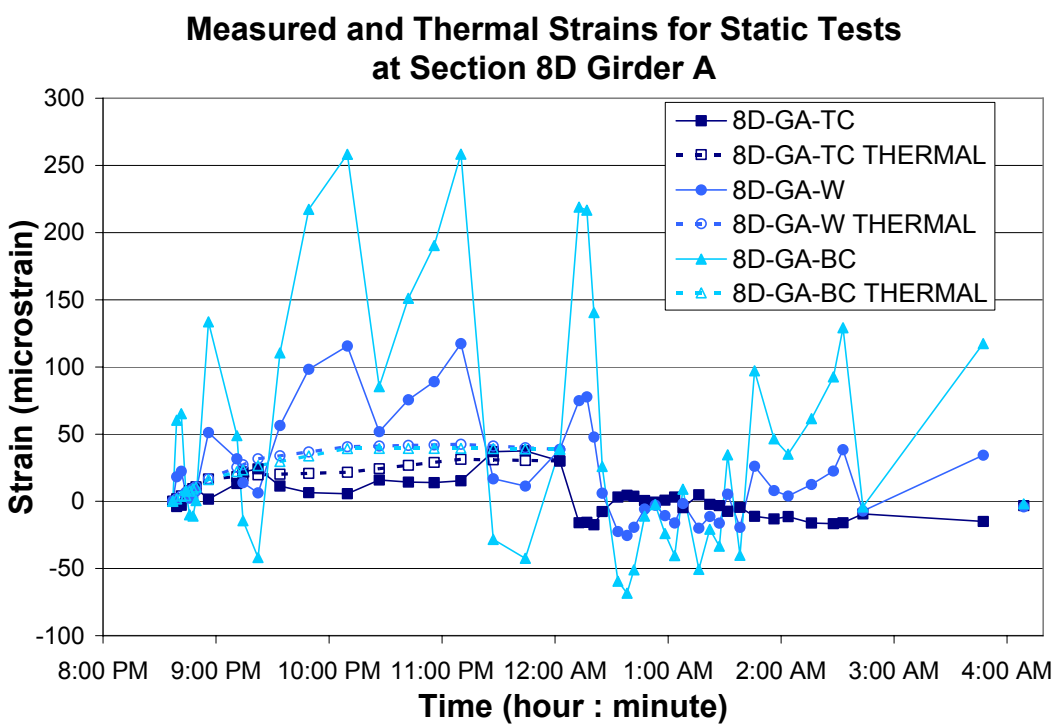


Figure D-42

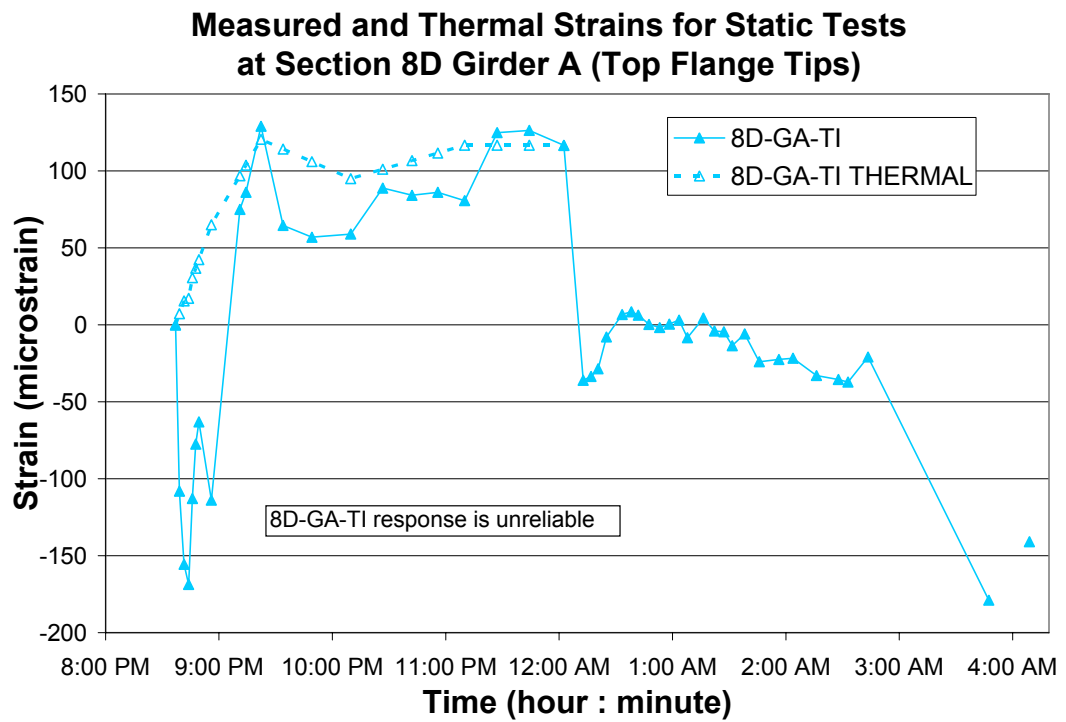


Figure D-43

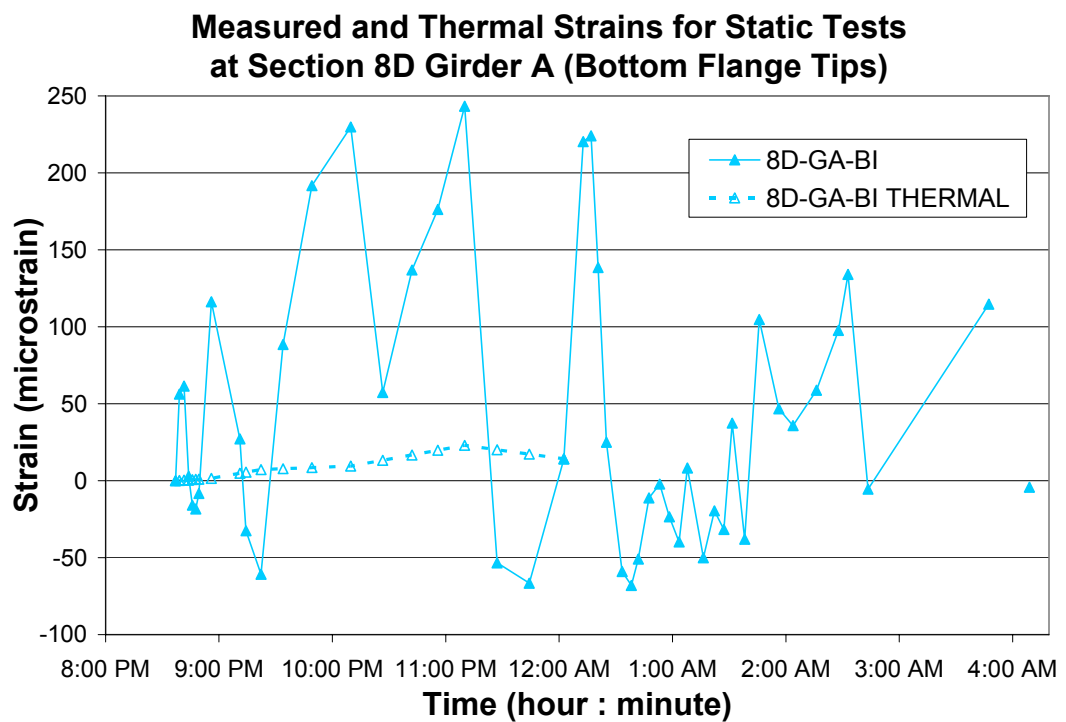


Figure D-44

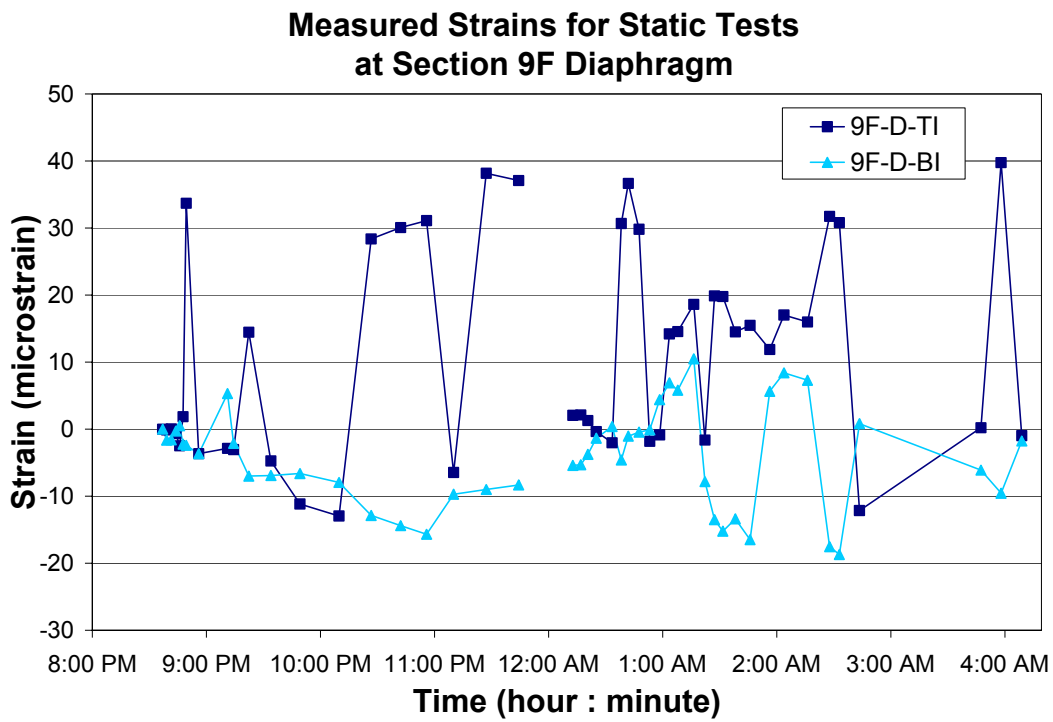


Figure D-45

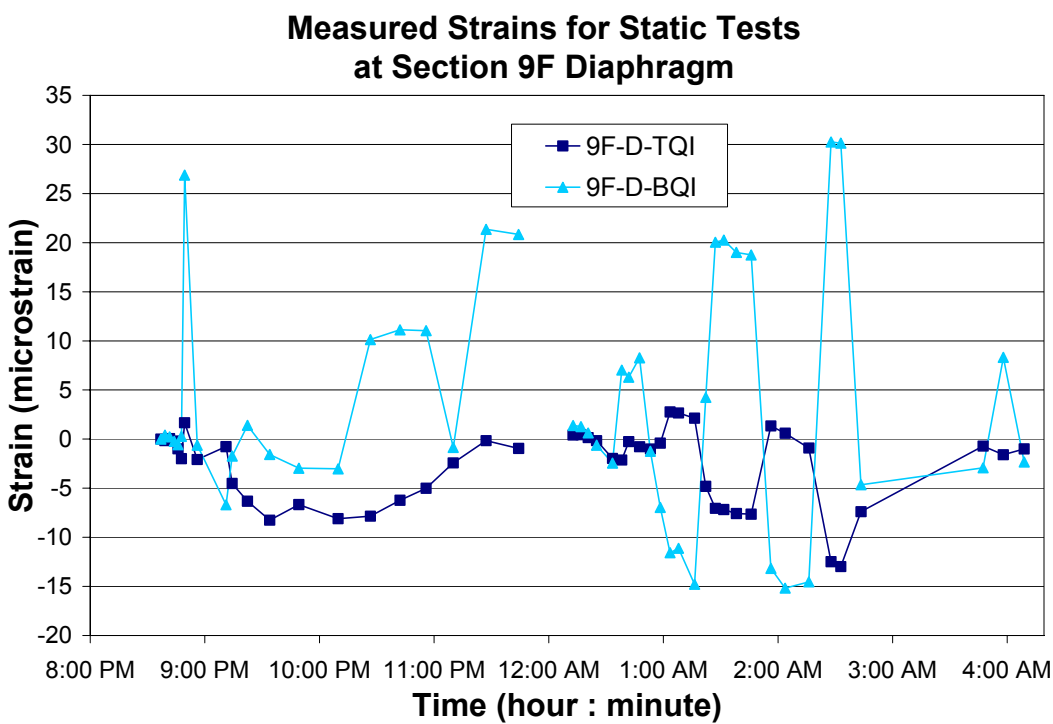


Figure D-46

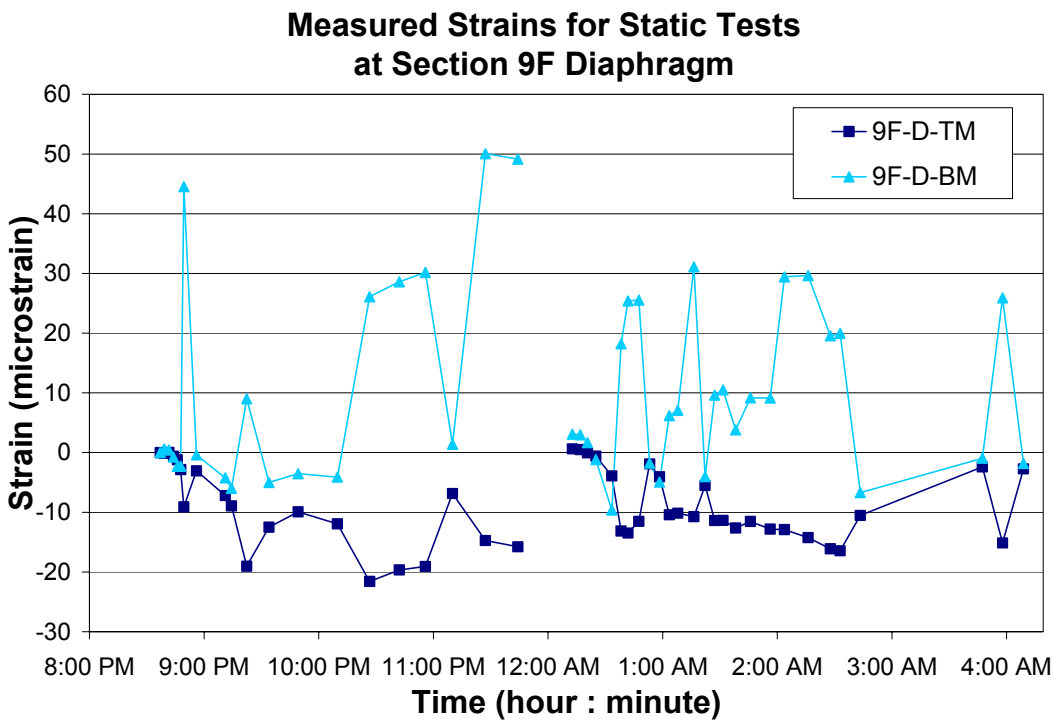


Figure D-47

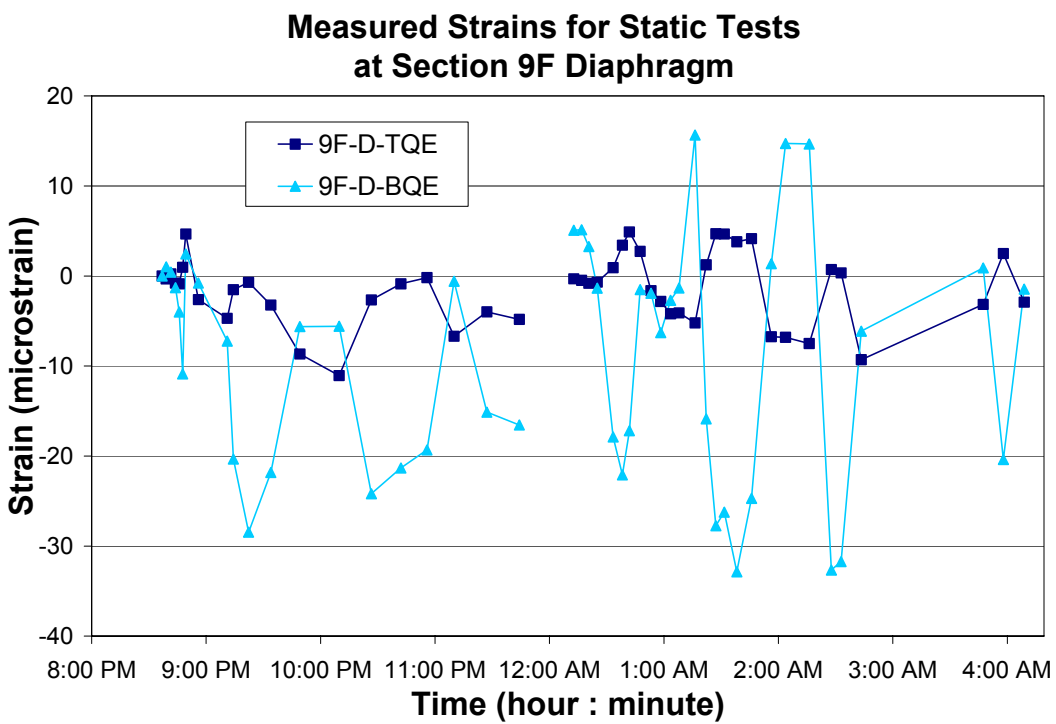


Figure D-48

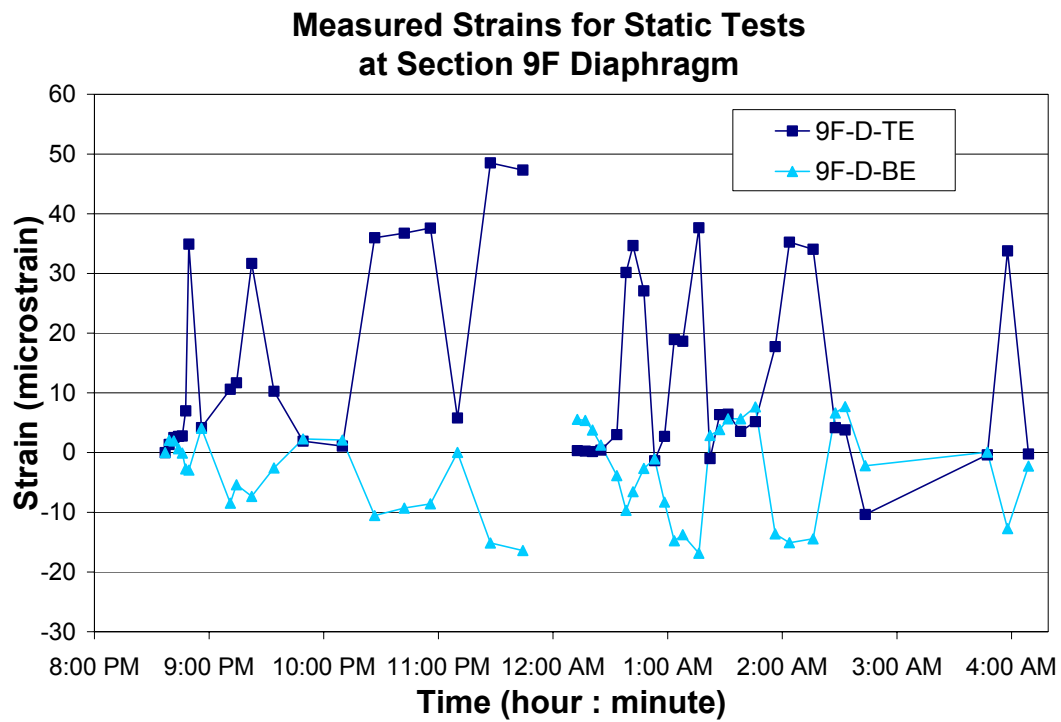


Figure D-49

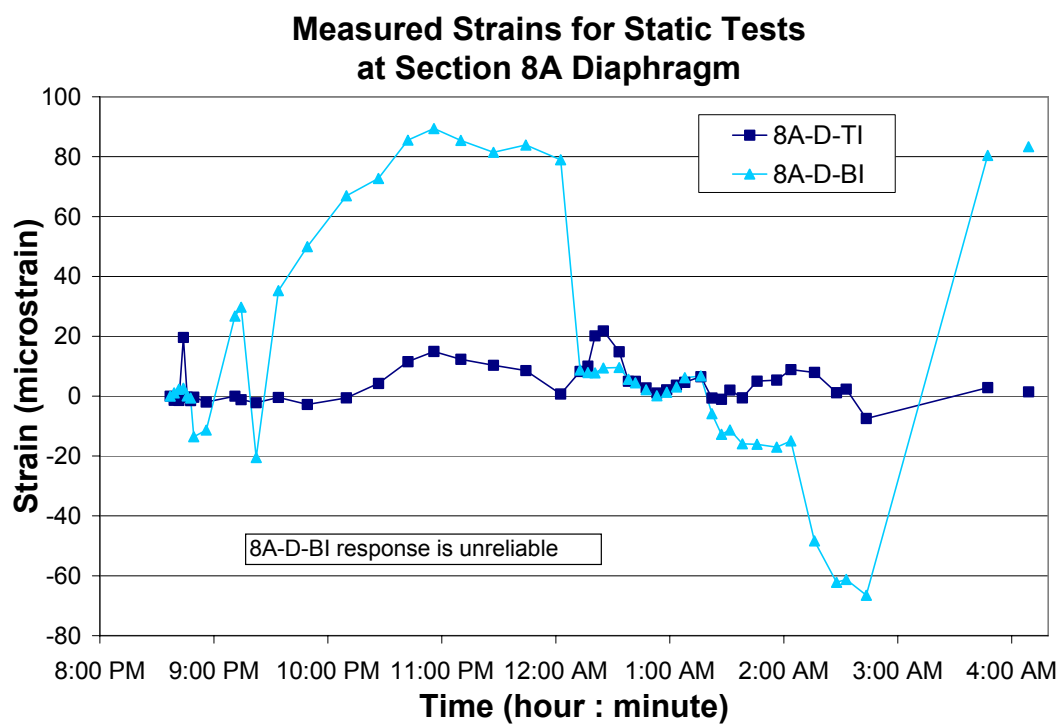


Figure D-50

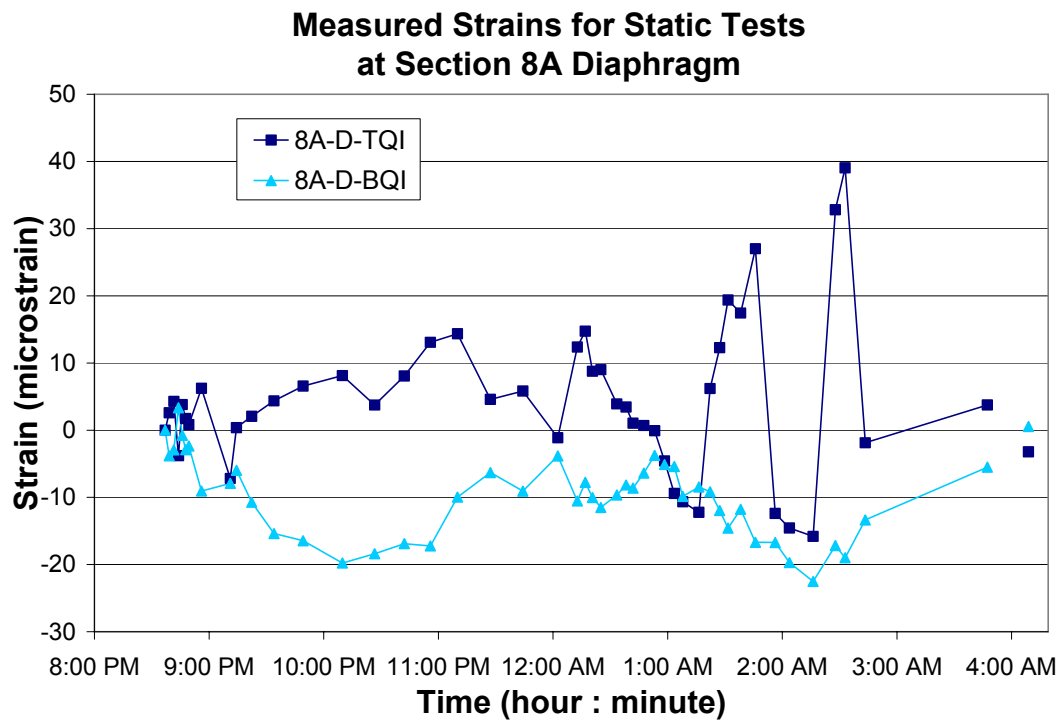


Figure D-51

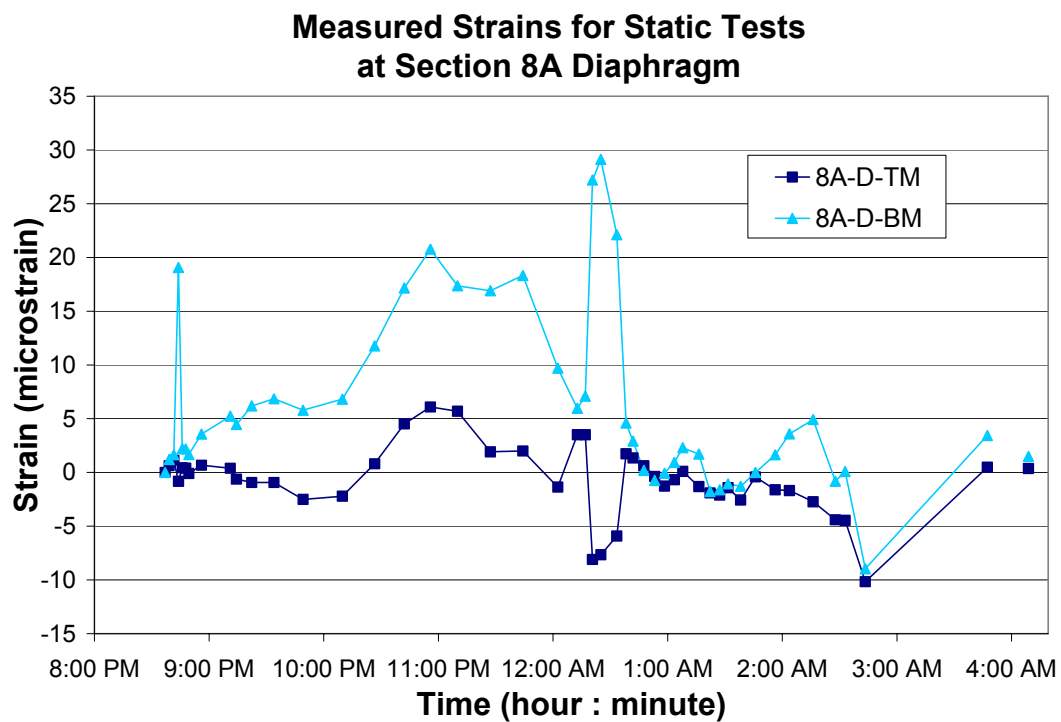


Figure D-52

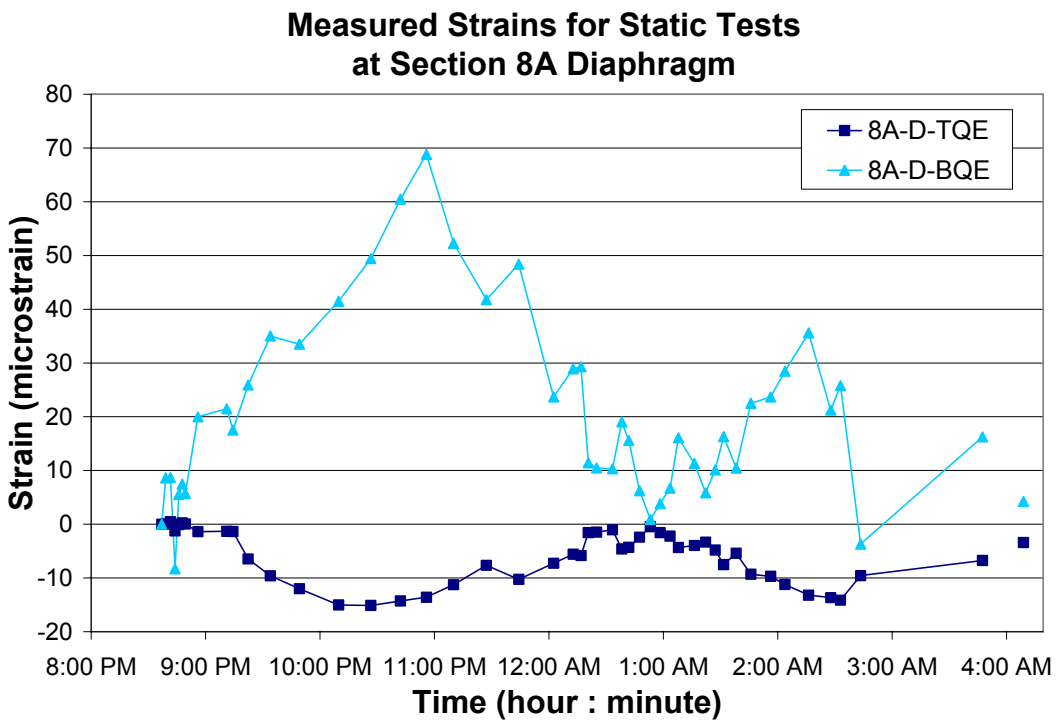


Figure D-53

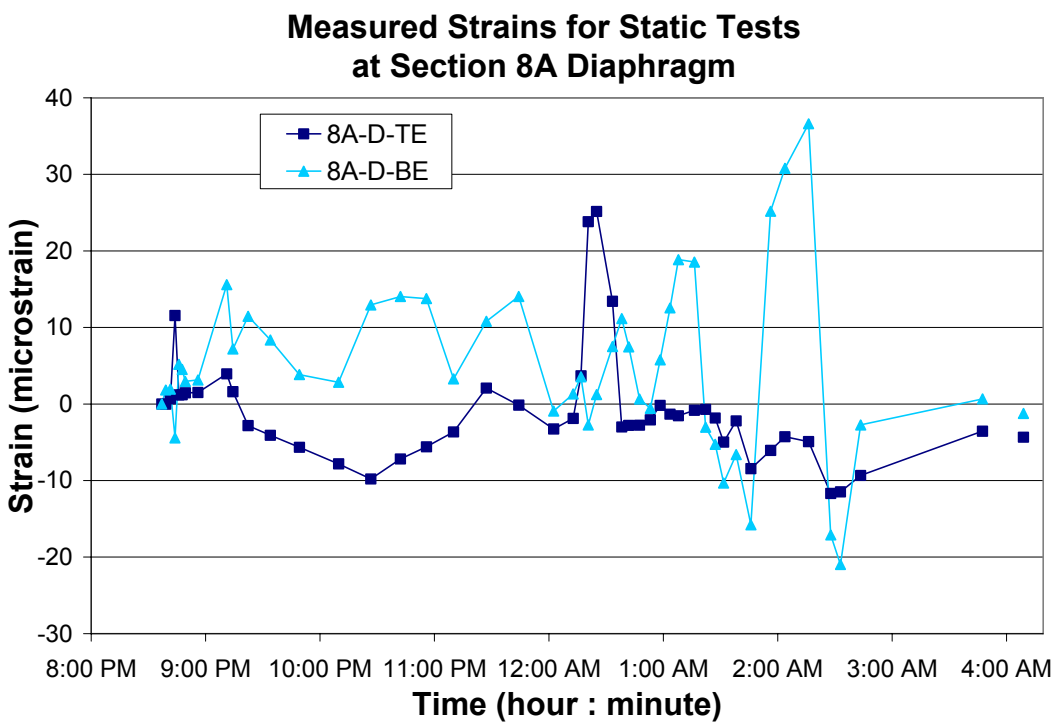


Figure D-54

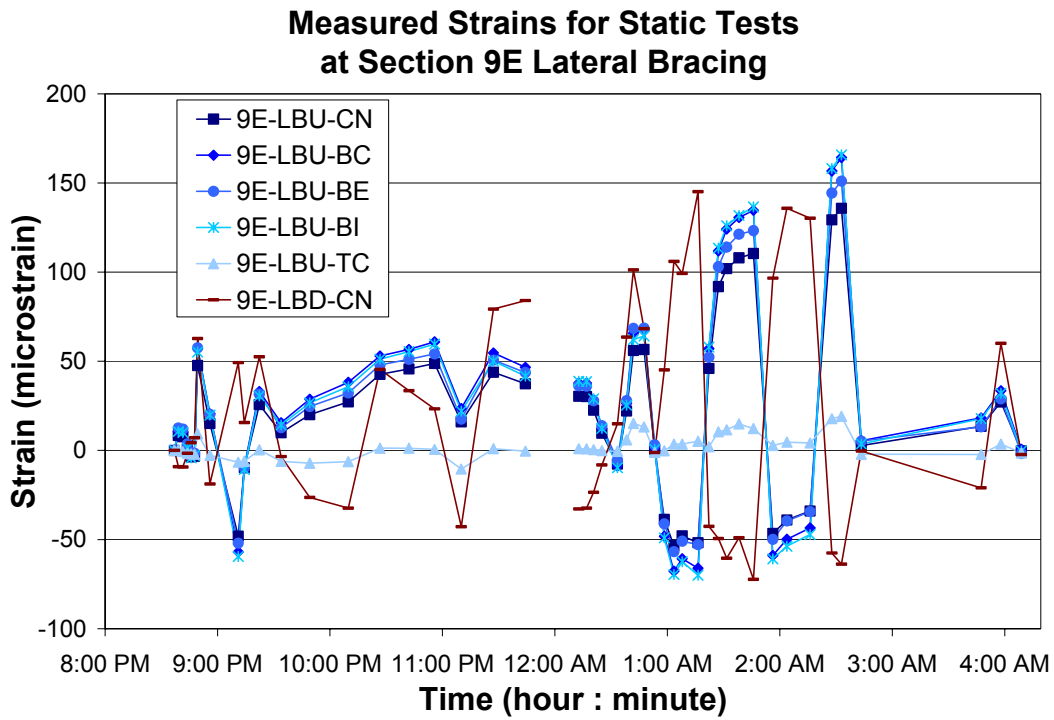


Figure D-55

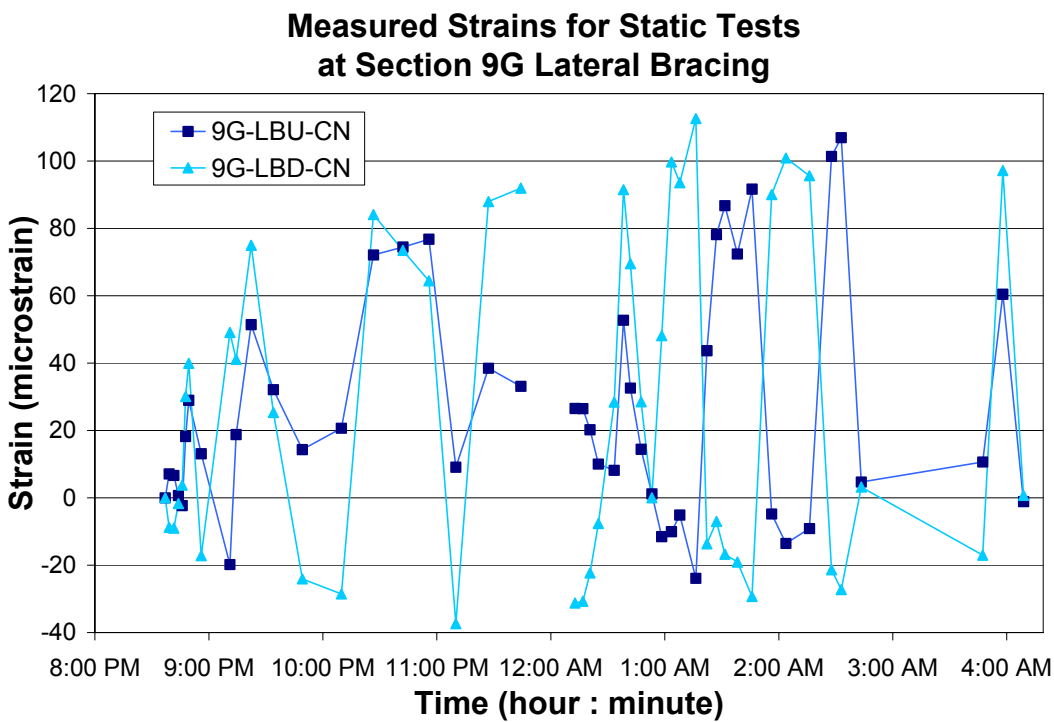


Figure D-56

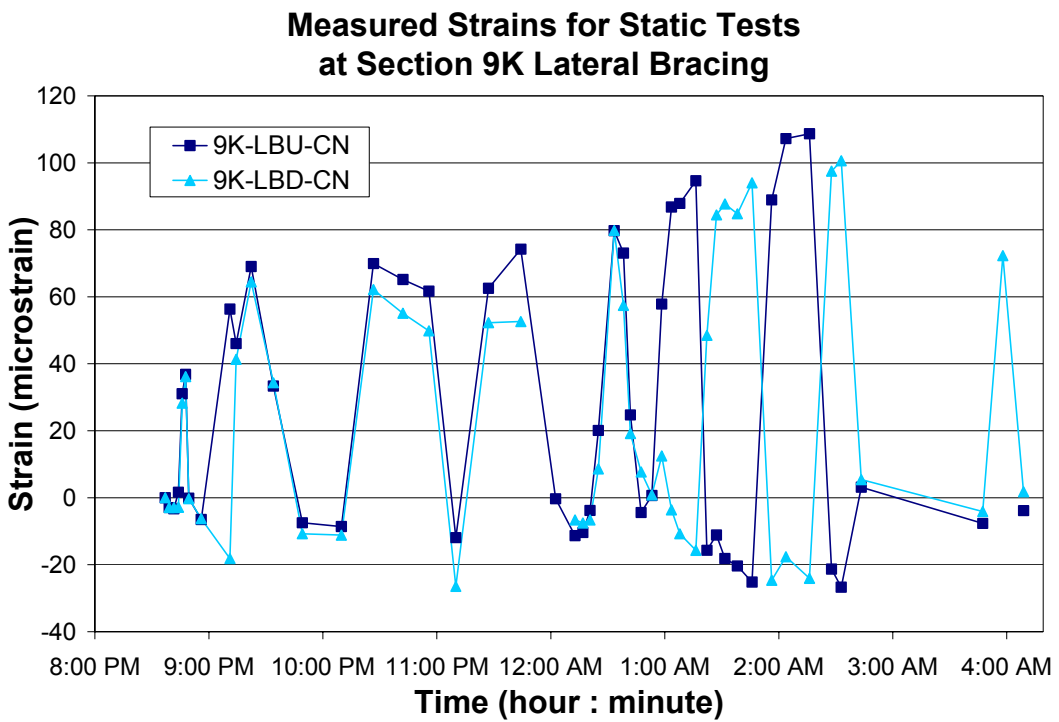


Figure D-57

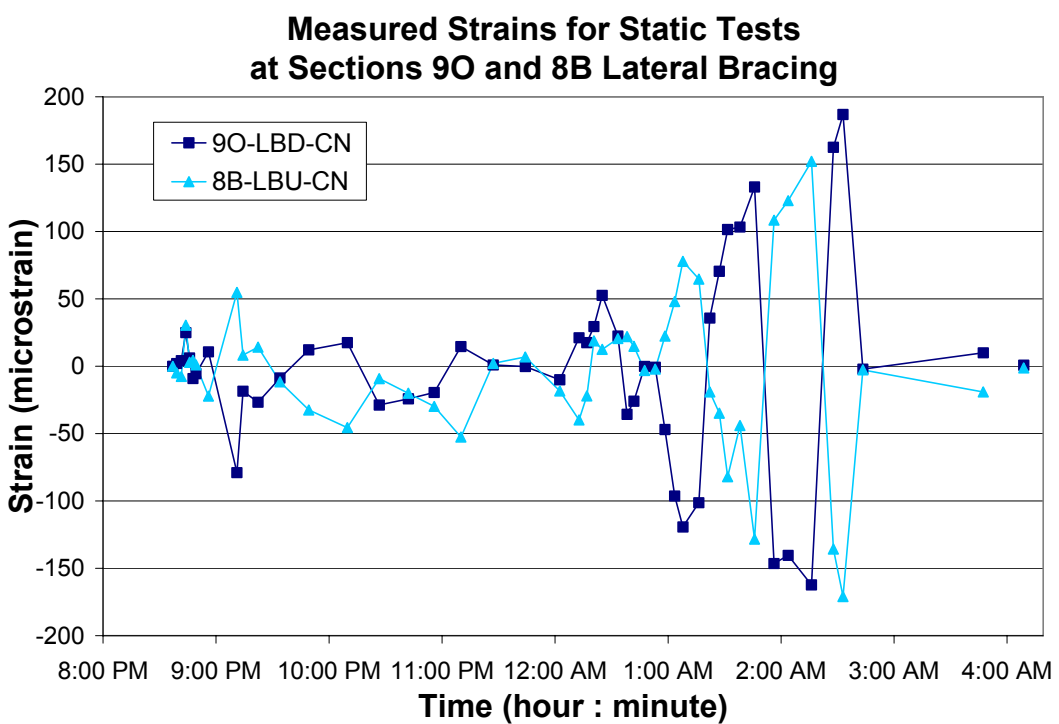


Figure D-58

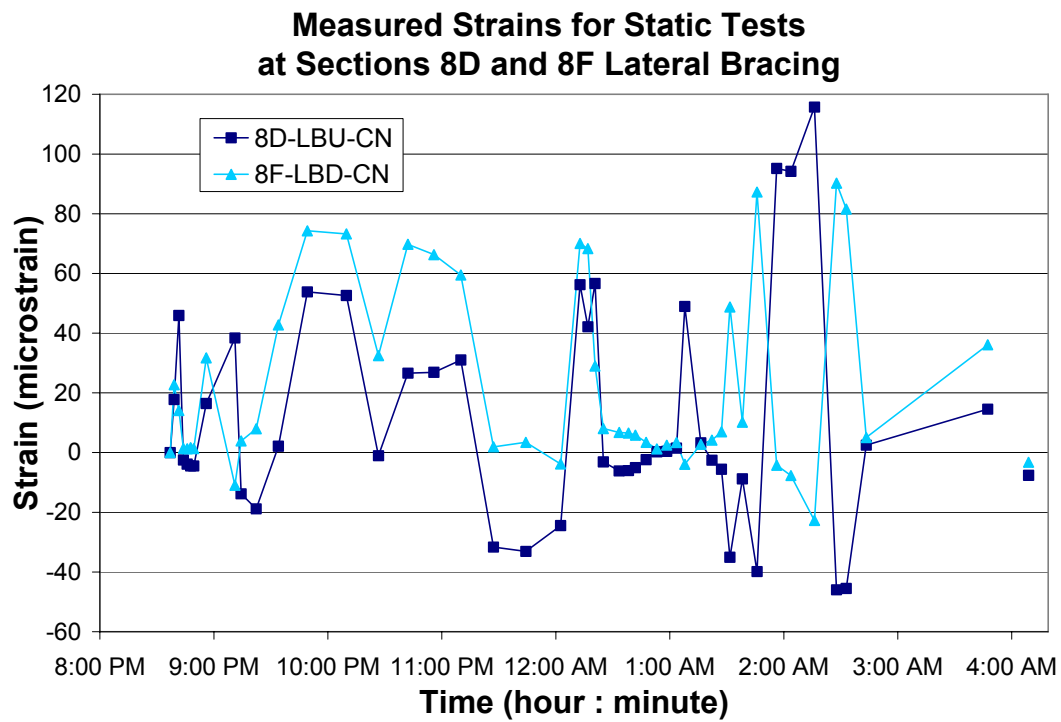


Figure D-59

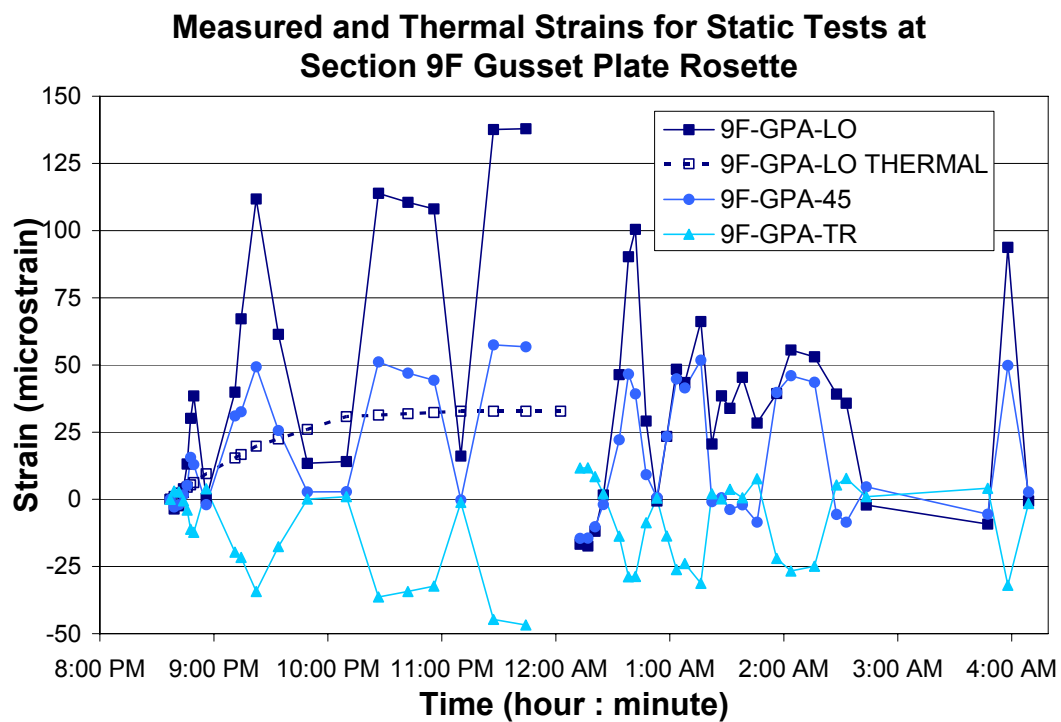


Figure D-60

**Measured and Thermal Strains for Static Tests
at Section 9F Gusset Tips**

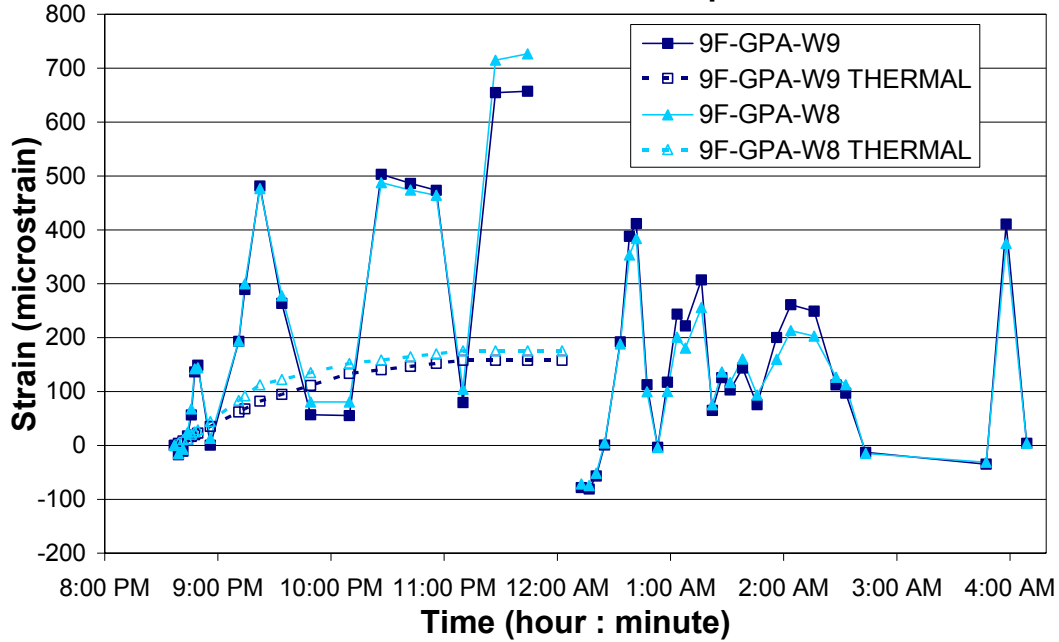


Figure D-61

**Measured Strains for Static Tests
at Section 9F Web Gaps**

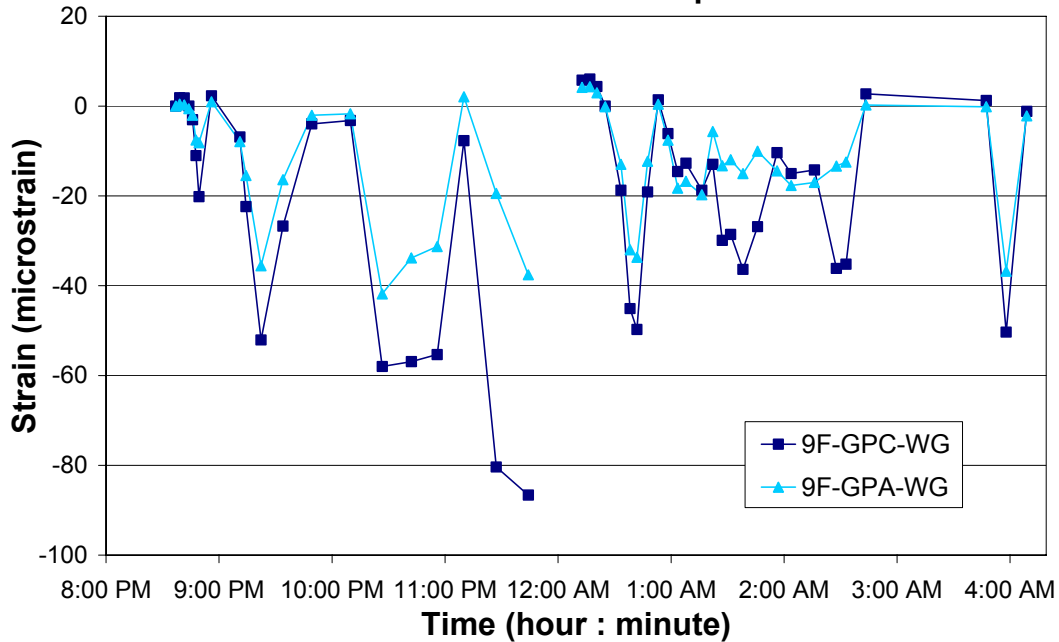


Figure D-62

**Measured and Thermal Strains for Static Tests
at Sections 9I and 8E Web Gaps**

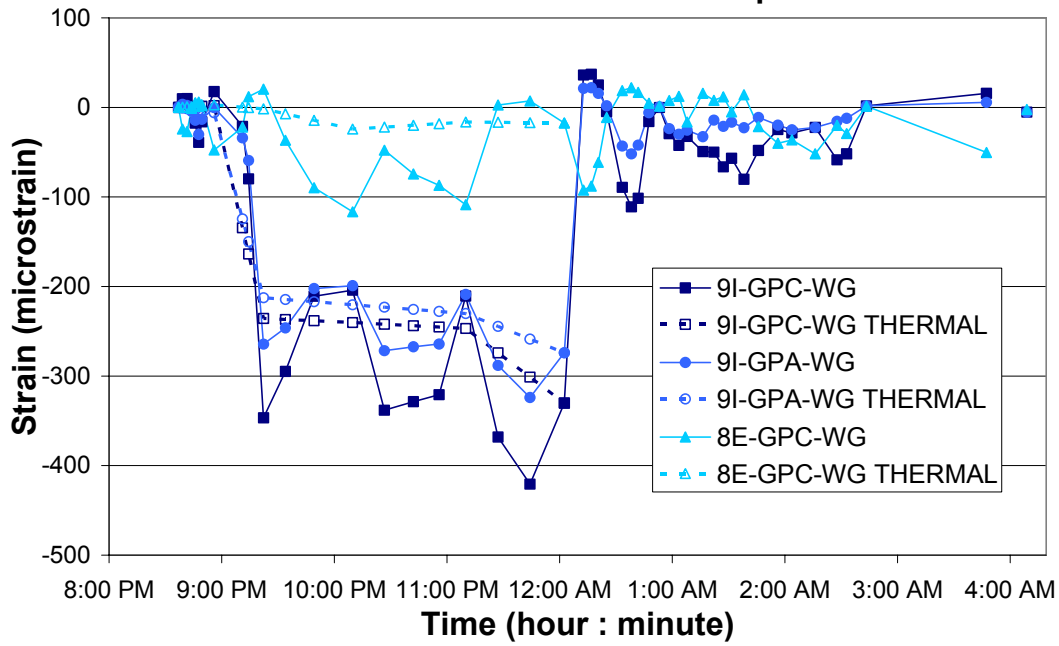


Figure D-63

Appendix E

Dynamic Test Data

This appendix contains recorded dynamic test data from the testing of Minnesota Department of Transportation Bridge No. 69824 in Duluth, Minnesota, on July 14th-15th, 2004. Section E.1 contains the plots for the TC and BC gages used for determining the girder and diaphragm neutral axis positions in Chapter 6 of this report. Section E.2 provides tables for the maximum and minimum strains in the dynamic and static tests, along with the calculated dynamic impact factors (DIF). If the static strain magnitude is less than 25 μ strain, a DIF is not calculated and is marked by the term *low static* in these tables.

Due to unexpected data recording issues (see Chapter 5), none of the strain gage data for tests D4 and D10 was recorded, and approximately half of the strain gage data was not recorded for tests D1, D5, D6, D7, and D12. Only gages that were recorded are provided in the plots and tables of this appendix.

E.1 Dynamic Data for Neutral Axis Locations

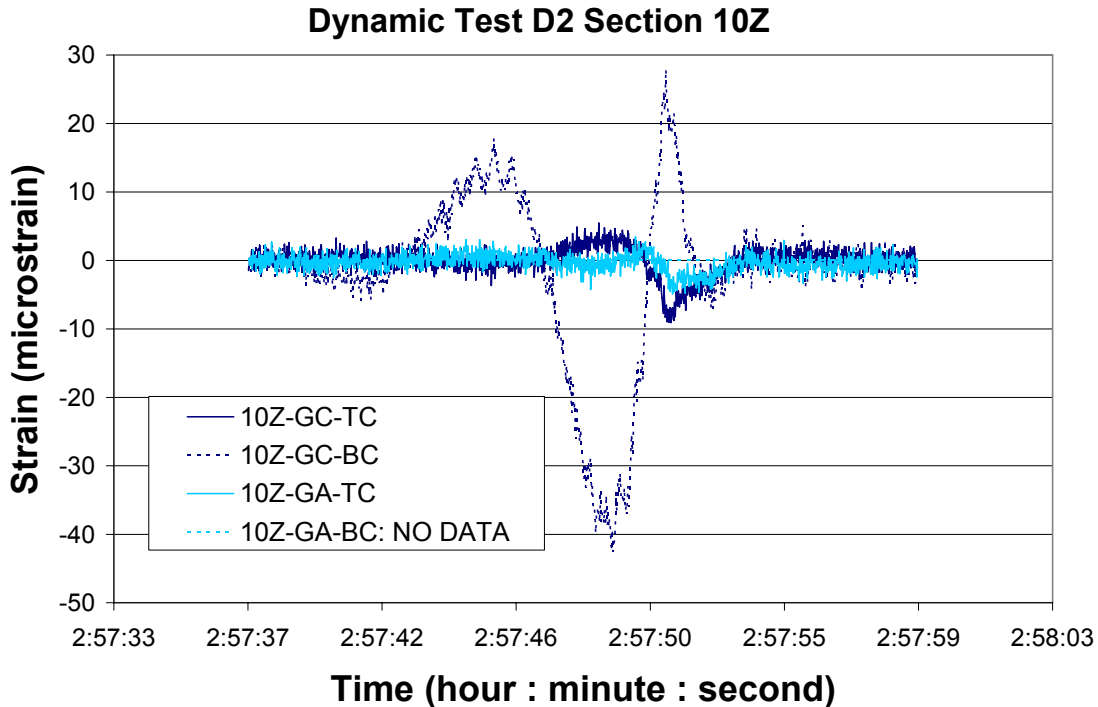


Figure E-1

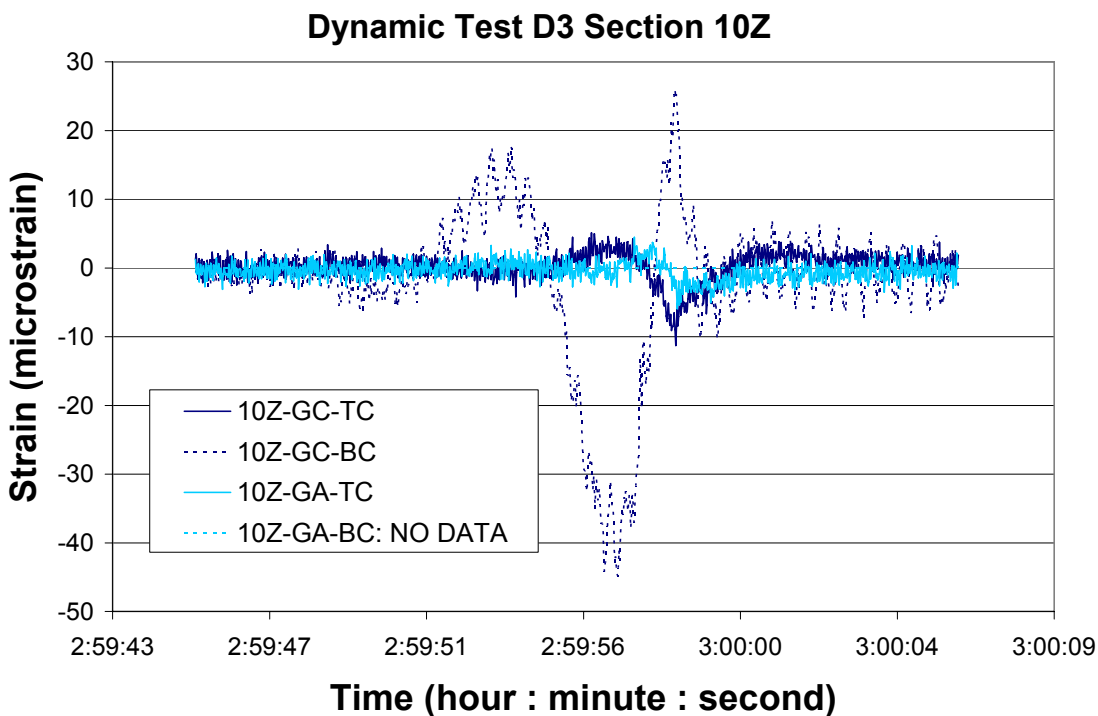


Figure E-2

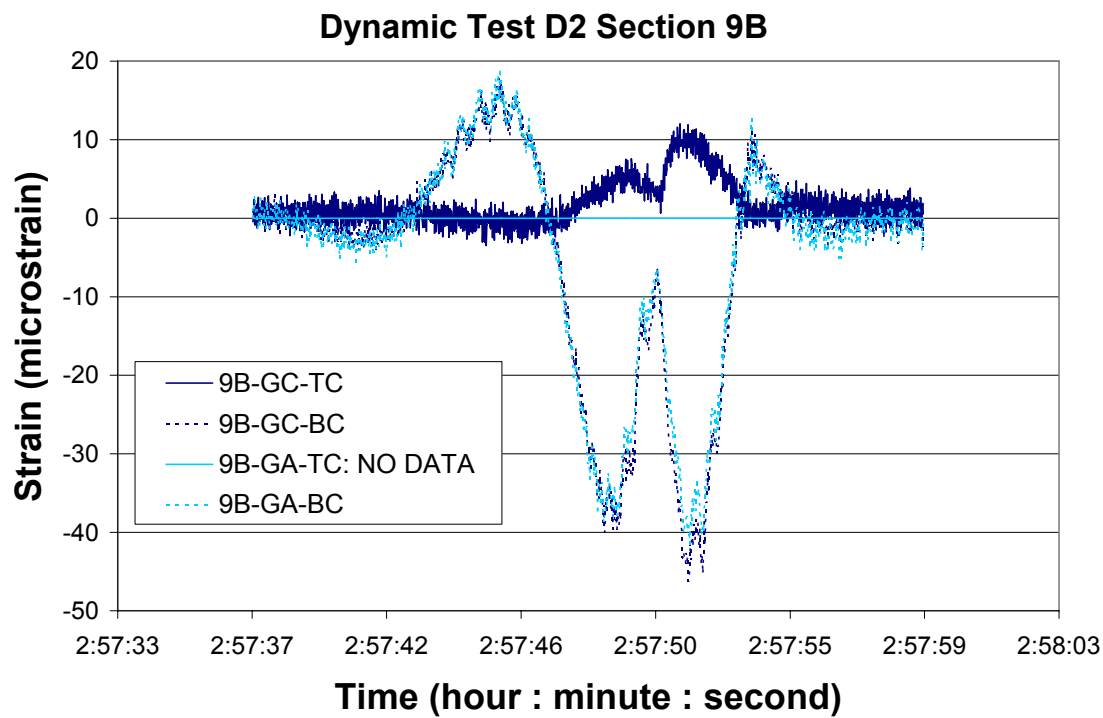


Figure E-3

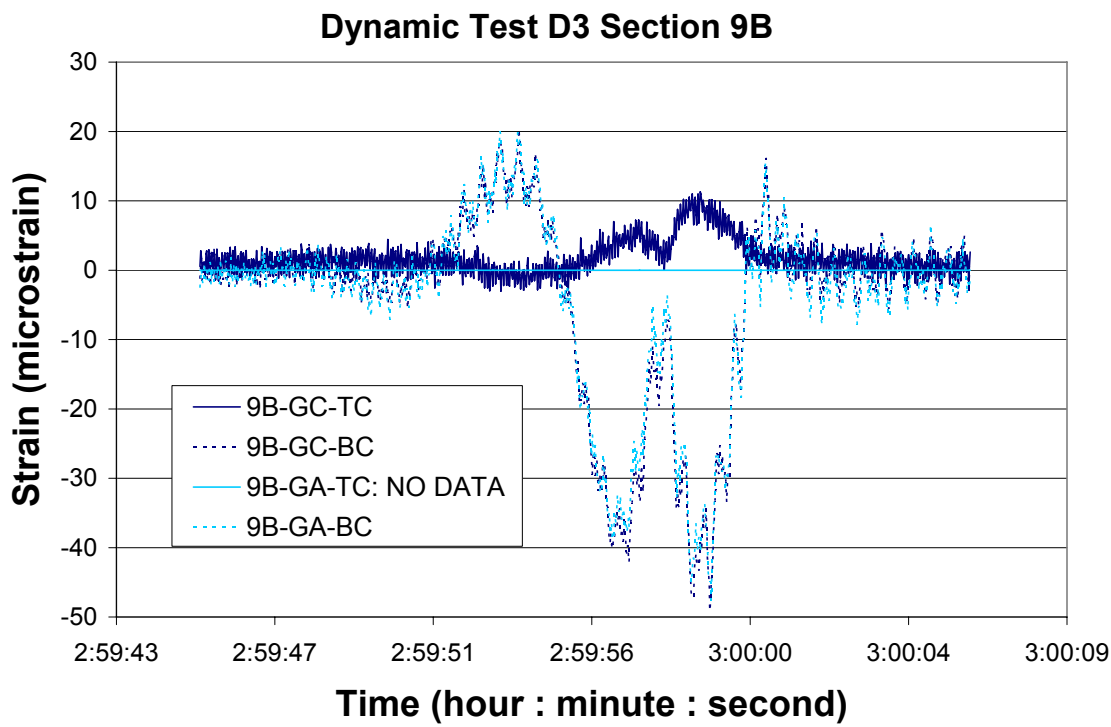


Figure E-4

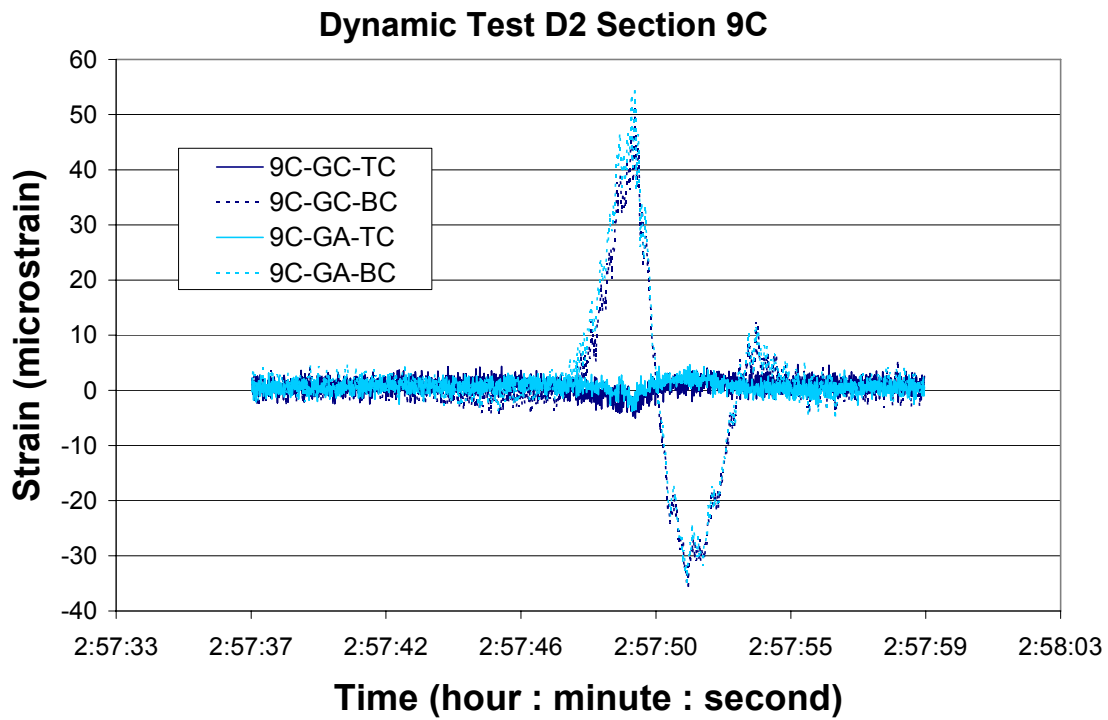


Figure E-5

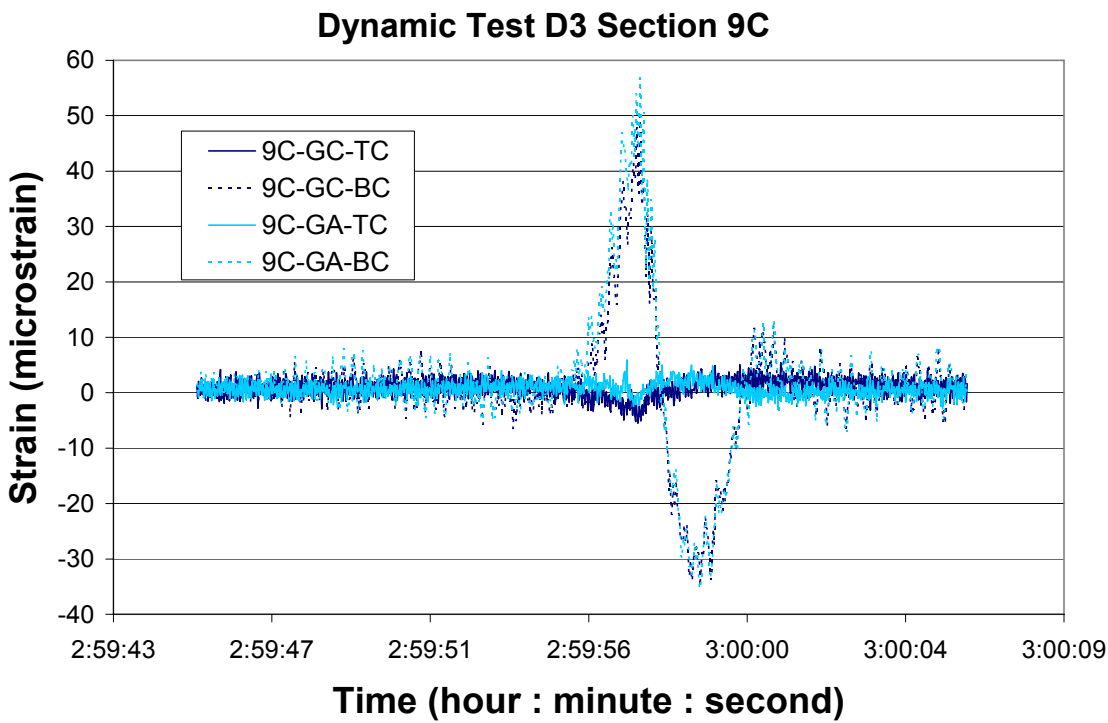


Figure E-6

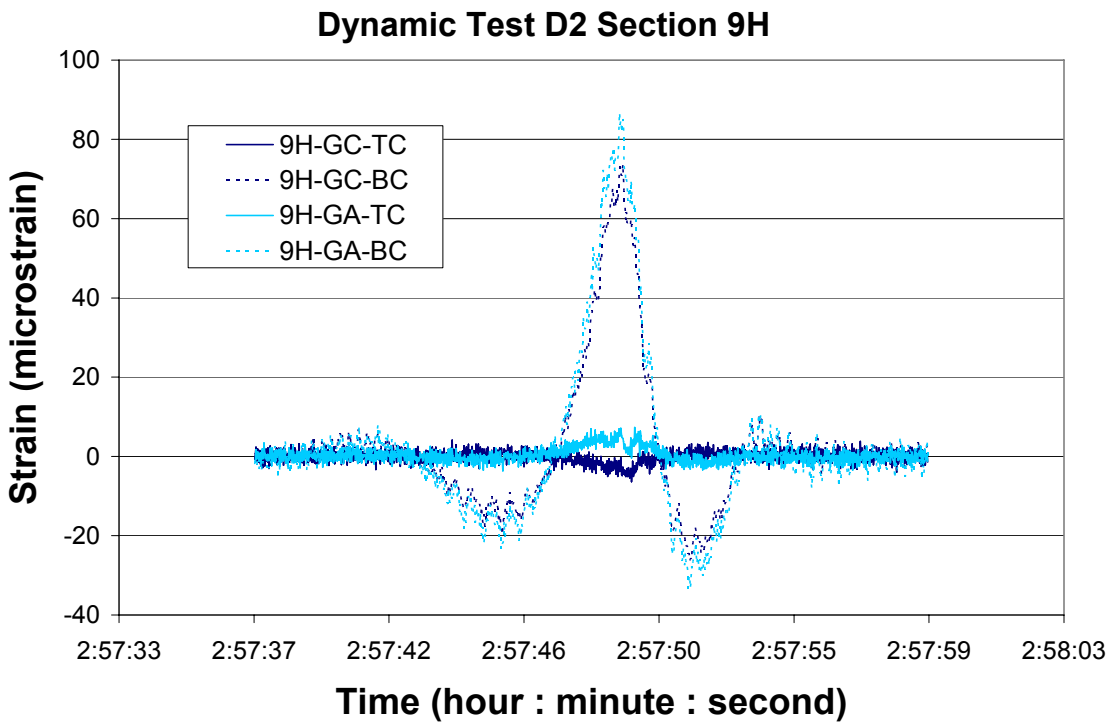


Figure E-7

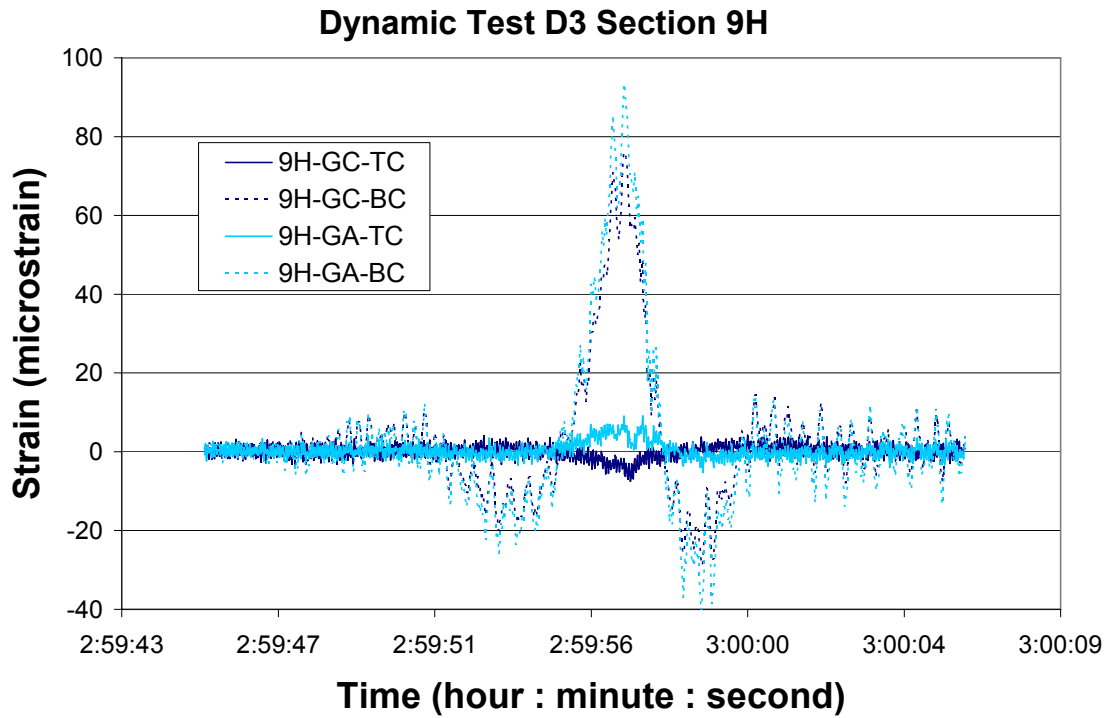


Figure E-8

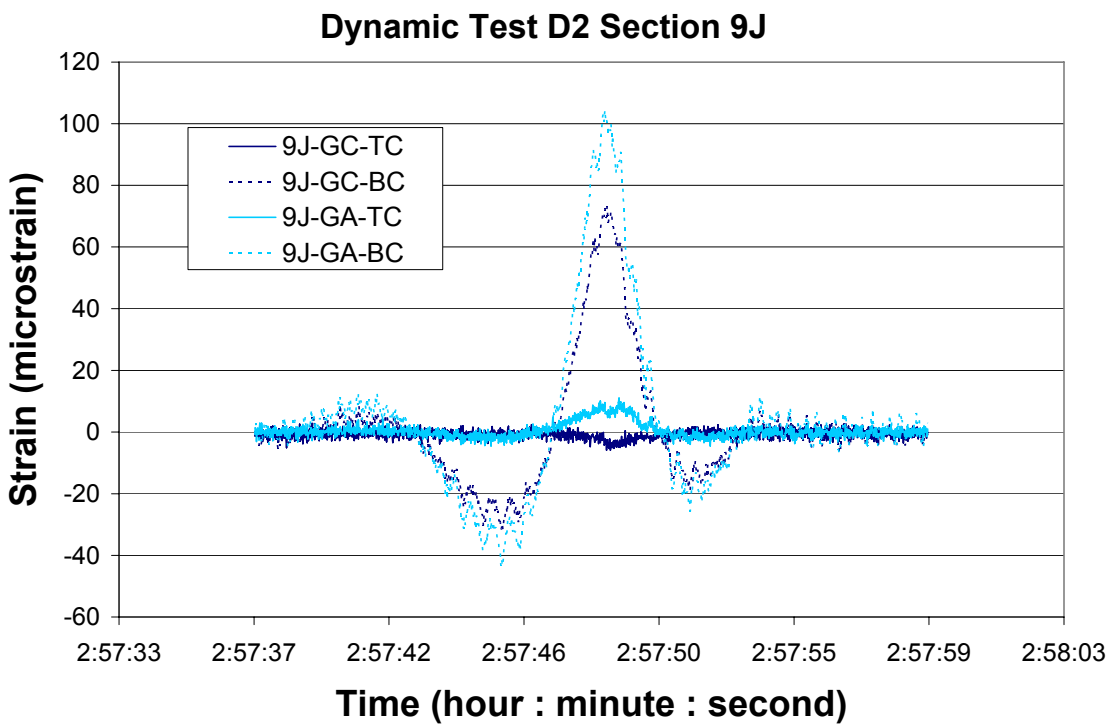


Figure E-9

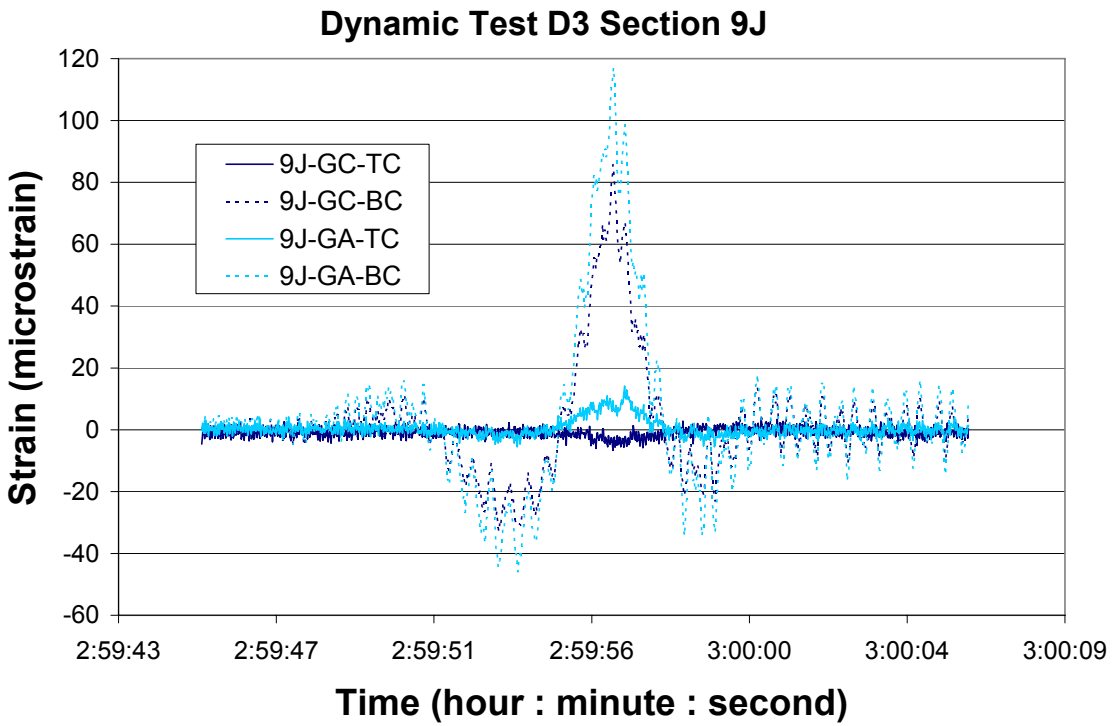


Figure E-10

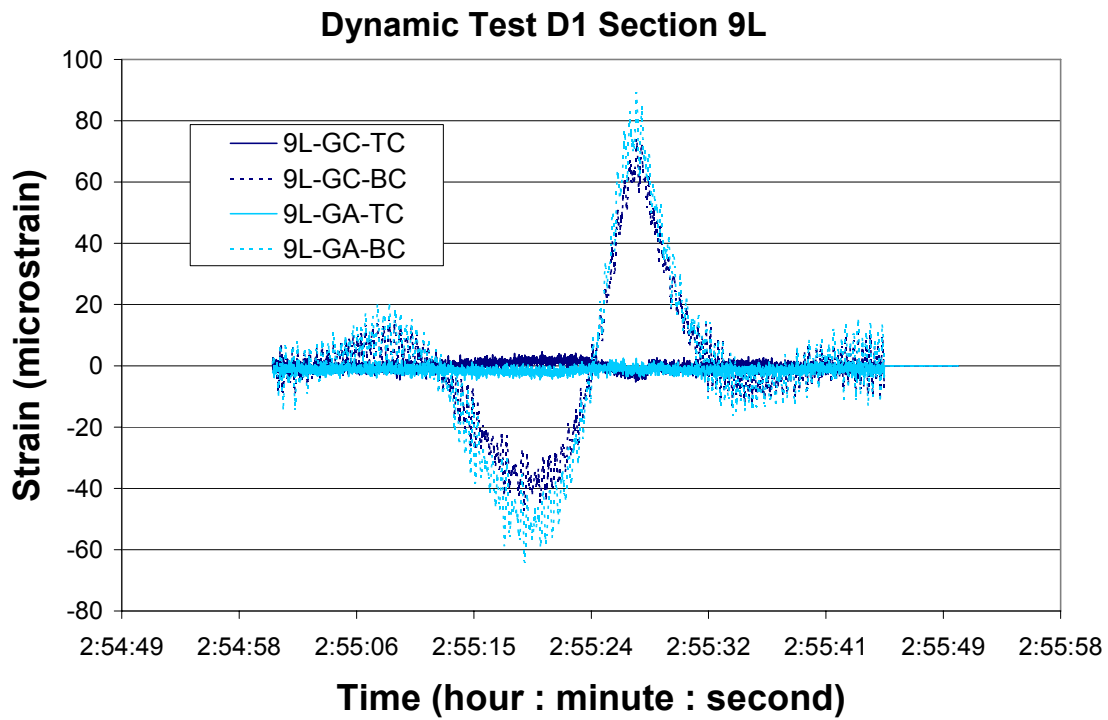


Figure E-11

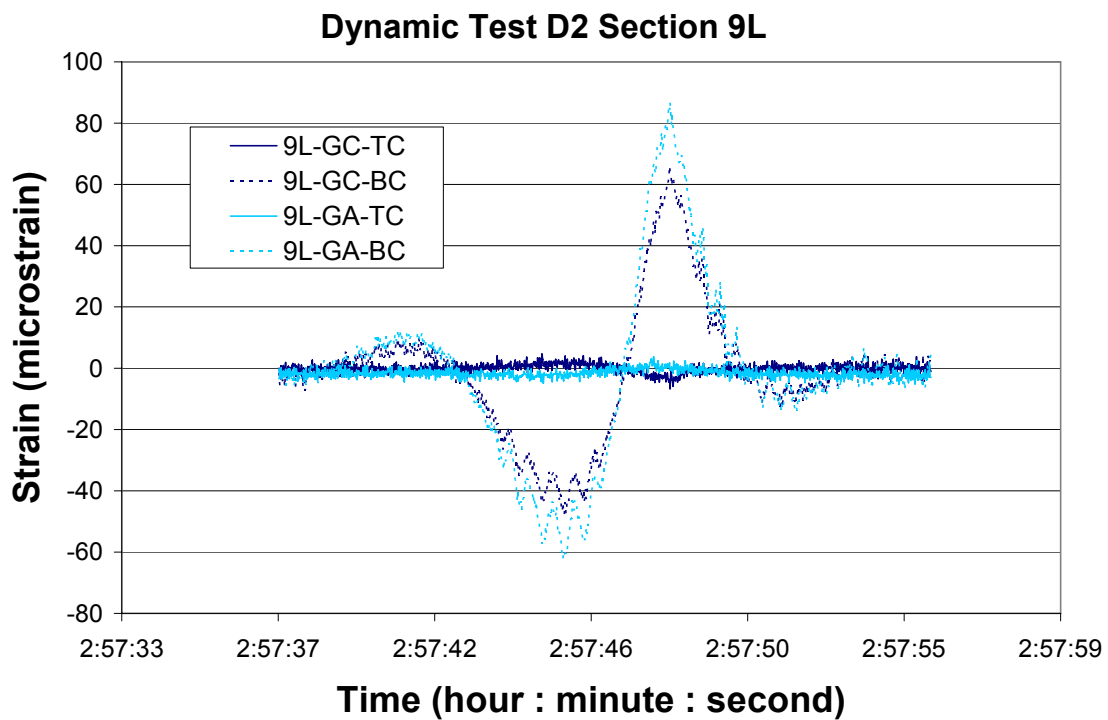


Figure E-12

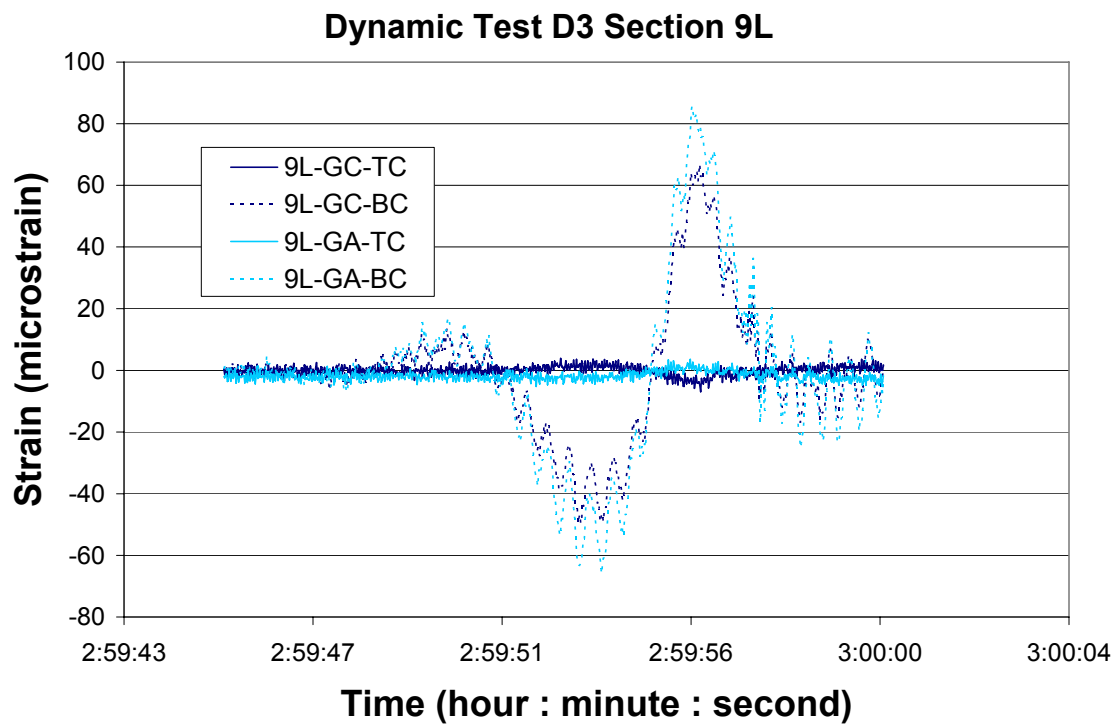


Figure E-13

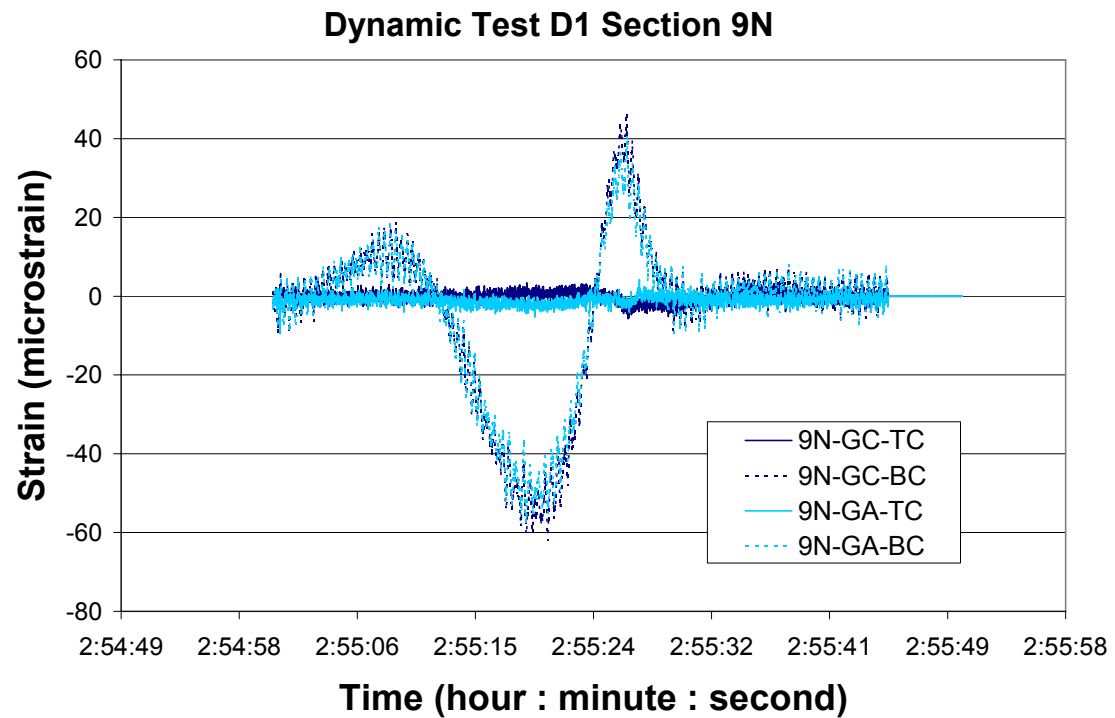


Figure E-14

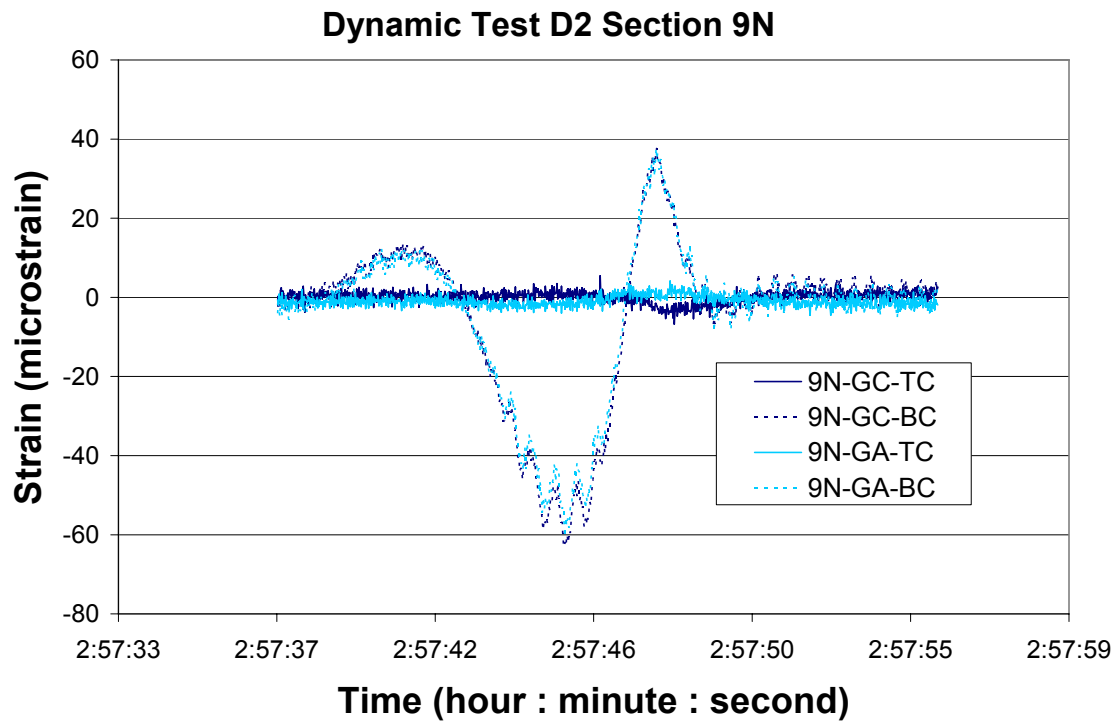


Figure E-15

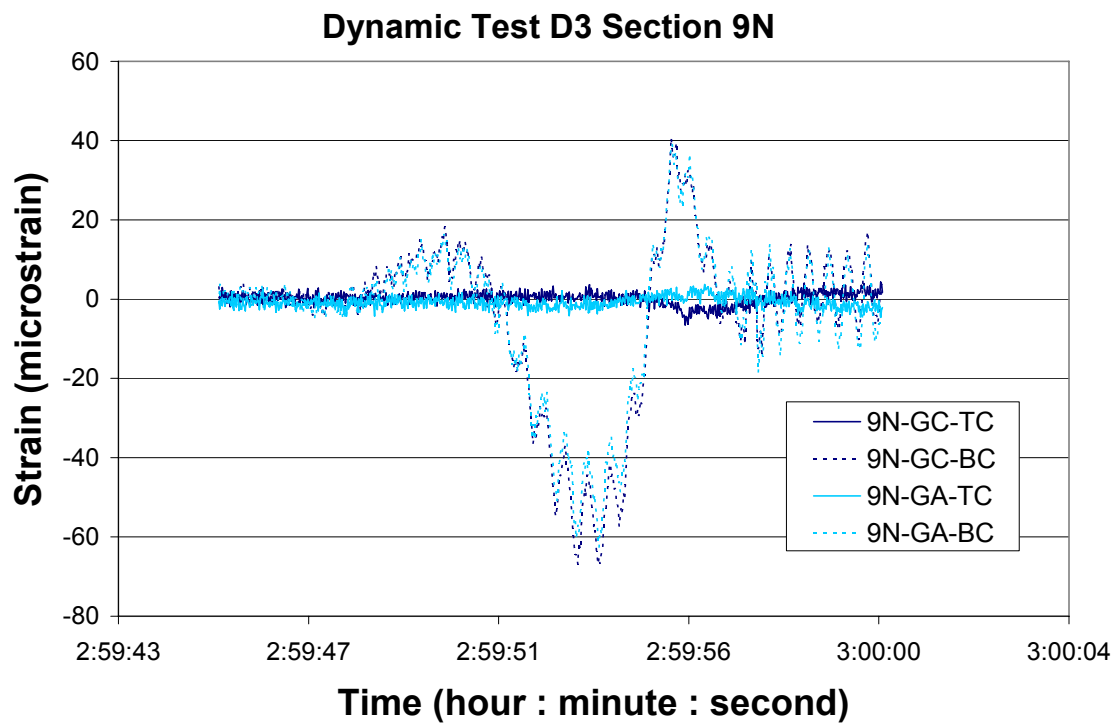


Figure E-16

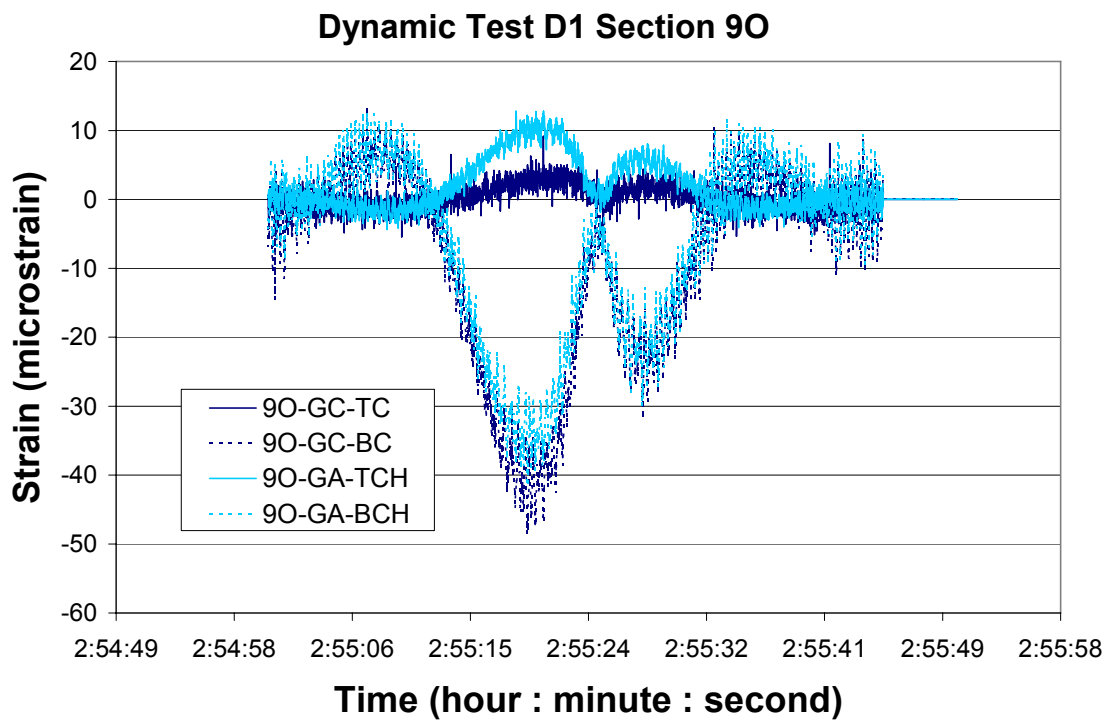


Figure E-17

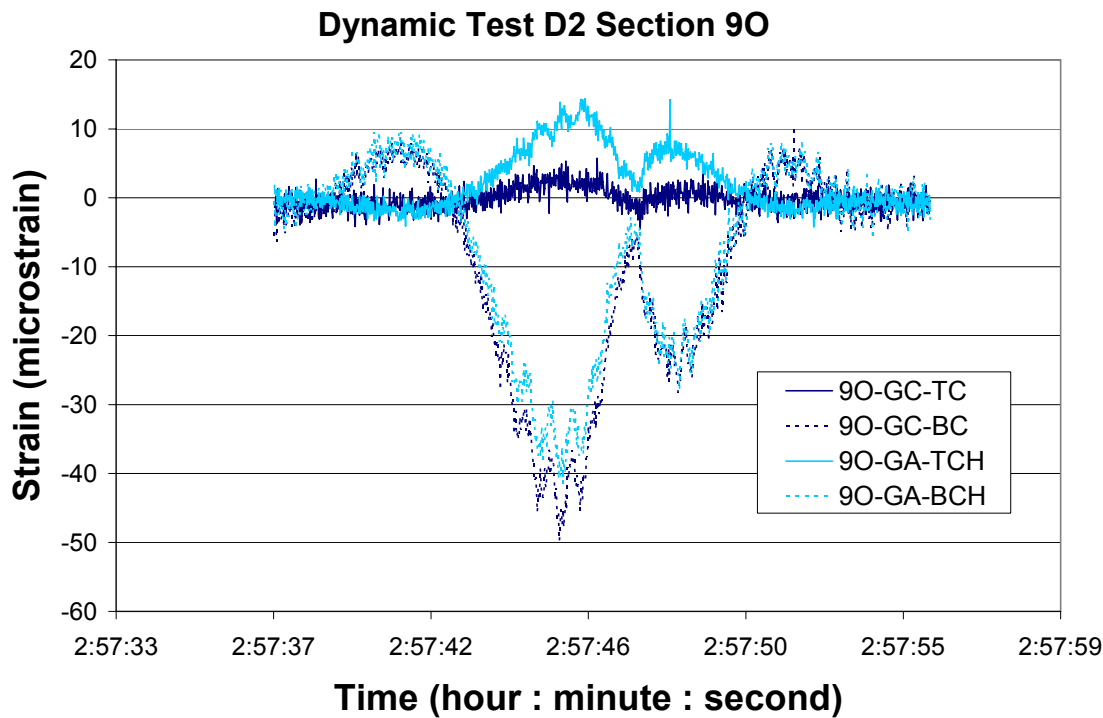


Figure E-18

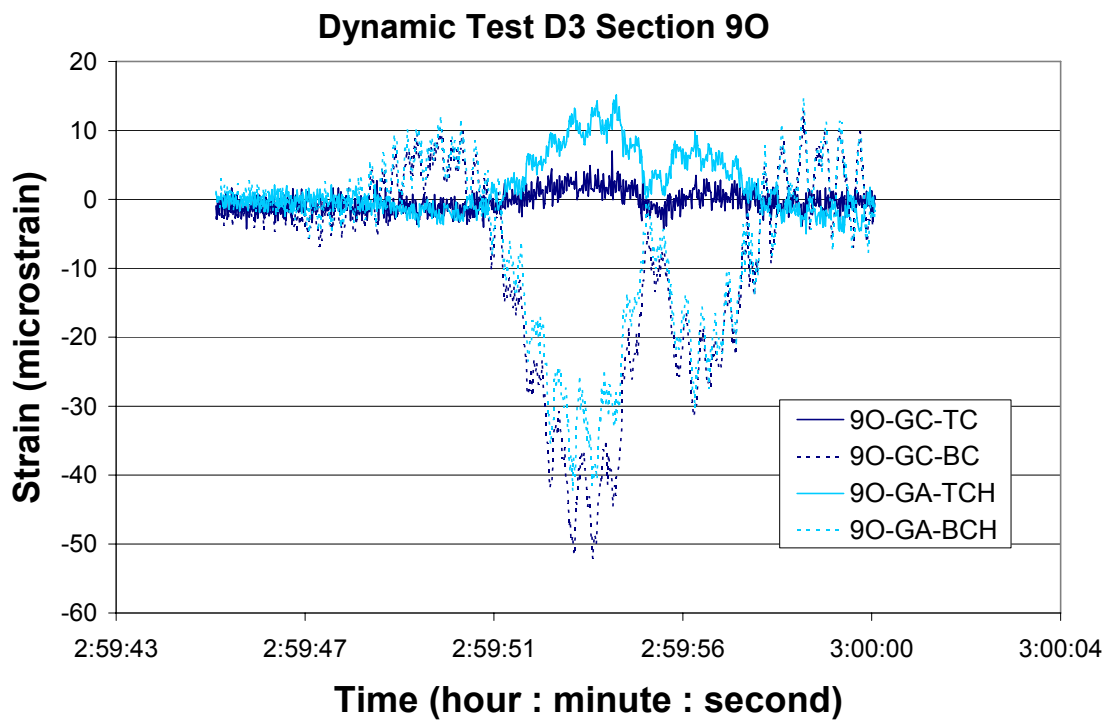


Figure E-19

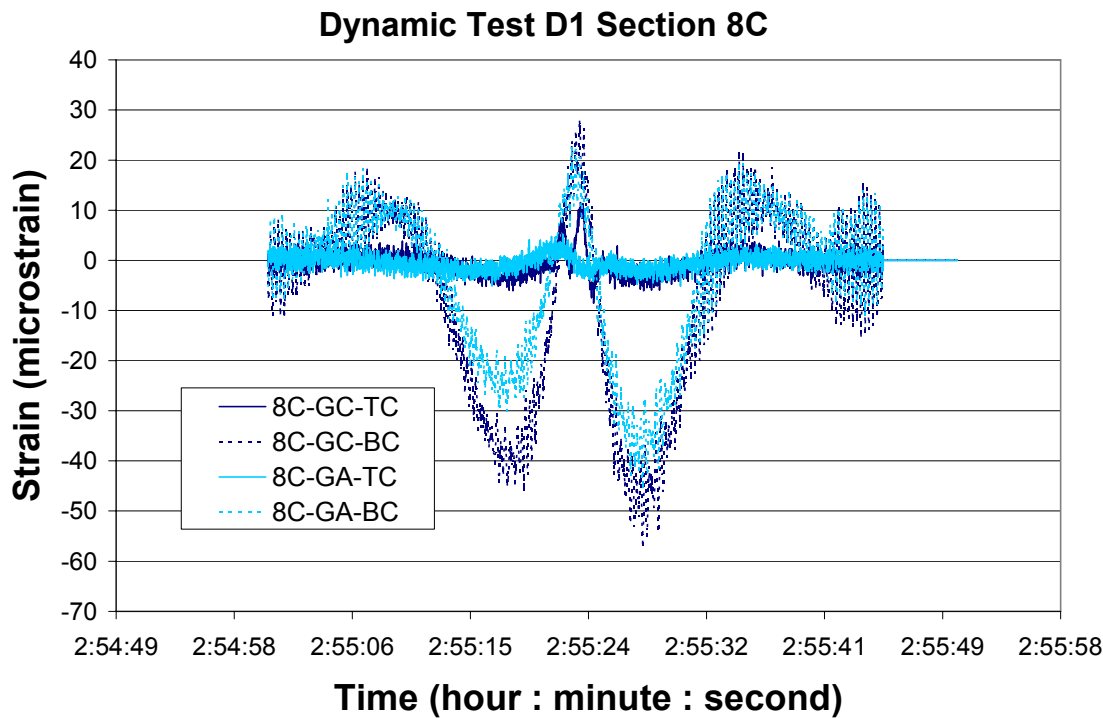


Figure E-20

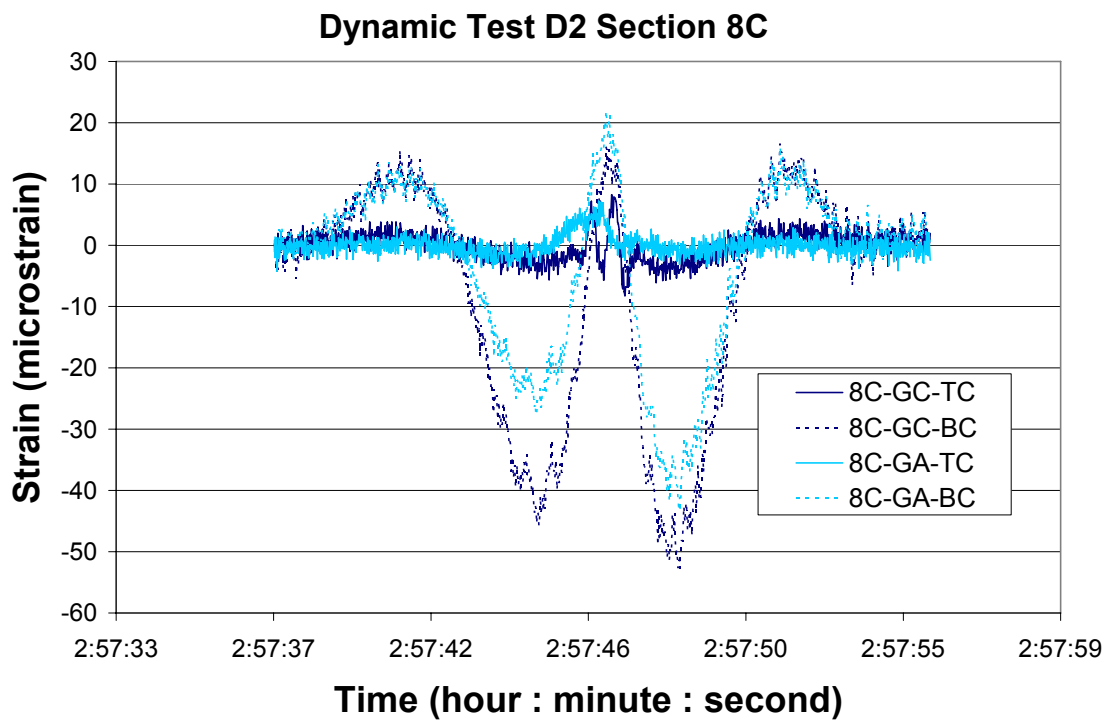


Figure E-21

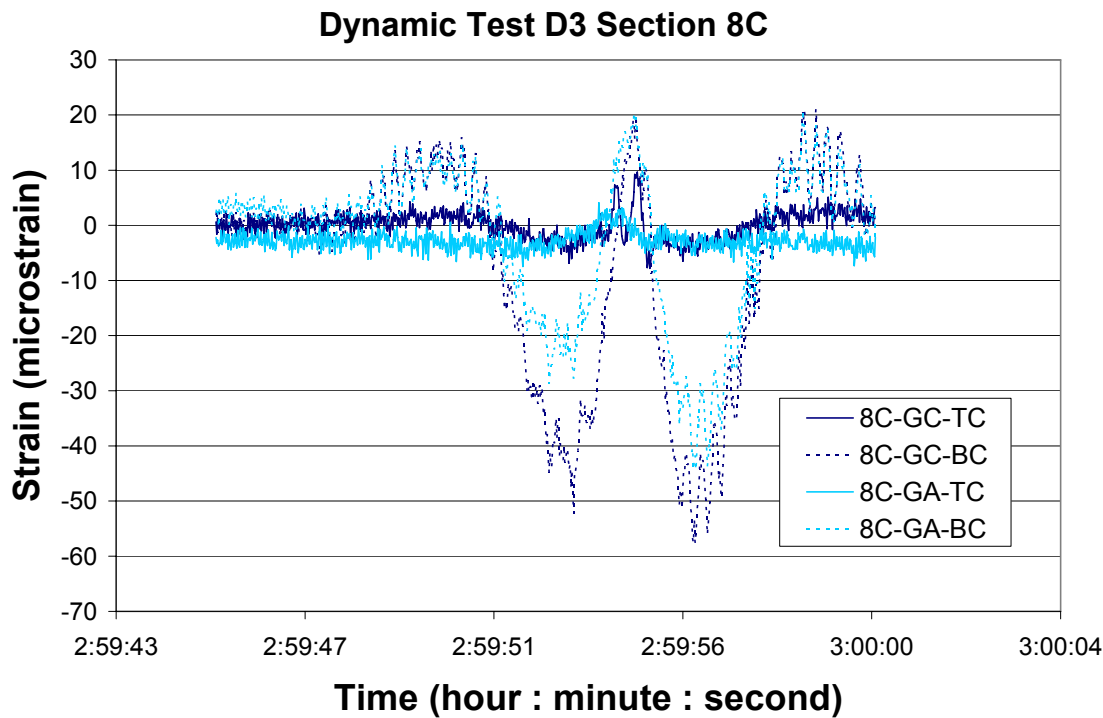


Figure E-22

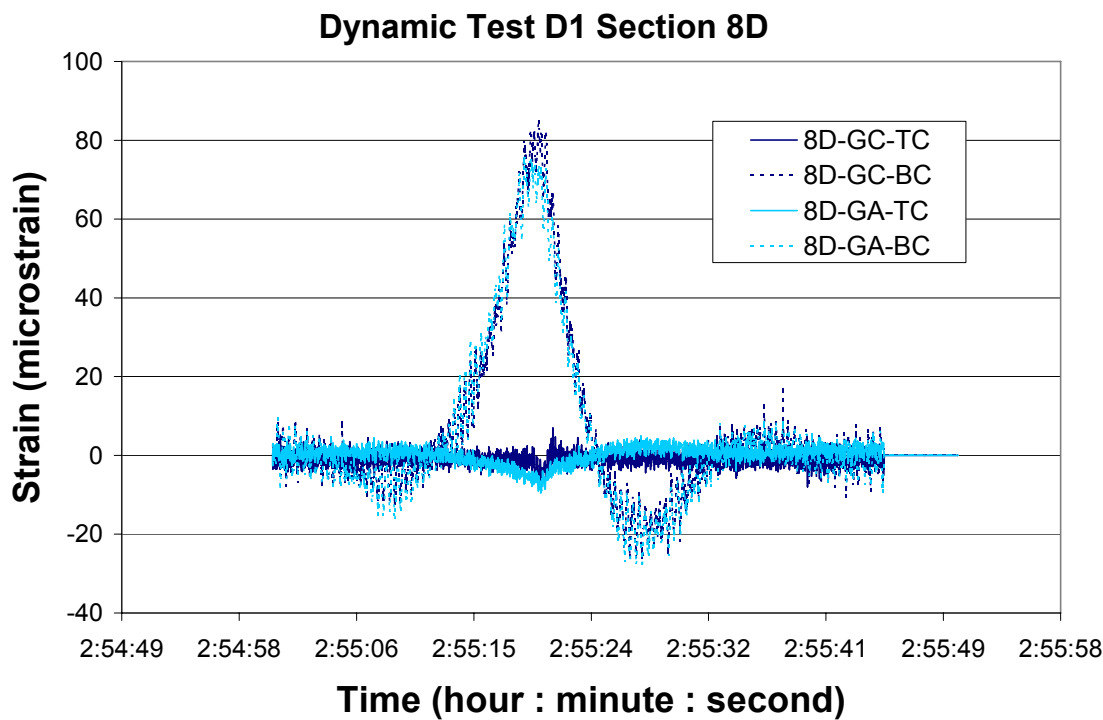


Figure E-23

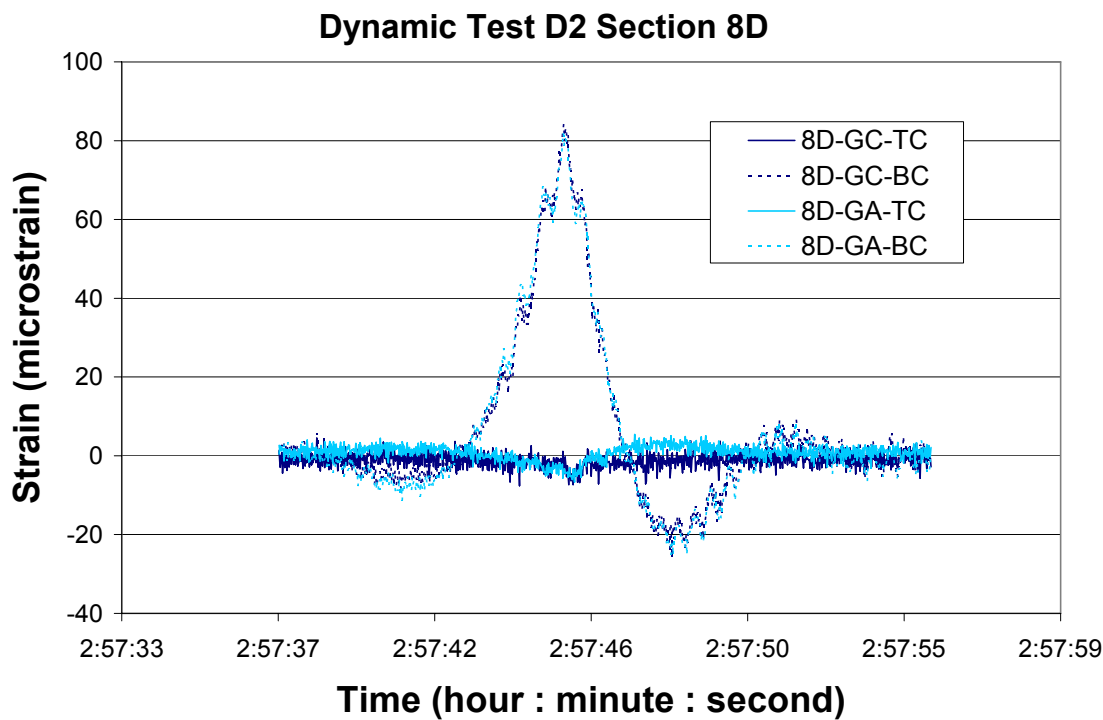


Figure E-24

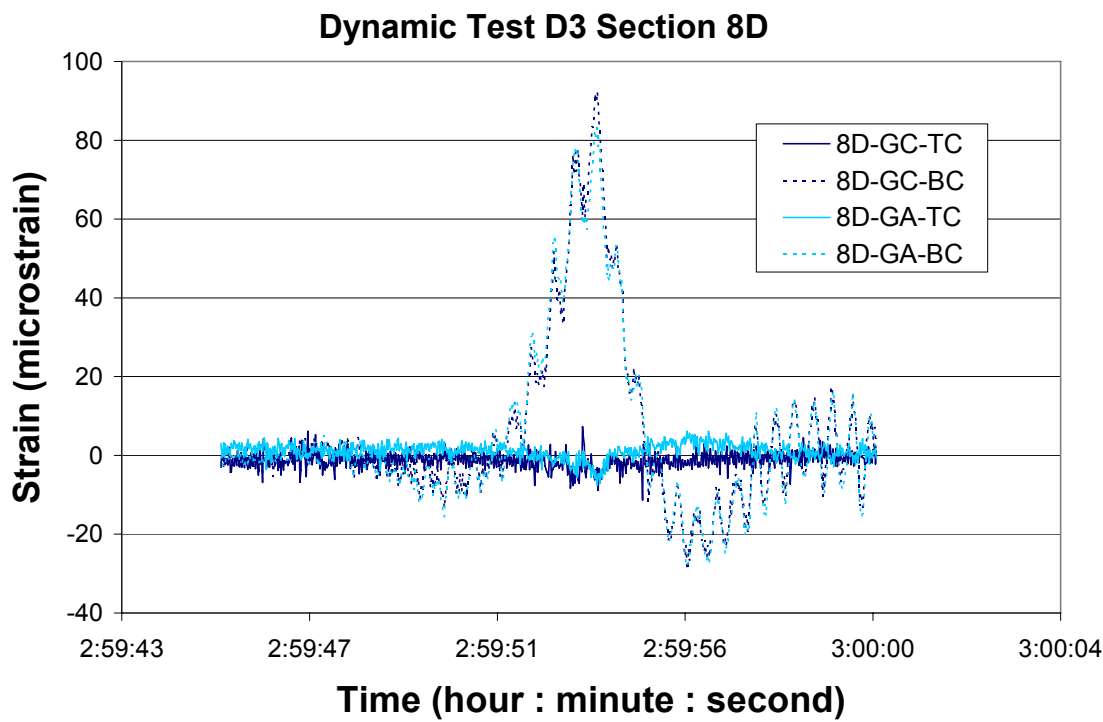


Figure E-25

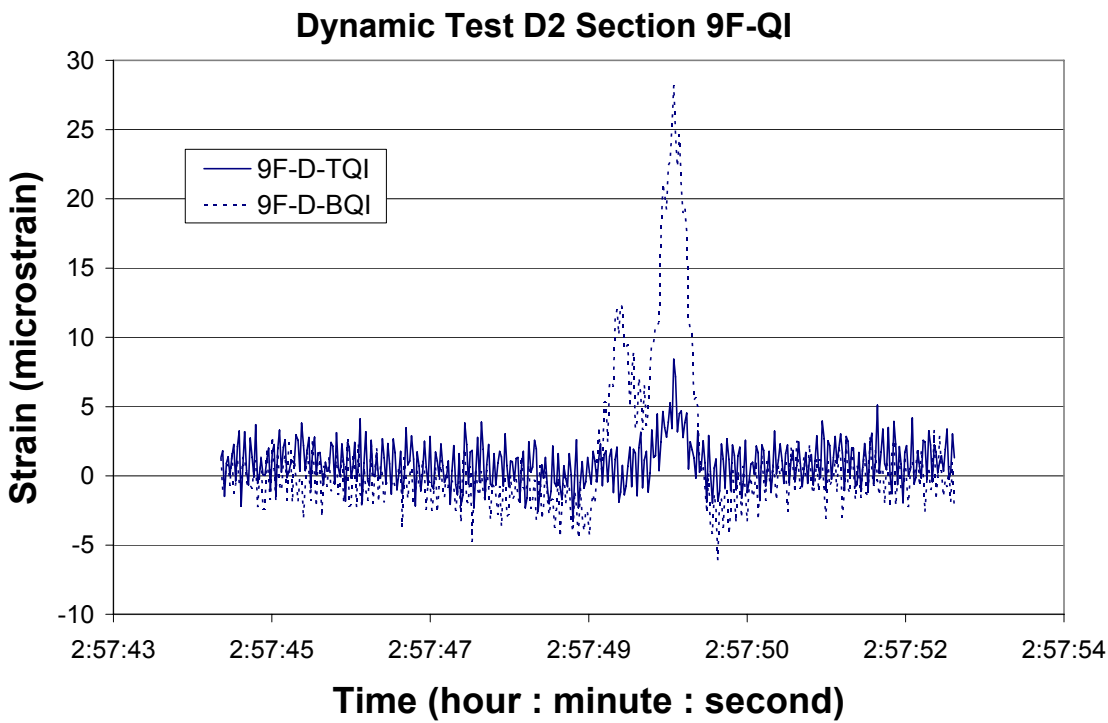


Figure E-26

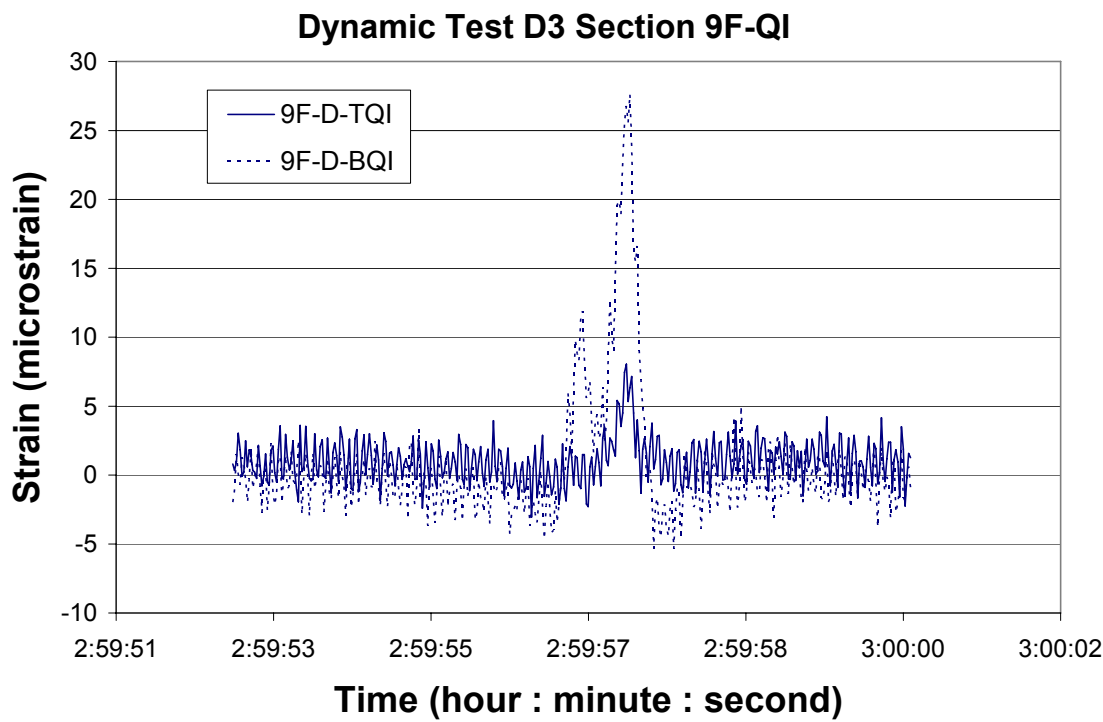


Figure E-27

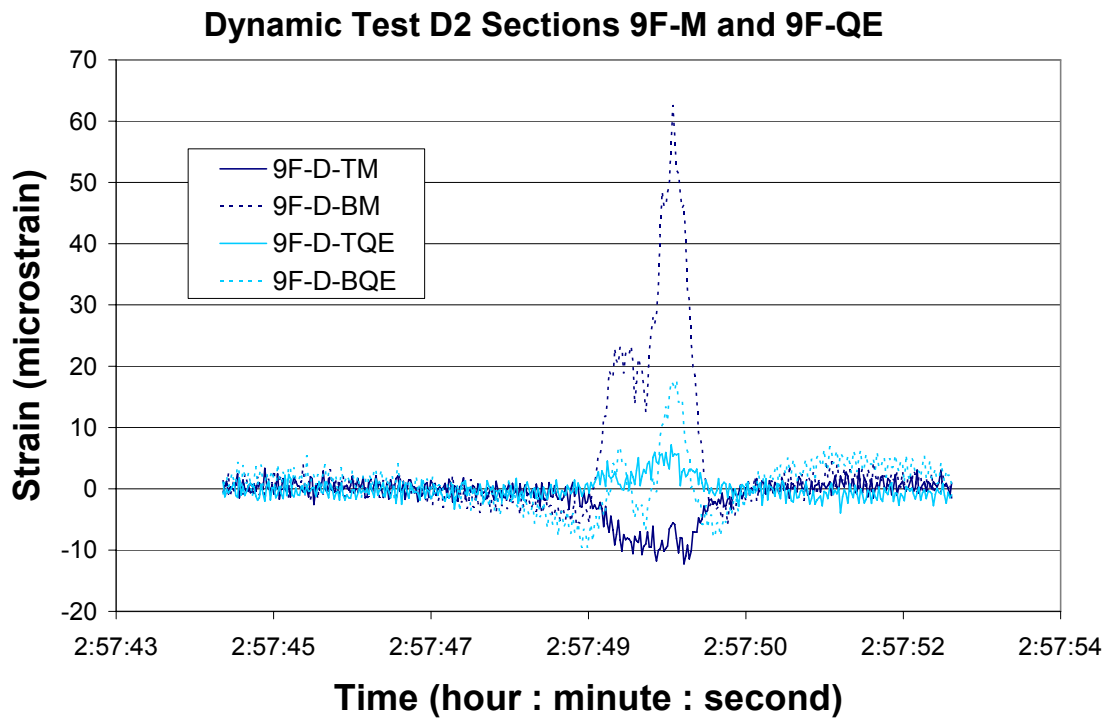


Figure E-28

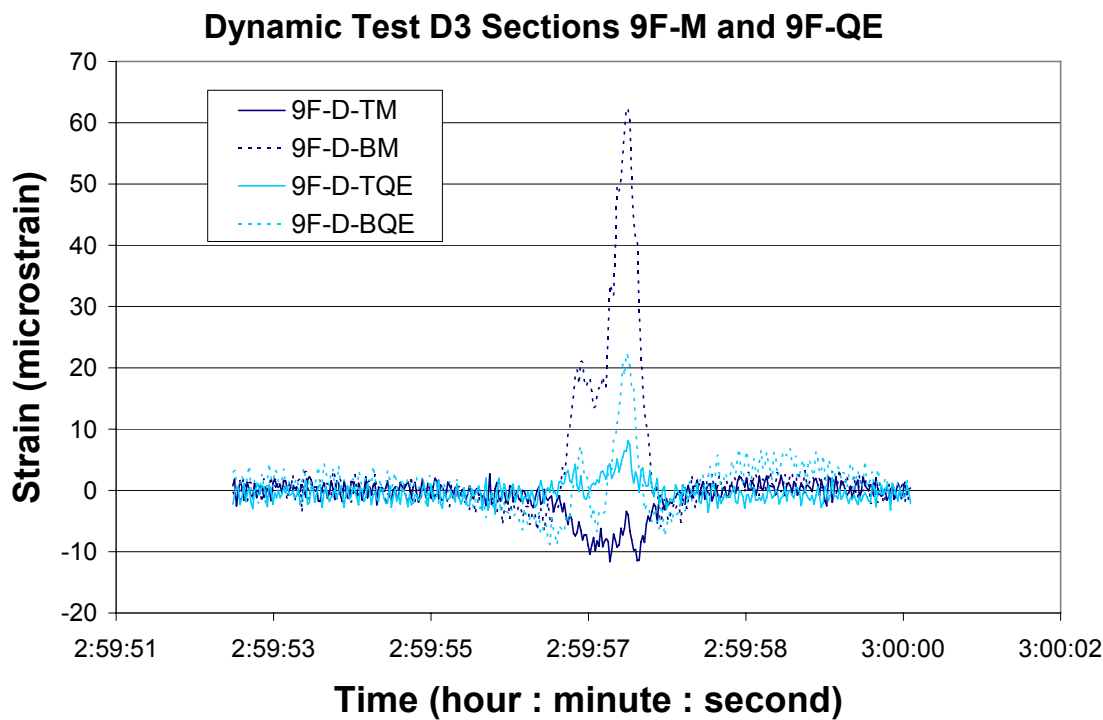


Figure E-29

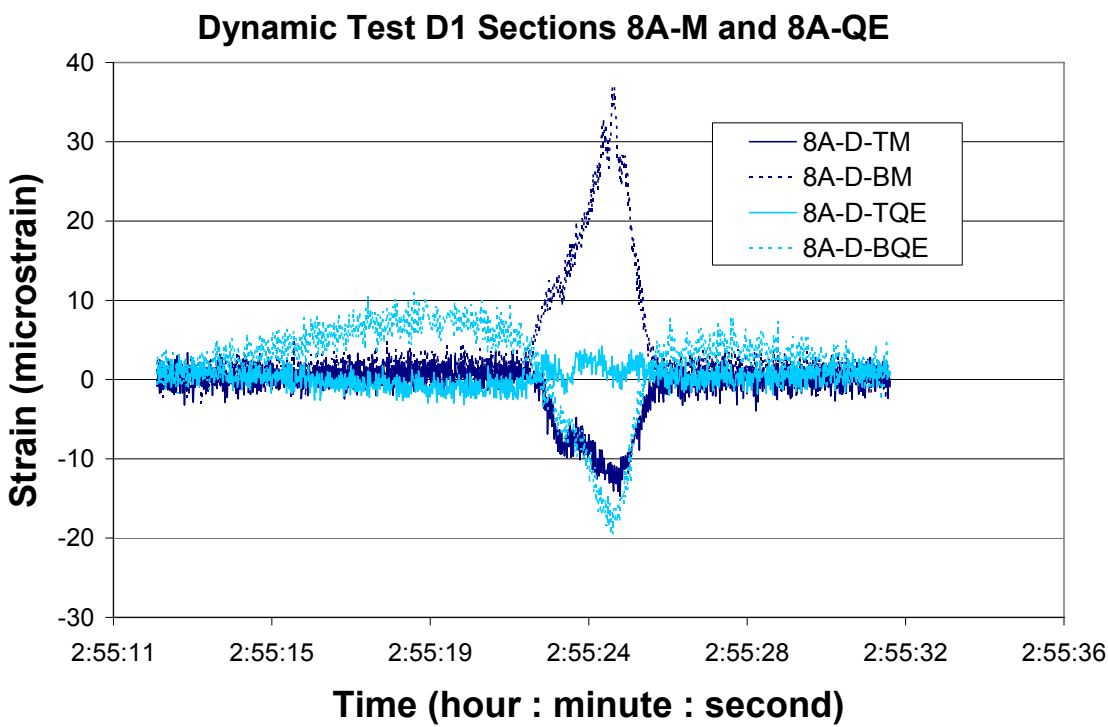


Figure E-30

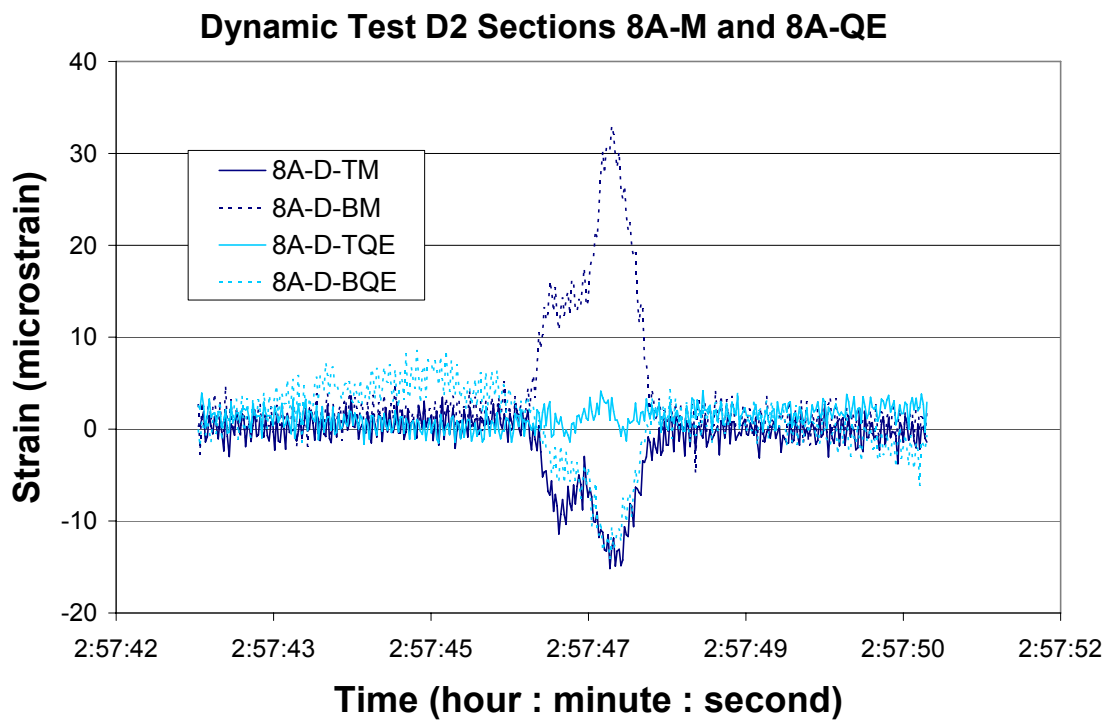


Figure E-31

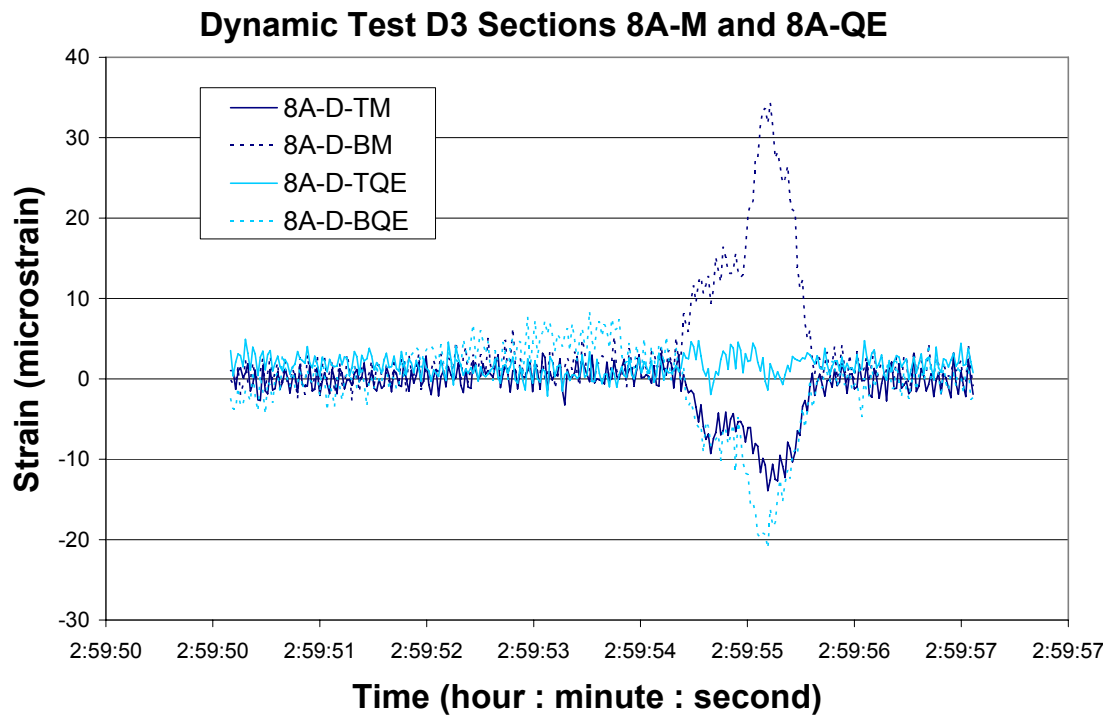


Figure E-32

E.2 Dynamic Impact Factors

Dynamic Impact Factors for Dynamic Test D1 vs Static Subset S1-S6							
Location	Gage	Maximum Strain ($\mu\epsilon$)		Minimum Strain ($\mu\epsilon$)		+ DIF	- DIF
		+ Static	+ Dynamic	- Static	- Dynamic		
GC BC	9L-GC-BC	57.2	73.9	-37.7	-47.3	1.29	1.25
	9N-GC-BC	43.4	46.5	-53.5	-62.2	1.07	1.16
	9O-GC-BC	-9.2	13.5	-40.7	-48.5	low static	1.19
	8C-GC-BC	10.7	28.2	-47.6	-57.3	low static	1.20
	8D-GC-BC	71.3	85.4	-19.2	-26.3	1.20	low static
GA BC	9L-GA-BC	65.4	89.3	-48.4	-64.3	1.37	1.33
	9N-GA-BC	30.6	40.8	-46.6	-57.7	1.33	1.24
	9O-GA-BCH	-5.0	12.6	-32.1	-41.6	low static	1.30
	9O-GA-BC45	-5.8	13.5	-29.6	-42.9	low static	1.45
	9O-GA-BCV	11.6	8.8	-6.7	-7.8	low static	low static
	8C-GA-BC	6.6	22.7	-33.8	-45.6	low static	1.35
	8D-GA-BC	61.4	76.1	-20.1	-27.9	1.24	low static
GC TC	9L-GC-TC	2.0	4.6	-1.5	-5.2	low static	low static
	9N-GC-TC	1.9	4.2	0.3	-5.7	low static	low static
	9O-GC-TC	3.2	9.2	-0.6	-5.4	low static	low static
	8C-GC-TC	-2.7	11.6	-5.9	-8.5	low static	low static
	8D-GC-TC	-0.7	7.0	-2.5	-8.0	low static	low static
GA TC	9L-GA-TC	1.8	2.4	-1.5	-5.2	low static	low static
	9N-GA-TC	3.3	4.2	0.4	-9.5	low static	low static
	9O-GA-TCH	12.3	12.8	4.0	-4.4	low static	low static
	9O-GA-TC45	-3.3	8.8	-29.9	-39.8	low static	1.33
	9O-GA-TCV	7.0	6.4	-15.7	-21.7	low static	low static
	8C-GA-TC	3.3	5.2	0.2	-5.1	low static	low static
	8D-GA-TC	0.0	5.0	-6.9	-9.5	low static	low static
GC BE	9O-GC-BE	-1.2	17.3	-46.7	-54.6	low static	1.17
	8D-GC-BE	77.5	92.0	-20.1	-27.9	1.19	low static
GC BI	9O-GC-BI	-12.0	14.5	-43.4	-51.6	low static	1.19
	8D-GC-BI	77.3	112.3	-22.5	-29.0	1.45	low static
GA BE	9O-GA-BE	-7.1	13.9	-33.0	-41.9	low static	1.27
GA BI	9O-GA-BI	-1.2	13.7	-37.6	-42.8	low static	1.14
8D-GA-BI	61.1	59.6	-19.2	-4.8	0.98	low static	
GC TE	9O-GC-TE	2.3	9.1	-3.3	-5.4	low static	low static
8D-GC-TE	-2.1	4.6	-7.6	-14.0	low static	low static	
GC TI	9O-GC-TI	3.5	13.0	-0.9	-5.6	low static	low static
8D-GC-TI	-1.5	3.9	-5.2	-10.0	low static	low static	
GA TE	9O-GA-TE	13.2	14.6	0.3	-4.8	low static	low static
GA TI	9O-GA-TI	11.5	15.4	2.5	-3.8	low static	low static
GC W	9O-GC-W	14.2	19.0	1.5	-8.4	low static	low static
8D-GC-W	32.3	43.0	-8.4	-14.9	1.33	low static	
GA W	9O-GA-WH	7.7	11.0	-7.4	-6.0	low static	low static
	9O-GA-W45	12.7	11.7	-14.3	-19.0	low static	low static
	9O-GA-WV	14.2	15.6	-3.9	-7.2	low static	low static
	8D-GA-W	18.3	26.9	-6.5	-11.8	low static	low static
8A Diaphragm	8A-D-TI	19.6	27.3	-1.5	-2.8	low static	low static
	8A-D-TQI	4.3	7.7	-3.8	-10.4	low static	low static
	8A-D-BQI	3.3	3.2	-3.8	-6.8	low static	low static
	8A-D-TM	1.1	4.0	-0.8	-14.7	low static	low static
	8A-D-BM	19.1	36.9	1.2	-3.6	low static	low static
	8A-D-TQE	0.5	4.5	-1.2	-3.1	low static	low static
	8A-D-BQE	8.7	11.0	-8.3	-19.6	low static	low static
	8A-D-TE	11.6	24.7	0.0	-1.7	low static	low static
	8A-D-BE	5.2	7.9	-4.4	-12.5	low static	low static
Lateral Bracing	9K-LBU-CN	36.8	66.9	-3.3	-9.0	1.82	low static
	9O-LBD-CN	24.9	42.7	-9.2	-18.7	low static	low static
	8B-LBU-CN	30.5	39.8	-7.6	-19.1	1.30	low static
	8D-LBU-CN	45.9	59.6	-4.5	-4.8	1.30	low static
	8F-LBD-CN	22.7	77.1	1.3	-8.4	low static	low static
Web Gap	9I-GPC-WG	9.5	14.1	-40.1	-49.4	low static	1.23
	8E-GPC-WG	4.4	11.2	-27.7	-37.9	low static	1.37
	9I-GPA-WG	4.2	11.9	-26.9	-27.5	low static	1.02

Table E-1

Dynamic Impact Factors for Dynamic Test D2 vs Static Subset S1-S6							
Location	Gage	Maximum Strain ($\mu\epsilon$)		Minimum Strain ($\mu\epsilon$)		+ DIF	- DIF
		+ Static	+ Dynamic	- Static	- Dynamic		
GC BC	10Z-GC-BC	13.5	27.9	-34.4	-42.6	low static	1.24
	9B-GC-BC	13.7	17.8	-34.9	-46.3	low static	1.33
	9C-GC-BC	48.6	51.0	-2.3	-36.2	1.05	low static
	9H-GC-BC	65.5	73.8	-13.8	-26.4	1.13	low static
	9J-GC-BC	79.8	73.3	-24.3	-31.8	0.92	low static
	9L-GC-BC	57.2	66.0	-37.7	-47.7	1.15	1.26
	9N-GC-BC	43.4	37.8	-53.5	-63.0	0.87	1.18
	9O-GC-BC	-9.2	10.4	-40.7	-49.8	low static	1.22
	8C-GC-BC	10.7	16.6	-47.6	-52.8	low static	1.11
	8D-GC-BC	71.3	84.2	-19.2	-26.0	1.18	low static
GA BC	9B-GA-BC	15.1	19.1	-33.1	-41.5	low static	1.26
	9C-GA-BC	40.7	55.0	-1.2	-34.8	1.35	low static
	9H-GA-BC	72.6	86.8	-16.8	-33.3	1.20	low static
	9J-GA-BC	98.0	104.5	-33.6	-43.4	1.07	1.29
	9L-GA-BC	65.4	86.9	-48.4	-62.3	1.33	1.29
	9N-GA-BC	30.6	37.8	-46.6	-60.5	1.23	1.30
	9O-GA-BCH	-5.0	9.6	-32.1	-41.4	low static	1.29
	9O-GA-BC45	-5.8	10.9	-29.6	-40.7	low static	1.38
	9O-GA-BCV	11.6	9.6	-6.7	-7.1	low static	low static
	8C-GA-BC	6.6	22.0	-33.8	-43.5	low static	1.28
GC TC	8D-GA-BC	61.4	82.0	-20.1	-25.4	1.34	low static
	10Z-GC-TC	3.8	5.4	-0.8	-9.1	low static	low static
	9B-GC-TC	3.1	12.0	-3.4	-3.5	low static	low static
	9C-GC-TC	-0.1	4.7	-3.7	-5.0	low static	low static
	9H-GC-TC	0.3	4.1	-2.7	-6.4	low static	low static
	9J-GC-TC	0.8	2.8	-2.0	-5.9	low static	low static
	9L-GC-TC	2.0	4.7	-1.5	-6.7	low static	low static
	9N-GC-TC	1.9	5.5	0.3	-6.8	low static	low static
	9O-GC-TC	3.2	5.7	-0.6	-4.5	low static	low static
	8C-GC-TC	-2.7	8.3	-5.9	-8.2	low static	low static
GA TC	8D-GC-TC	-0.7	4.5	-2.5	-7.6	low static	low static
	10Z-GA-TC	2.6	3.4	-3.2	-4.9	low static	low static
	9C-GA-TC	0.8	4.6	-3.2	-3.8	low static	low static
	9H-GA-TC	6.7	7.3	-0.6	-3.9	low static	low static
	9J-GA-TC	7.0	11.0	-1.1	-4.5	low static	low static
	9L-GA-TC	1.8	3.8	-1.5	-5.2	low static	low static
	9N-GA-TC	3.3	4.1	0.4	-4.5	low static	low static
	9O-GA-TCH	12.3	14.4	4.0	-4.2	low static	low static
	9O-GA-TC45	-3.3	7.2	-29.9	-42.9	low static	1.43
	9O-GA-TCV	7.0	4.1	-15.7	-22.7	low static	low static
GC BE	8C-GA-TC	3.3	7.2	0.2	-4.2	low static	low static
	8D-GA-TC	0.0	5.4	-6.9	-6.7	low static	low static
	9B-GC-BE	13.1	18.3	-43.6	-54.0	low static	1.24
	9J-GC-BE	96.0	88.7	-28.0	-35.3	0.92	1.26
GC BI	9O-GC-BE	-1.2	12.3	-46.7	-56.4	low static	1.21
	8D-GC-BE	77.5	96.0	-20.1	-24.1	1.24	low static
	9B-GC-BI	14.7	18.1	-32.7	-43.1	low static	1.32
	9J-GC-BI	84.8	89.8	-27.8	-35.9	1.06	1.29
GA BE	9O-GC-BI	-12.0	11.4	-43.4	-49.9	low static	1.15
	8D-GC-BI	77.3	103.4	-22.5	-25.7	1.34	low static
	9B-GA-BE	15.4	18.4	-33.7	-42.5	low static	1.26
GA BI	9J-GA-BE	95.9	108.7	-35.7	-46.9	1.13	1.32
	9O-GA-BE	-7.1	12.3	-33.0	-42.7	low static	1.29
	9B-GA-BI	14.3	19.3	-30.5	-37.3	low static	1.23
GA BI	9J-GA-BI	76.2	87.0	-27.3	-36.1	1.14	1.32
	9O-GA-BI	-1.2	10.3	-37.6	-43.9	low static	1.17
	8D-GA-BI	61.1	48.4	-19.2	-3.5	0.79	low static
GC TE	9B-GC-TE	5.9	13.8	-3.9	-2.8	low static	low static
	9J-GC-TE	-0.1	4.6	-5.9	-8.2	low static	low static
	9O-GC-TE	2.3	8.0	-3.3	-1.5	low static	low static
	8D-GC-TE	-2.1	2.6	-7.6	-14.7	low static	low static

continued on next page

Table E-2

Dynamic Impact Factors for Dynamic Test D2 vs Static Subset S1-S6 (continued)								
Location	Gage	Maximum Strain ($\mu\epsilon$)		Minimum Strain ($\mu\epsilon$)			+ DIF	- DIF
		+ Static	+ Dynamic	- Static	- Dynamic			
GC TI	9B-GC-TI	2.3	14.6	-4.3	-3.8	low static	low static	
	9J-GC-TI	-0.1	4.1	-4.6	-5.8	low static	low static	
	9O-GC-TI	3.5	5.7	-0.9	-6.1	low static	low static	
	8D-GC-TI	-1.5	6.1	-5.2	-15.0	low static	low static	
GA TE	9B-GA-TE	-1.7	7.9	-3.2	-4.1	low static	low static	
	9J-GA-TE	0.0	6.2	-3.9	-5.9	low static	low static	
	9O-GA-TE	13.2	16.5	0.3	-4.8	low static	low static	
GA TI	9O-GA-TI	11.5	15.6	2.5	-2.9	low static	low static	
GC W	9B-GC-W	8.1	12.1	-3.3	-3.7	low static	low static	
	9J-GC-W	3.9	8.5	-10.4	-11.9	low static	low static	
	9O-GC-W	14.2	17.6	1.5	-6.8	low static	low static	
	8D-GC-W	32.3	41.9	-8.4	-13.7	1.30	low static	
GA W	9B-GA-W	10.9	14.2	-16.6	-26.6	low static	low static	
	9J-GA-W	55.1	73.9	-17.2	-30.1	1.34	low static	
	9O-GA-WH	7.7	11.7	-7.4	-4.8	low static	low static	
	9O-GA-W45	12.7	11.9	-14.3	-20.7	low static	low static	
	9O-GA-WV	14.2	14.6	-3.9	-6.5	low static	low static	
	8D-GA-W	18.3	29.5	-6.5	-10.7	low static	low static	
9F Diaphragm	9F-D-TI	33.7	49.0	-2.5	-3.7	1.45	low static	
	9F-D-BI	0.5	5.0	-2.4	-8.4	low static	low static	
	9F-D-TQI	1.7	8.4	-2.0	-3.3	low static	low static	
	9F-D-BQI	26.9	28.2	-0.6	-6.1	1.05	low static	
	9F-D-TM	0.0	3.4	-9.1	-12.2	low static	low static	
	9F-D-BM	44.5	62.6	-2.3	-6.1	1.41	low static	
	9F-D-TQE	4.7	7.1	-0.9	-3.9	low static	low static	
	9F-D-BQE	2.5	17.7	-10.9	-9.7	low static	low static	
	9F-D-TE	34.9	40.9	1.4	-2.2	1.17	low static	
	9F-D-BE	2.1	4.2	-2.9	-10.7	low static	low static	
8A Diaphragm	8A-D-TI	19.6	27.3	-1.5	-3.7	low static	low static	
	8A-D-TQI	4.3	7.5	-3.8	-8.9	low static	low static	
	8A-D-BQI	3.3	4.7	-3.8	-7.7	low static	low static	
	8A-D-TM	1.1	3.6	-0.8	-15.2	low static	low static	
	8A-D-BM	19.1	33.0	1.2	-4.8	low static	low static	
	8A-D-TQE	0.5	5.4	-1.2	-1.6	low static	low static	
	8A-D-BQE	8.7	8.6	-8.3	-14.1	low static	low static	
	8A-D-TE	11.6	27.6	0.0	--	low static	--	
	8A-D-BE	5.2	7.9	-4.4	-12.8	low static	low static	
Lateral Bracing	9E-LBU-CN	47.6	57.9	-3.6	-16.7	1.21	low static	
	9E-LBU-BC	57.3	69.0	-3.3	-18.4	1.20	low static	
	9E-LBU-BE	57.5	66.6	-1.6	-18.5	1.16	low static	
	9E-LBU-BI	55.2	64.4	-4.1	-20.9	1.17	low static	
	9E-LBU-TC	9.3	16.2	-2.1	-6.8	low static	low static	
	9E-LBD-CN	62.8	79.1	-9.3	-13.6	1.26	low static	
	9G-LBU-CN	28.9	49.3	-2.3	-12.8	1.70	low static	
	9G-LBD-CN	39.9	71.5	-9.0	-11.6	1.79	low static	
	9K-LBU-CN	36.8	63.1	-3.3	-8.7	1.71	low static	
	9K-LBD-CN	36.2	59.0	-3.0	-9.2	1.63	low static	
	9O-LBD-CN	24.9	41.8	-9.2	-22.7	low static	low static	
	8B-LBU-CN	30.5	38.2	-7.6	-17.1	1.25	low static	
	8D-LBU-CN	45.9	48.4	-4.5	-3.5	1.05	low static	
	8F-LBD-CN	22.7	68.9	1.3	-8.8	low static	low static	
Web Gap	9F-GPC-WG	1.9	10.6	-20.2	-22.5	low static	low static	
	9I-GPC-WG	9.5	13.3	-40.1	-43.3	low static	1.08	
	8E-GPC-WG	4.4	14.2	-27.7	-37.6	low static	1.36	
	9F-GPA-WG	0.4	5.4	-8.1	-20.0	low static	low static	
	9I-GPA-WG	4.2	8.4	-26.9	-29.7	low static	1.11	
Gusset Plate	9F-GPA-LO	32.3	38.6	-4.7	-21.1	1.20	low static	
	9F-GPA-TR	3.1	6.8	-12.3	-17.3	low static	low static	
	9F-GPA-45	15.6	28.7	-2.9	-5.9	low static	low static	
	9F-GPA-W9	125.9	179.0	-21.1	-78.3	1.42	low static	
	9F-GPA-W8	117.0	147.9	-20.4	-74.0	1.26	low static	

Table E-3

Dynamic Impact Factors for Dynamic Test D3 vs Static Subset S1-S6							
Location	Gage	Maximum Strain ($\mu\epsilon$)		Minimum Strain ($\mu\epsilon$)		+ DIF	- DIF
		+ Static	+ Dynamic	- Static	- Dynamic		
GC BC	10Z-GC-BC	13.5	26.0	-34.4	-44.9	low static	1.31
	9B-GC-BC	13.7	20.3	-34.9	-49.1	low static	1.41
	9C-GC-BC	48.6	50.1	-2.3	-34.9	1.03	low static
	9H-GC-BC	65.5	76.0	-13.8	-28.9	1.16	low static
	9J-GC-BC	79.8	85.8	-24.3	-33.0	1.08	low static
	9L-GC-BC	57.2	66.9	-37.7	-49.7	1.17	1.32
	9N-GC-BC	43.4	40.8	-53.5	-67.0	0.94	1.25
	9O-GC-BC	-9.2	13.0	-40.7	-52.2	low static	1.28
	8C-GC-BC	10.7	21.1	-47.6	-57.6	low static	1.21
	8D-GC-BC	71.3	92.4	-19.2	-29.0	1.30	low static
GA BC	9B-GA-BC	15.1	20.0	-33.1	-47.6	low static	1.44
	9C-GA-BC	40.7	57.0	-1.2	-35.4	1.40	low static
	9H-GA-BC	72.6	93.5	-16.8	-40.4	1.29	low static
	9J-GA-BC	98.0	117.1	-33.6	-46.1	1.19	1.37
	9L-GA-BC	65.4	85.7	-48.4	-65.9	1.31	1.36
	9N-GA-BC	30.6	39.1	-46.6	-62.7	1.28	1.34
	9O-GA-BCH	-5.0	14.8	-32.1	-42.4	low static	1.32
	9O-GA-BC45	-5.8	15.8	-29.6	-43.6	low static	1.47
	9O-GA-BCV	11.6	8.2	-6.7	-9.4	low static	low static
	8C-GA-BC	6.6	20.8	-33.8	-44.4	low static	1.31
GC TC	8D-GA-BC	61.4	83.4	-20.1	-28.2	1.36	low static
	10Z-GC-TC	3.8	5.1	-0.8	-11.3	low static	low static
	9B-GC-TC	3.1	11.3	-3.4	-3.0	low static	low static
	9C-GC-TC	-0.1	5.4	-3.7	-5.4	low static	low static
	9H-GC-TC	0.3	4.2	-2.7	-7.5	low static	low static
	9J-GC-TC	0.8	3.5	-2.0	-6.6	low static	low static
	9L-GC-TC	2.0	3.9	-1.5	-6.9	low static	low static
	9N-GC-TC	1.9	4.3	0.3	-6.5	low static	low static
	9O-GC-TC	3.2	7.0	-0.6	-4.2	low static	low static
	8C-GC-TC	-2.7	9.6	-5.9	-7.8	low static	low static
GA TC	8D-GC-TC	-0.7	7.3	-2.5	-11.3	low static	low static
	10Z-GA-TC	2.6	4.5	-3.2	-5.9	low static	low static
	9C-GA-TC	0.8	5.9	-3.2	-2.4	low static	low static
	9H-GA-TC	6.7	9.1	-0.6	-5.3	low static	low static
	9J-GA-TC	7.0	14.1	-1.1	-5.4	low static	low static
	9L-GA-TC	1.8	3.6	-1.5	-5.3	low static	low static
	9N-GA-TC	3.3	3.7	0.4	-4.6	low static	low static
	9O-GA-TCH	12.3	15.1	4.0	-5.0	low static	low static
	9O-GA-TC45	-3.3	7.7	-29.9	-39.1	low static	1.31
	9O-GA-TCV	7.0	6.9	-15.7	-21.8	low static	low static
GC BE	8C-GA-TC	3.3	4.1	0.2	-7.4	low static	low static
	8D-GA-TC	0.0	6.1	-6.9	-7.5	low static	low static
	9B-GC-BE	13.1	19.7	-43.6	-59.1	low static	1.36
	9J-GC-BE	96.0	94.4	-28.0	-34.7	0.98	1.24
GC BI	9O-GC-BE	-1.2	15.4	-46.7	-58.7	low static	1.26
	8D-GC-BE	77.5	85.5	-20.1	-27.7	1.10	low static
	9B-GC-BI	14.7	20.0	-32.7	-44.3	low static	1.36
	9J-GC-BI	84.8	99.0	-27.8	-36.7	1.17	1.32
GA BE	9O-GC-BI	-12.0	15.4	-43.4	-55.3	low static	1.27
	8D-GC-BI	77.3	116.9	-22.5	-29.1	1.51	low static
	9B-GA-BE	15.4	21.1	-33.7	-49.0	low static	1.45
	9J-GA-BE	95.9	122.2	-35.7	-47.4	1.27	1.33
GA BI	9O-GA-BE	-7.1	15.3	-33.0	-43.3	low static	1.31
	9B-GA-BI	14.3	22.3	-30.5	-42.7	low static	1.40
	9J-GA-BI	76.2	90.7	-27.3	-37.8	1.19	1.39
	9O-GA-BI	-1.2	15.8	-37.6	-44.5	low static	1.18
GC TE	8D-GA-BI	61.1	52.7	-19.2	-4.6	0.86	low static
	9B-GC-TE	5.9	13.5	-3.9	-2.7	low static	low static
	9J-GC-TE	-0.1	4.9	-5.9	-10.2	low static	low static
	9O-GC-TE	2.3	8.1	-3.3	-1.6	low static	low static
continued on next page							

Table E-4

Dynamic Impact Factors for Dynamic Test D3 vs Static Subset S1-S6 (continued)								
Location	Gage	Maximum Strain ($\mu\epsilon$)		Minimum Strain ($\mu\epsilon$)		+ DIF	- DIF	
		+ Static	+ Dynamic	- Static	- Dynamic			
GC TI	9B-GC-TI	2.3	12.2	-4.3	-3.2	low static	low static	
	9J-GC-TI	-0.1	4.0	-4.6	-6.4	low static	low static	
	9O-GC-TI	3.5	6.7	-0.9	-4.2	low static	low static	
	8D-GC-TI	-1.5	6.0	-5.2	-11.6	low static	low static	
GA TE	9B-GA-TE	-1.7	8.9	-3.2	-4.9	low static	low static	
	9J-GA-TE	0.0	5.1	-3.9	-6.1	low static	low static	
	9O-GA-TE	13.2	17.3	0.3	-5.2	low static	low static	
GA TI	9O-GA-TI	11.5	15.8	2.5	-4.9	low static	low static	
GC W	9B-GC-W	8.1	12.7	-3.3	-3.5	low static	low static	
	9J-GC-W	3.9	7.4	-10.4	-10.4	low static	low static	
	9O-GC-W	14.2	18.6	1.5	-8.2	low static	low static	
	8D-GC-W	32.3	45.7	-8.4	-14.4	1.41	low static	
GA W	9B-GA-W	10.9	15.9	-16.6	-28.1	low static	low static	
	9J-GA-W	55.1	83.2	-17.2	-30.3	1.51	low static	
	9O-GA-WH	7.7	10.7	-7.4	-5.7	low static	low static	
	9O-GA-W45	12.7	12.6	-14.3	-20.2	low static	low static	
	9O-GA-WV	14.2	15.1	-3.9	-9.3	low static	low static	
	8D-GA-W	18.3	29.5	-6.5	-10.6	low static	low static	
9F Diaphragm	9F-D-TI	33.7	47.2	-2.5	-3.8	1.40	low static	
	9F-D-BI	0.5	9.0	-2.4	-9.6	low static	low static	
	9F-D-TQI	1.7	8.0	-2.0	-3.1	low static	low static	
	9F-D-BQI	26.9	27.6	-0.6	-5.4	1.03	low static	
	9F-D-TM	0.0	2.8	-9.1	-11.6	low static	low static	
	9F-D-BM	44.5	62.4	-2.3	-6.7	1.40	low static	
	9F-D-TQE	4.7	8.1	-0.9	-3.9	low static	low static	
	9F-D-BQE	2.5	22.4	-10.9	-8.9	low static	low static	
	9F-D-TE	34.9	40.6	1.4	-2.1	1.16	low static	
	9F-D-BE	2.1	9.1	-2.9	-11.1	low static	low static	
8A Diaphragm	8A-D-TI	19.6	27.5	-1.5	-1.7	low static	low static	
	8A-D-TQI	4.3	7.8	-3.8	-9.4	low static	low static	
	8A-D-BQI	3.3	6.1	-3.8	-4.0	low static	low static	
	8A-D-TM	1.1	3.5	-0.8	-13.9	low static	low static	
	8A-D-BM	19.1	34.3	1.2	-3.4	low static	low static	
	8A-D-TQE	0.5	5.9	-1.2	-2.5	low static	low static	
	8A-D-BQE	8.7	8.4	-8.3	-21.1	low static	low static	
	8A-D-TE	11.6	25.4	0.0	--	low static	--	
	8A-D-BE	5.2	7.2	-4.4	-14.5	low static	low static	
Lateral Bracing	9E-LBU-CN	47.6	59.0	-3.6	-13.0	1.24	low static	
	9E-LBU-BC	57.3	72.4	-3.3	-15.6	1.26	low static	
	9E-LBU-BE	57.5	68.5	-1.6	-16.1	1.19	low static	
	9E-LBU-BI	55.2	68.5	-4.1	-16.8	1.24	low static	
	9E-LBU-TC	9.3	15.3	-2.1	-8.0	low static	low static	
	9E-LBD-CN	62.8	80.7	-9.3	-19.4	1.29	low static	
	9G-LBU-CN	28.9	48.7	-2.3	-14.2	1.68	low static	
	9G-LBD-CN	39.9	70.1	-9.0	-12.5	1.76	low static	
	9K-LBU-CN	36.8	65.8	-3.3	-11.0	1.79	low static	
	9K-LBD-CN	36.2	65.1	-3.0	-11.0	1.80	low static	
	9O-LBD-CN	24.9	46.6	-9.2	-17.3	low static	low static	
	8B-LBU-CN	30.5	39.7	-7.6	-16.0	1.30	low static	
	8D-LBU-CN	45.9	52.7	-4.5	-4.6	1.15	low static	
Web Gap	9F-GPC-WG	1.9	10.7	-20.2	-22.4	low static	low static	
	9I-GPC-WG	9.5	13.3	-40.1	-46.9	low static	1.17	
	8E-GPC-WG	4.4	12.0	-27.7	-41.0	low static	1.48	
	9F-GPA-WG	0.4	5.7	-8.1	-19.5	low static	low static	
	9I-GPA-WG	4.2	10.5	-26.9	-29.9	low static	1.11	
Gusset Plate	9F-GPA-LO	32.3	40.4	-4.7	-23.2	1.25	low static	
	9F-GPA-TR	3.1	16.8	-12.3	-22.1	low static	low static	
	9F-GPA-45	15.6	28.3	-2.9	-9.8	low static	low static	
	9F-GPA-W9	125.9	187.5	-21.1	-89.1	1.49	low static	
	9F-GPA-W8	117.0	157.8	-20.4	-89.6	1.35	low static	

Table E-5

Dynamic Impact Factors for Dynamic Test D5 vs Static Subset S1-S6							
Location	Gage	Maximum Strain ($\mu\epsilon$)		Minimum Strain ($\mu\epsilon$)		+ DIF	- DIF
		+ Static	+ Dynamic	- Static	- Dynamic		
GC BC	9L-GC-BC	57.2	73.6	-37.7	-48.0	1.29	1.27
	9N-GC-BC	43.4	40.9	-53.5	-58.1	0.94	1.09
	9O-GC-BC	-9.2	15.7	-40.7	-47.5	low static	1.17
	8C-GC-BC	10.7	31.2	-47.6	-72.6	low static	1.53
	8D-GC-BC	71.3	76.8	-19.2	-32.8	1.08	low static
GA BC	9L-GA-BC	65.4	87.9	-48.4	-66.1	1.34	1.37
	9N-GA-BC	30.6	36.0	-46.6	-57.1	1.18	1.23
	9O-GA-BCH	-5.0	17.2	-32.1	-45.4	low static	1.42
	9O-GA-BC45	-5.8	22.6	-29.6	-55.7	low static	1.88
	9O-GA-BCV	11.6	8.6	-6.7	-9.8	low static	low static
	8C-GA-BC	6.6	27.5	-33.8	-62.4	low static	1.84
GC TC	9L-GC-TC	2.0	4.4	-1.5	-5.5	low static	low static
	9N-GC-TC	1.9	4.7	0.3	-5.2	low static	low static
	9O-GC-TC	3.2	16.7	-0.6	-8.7	low static	low static
	8C-GC-TC	-2.7	8.1	-5.9	-7.2	low static	low static
	8D-GC-TC	-0.7	5.1	-2.5	-8.9	low static	low static
GA TC	9L-GA-TC	1.8	1.2	-1.5	-6.7	low static	low static
	9N-GA-TC	3.3	6.3	0.4	-6.2	low static	low static
	9O-GA-TCH	12.3	14.5	4.0	-6.6	low static	low static
	9O-GA-TC45	-3.3	12.9	-29.9	-42.1	low static	1.41
	9O-GA-TCV	7.0	9.8	-15.7	-31.5	low static	low static
	8C-GA-TC	3.3	7.3	0.2	-10.6	low static	low static
GC BE	9O-GC-BE	-1.2	17.2	-46.7	-53.9	low static	1.15
	8D-GC-BE	77.5	86.4	-20.1	-32.0	1.11	low static
	GC BI	9O-GC-BI	-12.0	18.9	-43.4	-49.1	low static
GA BE	8D-GC-BI	77.3	96.2	-22.5	-35.0	1.24	low static
	9O-GA-BE	-7.1	17.9	-33.0	-43.7	low static	1.32
	9O-GA-BI	-1.2	18.4	-37.6	-46.4	low static	1.24
GA BI	8D-GA-BI	61.1	54.1	-19.2	-9.2	0.89	low static
	9O-GC-TE	2.3	7.3	-3.3	-4.1	low static	low static
	8D-GC-TE	-2.1	15.2	-7.6	-14.7	low static	low static
GC TI	9O-GC-TI	3.5	4.5	-0.9	-8.2	low static	low static
	8D-GC-TI	-1.5	4.8	-5.2	-10.3	low static	low static
GA TE	9O-GA-TE	13.2	14.7	0.3	-11.2	low static	low static
	9O-GA-TI	11.5	15.1	2.5	-14.1	low static	low static
GC W	9O-GC-W	14.2	18.9	1.5	-11.1	low static	low static
	8D-GC-W	32.3	39.4	-8.4	-14.6	1.22	low static
GA W	9O-GA-WH	7.7	15.1	-7.4	-6.7	low static	low static
	9O-GA-W45	12.7	11.3	-14.3	-19.6	low static	low static
	9O-GA-WV	14.2	22.3	-3.9	-10.4	low static	low static
	8D-GA-W	18.3	27.5	-6.5	-14.7	low static	low static
8A Diaphragm	8A-D-TI	19.6	26.7	-1.5	-2.2	low static	low static
	8A-D-TQI	4.3	7.3	-3.8	-10.8	low static	low static
	8A-D-BQI	3.3	5.6	-3.8	-8.6	low static	low static
	8A-D-TM	1.1	5.9	-0.8	-15.7	low static	low static
	8A-D-BM	19.1	35.3	1.2	-4.7	low static	low static
	8A-D-TQE	0.5	4.6	-1.2	-3.6	low static	low static
	8A-D-BQE	8.7	11.4	-8.3	-13.8	low static	low static
	8A-D-TE	11.6	26.8	0.0	-1.8	low static	low static
Lateral Bracing	8A-D-BE	5.2	8.1	-4.4	-12.1	low static	low static
	9K-LBD-CN	36.8	68.4	-3.3	-10.5	1.86	low static
	9O-LBD-CN	24.9	39.2	-9.2	-29.8	low static	low static
	8B-LBU-CN	30.5	35.2	-7.6	-28.9	1.15	low static
	8D-LBU-CN	45.9	54.1	-4.5	-9.2	1.18	low static
Web Gap	8F-LBD-CN	22.7	78.3	1.3	-8.5	low static	low static
	9I-GPC-WG	9.5	14.9	-40.1	-54.7	low static	1.36
	8E-GPC-WG	4.4	12.0	-27.7	-35.0	low static	1.26
Web Gap	9I-GPA-WG	4.2	10.0	-26.9	-32.9	low static	1.23

Table E-6

Dynamic Impact Factors for Dynamic Test D6 vs Static Subset S1-S6							
Location	Gage	Maximum Strain ($\mu\epsilon$)		Minimum Strain ($\mu\epsilon$)		+ DIF	- DIF
		+ Static	+ Dynamic	- Static	- Dynamic		
GC BC	10Z-GC-BC	13.5	38.5	-34.4	-58.3	low static	1.70
	9B-GC-BC	13.7	18.0	-34.9	-62.0	low static	1.78
	9C-GC-BC	48.6	74.1	-2.3	-34.4	1.53	low static
	9H-GC-BC	65.5	121.0	-13.8	-33.9	1.85	low static
	9J-GC-BC	79.8	112.4	-24.3	-36.4	1.41	low static
GA BC	9B-GA-BC	15.1	19.3	-33.1	-59.0	low static	1.79
	9C-GA-BC	40.7	64.9	-1.2	-34.1	1.59	low static
	9H-GA-BC	72.6	126.2	-16.8	-42.1	1.74	low static
	9J-GA-BC	98.0	143.4	-33.6	-50.9	1.46	1.52
GC TC	10Z-GC-TC	3.8	9.3	-0.8	-13.7	low static	low static
	9B-GC-TC	3.1	15.9	-3.4	-5.7	low static	low static
	9C-GC-TC	-0.1	10.7	-3.7	-5.2	low static	low static
	9H-GC-TC	0.3	17.7	-2.7	-7.0	low static	low static
	9J-GC-TC	0.8	1.2	-2.0	-8.7	low static	low static
GA TC	10Z-GA-TC	2.6	2.6	-3.2	-7.6	low static	low static
	9C-GA-TC	0.8	3.9	-3.2	-7.9	low static	low static
	9H-GA-TC	6.7	4.5	-0.6	-7.0	low static	low static
	9J-GA-TC	7.0	10.9	-1.1	-6.8	low static	low static
GC BE	9B-GC-BE	13.1	19.2	-43.6	-72.6	low static	1.67
	9J-GC-BE	96.0	120.9	-28.0	-37.2	1.26	1.33
GC BI	9B-GC-BI	14.7	19.7	-32.7	-56.9	low static	1.74
	9J-GC-BI	84.8	141.2	-27.8	-39.3	1.67	1.41
GA BE	9B-GA-BE	15.4	20.2	-33.7	-57.4	low static	1.70
	9J-GA-BE	95.9	158.2	-35.7	-50.7	1.65	1.42
GA BI	9B-GA-BI	14.3	20.7	-30.5	-53.2	low static	1.75
	9J-GA-BI	76.2	109.6	-27.3	-40.6	1.44	1.49
GC TE	9B-GC-TE	5.9	17.2	-3.9	-6.5	low static	low static
	9J-GC-TE	-0.1	2.4	-5.9	-12.8	low static	low static
GC TI	9B-GC-TI	2.3	15.3	-4.3	-5.1	low static	low static
	9J-GC-TI	-0.1	2.5	-4.6	-6.4	low static	low static
GA TE	9B-GA-TE	-1.7	6.4	-3.2	-6.8	low static	low static
	9J-GA-TE	0.0	2.7	-3.9	-9.6	low static	low static
GC W	9B-GC-W	8.1	16.6	-3.3	-4.1	low static	low static
	9J-GC-W	3.9	5.9	-10.4	-15.4	low static	low static
GA W	9B-GA-W	10.9	15.9	-16.6	-35.7	low static	low static
	9J-GA-W	55.1	106.9	-17.2	-31.9	1.94	low static
9F Diaphragm	9F-D-TI	33.7	57.2	-2.5	-5.8	1.70	low static
	9F-D-BI	0.5	4.8	-2.4	-12.7	low static	low static
	9F-D-TQI	1.7	9.7	-2.0	-6.0	low static	low static
	9F-D-BQI	26.9	41.9	-0.6	-6.3	1.56	low static
	9F-D-TM	0.0	1.3	-9.1	-13.7	low static	low static
	9F-D-BM	44.5	68.0	-2.3	-7.8	1.53	low static
	9F-D-TQE	4.7	6.1	-0.9	-5.8	low static	low static
	9F-D-BQE	2.5	6.9	-10.9	-15.6	low static	low static
	9F-D-TE	34.9	36.4	1.4	-4.0	1.04	low static
	9F-D-BE	2.1	3.2	-2.9	-13.7	low static	low static
Lateral Bracing	9E-LBU-CN	47.6	70.6	-3.6	-9.7	1.48	low static
	9E-LBU-BC	57.3	82.6	-3.3	-11.3	1.44	low static
	9E-LBU-BE	57.5	79.5	-1.6	-12.5	1.38	low static
	9E-LBU-BI	55.2	80.4	-4.1	-13.4	1.46	low static
	9E-LBU-TC	9.3	16.6	-2.1	-5.3	low static	low static
	9E-LBD-CN	62.8	82.4	-9.3	-16.2	1.31	low static
	9G-LBU-CN	28.9	67.4	-2.3	-7.7	2.33	low static
	9G-LBD-CN	39.9	92.6	-9.0	-13.1	2.32	low static
	9K-LBD-CN	36.2	69.8	-3.0	-10.3	1.93	low static
Web Gap	9F-GPC-WG	1.9	10.8	-20.2	-33.6	low static	low static
	9F-GPA-WG	0.4	4.9	-8.1	-26.0	low static	low static
Gusset Plate	9F-GPA-LO	32.3	53.2	-4.7	-22.0	1.65	low static
	9F-GPA-TR	3.1	8.9	-12.3	-26.1	low static	low static
	9F-GPA-45	15.6	38.7	-2.9	-9.5	low static	low static
	9F-GPA-W9	125.9	244.6	-21.1	-87.0	1.94	low static
	9F-GPA-W8	117.0	213.0	-20.4	-86.8	1.82	low static

Table E-7

Dynamic Impact Factors for Dynamic Test D7 vs Static Subset S1-S6							
Location	Gage	Maximum Strain ($\mu\epsilon$)		Minimum Strain ($\mu\epsilon$)		+ DIF	- DIF
		+ Static	+ Dynamic	- Static	- Dynamic		
GC BC	9L-GC-BC	57.2	69.0	-37.7	-44.2	1.21	1.17
	9N-GC-BC	43.4	41.7	-53.5	-58.0	0.96	1.08
	9O-GC-BC	-9.2	8.4	-40.7	-45.0	low static	1.11
	8C-GC-BC	10.7	21.5	-47.6	-57.3	low static	1.20
	8D-GC-BC	71.3	77.9	-19.2	-22.8	1.09	low static
GA BC	9L-GA-BC	65.4	79.2	-48.4	-56.7	1.21	1.17
	9N-GA-BC	30.6	36.4	-46.6	-54.8	1.19	1.18
	9O-GA-BCH	-5.0	11.7	-32.1	-40.0	low static	1.25
	9O-GA-BC45	-5.8	12.0	-29.6	-41.8	low static	1.41
	9O-GA-BCV	11.6	10.6	-6.7	-11.6	low static	low static
	8C-GA-BC	6.6	19.0	-33.8	-43.8	low static	1.29
	8D-GA-BC	61.4	74.6	-20.1	-24.0	1.22	low static
GC TC	9L-GC-TC	2.0	4.5	-1.5	-5.9	low static	low static
	9N-GC-TC	1.9	4.8	0.3	-5.0	low static	low static
	9O-GC-TC	3.2	7.2	-0.6	-8.2	low static	low static
	8C-GC-TC	-2.7	9.8	-5.9	-7.5	low static	low static
	8D-GC-TC	-0.7	6.3	-2.5	-10.8	low static	low static
GA TC	9L-GA-TC	1.8	1.2	-1.5	-6.6	low static	low static
	9N-GA-TC	3.3	2.6	0.4	-5.6	low static	low static
	9O-GA-TCH	12.3	12.7	4.0	-5.4	low static	low static
	9O-GA-TC45	-3.3	6.8	-29.9	-38.3	low static	1.28
	9O-GA-TCV	7.0	6.6	-15.7	-21.2	low static	low static
	8C-GA-TC	3.3	3.0	0.2	-8.0	low static	low static
	8D-GA-TC	0.0	4.1	-6.9	-9.9	low static	low static
GC BE	9O-GC-BE	-1.2	11.3	-46.7	-52.4	low static	1.12
	8D-GC-BE	77.5	85.4	-20.1	-23.2	1.10	low static
GC BI	9O-GC-BI	-12.0	12.3	-43.4	-47.6	low static	1.10
	8D-GC-BI	77.3	99.2	-22.5	-24.1	1.28	low static
GA BE	9O-GA-BE	-7.1	13.3	-33.0	-39.7	low static	1.20
GA BI	9O-GA-BI	-1.2	10.5	-37.6	-41.4	low static	1.10
8D-GA-BI	61.1	50.2	-19.2	-7.4	0.82	low static	
GC TE	9O-GC-TE	2.3	7.8	-3.3	-5.1	low static	low static
	8D-GC-TE	-2.1	1.3	-7.6	-14.8	low static	low static
GC TI	9O-GC-TI	3.5	10.9	-0.9	-7.5	low static	low static
	8D-GC-TI	-1.5	4.5	-5.2	-10.3	low static	low static
GA TE	9O-GA-TE	13.2	14.3	0.3	-6.9	low static	low static
GA TI	9O-GA-TI	11.5	14.9	2.5	-4.4	low static	low static
GC W	9O-GC-W	14.2	18.4	1.5	-8.8	low static	low static
	8D-GC-W	32.3	38.3	-8.4	-14.0	1.19	low static
GA W	9O-GA-WH	7.7	12.0	-7.4	-6.0	low static	low static
	9O-GA-W45	12.7	9.4	-14.3	-20.6	low static	low static
	9O-GA-WV	14.2	15.6	-3.9	-7.1	low static	low static
	8D-GA-W	18.3	25.0	-6.5	-12.8	low static	low static
8A Diaphragm	8A-D-TI	19.6	27.3	-1.5	-2.4	low static	low static
	8A-D-TQI	4.3	5.6	-3.8	-11.1	low static	low static
	8A-D-BQI	3.3	4.0	-3.8	-6.4	low static	low static
	8A-D-TM	1.1	4.0	-0.8	-15.8	low static	low static
	8A-D-BM	19.1	31.3	1.2	-3.4	low static	low static
	8A-D-TQE	0.5	3.4	-1.2	-3.8	low static	low static
	8A-D-BQE	8.7	11.0	-8.3	-16.0	low static	low static
	8A-D-TE	11.6	22.4	0.0	-2.5	low static	low static
Lateral Bracing	8A-D-BE	5.2	7.4	-4.4	-10.9	low static	low static
	9K-LBU-CN	36.8	63.0	-3.3	-8.2	1.71	low static
	9O-LBD-CN	24.9	38.7	-9.2	-23.4	low static	low static
	8B-LBU-CN	30.5	34.9	-7.6	-18.8	1.14	low static
	8D-LBU-CN	45.9	50.2	-4.5	-7.4	1.09	low static
Web Gap	8F-LBD-CN	22.7	73.3	1.3	-5.9	low static	low static
	9I-GPC-WG	9.5	11.1	-40.1	-49.7	low static	1.24
	8E-GPC-WG	4.4	8.4	-27.7	-35.1	low static	1.27
	9I-GPA-WG	4.2	11.5	-26.9	-27.8	low static	1.03

Table E-8

Dynamic Impact Factors for Dynamic Test D8 vs Static Subset S1-S6							
Location	Gage	Maximum Strain ($\mu\epsilon$)		Minimum Strain ($\mu\epsilon$)		+ DIF	- DIF
		+ Static	+ Dynamic	- Static	- Dynamic		
GC BC	10Z-GC-BC	13.5	29.1	-34.4	-48.2	low static	1.40
	9B-GC-BC	13.7	19.3	-34.9	-46.6	low static	1.33
	9C-GC-BC	48.6	56.7	-2.3	-37.3	1.17	low static
	9H-GC-BC	65.5	91.0	-13.8	-30.8	1.39	low static
	9J-GC-BC	79.8	81.3	-24.3	-34.5	1.02	low static
	9L-GC-BC	57.2	66.6	-37.7	-50.2	1.16	1.33
	9N-GC-BC	43.4	40.3	-53.5	-61.6	0.93	1.15
	9O-GC-BC	-9.2	13.1	-40.7	-46.7	low static	1.15
	8C-GC-BC	10.7	22.5	-47.6	-62.5	low static	1.31
	8D-GC-BC	71.3	79.8	-19.2	-28.0	1.12	low static
GA BC	9B-GA-BC	15.1	19.8	-33.1	-42.8	low static	1.29
	9C-GA-BC	40.7	62.8	-1.2	-36.6	1.54	low static
	9H-GA-BC	72.6	102.9	-16.8	-39.2	1.42	low static
	9J-GA-BC	98.0	114.9	-33.6	-46.2	1.17	1.38
	9L-GA-BC	65.4	90.8	-48.4	-65.3	1.39	1.35
	9N-GA-BC	30.6	38.3	-46.6	-63.6	1.25	1.37
	9O-GA-BCH	-5.0	12.4	-32.1	-44.0	low static	1.37
	9O-GA-BC45	-5.8	14.2	-29.6	-49.0	low static	1.66
	9O-GA-BCV	11.6	16.3	-6.7	-15.2	low static	low static
	8C-GA-BC	6.6	26.3	-33.8	-48.5	low static	1.43
GC TC	9D-GC-TC	61.4	87.3	-20.1	-32.5	1.42	low static
	9B-GC-TC	3.8	4.2	-0.8	-12.8	low static	low static
	9C-GC-TC	3.1	11.2	-3.4	-4.7	low static	low static
	9H-GC-TC	-0.1	3.5	-3.7	-6.4	low static	low static
	9J-GC-TC	0.3	3.0	-2.7	-8.6	low static	low static
	9L-GC-TC	0.8	2.2	-2.0	-8.4	low static	low static
	9N-GC-TC	2.0	3.7	-1.5	-6.8	low static	low static
	9O-GC-TC	1.9	5.5	0.3	-5.9	low static	low static
	8C-GC-TC	3.2	2.7	-0.6	-6.3	low static	low static
	8D-GC-TC	-2.7	6.5	-5.9	-7.0	low static	low static
GA TC	9E-GA-TC	2.6	3.3	-3.2	-6.1	low static	low static
	9C-GA-TC	0.8	4.1	-3.2	-4.8	low static	low static
	9H-GA-TC	6.7	7.1	-0.6	-5.1	low static	low static
	9J-GA-TC	7.0	11.2	-1.1	-5.5	low static	low static
	9L-GA-TC	1.8	1.9	-1.5	-7.3	low static	low static
	9N-GA-TC	3.3	3.1	0.4	-6.1	low static	low static
	9O-GA-TCH	12.3	14.8	4.0	-5.4	low static	low static
	9O-GA-TC45	-3.3	8.0	-29.9	-43.5	low static	1.45
	9O-GA-TCV	7.0	6.8	-15.7	-26.6	low static	low static
	8C-GA-TC	3.3	4.2	0.2	-8.1	low static	low static
GC BE	9F-GC-BE	0.0	3.1	-6.9	-10.9	low static	low static
	9B-GC-BE	13.1	19.4	-43.6	-55.9	low static	1.28
	9J-GC-BE	96.0	94.8	-28.0	-36.8	0.99	1.31
	9O-GC-BE	-1.2	12.9	-46.7	-55.9	low static	1.20
GC BI	9G-GC-BI	77.5	88.0	-20.1	-28.1	1.13	low static
	9B-GC-BI	14.7	18.1	-32.7	-43.4	low static	1.33
	9J-GC-BI	84.8	101.3	-27.8	-38.3	1.19	1.38
	9O-GC-BI	-12.0	13.8	-43.4	-46.2	low static	1.06
GA BE	9H-GA-BE	77.3	96.2	-22.5	-30.6	1.24	low static
	9B-GA-BE	15.4	19.7	-33.7	-42.9	low static	1.27
	9J-GA-BE	95.9	125.1	-35.7	-48.8	1.30	1.37
	9O-GA-BE	-7.1	12.4	-33.0	-45.2	low static	1.37
GA BI	9I-GA-BI	14.3	20.0	-30.5	-41.7	low static	1.37
	9J-GA-BI	76.2	91.5	-27.3	-40.4	1.20	1.48
	9O-GA-BI	-1.2	12.6	-37.6	-44.0	low static	1.17
	8D-GA-BI	61.1	52.0	-19.2	-14.1	0.85	low static
GC TE	9K-GC-TE	5.9	12.6	-3.9	-5.1	low static	low static
	9J-GC-TE	-0.1	2.7	-5.9	-13.1	low static	low static
	9O-GC-TE	2.3	5.4	-3.3	-4.2	low static	low static
	8D-GC-TE	-2.1	1.9	-7.6	-15.7	low static	low static

continued on next page

Table E-9

Dynamic Impact Factors for Dynamic Test D8 vs Static Subset S1-S6 (continued)							
Location	Gage	Maximum Strain ($\mu\epsilon$)		Minimum Strain ($\mu\epsilon$)		+ DIF	- DIF
		+ Static	+ Dynamic	- Static	- Dynamic		
GC TI	9B-GC-TI	2.3	12.7	-4.3	-4.2	low static	low static
	9J-GC-TI	-0.1	2.9	-4.6	-6.3	low static	low static
	9O-GC-TI	3.5	3.1	-0.9	-8.4	low static	low static
	8D-GC-TI	-1.5	2.1	-5.2	-11.4	low static	low static
GA TE	9B-GA-TE	-1.7	6.9	-3.2	-6.0	low static	low static
	9J-GA-TE	0.0	3.7	-3.9	-7.0	low static	low static
	9O-GA-TE	13.2	15.1	0.3	-8.3	low static	low static
GA TI	9O-GA-TI	11.5	16.2	2.5	-5.8	low static	low static
GC W	9B-GC-W	8.1	11.7	-3.3	-4.8	low static	low static
	9J-GC-W	3.9	5.4	-10.4	-14.8	low static	low static
	9O-GC-W	14.2	16.3	1.5	-10.6	low static	low static
	8D-GC-W	32.3	39.6	-8.4	-13.6	1.23	low static
GA W	9B-GA-W	10.9	15.9	-16.6	-26.2	low static	low static
	9J-GA-W	55.1	86.1	-17.2	-30.5	1.56	low static
	9O-GA-WH	7.7	19.7	-7.4	-8.3	low static	low static
	9O-GA-W45	12.7	10.6	-14.3	-21.4	low static	low static
	9O-GA-WV	14.2	20.0	-3.9	-8.8	low static	low static
	8D-GA-W	18.3	29.1	-6.5	-13.2	low static	low static
9F Diaphragm	9F-D-TI	33.7	48.9	-2.5	-4.3	1.45	low static
	9F-D-BI	0.5	8.5	-2.4	-10.1	low static	low static
	9F-D-TQI	1.7	7.2	-2.0	-4.5	low static	low static
	9F-D-BQI	26.9	23.2	-0.6	-7.2	0.86	low static
	9F-D-TM	0.0	1.4	-9.1	-13.7	low static	low static
	9F-D-BM	44.5	56.2	-2.3	-9.8	1.26	low static
	9F-D-TQE	4.7	5.3	-0.9	-5.5	low static	low static
	9F-D-BQE	2.5	18.8	-10.9	-13.5	low static	low static
	9F-D-TE	34.9	40.3	1.4	-3.7	1.15	low static
	9F-D-BE	2.1	5.2	-2.9	-11.5	low static	low static
8A Diaphragm	8A-D-TI	19.6	25.6	-1.5	-2.9	low static	low static
	8A-D-TQI	4.3	7.1	-3.8	-12.4	low static	low static
	8A-D-BQI	3.3	4.4	-3.8	-7.4	low static	low static
	8A-D-TM	1.1	2.8	-0.8	-16.0	low static	low static
	8A-D-BM	19.1	35.5	1.2	-4.3	low static	low static
	8A-D-TQE	0.5	3.4	-1.2	-4.2	low static	low static
	8A-D-BQE	8.7	9.5	-8.3	-17.0	low static	low static
	8A-D-TE	11.6	26.8	0.0	-2.6	low static	low static
	8A-D-BE	5.2	6.3	-4.4	-14.6	low static	low static
Lateral Bracing	9E-LBU-CN	47.6	59.0	-3.6	-16.8	1.24	low static
	9E-LBU-BC	57.3	70.2	-3.3	-19.5	1.23	low static
	9E-LBU-BE	57.5	66.5	-1.6	-18.3	1.16	low static
	9E-LBU-BI	55.2	72.0	-4.1	-20.8	1.30	low static
	9E-LBU-TC	9.3	19.5	-2.1	-9.2	low static	low static
	9E-LBD-CN	62.8	88.3	-9.3	-15.1	1.41	low static
	9G-LBU-CN	28.9	64.0	-2.3	-13.1	2.21	low static
	9G-LBD-CN	39.9	89.9	-9.0	-11.3	2.25	low static
	9K-LBU-CN	36.8	69.4	-3.3	-10.8	1.88	low static
	9K-LBD-CN	36.2	73.5	-3.0	-10.8	2.03	low static
	9O-LBD-CN	24.9	47.6	-9.2	-21.2	low static	low static
	8B-LBU-CN	30.5	37.5	-7.6	-26.9	1.23	low static
	8D-LBU-CN	45.9	52.0	-4.5	-14.1	1.13	low static
	8F-LBD-CN	22.7	78.4	1.3	-7.1	low static	low static
Web Gap	9F-GPC-WG	1.9	10.9	-20.2	-25.6	low static	low static
	9I-GPC-WG	9.5	13.3	-40.1	-54.0	low static	1.35
	8E-GPC-WG	4.4	8.8	-27.7	-36.8	low static	1.33
	9F-GPA-WG	0.4	4.6	-8.1	-23.3	low static	low static
	9I-GPA-WG	4.2	10.7	-26.9	-28.6	low static	1.06
Gusset Plate	9F-GPA-LO	32.3	47.2	-4.7	-23.4	1.46	low static
	9F-GPA-TR	3.1	13.8	-12.3	-23.9	low static	low static
	9F-GPA-45	15.6	34.1	-2.9	-7.9	low static	low static
	9F-GPA-W9	125.9	221.0	-21.1	-87.0	1.76	low static
	9F-GPA-W8	117.0	180.5	-20.4	-84.5	1.54	low static

Table E-10

Dynamic Impact Factors for Dynamic Test D9 vs Static Subset S1-S6							
Location	Gage	Maximum Strain ($\mu\epsilon$)		Minimum Strain ($\mu\epsilon$)		+ DIF	- DIF
		+ Static	+ Dynamic	- Static	- Dynamic		
GC BC	10Z-GC-BC	13.5	29.3	-34.4	-48.3	low static	1.40
	9B-GC-BC	13.7	17.4	-34.9	-47.3	low static	1.35
	9C-GC-BC	48.6	52.1	-2.3	-37.5	1.07	low static
	9H-GC-BC	65.5	81.0	-13.8	-31.2	1.24	low static
	9J-GC-BC	79.8	83.9	-24.3	-29.8	1.05	low static
	9L-GC-BC	57.2	70.9	-37.7	-45.7	1.24	1.21
	9N-GC-BC	43.4	39.4	-53.5	-60.9	0.91	1.14
	9O-GC-BC	-9.2	11.9	-40.7	-46.0	low static	1.13
	8C-GC-BC	10.7	25.7	-47.6	-56.1	low static	1.18
	8D-GC-BC	71.3	81.1	-19.2	-27.6	1.14	low static
GA BC	9B-GA-BC	15.1	18.8	-33.1	-42.8	low static	1.30
	9C-GA-BC	40.7	63.1	-1.2	-35.3	1.55	low static
	9H-GA-BC	72.6	88.2	-16.8	-40.9	1.21	low static
	9J-GA-BC	98.0	109.4	-33.6	-40.5	1.12	1.21
	9L-GA-BC	65.4	86.2	-48.4	-58.6	1.32	1.21
	9N-GA-BC	30.6	38.9	-46.6	-56.1	1.27	1.20
	9O-GA-BCH	-5.0	13.6	-32.1	-40.4	low static	1.26
	9O-GA-BC45	-5.8	14.3	-29.6	-41.5	low static	1.40
	9O-GA-BCV	11.6	15.8	-6.7	-12.6	low static	low static
	8C-GA-BC	6.6	23.3	-33.8	-45.8	low static	1.35
GC TC	8D-GA-BC	61.4	78.5	-20.1	-32.1	1.28	low static
	10Z-GC-TC	3.8	4.7	-0.8	-12.9	low static	low static
	9B-GC-TC	3.1	11.0	-3.4	-4.3	low static	low static
	9C-GC-TC	-0.1	11.9	-3.7	-6.2	low static	low static
	9H-GC-TC	0.3	16.0	-2.7	-7.5	low static	low static
	9J-GC-TC	0.8	1.4	-2.0	-8.8	low static	low static
	9L-GC-TC	2.0	3.6	-1.5	-5.7	low static	low static
	9N-GC-TC	1.9	3.8	0.3	-5.4	low static	low static
	9O-GC-TC	3.2	2.4	-0.6	-7.5	low static	low static
	8C-GC-TC	-2.7	7.2	-5.9	-8.8	low static	low static
GA TC	8D-GC-TC	-0.7	6.6	-2.5	-9.5	low static	low static
	10Z-GA-TC	2.6	3.4	-3.2	-5.9	low static	low static
	9C-GA-TC	0.8	4.6	-3.2	-5.5	low static	low static
	9H-GA-TC	6.7	5.9	-0.6	-5.3	low static	low static
	9J-GA-TC	7.0	11.1	-1.1	-6.1	low static	low static
	9L-GA-TC	1.8	1.0	-1.5	-7.1	low static	low static
	9N-GA-TC	3.3	2.4	0.4	-5.7	low static	low static
	9O-GA-TCH	12.3	12.7	4.0	-5.7	low static	low static
	9O-GA-TC45	-3.3	9.1	-29.9	-43.0	low static	1.44
	9O-GA-TCV	7.0	8.3	-15.7	-24.6	low static	low static
GC BE	8C-GA-TC	3.3	3.8	0.2	-8.3	low static	low static
	8D-GA-TC	0.0	3.2	-6.9	-10.1	low static	low static
	9B-GC-BE	13.1	18.5	-43.6	-53.7	low static	1.23
	9J-GC-BE	96.0	89.6	-28.0	-31.5	0.93	1.13
	9O-GC-BE	-1.2	12.6	-46.7	-52.6	low static	1.13
	8D-GC-BE	77.5	91.8	-20.1	-29.5	1.18	low static
	9B-GC-BI	14.7	16.7	-32.7	-47.3	low static	1.45
	9J-GC-BI	84.8	111.3	-27.8	-34.4	1.31	1.24
	9O-GC-BI	-12.0	15.1	-43.4	-48.4	low static	1.12
	8D-GC-BI	77.3	98.8	-22.5	-30.4	1.28	low static
GA BE	9B-GA-BE	15.4	18.9	-33.7	-44.1	low static	1.31
	9J-GA-BE	95.9	126.6	-35.7	-42.4	1.32	1.19
	9O-GA-BE	-7.1	15.9	-33.0	-41.2	low static	1.25
GA BI	9B-GA-BI	14.3	18.5	-30.5	-39.4	low static	1.29
	9J-GA-BI	76.2	83.1	-27.3	-34.8	1.09	1.28
	9O-GA-BI	-1.2	13.6	-37.6	-42.7	low static	1.14
	8D-GA-BI	61.1	53.0	-19.2	-8.9	0.87	low static
GC TE	9B-GC-TE	5.9	11.4	-3.9	-4.7	low static	low static
	9J-GC-TE	-0.1	1.9	-5.9	-12.7	low static	low static
	9O-GC-TE	2.3	6.5	-3.3	-4.5	low static	low static
	8D-GC-TE	-2.1	1.7	-7.6	-15.7	low static	low static

Table E-11

Dynamic Impact Factors for Dynamic Test D9 vs Static Subset S1-S6 (continued)							
Location	Gage	Maximum Strain ($\mu\epsilon$)		Minimum Strain ($\mu\epsilon$)		+ DIF	- DIF
		+ Static	+ Dynamic	- Static	- Dynamic		
GC TI	9B-GC-TI	2.3	11.9	-4.3	-4.4	low static	low static
	9J-GC-TI	-0.1	3.8	-4.6	-7.4	low static	low static
	9O-GC-TI	3.5	2.1	-0.9	-7.8	low static	low static
	8D-GC-TI	-1.5	3.3	-5.2	-11.3	low static	low static
GA TE	9B-GA-TE	-1.7	8.0	-3.2	-5.8	low static	low static
	9J-GA-TE	0.0	4.1	-3.9	-7.3	low static	low static
	9O-GA-TE	13.2	13.3	0.3	-8.1	low static	low static
GA TI	9O-GA-TI	11.5	13.4	2.5	-5.5	low static	low static
GC W	9B-GC-W	8.1	11.3	-3.3	-4.2	low static	low static
	9J-GC-W	3.9	5.2	-10.4	-14.3	low static	low static
	9O-GC-W	14.2	16.1	1.5	-10.3	low static	low static
	8D-GC-W	32.3	42.2	-8.4	-14.9	1.31	low static
GA W	9B-GA-W	10.9	15.5	-16.6	-25.9	low static	low static
	9J-GA-W	55.1	79.3	-17.2	-25.7	1.44	low static
	9O-GA-WH	7.7	13.0	-7.4	-9.4	low static	low static
	9O-GA-W45	12.7	9.6	-14.3	-22.1	low static	low static
	9O-GA-WV	14.2	15.5	-3.9	-10.4	low static	low static
	8D-GA-W	18.3	26.4	-6.5	-12.4	low static	low static
9F Diaphragm	9F-D-TI	33.7	51.6	-2.5	-5.3	1.53	low static
	9F-D-BI	0.5	5.5	-2.4	-11.1	low static	low static
	9F-D-TQI	1.7	8.5	-2.0	-4.6	low static	low static
	9F-D-BQI	26.9	29.0	-0.6	-6.5	1.08	low static
	9F-D-TM	0.0	0.8	-9.1	-15.0	low static	low static
	9F-D-BM	44.5	60.1	-2.3	-8.5	1.35	low static
	9F-D-TQE	4.7	4.3	-0.9	-5.7	low static	low static
	9F-D-BQE	2.5	16.6	-10.9	-12.5	low static	low static
	9F-D-TE	34.9	39.9	1.4	-3.9	1.14	low static
	9F-D-BE	2.1	4.5	-2.9	-13.3	low static	low static
8A Diaphragm	8A-D-TI	19.6	25.3	-1.5	-3.6	low static	low static
	8A-D-TQI	4.3	6.3	-3.8	-10.9	low static	low static
	8A-D-BQI	3.3	4.4	-3.8	-7.0	low static	low static
	8A-D-TM	1.1	3.8	-0.8	-16.7	low static	low static
	8A-D-BM	19.1	32.1	1.2	-5.0	low static	low static
	8A-D-TQE	0.5	2.9	-1.2	-3.4	low static	low static
	8A-D-BQE	8.7	9.8	-8.3	-16.2	low static	low static
	8A-D-TE	11.6	24.6	0.0	-2.6	low static	low static
	8A-D-BE	5.2	7.4	-4.4	-14.1	low static	low static
Lateral Bracing	9E-LBU-CN	47.6	70.3	-3.6	-16.0	1.47	low static
	9E-LBU-BC	57.3	83.7	-3.3	-18.8	1.46	low static
	9E-LBU-BE	57.5	80.7	-1.6	-17.3	1.40	low static
	9E-LBU-BI	55.2	78.8	-4.1	-21.9	1.43	low static
	9E-LBU-TC	9.3	18.0	-2.1	-8.1	low static	low static
	9E-LBD-CN	62.8	92.7	-9.3	-13.7	1.48	low static
	9G-LBU-CN	28.9	60.9	-2.3	-11.9	2.11	low static
	9G-LBD-CN	39.9	79.2	-9.0	-10.4	1.98	low static
	9K-LBU-CN	36.8	68.0	-3.3	-8.7	1.85	low static
	9K-LBD-CN	36.2	65.3	-3.0	-12.5	1.80	low static
	9O-LBD-CN	24.9	39.8	-9.2	-20.7	low static	low static
	8B-LBU-CN	30.5	39.4	-7.6	-18.3	1.29	low static
	8D-LBU-CN	45.9	53.0	-4.5	-8.9	1.15	low static
	8F-LBD-CN	22.7	75.7	1.3	-8.0	low static	low static
Web Gap	9F-GPC-WG	1.9	11.3	-20.2	-24.6	low static	low static
	9I-GPC-WG	9.5	11.3	-40.1	-52.9	low static	1.32
	8E-GPC-WG	4.4	10.1	-27.7	-37.2	low static	1.34
	9F-GPA-WG	0.4	4.9	-8.1	-20.4	low static	low static
	9I-GPA-WG	4.2	6.5	-26.9	-27.0	low static	1.01
Gusset Plate	9F-GPA-LO	32.3	47.6	-4.7	-22.7	1.48	low static
	9F-GPA-TR	3.1	11.3	-12.3	-26.0	low static	low static
	9F-GPA-45	15.6	30.1	-2.9	-7.1	low static	low static
	9F-GPA-W9	125.9	195.9	-21.1	-89.1	1.56	low static
	9F-GPA-W8	117.0	166.2	-20.4	-83.3	1.42	low static

Table E-12

Dynamic Impact Factors for Dynamic Test D11 vs Static Subset S1-S5								
Location	Gage	Maximum Strain ($\mu\epsilon$)		Minimum Strain ($\mu\epsilon$)		+ DIF	- DIF	
		+ Static	+ Dynamic	- Static	- Dynamic			
GC BC	10Z-GC-BC	13.5	15.1	-34.4	-30.7	low static	0.89	
	9B-GC-BC	13.7	16.5	-34.9	-30.0	low static	0.86	
	9C-GC-BC	20.1	11.2	-2.3	-4.0	low static	low static	
	9H-GC-BC	65.5	36.5	-13.8	-15.4	0.56	low static	
	9J-GC-BC	79.8	56.9	-24.3	-29.0	0.71	low static	
	9L-GC-BC	57.2	66.9	-37.7	-44.1	1.17	1.17	
	9N-GC-BC	43.4	40.9	-53.5	-56.3	0.94	1.05	
	9O-GC-BC	-9.2	9.2	-40.7	-46.6	low static	1.15	
	8C-GC-BC	10.7	19.9	-47.6	-50.8	low static	1.07	
	8D-GC-BC	71.3	77.5	-19.2	-26.4	1.09	low static	
GA BC	9B-GA-BC	15.1	17.4	-33.1	-32.4	low static	0.98	
	9C-GA-BC	21.1	12.5	-1.2	-2.5	low static	low static	
	9H-GA-BC	72.6	43.5	-16.8	-19.9	0.60	low static	
	9J-GA-BC	98.0	84.4	-33.6	-37.5	0.86	1.12	
	9L-GA-BC	65.4	88.4	-48.4	-55.6	1.35	1.15	
	9N-GA-BC	30.6	36.5	-46.6	-56.0	1.19	1.20	
	9O-GA-BCH	-5.0	10.9	-32.1	-39.9	low static	1.24	
	9O-GA-BC45	-6.4	10.6	-29.6	-44.1	low static	1.49	
	9O-GA-BCV	11.6	7.9	-6.7	-7.7	low static	low static	
	8C-GA-BC	6.6	21.4	-33.8	-41.8	low static	1.24	
GC TC	9D-GC-TC	61.4	74.1	-20.1	-30.9	1.21	low static	
	9B-GC-TC	3.8	4.0	-0.8	-4.4	low static	low static	
	9C-GC-TC	2.0	5.4	-3.4	-4.7	low static	low static	
	9H-GC-TC	-0.1	3.7	-1.2	-3.9	low static	low static	
	9J-GC-TC	0.3	2.8	-2.7	-6.2	low static	low static	
	9L-GC-TC	0.8	1.8	-2.0	-6.9	low static	low static	
	9N-GC-TC	2.0	4.3	-1.5	-5.8	low static	low static	
	9O-GC-TC	1.9	4.8	0.3	-5.1	low static	low static	
	8C-GC-TC	3.2	2.7	0.1	-8.1	low static	low static	
	8D-GC-TC	-2.7	8.6	-5.9	-7.9	low static	low static	
GA TC	9D-GA-TC	-0.7	6.0	-2.5	-10.5	low static	low static	
	10Z-GA-TC	2.6	2.0	-3.2	-5.6	low static	low static	
	9C-GA-TC	0.8	3.4	-0.8	-4.4	low static	low static	
	9H-GA-TC	6.7	4.1	-0.6	-4.9	low static	low static	
	9J-GA-TC	7.0	6.4	-1.1	-5.8	low static	low static	
	9L-GA-TC	1.8	1.1	-0.5	-8.9	low static	low static	
	9N-GA-TC	3.3	3.9	0.4	-6.8	low static	low static	
	9O-GA-TCH	12.3	12.7	4.7	-6.3	low static	low static	
	9O-GA-TC45	-3.3	2.9	-29.9	-43.1	low static	1.44	
	9O-GA-TCV	7.0	5.1	-15.7	-22.6	low static	low static	
GC BE	9C-GC-BE	3.3	2.6	0.2	-9.4	low static	low static	
	9D-GC-BE	0.0	37.6	-6.9	-11.6	low static	low static	
	9B-GC-BE	13.1	17.3	-43.6	-32.0	low static	0.74	
	9J-GC-BE	96.0	67.9	-28.0	-28.9	0.71	1.03	
GC BI	9O-GC-BI	-1.2	11.4	-46.7	-51.8	low static	1.11	
	9D-GC-BI	77.5	90.0	-20.1	-26.7	1.16	low static	
	9B-GC-BI	14.7	15.9	-32.7	-31.9	low static	0.98	
	9J-GC-BI	84.8	62.8	-27.8	-31.7	0.74	1.14	
GA BE	9O-GC-BI	-20.2	11.4	-43.4	-46.3	low static	1.07	
	9D-GC-BI	77.3	101.4	-22.5	-32.0	1.31	low static	
	9B-GA-BE	15.4	18.8	-33.7	-29.8	low static	0.88	
GA BI	9J-GA-BE	95.9	83.1	-35.7	-39.5	0.87	1.11	
	9O-GA-BE	-14.1	14.0	-33.0	-39.3	low static	1.19	
	9B-GA-BI	14.3	18.3	-30.5	-30.5	low static	1.00	
GA BI	9J-GA-BI	76.2	67.2	-27.3	-32.3	0.88	1.18	
	9O-GA-BI	-1.2	10.0	-37.6	-42.5	low static	1.13	
	8D-GA-BI	61.1	47.8	-19.2	-8.8	0.78	low static	
GC TE	9B-GC-TE	3.9	4.7	-3.9	-4.4	low static	low static	
	9J-GC-TE	-0.1	1.5	-5.9	-5.9	low static	low static	
	9O-GC-TE	2.3	7.0	-3.3	-4.7	low static	low static	
	8D-GC-TE	-2.1	1.0	-7.6	-15.7	low static	low static	

continued on next page

Table E-13

Dynamic Impact Factors for Dynamic Test D11 vs Static Subset S1-S5 (continued)							
Location	Gage	Maximum Strain ($\mu\epsilon$)		Minimum Strain ($\mu\epsilon$)		+ DIF	- DIF
		+ Static	+ Dynamic	- Static	- Dynamic		
GC TI	9B-GC-TI	2.3	6.2	-4.3	-4.8	low static	low static
	9J-GC-TI	-0.1	2.6	-4.6	-6.3	low static	low static
	9O-GC-TI	3.5	4.0	0.5	-8.8	low static	low static
	8D-GC-TI	-1.5	2.9	-5.2	-11.8	low static	low static
GA TE	9B-GA-TE	-1.7	-0.2	-3.1	-7.2	low static	low static
	9J-GA-TE	0.0	2.8	-2.7	-5.0	low static	low static
	9O-GA-TE	13.2	12.8	0.3	-8.4	low static	low static
GA TI	9O-GA-TI	11.5	14.1	3.5	-6.0	low static	low static
GC W	9B-GC-W	4.6	5.0	-3.3	-5.3	low static	low static
	9J-GC-W	3.9	4.6	-10.4	-11.2	low static	low static
	9O-GC-W	14.2	15.7	5.6	-10.7	low static	low static
	8D-GC-W	32.3	38.2	-8.4	-15.0	1.18	low static
GA W	9B-GA-W	10.9	15.2	-16.6	-19.7	low static	low static
	9J-GA-W	55.1	57.5	-17.2	-24.3	1.04	low static
	9O-GA-WH	7.7	11.4	-2.3	-4.9	low static	low static
	9O-GA-W45	12.7	9.7	-14.3	-22.1	low static	low static
	9O-GA-WV	14.2	13.8	-3.4	-8.4	low static	low static
	8D-GA-W	18.3	25.1	-6.5	-14.2	low static	low static
9F Diaphragm	9F-D-TI	1.8	3.5	-2.5	-5.5	low static	low static
	9F-D-BI	0.5	4.7	-2.2	-6.2	low static	low static
	9F-D-TQI	0.1	3.2	-2.0	-5.1	low static	low static
	9F-D-BQI	0.4	2.5	-0.6	-6.6	low static	low static
	9F-D-TM	0.0	1.0	-2.8	-6.5	low static	low static
	9F-D-BM	0.6	2.2	-2.3	-7.1	low static	low static
	9F-D-TQE	1.0	0.6	-0.9	-6.2	low static	low static
	9F-D-BQE	1.0	3.3	-10.9	-8.3	low static	low static
	9F-D-TE	7.0	3.1	1.4	-3.9	low static	low static
	9F-D-BE	2.1	3.9	-2.7	-7.3	low static	low static
8A Diaphragm	8A-D-TI	19.6	26.2	-1.5	-2.1	low static	low static
	8A-D-TQI	4.3	6.2	-3.8	-12.6	low static	low static
	8A-D-BQI	3.3	2.9	-3.8	-12.2	low static	low static
	8A-D-TM	1.1	3.4	-0.8	-16.4	low static	low static
	8A-D-BM	19.1	34.7	1.2	-2.8	low static	low static
	8A-D-TQE	0.5	2.7	-1.2	-5.6	low static	low static
	8A-D-BQE	8.7	11.3	-8.3	-13.1	low static	low static
	8A-D-TE	11.6	23.6	0.0	-3.0	low static	low static
	8A-D-BE	5.2	8.3	-4.4	-12.3	low static	low static
	9E-LBU-CN	8.4	11.7	-3.6	-16.6	low static	low static
Lateral Bracing	9E-LBU-BC	10.6	14.5	-3.3	-19.0	low static	low static
	9E-LBU-BE	12.6	10.8	-1.6	-19.2	low static	low static
	9E-LBU-BI	10.6	13.1	-4.1	-20.2	low static	low static
	9E-LBU-TC	0.2	2.6	-2.1	-4.8	low static	low static
	9E-LBD-CN	7.1	18.3	-9.3	-14.2	low static	low static
	9G-LBU-CN	18.2	9.0	-2.3	-15.8	low static	low static
	9G-LBD-CN	30.1	18.6	-9.0	-10.7	0.62	low static
	9K-LBU-CN	36.8	58.3	-3.3	-7.7	1.58	low static
	9K-LBD-CN	36.2	57.1	-3.0	-3.0	1.58	low static
	9O-LBD-CN	24.9	33.5	-9.2	-23.2	low static	low static
	8B-LBU-CN	30.5	38.7	-7.6	-21.6	1.27	low static
	8D-LBU-CN	45.9	47.8	-4.5	-8.8	1.04	low static
	8F-LBD-CN	22.7	67.3	1.3	-6.9	low static	low static
Web Gap	9F-GPC-WG	1.9	3.3	-11.0	-8.2	low static	low static
	9I-GPC-WG	9.5	10.8	-40.1	-30.8	low static	0.77
	8E-GPC-WG	4.4	9.3	-27.7	-37.4	low static	1.35
	9F-GPA-WG	0.4	1.8	-7.6	-8.4	low static	low static
	9I-GPA-WG	4.2	5.3	-26.9	-20.6	low static	0.77
Gusset Plate	9F-GPA-LO	24.7	14.9	-4.7	-7.8	low static	low static
	9F-GPA-TR	3.1	4.6	-11.2	-10.0	low static	low static
	9F-GPA-45	15.6	13.7	-2.9	-4.1	low static	low static
	9F-GPA-W9	116.6	63.7	-21.1	-23.6	0.55	low static
	9F-GPA-W8	117.0	62.7	-20.4	-22.0	0.54	low static

Table E-14

Dynamic Impact Factors for Dynamic Test D12 vs Static Subset S1-S5							
Location	Gage	Maximum Strain ($\mu\epsilon$)		Minimum Strain ($\mu\epsilon$)		+ DIF	- DIF
		+ Static	+ Dynamic	- Static	- Dynamic		
GC BC	10Z-GC-BC	13.5	15.8	-34.4	-25.6	low static	0.74
	9B-GC-BC	13.7	18.6	-34.9	-26.9	low static	0.77
	9C-GC-BC	20.1	10.0	-2.3	-4.8	low static	low static
	9H-GC-BC	65.5	29.1	-13.8	-18.6	0.44	low static
	9J-GC-BC	79.8	45.6	-24.3	-30.2	0.57	low static
GA BC	9B-GA-BC	15.1	18.5	-33.1	-29.1	low static	0.88
	9C-GA-BC	21.1	10.5	-1.2	-4.4	low static	low static
	9H-GA-BC	72.6	36.0	-16.8	-24.1	0.50	low static
	9J-GA-BC	98.0	69.3	-33.6	-40.0	0.71	1.19
GC TC	10Z-GC-TC	3.8	3.0	-0.8	-4.9	low static	low static
	9B-GC-TC	2.0	4.4	-3.4	-4.6	low static	low static
	9C-GC-TC	-0.1	3.2	-1.2	-4.5	low static	low static
	9H-GC-TC	0.3	2.9	-2.7	-5.6	low static	low static
	9J-GC-TC	0.8	1.5	-2.0	-6.6	low static	low static
GA TC	10Z-GA-TC	2.6	1.7	-3.2	-5.6	low static	low static
	9C-GA-TC	0.8	3.9	-0.8	-3.9	low static	low static
	9H-GA-TC	6.7	3.7	-0.6	-4.8	low static	low static
	9J-GA-TC	7.0	7.1	-1.1	-6.5	low static	low static
GC BE	9B-GC-BE	13.1	18.4	-43.6	-28.5	low static	0.65
	9J-GC-BE	96.0	57.0	-28.0	-32.4	0.59	1.16
GC BI	9B-GC-BI	14.7	16.1	-32.7	-27.2	low static	0.83
	9J-GC-BI	84.8	49.2	-27.8	-35.2	0.58	1.26
GA BE	9B-GA-BE	15.4	20.3	-33.7	-26.9	low static	0.80
	9J-GA-BE	95.9	68.6	-35.7	-44.7	0.72	1.25
GA BI	9B-GA-BI	14.3	19.8	-30.5	-27.7	low static	0.91
	9J-GA-BI	76.2	59.1	-27.3	-35.0	0.78	1.28
GC TE	9B-GC-TE	3.9	3.4	-3.9	-5.1	low static	low static
	9J-GC-TE	-0.1	1.9	-5.9	-5.5	low static	low static
GC TI	9B-GC-TI	2.3	5.4	-4.3	-4.4	low static	low static
	9J-GC-TI	-0.1	2.4	-4.6	-5.3	low static	low static
GA TE	9B-GA-TE	-1.7	0.4	-3.1	-6.5	low static	low static
	9J-GA-TE	0.0	4.2	-2.7	-5.2	low static	low static
GC W	9B-GC-W	4.6	4.4	-3.3	-4.6	low static	low static
	9J-GC-W	3.9	5.3	-10.4	-11.3	low static	low static
GA W	9B-GA-W	10.9	16.4	-16.6	-17.5	low static	low static
	9J-GA-W	55.1	48.3	-17.2	-25.9	0.88	low static
9F Diaphragm	9F-D-TI	1.8	2.9	-2.5	-5.1	low static	low static
	9F-D-BI	0.5	4.3	-2.2	-6.5	low static	low static
	9F-D-TQI	0.1	3.5	-2.0	-4.8	low static	low static
	9F-D-BQI	0.4	2.3	-0.6	-6.3	low static	low static
	9F-D-TM	0.0	1.4	-2.8	-5.8	low static	low static
	9F-D-BM	0.6	2.6	-2.3	-6.9	low static	low static
	9F-D-TQE	1.0	0.8	-0.9	-6.1	low static	low static
	9F-D-BQE	1.0	3.7	-10.9	-7.1	low static	low static
	9F-D-TE	7.0	2.9	1.4	-3.4	low static	low static
	9F-D-BE	2.1	1.9	-2.7	-7.7	low static	low static
Lateral Bracing	9E-LBU-CN	8.4	12.8	-3.6	-16.7	low static	low static
	9E-LBU-BC	10.6	14.8	-3.3	-19.7	low static	low static
	9E-LBU-BE	12.6	10.2	-1.6	-19.2	low static	low static
	9E-LBU-BI	10.6	13.6	-4.1	-20.7	low static	low static
	9E-LBU-TC	0.2	1.8	-2.1	-4.9	low static	low static
	9E-LBD-CN	7.1	17.6	-9.3	-15.3	low static	low static
	9G-LBU-CN	18.2	9.7	-2.3	-15.4	low static	low static
	9G-LBD-CN	30.1	17.6	-9.0	-10.9	0.59	low static
	9K-LBD-CN	36.2	41.4	-3.0	-5.1	1.14	low static
Web Gap	9F-GPC-WG	1.9	3.3	-11.0	-6.7	low static	low static
	9F-GPA-WG	0.4	1.9	-7.6	-7.2	low static	low static
Gusset Plate	9F-GPA-LO	24.7	12.0	-4.7	-8.0	low static	low static
	9F-GPA-TR	3.1	4.8	-11.2	-9.2	low static	low static
	9F-GPA-45	15.6	12.5	-2.9	-4.2	low static	low static
	9F-GPA-W9	116.6	55.6	-21.1	-29.9	0.48	low static
	9F-GPA-W8	117.0	51.2	-20.4	-26.4	0.44	low static

Table E-15

Dynamic Impact Factors for Dynamic Test D13 vs Static Subset S1-S5								
Location	Gage	Maximum Strain ($\mu\epsilon$)		Minimum Strain ($\mu\epsilon$)		+ DIF	- DIF	
		+ Static	+ Dynamic	- Static	- Dynamic			
GC BC	10Z-GC-BC	13.5	30.6	-34.4	-53.3	low static	1.55	
	9B-GC-BC	13.7	18.8	-34.9	-53.8	low static	1.54	
	9C-GC-BC	20.1	53.0	-2.3	-28.9	low static	low static	
	9H-GC-BC	65.5	67.2	-13.8	-22.0	1.03	low static	
	9J-GC-BC	79.8	77.4	-24.3	-32.8	0.97	low static	
	9L-GC-BC	57.2	54.0	-37.7	-53.9	0.94	1.43	
	9N-GC-BC	43.4	35.7	-53.5	-63.8	0.82	1.19	
	9O-GC-BC	-9.2	12.2	-40.7	-53.7	low static	1.32	
	8C-GC-BC	10.7	22.7	-47.6	-53.9	low static	1.13	
	8D-GC-BC	71.3	70.6	-19.2	-24.1	0.99	low static	
GA BC	9B-GA-BC	15.1	19.3	-33.1	-53.9	low static	1.63	
	9C-GA-BC	21.1	55.4	-1.2	-28.6	low static	low static	
	9H-GA-BC	72.6	92.1	-16.8	-28.8	1.27	low static	
	9J-GA-BC	98.0	128.4	-33.6	-53.5	1.31	1.59	
	9L-GA-BC	65.4	94.5	-48.4	-64.4	1.44	1.33	
	9N-GA-BC	30.6	44.5	-46.6	-63.5	1.45	1.36	
	9O-GA-BCH	-5.0	16.8	-32.1	-53.7	low static	1.67	
	9O-GA-BC45	-6.4	14.1	-29.6	-53.8	low static	1.82	
	9O-GA-BCV	11.6	12.4	-6.7	-7.3	low static	low static	
	8C-GA-BC	6.6	26.5	-33.8	-50.2	low static	1.48	
GC TC	9D-GC-TC	61.4	88.2	-20.1	-27.0	1.44	low static	
	9B-GC-TC	3.8	2.5	-0.8	-12.1	low static	low static	
	9C-GC-TC	2.0	13.1	-3.4	-5.3	low static	low static	
	9H-GC-TC	-0.1	4.6	-1.2	-8.3	low static	low static	
	9J-GC-TC	0.3	3.3	-2.7	-8.7	low static	low static	
	9L-GC-TC	0.8	2.4	-2.0	-8.1	low static	low static	
	9N-GC-TC	2.0	3.4	-1.5	-6.7	low static	low static	
	9O-GC-TC	1.9	4.4	0.3	-4.6	low static	low static	
	8C-GC-TC	3.2	4.1	0.1	-9.7	low static	low static	
	8D-GC-TC	-2.7	4.1	-5.9	-8.8	low static	low static	
GA TC	9E-GA-TC	2.6	1.8	-3.2	-8.9	low static	low static	
	9C-GA-TC	0.8	3.3	-0.8	-5.8	low static	low static	
	9H-GA-TC	6.7	6.1	-0.6	-6.4	low static	low static	
	9J-GA-TC	7.0	11.5	-1.1	-6.4	low static	low static	
	9L-GA-TC	1.8	3.1	-0.5	-7.0	low static	low static	
	9N-GA-TC	3.3	4.6	0.4	-5.7	low static	low static	
	9O-GA-TCH	12.3	18.1	4.7	-6.8	low static	low static	
	9O-GA-TC45	-3.3	6.4	-29.9	-53.1	low static	1.77	
	9O-GA-TCV	7.0	8.6	-15.7	-24.6	low static	low static	
	8C-GA-TC	3.3	6.4	0.2	-7.9	low static	low static	
GC BE	9F-GC-BE	0.0	1.5	-6.9	-11.1	low static	low static	
	9B-GC-BE	13.1	19.7	-43.6	-54.0	low static	1.24	
	9J-GC-BE	96.0	89.0	-28.0	-35.1	0.93	1.25	
	9O-GC-BE	-1.2	13.6	-46.7	-57.6	low static	1.23	
GC BI	9G-GC-BI	77.5	74.2	-20.1	-24.7	0.96	low static	
	9B-GC-BI	14.7	17.2	-32.7	-54.0	low static	1.65	
	9J-GC-BI	84.8	86.1	-27.8	-38.6	1.02	1.39	
	9O-GC-BI	-20.2	16.8	-43.4	-53.9	low static	1.24	
GA BE	9H-GA-BE	77.3	90.2	-22.5	-25.1	1.17	low static	
	9B-GA-BE	15.4	20.5	-33.7	-53.9	low static	1.60	
	9J-GA-BE	95.9	129.1	-35.7	-53.5	1.35	1.50	
	9O-GA-BE	-14.1	17.7	-33.0	-54.0	low static	1.64	
GA BI	9I-GA-BI	14.3	19.6	-30.5	-47.6	low static	1.56	
	9J-GA-BI	76.2	103.7	-27.3	-39.0	1.36	1.43	
	9O-GA-BI	-1.2	14.4	-37.6	-53.9	low static	1.43	
	8D-GA-BI	61.1	53.5	-19.2	-21.7	0.88	low static	
GC TE	9K-GC-TE	3.9	13.6	-3.9	-5.8	low static	low static	
	9J-GC-TE	-0.1	2.4	-5.9	-10.5	low static	low static	
	9O-GC-TE	2.3	3.9	-3.3	-7.9	low static	low static	
	8D-GC-TE	-2.1	0.9	-7.6	-18.3	low static	low static	

continued on next page

Table E-16

Dynamic Impact Factors for Dynamic Test D13 vs Static Subset S1-S5								
Location	Gage	Maximum Strain ($\mu\epsilon$)		Minimum Strain ($\mu\epsilon$)		+ DIF	- DIF	
		+ Static	+ Dynamic	- Static	- Dynamic			
GC TI	9B-GC-TI	2.3	14.7	-4.3	-4.7	low static	low static	
	9J-GC-TI	-0.1	3.7	-4.6	-7.9	low static	low static	
	9O-GC-TI	3.5	6.1	0.5	-8.7	low static	low static	
	8D-GC-TI	-1.5	3.6	-5.2	-13.4	low static	low static	
GA TE	9B-GA-TE	-1.7	6.9	-3.1	-6.7	low static	low static	
	9J-GA-TE	0.0	5.2	-2.7	-7.0	low static	low static	
	9O-GA-TE	13.2	16.8	0.3	-8.5	low static	low static	
GA TI	9O-GA-TI	11.5	16.2	3.5	-8.9	low static	low static	
GC W	9B-GC-W	4.6	9.3	-3.3	-5.7	low static	low static	
	9J-GC-W	3.9	4.2	-10.4	-12.4	low static	low static	
	9O-GC-W	14.2	11.5	5.6	-13.8	low static	low static	
	8D-GC-W	32.3	33.1	-8.4	-14.2	1.03	low static	
GA W	9B-GA-W	10.9	16.4	-16.6	-28.7	low static	low static	
	9J-GA-W	55.1	93.3	-17.2	-28.2	1.69	low static	
	9O-GA-WH	7.7	13.5	-2.3	-6.2	low static	low static	
	9O-GA-W45	12.7	9.8	-14.3	-25.0	low static	low static	
	9O-GA-WV	14.2	14.7	-3.4	-9.1	low static	low static	
	8D-GA-W	18.3	28.9	-6.5	-13.5	low static	low static	
9F Diaphragm	9F-D-TI	1.8	53.2	-2.5	-5.0	low static	low static	
	9F-D-BI	0.5	5.8	-2.2	-7.4	low static	low static	
	9F-D-TQI	0.1	3.6	-2.0	-4.6	low static	low static	
	9F-D-BQI	0.4	10.6	-0.6	-9.8	low static	low static	
	9F-D-TM	0.0	1.0	-2.8	-15.4	low static	low static	
	9F-D-BM	0.6	40.6	-2.3	-8.6	low static	low static	
	9F-D-TQE	1.0	1.7	-0.9	-6.4	low static	low static	
	9F-D-BQE	1.0	16.4	-10.9	-12.0	low static	low static	
	9F-D-TE	7.0	37.9	1.4	-3.4	low static	low static	
	9F-D-BE	2.1	2.7	-2.7	-11.9	low static	low static	
8A Diaphragm	8A-D-TI	19.6	23.9	-1.5	-3.6	low static	low static	
	8A-D-TQI	4.3	8.3	-3.8	-13.9	low static	low static	
	8A-D-BQI	3.3	7.5	-3.8	-17.8	low static	low static	
	8A-D-TM	1.1	2.8	-0.8	-16.0	low static	low static	
	8A-D-BM	19.1	36.2	1.2	-4.2	low static	low static	
	8A-D-TQE	0.5	1.8	-1.2	-5.8	low static	low static	
	8A-D-BQE	8.7	10.5	-8.3	-7.8	low static	low static	
	8A-D-TE	11.6	26.4	0.0	-4.5	low static	low static	
	8A-D-BE	5.2	8.2	-4.4	-14.1	low static	low static	
	9E-LBU-CN	8.4	53.8	-3.6	-28.3	low static	low static	
Lateral Bracing	9E-LBU-BC	10.6	60.3	-3.3	-35.1	low static	low static	
	9E-LBU-BE	12.6	55.7	-1.6	-35.4	low static	low static	
	9E-LBU-BI	10.6	57.8	-4.1	-35.2	low static	low static	
	9E-LBU-TC	0.2	12.3	-2.1	-5.7	low static	low static	
	9E-LBD-CN	7.1	81.5	-9.3	-14.8	low static	low static	
	9G-LBU-CN	18.2	39.2	-2.3	-22.8	low static	low static	
	9G-LBD-CN	30.1	69.5	-9.0	-11.5	2.31	low static	
	9K-LBU-CN	36.8	61.3	-3.3	-12.3	1.67	low static	
	9K-LBD-CN	36.2	53.8	-3.0	-25.0	1.49	low static	
	9O-LBD-CN	24.9	34.3	-9.2	-38.6	low static	low static	
	8B-LBU-CN	30.5	28.5	-7.6	-39.8	0.93	low static	
	8D-LBU-CN	45.9	53.5	-4.5	-21.7	1.17	low static	
	8F-LBD-CN	22.7	69.7	1.3	-10.6	low static	low static	
Web Gap	9F-GPC-WG	1.9	8.4	-11.0	-20.8	low static	low static	
	9I-GPC-WG	9.5	13.6	-40.1	-53.9	low static	1.34	
	8E-GPC-WG	4.4	7.6	-27.7	-33.6	low static	1.22	
	9F-GPA-WG	0.4	4.4	-7.6	-21.1	low static	low static	
	9I-GPA-WG	4.2	11.0	-26.9	-32.2	low static	1.20	
Gusset Plate	9F-GPA-LO	24.7	40.7	-4.7	-18.5	low static	low static	
	9F-GPA-TR	3.1	7.9	-11.2	-21.5	low static	low static	
	9F-GPA-45	15.6	30.0	-2.9	-6.1	low static	low static	
	9F-GPA-W9	116.6	186.4	-21.1	-63.4	1.60	low static	
	9F-GPA-W8	117.0	161.7	-20.4	-61.0	1.38	low static	

Table E-17

Appendix F
Results for Computed and Measured Static Test Data

This appendix provides the final measured static test data for the testing of Mn/DOT Bridge No. 69824 on July 14-15th, 2004, along with comparisons to the computed results from the Final Modal (FM) and Final Model – Rating (FMR) analytical models of the bridge using UMN Program. See Chapter 7 for more details on the computational models.

Since the displacement instruments only provided voltage readings (except for the total stations), an offset value had to be subtracted from the readings for each test to determine the displacements. For the plots in this appendix, the Zero reading value most closely following a specific test is used as the offset. For example, Zero 1 readings are subtracted from the data for tests T1 through T19 to get the displacements and Zero 2 readings are subtracted from the data for tests T20 through T27, etc. Displacements from the total stations are calculated using trigonometry. Displacement measurements are provided in radians for rotations and inches for deflections. The strain gage data in this appendix have had the thermal effects removed as described in Chapter 5 and have been converted to stress by using Hooke's Law with a modulus of elasticity for steel of $E_s = 29000$ ksi and a Poisson's ratio of 0.3. All stress values are in units of ksi.

Due to unexpected data recording issues (see Chapter 5), approximately half of the strain gage data was not recorded at 3:57:56 a.m. for Static Test S17 (T56). Missed data can be identified on the data plots in this appendix as a discontinuity in the line.

Section F.1 of this appendix provides plots of the measured static test data for all instruments used during testing. Measured static test data is plotted per test (see Chapter 5 for the configurations of Static Tests S1 through S43) using solid shapes and connected with solid lines. Computed results are also provided in these plots for instruments for which analysis was completed and are shown with hollow shapes and connected by dashed lines. FM analysis results are provided for all such instruments. Following the FM results are plots of the FMR results for the girder strain gages in the negative moment regions at Sections 10Z, 9B, 9N, 9O, and 8C for each girder. No other comparisons are provided for the FMR results since all other results are identical to the results for the FM analysis. Recall from Chapter 7 that the only difference between the FM and FMR analyses was that for the FMR analysis the girder flexural stresses in the negative moment regions were determined based on the section properties for the steel beam and reinforcement only, while for the FM analysis the stresses in both of these regions were based on composite section properties with the concrete effective in tension.

The plots in Section F.1 are organized as described below (analysis is for the FM model unless indicated otherwise):

- Girder Rotations: Figure F-1
- Vertical Deflections: Figure F-2 to Figure F-4
- Steel-Concrete Slip: Figure F-5
- Bearing Movement: Figure F-6
- Girder Stresses: Figure F-7 to Figure F-44
- Diaphragm Stresses: Figure F-45 to Figure F-54
- Lateral Wind Bracing Stresses: Figure F-55 to Figure F-60
- Gusset Plate Stresses: Figure F-61 to Figure F-62

- Web Gap Stresses: Figure F-63 to Figure F-64
- FMR Girder Stresses: Figure F-65 to Figure F-84

Plots are ordered from Section 10Z toward Section 8F for each of the above groups.

Section F.2 provides comparisons between the measured and computational results in tabular form. All forty-three static test results are shown for the measured and computed FM values of each gage that had analytical values computed. FMR comparisons for the girder strain gages in the negative moment regions at Sections 10Z, 9B, 9N, 9O, and 8C for each girder are provided following the FM comparisons. Percent error calculations are made for each comparison that has the measured value greater than a minimum magnitude. The minimum magnitude was set at 0.0001 radians for rotations, 0.10 inches for girder deflections, and 0.30 ksi for stresses. The percent error was calculated using:

$$\text{Percent Error} = \frac{\text{Computed} - \text{Measured}}{\text{Measured}} \cdot 100\% \quad (\text{F-1})$$

Therefore, comparisons with a positive *Percent Error* are overestimated by the analysis and comparisons with a negative *Percent Error* are underestimated. The maximum and minimum *Percent Errors* are tabulated for each instrument along with the average and standard deviation of the calculated values.

The tables in Section F.2 are grouped as described below (comparisons are made with the FM model unless indicated otherwise):

- Girder Rotations: Table F-1
- Vertical Deflections: Table F-2 to Table F-4
- Girder Stresses: Table F-5 to Table F-39
- Diaphragm Stresses: Table F-40 to Table F-49
- Lateral Wind Bracing Stresses: Table F-50 to Table F-54
- FMR Girder Stresses: Table F-55 to Table F-70

Tables are organized by section beginning at 10Z and going toward Section 8F within each of the above categories.

F.1 Plots of Computed (FM,FMR) versus Measured Static Test Data

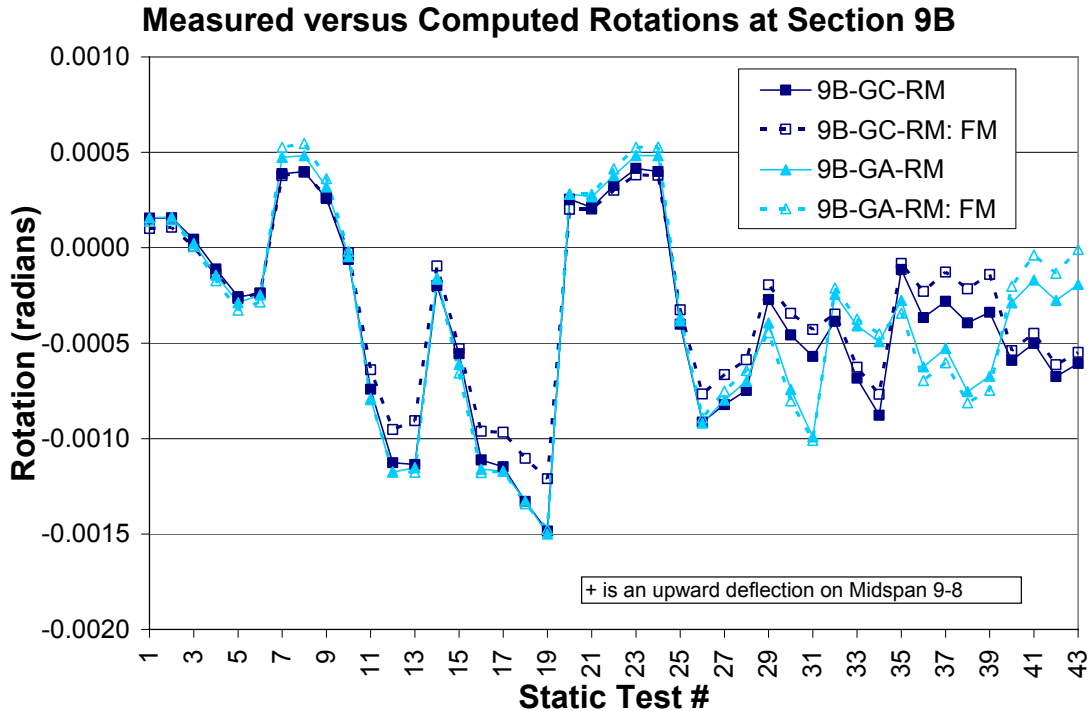


Figure F-1

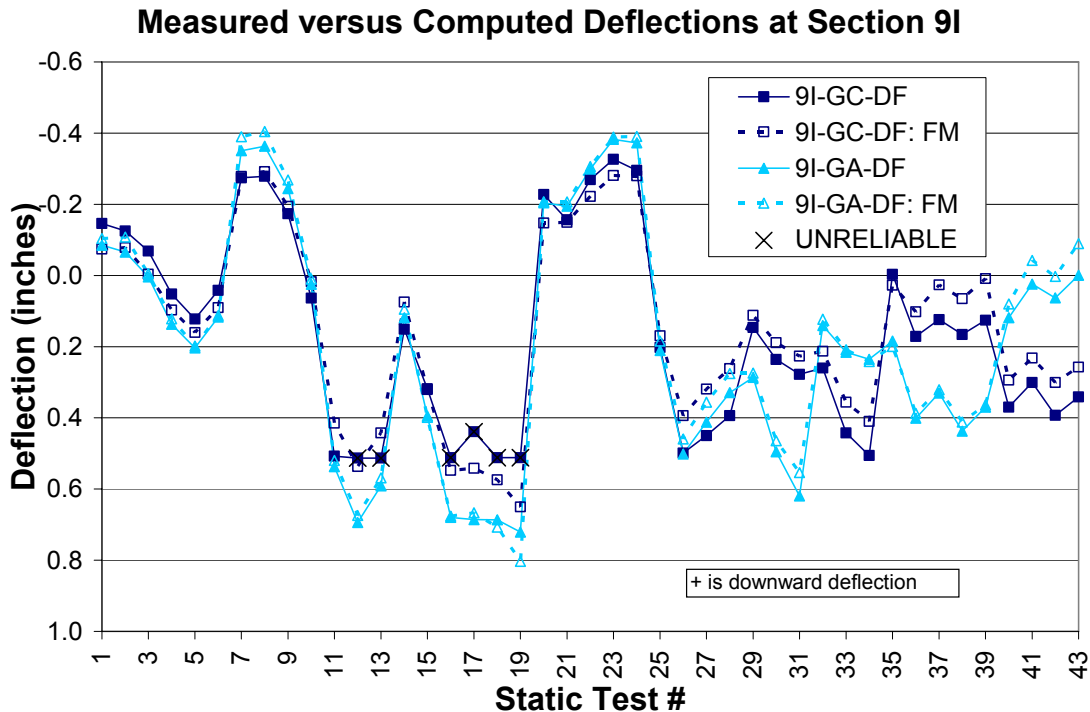


Figure F-2

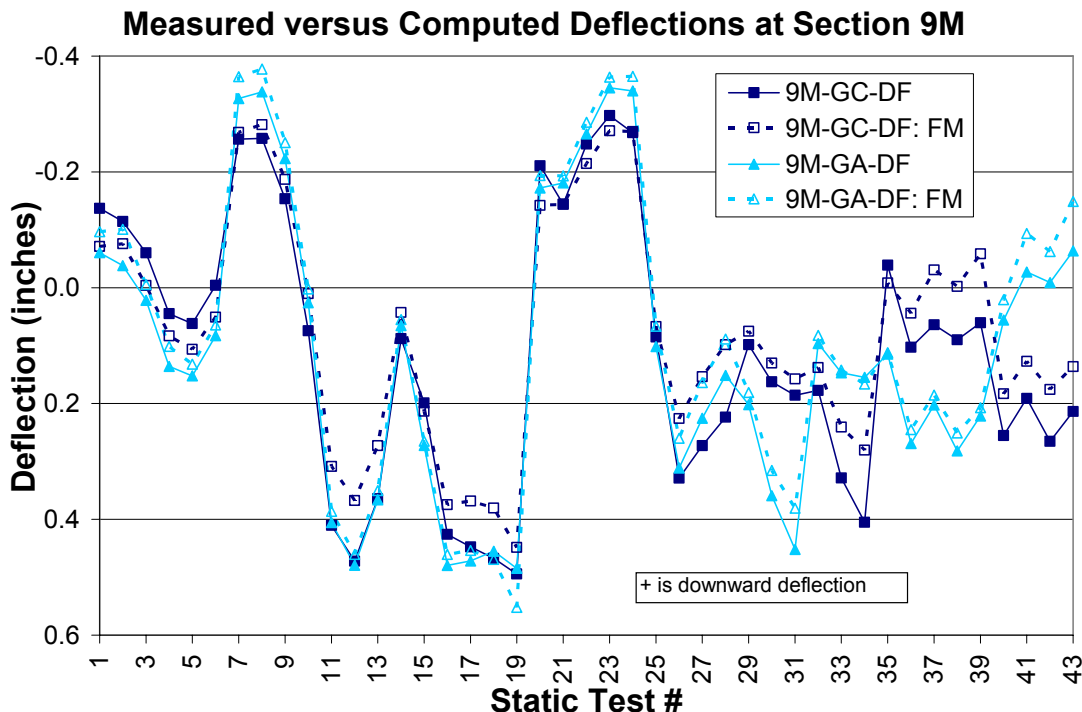


Figure F-3

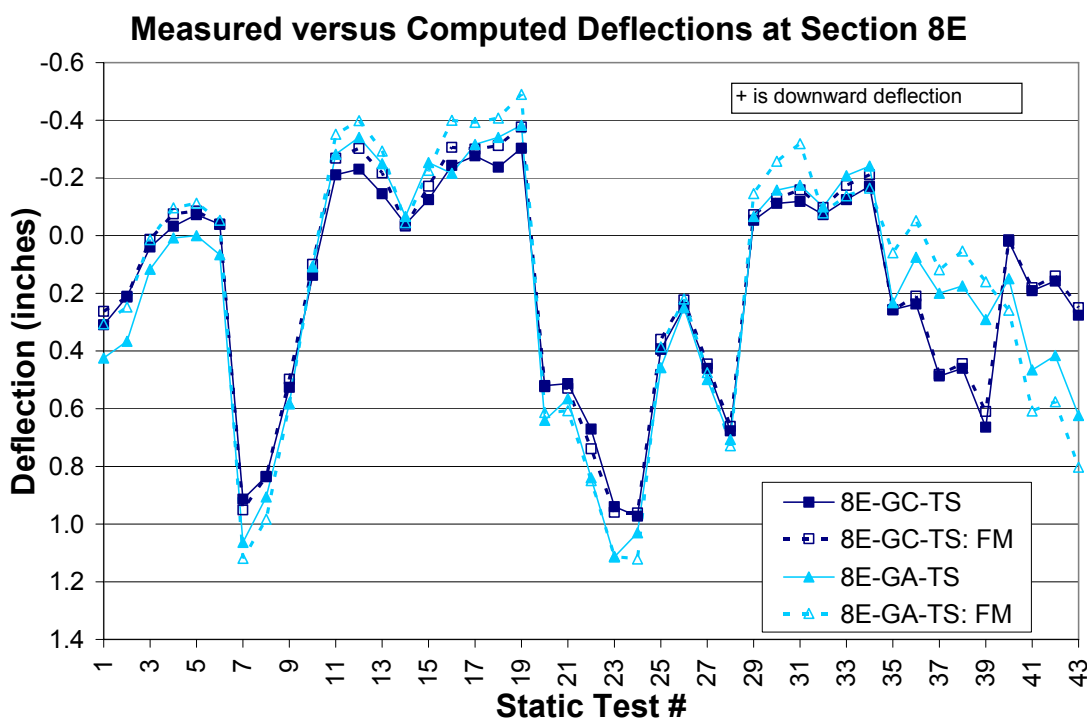


Figure F-4

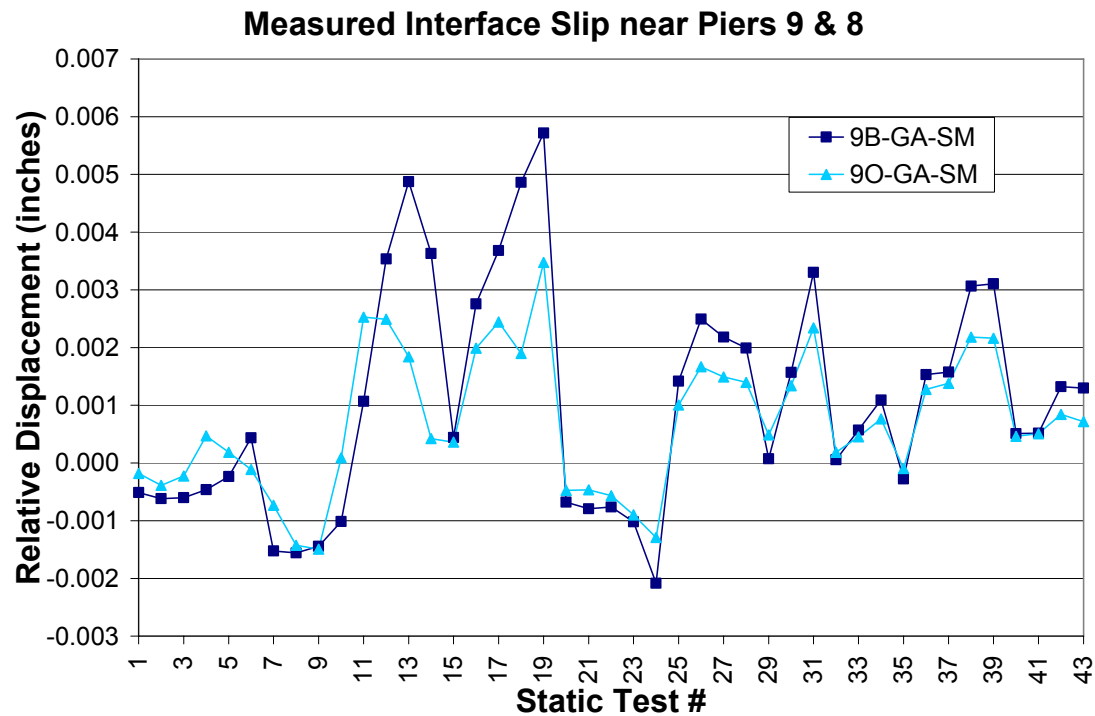


Figure F-5

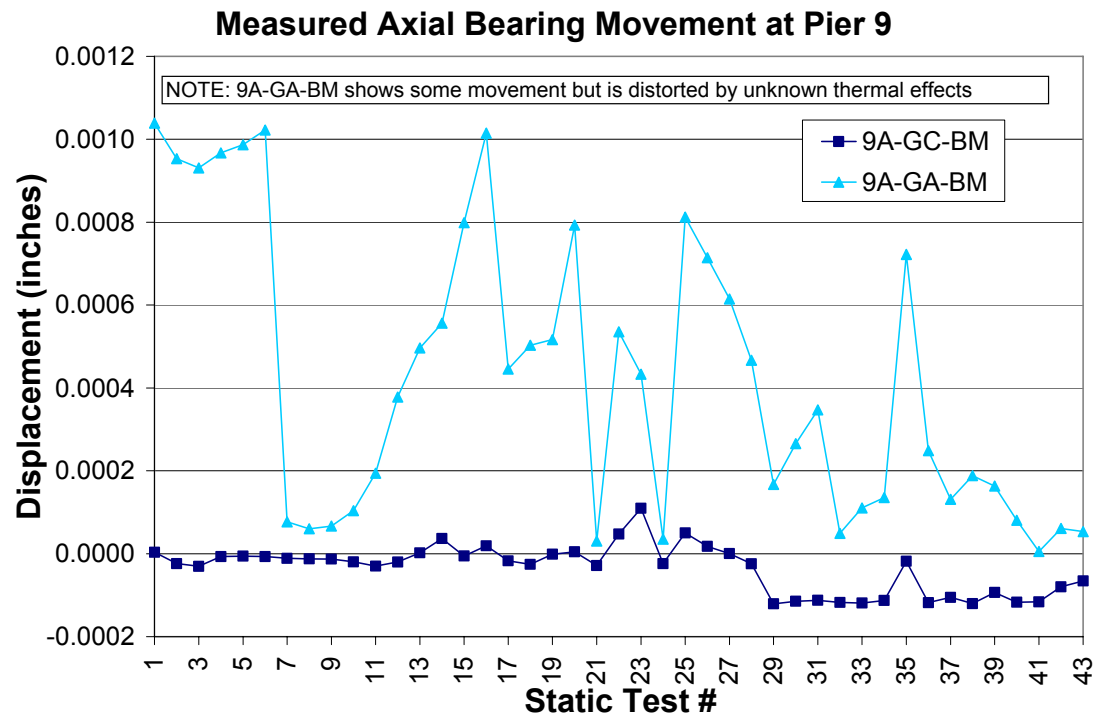


Figure F-6

**Measured versus Computed Stress
at Section 10Z Girder C**

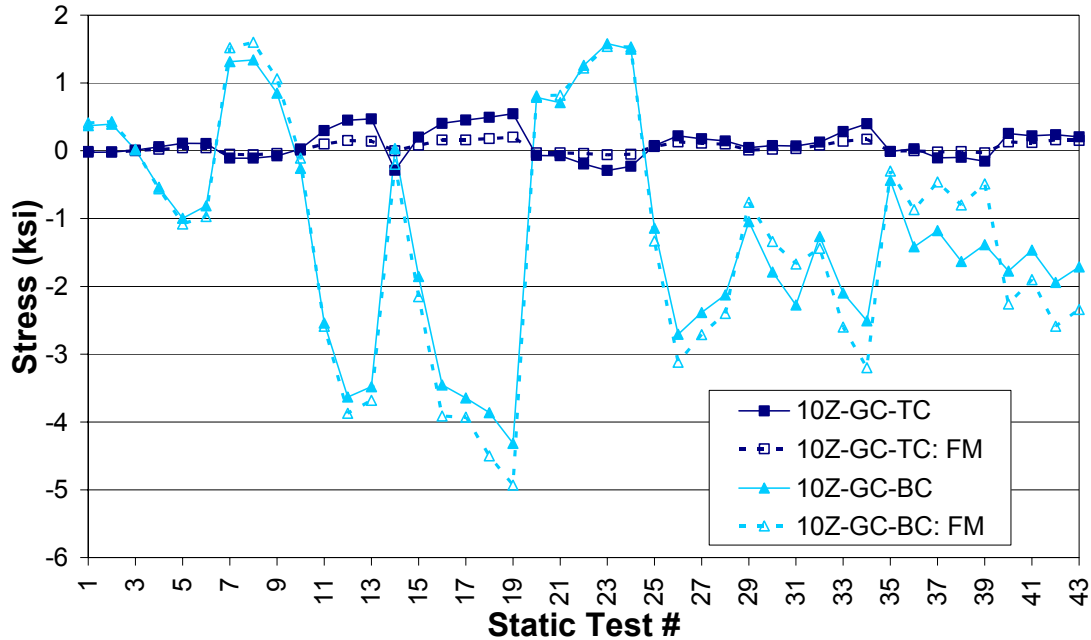


Figure F-7

**Measured versus Computed Stress
at Section 10Z Girder A**

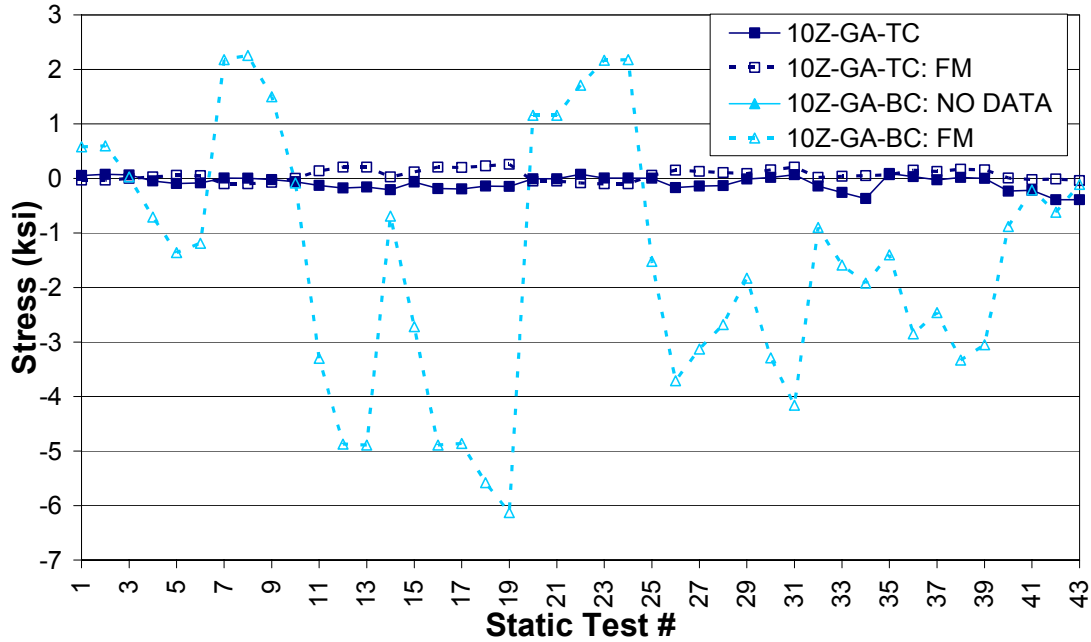


Figure F-8

**Measured versus Computed Stress
at Section 9B Girder C**

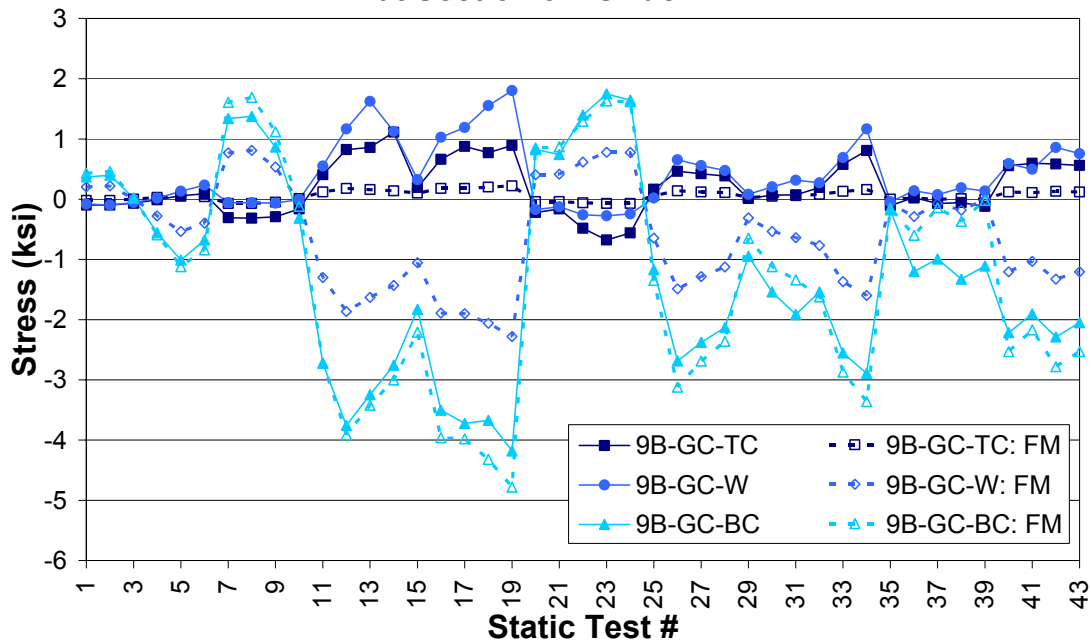


Figure F-9

**Measured versus Computed Stress
at Section 9B Girder C - Top Flange Tips**

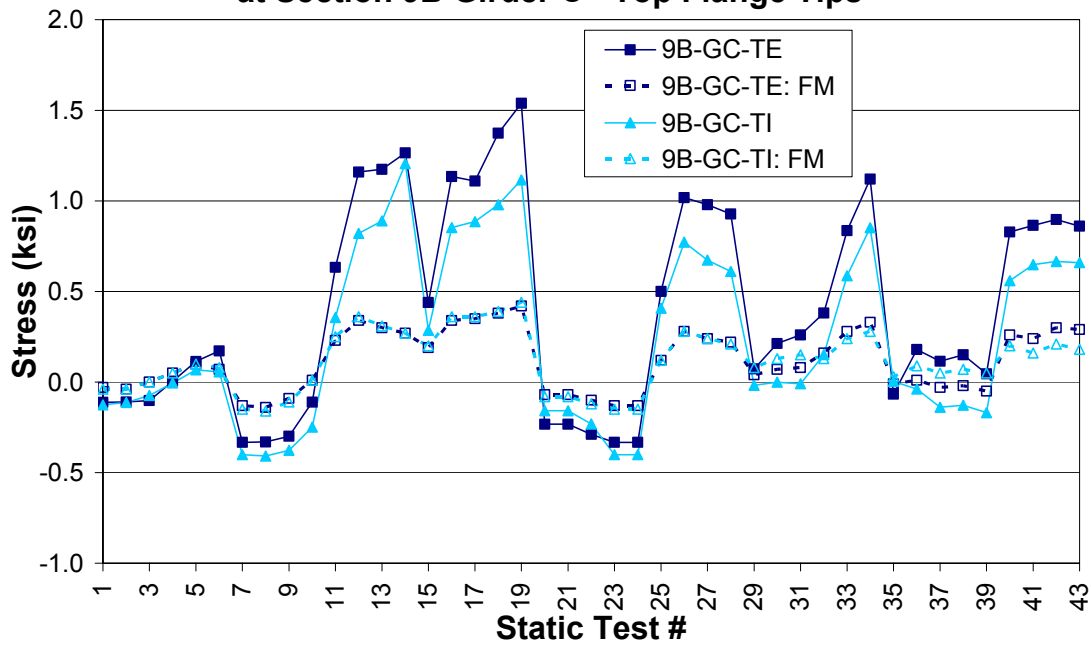


Figure F-10

**Measured versus Computed Stress
at Section 9B Girder C - Bottom Flange Tips**

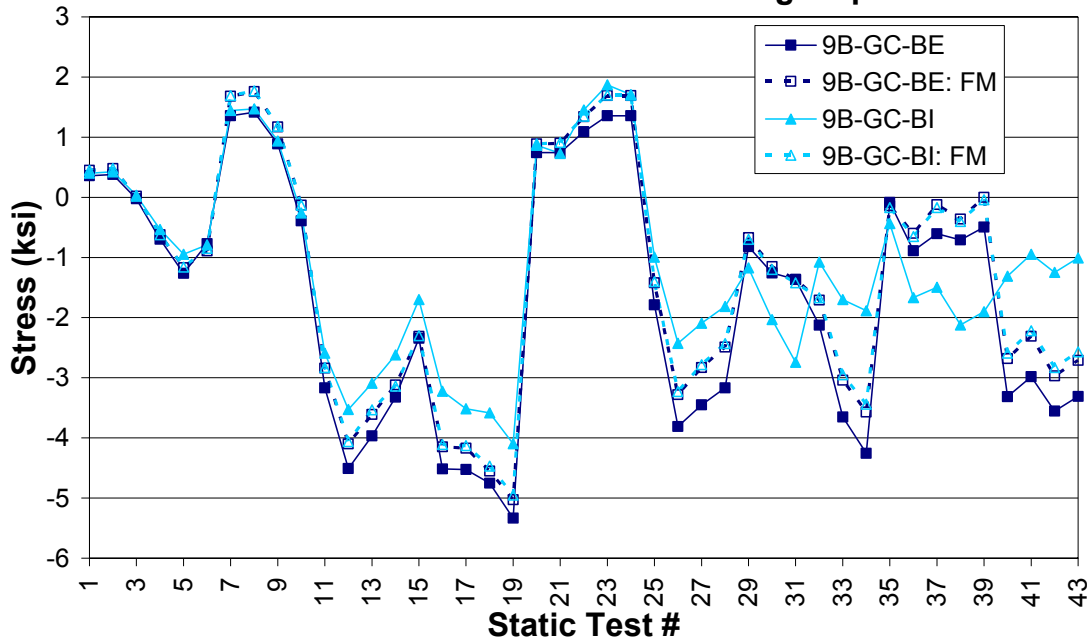


Figure F-11

**Measured versus Computed Stress
at Section 9B Girder A**

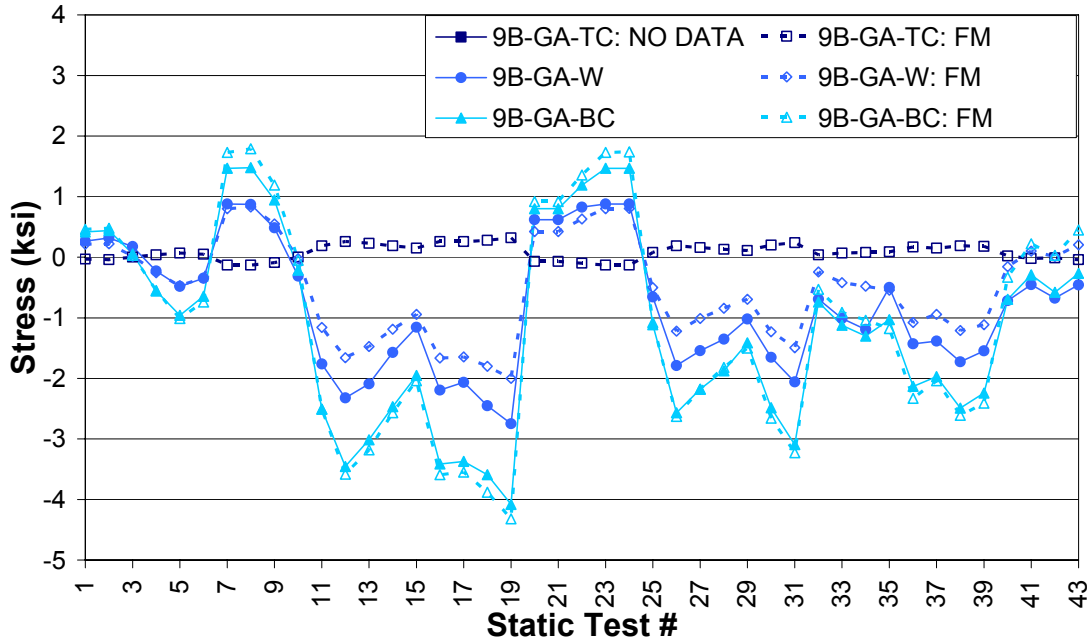


Figure F-12

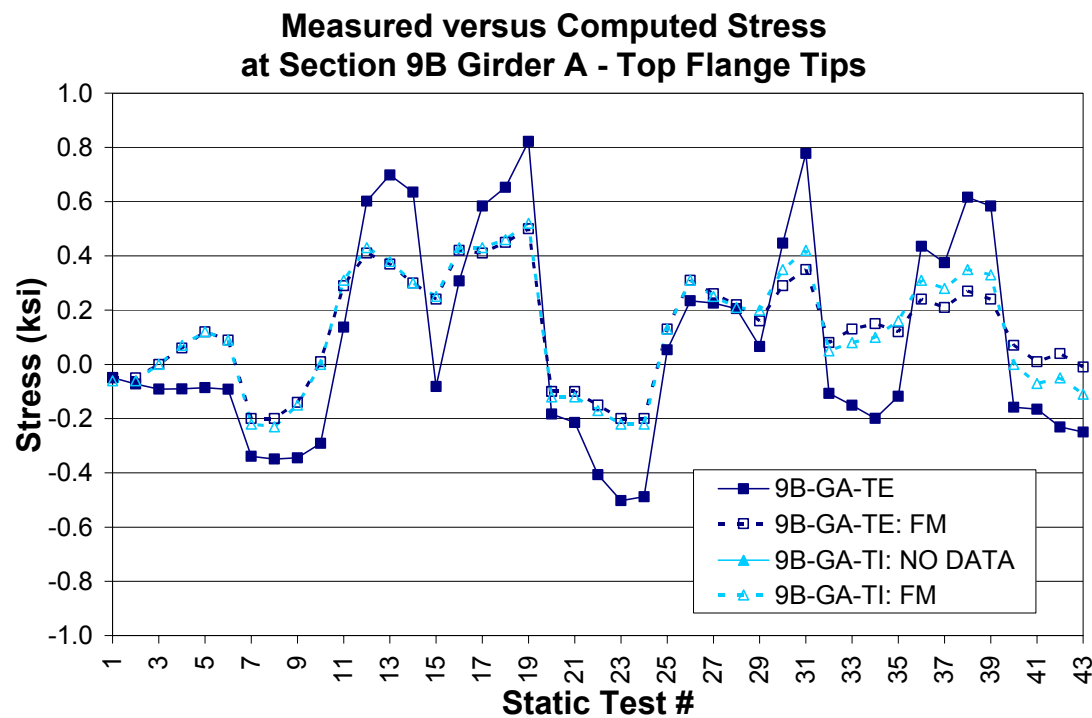


Figure F-13

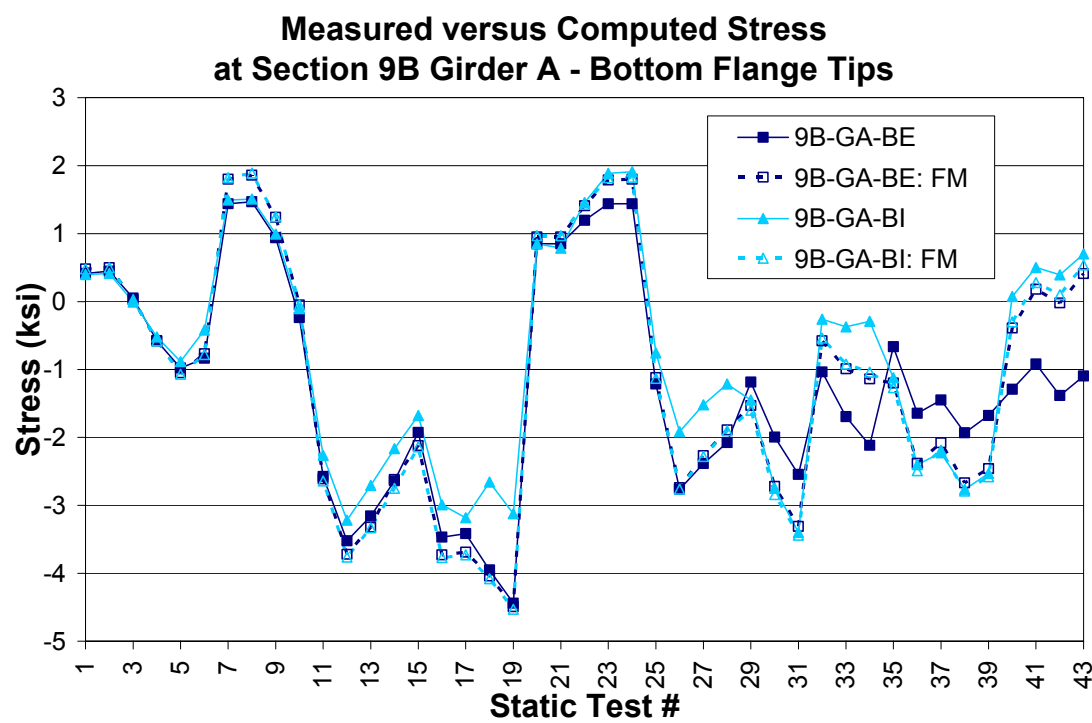


Figure F-14

Measured versus Computed Stress at Section 9C Girder C

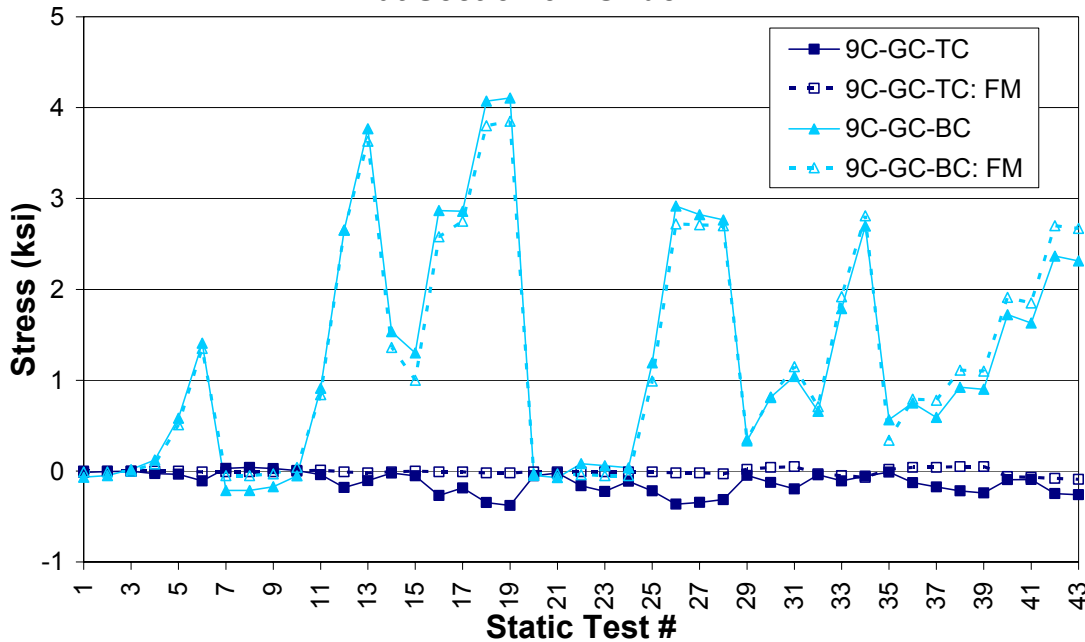


Figure F-15

Measured versus Computed Stress at Section 9C Girder A

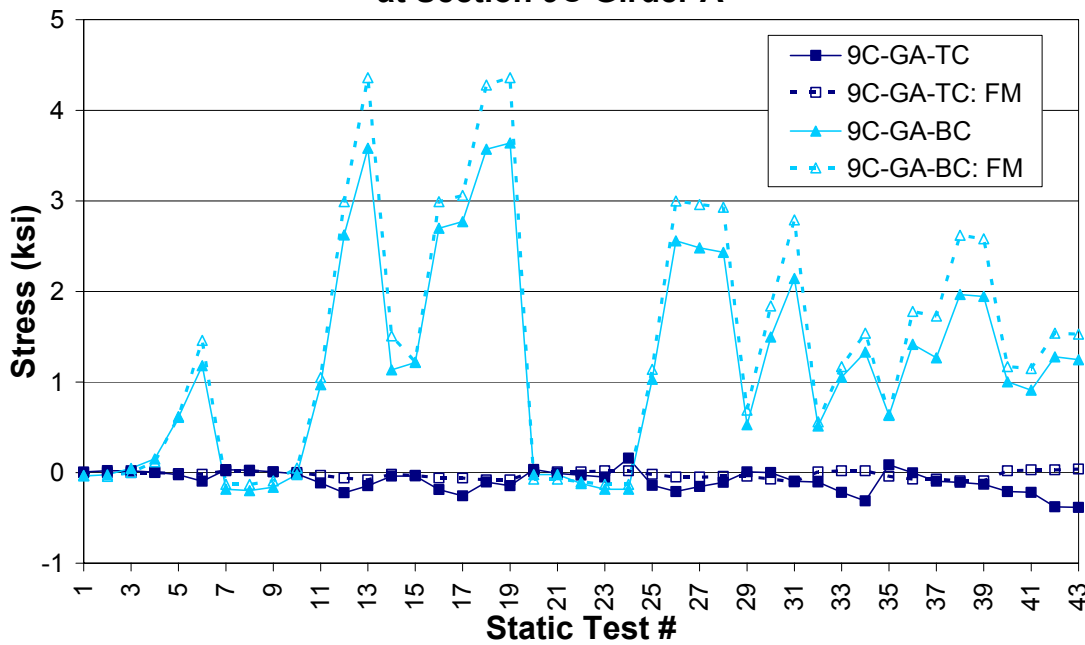


Figure F-16

**Measured versus Computed Stress
at Section 9H Girder C**

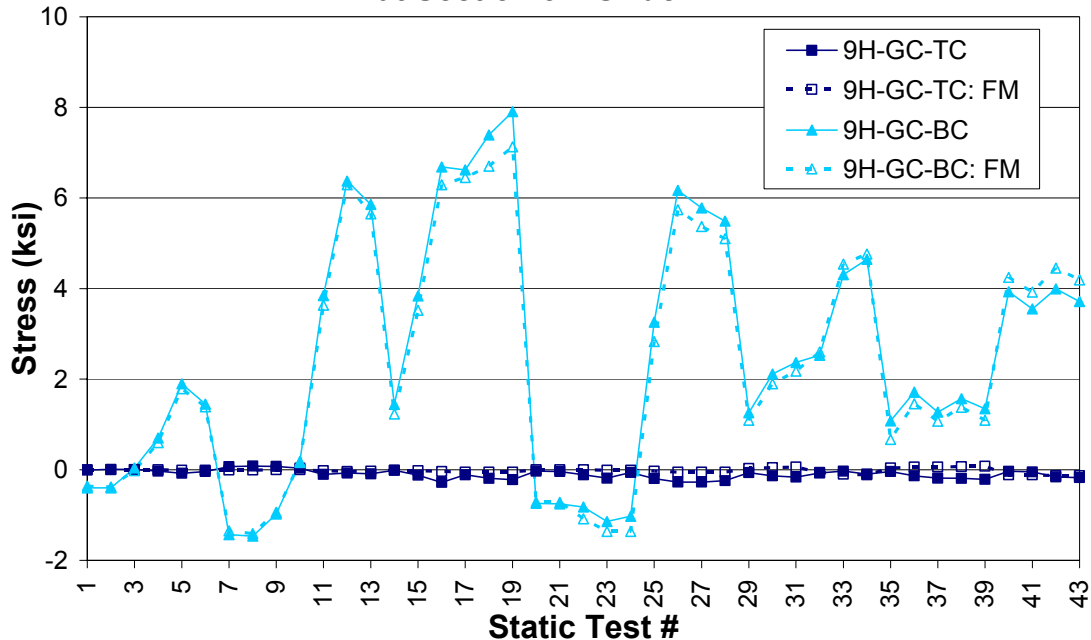


Figure F-17

**Measured versus Computed Stress
at Section 9H Girder A**

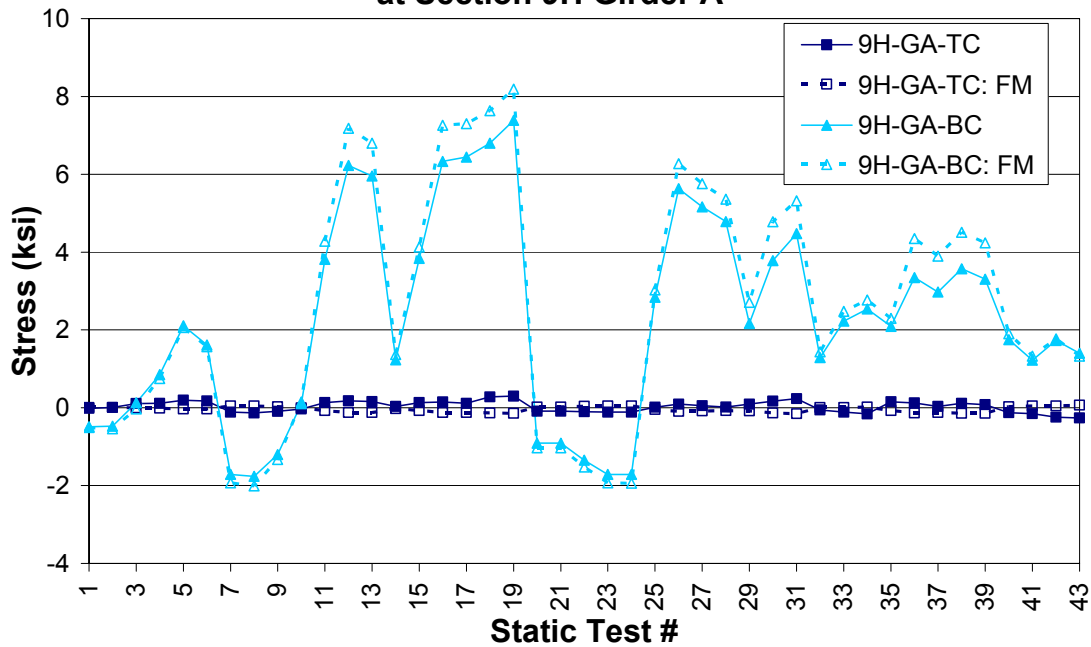


Figure F-18

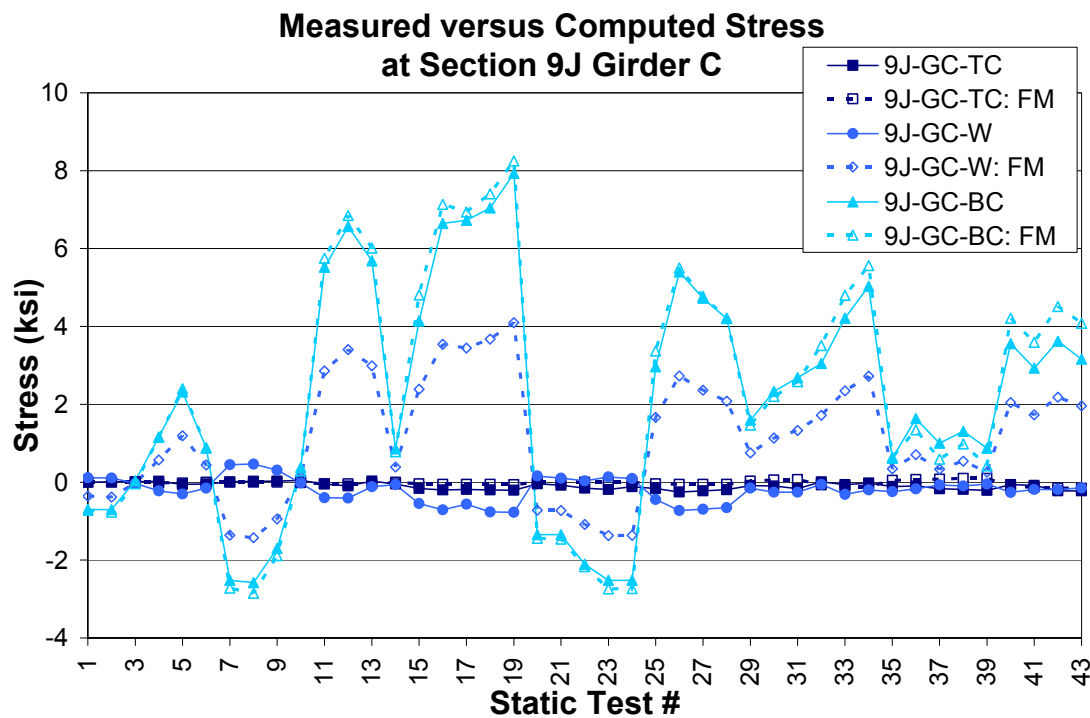


Figure F-19

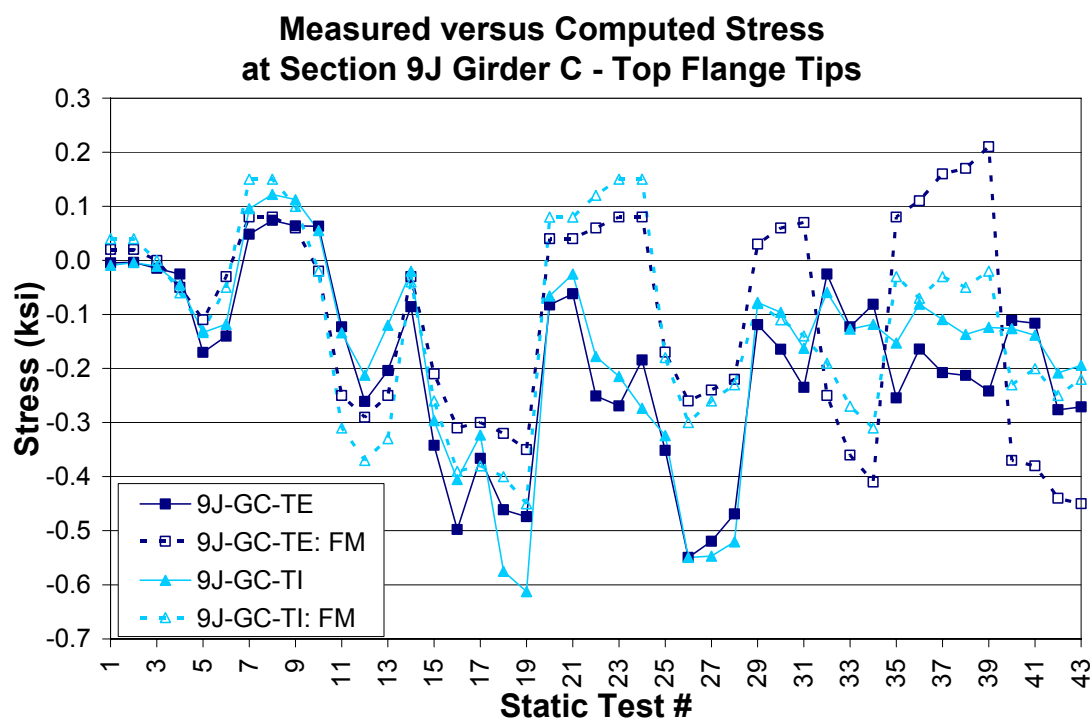


Figure F-20

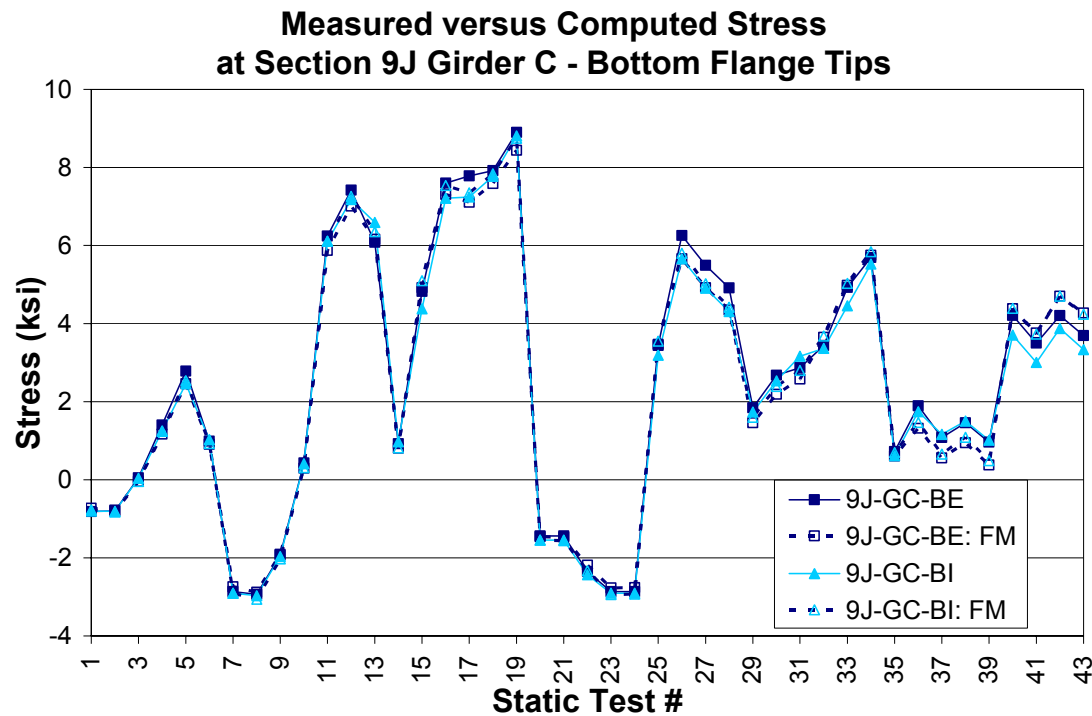


Figure F-21

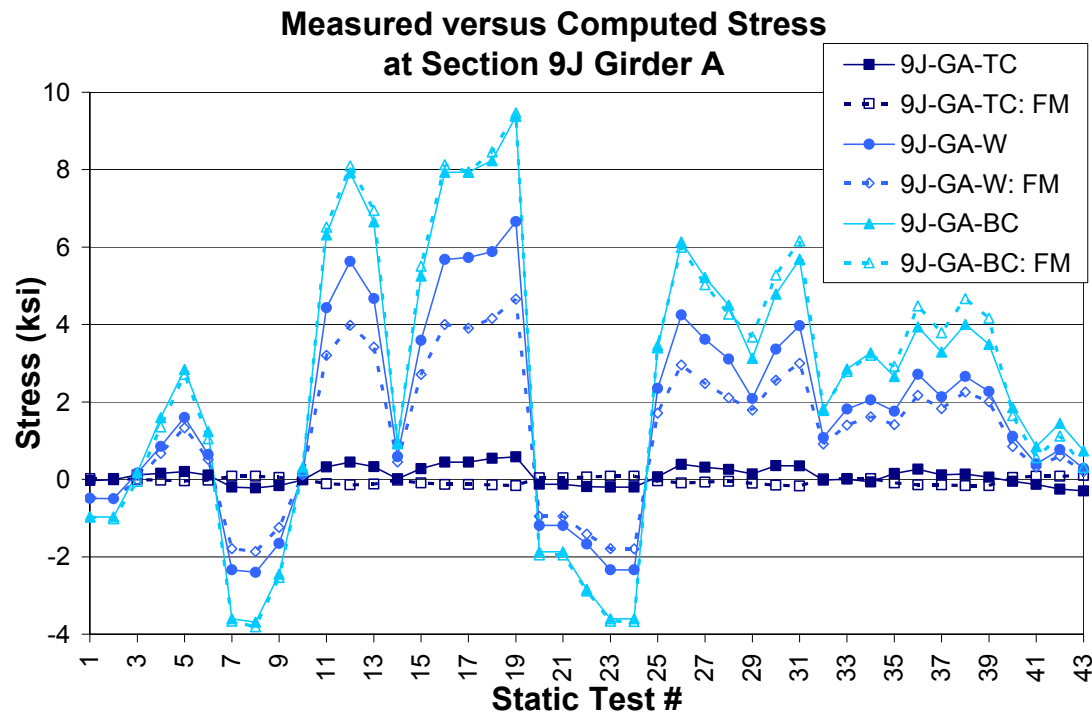


Figure F-22

**Measured versus Computed Stress
at Section 9J Girder A - Top Flange Tips**

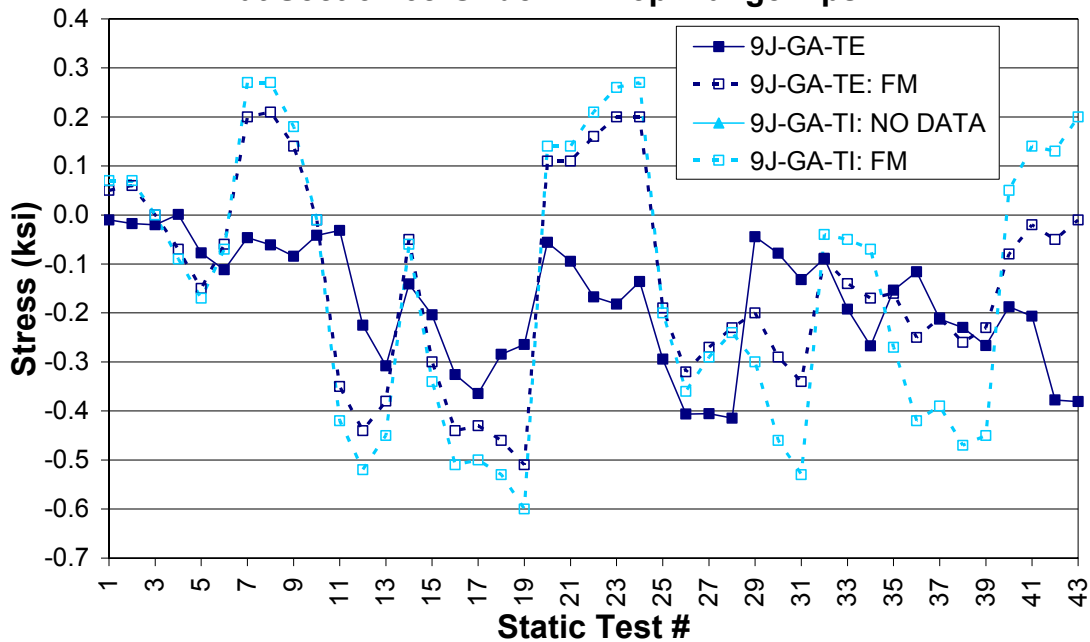


Figure F-23

**Measured versus Computed Stress
at Section 9J Girder A - Bottom Flange Tips**

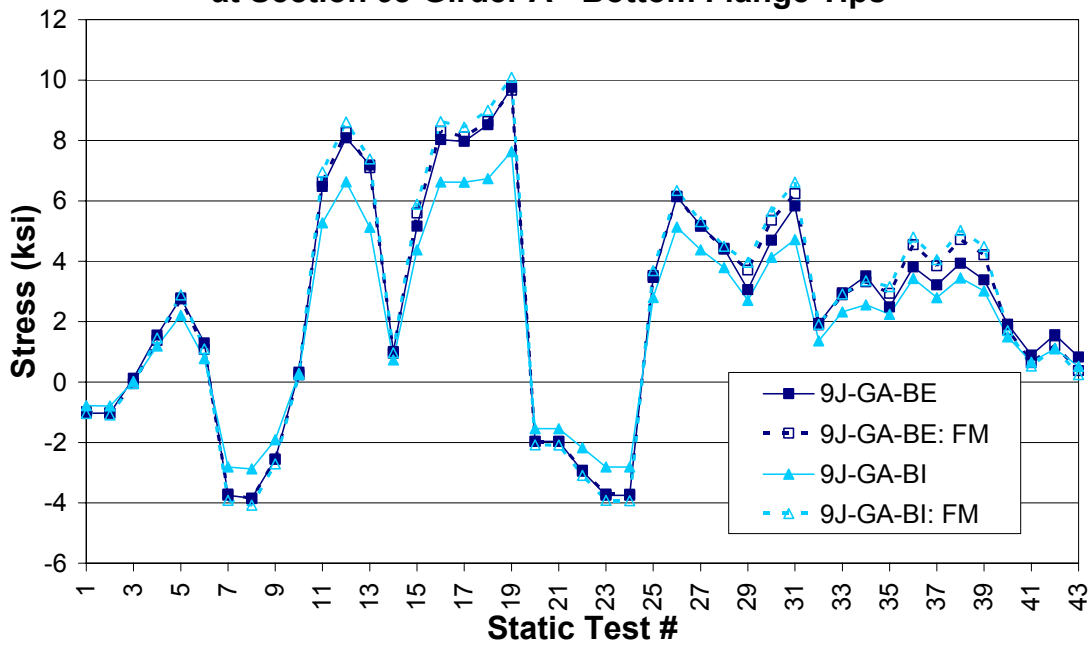


Figure F-24

**Measured versus Computed Stress
at Section 9L Girder C**

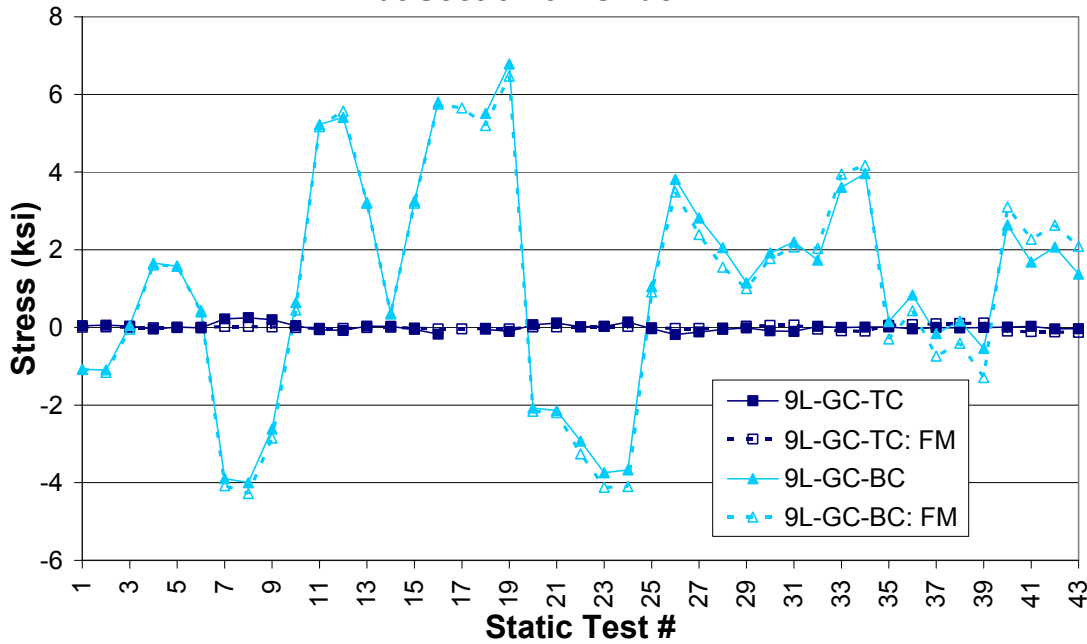


Figure F-25

**Measured versus Computed Stress
at Section 9L Girder A**

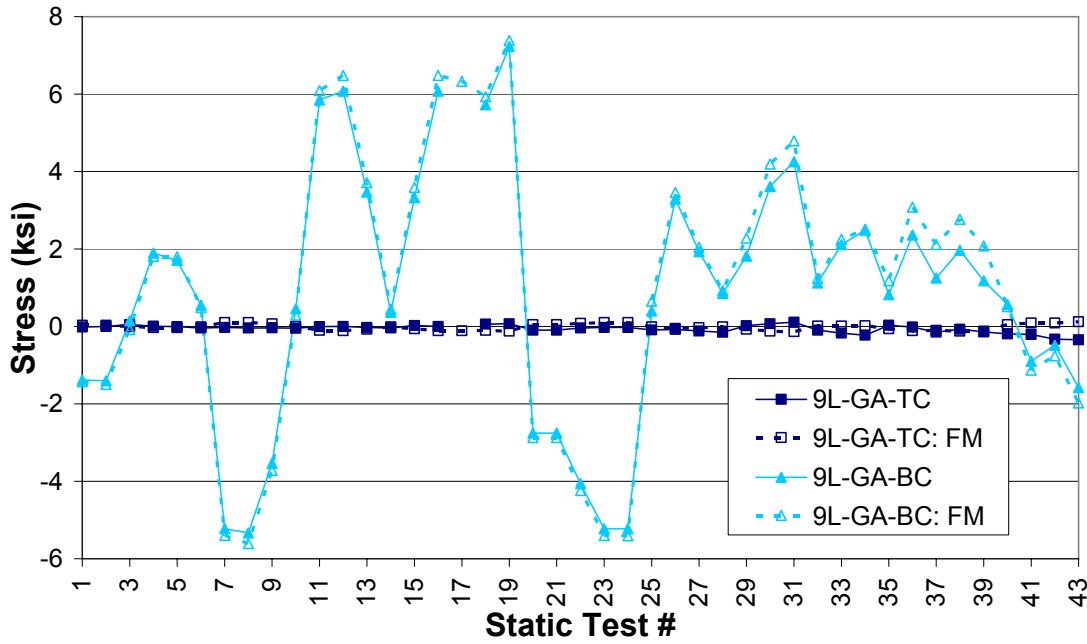


Figure F-26

**Measured versus Computed Stress
at Section 9N Girder C**

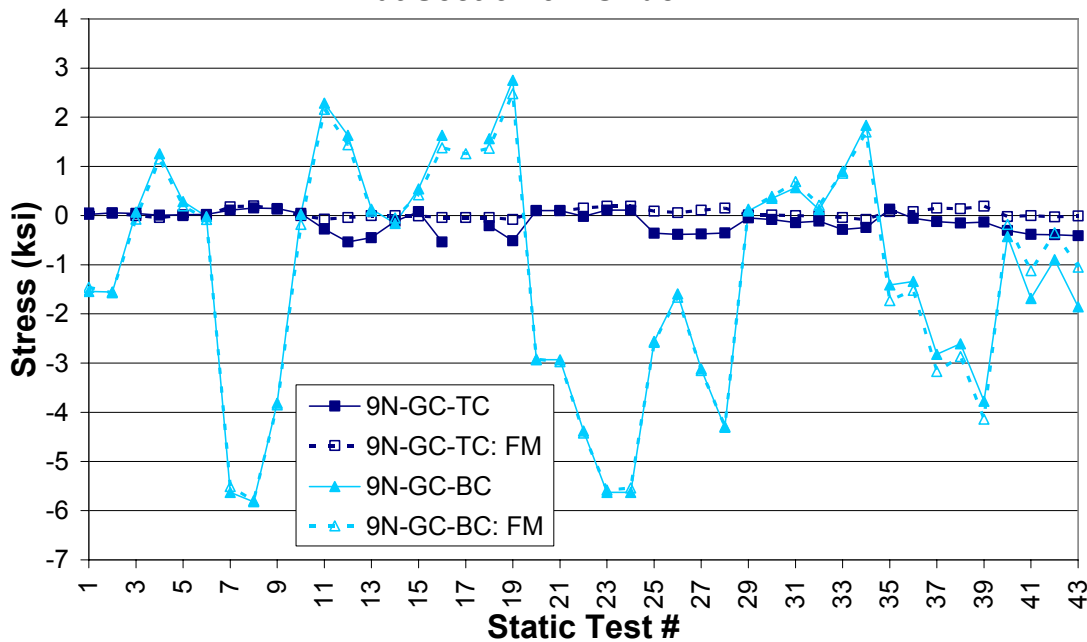


Figure F-27

**Measured versus Computed Stress
at Section 9N Girder A**

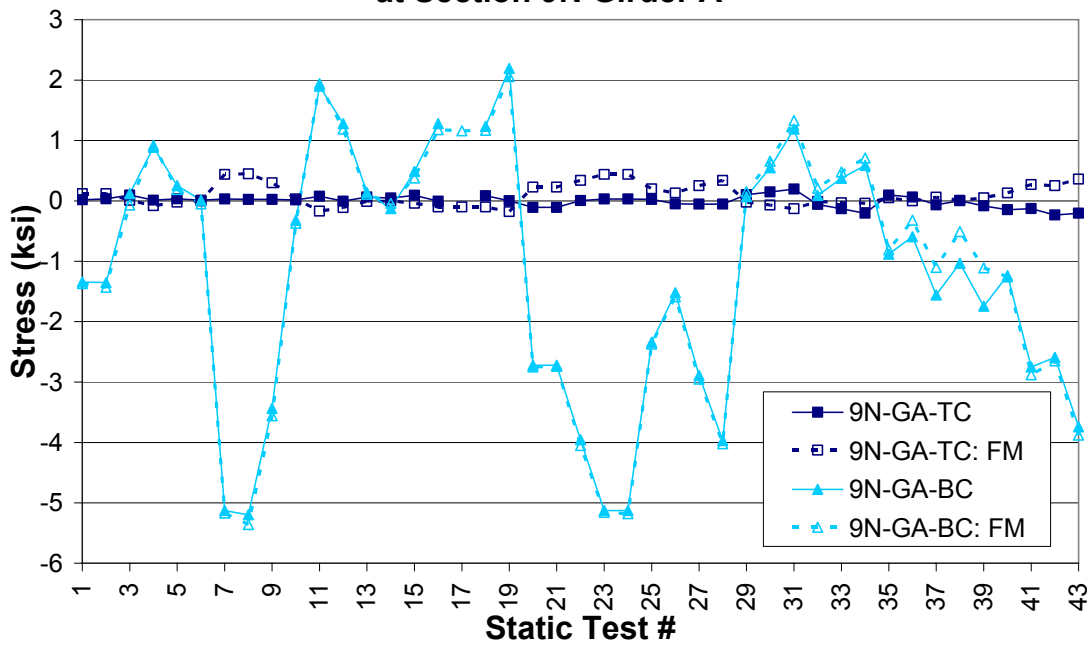


Figure F-28

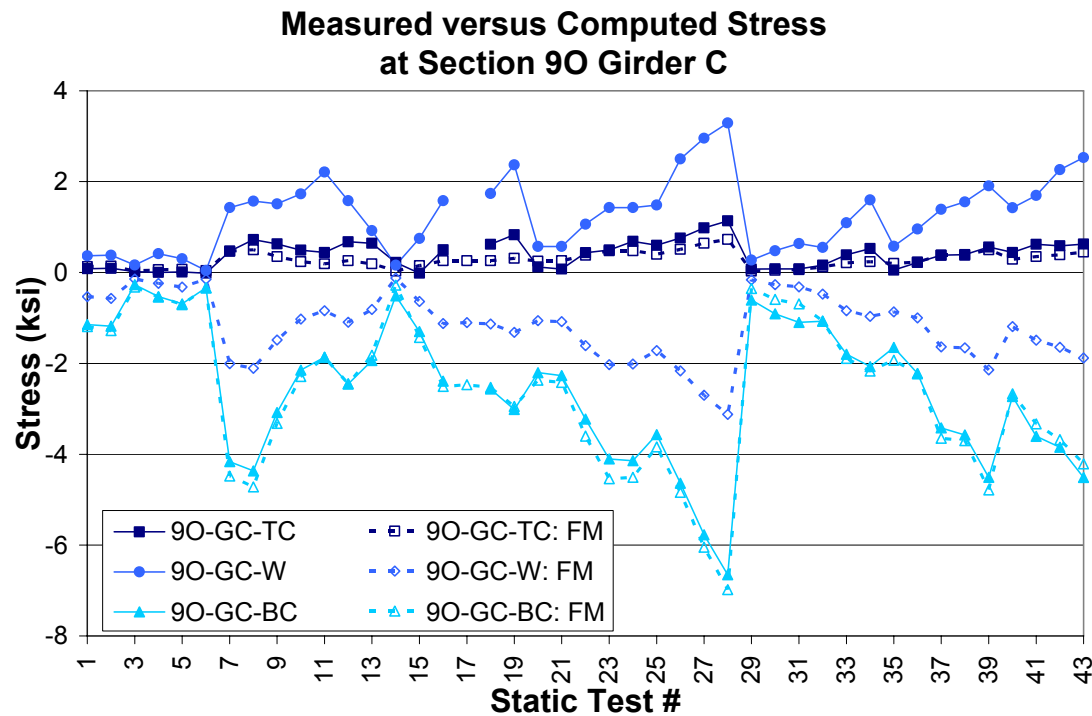


Figure F-29

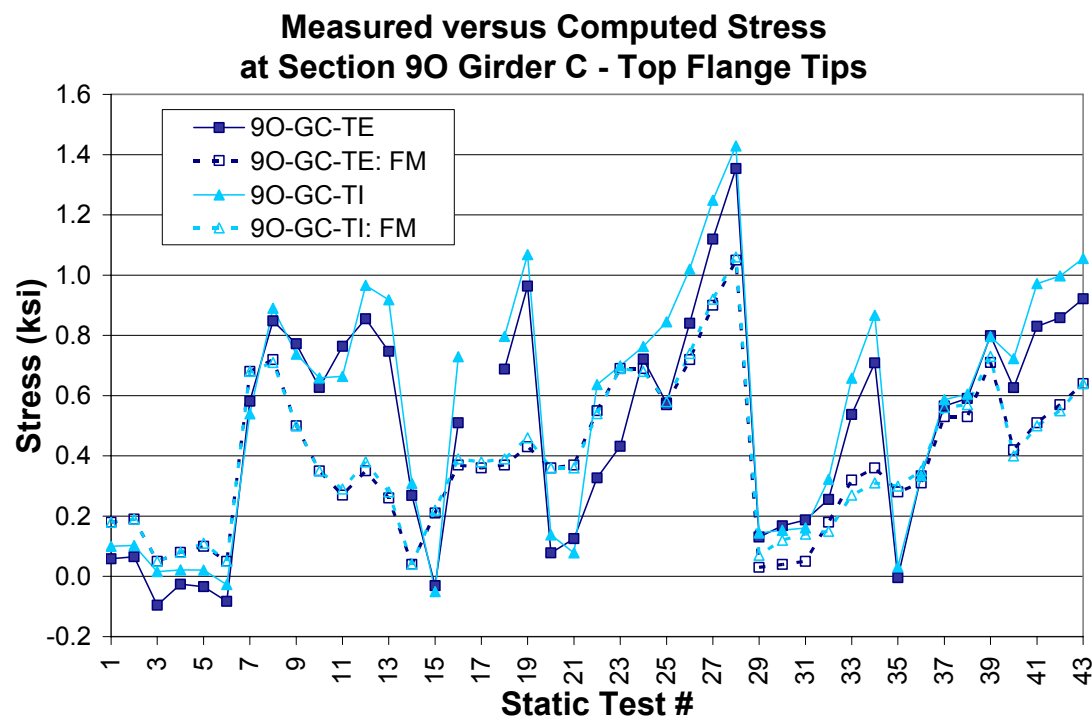


Figure F-30

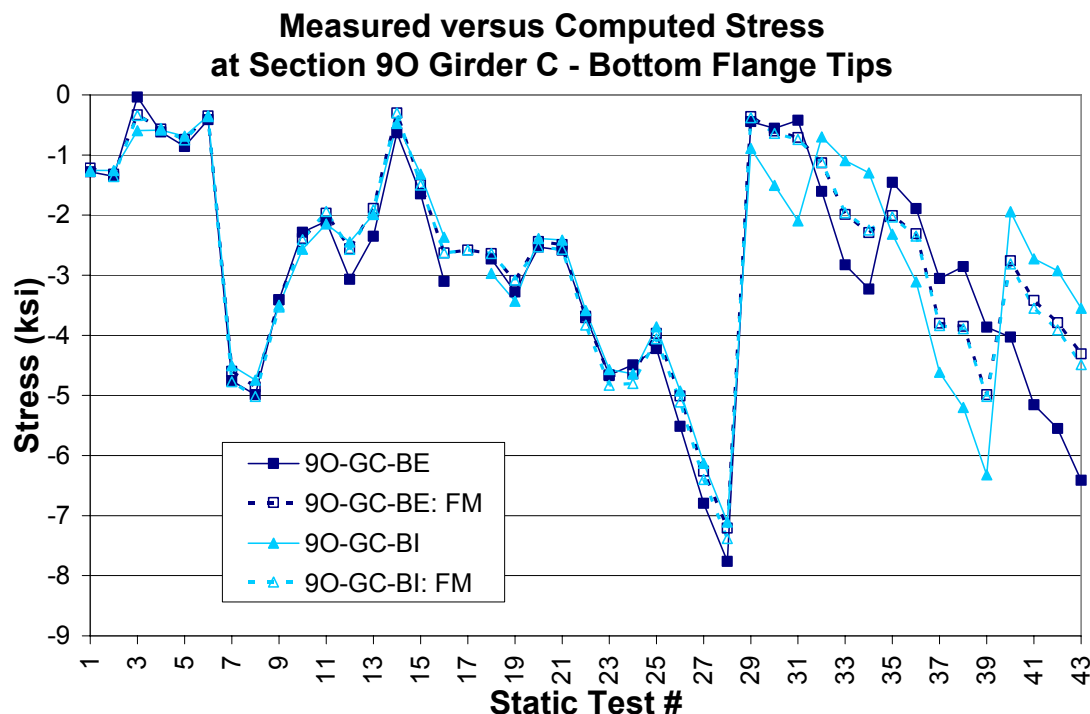


Figure F-31

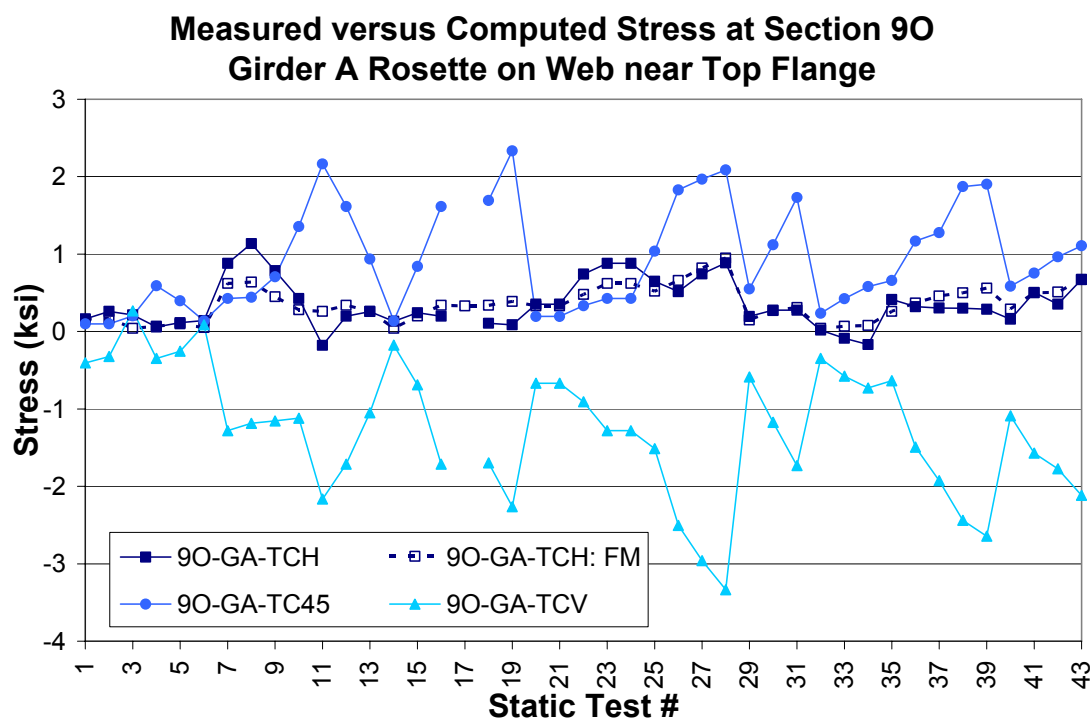


Figure F-32

**Measured versus Computed Stress at Section 9O
Girder A Rosette on Web at Mid-Height**

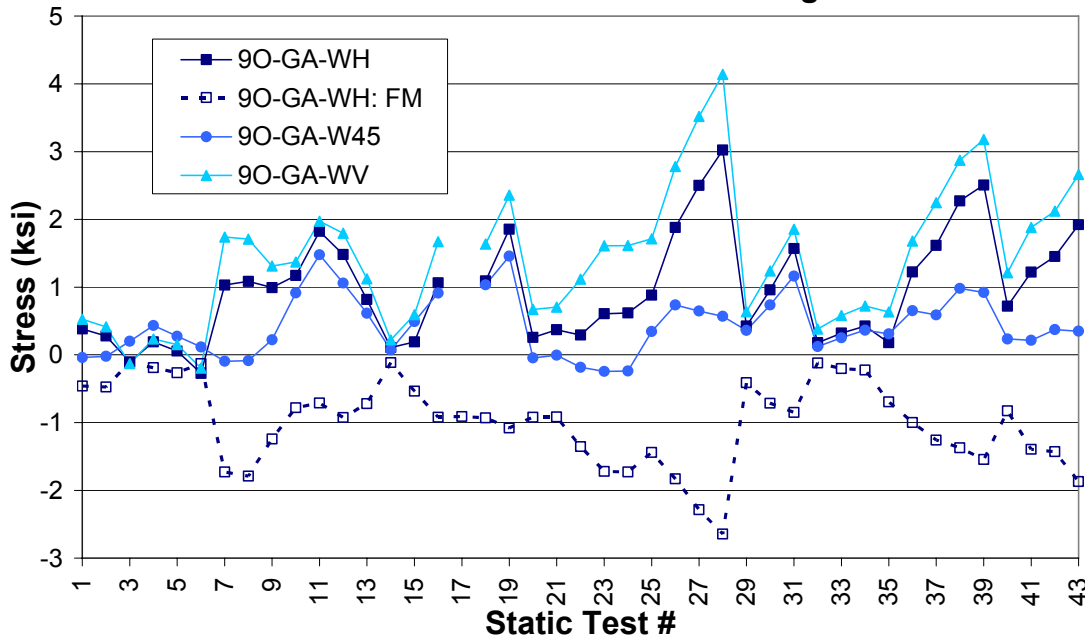


Figure F-33

**Measured versus Computed Stress at Section 9O
Girder A Rosette on Web near Bottom Flange)**

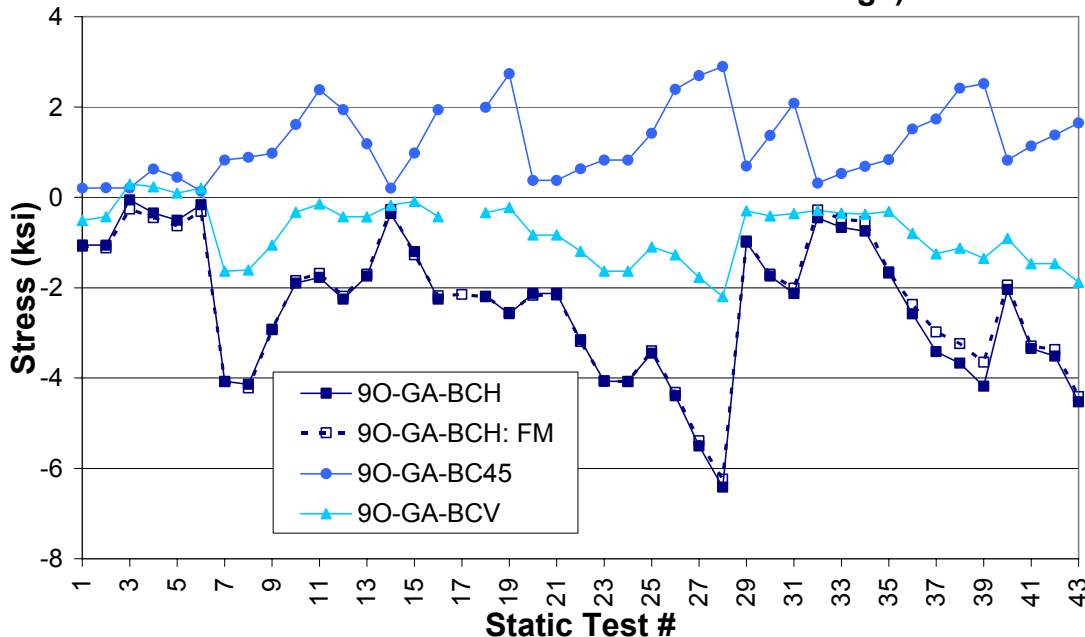


Figure F-34

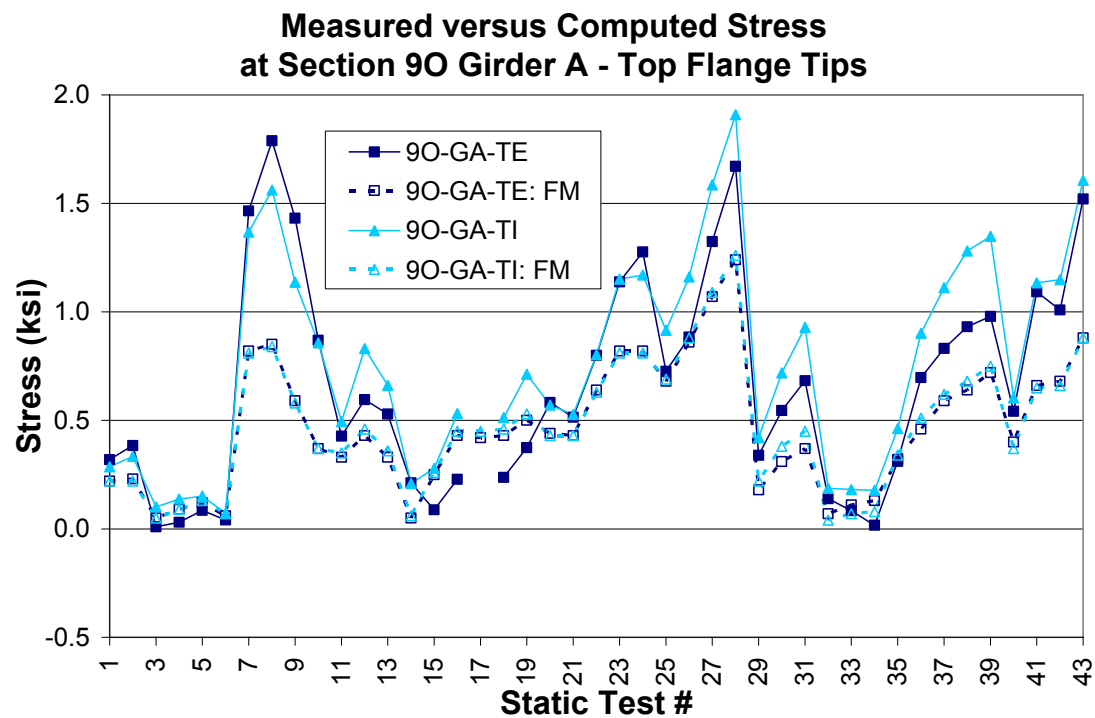


Figure F-35

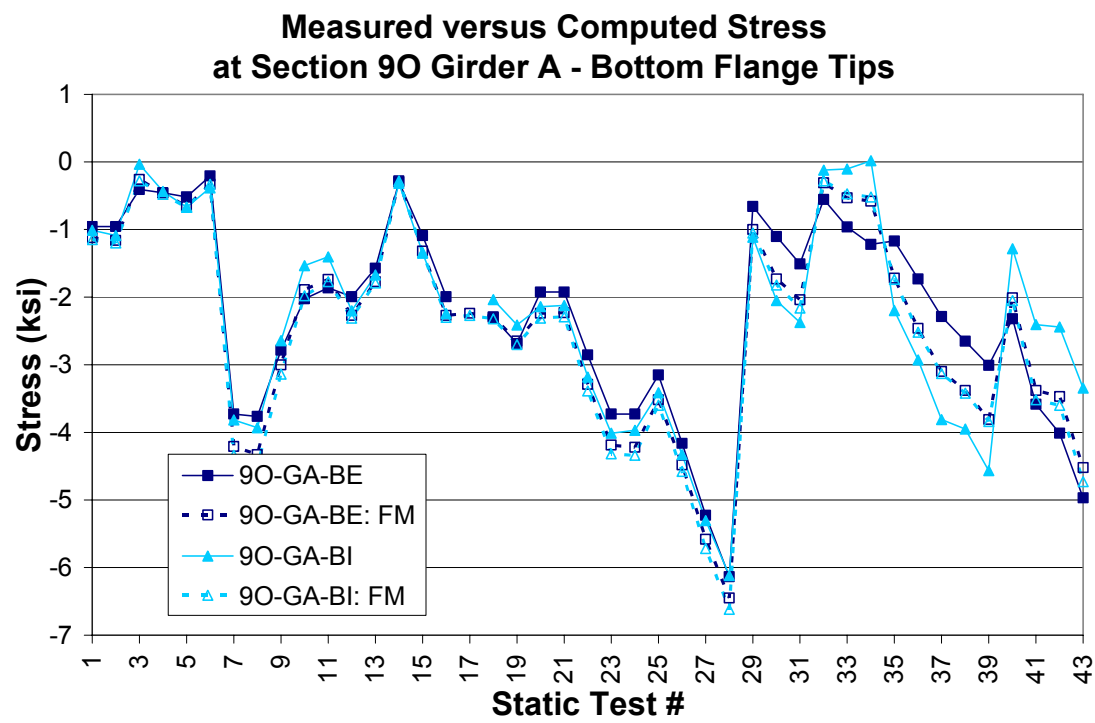


Figure F-36

Measured versus Computed Stress at Section 8C Girder C

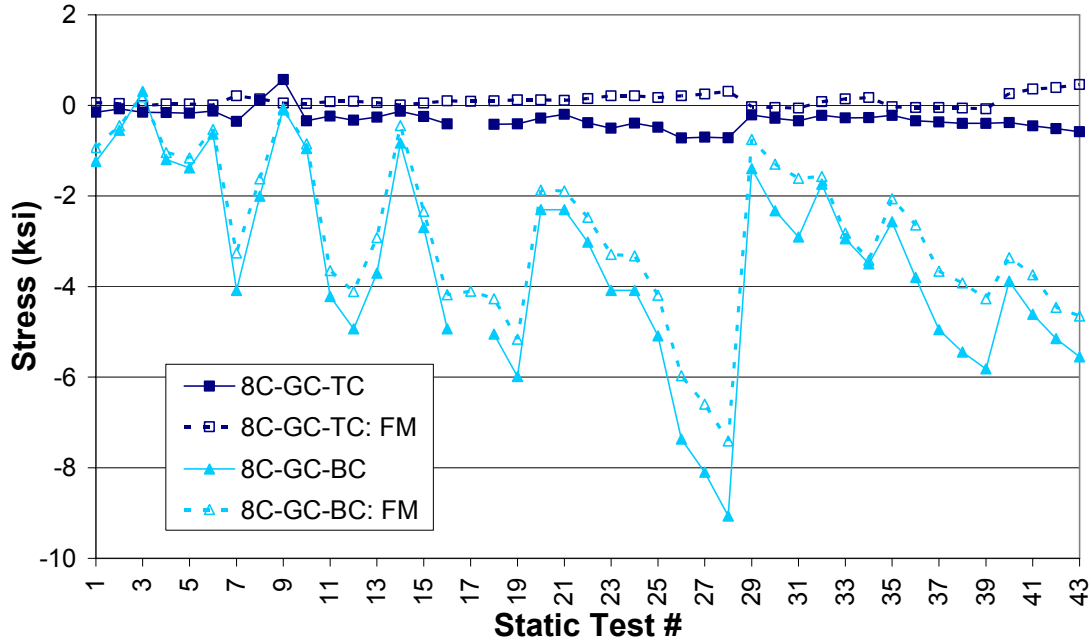


Figure F-37

Measured versus Computed Stress at Section 8C Girder A

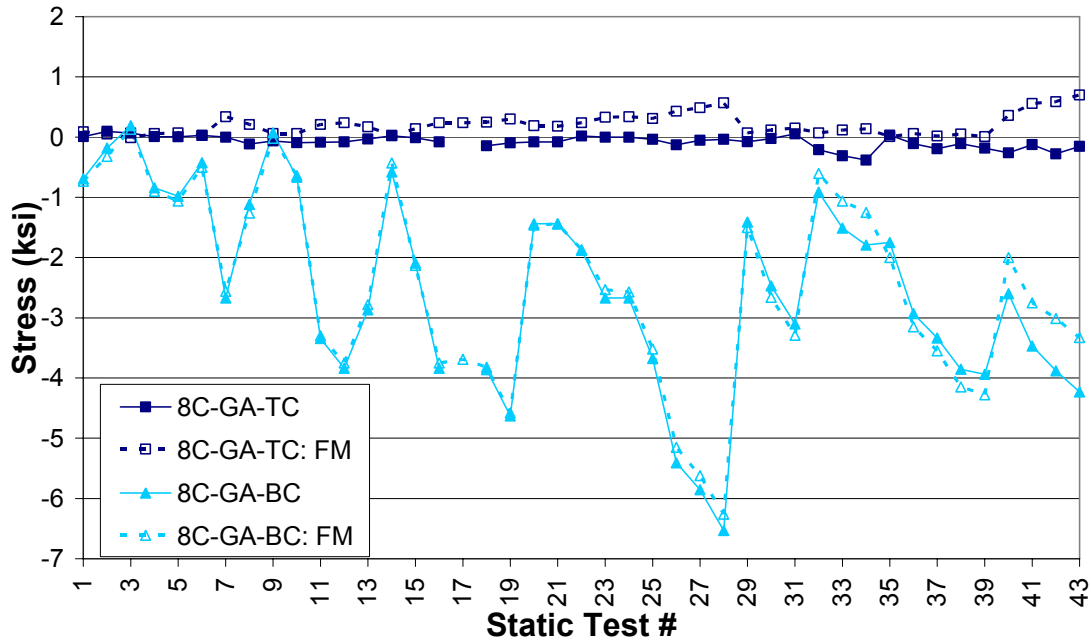


Figure F-38

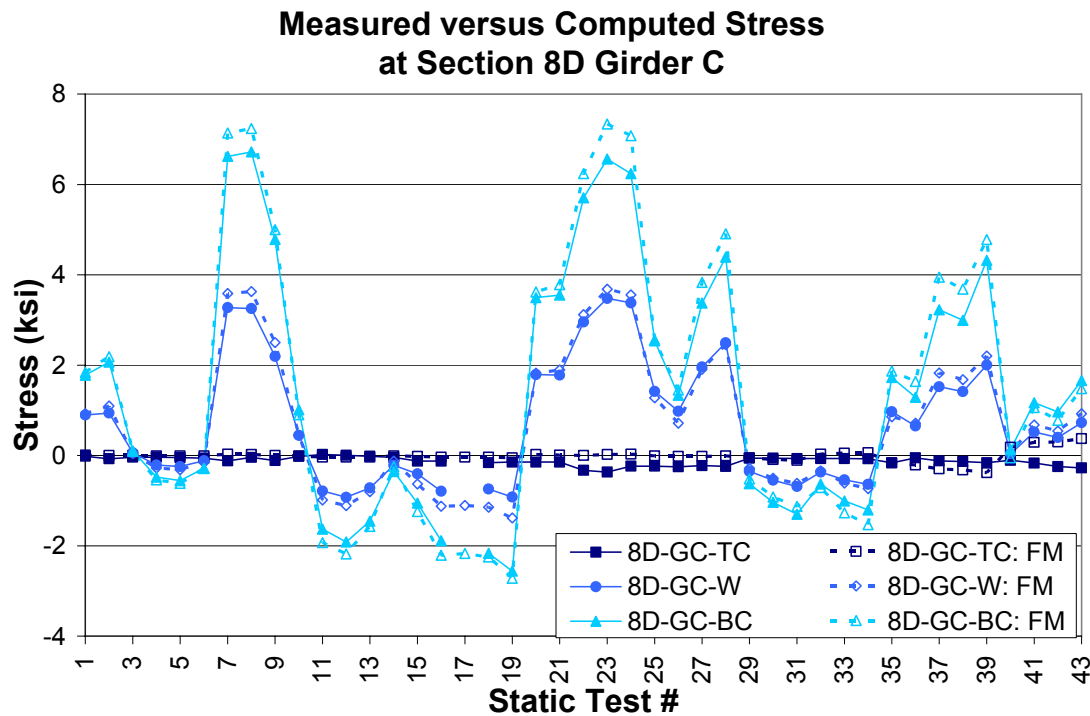


Figure F-39

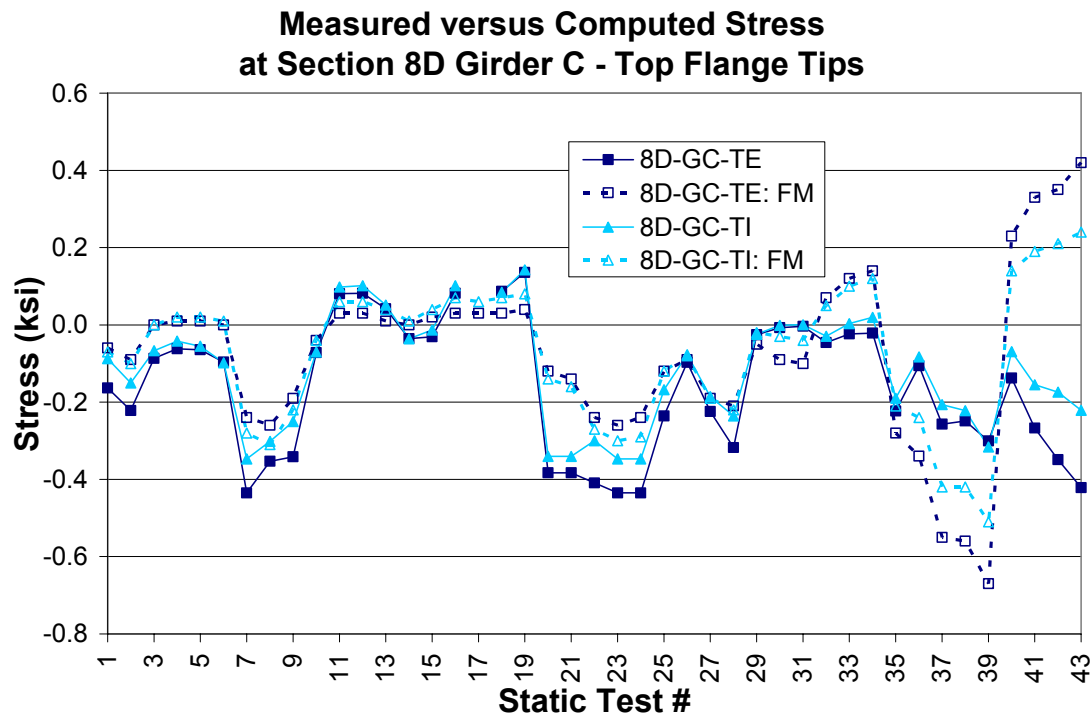


Figure F-40

**Measured versus Computed Stress
at Section 8D Girder C - Bottom Flange Tips**

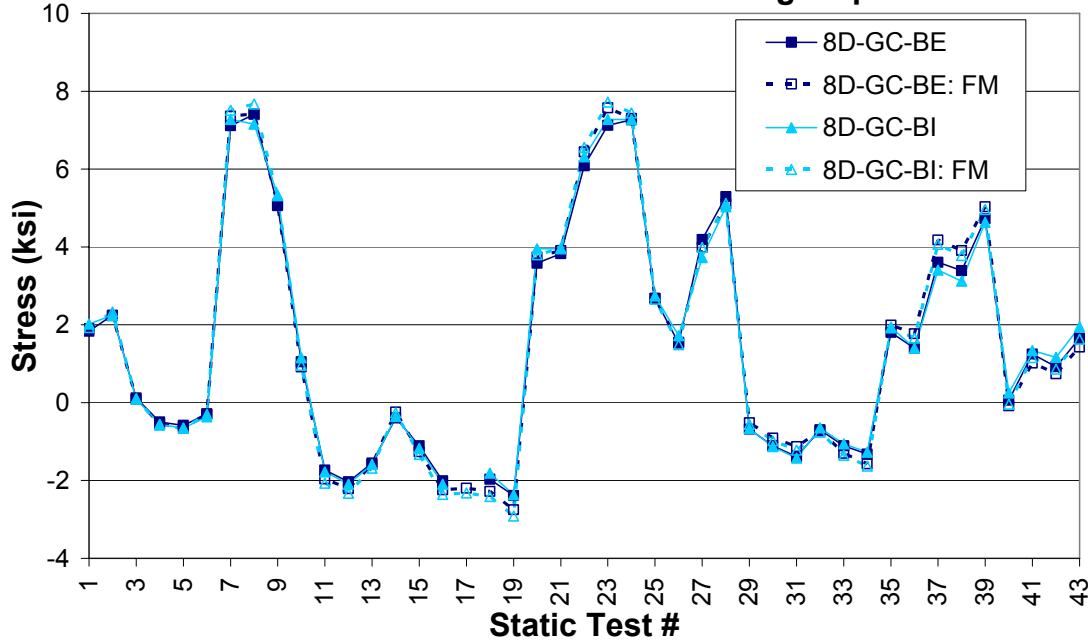


Figure F-41

**Measured versus Computed Stress
at Section 8D Girder A**

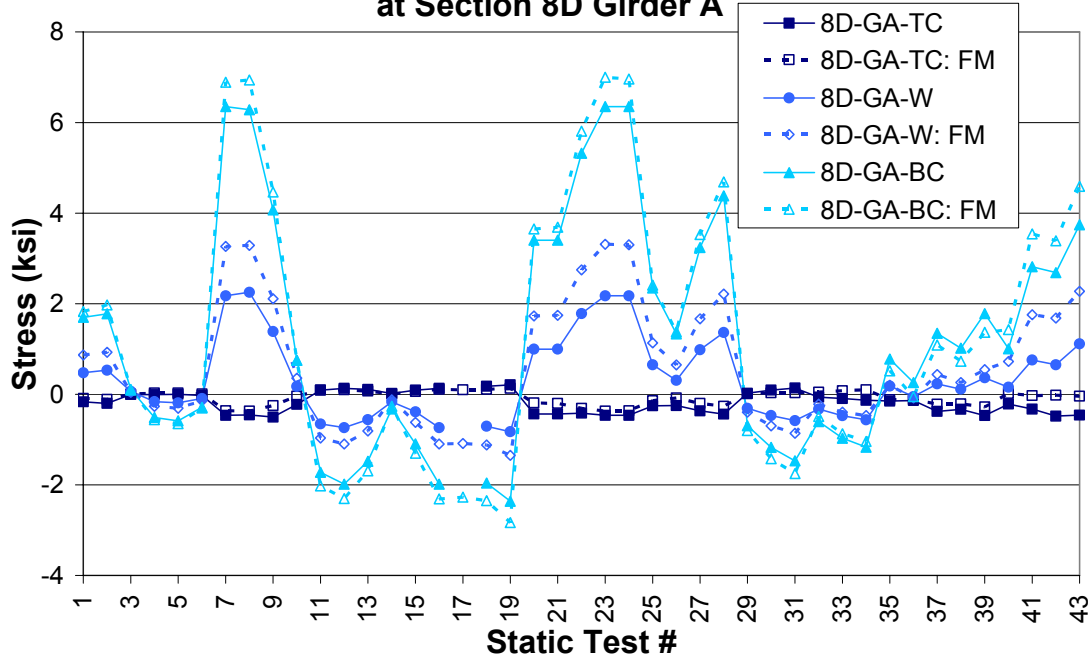


Figure F-42

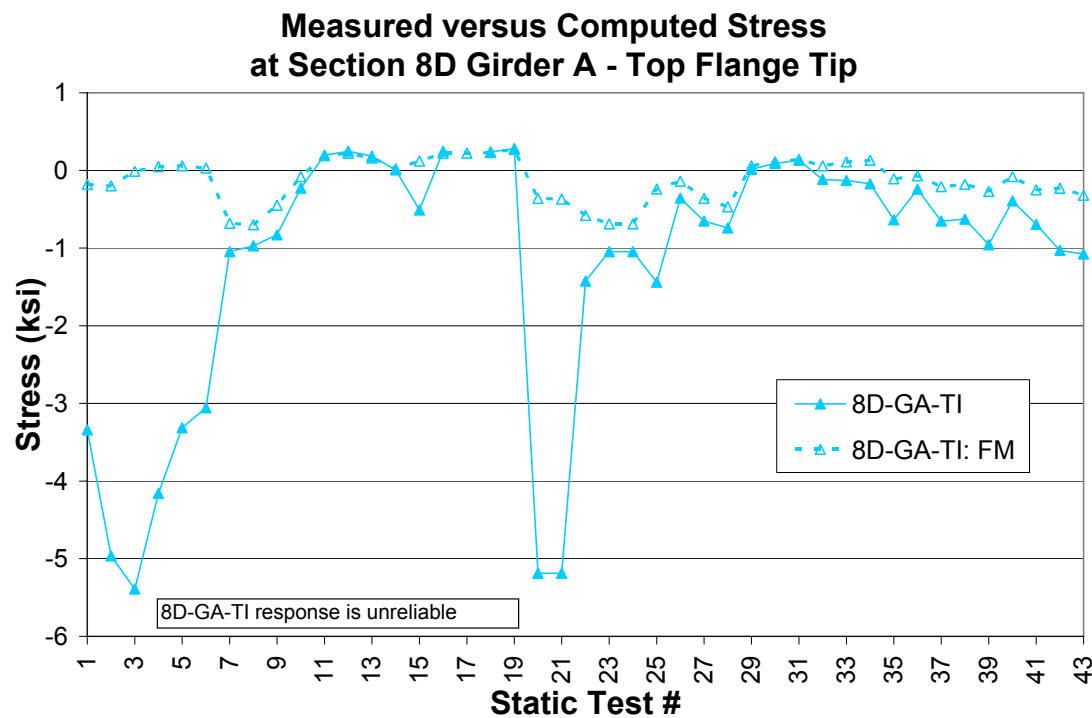


Figure F-43

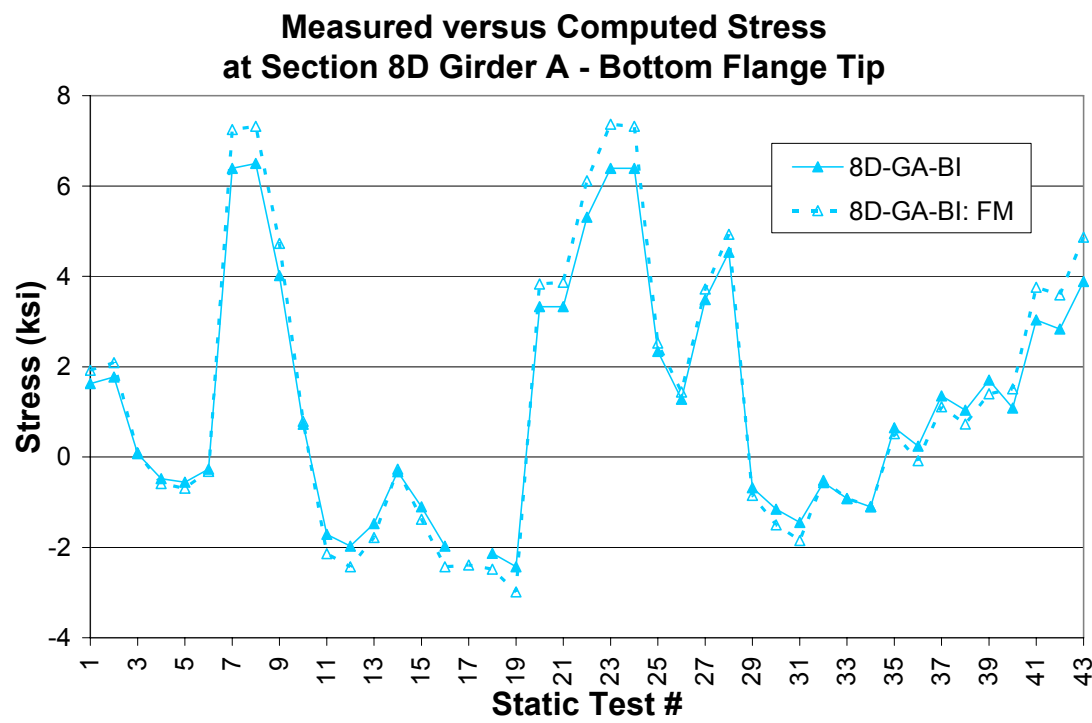


Figure F-44

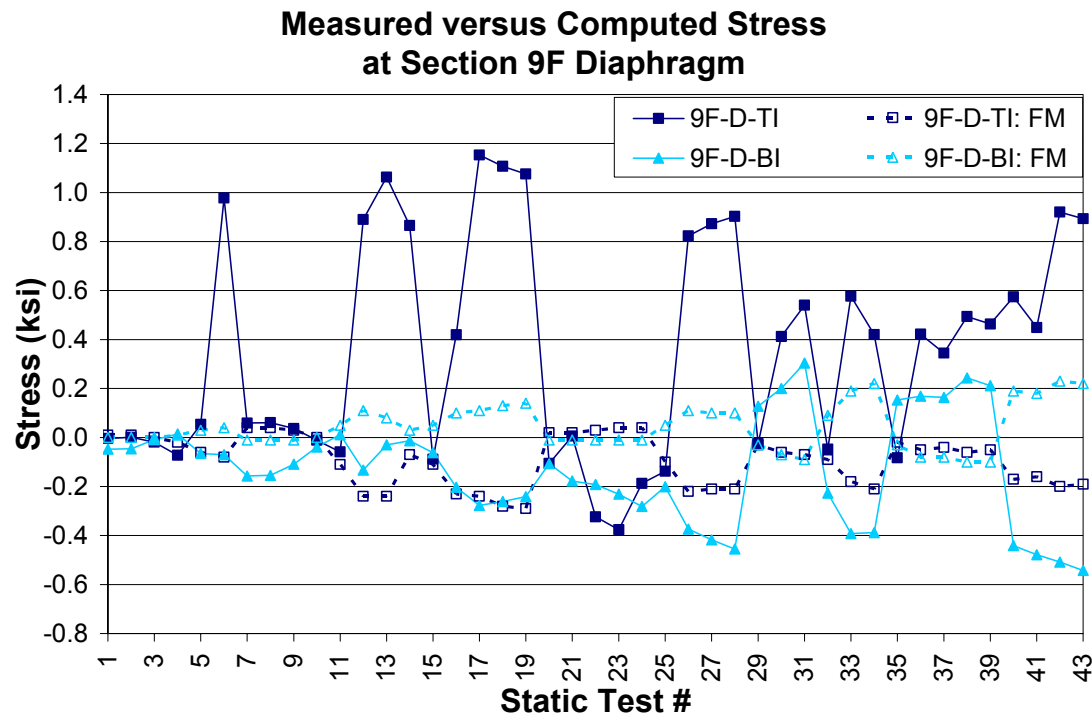


Figure F-45

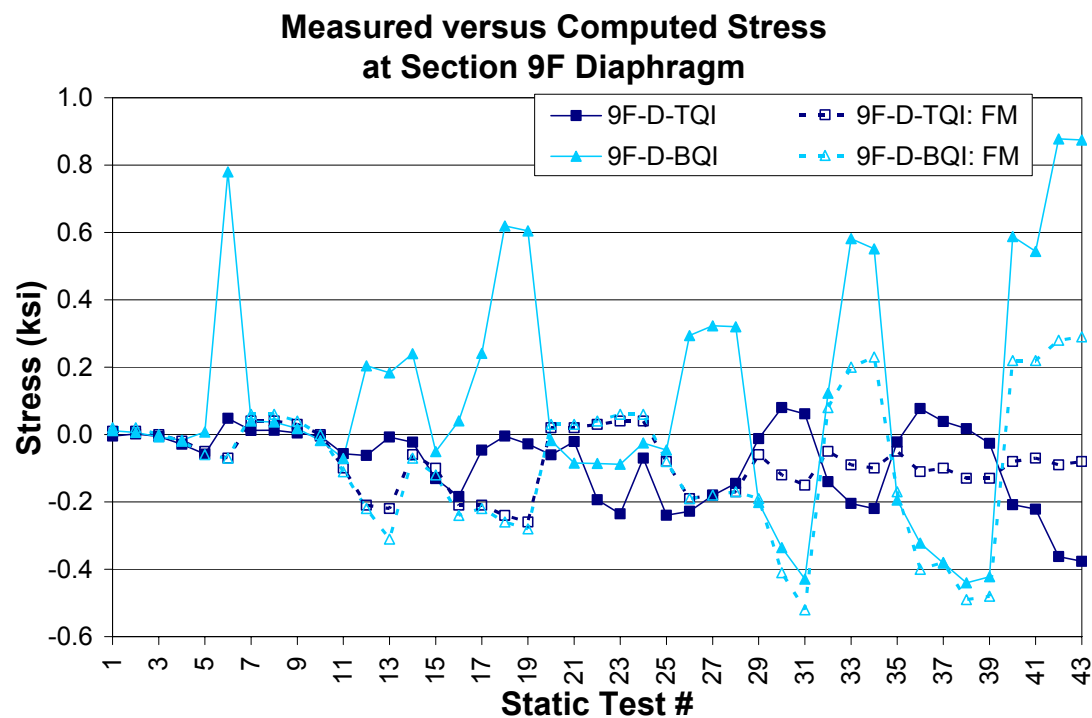


Figure F-46

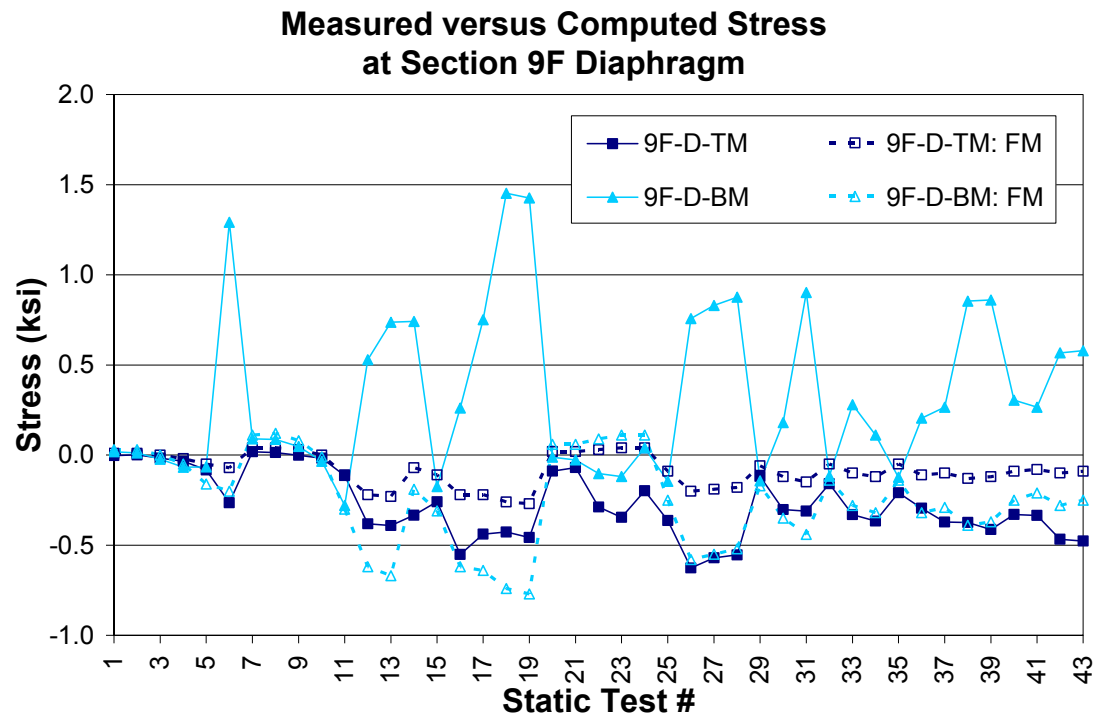


Figure F-47

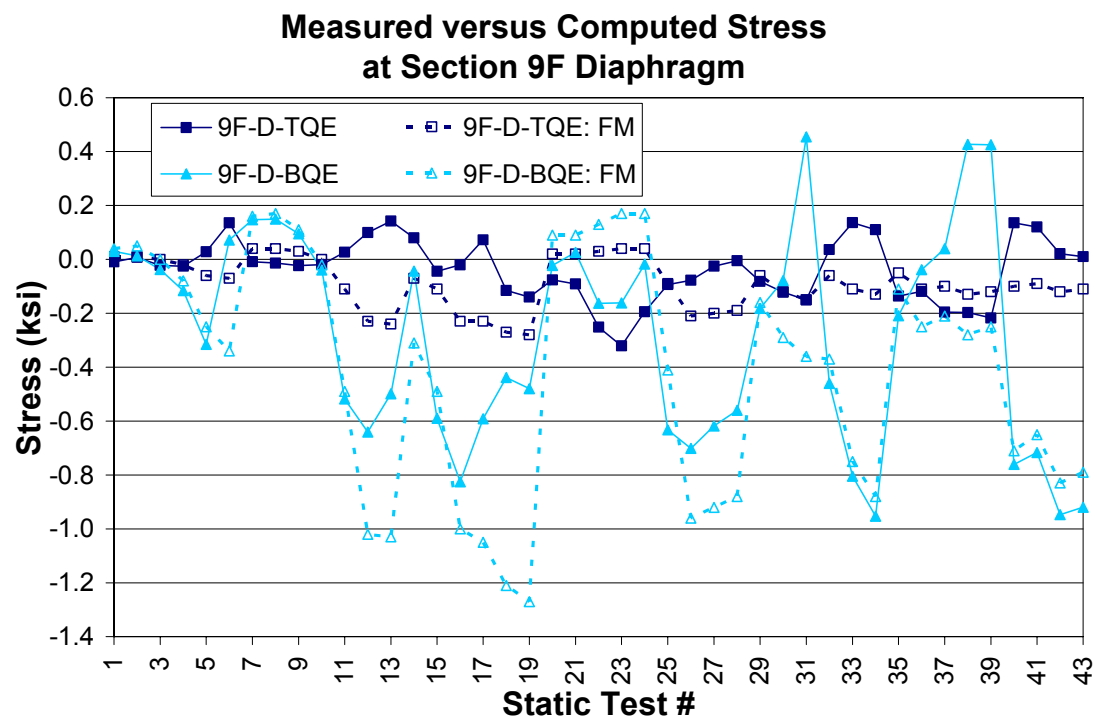


Figure F-48

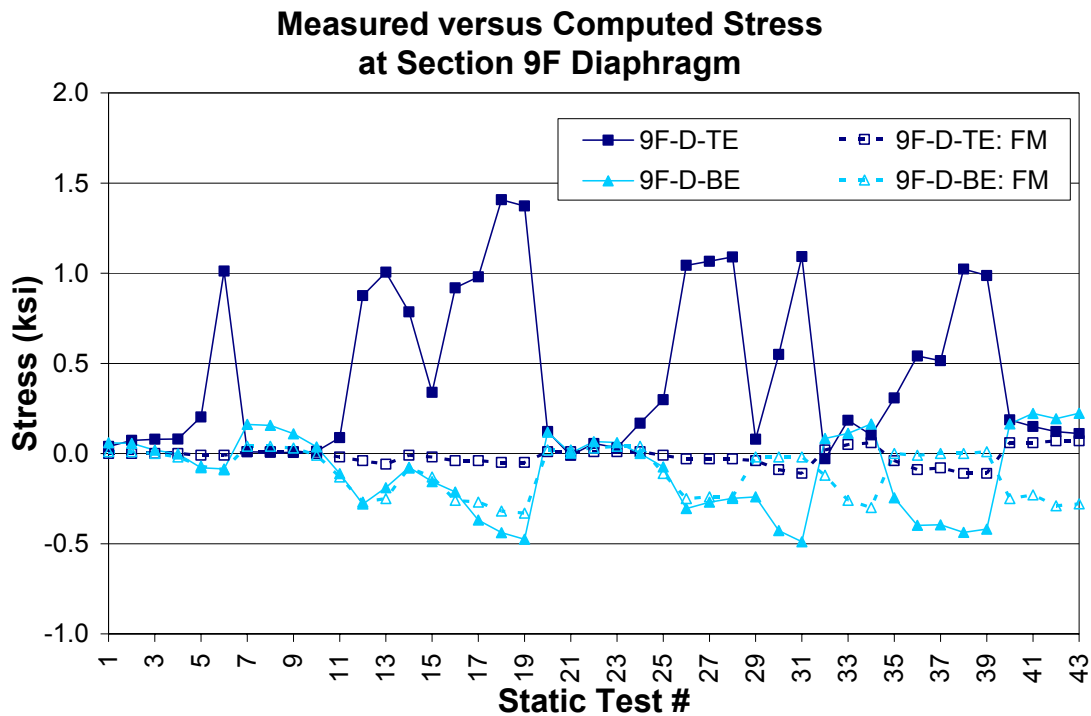


Figure F-49

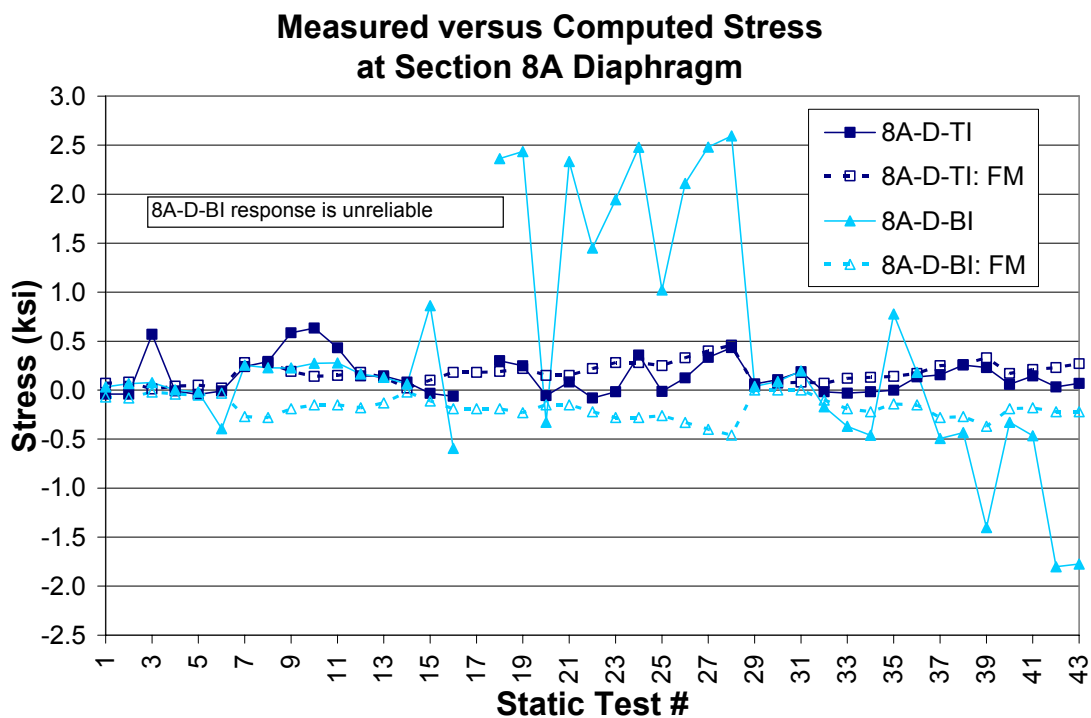


Figure F-50

**Measured versus Computed Stress
at Section 8A Diaphragm**

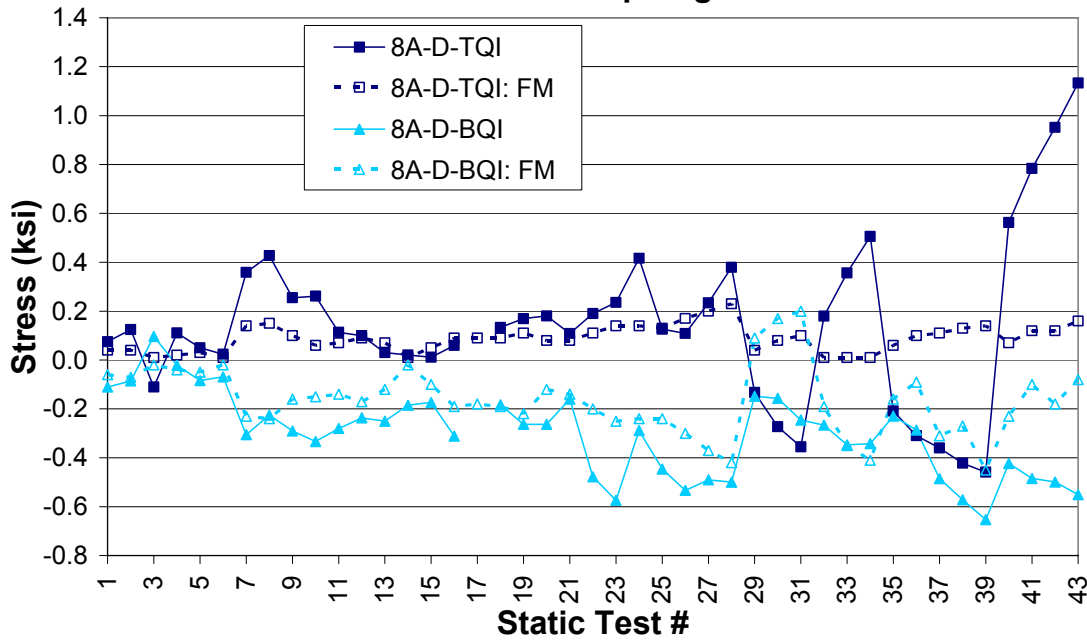


Figure F-51

**Measured versus Computed Stress
at Section 8A Diaphragm**

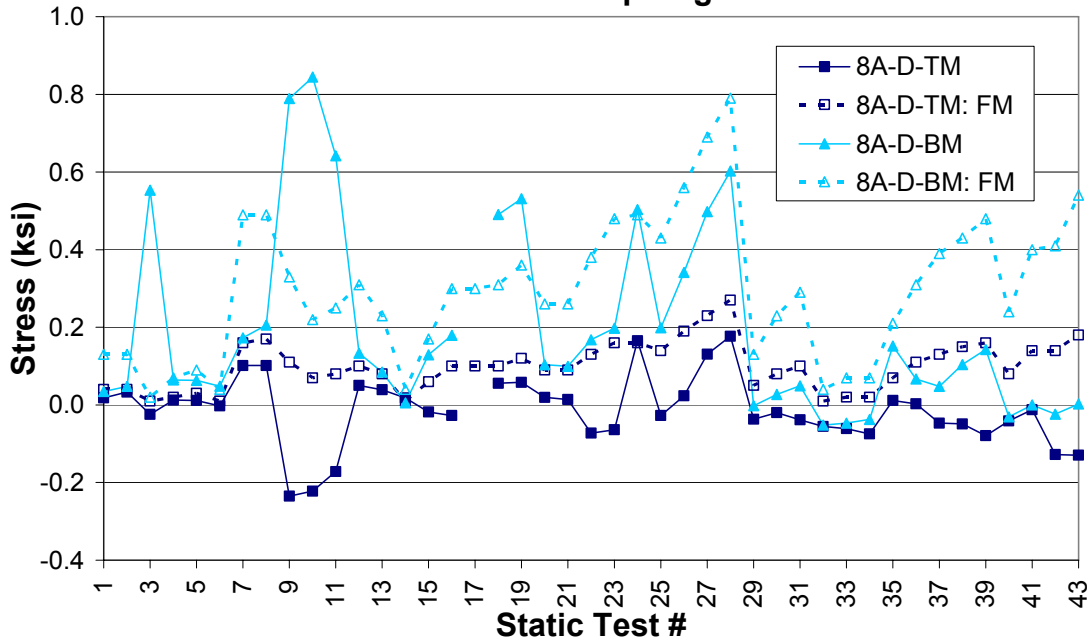


Figure F-52

**Measured versus Computed Stress
at Section 8A Diaphragm**

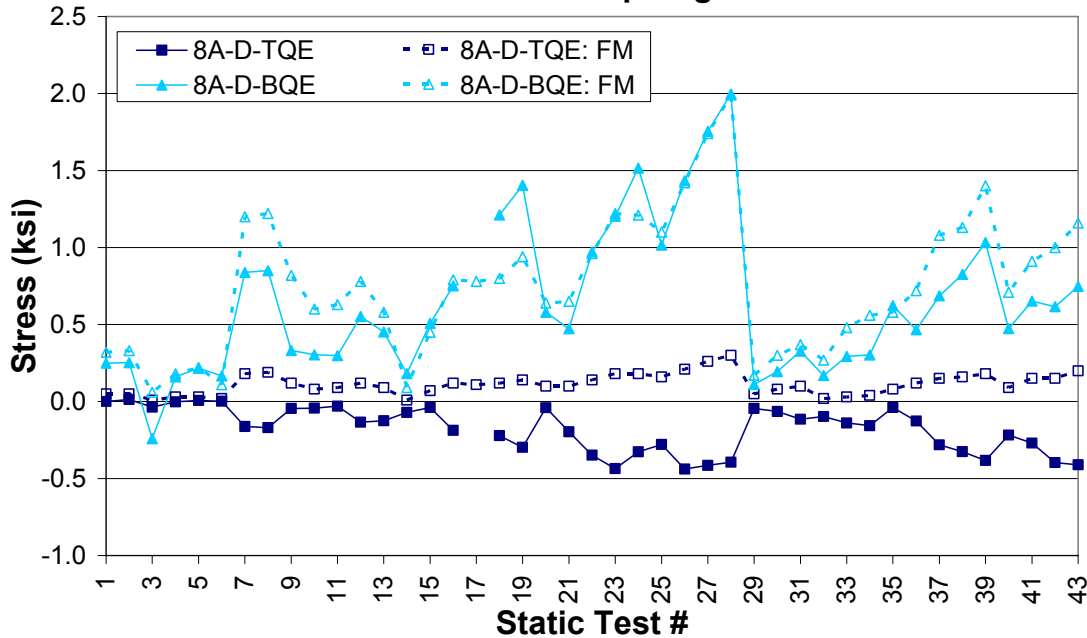


Figure F-53

**Measured versus Computed Stress
at Section 8A Diaphragm**

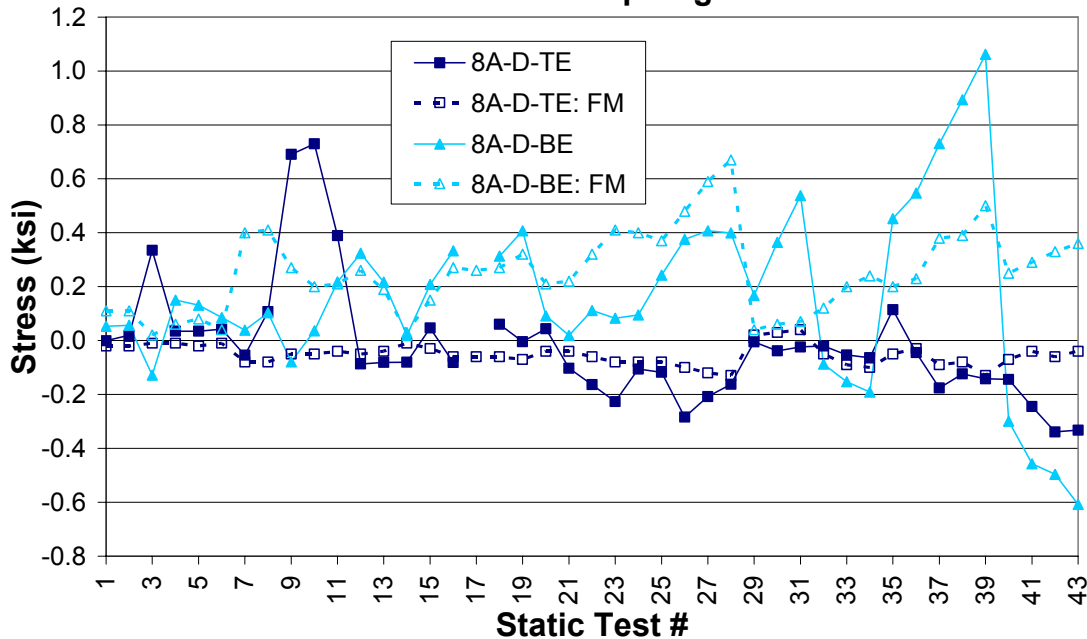


Figure F-54

**Measured versus Computed Stress at Section 9E
Lateral Bracing (5 gages)**

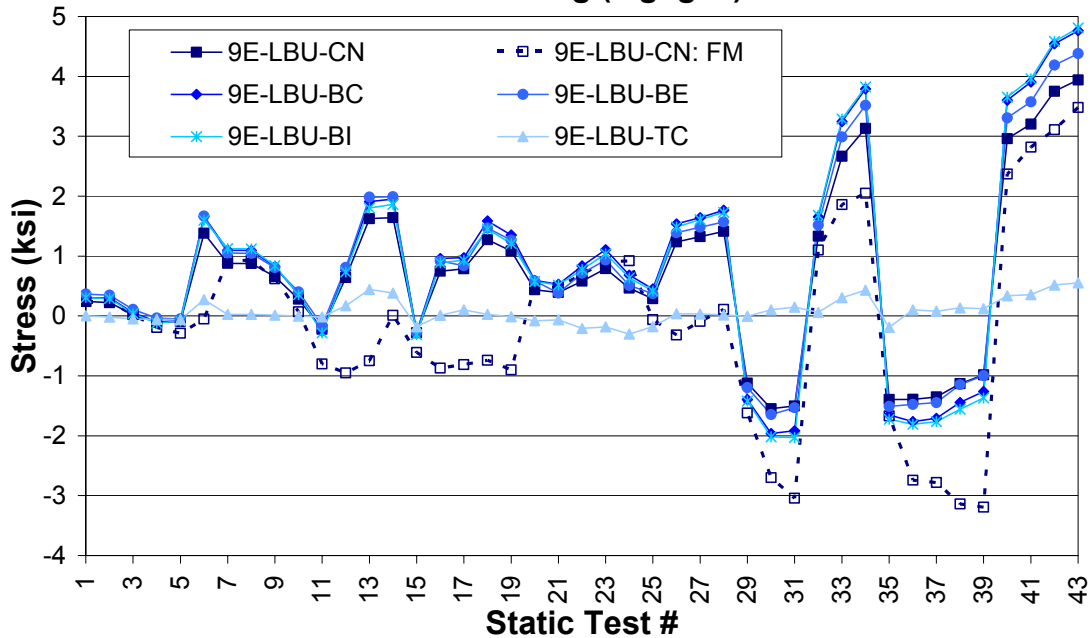


Figure F-55

**Measured versus Computed Stress at Section 9E
Lateral Bracing**

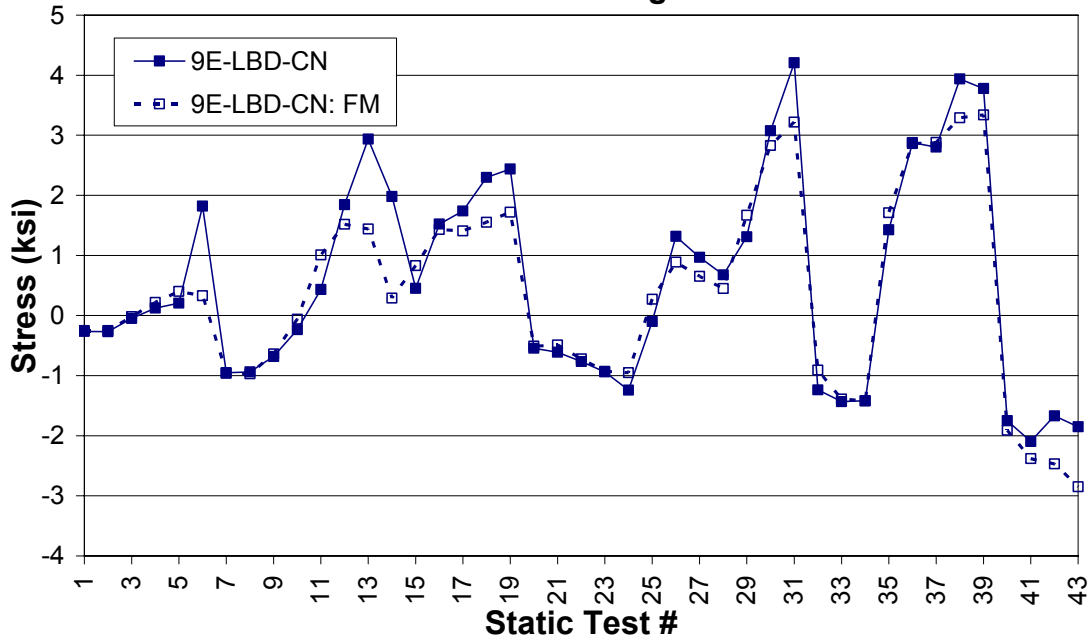


Figure F-56

**Measured versus Computed Stress at Section 9G
Lateral Bracing**

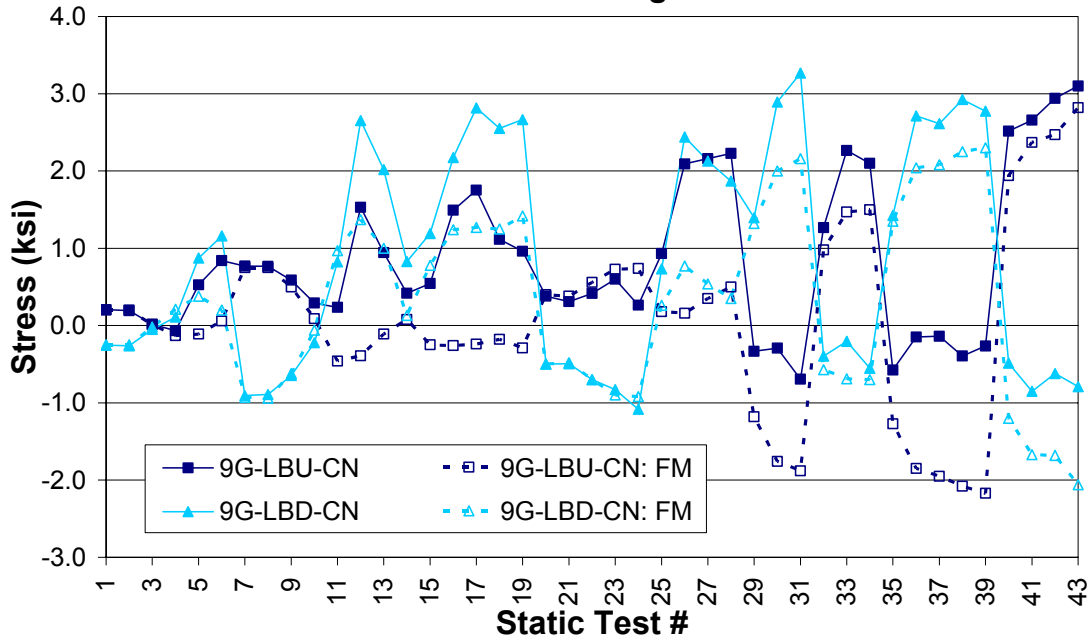


Figure F-57

**Measured versus Computed Stress at Section 9K
Lateral Bracing**

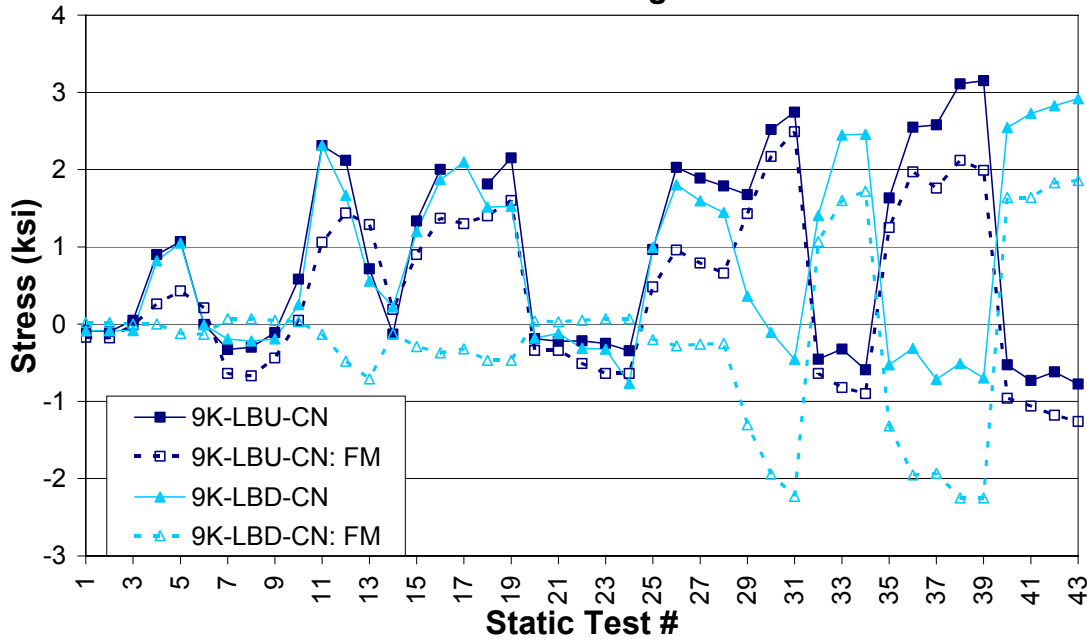


Figure F-58

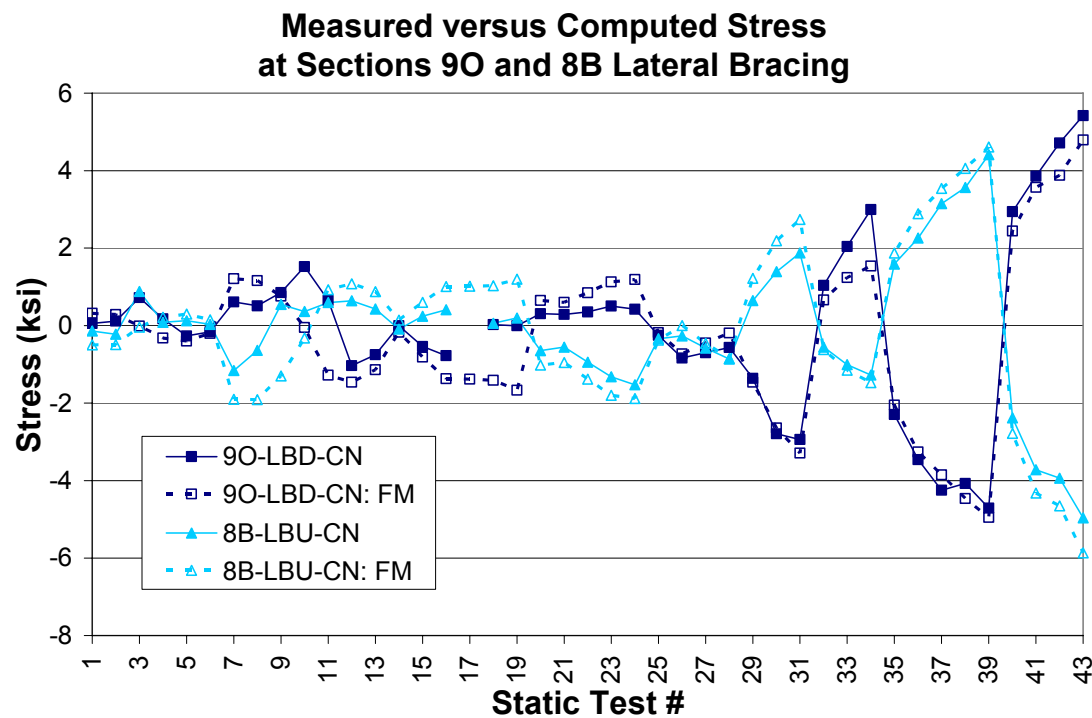


Figure F-59

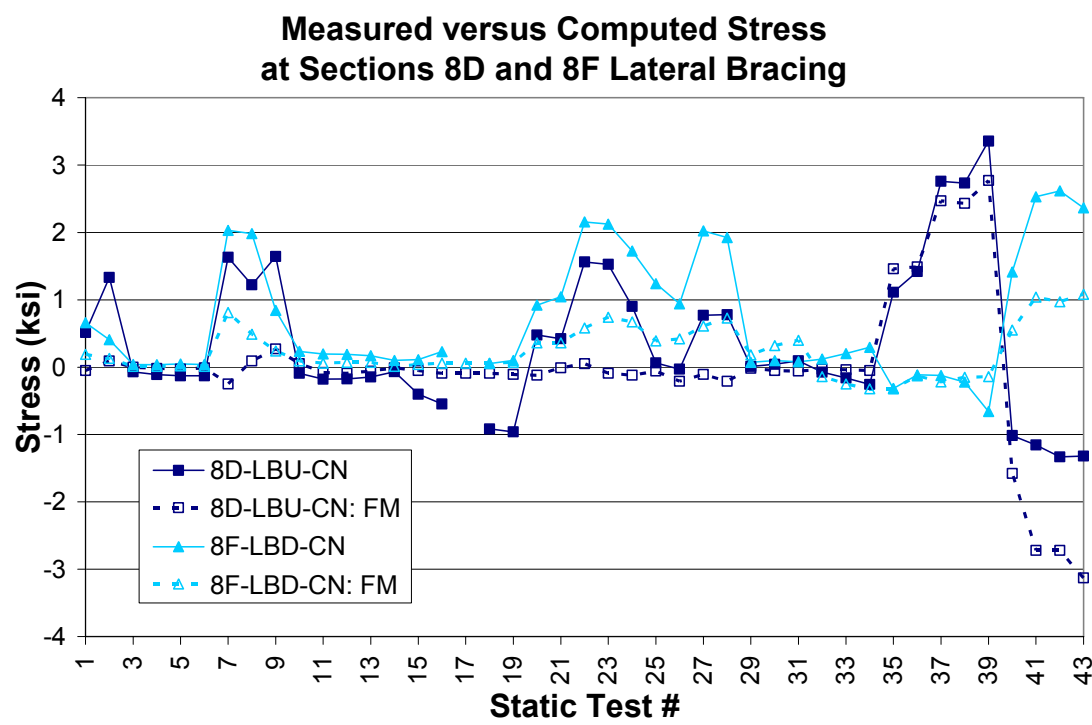


Figure F-60

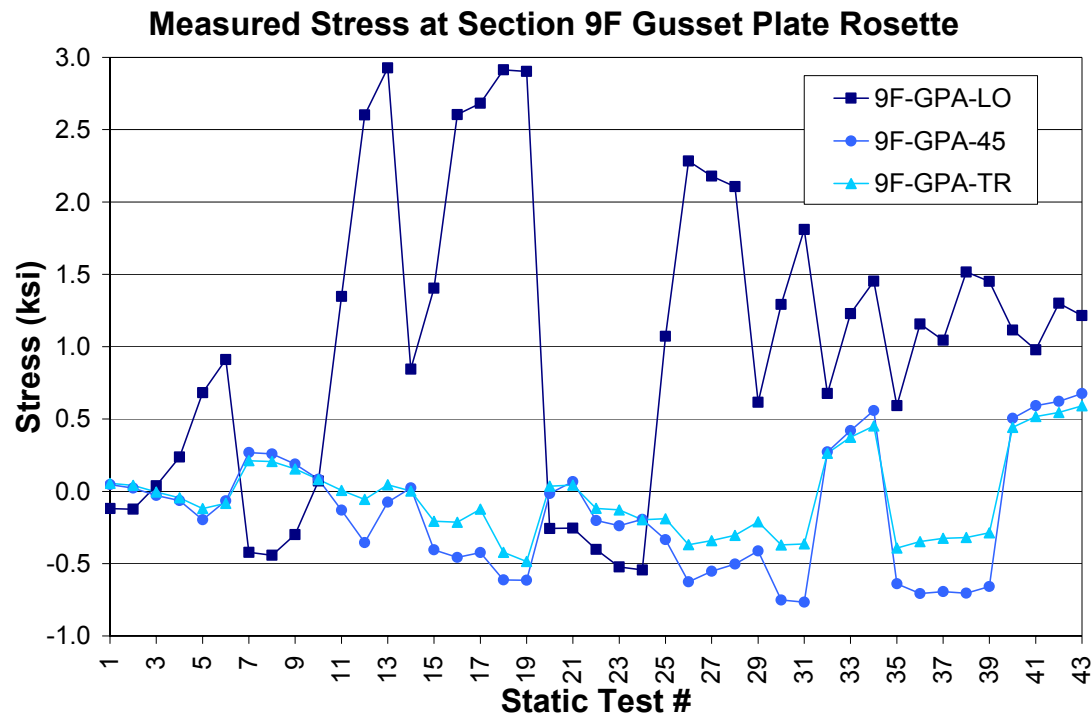


Figure F-61

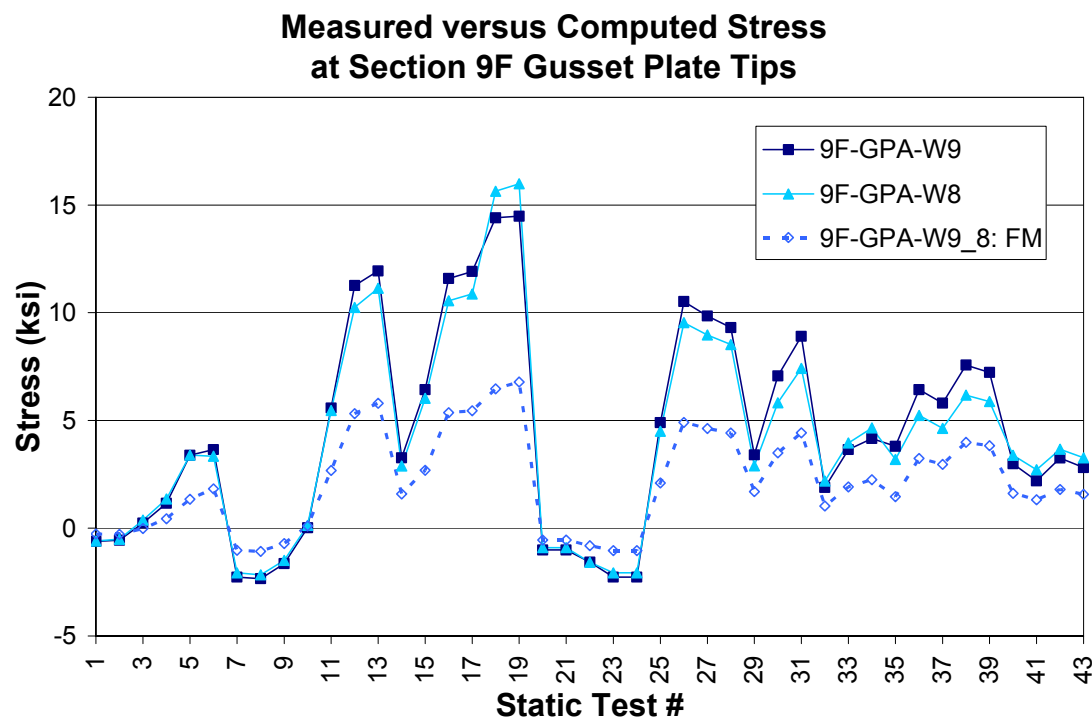


Figure F-62

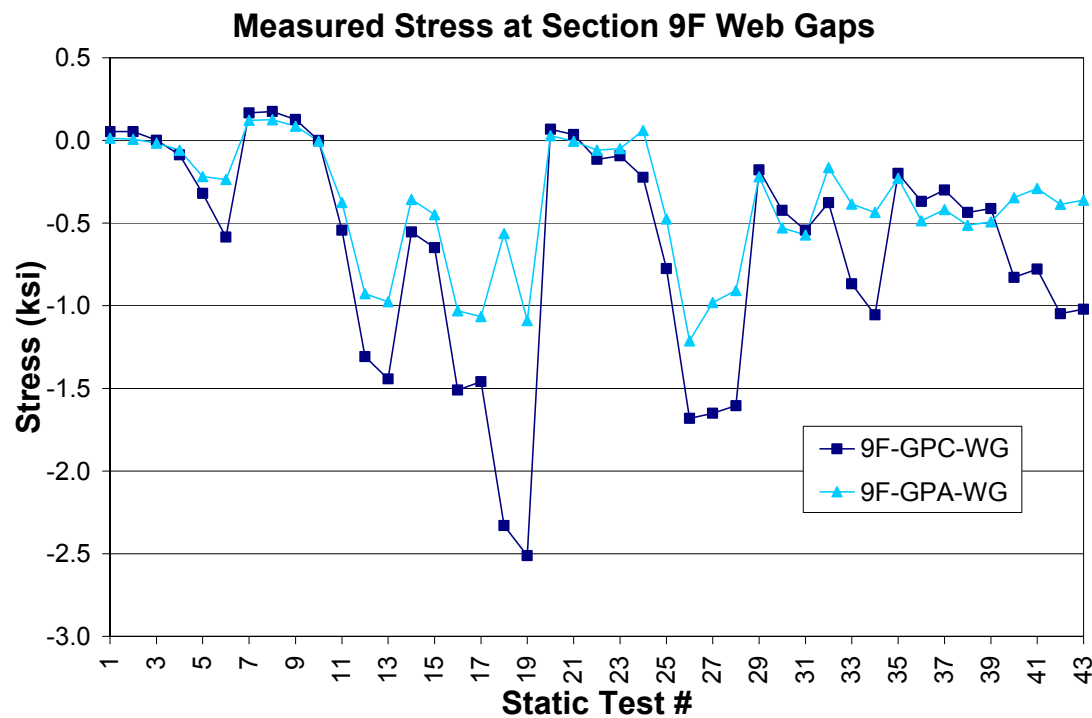


Figure F-63

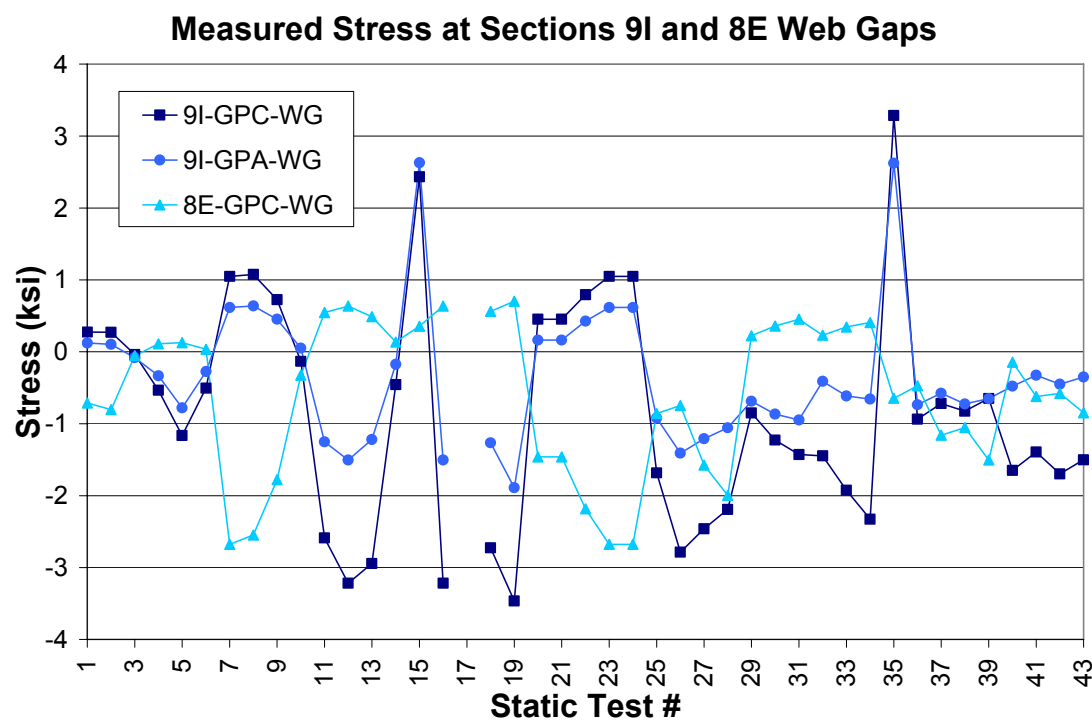


Figure F-64

**Measured versus Computed (Rating Model) Stress
at Section 10Z Girder C**

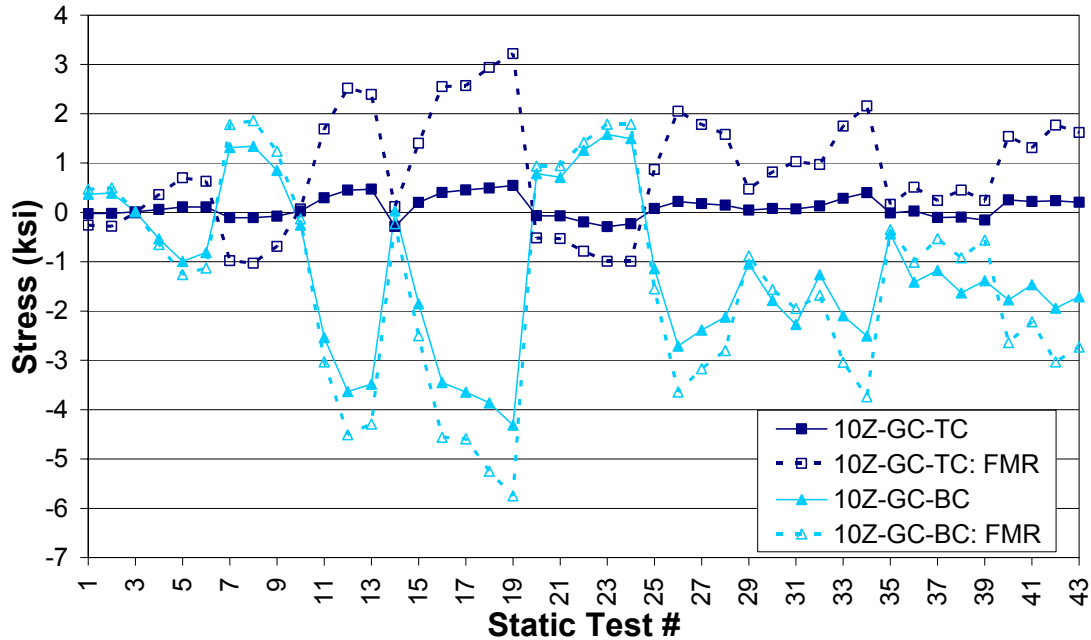


Figure F-65

**Measured versus Computed (Rating Model) Stress
at Section 10Z Girder A**

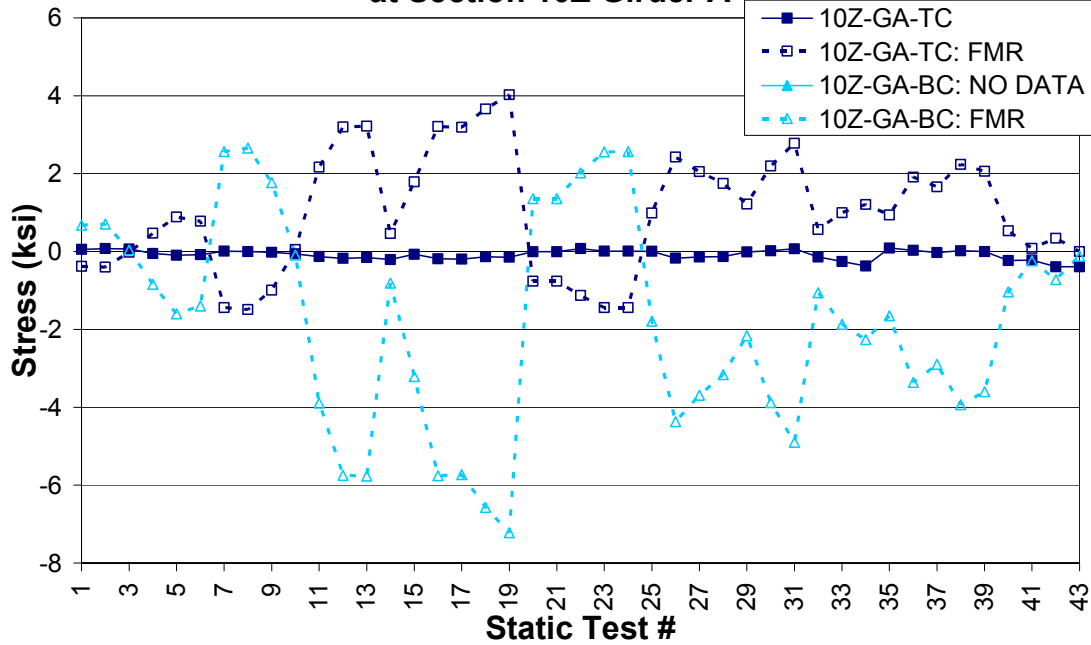


Figure F-66

**Measured versus Computed (Rating Model) Stress
at Section 9B Girder C**

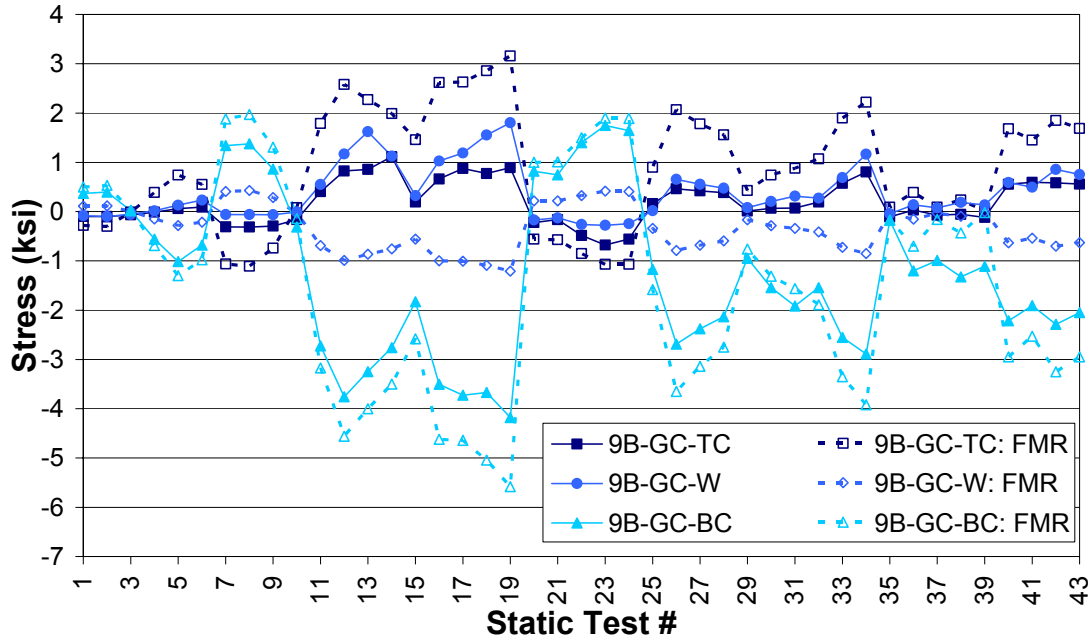


Figure F-67

**Measured versus Computed (Rating Model) Stress
at Section 9B Girder C - Top Flange Tips**

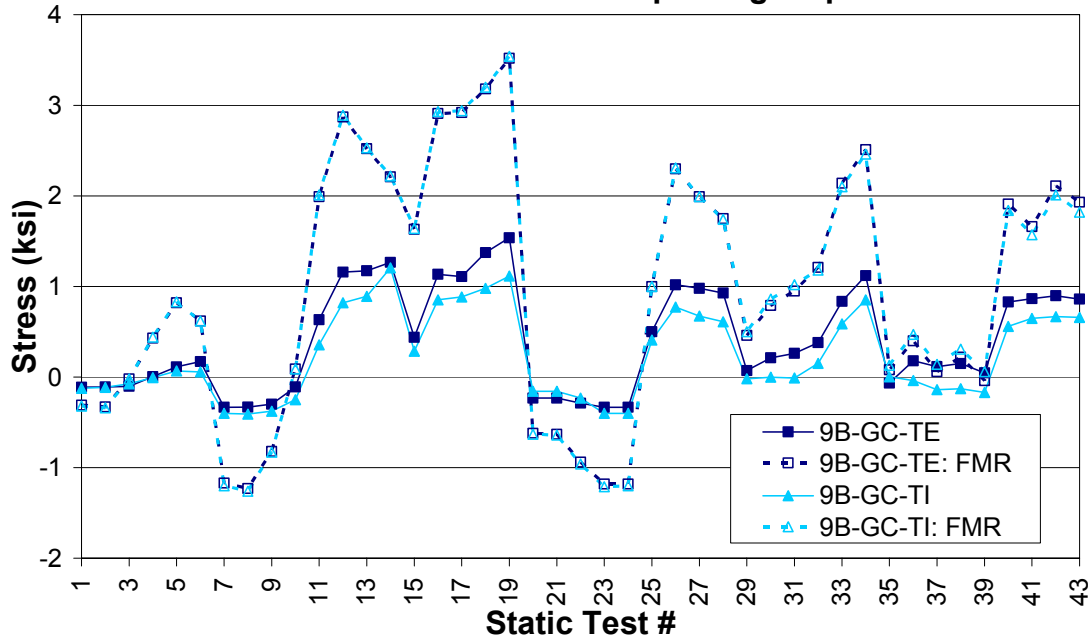


Figure F-68

**Measured versus Computed (Rating Model) Stress
at Section 9B Girder C - Bottom Flange Tips**

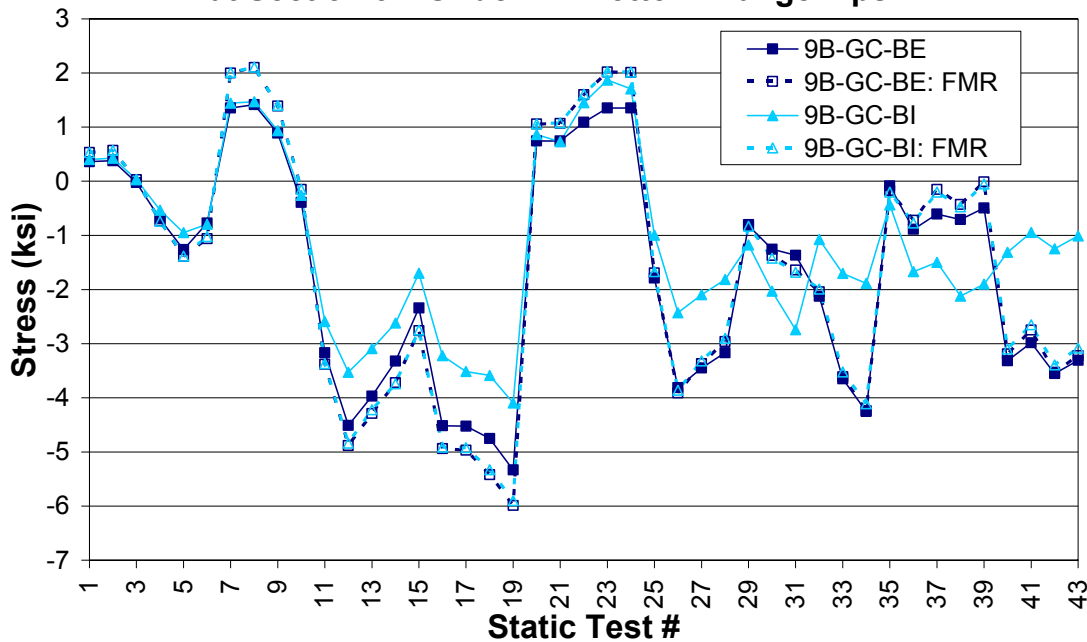


Figure F-69

**Measured versus Computed (Rating Model) Stress
at Section 9B Girder A**

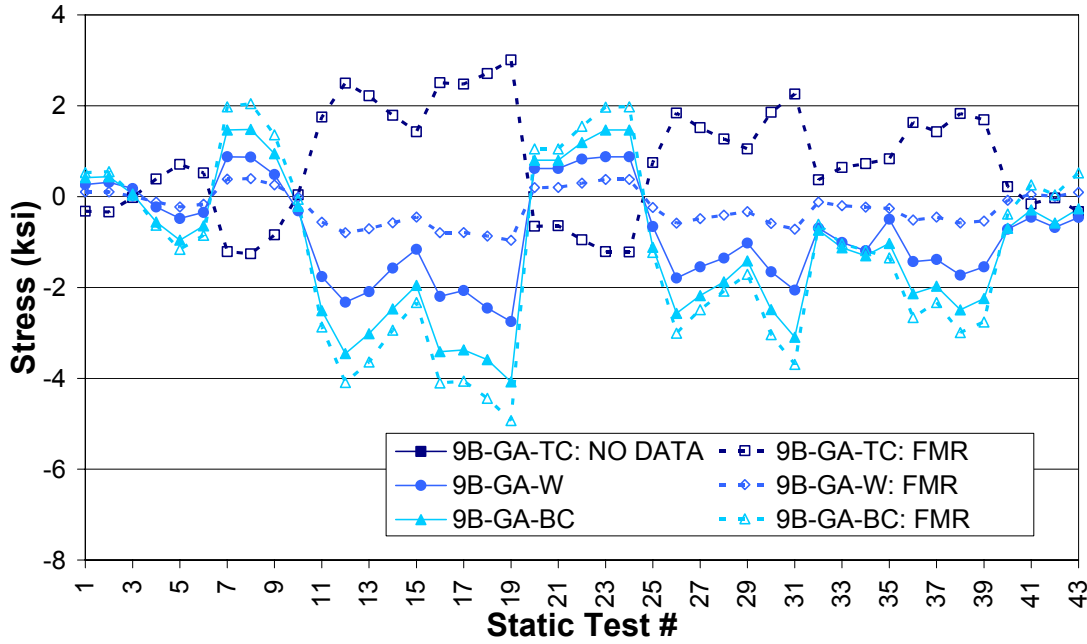


Figure F-70

**Measured versus Computed (Rating Model) Stress
at Section 9B Girder A - Top Flange Tips**

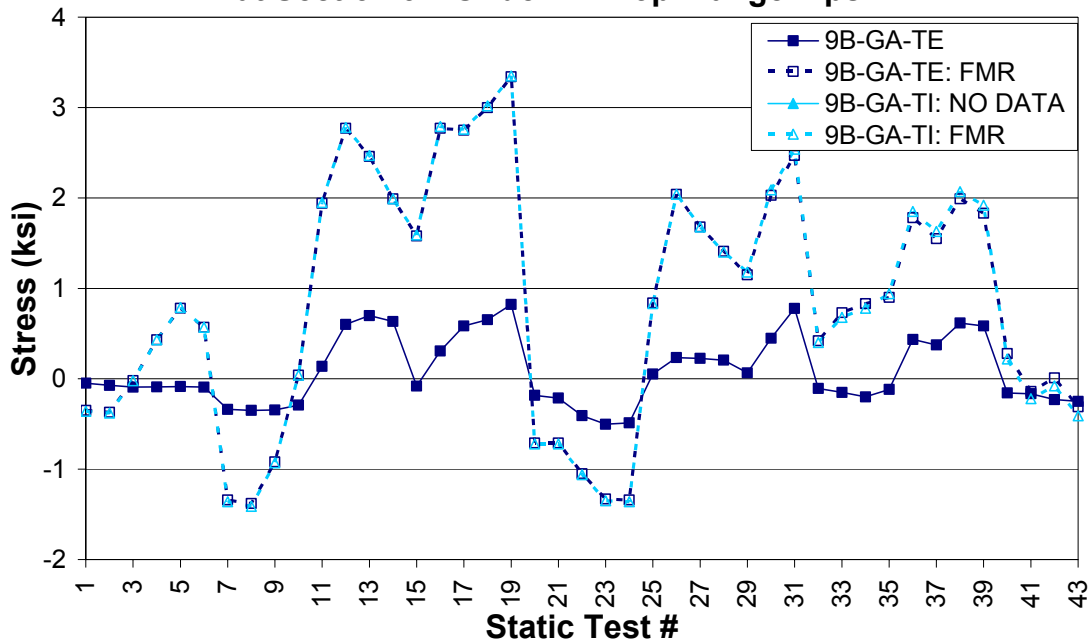


Figure F-71

**Measured versus Computed (Rating Model) Stress
at Section 9B Girder A - Bottom Flange Tips**

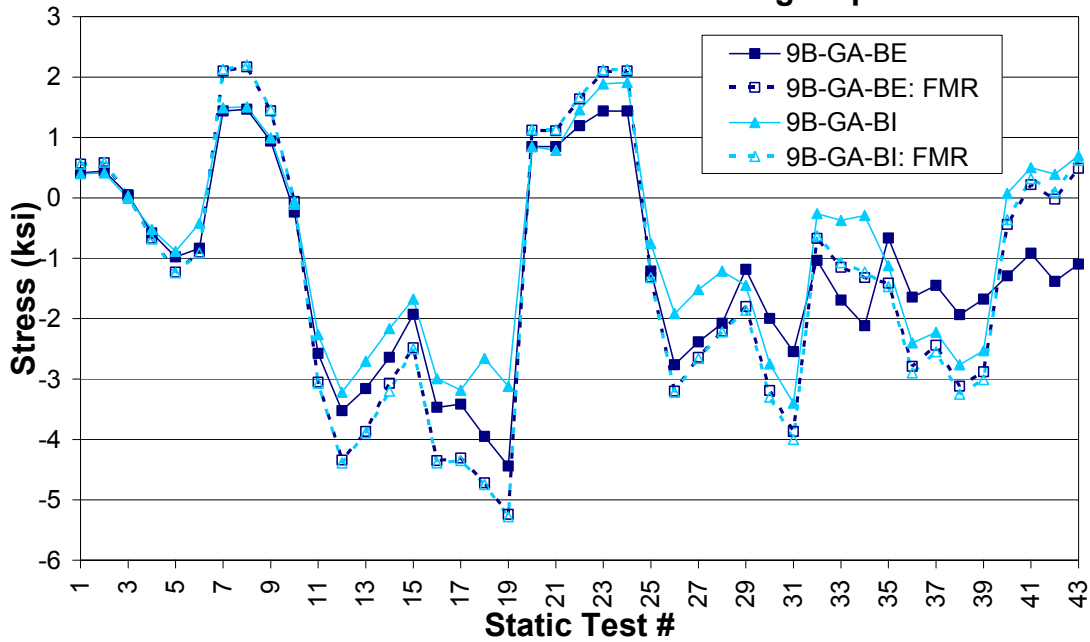


Figure F-72

**Measured versus Computed (Rating Model) Stress
at Section 9N Girder C**

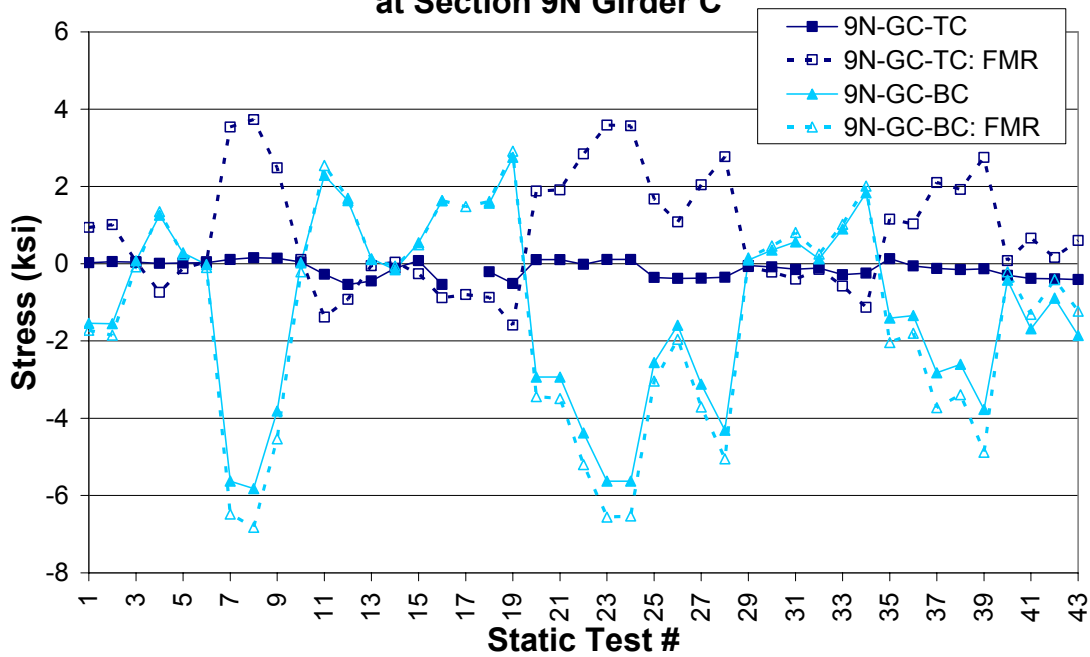


Figure F-73

**Measured versus Computed (Rating Model) Stress
at Section 9N Girder A**

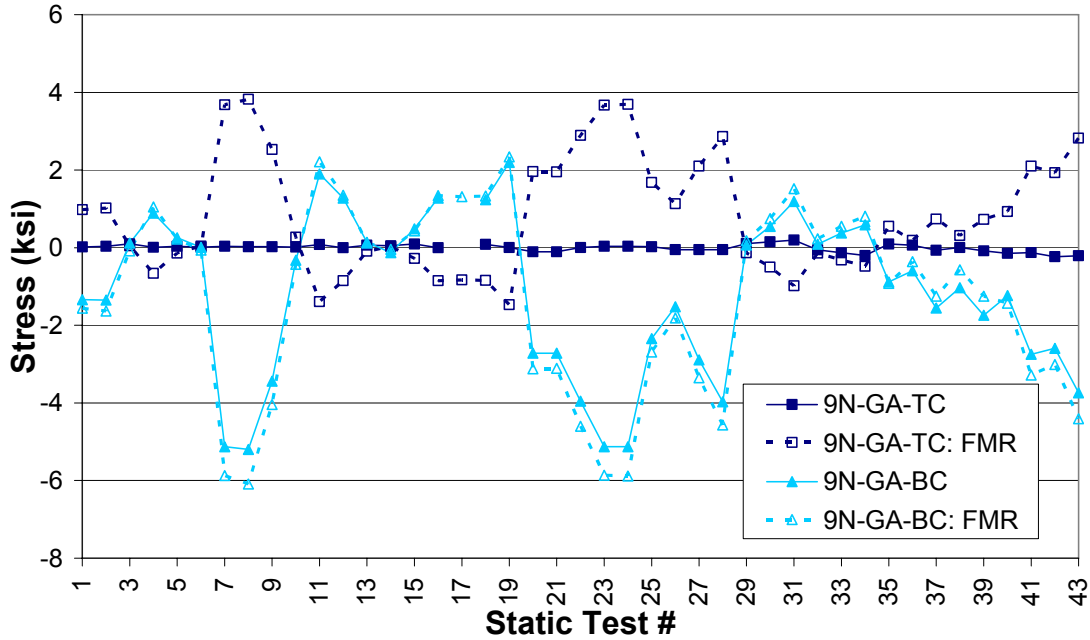


Figure F-74

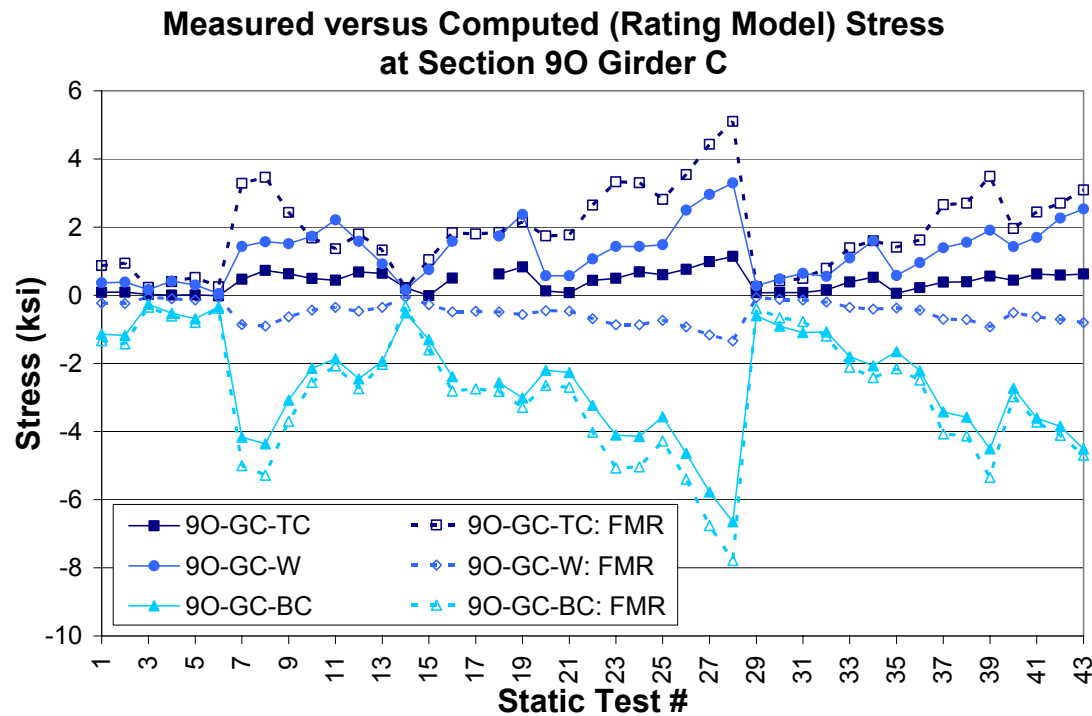


Figure F-75

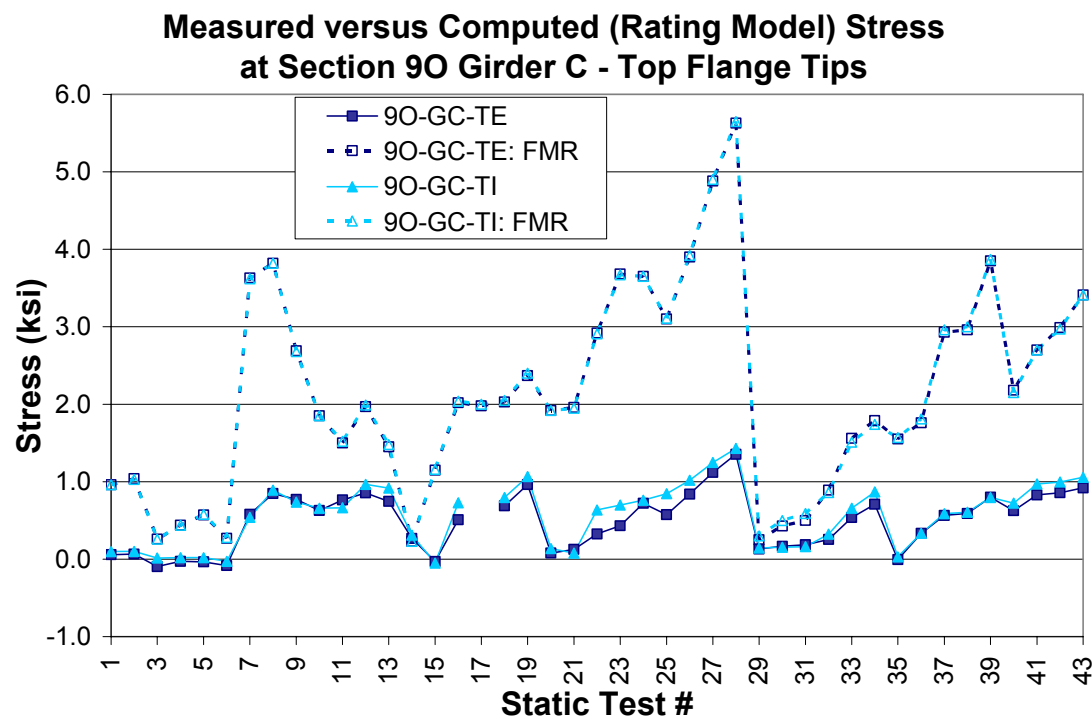


Figure F-76

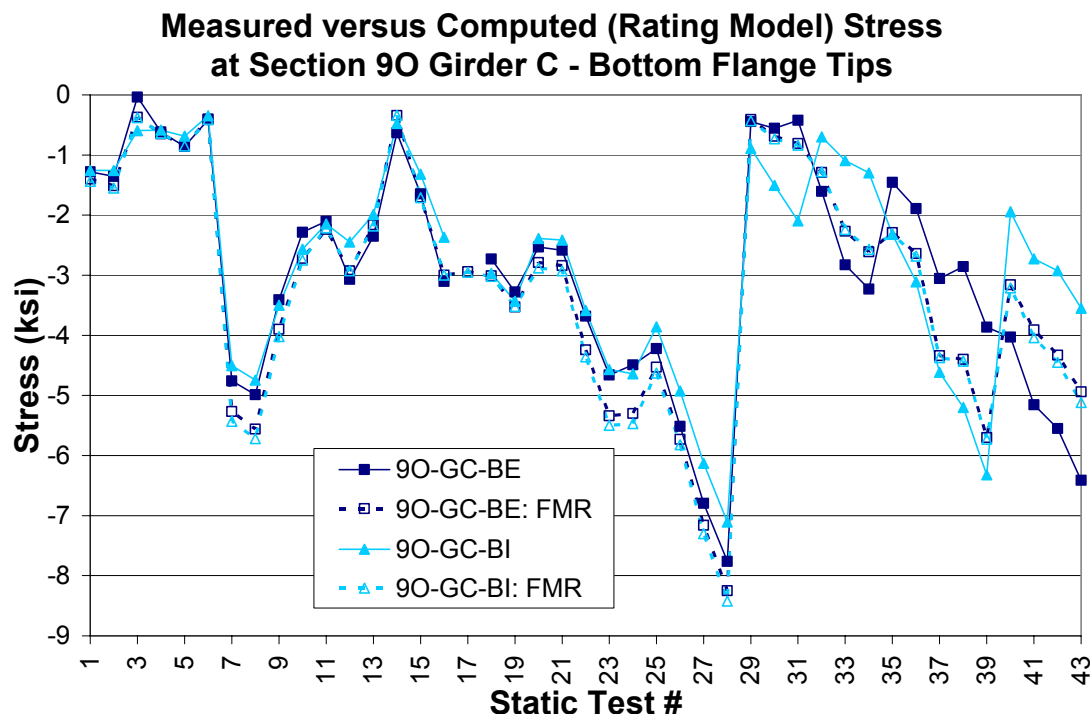


Figure F-77

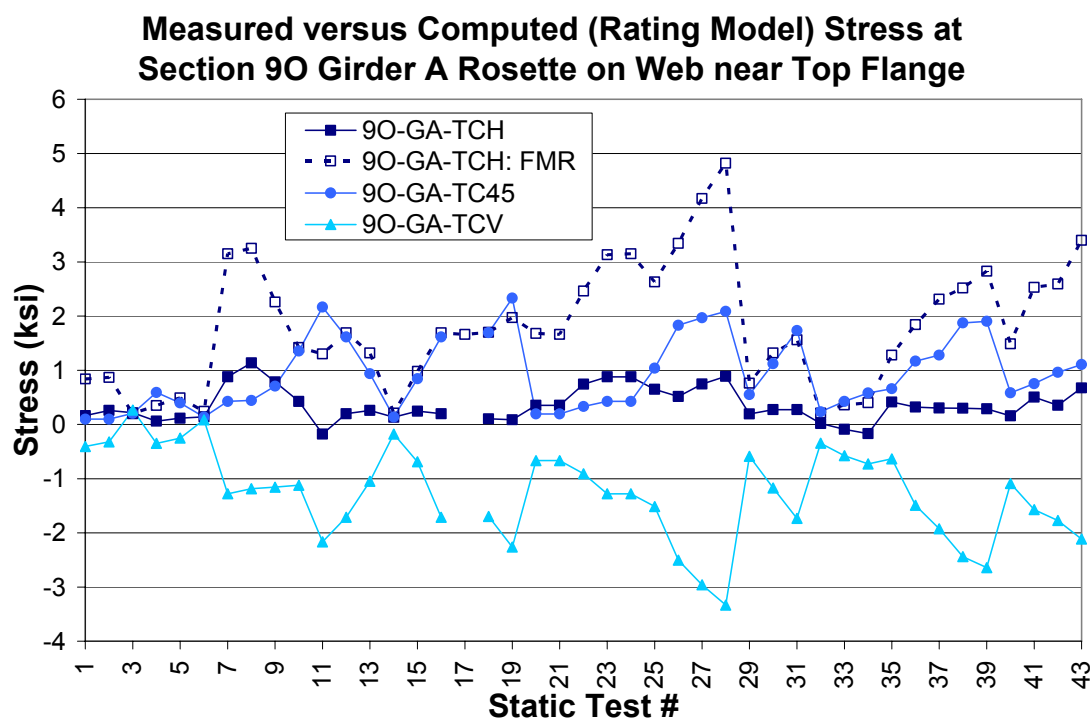


Figure F-78

Measured versus Computed (Rating Model) Stress at Section 9O Girder A Rosette on Web at Mid-Height

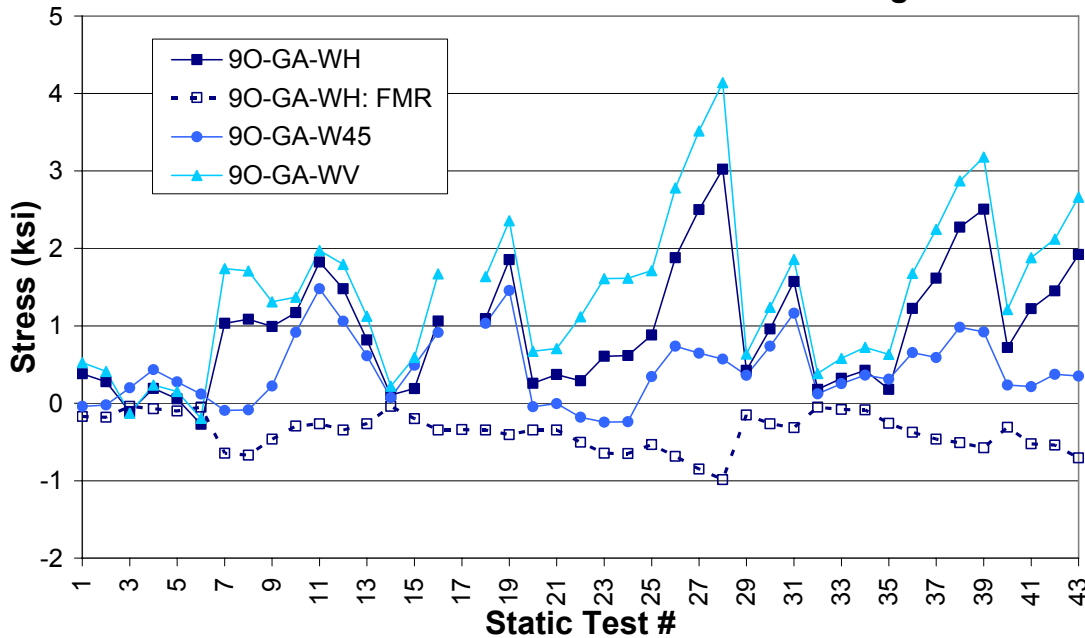


Figure F-79

Measured versus Computed (Rating Model) Stress at Section 9O Girder A Rosette on Web near Bottom Flange

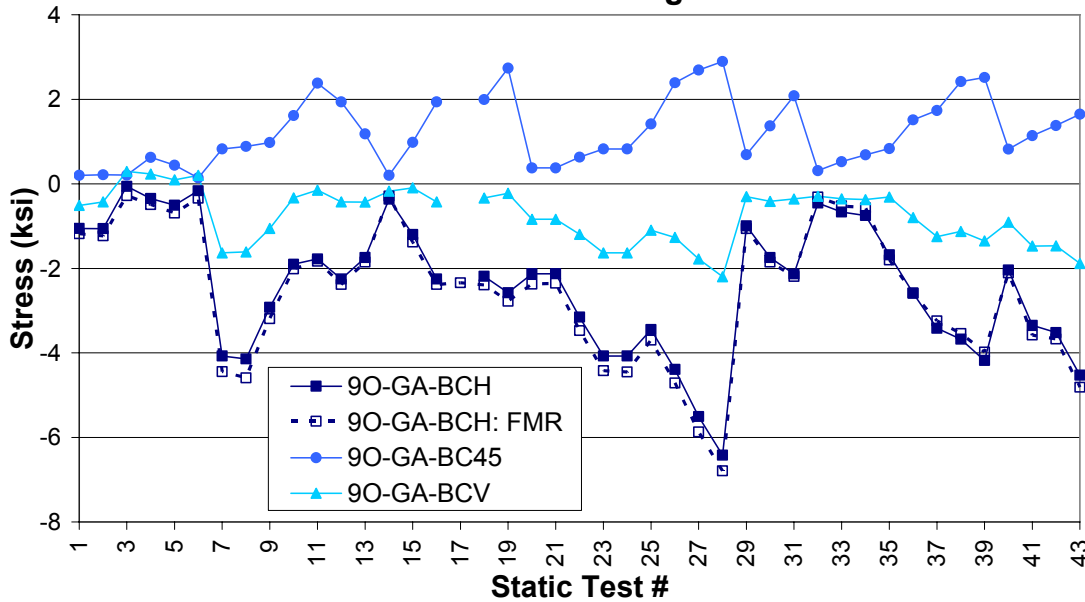


Figure F-80

**Measured versus Computed (Rating Model) Stress
at Section 9O Girder A - Top Flange Tips**

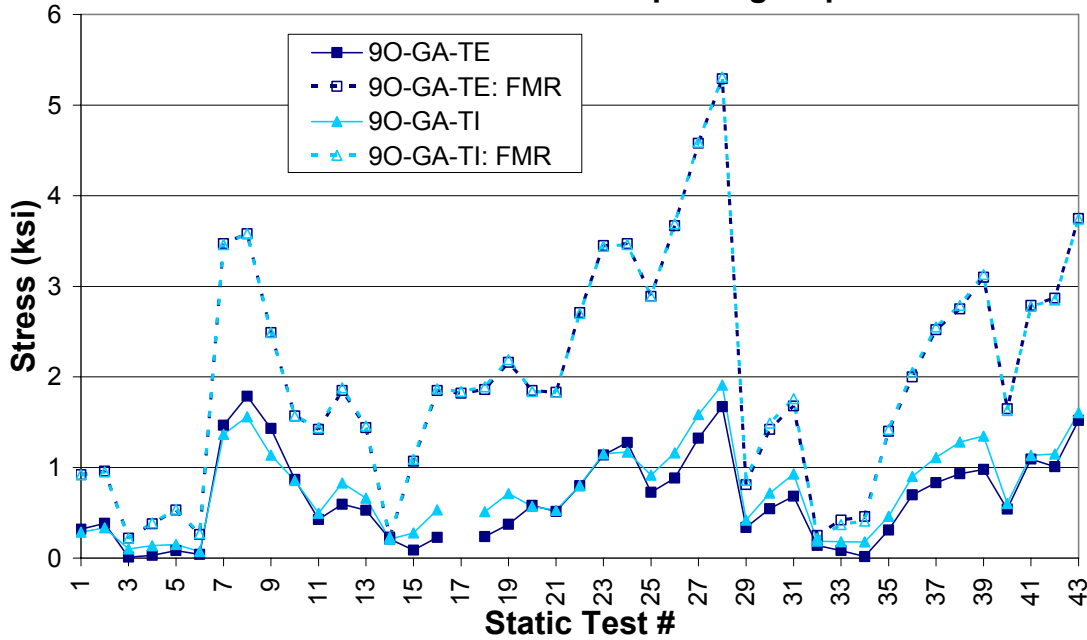


Figure F-81

**Measured versus Computed (Rating Model) Stress
at Section 9O Girder A - Bottom Flange Tips**

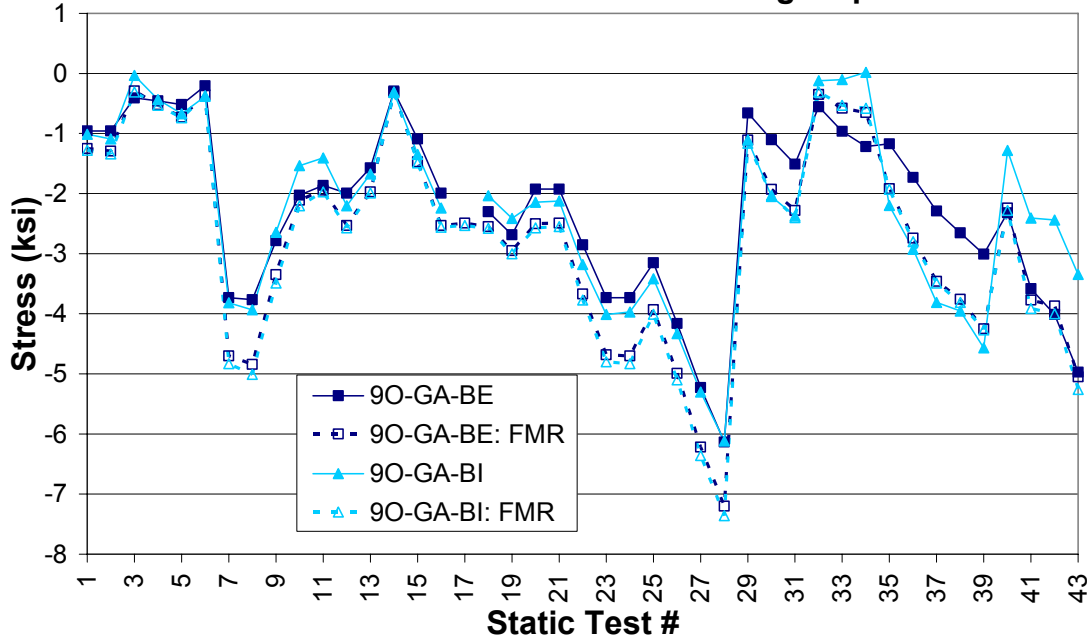


Figure F-82

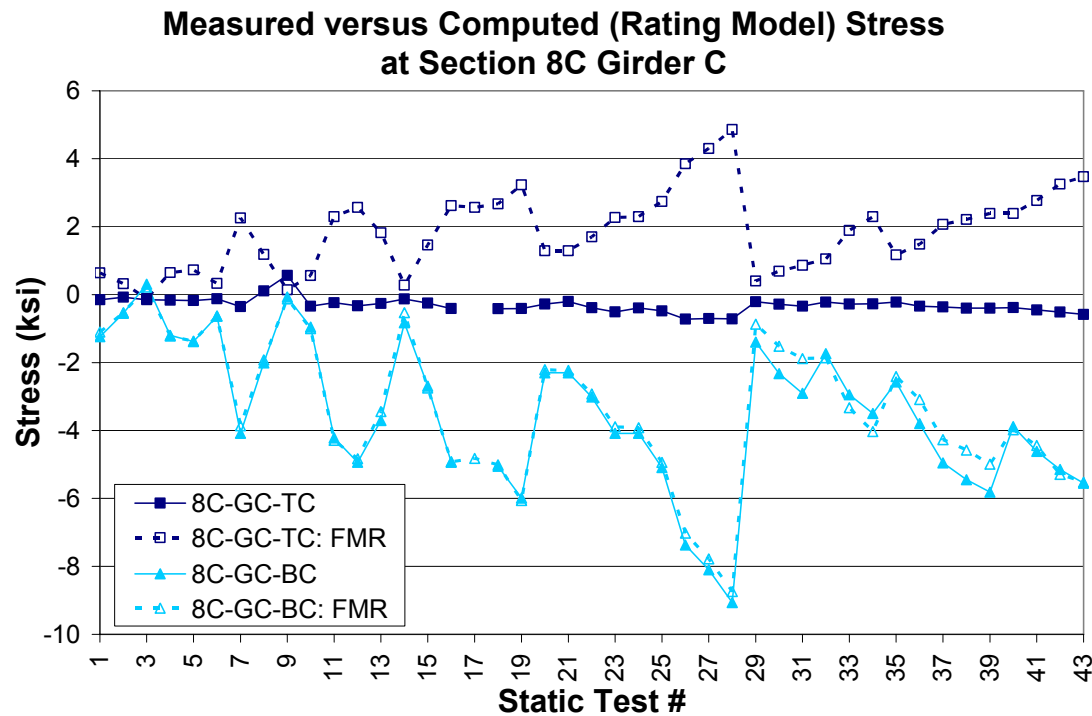


Figure F-83

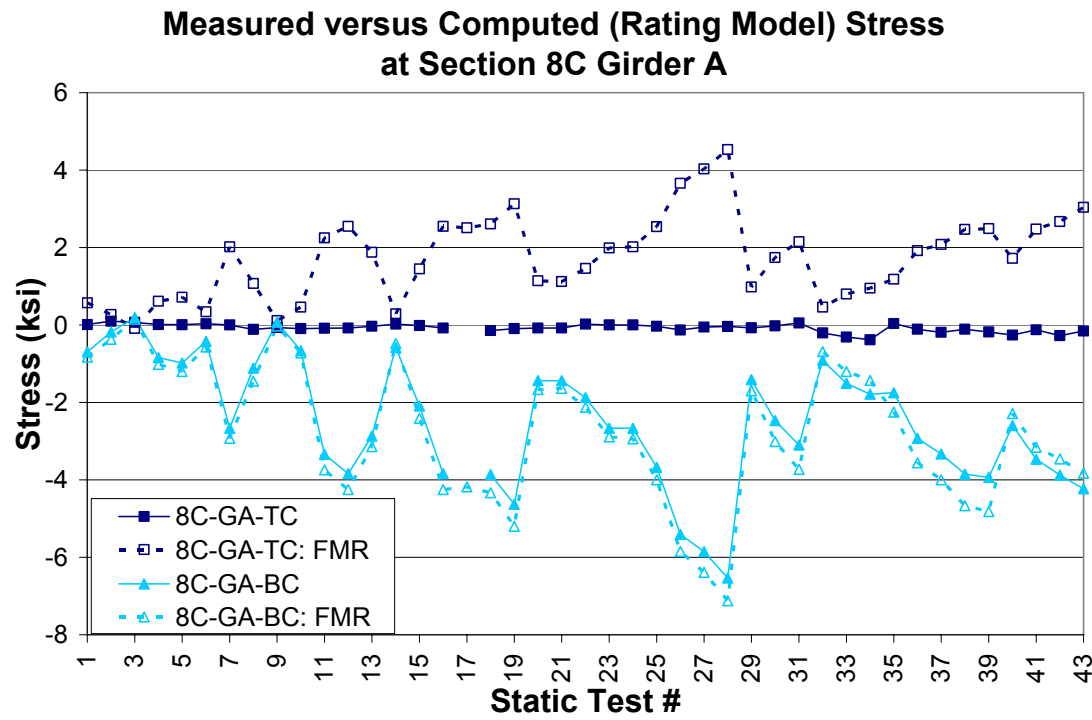


Figure F-84

F.2 Tables of Computed (FM,FMR) versus Measured Static Test Data

Test	9B-GC-RM (radians)			9B-GA-RM (radians)		
	Measured	FM	% Error	Measured	FM	% Error
1	0.00015	0.00010	-35.1%	0.00016	0.00014	-10.6%
2	0.00016	0.00011	-32.1%	0.00016	0.00015	-9.1%
3	0.00004	0.00001	--	0.00002	0.00001	--
4	-0.00011	-0.00014	24.2%	-0.00014	-0.00017	20.4%
5	-0.00026	-0.00027	3.8%	-0.00029	-0.00033	13.8%
6	-0.00024	-0.00024	-1.4%	-0.00025	-0.00028	15.0%
7	0.00039	0.00038	-2.6%	0.00047	0.00053	11.1%
8	0.00040	0.00040	-0.6%	0.00048	0.00055	13.4%
9	0.00026	0.00026	2.0%	0.00032	0.00036	13.8%
10	-0.00006	-0.00003	--	-0.00005	-0.00002	--
11	-0.00074	-0.00064	-13.7%	-0.00079	-0.00080	0.7%
12	-0.00113	-0.00095	-15.5%	-0.00118	-0.00117	-0.1%
13	-0.00114	-0.00091	-20.2%	-0.00115	-0.00118	2.1%
14	-0.00020	-0.00010	-51.5%	-0.00016	-0.00016	-3.7%
15	-0.00056	-0.00053	-4.8%	-0.00061	-0.00066	7.4%
16	-0.00111	-0.00096	-13.5%	-0.00116	-0.00118	1.4%
17	-0.00115	-0.00097	-15.8%	-0.00117	-0.00117	0.0%
18	-0.00133	-0.00110	-17.0%	-0.00133	-0.00134	1.1%
19	-0.00148	-0.00121	-18.5%	-0.00150	-0.00148	-1.7%
20	0.00025	0.00020	-21.0%	0.00028	0.00028	-0.6%
21	0.00021	0.00020	-4.1%	0.00027	0.00028	4.9%
22	0.00033	0.00030	-7.4%	0.00038	0.00041	9.5%
23	0.00042	0.00038	-8.4%	0.00048	0.00053	8.8%
24	0.00040	0.00038	-4.8%	0.00048	0.00053	9.5%
25	-0.00040	-0.00033	-18.8%	-0.00038	-0.00036	-4.9%
26	-0.00091	-0.00077	-16.1%	-0.00092	-0.00089	-3.0%
27	-0.00082	-0.00066	-19.1%	-0.00080	-0.00075	-5.8%
28	-0.00075	-0.00059	-21.5%	-0.00070	-0.00064	-8.1%
29	-0.00027	-0.00019	-28.8%	-0.00039	-0.00045	13.0%
30	-0.00046	-0.00034	-24.8%	-0.00074	-0.00080	8.0%
31	-0.00057	-0.00043	-24.8%	-0.00099	-0.00101	1.9%
32	-0.00039	-0.00035	-9.9%	-0.00024	-0.00021	-13.6%
33	-0.00068	-0.00063	-8.4%	-0.00041	-0.00037	-8.6%
34	-0.00088	-0.00077	-12.5%	-0.00049	-0.00045	-8.3%
35	-0.00011	-0.00008	-28.1%	-0.00028	-0.00034	24.1%
36	-0.00037	-0.00023	-37.6%	-0.00062	-0.00070	11.6%
37	-0.00028	-0.00013	-54.5%	-0.00053	-0.00060	14.3%
38	-0.00039	-0.00022	-45.3%	-0.00075	-0.00081	7.7%
39	-0.00034	-0.00014	-58.5%	-0.00067	-0.00075	11.0%
40	-0.00059	-0.00054	-8.6%	-0.00029	-0.00020	-29.9%
41	-0.00050	-0.00045	-10.4%	-0.00017	-0.00004	-77.6%
42	-0.00068	-0.00061	-9.3%	-0.00028	-0.00013	-51.8%
43	-0.00061	-0.00055	-9.5%	-0.00019	-0.00001	-95.3%
	min = -58.5%		min = -95.3%			
	max = 24.2%		max = 24.1%			
	average = -17.2%		average = -2.6%			
	st. dev. = 16.2%		st. dev. = 23.2%			

Table F-1: Computed (FM) versus Measured Results for Static Test Rotations at Section 9B

Test	9I-GC-DF (inches)			9I-GA-DF (inches)		
	Measured	FM	% Error	Measured	FM	% Error
1	-0.146	-0.074	-49.2%	-0.085	-0.104	--
2	-0.125	-0.079	-36.9%	-0.066	-0.108	--
3	-0.069	-0.004	--	0.004	-0.006	--
4	0.052	0.097	--	0.137	0.122	-11.2%
5	0.122	0.160	31.2%	0.204	0.198	-2.7%
6	0.042	0.090	--	0.117	0.113	-3.4%
7	-0.274	-0.278	1.5%	-0.351	-0.390	11.2%
8	-0.279	-0.292	4.7%	-0.363	-0.405	11.3%
9	-0.174	-0.194	11.7%	-0.244	-0.269	10.1%
10	0.063	0.018	--	0.024	0.010	--
11	0.508	0.415	-18.2%	0.537	0.520	-3.3%
12	0.513	0.537	4.5%	0.694	0.675	-2.8%
13	0.513	0.442	-13.8%	0.591	0.569	-3.7%
14	0.151	0.074	-50.8%	0.119	0.095	-19.9%
15	0.318	0.320	0.6%	0.395	0.399	1.0%
16	0.512	0.548	7.0%	0.680	0.676	-0.6%
17	0.439	0.542	23.4%	0.686	0.667	-2.8%
18	0.512	0.574	12.1%	0.687	0.708	3.0%
19	0.512	0.650	27.0%	0.721	0.804	11.5%
20	-0.228	-0.148	-35.2%	-0.204	-0.207	1.5%
21	-0.156	-0.150	-4.3%	-0.195	-0.207	6.2%
22	-0.269	-0.222	-17.5%	-0.299	-0.306	2.3%
23	-0.326	-0.281	-13.9%	-0.383	-0.389	1.8%
24	-0.295	-0.280	-5.2%	-0.373	-0.391	4.9%
25	0.202	0.169	-16.3%	0.211	0.185	-12.4%
26	0.499	0.394	-21.0%	0.502	0.459	-8.5%
27	0.450	0.319	-29.0%	0.412	0.356	-13.5%
28	0.394	0.262	-33.5%	0.329	0.276	-16.3%
29	0.146	0.112	-23.3%	0.287	0.274	-4.2%
30	0.236	0.189	-19.9%	0.496	0.465	-6.3%
31	0.278	0.227	-18.4%	0.619	0.554	-10.6%
32	0.260	0.213	-18.2%	0.140	0.123	-12.3%
33	0.442	0.356	-19.5%	0.215	0.208	-3.3%
34	0.506	0.410	-19.0%	0.235	0.242	2.8%
35	-0.003	0.027	--	0.185	0.200	8.1%
36	0.171	0.102	-40.4%	0.401	0.388	-3.3%
37	0.124	0.026	-79.0%	0.330	0.321	-2.8%
38	0.166	0.065	-60.5%	0.437	0.412	-5.9%
39	0.126	0.009	-93.2%	0.370	0.364	-1.7%
40	0.370	0.294	-20.4%	0.119	0.080	-32.7%
41	0.301	0.232	-22.9%	0.024	-0.042	--
42	0.393	0.301	-23.5%	0.063	0.002	--
43	0.341	0.257	-24.6%	-0.001	-0.089	--
	min = -93.2% max = 31.2% average = -23.9% st. dev. = 24.2%			min = -32.7% max = 11.5% average = -3.0% st. dev. = 9.2%		

NOTE: data from tests 12,13, and 16-19 excluded for 9I-GC-DF calculations since string potentiometer was out of range

Table F-2: Computed (FM) versus Measured Results for Static Test Deflections at Section 9I

Test	9M-GC-DF (inches)			9M-GA-DF (inches)		
	Measured	FM	% Error	Measured	FM	% Error
1	-0.137	-0.071	-48.0%	-0.061	-0.097	--
2	-0.114	-0.076	-33.5%	-0.038	-0.101	--
3	-0.060	-0.004	--	0.022	-0.006	--
4	0.045	0.083	--	0.136	0.101	-25.3%
5	0.062	0.107	--	0.152	0.132	-13.3%
6	-0.004	0.051	--	0.083	0.064	--
7	-0.257	-0.268	4.5%	-0.327	-0.365	11.6%
8	-0.258	-0.282	9.2%	-0.338	-0.378	11.7%
9	-0.154	-0.187	21.8%	-0.223	-0.251	12.4%
10	0.074	0.010	--	0.026	0.002	--
11	0.410	0.308	-24.9%	0.406	0.386	-4.8%
12	0.472	0.368	-22.1%	0.479	0.461	-3.9%
13	0.365	0.273	-25.2%	0.366	0.351	-4.3%
14	0.088	0.043	--	0.065	0.055	--
15	0.199	0.214	7.4%	0.272	0.265	-2.6%
16	0.426	0.375	-12.0%	0.480	0.461	-3.9%
17	0.448	0.368	-17.7%	0.472	0.454	-3.8%
18	0.467	0.380	-18.6%	0.455	0.469	3.1%
19	0.494	0.448	-9.3%	0.485	0.552	13.9%
20	-0.211	-0.142	-32.5%	-0.172	-0.194	12.6%
21	-0.144	-0.144	0.0%	-0.181	-0.193	6.8%
22	-0.248	-0.214	-13.6%	-0.266	-0.286	7.6%
23	-0.297	-0.271	-8.9%	-0.345	-0.364	5.4%
24	-0.268	-0.270	0.8%	-0.340	-0.365	7.5%
25	0.085	0.067	--	0.102	0.067	-34.4%
26	0.329	0.226	-31.3%	0.311	0.260	-16.5%
27	0.273	0.154	-43.7%	0.225	0.164	-27.3%
28	0.224	0.098	-56.1%	0.151	0.088	-41.6%
29	0.098	0.075	--	0.202	0.181	-10.3%
30	0.163	0.130	-20.1%	0.359	0.316	-12.1%
31	0.186	0.157	-15.3%	0.452	0.381	-15.7%
32	0.177	0.138	-22.3%	0.096	0.082	--
33	0.328	0.241	-26.7%	0.147	0.142	-3.2%
34	0.405	0.280	-30.7%	0.155	0.166	7.3%
35	-0.039	-0.008	--	0.114	0.112	-2.1%
36	0.103	0.044	-57.2%	0.269	0.245	-8.9%
37	0.064	-0.031	--	0.203	0.186	-8.4%
38	0.090	-0.002	--	0.282	0.251	-11.0%
39	0.061	-0.058	--	0.222	0.207	-6.5%
40	0.255	0.183	-28.3%	0.056	0.021	--
41	0.191	0.127	-33.4%	-0.027	-0.094	--
42	0.265	0.176	-33.8%	-0.009	-0.063	--
43	0.214	0.136	-36.3%	-0.064	-0.149	--
		min =	-57.2%			min = -41.6%
		max =	21.8%			max = 13.9%
		average =	-21.2%			average = -5.0%
		st. dev. =	18.4%			st. dev. = 13.6%

Table F-3: Computed (FM) versus Measured Results for Static Test Deflections at Section 9M

Test	8E-GC-TS (inches)			8E-GA-TS (inches)		
	Measured	FM	% Error	Measured	FM	% Error
1	0.309	0.262	-15.2%	0.424	0.306	-27.8%
2	0.211	0.213	1.3%	0.366	0.248	-32.3%
3	0.039	0.012	--	0.116	0.014	-87.8%
4	-0.033	-0.075	--	0.008	-0.096	--
5	-0.072	-0.086	--	0.000	-0.113	--
6	-0.039	-0.040	--	0.067	-0.053	--
7	0.914	0.951	4.1%	1.064	1.119	5.2%
8	0.835	0.836	0.2%	0.906	0.983	8.5%
9	0.526	0.498	-5.4%	0.582	0.583	0.2%
10	0.138	0.100	-27.8%	0.108	0.106	-2.2%
11	-0.211	-0.268	27.3%	-0.283	-0.351	24.2%
12	-0.230	-0.302	31.3%	-0.341	-0.399	16.9%
13	-0.145	-0.217	50.1%	-0.249	-0.293	17.5%
14	-0.039	-0.033	--	-0.067	-0.045	--
15	-0.125	-0.172	37.3%	-0.254	-0.226	-10.9%
16	-0.244	-0.306	25.7%	-0.216	-0.399	84.7%
17	-0.276	-0.300	8.7%	-0.316	-0.393	24.4%
18	-0.237	-0.312	31.8%	-0.341	-0.408	19.6%
19	-0.303	-0.377	24.4%	-0.383	-0.489	27.9%
20	0.520	0.524	0.8%	0.640	0.613	-4.2%
21	0.513	0.529	3.2%	0.565	0.607	7.5%
22	0.671	0.739	10.2%	0.839	0.850	1.2%
23	0.940	0.959	2.1%	1.113	1.112	-0.1%
24	0.973	0.961	-1.2%	1.030	1.121	8.8%
25	0.395	0.360	-8.8%	0.457	0.386	-15.7%
26	0.250	0.223	-10.6%	0.249	0.220	-11.8%
27	0.460	0.445	-3.3%	0.499	0.475	-4.7%
28	0.677	0.661	-2.4%	0.706	0.728	3.1%
29	-0.053	-0.073	--	-0.067	-0.146	--
30	-0.112	-0.128	14.4%	-0.158	-0.258	63.4%
31	-0.118	-0.158	33.7%	-0.175	-0.319	82.7%
32	-0.072	-0.098	--	-0.100	-0.078	--
33	-0.125	-0.174	39.5%	-0.208	-0.138	-33.5%
34	-0.171	-0.211	23.1%	-0.241	-0.165	-31.7%
35	0.257	0.258	0.4%	0.233	0.059	-74.6%
36	0.237	0.210	-11.4%	0.075	-0.052	--
37	0.487	0.481	-1.1%	0.200	0.119	-40.6%
38	0.460	0.444	-3.5%	0.175	0.053	-69.5%
39	0.664	0.610	-8.1%	0.291	0.160	-45.1%
40	0.020	0.015	--	0.150	0.259	72.8%
41	0.191	0.181	-5.3%	0.465	0.608	30.6%
42	0.158	0.140	-11.4%	0.416	0.576	38.6%
43	0.276	0.250	-9.5%	0.623	0.803	28.8%
	min = -27.8%		min = -87.8%			
	max = 50.1%		max = 84.7%			
	average = 7.0%		average = 2.1%			
	st. dev. = 18.2%		st. dev. = 39.4%			

Table F-4: Computed (FM) versus Measured Results for Static Test Deflections at Section 8E

Test	10Z-GC-TC (ksi)			10Z-GC-BC (ksi)		
	Measured	FM	% Error	Measured	FM	% Error
1	-0.02	-0.01	--	0.37	0.41	11.0%
2	-0.02	-0.02	--	0.39	0.43	9.6%
3	0.01	0.00	--	0.01	0.02	--
4	0.06	0.02	--	-0.54	-0.56	4.3%
5	0.11	0.04	--	-1.00	-1.08	8.4%
6	0.11	0.04	--	-0.81	-0.97	19.6%
7	-0.11	-0.05	--	1.31	1.52	15.7%
8	-0.11	-0.06	--	1.34	1.60	19.3%
9	-0.08	-0.04	--	0.85	1.06	24.8%
10	0.03	0.01	--	-0.26	-0.11	--
11	0.30	0.10	--	-2.54	-2.59	2.0%
12	0.45	0.15	-66.6%	-3.63	-3.87	6.5%
13	0.47	0.14	-70.3%	-3.48	-3.68	5.7%
14	-0.29	0.00	--	0.03	-0.20	--
15	0.20	0.08	--	-1.86	-2.15	15.9%
16	0.40	0.16	-60.3%	-3.45	-3.91	13.3%
17	0.45	0.16	-64.8%	-3.65	-3.93	7.8%
18	0.49	0.18	-63.6%	-3.86	-4.50	16.5%
19	0.54	0.20	-63.3%	-4.31	-4.93	14.3%
20	-0.07	-0.03	--	0.79	0.81	2.9%
21	-0.07	-0.03	--	0.71	0.82	15.6%
22	-0.20	-0.04	--	1.26	1.22	-3.2%
23	-0.29	-0.06	--	1.58	1.54	-2.6%
24	-0.23	-0.05	--	1.50	1.53	2.1%
25	0.08	0.06	--	-1.14	-1.33	16.4%
26	0.22	0.13	--	-2.71	-3.12	15.2%
27	0.18	0.11	--	-2.38	-2.71	13.7%
28	0.14	0.10	--	-2.13	-2.40	12.9%
29	0.05	0.01	--	-1.05	-0.76	-27.3%
30	0.08	0.02	--	-1.79	-1.34	-25.0%
31	0.07	0.03	--	-2.27	-1.67	-26.6%
32	0.13	0.08	--	-1.27	-1.44	13.8%
33	0.28	0.14	--	-2.10	-2.60	24.0%
34	0.40	0.17	-57.4%	-2.51	-3.20	27.6%
35	-0.01	-0.01	--	-0.44	-0.30	-31.3%
36	0.03	0.00	--	-1.42	-0.87	-38.6%
37	-0.10	-0.02	--	-1.18	-0.46	-61.0%
38	-0.10	-0.01	--	-1.63	-0.80	-51.0%
39	-0.16	-0.03	--	-1.38	-0.49	-64.6%
40	0.25	0.13	--	-1.78	-2.26	27.3%
41	0.22	0.12	--	-1.46	-1.90	29.7%
42	0.24	0.16	--	-1.94	-2.59	33.5%
43	0.21	0.15	--	-1.71	-2.34	36.6%
	min = -70.3%		min = -64.6%			
	max = -57.4%		max = 36.6%			
	average = -63.7%		average = 3.4%			
	st. dev. = 3.9%		st. dev. = 24.6%			

Table F-5: Computed (FM) versus Measured Results for Static Test Stresses at Section 10Z

	10Z-GA-TC (ksi)			10Z-GA-BC: NO DATA (ksi)		
Test	Measured	FM	% Error	Measured	FM	% Error
1	0.06	-0.03	--	--	0.58	--
2	0.08	-0.03	--	--	0.60	--
3	0.07	0.00	--	--	0.03	--
4	-0.05	0.03	--	--	-0.71	--
5	-0.09	0.06	--	--	-1.36	--
6	-0.08	0.05	--	--	-1.19	--
7	0.01	-0.10	--	--	2.18	--
8	0.00	-0.10	--	--	2.26	--
9	-0.02	-0.07	--	--	1.50	--
10	-0.06	0.00	--	--	-0.08	--
11	-0.13	0.14	--	--	-3.30	--
12	-0.18	0.21	--	--	-4.87	--
13	-0.16	0.21	--	--	-4.89	--
14	-0.21	0.03	--	--	-0.69	--
15	-0.07	0.12	--	--	-2.72	--
16	-0.18	0.21	--	--	-4.89	--
17	-0.19	0.20	--	--	-4.86	--
18	-0.14	0.23	--	--	-5.58	--
19	-0.15	0.26	--	--	-6.13	--
20	-0.01	-0.05	--	--	1.16	--
21	-0.01	-0.05	--	--	1.16	--
22	0.08	-0.08	--	--	1.71	--
23	0.01	-0.10	--	--	2.17	--
24	0.01	-0.10	--	--	2.18	--
25	0.01	0.06	--	--	-1.52	--
26	-0.17	0.15	--	--	-3.71	--
27	-0.14	0.13	--	--	-3.13	--
28	-0.13	0.11	--	--	-2.68	--
29	-0.01	0.09	--	--	-1.83	--
30	0.02	0.16	--	--	-3.29	--
31	0.07	0.21	--	--	-4.16	--
32	-0.14	0.02	--	--	-0.90	--
33	-0.26	0.04	--	--	-1.59	--
34	-0.37	0.05	-113.5%	--	-1.92	--
35	0.09	0.07	--	--	-1.40	--
36	0.03	0.15	--	--	-2.85	--
37	-0.03	0.13	--	--	-2.46	--
38	0.02	0.17	--	--	-3.33	--
39	0.00	0.16	--	--	-3.05	--
40	-0.23	0.01	--	--	-0.88	--
41	-0.22	-0.02	--	--	-0.21	--
42	-0.39	-0.01	-97.4%	--	-0.62	--
43	-0.39	-0.04	-89.7%	--	-0.11	--
	min = -113.5%			min = --		
	max = -89.7%			max = --		
	average = -100.2%			average = --		
	st. dev. = 9.9%			st. dev. = --		

Table F-6: Computed (FM) versus Measured Results for Static Test Stresses at Section 10Z

	9B-GC-TC			(ksi)			9B-GC-W			(ksi)			9B-GC-BC			(ksi)		
Test	Measured	FM	% Error	Measured	FM	% Error	Measured	FM	% Error	Measured	FM	% Error	Measured	FM	% Error	Measured	FM	% Error
1	-0.10	-0.02	--	-0.08	0.21	--	0.37	0.43	16.2%									
2	-0.10	-0.02	--	-0.10	0.22	--	0.40	0.46	15.7%									
3	-0.07	0.00	--	-0.06	0.01	--	0.02	0.02	--									
4	-0.01	0.03	--	0.02	-0.28	--	-0.56	-0.59	5.8%									
5	0.06	0.05	--	0.13	-0.54	--	-1.01	-1.12	10.6%									
6	0.09	0.04	--	0.23	-0.40	--	-0.68	-0.84	24.2%									
7	-0.31	-0.07	-77.3%	-0.06	0.77	--	1.34	1.61	20.3%									
8	-0.31	-0.07	-77.7%	-0.06	0.81	--	1.38	1.69	22.8%									
9	-0.29	-0.05	--	-0.06	0.54	--	0.86	1.12	29.6%									
10	-0.16	0.01	--	-0.01	-0.06	--	-0.31	-0.12	-61.7%									
11	0.41	0.12	-70.4%	0.55	-1.30	-335.9%	-2.72	-2.72	-0.1%									
12	0.83	0.18	-78.2%	1.17	-1.87	-259.6%	-3.76	-3.91	4.1%									
13	0.86	0.16	-81.4%	1.62	-1.63	-200.4%	-3.25	-3.42	5.4%									
14	1.11	0.14	-87.4%	1.12	-1.43	-227.2%	-2.76	-3.00	8.8%									
15	0.20	0.10	--	0.32	-1.06	-425.7%	-1.83	-2.21	20.9%									
16	0.66	0.18	-72.8%	1.03	-1.89	-283.9%	-3.50	-3.96	13.0%									
17	0.88	0.18	-79.4%	1.19	-1.90	-259.8%	-3.72	-3.98	6.9%									
18	0.77	0.20	-74.1%	1.55	-2.06	-232.7%	-3.67	-4.32	17.7%									
19	0.89	0.22	-75.3%	1.80	-2.28	-226.3%	-4.18	-4.78	14.4%									
20	-0.22	-0.04	--	-0.17	0.41	--	0.82	0.85	3.3%									
21	-0.16	-0.04	--	-0.13	0.42	--	0.74	0.87	16.9%									
22	-0.48	-0.06	-87.5%	-0.26	0.62	--	1.40	1.29	-7.8%									
23	-0.68	-0.07	-89.7%	-0.28	0.78	--	1.75	1.63	-6.8%									
24	-0.56	-0.07	-87.5%	-0.24	0.78	--	1.64	1.62	-1.4%									
25	0.16	0.06	--	0.02	-0.65	--	-1.17	-1.35	15.2%									
26	0.46	0.14	-69.8%	0.65	-1.49	-327.5%	-2.69	-3.12	16.1%									
27	0.42	0.12	-71.5%	0.56	-1.29	-331.0%	-2.38	-2.69	13.1%									
28	0.39	0.11	-71.4%	0.48	-1.13	-335.8%	-2.13	-2.36	10.7%									
29	0.01	0.03	--	0.08	-0.31	--	-0.95	-0.65	-31.3%									
30	0.07	0.05	--	0.21	-0.54	--	-1.54	-1.12	-27.4%									
31	0.07	0.06	--	0.31	-0.64	-303.2%	-1.91	-1.34	-30.0%									
32	0.19	0.08	--	0.27	-0.77	--	-1.54	-1.62	5.2%									
33	0.58	0.13	-77.4%	0.69	-1.37	-298.7%	-2.55	-2.87	12.5%									
34	0.81	0.16	-80.2%	1.17	-1.60	-237.1%	-2.89	-3.36	16.3%									
35	-0.11	0.00	--	-0.04	-0.08	--	-0.18	-0.15	--									
36	0.03	0.02	--	0.14	-0.29	--	-1.20	-0.60	-50.0%									
37	-0.07	0.00	--	0.08	-0.07	--	-0.99	-0.14	-85.9%									
38	-0.06	0.01	--	0.19	-0.18	--	-1.33	-0.37	-72.1%									
39	-0.12	0.00	--	0.14	-0.01	--	-1.11	-0.02	-98.2%									
40	0.56	0.12	-78.4%	0.59	-1.21	-304.1%	-2.22	-2.53	14.1%									
41	0.60	0.11	-81.5%	0.49	-1.03	-308.2%	-1.91	-2.17	13.9%									
42	0.58	0.13	-77.7%	0.86	-1.33	-254.3%	-2.29	-2.78	21.5%									
43	0.56	0.12	-78.6%	0.76	-1.21	-259.5%	-2.05	-2.53	23.5%									
	min = -89.7%			min = -425.7%			min = -98.2%			max = -69.8%			max = 29.6%			average = -78.4%		
	st. dev. = 5.6%			st. dev. = 52.4%			st. dev. = 30.6%			average = -1.3%			st. dev. =					

Table F-7: Computed (FM) versus Measured Results for Static Test Stresses at Section 9B

Test	9B-GC-TI (ksi)			9B-GC-TE (ksi)		
	Measured	FM	% Error	Measured	FM	% Error
1	-0.13	-0.04	--	-0.11	-0.03	--
2	-0.11	-0.04	--	-0.11	-0.04	--
3	-0.07	0.00	--	-0.10	0.00	--
4	-0.01	0.05	--	0.00	0.05	--
5	0.07	0.10	--	0.11	0.10	--
6	0.06	0.08	--	0.17	0.07	--
7	-0.40	-0.15	-62.5%	-0.33	-0.13	-61.0%
8	-0.41	-0.16	-60.8%	-0.33	-0.14	-57.7%
9	-0.38	-0.11	-70.8%	-0.30	-0.09	--
10	-0.25	0.01	--	-0.11	0.01	--
11	0.36	0.25	-29.8%	0.63	0.23	-63.7%
12	0.82	0.36	-56.1%	1.16	0.34	-70.7%
13	0.89	0.31	-65.2%	1.17	0.30	-74.4%
14	1.21	0.27	-77.6%	1.27	0.27	-78.7%
15	0.29	0.20	--	0.44	0.19	-56.7%
16	0.85	0.36	-57.8%	1.13	0.34	-70.0%
17	0.89	0.36	-59.3%	1.11	0.35	-68.5%
18	0.98	0.39	-60.2%	1.37	0.38	-72.3%
19	1.12	0.44	-60.6%	1.54	0.42	-72.7%
20	-0.16	-0.08	--	-0.23	-0.07	--
21	-0.16	-0.08	--	-0.23	-0.07	--
22	-0.23	-0.12	--	-0.29	-0.10	--
23	-0.40	-0.15	-62.5%	-0.33	-0.13	-61.0%
24	-0.40	-0.15	-62.5%	-0.33	-0.13	-61.0%
25	0.41	0.12	-70.5%	0.50	0.12	-76.0%
26	0.77	0.28	-63.7%	1.02	0.28	-72.5%
27	0.67	0.24	-64.3%	0.98	0.24	-75.5%
28	0.61	0.21	-65.6%	0.93	0.22	-76.3%
29	-0.02	0.08	--	0.07	0.04	--
30	0.00	0.13	--	0.21	0.07	--
31	-0.01	0.15	--	0.26	0.08	--
32	0.15	0.13	--	0.38	0.16	-58.0%
33	0.59	0.24	-59.1%	0.84	0.28	-66.5%
34	0.85	0.28	-67.1%	1.12	0.33	-70.5%
35	0.00	0.03	--	-0.07	-0.01	--
36	-0.04	0.09	--	0.18	0.01	--
37	-0.14	0.05	--	0.11	-0.03	--
38	-0.13	0.07	--	0.15	-0.02	--
39	-0.17	0.05	--	0.05	-0.05	--
40	0.56	0.20	-64.3%	0.83	0.26	-68.6%
41	0.65	0.16	-75.3%	0.86	0.24	-72.3%
42	0.67	0.21	-68.5%	0.90	0.30	-66.5%
43	0.66	0.18	-72.7%	0.86	0.29	-66.3%
	min = -77.6%			min = -78.7%		
	max = -29.8%			max = -56.7%		
	average = -63.3%			average = -68.2%		
	st. dev. = 9.0%			st. dev. = 6.3%		

Table F-8: Computed (FM) versus Measured Results for Static Test Stresses at Section 9B

Test	9B-GC-BI (ksi)			9B-GC-BE (ksi)		
	Measured	FM	% Error	Measured	FM	% Error
1	0.40	0.45	12.4%	0.36	0.45	24.6%
2	0.43	0.48	12.9%	0.38	0.48	26.3%
3	0.03	0.02	--	-0.02	0.02	--
4	-0.53	-0.62	16.2%	-0.69	-0.62	-10.8%
5	-0.95	-1.16	22.5%	-1.26	-1.17	-7.4%
6	-0.79	-0.85	7.4%	-0.77	-0.89	15.5%
7	1.45	1.69	16.9%	1.36	1.68	24.0%
8	1.47	1.77	20.3%	1.42	1.76	24.3%
9	0.94	1.18	26.1%	0.89	1.17	31.7%
10	-0.26	-0.13	--	-0.39	-0.13	-66.6%
11	-2.59	-2.83	9.3%	-3.17	-2.84	-10.3%
12	-3.53	-4.06	15.1%	-4.51	-4.10	-9.1%
13	-3.09	-3.53	14.2%	-3.97	-3.61	-9.0%
14	-2.62	-3.14	19.8%	-3.32	-3.12	-6.1%
15	-1.70	-2.30	35.4%	-2.34	-2.31	-1.4%
16	-3.22	-4.11	27.5%	-4.52	-4.15	-8.1%
17	-3.51	-4.13	17.5%	-4.52	-4.17	-7.8%
18	-3.59	-4.47	24.7%	-4.75	-4.55	-4.2%
19	-4.10	-4.95	20.8%	-5.33	-5.03	-5.7%
20	0.86	0.89	2.9%	0.74	0.89	19.7%
21	0.73	0.91	24.6%	0.74	0.90	21.0%
22	1.45	1.35	-7.1%	1.09	1.34	22.9%
23	1.87	1.70	-9.1%	1.36	1.69	24.7%
24	1.71	1.70	-0.5%	1.36	1.69	24.7%
25	-1.00	-1.40	40.7%	-1.79	-1.42	-20.5%
26	-2.43	-3.23	33.0%	-3.81	-3.28	-14.0%
27	-2.09	-2.78	32.8%	-3.45	-2.83	-18.0%
28	-1.81	-2.43	34.0%	-3.17	-2.49	-21.4%
29	-1.17	-0.70	-40.4%	-0.82	-0.67	-18.3%
30	-2.03	-1.20	-40.9%	-1.26	-1.15	-8.5%
31	-2.74	-1.42	-48.2%	-1.37	-1.37	0.3%
32	-1.08	-1.67	55.3%	-2.13	-1.71	-19.6%
33	-1.70	-2.95	73.4%	-3.65	-3.04	-16.7%
34	-1.88	-3.44	82.5%	-4.25	-3.57	-16.1%
35	-0.43	-0.17	-60.9%	-0.09	-0.14	--
36	-1.67	-0.65	-61.0%	-0.89	-0.60	-32.3%
37	-1.50	-0.17	-88.6%	-0.60	-0.12	-80.1%
38	-2.12	-0.40	-81.2%	-0.71	-0.36	-49.1%
39	-1.90	-0.04	-97.9%	-0.49	0.00	-100.0%
40	-1.31	-2.59	97.5%	-3.31	-2.68	-19.1%
41	-0.94	-2.22	135.0%	-2.98	-2.31	-22.6%
42	-1.25	-2.83	126.8%	-3.55	-2.97	-16.4%
43	-1.01	-2.57	155.0%	-3.31	-2.71	-18.1%
	min = -97.9%		min = -100.0%		max = 31.7%	
	max = 155.0%		average = -9.2%		st. dev. = 27.9%	
	average = 16.5%		st. dev. = 54.4%			

Table F-9: Computed (FM) versus Measured Results for Static Test Stresses at Section 9B

	9B-GA-TC: NO DATA (ksi)			9B-GA-W (ksi)			9B-GA-BC (ksi)		
Test	Measured	FM	% Error	Measured	FM	% Error	Measured	FM	% Error
1	--	-0.03	--	0.27	0.22	--	0.42	0.46	10.2%
2	--	-0.04	--	0.32	0.22	-30.6%	0.44	0.48	9.4%
3	--	0.00	--	0.18	0.02	--	0.06	0.03	--
4	--	0.04	--	-0.23	-0.26	--	-0.56	-0.55	-1.2%
5	--	0.07	--	-0.48	-0.47	-2.5%	-0.96	-1.01	5.3%
6	--	0.05	--	-0.35	-0.35	-0.5%	-0.64	-0.74	15.2%
7	--	-0.13	--	0.88	0.80	-8.8%	1.47	1.73	17.7%
8	--	-0.13	--	0.87	0.83	-4.7%	1.48	1.79	21.0%
9	--	-0.09	--	0.49	0.55	13.1%	0.95	1.19	25.8%
10	--	0.00	--	-0.31	-0.03	-92.0%	-0.22	-0.05	--
11	--	0.19	--	-1.76	-1.16	-34.1%	-2.51	-2.51	0.1%
12	--	0.26	--	-2.32	-1.66	-28.6%	-3.46	-3.58	3.6%
13	--	0.23	--	-2.09	-1.48	-29.5%	-3.02	-3.18	5.5%
14	--	0.19	--	-1.57	-1.19	-24.4%	-2.47	-2.57	4.1%
15	--	0.15	--	-1.16	-0.95	-18.4%	-1.95	-2.04	4.4%
16	--	0.26	--	-2.19	-1.67	-24.1%	-3.41	-3.59	5.2%
17	--	0.26	--	-2.06	-1.65	-20.3%	-3.37	-3.55	5.3%
18	--	0.28	--	-2.45	-1.80	-26.6%	-3.59	-3.88	8.1%
19	--	0.32	--	-2.75	-2.00	-27.3%	-4.08	-4.32	5.9%
20	--	-0.07	--	0.62	0.43	-31.6%	0.80	0.92	14.8%
21	--	-0.07	--	0.62	0.43	-31.6%	0.80	0.92	14.8%
22	--	-0.10	--	0.83	0.63	-23.7%	1.19	1.36	14.0%
23	--	-0.13	--	0.88	0.80	-8.8%	1.47	1.73	17.7%
24	--	-0.13	--	0.88	0.81	-8.2%	1.47	1.74	18.4%
25	--	0.08	--	-0.66	-0.50	-23.9%	-1.11	-1.08	-3.1%
26	--	0.19	--	-1.79	-1.22	-31.8%	-2.57	-2.63	2.4%
27	--	0.16	--	-1.54	-1.01	-34.6%	-2.18	-2.18	0.0%
28	--	0.13	--	-1.35	-0.85	-37.5%	-1.88	-1.82	-3.0%
29	--	0.11	--	-1.02	-0.70	-31.9%	-1.41	-1.50	6.1%
30	--	0.20	--	-1.65	-1.23	-25.6%	-2.48	-2.66	7.1%
31	--	0.24	--	-2.06	-1.50	-27.3%	-3.10	-3.23	4.4%
32	--	0.04	--	-0.69	-0.25	-64.6%	-0.74	-0.53	-28.3%
33	--	0.07	--	-1.01	-0.42	-58.4%	-1.13	-0.91	-19.2%
34	--	0.08	--	-1.19	-0.48	-59.7%	-1.30	-1.04	-20.1%
35	--	0.09	--	-0.50	-0.55	9.5%	-1.03	-1.18	14.4%
36	--	0.17	--	-1.43	-1.08	-24.5%	-2.13	-2.33	9.2%
37	--	0.15	--	-1.38	-0.95	-31.7%	-1.97	-2.04	3.4%
38	--	0.19	--	-1.73	-1.21	-29.9%	-2.49	-2.61	4.7%
39	--	0.18	--	-1.55	-1.12	-27.9%	-2.24	-2.41	7.4%
40	--	0.02	--	-0.72	-0.16	-78.4%	-0.70	-0.33	-52.6%
41	--	-0.02	--	-0.45	0.10	-122.0%	-0.29	0.22	--
42	--	-0.01	--	-0.68	0.01	-101.5%	-0.58	0.03	-105.2%
43	--	-0.04	--	-0.46	0.21	-144.8%	-0.27	0.45	--
	min = --			min = -144.8%			min = -105.2%		
	max = --			max = 13.1%			max = 25.8%		
	average = --			average = -35.2%			average = 1.4%		
	st. dev. = --			st. dev. = 32.5%			st. dev. = 22.2%		

Table F-10: Computed (FM) versus Measured Results for Static Test Stresses at Section 9B

Test	9B-GA-TI: NO DATA (ksi)			9B-GA-TE (ksi)		
	Measured	FM	% Error	Measured	FM	% Error
1	--	-0.06	--	-0.05	-0.05	--
2	--	-0.06	--	-0.07	-0.05	--
3	--	0.00	--	-0.09	0.00	--
4	--	0.07	--	-0.09	0.06	--
5	--	0.12	--	-0.09	0.12	--
6	--	0.09	--	-0.09	0.09	--
7	--	-0.22	--	-0.34	-0.20	-40.9%
8	--	-0.23	--	-0.35	-0.20	-42.7%
9	--	-0.15	--	-0.34	-0.14	-59.4%
10	--	0.00	--	-0.29	0.01	--
11	--	0.31	--	0.14	0.29	--
12	--	0.43	--	0.60	0.41	-31.9%
13	--	0.38	--	0.70	0.37	-47.0%
14	--	0.30	--	0.63	0.30	-52.7%
15	--	0.25	--	-0.08	0.24	--
16	--	0.43	--	0.31	0.42	36.4%
17	--	0.43	--	0.58	0.41	-29.8%
18	--	0.46	--	0.65	0.45	-31.0%
19	--	0.52	--	0.82	0.50	-39.2%
20	--	-0.12	--	-0.18	-0.10	--
21	--	-0.12	--	-0.21	-0.10	--
22	--	-0.17	--	-0.41	-0.15	-63.1%
23	--	-0.22	--	-0.50	-0.20	-60.2%
24	--	-0.22	--	-0.49	-0.20	-59.0%
25	--	0.13	--	0.05	0.13	--
26	--	0.31	--	0.23	0.31	--
27	--	0.25	--	0.23	0.26	--
28	--	0.21	--	0.21	0.22	--
29	--	0.20	--	0.07	0.16	--
30	--	0.35	--	0.45	0.29	-35.1%
31	--	0.42	--	0.78	0.35	-55.0%
32	--	0.05	--	-0.11	0.08	--
33	--	0.08	--	-0.15	0.13	--
34	--	0.10	--	-0.20	0.15	--
35	--	0.16	--	-0.12	0.12	--
36	--	0.31	--	0.44	0.24	-44.8%
37	--	0.28	--	0.38	0.21	-44.0%
38	--	0.35	--	0.62	0.27	-56.2%
39	--	0.33	--	0.58	0.24	-58.9%
40	--	0.00	--	-0.16	0.07	--
41	--	-0.07	--	-0.17	0.01	--
42	--	-0.05	--	-0.23	0.04	--
43	--	-0.11	--	-0.25	-0.01	--
	min = --			min = -63.1%		
	max = --			max = 36.4%		
	average = --			average = -42.9%		
	st. dev. = --			st. dev. = 21.4%		

Table F-11: Computed (FM) versus Measured Results for Static Test Stresses at Section 9B

Test	9B-GA-BI (ksi)			9B-GA-BE (ksi)		
	Measured	FM	% Error	Measured	FM	% Error
1	0.40	0.48	20.1%	0.41	0.48	16.4%
2	0.41	0.50	20.7%	0.45	0.50	12.0%
3	-0.01	0.03	--	0.05	0.03	--
4	-0.52	-0.58	11.5%	-0.58	-0.58	0.0%
5	-0.88	-1.07	21.2%	-0.98	-1.05	7.3%
6	-0.42	-0.78	85.0%	-0.84	-0.77	-7.8%
7	1.49	1.82	21.8%	1.44	1.80	25.1%
8	1.51	1.89	25.4%	1.47	1.86	26.7%
9	0.99	1.25	25.7%	0.94	1.24	31.9%
10	-0.11	-0.05	--	-0.24	-0.05	--
11	-2.26	-2.64	16.6%	-2.57	-2.61	1.4%
12	-3.22	-3.76	16.8%	-3.52	-3.72	5.6%
13	-2.71	-3.33	23.1%	-3.16	-3.32	5.1%
14	-2.16	-2.75	27.1%	-2.64	-2.62	-0.8%
15	-1.68	-2.14	27.7%	-1.93	-2.12	10.0%
16	-2.99	-3.77	26.0%	-3.47	-3.73	7.6%
17	-3.18	-3.73	17.1%	-3.41	-3.69	8.1%
18	-2.66	-4.08	53.5%	-3.95	-4.04	2.3%
19	-3.12	-4.53	45.0%	-4.44	-4.49	1.1%
20	0.85	0.97	14.0%	0.85	0.95	11.7%
21	0.79	0.97	23.2%	0.85	0.95	11.7%
22	1.46	1.43	-1.8%	1.20	1.41	18.0%
23	1.89	1.82	-3.6%	1.44	1.79	24.4%
24	1.91	1.83	-4.2%	1.44	1.80	25.1%
25	-0.76	-1.13	49.2%	-1.21	-1.12	-7.6%
26	-1.91	-2.76	44.2%	-2.76	-2.74	-0.8%
27	-1.52	-2.28	50.1%	-2.38	-2.27	-4.8%
28	-1.21	-1.90	56.5%	-2.08	-1.89	-9.0%
29	-1.45	-1.60	10.3%	-1.18	-1.53	29.2%
30	-2.75	-2.84	3.3%	-2.00	-2.72	36.3%
31	-3.40	-3.44	1.2%	-2.55	-3.31	30.0%
32	-0.26	-0.54	--	-1.04	-0.58	-44.0%
33	-0.37	-0.92	146.5%	-1.69	-0.99	-41.5%
34	-0.29	-1.04	--	-2.12	-1.14	-46.1%
35	-1.12	-1.27	13.2%	-0.66	-1.20	80.7%
36	-2.40	-2.49	3.7%	-1.64	-2.38	44.7%
37	-2.23	-2.19	-1.6%	-1.45	-2.08	43.3%
38	-2.76	-2.79	1.0%	-1.93	-2.67	38.0%
39	-2.53	-2.58	1.9%	-1.68	-2.46	46.8%
40	0.07	-0.30	--	-1.29	-0.39	-69.8%
41	0.50	0.28	-44.2%	-0.92	0.18	-119.6%
42	0.39	0.10	-74.5%	-1.38	-0.02	-98.6%
43	0.70	0.54	-23.0%	-1.10	0.41	-137.4%
	min = -74.5%		min = -137.4%			
	max = 146.5%		max = 80.7%			
	average = 19.7%		average = 0.3%			
	st. dev. = 34.3%		st. dev. = 43.0%			

Table F-12: Computed (FM) versus Measured Results for Static Test Stresses at Section 9B

Test	9C-GC-TC (ksi)			9C-GC-BC (ksi)		
	Measured	FM	% Error	Measured	FM	% Error
1	-0.01	0.00	--	-0.07	-0.01	--
2	-0.01	0.00	--	-0.05	-0.01	--
3	0.00	0.00	--	0.02	0.00	--
4	-0.03	0.00	--	0.12	0.08	--
5	-0.03	0.00	--	0.58	0.51	-12.5%
6	-0.11	-0.01	--	1.41	1.35	-4.1%
7	0.03	-0.01	--	-0.21	-0.05	--
8	0.04	-0.01	--	-0.21	-0.05	--
9	0.03	-0.01	--	-0.17	-0.03	--
10	0.01	0.00	--	-0.05	0.04	--
11	-0.04	0.01	--	0.91	0.84	-7.8%
12	-0.18	-0.01	--	2.65	2.65	-0.1%
13	-0.11	-0.02	--	3.77	3.63	-3.7%
14	-0.02	-0.01	--	1.53	1.36	-11.3%
15	-0.05	0.00	--	1.30	1.00	-23.0%
16	-0.27	-0.01	--	2.87	2.58	-10.0%
17	-0.18	-0.01	--	2.86	2.75	-3.8%
18	-0.35	-0.02	-94.2%	4.07	3.80	-6.6%
19	-0.38	-0.02	-94.7%	4.11	3.85	-6.2%
20	-0.05	-0.01	--	-0.05	-0.03	--
21	-0.02	-0.01	--	-0.07	-0.03	--
22	-0.16	-0.01	--	0.08	-0.04	--
23	-0.22	-0.01	--	0.06	-0.05	--
24	-0.11	-0.01	--	0.04	-0.05	--
25	-0.22	-0.01	--	1.19	0.99	-16.8%
26	-0.36	-0.02	-94.5%	2.92	2.72	-6.8%
27	-0.34	-0.02	-94.2%	2.82	2.71	-3.9%
28	-0.31	-0.03	-90.5%	2.76	2.70	-2.3%
29	-0.05	0.02	--	0.33	0.35	4.9%
30	-0.12	0.04	--	0.81	0.81	-0.4%
31	-0.20	0.05	--	1.04	1.15	10.3%
32	-0.04	-0.03	--	0.66	0.71	8.0%
33	-0.11	-0.05	--	1.79	1.92	7.4%
34	-0.06	-0.07	--	2.70	2.81	4.2%
35	-0.01	0.02	--	0.57	0.34	-39.9%
36	-0.13	0.04	--	0.75	0.79	5.5%
37	-0.17	0.04	--	0.59	0.78	32.0%
38	-0.22	0.05	--	0.92	1.11	20.5%
39	-0.24	0.05	--	0.90	1.10	22.2%
40	-0.10	-0.06	--	1.72	1.91	10.9%
41	-0.09	-0.07	--	1.63	1.85	13.5%
42	-0.25	-0.08	--	2.37	2.70	14.1%
43	-0.26	-0.09	--	2.31	2.67	15.4%
	min = -94.7% max = -90.5% average = -93.6% st. dev. = 1.6%			min = -39.9% max = 32.0% average = 0.3% st. dev. = 14.2%		

Table F-13: Computed (FM) versus Measured Results for Static Test Stresses at Section 9C

Test	9C-GA-TC (ksi)			9C-GA-BC (ksi)		
	Measured	FM	% Error	Measured	FM	% Error
1	0.01	0.00	--	-0.04	-0.03	--
2	0.02	0.00	--	-0.02	-0.04	--
3	0.02	0.00	--	0.05	0.00	--
4	0.00	0.00	--	0.15	0.12	--
5	-0.02	-0.01	--	0.61	0.62	1.5%
6	-0.09	-0.02	--	1.18	1.46	23.6%
7	0.03	0.02	--	-0.18	-0.13	--
8	0.03	0.02	--	-0.20	-0.13	--
9	0.01	0.01	--	-0.16	-0.09	--
10	-0.01	0.00	--	-0.02	0.05	--
11	-0.11	-0.03	--	0.97	1.05	8.2%
12	-0.22	-0.06	--	2.62	2.99	13.9%
13	-0.14	-0.08	--	3.58	4.36	21.7%
14	-0.04	-0.02	--	1.13	1.51	33.1%
15	-0.04	-0.03	--	1.22	1.22	0.3%
16	-0.19	-0.06	--	2.70	2.99	10.8%
17	-0.26	-0.06	--	2.77	3.06	10.5%
18	-0.10	-0.08	--	3.57	4.28	19.9%
19	-0.14	-0.08	--	3.64	4.36	19.8%
20	0.03	0.01	--	-0.02	-0.07	--
21	-0.01	0.01	--	-0.02	-0.07	--
22	-0.03	0.01	--	-0.12	-0.10	--
23	-0.05	0.02	--	-0.18	-0.13	--
24	0.16	0.02	--	-0.18	-0.13	--
25	-0.14	-0.02	--	1.03	1.14	10.5%
26	-0.21	-0.05	--	2.56	3.00	17.2%
27	-0.15	-0.05	--	2.48	2.96	19.3%
28	-0.11	-0.04	--	2.43	2.93	20.5%
29	0.01	-0.04	--	0.53	0.69	30.7%
30	0.00	-0.07	--	1.50	1.84	22.9%
31	-0.09	-0.10	--	2.14	2.79	30.1%
32	-0.10	0.01	--	0.51	0.56	8.8%
33	-0.22	0.02	--	1.05	1.17	11.0%
34	-0.31	0.02	-106.4%	1.33	1.54	15.7%
35	0.09	-0.04	--	0.63	0.64	1.3%
36	0.00	-0.07	--	1.42	1.78	25.7%
37	-0.09	-0.07	--	1.27	1.73	36.5%
38	-0.11	-0.09	--	1.97	2.62	33.2%
39	-0.13	-0.09	--	1.94	2.58	32.7%
40	-0.21	0.02	--	1.00	1.17	16.6%
41	-0.22	0.03	--	0.91	1.15	26.3%
42	-0.38	0.03	-107.9%	1.28	1.54	20.4%
43	-0.38	0.04	-110.4%	1.25	1.53	22.8%
	min = -110.4%			min = 0.3%		
	max = -106.4%			max = 36.5%		
	average = -108.3%			average = 18.8%		
	st. dev. = 1.6%			st. dev. = 9.7%		

Table F-14: Computed (FM) versus Measured Results for Static Test Stresses at Section 9C

Test	9H-GC-TC (ksi)			9H-GC-BC (ksi)		
	Measured	FM	% Error	Measured	FM	% Error
1	-0.01	0.00	--	-0.40	-0.36	-9.8%
2	0.01	0.00	--	-0.40	-0.38	-4.7%
3	0.01	0.00	--	0.04	-0.02	--
4	-0.03	0.00	--	0.70	0.60	-14.4%
5	-0.08	-0.01	--	1.90	1.79	-5.7%
6	-0.04	-0.01	--	1.45	1.39	-4.2%
7	0.07	-0.01	--	-1.43	-1.35	-5.7%
8	0.08	-0.01	--	-1.46	-1.41	-3.7%
9	0.07	0.00	--	-0.98	-0.94	-3.8%
10	0.03	0.00	--	0.19	0.16	--
11	-0.10	-0.02	--	3.84	3.63	-5.6%
12	-0.07	-0.04	--	6.37	6.29	-1.3%
13	-0.09	-0.03	--	5.86	5.65	-3.5%
14	-0.01	-0.01	--	1.44	1.23	-14.6%
15	-0.12	-0.02	--	3.84	3.52	-8.3%
16	-0.28	-0.04	--	6.69	6.29	-5.9%
17	-0.11	-0.05	--	6.62	6.45	-2.6%
18	-0.19	-0.05	--	7.39	6.70	-9.3%
19	-0.22	-0.05	--	7.90	7.13	-9.8%
20	-0.03	0.00	--	-0.74	-0.71	-4.1%
21	-0.04	0.00	--	-0.75	-0.72	-4.5%
22	-0.11	0.00	--	-0.82	-1.08	30.9%
23	-0.19	-0.01	--	-1.14	-1.36	19.2%
24	-0.06	-0.01	--	-1.02	-1.36	32.8%
25	-0.19	-0.03	--	3.26	2.83	-13.1%
26	-0.27	-0.05	--	6.17	5.74	-6.9%
27	-0.27	-0.05	--	5.78	5.37	-7.1%
28	-0.24	-0.05	--	5.49	5.10	-7.1%
29	-0.06	0.03	--	1.26	1.09	-13.4%
30	-0.13	0.05	--	2.11	1.90	-10.0%
31	-0.17	0.06	--	2.37	2.18	-8.0%
32	-0.07	-0.06	--	2.53	2.60	2.8%
33	-0.03	-0.10	--	4.31	4.54	5.4%
34	-0.09	-0.11	--	4.65	4.76	2.5%
35	-0.04	0.04	--	1.08	0.67	-37.9%
36	-0.13	0.06	--	1.71	1.46	-14.7%
37	-0.18	0.06	--	1.27	1.07	-16.0%
38	-0.19	0.07	--	1.57	1.38	-12.2%
39	-0.21	0.08	--	1.35	1.09	-19.1%
40	-0.03	-0.11	--	3.93	4.25	8.1%
41	-0.04	-0.11	--	3.55	3.92	10.4%
42	-0.16	-0.13	--	3.99	4.45	11.4%
43	-0.17	-0.13	--	3.71	4.19	12.8%
	min = 0.0%		min = -37.9%		max = 32.8%	
	max = 0.0%		average = -3.7%		st. dev. = 12.6%	
	average = --		st. dev. = --			

Table F-15: Computed (FM) versus Measured Results for Static Test Stresses at Section 9H

Test	9H-GA-TC (ksi)			9H-GA-BC (ksi)		
	Measured	FM	% Error	Measured	FM	% Error
1	-0.02	0.01	--	-0.49	-0.51	4.9%
2	0.01	0.01	--	-0.47	-0.54	14.3%
3	0.11	0.00	--	0.13	-0.03	--
4	0.11	-0.01	--	0.85	0.75	-12.1%
5	0.20	-0.03	--	2.11	2.06	-2.2%
6	0.18	-0.03	--	1.62	1.57	-2.9%
7	-0.11	0.05	--	-1.71	-1.93	12.7%
8	-0.13	0.05	--	-1.76	-2.01	14.0%
9	-0.09	0.03	--	-1.20	-1.33	10.7%
10	-0.03	0.00	--	0.11	0.15	--
11	0.14	-0.07	--	3.82	4.28	12.2%
12	0.18	-0.12	--	6.23	7.18	15.3%
13	0.16	-0.12	--	5.96	6.80	14.2%
14	0.03	-0.02	--	1.23	1.37	11.3%
15	0.13	-0.07	--	3.84	4.13	7.7%
16	0.15	-0.12	--	6.33	7.26	14.6%
17	0.12	-0.12	--	6.44	7.30	13.3%
18	0.28	-0.13	--	6.80	7.63	12.2%
19	0.30	-0.14	--	7.39	8.19	10.9%
20	-0.09	0.02	--	-0.91	-1.03	13.4%
21	-0.09	0.02	--	-0.91	-1.03	13.4%
22	-0.10	0.04	--	-1.34	-1.52	13.0%
23	-0.11	0.05	--	-1.71	-1.93	12.7%
24	-0.11	0.05	--	-1.71	-1.94	13.2%
25	0.01	-0.04	--	2.84	3.03	6.7%
26	0.10	-0.09	--	5.63	6.27	11.4%
27	0.05	-0.08	--	5.16	5.76	11.6%
28	0.02	-0.07	--	4.78	5.36	12.0%
29	0.10	-0.08	--	2.17	2.71	25.1%
30	0.17	-0.13	--	3.78	4.78	26.3%
31	0.24	-0.15	--	4.47	5.32	18.9%
32	-0.06	0.01	--	1.29	1.44	11.6%
33	-0.11	0.01	--	2.23	2.48	11.3%
34	-0.16	0.02	--	2.54	2.77	9.2%
35	0.15	-0.07	--	2.09	2.30	9.9%
36	0.12	-0.13	--	3.35	4.35	30.0%
37	0.03	-0.12	--	2.98	3.90	31.0%
38	0.11	-0.14	--	3.57	4.51	26.3%
39	0.08	-0.14	--	3.31	4.24	28.3%
40	-0.12	0.03	--	1.75	1.90	8.7%
41	-0.15	0.05	--	1.23	1.33	8.5%
42	-0.24	0.05	--	1.73	1.77	2.3%
43	-0.26	0.07	--	1.40	1.33	-5.1%
	min = 0.0%		min = -12.1%		max = 31.0%	
	max = 0.0%		average = 12.2%		st. dev. = 8.8%	
	average = --		st. dev. = --			

Table F-16: Computed (FM) versus Measured Results for Static Test Stresses at Section 9H

	9J-GC-TC			(ksi)			9J-GC-W			(ksi)			9J-GC-BC			(ksi)		
Test	Measured	FM	% Error	Measured	FM	% Error	Measured	FM	% Error	Measured	FM	% Error	Measured	FM	% Error	Measured	FM	% Error
1	0.00	0.00	--	0.11	-0.01	--	-0.70	-0.72	2.6%									
2	0.01	0.00	--	0.11	-0.01	--	-0.70	-0.77	9.5%									
3	0.01	0.00	--	-0.03	0.00	--	0.04	-0.04	--									
4	0.02	-0.01	--	-0.22	0.01	--	1.16	1.15	-0.7%									
5	-0.06	-0.02	--	-0.30	0.01	-103.3%	2.31	2.40	3.7%									
6	-0.05	0.00	--	-0.15	0.01	--	0.88	0.88	-0.1%									
7	0.01	0.00	--	0.45	-0.04	-107.8%	-2.52	-2.72	7.9%									
8	0.02	0.00	--	0.47	-0.04	-107.5%	-2.58	-2.85	10.5%									
9	0.03	0.00	--	0.31	-0.02	-106.4%	-1.70	-1.89	10.9%									
10	0.05	-0.01	--	-0.02	0.00	--	0.38	0.29	-23.6%									
11	-0.05	-0.04	--	-0.40	0.03	-107.5%	5.51	5.75	4.3%									
12	-0.10	-0.04	--	-0.41	0.04	-109.8%	6.56	6.85	4.4%									
13	0.03	-0.04	--	-0.12	0.04	--	5.69	6.01	5.7%									
14	-0.05	0.00	--	-0.06	0.01	--	0.86	0.78	-9.1%									
15	-0.16	-0.04	--	-0.55	0.03	-104.6%	4.14	4.81	16.2%									
16	-0.20	-0.05	--	-0.71	0.04	-105.6%	6.64	7.13	7.3%									
17	-0.19	-0.05	--	-0.56	0.04	-107.1%	6.72	6.94	3.2%									
18	-0.20	-0.05	--	-0.77	0.04	-105.2%	7.04	7.40	5.1%									
19	-0.21	-0.06	--	-0.78	0.05	-106.4%	7.93	8.25	4.1%									
20	-0.04	0.00	--	0.16	-0.02	--	-1.35	-1.44	6.7%									
21	-0.07	0.00	--	0.10	-0.02	--	-1.35	-1.46	8.2%									
22	-0.15	0.00	--	0.03	-0.03	--	-2.11	-2.17	2.9%									
23	-0.19	0.00	--	0.14	-0.04	--	-2.52	-2.74	8.7%									
24	-0.12	0.00	--	0.09	-0.04	--	-2.52	-2.73	8.3%									
25	-0.16	-0.04	--	-0.44	0.00	-101.1%	2.96	3.37	13.8%									
26	-0.25	-0.05	--	-0.73	0.02	-102.7%	5.40	5.50	1.9%									
27	-0.22	-0.05	--	-0.69	0.01	-101.4%	4.72	4.77	1.0%									
28	-0.19	-0.05	--	-0.66	0.01	-100.8%	4.20	4.21	0.3%									
29	-0.09	0.03	--	-0.15	0.06	--	1.59	1.47	-7.7%									
30	-0.09	0.06	--	-0.26	0.09	--	2.33	2.20	-5.7%									
31	-0.17	0.07	--	-0.26	0.11	--	2.68	2.58	-3.7%									
32	0.01	-0.07	--	-0.06	-0.03	--	3.05	3.51	15.3%									
33	-0.06	-0.11	--	-0.32	-0.05	-85.7%	4.21	4.80	13.9%									
34	-0.02	-0.12	--	-0.20	-0.05	--	5.03	5.56	10.6%									
35	-0.11	0.05	--	-0.24	0.06	--	0.61	0.64	5.3%									
36	-0.10	0.07	--	-0.17	0.09	--	1.63	1.34	-18.0%									
37	-0.17	0.08	--	-0.07	0.10	--	1.00	0.59	-41.0%									
38	-0.19	0.10	--	-0.10	0.11	--	1.31	0.98	-25.0%									
39	-0.21	0.10	--	-0.05	0.12	--	0.87	0.42	-51.8%									
40	-0.06	-0.12	--	-0.27	-0.07	--	3.56	4.21	18.3%									
41	-0.08	-0.13	--	-0.19	-0.09	--	2.93	3.59	22.7%									
42	-0.22	-0.15	--	-0.19	-0.10	--	3.62	4.51	24.6%									
43	-0.22	-0.16	--	-0.15	-0.12	--	3.16	4.08	29.2%									
	min = 0.0%			min = -109.8%			min = -51.8%			max = 0.0%			max = 29.2%			average = 2.4%		
	st. dev. = --			st. dev. = 5.4%			st. dev. = 15.4%											

Table F-17: Computed (FM) versus Measured Results for Static Test Stresses at Section 9J

Test	9J-GC-TI (ksi)			9J-GC-TE (ksi)		
	Measured	FM	% Error	Measured	FM	% Error
1	-0.01	0.04	--	0.00	0.02	--
2	0.00	0.04	--	0.00	0.02	--
3	-0.01	0.00	--	-0.01	0.00	--
4	-0.05	-0.06	--	-0.03	-0.05	--
5	-0.13	-0.13	--	-0.17	-0.11	--
6	-0.12	-0.05	--	-0.14	-0.03	--
7	0.10	0.15	--	0.05	0.08	--
8	0.12	0.15	--	0.07	0.08	--
9	0.11	0.10	--	0.06	0.06	--
10	0.06	-0.02	--	0.06	-0.02	--
11	-0.13	-0.31	--	-0.12	-0.25	--
12	-0.21	-0.37	--	-0.26	-0.29	--
13	-0.12	-0.33	--	-0.20	-0.25	--
14	-0.02	-0.04	--	-0.09	-0.03	--
15	-0.30	-0.26	--	-0.34	-0.21	-38.6%
16	-0.41	-0.39	-3.8%	-0.50	-0.31	-37.7%
17	-0.32	-0.38	17.7%	-0.37	-0.30	-18.1%
18	-0.58	-0.40	-30.4%	-0.46	-0.32	-30.6%
19	-0.61	-0.45	-26.5%	-0.47	-0.35	-26.1%
20	-0.07	0.08	--	-0.08	0.04	--
21	-0.03	0.08	--	-0.06	0.04	--
22	-0.18	0.12	--	-0.25	0.06	--
23	-0.21	0.15	--	-0.27	0.08	--
24	-0.27	0.15	--	-0.18	0.08	--
25	-0.32	-0.18	-44.5%	-0.35	-0.17	-51.6%
26	-0.55	-0.30	-45.4%	-0.55	-0.26	-52.7%
27	-0.55	-0.26	-52.5%	-0.52	-0.24	-53.8%
28	-0.52	-0.23	-55.8%	-0.47	-0.22	-53.1%
29	-0.08	-0.08	--	-0.12	0.03	--
30	-0.10	-0.11	--	-0.16	0.06	--
31	-0.16	-0.14	--	-0.24	0.07	--
32	-0.06	-0.19	--	-0.03	-0.25	--
33	-0.13	-0.27	--	-0.12	-0.36	--
34	-0.12	-0.31	--	-0.08	-0.41	--
35	-0.15	-0.03	--	-0.25	0.08	--
36	-0.08	-0.07	--	-0.16	0.11	--
37	-0.11	-0.03	--	-0.21	0.16	--
38	-0.14	-0.05	--	-0.21	0.17	--
39	-0.12	-0.02	--	-0.24	0.21	--
40	-0.13	-0.23	--	-0.11	-0.37	--
41	-0.14	-0.20	--	-0.12	-0.38	--
42	-0.21	-0.25	--	-0.28	-0.44	--
43	-0.19	-0.22	--	-0.27	-0.45	--
	min = -55.8%		min = -53.8%			
	max = 17.7%		max = -18.1%			
	average = -30.2%		average = -40.3%			
	st. dev. = 24.0%		st. dev. = 12.6%			

Table F-18: Computed (FM) versus Measured Results for Static Test Stresses at Section 9J

	9J-GC-BI (ksi)			9J-GC-BE (ksi)		
Test	Measured	FM	% Error	Measured	FM	% Error
1	-0.80	-0.77	-4.0%	-0.81	-0.73	-10.0%
2	-0.81	-0.83	2.9%	-0.80	-0.78	-2.4%
3	0.04	-0.04	--	0.05	-0.04	--
4	1.25	1.24	-1.0%	1.40	1.17	-16.6%
5	2.46	2.54	3.3%	2.78	2.46	-11.6%
6	1.03	0.93	-9.4%	0.99	0.91	-7.9%
7	-2.90	-2.91	0.3%	-2.87	-2.74	-4.4%
8	-2.97	-3.06	3.0%	-2.93	-2.88	-1.9%
9	-1.97	-2.03	3.3%	-1.93	-1.91	-1.0%
10	0.42	0.31	-25.4%	0.43	0.30	-30.9%
11	6.11	6.11	0.0%	6.24	5.87	-6.0%
12	7.18	7.26	1.1%	7.42	7.01	-5.5%
13	6.59	6.35	-3.7%	6.08	6.16	1.3%
14	0.97	0.82	-15.8%	0.93	0.81	-12.5%
15	4.38	5.10	16.5%	4.83	4.92	1.9%
16	7.21	7.54	4.6%	7.60	7.31	-3.8%
17	7.24	7.35	1.5%	7.78	7.11	-8.7%
18	7.77	7.84	0.9%	7.92	7.59	-4.2%
19	8.81	8.75	-0.7%	8.90	8.44	-5.2%
20	-1.54	-1.55	0.4%	-1.44	-1.46	1.6%
21	-1.54	-1.56	1.1%	-1.44	-1.47	2.3%
22	-2.44	-2.33	-4.4%	-2.35	-2.19	-6.8%
23	-2.90	-2.94	1.3%	-2.87	-2.77	-3.3%
24	-2.90	-2.93	1.0%	-2.87	-2.76	-3.7%
25	3.19	3.55	11.2%	3.44	3.47	0.9%
26	5.66	5.80	2.5%	6.26	5.66	-9.5%
27	4.91	5.02	2.3%	5.49	4.92	-10.4%
28	4.31	4.42	2.5%	4.92	4.35	-11.5%
29	1.74	1.60	-7.9%	1.84	1.46	-20.7%
30	2.53	2.39	-5.7%	2.68	2.19	-18.2%
31	3.17	2.80	-11.5%	2.87	2.58	-10.2%
32	3.36	3.68	9.4%	3.44	3.65	6.1%
33	4.46	5.03	12.8%	4.93	4.98	1.1%
34	5.53	5.84	5.7%	5.69	5.75	1.0%
35	0.62	0.70	12.8%	0.72	0.61	-15.5%
36	1.75	1.47	-15.8%	1.89	1.32	-30.3%
37	1.17	0.66	-43.4%	1.08	0.56	-48.3%
38	1.51	1.09	-27.6%	1.46	0.95	-34.8%
39	1.01	0.49	-51.6%	0.96	0.38	-60.5%
40	3.71	4.39	18.4%	4.21	4.38	4.0%
41	3.00	3.73	24.2%	3.50	3.76	7.4%
42	3.87	4.70	21.3%	4.21	4.70	11.7%
43	3.34	4.24	27.1%	3.70	4.27	15.5%
	min = -51.6%		min = -60.5%		max = 27.1%	
	max = 27.1%		max = 15.5%		average = -0.9%	
	average = -0.9%		average = -8.6%		st. dev. = 15.3%	
	st. dev. = 15.3%		st. dev. = 14.6%			

Table F-19: Computed (FM) versus Measured Results for Static Test Stresses at Section 9J

	9J-GA-TC			(ksi)			9J-GA-W			(ksi)			9J-GA-BC			(ksi)		
Test	Measured	FM	% Error	Measured	FM	% Error	Measured	FM	% Error	Measured	FM	% Error	Measured	FM	% Error	Measured	FM	% Error
1	-0.03	0.02	--	-0.49	-0.48	-3.2%	-0.97	-0.97	-0.4%									
2	-0.01	0.02	--	-0.50	-0.50	0.1%	-0.97	-1.02	5.4%									
3	0.12	0.00	--	0.16	-0.03	--	0.18	-0.05	--									
4	0.16	-0.02	--	0.85	0.67	-21.3%	1.60	1.36	-14.8%									
5	0.20	-0.04	--	1.60	1.34	-16.5%	2.84	2.71	-4.6%									
6	0.11	-0.02	--	0.64	0.52	-19.8%	1.24	1.05	-15.0%									
7	-0.20	0.08	--	-2.33	-1.79	-23.3%	-3.60	-3.66	1.6%									
8	-0.22	0.08	--	-2.40	-1.87	-22.4%	-3.69	-3.81	3.3%									
9	-0.16	0.05	--	-1.66	-1.24	-25.1%	-2.45	-2.53	3.4%									
10	-0.02	0.00	--	0.14	0.12	--	0.32	0.23	-28.3%									
11	0.33	-0.11	-133.8%	4.44	3.21	-27.8%	6.31	6.52	3.3%									
12	0.45	-0.14	-131.4%	5.63	3.98	-29.3%	7.92	8.10	2.2%									
13	0.33	-0.12	-136.5%	4.67	3.42	-26.9%	6.65	6.95	4.4%									
14	0.01	-0.02	--	0.59	0.45	-23.5%	0.94	0.92	-2.4%									
15	0.28	-0.09	--	3.59	2.71	-24.5%	5.25	5.51	4.9%									
16	0.44	-0.13	-129.2%	5.68	4.00	-29.6%	7.93	8.13	2.5%									
17	0.44	-0.13	-129.3%	5.73	3.91	-31.9%	7.93	7.94	0.1%									
18	0.55	-0.14	-125.6%	5.89	4.16	-29.3%	8.23	8.46	2.7%									
19	0.58	-0.16	-127.6%	6.66	4.66	-30.1%	9.38	9.47	1.0%									
20	-0.13	0.04	--	-1.19	-0.96	-19.7%	-1.87	-1.95	4.2%									
21	-0.13	0.04	--	-1.19	-0.96	-19.7%	-1.87	-1.95	4.2%									
22	-0.18	0.06	--	-1.67	-1.41	-15.6%	-2.84	-2.88	1.4%									
23	-0.20	0.08	--	-2.33	-1.79	-23.3%	-3.60	-3.66	1.6%									
24	-0.20	0.08	--	-2.33	-1.80	-23.1%	-3.60	-3.67	1.9%									
25	0.07	-0.04	--	2.35	1.71	-27.3%	3.40	3.46	1.9%									
26	0.39	-0.09	-123.1%	4.25	2.96	-30.4%	6.13	6.00	-2.2%									
27	0.31	-0.07	-122.3%	3.62	2.48	-31.4%	5.22	5.03	-3.6%									
28	0.26	-0.05	--	3.11	2.11	-32.1%	4.50	4.27	-5.1%									
29	0.14	-0.10	--	2.09	1.79	-14.4%	3.13	3.68	17.7%									
30	0.35	-0.15	-142.4%	3.37	2.57	-23.8%	4.79	5.28	10.2%									
31	0.35	-0.17	-148.9%	3.97	3.00	-24.6%	5.69	6.16	8.4%									
32	-0.02	0.01	--	1.08	0.92	-15.3%	1.78	1.82	2.1%									
33	0.01	0.02	--	1.82	1.41	-22.7%	2.85	2.79	-2.2%									
34	-0.06	0.02	--	2.05	1.62	-21.4%	3.27	3.21	-1.8%									
35	0.15	-0.09	--	1.76	1.42	-19.7%	2.66	2.92	9.8%									
36	0.26	-0.14	--	2.72	2.17	-20.1%	3.94	4.48	13.7%									
37	0.11	-0.14	--	2.14	1.83	-14.5%	3.29	3.79	15.3%									
38	0.14	-0.16	--	2.66	2.26	-15.2%	4.01	4.67	16.5%									
39	0.06	-0.16	--	2.27	2.01	-11.6%	3.49	4.17	19.6%									
40	-0.05	0.05	--	1.11	0.85	-23.5%	1.85	1.65	-11.0%									
41	-0.13	0.08	--	0.40	0.32	-20.1%	0.85	0.56	-33.9%									
42	-0.25	0.08	--	0.77	0.60	-21.9%	1.45	1.12	-22.8%									
43	-0.30	0.10	--	0.28	0.21	--	0.74	0.31	-57.9%									
	min = -148.9%			min = -32.1%			min = -57.9%			max = 19.6%			max = 14.0%			st. dev. = 7.8%		

Table F-20: Computed (FM) versus Measured Results for Static Test Stresses at Section 9J

Test	9J-GA-TI: NO DATA (ksi)			9J-GA-TE (ksi)		
	Measured	FM	% Error	Measured	FM	% Error
1	--	0.07	--	-0.01	0.05	--
2	--	0.07	--	-0.02	0.06	--
3	--	0.00	--	-0.02	0.00	--
4	--	-0.09	--	0.00	-0.07	--
5	--	-0.17	--	-0.08	-0.15	--
6	--	-0.07	--	-0.11	-0.06	--
7	--	0.27	--	-0.05	0.20	--
8	--	0.27	--	-0.06	0.21	--
9	--	0.18	--	-0.08	0.14	--
10	--	-0.01	--	-0.04	-0.01	--
11	--	-0.42	--	-0.03	-0.35	--
12	--	-0.52	--	-0.22	-0.44	--
13	--	-0.45	--	-0.31	-0.38	23.4%
14	--	-0.06	--	-0.14	-0.05	--
15	--	-0.34	--	-0.20	-0.30	--
16	--	-0.51	--	-0.33	-0.44	35.0%
17	--	-0.50	--	-0.36	-0.43	18.0%
18	--	-0.53	--	-0.28	-0.46	--
19	--	-0.60	--	-0.26	-0.51	--
20	--	0.14	--	-0.06	0.11	--
21	--	0.14	--	-0.09	0.11	--
22	--	0.21	--	-0.17	0.16	--
23	--	0.26	--	-0.18	0.20	--
24	--	0.27	--	-0.14	0.20	--
25	--	-0.20	--	-0.29	-0.19	--
26	--	-0.36	--	-0.41	-0.32	-21.3%
27	--	-0.29	--	-0.41	-0.27	-33.4%
28	--	-0.24	--	-0.41	-0.23	-44.5%
29	--	-0.30	--	-0.04	-0.20	--
30	--	-0.46	--	-0.08	-0.29	--
31	--	-0.53	--	-0.13	-0.34	--
32	--	-0.04	--	-0.09	-0.09	--
33	--	-0.05	--	-0.19	-0.14	--
34	--	-0.07	--	-0.27	-0.17	--
35	--	-0.27	--	-0.15	-0.16	--
36	--	-0.42	--	-0.12	-0.25	--
37	--	-0.39	--	-0.21	-0.21	--
38	--	-0.47	--	-0.23	-0.26	--
39	--	-0.45	--	-0.27	-0.23	--
40	--	0.05	--	-0.19	-0.08	--
41	--	0.14	--	-0.21	-0.02	--
42	--	0.13	--	-0.38	-0.05	-86.8%
43	--	0.20	--	-0.38	-0.01	-97.4%
	min = --		min = -97.4%			
	max = --		max = 35.0%			
	average = --		average = -25.9%			
	st. dev. = --		st. dev. = 46.5%			

Table F-21: Computed (FM) versus Measured Results for Static Test Stresses at Section 9J

Test	9J-GA-BI (ksi)			9J-GA-BE (ksi)		
	Measured	FM	% Error	Measured	FM	% Error
1	-0.78	-1.04	33.3%	-1.03	-0.99	-4.3%
2	-0.79	-1.09	37.8%	-1.02	-1.03	0.6%
3	0.02	-0.05	--	0.13	-0.05	--
4	1.19	1.46	22.6%	1.56	1.38	-11.4%
5	2.21	2.89	30.8%	2.78	2.75	-1.1%
6	0.78	1.10	40.9%	1.30	1.08	-16.7%
7	-2.81	-3.92	39.4%	-3.75	-3.71	-1.0%
8	-2.87	-4.08	42.0%	-3.84	-3.86	0.4%
9	-1.91	-2.71	41.8%	-2.56	-2.56	0.1%
10	0.29	0.25	--	0.32	0.24	-26.1%
11	5.27	6.96	32.0%	6.47	6.64	2.6%
12	6.63	8.61	29.8%	8.08	8.27	2.3%
13	5.13	7.39	44.2%	7.19	7.10	-1.2%
14	0.73	0.97	32.9%	1.01	0.95	-6.0%
15	4.38	5.89	34.5%	5.16	5.60	8.5%
16	6.63	8.63	30.2%	8.03	8.31	3.5%
17	6.62	8.44	27.5%	7.97	8.12	1.9%
18	6.73	9.00	33.6%	8.52	8.63	1.3%
19	7.63	10.09	32.2%	9.76	9.66	-1.1%
20	-1.54	-2.08	35.0%	-1.96	-1.97	0.4%
21	-1.54	-2.09	35.6%	-1.96	-1.97	0.4%
22	-2.18	-3.09	41.8%	-2.95	-2.92	-1.2%
23	-2.81	-3.92	39.4%	-3.75	-3.71	-1.0%
24	-2.81	-3.93	39.8%	-3.75	-3.72	-0.7%
25	2.80	3.69	31.7%	3.47	3.53	1.9%
26	5.13	6.35	23.8%	6.14	6.15	0.1%
27	4.38	5.31	21.3%	5.19	5.16	-0.5%
28	3.79	4.50	18.7%	4.43	4.40	-0.6%
29	2.71	3.97	46.8%	3.06	3.71	21.1%
30	4.13	5.65	36.9%	4.70	5.36	14.1%
31	4.71	6.62	40.4%	5.83	6.24	7.1%
32	1.37	1.91	39.9%	1.94	1.89	-2.8%
33	2.32	2.92	25.7%	2.95	2.89	-2.1%
34	2.56	3.36	31.5%	3.51	3.32	-5.4%
35	2.25	3.16	40.5%	2.48	2.94	18.4%
36	3.43	4.80	40.0%	3.81	4.55	19.5%
37	2.80	4.06	45.1%	3.22	3.85	19.7%
38	3.45	5.02	45.4%	3.93	4.72	20.1%
39	3.02	4.49	48.8%	3.39	4.21	24.3%
40	1.49	1.70	13.7%	1.92	1.74	-9.3%
41	0.66	0.53	-20.1%	0.89	0.64	-28.4%
42	1.10	1.12	1.6%	1.57	1.21	-22.9%
43	0.52	0.25	-52.2%	0.83	0.38	-54.3%
	min = -52.2%		min = -54.3%			
	max = 48.8%		max = 24.3%			
	average = 30.6%		average = -0.7%			
	st. dev. = 18.1%		st. dev. = 14.2%			

Table F-22: Computed (FM) versus Measured Results for Static Test Stresses at Section 9J

	9L-GC-TC			(ksi)			9L-GC-BC			(ksi)		
Test	Measured	FM	% Error	Measured	FM	% Error	Measured	FM	% Error	Measured	% Error	
1	0.04	0.00	--		-1.08	-1.08	-	-	-	-	-0.1%	
2	0.06	0.01	--		-1.09	-1.16	-	-	-	-	6.0%	
3	0.03	0.00	--		0.05	-0.05	--	--	--	--	--	
4	-0.04	-0.01	--		1.66	1.61	-	-	-	-	-2.9%	
5	0.00	-0.01	--		1.58	1.58	-	-	-	-	0.3%	
6	-0.01	0.00	--		0.43	0.40	-	-	-	-	-7.6%	
7	0.22	0.02	--		-3.89	-4.08	-	-	-	-	4.9%	
8	0.25	0.02	--		-4.00	-4.28	-	-	-	-	7.0%	
9	0.20	0.01	--		-2.61	-2.85	-	-	-	-	9.1%	
10	0.04	-0.01	--		0.64	0.45	-	-	-	-	-29.8%	
11	-0.06	-0.03	--		5.22	5.17	-	-	-	-	-1.0%	
12	-0.08	-0.03	--		5.41	5.57	-	-	-	-	3.0%	
13	0.03	-0.01	--		3.22	3.20	-	-	-	-	-0.5%	
14	0.03	0.00	--		0.35	0.36	-	-	-	-	3.0%	
15	-0.05	-0.02	--		3.25	3.20	-	-	-	-	-1.6%	
16	-0.17	-0.04	--		5.80	5.75	-	-	-	-	-0.9%	
17	0.00	-0.04	--		0.00	5.65	--	--	--	--	--	
18	-0.05	-0.03	--		5.51	5.20	-	-	-	-	-5.6%	
19	-0.10	-0.04	--		6.78	6.47	-	-	-	-	-4.6%	
20	0.07	0.01	--		-2.08	-2.16	-	-	-	-	4.1%	
21	0.11	0.01	--		-2.14	-2.19	-	-	-	-	2.3%	
22	0.01	0.01	--		-2.92	-3.26	-	-	-	-	11.5%	
23	0.03	0.02	--		-3.74	-4.12	-	-	-	-	10.1%	
24	0.13	0.02	--		-3.67	-4.10	-	-	-	-	11.7%	
25	-0.03	-0.01	--		1.05	0.91	-	-	-	-	-13.0%	
26	-0.18	-0.03	--		3.82	3.49	-	-	-	-	-8.5%	
27	-0.12	-0.03	--		2.82	2.39	-	-	-	-	-15.2%	
28	-0.06	-0.02	--		2.06	1.55	-	-	-	-	-24.6%	
29	-0.01	0.03	--		1.15	1.00	-	-	-	-	-12.9%	
30	-0.09	0.05	--		1.92	1.77	-	-	-	-	-7.8%	
31	-0.10	0.06	--		2.20	2.07	-	-	-	-	-5.9%	
32	0.03	-0.05	--		1.73	2.04	-	-	-	-	17.7%	
33	0.00	-0.09	--		3.61	3.95	-	-	-	-	9.5%	
34	0.01	-0.10	--		3.96	4.17	-	-	-	-	5.4%	
35	0.01	0.05	--		0.15	-0.30	--	--	--	--	--	
36	-0.04	0.07	--		0.83	0.43	-	-	-	-	-48.5%	
37	0.00	0.09	--		-0.16	-0.74	--	--	--	--	--	
38	-0.01	0.10	--		0.16	-0.41	--	--	--	--	--	
39	-0.01	0.11	--		-0.54	-1.29	-	-	-	-	138.2%	
40	0.01	-0.10	--		2.64	3.10	-	-	-	-	17.5%	
41	0.03	-0.11	--		1.68	2.27	-	-	-	-	35.2%	
42	-0.04	-0.12	--		2.07	2.63	-	-	-	-	27.1%	
43	-0.03	-0.13	--		1.38	2.09	-	-	-	-	51.9%	
	min = 0.0%			min = -48.5%			max = 0.0%			max = 138.2%		
	average = --			average = 4.8%			st. dev. = --			st. dev. = 27.6%		

Table F-23: Computed (FM) versus Measured Results for Static Test Stresses at Section 9L

Test	9L-GA-TC (ksi)			9L-GA-BC (ksi)		
	Measured	FM	% Error	Measured	FM	% Error
1	-0.02	0.03	--	-1.39	-1.43	3.2%
2	0.00	0.03	--	-1.40	-1.50	6.8%
3	0.05	0.00	--	0.14	-0.08	--
4	0.00	-0.03	--	1.90	1.81	-4.6%
5	-0.01	-0.03	--	1.71	1.80	5.5%
6	-0.04	-0.01	--	0.55	0.49	-10.6%
7	-0.02	0.10	--	-5.23	-5.40	3.3%
8	-0.04	0.10	--	-5.33	-5.61	5.2%
9	-0.04	0.07	--	-3.54	-3.72	5.2%
10	-0.04	0.00	--	0.46	0.29	-36.8%
11	-0.01	-0.10	--	5.85	6.09	4.1%
12	0.00	-0.11	--	6.08	6.48	6.7%
13	-0.03	-0.07	--	3.47	3.71	6.9%
14	-0.04	-0.01	--	0.37	0.44	19.9%
15	0.02	-0.06	--	3.32	3.59	8.1%
16	0.00	-0.11	--	6.08	6.48	6.7%
17	0.00	-0.11	--	0.00	6.33	--
18	0.06	-0.10	--	5.72	5.93	3.6%
19	0.07	-0.12	--	7.23	7.39	2.2%
20	-0.10	0.05	--	-2.76	-2.87	4.1%
21	-0.10	0.05	--	-2.76	-2.87	4.1%
22	-0.04	0.08	--	-4.06	-4.24	4.3%
23	-0.02	0.10	--	-5.23	-5.40	3.3%
24	-0.02	0.10	--	-5.23	-5.41	3.4%
25	-0.09	-0.01	--	0.40	0.65	64.4%
26	-0.08	-0.05	--	3.29	3.46	5.1%
27	-0.12	-0.03	--	1.93	2.04	5.7%
28	-0.15	-0.01	--	0.85	0.92	7.9%
29	0.02	-0.07	--	1.81	2.28	25.8%
30	0.07	-0.12	--	3.62	4.19	15.9%
31	0.11	-0.14	--	4.26	4.79	12.5%
32	-0.10	0.01	--	1.12	1.24	10.5%
33	-0.17	0.01	--	2.11	2.25	6.5%
34	-0.23	0.02	--	2.49	2.51	0.9%
35	0.03	-0.06	--	0.82	1.18	43.9%
36	-0.02	-0.11	--	2.36	3.08	30.5%
37	-0.15	-0.10	--	1.25	2.11	68.8%
38	-0.07	-0.12	--	1.97	2.77	40.7%
39	-0.14	-0.12	--	1.18	2.08	76.6%
40	-0.19	0.05	--	0.57	0.51	-10.2%
41	-0.21	0.09	--	-0.90	-1.13	25.8%
42	-0.33	0.09	-127.1%	-0.48	-0.76	56.7%
43	-0.35	0.12	-134.7%	-1.58	-1.98	25.2%
	min = -134.7%			min = -36.8%		
	max = -127.1%			max = 76.6%		
	average = -130.9%			average = 13.8%		
	st. dev. = 3.8%			st. dev. = 21.9%		

Table F-24: Computed (FM) versus Measured Results for Static Test Stresses at Section 9L

Test	9N-GC-TC (ksi)			9N-GC-BC (ksi)		
	Measured	FM	% Error	Measured	FM	% Error
1	0.02	0.05	--	-1.54	-1.46	-5.3%
2	0.06	0.05	--	-1.55	-1.57	1.2%
3	0.04	0.00	--	0.07	-0.07	--
4	0.01	-0.04	--	1.26	1.15	-8.5%
5	0.02	0.00	--	0.28	0.20	--
6	0.02	0.00	--	-0.02	-0.08	--
7	0.11	0.18	--	-5.63	-5.51	-2.1%
8	0.15	0.20	--	-5.82	-5.80	-0.4%
9	0.14	0.13	--	-3.81	-3.85	1.0%
10	0.04	0.00	--	0.03	-0.18	--
11	-0.27	-0.07	--	2.29	2.16	-5.5%
12	-0.54	-0.04	-92.6%	1.63	1.44	-11.8%
13	-0.45	0.00	-100.0%	0.13	0.09	--
14	-0.12	0.00	--	-0.16	-0.05	--
15	0.08	-0.01	--	0.54	0.42	-22.6%
16	-0.54	-0.04	-92.6%	1.63	1.38	-15.5%
17	0.00	-0.04	--	0.00	1.26	--
18	-0.21	-0.04	--	1.57	1.37	-12.5%
19	-0.51	-0.08	-84.4%	2.75	2.48	-10.0%
20	0.10	0.10	--	-2.93	-2.92	-0.5%
21	0.10	0.10	--	-2.93	-2.97	1.2%
22	-0.02	0.15	--	-4.38	-4.42	0.9%
23	0.11	0.19	--	-5.63	-5.58	-0.9%
24	0.11	0.19	--	-5.63	-5.54	-1.6%
25	-0.36	0.09	-125.2%	-2.56	-2.58	0.9%
26	-0.38	0.06	-115.7%	-1.59	-1.66	4.2%
27	-0.37	0.11	-129.4%	-3.12	-3.15	1.1%
28	-0.35	0.15	-142.6%	-4.31	-4.29	-0.4%
29	-0.05	0.01	--	0.09	0.13	--
30	-0.08	0.01	--	0.35	0.39	11.1%
31	-0.14	0.00	--	0.57	0.69	21.6%
32	-0.11	-0.01	--	0.12	0.21	--
33	-0.28	-0.04	--	0.90	0.86	-4.3%
34	-0.24	-0.08	--	1.83	1.70	-7.3%
35	0.13	0.08	--	-1.41	-1.73	22.8%
36	-0.06	0.08	--	-1.34	-1.52	13.5%
37	-0.12	0.15	--	-2.82	-3.17	12.4%
38	-0.15	0.14	--	-2.61	-2.87	10.1%
39	-0.13	0.19	--	-3.77	-4.14	9.7%
40	-0.30	-0.02	-93.4%	-0.42	-0.18	-57.6%
41	-0.38	0.00	-100.0%	-1.69	-1.12	-33.6%
42	-0.39	-0.03	-92.3%	-0.89	-0.35	-60.8%
43	-0.41	-0.01	-97.6%	-1.86	-1.05	-43.4%
	min = -142.6%			min = -60.8%		
	max = -84.4%			max = 22.8%		
	average = -105.5%			average = -5.7%		
	st. dev. = 17.5%			st. dev. = 18.8%		

Table F-25: Computed (FM) versus Measured Results for Static Test Stresses at Section 9N

Test	9N-GA-TC (ksi)			9N-GA-BC (ksi)		
	Measured	FM	% Error	Measured	FM	% Error
1	0.02	0.12	--	-1.34	-1.37	2.1%
2	0.03	0.12	--	-1.35	-1.43	5.8%
3	0.10	0.01	--	0.12	-0.07	--
4	0.01	-0.08	--	0.89	0.92	3.6%
5	0.04	-0.02	--	0.25	0.19	--
6	0.01	0.00	--	0.01	-0.05	--
7	0.03	0.44	--	-5.13	-5.17	0.8%
8	0.02	0.45	--	-5.20	-5.36	3.1%
9	0.02	0.30	--	-3.44	-3.56	3.6%
10	0.02	0.03	--	-0.32	-0.37	14.7%
11	0.08	-0.17	--	1.90	1.94	2.0%
12	0.00	-0.11	--	1.28	1.19	-6.9%
13	0.06	-0.01	--	0.14	0.11	--
14	0.05	0.00	--	-0.13	-0.04	--
15	0.09	-0.04	--	0.49	0.38	-22.2%
16	0.00	-0.10	--	1.28	1.18	-7.7%
17	0.00	-0.10	--	0.00	1.16	--
18	0.09	-0.10	--	1.24	1.17	-5.3%
19	0.00	-0.18	--	2.20	2.06	-6.2%
20	-0.11	0.23	--	-2.72	-2.75	1.1%
21	-0.11	0.23	--	-2.72	-2.74	0.7%
22	0.01	0.34	--	-3.96	-4.05	2.4%
23	0.03	0.44	--	-5.13	-5.16	0.6%
24	0.03	0.44	--	-5.13	-5.18	1.0%
25	0.02	0.20	--	-2.34	-2.37	1.3%
26	-0.05	0.13	--	-1.52	-1.59	4.5%
27	-0.05	0.25	--	-2.89	-2.95	2.1%
28	-0.05	0.34	--	-3.97	-4.02	1.3%
29	0.10	-0.02	--	0.07	0.15	--
30	0.15	-0.07	--	0.55	0.66	20.1%
31	0.20	-0.13	--	1.19	1.33	11.9%
32	-0.06	-0.01	--	0.09	0.21	--
33	-0.13	-0.03	--	0.37	0.48	28.5%
34	-0.20	-0.04	--	0.59	0.71	20.8%
35	0.10	0.05	--	-0.88	-0.81	-8.0%
36	0.06	0.00	--	-0.59	-0.32	-46.1%
37	-0.07	0.06	--	-1.56	-1.10	-29.3%
38	0.00	0.01	--	-1.03	-0.51	-50.6%
39	-0.08	0.05	--	-1.74	-1.11	-36.3%
40	-0.15	0.13	--	-1.24	-1.26	2.0%
41	-0.13	0.27	--	-2.75	-2.88	4.7%
42	-0.24	0.25	--	-2.59	-2.65	2.3%
43	-0.21	0.36	--	-3.74	-3.88	3.8%
	min = 0.0%		min = -50.6%			
	max = 0.0%		max = 28.5%			
	average = --		average = -2.1%			
	st. dev. = --		st. dev. = 16.6%			

Table F-26: Computed (FM) versus Measured Results for Static Test Stresses at Section 9N

	9O-GC-TC			(ksi)			9O-GC-W			(ksi)			9O-GC-BC			(ksi)		
Test	Measured	FM	% Error	Measured	FM	% Error	Measured	FM	% Error	Measured	FM	% Error	Measured	FM	% Error	Measured	FM	% Error
1	0.08	0.13	--		0.37	-0.53	-244.2%		-1.15	-1.19	3.9%							
2	0.09	0.14	--		0.38	-0.57	-249.4%		-1.18	-1.28	8.4%							
3	0.02	0.03	--		0.16	-0.15	--		-0.27	-0.32	--							
4	0.00	0.06	--		0.41	-0.24	-158.2%		-0.53	-0.54	1.5%							
5	0.01	0.07	--		0.30	-0.32	-205.8%		-0.69	-0.71	3.0%							
6	-0.02	0.04	--		0.04	-0.15	--		-0.34	-0.34	-0.1%							
7	0.47	0.47	0.9%		1.43	-2.01	-240.3%		-4.17	-4.48	7.5%							
8	0.72	0.50	-30.9%		1.57	-2.11	-234.4%		-4.37	-4.72	8.1%							
9	0.63	0.35	-44.2%		1.51	-1.49	-198.4%		-3.08	-3.32	7.7%							
10	0.49	0.24	-51.1%		1.73	-1.03	-159.2%		-2.15	-2.29	6.6%							
11	0.44	0.19	-57.0%		2.21	-0.84	-138.0%		-1.86	-1.87	0.3%							
12	0.68	0.26	-61.7%		1.58	-1.10	-169.4%		-2.45	-2.45	-0.1%							
13	0.64	0.19	-70.4%		0.92	-0.82	-188.6%		-1.94	-1.82	-6.1%							
14	0.22	0.03	--		0.16	-0.13	--		-0.52	-0.28	-45.7%							
15	-0.01	0.15	--		0.75	-0.64	-185.2%		-1.30	-1.43	9.8%							
16	0.50	0.26	-48.2%		1.58	-1.13	-171.3%		-2.39	-2.51	4.9%							
17	0.00	0.26	--		0.00	-1.11	--		0.00	-2.47	--							
18	0.62	0.26	-58.1%		1.74	-1.14	-165.3%		-2.56	-2.53	-1.3%							
19	0.83	0.31	-62.7%		2.37	-1.32	-155.7%		-3.02	-2.95	-2.2%							
20	0.12	0.25	--		0.57	-1.06	-285.3%		-2.20	-2.37	7.6%							
21	0.07	0.26	--		0.57	-1.08	-288.8%		-2.27	-2.42	6.6%							
22	0.43	0.38	-12.5%		1.06	-1.61	-251.4%		-3.23	-3.60	11.5%							
23	0.50	0.48	-3.4%		1.43	-2.03	-242.1%		-4.10	-4.54	10.6%							
24	0.69	0.48	-30.0%		1.43	-2.02	-241.0%		-4.15	-4.51	8.8%							
25	0.60	0.40	-33.3%		1.48	-1.72	-216.0%		-3.57	-3.84	7.6%							
26	0.76	0.51	-32.9%		2.50	-2.17	-186.7%		-4.64	-4.84	4.4%							
27	0.98	0.64	-34.8%		2.96	-2.71	-191.5%		-5.77	-6.05	4.8%							
28	1.14	0.73	-35.8%		3.29	-3.13	-194.9%		-6.65	-6.98	4.9%							
29	0.07	0.03	--		0.27	-0.16	--		-0.60	-0.35	-42.1%							
30	0.08	0.05	--		0.48	-0.27	-156.6%		-0.91	-0.59	-35.2%							
31	0.08	0.06	--		0.64	-0.32	-149.2%		-1.10	-0.69	-37.2%							
32	0.16	0.12	--		0.55	-0.48	-186.0%		-1.07	-1.07	-0.4%							
33	0.39	0.21	-46.1%		1.09	-0.84	-176.8%		-1.80	-1.89	4.9%							
34	0.52	0.24	-54.3%		1.60	-0.97	-160.5%		-2.07	-2.17	4.9%							
35	0.05	0.20	--		0.58	-0.87	-250.1%		-1.65	-1.93	16.9%							
36	0.22	0.23	--		0.96	-1.00	-204.4%		-2.22	-2.23	0.3%							
37	0.38	0.38	-0.3%		1.39	-1.64	-217.5%		-3.42	-3.65	6.6%							
38	0.39	0.38	-3.3%		1.55	-1.66	-206.8%		-3.58	-3.70	3.4%							
39	0.56	0.50	-10.5%		1.90	-2.15	-212.6%		-4.51	-4.79	6.2%							
40	0.44	0.29	-34.4%		1.42	-1.19	-183.5%		-2.73	-2.67	-2.2%							
41	0.62	0.35	-43.7%		1.70	-1.49	-187.9%		-3.61	-3.33	-7.6%							
42	0.59	0.39	-33.4%		2.26	-1.65	-172.7%		-3.85	-3.68	-4.3%							
43	0.62	0.45	-27.9%		2.53	-1.88	-174.3%		-4.51	-4.21	-6.7%							
	min = -70.4%			min = -288.8%			min = -45.7%			max = 0.9%			max = 16.9%			average = -35.4%		
	st. dev. = 20.1%			st. dev. = 37.4%			st. dev. = 14.0%			average = -0.5%			st. dev. = 14.0%					

Table F-27: Computed (FM) versus Measured Results for Static Test Stresses at Section 9O

Test	9O-GC-TI (ksi)			9O-GC-TE (ksi)		
	Measured	FM	% Error	Measured	FM	% Error
1	0.10	0.18	--	0.06	0.18	--
2	0.10	0.19	--	0.07	0.19	--
3	0.02	0.05	--	-0.10	0.05	--
4	0.02	0.08	--	-0.03	0.08	--
5	0.02	0.11	--	-0.03	0.10	--
6	-0.03	0.05	--	-0.08	0.05	--
7	0.54	0.68	26.0%	0.58	0.68	17.0%
8	0.89	0.71	-20.3%	0.85	0.72	-15.1%
9	0.74	0.50	-32.2%	0.77	0.50	-35.3%
10	0.66	0.35	-46.9%	0.63	0.35	-44.2%
11	0.66	0.29	-56.3%	0.76	0.27	-64.6%
12	0.97	0.38	-60.7%	0.86	0.35	-59.1%
13	0.92	0.28	-69.5%	0.75	0.26	-65.2%
14	0.31	0.04	-87.1%	0.27	0.04	--
15	-0.05	0.22	--	-0.03	0.21	--
16	0.73	0.39	-46.5%	0.51	0.37	-27.4%
17	0.00	0.38	--	0.00	0.36	--
18	0.80	0.39	-51.1%	0.69	0.37	-46.2%
19	1.07	0.46	-56.9%	0.96	0.43	-55.4%
20	0.14	0.36	--	0.08	0.36	--
21	0.08	0.36	--	0.13	0.37	--
22	0.64	0.54	-15.2%	0.33	0.55	68.2%
23	0.70	0.69	-1.3%	0.43	0.69	59.7%
24	0.76	0.68	-10.9%	0.72	0.69	-4.3%
25	0.84	0.58	-31.4%	0.58	0.57	-0.9%
26	1.02	0.74	-27.4%	0.84	0.72	-14.3%
27	1.25	0.92	-26.3%	1.12	0.90	-19.6%
28	1.43	1.06	-25.8%	1.35	1.05	-22.4%
29	0.14	0.07	--	0.13	0.03	--
30	0.15	0.12	--	0.17	0.04	--
31	0.16	0.14	--	0.19	0.05	--
32	0.32	0.15	-53.5%	0.26	0.18	--
33	0.66	0.27	-59.0%	0.54	0.32	-40.5%
34	0.87	0.31	-64.2%	0.71	0.36	-49.2%
35	0.03	0.30	--	0.00	0.28	--
36	0.33	0.35	4.8%	0.33	0.31	-7.0%
37	0.59	0.56	-4.6%	0.57	0.53	-6.3%
38	0.61	0.57	-5.8%	0.59	0.53	-10.3%
39	0.80	0.73	-8.3%	0.80	0.71	-11.1%
40	0.72	0.40	-44.7%	0.63	0.42	-32.9%
41	0.97	0.50	-48.5%	0.83	0.51	-38.5%
42	1.00	0.55	-44.8%	0.86	0.57	-33.6%
43	1.06	0.64	-39.4%	0.92	0.64	-30.6%
	min = -87.1%		min = -65.2%		max = 26.0%	
	max = 26.0%		max = 68.2%		average = -34.8%	
	average = -34.8%		average = -21.8%		st. dev. = 25.3%	
	st. dev. = 25.3%		st. dev. = 31.7%			

Table F-28: Computed (FM) versus Measured Results for Static Test Stresses at Section 9O

Test	9O-GC-BI (ksi)			9O-GC-BE (ksi)		
	Measured	FM	% Error	Measured	FM	% Error
1	-1.26	-1.27	0.9%	-1.28	-1.22	-4.8%
2	-1.26	-1.36	8.1%	-1.35	-1.32	-2.5%
3	-0.59	-0.34	-42.8%	-0.04	-0.33	--
4	-0.59	-0.56	-4.4%	-0.62	-0.57	-7.9%
5	-0.69	-0.75	9.4%	-0.86	-0.74	-13.7%
6	-0.35	-0.36	3.5%	-0.41	-0.35	-15.2%
7	-4.50	-4.77	5.9%	-4.76	-4.60	-3.4%
8	-4.75	-5.02	5.8%	-4.99	-4.86	-2.6%
9	-3.50	-3.53	0.8%	-3.41	-3.41	0.0%
10	-2.57	-2.41	-6.2%	-2.29	-2.39	4.6%
11	-2.15	-1.94	-9.6%	-2.10	-1.97	-6.3%
12	-2.45	-2.57	5.0%	-3.07	-2.56	-16.6%
13	-1.99	-1.91	-3.9%	-2.35	-1.89	-19.7%
14	-0.47	-0.30	-36.6%	-0.63	-0.30	-52.5%
15	-1.32	-1.50	13.7%	-1.65	-1.49	-9.6%
16	-2.37	-2.63	11.0%	-3.10	-2.63	-15.2%
17	0.00	-2.58	--	0.00	-2.58	--
18	-2.97	-2.64	-11.1%	-2.73	-2.64	-3.3%
19	-3.43	-3.08	-10.3%	-3.28	-3.09	-5.8%
20	-2.39	-2.53	5.9%	-2.53	-2.44	-3.6%
21	-2.41	-2.57	6.4%	-2.58	-2.49	-3.6%
22	-3.59	-3.83	6.7%	-3.68	-3.71	0.7%
23	-4.57	-4.83	5.7%	-4.66	-4.67	0.2%
24	-4.64	-4.80	3.4%	-4.49	-4.64	3.3%
25	-3.86	-4.06	5.2%	-4.22	-3.97	-6.0%
26	-4.93	-5.11	3.7%	-5.52	-5.01	-9.2%
27	-6.13	-6.40	4.4%	-6.80	-6.26	-7.9%
28	-7.11	-7.38	3.8%	-7.76	-7.21	-7.1%
29	-0.89	-0.38	-57.3%	-0.44	-0.36	-18.9%
30	-1.51	-0.64	-57.5%	-0.55	-0.60	8.2%
31	-2.10	-0.74	-64.7%	-0.42	-0.71	67.6%
32	-0.70	-1.12	59.9%	-1.61	-1.13	-29.6%
33	-1.09	-1.96	79.4%	-2.83	-1.99	-29.7%
34	-1.30	-2.25	73.6%	-3.23	-2.29	-29.1%
35	-2.32	-2.03	-12.4%	-1.46	-2.01	38.1%
36	-3.11	-2.35	-24.4%	-1.89	-2.31	22.0%
37	-4.61	-3.84	-16.8%	-3.06	-3.80	24.4%
38	-5.20	-3.89	-25.2%	-2.86	-3.85	34.7%
39	-6.32	-5.02	-20.6%	-3.86	-4.99	29.1%
40	-1.94	-2.81	44.7%	-4.03	-2.76	-31.5%
41	-2.73	-3.55	30.2%	-5.16	-3.42	-33.7%
42	-2.92	-3.91	33.7%	-5.55	-3.79	-31.7%
43	-3.55	-4.49	26.5%	-6.41	-4.31	-32.8%
	min = -64.7%			min = -52.5%		
	max = 79.4%			max = 67.6%		
	average = 1.3%			average = -5.4%		
	st. dev. = 29.8%			st. dev. = 22.0%		

Table F-29: Computed (FM) versus Measured Results for Static Test Stresses at Section 9O

	9O-GA-TCH			(ksi)			9O-GA-WH			(ksi)			9O-GA-BCH			(ksi)		
Test	Measured	FM	% Error	Measured	FM	% Error	Measured	FM	% Error	Measured	FM	% Error	Measured	FM	% Error	Measured	FM	% Error
1	0.16	0.16	--		0.38	-0.46	-220.7%		-1.06	-1.08	2.3%							
2	0.26	0.17	--		0.28	-0.48	--		-1.06	-1.12	5.9%							
3	0.22	0.04	--		-0.11	-0.11	--		-0.06	-0.26	--							
4	0.06	0.07	--		0.19	-0.19	--		-0.35	-0.45	29.7%							
5	0.11	0.10	--		0.06	-0.27	--		-0.51	-0.63	24.7%							
6	0.14	0.05	--		-0.27	-0.13	--		-0.16	-0.31	--							
7	0.88	0.62	-29.6%		1.03	-1.73	-267.8%		-4.07	-4.08	0.2%							
8	1.13	0.64	-43.6%		1.08	-1.79	-265.1%		-4.14	-4.22	1.9%							
9	0.79	0.45	-42.7%		0.99	-1.24	-225.1%		-2.92	-2.93	0.3%							
10	0.43	0.28	-34.3%		1.17	-0.78	-166.6%		-1.90	-1.84	-3.1%							
11	-0.18	0.26	--		1.82	-0.71	-138.9%		-1.77	-1.68	-5.3%							
12	0.20	0.34	--		1.48	-0.93	-162.5%		-2.25	-2.19	-2.8%							
13	0.26	0.26	--		0.82	-0.72	-188.0%		-1.74	-1.70	-2.6%							
14	0.13	0.04	--		0.11	-0.12	--		-0.36	-0.27	-25.1%							
15	0.24	0.20	--		0.19	-0.54	--		-1.20	-1.27	5.8%							
16	0.20	0.34	--		1.06	-0.92	-186.5%		-2.25	-2.18	-3.3%							
17	0.00	0.33	--		0.00	-0.91	--		0.00	-2.15	--							
18	0.11	0.34	--		1.09	-0.93	-185.2%		-2.19	-2.20	0.6%							
19	0.09	0.39	--		1.85	-1.08	-158.2%		-2.58	-2.55	-1.0%							
20	0.35	0.33	-6.6%		0.26	-0.92	--		-2.13	-2.17	1.9%							
21	0.35	0.33	-6.6%		0.37	-0.92	-347.1%		-2.13	-2.16	1.5%							
22	0.74	0.48	-35.3%		0.29	-1.36	--		-3.15	-3.19	1.2%							
23	0.88	0.62	-29.6%		0.61	-1.72	-384.3%		-4.07	-4.06	-0.3%							
24	0.88	0.62	-29.6%		0.62	-1.73	-380.5%		-4.07	-4.08	0.2%							
25	0.65	0.52	-19.8%		0.88	-1.44	-263.6%		-3.45	-3.40	-1.5%							
26	0.51	0.66	28.3%		1.88	-1.83	-197.4%		-4.39	-4.32	-1.7%							
27	0.74	0.82	10.1%		2.50	-2.29	-191.4%		-5.50	-5.39	-2.1%							
28	0.89	0.95	7.1%		3.02	-2.65	-187.5%		-6.42	-6.24	-2.8%							
29	0.19	0.15	--		0.43	-0.41	-196.4%		-1.00	-0.97	-2.5%							
30	0.27	0.27	--		0.96	-0.72	-174.6%		-1.74	-1.70	-2.5%							
31	0.27	0.31	--		1.57	-0.85	-154.1%		-2.13	-2.01	-5.7%							
32	0.02	0.04	--		0.18	-0.12	--		-0.45	-0.28	-38.3%							
33	-0.09	0.07	--		0.32	-0.21	-163.9%		-0.67	-0.48	-28.1%							
34	-0.17	0.08	--		0.42	-0.23	-153.1%		-0.75	-0.53	-29.4%							
35	0.41	0.26	-37.3%		0.18	-0.70	--		-1.68	-1.65	-1.6%							
36	0.32	0.37	14.8%		1.22	-1.00	-181.7%		-2.58	-2.37	-8.2%							
37	0.30	0.46	51.3%		1.62	-1.26	-178.0%		-3.42	-2.98	-12.7%							
38	0.30	0.50	66.2%		2.27	-1.37	-160.2%		-3.67	-3.24	-11.8%							
39	0.29	0.56	--		2.51	-1.55	-161.7%		-4.18	-3.65	-12.7%							
40	0.16	0.29	--		0.72	-0.83	-214.9%		-2.04	-1.94	-4.9%							
41	0.50	0.50	-0.9%		1.22	-1.40	-214.3%		-3.35	-3.29	-1.7%							
42	0.35	0.51	44.2%		1.45	-1.43	-198.6%		-3.52	-3.37	-4.2%							
43	0.67	0.67	-0.6%		1.92	-1.87	-197.4%		-4.53	-4.41	-2.6%							
	min = -43.6%			min = -384.3%			min = -38.3%			max = 66.2%			max = 29.7%			average = -4.7%		
	st. dev. = 31.9%			st. dev. = 62.0%			st. dev. = 11.8%			average = -3.6%			st. dev. =					

Table F-30: Computed (FM) versus Measured Results for Static Test Stresses at Section 9O

Test	9O-GA-TI (ksi)			9O-GA-TE (ksi)		
	Measured	FM	% Error	Measured	FM	% Error
1	0.29	0.22	--	0.32	0.22	-31.0%
2	0.33	0.22	-34.1%	0.38	0.23	-40.1%
3	0.10	0.05	--	0.01	0.05	--
4	0.14	0.09	--	0.03	0.09	--
5	0.15	0.13	--	0.08	0.12	--
6	0.07	0.07	--	0.04	0.06	--
7	1.37	0.81	-40.8%	1.47	0.82	-44.0%
8	1.56	0.84	-46.2%	1.79	0.85	-52.5%
9	1.14	0.58	-49.0%	1.43	0.59	-58.8%
10	0.86	0.37	-56.9%	0.87	0.37	-57.5%
11	0.49	0.35	-29.3%	0.43	0.33	-22.7%
12	0.83	0.46	-44.6%	0.60	0.43	-27.8%
13	0.66	0.36	-45.6%	0.53	0.33	-37.6%
14	0.21	0.06	--	0.21	0.05	--
15	0.28	0.26	--	0.09	0.25	--
16	0.53	0.45	-15.3%	0.23	0.43	--
17	0.00	0.45	--	0.00	0.42	--
18	0.51	0.46	-10.3%	0.24	0.43	--
19	0.71	0.53	-25.6%	0.37	0.50	33.8%
20	0.57	0.43	-24.6%	0.58	0.44	-24.4%
21	0.53	0.43	-18.5%	0.51	0.43	-16.4%
22	0.80	0.63	-21.5%	0.80	0.64	-20.0%
23	1.15	0.81	-29.6%	1.14	0.82	-28.0%
24	1.17	0.81	-30.8%	1.28	0.82	-35.8%
25	0.92	0.69	-24.6%	0.73	0.68	-6.4%
26	1.16	0.88	-24.2%	0.88	0.86	-2.7%
27	1.59	1.09	-31.2%	1.32	1.07	-19.2%
28	1.91	1.26	-34.0%	1.67	1.24	-25.8%
29	0.42	0.22	-47.7%	0.34	0.18	-46.9%
30	0.72	0.38	-47.1%	0.54	0.31	-43.1%
31	0.93	0.45	-51.6%	0.68	0.37	-45.8%
32	0.19	0.04	--	0.14	0.07	--
33	0.18	0.07	--	0.08	0.11	--
34	0.18	0.08	--	0.02	0.13	--
35	0.46	0.34	-26.4%	0.31	0.32	2.8%
36	0.90	0.51	-43.5%	0.70	0.46	-34.1%
37	1.11	0.62	-44.2%	0.83	0.59	-29.0%
38	1.28	0.68	-46.9%	0.93	0.64	-31.3%
39	1.35	0.75	-44.4%	0.98	0.72	-26.4%
40	0.60	0.37	-38.7%	0.54	0.40	-26.2%
41	1.13	0.65	-42.7%	1.09	0.66	-39.6%
42	1.15	0.66	-42.5%	1.01	0.68	-32.6%
43	1.61	0.88	-45.2%	1.52	0.88	-42.1%
	min = -56.9%		min = -58.8%			
	max = -10.3%		max = 33.8%			
	average = -36.2%		average = -29.4%			
	st. dev. = 11.5%		st. dev. = 18.3%			

Table F-31: Computed (FM) versus Measured Results for Static Test Stresses at Section 9O

Test	9O-GA-BI (ksi)			9O-GA-BE (ksi)		
	Measured	FM	% Error	Measured	FM	% Error
1	-1.01	-1.15	13.7%	-0.96	-1.12	17.1%
2	-1.09	-1.20	10.1%	-0.96	-1.16	21.4%
3	-0.03	-0.28	--	-0.41	-0.26	-36.3%
4	-0.43	-0.48	10.4%	-0.46	-0.46	1.0%
5	-0.67	-0.67	0.0%	-0.52	-0.66	27.5%
6	-0.38	-0.33	-13.7%	-0.21	-0.33	--
7	-3.82	-4.34	13.7%	-3.73	-4.21	12.8%
8	-3.93	-4.51	14.7%	-3.76	-4.33	15.0%
9	-2.64	-3.14	18.8%	-2.78	-3.00	7.8%
10	-1.53	-1.98	29.0%	-2.03	-1.89	-6.7%
11	-1.40	-1.77	26.0%	-1.86	-1.74	-6.7%
12	-2.20	-2.31	4.9%	-1.99	-2.27	13.9%
13	-1.67	-1.79	7.1%	-1.57	-1.77	12.7%
14	-0.32	-0.28	-11.3%	-0.29	-0.28	--
15	-1.35	-1.34	-0.6%	-1.09	-1.32	21.2%
16	-2.24	-2.30	2.6%	-1.99	-2.27	13.9%
17	0.00	-2.27	--	0.00	-2.24	--
18	-2.04	-2.32	14.0%	-2.30	-2.29	-0.6%
19	-2.41	-2.70	12.0%	-2.69	-2.65	-1.4%
20	-2.14	-2.31	7.9%	-1.92	-2.24	16.4%
21	-2.12	-2.29	7.8%	-1.92	-2.23	15.9%
22	-3.18	-3.39	6.6%	-2.85	-3.29	15.3%
23	-4.01	-4.32	7.7%	-3.73	-4.19	12.3%
24	-3.97	-4.34	9.4%	-3.73	-4.22	13.1%
25	-3.42	-3.60	5.4%	-3.15	-3.52	11.7%
26	-4.33	-4.58	5.8%	-4.16	-4.48	7.6%
27	-5.30	-5.72	7.8%	-5.23	-5.58	6.8%
28	-6.12	-6.62	8.2%	-6.14	-6.45	5.1%
29	-1.11	-1.05	-5.5%	-0.66	-1.00	52.1%
30	-2.05	-1.82	-11.2%	-1.10	-1.73	56.8%
31	-2.38	-2.16	-9.1%	-1.51	-2.04	35.3%
32	-0.12	-0.28	--	-0.55	-0.31	-44.1%
33	-0.10	-0.47	--	-0.96	-0.53	-44.9%
34	0.02	-0.52	--	-1.22	-0.58	-52.4%
35	-2.20	-1.74	-20.8%	-1.17	-1.72	47.0%
36	-2.93	-2.52	-13.9%	-1.73	-2.46	42.1%
37	-3.81	-3.13	-17.9%	-2.29	-3.10	35.5%
38	-3.95	-3.42	-13.5%	-2.65	-3.38	27.5%
39	-4.57	-3.84	-15.9%	-3.01	-3.81	26.6%
40	-1.28	-2.05	59.9%	-2.32	-2.01	-13.3%
41	-2.41	-3.52	46.2%	-3.58	-3.38	-5.7%
42	-2.44	-3.60	47.6%	-4.01	-3.47	-13.5%
43	-3.35	-4.73	41.4%	-4.97	-4.52	-9.0%
	min = -20.8%		min = -52.4%		max = 59.9%	
	max = 59.9%		max = 56.8%		average = 8.0%	
	average = 8.0%		average = 8.9%		st. dev. = 18.3%	
	st. dev. = 18.3%		st. dev. = 24.3%			

Table F-32: Computed (FM) versus Measured Results for Static Test Stresses at Section 9O

Test	8C-GC-TC (ksi)			8C-GC-BC (ksi)		
	Measured	FM	% Error	Measured	FM	% Error
1	-0.15	0.06	--	-1.24	-0.93	-25.0%
2	-0.08	0.04	--	-0.55	-0.45	-17.8%
3	-0.15	-0.01	--	0.31	0.19	-38.7%
4	-0.16	0.03	--	-1.20	-1.04	-13.1%
5	-0.17	0.03	--	-1.38	-1.16	-15.9%
6	-0.12	0.01	--	-0.63	-0.53	-16.5%
7	-0.35	0.21	-159.6%	-4.09	-3.26	-20.2%
8	0.11	0.14	--	-2.01	-1.62	-19.3%
9	0.57	0.05	-91.2%	-0.07	-0.10	--
10	-0.34	0.04	-111.8%	-0.95	-0.85	-10.9%
11	-0.24	0.08	--	-4.22	-3.65	-13.5%
12	-0.33	0.09	-127.4%	-4.93	-4.11	-16.7%
13	-0.26	0.06	--	-3.71	-2.92	-21.2%
14	-0.13	0.01	--	-0.83	-0.45	-46.0%
15	-0.25	0.05	--	-2.69	-2.34	-13.1%
16	-0.41	0.10	-124.5%	-4.93	-4.18	-15.3%
17	0.00	0.09	--	0.00	-4.10	--
18	-0.42	0.10	-123.9%	-5.05	-4.27	-15.5%
19	-0.41	0.12	-129.2%	-5.99	-5.16	-13.8%
20	-0.28	0.12	--	-2.30	-1.87	-18.8%
21	-0.20	0.11	--	-2.30	-1.89	-17.9%
22	-0.39	0.15	-138.8%	-3.02	-2.47	-18.1%
23	-0.51	0.21	-141.5%	-4.09	-3.29	-19.5%
24	-0.39	0.21	-153.4%	-4.09	-3.32	-18.7%
25	-0.48	0.17	-135.3%	-5.09	-4.19	-17.7%
26	-0.72	0.21	-129.2%	-7.36	-5.97	-18.9%
27	-0.70	0.25	-135.5%	-8.10	-6.60	-18.5%
28	-0.71	0.31	-143.4%	-9.07	-7.41	-18.3%
29	-0.21	-0.03	--	-1.40	-0.75	-46.4%
30	-0.28	-0.05	--	-2.32	-1.30	-44.0%
31	-0.34	-0.06	-82.3%	-2.91	-1.61	-44.6%
32	-0.22	0.08	--	-1.74	-1.57	-9.8%
33	-0.28	0.14	--	-2.95	-2.82	-4.3%
34	-0.27	0.17	--	-3.50	-3.42	-2.2%
35	-0.22	-0.03	--	-2.57	-2.06	-19.8%
36	-0.34	-0.05	-85.4%	-3.80	-2.64	-30.5%
37	-0.37	-0.05	-86.3%	-4.95	-3.66	-26.1%
38	-0.40	-0.06	-85.0%	-5.45	-3.92	-28.0%
39	-0.40	-0.08	-79.9%	-5.82	-4.27	-26.6%
40	-0.38	0.26	-168.1%	-3.88	-3.36	-13.4%
41	-0.45	0.36	-179.5%	-4.61	-3.74	-18.9%
42	-0.51	0.39	-175.8%	-5.15	-4.46	-13.4%
43	-0.58	0.46	-178.7%	-5.55	-4.65	-16.2%
	min = -179.5%			min = -46.4%		
	max = -79.9%			max = -2.2%		
	average = -128.9%			average = -20.6%		
	st. dev. = 31.5%			st. dev. = 10.3%		

Table F-33: Computed (FM) versus Measured Results for Static Test Stresses at Section 8C

Test	8C-GA-TC (ksi)			8C-GA-BC (ksi)		
	Measured	FM	% Error	Measured	FM	% Error
1	0.01	0.09	--	-0.69	-0.73	5.3%
2	0.10	0.05	--	-0.18	-0.32	--
3	0.07	-0.01	--	0.19	0.13	--
4	0.01	0.06	--	-0.84	-0.90	7.1%
5	0.01	0.07	--	-0.98	-1.06	8.0%
6	0.03	0.03	--	-0.42	-0.50	18.4%
7	0.00	0.34	--	-2.67	-2.56	-4.1%
8	-0.11	0.21	--	-1.12	-1.26	12.9%
9	-0.06	0.06	--	0.07	-0.02	--
10	-0.09	0.06	--	-0.67	-0.64	-4.0%
11	-0.09	0.21	--	-3.34	-3.30	-1.3%
12	-0.08	0.24	--	-3.84	-3.75	-2.3%
13	-0.03	0.17	--	-2.87	-2.78	-3.1%
14	0.02	0.03	--	-0.58	-0.43	-25.5%
15	-0.01	0.14	--	-2.09	-2.13	1.8%
16	-0.08	0.24	--	-3.84	-3.75	-2.3%
17	0.00	0.24	--	0.00	-3.69	--
18	-0.14	0.25	--	-3.86	-3.82	-1.1%
19	-0.10	0.30	--	-4.63	-4.58	-1.0%
20	-0.08	0.19	--	-1.44	-1.46	1.5%
21	-0.08	0.18	--	-1.44	-1.44	0.1%
22	0.02	0.24	--	-1.88	-1.87	-0.4%
23	0.00	0.33	--	-2.67	-2.53	-5.2%
24	0.00	0.34	--	-2.67	-2.57	-3.7%
25	-0.04	0.31	--	-3.67	-3.52	-4.2%
26	-0.13	0.43	--	-5.41	-5.15	-4.8%
27	-0.05	0.49	--	-5.85	-5.62	-4.0%
28	-0.04	0.57	--	-6.53	-6.26	-4.2%
29	-0.08	0.07	--	-1.41	-1.50	6.4%
30	-0.02	0.12	--	-2.47	-2.66	7.7%
31	0.05	0.15	--	-3.10	-3.29	6.0%
32	-0.21	0.07	--	-0.91	-0.60	-34.3%
33	-0.31	0.12	-138.8%	-1.51	-1.06	-29.7%
34	-0.38	0.14	-136.8%	-1.79	-1.25	-30.2%
35	0.04	0.01	--	-1.75	-2.00	14.3%
36	-0.11	0.06	--	-2.93	-3.15	7.5%
37	-0.19	0.02	--	-3.34	-3.55	6.4%
38	-0.11	0.05	--	-3.85	-4.15	7.7%
39	-0.18	0.01	--	-3.94	-4.28	8.7%
40	-0.26	0.36	--	-2.60	-2.00	-23.0%
41	-0.12	0.56	--	-3.47	-2.75	-20.7%
42	-0.28	0.59	--	-3.88	-3.01	-22.4%
43	-0.15	0.70	--	-4.23	-3.33	-21.3%
	min = -138.8% max = -136.8% average = -137.8% st. dev. = 1.0%			min = -34.3% max = 18.4% average = -3.4% st. dev. = 12.9%		

Table F-34: Computed (FM) versus Measured Results for Static Test Stresses at Section 8C

	8D-GC-TC			(ksi)			8D-GC-W			(ksi)			8D-GC-BC			(ksi)		
Test	Measured	FM	% Error	Measured	FM	% Error	Measured	FM	% Error	Measured	FM	% Error	Measured	FM	% Error	Measured	FM	% Error
1	-0.02	0.01	--	0.89	0.93	3.5%	1.78	1.84	3.4%									
2	-0.07	0.00	--	0.94	1.10	16.9%	2.07	2.19	5.9%									
3	-0.04	0.00	--	0.06	0.05	--	0.10	0.09	--									
4	-0.04	-0.01	--	-0.21	-0.28	--	-0.48	-0.54	12.9%									
5	-0.05	-0.01	--	-0.24	-0.32	--	-0.56	-0.62	11.1%									
6	-0.06	-0.01	--	-0.12	-0.15	--	-0.29	-0.29	--									
7	-0.12	0.03	--	3.28	3.59	9.5%	6.62	7.14	7.8%									
8	-0.04	0.02	--	3.25	3.63	11.6%	6.72	7.24	7.7%									
9	-0.11	0.00	--	2.19	2.50	14.1%	4.78	5.00	4.5%									
10	-0.02	-0.01	--	0.45	0.45	-0.1%	1.01	0.90	-11.0%									
11	0.02	-0.04	--	-0.79	-0.99	25.2%	-1.63	-1.93	18.2%									
12	0.00	-0.04	--	-0.93	-1.11	19.9%	-1.91	-2.18	13.9%									
13	-0.02	-0.04	--	-0.72	-0.81	11.9%	-1.45	-1.57	8.2%									
14	-0.04	-0.01	--	-0.21	-0.13	--	-0.35	-0.24	-32.2%									
15	-0.12	-0.02	--	-0.41	-0.63	54.8%	-1.06	-1.24	17.5%									
16	-0.13	-0.04	--	-0.79	-1.13	42.5%	-1.88	-2.21	17.3%									
17	0.00	-0.04	--	0.00	-1.11	--	0.00	-2.17	--									
18	-0.16	-0.04	--	-0.74	-1.15	54.0%	-2.17	-2.25	3.9%									
19	-0.15	-0.05	--	-0.92	-1.39	50.2%	-2.56	-2.72	6.3%									
20	-0.15	0.02	--	1.79	1.82	1.5%	3.49	3.62	3.6%									
21	-0.15	0.01	--	1.78	1.90	6.6%	3.55	3.78	6.5%									
22	-0.33	0.00	-100.0%	2.96	3.12	5.6%	5.70	6.24	9.4%									
23	-0.37	0.02	-105.5%	3.48	3.68	5.8%	6.56	7.34	11.9%									
24	-0.24	0.03	--	3.38	3.56	5.2%	6.24	7.08	13.5%									
25	-0.24	-0.01	--	1.42	1.28	-10.0%	2.54	2.56	0.9%									
26	-0.25	-0.02	--	0.98	0.72	-26.9%	1.33	1.45	8.7%									
27	-0.23	-0.02	--	1.96	1.91	-2.8%	3.37	3.83	13.5%									
28	-0.24	-0.01	--	2.49	2.45	-1.8%	4.39	4.91	11.9%									
29	-0.06	-0.05	--	-0.35	-0.29	-18.6%	-0.63	-0.52	-17.0%									
30	-0.06	-0.09	--	-0.55	-0.51	-8.1%	-1.04	-0.92	-11.5%									
31	-0.07	-0.11	--	-0.69	-0.62	-9.6%	-1.30	-1.13	-13.3%									
32	-0.07	0.03	--	-0.37	-0.34	-7.0%	-0.63	-0.71	12.3%									
33	-0.07	0.05	--	-0.54	-0.61	12.7%	-1.01	-1.27	25.8%									
34	-0.07	0.06	--	-0.64	-0.74	14.9%	-1.21	-1.53	26.9%									
35	-0.16	-0.16	--	0.97	0.86	-11.8%	1.73	1.87	8.3%									
36	-0.05	-0.21	--	0.65	0.72	9.8%	1.29	1.64	27.4%									
37	-0.12	-0.30	--	1.52	1.83	19.8%	3.23	3.95	22.4%									
38	-0.14	-0.32	--	1.41	1.68	18.9%	2.99	3.68	22.9%									
39	-0.16	-0.38	--	2.00	2.20	10.0%	4.32	4.78	10.6%									
40	-0.11	0.18	--	0.04	0.07	--	0.13	-0.05	--									
41	-0.17	0.29	--	0.52	0.68	30.4%	1.17	1.06	-9.1%									
42	-0.25	0.30	--	0.40	0.54	35.1%	0.96	0.78	-19.2%									
43	-0.28	0.37	--	0.73	0.93	27.1%	1.66	1.48	-10.8%									
	min = -105.5%			min = -26.9%			min = -32.2%			max = 54.8%			max = 27.4%			average = 11.7%		
	max = -100.0%			average = 19.1%			st. dev. = 13.2%			st. dev. = 2.7%			st. dev. = 6.4%			st. dev. = 2.7%		

Table F-35: Computed (FM) versus Measured Results for Static Test Stresses at Section 8D

Test	8D-GC-TI			8D-GC-TE		
	Measured	FM	% Error	Measured	FM	% Error
1	-0.09	-0.07	--	-0.16	-0.06	--
2	-0.15	-0.10	--	-0.22	-0.09	--
3	-0.07	0.00	--	-0.09	0.00	--
4	-0.04	0.02	--	-0.06	0.01	--
5	-0.06	0.02	--	-0.06	0.01	--
6	-0.10	0.01	--	-0.10	0.00	--
7	-0.35	-0.28	-19.3%	-0.43	-0.24	-44.8%
8	-0.30	-0.31	2.9%	-0.35	-0.26	-26.3%
9	-0.25	-0.22	--	-0.34	-0.19	-44.3%
10	-0.07	-0.04	--	-0.07	-0.04	--
11	0.10	0.06	--	0.08	0.03	--
12	0.10	0.06	--	0.08	0.03	--
13	0.05	0.04	--	0.04	0.01	--
14	-0.04	0.01	--	-0.04	0.00	--
15	-0.01	0.04	--	-0.03	0.02	--
16	0.10	0.07	--	0.08	0.03	--
17	0.00	0.06	--	0.00	0.03	--
18	0.08	0.07	--	0.09	0.03	--
19	0.14	0.08	--	0.14	0.04	--
20	-0.34	-0.14	-58.9%	-0.38	-0.12	-68.6%
21	-0.34	-0.16	-53.0%	-0.38	-0.14	-63.4%
22	-0.30	-0.27	--	-0.41	-0.24	-41.3%
23	-0.35	-0.30	-13.5%	-0.43	-0.26	-40.2%
24	-0.35	-0.29	-16.4%	-0.43	-0.24	-44.8%
25	-0.17	-0.12	--	-0.24	-0.12	--
26	-0.08	-0.08	--	-0.10	-0.09	--
27	-0.19	-0.19	--	-0.22	-0.19	--
28	-0.24	-0.22	--	-0.32	-0.21	-33.9%
29	-0.02	-0.02	--	-0.03	-0.05	--
30	0.00	-0.03	--	-0.01	-0.09	--
31	0.00	-0.04	--	0.00	-0.10	--
32	-0.03	0.05	--	-0.05	0.07	--
33	0.00	0.10	--	-0.02	0.12	--
34	0.02	0.12	--	-0.02	0.14	--
35	-0.19	-0.21	--	-0.22	-0.28	--
36	-0.08	-0.24	--	-0.11	-0.34	--
37	-0.21	-0.42	--	-0.26	-0.55	--
38	-0.22	-0.42	--	-0.25	-0.56	--
39	-0.32	-0.51	61.4%	-0.30	-0.67	122.8%
40	-0.07	0.14	--	-0.14	0.23	--
41	-0.15	0.19	--	-0.27	0.33	--
42	-0.17	0.21	--	-0.35	0.35	-200.3%
43	-0.22	0.24	--	-0.42	0.42	-199.7%
	min = -58.9%		min = -200.3%			
	max = 61.4%		max = 122.8%			
	average = -13.8%		average = -57.1%			
	st. dev. = 36.9%		st. dev. = 79.5%			

Table F-36: Computed (FM) versus Measured Results for Static Test Stresses at Section 8D

Test	8D-GC-BI			8D-GC-BE		
	Measured	FM	% Error	Measured	FM	% Error
1	2.02	1.93	-4.4%	1.84	1.90	3.5%
2	2.24	2.33	3.9%	2.25	2.23	-0.8%
3	0.09	0.10	--	0.12	0.09	--
4	-0.56	-0.58	3.6%	-0.50	-0.55	11.1%
5	-0.65	-0.66	1.2%	-0.58	-0.63	8.2%
6	-0.36	-0.30	-17.0%	-0.29	-0.29	--
7	7.28	7.51	3.2%	7.11	7.36	3.5%
8	7.15	7.67	7.2%	7.40	7.42	0.2%
9	5.33	5.32	-0.1%	5.06	5.10	0.8%
10	1.15	0.96	-16.7%	1.05	0.92	-12.1%
11	-1.78	-2.07	16.4%	-1.73	-1.96	13.0%
12	-2.10	-2.33	11.2%	-2.04	-2.21	8.6%
13	-1.58	-1.68	6.1%	-1.55	-1.59	2.5%
14	-0.36	-0.26	-27.6%	-0.39	-0.24	-38.6%
15	-1.18	-1.33	13.1%	-1.11	-1.26	13.4%
16	-2.10	-2.36	12.6%	-2.01	-2.24	11.6%
17	0.00	-2.32	--	0.00	-2.20	--
18	-1.81	-2.41	33.1%	-1.97	-2.28	15.9%
19	-2.36	-2.91	23.2%	-2.38	-2.75	15.4%
20	3.95	3.80	-3.9%	3.58	3.74	4.5%
21	3.95	3.97	0.4%	3.83	3.91	2.2%
22	6.31	6.56	3.9%	6.08	6.44	5.8%
23	7.28	7.72	6.1%	7.13	7.57	6.2%
24	7.28	7.44	2.3%	7.27	7.30	0.5%
25	2.75	2.66	-3.1%	2.68	2.68	0.0%
26	1.72	1.49	-13.4%	1.53	1.55	1.4%
27	3.73	3.99	7.0%	4.19	3.99	-4.7%
28	5.03	5.12	1.7%	5.29	5.10	-3.6%
29	-0.67	-0.56	-16.4%	-0.68	-0.52	-23.7%
30	-1.13	-0.98	-13.4%	-1.11	-0.91	-18.1%
31	-1.42	-1.22	-14.3%	-1.39	-1.13	-18.4%
32	-0.65	-0.76	17.0%	-0.70	-0.73	4.7%
33	-1.06	-1.35	27.4%	-1.11	-1.30	17.3%
34	-1.27	-1.63	28.5%	-1.32	-1.57	18.7%
35	1.94	1.92	-1.0%	1.81	1.99	10.2%
36	1.40	1.66	18.6%	1.40	1.77	26.5%
37	3.41	4.07	19.4%	3.61	4.18	15.9%
38	3.12	3.78	21.2%	3.39	3.91	15.2%
39	4.64	4.96	7.0%	4.73	5.03	6.4%
40	0.25	-0.04	--	0.07	-0.08	--
41	1.34	1.16	-13.2%	1.25	1.02	-18.2%
42	1.16	0.86	-26.2%	0.92	0.74	-19.9%
43	1.95	1.63	-16.3%	1.65	1.43	-13.5%
	min = -27.6%			min = -38.6%		
	max = 33.1%			max = 26.5%		
	average = 2.7%			average = 1.8%		
	st. dev. = 14.8%			st. dev. = 13.5%		

Table F-37: Computed (FM) versus Measured Results for Static Test Stresses at Section 8D

	8D-GA-TC			(ksi)			8D-GA-W			(ksi)			8D-GA-BC			(ksi)		
Test	Measured	FM	% Error	Measured	FM	% Error	Measured	FM	% Error	Measured	FM	% Error	Measured	FM	% Error	Measured	FM	% Error
1	-0.17	-0.09	--		0.48	0.87	82.8%		1.70	1.83	7.7%							
2	-0.20	-0.11	--		0.53	0.93	75.0%		1.78	1.97	10.7%							
3	0.00	0.00	--		0.06	0.05	--		0.11	0.09	--							
4	-0.01	0.03	--		-0.16	-0.27	--		-0.51	-0.56	9.7%							
5	0.00	0.03	--		-0.19	-0.31	--		-0.58	-0.65	11.4%							
6	-0.03	0.01	--		-0.09	-0.15	--		-0.29	-0.30	--							
7	-0.46	-0.36	-22.3%		2.17	3.27	50.2%		6.35	6.89	8.5%							
8	-0.45	-0.37	-18.4%		2.25	3.29	45.7%		6.28	6.94	10.4%							
9	-0.50	-0.25	-50.5%		1.39	2.11	52.1%		4.07	4.47	9.8%							
10	-0.22	-0.04	--		0.18	0.36	--		0.75	0.75	-0.2%							
11	0.09	0.09	--		-0.65	-0.97	47.8%		-1.72	-2.02	17.2%							
12	0.13	0.10	--		-0.74	-1.10	49.2%		-1.98	-2.30	15.9%							
13	0.11	0.07	--		-0.56	-0.81	44.5%		-1.48	-1.69	14.3%							
14	0.02	0.01	--		-0.17	-0.13	--		-0.32	-0.26	-18.8%							
15	0.09	0.06	--		-0.39	-0.62	59.6%		-1.10	-1.30	18.7%							
16	0.13	0.11	--		-0.74	-1.10	49.2%		-1.98	-2.31	16.4%							
17	0.00	0.10	--		0.00	-1.09	--		0.00	-2.27	--							
18	0.18	0.11	--		-0.71	-1.12	58.3%		-1.96	-2.35	19.9%							
19	0.21	0.13	--		-0.83	-1.35	62.9%		-2.36	-2.83	19.8%							
20	-0.44	-0.19	-56.3%		1.00	1.73	73.7%		3.41	3.65	7.2%							
21	-0.44	-0.20	-54.0%		1.00	1.75	75.2%		3.41	3.69	8.4%							
22	-0.42	-0.31	-25.5%		1.78	2.75	54.2%		5.32	5.81	9.1%							
23	-0.46	-0.37	-20.1%		2.17	3.32	52.5%		6.35	7.00	10.2%							
24	-0.46	-0.36	-22.3%		2.17	3.30	51.9%		6.35	6.96	9.6%							
25	-0.25	-0.14	--		0.65	1.14	74.0%		2.35	2.41	2.7%							
26	-0.25	-0.08	--		0.31	0.65	109.9%		1.33	1.38	3.4%							
27	-0.36	-0.20	-45.0%		0.98	1.67	69.2%		3.24	3.53	8.9%							
28	-0.44	-0.26	-40.6%		1.36	2.22	62.3%		4.38	4.69	7.1%							
29	0.02	0.01	--		-0.31	-0.40	27.3%		-0.69	-0.80	15.2%							
30	0.09	0.03	--		-0.47	-0.70	48.4%		-1.17	-1.42	21.0%							
31	0.14	0.03	--		-0.58	-0.86	48.4%		-1.47	-1.75	19.2%							
32	-0.07	0.05	--		-0.33	-0.22	-33.0%		-0.60	-0.49	-18.8%							
33	-0.09	0.08	--		-0.47	-0.40	-16.2%		-0.97	-0.87	-10.3%							
34	-0.13	0.10	--		-0.56	-0.47	-16.6%		-1.17	-1.04	-10.9%							
35	-0.15	-0.12	--		0.18	0.20	--		0.78	0.52	-33.0%							
36	-0.14	-0.11	--		-0.05	-0.08	--		0.26	-0.05	--							
37	-0.38	-0.22	-42.1%		0.23	0.44	--		1.35	1.09	-19.1%							
38	-0.33	-0.21	-36.4%		0.11	0.26	--		1.02	0.73	-28.2%							
39	-0.47	-0.28	-40.3%		0.36	0.55	50.6%		1.78	1.37	-23.2%							
40	-0.22	0.02	--		0.15	0.73	--		1.01	1.43	42.2%							
41	-0.32	-0.03	-90.8%		0.76	1.76	132.1%		2.82	3.54	25.7%							
42	-0.48	-0.02	-95.9%		0.65	1.69	157.7%		2.69	3.39	26.2%							
43	-0.46	-0.04	-91.3%		1.11	2.28	104.2%		3.75	4.59	22.5%							
	min = -95.9%			min = -33.0%			min = -33.0%			max = -18.4%			max = 42.2%			average = 6.8%		
	average = -47.0%			average = 58.2%			st. dev. = 37.4%			st. dev. = 24.8%			st. dev. = 16.0%					

Table F-38: Computed (FM) versus Measured Results for Static Test Stresses at Section 8D

Test	8D-GA-TI (ksi)			8D-GA-BI (ksi)		
	Measured	FM	% Error	Measured	FM	% Error
1	-3.34	-0.18	-94.6%	1.63	1.92	18.1%
2	-4.96	-0.20	-96.0%	1.77	2.09	18.0%
3	-5.39	-0.01	-99.8%	0.07	0.09	--
4	-4.16	0.05	-101.2%	-0.48	-0.59	22.4%
5	-3.31	0.06	-101.8%	-0.56	-0.69	23.7%
6	-3.06	0.03	-101.0%	-0.27	-0.32	--
7	-1.04	-0.68	-34.9%	6.39	7.25	13.4%
8	-0.97	-0.70	-28.0%	6.50	7.32	12.7%
9	-0.83	-0.45	-45.7%	4.02	4.73	17.7%
10	-0.23	-0.08	--	0.73	0.79	9.0%
11	0.19	0.19	--	-1.71	-2.14	25.0%
12	0.25	0.22	--	-1.97	-2.43	23.2%
13	0.18	0.16	--	-1.48	-1.78	20.6%
14	0.01	0.02	--	-0.32	-0.27	-16.8%
15	-0.51	0.12	-123.6%	-1.10	-1.38	25.0%
16	0.25	0.22	--	-1.97	-2.43	23.2%
17	0.00	0.22	--	0.00	-2.39	--
18	0.24	0.23	--	-2.13	-2.48	16.4%
19	0.28	0.27	--	-2.43	-2.99	23.0%
20	-5.19	-0.36	-93.1%	3.33	3.83	15.1%
21	-5.19	-0.37	-92.9%	3.33	3.87	16.3%
22	-1.42	-0.58	-59.3%	5.31	6.12	15.2%
23	-1.04	-0.69	-33.9%	6.39	7.37	15.3%
24	-1.04	-0.69	-33.9%	6.39	7.32	14.5%
25	-1.44	-0.24	-83.3%	2.34	2.52	7.6%
26	-0.35	-0.14	-60.6%	1.28	1.44	12.6%
27	-0.65	-0.36	-44.8%	3.49	3.72	6.7%
28	-0.74	-0.47	-36.4%	4.54	4.93	8.7%
29	0.01	0.06	--	-0.68	-0.85	25.1%
30	0.09	0.11	--	-1.15	-1.50	30.0%
31	0.13	0.14	--	-1.45	-1.85	27.5%
32	-0.12	0.06	--	-0.57	-0.52	-8.2%
33	-0.13	0.11	--	-0.92	-0.92	0.2%
34	-0.17	0.13	--	-1.10	-1.10	-0.2%
35	-0.63	-0.11	-82.6%	0.65	0.52	-19.7%
36	-0.24	-0.07	--	0.24	-0.08	--
37	-0.65	-0.21	-67.8%	1.36	1.11	-18.1%
38	-0.63	-0.18	-71.3%	1.04	0.73	-29.6%
39	-0.96	-0.27	-71.8%	1.70	1.40	-17.9%
40	-0.39	-0.08	-79.6%	1.09	1.51	39.1%
41	-0.70	-0.25	-64.0%	3.04	3.76	23.8%
42	-1.03	-0.23	-77.7%	2.83	3.59	26.8%
43	-1.08	-0.32	-70.3%	3.89	4.87	25.2%
	min = -123.6%			min = -29.6%		
	max = -28.0%			max = 39.1%		
	average = -72.2%			average = 12.6%		
	st. dev. = 25.5%			st. dev. = 15.5%		

NOTE: 8D-GA-TI response is unreliable

Table F-39: Computed (FM) versus Measured Results for Static Test Stresses at Section 8D

Test	9F-D-TI (ksi)			9F-D-BI (ksi)		
	Measured	FM	% Error	Measured	FM	% Error
1	0.00	0.01	--	-0.05	0.00	--
2	0.00	0.01	--	-0.05	0.00	--
3	-0.02	0.00	--	-0.01	0.00	--
4	-0.07	-0.02	--	0.01	0.01	--
5	0.05	-0.06	--	-0.06	0.03	--
6	0.98	-0.08	-108.2%	-0.07	0.04	--
7	0.06	0.04	--	-0.16	-0.01	--
8	0.06	0.04	--	-0.15	-0.01	--
9	0.04	0.03	--	-0.11	-0.01	--
10	-0.01	0.00	--	-0.04	0.00	--
11	-0.06	-0.11	--	0.01	0.05	--
12	0.89	-0.24	-127.0%	-0.13	0.11	--
13	1.06	-0.24	-122.6%	-0.03	0.08	--
14	0.86	-0.07	-108.1%	-0.01	0.03	--
15	-0.09	-0.11	--	-0.06	0.05	--
16	0.42	-0.23	-154.9%	-0.20	0.10	--
17	1.15	-0.24	-120.8%	-0.28	0.11	--
18	1.11	-0.28	-125.3%	-0.26	0.13	--
19	1.08	-0.29	-127.0%	-0.24	0.14	--
20	-0.11	0.02	--	-0.11	-0.01	--
21	0.01	0.02	--	-0.18	-0.01	--
22	-0.32	0.03	-109.3%	-0.19	-0.01	--
23	-0.38	0.04	-110.6%	-0.23	-0.01	--
24	-0.19	0.04	--	-0.28	-0.01	--
25	-0.14	-0.10	--	-0.20	0.05	--
26	0.82	-0.22	-126.7%	-0.37	0.11	-129.5%
27	0.87	-0.21	-124.1%	-0.42	0.10	-124.0%
28	0.90	-0.21	-123.3%	-0.45	0.10	-122.0%
29	-0.02	-0.03	--	0.13	-0.03	--
30	0.41	-0.06	-114.6%	0.20	-0.07	--
31	0.54	-0.07	-113.0%	0.30	-0.09	-129.6%
32	-0.05	-0.09	--	-0.23	0.09	--
33	0.58	-0.18	-131.2%	-0.39	0.19	-148.5%
34	0.42	-0.21	-149.9%	-0.39	0.22	-156.7%
35	-0.08	-0.02	--	0.15	-0.03	--
36	0.42	-0.05	-111.8%	0.17	-0.08	--
37	0.34	-0.04	-111.6%	0.16	-0.08	--
38	0.49	-0.06	-112.2%	0.24	-0.10	--
39	0.46	-0.05	-110.8%	0.21	-0.10	--
40	0.57	-0.17	-129.6%	-0.44	0.19	-143.0%
41	0.45	-0.16	-135.6%	-0.48	0.18	-137.6%
42	0.92	-0.20	-121.7%	-0.51	0.23	-145.2%
43	0.89	-0.19	-121.3%	-0.54	0.22	-140.6%
	min = -154.9%			min = -156.7%		
	max = -108.1%			max = -122.0%		
	average = -122.0%			average = -137.7%		
	st. dev. = 11.9%			st. dev. = 10.7%		

Table F-40: Computed (FM) versus Measured Results for Static Test Stresses at Section 9F

Test	9F-D-TQI (ksi)			9F-D-BQI (ksi)		
	Measured	FM	% Error	Measured	FM	% Error
1	0.00	0.01	--	0.01	0.02	--
2	0.00	0.01	--	0.01	0.02	--
3	-0.01	0.00	--	-0.01	0.00	--
4	-0.03	-0.02	--	-0.02	-0.02	--
5	-0.06	-0.05	--	0.01	-0.06	--
6	0.05	-0.07	--	0.78	-0.07	-109.0%
7	0.01	0.04	--	0.04	0.06	--
8	0.01	0.04	--	0.04	0.06	--
9	0.00	0.03	--	0.02	0.04	--
10	0.00	0.00	--	-0.02	0.00	--
11	-0.06	-0.10	--	-0.07	-0.11	--
12	-0.06	-0.21	--	0.20	-0.22	--
13	-0.01	-0.22	--	0.18	-0.31	--
14	-0.02	-0.06	--	0.24	-0.07	--
15	-0.13	-0.10	--	-0.05	-0.12	--
16	-0.18	-0.21	--	0.04	-0.24	--
17	-0.05	-0.21	--	0.24	-0.22	--
18	0.00	-0.24	--	0.62	-0.26	-142.0%
19	-0.03	-0.26	--	0.60	-0.28	-146.3%
20	-0.06	0.02	--	-0.02	0.03	--
21	-0.02	0.02	--	-0.08	0.03	--
22	-0.19	0.03	--	-0.09	0.04	--
23	-0.24	0.04	--	-0.09	0.06	--
24	-0.07	0.04	--	-0.02	0.06	--
25	-0.24	-0.08	--	-0.05	-0.08	--
26	-0.23	-0.19	--	0.29	-0.19	--
27	-0.18	-0.18	--	0.32	-0.18	-155.8%
28	-0.15	-0.17	--	0.32	-0.17	-153.1%
29	-0.01	-0.06	--	-0.20	-0.19	--
30	0.08	-0.12	--	-0.34	-0.41	22.2%
31	0.06	-0.15	--	-0.43	-0.52	21.3%
32	-0.14	-0.05	--	0.12	0.08	--
33	-0.20	-0.09	--	0.58	0.20	-65.6%
34	-0.22	-0.10	--	0.55	0.23	-58.3%
35	-0.02	-0.05	--	-0.19	-0.17	--
36	0.08	-0.11	--	-0.32	-0.40	24.0%
37	0.04	-0.10	--	-0.38	-0.38	-0.4%
38	0.02	-0.13	--	-0.44	-0.49	11.3%
39	-0.03	-0.13	--	-0.42	-0.48	13.8%
40	-0.21	-0.08	--	0.59	0.22	-62.6%
41	-0.22	-0.07	--	0.54	0.22	-59.5%
42	-0.36	-0.09	-75.2%	0.88	0.28	-68.1%
43	-0.38	-0.08	-78.7%	0.87	0.29	-66.8%
	min = -78.7%			min = -155.8%		
	max = -75.2%			max = 24.0%		
	average = -76.9%			average = -58.5%		
	st. dev. = 1.8%			st. dev. = 63.7%		

Table F-41: Computed (FM) versus Measured Results for Static Test Stresses at Section 9F

Test	9F-D-TM (ksi)			9F-D-BM (ksi)		
	Measured	FM	% Error	Measured	FM	% Error
1	0.00	0.01	--	0.02	0.03	--
2	0.00	0.01	--	0.01	0.03	--
3	-0.02	0.00	--	-0.02	0.00	--
4	-0.03	-0.02	--	-0.07	-0.05	--
5	-0.08	-0.05	--	-0.07	-0.16	--
6	-0.26	-0.07	--	1.29	-0.20	-115.5%
7	0.02	0.04	--	0.09	0.11	--
8	0.01	0.04	--	0.09	0.12	--
9	0.00	0.03	--	0.05	0.08	--
10	-0.02	0.00	--	-0.03	-0.01	--
11	-0.11	-0.11	--	-0.28	-0.30	--
12	-0.38	-0.22	-42.3%	0.53	-0.62	-217.3%
13	-0.39	-0.23	-41.2%	0.74	-0.67	-191.0%
14	-0.33	-0.07	-79.0%	0.74	-0.19	-125.6%
15	-0.26	-0.11	--	-0.17	-0.31	--
16	-0.55	-0.22	-60.1%	0.26	-0.62	--
17	-0.44	-0.22	-49.9%	0.75	-0.64	-185.2%
18	-0.43	-0.26	-39.2%	1.45	-0.74	-151.0%
19	-0.46	-0.27	-41.0%	1.43	-0.77	-154.0%
20	-0.09	0.02	--	-0.01	0.06	--
21	-0.07	0.02	--	-0.03	0.06	--
22	-0.29	0.03	--	-0.10	0.09	--
23	-0.35	0.04	-111.6%	-0.12	0.11	--
24	-0.20	0.04	--	0.04	0.11	--
25	-0.36	-0.09	-75.2%	-0.15	-0.25	--
26	-0.63	-0.20	-68.0%	0.76	-0.58	-176.6%
27	-0.57	-0.19	-66.7%	0.83	-0.55	-166.3%
28	-0.55	-0.18	-67.5%	0.88	-0.52	-159.4%
29	-0.12	-0.06	--	-0.14	-0.17	--
30	-0.30	-0.12	-60.3%	0.18	-0.35	--
31	-0.31	-0.15	-51.8%	0.90	-0.44	-148.8%
32	-0.16	-0.05	--	-0.12	-0.14	--
33	-0.33	-0.10	-69.7%	0.28	-0.28	--
34	-0.37	-0.12	-67.2%	0.11	-0.32	--
35	-0.21	-0.05	--	-0.12	-0.14	--
36	-0.29	-0.11	--	0.20	-0.32	--
37	-0.37	-0.10	-73.1%	0.26	-0.29	--
38	-0.37	-0.13	-65.2%	0.85	-0.39	-145.7%
39	-0.41	-0.12	-70.9%	0.86	-0.37	-143.0%
40	-0.33	-0.09	-72.7%	0.30	-0.25	-182.2%
41	-0.33	-0.08	-76.1%	0.27	-0.21	--
42	-0.47	-0.10	-78.6%	0.57	-0.28	-149.4%
43	-0.48	-0.09	-81.1%	0.58	-0.25	-143.2%
	min = -111.6%			min = -217.3%		
	max = -39.2%			max = -115.5%		
	average = -65.6%			average = -159.6%		
	st. dev. = 16.2%			st. dev. = 25.0%		

Table F-42: Computed (FM) versus Measured Results for Static Test Stresses at Section 9F

Test	9F-D-TQE (ksi)			9F-D-BQE (ksi)		
	Measured	FM	% Error	Measured	FM	% Error
1	-0.01	0.01	--	0.03	0.04	--
2	0.01	0.01	--	0.01	0.05	--
3	-0.02	0.00	--	-0.04	0.00	--
4	-0.03	-0.02	--	-0.12	-0.08	--
5	0.03	-0.06	--	-0.32	-0.25	-20.7%
6	0.14	-0.07	--	0.07	-0.34	--
7	-0.01	0.04	--	0.15	0.16	--
8	-0.01	0.04	--	0.15	0.17	--
9	-0.02	0.03	--	0.09	0.11	--
10	-0.02	0.00	--	-0.04	-0.02	--
11	0.03	-0.11	--	-0.52	-0.49	-5.5%
12	0.10	-0.23	--	-0.64	-1.02	59.3%
13	0.14	-0.24	--	-0.50	-1.03	106.6%
14	0.08	-0.07	--	-0.04	-0.31	--
15	-0.04	-0.11	--	-0.59	-0.49	-16.9%
16	-0.02	-0.23	--	-0.83	-1.00	21.2%
17	0.07	-0.23	--	-0.59	-1.05	77.6%
18	-0.12	-0.27	--	-0.44	-1.21	176.0%
19	-0.14	-0.28	--	-0.48	-1.27	164.6%
20	-0.08	0.02	--	-0.02	0.09	--
21	-0.09	0.02	--	0.03	0.09	--
22	-0.25	0.03	--	-0.16	0.13	--
23	-0.32	0.04	-112.5%	-0.16	0.17	--
24	-0.19	0.04	--	-0.02	0.17	--
25	-0.09	-0.09	--	-0.63	-0.41	-35.2%
26	-0.08	-0.21	--	-0.70	-0.96	36.9%
27	-0.03	-0.20	--	-0.62	-0.92	48.8%
28	-0.01	-0.19	--	-0.56	-0.88	57.1%
29	-0.08	-0.06	--	-0.18	-0.16	--
30	-0.12	-0.12	--	-0.08	-0.29	--
31	-0.15	-0.15	--	0.45	-0.36	-179.2%
32	0.04	-0.06	--	-0.46	-0.37	-19.6%
33	0.14	-0.11	--	-0.80	-0.75	-6.8%
34	0.11	-0.13	--	-0.95	-0.88	-7.6%
35	-0.14	-0.05	--	-0.21	-0.11	--
36	-0.12	-0.11	--	-0.04	-0.25	--
37	-0.20	-0.10	--	0.04	-0.21	--
38	-0.20	-0.13	--	0.43	-0.28	-165.6%
39	-0.22	-0.12	--	0.43	-0.25	-158.8%
40	0.14	-0.10	--	-0.76	-0.71	-6.7%
41	0.12	-0.09	--	-0.72	-0.65	-9.3%
42	0.02	-0.12	--	-0.95	-0.83	-12.4%
43	0.01	-0.11	--	-0.92	-0.79	-14.1%
	min = -112.5%			min = -179.2%		
	max = -112.5%			max = 176.0%		
	average = -112.5%			average = 3.9%		
	st. dev. = 0.0%			st. dev. = 86.9%		

Table F-43: Computed (FM) versus Measured Results for Static Test Stresses at Section 9F

Test	9F-D-TE (ksi)			9F-D-BE (ksi)		
	Measured	FM	% Error	Measured	FM	% Error
1	0.04	0.00	--	0.06	0.01	--
2	0.07	0.00	--	0.06	0.01	--
3	0.08	0.00	--	0.02	0.00	--
4	0.08	0.00	--	0.00	-0.02	--
5	0.20	-0.01	--	-0.08	-0.07	--
6	1.01	-0.01	-101.0%	-0.09	-0.09	--
7	0.01	0.01	--	0.16	0.04	--
8	0.01	0.01	--	0.16	0.04	--
9	0.00	0.01	--	0.11	0.03	--
10	0.01	0.00	--	0.04	-0.01	--
11	0.09	-0.02	--	-0.11	-0.13	--
12	0.88	-0.04	-104.6%	-0.28	-0.27	--
13	1.01	-0.06	-106.0%	-0.19	-0.25	--
14	0.79	-0.01	-101.3%	-0.08	-0.08	--
15	0.34	-0.02	-105.9%	-0.16	-0.13	--
16	0.92	-0.04	-104.4%	-0.21	-0.26	--
17	0.98	-0.04	-104.1%	-0.37	-0.27	-26.9%
18	1.41	-0.05	-103.6%	-0.44	-0.32	-27.1%
19	1.37	-0.05	-103.6%	-0.48	-0.33	-30.7%
20	0.12	0.01	--	0.12	0.02	--
21	-0.01	0.01	--	0.00	0.02	--
22	0.06	0.01	--	0.07	0.03	--
23	0.03	0.01	--	0.06	0.04	--
24	0.17	0.01	--	0.00	0.04	--
25	0.30	-0.01	--	-0.07	-0.11	--
26	1.04	-0.03	-102.9%	-0.31	-0.25	-18.3%
27	1.07	-0.03	-102.8%	-0.27	-0.24	--
28	1.09	-0.03	-102.8%	-0.25	-0.24	--
29	0.08	-0.04	--	-0.24	-0.02	--
30	0.55	-0.09	-116.4%	-0.43	-0.02	-95.3%
31	1.09	-0.11	-110.1%	-0.49	-0.02	-95.9%
32	-0.03	0.02	--	0.08	-0.12	--
33	0.18	0.05	--	0.11	-0.26	--
34	0.10	0.06	--	0.16	-0.30	--
35	0.31	-0.04	-113.0%	-0.25	0.00	--
36	0.54	-0.09	-116.6%	-0.40	-0.01	-97.5%
37	0.51	-0.08	-115.5%	-0.40	0.00	-100.0%
38	1.02	-0.11	-110.8%	-0.44	0.00	-100.0%
39	0.99	-0.11	-111.1%	-0.42	0.01	-102.4%
40	0.19	0.06	--	0.16	-0.25	--
41	0.15	0.06	--	0.22	-0.23	--
42	0.12	0.07	--	0.19	-0.29	--
43	0.11	0.07	--	0.22	-0.28	--
	min = -116.6%			min = -102.4%		
	max = -101.0%			max = -18.3%		
	average = -107.2%			average = -69.4%		
	st. dev. = 5.1%			st. dev. = 35.8%		

Table F-44: Computed (FM) versus Measured Results for Static Test Stresses at Section 9F

Test	8A-D-TI (ksi)			8A-D-BI (ksi)		
	Measured	FM	% Error	Measured	FM	% Error
1	-0.04	0.07	--	0.03	-0.07	--
2	-0.04	0.08	--	0.07	-0.08	--
3	0.57	0.01	-98.2%	0.08	-0.02	--
4	-0.01	0.04	--	0.00	-0.04	--
5	-0.04	0.05	--	-0.02	-0.05	--
6	-0.01	0.02	--	-0.39	-0.03	-92.4%
7	0.24	0.28	--	0.25	-0.27	--
8	0.29	0.28	--	0.23	-0.28	--
9	0.58	0.19	-67.5%	0.23	-0.19	--
10	0.63	0.14	-77.9%	0.27	-0.15	--
11	0.43	0.15	-65.1%	0.28	-0.15	--
12	0.14	0.18	--	0.16	-0.18	--
13	0.14	0.13	--	0.13	-0.13	--
14	0.08	0.02	--	0.06	-0.02	--
15	-0.03	0.10	--	0.86	-0.11	-112.8%
16	-0.06	0.18	--	-0.59	-0.19	-68.0%
17	0.00	0.18	--	0.00	-0.19	--
18	0.30	0.19	--	2.36	-0.19	-108.0%
19	0.25	0.22	--	2.43	-0.23	-109.5%
20	-0.06	0.15	--	-0.33	-0.15	-54.3%
21	0.08	0.15	--	2.33	-0.15	-106.4%
22	-0.08	0.22	--	1.45	-0.22	-115.2%
23	-0.02	0.28	--	1.94	-0.28	-114.4%
24	0.36	0.28	-21.6%	2.48	-0.28	-111.3%
25	-0.01	0.25	--	1.02	-0.26	-125.4%
26	0.12	0.33	--	2.11	-0.33	-115.6%
27	0.33	0.40	19.7%	2.48	-0.40	-116.1%
28	0.43	0.46	6.2%	2.59	-0.46	-117.7%
29	0.06	0.04	--	0.04	0.00	--
30	0.11	0.07	--	0.09	0.00	--
31	0.19	0.08	--	0.20	0.00	--
32	-0.02	0.07	--	-0.17	-0.10	--
33	-0.03	0.12	--	-0.37	-0.19	-48.7%
34	-0.02	0.13	--	-0.46	-0.22	-52.4%
35	0.00	0.14	--	0.78	-0.14	-118.0%
36	0.13	0.17	--	0.18	-0.15	--
37	0.16	0.25	--	-0.49	-0.28	-43.3%
38	0.26	0.26	--	-0.43	-0.27	-37.7%
39	0.23	0.33	--	-1.40	-0.37	-73.6%
40	0.06	0.17	--	-0.33	-0.19	-41.9%
41	0.15	0.21	--	-0.47	-0.18	-61.3%
42	0.03	0.23	--	-1.80	-0.22	-87.8%
43	0.07	0.27	--	-1.78	-0.22	-87.6%
	min = -98.2% max = 19.7% average = -43.5% st. dev. = 41.7%			min = -125.4% max = -37.7% average = -88.3% st. dev. = 29.2%		

NOTE: 8A-D-BI response is unreliable

Table F-45: Computed (FM) versus Measured Results for Static Test Stresses at Section 8A

Test	8A-D-TQI (ksi)			8A-D-BQI (ksi)		
	Measured	FM	% Error	Measured	FM	% Error
1	0.08	0.04	--	-0.11	-0.06	--
2	0.12	0.04	--	-0.09	-0.07	--
3	-0.11	0.01	--	0.10	-0.02	--
4	0.11	0.02	--	-0.02	-0.04	--
5	0.05	0.03	--	-0.08	-0.05	--
6	0.02	0.01	--	-0.07	-0.02	--
7	0.36	0.14	-61.0%	-0.31	-0.23	-24.8%
8	0.43	0.15	-64.9%	-0.23	-0.24	--
9	0.25	0.10	--	-0.29	-0.16	--
10	0.26	0.06	--	-0.33	-0.15	-55.0%
11	0.11	0.07	--	-0.28	-0.14	--
12	0.10	0.09	--	-0.24	-0.17	--
13	0.03	0.07	--	-0.25	-0.12	--
14	0.02	0.01	--	-0.18	-0.02	--
15	0.01	0.05	--	-0.17	-0.10	--
16	0.06	0.09	--	-0.31	-0.19	-38.9%
17	0.00	0.09	--	0.00	-0.18	--
18	0.13	0.09	--	-0.18	-0.19	--
19	0.17	0.11	--	-0.26	-0.22	--
20	0.18	0.08	--	-0.26	-0.12	--
21	0.11	0.08	--	-0.16	-0.14	--
22	0.19	0.11	--	-0.48	-0.20	-58.1%
23	0.24	0.14	--	-0.57	-0.25	-56.4%
24	0.42	0.14	-66.4%	-0.29	-0.24	--
25	0.13	0.13	--	-0.45	-0.24	-46.2%
26	0.11	0.17	--	-0.53	-0.30	-43.8%
27	0.23	0.20	--	-0.49	-0.37	-24.5%
28	0.38	0.23	-39.4%	-0.50	-0.42	-16.0%
29	-0.13	0.04	--	-0.15	0.09	--
30	-0.27	0.08	--	-0.16	0.17	--
31	-0.35	0.10	-128.2%	-0.25	0.20	--
32	0.18	0.01	--	-0.27	-0.19	--
33	0.36	0.01	-97.2%	-0.35	-0.35	0.9%
34	0.51	0.01	-98.0%	-0.34	-0.41	20.0%
35	-0.21	0.06	--	-0.23	-0.16	--
36	-0.31	0.10	-132.4%	-0.29	-0.09	--
37	-0.36	0.11	-130.6%	-0.48	-0.31	-36.1%
38	-0.42	0.13	-130.8%	-0.57	-0.27	-52.8%
39	-0.46	0.14	-130.5%	-0.65	-0.45	-31.1%
40	0.56	0.07	-87.6%	-0.42	-0.23	-45.6%
41	0.78	0.12	-84.7%	-0.48	-0.10	-79.4%
42	0.95	0.12	-87.4%	-0.50	-0.18	-63.9%
43	1.13	0.16	-85.9%	-0.55	-0.08	-85.5%
	min = -132.4%			min = -85.5%		
	max = -39.4%			max = 20.0%		
	average = -95.0%			average = -40.9%		
	st. dev. = 29.0%			st. dev. = 25.5%		

Table F-46: Computed (FM) versus Measured Results for Static Test Stresses at Section 8A

Test	8A-D-TM (ksi)			8A-D-BM (ksi)		
	Measured	FM	% Error	Measured	FM	% Error
1	0.02	0.04	--	0.03	0.13	--
2	0.03	0.04	--	0.05	0.13	--
3	-0.02	0.01	--	0.55	0.02	-96.4%
4	0.01	0.02	--	0.06	0.07	--
5	0.01	0.03	--	0.06	0.09	--
6	0.00	0.01	--	0.05	0.04	--
7	0.10	0.16	--	0.17	0.49	--
8	0.10	0.17	--	0.21	0.49	--
9	-0.23	0.11	--	0.79	0.33	-58.2%
10	-0.22	0.07	--	0.84	0.22	-74.0%
11	-0.17	0.08	--	0.64	0.25	-61.0%
12	0.05	0.10	--	0.13	0.31	--
13	0.04	0.08	--	0.08	0.23	--
14	0.02	0.01	--	0.01	0.04	--
15	-0.02	0.06	--	0.13	0.17	--
16	-0.03	0.10	--	0.18	0.30	--
17	0.00	0.10	--	0.00	0.30	--
18	0.06	0.10	--	0.49	0.31	-36.8%
19	0.06	0.12	--	0.53	0.36	-32.3%
20	0.02	0.09	--	0.10	0.26	--
21	0.01	0.09	--	0.10	0.26	--
22	-0.07	0.13	--	0.17	0.38	--
23	-0.06	0.16	--	0.20	0.48	--
24	0.17	0.16	--	0.50	0.49	-2.7%
25	-0.03	0.14	--	0.20	0.43	--
26	0.02	0.19	--	0.34	0.56	64.1%
27	0.13	0.23	--	0.50	0.69	38.6%
28	0.18	0.27	--	0.60	0.79	31.1%
29	-0.04	0.05	--	0.00	0.13	--
30	-0.02	0.08	--	0.03	0.23	--
31	-0.04	0.10	--	0.05	0.29	--
32	-0.06	0.01	--	-0.05	0.04	--
33	-0.06	0.02	--	-0.05	0.07	--
34	-0.07	0.02	--	-0.04	0.07	--
35	0.01	0.07	--	0.15	0.21	--
36	0.00	0.11	--	0.07	0.31	--
37	-0.05	0.13	--	0.05	0.39	--
38	-0.05	0.15	--	0.10	0.43	--
39	-0.08	0.16	--	0.14	0.48	--
40	-0.04	0.08	--	-0.03	0.24	--
41	-0.01	0.14	--	0.00	0.40	--
42	-0.13	0.14	--	-0.02	0.41	--
43	-0.13	0.18	--	0.00	0.54	--
	min = 0.0%		min = -96.4%		max = 64.1%	
	max = 0.0%		average = -22.7%		st. dev. = 50.7%	
	average = --		st. dev. = --			

Table F-47: Computed (FM) versus Measured Results for Static Test Stresses at Section 8A

Test	8A-D-TQE (ksi)			8A-D-BQE (ksi)		
	Measured	FM	% Error	Measured	FM	% Error
1	0.00	0.05	--	0.25	0.32	--
2	0.01	0.05	--	0.25	0.33	--
3	-0.04	0.01	--	-0.24	0.06	--
4	0.00	0.03	--	0.16	0.18	--
5	0.01	0.03	--	0.22	0.22	--
6	0.00	0.02	--	0.17	0.11	--
7	-0.16	0.18	--	0.84	1.20	43.1%
8	-0.17	0.19	--	0.85	1.22	43.6%
9	-0.05	0.12	--	0.33	0.82	147.7%
10	-0.04	0.08	--	0.30	0.60	97.8%
11	-0.03	0.09	--	0.30	0.63	--
12	-0.13	0.12	--	0.55	0.78	41.3%
13	-0.12	0.09	--	0.45	0.58	28.4%
14	-0.07	0.01	--	0.18	0.09	--
15	-0.04	0.07	--	0.51	0.45	-11.5%
16	-0.19	0.12	--	0.75	0.79	5.1%
17	0.00	0.11	--	0.00	0.78	--
18	-0.22	0.12	--	1.21	0.80	-34.0%
19	-0.30	0.14	--	1.40	0.94	-33.1%
20	-0.04	0.10	--	0.58	0.64	10.4%
21	-0.20	0.10	--	0.47	0.65	37.8%
22	-0.35	0.14	-140.2%	0.97	0.96	-1.2%
23	-0.44	0.18	-141.3%	1.20	1.22	1.4%
24	-0.33	0.18	-155.1%	1.52	1.21	-20.2%
25	-0.28	0.16	--	1.02	1.10	8.3%
26	-0.44	0.21	-147.9%	1.43	1.42	-0.9%
27	-0.41	0.26	-162.8%	1.75	1.74	-0.8%
28	-0.39	0.30	-176.1%	2.00	1.99	-0.3%
29	-0.05	0.05	--	0.11	0.17	--
30	-0.06	0.08	--	0.19	0.30	--
31	-0.11	0.10	--	0.33	0.37	12.9%
32	-0.10	0.02	--	0.17	0.27	--
33	-0.14	0.03	--	0.29	0.48	--
34	-0.16	0.04	--	0.30	0.56	84.9%
35	-0.04	0.08	--	0.62	0.58	-6.9%
36	-0.13	0.12	--	0.47	0.72	54.4%
37	-0.28	0.15	--	0.69	1.08	57.2%
38	-0.32	0.16	-149.2%	0.83	1.13	36.9%
39	-0.38	0.18	-147.0%	1.03	1.40	35.6%
40	-0.22	0.09	--	0.47	0.71	50.1%
41	-0.27	0.15	--	0.65	0.91	39.5%
42	-0.40	0.15	-137.8%	0.62	1.00	62.4%
43	-0.41	0.20	-148.7%	0.75	1.16	55.1%
	min = -176.1%			min = -34.0%		
	max = -137.8%			max = 147.7%		
	average = -150.6%			average = 28.2%		
	st. dev. = 11.0%			st. dev. = 39.0%		

Table F-48: Computed (FM) versus Measured Results for Static Test Stresses at Section 8A

Test	8A-D-TE (ksi)			8A-D-BE (ksi)		
	Measured	FM	% Error	Measured	FM	% Error
1	0.00	-0.02	--	0.05	0.11	--
2	0.02	-0.02	--	0.06	0.11	--
3	0.34	-0.01	-103.0%	-0.13	0.02	--
4	0.03	-0.01	--	0.15	0.06	--
5	0.03	-0.02	--	0.13	0.08	--
6	0.04	-0.01	--	0.09	0.04	--
7	-0.05	-0.08	--	0.04	0.40	--
8	0.11	-0.08	--	0.10	0.41	--
9	0.69	-0.05	-107.2%	-0.08	0.27	--
10	0.73	-0.05	-106.9%	0.04	0.20	--
11	0.39	-0.04	-110.3%	0.22	0.21	--
12	-0.09	-0.05	--	0.32	0.26	-19.7%
13	-0.08	-0.04	--	0.22	0.19	--
14	-0.08	-0.01	--	0.02	0.03	--
15	0.05	-0.03	--	0.21	0.15	--
16	-0.08	-0.06	--	0.33	0.27	-18.7%
17	0.00	-0.06	--	0.00	0.26	--
18	0.06	-0.06	--	0.31	0.27	-13.8%
19	0.00	-0.07	--	0.41	0.32	-21.4%
20	0.04	-0.04	--	0.09	0.21	--
21	-0.10	-0.04	--	0.02	0.22	--
22	-0.16	-0.06	--	0.11	0.32	--
23	-0.23	-0.08	--	0.08	0.41	--
24	-0.11	-0.08	--	0.09	0.40	--
25	-0.12	-0.08	--	0.24	0.37	--
26	-0.28	-0.10	--	0.38	0.48	27.9%
27	-0.21	-0.12	--	0.41	0.59	44.9%
28	-0.16	-0.13	--	0.40	0.67	67.7%
29	-0.01	0.02	--	0.17	0.04	--
30	-0.04	0.03	--	0.36	0.06	-83.5%
31	-0.02	0.04	--	0.54	0.07	-87.0%
32	-0.02	-0.05	--	-0.09	0.12	--
33	-0.05	-0.09	--	-0.15	0.20	--
34	-0.06	-0.10	--	-0.19	0.24	--
35	0.11	-0.05	--	0.45	0.20	-55.7%
36	-0.04	-0.03	--	0.55	0.23	-57.9%
37	-0.18	-0.09	--	0.73	0.38	-48.0%
38	-0.12	-0.08	--	0.89	0.39	-56.3%
39	-0.14	-0.13	--	1.06	0.50	-52.9%
40	-0.14	-0.07	--	-0.30	0.25	--
41	-0.24	-0.04	--	-0.46	0.29	-163.4%
42	-0.34	-0.06	-82.3%	-0.50	0.33	-166.5%
43	-0.33	-0.04	-88.0%	-0.61	0.36	-159.2%
	min = -110.3%			min = -166.5%		
	max = -82.3%			max = 67.7%		
	average = -99.6%			average = -50.8%		
	st. dev. = 10.6%			st. dev. = 66.0%		

Table F-49: Computed (FM) versus Measured Results for Static Test Stresses at Section 8A

Test	9E-LBU-CN (ksi)			9E-LBD-CN (ksi)		
	Measured	FM	% Error	Measured	FM	% Error
1	0.24	0.24	--	-0.26	-0.25	--
2	0.22	0.24	--	-0.27	-0.25	--
3	0.02	0.02	--	-0.05	-0.02	--
4	-0.10	-0.19	--	0.13	0.22	--
5	-0.09	-0.29	--	0.21	0.40	--
6	1.38	-0.05	-103.6%	1.82	0.33	-81.9%
7	0.88	0.92	4.6%	-0.95	-0.96	0.8%
8	0.88	0.93	6.2%	-0.94	-0.97	3.2%
9	0.66	0.62	-5.4%	-0.68	-0.64	-6.1%
10	0.28	0.07	--	-0.24	-0.06	--
11	-0.22	-0.80	--	0.43	1.01	133.0%
12	0.64	-0.95	-248.1%	1.84	1.52	-17.6%
13	1.62	-0.75	-146.2%	2.94	1.44	-51.0%
14	1.64	0.01	-99.4%	1.98	0.29	-85.4%
15	-0.28	-0.61	--	0.45	0.83	83.1%
16	0.75	-0.87	-216.5%	1.52	1.43	-6.1%
17	0.79	-0.81	-202.8%	1.74	1.41	-19.0%
18	1.27	-0.74	-158.2%	2.30	1.55	-32.6%
19	1.08	-0.90	-183.0%	2.44	1.72	-29.4%
20	0.44	0.49	11.6%	-0.55	-0.51	-6.4%
21	0.39	0.48	22.3%	-0.61	-0.49	-19.5%
22	0.58	0.70	20.2%	-0.76	-0.72	-5.8%
23	0.79	0.90	14.0%	-0.94	-0.93	-0.9%
24	0.47	0.92	97.6%	-1.24	-0.95	-23.4%
25	0.29	-0.06	--	-0.10	0.27	--
26	1.24	-0.32	-125.9%	1.32	0.89	-32.5%
27	1.33	-0.09	-106.8%	0.97	0.65	-33.1%
28	1.41	0.11	-92.2%	0.68	0.45	-33.5%
29	-1.12	-1.62	44.4%	1.31	1.67	27.4%
30	-1.55	-2.70	74.3%	3.07	2.83	-8.0%
31	-1.50	-3.04	102.6%	4.21	3.22	-23.5%
32	1.33	1.10	-17.5%	-1.24	-0.91	-26.4%
33	2.66	1.86	-30.2%	-1.43	-1.39	-3.1%
34	3.13	2.05	-34.6%	-1.42	-1.42	0.1%
35	-1.39	-1.67	19.9%	1.43	1.71	19.7%
36	-1.39	-2.74	97.1%	2.88	2.86	-0.6%
37	-1.35	-2.78	105.6%	2.80	2.88	2.8%
38	-1.13	-3.14	177.6%	3.94	3.29	-16.5%
39	-0.98	-3.19	223.9%	3.78	3.34	-11.6%
40	2.96	2.37	-19.9%	-1.75	-1.91	9.0%
41	3.20	2.82	-12.0%	-2.10	-2.38	13.6%
42	3.75	3.11	-17.1%	-1.67	-2.47	48.1%
43	3.94	3.48	-11.7%	-1.85	-2.85	54.0%
	min = -248.1%			min = -85.4%		
	max = 223.9%			max = 133.0%		
	average = -23.8%			average = -5.0%		
	st. dev. = 108.7%			st. dev. = 39.3%		

Table F-50: Computed (FM) versus Measured Results for Static Test Stresses at Section 9E

Test	9G-LBU-CN (ksi)			9G-LBD-CN (ksi)		
	Measured	FM	% Error	Measured	FM	% Error
1	0.21	0.20	--	-0.25	-0.25	--
2	0.19	0.20	--	-0.26	-0.25	--
3	0.02	0.01	--	-0.05	-0.02	--
4	-0.07	-0.13	--	0.11	0.21	--
5	0.53	-0.11	-120.8%	0.87	0.38	-56.5%
6	0.84	0.06	-92.9%	1.16	0.20	-82.7%
7	0.77	0.75	-2.5%	-0.91	-0.93	2.7%
8	0.77	0.75	-2.3%	-0.89	-0.94	5.5%
9	0.59	0.50	-14.7%	-0.65	-0.62	-4.1%
10	0.29	0.09	--	-0.22	-0.06	--
11	0.24	-0.46	--	0.82	0.97	17.7%
12	1.53	-0.39	-125.5%	2.65	1.37	-48.4%
13	0.94	-0.11	-111.6%	2.02	1.00	-50.4%
14	0.42	0.08	-80.9%	0.83	0.13	-84.3%
15	0.54	-0.25	-145.9%	1.19	0.78	-34.6%
16	1.49	-0.26	-117.4%	2.17	1.24	-43.0%
17	1.75	-0.24	-113.7%	2.82	1.27	-54.9%
18	1.12	-0.18	-116.1%	2.55	1.25	-51.0%
19	0.96	-0.29	-130.2%	2.67	1.42	-46.7%
20	0.38	0.40	5.6%	-0.50	-0.50	0.3%
21	0.31	0.38	23.3%	-0.49	-0.48	-2.8%
22	0.42	0.56	34.9%	-0.70	-0.70	0.2%
23	0.60	0.73	21.9%	-0.83	-0.90	8.7%
24	0.26	0.74	--	-1.08	-0.92	-15.1%
25	0.93	0.18	-80.7%	0.73	0.26	-64.6%
26	2.09	0.16	-92.4%	2.44	0.77	-68.4%
27	2.16	0.35	-83.8%	2.13	0.54	-74.7%
28	2.23	0.50	-77.5%	1.87	0.35	-81.3%
29	-0.33	-1.18	253.2%	1.40	1.32	-5.5%
30	-0.29	-1.76	--	2.89	2.00	-30.8%
31	-0.69	-1.88	171.0%	3.27	2.16	-33.9%
32	1.27	0.98	-22.6%	-0.40	-0.57	43.9%
33	2.27	1.47	-35.1%	-0.20	-0.69	--
34	2.10	1.50	-28.6%	-0.55	-0.70	26.6%
35	-0.57	-1.27	120.9%	1.42	1.35	-5.2%
36	-0.15	-1.85	--	2.71	2.04	-24.8%
37	-0.14	-1.95	--	2.61	2.08	-20.4%
38	-0.39	-2.08	429.0%	2.93	2.25	-23.1%
39	-0.26	-2.17	--	2.77	2.30	-17.1%
40	2.52	1.94	-22.9%	-0.49	-1.20	146.7%
41	2.66	2.37	-10.8%	-0.85	-1.67	96.4%
42	2.94	2.47	-16.0%	-0.62	-1.68	171.0%
43	3.10	2.82	-9.1%	-0.79	-2.06	160.4%
	min = -145.9%			min = -84.3%		
	max = 429.0%			max = 171.0%		
	average = -18.6%			average = -9.3%		
	st. dev. = 118.8%			st. dev. = 62.3%		

Table F-51: Computed (FM) versus Measured Results for Static Test Stresses at Section 9G

Test	9K-LBU-CN (ksi)			9K-LBD-CN (ksi)		
	Measured	FM	% Error	Measured	FM	% Error
1	-0.09	-0.17	--	-0.09	0.02	--
2	-0.10	-0.18	--	-0.09	0.02	--
3	0.05	-0.01	--	-0.08	0.00	--
4	0.90	0.26	-71.1%	0.82	0.00	-100.0%
5	1.07	0.43	-59.7%	1.05	-0.12	-111.4%
6	0.00	0.21	--	-0.01	-0.13	--
7	-0.33	-0.64	95.0%	-0.19	0.07	--
8	-0.30	-0.67	122.9%	-0.22	0.07	--
9	-0.11	-0.44	--	-0.19	0.05	--
10	0.58	0.05	-91.4%	0.25	0.03	--
11	2.31	1.06	-54.2%	2.31	-0.13	-105.6%
12	2.12	1.44	-32.0%	1.67	-0.48	-128.8%
13	0.72	1.29	79.9%	0.56	-0.71	-227.8%
14	-0.13	0.19	--	0.22	-0.12	--
15	1.33	0.90	-32.6%	1.20	-0.29	-124.2%
16	2.00	1.37	-31.6%	1.87	-0.37	-119.8%
17	0.00	1.30	--	2.10	-0.32	-115.3%
18	1.81	1.40	-22.8%	1.52	-0.47	-131.0%
19	2.15	1.60	-25.7%	1.53	-0.47	-130.8%
20	-0.19	-0.34	--	-0.18	0.04	--
21	-0.22	-0.34	--	-0.12	0.03	--
22	-0.22	-0.51	--	-0.31	0.05	-116.0%
23	-0.25	-0.64	--	-0.32	0.07	-121.6%
24	-0.35	-0.64	85.1%	-0.77	0.07	-109.1%
25	0.97	0.48	-50.4%	1.00	-0.20	-120.1%
26	2.03	0.96	-52.7%	1.80	-0.28	-115.5%
27	1.89	0.79	-58.2%	1.60	-0.26	-116.3%
28	1.79	0.66	-63.1%	1.45	-0.25	-117.3%
29	1.68	1.43	-14.7%	0.36	-1.30	-459.8%
30	2.52	2.17	-13.8%	-0.11	-1.94	--
31	2.74	2.49	-9.3%	-0.46	-2.23	389.5%
32	-0.46	-0.64	40.6%	1.41	1.07	-23.9%
33	-0.32	-0.82	153.8%	2.45	1.60	-34.7%
34	-0.59	-0.90	52.2%	2.46	1.72	-30.0%
35	1.63	1.25	-23.5%	-0.53	-1.32	150.3%
36	2.55	1.97	-22.7%	-0.31	-1.95	524.6%
37	2.58	1.76	-31.7%	-0.71	-1.93	170.0%
38	3.11	2.12	-31.8%	-0.51	-2.25	340.3%
39	3.15	1.99	-36.9%	-0.70	-2.25	222.5%
40	-0.53	-0.96	82.2%	2.54	1.64	-35.5%
41	-0.73	-1.06	45.1%	2.73	1.64	-39.9%
42	-0.62	-1.18	91.0%	2.83	1.83	-35.3%
43	-0.78	-1.26	62.6%	2.92	1.86	-36.3%
	min = -91.4% max = 153.8% average = 2.5% st. dev. = 63.3%			min = -459.8% max = 524.6% average = -32.5% st. dev. = 188.8%		

Table F-52: Computed (FM) versus Measured Results for Static Test Stresses at Section 9K

Test	9O-LBD-CN (ksi)			8B-LBU-CN (ksi)		
	Measured	FM	% Error	Measured	FM	% Error
1	0.06	0.32	--	-0.14	-0.50	--
2	0.12	0.29	--	-0.22	-0.49	--
3	0.72	-0.01	-101.4%	0.89	-0.04	-104.5%
4	0.18	-0.32	--	0.09	0.22	--
5	-0.27	-0.40	--	0.13	0.30	--
6	-0.16	-0.20	--	0.03	0.15	--
7	0.61	1.21	97.5%	-1.16	-1.90	64.3%
8	0.51	1.16	128.6%	-0.64	-1.91	199.3%
9	0.85	0.76	-11.0%	0.55	-1.30	-337.6%
10	1.53	-0.05	-103.3%	0.36	-0.32	-188.2%
11	0.65	-1.28	-296.5%	0.60	0.93	56.1%
12	-1.04	-1.46	41.1%	0.64	1.08	69.1%
13	-0.75	-1.14	51.5%	0.43	0.88	105.5%
14	0.00	-0.17	--	-0.09	0.14	--
15	-0.54	-0.81	50.4%	0.24	0.60	--
16	-0.78	-1.37	76.7%	0.41	1.01	146.1%
17	0.00	-1.38	--	0.00	1.02	--
18	0.03	-1.41	--	0.06	1.03	--
19	-0.01	-1.67	--	0.20	1.20	--
20	0.31	0.65	109.3%	-0.64	-1.02	58.7%
21	0.29	0.60	--	-0.55	-0.95	71.8%
22	0.35	0.85	140.6%	-0.94	-1.38	46.5%
23	0.51	1.13	123.0%	-1.32	-1.80	36.1%
24	0.42	1.19	180.7%	-1.53	-1.88	23.2%
25	-0.25	-0.18	--	-0.34	-0.37	9.9%
26	-0.84	-0.73	-12.6%	-0.27	0.00	--
27	-0.70	-0.45	-35.9%	-0.58	-0.46	-20.7%
28	-0.56	-0.19	-66.3%	-0.86	-0.85	-1.6%
29	-1.36	-1.46	7.1%	0.65	1.22	88.2%
30	-2.79	-2.64	-5.5%	1.39	2.19	57.2%
31	-2.94	-3.29	11.9%	1.88	2.74	46.0%
32	1.04	0.66	-36.3%	-0.55	-0.62	12.4%
33	2.04	1.24	-39.3%	-1.01	-1.15	13.9%
34	3.00	1.54	-48.6%	-1.28	-1.47	15.2%
35	-2.29	-2.05	-10.5%	1.59	1.87	17.5%
36	-3.46	-3.26	-5.8%	2.26	2.89	28.0%
37	-4.25	-3.85	-9.4%	3.15	3.54	12.6%
38	-4.07	-4.46	9.5%	3.57	4.06	13.9%
39	-4.71	-4.95	5.2%	4.41	4.61	4.5%
40	2.94	2.44	-17.1%	-2.38	-2.78	16.8%
41	3.86	3.57	-7.5%	-3.72	-4.32	16.1%
42	4.71	3.88	-17.7%	-3.94	-4.65	18.2%
43	5.42	4.79	-11.6%	-4.96	-5.87	18.4%
	min = -296.5%			min = -337.6%		
	max = 180.7%			max = 199.3%		
	average = 6.1%			average = 19.2%		
	st. dev. = 86.3%			st. dev. = 90.6%		

Table F-53: Computed (FM) versus Measured Results for Static Test Stresses at Section 9O and 8B

Test	8D-LBU-CN (ksi)			8F-LBD-CN (ksi)		
	Measured	FM	% Error	Measured	FM	% Error
1	0.52	-0.05	-109.7%	0.66	0.19	-71.2%
2	1.33	0.09	-93.2%	0.41	0.13	-68.2%
3	-0.07	0.00	--	0.04	0.01	--
4	-0.11	-0.02	--	0.04	0.01	--
5	-0.13	-0.03	--	0.05	0.02	--
6	-0.13	-0.01	--	0.04	0.01	--
7	1.63	-0.25	-115.3%	2.03	0.81	-60.1%
8	1.22	0.09	-92.6%	1.98	0.49	-75.3%
9	1.64	0.27	-83.6%	0.84	0.24	-71.5%
10	-0.09	0.05	--	0.23	0.09	--
11	-0.18	-0.08	--	0.20	0.06	--
12	-0.18	-0.09	--	0.19	0.07	--
13	-0.15	-0.06	--	0.17	0.07	--
14	-0.07	-0.01	--	0.10	0.01	--
15	-0.40	-0.05	-87.5%	0.11	0.04	--
16	-0.55	-0.09	-83.5%	0.23	0.06	--
17	0.00	-0.09	--	0.00	0.06	--
18	-0.92	-0.09	-90.2%	0.06	0.06	--
19	-0.96	-0.11	-88.5%	0.10	0.07	--
20	0.48	-0.12	-125.2%	0.92	0.36	-60.9%
21	0.42	-0.01	-102.4%	1.05	0.36	-65.6%
22	1.56	0.05	-96.8%	2.15	0.58	-73.1%
23	1.53	-0.09	-105.9%	2.12	0.74	-65.2%
24	0.90	-0.12	-113.3%	1.72	0.67	-61.2%
25	0.06	-0.06	--	1.24	0.39	-68.5%
26	-0.03	-0.21	--	0.94	0.42	-55.4%
27	0.77	-0.11	-114.3%	2.02	0.61	-69.9%
28	0.78	-0.21	-126.9%	1.92	0.73	-62.0%
29	0.01	-0.02	--	0.07	0.18	--
30	0.04	-0.05	--	0.10	0.32	--
31	0.09	-0.06	--	0.08	0.40	--
32	-0.07	-0.03	--	0.12	-0.14	--
33	-0.16	-0.04	--	0.20	-0.25	--
34	-0.26	-0.05	--	0.29	-0.32	--
35	1.11	1.46	31.2%	-0.32	-0.32	0.8%
36	1.42	1.49	5.0%	-0.11	-0.13	--
37	2.76	2.47	-10.5%	-0.12	-0.22	--
38	2.73	2.43	-11.1%	-0.22	-0.15	--
39	3.36	2.77	-17.5%	-0.66	-0.14	-78.8%
40	-1.02	-1.58	55.4%	1.41	0.55	-61.1%
41	-1.16	-2.72	135.2%	2.53	1.04	-58.9%
42	-1.33	-2.72	104.0%	2.62	0.97	-62.9%
43	-1.32	-3.13	137.1%	2.37	1.08	-54.4%
	min = -126.9%			min = -78.8%		
	max = 137.1%			max = 0.8%		
	average = -48.0%			average = -62.2%		
	st. dev. = 81.0%			st. dev. = 15.8%		

Table F-54: Computed (FM) versus Measured Results for Static Test Stresses at Section 8D and 8F

Test	10Z-GC-TC (ksi)			10Z-GC-BC (ksi)		
	Measured	FMR	% Error	Measured	FMR	% Error
1	-0.02	-0.26	--	0.37	0.47	27.2%
2	-0.02	-0.28	--	0.39	0.50	27.4%
3	0.01	-0.01	--	0.01	0.02	--
4	0.06	0.36	--	-0.54	-0.65	21.0%
5	0.11	0.70	--	-1.00	-1.26	26.5%
6	0.11	0.63	--	-0.81	-1.13	39.3%
7	-0.11	-0.98	--	1.31	1.78	35.5%
8	-0.11	-1.03	--	1.34	1.86	38.7%
9	-0.08	-0.69	--	0.85	1.24	46.0%
10	0.03	0.07	--	-0.26	-0.13	--
11	0.30	1.69	--	-2.54	-3.03	19.3%
12	0.45	2.52	461.1%	-3.63	-4.51	24.1%
13	0.47	2.39	407.8%	-3.48	-4.29	23.3%
14	-0.29	0.12	--	0.03	-0.23	--
15	0.20	1.40	--	-1.86	-2.50	34.7%
16	0.40	2.55	532.9%	-3.45	-4.56	32.1%
17	0.45	2.57	465.9%	-3.65	-4.59	25.9%
18	0.49	2.94	494.7%	-3.86	-5.25	35.9%
19	0.54	3.22	491.0%	-4.31	-5.75	33.3%
20	-0.07	-0.52	--	0.79	0.94	19.4%
21	-0.07	-0.53	--	0.71	0.95	33.9%
22	-0.20	-0.79	--	1.26	1.42	12.7%
23	-0.29	-0.99	--	1.58	1.79	13.2%
24	-0.23	-0.99	--	1.50	1.79	19.5%
25	0.08	0.87	--	-1.14	-1.55	35.6%
26	0.22	2.05	--	-2.71	-3.64	34.4%
27	0.18	1.78	--	-2.38	-3.17	33.0%
28	0.14	1.58	--	-2.13	-2.80	31.7%
29	0.05	0.47	--	-1.05	-0.88	-15.8%
30	0.08	0.82	--	-1.79	-1.56	-12.7%
31	0.07	1.03	--	-2.27	-1.95	-14.3%
32	0.13	0.97	--	-1.27	-1.68	32.8%
33	0.28	1.75	--	-2.10	-3.04	44.9%
34	0.40	2.16	441.8%	-2.51	-3.74	49.1%
35	-0.01	0.16	--	-0.44	-0.35	-19.8%
36	0.03	0.51	--	-1.42	-1.01	-28.7%
37	-0.10	0.24	--	-1.18	-0.53	-55.0%
38	-0.10	0.45	--	-1.63	-0.92	-43.6%
39	-0.16	0.24	--	-1.38	-0.56	-59.6%
40	0.25	1.54	--	-1.78	-2.64	48.7%
41	0.22	1.31	--	-1.46	-2.22	51.5%
42	0.24	1.77	--	-1.94	-3.03	56.2%
43	0.21	1.62	--	-1.71	-2.73	59.4%
	min = 407.8%		min = -59.6%			
	max = 532.9%		max = 59.4%			
	average = 470.8%		average = 20.4%			
	st. dev. = 37.3%		st. dev. = 28.9%			

Table F-55: Computed (FMR) versus Measured Results for Static Test Stresses at Section 10Z

	10Z-GA-TC (ksi)			10Z-GA-BC: NO DATA (ksi)		
Test	Measured	FMR	% Error	Measured	FMR	% Error
1	0.06	-0.38	--	--	0.68	--
2	0.08	-0.40	--	--	0.71	--
3	0.07	-0.02	--	--	0.04	--
4	-0.05	0.47	--	--	-0.84	--
5	-0.09	0.89	--	--	-1.60	--
6	-0.08	0.78	--	--	-1.40	--
7	0.01	-1.44	--	--	2.57	--
8	0.00	-1.49	--	--	2.66	--
9	-0.02	-0.99	--	--	1.77	--
10	-0.06	0.05	--	--	-0.09	--
11	-0.13	2.17	--	--	-3.89	--
12	-0.18	3.20	--	--	-5.75	--
13	-0.16	3.22	--	--	-5.77	--
14	-0.21	0.46	--	--	-0.81	--
15	-0.07	1.79	--	--	-3.21	--
16	-0.18	3.21	--	--	-5.76	--
17	-0.19	3.19	--	--	-5.73	--
18	-0.14	3.66	--	--	-6.57	--
19	-0.15	4.03	--	--	-7.22	--
20	-0.01	-0.76	--	--	1.36	--
21	-0.01	-0.76	--	--	1.36	--
22	0.08	-1.13	--	--	2.02	--
23	0.01	-1.44	--	--	2.56	--
24	0.01	-1.44	--	--	2.57	--
25	0.01	0.99	--	--	-1.79	--
26	-0.17	2.43	--	--	-4.37	--
27	-0.14	2.05	--	--	-3.69	--
28	-0.13	1.75	--	--	-3.16	--
29	-0.01	1.22	--	--	-2.16	--
30	0.02	2.20	--	--	-3.88	--
31	0.07	2.78	--	--	-4.90	--
32	-0.14	0.57	--	--	-1.06	--
33	-0.26	1.00	--	--	-1.87	--
34	-0.37	1.21	-427.2%	--	-2.26	--
35	0.09	0.94	--	--	-1.65	--
36	0.03	1.91	--	--	-3.36	--
37	-0.03	1.66	--	--	-2.90	--
38	0.02	2.24	--	--	-3.93	--
39	0.00	2.06	--	--	-3.60	--
40	-0.23	0.53	--	--	-1.04	--
41	-0.22	0.08	--	--	-0.24	--
42	-0.39	0.34	-187.2%	--	-0.72	--
43	-0.39	0.00	-100.0%	--	-0.12	--
	min = -427.2%			min = --		
	max = -100.0%			max = --		
	average = -238.1%			average = --		
	st. dev. = 138.4%			st. dev. = --		

Table F-56: Computed (FMR) versus Measured Results for Static Test Stresses at Section 10Z

	9B-GC-TC			(ksi)			9B-GC-W			(ksi)			9B-GC-BC			(ksi)		
Test	Measured	FMR	% Error	Measured	FMR	% Error	Measured	FMR	% Error	Measured	FMR	% Error	Measured	FMR	% Error	Measured	FMR	% Error
1	-0.10	-0.28	--		-0.08	0.11	--			0.37	0.50	35.1%						
2	-0.10	-0.30	--		-0.10	0.12	--			0.40	0.53	33.3%						
3	-0.07	-0.01	--		-0.06	0.01	--			0.02	0.03	--						
4	-0.01	0.39	--		0.02	-0.15	--			-0.56	-0.69	23.7%						
5	0.06	0.74	--		0.13	-0.28	--			-1.01	-1.30	28.4%						
6	0.09	0.55	--		0.23	-0.22	--			-0.68	-0.98	44.9%						
7	-0.31	-1.06	243.4%		-0.06	0.41	--			1.34	1.88	40.5%						
8	-0.31	-1.11	253.0%		-0.06	0.43	--			1.38	1.97	43.1%						
9	-0.29	-0.74	--		-0.06	0.29	--			0.86	1.31	51.5%						
10	-0.16	0.08	--		-0.01	-0.03	--			-0.31	-0.14	-55.3%						
11	0.41	1.79	341.6%		0.55	-0.69	-225.2%			-2.72	-3.17	16.5%						
12	0.83	2.58	212.6%		1.17	-0.99	-184.7%			-3.76	-4.56	21.4%						
13	0.86	2.27	164.5%		1.62	-0.87	-153.3%			-3.25	-4.00	23.2%						
14	1.11	1.99	78.9%		1.12	-0.76	-167.2%			-2.76	-3.50	26.9%						
15	0.20	1.46	--		0.32	-0.56	-272.9%			-1.83	-2.58	41.1%						
16	0.66	2.62	296.4%		1.03	-1.00	-197.3%			-3.50	-4.62	31.8%						
17	0.88	2.63	200.3%		1.19	-1.01	-184.5%			-3.72	-4.64	24.6%						
18	0.77	2.86	270.2%		1.55	-1.09	-170.2%			-3.67	-5.04	37.3%						
19	0.89	3.16	254.7%		1.80	-1.21	-167.0%			-4.18	-5.58	33.5%						
20	-0.22	-0.56	--		-0.17	0.22	--			0.82	1.00	21.5%						
21	-0.16	-0.57	--		-0.13	0.22	--			0.74	1.01	35.7%						
22	-0.48	-0.85	76.4%		-0.26	0.33	--			1.40	1.50	7.2%						
23	-0.68	-1.07	57.6%		-0.28	0.42	--			1.75	1.90	8.6%						
24	-0.56	-1.07	91.2%		-0.24	0.41	--			1.64	1.89	15.0%						
25	0.16	0.90	--		0.02	-0.34	--			-1.17	-1.58	34.9%						
26	0.46	2.07	346.5%		0.65	-0.79	-220.6%			-2.69	-3.65	35.8%						
27	0.42	1.78	323.2%		0.56	-0.68	-222.3%			-2.38	-3.14	32.0%						
28	0.39	1.56	304.9%		0.48	-0.60	-224.7%			-2.13	-2.75	29.0%						
29	0.01	0.43	--		0.08	-0.17	--			-0.95	-0.76	-19.7%						
30	0.07	0.74	--		0.21	-0.29	--			-1.54	-1.31	-15.0%						
31	0.07	0.88	--		0.31	-0.34	-208.0%			-1.91	-1.56	-18.5%						
32	0.19	1.07	--		0.27	-0.41	--			-1.54	-1.89	22.7%						
33	0.58	1.90	229.9%		0.69	-0.73	-205.1%			-2.55	-3.35	31.3%						
34	0.81	2.22	175.3%		1.17	-0.85	-172.8%			-2.89	-3.92	35.6%						
35	-0.11	0.09	--		-0.04	-0.04	--			-0.18	-0.17	--						
36	0.03	0.39	--		0.14	-0.16	--			-1.20	-0.70	-41.6%						
37	-0.07	0.09	--		0.08	-0.04	--			-0.99	-0.16	-83.9%						
38	-0.06	0.24	--		0.19	-0.10	--			-1.33	-0.43	-67.6%						
39	-0.12	0.01	--		0.14	-0.01	--			-1.11	-0.02	-98.2%						
40	0.56	1.68	202.5%		0.59	-0.64	-207.6%			-2.22	-2.95	33.1%						
41	0.60	1.45	143.4%		0.49	-0.54	-209.1%			-1.91	-2.53	32.8%						
42	0.58	1.85	217.1%		0.86	-0.70	-181.5%			-2.29	-3.25	42.1%						
43	0.56	1.69	201.8%		0.76	-0.63	-183.4%			-2.05	-2.95	44.0%						
	min = 57.6%			min = -272.9%			min = -98.2%			max = 346.5%			max = 51.5%			average = 213.0%		
	st. dev. = 83.8%			st. dev. = 27.8%			st. dev. = 35.8%			average = 15.1%			st. dev. = 35.8%					

Table F-57: Computed (FMR) versus Measured Results for Static Test Stresses at Section 9B

Test	9B-GC-TI			9B-GC-TE		
	Measured	FMR	% Error	Measured	FMR	% Error
1	-0.13	-0.32	--	-0.11	-0.31	--
2	-0.11	-0.34	--	-0.11	-0.33	--
3	-0.07	-0.02	--	-0.10	-0.02	--
4	-0.01	0.44	--	0.00	0.43	--
5	0.07	0.83	--	0.11	0.82	--
6	0.06	0.62	--	0.17	0.62	--
7	-0.40	-1.20	199.7%	-0.33	-1.17	251.2%
8	-0.41	-1.26	208.7%	-0.33	-1.23	271.8%
9	-0.38	-0.83	120.3%	-0.30	-0.82	--
10	-0.25	0.09	--	-0.11	0.09	--
11	0.36	2.01	464.5%	0.63	1.99	214.3%
12	0.82	2.89	252.3%	1.16	2.87	147.6%
13	0.89	2.53	184.2%	1.17	2.52	114.7%
14	1.21	2.22	84.1%	1.27	2.21	74.7%
15	0.29	1.64	--	0.44	1.63	271.4%
16	0.85	2.93	243.6%	1.13	2.91	156.5%
17	0.89	2.94	232.1%	1.11	2.92	163.1%
18	0.98	3.20	226.8%	1.37	3.18	131.4%
19	1.12	3.54	217.3%	1.54	3.52	128.8%
20	-0.16	-0.63	--	-0.23	-0.62	--
21	-0.16	-0.64	--	-0.23	-0.63	--
22	-0.23	-0.96	--	-0.29	-0.94	--
23	-0.40	-1.21	202.2%	-0.33	-1.18	254.2%
24	-0.40	-1.20	199.7%	-0.33	-1.18	254.2%
25	0.41	1.00	145.4%	0.50	1.00	99.7%
26	0.77	2.31	199.2%	1.02	2.30	125.8%
27	0.67	1.99	195.8%	0.98	1.99	103.2%
28	0.61	1.74	184.9%	0.93	1.75	88.7%
29	-0.02	0.50	--	0.07	0.46	--
30	0.00	0.86	--	0.21	0.79	--
31	-0.01	1.02	--	0.26	0.95	--
32	0.15	1.18	--	0.38	1.21	218.0%
33	0.59	2.10	258.2%	0.84	2.14	156.1%
34	0.85	2.46	188.8%	1.12	2.51	124.1%
35	0.00	0.13	--	-0.07	0.08	--
36	-0.04	0.47	--	0.18	0.40	--
37	-0.14	0.14	--	0.11	0.06	--
38	-0.13	0.31	--	0.15	0.22	--
39	-0.17	0.06	--	0.05	-0.04	--
40	0.56	1.84	228.6%	0.83	1.91	130.5%
41	0.65	1.57	142.2%	0.86	1.66	91.9%
42	0.67	2.01	201.8%	0.90	2.11	135.3%
43	0.66	1.82	176.2%	0.86	1.93	124.3%
	min = 84.1% max = 464.5% average = 206.8% st. dev. = 68.2%			min = 74.7% max = 271.8% average = 159.6% st. dev. = 61.4%		

Table F-58: Computed (FMR) versus Measured Results for Static Test Stresses at Section 9B

Test	9B-GC-BI (ksi)			9B-GC-BE (ksi)		
	Measured	FMR	% Error	Measured	FMR	% Error
1	0.40	0.53	32.4%	0.36	0.53	46.8%
2	0.43	0.57	34.0%	0.38	0.57	50.0%
3	0.03	0.03	--	-0.02	0.03	--
4	-0.53	-0.74	38.7%	-0.69	-0.74	6.5%
5	-0.95	-1.38	45.7%	-1.26	-1.39	10.0%
6	-0.79	-1.02	28.8%	-0.77	-1.06	37.5%
7	1.45	2.01	39.0%	1.36	2.00	47.6%
8	1.47	2.11	43.5%	1.42	2.10	48.4%
9	0.94	1.40	49.6%	0.89	1.39	56.5%
10	-0.26	-0.15	--	-0.39	-0.15	-61.5%
11	-2.59	-3.37	30.1%	-3.17	-3.38	6.7%
12	-3.53	-4.84	37.2%	-4.51	-4.88	8.2%
13	-3.09	-4.22	36.5%	-3.97	-4.29	8.1%
14	-2.62	-3.74	42.7%	-3.32	-3.72	11.9%
15	-1.70	-2.75	61.9%	-2.34	-2.76	17.8%
16	-3.22	-4.91	52.3%	-4.52	-4.94	9.4%
17	-3.51	-4.92	40.0%	-4.52	-4.97	9.8%
18	-3.59	-5.33	48.7%	-4.75	-5.42	14.1%
19	-4.10	-5.90	44.0%	-5.33	-5.99	12.3%
20	0.86	1.06	22.6%	0.74	1.06	42.6%
21	0.73	1.08	47.9%	0.74	1.07	43.9%
22	1.45	1.61	10.8%	1.09	1.60	46.8%
23	1.87	2.03	8.6%	1.36	2.02	49.1%
24	1.71	2.02	18.2%	1.36	2.01	48.3%
25	-1.00	-1.67	67.8%	-1.79	-1.69	-5.4%
26	-2.43	-3.86	59.0%	-3.81	-3.91	2.6%
27	-2.09	-3.32	58.5%	-3.45	-3.37	-2.3%
28	-1.81	-2.90	59.9%	-3.17	-2.96	-6.5%
29	-1.17	-0.83	-29.3%	-0.82	-0.80	-2.4%
30	-2.03	-1.42	-30.0%	-1.26	-1.37	9.0%
31	-2.74	-1.68	-38.7%	-1.37	-1.64	20.1%
32	-1.08	-1.99	85.0%	-2.13	-2.04	-4.0%
33	-1.70	-3.52	106.9%	-3.65	-3.61	-1.1%
34	-1.88	-4.11	118.1%	-4.25	-4.24	-0.3%
35	-0.43	-0.20	-54.0%	-0.09	-0.17	--
36	-1.67	-0.77	-53.8%	-0.89	-0.72	-18.8%
37	-1.50	-0.20	-86.6%	-0.60	-0.15	-75.2%
38	-2.12	-0.47	-77.9%	-0.71	-0.43	-39.2%
39	-1.90	-0.05	-97.4%	-0.49	-0.01	-98.0%
40	-1.31	-3.10	136.4%	-3.31	-3.19	-3.7%
41	-0.94	-2.65	180.5%	-2.98	-2.75	-7.8%
42	-1.25	-3.39	171.7%	-3.55	-3.53	-0.7%
43	-1.01	-3.08	205.6%	-3.31	-3.22	-2.7%
	min = -97.4%		min = -98.0%			
	max = 205.6%		max = 56.5%			
	average = 38.9%		average = 8.2%			
	st. dev. = 65.2%		st. dev. = 33.0%			

Table F-59: Computed (FMR) versus Measured Results for Static Test Stresses at Section 9B

	9B-GA-TC: NO DATA (ksi)			9B-GA-W (ksi)			9B-GA-BC (ksi)		
Test	Measured	FMR	% Error	Measured	FMR	% Error	Measured	FMR	% Error
1	--	-0.32	--	0.27	0.11	--	0.42	0.53	27.0%
2	--	-0.34	--	0.32	0.11	-66.9%	0.44	0.55	25.4%
3	--	-0.02	--	0.18	0.01	--	0.06	0.03	--
4	--	0.39	--	-0.23	-0.12	--	-0.56	-0.63	13.2%
5	--	0.71	--	-0.48	-0.23	-53.3%	-0.96	-1.16	21.0%
6	--	0.52	--	-0.35	-0.17	-52.4%	-0.64	-0.85	32.3%
7	--	-1.21	--	0.88	0.39	-56.1%	1.47	1.98	34.8%
8	--	-1.26	--	0.87	0.40	-54.7%	1.48	2.05	38.6%
9	--	-0.84	--	0.49	0.26	-46.5%	0.95	1.36	43.7%
10	--	0.04	--	-0.31	-0.01	-96.8%	-0.22	-0.06	--
11	--	1.75	--	-1.76	-0.56	-68.2%	-2.51	-2.87	14.4%
12	--	2.50	--	-2.32	-0.80	-65.8%	-3.46	-4.09	18.3%
13	--	2.22	--	-2.09	-0.71	-66.1%	-3.02	-3.64	20.7%
14	--	1.79	--	-1.57	-0.58	-63.5%	-2.47	-2.94	19.0%
15	--	1.43	--	-1.16	-0.45	-61.1%	-1.95	-2.33	19.3%
16	--	2.51	--	-2.19	-0.80	-63.8%	-3.41	-4.10	20.1%
17	--	2.48	--	-2.06	-0.79	-61.7%	-3.37	-4.06	20.4%
18	--	2.71	--	-2.45	-0.87	-64.7%	-3.59	-4.44	23.7%
19	--	3.01	--	-2.75	-0.96	-65.1%	-4.08	-4.93	20.8%
20	--	-0.65	--	0.62	0.20	-67.8%	0.80	1.05	31.0%
21	--	-0.64	--	0.62	0.21	-67.0%	0.80	1.05	31.0%
22	--	-0.95	--	0.83	0.30	-63.7%	1.19	1.55	29.9%
23	--	-1.21	--	0.88	0.38	-56.7%	1.47	1.97	34.1%
24	--	-1.22	--	0.88	0.38	-56.7%	1.47	1.98	34.8%
25	--	0.75	--	-0.66	-0.24	-63.5%	-1.11	-1.23	10.4%
26	--	1.84	--	-1.79	-0.59	-67.3%	-2.57	-3.01	17.1%
27	--	1.52	--	-1.54	-0.49	-68.6%	-2.18	-2.49	14.2%
28	--	1.27	--	-1.35	-0.41	-70.0%	-1.88	-2.08	10.9%
29	--	1.05	--	-1.02	-0.33	-67.7%	-1.41	-1.71	21.0%
30	--	1.86	--	-1.65	-0.59	-64.3%	-2.48	-3.04	22.4%
31	--	2.26	--	-2.06	-0.72	-65.3%	-3.10	-3.69	19.2%
32	--	0.37	--	-0.69	-0.12	-82.6%	-0.74	-0.61	-17.5%
33	--	0.64	--	-1.01	-0.20	-80.2%	-1.13	-1.04	-7.6%
34	--	0.73	--	-1.19	-0.23	-80.7%	-1.30	-1.19	-8.5%
35	--	0.83	--	-0.50	-0.26	-47.8%	-1.03	-1.35	30.9%
36	--	1.63	--	-1.43	-0.52	-64.0%	-2.13	-2.66	24.6%
37	--	1.43	--	-1.38	-0.45	-67.5%	-1.97	-2.33	18.1%
38	--	1.83	--	-1.73	-0.58	-66.4%	-2.49	-2.99	20.0%
39	--	1.69	--	-1.55	-0.54	-65.4%	-2.24	-2.76	23.0%
40	--	0.22	--	-0.72	-0.08	-88.8%	-0.70	-0.38	-45.4%
41	--	-0.16	--	-0.45	0.05	-111.0%	-0.29	0.26	--
42	--	-0.03	--	-0.68	0.01	-100.7%	-0.58	0.04	-106.9%
43	--	-0.33	--	-0.46	0.10	-120.8%	-0.27	0.52	--
	min = --			min = -120.8%			min = -106.9%		
	max = --			max = -46.5%			max = 43.7%		
	average = --			average = -69.0%			average = 15.9%		
	st. dev. = --			st. dev. = 15.5%			st. dev. = 25.5%		

Table F-60: Computed (FMR) versus Measured Results for Static Test Stresses at Section 9B

Test	9B-GA-TI: NO DATA (ksi)			9B-GA-TE (ksi)		
	Measured	FMR	% Error	Measured	FMR	% Error
1	--	-0.36	--	-0.05	-0.35	--
2	--	-0.38	--	-0.07	-0.37	--
3	--	-0.02	--	-0.09	-0.02	--
4	--	0.43	--	-0.09	0.43	--
5	--	0.79	--	-0.09	0.78	--
6	--	0.57	--	-0.09	0.57	--
7	--	-1.36	--	-0.34	-1.34	295.9%
8	--	-1.41	--	-0.35	-1.38	295.4%
9	--	-0.93	--	-0.34	-0.92	166.9%
10	--	0.04	--	-0.29	0.04	--
11	--	1.95	--	0.14	1.94	--
12	--	2.78	--	0.60	2.77	360.3%
13	--	2.47	--	0.70	2.46	252.2%
14	--	1.99	--	0.63	1.99	213.5%
15	--	1.59	--	-0.08	1.58	--
16	--	2.79	--	0.31	2.77	799.7%
17	--	2.76	--	0.58	2.75	371.1%
18	--	3.02	--	0.65	3.00	359.7%
19	--	3.35	--	0.82	3.34	306.3%
20	--	-0.72	--	-0.18	-0.71	--
21	--	-0.72	--	-0.21	-0.71	--
22	--	-1.06	--	-0.41	-1.05	158.2%
23	--	-1.35	--	-0.50	-1.33	164.8%
24	--	-1.36	--	-0.49	-1.34	174.5%
25	--	0.83	--	0.05	0.84	--
26	--	2.04	--	0.23	2.04	--
27	--	1.68	--	0.23	1.68	--
28	--	1.40	--	0.21	1.41	--
29	--	1.18	--	0.07	1.15	--
30	--	2.09	--	0.45	2.03	354.2%
31	--	2.54	--	0.78	2.47	217.6%
32	--	0.40	--	-0.11	0.42	--
33	--	0.68	--	-0.15	0.73	--
34	--	0.78	--	-0.20	0.83	--
35	--	0.94	--	-0.12	0.90	--
36	--	1.85	--	0.44	1.78	309.1%
37	--	1.63	--	0.38	1.55	313.2%
38	--	2.07	--	0.62	1.99	223.0%
39	--	1.92	--	0.58	1.83	213.5%
40	--	0.22	--	-0.16	0.28	--
41	--	-0.22	--	-0.17	-0.14	--
42	--	-0.08	--	-0.23	0.01	--
43	--	-0.41	--	-0.25	-0.31	--
	min = --			min = 158.2%		
	max = --			max = 799.7%		
	average = --			average = 292.1%		
	st. dev. = --			st. dev. = 138.8%		

Table F-61: Computed (FMR) versus Measured Results for Static Test Stresses at Section 9B

Test	9B-GA-BI			9B-GA-BE		
	Measured	FMR	% Error	Measured	FMR	% Error
1	0.40	0.56	40.1%	0.41	0.56	35.7%
2	0.41	0.59	42.5%	0.45	0.58	29.9%
3	-0.01	0.03	--	0.05	0.03	--
4	-0.52	-0.68	30.7%	-0.58	-0.67	15.5%
5	-0.88	-1.24	40.4%	-0.98	-1.23	25.7%
6	-0.42	-0.91	115.9%	-0.84	-0.90	7.7%
7	1.49	2.13	42.5%	1.44	2.10	46.0%
8	1.51	2.20	46.0%	1.47	2.17	47.9%
9	0.99	1.46	46.8%	0.94	1.44	53.2%
10	-0.11	-0.06	--	-0.24	-0.06	--
11	-2.26	-3.07	35.6%	-2.57	-3.05	18.5%
12	-3.22	-4.39	36.4%	-3.52	-4.34	23.2%
13	-2.71	-3.89	43.7%	-3.16	-3.87	22.5%
14	-2.16	-3.20	47.8%	-2.64	-3.07	16.2%
15	-1.68	-2.50	49.1%	-1.93	-2.48	28.7%
16	-2.99	-4.39	46.7%	-3.47	-4.35	25.4%
17	-3.18	-4.35	36.6%	-3.41	-4.31	26.2%
18	-2.66	-4.75	78.7%	-3.95	-4.72	19.5%
19	-3.12	-5.28	69.1%	-4.44	-5.24	18.0%
20	0.85	1.13	32.8%	0.85	1.12	31.6%
21	0.79	1.13	43.6%	0.85	1.11	30.5%
22	1.46	1.67	14.7%	1.20	1.64	37.2%
23	1.89	2.12	12.3%	1.44	2.09	45.3%
24	1.91	2.13	11.5%	1.44	2.10	46.0%
25	-0.76	-1.32	74.3%	-1.21	-1.31	8.0%
26	-1.91	-3.22	68.2%	-2.76	-3.20	15.8%
27	-1.52	-2.66	75.1%	-2.38	-2.64	10.7%
28	-1.21	-2.22	82.9%	-2.08	-2.21	6.4%
29	-1.45	-1.86	28.3%	-1.18	-1.80	52.0%
30	-2.75	-3.30	20.0%	-2.00	-3.19	59.8%
31	-3.40	-4.00	17.7%	-2.55	-3.87	52.0%
32	-0.26	-0.63	--	-1.04	-0.67	-35.3%
33	-0.37	-1.07	186.7%	-1.69	-1.15	-32.1%
34	-0.29	-1.23	--	-2.12	-1.32	-37.6%
35	-1.12	-1.47	31.0%	-0.66	-1.41	112.3%
36	-2.40	-2.90	20.7%	-1.64	-2.79	69.7%
37	-2.23	-2.55	14.6%	-1.45	-2.44	68.1%
38	-2.76	-3.25	17.7%	-1.93	-3.12	61.3%
39	-2.53	-3.01	18.9%	-1.68	-2.88	71.9%
40	0.07	-0.36	--	-1.29	-0.44	-65.9%
41	0.50	0.32	-36.2%	-0.92	0.22	-124.0%
42	0.39	0.10	-74.5%	-1.38	-0.02	-98.6%
43	0.70	0.62	-11.6%	-1.10	0.49	-144.7%
		min =	-74.5%		min =	-144.7%
		max =	186.7%		max =	112.3%
		average =	39.4%		average =	17.1%
		st. dev. =	40.4%		st. dev. =	50.6%

Table F-62: Computed (FMR) versus Measured Results for Static Test Stresses at Section 9B

Test	9N-GC-TC (ksi)			9N-GC-BC (ksi)		
	Measured	FMR	% Error	Measured	FMR	% Error
1	0.02	0.94	--	-1.54	-1.72	11.6%
2	0.06	1.01	--	-1.55	-1.85	19.2%
3	0.04	0.05	--	0.07	-0.08	--
4	0.01	-0.74	--	1.26	1.35	7.4%
5	0.02	-0.13	--	0.28	0.23	--
6	0.02	0.05	--	-0.02	-0.10	--
7	0.11	3.54	--	-5.63	-6.48	15.1%
8	0.15	3.73	--	-5.82	-6.82	17.1%
9	0.14	2.48	--	-3.81	-4.53	18.8%
10	0.04	0.11	--	0.03	-0.21	--
11	-0.27	-1.38	--	2.29	2.54	11.1%
12	-0.54	-0.92	71.3%	1.63	1.69	3.5%
13	-0.45	-0.05	-88.9%	0.13	0.11	--
14	-0.12	0.04	--	-0.16	-0.06	--
15	0.08	-0.26	--	0.54	0.49	-9.7%
16	-0.54	-0.88	63.8%	1.63	1.63	-0.2%
17	0.00	-0.80	--	0.00	1.48	--
18	-0.21	-0.87	--	1.57	1.61	2.8%
19	-0.51	-1.59	209.3%	2.75	2.91	5.6%
20	0.10	1.88	--	-2.93	-3.44	17.2%
21	0.10	1.91	--	-2.93	-3.49	18.9%
22	-0.02	2.84	--	-4.38	-5.20	18.7%
23	0.11	3.59	--	-5.63	-6.56	16.5%
24	0.11	3.57	--	-5.63	-6.53	16.0%
25	-0.36	1.67	-568.5%	-2.56	-3.04	18.9%
26	-0.38	1.08	-381.9%	-1.59	-1.96	23.0%
27	-0.37	2.04	-645.7%	-3.12	-3.71	19.0%
28	-0.35	2.77	-885.9%	-4.31	-5.05	17.2%
29	-0.05	-0.07	--	0.09	0.15	--
30	-0.08	-0.22	--	0.35	0.46	31.1%
31	-0.14	-0.40	--	0.57	0.81	42.8%
32	-0.11	-0.15	--	0.12	0.25	--
33	-0.28	-0.58	--	0.90	1.02	13.5%
34	-0.24	-1.13	--	1.83	2.01	9.6%
35	0.13	1.15	--	-1.41	-2.04	44.8%
36	-0.06	1.03	--	-1.34	-1.80	34.4%
37	-0.12	2.10	--	-2.82	-3.73	32.3%
38	-0.15	1.92	--	-2.61	-3.39	30.1%
39	-0.13	2.75	--	-3.77	-4.88	29.4%
40	-0.30	0.08	-126.5%	-0.42	-0.21	-50.5%
41	-0.38	0.66	-272.7%	-1.69	-1.31	-22.3%
42	-0.39	0.16	-141.0%	-0.89	-0.41	-54.1%
43	-0.41	0.60	-246.5%	-1.86	-1.23	-33.7%
	min = -885.9%			min = -54.1%		
	max = 209.3%			max = 44.8%		
	average = -251.1%			average = 11.0%		
	st. dev. = 309.0%			st. dev. = 22.2%		

Table F-63: Computed (FMR) versus Measured Results for Static Test Stresses at Section 9N

Test	9N-GA-TC (ksi)			9N-GA-BC (ksi)		
	Measured	FMR	% Error	Measured	FMR	% Error
1	0.02	0.98	--	-1.34	-1.56	16.3%
2	0.03	1.02	--	-1.35	-1.63	20.6%
3	0.10	0.05	--	0.12	-0.08	--
4	0.01	-0.66	--	0.89	1.05	18.2%
5	0.04	-0.14	--	0.25	0.22	--
6	0.01	0.04	--	0.01	-0.06	--
7	0.03	3.68	--	-5.13	-5.87	14.5%
8	0.02	3.82	--	-5.20	-6.09	17.2%
9	0.02	2.53	--	-3.44	-4.04	17.6%
10	0.02	0.27	--	-0.32	-0.43	33.2%
11	0.08	-1.39	--	1.90	2.21	16.2%
12	0.00	-0.85	--	1.28	1.35	5.6%
13	0.06	-0.09	--	0.14	0.12	--
14	0.05	0.03	--	-0.13	-0.04	--
15	0.09	-0.28	--	0.49	0.43	-12.0%
16	0.00	-0.85	--	1.28	1.34	4.8%
17	0.00	-0.83	--	0.00	1.31	--
18	0.09	-0.84	--	1.24	1.33	7.7%
19	0.00	-1.47	--	2.20	2.34	6.6%
20	-0.11	1.96	--	-2.72	-3.12	14.7%
21	-0.11	1.95	--	-2.72	-3.11	14.3%
22	0.01	2.89	--	-3.96	-4.60	16.3%
23	0.03	3.67	--	-5.13	-5.86	14.3%
24	0.03	3.69	--	-5.13	-5.88	14.7%
25	0.02	1.68	--	-2.34	-2.69	15.0%
26	-0.05	1.13	--	-1.52	-1.81	18.9%
27	-0.05	2.10	--	-2.89	-3.35	16.0%
28	-0.05	2.86	--	-3.97	-4.57	15.2%
29	0.10	-0.13	--	0.07	0.18	--
30	0.15	-0.50	--	0.55	0.75	36.5%
31	0.20	-0.98	--	1.19	1.52	27.9%
32	-0.06	-0.14	--	0.09	0.23	--
33	-0.13	-0.32	--	0.37	0.55	47.2%
34	-0.20	-0.48	--	0.59	0.81	37.8%
35	0.10	0.55	--	-0.88	-0.92	4.5%
36	0.06	0.19	--	-0.59	-0.36	-39.3%
37	-0.07	0.74	--	-1.56	-1.25	-19.7%
38	0.00	0.31	--	-1.03	-0.57	-44.7%
39	-0.08	0.73	--	-1.74	-1.25	-28.3%
40	-0.15	0.93	--	-1.24	-1.43	15.8%
41	-0.13	2.10	--	-2.75	-3.28	19.3%
42	-0.24	1.93	--	-2.59	-3.01	16.2%
43	-0.21	2.82	--	-3.74	-4.41	17.9%
	min = 0.0%		min = -44.7%			
	max = 0.0%		max = 47.2%			
	average = --		average = 11.3%			
	st. dev. = --		st. dev. = 19.2%			

Table F-64: Computed (FMR) versus Measured Results for Static Test Stresses at Section 9N

	9O-GC-TC			(ksi)			9O-GC-W			(ksi)			9O-GC-BC			(ksi)		
Test	Measured	FMR	% Error	Measured	FMR	% Error	Measured	FMR	% Error	Measured	FMR	% Error	Measured	FMR	% Error	Measured	FMR	% Error
1	0.08	0.87	--		0.37	-0.23	-162.6%		-1.15	-1.33	16.1%							
2	0.09	0.94	--		0.38	-0.25	-164.2%		-1.18	-1.43	21.1%							
3	0.02	0.23	--		0.16	-0.06	--		-0.27	-0.35	--							
4	0.00	0.40	--		0.41	-0.11	-125.5%		-0.53	-0.61	14.6%							
5	0.01	0.52	--		0.30	-0.14	-146.3%		-0.69	-0.80	16.0%							
6	-0.02	0.25	--		0.04	-0.07	--		-0.34	-0.38	11.7%							
7	0.47	3.28	604.3%		1.43	-0.86	-160.2%		-4.17	-5.00	20.0%							
8	0.72	3.46	378.2%		1.57	-0.91	-157.9%		-4.37	-5.28	20.9%							
9	0.63	2.43	287.1%		1.51	-0.64	-142.1%		-3.08	-3.70	20.1%							
10	0.49	1.68	242.5%		1.73	-0.44	-125.4%		-2.15	-2.56	19.1%							
11	0.44	1.36	208.0%		2.21	-0.36	-116.3%		-1.86	-2.08	11.6%							
12	0.68	1.79	164.0%		1.58	-0.48	-130.1%		-2.45	-2.74	11.7%							
13	0.64	1.32	105.8%		0.92	-0.36	-138.6%		-1.94	-2.03	4.8%							
14	0.22	0.21	--		0.16	-0.06	--		-0.52	-0.32	-37.9%							
15	-0.01	1.04	--		0.75	-0.28	-137.3%		-1.30	-1.60	22.9%							
16	0.50	1.83	264.3%		1.58	-0.49	-131.1%		-2.39	-2.81	17.5%							
17	0.00	1.80	--		0.00	-0.48	--		0.00	-2.75	--							
18	0.62	1.84	196.3%		1.74	-0.49	-128.2%		-2.56	-2.82	10.0%							
19	0.83	2.15	158.7%		2.37	-0.57	-124.0%		-3.02	-3.29	9.0%							
20	0.12	1.74	--		0.57	-0.46	-179.6%		-2.20	-2.65	20.3%							
21	0.07	1.77	--		0.57	-0.47	-181.3%		-2.27	-2.70	19.0%							
22	0.43	2.64	508.2%		1.06	-0.69	-164.9%		-3.23	-4.02	24.5%							
23	0.50	3.33	570.1%		1.43	-0.87	-160.9%		-4.10	-5.07	23.5%							
24	0.69	3.30	381.0%		1.43	-0.87	-160.9%		-4.15	-5.04	21.6%							
25	0.60	2.81	368.6%		1.48	-0.74	-149.6%		-3.57	-4.28	20.0%							
26	0.76	3.54	365.8%		2.50	-0.93	-137.2%		-4.64	-5.40	16.4%							
27	0.98	4.43	351.0%		2.96	-1.17	-139.4%		-5.77	-6.76	17.1%							
28	1.14	5.10	348.4%		3.29	-1.35	-140.9%		-6.65	-7.79	17.1%							
29	0.07	0.25	--		0.27	-0.07	--		-0.60	-0.39	-35.5%							
30	0.08	0.42	--		0.48	-0.12	-125.2%		-0.91	-0.66	-27.5%							
31	0.08	0.49	--		0.64	-0.14	-121.9%		-1.10	-0.77	-30.0%							
32	0.16	0.79	--		0.55	-0.21	-137.1%		-1.07	-1.20	11.7%							
33	0.39	1.39	256.7%		1.09	-0.36	-132.9%		-1.80	-2.11	17.1%							
34	0.52	1.60	204.8%		1.60	-0.41	-125.7%		-2.07	-2.42	16.9%							
35	0.05	1.41	--		0.58	-0.38	-165.1%		-1.65	-2.16	30.8%							
36	0.22	1.62	--		0.96	-0.44	-145.4%		-2.22	-2.49	12.0%							
37	0.38	2.66	598.2%		1.39	-0.71	-150.6%		-3.42	-4.07	18.9%							
38	0.39	2.70	587.1%		1.55	-0.72	-146.0%		-3.58	-4.13	15.5%							
39	0.56	3.49	524.4%		1.90	-0.93	-148.8%		-4.51	-5.35	18.7%							
40	0.44	1.96	343.4%		1.42	-0.51	-135.8%		-2.73	-2.98	9.1%							
41	0.62	2.44	292.7%		1.70	-0.64	-137.7%		-3.61	-3.72	3.2%							
42	0.59	2.70	361.1%		2.26	-0.71	-131.1%		-3.85	-4.11	6.8%							
43	0.62	3.09	395.3%		2.53	-0.81	-131.8%		-4.51	-4.70	4.1%							
	min = 105.8%			min = -181.3%			min = -37.9%			max = 604.3%			max = 30.8%			average = 11.2%		
	average = 348.7%			st. dev. = 141.6%			st. dev. = 16.1%			st. dev. = 15.6%								

Table F-65: Computed (FMR) versus Measured Results for Static Test Stresses at Section 9O

Test	9O-GC-TI (ksi)			9O-GC-TE (ksi)		
	Measured	FMR	% Error	Measured	FMR	% Error
1	0.10	0.96	--	0.06	0.96	--
2	0.10	1.03	--	0.07	1.04	--
3	0.02	0.26	--	-0.10	0.26	--
4	0.02	0.44	--	-0.03	0.44	--
5	0.02	0.58	--	-0.03	0.57	--
6	-0.03	0.28	--	-0.08	0.27	--
7	0.54	3.62	570.6%	0.58	3.63	524.3%
8	0.89	3.82	329.0%	0.85	3.82	350.5%
9	0.74	2.68	263.2%	0.77	2.69	248.2%
10	0.66	1.85	180.8%	0.63	1.85	195.0%
11	0.66	1.52	129.0%	0.76	1.50	96.4%
12	0.97	1.99	105.9%	0.86	1.97	130.3%
13	0.92	1.48	61.2%	0.75	1.45	94.0%
14	0.31	0.23	-25.8%	0.27	0.23	--
15	-0.05	1.16	--	-0.03	1.15	--
16	0.73	2.04	179.6%	0.51	2.02	296.1%
17	0.00	2.00	--	0.00	1.98	--
18	0.80	2.05	157.2%	0.69	2.03	195.0%
19	1.07	2.40	124.8%	0.96	2.37	146.0%
20	0.14	1.92	--	0.08	1.92	--
21	0.08	1.95	--	0.13	1.96	--
22	0.64	2.91	356.9%	0.33	2.92	793.0%
23	0.70	3.67	425.0%	0.43	3.68	751.9%
24	0.76	3.65	378.2%	0.72	3.65	406.3%
25	0.84	3.11	268.1%	0.58	3.10	439.0%
26	1.02	3.92	284.4%	0.84	3.90	364.0%
27	1.25	4.90	292.3%	1.12	4.88	335.9%
28	1.43	5.65	295.4%	1.35	5.63	315.9%
29	0.14	0.30	--	0.13	0.25	--
30	0.15	0.50	--	0.17	0.43	--
31	0.16	0.59	--	0.19	0.50	--
32	0.32	0.86	166.6%	0.26	0.89	--
33	0.66	1.51	129.4%	0.54	1.56	190.0%
34	0.87	1.74	100.7%	0.71	1.79	152.6%
35	0.03	1.57	--	0.00	1.55	--
36	0.33	1.81	441.8%	0.33	1.76	428.0%
37	0.59	2.96	404.2%	0.57	2.93	418.2%
38	0.61	3.00	395.6%	0.59	2.96	401.2%
39	0.80	3.87	386.1%	0.80	3.85	381.8%
40	0.72	2.15	197.3%	0.63	2.18	248.2%
41	0.97	2.70	177.9%	0.83	2.70	225.4%
42	1.00	2.97	197.8%	0.86	2.99	248.2%
43	1.06	3.41	223.0%	0.92	3.41	270.0%
	min = -25.8%		min = 94.0%		max = 793.0%	
	max = 570.6%		average = 320.2%		st. dev. = 169.9%	
	average = 248.2%		st. dev. = 132.6%			

Table F-66: Computed (FMR) versus Measured Results for Static Test Stresses at Section 9O

Test	9O-GC-BI (ksi)			9O-GC-BE (ksi)		
	Measured	FMR	% Error	Measured	FMR	% Error
1	-1.26	-1.44	14.4%	-1.28	-1.40	9.3%
2	-1.26	-1.55	23.2%	-1.35	-1.51	11.5%
3	-0.59	-0.38	-36.1%	-0.04	-0.37	--
4	-0.59	-0.64	9.3%	-0.62	-0.65	5.0%
5	-0.69	-0.85	24.0%	-0.86	-0.85	-0.9%
6	-0.35	-0.41	17.9%	-0.41	-0.40	-3.0%
7	-4.50	-5.43	20.6%	-4.76	-5.27	10.7%
8	-4.75	-5.72	20.5%	-4.99	-5.56	11.4%
9	-3.50	-4.02	14.8%	-3.41	-3.90	14.4%
10	-2.57	-2.75	7.0%	-2.29	-2.72	19.0%
11	-2.15	-2.21	2.9%	-2.10	-2.24	6.6%
12	-2.45	-2.93	19.7%	-3.07	-2.93	-4.5%
13	-1.99	-2.18	9.7%	-2.35	-2.16	-8.2%
14	-0.47	-0.34	-28.1%	-0.63	-0.34	-46.2%
15	-1.32	-1.71	29.7%	-1.65	-1.70	3.2%
16	-2.37	-3.00	26.6%	-3.10	-3.00	-3.3%
17	0.00	-2.95	--	0.00	-2.94	--
18	-2.97	-3.02	1.7%	-2.73	-3.01	10.2%
19	-3.43	-3.52	2.5%	-3.28	-3.53	7.6%
20	-2.39	-2.88	20.5%	-2.53	-2.79	10.2%
21	-2.41	-2.93	21.3%	-2.58	-2.84	9.9%
22	-3.59	-4.36	21.5%	-3.68	-4.24	15.1%
23	-4.57	-5.50	20.3%	-4.66	-5.34	14.6%
24	-4.64	-5.47	17.9%	-4.49	-5.30	18.0%
25	-3.86	-4.63	20.0%	-4.22	-4.53	7.3%
26	-4.93	-5.82	18.1%	-5.52	-5.73	3.9%
27	-6.13	-7.30	19.1%	-6.80	-7.16	5.3%
28	-7.11	-8.42	18.5%	-7.76	-8.25	6.3%
29	-0.89	-0.43	-51.7%	-0.44	-0.41	-7.6%
30	-1.51	-0.73	-51.5%	-0.55	-0.69	24.5%
31	-2.10	-0.84	-59.9%	-0.42	-0.81	91.2%
32	-0.70	-1.28	82.8%	-1.61	-1.29	-19.7%
33	-1.09	-2.24	105.0%	-2.83	-2.27	-19.8%
34	-1.30	-2.57	98.3%	-3.23	-2.61	-19.2%
35	-2.32	-2.32	0.1%	-1.46	-2.29	57.4%
36	-3.11	-2.68	-13.8%	-1.89	-2.64	39.4%
37	-4.61	-4.37	-5.3%	-3.06	-4.34	42.0%
38	-5.20	-4.43	-14.8%	-2.86	-4.40	53.9%
39	-6.32	-5.73	-9.3%	-3.86	-5.70	47.5%
40	-1.94	-3.21	65.2%	-4.03	-3.16	-21.6%
41	-2.73	-4.04	48.1%	-5.16	-3.91	-24.2%
42	-2.92	-4.45	52.2%	-5.55	-4.33	-22.0%
43	-3.55	-5.12	44.2%	-6.41	-4.94	-23.0%
	min = -59.9%		min = -46.2%			
	max = 105.0%		max = 91.2%			
	average = 15.4%		average = 8.1%			
	st. dev. = 34.1%		st. dev. = 25.1%			

Table F-67: Computed (FMR) versus Measured Results for Static Test Stresses at Section 9O

	9O-GA-TCH (ksi)			9O-GA-WH (ksi)			9O-GA-BCH (ksi)		
Test	Measured	FMR	% Error	Measured	FMR	% Error	Measured	FMR	% Error
1	0.16	0.84	--	0.38	-0.17	-144.6%	-1.06	-1.18	11.8%
2	0.26	0.87	--	0.28	-0.18	--	-1.06	-1.23	16.2%
3	0.22	0.20	--	-0.11	-0.04	--	-0.06	-0.28	--
4	0.06	0.35	--	0.19	-0.07	--	-0.35	-0.49	41.2%
5	0.11	0.49	--	0.06	-0.10	--	-0.51	-0.69	36.6%
6	0.14	0.24	--	-0.27	-0.05	--	-0.16	-0.34	--
7	0.88	3.15	257.6%	1.03	-0.65	-162.6%	-4.07	-4.44	9.0%
8	1.13	3.25	186.4%	1.08	-0.67	-161.8%	-4.14	-4.59	10.9%
9	0.79	2.26	187.9%	0.99	-0.47	-146.9%	-2.92	-3.19	9.2%
10	0.43	1.42	233.0%	1.17	-0.30	-125.2%	-1.90	-2.01	5.8%
11	-0.18	1.30	--	1.82	-0.27	-114.5%	-1.77	-1.83	3.1%
12	0.20	1.69	--	1.48	-0.35	-123.3%	-2.25	-2.38	5.6%
13	0.26	1.32	--	0.82	-0.27	-132.4%	-1.74	-1.85	6.0%
14	0.13	0.21	--	0.11	-0.04	--	-0.36	-0.29	-19.5%
15	0.24	0.98	--	0.19	-0.20	--	-1.20	-1.38	14.9%
16	0.20	1.69	--	1.06	-0.35	-132.4%	-2.25	-2.38	5.6%
17	0.00	1.66	--	0.00	-0.34	--	0.00	-2.34	--
18	0.11	1.70	--	1.09	-0.35	-131.6%	-2.19	-2.39	9.3%
19	0.09	1.97	--	1.85	-0.41	-121.8%	-2.58	-2.78	7.9%
20	0.35	1.68	375.5%	0.26	-0.35	--	-2.13	-2.37	11.3%
21	0.35	1.66	369.8%	0.37	-0.35	-193.2%	-2.13	-2.35	10.4%
22	0.74	2.46	231.5%	0.29	-0.51	--	-3.15	-3.47	10.1%
23	0.88	3.13	255.3%	0.61	-0.65	-206.6%	-4.07	-4.42	8.5%
24	0.88	3.15	257.6%	0.62	-0.65	-205.4%	-4.07	-4.45	9.2%
25	0.65	2.63	305.5%	0.88	-0.54	-160.8%	-3.45	-3.70	7.2%
26	0.51	3.34	549.5%	1.88	-0.69	-136.4%	-4.39	-4.71	7.2%
27	0.74	4.17	459.9%	2.50	-0.85	-134.0%	-5.50	-5.87	6.6%
28	0.89	4.82	443.5%	3.02	-0.99	-132.6%	-6.42	-6.79	5.8%
29	0.19	0.76	--	0.43	-0.15	-135.3%	-1.00	-1.06	6.5%
30	0.27	1.32	--	0.96	-0.27	-127.6%	-1.74	-1.85	6.1%
31	0.27	1.56	--	1.57	-0.32	-120.1%	-2.13	-2.19	2.7%
32	0.02	0.21	--	0.18	-0.05	--	-0.45	-0.31	-31.7%
33	-0.09	0.36	--	0.32	-0.08	-124.9%	-0.67	-0.52	-22.1%
34	-0.17	0.40	--	0.42	-0.09	-120.1%	-0.75	-0.57	-24.0%
35	0.41	1.28	208.5%	0.18	-0.26	--	-1.68	-1.80	7.4%
36	0.32	1.84	471.0%	1.22	-0.38	-130.7%	-2.58	-2.59	0.3%
37	0.30	2.31	659.9%	1.62	-0.47	-128.8%	-3.42	-3.24	-5.1%
38	0.30	2.52	737.6%	2.27	-0.51	-122.4%	-3.67	-3.54	-3.6%
39	0.29	2.83	--	2.51	-0.58	-122.9%	-4.18	-3.98	-4.8%
40	0.16	1.49	--	0.72	-0.31	-143.2%	-2.04	-2.11	3.5%
41	0.50	2.53	401.2%	1.22	-0.53	-143.0%	-3.35	-3.58	7.0%
42	0.35	2.59	632.4%	1.45	-0.54	-137.2%	-3.52	-3.67	4.4%
43	0.67	3.40	404.4%	1.92	-0.71	-136.7%	-4.53	-4.81	6.3%
	min = 186.4%			min = -206.6%			min = -31.7%		
	max = 737.6%			max = -114.5%			max = 41.2%		
	average = 381.4%			average = -140.6%			average = 5.1%		
	st. dev. = 160.8%			st. dev. = 23.3%			st. dev. = 12.9%		

Table F-68: Computed (FMR) versus Measured Results for Static Test Stresses at Section 9O

Test	9O-GA-TI (ksi)			9O-GA-TE (ksi)		
	Measured	FMR	% Error	Measured	FMR	% Error
1	0.29	0.92	--	0.32	0.92	188.4%
2	0.33	0.95	184.4%	0.38	0.96	149.9%
3	0.10	0.22	--	0.01	0.22	--
4	0.14	0.39	--	0.03	0.38	--
5	0.15	0.54	--	0.08	0.53	--
6	0.07	0.27	--	0.04	0.26	--
7	1.37	3.46	153.0%	1.47	3.47	136.8%
8	1.56	3.58	129.2%	1.79	3.58	100.2%
9	1.14	2.49	119.0%	1.43	2.49	73.9%
10	0.86	1.57	83.1%	0.87	1.57	80.5%
11	0.49	1.44	191.0%	0.43	1.42	232.5%
12	0.83	1.88	126.4%	0.60	1.85	210.7%
13	0.66	1.46	120.8%	0.53	1.44	172.2%
14	0.21	0.23	--	0.21	0.23	--
15	0.28	1.09	--	0.09	1.07	--
16	0.53	1.87	251.8%	0.23	1.85	--
17	0.00	1.84	--	0.00	1.82	--
18	0.51	1.89	268.6%	0.24	1.86	--
19	0.71	2.19	207.3%	0.37	2.16	478.0%
20	0.57	1.84	222.6%	0.58	1.85	218.0%
21	0.53	1.83	246.8%	0.51	1.83	255.8%
22	0.80	2.70	236.2%	0.80	2.71	238.9%
23	1.15	3.44	198.9%	1.14	3.45	203.0%
24	1.17	3.46	195.8%	1.28	3.47	171.9%
25	0.92	2.89	215.7%	0.73	2.89	297.8%
26	1.16	3.69	217.8%	0.88	3.67	315.2%
27	1.59	4.59	189.6%	1.32	4.58	245.9%
28	1.91	5.31	178.1%	1.67	5.29	216.6%
29	0.42	0.86	104.3%	0.34	0.81	139.0%
30	0.72	1.49	107.4%	0.54	1.42	160.6%
31	0.93	1.76	89.5%	0.68	1.68	146.0%
32	0.19	0.22	--	0.14	0.25	--
33	0.18	0.37	--	0.08	0.42	--
34	0.18	0.41	--	0.02	0.46	--
35	0.46	1.42	207.4%	0.31	1.40	349.8%
36	0.90	2.05	127.3%	0.70	2.00	186.7%
37	1.11	2.55	129.5%	0.83	2.52	203.1%
38	1.28	2.79	117.9%	0.93	2.75	195.3%
39	1.35	3.13	132.2%	0.98	3.10	216.7%
40	0.60	1.63	170.1%	0.54	1.65	204.6%
41	1.13	2.78	145.2%	1.09	2.79	155.3%
42	1.15	2.85	148.1%	1.01	2.87	184.6%
43	1.61	3.74	132.7%	1.52	3.75	146.7%
	min = 83.1% max = 268.6% average = 167.1% st. dev. = 50.1%			min = 73.9% max = 478.0% average = 202.4% st. dev. = 78.9%		

Table F-69: Computed (FMR) versus Measured Results for Static Test Stresses at Section 9O

Test	9O-GA-BI (ksi)			9O-GA-BE (ksi)		
	Measured	FMR	% Error	Measured	FMR	% Error
1	-1.01	-1.28	26.5%	-0.96	-1.25	30.7%
2	-1.09	-1.34	23.0%	-0.96	-1.29	35.0%
3	-0.03	-0.31	--	-0.41	-0.29	-29.0%
4	-0.43	-0.53	22.0%	-0.46	-0.52	14.2%
5	-0.67	-0.74	10.4%	-0.52	-0.73	41.0%
6	-0.38	-0.37	-3.3%	-0.21	-0.36	--
7	-3.82	-4.83	26.5%	-3.73	-4.70	26.0%
8	-3.93	-5.01	27.4%	-3.76	-4.84	28.6%
9	-2.64	-3.49	32.0%	-2.78	-3.35	20.4%
10	-1.53	-2.20	43.3%	-2.03	-2.11	4.2%
11	-1.40	-1.97	40.3%	-1.86	-1.94	4.1%
12	-2.20	-2.57	16.8%	-1.99	-2.53	26.9%
13	-1.67	-1.99	19.1%	-1.57	-1.97	25.4%
14	-0.32	-0.31	-1.8%	-0.29	-0.31	--
15	-1.35	-1.49	10.5%	-1.09	-1.47	35.0%
16	-2.24	-2.56	14.2%	-1.99	-2.53	26.9%
17	0.00	-2.53	--	0.00	-2.49	--
18	-2.04	-2.58	26.7%	-2.30	-2.55	10.7%
19	-2.41	-3.00	24.4%	-2.69	-2.95	9.8%
20	-2.14	-2.57	20.0%	-1.92	-2.50	29.9%
21	-2.12	-2.55	20.0%	-1.92	-2.49	29.4%
22	-3.18	-3.77	18.6%	-2.85	-3.67	28.6%
23	-4.01	-4.80	19.6%	-3.73	-4.68	25.4%
24	-3.97	-4.83	21.7%	-3.73	-4.70	26.0%
25	-3.42	-4.01	17.4%	-3.15	-3.93	24.7%
26	-4.33	-5.10	17.8%	-4.16	-4.99	19.9%
27	-5.30	-6.36	19.9%	-5.23	-6.22	19.0%
28	-6.12	-7.36	20.3%	-6.14	-7.20	17.4%
29	-1.11	-1.16	4.4%	-0.66	-1.11	68.8%
30	-2.05	-2.03	-1.0%	-1.10	-1.93	74.9%
31	-2.38	-2.40	1.0%	-1.51	-2.28	51.2%
32	-0.12	-0.31	--	-0.55	-0.35	-36.9%
33	-0.10	-0.53	--	-0.96	-0.58	-39.7%
34	0.02	-0.58	--	-1.22	-0.65	-46.6%
35	-2.20	-1.93	-12.2%	-1.17	-1.92	64.1%
36	-2.93	-2.80	-4.4%	-1.73	-2.74	58.3%
37	-3.81	-3.49	-8.4%	-2.29	-3.46	51.2%
38	-3.95	-3.81	-3.6%	-2.65	-3.76	41.8%
39	-4.57	-4.27	-6.5%	-3.01	-4.25	41.2%
40	-1.28	-2.28	77.8%	-2.32	-2.24	-3.4%
41	-2.41	-3.91	62.4%	-3.58	-3.77	5.2%
42	-2.44	-4.00	64.0%	-4.01	-3.87	-3.6%
43	-3.35	-5.26	57.2%	-4.97	-5.05	1.6%
	min = -12.2%		min = -46.6%			
	max = 77.8%		max = 74.9%			
	average = 20.1%		average = 21.5%			
	st. dev. = 20.4%		st. dev. = 27.0%			

Table F-70: Computed (FMR) versus Measured Results for Static Test Stresses at Section 9O

Appendix G

Strength Check Procedures of Composite Steel Curved Girder

Bridge Components for Load Rating

As published in Appendix B of Freisinger et al. (2004)

This appendix summarizes the strength check procedures for checking the components of Mn/DOT Bridge Number 69824 so as to assess the load rating of the bridge according to current load rating procedures. The following procedures are used to assess the rating of this bridge:

- The AASHTO Manual for Condition Evaluation and Load Resistance Factor Rating of Highway Bridges (LRFR) 2003, which directs users to the 1998 AASHTO LRFD Specifications, is used as the primary rating procedure for all bridge components. The 1998 AASHTO LRFD has been augmented with a new section 6.10 to assess the strength of an I-girder. The new section 6.10 has been balloted by AASHTO, but has not yet been published.
- Provisions from the AASHTO Guide Specifications for Horizontally Curved Steel Girder Highway Bridges (CGG) 2003, which is based on LFD methodology and directs users to AASHTO Standard Specifications 2002 for some provisions, have been incorporated as noted.
- This report provides photos and descriptions of each bridge component being checked, and the basic equations used to determine the strength of the component are summarized (service and fatigue conditions are not included in this report).

See above codes for variable definitions that are not listed in the following report.

MAIN GIRDER

From plans:

- Unit consists of five spans
- Web is 78"x ½" plate with the exception of pier 6-5 in which the girder tapers to a smaller size
- Flanges are 18"x 7/8" with the exception of the increased thicknesses over the piers
- Spans also vary in length



Influences the bridge behavior

- Shear resistance for strength limit state in LRFD is governed by the web
- Flexure resistance for strength limit state in LRFD is governed by the flanges

Current Mn/DOT Evaluation includes

- The BARS program does check shear and flexure based on the load factor method
- The flange strength in the BARS program is reduced to account for curvature of the bridge

Proposed Evaluation includes

- Shear
 - o Check the shear along the girder taking care to calculate the correct resistance for stiffened interior and end panel locations (LRFD 6.10.9)
 - o Check shear resistance (LRFD 6.10.9.1)
 - For interior panel fulfilling the tension-field requirement (LRFD 6.10.9.3.2)

$$\frac{2Dt_w}{(b_{fc}t_{fc} + b_{fi}t_{fi})} \leq 2.5$$

$$V_r = \varphi_v V_n = 1.00 \left(V_p \left[C + \frac{0.87(1-C)}{\sqrt{1 + \left(\frac{d_o}{D} \right)^2}} \right] \right)$$

where,

$$V_p = 0.58 F_{yw} D t_w$$

C = Ratio of shear buckling resistance to the shear yield strength (See AASHTO 6.10 for equations)

- For interior panel that does not meet tension-field requirement and end panels (LRFD 6.10.9.2,3,4)

$$V_r = \varphi_v V_n = 1.00 (V_p C)$$

- NOTE: For now, tension-field will not be used in main curved girder calculations. So the shear along the girder will be calculated as an end panel.
 - Flexure (Note: The main girders in this bridge are noncompact)
 - For composite noncompact section in positive flexure (LRFD 6.10.7.2.1)
 - In compression (resistance factor is 1.00 for flexure in all cases)
$$f_{bu} \leq \phi_f F_{nc}$$

where F_{nc} is the compression resistance of a fully braced flange

$$F_{nc} = R_b R_h F_{yc}$$
 - In tension
 - For composite section in negative flexure
 - In compression for partially braced flanges (LRFD 6.10.8.1.1)
$$f_{bu} + \frac{1}{3} f_l \leq \phi_f F_{nt}$$

where F_{nt} is the tension resistance

$$F_{nt} = R_h F_{yt}$$
- For composite section in negative flexure
- In compression for partially braced flanges (LRFD 6.10.8.1.1)
- $$f_{bu} + \frac{1}{3} f_l \leq \phi_f F_{nc}$$
- where F_{nc} is the smaller of local buckling or lateral torsional resistance
- Local Buckling Resistance
- If $\lambda_f \leq \lambda_{pf}$:
- $$F_{nc} = R_b R_h F_{yc}$$
- Otherwise:
- $$F_{nc} = \left[1 - \left(1 - \frac{F_{yr}}{R_h F_{yc}} \right) \left(\frac{\lambda_r - \lambda_{pf}}{\lambda_{rf} - \lambda_{pf}} \right) \right] R_b R_h F_{yc}$$
- where,
- $$\lambda_f = \frac{b_{fc}}{2t_{fc}}$$
- $$\lambda_{pf} = 0.38 \sqrt{\frac{E}{F_{yc}}}$$
- $$\lambda_{rf} = 0.56 \sqrt{\frac{E}{F_{yr}}}$$
- Lateral Torsional Buckling Resistance
- If $L_b \leq L_p$:
- $$F_{nc} = R_b R_h F_{yc}$$
- If $L_p < L_b \leq L_r$:
- $$F_{nc} = C_b \left[1 - \left(1 - \frac{F_{yr}}{R_h F_{yc}} \right) \left(\frac{L_b - L_p}{L_r - L_p} \right) \right] R_b R_h F_{yc} \leq R_b R_h F_{yc}$$

Otherwise:

$$F_{nc} = F_{cr} \leq R_b R_h F_{yc}$$

where,

L_b = unbraced length

$$L_p = r_t \sqrt{\frac{E}{F_{yc}}}$$

$$L_r = r_t \pi \sqrt{\frac{E}{F_{yr}}}$$

$$F_{cr} = \frac{C_b R_b \pi^2 E}{\left(\frac{L_b}{r_t}\right)^2}$$

- In tension for continuously braced flanges (LRFD 6.10.8.1.3)

$$f_{bu} \leq \phi_f R_h F_{yf}$$

where F_{yf} is the strength of the tension flange

- Ductility Requirement (LRFD 6.10.7.3)

$$D_p \leq 0.42 D_t$$

CGG Provisions

- Shear
 - Check shear resistance – tension-field action is not allowed at this time in the CGG (CGG 6.3.2)

$$V_{cr} = V_p C$$

$$V_p = 0.58 F_{yw} D t_w$$

- Flexure
 - General (CGG 5.1)
 - Limits on total factored lateral flange bending stress, f_l , and the largest computed factored average flange stress, f_b

$$f_l \leq 0.5 F_y$$

$$f_b \leq F_{cr}$$

If $f_b > \text{MIN}(0.33F_y, 17 \text{ ksi})$ also check:

$$\left| \frac{f_l}{f_b} \right| \leq 0.5$$

- Compact - Partially Braced Compression Flange (CGG 5.2.1)

$$F_{cr} = \min(F_{cr1}, F_{cr2})$$

$$F_{cr1} = F_{bs} \overline{\rho_b} \overline{\rho_w}$$

$$\overline{\rho_b} = \frac{1}{1 + \frac{12l}{b_f} \left(1 + \frac{2l}{b_f} \right) \left(\frac{l}{R} - 0.01 \right)^2}$$

$$\overline{\rho_w} = 0.95 + 18 \left(0.1 + \frac{l}{R} \right)^2 + \frac{f_l}{f_b} \frac{0.3 - 1.2 \frac{l}{R} \frac{l}{b_f}}{\overline{\rho_b} \left(\frac{F_{bs}}{F_y} \right)}$$

$$\overline{\rho_b} \overline{\rho_w} \leq 1.0$$

$$F_{bs} = F_y (1 - 3\lambda^2)$$

$$\lambda = \frac{1}{\pi} \left(\frac{12l}{b_f} \right) \sqrt{\frac{F_y}{E}}$$

$$F_{cr2} = F_y - \frac{|f_l|}{3}$$

- Noncompact – Partially Braced Compression Flange (CGG 5.2.2)

$$\frac{b_f}{t_f} \leq 1.02 \sqrt{\frac{E}{(f_b + f_l)}} \leq 23$$

$$F_{cr} = \min(F_{cr1}, F_{cr2})$$

$$F_{cr1} = F_{bs} \rho_b \rho_w$$

$$\rho_b = \frac{1}{1 + \frac{l}{R} \frac{12l}{R}}$$

If f_l/f_b is greater than or equal to zero, $p_w = \min(p_{w1}, p_{w2})$

If f_l/f_b is less than zero, $p_w = p_{w1}$

$$\rho_{w1} = \frac{1}{1 - \frac{f_l}{f_b} \left(1 - \frac{12l}{75b_f} \right)}$$

$$\rho_{w2} = \frac{0.95 + \frac{\frac{12l}{b_f}}{30 + 8000 \left(0.1 - \frac{l}{R} \right)^2}}{1 + 0.6 \left(\frac{f_l}{f_b} \right)}$$

$$F_{cr2} = F_y - |f_l|$$

- Partially Braced Tension Flange (CGG 5.3)

$$F_{cr} = \min(F_{cr1}, F_{cr2})$$

$$F_{cr1} = F_y \overline{\rho_b \rho_w}$$

$$F_{cr2} = F_y - \frac{|f_l|}{3}$$

- Continuously Braced Flanges (tension or compression) (CGG 5.4)
 - Lateral flange bending stresses need not be considered after flange is continuously braced

$$F_{cr} = F_y$$

- Web Bending Stress for transversely stiffened webs
 - Critical compressive strength (CGG 6.3.1)

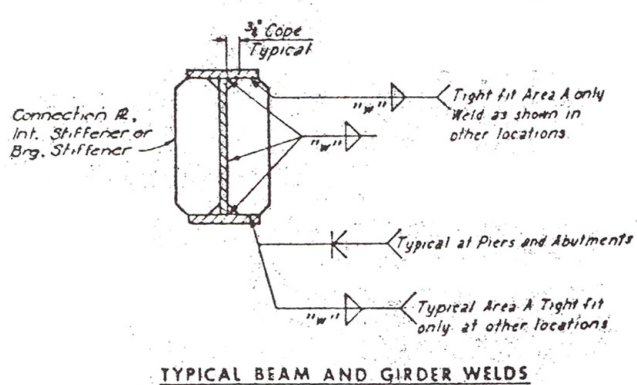
$$F_{cr} = \frac{0.9Ek}{\left(\frac{D}{t_w} \right)^2} \leq F_y$$

- Maximum tensile longitudinal stress must be less than F_y (CGG 6.1)

INTERMEDIATE STIFFENER

From plans:

- 1 stiffener located between diaphragms
- Not welded to tension flange in positive or negative region
- PL 5" x 3/8" typical (inside only)



Note: Weld "W" shall be the minimum size fillet weld as specified in current A.W.S. Specifications unless otherwise specified on the plans. The minimum size of any fillet weld shall be 1".

Influences the bridge behavior

- Shear resistance for strength limit state in LRFD

Current Mn/DOT Evaluation includes

- The BARS program does check shear, but the stiffeners are not checked directly by the program

Proposed Evaluation includes

- Check stiffener dimensions
 - o Projecting width (LRFD 6.10.11.1.2)

$$b_t \geq 2.0 + \frac{d}{30}$$

$$16t_p \geq b_t \geq \frac{b_f}{4}$$
 - o Moment of inertia (LRFD 6.10.11.1.3)

$$I_t \geq d_o t_w^3 J$$
 - o Area, if tension-field action is specified (LRFD 6.10.11.1.4)

$$A_s \geq \left[1.5B \frac{D}{t_w} (1-C) \left(\frac{V_u}{V_r} \right) - 18 \right] \frac{F_{yw}}{F_{crs}} t_w^2$$
- Check weld strength of fillet weld (LRFD 6.13.3.2.4)

$$R_r = \phi R_n = 0.6 \phi_{e2} F_{exx} t_e L \quad \phi_{e2} = 0.8$$

- Check shear resistance of base metal (LRFD 6.13.5.3)

$$R_r = \phi R_n = 1.00 * 0.58 A_g F_y$$

CGG Provisions

- Check stiffener dimensions (CGG 6.5)
 - o Width-to-thickness ratio

$$\frac{b_s}{t_s} \leq 0.48 \sqrt{\frac{E}{F_y}}$$

- o Width and thickness dimensions

$$b_s \geq 2 + \frac{D}{30} \text{ and } \frac{1}{4} b_f$$

$$t_s \leq \frac{b_f - t_w}{2} - 1$$

- o Moment of inertia

$$I_{ts} = d_o t_w^3 J$$

$$J = \left[\left(\frac{1.58}{\frac{d}{D}} \right)^2 - 2 \right] X \geq 0.5$$

If a is less than or equal to 0.78

$$X = 1.0$$

If a is greater than 0.78, but less than or equal to 1.0

$$X = 1 + \left(\frac{a - 0.78}{1775} \right) Z^4$$

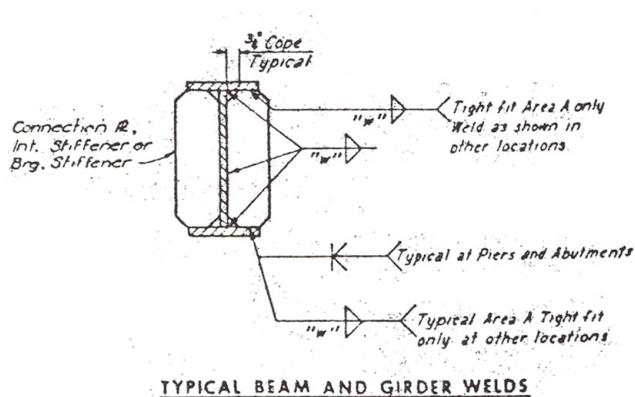
$$a = \frac{d_o}{D}$$

$$Z=\frac{0.079d_o^2}{Rt_w}\leq10$$

DIAPHRAGM STIFFENER

From plans:

- Used as the connection plate to attach the diaphragms to the web of the girder
- Located about every 11'-13' along girder
- Not welded to tension flange in positive or negative region
- PL 8.5" x 1/2" typical (inside only)



Note: Weld "w" shall be the minimum size fillet weld as specified in current A.W.S. Specifications unless otherwise specified on the plans. The minimum size of any fillet weld shall be 1".

Influences the bridge behavior

- Stiffener influences shear resistance for strength limit state in LRFD
- Connection influences moment and shear being passed from the diaphragms into the main girder

Current Mn/DOT Evaluation includes

- The BARS program does check shear, but the stiffener is not checked directly by the program. The connection is not checked in the program either. It must be assumed to be sufficient.

Proposed Evaluation includes

- Special connection stiffener provision (LRFD 6.10.11.1.1)
 - o If the following is met, the connection plate must only satisfy the provisions in 6.10.11.2. Otherwise all provisions apply.

$$\frac{D}{t_w} \leq 2.5 \sqrt{\frac{E}{F_{yw}}}$$

- Check stiffener dimensions
 - o Projecting width (LRFD 6.10.11.1.2)

$$b_t \geq 2.0 + \frac{d}{30}$$

$$16t_p \geq b_t \geq \frac{b_f}{4}$$

- Moment of inertia (LRFD 6.10.11.1.3)

$$I_t \geq d_0 t_w^3 J$$

- Area, if tension field action is specified (LRFD 6.10.11.1.4)

$$A_s \geq \left[1.5B \frac{D}{t_w} (1-C) \left(\frac{V_u}{V_r} \right) - 18 \right] \frac{F_{yw}}{F_{crs}} t_w^2$$

- Check eccentrically loaded bolt group for shear and moment at end of diaphragm
 - Use elastic method of eccentrically loaded bolt groups to obtain force on each bolt
 - Slip Resistance at service loads (LRFD 6.13.2.8)

$$R_r = K_h K_s N_s P_t$$

- Bearing Resistance (LRFD 6.13.2.9)

If $L_c < 2 * \text{diameter of bolt}$

$$R_r = \phi_{bb} R_n = \phi_{bb} (1.2 L_c t F_u) \quad \phi_{bb} = 0.8$$

- Shear Resistance (LRFD 6.13.2.7)

If bolts are excluded from plane:

$$R_r = \phi_s R_n = \phi_s (0.48 A_b F_{ub} N_s) \quad \phi_s = 0.80$$

- Check weld for shear and moment at end of diaphragm (LRFD 6.13.3.2.4)
 - Use vector addition to obtain the total force on the weld

$$R_r = \phi R_n = 0.6 \phi_{e2} F_{exx} t_e L \quad \phi_{e2} = 0.8$$

- Check shear resistance of base metal (LRFD 6.13.5.3)

$$R_r = \phi R_n = 1.00 * 0.58 A_g F_y$$

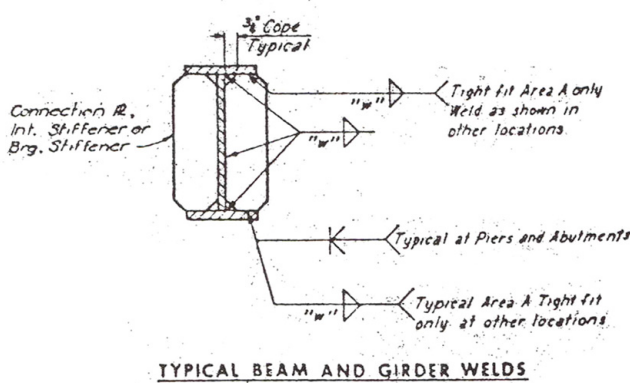
CGG Provisions

- Same stiffener provisions listed for the intermediate stiffeners – see the equations above.
- Design connection according to the provisions in AASHTO Standard Specifications

BEARING STIFFENER

From plans:

- 1 pair located on each girder at each pier
- Not welded to tension flange in positive or negative region
- PL 8.5" x varying thickness (inside and outside)



Influences the bridge behavior

- Shear resistance for strength limit state in LRFD

Current Mn/DOT Evaluation includes

- The BARS program does check shear, but the stiffeners are not checked directly.

Proposed Evaluation includes

- Check stiffener dimensions
 - o Projecting width (LRFD 6.10.11.2.2)

$$b_f < 0.48t_p \sqrt{\frac{E}{F_{ys}}}$$

- Check bearing resistance (LRFD 6.10.11.2.3)

$$(R_{sb})_r = \phi_b (R_{sb})_n = 1.00(1.4A_{pn}F_{ys})$$

- Check axial resistance as a compression member (LRFD 6.10.11.2.4)
 - o K=0.75, Effective web is 18*t_w centered on stiffeners

$$P_r = \phi_c P_n = 0.9P_n$$

If lambda < 2.25

$$P_n = 0.66^\lambda F_y A_s$$

Else

$$P_n = \frac{0.88F_y A_s}{\lambda}$$

$$\lambda = \left[\frac{KL}{r_s \pi} \right]^2 \frac{F_y}{E}$$

- Check weld strength of fillet weld (LRFD 6.13.3.2.4)

$$R_r = \phi R_n = 0.6 \phi_{e2} F_{exx} t_e L \quad \phi_{e2} = 0.8$$

- Check shear resistance of base metal (LRFD 6.13.5.3)

$$R_r = \phi R_n = 1.00 * 0.58 A_g F_y$$

CGG Provisions

- Check stiffener dimensions (CGG 6.7 – refers to CGG 6.5)
 - o Width-to-thickness ratio

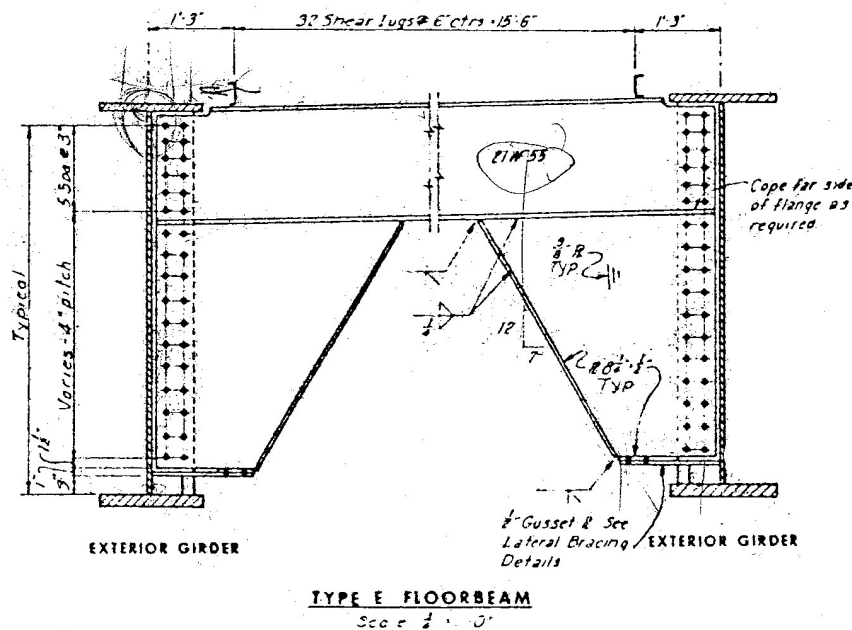
$$\frac{b_s}{t_s} \leq 0.48 \sqrt{\frac{E}{F_y}}$$

- Bearing Resistance
 - o $18*t_w$ centrally located portion of the web can be considered effective between the stiffeners
 - o Factored bearing stress shall be less than $1.35*F_y$
- Axial Resistance
 - o Applied concentrically with respect to centroidal axes of bearing stiffener
 - Design as a centrally loaded compression member according to AASHTO 10.54.1 with $K=0.75$
 - o Eccentrically loaded concentrated load
 - Consider stiffener as a beam-column according to AASHTO 10.54.2 with $K=0.75$ and $C=1.0$

DIAPHRAGMS (OR FLOORBEAMS)

From plans:

- Located about every 11-12' along girder
- Connected to girder through the connection stiffener
- Consists of a W21x55, with knee beams made of 3/8" thick plates as shown in detail below



Influences the bridge behavior

- Flexural Moment and Shear shall be evaluated for strength limit state in LRFD

Current Mn/DOT Evaluation includes

- BARS does not check the diaphragm specifically.

Proposed Evaluation includes

- Same calculations as for the main girder, but $f_i=0$ since there is no warping being considered in the diaphragms. See above proposed evaluation for the main girder for more details, except as noted below:

- Since the midspan diaphragm section is compact, in the positive flexure region (LRFD 6.10.7.1.1)

$$M_u \leq \phi_f * M_n$$

where M_n is determined through equations involving the yield moment and the plastic moment

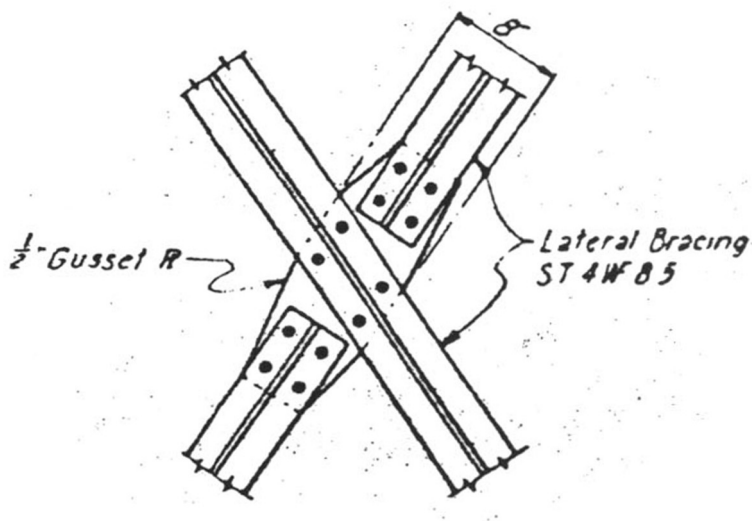
CGG Provisions

- Design according to the provisions in AASHTO Standard Specifications

LATERAL BRACING AND CONNECTION AT CROSSING

From plans:

- Lateral bracing is connected at their crossing point between girders
- All connections are bolted



Influences the bridge behavior

- Axial resistance for strength limit state in LRFD

Current Mn/DOT Evaluation includes

- The BARS program does not check the connections separately. The program must assume that the connections are sufficient to carry the loads.

Proposed Evaluation includes

- Tension Member (LRFR 6.6.6)
 - o Check yielding on gross section and fracture on net section (LRFD 6.8.2)

$$P_r = \phi_t P_n = 0.95 F_y A_g$$

$$P_r = \phi_u P_n = 0.8 F_u A_n U$$
 - o Block shear rupture resistance (LRFD 6.13.4)
 - If $A_{tn} \geq 0.58 * A_{vn}$

$$R_r = \phi_{bs} R_n = 0.8(0.58 F_y A_{vg} + F_u A_{tn})$$
 - Else

$$R_r = \phi_{bs} R_n = 0.8(0.58 F_u A_{vn} + F_y A_{tg})$$
- Non-composite compression member (LRFR 6.6.7)

- Check as non-slender or slender element as appropriate for largest compressive load without buckling (LRFD 6.9.4.2)

$$P_r = \phi_c P_n = 0.9 P_n$$

If $\lambda < 2.25$ $P_n = 0.66^\lambda F_y A_s$

Else $P_n = \frac{0.88 F_y A_s}{\lambda}$

$$\lambda = \left[\frac{KL}{r\pi} \right]^2 \frac{F_y}{E}$$

- Check connection plate for yielding, fracture, block shear, and compression using the equations listed above but using the Whitmore section for the effective area of the gusset plate
- Check bolts
 - Slip Resistance at service loads (LRFD 6.13.2.8)

$$R_r = K_h K_s N_s P_t$$
 - Bearing Resistance (LRFD 6.13.2.9)

If $L_c < 2 * \text{diameter of bolt}$

$$R_r = \phi_{bb} R_n = \phi_{bb} (1.2 L_c t F_u) \quad \phi_{bb} = 0.8$$
 - Shear Resistance (LRFD 6.13.2.7)

If bolts are excluded from plane:

$$R_r = \phi_s R_n = \phi_s (0.48 A_b F_{ub} N_s) \quad \phi_s = 0.80$$

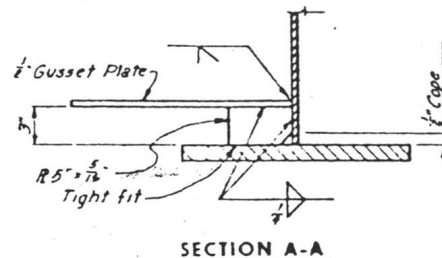
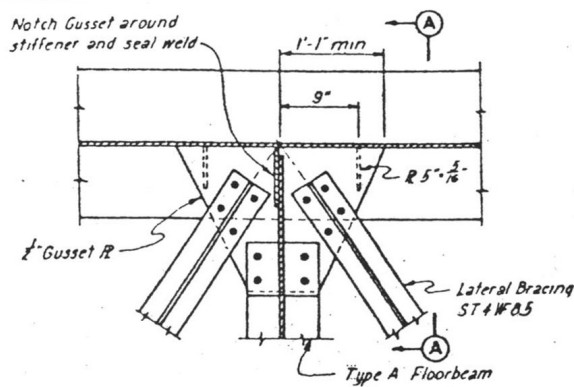
CGG Provisions

- Design according to the provisions in AASHTO Standard Specifications

SHELF PLATE CONNECTION

From plans:

- Located at each diaphragm to connect bottom of diaphragm and lateral bracing to main girders
- All connections are bolted



Note:
Lateral Bracing, Floorbeam, and
Girder Stiffener not shown in section

Influences the bridge behavior

- Axial resistance for strength limit state in LRFD

Current Mn/DOT Evaluation includes

- The BARS program does not check the connections separately. The program must assume that the connections are sufficient to carry the loads.

Proposed Evaluation includes

- For the lateral bracing connection and the diaphragm connection to the gusset plate:
 - o Check connection plate for yielding, fracture, block shear, and compression using the whitmore section
 - Tension Member (LRFR 6.6.6)
 - Check yielding on gross section and fracture on net section (LRFD 6.8.2)

$$P_r = \phi_t P_n = 0.95 F_y A_g$$

$$P_r = \phi_u P_n = 0.8 F_u A_n U$$

Block shear rupture resistance (LRFD 6.13.4)

If $A_{tn} \geq 0.58 * A_{vn}$

$$R_r = \phi_{bs} R_n = 0.8(0.58 F_y A_{vg} + F_u A_{tn})$$

Else

$$R_r = \phi_{bs} R_n = 0.8(0.58 F_u A_{vn} + F_y A_{tg})$$

- Check as non-slender or slender element as appropriate for largest compressive load without buckling (LRFD 6.9.4.2)

$$P_r = \phi_c P_n = 0.9 P_n$$

$$\text{If } \lambda < 2.25 \quad P_n = 0.66^2 F_y A_s$$

$$\text{Else} \quad P_n = \frac{0.88 F_y A_s}{\lambda}$$

$$\lambda = \left[\frac{KL}{r\pi} \right]^2 \frac{F_y}{E}$$

- Check bolts connection the lateral bracing and the diaphragm

- Slip Resistance at service loads (LRFD 6.13.2.8)

$$R_r = K_h K_s N_s P_t$$

- Bearing Resistance (LRFD 6.13.2.9)

If $L_c < 2 * \text{diameter of bolt}$

$$R_r = \phi_{bb} R_n = \phi_{bb} (1.2 L_c t F_u) \quad \phi_{bb} = 0.8$$

- Shear Resistance (LRFD 6.13.2.7)

If bolts are excluded from plane:

$$R_r = \phi_s R_n = \phi_s (0.48 A_b F_{ub} N_s) \quad \phi_s = 0.80$$

- Check welds (LRFD 6.13.3.2.4)

- Determine the resultant forces on the welds parallel and perpendicular to the main girder

$$R_r = \phi R_n = 0.6 \phi_{e2} F_{exx} t_e L \quad \phi_{e2} = 0.8$$

- Check shear resistance of base metal (LRFD 6.13.5.3)

$$R_r = \phi R_n = 1.00 * 0.58 A_g F_y$$

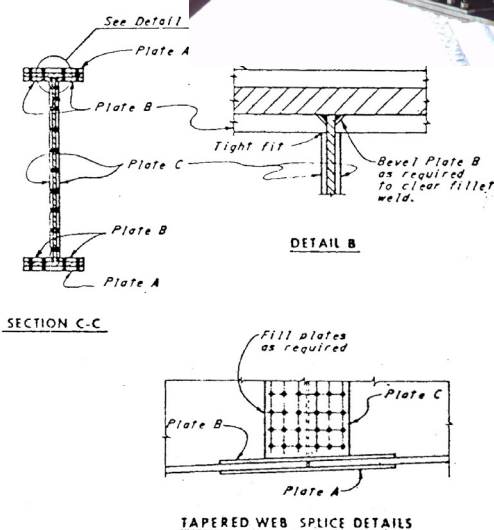
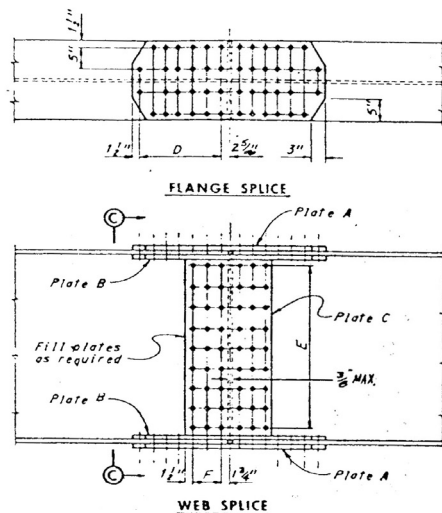
CGG Provisions

- Design according to the provisions in AASHTO Standard Specifications

FIELD SPLICE

From plans:

- Bolted connection between web and flanges



FLANGE SPLICES			
FLANGE PLATE	BOLTED OR RIVETED ALTERNATE PLATE A	PLATE C	PLATE B
18" x 2"	18" x 2"	5"	5 Spcs @ 3"
			D

When splicing plates of unequal thickness, the splice for the smaller plate shall be used. Use fill plates as required at these locations. Fill plates shall not be extended beyond flange splice plates.

WEB SPLICES							
WEB PLATE	BOLTED ALTERNATE			RIVETED ALTERNATE			
	PLATE C	E	F	PLATE C	E	F	
69 1/8" x 2"	19 1/8"	15 Spcs @ 4 1/2"	2 Spcs @ 3"	25 1/8" x 2"	16 Spcs @ 4"	3 Spcs @ 3"	
70 1/8" x 2"	19 1/8"	16 Spcs @ 4 1/2"	2 Spcs @ 3"	25 1/8" x 2"	18 Spcs @ 4"	3 Spcs @ 3"	

(1) Web depth is approximate only. Use this splice for Field Splice 4.

GIRDER FIELD SPLICES

Influences the bridge behavior

- Flexural moment and shear force shall be evaluated for strength limit state in LRFD

Current Mn/DOT Evaluation includes

- The BARS program does not check connections specifically.

Proposed Evaluation includes

- Check the field splice according to (LRFD 6.13.6)
- Flange Splice

- Controlling flange (with larger ratio of elastic flexural stress to factored flexural resistance) is proportioned to provide a minimum resistance of the design stress, F_{cf} , times the effective area specified in LRFD 6.10.3.6 (LRFD 6.13.6.1.4c)

$$F_{cf} = \frac{\left(\left| \frac{f_{cf}}{R_h} \right| + \alpha \phi_f F_{yf} \right)}{2} \geq 0.75 \alpha \phi_f F_{yf}$$

- Then check for compression with $L_u=0$
- Noncontrolling flange

$$F_{ncf} = R_{cf} \left| \frac{f_{ncf}}{R_h} \right| \geq 0.75 \alpha \phi_f F_{yf}$$

- Then check for yielding, fracture, and block shear on the flange section
- Bolts

- Slip Resistance at service loads (LRFD 6.13.2.8)

$$R_r = K_h K_s N_s P_t$$

- Bearing Resistance (LRFD 6.13.2.9)

If $L_c < 2 \times \text{diameter of bolt}$

$$R_r = \phi_{bb} R_n = \phi_{bb} (1.2 L_c t F_u) \quad \phi_{bb} = 0.8$$

- Shear Resistance (LRFD 6.13.2.7)

If bolts are excluded from plane:

$$R_r = \phi_s R_n = \phi_s (0.48 A_b F_{ub} N_s) \quad \phi_s = 0.80$$

- Web Splice (LRFD 6.13.6.1.4b and C6.13.6.1.4b)

- Determine design forces for the web splice plates and bolts

- Shear Force

- If $V_u < 0.5 * V_r$ then: $V_{uw} = 1.5 * V_u$
- Else, $V_{uw} = (1/2) * (V_u + V_r)$

- Design Moment

$$M_{uw} = \frac{t_w D^2}{2} \left| R_h F_{cf} - R_{cf} f_{ncf} \right|$$

- Design Horizontal Force (to balance moment)

$$H_{uw} = \frac{t_w D}{2} (R_h F_{cf} + R_{cf} f_{ncf})$$

- Bolts – check slip resistance, bearing resistance, and shear resistance against the force determined from vector addition in the extreme bolt from the forces calculated above
- Web Plate
 - Flexure due to web moment and horizontal force against the yield strength of the steel

$$f = \frac{M_{uw}}{Spl} + \frac{H_{uw}}{Apl} < \phi f_y$$

- Shear due to yielding, fracture, and block shear
 - Check yielding on gross section and fracture on net section (LRFD 6.8.2)

$$P_r = \phi_t P_n = 0.95 F_y A_g$$

$$P_r = \phi_u P_n = 0.8 F_u A_n U$$
 - Block shear rupture resistance (LRFD 6.13.4)

If $A_{tn} \geq 0.58 * A_{vn}$

$$R_r = \phi_{bs} R_n = 0.8(0.58 F_y A_{vg} + F_u A_{tn})$$

Else

$$R_r = \phi_{bs} R_n = 0.8(0.58 F_u A_{vn} + F_y A_{tg})$$

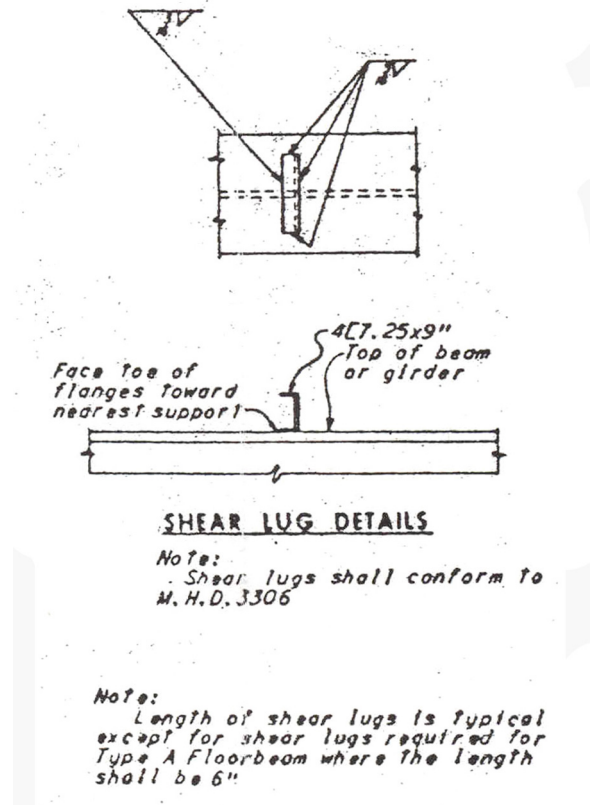
CGG Provisions

- Design according to the provisions in AASHTO Standard Specifications

SHEAR LUGS

From plans:

- Located along main girders and diaphragms as various spacing
- No shear lugs located in negative region



Influences the bridge behavior

- Shear resistance of stud for strength limit state in LRFD

Current Mn/DOT Evaluation includes

- The BARS program does check shear and flexure, but the program does not check the shear lugs separately. The program must assume that there are adequate shear lugs to transfer the forces between the steel and concrete.

Proposed Evaluation includes

- Check number of lugs required, between the point of maximum moment and each adjacent point of zero moment, for strength limit state determined by dividing the total nominal shear force, P (maximum force the concrete or steel can support), by the factored shear resistance of one shear connector, Q_r (LRFD 6.10.10.4.1)
 - o Shear channel connector strength, Q_r

$$Q_r = \phi_{sc} Q_n = 0.85 \left(0.3(t_f + 0.5t_w) L_c \sqrt{f'_c E_c} \right)$$

- o Total nominal shear force, P

$$P = P_p = \min(P_{1p}, P_{2p})$$

$$P_{1p} = 0.85 f'_c b_s t_s$$

$$P_{2p} = F_{yw}Dt_w + F_{yt}b_{ft}t_{ft} + F_{yc}b_{fc}t_{fc}$$

- If the shear lugs on the bridge are less than the shear lugs required for full composite action, then the load transferred due to partial composite action will be investigated.

CGG Provisions

- Shear lugs are required along the length of the girder (positive and negative moment regions), but in this case only the positive moment region has shear lugs
- Check number of lugs required, between the point of maximum moment and an adjacent end of the girder, for strength limit state determined by dividing the total nominal shear force, P (maximum force the concrete or steel can support with the additional radial force taken into account), by the factored shear resistance of one shear connector, S_r (LRFD 6.10.10.4.1)
 - o Shear channel connector strength, S_r (AASHTO 10.38.5.1.2)

$$S_r = \phi_{sc} S_u = 0.85 \left(550 \left(h + \frac{t}{2} \right) W \sqrt{f'_c} \right)$$

- o Total nominal shear force, P

$$P = \sqrt{P_p^2 + F_p^2}$$

$$\overline{P_p} = \min(P_{1p}, P_{2p})$$

$$P_{1p} = F_y A_s$$

$$P_{2p} = 0.85 f'_c b_d t_d$$

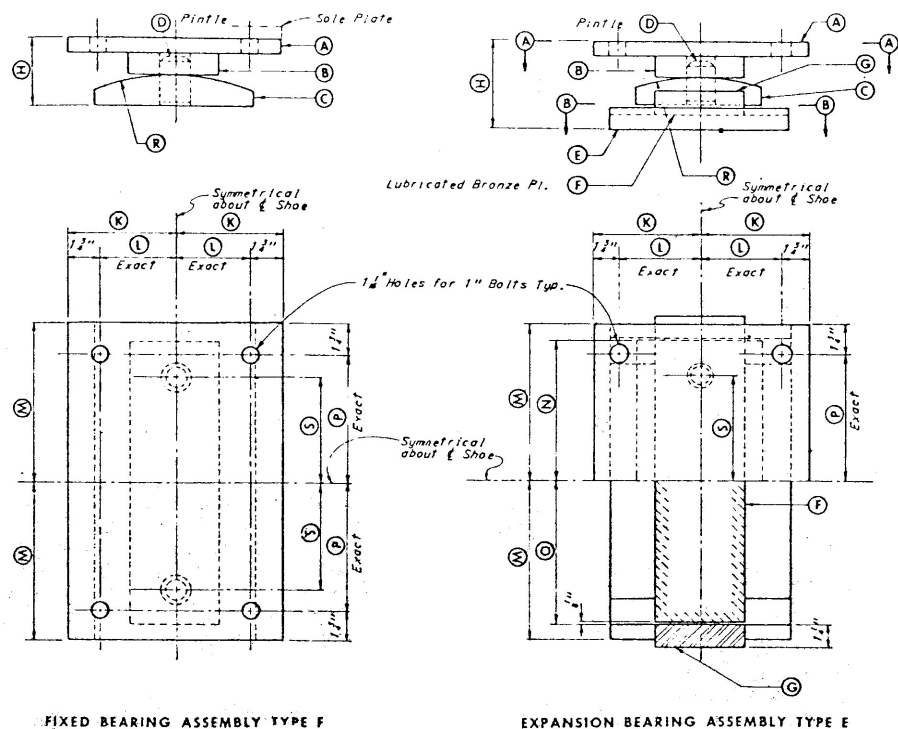
$$\overline{F_p} = \overline{P_p} \frac{L_p}{R}$$

- If the shear lugs on the bridge are less than the shear lugs required for full composite action, then the load transferred due to partial composite action will be investigated.

BEARINGS

From plans:

- Located at each pier
- Fixed (Type F) – Piers 7 and 8
- Expansion (Roller, Type E) – Piers 5, 6, 9, and 10



Influences the bridge behavior

- Bearing resistance of force transfer between girders and piers for strength limit state in LRFD

Current Mn/DOT Evaluation includes

- The BARS program must assume that the bearings are adequate to transfer the force between the girders and the piers.

Proposed Evaluation includes

- Determining the longitudinal forces, lateral forces, and vertical forces acting on the bearing from the forces acting through the lateral bracing, the diaphragms, and the main girder
- Check the shear resistance of the bolts connecting the sole plate to the top bearing plate (LRFD 6.13.2.7)

If bolts are excluded from plane:

$$R_r = \phi_s R_n = \phi_s (0.48 A_b F_{ub} N_s) \quad \phi_s = 0.80$$

- Check welds connecting the main girder to the sole plate (LRFD 6.13.3.2.4)

$$R_r = \phi R_n = 0.6 \phi_{e2} F_{exx} t_e L \quad \phi_{e2} = 0.8$$

- Check shear resistance of base metal (LRFD 6.13.5.3)

$$R_r = \phi R_n = 1.00 * 0.58 A_g F_y$$

- Check the shear resistance of the pintle (LRFD 6.13.2.7)

If bolts are excluded from plane:

$$R_r = \phi_s R_n = \phi_s (0.48 A_b F_{ub} N_s) \quad \phi_s = 0.80$$

- Check the bearing on the concrete pier cap (LRFD 5.7.5), conservatively ignoring the confinement reinforcement

$$P_r = \phi P_n = 0.70 (0.85 f'_c A_l m)$$

CGG Provisions

- Design according to the provisions in AASHTO Standard Specifications